USGS
science for a changing world

Prepared in cooperation with the Harris-Galveston Subsidence District and the Fort Bend Subsidence District

Hydrogeology, Land-Surface Subsidence, and Documentation of the Gulf Coast Land Subsidence and Groundwater-Flow (GULF) Model, Southeast Texas, 1897–2018

Professional Paper 1877
Version 1.1, November 2023

U.S. Department of the Interior
U.S. Geological Survey

Hydrogeology, Land-Surface Subsidence, and Documentation of the Gulf Coast Land Subsidence and Groundwater-Flow (GULF) Model, Southeast Texas, 1897–2018

By John H. Ellis, Jacob E. Knight, Jeremy T. White, Michelle Sneed, Joseph D. Hughes, Jason K. Ramage, Christopher L. Braun, Andrew Teeple, Linzy Foster, Samuel H. Rendon, and Justin Brandt

Prepared in cooperation with the Harris-Galveston Subsidence District and the Fort Bend Subsidence District

Professional Paper 1877
Version 1.1, November 2023

U.S. Department of the Interior
U.S. Geological Survey

U.S. Geological Survey, Reston, Virginia: 2023
Revised: November 2023 (ver. 1.1)

For more information on the USGS—the Federal source for science about the Earth, its natural and living resources, natural hazards, and the environment—visit https://www.usgs.gov or call 1–888–ASK–USGS.

For an overview of USGS information products, including maps, imagery, and publications, visit https://store.usgs.gov/.

Suggested citation:
Ellis, J.H., Knight, J.E., White, J.T., Sneed, M., Hughes, J.D., Ramage, J.K., Braun, C.L., Teeple, A., Foster, L., Rendon, S.H., and Brandt, J., 2023, Hydrogeology, land-surface subsidence, and documentation of the Gulf Coast Land Subsidence and Groundwater-Flow (GULF) model, southeast Texas, 1897–2018 (ver. 1.1, November 2023): U.S. Geological Survey Professional Paper 1877, 425 p., https://doi.org/10.3133/pp1877.

Associated data for this publication::
Knight, J.E., Ellis, J.H., White, J.T., Sneed, M., Hughes, J.D., Ramage, J.K., Braun, C.L., Teeple, A.P., Foster, L., Rendon, S.H., Brandt, J., Duncan, L.L., Traylor, J.P., and Pattison, C.N., 2023, MODFLOW 6 model and ensemble used in the simulation of groundwater flow and land-surface subsidence in the northern part of the Gulf Coast aquifer system, 1897–2018: U.S. Geological Survey data release, https://doi.org/10.5066/P9XM8A1P.

ISSN 2330-7102 (online)

Acknowledgments

The project documented in this report was conducted as part of the U.S. Geological Survey (USGS) Cooperative Water Program, in cooperation with the Harris-Galveston and Fort Bend Subsidence Districts. The authors appreciate the support and feedback of Michael Turco, Christina Petersen, Ashley Greuter, and the staff at the subsidence districts. The authors are grateful for the contributions of the Texas Water Development Board Groundwater Management Area 14 districts. The authors thank the staff at INTERA Incorporated for their reports on the stratigraphy, subsidence parameters, and groundwater use in the northern part of the Gulf Coast aquifer system in Texas. The authors thank Larry French, Natalie Ballew, Cindy Ridgeway, Daryn Hardwick, Shirley Wade, and others at the Texas Water Development Board for their assistance with the Groundwater Availability Model process, technical reviews, and feedback at multiple points during this project. The authors also acknowledge the report reviewers for their comments which have improved this manuscript.

The authors acknowledge the assistance of numerous USGS personnel, including Dexter Brown (USGS, retired), Natalie Houston, Sam Wallace, Martha Nielsen, Jeff East, John Gordon, and others for assistance with field work, water-use analysis, system conceptualization, data analysis, spatial datasets, and report review. The authors also acknowledge the many hours of assistance provided by Laura Coplin for locating historical data and for designing the illustrations in this report. The authors acknowledge and appreciate the professionalism, experience, and dedication of these colleagues.

Contents

Sidebar

Figures

Tables

Conversion Factors

U.S. customary units to International System of Units

Multiply	By	To obtain
	Length	
inch (in.)	2.54	centimeter (cm)
foot (ft)	0.3048	meter (m)
mile (mi)	1.609	kilometer (km)
	Area	
acre	4,047	square meter (m^2)
acre	0.4047	hectare (ha)
square foot (ft^2)	929.0	square centimeter (cm^2)
square foot (ft^2)	0.09290	square meter (m^2)
square mile (mi^2)	259.0	hectare (ha)
	Volume	
gallon (gal)	0.003785	cubic meter (m^3)
acre-foot (acre-ft)	1,233	cubic meter (m^3)
	Flow rate	
acre-foot per year (acre-ft/yr)	1,233	cubic meter per year (m^3/yr)
acre-foot per year (acre-ft/yr)	0.001233	cubic hectometer per year (hm^3/yr)
foot per day (ft/d)	0.3048	meter per day (m/d)
foot per year (ft/yr)	0.3048	meter per year (m/yr)
cubic foot per second (ft^3/s)	0.02832	cubic meter per second (m^3/s)
million gallons per day (Mgal/d)	3,785	cubic meter (m^3)
inch per year (in/yr)	25.4	millimeter per year (mm/yr)
	Hydraulic conductivity	
foot per day (ft/d)	0.3048	meter per day (m/d)
	Hydraulic gradient	
foot per mile (ft/mi)	0.1894	meter per kilometer (m/km)
	Transmissivity	
foot squared per day (ft^2/d)	0.09290	meter squared per day (m^2/d)

International System of Units to U.S. customary units

Multiply	By	To obtain
	Length	
centimeter (cm)	0.3937	inch (in.)
millimeter (mm)	0.03937	inch (in.)
meter (m)	3.281	foot (ft)
kilometer (km)	0.6214	mile (mi)
kilometer (km)	0.5400	mile, nautical (nmi)
meter (m)	1.094	yard (yd)
	Area	
square kilometer (km^2)	247.1	acre
	Flow rate	
millimeter per year (mm/yr)	0.03937	inch per year (in/yr)

Datum

Vertical coordinate information is referenced to the National Geodetic Vertical Datum of 1929 (NGVD 1929) or to the North American Vertical Datum of 1988 (NAVD 88).

Horizontal coordinate information is referenced to the North American Datum of 1983 (NAD 83).

Elevation, as used in this report, refers to distance above the vertical datum in the context of compaction, subsidence, and vertical displacement and also refers to the height of the land surface above the vertical datum.

Altitude, as used in this report, refers to distance above the vertical datum in the context of groundwater-monitoring well depths and screened intervals and water-table surfaces.

Abbreviations

AMOCO	American Oil Company
bls	below land surface
CORS	Continuously Operating Reference Station
CSUB	Skeletal Storage, Compaction, and Subsidence
FBSD	Fort Bend Subsidence District
GAM	Groundwater Availability Model
GCD	groundwater conservation district
GHB	General-Head Boundary
GNSS	Global Navigation Satellite System
GPS	Global Positioning System
GULF model	Gulf Coast Land Subsidence and Groundwater-Flow model
HAGM	Houston Area Groundwater Model
HGSD	Harris-Galveston Subsidence District
IBS	Interbed-Storage package
IES	iterative ensemble smoother
InSAR	interferometric synthetic aperture radar
Kh	horizontal hydraulic conductivity
Kv	vertical hydraulic conductivity
LSGCD	Lone Star Groundwater Conservation District
NGC-GAM	Northern Gulf Coast Groundwater Availability Model
NGS	National Geodetic Survey
NOAA	National Oceanic and Atmospheric Administration
NWIS	National Water Information System
SAR	synthetic aperture radar
SUB	Subsidence and Aquifer-System Compaction Package
SUB-WT	Subsidence and Aquifer-System Compaction Package (SUB-WT) for Water-Table Aquifers
SWB	Soil-Water-Balance
TWDB	Texas Water Development Board
USGS	U.S. Geological Survey

Hydrogeology, Land-Surface Subsidence, and Documentation of the Gulf Coast Land Subsidence and Groundwater-Flow (GULF) Model, Southeast Texas, 1897–2018

By John H. Ellis,[1] Jacob E. Knight,[1] Jeremy T. White,[2] Michelle Sneed,[1] Joseph D. Hughes,[1] Jason K. Ramage,[1] Christopher L. Braun,[1] Andrew Teeple,[1] Linzy Foster,[1] Samuel H. Rendon,[1] and Justin Brandt[1]

Executive Summary

As a part of the Texas Water Development Board groundwater availability modeling program, the U.S. Geological Survey developed the Gulf Coast Land Subsidence and Groundwater-Flow model (hereinafter, the "GULF model") and ensemble to simulate groundwater flow and land-surface subsidence in the northern part of the Gulf Coast aquifer system (the study area) in Texas from predevelopment (1897) through 2018. Since the publication of a previous groundwater model for the greater Houston area in 2012, there have been changes to the distribution of groundwater withdrawals and advances in modeling tools. To reflect these changes and to simulate more recent conditions, the GULF model was developed in cooperation with the Harris-Galveston and Fort Bend Subsidence Districts to provide an updated Groundwater Availability Model.

Since the early 1900s, most of the groundwater withdrawals in the study area have been from three of the hydrogeologic units that compose the Gulf Coast aquifer system—the Chicot, Evangeline, and Jasper aquifers and, more recently, from the Catahoula confining unit. Withdrawals from these hydrogeologic units are used for municipal supply, commercial and industrial use, and irrigation purposes. Withdrawals of large quantities of groundwater in the greater Houston area have caused widespread groundwater-level declines in the Chicot, Evangeline, and Jasper aquifers of more than 300 feet (ft). Early development of the aquifer system, which began before 1900, resulted in nearly 50 percent of the eventual historical groundwater-level minimums having been reached as early as 1946 in some areas. These groundwater-level declines led to more than 9 ft of land-surface subsidence—historically in central and southeastern Harris County and Galveston County, but more recently in northern, northwestern, and western Harris County, Montgomery County, and northern Fort Bend County—from depressurization and compaction of clay and silt layers interbedded in the aquifer sediments.

In a generalized conceptual model of the Gulf Coast aquifer system, water enters the groundwater system in topographically high outcrops of the hydrogeologic units in the northwestern part of the aquifer system. Groundwater that does not discharge to streams flows to intermediate and deep zones of the aquifer system southeastward of the outcrop areas where it is discharged by wells and by upward leakage in topographically low areas near the coast. The uppermost parts of the aquifer system, which include outcrop areas, are under water-table (unconfined) conditions where the groundwater is not confined under pressure. As depth increases in the aquifer system and interbedded clay and silt layers accumulate, water-table conditions evolve into confined conditions where the groundwater is under pressure.

Groundwater flow and land-surface subsidence in the GULF model and ensemble were simulated by using MODFLOW 6 with the Skeletal Storage, Compaction, and Subsidence package. The model consists of six layers, one for each of the five hydrogeologic units in the northern part of the Gulf Coast aquifer system and a surficial top layer that includes part of each hydrogeologic unit. Transient groundwater flow was simulated during 1897–2018 by using a combination of multiyear, annual, and monthly stress periods. An initial steady-state stress period was configured to represent predevelopment mean annual inflows and outflows. The subsidence package used in the GULF model and ensemble uses a head-based subsidence formulation that simulates the delayed drainage response from clay and silt sediment to changes in groundwater levels.

The GULF model and ensemble were history matched to groundwater-level observations at selected wells, land-surface subsidence at benchmarks, aquifer compaction at borehole extensometers, and vertical displacement from Global Positioning System stations. A Bayesian framework was used to represent uncertainty in modeled parameters and simulated

[1]U.S. Geological Survey.

[2]INTERA Incorporated.

outputs of interest. History matching and uncertainty quantification were performed by using a Monte Carlo approach enabled through iterative ensemble smoother software to produce an ensemble of models fit to historical data. The iterative ensemble smoother substantially reduced the computational demand of parameter estimation by approximating the first-order relation between model inputs and outputs, thereby allowing 183,207 adjustable parameters to be used for history matching at a relatively low computational and time cost.

The history-matched parameter values are within the ranges of previously published values and agree with the current understanding of the spatial and temporal patterns of parameter uncertainty for the Gulf Coast aquifer system. A good agreement between the observed (or estimated) and simulated groundwater levels, land-surface subsidence, compaction, and vertical displacement was obtained across the modeled area based on qualitative and quantitative comparisons. Ensemble mean annual groundwater-flow rates to the Chicot, Evangeline, Jasper aquifers and Catahoula confining unit were 0.0–0.49 inch (in.), 0.09–0.33 in., 0.01–0.07 in., and 0.01–0.05 in., respectively. GULF model mean annual groundwater-flow rates to the Chicot, Evangeline, and Jasper aquifers and Catahoula confining unit were 0.31 in., 0.19 in., 0.03 in., and 0.03 in., respectively.

The GULF-model-simulated recharge to the outcrop area was the largest inflow (75 percent), and recharge to other areas was 25 percent of the model inflow. The simulated outflows included (1) net surface-water/groundwater exchange with study area streams (50 percent), (2) groundwater use (49 percent), and (3) net surface-water/groundwater exchange with the Gulf of Mexico (1 percent). The sum of the simulated values of the outflows (1,041,973 acre-feet per year [acre-ft/yr]) and the elastic expansion of the fine-grained sediment and numerical solver error (339 acre-ft/yr) minus the inflows (654,172 acre-ft/yr) represents the reduction of storage from the Gulf Coast aquifer system (388,140 acre-ft/yr). Most of the storage depletion is caused by the long-term groundwater-level declines that have resulted primarily in inelastic compaction.

The GULF model was used to estimate Jasper aquifer compaction at selected benchmarks in Montgomery County and northern Harris County, which are the primary locations of Jasper aquifer groundwater use. Simulated Jasper aquifer compaction in northern Harris County was between 0.2 and 0.5 ft, or between about 5 and 16 percent of simulated subsidence at the benchmark locations. Simulated Jasper aquifer compaction in Montgomery County was between 0.8 and 1.2 ft, or between about 33 and 57 percent of simulated subsidence at the benchmark locations.

Introduction

Groundwater from the Gulf Coast aquifer system—defined by the Texas Water Development Board (TWDB) as the Chicot aquifer, Evangeline aquifer, Burkeville confining unit, Jasper aquifer, and Catahoula confining unit (Ashworth and Hopkins, 1995)—is an important resource along the northern part of the Gulf Coast of Texas. Groundwater withdrawn from this system has been an important source of water for municipal supply, commercial and industrial use, and irrigation use since the early 1900s. The greater Houston area (fig. 1) in southeast Texas encompasses about 7,854 square miles (mi^2) and had an estimated population of about 7.1 million in 2020 (U.S. Census Bureau, 2020). The surrounding area contains more than 30 cities, including Beaumont, Galveston, Port Arthur, and Conroe, Tex. Between 2010 and 2019, the Houston metropolitan statistical area population grew by about 1.15 million people (U.S. Census Bureau, 2020); therefore, as the population of this area continues to expand, management practices that lead to sustainable use of groundwater are critically important.

Groundwater from the Gulf Coast aquifer system has been used in the greater Houston area for municipal supply, commercial and industrial use, and irrigation for more than 120 years. The Gulf Coast aquifer system has an abundance of groundwater; however, groundwater withdrawals (synonymous in this report with "groundwater use") have resulted in potentiometric surface declines in the Chicot, Evangeline, and Jasper aquifers, and associated land-surface subsidence (referred to hereinafter as "subsidence"), which causes a decrease in land-surface elevation from depressurization and compaction of interbedded clays and silts in these aquifers. The adverse effects of groundwater withdrawals led to the 1975 establishment of the Harris-Galveston Coastal Subsidence District (after 2005, the Harris-Galveston Subsidence District [HGSD], used hereinafter) to provide groundwater management and regulation. An additional subsidence district, the Fort Bend Subsidence District (FBSD), was established in 1989, along with 11 groundwater conservation districts between 2001 and 2014.

Since 1999, the TWDB has been tasked with developing numerical groundwater-flow models (hereinafter referred to as "groundwater models") of the aquifers in Texas through the groundwater availability modeling program. The Groundwater Availability Models (GAMs) and associated reports include extensive documentation on the aquifers' hydrogeologic and hydraulic properties; such properties are surface and subsurface geology, aquifer conceptualization including inflows (such as recharge, lateral flow, seepage from streams) and outflows (such as seepage to streams, groundwater use), the hydrogeologic framework (hydrogeologic unit geospatial extent, bed orientation, unit thickness), construction, and calibration (or "history matching") of the GAM. Pursuant to Texas Water Code §36.1132, the TWDB uses the GAMs to estimate the modeled available groundwater. Results from the groundwater availability modeling program are intended to be a tool that water-resource managers can use to address future groundwater availability issues.

The Gulf Coast Land Subsidence and Groundwater-Flow model (referred to hereinafter as the "GULF model") and ensemble described in this report and documented in a

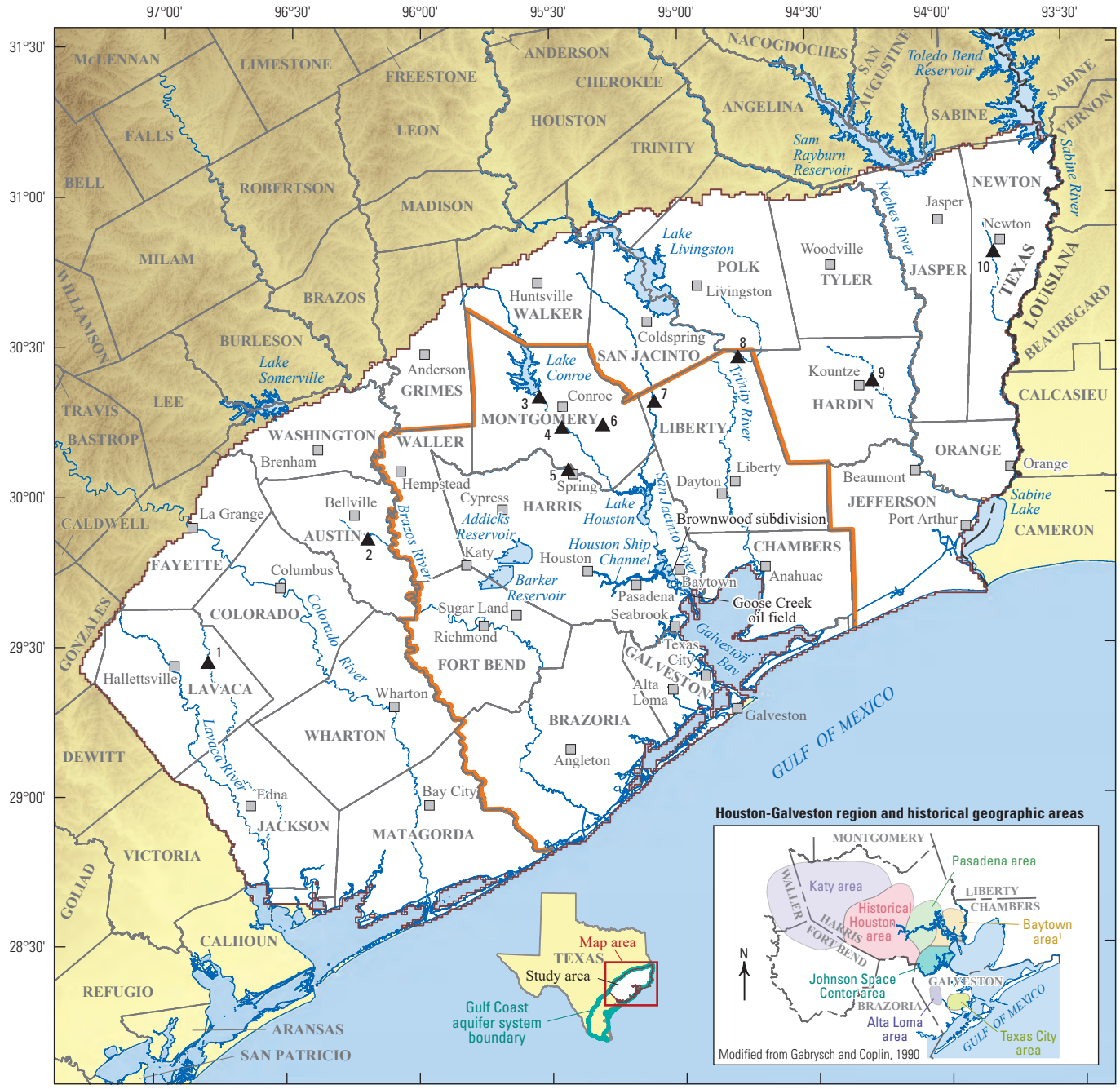

Base modified from U.S. Geological Survey (USGS) digital data
Albers Equal-Area Conic projection
Standard parallels 29°30' N. and 45°30' N.
Central meridian 96°00' W.
North American Datum of 1983

Gulf Coast aquifer system boundary modified from Casarez (2020)
Hydrography modified from Horizon Systems Corporation (2020)
Shaded relief derived from USGS (2021a)

0 20 40 60 MILES
0 20 40 60 KILOMETERS

EXPLANATION

- **Gulf Coast Land Subsidence and Groundwater-Flow model area**—The northern part of the Gulf Coast aquifer system, synonymous with the "study area"
- **Greater Houston area boundary**
- 3 **USGS streamgage and map number (USGS, 2021b)**

Map number	USGS station number	Station name
1	08164300	Navidad River near Hallettsville, Texas
2	08111700	Mill Creek near Bellville, Texas
3	08067650	West Fork San Jacinto River below Lake Conroe near Conroe, Texas
4	08068000	West Fork San Jacinto River near Conroe, Texas
5	08068500	Spring Creek near Spring, Texas
6	08070500	Caney Creek near Splendora, Texas
7	08070000	East Fork San Jacinto River near Cleveland, Texas
8	08066300	Menard Creek near Rye, Texas
9	08041500	Village Creek near Kountze, Texas
10	08029500	Big Cow Creek near Newton, Texas

[1]Prior to Gabrysch (1972), the reported groundwater use for the Baytown area also included the La Porte area, which is approximately spatially contiguous with the Johnson Space Center area. Groundwater use in the Johnson Space Center area was subdivided from the Baytown area in Gabrysch (1972), and the groundwater use was redistributed into these two areas beginning in 1960.

Figure 1. The Gulf Coast aquifer system study area and selected U.S. Geological Survey streamgages in southeast Texas.

companion data release (Knight and others, 2023) is the most recent groundwater model in a series of GAMs for the northern part of the Gulf Coast aquifer system (for brevity, referred to hereinafter as the "Gulf Coast aquifer system") described in the "Previous Hydrogeologic Modeling" section of this report. A previous groundwater model for the greater Houston area is referred to as the "Houston Area Groundwater Model" (HAGM) (Kasmarek, 2012); since the development of the HAGM, there have been changes to the distribution of groundwater withdrawals and advances in modeling tools. To reflect these changes and simulate more recent conditions, the GULF model and ensemble were developed by the U.S. Geological Survey (USGS) in cooperation with the Harris-Galveston and Fort Bend Subsidence Districts to provide an updated model for use as a GAM. This report documents the hydrogeology of the Gulf Coast aquifer system and the simulation of groundwater flow and subsidence using the GULF model and an ensemble from predevelopment (generally before 1900) through 2018.

Purpose and Scope

This report presents the results of an investigation of the occurrence and movement of groundwater and extent of subsidence during 1897–2018 caused by aquifer-system compaction in the Gulf Coast aquifer system and includes descriptions of the aquifer hydrogeology and development of a groundwater-flow model (the GULF model) primarily for a 28-county area in southeast Texas that includes the greater Houston area. This report describes how the GULF model could be used to evaluate future groundwater availability and subsidence under various potential future conditions for the Gulf Coast aquifer system (synonymous with "study area" and "model area" in this report). Specifically, the report includes (1) a description of the hydrogeology (including the geologic and hydrologic units, groundwater use, groundwater levels, streamflow, recharge, groundwater flow, and subsidence based on available information), (2) a description of groundwater-flow simulation, including primarily the construction and discretization of the GULF model, historical observations, history matching, and uncertainty when the GULF model is used to simulate regional patterns of groundwater occurrence and flow and subsidence, and (3) documentation of the uncertainty of system response to groundwater development at a regional scale to inform water-management decisions. In this report the term "groundwater development" refers to the installation of groundwater wells and associated infrastructure needed to supply water for a wide range of uses including municipal, industrial, and agricultural needs. Groundwater model files and all required software to perform the simulations described in this report are documented in Knight and others (2023).

Study Area

The study area (the white shaded area on fig. 1) consists of about 22,770 mi^2 (14.6 million acres) of Gulf Coast aquifer system sedimentary deposits primarily in 28 counties in southeast Texas.

The greater Houston area is the dominant feature of the study area and includes Brazoria, Fort Bend, Galveston, Harris, and Montgomery Counties and parts of Chambers, Waller, and Liberty Counties (fig. 1). The northern boundary of the study area is the outcrop (appearance at the surface of a geologic unit) of the Catahoula confining unit described in Casarez (2020). The northeastern boundary of the study area is the Texas–Louisiana boundary, which coincides with the Sabine River. The southwestern boundary of the study area is the western extent of Lavaca and Jackson Counties. The southern boundary is the nearshore area of the Gulf of Mexico. The study area also includes the alluvium and terrace deposits of multiple streams that overlie the sediment of the Gulf Coast aquifer system. These major streams include, from west to east, the Lavaca, Colorado, Brazos, San Jacinto, Trinity, Neches, and Sabine Rivers, as well as smaller streams and tributaries, some of which have streamflow and base-flow information presented in this report. Several large reservoirs in the study area include, from west to east, Barker Reservoir, Addicks Reservoir, Lake Conroe, Lake Houston, and Lake Livingston (Dowell, 1964; TWDB, 1998).

The physiography of the study area is characterized by a gently sloping coastal plain dissected by surface-water features such as incised drainage channels, streams, and associated tributaries. Land-surface elevations in the study area (fig. 2) range from about 0 to about 600 feet (ft) above the North American Vertical Datum of 1988 (NAVD 88) (USGS, 2021a), and the mean land-surface gradient is about 2 feet per mile (ft/mi) (Rose, 1943). Land-surface elevations are highest near the northwestern boundary of the study area between the Brazos and Colorado Rivers (fig. 2).

The study area contains all or parts of 11 groundwater conservation districts (GCDs) (fig. 3) (TWDB, 2019), listed in order of establishment by the Texas Legislature: Fayette County GCD (2001), Texana GCD (2001), Coastal Plains GCD (2001), Lone Star GCD (LSGCD) (2001), Coastal Bend GCD (2001), Bluebonnet GCD (2002), Southeast Texas GCD (2004), Brazoria County GCD (2005), Lower Trinity GCD (2006), Colorado County GCD (2007), and Calhoun County GCD (2014). Additionally, the study area contains two subsidence districts: HGSD and FBSD, established in 1975 and 1989, respectively. The primary purpose of the HGSD and the FBSD is to control subsidence in Harris, Galveston, and Fort Bend Counties by providing groundwater regulation in five jurisdictional areas. HGSD Regulatory Areas 1 and 2, enacted in 1999, require that groundwater withdrawals compose no more than 10 and 20 percent, respectively, of the water used to meet demand (HGSD Regulatory Areas 1 and 2 have already converted to surface water). Since 2010, Area 3, which was also enacted in 1999, has required that

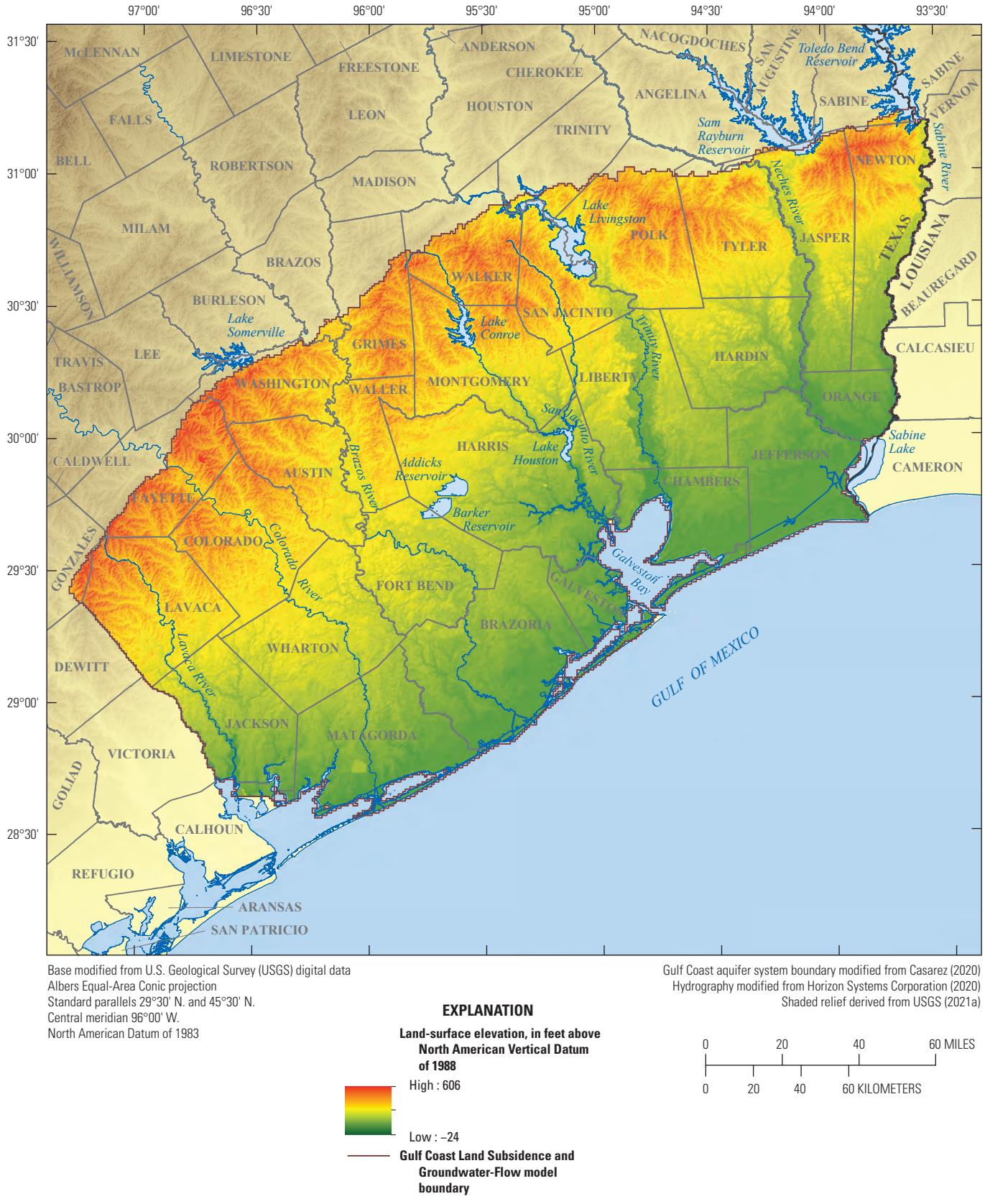

Base modified from U.S. Geological Survey (USGS) digital data
Albers Equal-Area Conic projection
Standard parallels 29°30' N. and 45°30' N.
Central meridian 96°00' W.
North American Datum of 1983

Gulf Coast aquifer system boundary modified from Casarez (2020)
Hydrography modified from Horizon Systems Corporation (2020)
Shaded relief derived from USGS (2021a)

EXPLANATION

Land-surface elevation, in feet above North American Vertical Datum of 1988

High : 606

Low : –24

Gulf Coast Land Subsidence and Groundwater-Flow model boundary

0 20 40 60 MILES

0 20 40 60 KILOMETERS

Figure 2. Elevation of the land surface in the Gulf Coast aquifer system study area in southeast Texas.

groundwater withdrawals compose no more than 70 percent of the water used to meet demand through 2025 (fig. 3) (HGSD, 2013). Beginning in 2025, groundwater withdrawals in Area 3 will be required to compose no more than 40 percent of the water used to meet demand (fig. 3) (HGSD, 2013). FBSD Regulatory Area A requires that groundwater withdrawals compose no more than 70 percent of water used to meet demand (as of 2014), with groundwater withdrawals slated to decrease to 40 percent of the water used to meet demand by 2025 (FBSD, 2013). FBSD Regulatory Area B permits are not subject to groundwater reduction requirements (FBSD, 2013).

Land-cover data for the study area were obtained from the CropScape database (National Agricultural Statistics Service, 2021) (fig. 4). This database included land-cover characteristics at a 30-meter resolution for land overlying the Gulf Coast aquifer system. Land-cover and crop data were used for 2004, 2011, and 2018 to provide a generalized estimate during 2004–2018. During this period, the land cover (14.6 million acres) was primarily grass/pasture (25.7 percent), wetlands (20.4 percent), forest (19.4 percent), developed (14.1 percent), cropland (13.8 percent), and shrubland (6.7 percent).

Cotton, which accounted for 14.1 percent of cropland by area, was the dominant crop type overlying the Gulf Coast aquifer system. Corn (13.1 percent), rice (12.5 percent), hay (12.0 percent), and sorghum (6.0 percent) were the only other crop types accounting for at least 5 percent of cropland by area (fig. 4). About 35 percent of cropland by area was fallow or idle. Although crop types could change depending on economic conditions and hydrologic factors such as flooding or drought conditions, the percentages of total crop land cover and individual crop types did not change substantially during 2004–18, the period for which data were available (National Agricultural Statistics Service, 2021).

The climate in the greater Houston area (fig. 1) is subtropical, and the mean annual precipitation for 1897–2018 was 48 inches (in.) (fig. 5) (National Climatic Data Center, 2019). A substantial period of above-mean annual precipitation occurred generally after about 1973, whereas substantial periods of below-mean annual precipitation occurred between about 1950 and 1970. During 1897–2018, mean monthly precipitation was greatest in May (4.7 in.) and least in February and March (3.3 in.) (fig. 6) (National Climatic Data Center, 2019).

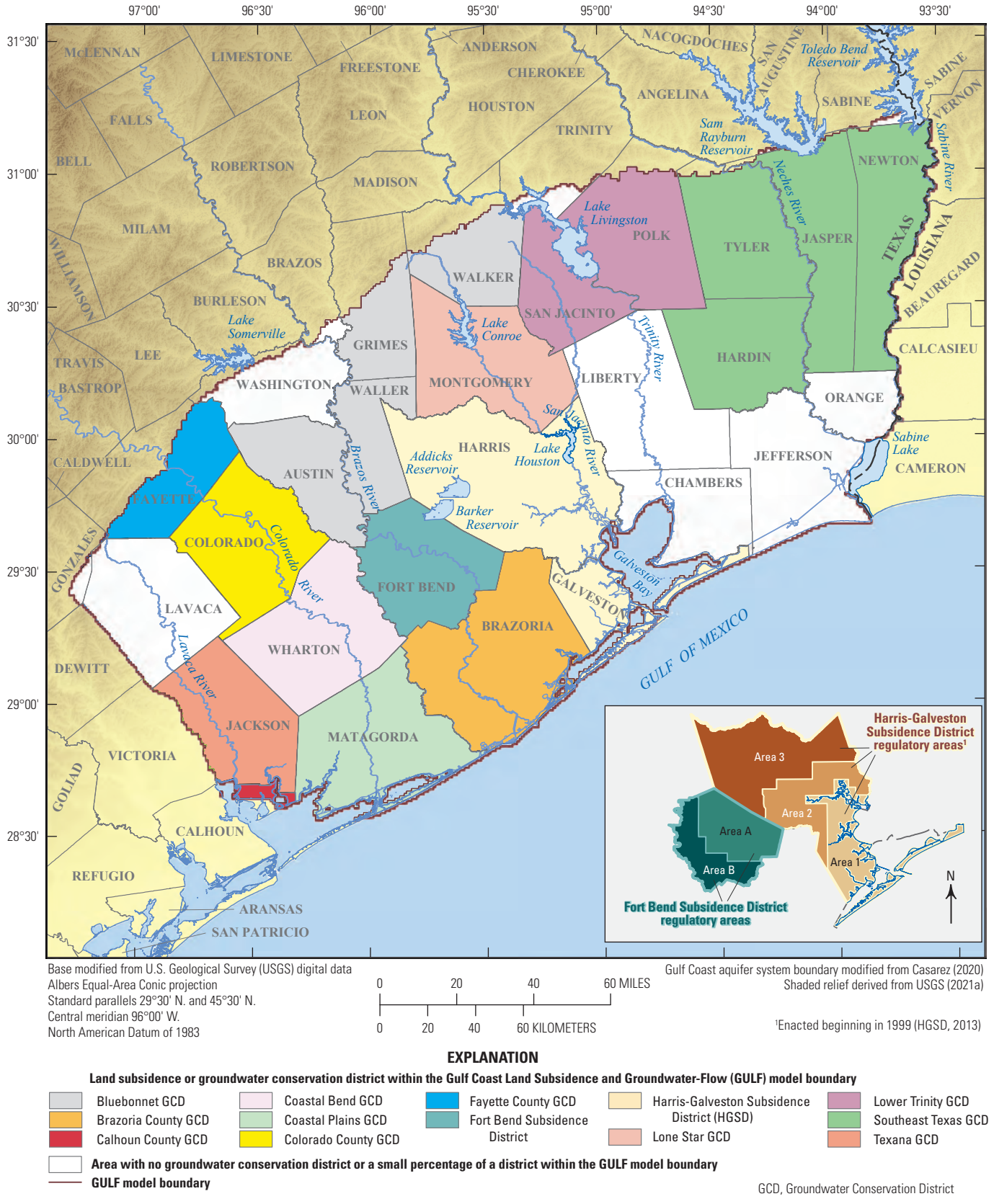

Base modified from U.S. Geological Survey (USGS) digital data
Albers Equal-Area Conic projection
Standard parallels 29°30' N. and 45°30' N.
Central meridian 96°00' W.
North American Datum of 1983

0 20 40 60 MILES
0 20 40 60 KILOMETERS

Gulf Coast aquifer system boundary modified from Casarez (2020)
Shaded relief derived from USGS (2021a)

[1]Enacted beginning in 1999 (HGSD, 2013)

EXPLANATION

Land subsidence or groundwater conservation district within the Gulf Coast Land Subsidence and Groundwater-Flow (GULF) model boundary

- Bluebonnet GCD
- Brazoria County GCD
- Calhoun County GCD
- Coastal Bend GCD
- Coastal Plains GCD
- Colorado County GCD
- Fayette County GCD
- Fort Bend Subsidence District
- Harris-Galveston Subsidence District (HGSD)
- Lone Star GCD
- Lower Trinity GCD
- Southeast Texas GCD
- Texana GCD

Area with no groundwater conservation district or a small percentage of a district within the GULF model boundary

GULF model boundary

GCD, Groundwater Conservation District

Figure 3. Land subsidence and groundwater conservation districts within the Gulf Coast aquifer system study area in southeast Texas.

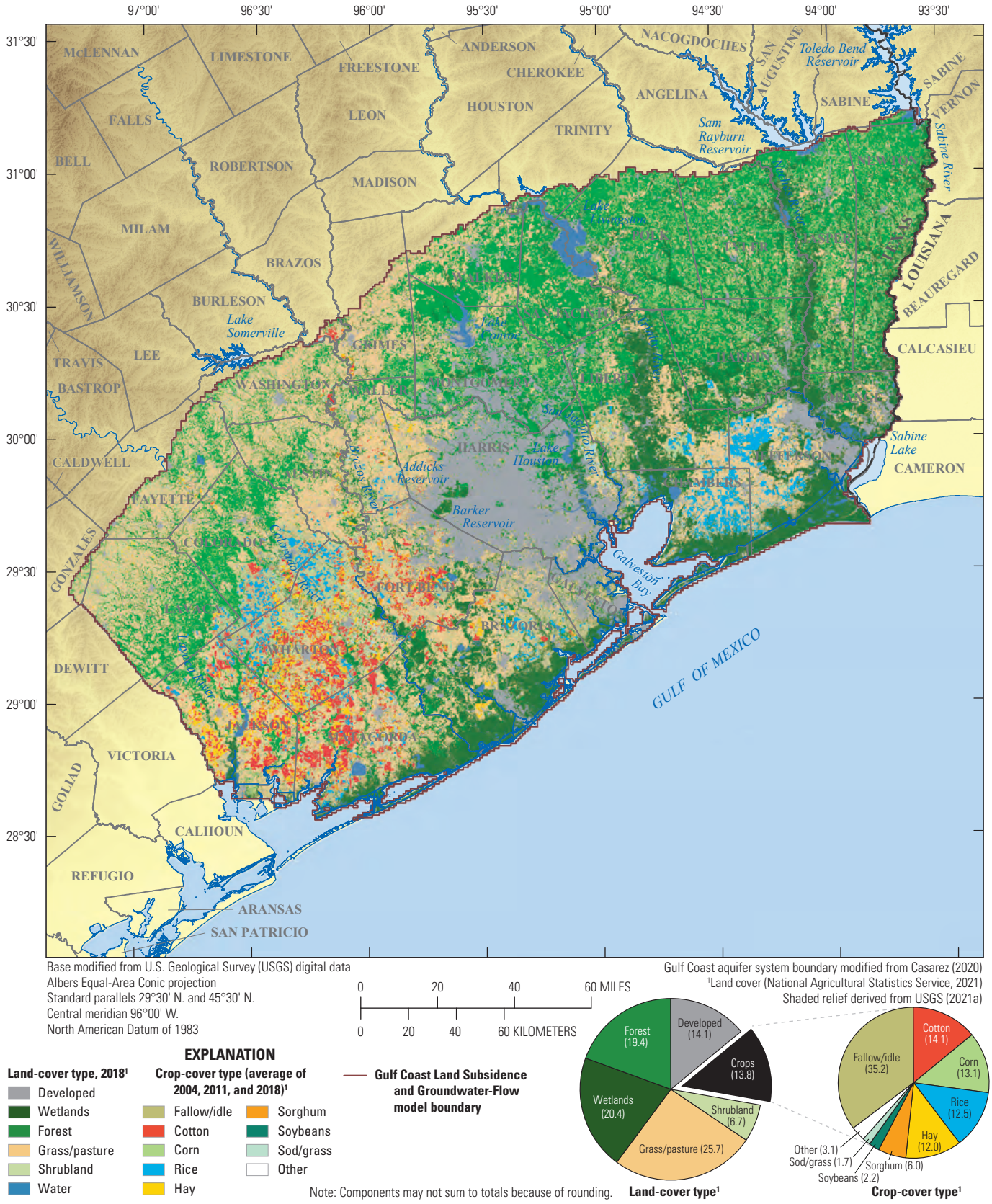

Figure 4. Land-cover and crop-cover type within the Gulf Coast aquifer system study area in southeast Texas.

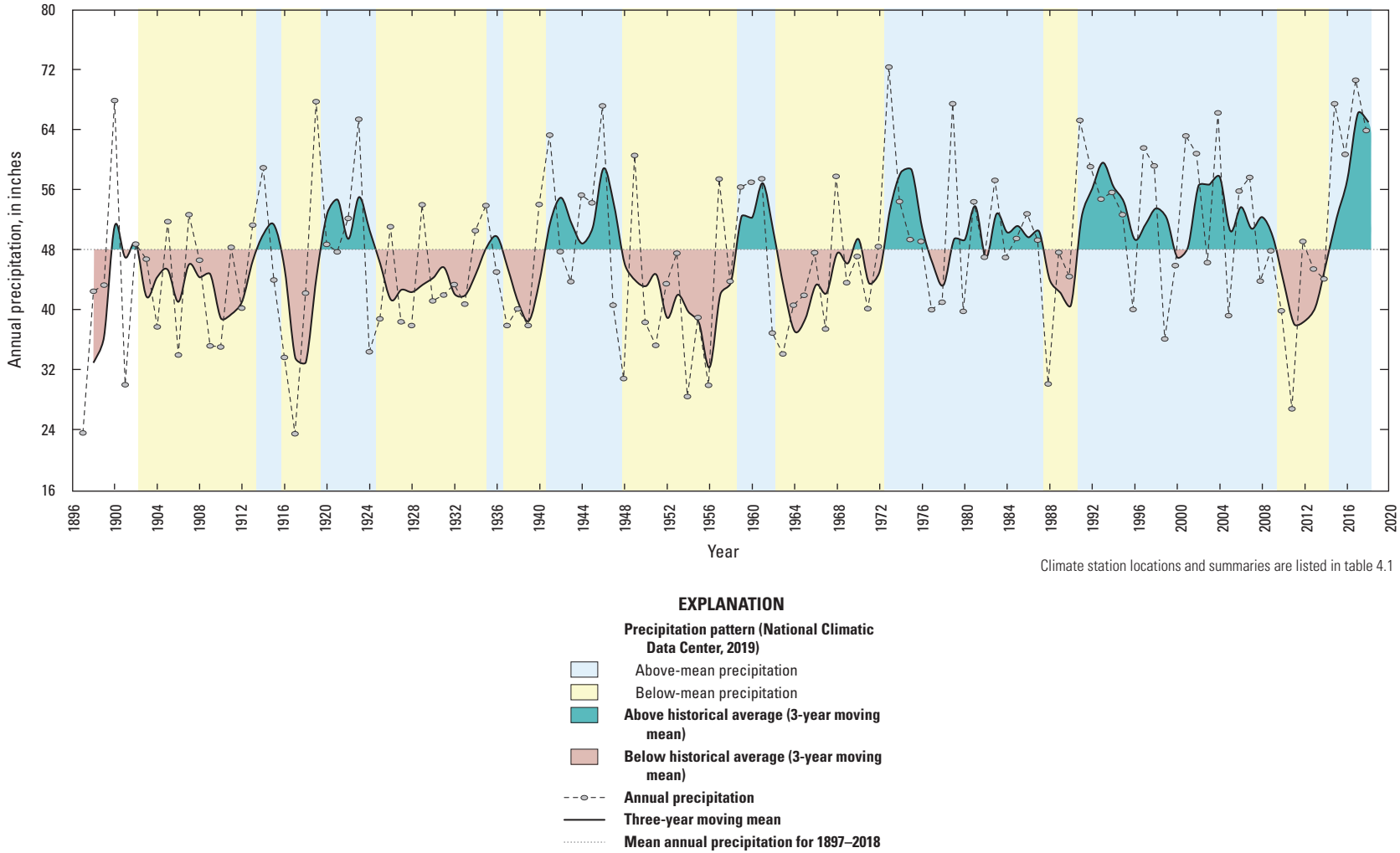

Figure 5. Precipitation and climate characteristics for the Gulf Coast aquifer system study area in southeast Texas, 1897–2018.

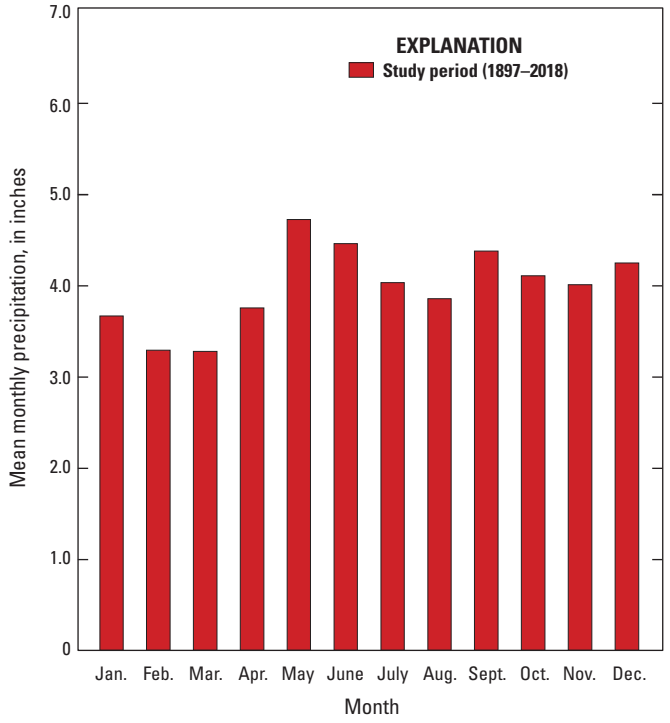

Figure 6. Mean monthly precipitation for the Gulf Coast aquifer system study area in southeast Texas, 1897–2018.

Hydrogeology

The general direction of groundwater flow in the Gulf Coast aquifer system is from the northwest to the southeast along a gradient approximately perpendicular to the coastline. Most of the water that infiltrates downward to the saturated zone flows relatively short distances through shallow zones and discharges to streams in the study area. Precipitation entering the saturated zone through the hydrogeologic unit outcrop area (hereinafter referred to as the "outcrop area") flows downward to depth, then laterally in the intermediate and deep aquifer systems in a southeast direction towards the coast. This groundwater is discharged by wells (particularly since the transition to substantial groundwater development starting about 1946) (Lang and others, 1950) and by upward leakage in topographically low areas near the coast (mainly during predevelopment and early development conditions, less so since about 1946). Near the coastline and at depth, denser saline water is present in the sediments and forms an effective boundary to continued downdip flow. The presence of saline water causes the less dense freshwater to be redirected upward as diffuse leakage, which is eventually discharged in coastal areas and Galveston Bay (Kasmarek and Strom, 2002).

Geologic and Hydrogeologic Units

In the study area, the Gulf Coast aquifer system is contained in discontinuous Quaternary- and Tertiary-age sedimentary deposits (fig. 7) of sands and interbedded clays and silts (clays and silts are commonly referred to as "fine-grained sediments") of fluvial deltaic or shallow marine origin. Changes in land-surface elevations related to natural subsidence of the depositional basin and sea-level transitions created cycles of sedimentation facies. During periods of sea-level decline, fluvial deltaic processes deposited continental sediments (mostly sand); during periods of rising sea level, marine sediments (mostly fine-grained sediment) were deposited, and continental sediments were reworked. As a result, the aquifer system has a high degree of heterogeneity areally and vertically (Sellards and others, 1932), and the sand and fine-grained units (or a thickness of fine-grained sediment) are not persistent in lithologic composition or thickness and grade together laterally and vertically within short distances (Gabrysch, 1967).

The Gulf Coast aquifer system hydrogeologic units include the Chicot aquifer, the Evangeline aquifer, the Burkeville confining unit, the Jasper aquifer, and the Catahoula confining unit (figs. 8–9). The Gulf Coast aquifer system is generally under water-table conditions (the groundwater is not confined under pressure, and atmospheric pressure conditions prevail) where each unit crops out at the surface—essentially in the northern part the study area (fig. 8). As depth increases in the aquifer system and interbedded fine-grained sediment accumulates, pressure conditions evolve from unconfined water-table conditions into confined conditions where the groundwater is under artesian pressure that can far exceed atmospheric pressure (Carr and others, 1985). Thus, the aquifer system becomes confined at some distance downdip. The configuration of the outcrop area on figure 8 is a simplification of the surface geology (fig. 7) and is based on the aquifer extents from Casarez (2020). The outcrop area of the geologic units that contain the Chicot aquifer (fig. 8) is defined as the areal extent from Noble and others (1996)—which includes the Lissie Formation and Willis Sand—bounded by the updip limit of the Chicot aquifer from Casarez (2020). The vertical thickness of each hydrogeologic unit (fig. 9) and where the tops and bases of different hydrogeologic units meet (hereinafter referred to as "contacts"), represented by spatially interpolated surfaces, were determined as a part of this study on the basis of stratigraphic contacts described by Young and Draper (2020) that were documented in Teeple and others (2021) and appendix 1 of this report.

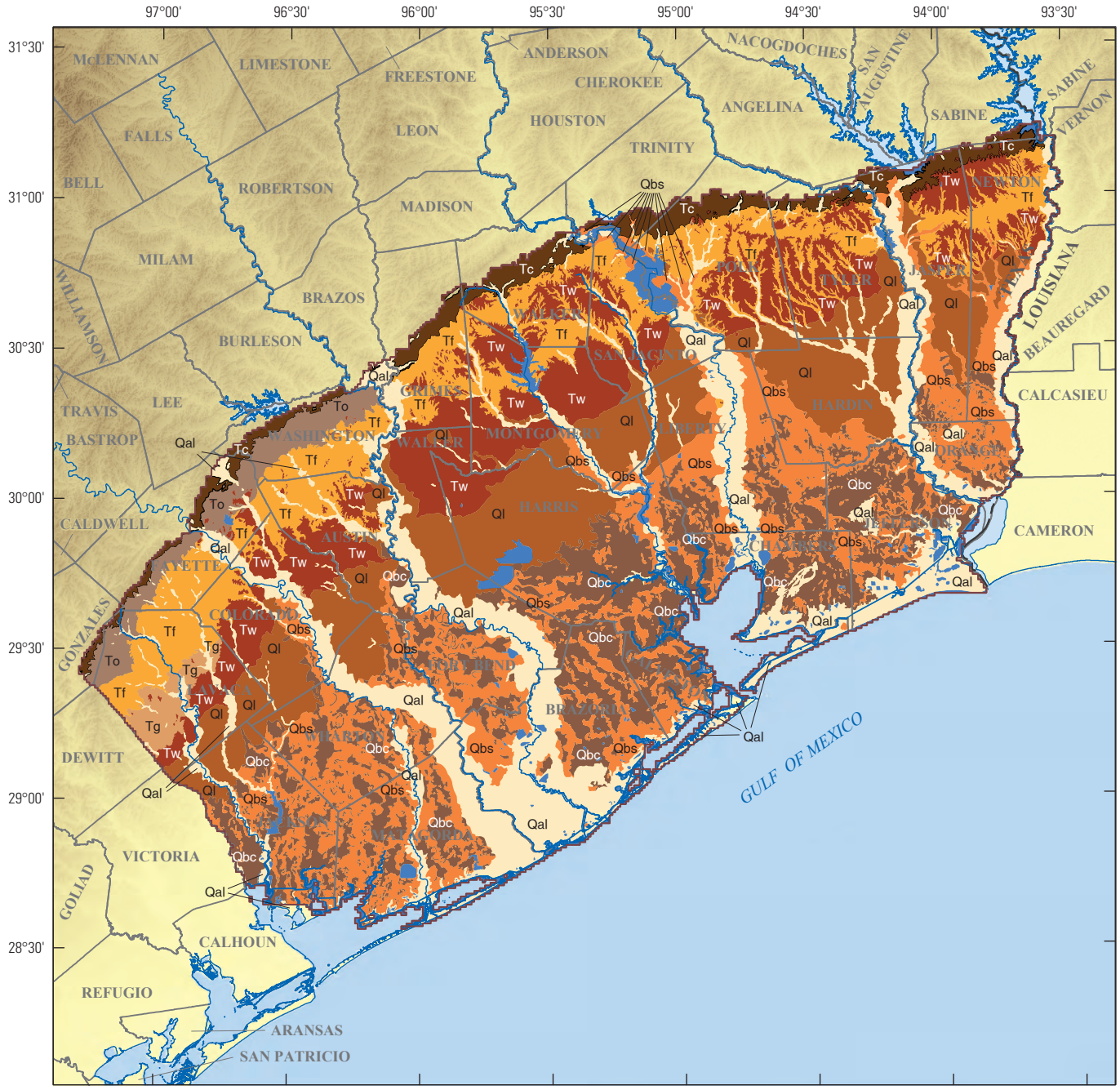

Base modified from U.S. Geological Survey (USGS) digital data
Albers Equal-Area Conic projection
Standard parallels 29°30' N. and 45°30' N.
Central meridian 96°00' W.
North American Datum of 1983

Gulf Coast aquifer system boundary modified from Casarez (2020)
Geology from Stoeser and others (2005)
Shaded relief derived from USGS (2021a)

0 20 40 60 MILES
0 20 40 60 KILOMETERS

EXPLANATION

Quaternary

- Qal — Alluvium, terrace, beach sand, dune sand
- Qbc — Beaumont Formation (fine-grained fraction)
- Qbs — Beaumont Formation (coarse-grained fraction)
- Ql — Lissie Formation

Tertiary

- Tw — Willis Sand (Pliocene)—Pow*
- Tg — Goliad Sand (Miocene)—Mg*
- Tf — Fleming Formation (Miocene)—Mf*
- To — Oakville Sandstone (Miocene)—Mo*
- Tc — Catahoula Formation (Oligocene)—Oc*

Water

Gulf Coast Land Subsidence and Groundwater-Flow model boundary

*Abbreviation for geologic unit used by the University of Texas, Bureau of Economic Geology

Figure 7. Surficial geologic units of the Gulf Coast aquifer system within the study area in southeast Texas.

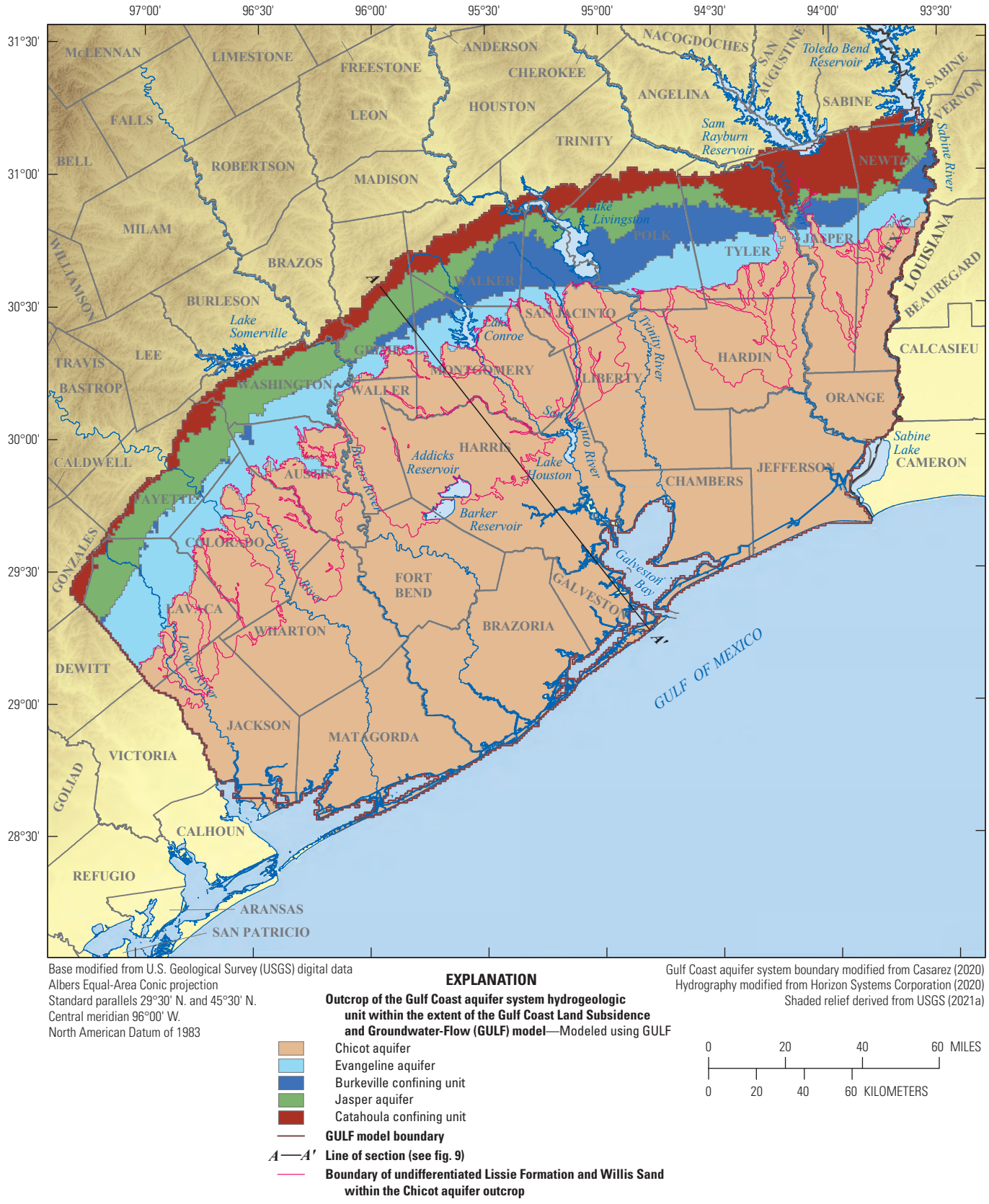

Base modified from U.S. Geological Survey (USGS) digital data
Albers Equal-Area Conic projection
Standard parallels 29°30' N. and 45°30' N.
Central meridian 96°00' W.
North American Datum of 1983

Gulf Coast aquifer system boundary modified from Casarez (2020)
Hydrography modified from Horizon Systems Corporation (2020)
Shaded relief derived from USGS (2021a)

EXPLANATION

Outcrop of the Gulf Coast aquifer system hydrogeologic unit within the extent of the Gulf Coast Land Subsidence and Groundwater-Flow (GULF) model—Modeled using GULF

- Chicot aquifer
- Evangeline aquifer
- Burkeville confining unit
- Jasper aquifer
- Catahoula confining unit

GULF model boundary

A—*A'* **Line of section (see fig. 9)**

Boundary of undifferentiated Lissie Formation and Willis Sand within the Chicot aquifer outcrop

0 20 40 60 MILES

0 20 40 60 KILOMETERS

Figure 8. Extent and outcrop area of the geologic units that contain the Gulf Coast aquifer system in the study area in southeast Texas.

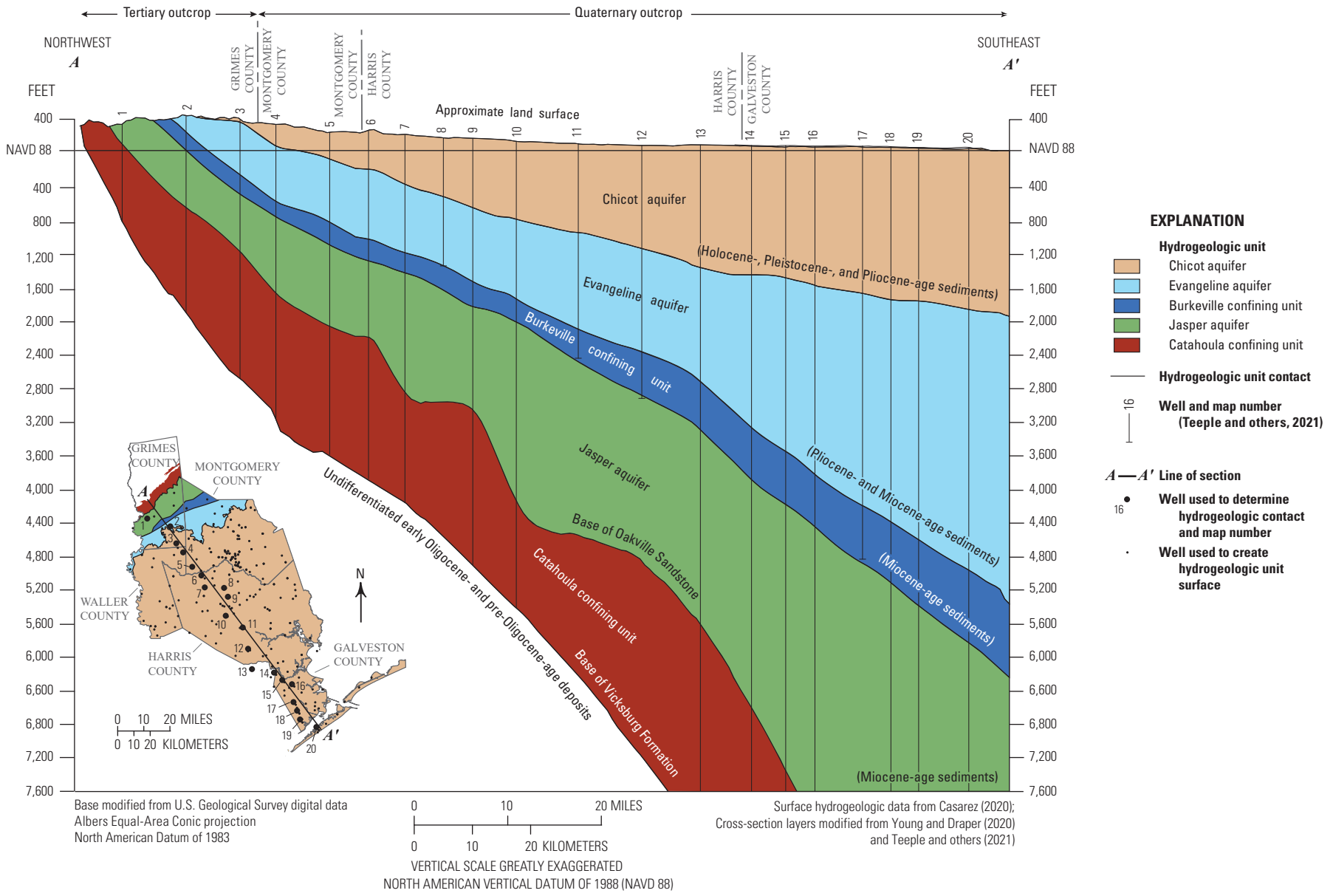

Figure 9. Hydrogeologic cross section of the Gulf Coast aquifer system within the study area in southeast Texas.

History of the Geologic and Hydrogeologic Units

The geologic and hydrogeologic units of the Gulf Coast aquifer system (figs. 7–8) have been studied for more than 100 years and were first extensively described in Deussen (1914). Prior to the publication of Turcan and others (1966), however, the aquifers and confining units of this system were not formally named as distinct hydrogeologic units. Rather, the water-bearing and confining units were classified by geologic formation in early reports generally prior to 1943 and thereafter were delineated by using geophysical logs and grouped into hydrogeologic "zones" (fig. 10). These grouped zones then formed the basis for the establishment of the current (2023) hydrogeologic units. A simplified correlation of the various geologic and hydrogeologic units and naming based on published reports describing the Gulf Coast aquifer system is presented in figure 10. All geologic units presented herein use a standardized catalog of established geologic unit naming (USGS, 2019); differences might exist between some of the geologic names presented in this report compared to those in previously published reports.

Deussen (1914) presented a stratigraphic column including the Catahoula Formation (named by Veatch, 1906), Fleming Formation (named by Kennedy, 1892), Lissie Formation (named by Deussen, 1914), and Beaumont Formation (named by Hayes and Kennedy, 1903). Sellards and others (1932) characterized the Frio Formation, Oakville Sandstone, Lagarto Clay (all three named by Dumble, 1894), Goliad Sand, Citronelle group sands (present-day Willis Sand), and Beaumont and Lissie Formations. Doering (1935) named the Willis Sand in place of the previous Citronelle group sands designation and provided the first compilation of the modern-day names of the geologic formations that contain the Chicot, Evangeline, and Jasper aquifers and Burkeville confining unit. Darton and others (1937) presented a map of the Gulf Coast aquifer system geologic formations and surface outcrops in Texas.

Rose (1943) mapped the vertical sequence of the Gulf Coast aquifer system geologic strata based on a well-log analysis. The strata were then grouped into zones based on sand content and permeability, although they remained uncorrelated with outcrops at the surface. From that report, Zones 6–7 approximately correspond to the Chicot aquifer; Zones 3–5 approximately correspond to the Evangeline aquifer; Zone 2 is the Burkeville confining unit, and Zone 1 is the Jasper aquifer (fig. 10). A similar zonal classification system was used in White and others (1944) and added surface outcrop correlation to the described hydrogeologic units and reduced the number of zones representing the Chicot and Evangeline aquifers (fig. 10). In that report, Zone 6 likely corresponds to the Beaumont Formation of the Chicot aquifer, Zones 3 and 5 likely correspond to a combination of the Chicot and Evangeline aquifers, Zone 2 corresponds to the Burkeville confining unit (Anders and others, 1968), and Zone 1 likely corresponds to the upper part of the Jasper aquifer of Jorgensen (1975) (fig. 10). Lang and others (1950) used the same zonal classifications as Rose (1943) and added geologic units, including the Beaumont Formation and what Lang and others referred to as the "Alta Loma Sand," hereinafter referred to as the "Alta Loma Sand of Lang and others (1950)." The Alta Loma Sand of Lang and others (1950) is present in the lower part of the Chicot aquifer in Galveston County and in southeastern Harris County (Jorgensen, 1975). Lang and others (1950) also described the surface outcrop correlation to the geologic units and extended the published cross section laterally to the Gulf of Mexico nearshore area and vertically to include the Catahoula confining unit. Lang and others (1950) were also among the earliest authors to correlate the vertical sequence of strata with the surface outcrop of each zone. The zonal classifications of Lang and others (1950) are described in table 1 of Carr and others (1985).

Wood and Gabrysch (1965) simplified the hydrogeologic "zones" used in previous reports and grouped each of these zones into a "Heavily pumped layer." Turcan and others (1966) formalized the present-day aquifer unit naming convention by correlating established hydrogeologic units in Louisiana across State lines to the previously studied Texas Gulf Coast area. The Chicot and Evangeline aquifer designations in Texas were first applied in Turcan and others (1966) and were previously named by Jones and others (1954) for these units in Louisiana. The term "Jasper aquifer" was also first used in Turcan and others (1966) as the lower part of the Lagarto Clay and Oakville Sandstone. That report also included the Catahoula confining unit as a hydrogeologic formation of the Gulf Coast aquifer. Subsequent reports since 1967, whether describing the Gulf Coast aquifer system in individual counties or as an entire system, have generally used the naming convention from Turcan and others (1966). Jorgensen (1975) subdivided the Chicot aquifer into an upper part, which generally included the areal extent of the Beaumont Formation and a small part of the Montgomery Formation, and a lower part containing the Alta Loma Sand of Lang and others (1950) and Willis Sand. Jorgensen (1975) also subdivided the Jasper aquifer based on Popkin (1971).

Baker (1979) constructed 11 stratigraphic cross sections depicting the Gulf Coast hydrogeologic units defined by Turcan and others (1966) from the surface outcrop to the Gulf of Mexico nearshore. Baker (1979) was among the first reports to establish an aquifer-wide hydrostratigraphic framework and subsurface delineation of the previously named hydrogeologic units. Carr and others (1985) provided further refinement of the Baker (1979) cross sections and has been often used to describe the stratigraphy of the Gulf Coast aquifer system since its publication. Kasmarek and Strom (2002) used the stratigraphy primarily from Carr and others (1985).

Young and Draper (2020) updated the Gulf Coast aquifer system geologic stratigraphy and hydrogeologic unit thicknesses; their report featured a coupled chronostratigraphic and lithostratigraphic approach. The approach from Young and Draper (2020) built on an existing hydrogeologic framework from Young and others (2014), which in turn was based on the work of Young and others (2012) and differs from earlier

[--, Not applicable or unknown]

Geologic classification[1]			Published geologic and hydrogeologic units										
System	Series	Geologic unit	Rose (1943)	White and others (1944)	Lang and others (1950)	Wood and Gabrysch (1965)	Turcan and others (1966)	Jorgensen (1975)	Baker (1979)	Carr and others (1985)	Kasmarek and Strom (2002)	Units from this report[2]	
												Hydrogeologic	Geologic
Quaternary	Holocene	Alluvium				Confining layer, Alta Loma Sand[3]	Chicot aquifer	Chicot aquifer (upper part)	Chicot aquifer	Chicot aquifer	Chicot aquifer	Chicot aquifer	Alluvium
	Pleistocene	Beaumont Formation		Zone 6	Beaumont Formation[4] / Alta Loma Sand								Beaumont Formation
		Lissie Formation: Montgomery Formation / Bentley Formation						Chicot aquifer (lower part)					Lissie Formation
Tertiary	Pliocene	Willis Sand	Zones 6–7		Zones 6–7								Willis Sand
	Miocene	Goliad Sand	Zones 3–5	Zones 3 and 5	Zones 3–5	Heavily pumped layer	Evangeline aquifer	Evangeline aquifer	Evangeline aquifer	Evangeline aquifer	Evangeline aquifer	Evangeline aquifer	Goliad Sand (upper part) / Goliad Sand (lower part)
		Fleming Formation / Lagarto Clay	Zone 2	Zone 2	Zone 2	Zone 2	Burkeville confining unit	Burkeville confining unit	Burkeville confining unit	Burkeville confining unit	Burkeville confining unit	Burkeville confining unit	Lagarto Clay (upper part) / Lagarto Clay (middle part) / Lagarto Clay (lower part)
		Oakville Sandstone	Zone 1	Zone 1[5]	Zone 1		Jasper aquifer	Jasper aquifer (upper part) / Jasper aquifer (lower part)	Jasper aquifer	--[7]	Jasper aquifer	Jasper aquifer	Oakville Sandstone
	Oligocene	Catahoula Formation / Frio Formation			Catahoula Formation	--[6]	Unnamed aquiclude[8]	--[9]	Catahoula confining unit	--[7]	--[10]	Catahoula confining unit	Frio Formation
		Vicksburg Formation											Vicksburg Formation

[1]Names of geologic units are from the U.S. Geological Survey National Geologic Map Database (USGS, 2019). The series associated with the geologic units are from Young and Draper (2020). In Young and Draper (2020), a small part of the Goliad Sand is described of Pliocene age. Stoeser and others (2005) describes the Goliad Sand of Miocene age, as shown on figure 7.

[2]Geologic and hydrogeologic unit stratigraphy from this report is modified from Young and Draper (2020) and Young and others (2012, 2014).

[3]This characterization is provided in Carr and others (1985).

[4]The Beaumont Formation in Lang and others (1950) is interpreted in Carr and others (1985) to include the "Alta Loma Sand" described in Lang and others (1950). This characterization is also repeated in Petitt and Winslow (1955). Additionally, the zones shown for Lang and others (1950) are described in Carr and others (1985).

[5]The stratigraphic cross section from White and others (1944) does not appear to include the entirety of the Oakville Sandstone in the definition of the Jasper aquifer.

[6]The Catahoula Formation and Oakville Sandstone are recognized as water-bearing formations in Wood and Gabrysch (1965) but not as distinct hydrogeologic units. The Jasper aquifer was not named and recognized as an aquifer unit until Turcan and others (1966).

[7]These units are included in the stratigraphic cross sections from Carr and others (1985); however, they are absent from table 1 of that report used to describe the hydrogeologic units listed above.

[8]The term "unnamed aquiclude" is used in the stratigraphic column in table 1 of Turcan and others (1966); however, the Catahoula Formation description is applied to the geologic sediment in Jasper and Newton Counties in a stratigraphic cross section from that report.

[9]The Catahoula Formation is recognized as geologic formation in Jorgensen (1975), but is not included in table 1 of that report used to describe the hydrogeologic units.

[10]Not studied in Kasmarek and Strom (2002).

EXPLANATION

Hydrogeologic unit or equivalent precursor zone

- Chicot aquifer
- Evangeline aquifer
- Burkeville confining unit
- Jasper aquifer
- Catahoula confining unit

Figure 10. Geologic and hydrogeologic units of the Gulf Coast aquifer system within the study area in southeast Texas.

publications (Baker, 1979; Carr and others, 1985; Strom and others, 2003a; 2003b, 2003c) that exclusively used a lithostratigraphic approach to characterize the hydrogeologic framework. Young and others (2012) used various sources of information (geophysical logs, and marker beds defining coastal onlap) to subdivide the Lagarto Clay into upper, middle, and lower parts based primarily on chronostratigraphic considerations (fig. 10).

In his seminal assessment of structure of the Gulf Coast aquifer system, Baker (1979) determined the upper and lower boundaries of the Burkeville confining unit independently from time concepts and primarily based on lithostratigraphic considerations. In documenting his construction of the Burkeville confining unit, Baker (1979, p. 40) states:

> "* * * the entire thickness of sediment in the Burkeville confining system in some areas is younger than the entire thickness of sediment in the Burkeville in the other places. The configuration of the unit is highly irregular. Boundaries are not restricted to a single stratigraphic unit but transgress the Fleming [Lagarto Clay]-Oakville [Sandstone] contact in many places."

The Burkeville unit defined by Baker (1979) is a lithostratigraphic unit that is not bounded by isochronous boundaries; therefore, it cannot be accurately represented by a single chronostratigraphic formation defined by Young and others (2010, 2012). To create a "lithostratigraphic-based" Burkeville confining unit from the clays and sand sequences, Young and Draper (2020) correlated the sand and clay sequences in the upper, middle, and lower parts of the Lagarto Clay, and Oakville Sandstone based on a lithostratigraphic approach. This approach provides a practical integration of the lithostratigraphic and chronostratigraphic approaches to represent the conceptualization by Baker (1979) of the Burkeville confining unit.

The depiction of the hydrogeologic units containing the Evangeline aquifer by Young and Draper (2020) contains a considerable extent of the upper part of the Lagarto Clay, whereas previous reports (Turcan and others, 1966; Jorgensen, 1975; Baker, 1979; Carr and others, 1985) incorporated only a small part of the Lagarto Clay where there were interbedded layers of sand in the Fleming Formation into their definition of the Evangeline aquifer. Additionally, Young and Draper (2020) includes the entire Goliad Sand as one of the hydrogeologic units that contain the Evangeline aquifer.

Young and Draper (2020) define the base of the Chicot aquifer as the base of the Willis Sand following previous reports; however, additional geophysical logs (approximately 650 versus 290 original logs) were used to characterize the contact between the Chicot and Evangeline aquifers. Thus, Young and Draper (2020) thickness of the Chicot and Evangeline aquifers can differ substantially in some areas compared to previous studies.

The Jasper aquifer defined by Young and Draper (2020) is mostly contained in a large part of the Oakville Sandstone and the lower part of the Lagarto Clay, which is similar to the stratigraphy of Turcan and others (1966). Furthermore, Young and Draper (2020) wrote that the Vicksburg Formation at the base of the Gulf Coast aquifer system is another hydrogeologic unit that in part contains the Jasper aquifer—an update previously included in Young and others (2014).

Chicot Aquifer

The Chicot aquifer is the uppermost hydrogeologic unit in the Gulf Coast aquifer system and is contained in the geologic units from the land surface to the upper extent of the Evangeline aquifer. From oldest to youngest, the Chicot aquifer is contained in the Willis Sand, the Lissie Formation (which includes the Bentley and Montgomery Formations), the Beaumont Formation, and the alluvium (fig. 10). The base of the Chicot aquifer is the Pliocene-age Willis Sand.

The Willis Sand, which consists of Pliocene-age nonfossiliferous sand and sand beds with gravel, unconformably overlies the Goliad Sand and underlies the Lissie Formation (Doering, 1935). The origins of the sediment of this formation are similar to those of the Lissie and Beaumont Formations: namely, the accumulation of sediments through a cuesta and resulting deposition on a flat erosional plain (Doering, 1935). In the 15- to 20-mi-wide outcrop area, the Willis Sand is composed of stratified upward-fining gravelly coarse sand (Young and others, 2012). The Willis Sand dips towards the coast at a rate between 10 and 25 ft/mi (Doering, 1935) and ranges in thickness from about 100 ft in the outcrop area to 500 ft near the coastline (Young and others, 2012).

The Pleistocene-age Lissie Formation contains thick beds of sand and interbedded fine-grained sediment that unconformably overlie the Willis Sand and are unconformably overlain by the Beaumont Formation (fig. 10). The Lissie Formation sediments are continental in origin and dip towards the coast at a rate of about 5 to 20 ft/mi (Doering, 1935). The Lissie Formation crops out in a belt about 30 miles (mi) wide parallel to the Texas coastline about 50 mi inland from the coast and is the most areally extensive outcrop in the Gulf Coast aquifer system (Sellards and others, 1932). North of the Brazos River, the Lissie Formation has been mapped at the surface as the Montgomery and Bentley Formations (Young and others, 2012). The Lissie Formation is composed of more than 60 percent sand in the updip area and between 20 and 60 percent sand in downdip area near the shore (Young and others, 2012).

Overlying the Montgomery Formation is the Pleistocene-age Beaumont Formation (fig. 10), which is made up of poorly bedded, marly clay with interbedded sand generally between 400 and 900 ft thick (Sellards and others, 1932). These clay and sand intervals ("fine-grained fraction" and "coarse-grained fraction" shown on fig. 7) are generally continuous on a local scale. The strata of the Beaumont Formation are primarily riverine-derived deposits (natural levees and deltas), and to a lesser degree, marine and lagoonal deposits in bays and embayments between stream ridges (sand and silt deposits that form natural levees near the edge of the channel) and delta

banks (Sellards and others, 1932). In Harris and Galveston Counties, the highly clay areas of the Beaumont Formation represent delta-plain facies (Kreitler and others, 1977). The Beaumont Formation clay fraction is well exposed in deeper drainage ditches in Harris County and in surrounding areas (Sellards and others, 1932). The Beaumont Formation (clay fraction) confines the Chicot aquifer where it is present (fig. 7), generally in the downdip portion (lower half) of the study area bounded by the Gulf of Mexico.

The Holocene-age alluvium present in the river basins consists of gravels, buried sand, and point bar deposits with clay to gravel grain sizes, and is stratified with fine-grained sediments (clay and silt) in the upper part of the alluvium and sand and gravel in the lower part (Chowdhury and Turco, 2006). The surficial alluvium area can provide a hydraulic connection between surface water and the groundwater system (Chowdhury and Turco, 2006).

The updip extent of the outcrop area of geologic units that contain the Chicot aquifer follows the updip extent of the Lissie Formation (figs. 7–8) in the eastern part of the study area. However, the updip extent of the geologic units that contain the Chicot aquifer transitions in the Trinity River area to that of the updip extent of the Willis Sand and follows this contact westward to the GULF model boundary (figs. 7–8). This updip extent is similar to the updip extent described in Strom and others (2003a).

Evangeline Aquifer

The Evangeline aquifer underlies the Chicot aquifer and is contained in the upper part of the Miocene-age Lagarto Clay (a member of the Fleming Formation), in the lower part of the Miocene-age Goliad Sand, and the upper part of the predominantly Miocene-age Goliad Sand (fig. 10). The base of the Evangeline aquifer is the Miocene-age middle part of the Lagarto Clay (fig. 10).

Few descriptions of the Lagarto Clay other than in Sellards and others (1932) and Plummer (1932) are available; therefore, it is described here as a member of the more frequently reported Miocene-age Fleming Formation. The Fleming Formation extends throughout the Gulf Coast aquifer system in Texas and eastern Louisiana (Chowdhury and Turco, 2006). Together with the Oakville Sandstone, the Fleming Formation composes a major fluvial deltaic depositional episode (Young and others, 2012). Although the Fleming Formation is lithologically similar to the Oakville Sandstone, it is differentiated from the Oakville Sandstone in some places by a greater percentage of fine-grained sediment (Baker, 1979).

The Goliad Sand consists of about 80 percent sand, 10 percent clay, 5 percent gravel, and 5 percent calcium carbonate (Sellards and others, 1932). The upper part of the Goliad Sand consists of finer grained sands that are cemented with calcium carbonate (Hosman, 1996) and contains thinner bedded sandstone than the lower part of the Goliad Sand (Young and others, 2012). The Goliad Sand crops out in a belt about 15 mi wide in Lavaca County (Sellards and others, 1932) but is not present as a surface outcrop elsewhere in the study area (fig. 7). The Goliad Sand ranges in thickness from 200 ft at outcrop to about 1,400 ft near the coastline (Young and others, 2012).

The Goliad Sand does not generally crop out at the surface in any large spatial extent other than in one area in Lavaca County (fig. 7). The same applies to the upper part of the Lagarto Clay (Young and others, 2012). Rather, these units pinch out into the overlying Willis Sand (Young and others, 2012). Thus, rather than "outcrop" as a whole, the geologic units that contain the Evangeline aquifer are said to "subcrop," or become truncated at the surface by geologically younger units. However, for the purposes of conceptualization in this study and use in the GULF model, the geologic units that contain the Evangeline aquifer have a defined outcrop area (fig. 8) described by Casarez (2020). This configuration follows previous reports (Gabrysch, 1977; Baker, 1979; Strom and others, 2003b, Kasmarek and Robinson, 2004; Kasmarek, 2012) which show a generally well-defined outcrop area for the rocks that contain the Evangeline aquifer that is laterally extensive across the study area.

Burkeville Confining Unit

The Burkeville confining unit (named by Wesselman, 1967) includes the middle part of the Miocene-age Lagarto Clay, which is a member of the larger Fleming Formation (fig. 10). The Fleming Formation contains the Burkeville confining unit and the Evangeline aquifer towards updip areas (Chowdhury and Turco, 2006); therefore, the description of the Fleming Formation in the Evangeline aquifer section of this report generally applies to the Burkeville confining unit. The middle part of the Lagarto Clay was identified by Young and others (2010) as having a lower sand content than the upper and lower parts of this formation and dips at a rate of about 65 to 80 ft/mi (Young and others, 2012).

In most parts of the study area, the Burkeville confining unit is composed of many individual sand layers; however, because of the large percentage of finer grained units compared to the Jasper aquifer and overlying Evangeline aquifer, the name "Burkeville confining unit" is appropriate because this unit impedes groundwater (Baker, 1979) and is an effective barrier to the vertical flow of water (Turcan and others (1966). Compared to previous definitions of the Burkeville confining unit, the definition of this unit from Young and Draper (2020) includes a more regular thickening of the unit in the downdip direction and a downdip extent beyond the coastline.

Jasper Aquifer

The Jasper aquifer underlies the Burkeville confining unit and is composed of the Oakville Sandstone and the lower part of the Miocene-age Lagarto Clay (fig. 10). The Oakville Sandstone unconformably overlies the Catahoula Formation

and is overlain unconformably by the Lagarto Clay of the Fleming Formation (fig. 10) (Sellards and others, 1932). The exchange of water between the Jasper aquifer and the underlying units is largely impeded by the Catahoula confining unit (Baker, 1986). The Oakville Sandstone is mostly uniform in composition and includes about 40 percent sand, 30 percent clay, 20 percent marl, 5 percent shells, and 5 percent gravel (Sellards and others, 1932). The Jasper aquifer ranges in thickness from about 200 ft to about 3,200 ft (Baker, 1979). The Jasper aquifer contains dissolved solids of less than 3,000 milligrams per liter from the outcrop area of the geologic units that contain the aquifer to about 50 to 75 mi downdip from its outcrop, which approximately parallels the coastline and passes a few miles north of Beaumont and near the center of Houston (Baker, 1986).

In the study area, the Oakville Sandstone is mapped as a surface outcrop west of the Brazos River in Gonzales, Lavaca, Fayette, and Washington Counties; east of these counties, the Oakville Sandstone is not mapped as a surface outcrop (Baker, 1986) (fig. 7). The Oakville Sandstone is distinguished from the Lagarto Clay by an increased amount of crossbedding in the Oakville Sandstone compared to the Lagarto Clay, and thicker, more massive sand beds (Sellards and others, 1932).

Compared to the previous Jasper aquifer extents from Strom and others (2003c)—which were defined by Baker (1979)—the downdip vertical extent of the Jasper aquifer from Young and Draper (2020) and Young and others (2010, 2012) includes the upper part of the Catahoula Formation (fig. 9) which contains sand and sandy clay intervals. This downdip interval was previously included in the Catahoula Formation. Additionally, Strom and others (2003c) included a sandy (freshwater-bearing) part of the Catahoula Formation in the outcrop extent of the geologic units that contain the Jasper aquifer; this sandy layer of the Catahoula Formation was included in the Catahoula confining unit in this report and is discussed in Baker and others (1974) and Baker (1986) and is depicted in figure 4 in Baker (1979).

Catahoula Confining Unit

The Catahoula confining unit (named by Baker, 1979) is a pyroclastic unit composed of interbedded sand and fine-grained sediment (Baker, 1986) that is the basal unit of the Gulf Coast aquifer system (figs. 9–10). The Catahoula confining unit includes the Oligocene-age Catahoula and Vicksburg Formations (fig. 10) and includes about 60 percent tuff, 20–30 percent sandstone, 10–20 percent clay, and minor amounts of conglomerate (Sellards and others, 1932). The Catahoula confining unit is composed of sufficient fine-grained sediment to be considered a confining unit everywhere except near the outcrop area where a sandy layer is present as described in the Jasper Aquifer section of this report (Wood and others, 1963). The Catahoula confining unit is overlain unconformably by the Oakville Sandstone and the Lagarto Clay. Some reports assign the Catahoula confining unit as Miocene in age, whereas others identify the strata as Oligocene in age (Baker, 1979). For the purposes of this report, the units of the Catahoula confining unit are considered as Oligocene in age, based on Young and others (2010; 2012) (fig. 10). The contact between the Oligocene and underlying Eocene-aged sediments is mostly indistinguishable and based solely on lithology (Chowdhury and Turco, 2006), resulting in disputes regarding the ages of these units. Facies within the Catahoula Formation include the mud-dominated marine and nonmarine facies of the Frio Formation as well as sand-poor marine and nonmarine facies of the shallow subsurface extent of the Catahoula Formation and its deeper subsurface equivalent, the Frio Formation (Young and others, 2012).

The Catahoula Formation was described by Sellards and others (1932) as massive dark-colored greenish gray (or red or blue) clay with quantities of gypsum and calcareous concretions. The clays are noted to be laminated and interbedded with sands, sandy clays, and sandstone (Chowdhury and Turco, 2006). The thickness of the formation in outcrop varies from about 150 to 800 ft; beneath land surface, the thickness ranges from 250 to 600 ft (Sellards and others, 1932). The lowermost fine-grained unit of the Catahoula Formation, sometimes mapped in outcrop as the Frio Formation and equivalent in age to the Vicksburg Formation of the subsurface, is treated in this report as part of the Catahoula confining unit.

Groundwater Development

Since the early 1900s, most of the groundwater withdrawals in the study area have been from three of the hydrogeologic units that compose the Gulf Coast aquifer system—the Chicot, Evangeline, and Jasper aquifers and, more recently, from the Catahoula confining unit (fig. 10–12; table 1). Withdrawals from these units are used for municipal, domestic, commercial, industrial, irrigation, and livestock purposes. Groundwater withdrawals from the Catahoula confining unit are also an important source of water in Walker County, Montgomery County, and laterally adjacent counties. In 1950, Houston was one of only three cities in the United States with a population greater than 250,000 (the others were San Antonio, Tex., and Memphis, Tennessee) that were supplied exclusively by groundwater (Borchert, 1954). Daily mean groundwater use (hereinafter "groundwater use") for the study area is provided on table 1.

Although water-use patterns vary on a county scale, groundwater development over time in the study area can be described in terms of three periods: (1) predevelopment to early development, prior to about 1945, (2) concentrated development and transition to developed conditions from 1946 to 1974, and (3) regulation and alternative water supplies conversion (post-developed conditions), from 1975 to present (2023) (fig. 11).

The greater Houston area (fig. 1) has grown substantially since the publication of many earlier reports describing groundwater use (synonymous with "groundwater withdrawal") and water-level data for Houston and the surrounding

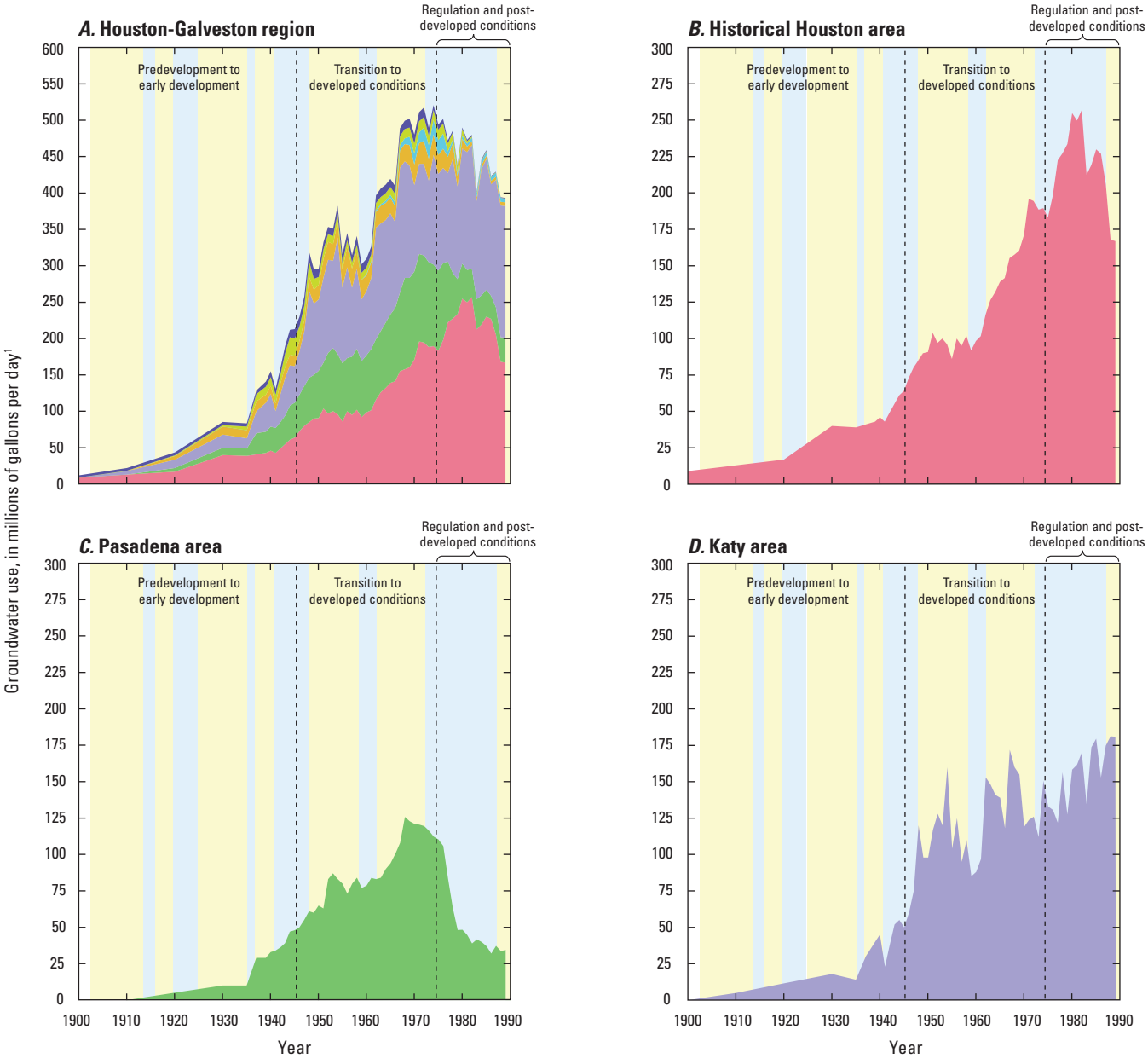

[1]Annual groundwater-use data for the historical geographic areas are included in table 1 for the period 1900–89. Groundwater-use data sources for the period 1900–89 are listed in appendix 2. Annual groundwater-use estimates, by county, for the period 1900–2020 are shown on figure 2.1.
[2]Prior to Gabrysch (1972), the reported groundwater use for the Baytown area also included the La Porte area, which is approximately spatially contiguous with the Johnson Space Center area. Groundwater use in the Johnson Space Center area was subdivided from the Baytown area in Gabrysch (1972), and the groundwater use was redistributed into these two areas beginning in 1960.

Figure 11. Temporal distribution of groundwater use for the *A*, Houston-Galveston region, *B*, historical Houston area, *C*, Pasadena area, *D*, Katy area, *E*, Baytown area, *F*, Johnson Space Center area, *G*, Texas City area, *H*, Alta Loma area, and *I*, the study area and greater Houston area in southeast Texas.

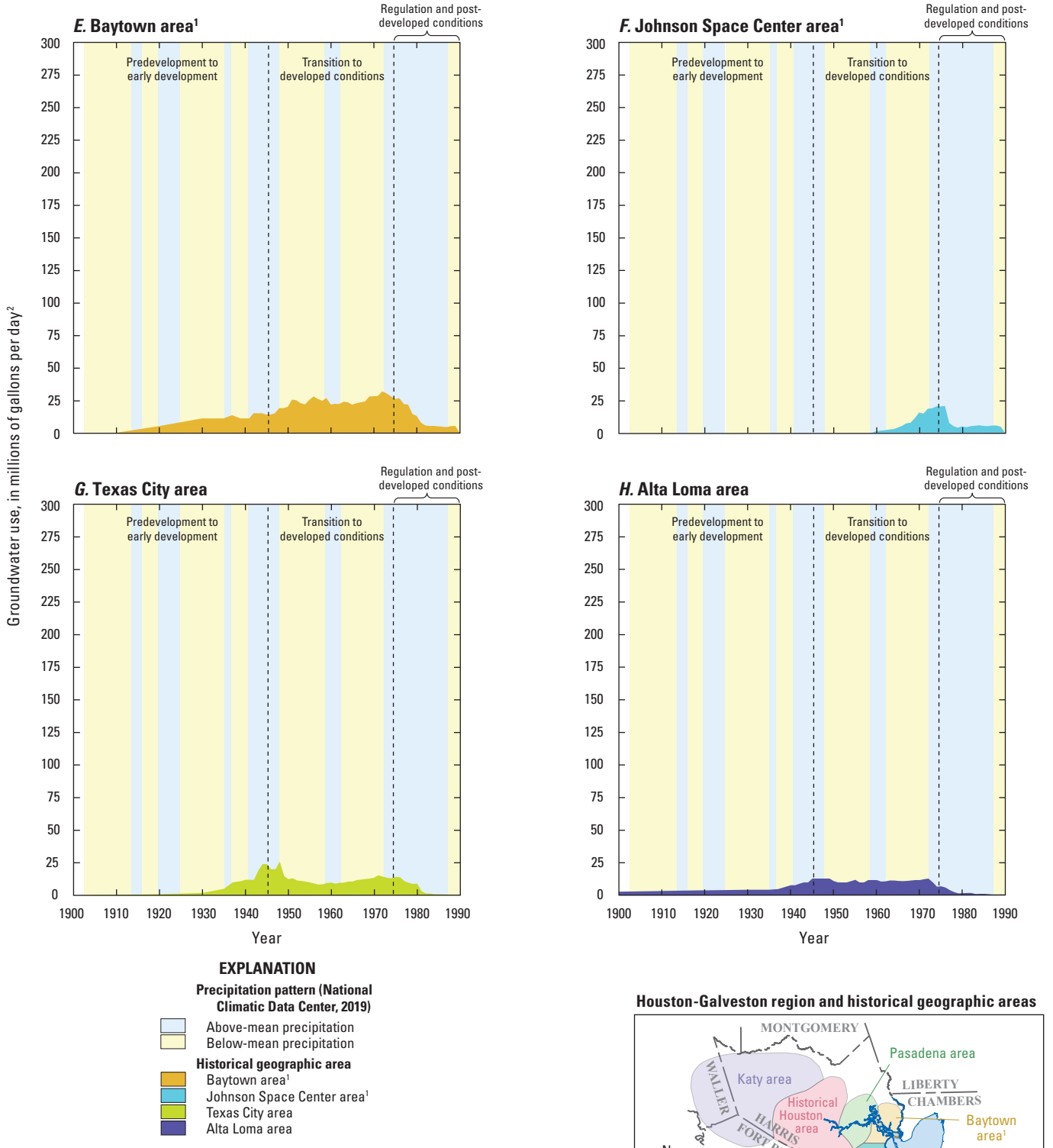

[1]Prior to Gabrysch (1972), the reported groundwater use for the Baytown area also included the La Porte area, which is approximately spatially contiguous with the Johnson Space Center area. Groundwater use in the Johnson Space Center area was subdivided from the Baytown area in Gabrysch (1972), and the groundwater use was redistributed into these two areas beginning in 1960.

[2]Annual groundwater-use data for the historical geographic areas are included in table 1 for the period 1900–89. Groundwater-use data sources for the period 1900–89 are listed in appendix 2.

Annual groundwater-use estimates, by county, for the period 1900–2020 are shown on figure 2.1.

Figure 11.—Continued

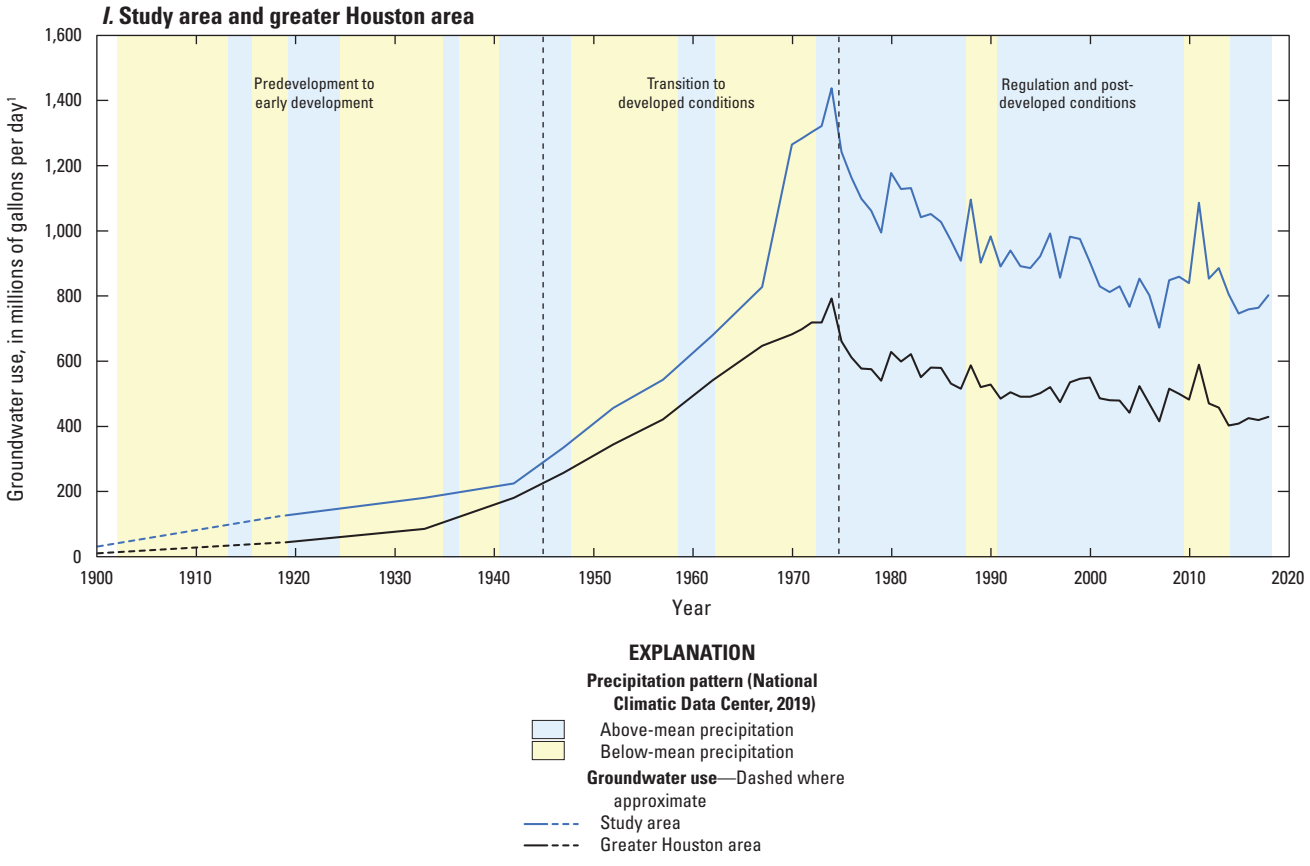

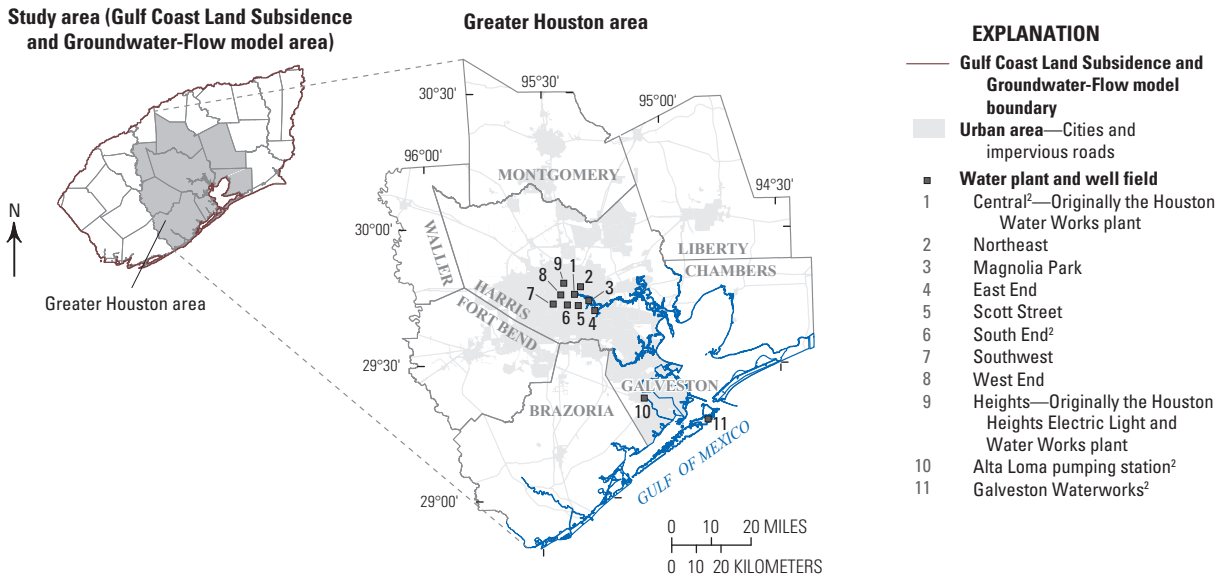

[1]Annual groundwater-use estimates, by county, for the period 1900–2020 are shown on figure 2.1.
Groundwater-use data for the study area and the greater Houston area are from Oliver and Harmon (2022).
[2]See photograph in the "Predevelopment to Early Development (1897–1945)" section of this report.

Figure 11.—Continued

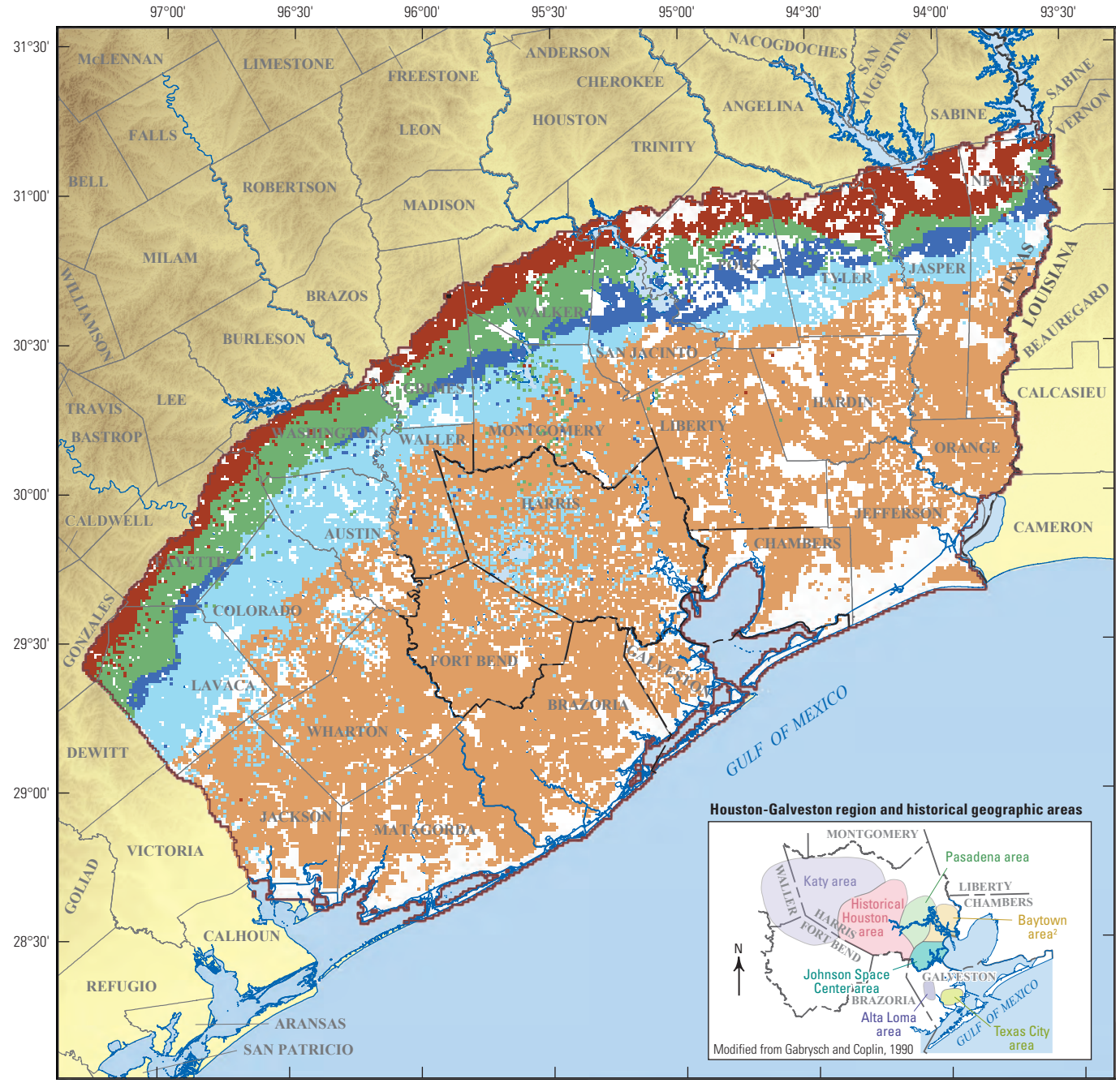

Base modified from U.S. Geological Survey (USGS) digital data
Albers Equal-Area Conic projection
Standard parallels 29°30' N. and 45°30' N.
Central meridian 96°00' W.
North American Datum of 1983

Gulf Coast aquifer system boundary modified from Casarez (2020)
Shaded relief derived from USGS (2021a)

EXPLANATION

Gulf Coast Land Subsidence and Groundwater-Flow (GULF) model area

Groundwater use, by hydrogeologic unit in which well is screened

- Chicot aquifer
- Evangeline aquifer[1]
- Burkeville confining unit
- Jasper aquifer
- Catahoula confining unit

0 20 40 60 MILES
0 20 40 60 KILOMETERS

[1]In northern Harris County and in southern Montgomery County (and laterally adjacent areas), substantial groundwater use occurs in the Evangeline aquifer that may not be fully represented by this generalized figure.
[2]Prior to Gabrysch (1972), the reported groundwater use for the Baytown area also included the La Porte area, which is approximately spatially contiguous with the Johnson Space Center area. Groundwater use in the Johnson Space Center area was subdivided from the Baytown area in Gabrysch (1972), and the groundwater use was redistributed into these two areas beginning in 1960.

Figure 12. Spatial distribution of permitted groundwater use by hydrogeologic unit for the Gulf Coast aquifer system study area in southeast Texas.

Table 1. Temporal distribution of groundwater use within the Gulf Coast aquifer system study area in southeast Texas, 1900–2018.

[Mgal/d, million gallons per day; --, not available; All groundwater use listed is reported as daily mean values. Groundwater-use periods for the values listed here are as follows: predevelopment to early development (1900–45), transition to developed conditions (1946–74), regulation and post-developed conditions (1975–2018)]

Year	Study area groundwater use (Mgal/d) (fig. 1)[1]	Greater Houston area groundwater use (Mgal/d) (fig. 11)[1,2]	Houston-Galveston region groundwater use (Mgal/d)[3,4]	Houston-Galveston region groundwater use (Mgal/d)[4]						
				Historical Houston area[5,6]	Pasadena area[6]	Katy area[6]	Baytown area[7]	Johnson Space Center area[7]	Texas City area	Alta Loma area
1900	--	--	12.0	9.0	0.0	0.0	0.0		0.0	3.0
1910	--	--	22.0	13.0	0.0	5.0	0.0		0.5	3.5
1920	--	--	43.5	17.0	5.0	11.5	5.0		1.0	4.0
1930	--	--	85.7	40.0	10.0	18.0	11.0		2.0	4.7
1935	--	--	83.5	39.0	10.0	14.0	11.0		5.0	4.5
1937	--	--	128	41.0	29.0	30.0	13.5		10.0	5.0
1939	--	--	140	43.0	29.0	40.0	11.0		11.0	5.8
1940			152	46.0	33.0	45.0	11.0		11.0	6.5
1941			131	43.0	34.0	23.0	11.0		12.0	8.0
1942	225	181	159	49.0	36.0	38.0	15.0		12.0	9.0
1943			190	55.0	39.0	52.0	15.0		19.0	10.0
1944			212	61.0	47.0	55.0	15.0		24.0	10.0
1945			213	64.0	48.0	50.0	14.0		24.0	13.0
1946			230	73.0	50.0	60.0	14.0		20.0	13.0
1947	335	258	258	80.0	55.0	75.0	15.0		20.0	13.0
1948			324	85.0	61.0	120	19.0		26.0	13.0
1949			295	90.0	60.0	98.0	19.0		15.0	13.0
1950			297	90.7	65.0	98.0	20.0		12.4	10.5
1951			332	104	63.0	117	25.5		13.1	10.0
1952	456	344	354	97.1	83.0	128	24.8		11.5	10.0
1953			351	100	87.0	120	22.8		11.2	10.0
1954			382	96.0	83.0	160	21.8		10.7	11.0
1955			317	86.0	80.0	104	25.2		10.0	12.0
1956			345	100	73.0	125	27.9		9.2	10.0
1957	543	421	314	95.0	80.0	95.0	26.0		8.4	10.0
1958			341	102	84.0	110	24.5		8.5	11.8
1959			302	92.0	77.0	85.0	26.7		9.5	11.8
1960			310	98.4	78.6	88.0	21.7	1.2	9.8	11.9
1961			326	102	83.9	97.0	22.3	1.6	9.0	10.7
1962	679	541	397	116	83.1	153	22.0	2.0	9.6	10.9
1963			406	126	84.0	148	23.9	2.4	9.9	11.5
1964			411	132	90.0	141	23.4	2.8	10.7	11.5
1965			419	139	94.0	139	21.6	3.9	10.6	11.3
1966			411	142	100	118	22.7	5.3	11.8	11.0
1967	828	647	489	155	108	172	23.4	7.3	12.1	11.2
1968			499	158	126	160	24.0	7.8	12.7	11.6
1969			502	160	123	155	27.8	11.2	12.9	11.9

Table 1. Temporal distribution of groundwater use within the Gulf Coast aquifer system study area in southeast Texas, 1900–2018. —Continued

[Mgal/d, million gallons per day; --, not available; All groundwater use listed is reported as daily mean values. Groundwater-use periods for the values listed here are as follows: predevelopment to early development (1900–45), transition to developed conditions (1946–74), regulation and post-developed conditions (1975–2018)]

Year	Study area groundwater use (Mgal/d) (fig. 1)[1]	Greater Houston area groundwater use (Mgal/d) (fig. 11)[1,2]	Houston-Galveston region groundwater use (Mgal/d)[3,4]	Houston-Galveston region groundwater use (Mgal/d)[4]						
				Historical Houston area[5,6]	Pasadena area[6]	Katy area[6]	Baytown area[7]	Johnson Space Center area[7]	Texas City area	Alta Loma area
1970	1,270	683	480	171	121	119	28.0	15.6	13.6	11.9
1971	1,280	699	511	196	120	124	28.4	14.7	15.5	12.5
1972	1,300	719	517	195	120	126	31.8	18.4	14.4	13.0
1973	1,320	719	490	189	116	112	30.3	18.7	13.5	10.2
1974	1,440	793	521	190	112	151	28.0	20.2	13.2	6.8
1975	1,240	661	494	183	110	133	26.1	20.2	14.3	7.1
1976	1,160	618	502	198	106	131	26.5	20.6	14.0	6.1
1977	1,100	584	472	223	83.3	122	22.1	7.5	11.0	4.1
1978	1,060	582	486	227	62.9	156	21.6	5.1	9.7	2.7
1979	995	548	438	234	48.1	127	14.4	4.0	8.9	1.6
1980	1,180	642	490	255	48.2	158	12.9	4.9	9.0	1.8
1981	1,130	611	473	250	44.7	162	7.7	4.2	3.2	2.0
1982	1,130	636	480	257	38.8	170	5.6	5.0	1.6	2.0
1983	1,040	565	402	213	41.6	135	5.3	5.4	1.4	1.2
1984	1,050	595	446	219	39.9	174	5.2	5.8	1.0	1.4
1985	1,030	593	459	230	37.0	180	4.9	5.2	0.9	1.4
1986	970	543	423	227	32.0	153	4.6	5.1	0.8	1.0
1987	908	527	429	206	37.2	175	4.4	5.5	0.7	0.7
1988	1,100	602	394	168	33.6	181	5.0	5.6	0.2	0.7
1989	903	533	393	167	34.4	181	5.2	4.6	0.3	0.9
1990	983	533	--	--	--	--	--	--	--	--
1991	891	487	--	--	--	--	--	--	--	--
1992	940	503	--	--	--	--	--	--	--	--
1993	892	491	--	--	--	--	--	--	--	--
1994	886	491	--	--	--	--	--	--	--	--
1995	922	502	--	--	--	--	--	--	--	--
1996	992	522	--	--	--	--	--	--	--	--
1997	857	474	--	--	--	--	--	--	--	--
1998	982	537	--	--	--	--	--	--	--	--
1999	975	546	--	--	--	--	--	--	--	--
2000	904	552	--	--	--	--	--	--	--	--
2001	830	486	--	--	--	--	--	--	--	--
2002	812	479	--	--	--	--	--	--	--	--
2003	830	474	--	--	--	--	--	--	--	--
2004	767	433	--	--	--	--	--	--	--	--
2005	853	522	--	--	--	--	--	--	--	--

Table 1. Temporal distribution of groundwater use within the Gulf Coast aquifer system study area in southeast Texas, 1900–2018. —Continued

[Mgal/d, million gallons per day; --, not available; All groundwater use listed is reported as daily mean values. Groundwater-use periods for the values listed here are as follows: predevelopment to early development (1900–45), transition to developed conditions (1946–74), regulation and post-developed conditions (1975–2018)]

Year	Study area groundwater use (Mgal/d) (fig. 1)[1]	Greater Houston area groundwater use (Mgal/d) (fig. 11)[1,2]	Houston-Galveston region groundwater use (Mgal/d)[3,4]	Houston-Galveston region groundwater use (Mgal/d)[4]						
				Historical Houston area[5,6]	Pasadena area[6]	Katy area[6]	Baytown area[7]	Johnson Space Center area[7]	Texas City area	Alta Loma area
2006	803	466	--	--	--	--	--	--	--	--
2007	704	408	--	--	--	--	--	--	--	--
2008	849	506	--	--	--	--	--	--	--	--
2009	859	499	--	--	--	--	--	--	--	--
2010	840	471	--	--	--	--	--	--	--	--
2011	1,090	578	--	--	--	--	--	--	--	--
2012	853	453	--	--	--	--	--	--	--	--
2013	886	444	--	--	--	--	--	--	--	--
2014	806	393	--	--	--	--	--	--	--	--
2015	747	400	--	--	--	--	--	--	--	--
2016	759	407	--	--	--	--	--	--	--	--
2017	764	402	--	--	--	--	--	--	--	--
2018	803	429	--	--	--	--	--	--	--	--

[1]Study area groundwater use is described in Oliver and Harmon (2022) and was distributed into the groundwater-flow model stress periods (described in the "Simulation of Groundwater Flow and Land-Surface Subsidence" section of this report). The groundwater-flow model stress periods do not align evenly with the time increments on this table prior to 1940; therefore, groundwater use for the study area prior to 1940 is not shown.

[2]Greater Houston area groundwater use was compiled from Oliver and Harmon (2022), Texas Water Development Board (2020a), and from selected groundwater conservation or subsidence districts shown on figure 3. The spatial extent of the greater Houston area is shown on figures 11 and 18.

[3]The spatial extent of the Houston-Galveston region and historical geographic areas is shown on figures 11 and 12. Groundwater use in the Houston-Galveston region is computed as the sum of the groundwater use in the historical geographic areas.

[4]The Houston-Galveston region defined in this report is approximately spatially contiguous with the "Houston District" defined in Wood and Gabrysch (1965) and subsequent reports. However, the "Houston District" defined in reports prior to 1965 did not generally include the Baytown, Texas City, or Alta Loma areas (except for Anders and Naftel [1962] which included the Baytown area). Groundwater-use totals in the Houston-Galveston region beginning with Gabrysch (1967) also included "other Galveston County areas." Additionally, groundwater-use totals in the Houston-Galveston region also included "other Harris areas" beginning with Gabrysch (1980a). These "other area" totals are not included in the Houston-Galveston region groundwater-use totals above. The references used to compile the Houston-Galveston groundwater use are listed in appendix 2.

[5]The area defined in this report as the "historical Houston area" (fig. 11) is roughly equivalent to the extent of Houston mentioned in reports from about 50 to 70 years ago, before rapid growth greatly increased the size of the Houston area. The "historical Houston area" in this report is synonymous with the "Houston area" used in many previous reports.

[6]The irrigation groundwater use for the Katy area generally occurred between early May and mid-September. Additionally, the groundwater use in the historical Houston area and Pasadena area is greater during the summer than at other times of the year. In order to compare groundwater use between each area, the withdrawals in the Houston, Pasadena, and Katy areas are reported as daily mean values for the entire year, as in Lang and others (1950).

[7]Prior to Gabrysch (1972), the reported groundwater use for the Baytown area also included the La Porte, Texas, area. The La Porte area is approximately spatially contiguous with the Johnson Space Center area. Groundwater use in the Johnson Space Center area was subdivided from the Baytown area in Gabrysch (1972), and the groundwater use was redistributed into these two areas beginning in 1960 in that report. This redistributed groundwater use is used in this table.

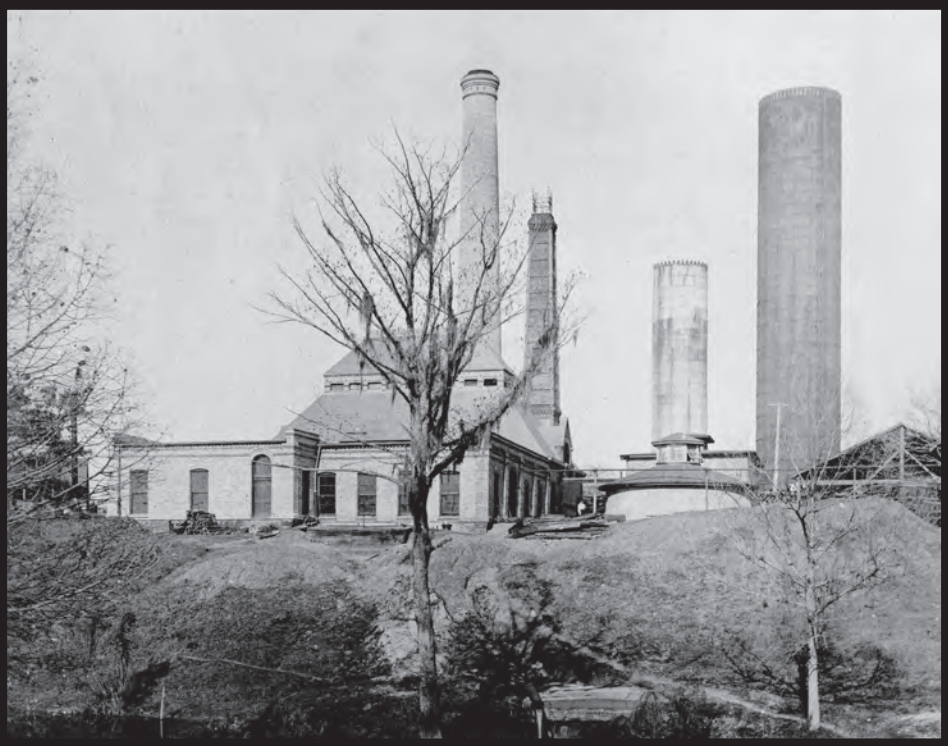

Photograph courtesy of the Houston Metropolitan Research Center (HMRC), Houston Public Library. Photograph MSS0114-0800 is used with permission from the MSS0114 HMRC Photo Collection.

View of the Houston Water Works plant. This is the original plant built in 1879, showing the 1879 and 1886 standpipes. The remains of this plant were placed on the National Register of Historic Places in 1976 (Texas Historical Commission, 2022). The exact photograph date is unknown.

Photograph by Henry Stark, courtesy of the Houston Metropolitan Research Center (HMRC), Houston Public Library. Photograph MSS0717-0183 is used with permission from the MSS0717 Views in Texas 1895-1896 Photo Collection.

Galveston Waterworks, circa 1895–1896. Water was supplied to this plant through an 18.7-mile-long pipe originating at the Alta Loma pumping station. The exact photograph date is unknown.

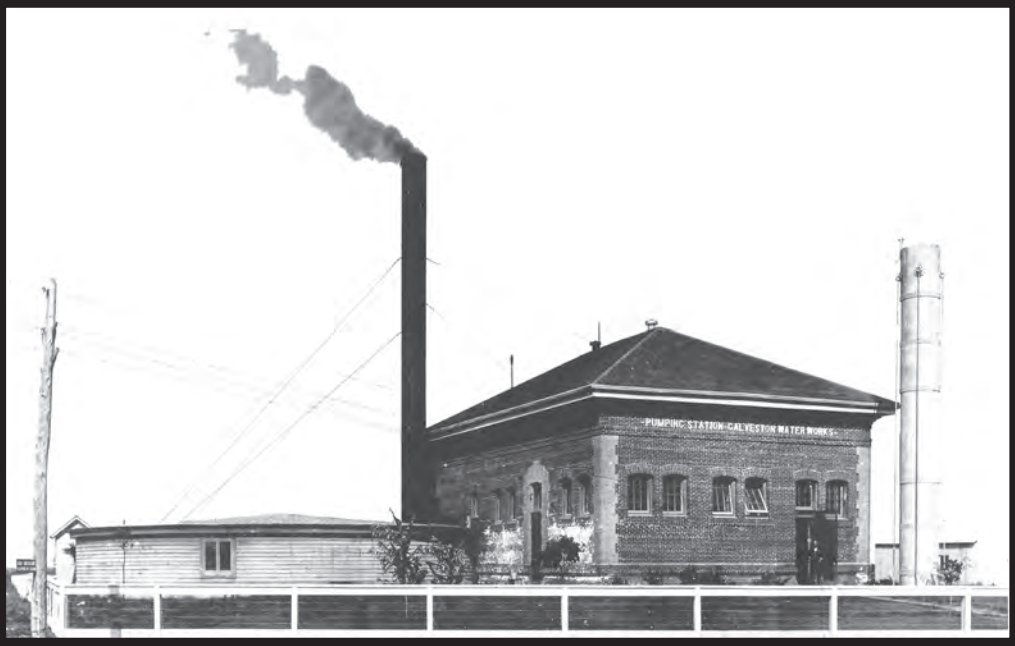

Photograph from the Santa Fe Area Historical Foundation, used with permission.

Alta Loma pumping station, circa 1895, before it was destroyed in the 1900 storm. The exact photograph date is unknown.

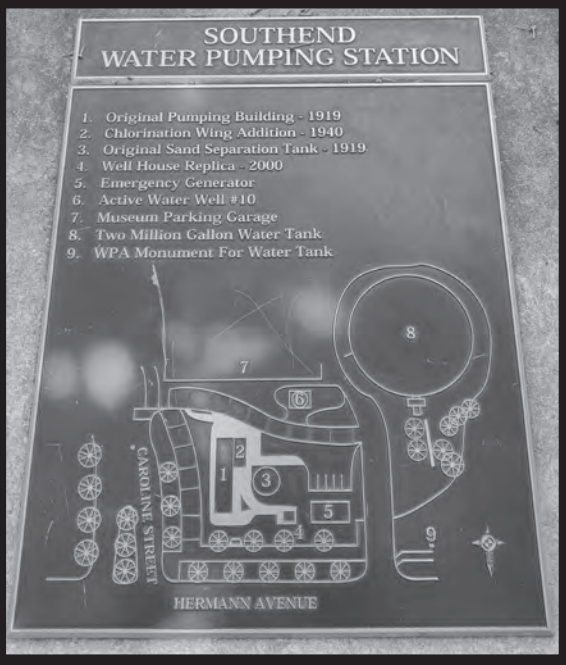

The South End water plant (3) constructed in 1919 (left) and the site plan of the South End water plant (right). The original pump house was restored in 2000. Photographs taken by John Ellis, U.S. Geological Survey, June 29, 2022.

cities. Therefore, descriptions from previously published reports (listed in appendix 2) describing these groundwater data have been updated to reflect present-day geographic locations. Additionally, the spatial extents of the seven historical geographic areas (historical Houston, Pasadena, Katy, Baytown [described in historical reports as the "Baytown-La Porte area"], Johnson Space Center [although groundwater use was included in the "Baytown" area until 1960], Texas City, and Alta Loma areas) used to describe groundwater use in this report are shown on figures 11*A*–11*H*, which are modified from Gabrysch and Coplin (1990). Collectively, these areas are known as the "Houston-Galveston region." The Houston-Galveston region defined in this report (fig. 12) is approximately spatially contiguous with the "Houston District" defined in Wood and Gabrysch (1965) and subsequent reports. A list of references for groundwater-use data described in this section is presented in appendix 2.

Predevelopment to Early Development (1897–1945)

The first municipal supply well in the Houston-Galveston region was drilled in 1886 at the Houston Water Works plant (Central water plant and well field on fig. 11*I*), which had initially been established in 1879 by the Houston Water Works Company to provide surface water sourced from the Houston Ship Channel (fig. 1) (Lang and others 1950; in their report, Lang and others referred to the Houston Ship Channel as Buffalo Bayou). A well field of about 14 wells was completed by 1890, which was expanded to 38 wells by 1897—all of which were drilled to depths between 80 and 1,135 ft on a 14-acre tract containing the Houston Water Works plant (Baker, 1891, 1897; Deussen, 1914; Lang and others, 1950). In 1893, municipal groundwater was first provided from a deep artesian well at the nearby Houston Heights Electric Light and Water Works plant (Heights water plant and well field on fig. 11*I*) (Archaeological & Historical Commission, 2015). In 1893, groundwater use also began in Texas City (Rose, 1943, as cited in Petitt and Winslow, 1955). During 1894–95, the City of Galveston (fig. 1) began drilling and development of the first of 30 wells and a pump station in the Alta Loma area (Alta Loma pumping station; fig. 11*I*) after previously establishing a pump station (Galveston Waterworks; fig. 11*I*) and 7 municipal supply wells in 1888 that produced highly mineralized water (Petitt and Winslow, 1955; McDougal, 2018). Groundwater use from these wells in the Alta Loma area was about 1.6 million gallons per day (Mgal/d) by 1895 (Petitt and Winslow, 1955; Gabrysch and Bonnet, 1975). Groundwater began to be used to irrigate rice in the Katy area in 1902 after about 75 acres were planted, which expanded to 400 acres by 1905 (Lang and others, 1950). In October 1906, the City of Houston purchased the Houston Water Works Company wells (55 wells listed in Taylor, 1907), and during that year (from January to December), about 11.0 Mgal/d of groundwater was used in the historical Houston area (Gabrysch and Coplin, 1990) and was supplied from the Central well field (fig. 11*I*). The development of groundwater to supply industry in the Pasadena area began at an oil refinery in 1916, the year after the Houston Ship Channel was opened (Lang and others, 1950). In the Baytown area, industrial groundwater use began about 1918 (Gabrysch and Bonnet, 1975). In 1918, the City of Houston annexed the land in and near the Houston Heights Electric Light and Water Works plant (fig. 11*I*), thereby adding this water plant to its well network. Additionally, the City of Houston added additional groundwater capacity to its well network through operations at the South End and West End water plants during 1919 (fig. 11*I*).

Groundwater use in the Houston-Galveston region greatly increased during 1920–30 (table 1) to keep up with the substantial population growth rate that was nearly three times that of the typical city in the United States (Howson, 1938). In 1920, groundwater use in the Houston-Galveston region totaled about 43.5 Mgal/d, including about 22.0 Mgal/d in the historical Houston and Pasadena areas (collectively), about 11.5 Mgal/d in the Katy area, about 5.0 Mgal/d in the Baytown area, about 1.0 Mgal/d in the Texas City area, and about 4.0 Mgal/d in the Alta Loma area (fig. 11; table 1) (Goines and others, 1951). In 1920, the Texas City area groundwater use was supplied by about 10 industrial wells distributed among the sites of a railroad, an oil refinery, and a water plant (Petitt and Winslow, 1955). Substantial groundwater use first

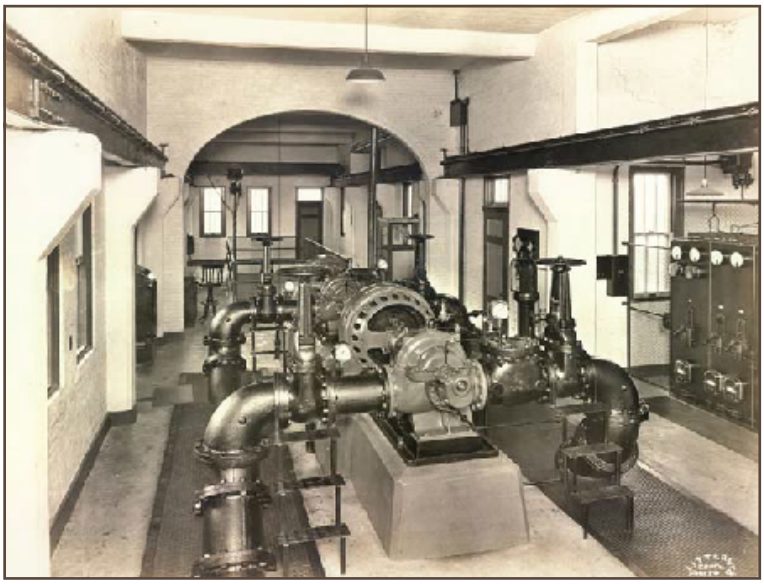

Photo courtesy of City of Houston E.B. Cape Center, used with permission.

Interior of the City of Houston Central Water Plant (fig. 11*I*) at 33 Artesian Street, circa 1936.

occurred in the Baytown area after operations commenced at the Humble Oil and Refining Company (hereinafter, "Humble Oil") refinery in 1920. After the Houston Ship Channel was dredged in 1925 by the U.S. Army Corps of Engineers to enlarge the channel, the improved access to the Gulf of Mexico resulted in major industrial development (and greater groundwater withdrawals to supply industrial water use) in the Pasadena, Baytown, and Texas City areas (Galloway and others, 1999). In the historical Houston area, municipal supply became available at the Scott Street water plant in 1926, and the Magnolia Park water plant the same year after annexation of the land in and near the Magnolia Park water plant (fig. 11*I*). Groundwater use at three additional oil refineries commenced in the Pasadena area prior to 1927 (Rose, 1943).

Groundwater use in 1930 in the Houston-Galveston region was about 85.7 Mgal/d, or nearly twice the groundwater use in 1920 (table 1). The total groundwater use in 1930 included about 50.0 Mgal/d in the historical Houston and Pasadena areas (collectively), about 18.0 Mgal/d in the Katy area (White and others, 1944; Lang and others, 1950), about 11.0 Mgal/d in the Baytown area, about 2.0 Mgal/d in the Texas City area, and about 4.7 Mgal/d in the Alta Loma area (White and others, 1939; Goines and others, 1951) (fig. 11; table 1). The groundwater used in the historical Houston and Pasadena areas was withdrawn from about 185 wells (collectively); groundwater used in the Baytown area was primarily from about 9 wells at the Humble Oil refinery (White and others, 1939). In the historical Houston area, municipal groundwater use in 1931 was about 25.4 Mgal/d, which was supplied primarily from six well fields and the recently completed East End and Northeast water plants (fig. 11*I*) (White and others, 1939). In the Katy area, groundwater from about 45 wells was used to irrigate approximately 9,000 acres in 1930 (Lang and others, 1950). Groundwater use in the Texas City area increased rapidly to about 4.0 Mgal/d by 1934 after operations commenced at the Pan American Refinery in Texas City (later the "American Oil Company [AMOCO] refinery" in various reports) (Rose, 1949). In 1935, groundwater use in the historical Houston and Pasadena areas was about the same as in 1930, and groundwater use in the Katy area had decreased from 1930 levels to about 14.0 Mgal/d (fig. 11; table 1) (Lang and others, 1950), attributed to decreased industrial activity during the Great Depression (Fugate, 1941).

Beginning in 1937 in the Houston-Galveston region, groundwater use rapidly expanded; during the following 8 years, groundwater use increased by nearly 70 percent (fig. 11; table 1). In 1937, groundwater use in the Houston-Galveston region totaled about 128 Mgal/d, including about 70.0 Mgal/d in the historical Houston and Pasadena areas (collectively), about 30.0 Mgal/d in the Katy area (Lang and others, 1950), about 13.5 Mgal/d in the Baytown area (White and others, 1939), about 10.0 Mgal/d in the Texas City area, and about 5.0 Mgal/d in the Alta Loma area (Goines and others, 1951; Gabrysch, 1967) (fig. 11; table 1). By 1937, groundwater use in the Pasadena area had increased by about 19.0 Mgal/d since 1935 after groundwater withdrawals from nine new wells began supporting the operation of a large paper mill (table 3.1) (White and others, 1944). This mill remained the largest industrial user of groundwater in the Pasadena area until 1954 (Anders and Naftel, 1962).

In 1940, groundwater use in the Houston-Galveston region totaled about 152 Mgal/d, or about 83 percent more groundwater use than in 1935 (fig. 11; table 1). This groundwater use in 1940 included about 79.0 Mgal/d in the historical Houston and Pasadena areas (collectively), about 45.0 Mgal/d in the Katy area (Lang and others, 1950), about 11.0 Mgal/d in the Baytown area (Goines and others, 1951), about 11.0 Mgal/d in the Texas City area (AMOCO, 1958; Gabrysch, 1967), and about 6.5 Mgal/d in the Alta Loma area (Goines and others, 1951) (fig. 11; table 1). In the Pasadena area, surface water from the San Jacinto River became available in 1942; however, total surface-water use was less than 20 Mgal/d until the construction of Lake Houston in 1953 (Gabrysch, 1967). Beginning in 1943 in the historical Houston area, additional municipal wells were drilled at the Northeast, East End, and South End well fields (fig. 11*I*), including a 2,060-ft well at the East End well field that was then the deepest municipal production well in the Houston-Galveston region (Rose and Alexander, 1944). In the Texas City area groundwater use doubled between 1941 and 1944 (table 1) as a result of increased use at existing water plants, and after operations commenced in 1941 at the Union Carbide Refinery (referred to as the "Carbide and Carbon Chemicals Company refinery" in various reports) and at two other industrial plants in 1943 (Petitt and Winslow, 1955; AMOCO, 1958).

In 1945, groundwater use in the Houston-Galveston region totaled about 213 Mgal/d, including about 112 Mgal/d in the historical Houston and Pasadena areas (collectively), about 50.0 Mgal/d in the Katy area (Lang and others, 1950), about 14.0 Mgal/d in the Baytown area (Goines and others, 1951), about 24.0 Mgal/d in the Texas City area (Rose, 1949; Gabrysch, 1967), and about 13.0 Mgal/d in the Alta Loma area (Gabrysch, 1967) (fig. 11; table 1). In the historical Houston area, seven municipal wells were drilled and completed at the new Southwest well field (fig. 11*I*) during 1945–46 (Lang and Sundstrom, 1946). In the Katy area in 1945, about 123 wells were used for irrigation of approximately 34,320 acres (Lang and others, 1950). Most of the groundwater use in 1946 in the historical Houston and Pasadena areas was from about 300 wells, compared to about 239 wells in 1930 (Lang and Sundstrom, 1946).

Transition to Developed Conditions (1946–1974)

In 1946, the groundwater use in the Houston-Galveston region entered a period of resumed rapid expansion that had begun about 1937 before slowing briefly during 1945 (fig. 11; table 1). During 1946–49, about 95 large-capacity wells were drilled in the historical Houston, Pasadena, and Katy areas (Lang and others, 1950). Municipal supply increased during 1946–49 through the development of 16 municipal production wells; the placement and depth of these 16 wells were based

on the results of exploratory well drilling (described in Rose and others, 1944). Four of these production wells were drilled and completed at the East End well field (fig. 11*I*), including a 2,580-ft well that was then the deepest municipal production well in the Houston-Galveston region. An additional six wells at the Northeast well field and two wells at the Southwest well field (fig. 11*I*) were drilled and completed (Lang and others, 1950). Based on the recognition that subsidence in the Texas City area was becoming a problem and to counteract issues of saltwater intrusion, delivery of surface water from the Brazos River began in 1948 to the Texas City area through a 50-mi-long canal (AMOCO, 1958; Wood, 1958b). These surface-water deliveries resulted in a rapid decrease of groundwater use in the Texas City area from a historical peak of about 26.0 Mgal/d in 1948 to about 11.5 Mgal/d in 1952, and to about 8.4 Mgal/d in 1957 (fig. 11; table 1) (AMOCO, 1958; Petitt and Winslow, 1955).

In 1950, groundwater use in the Houston-Galveston region totaled about 297 Mgal/d, including about 156 Mgal/d in the historical Houston and Pasadena areas (collectively), about 98.0 Mgal/d in the Katy area (Doyel and others, 1954), about 20.0 Mgal/d in the Baytown area (Goines and others, 1951), about 12.4 Mgal/d in the Texas City area, and about 10.5 Mgal/d in the Alta Loma area (AMOCO, 1958) (fig. 11; table 1). Surface-water deliveries to the historical Houston and Pasadena areas increased from 20.0 to 33.0 Mgal/d after the construction of Lake Houston in 1953. In 1954, municipal surface-water supplies also became available in the historical Houston and Pasadena areas (Anders and Naftel, 1962) for the first time since 1904, when surface water was still provided by the Houston Water Works plant (fig. 11*I*). In the Katy area, more groundwater was produced in 1954 (160 Mgal/d) than had been withdrawn in previous years because of an increased acreage of rice and pervasive drought conditions (fig. 11; table 1) (Wood, 1958a).

In 1955, groundwater use in the Houston-Galveston region totaled about 317 Mgal/d, including about 86.0 Mgal/d in the historical Houston area, about 80.0 Mgal/d in the Pasadena area, about 104 Mgal/d in the Katy area, about 25.2 Mgal/d in the Baytown area (Wood 1958a; Anders and Naftel, 1962), about 10.0 Mgal/d in the Texas City area (Gabrysch, 1967), and about 12.0 Mgal/d in the Alta Loma area (Wood, 1958b) (fig. 11; table 1). The surface-water supply from Lake Houston resulted in reduced groundwater use from 1954 until 1960 (except for 1958) for the historical Houston and Pasadena areas (Anders and Naftel, 1962) (fig. 11; table 1). Baytown area groundwater use peaked for the first time in 1956, and this annual groundwater withdrawal volume was not exceeded until 1966 in the combined usage for the Baytown and the Johnson Space Center areas (fig. 11; table 1).

In 1960, groundwater use in the Houston-Galveston region totaled about 310 Mgal/d, similar to the groundwater use (about 317 Mgal/d) in 1955 (fig. 11; table 1). This groundwater use included about 98.4 Mgal/d in the historical Houston area, about 78.6 Mgal/d in the Pasadena area, about 88.0 Mgal/d in the Katy area, about 21.7 Mgal/d in the Baytown area, about 1.2 Mgal/d in the Johnson Space Center area, about 9.8 Mgal/d in the Texas City area, and about 11.9 Mgal/d in the Alta Loma area (fig. 11; table 1) (Gabrysch, 1972). In 1960, surface water supplied 24 percent of the municipal water demand that was previously pumped from groundwater wells by the City of Houston (in the historical Houston area) and 46 percent of the water used for industry in the Pasadena area (Anders and Naftel, 1962). During 1960–64, groundwater use greatly increased in the historical Houston, Pasadena, and Katy areas (fig. 11; table 1); combined groundwater withdrawals in these areas increased about 37 percent between 1960 and 1964.

Installation of production well 8 (Texas Water Development Board well 6520303) by Texas Water Well Company on January 11, 1947, at the Southwest well field (fig. 11*I*). At the time this photograph was taken, Schlumberger was running an electrical log survey. Photograph by the U.S. Geological Survey, January 11, 1947.

In 1963, about 79 Mgal/d of groundwater was used in Jackson County, nearly all of which was for irrigation, representing about a fourfold increase in groundwater use since 1945 (Baker, 1965). The increase in groundwater use is demonstrated by the rapid increase in the number of irrigation wells used to provide irrigation water in the county; in 1942, only 23 irrigation wells were in Jackson County, compared to 246 in 1963 (Follett and Cumley, 1943; Baker, 1965). In 1966, about 6.2 Mgal/d of groundwater was used in Montgomery County (Popkin, 1971); this usage increased to about 9.0 Mgal/d by 1974 (TWDB, 2020a). Groundwater use in Brazoria County in 1966 was about 36.3 Mgal/d (Sandeen and Wesselman, 1973). In Liberty County during 1946–65, groundwater use, generally for rice irrigation, increased greatly from about 5.2 to about 52 Mgal/d (Anders and others, 1968).

In 1965, groundwater use in the Houston-Galveston region totaled about 419 Mgal/d, including about 139 Mgal/d in the historical Houston area, about 94.0 Mgal/d in the Pasadena area, about 139 Mgal/d in the Katy area, about 21.6 Mgal/d in the Baytown area, about 3.9 Mgal/d in the Johnson Space Center area, about 10.6 Mgal/d in the Texas City area, and about 11.3 Mgal/d in the Alta Loma area (fig. 11; table 1) (Gabrysch, 1972). Groundwater-use totals in Liberty and Chambers Counties in 1965 were about 51.2 Mgal/d (Anders and others, 1968) and 4.0 Mgal/d (Wesselman and Aronow, 1971), respectively.

By 1970, groundwater use in the Houston-Galveston region totaled about 480 Mgal/d, including about 171 Mgal/d in the historical Houston area, about 121 Mgal/d in the Pasadena area, about 119 Mgal/d in the Katy area, about 28.0 Mgal/d in the Baytown area, about 15.6 Mgal/d in the Johnson Space Center area, about 13.6 Mgal/d in the Texas City area, and about 11.9 Mgal/d in the Alta Loma area (fig. 11; table 1) (Gabrysch, 1980a). The City of Galveston began using surface water in 1973, resulting in rapid decreases in groundwater use in the Alta Loma area thereafter (fig. 11*H*) (Gabrysch and Bonnet, 1975.

During the early 1970s, groundwater use in the Houston-Galveston region increased through 1974 when groundwater use totaled about 521 Mgal/d, including about 190 Mgal/d in the historical Houston area, about 112 Mgal/d in the Pasadena area, about 151 Mgal/d in the Katy area, about 28.0 Mgal/d in the Baytown area, about 20.2 Mgal/d in the Johnson Space Center area, about 13.2 Mgal/d in the Texas City area, and about 6.8 Mgal/d in the Alta Loma area (fig. 11; table 1) (Gabrysch, 1980a). The groundwater use in 1974 represents the historical peak of water use in the Houston-Galveston region (table 1).

Regulation and Post-Developed Conditions (1975–Present)

The period from about 1975 through the present (2023) marked a shift in water-use sources from groundwater to surface water in the Houston-Galveston region. The more widespread availability of surface water—first from the San Jacinto River in 1942 and the Brazos River in 1948, followed by Lake Houston in 1953, and later from Lake Livingston in late 1976—resulted in reduced groundwater use in the Pasadena, Baytown, Texas City, and Alta Loma areas (Gabrysch and Coplin, 1990). Coincident with additional surface-water availability was the introduction of groundwater regulation with the 1975 formation of the Harris-Galveston Subsidence District (HGSD), the first district of its kind in the United States (Coplin and Galloway, 1999). The HGSD established a regulatory Area of Concentrated Emphasis in the eastern part of the historical Houston area, and the Pasadena, Baytown, Johnson Space Center, Texas City, and Alta Loma areas based on the 1976 HGSD Regulatory Plan (HGSD, 2013). The water regulation of these areas and emphasis on increased reliance on surface-water supplies occurred concurrently with increased population growth and groundwater use in northern and western Harris County, southern Montgomery County, and eastern Fort Bend County.

In the Area of Concentrated Emphasis, the transition from relying on groundwater to relying mostly on surface water was rapidly completed in a few years. In the Pasadena area, groundwater use decreased from about 106 Mgal/d in 1976 to about 48.1 Mgal/d in 1979, with water from Lake Livingston taking the place of most of the groundwater (fig. 11; table 1) (Gabrysch, 1982a, b). Similarly, groundwater use in the Baytown, Johnson Space Center, and Texas City areas during 1975–79 decreased from about 26.5 to 14.4 Mgal/d, from about 20.6 to 4.0 Mgal/d, and from about 14.0 to 8.9 Mgal/d, respectively, as a direct result of increases in surface-water use (fig. 11; table 1) (Gabrysch, 1982a).

Although groundwater use decreased during 1975–79 in Pasadena, Baytown, and the Johnson Space Center areas, the rate of groundwater use in the historical Houston area, as well as in northern and western Harris County, continued to increase, in part because of the relocation of well fields (Gabrysch, 1982a) and population growth. The 438 Mgal/d of groundwater use in the Houston-Galveston region in 1979 included about 234 Mgal/d in the historical Houston area, about 48.1 Mgal/d in the Pasadena area, about 127 Mgal/d in the Katy area, about 14.4 Mgal/d in the Baytown area, about 4.0 Mgal/d in the Johnson Space Center area, about 8.9 Mgal/d in the Texas City area, and about 1.6 Mgal/d in the Alta Loma area (fig. 11; table 1) (Gabrysch, 1980a).

Groundwater use in the historical Houston area generally continued to increase until 1982, when a historical high of about 257 Mgal/d was withdrawn, after which groundwater use declined to about 206 Mgal/d in 1987 (fig. 11; table 1) (Gabrysch and Coplin, 1990). Three years later, HGSD's 1985 regulatory plan created Regulatory Areas 1 and 2 from the 1976 Area of Concentrated Emphasis, and six other regulatory areas that were combined into Regulatory Area 3 in 1999 (fig. 3) (HGSD, 2013). Groundwater use in the Pasadena area peaked at about 126 Mgal/d in 1968, decreased slowly during 1969–76, then rapidly during 1977–78, and was down to about 37.2 Mgal/d by 1987 (fig. 11; table 1) (Gabrysch and Coplin, 1990). The pattern of groundwater use in the Baytown area was similar to that of the Pasadena area; groundwater in the Baytown area peaked at about 31.8 Mgal/d in 1972, and then decreased slowly until about 1978, then rapidly during 1979–81, and was down to about 4.4 Mgal/d by 1987 (fig. 11; table 1) (Gabrysch and Coplin, 1990). By 1987, groundwater use in the Johnson Space Center, Texas City, and Alta Loma areas had decreased to about 5.5, 0.7, and 0.7 Mgal/d, respectively (fig. 11; table 1) (Gabrysch and Coplin, 1990).

By 1990, combined annual groundwater use in the greater Houston area was about 533 Mgal/d, distributed as follows: about 25.5 Mgal/d in Brazoria County, about 4.6 Mgal/d in Chambers County, about 62.6 Mgal/d in Fort Bend County, about 4.5 Mgal/d in Galveston County, about 363 Mgal/d in Harris County, about 17.8 Mgal/d in Liberty County, about 25.5 Mgal/d in Montgomery County, and about 29.1 Mgal/d

in Waller County (fig. 2.1) (TWDB, 2020a). As described in the Introduction section of this report, the greater Houston area includes Brazoria, Fort Bend, Galveston, Harris, and Montgomery Counties and parts of Chambers, Waller, and Liberty Counties (figs. 1 and 11*I*). In 1990, Harris and Galveston Counties underwent an initial conversion to alternative water supplies (surface water) for 90 percent (HGSD Regulatory Area 1; fig. 3) or 80 percent (HGSD Regulatory Area 2; fig. 3) of total permitted water use. By 1995, groundwater use in the historical Houston area had declined to about 60 percent of the historical peak (Coplin and Galloway, 1999).

By 2000, combined annual groundwater use in the greater Houston area was about 552 Mgal/d, distributed as follows: about 32.0 Mgal/d in Brazoria County, about 4.7 Mgal/d in Chambers County, about 86.5 Mgal/d in Fort Bend County, about 4.1 Mgal/d in Galveston County, about 338 Mgal/d in Harris County, about 12.0 Mgal/d in Liberty County, about 49.8 Mgal/d in Montgomery County, and about 25.3 Mgal/d in Waller County (fig. 2.1) (TWDB, 2020a). By 2000, the bulk of the conversion requirements from groundwater to surface-water supplies for HGSD Regulatory Areas 1 and 2 (fig. 3) in Harris and Galveston Counties had been completed.

In 2010, combined annual groundwater use in the greater Houston area was about 471 Mgal/d (TWDB, 2020a), a decrease of about 15 percent from 2000, and about a 41-percent decrease from 1974 when annual groundwater use in the greater Houston area peaked at about 793 Mgal/d. Groundwater use in 2010 was distributed as follows: about 45.2 Mgal/d in Brazoria County, about 3.5 Mgal/d in Chambers County, about 99.3 Mgal/d in Fort Bend County, about 0.7 Mgal/d in Galveston County, about 225 Mgal/d in Harris County, about 8.2 Mgal/d in Liberty County, about 64.0 Mgal/d in Montgomery County, and about 25.5 Mgal/d in Waller County (fig. 2.1) (TWDB, 2020a).

In 2015, combined annual groundwater use in the greater Houston area was about 400 Mgal/d (TWDB, 2020a), a decrease of about 28 percent from 2000, and about a 50 percent decrease from 1974. The groundwater use in the greater Houston area in 2015 was distributed by county as follows: about 29.0 Mgal/d in Brazoria County, about 2.7 Mgal/d in Chambers County, about 71.4 Mgal/d in Fort Bend County, about 0.6 Mgal/d in Galveston County, about 212 Mgal/d in Harris County, about 7.8 Mgal/d in Liberty County, about 63.0 Mgal/d in Montgomery County, and about 13.1 Mgal/d in Waller County (fig. 2.1) (TWDB, 2020a).

Groundwater-Level Measurements

Groundwater levels in the study area have been extensively studied by the USGS and other entities since about 1931. All the groundwater-level data collected by the USGS are stored in the USGS National Water Information System (NWIS) database (USGS, 2021b). For the purposes of this report, the term "groundwater level" is synonymous with the depth to water measured in feet below land surface and applies to wells screened in either (1) an unconfined aquifer, where the upper water surface (water table) is at atmospheric pressure, or (2) a confined aquifer, where fine-grained units above and below the aquifer result in pressurized conditions so that the groundwater level in a well penetrating the aquifer will rise above the top of the aquifer. Prior to groundwater development, the groundwater level in the greater Houston area increased as the depth of the screened interval of the well increased, and the groundwater level in the more deeply screened aquifer units was greater than the groundwater level in the more shallowly screened aquifer units. With the advent of sustained groundwater development, however, intersecting cones of depression (Freeze and Cherry, 1979) around production wells merged to form a lower potentiometric surface (a hypothetical surface defined by the level to which water rises in observation wells) compared to the surface of the water table during antecedent (predevelopment) conditions. The changing altitude of the water-table surface has been mapped and published in a series of USGS-authored reports since 1932 (many of which were published in the TWDB or Texas State Board of Water Engineers report series), such as White and others (1939, 1944), Lang and Sundstrom (1946), Lang and others (1950), Petitt and Winslow (1955), Wood and Gabrysch (1965), Gabrysch (1967, 1972, 1980a, 1984), and Gabrysch and Coplin (1990).

The following sections describe study area groundwater levels from predevelopment through 2015 using information obtained from numerous historical reports. The present-day naming of the Gulf Coast aquifer hydrogeologic units was formalized in Turcan and others (1966) (fig. 10); therefore, reports describing groundwater-level changes prior to about 1966 generally did not follow this naming convention. Rather, these pre-1966 reports used either the "zones" from figure 10 or described the screened interval as a depth below land surface, or an elevation above NAVD 88. The classifications of the top and bottom depth intervals of the hydrogeologic units have changed over time, as discussed in the "History of the Geologic and Hydrogeologic Units" section, which complicates identifying the modern-day hydrogeologic unit in which the wells from the historical reports are screened. Therefore, rather than using the older naming convention that predates Turcan and others (1966), the groundwater-level changes described in reports published before about 1966 are generally not attributed to a specific hydrogeologic unit. Additionally, the groundwater levels from many of the wells described in historical reports are also plotted in figures in this report. Because the well identifiers used by the USGS and TWDB have changed between the publication of the historical reports and more recent reports, a "historical identifier" column is provided in table 3.1 to cross-reference historical and current (2023) well identifiers.

Groundwater levels and groundwater development are closely related over time. Thus, the three periods used to describe groundwater development—predevelopment to early development; transition to developed conditions; regulation and post-developed conditions—are used to

describe groundwater levels in the study area. Similar to the "Groundwater Development" section, locations from previously published reports describing groundwater data have been updated to reflect present-day geographic descriptions.

Predevelopment to Early Development (1897–1945)

From the early 1900s until about 1930, periodic measurements of groundwater levels were documented in the Houston-Galveston region. Groundwater-level data became more widely available beginning in December 1930 when systematic USGS groundwater measurement surveys began in cooperation with the Texas State Board of Water Engineers (predecessor to the Texas Water Commission) and the City of Houston (White and others, 1939, 1944). These groundwater measurement surveys were done by the USGS to investigate the rapid development of groundwater resources between 1930 and 1940 (fig. 11; table 1). Selected groundwater levels from these surveys are presented in figures 13–16. Although the hydrographs in these figures represent groundwater levels for a relatively small number of wells, many wells with at least one groundwater-level measurement before 1940 are listed in table 3.1. The spatial extents of the historical geographic areas used to describe water-level data are shown on figures 13–16 and are identified in table 3.1 for each well.

During predevelopment to early development conditions, flowing wells (where the potentiometric surface is above land surface) were common in much of the study area, such that artesian pressure was sufficient to sustain groundwater levels between 15 and 30 ft above land surface in some areas (White and others, 1939, 1944) and to sustain groundwater levels of much more than 30 ft above land surface in other areas (Wood and Gabrysch, 1965). Among the earliest published records regarding flowing wells in the study area are Singley (1893) and Taylor (1907). Singley (1893) lists 45 flowing wells in Galveston County. Taylor (1907) lists 140 flowing wells in Harris County, about 90 flowing wells in Galveston County, between 11 and 17 flowing wells in Chambers County, and a "wide distribution" of flowing wells in Brazoria County. Taylor (1907) also lists a few flowing wells in Austin, Colorado, Lavaca, Orange, Waller, and Wharton Counties. A list of historical flowing wells completed as shallow as 100 ft below land surface (bls) is provided in Taylor (1907). Deussen (1914) lists many flowing wells across the study area, particularly in Brazoria, Galveston, Hardin, Harris, Jefferson, and Polk Counties (fig. 1). Some of the flowing wells listed by Deussen (1914) were indicated by Rose (1943)

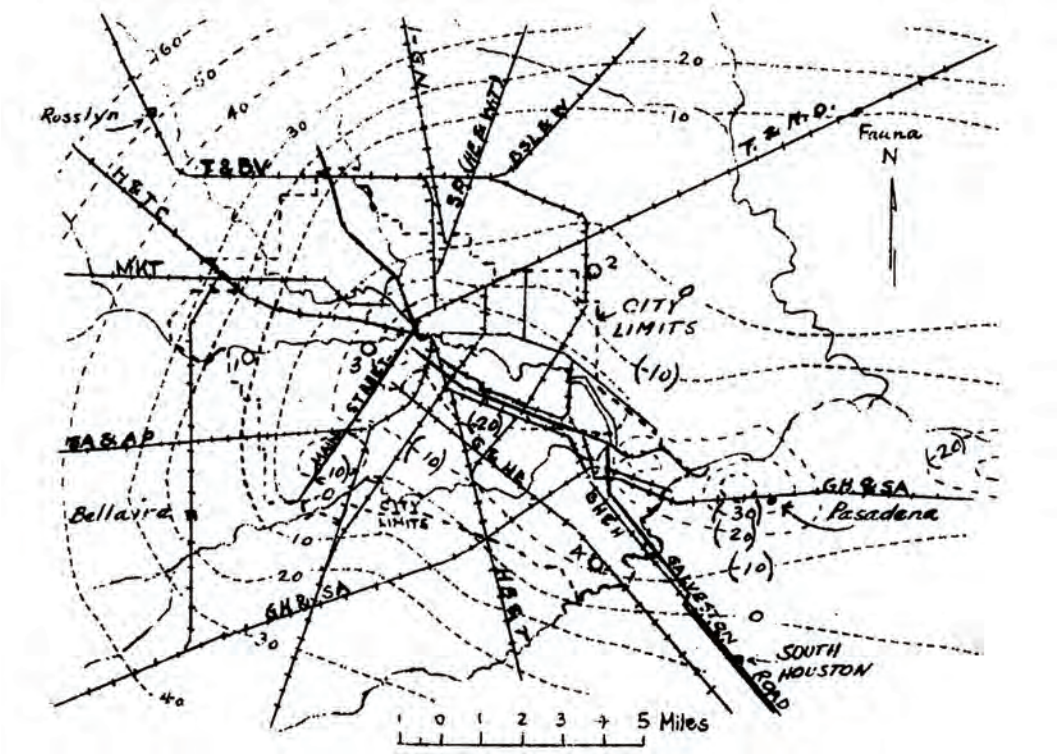

This image shows 1931 groundwater-level contours in the Houston-Galveston region and is included in White and others (1939). Well 1 in this image is TWDB well 6513824; well 2 is TWDB well 6514908, and well 3 is TWDB well 6513927 (table 3.1). Note that the groundwater-level contours are in feet above a vertical control datum that approximates sea level. Photograph by John Ellis, U.S. Geological Survey, August 21, 2022.

as having sufficient artesian pressure to raise the groundwater level to about 20 ft above land surface. In Montgomery County, Popkin (1971) lists an 1,800-ft-deep flowing well in 1902 (TWDB well 6053502; fig. 13*A*; table 3.1) screened in the Jasper aquifer south of Conroe (fig. 1), along with about 40 other flowing wells. During the early 1900s, Montgomery County groundwater levels in the Evangeline and Jasper aquifers were between about 5 and 10 ft and 20 and 45 ft above land surface, respectively (Popkin, 1971). In the Alta Loma area, the artesian pressure was sufficient to sustain groundwater levels 28 ft above land surface in 1900 (Petitt and Winslow, 1955).

Although flowing wells were present throughout the study area when Deussen (1914) was published, groundwater use in Harris County at the Houston Water Works plant (fig. 11*I*) necessitated airlift pumps on most of the wells by about 1904 (Municipal Engineering Company, 1904; Lang and others, 1950). In 1915, most of the wells in the Texas City area

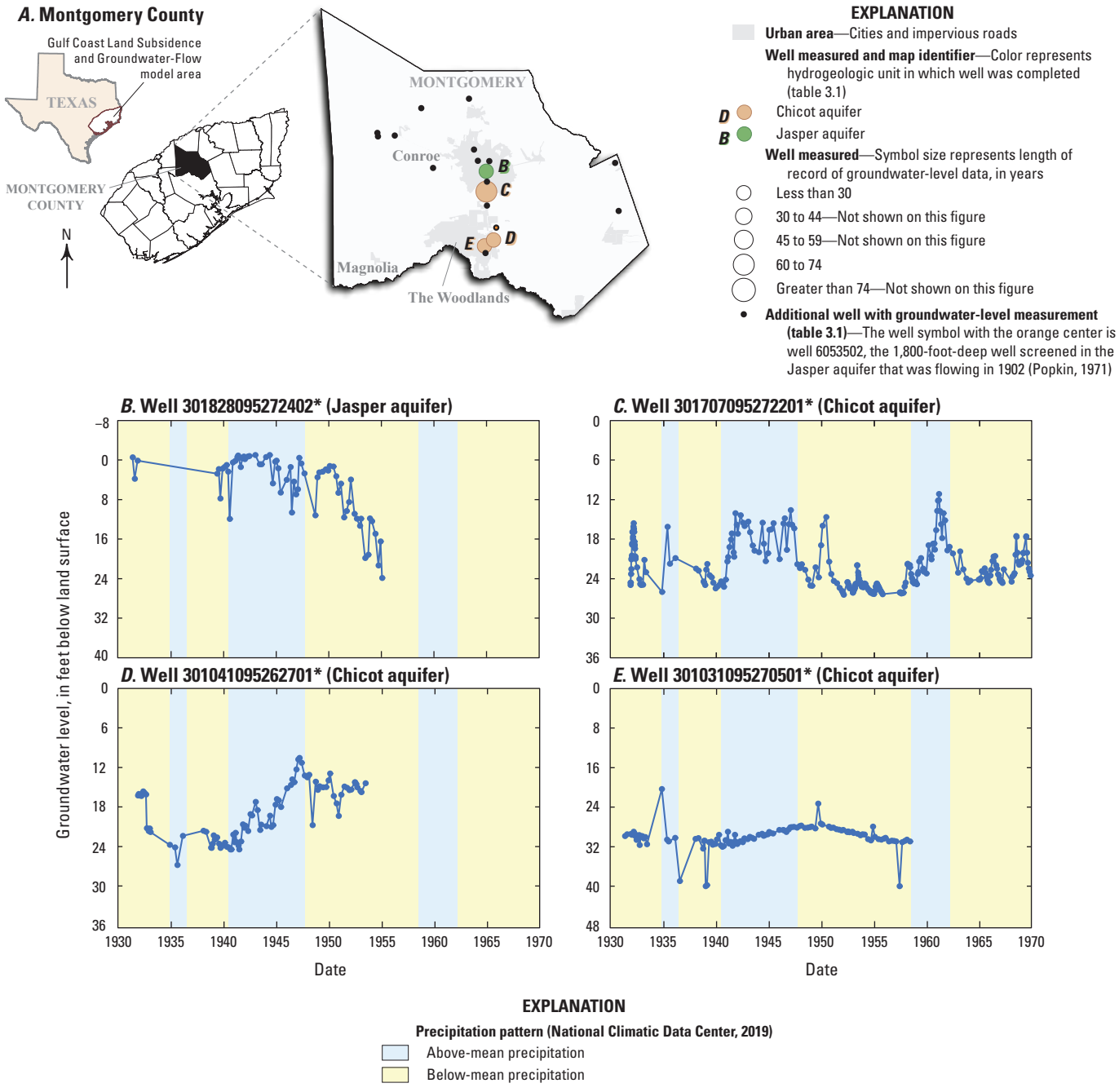

*Hydrograph labeled with 15-digit U.S. Geological Survey (USGS) well identifier shows data from the USGS (2021b).

Figure 13. Locations and hydrographs of groundwater levels for selected wells in Montgomery County from the early 1930s to 1970 in the Gulf Coast aquifer system study area in southeast Texas.

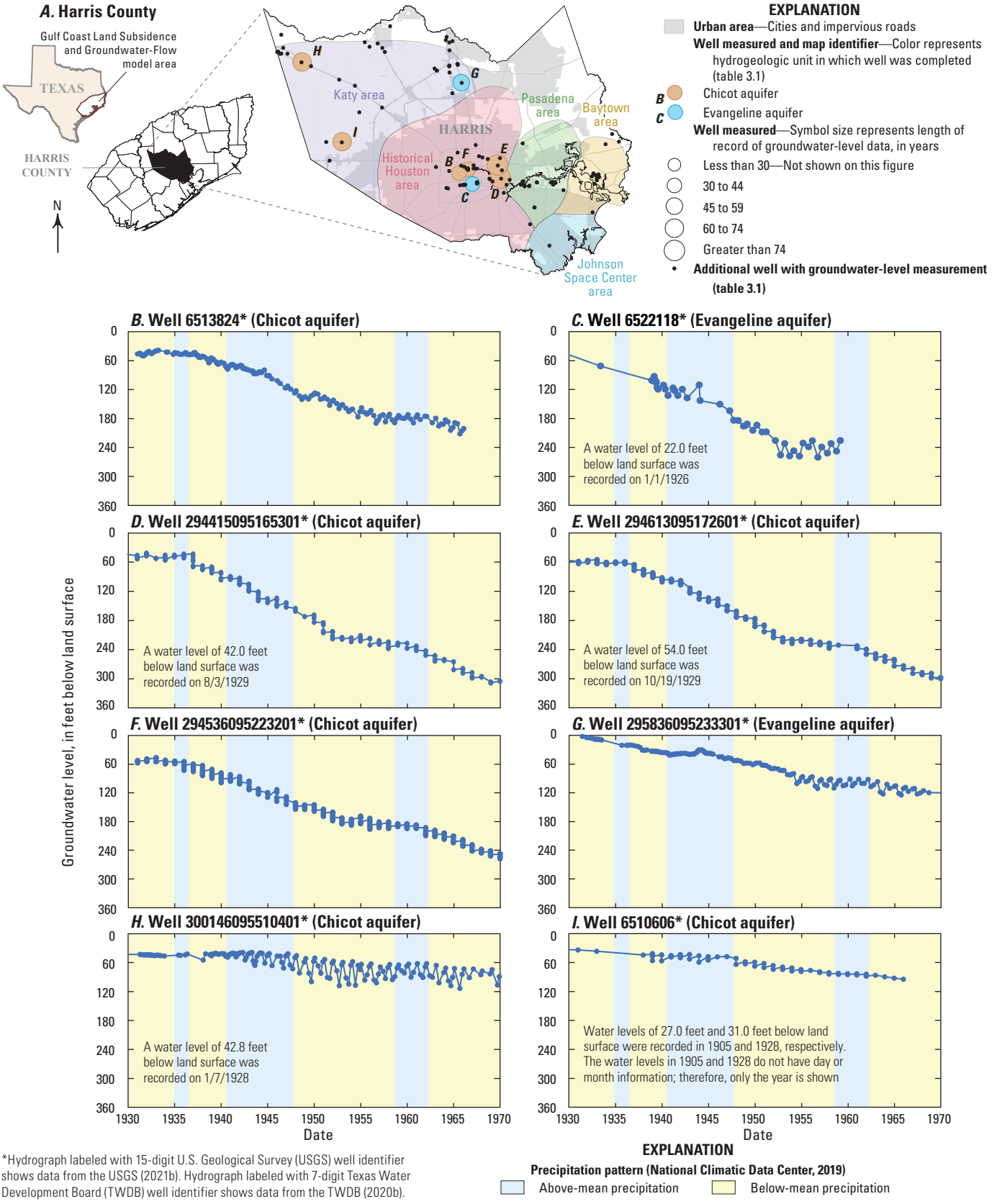

*Hydrograph labeled with 15-digit U.S. Geological Survey (USGS) well identifier shows data from the USGS (2021b). Hydrograph labeled with 7-digit Texas Water Development Board (TWDB) well identifier shows data from the TWDB (2020b).

Figure 14. Locations and hydrographs of groundwater levels for selected wells in Harris County from the early 1930s to 1970 in the Gulf Coast aquifer system study area in southeast Texas.

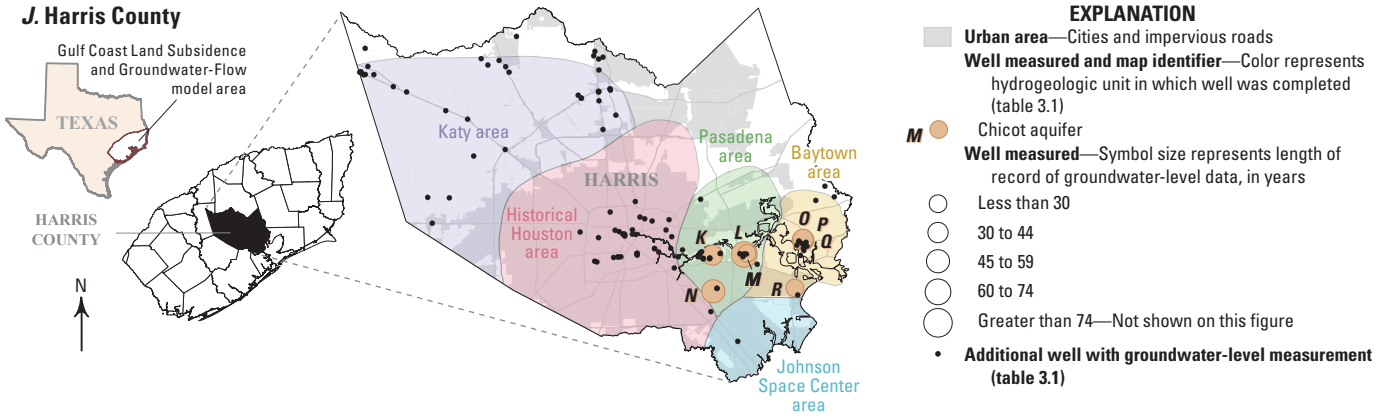

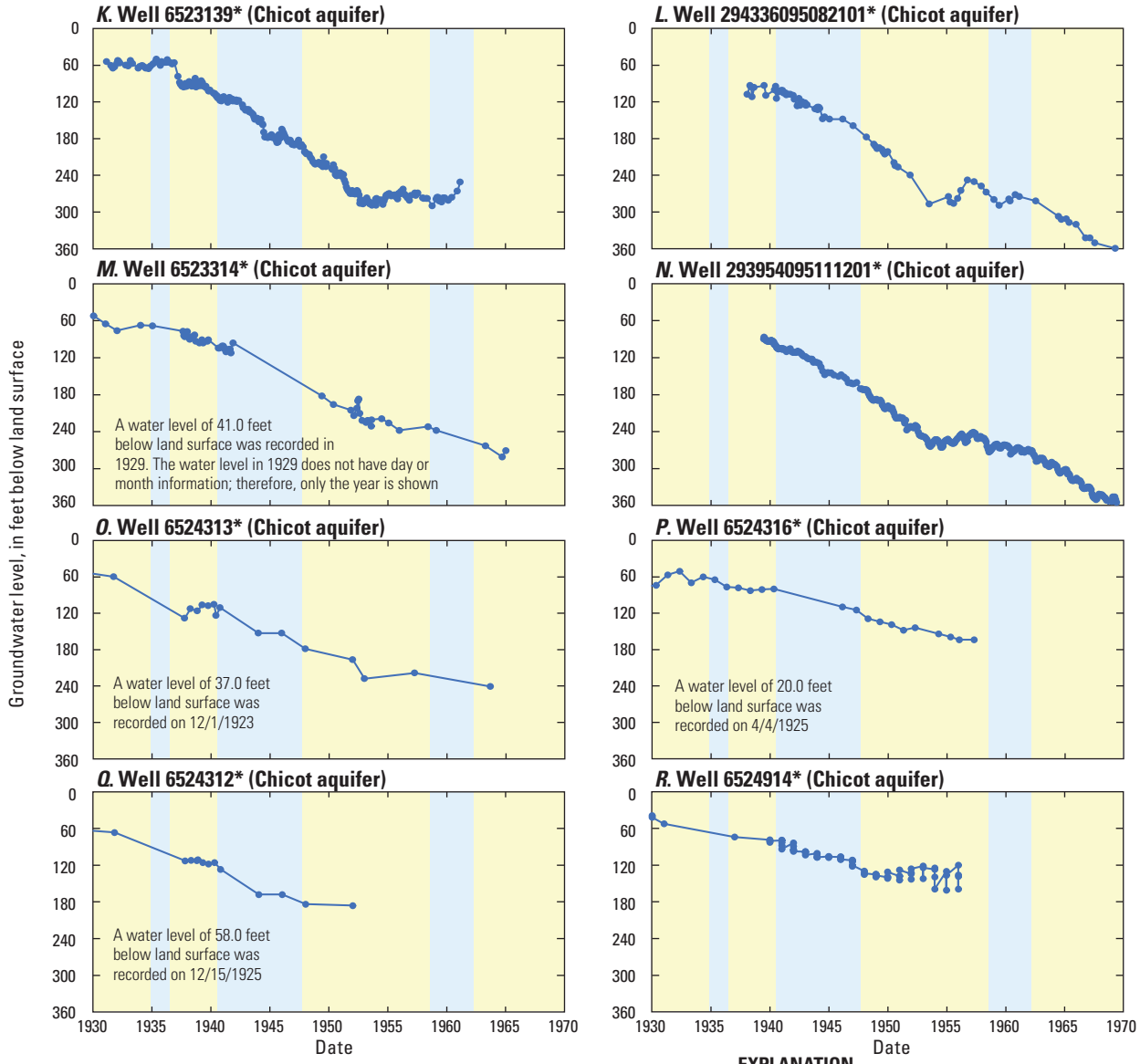

*Hydrograph labeled with 15-digit U.S. Geological Survey (USGS) well identifier shows data from the USGS (2021b). Hydrograph labeled with 7-digit Texas Water Development Board (TWDB) well identifier shows data from the TWDB (2020b).

Figure 14.—Continued

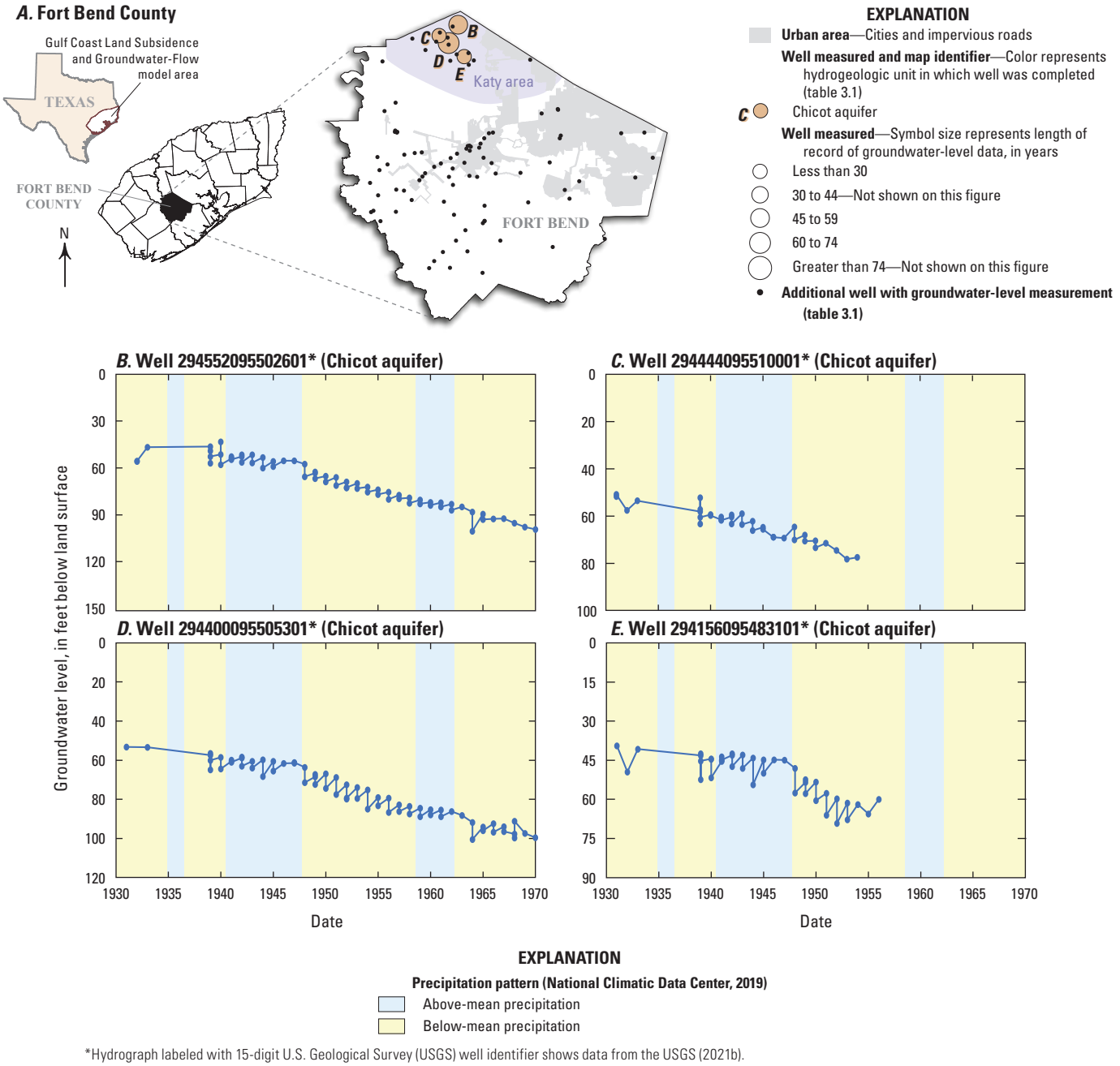

*Hydrograph labeled with 15-digit U.S. Geological Survey (USGS) well identifier shows data from the USGS (2021b).

Figure 15. Locations and hydrographs of groundwater levels for selected wells in Fort Bend County from the early 1930s to 1970 in the Gulf Coast aquifer system study area in southeast Texas.

still flowed, and the artesian pressure was sufficient to raise the groundwater level to as much as 8 ft above land surface. Between 1920 and 1930, increased groundwater use in the historical Houston and Pasadena areas (fig. 11; table 1) resulted in mean groundwater-level declines of about 4 feet per year (ft/yr) (White and others, 1944), although some localities had groundwater-level declines of as much as 7 ft/yr (Howson, 1938). By about 1930, groundwater levels in the historical Houston and Pasadena areas were about 50–60 ft bls (fig. 14) (White and others, 1939). In the Baytown area, groundwater levels declined by about 5 ft/yr between 1920 and 1930 due to increases in industrial and public supply groundwater use (White and others, 1939). As a result, groundwater levels in the Baytown area were also about 50–60 ft bls by about 1930 (fig. 14*O–R*) (White and others, 1939). In the Katy area, groundwater levels declined by about 5 ft during 1903–30. In Galveston County, where there had been sufficient artesian pressure to raise the groundwater level above land surface, the groundwater levels slowly declined and were generally

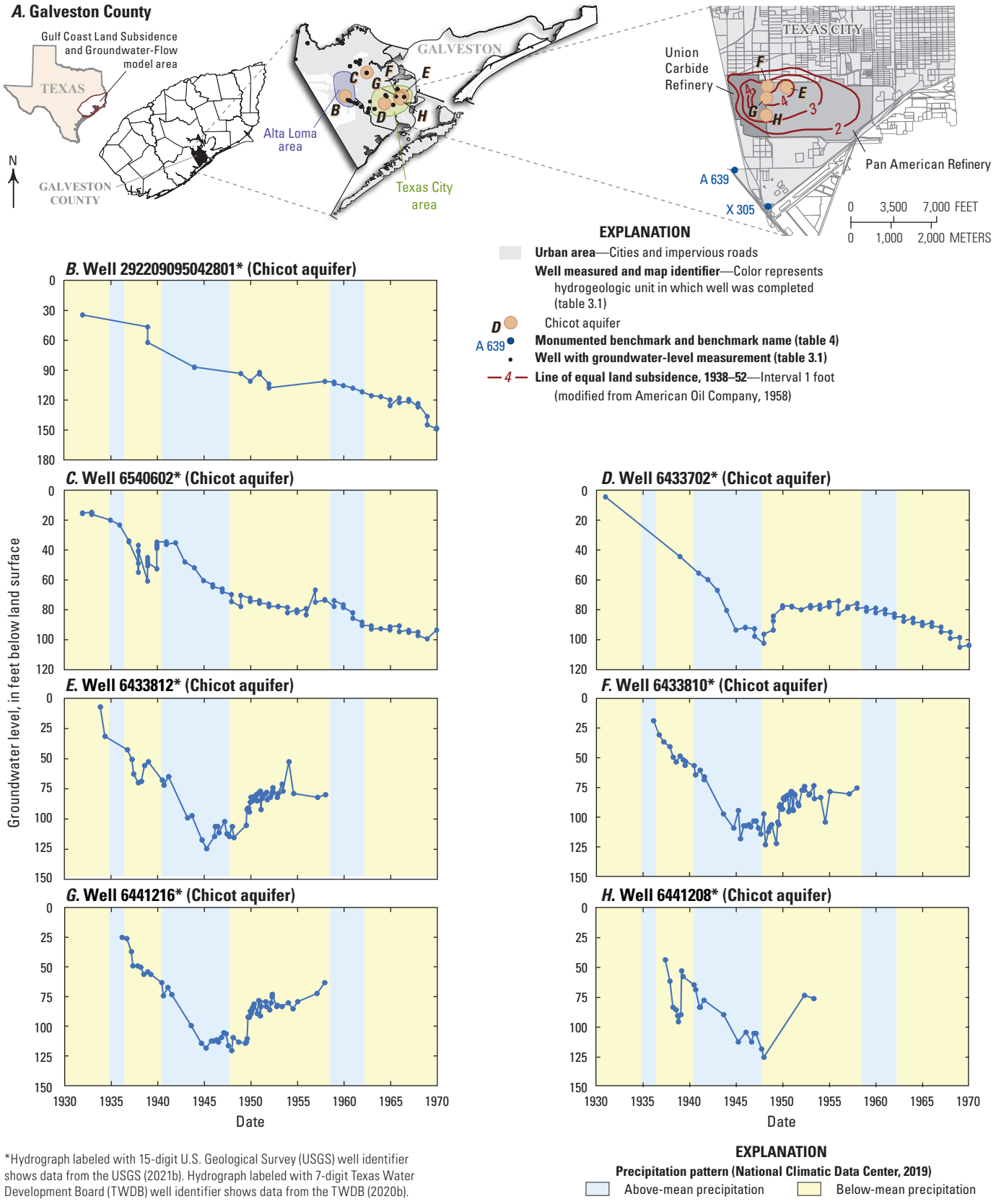

*Hydrograph labeled with 15-digit U.S. Geological Survey (USGS) well identifier shows data from the USGS (2021b). Hydrograph labeled with 7-digit Texas Water Development Board (TWDB) well identifier shows data from the TWDB (2020b).

Figure 16. Locations and hydrographs of groundwater levels for selected wells and approximate land subsidence near the Union Carbide and Pan American Refineries, 1938–52, in Galveston County in the Gulf Coast aquifer system study area in southeast Texas.

below land surface by 1930 (fig. 16) (Wood, 1956). The last flowing well in the Texas City area ceased to flow by 1931 (Rose, 1949).

During 1931–36, groundwater levels in the historical Houston and Pasadena areas did not change appreciably (fig. 14), primarily because of a pause in the growth of groundwater demands in these areas for industrial use during the Great Depression (White and others, 1939). Groundwater levels generally declined by less than 5 ft during 1931–36 in the Katy area (fig. 14*G–I*); these declines were attributed to irrigation groundwater use. Groundwater levels in the Baytown area declined by between 20 and 60 ft during 1931–36 (fig. 14*O–R*).

In 1937, a new period of sustained groundwater-level declines began because of the renewed rapid expansion of groundwater use in the Houston-Galveston region (fig. 11; table 1). During 1937–40, groundwater levels in the historical Houston area declined by 15–38 ft (fig. 14*B–F*) (White and others, 1944). The groundwater level at a well located about a half-mile from a paper mill in the Pasadena area (fig. 14*K*) declined by about 45 ft in 1937 and another 20 ft during 1938–40 after eight wells withdrawing 19 Mgal/d began operation at the mill (fig. 11*C*; table 1) (White and others, 1939). Although groundwater use in the Katy area increased from 30 to 45 Mgal/d between 1937 and 1940 (fig. 11*D*; table 1), groundwater-level declines during this period were generally less than 10 ft (figs. 14–15) (Lang and others, 1950). The groundwater levels in Galveston County that were previously near land surface in many wells had declined to about 45 to 50 ft bls by 1939 (fig. 16) (Petitt and Winslow, 1955). In the Texas City area, the development of groundwater resources increased rapidly during the 1930s, resulting in large-scale groundwater use and concurrent declines in groundwater levels (fig. 16*D–H*) (AMOCO, 1958).

Annual groundwater-level declines during 1940–45 in many of the areas that made up the Houston-Galveston region were generally greater compared to previous annual groundwater-level declines (figs. 14–16) as a result of large increases in groundwater use (fig. 11; table 1). During 1940–45, the mean groundwater-level decline was about 40 ft in the historical Houston area, about 55 ft in the Pasadena area, about 10 ft in the Katy area (Lang and others, 1950), about 30 ft in the Baytown area, and about 50 ft in the Texas City area (figs. 14–16).

Groundwater levels in Liberty County prior to 1940 were still generally near land surface (table 3.1), and about 15 flowing wells were reported in 1945 by Alexander (1950). In the Jasper aquifer, groundwater levels during 1939–40 were at or near land surface in Montgomery County (fig. 13*B*). In Brazoria County, flowing wells were still common in the late 1930s, but few remained after 1943 (Sandeen and Wesselman, 1973). Water-level declines in Brazoria County between 1931 and the mid-1940s were between about 50 and 180 ft in many areas where groundwater withdrawals were large, whereas areas distant from where large amounts of groundwater were withdrawn recorded about 10 ft of decline (Follett, 1947). Climate-related patterns are noticeable on hydrographs of groundwater levels for shallow wells in Montgomery County (fig. 13*C–E*) and in Harris County (fig. 14*H*), with groundwater levels rising during periods of above-mean precipitation.

Transition to Developed Conditions (1946–1974)

Many studies have recorded groundwater levels across the Gulf Coast aquifer system, and long-term groundwater-level data for the study area are widely available (fig. 17) during and after the 1946–74 period, particularly in the greater Houston area (geographic extent of fig. 18*A*). Many wells and associated groundwater-level data (depth to water in feet below land surface) are used to describe water-level patterns in the study area after 1946 (figs. 19–36, 51–52; table 2). The groundwater-level dataset (figs. 19–36, 51–52; table 2) includes hydrographs of groundwater levels from 129 wells, including 71 wells completed in the Chicot aquifer, 36 in the Evangeline aquifer, 1 in the Burkeville confining unit, 19 in the Jasper aquifer, and 2 in the Catahoula confining unit (table 2). The subset of groundwater levels from 129 wells represents a distributed subset (areally and vertically), and this set of wells generally has the longest period of groundwater-level data available in the study area. In table 2, wells are grouped according to the historical geographic areas as follows: Katy area (figs. 21–23, 31); historical Houston area (figs. 24–25); Pasadena area (fig. 26); Johnson Space Center area (fig. 27*B–D*); Baytown area (fig. 27*E–G*); Alta Loma area (fig. 33*B*, *E*); and Texas City area (fig. 33*C*).

Although the historical groundwater-level minimums for many wells in the Houston-Galveston region (fig. 18*B*) generally occurred in the mid- to late-1970s, prior groundwater-level declines were so extensive that by 1946 groundwater levels in some wells in the Houston and Pasadena areas had nearly reached 50 percent of their historical minimums based on a predevelopment groundwater level estimated at land surface. This is illustrated by the hydrographs of two groundwater levels (fig. 14*D–E*) that are continued on figure 25 (the same wells on both figures) and that are representative of the historical pattern of groundwater-level declines seen in many wells in the historical Houston area, Pasadena area, and Baytown area. The rapid expansion of groundwater use during 1937–52 resulted in the largest annual mean groundwater-level declines in the historical Houston area and Pasadena area (about 10 ft/yr and 14 ft/yr, respectively) during the study period. The annual mean groundwater-level declines during 1937–52 in these areas were somewhat greater than the annual mean declines during 1962–72 (each about 8 ft/yr), another period of rapid groundwater expansion and groundwater-level decline. Groundwater-level measurements have been made annually at well D since 1929 (figs. 14 and 25); well D has the longest continuous record of groundwater-level measurements of any the wells measured annually by the USGS in the greater Houston area.

During 1946–49, the mean groundwater-level decline was about 40 ft in the historical Houston area (figs. 14*B–F*, 24–25), about 50 ft in the Pasadena area (fig. 14*K–N*), about

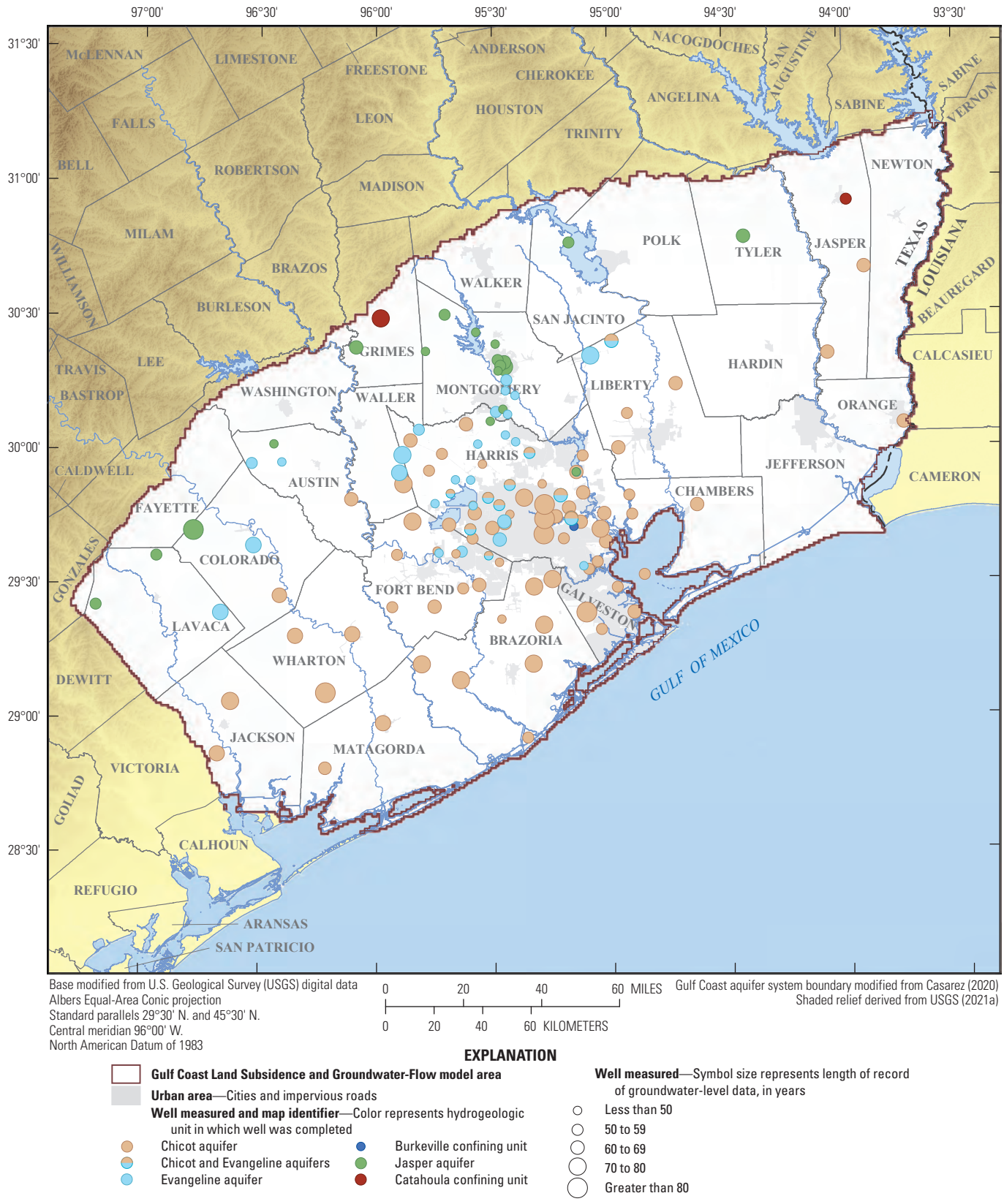

Figure 17. Locations of wells with long-term groundwater-level measurements within the Gulf Coast aquifer system study area in southeast Texas.

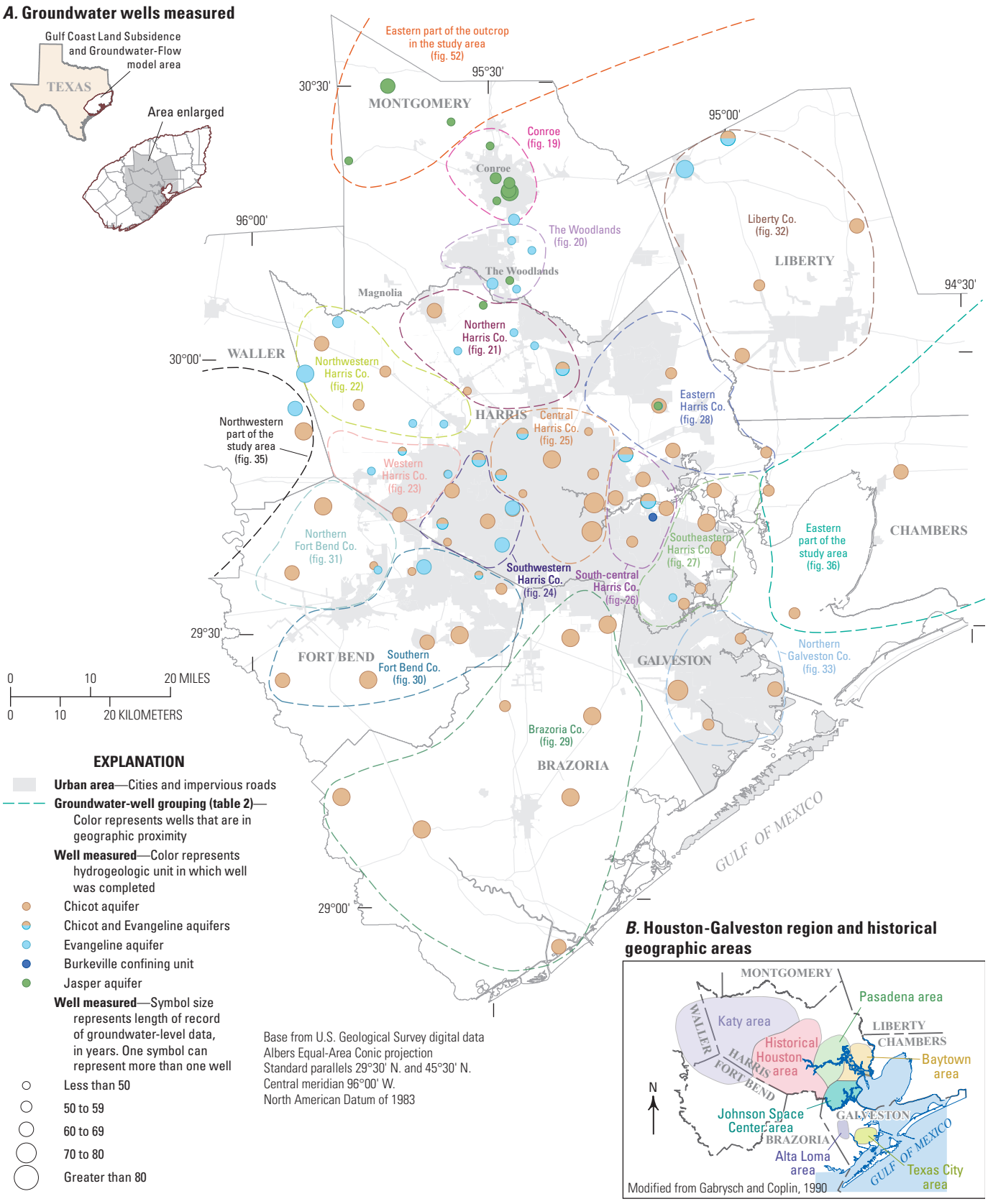

Figure 18. Locations of wells with long-term groundwater-level measurements in the greater Houston area within the Gulf Coast aquifer system study area in southeast Texas.

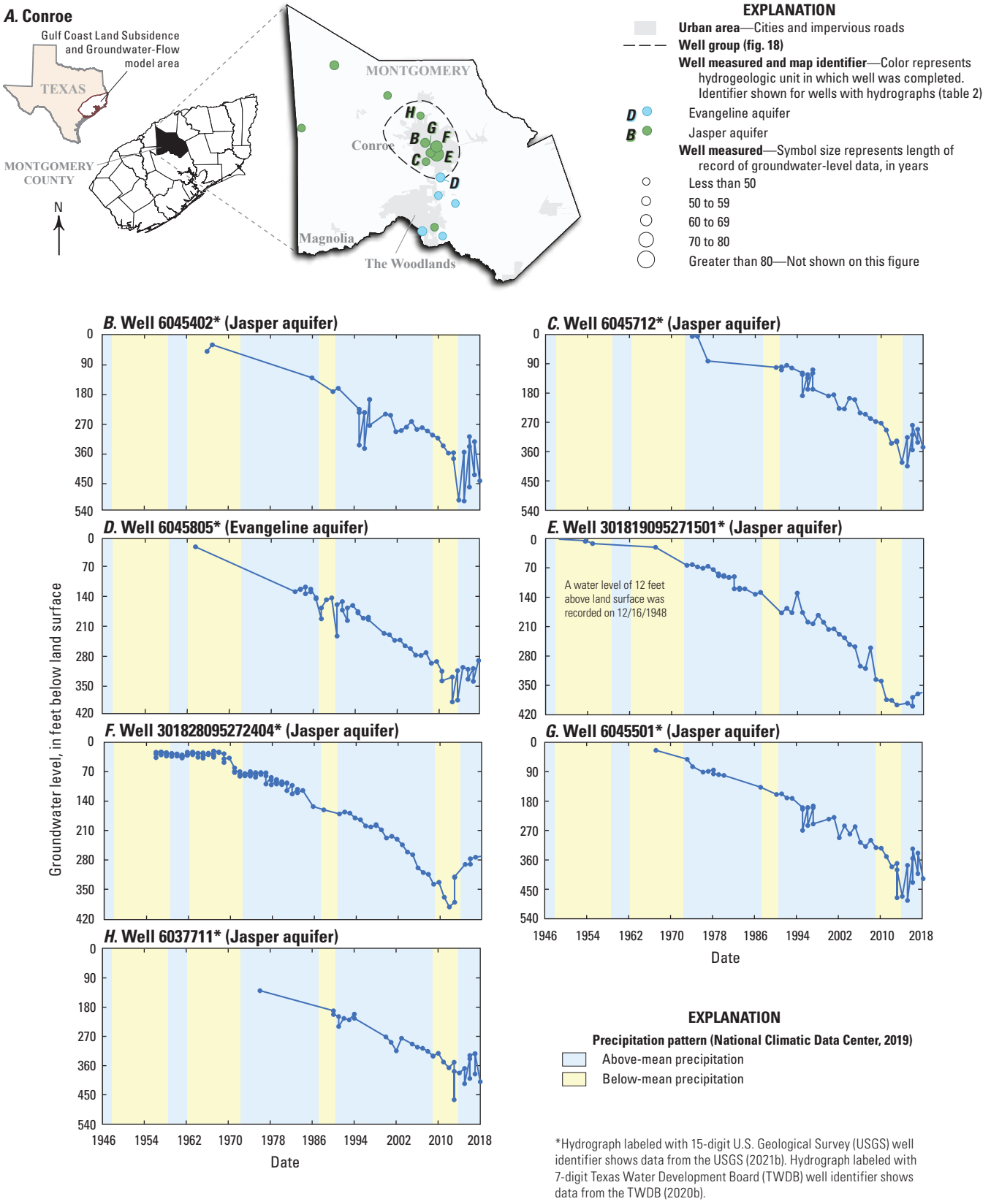

Figure 19. Depth to water for selected wells in and near Conroe, Texas.

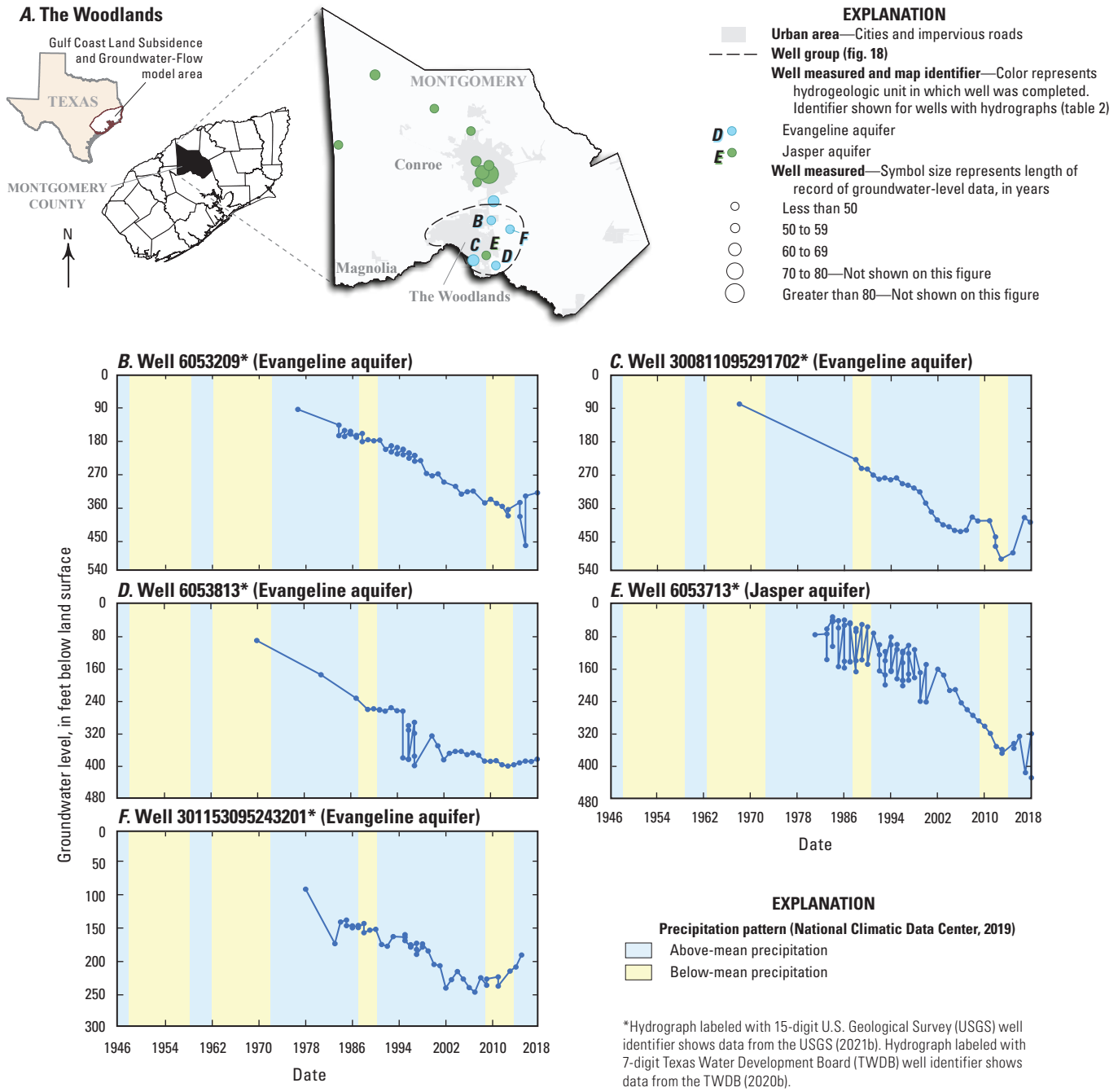

Figure 20. Depth to water for selected wells in and near The Woodlands in Montgomery County, Texas.

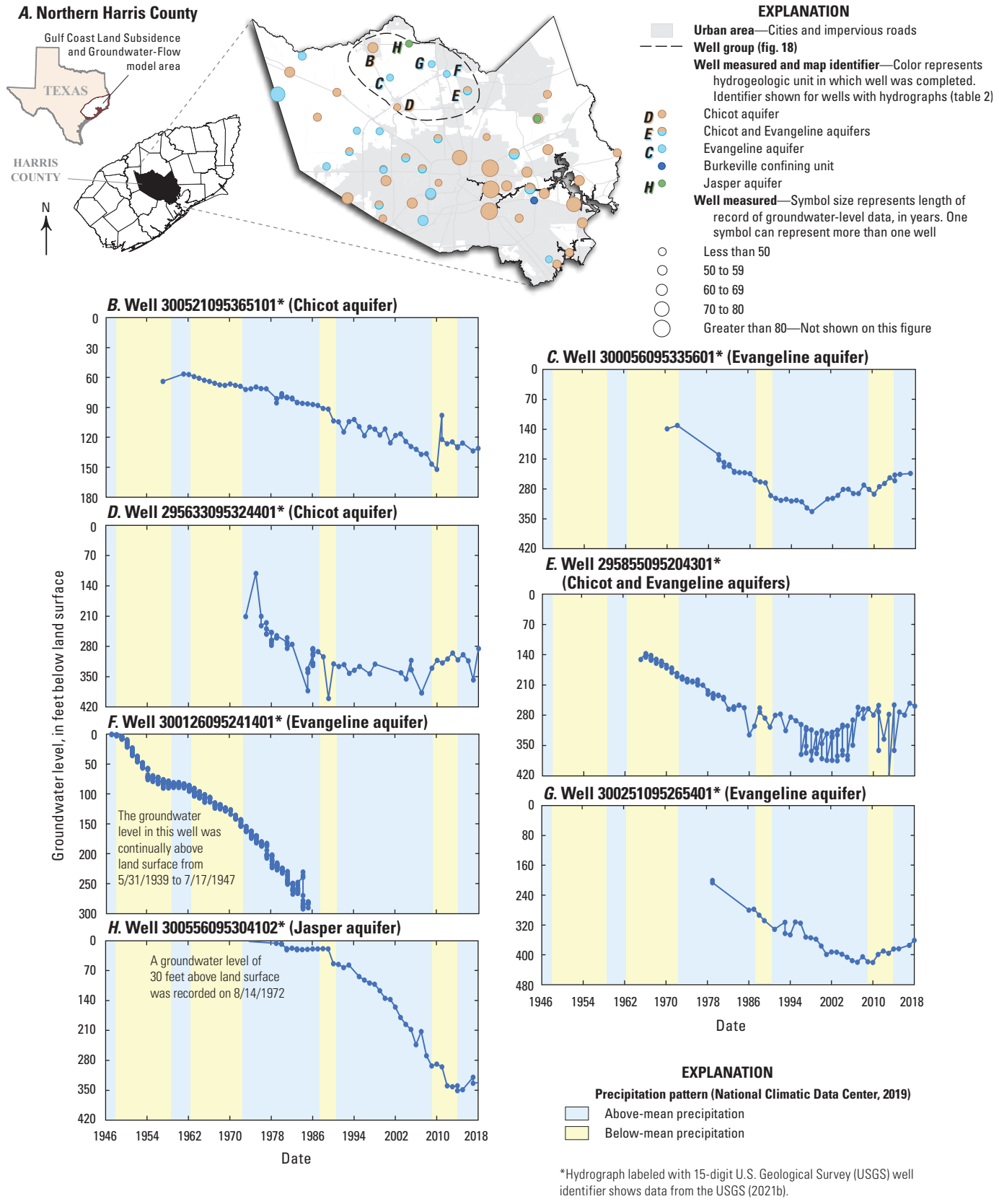

Figure 21. Depth to water for selected wells in and near northern Harris County, Texas.

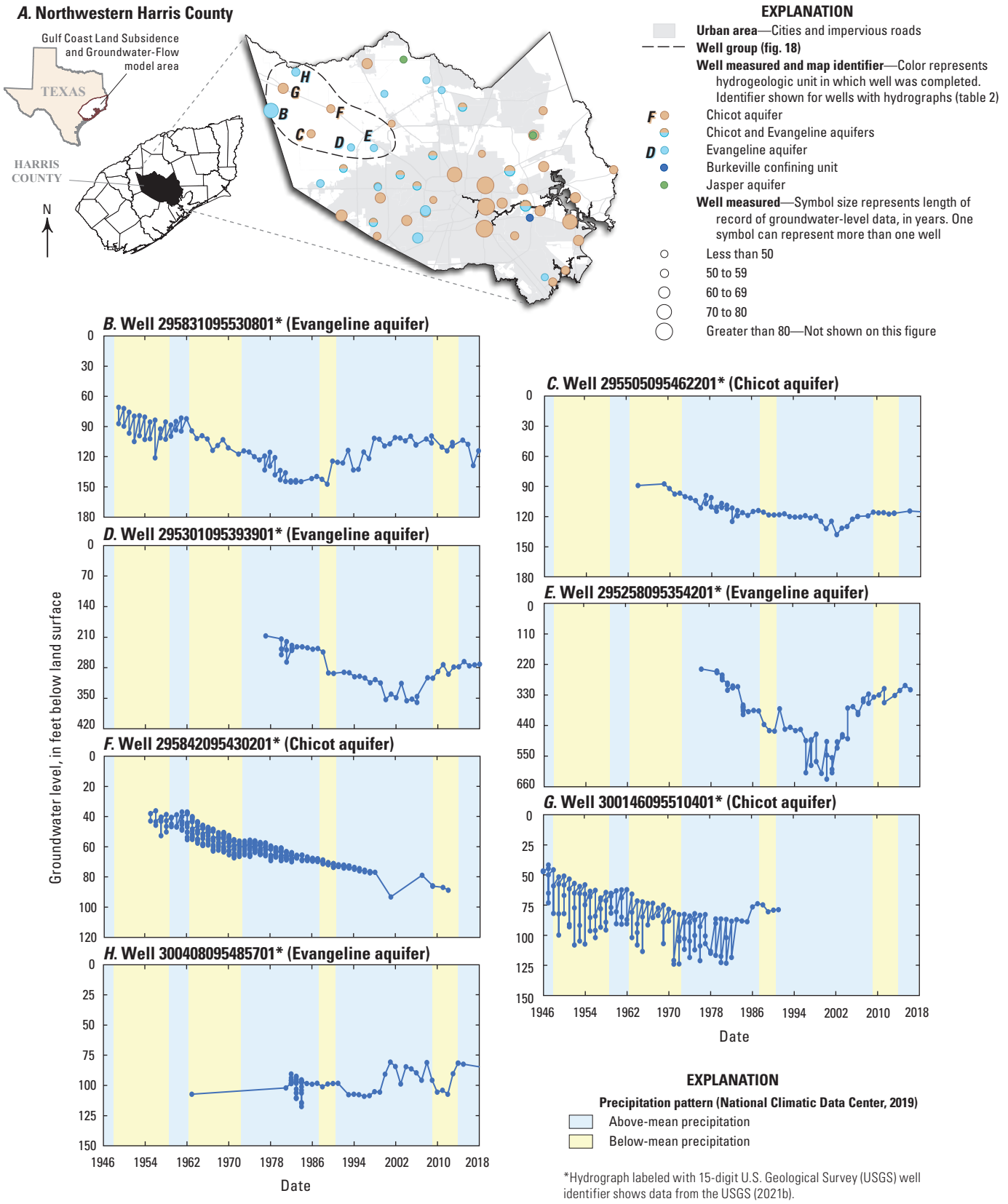

Figure 22. Depth to water for selected wells in and near northwestern Harris County, Texas.

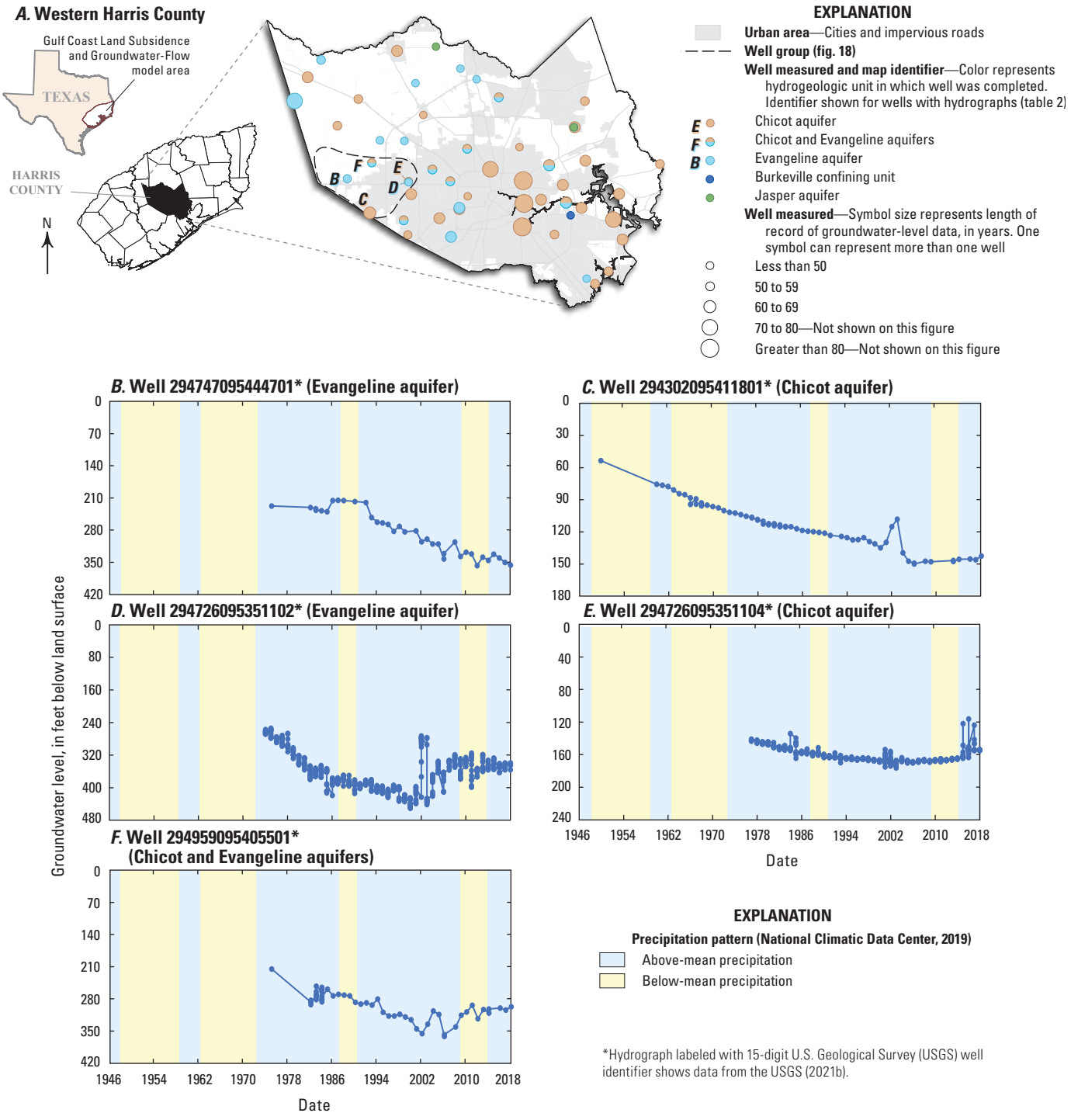

Figure 23. Depth to water for selected wells in and near western Harris County, Texas.

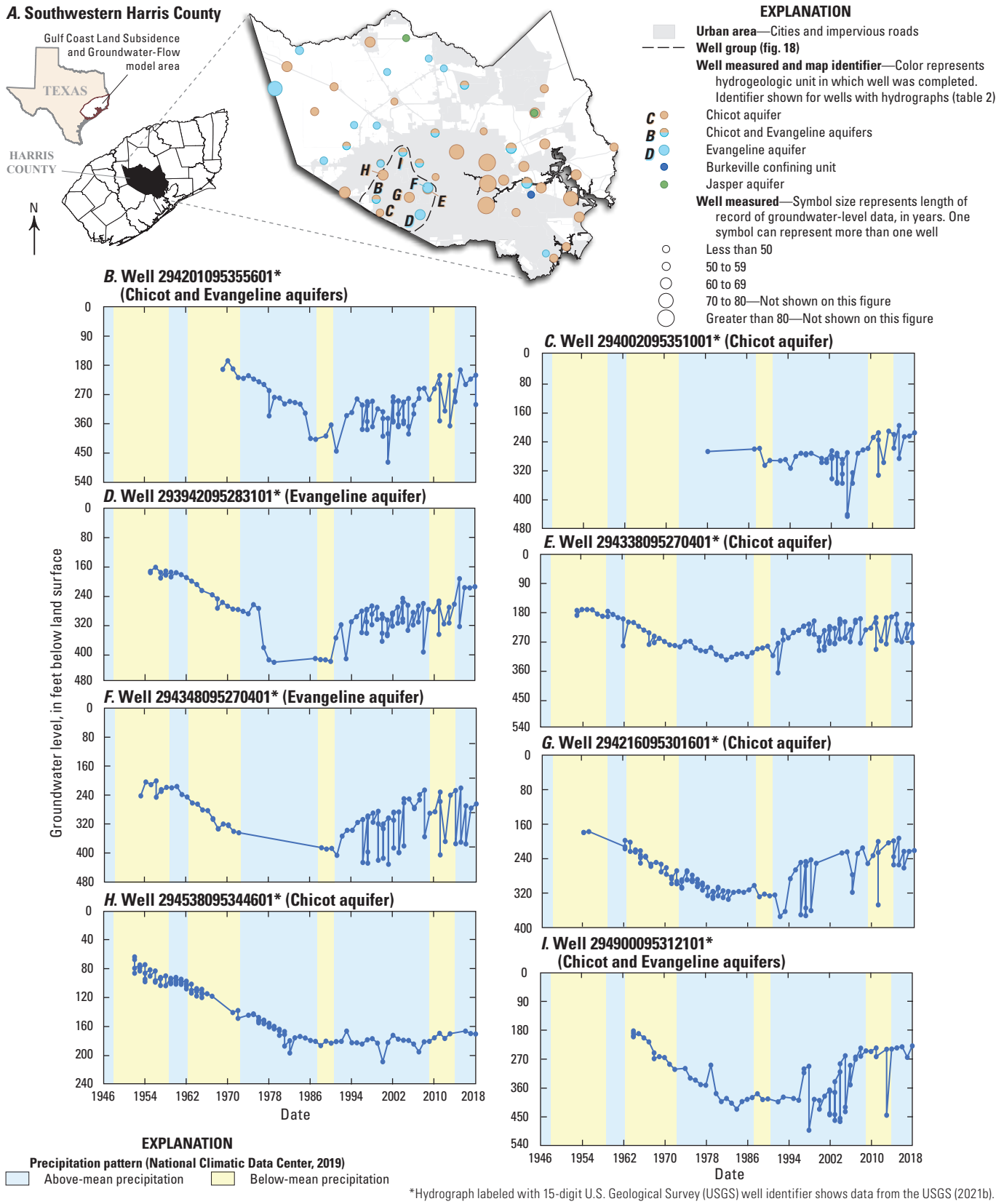

Figure 24. Depth to water for selected wells in and near southwestern Harris County, Texas.

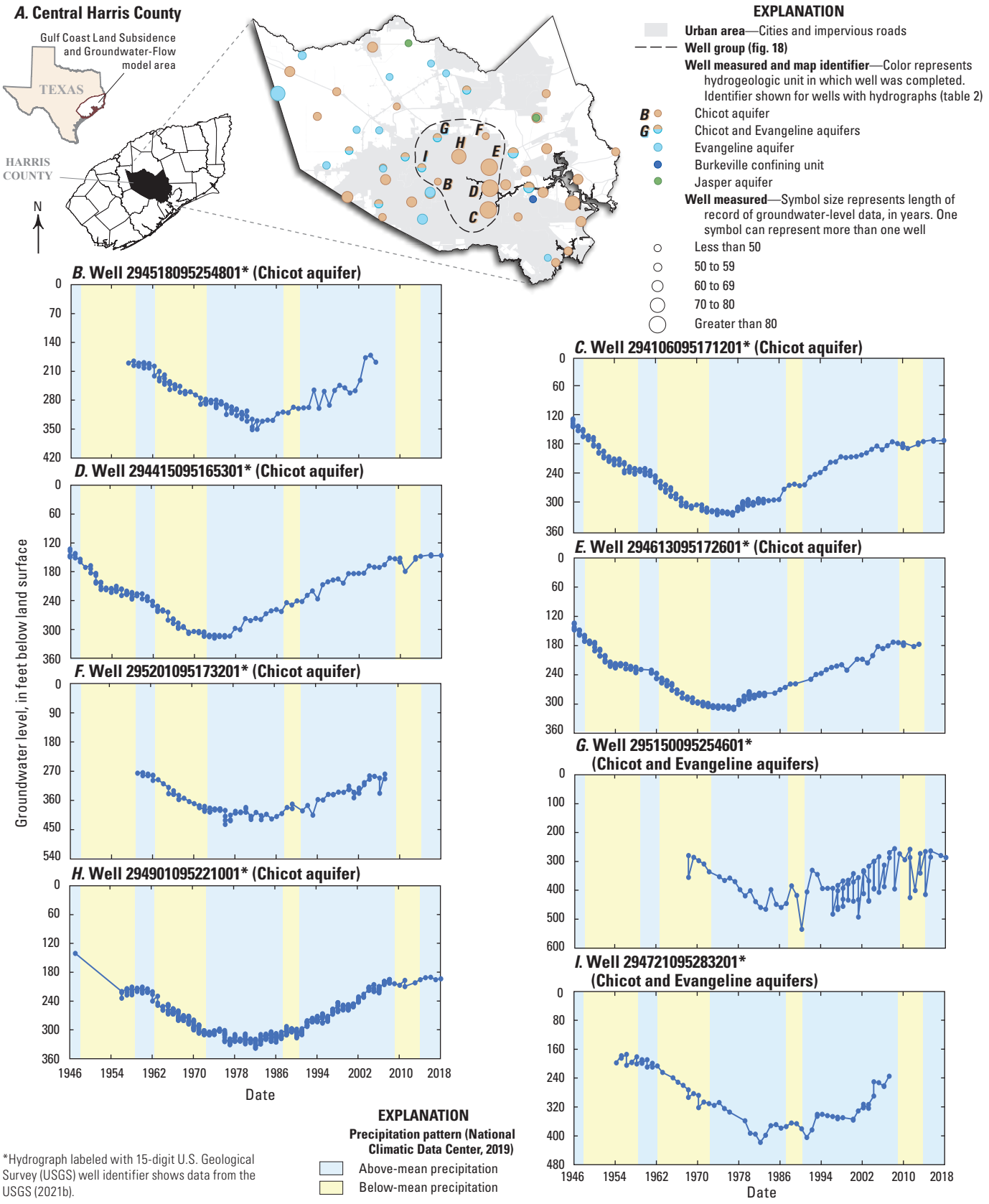

Figure 25. Depth to water for selected wells in and near central Harris County, Texas.

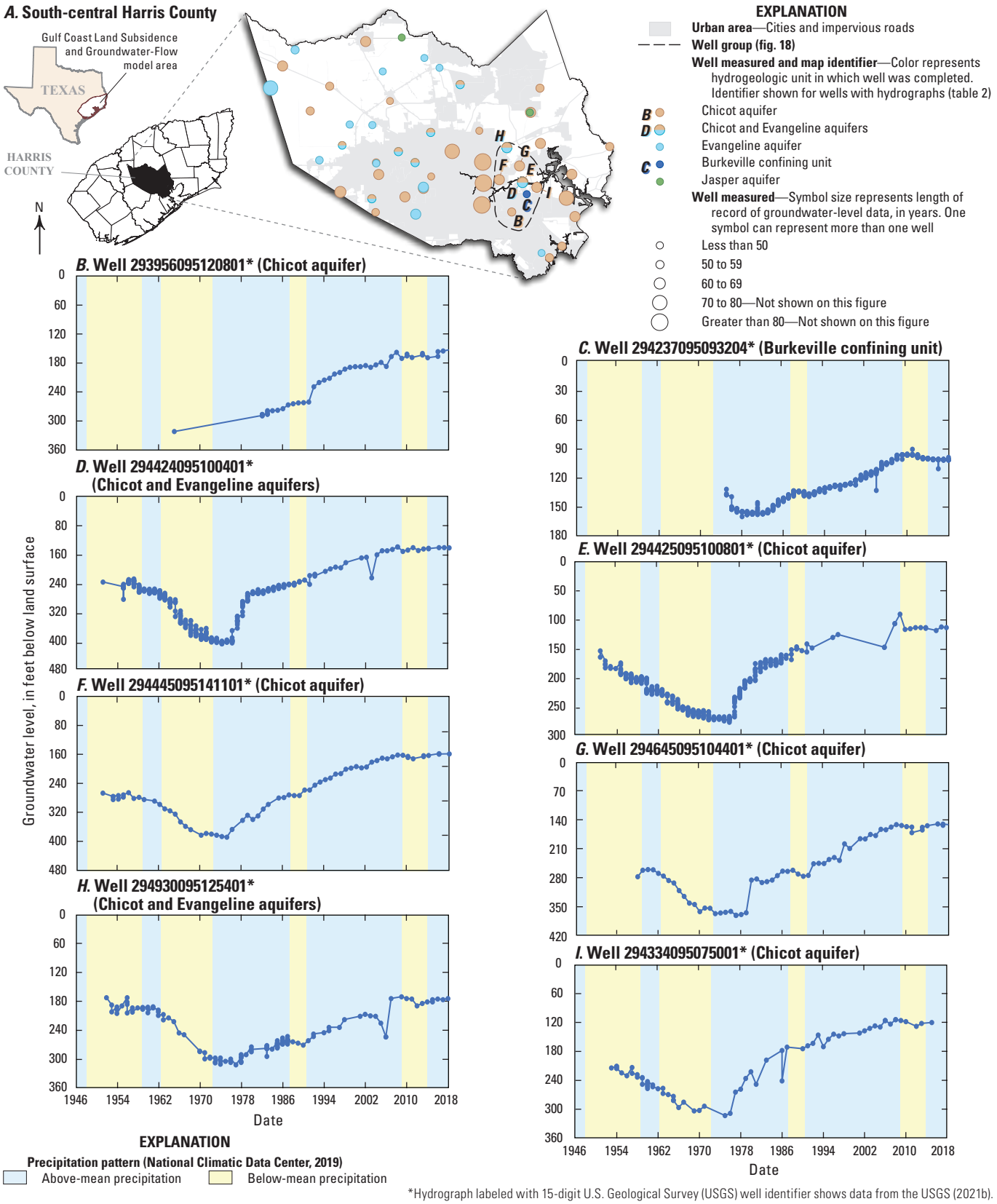

*Hydrograph labeled with 15-digit U.S. Geological Survey (USGS) well identifier shows data from the USGS (2021b).

Figure 26. Depth to water for selected wells in and near south-central Harris County, Texas.

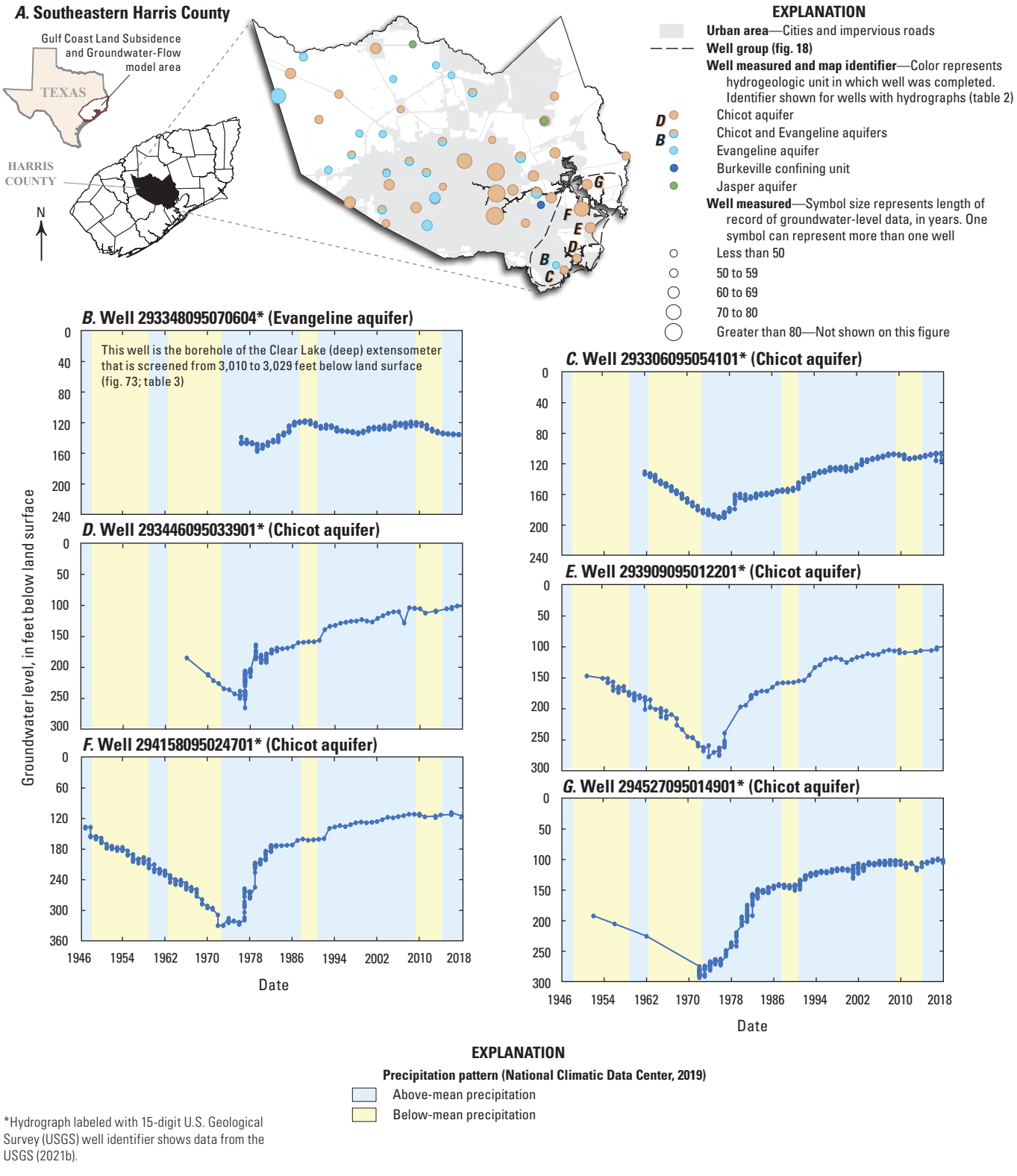

*Hydrograph labeled with 15-digit U.S. Geological Survey (USGS) well identifier shows data from the USGS (2021b).

Figure 27. Depth to water for selected wells in and near southeastern Harris County, Texas.

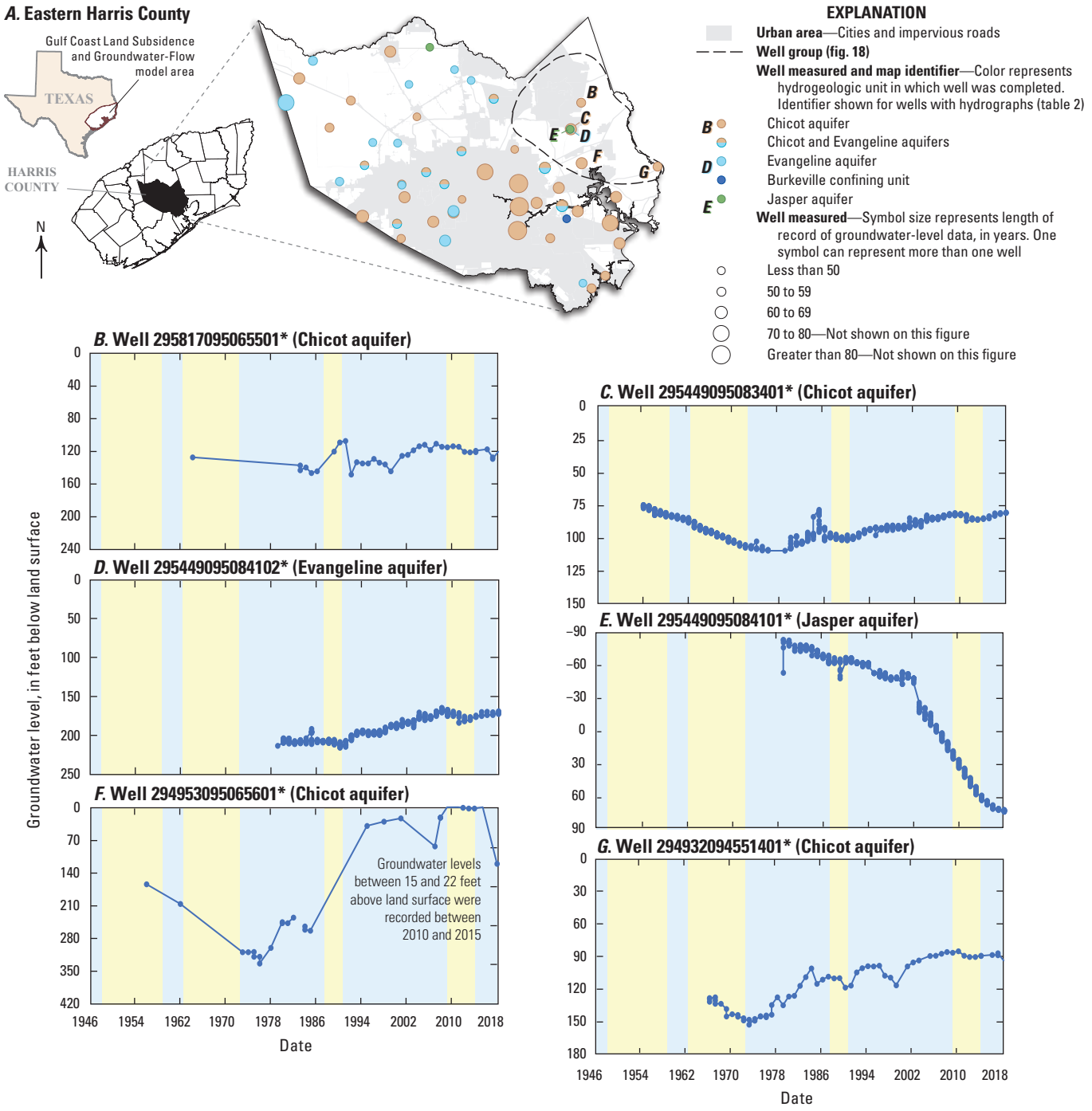

*Hydrograph labeled with 15-digit U.S. Geological Survey (USGS) well identifier shows data from the USGS (2021b).

Figure 28. Depth to water for selected wells in and near eastern Harris County, Texas.

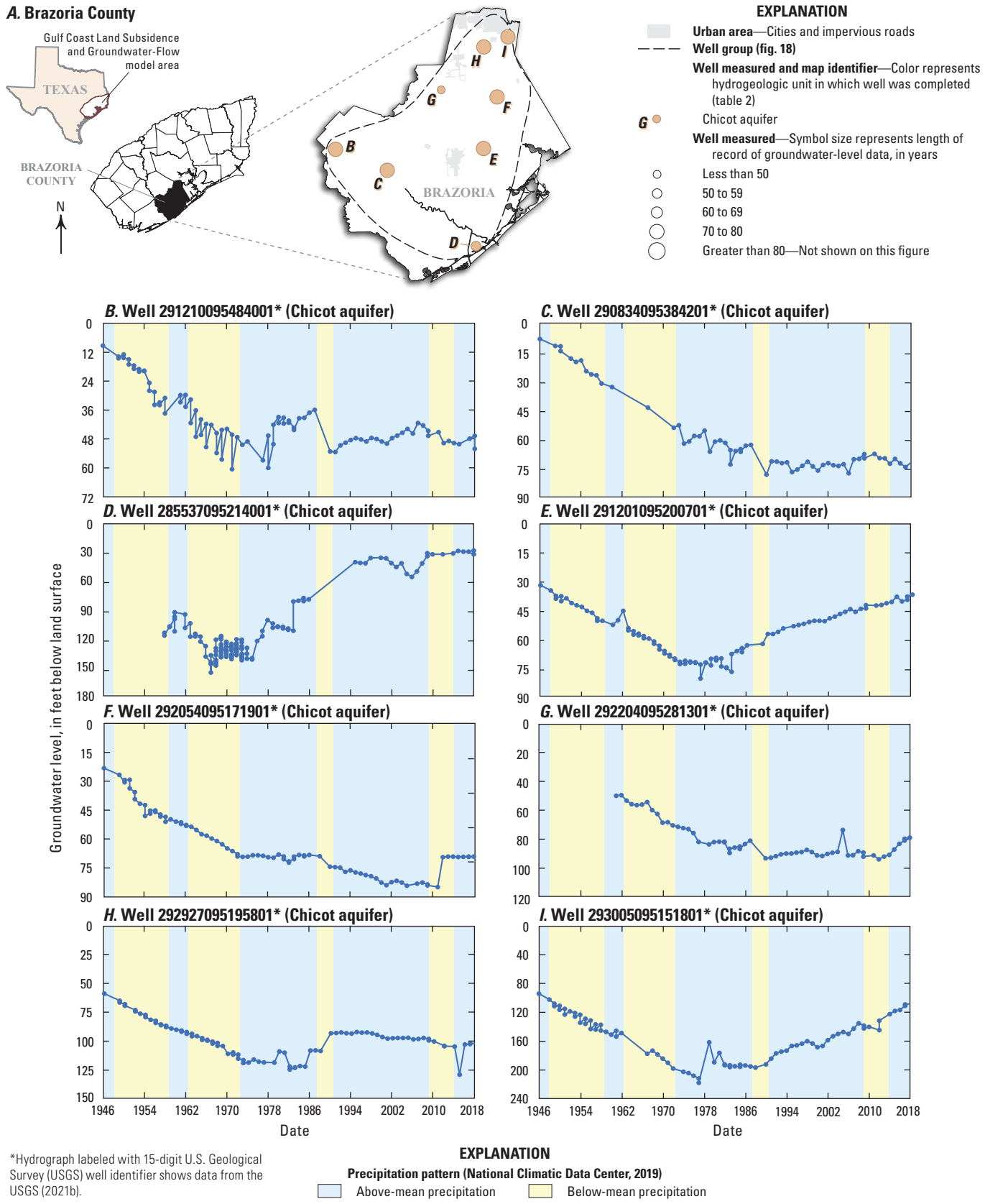

Figure 29. Depth to water for selected wells in and near Brazoria County, Texas.

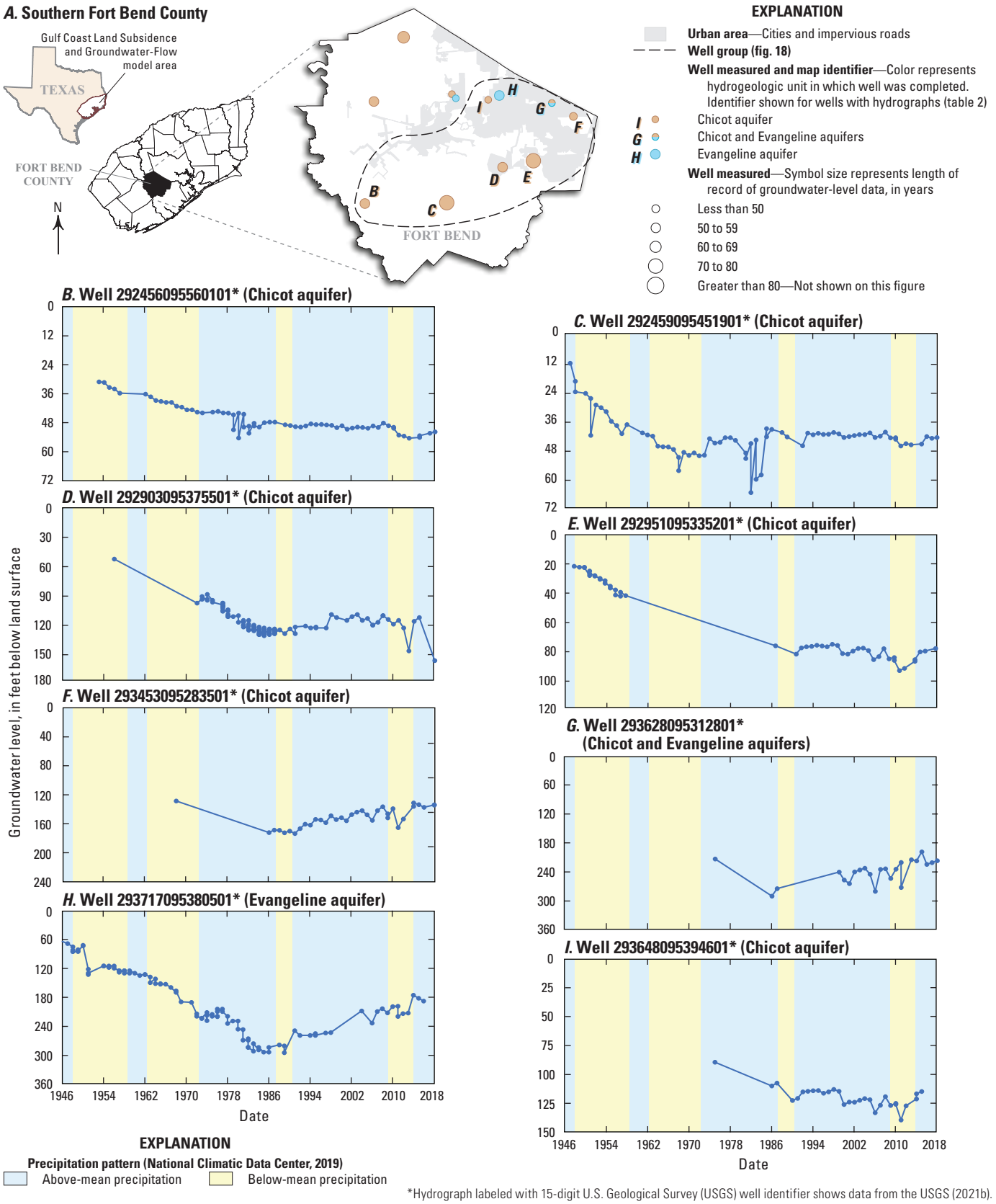

*Hydrograph labeled with 15-digit U.S. Geological Survey (USGS) well identifier shows data from the USGS (2021b).

Figure 30. Depth to water for selected wells in and near southern Fort Bend County, Texas.

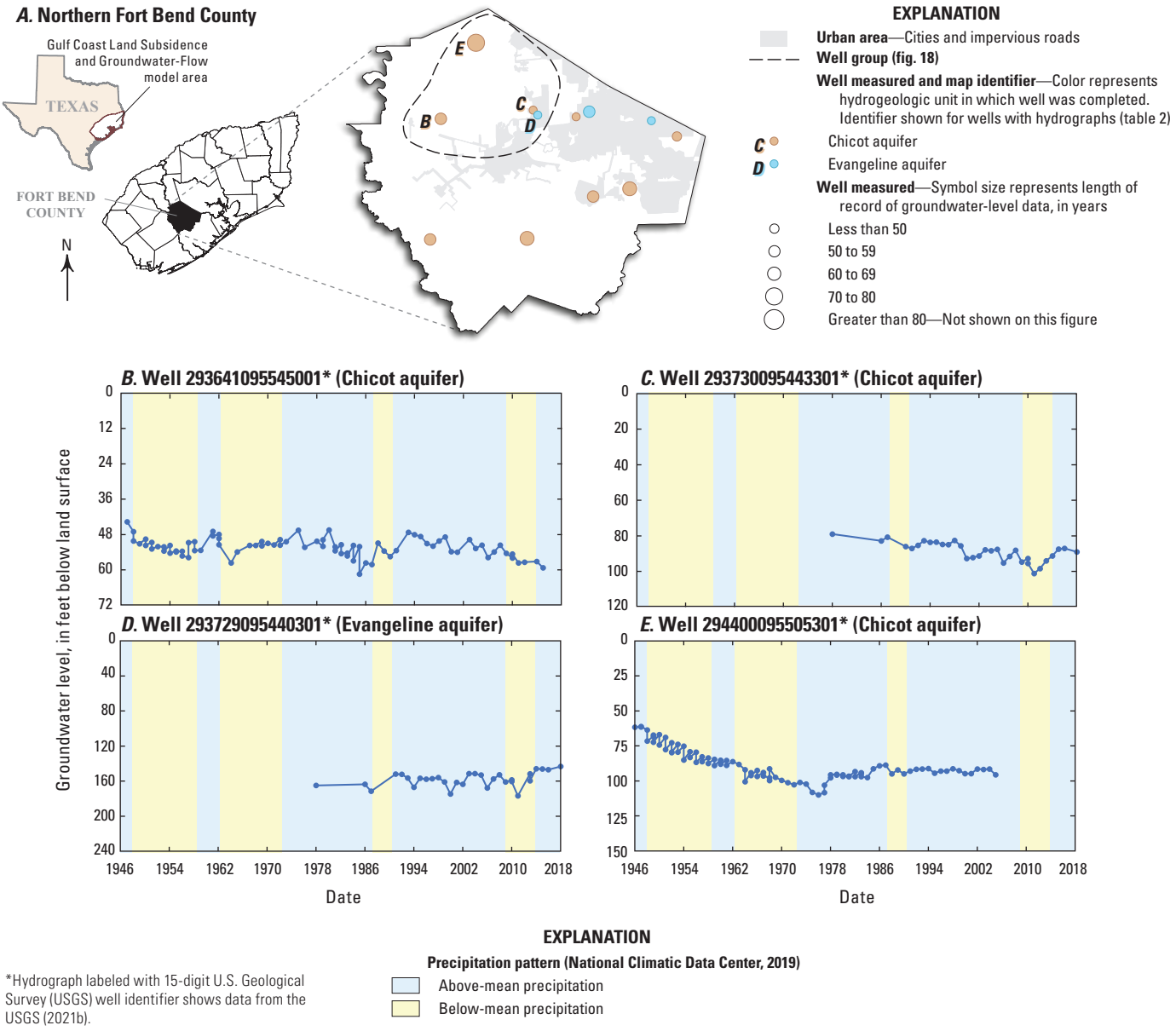

Figure 31. Depth to water for selected wells in and near northern Fort Bend County, Texas.

25 ft in the Baytown area (fig. 14*O–R*), and about 15 ft in the Katy area (fig. 15) (Lang and others, 1950). In the Texas City area, groundwater levels during 1946–48 were similar, and historical minimums prior to 1950 were reached during this period—generally about 115 ft bls (fig. 16). Surface-water deliveries from the Brazos River in the Texas City area began in 1948, however, resulting in a mean groundwater-level rise (recovery) of about 20 ft during 1948–49 (fig. 16*D–H*). The mean groundwater-level declines in Brazoria and Fort Bend Counties during this time were less than 10 ft (figs. 29–31). In Brazoria County, groundwater levels during this period were generally most shallow in the northwestern areas of the county and deepest in the northeastern areas nearest the border of Harris and Galveston Counties (Sandeen and Wesselman, 1973). In Montgomery County, many flowing wells in Conroe that were completed in the Jasper and Evangeline aquifers had ceased flowing by the mid-1940s and mid-1950s, respectively (fig. 13*B*) (Popkin, 1971).

The increased use of surface water beginning in 1954 after the construction of Lake Houston helped stabilize groundwater levels in the historical Houston and Pasadena areas compared to the previous period of sustained declines since about 1937 (figs. 14, 24–26). In the Houston and Pasadena areas, groundwater-level declines during 1957–61 were less than declines in previous years, averaging 2.6 ft (0.6 ft/year), compared to previous declines between 7 and 15 ft/yr (figs. 14, 25–26) (Anders and Naftel, 1962). Before 1954, the rate of groundwater-level decline in the historical

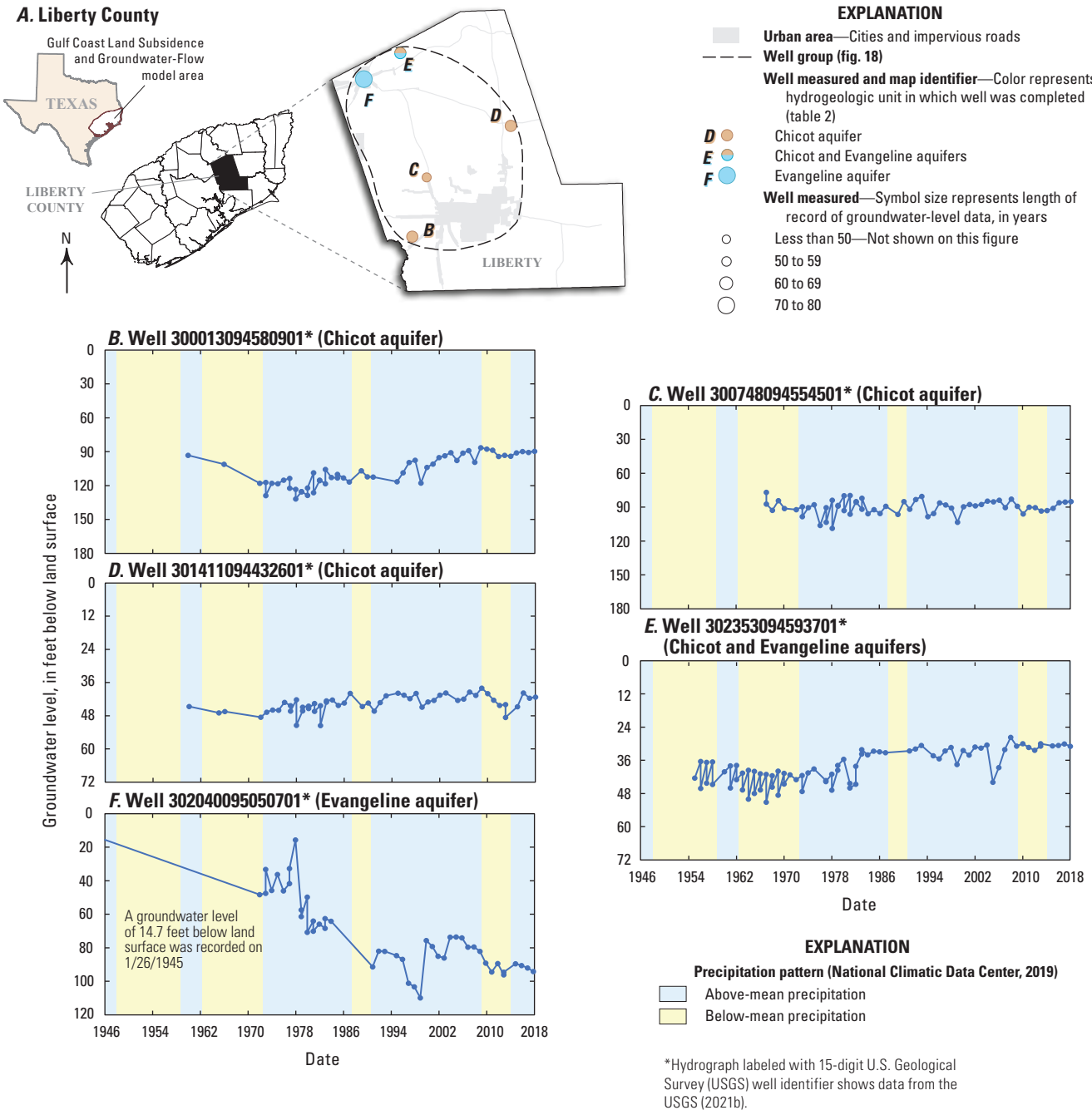

Figure 32. Depth to water for selected wells in and near Liberty County, Texas.

Houston area was about 7 ft/yr (Gabrysch, 1967), although some wells in the historical Houston area had greater annual declines of between 8 and 10 ft during 1946–47 and 1954–56 (figs. 24–25). In the Texas City area, groundwater levels rose between 35 and 40 ft at the Pan American refinery after the introduction of surface water from the Brazos River in 1948 (fig. 16*E–H*) (AMOCO, 1958).

Outside of the greater Houston area, groundwater-level declines occurred during the 1940s to 1960s, although these declines were lesser than the declines in the greater Houston area. In Colorado, Lavaca, and Wharton Counties, most previously flowing wells were no longer flowing by the mid-1940s, and additional groundwater-level declines began after 1947 (figs. 34–35) (Loskot and others, 1982). In the 1950s and 1960s, groundwater levels in Matagorda County declined (fig. 34) because of increased groundwater use for irrigation (Hammond, 1969). Groundwater-level declines of 200 ft by 1965 were noted in a well in southern Jasper County (fig. 36*F*) based on a starting groundwater level of about 38 ft above

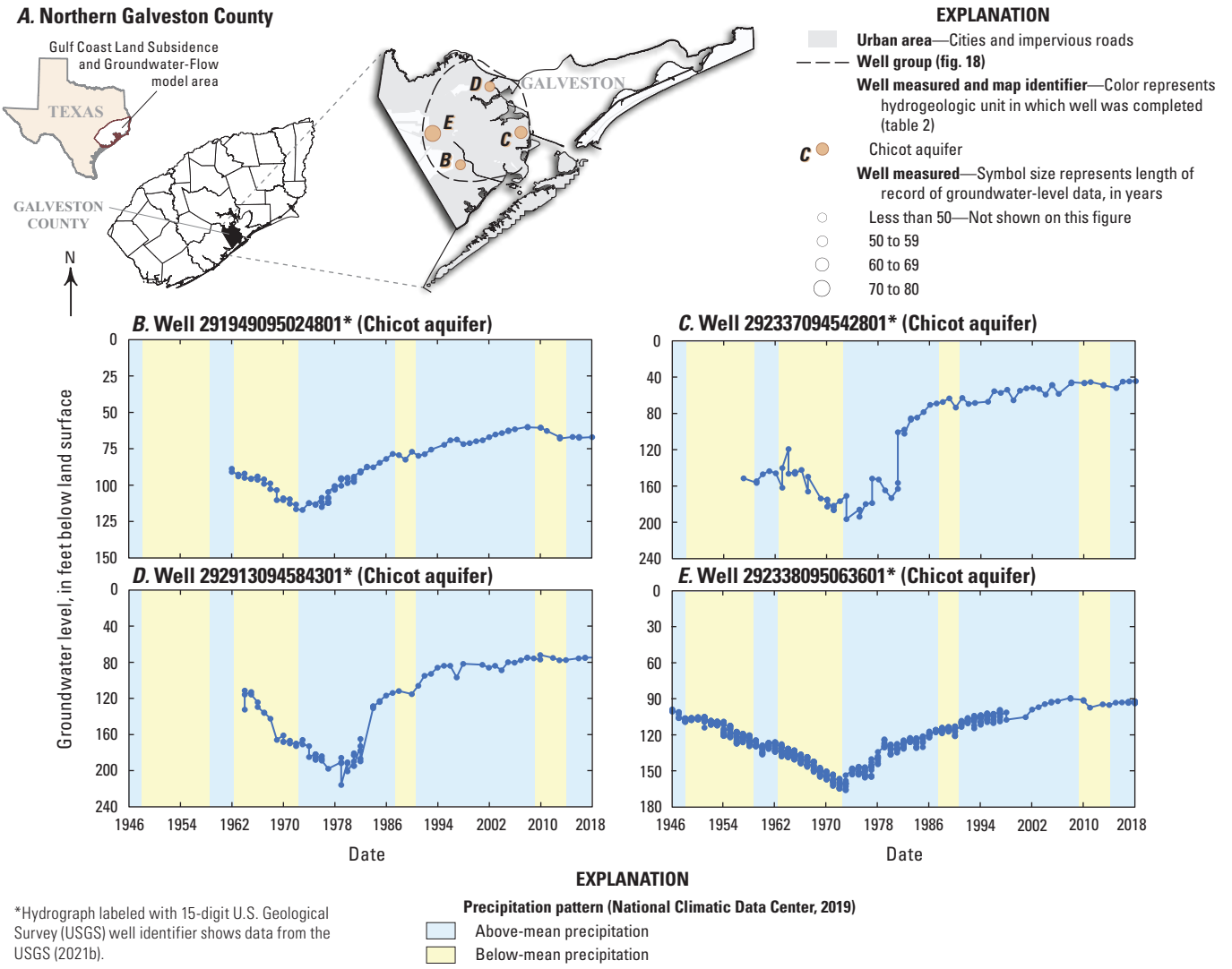

Figure 33. Depth to water for selected wells in and near northern Galveston County in southeast Texas.

land surface in 1947 noted in Wesselman (1967), although declines 10 mi from this well were less than half of this amount (Wesselman, 1967).

During 1953–61, the groundwater levels in the Katy area declined by a mean of 10.3 ft; however, the rate of decline slowed somewhat during 1957–61, when the mean decline was only 1.6 ft, in part because of increases in precipitation (figs. 14–15, 21–23, 31, 35) (Anders and Naftel, 1962). By 1961, groundwater levels had declined to more than 260 ft bls in parts of the Pasadena area (fig. 26) (Wood and Gabrysch, 1965). Groundwater levels in the Texas City area during 1950–62 remained steady or declined slightly (fig. 16*C*) (Anders and Naftel, 1963).

By the 1960s, substantial groundwater-level declines had occurred in most of the greater Houston area. Groundwater-level declines in the Pasadena area resulted in groundwater levels more than 300 ft bls by 1966 and groundwater-level declines of about 9–9.5 ft/yr since the early 1960s (fig. 26) (Wood and Gabrysch, 1965). Annual mean groundwater-level declines in the Baytown area were about 5 ft/yr through 1965 (fig. 27) (Gabrysch, 1967). In Brazoria County, groundwater levels in the Chicot aquifer declined by about 20–40 ft during 1946–67 (Sandeen and Wesselman, 1973), or about 1.3 to 4 ft/yr, and the mean groundwater level was about 80 ft bls in 1967 (fig. 29). In Chambers County, during 1941–66, groundwater levels declined more than 90 ft in the Chicot aquifer near Baytown (Wesselman and Aronow, 1971), whereas declines in other areas of Chambers County were generally less than 30 ft (fig. 36*D*) In Montgomery County between 1943 and 1966–67, groundwater levels declined 10 to 25 ft in the Evangeline aquifer in Conroe and between 40 and 50 ft for wells in the southeastern area of the county; however, about 40 wells drilled in Montgomery County to various depths continued to flow during 1966–67 (Popkin, 1971), most of which were located at or outside of the Conroe city limits. Near Conroe, groundwater levels declined by about 50 ft since predevelopment conditions in the Jasper aquifer and were about 30 ft bls in 1967 (fig. 19) (Popkin, 1971). Groundwater-level

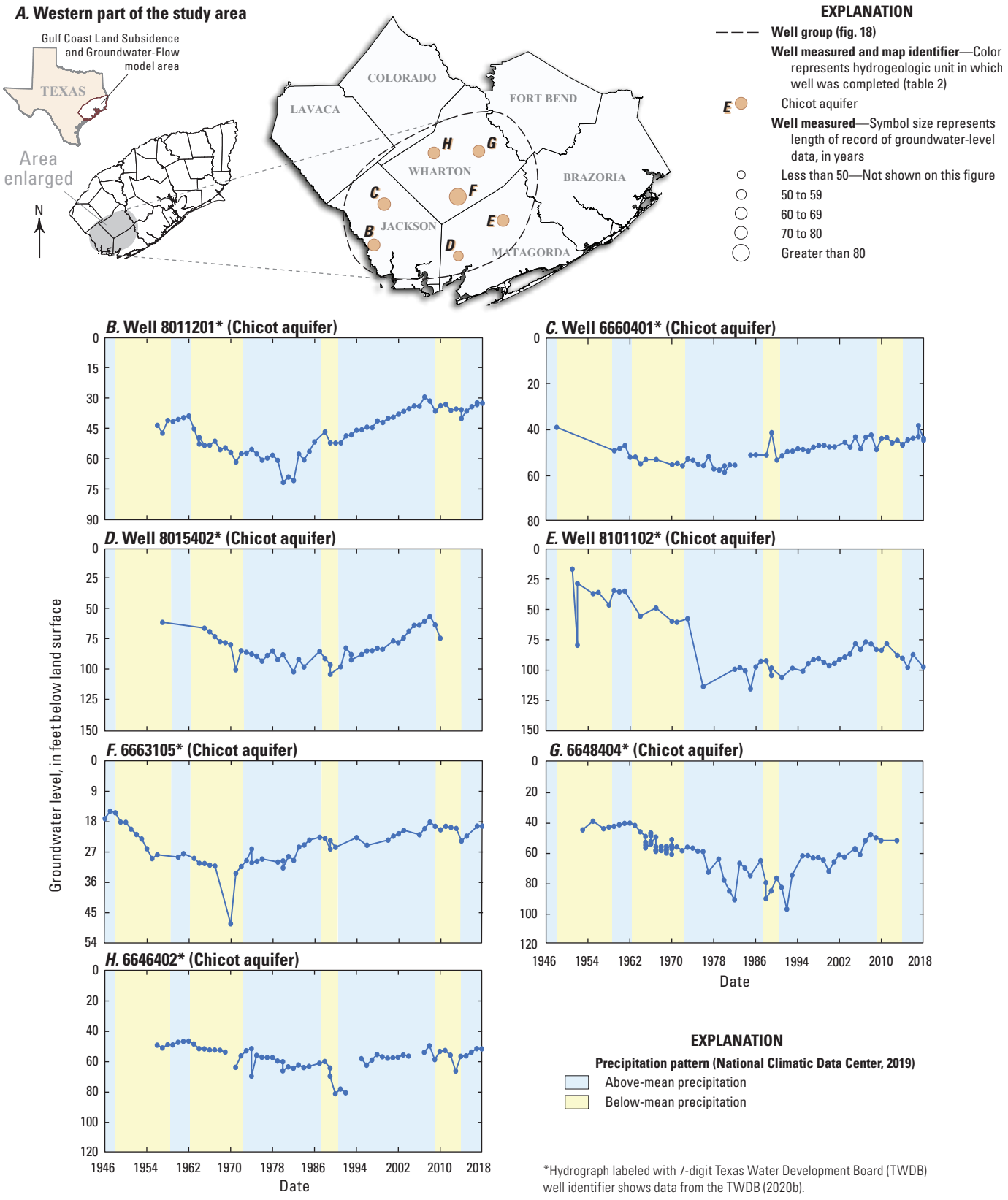

Figure 34. Depth to water for selected wells in and near the western part of the Gulf Coast aquifer system study area in southeast Texas.

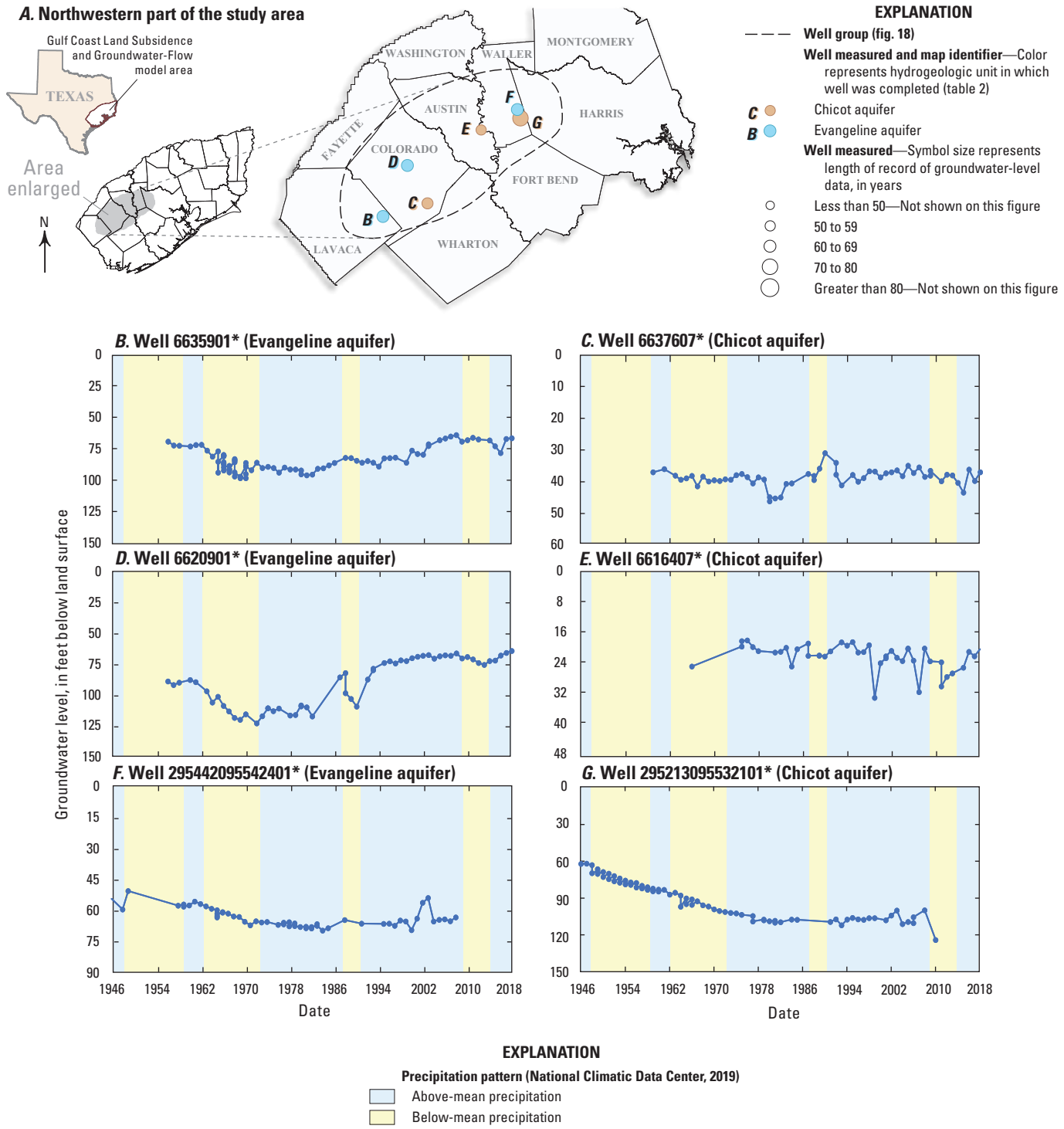

*Hydrograph labeled with 15-digit U.S. Geological Survey (USGS) well identifier shows data from the USGS (2021b). Hydrograph labeled with 7-digit Texas Water Development Board (TWDB) well identifier shows data from the TWDB (2020b).

Figure 35. Depth to water for selected wells in and near the northwestern part of the Gulf Coast aquifer system study area in southeast Texas.

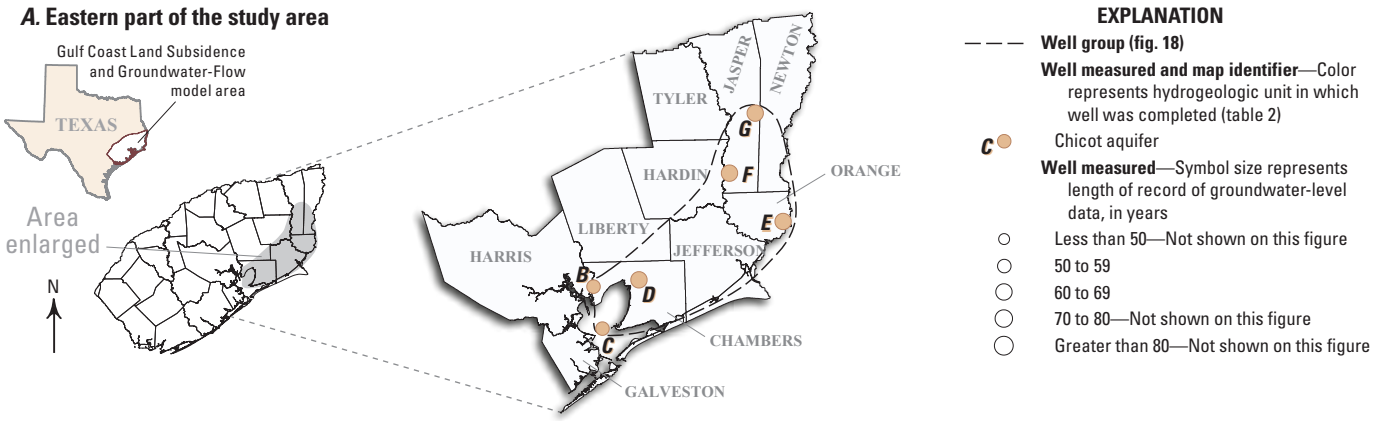

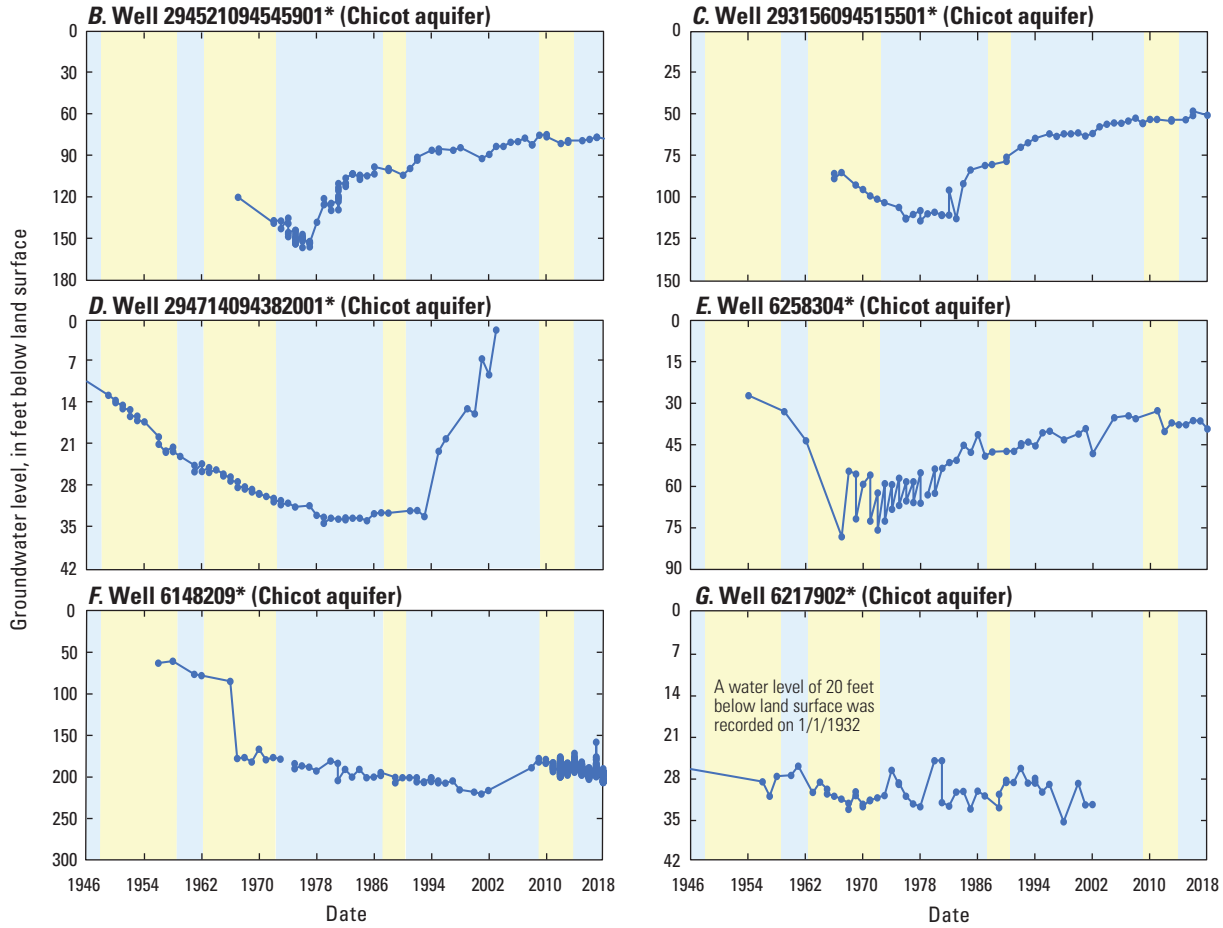

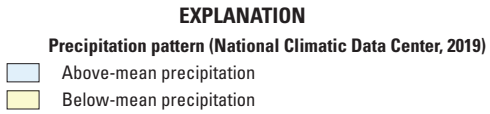

*Hydrograph labeled with 15-digit U.S. Geological Survey (USGS) well identifier shows data from the USGS (2021b). Hydrograph labeled with 7-digit Texas Water Development Board (TWDB) well identifier shows data from the TWDB (2020b).

Figure 36. Depth to water for selected wells in and near the eastern part of the Gulf Coast aquifer system study area in southeast Texas.

Table 2. Wells with long-term groundwater-level measurements within the Gulf Coast aquifer system study area in southeast Texas.

[USGS well ID is the well identifier used by the U.S. Geological Survey (USGS; 2021b); TWDB well ID is the well identifier used by the Texas Water Development Board (TWDB; 2020b); bls, below land surface; --, not available; conf., confining]

USGS well ID	TWDB well ID	Identifier for long-term wells in this report (figs. 19–36, 51–52)	County	Groundwater-well groups (fig. 18)	Historical geographic area (fig. 18*B*)[1]	Hydrogeologic unit	Period of record (may contain gaps) (month/year)		Well depth, in feet bls[3]
							Begin[2]	End	
301948095290101	6045402	B	Montgomery	Conroe (fig. 19)	--	Jasper aquifer	7/1966	1/2020	1,150
301720095285601	6045712	C	Montgomery		--	Jasper aquifer	3/1974	1/2020	1,245
301516095264301	6045805	D	Montgomery		--	Evangeline aquifer	10/1964	1/2020	702
301819095271501	[4]6045507	E	Montgomery		--	Jasper aquifer	12/1948	2/2019	1,280
301828095272404	[5]6045504	F	Montgomery		--	Jasper aquifer	6/1956	1/2020	1,221
301918095271901	6045501	G	Montgomery		--	Jasper aquifer	1/1967	1/2020	1,280
302320095294201	6037711	H	Montgomery		--	Jasper aquifer	11/1976	1/2020	1,093
301256095270401	6053209	B	Montgomery	The Woodlands (fig. 20)	--	Evangeline aquifer	5/1977	1/2020	1,000
300811095291702	6053708	C	Montgomery		--	Evangeline aquifer	3/1968	2/2020	1,180
300740095262701	6053813	D	Montgomery		--	Evangeline aquifer	10/1970	1/2020	996
300823095275001	6053713	E	Montgomery		--	Jasper aquifer	10/1981	1/2020	1,710
301153095243201	6053608	F	Montgomery		--	Evangeline aquifer	10/1978	2/2015	809
300521095365101	[6]6060103	B	Harris	Northern Harris County (fig. 21)	Katy area	Chicot aquifer	7/1957	1/2020	412
300056095335601	6060804	C	Harris			Evangeline aquifer	9/1970	2/2017	962
295633095324401	6504515	D	Harris			Chicot aquifer	7/1973	1/2020	703
295855095204301	6506102	E	Harris			Chicot and Evangeline aquifers	12/1965	1/2020	1,540
300126095241401	6061903	F	Harris			Evangeline aquifer	5/1939	8/1985	1,052
300251095265401	6061528	G	Harris			Evangeline aquifer	6/1979	2/2020	1,074
300556095304102	6060306	H	Harris			Jasper aquifer	8/1972	1/2020	1,612
295831095530801	6501302	B	Harris	Northwestern Harris County (fig. 22)	Katy area	Evangeline aquifer	3/1949	1/2020	1,007
295505095462201	6502612	C	Harris			Chicot aquifer	3/1964	1/2020	565
295301095393901	6503906	D	Harris			Evangeline aquifer	11/1977	2/2020	1,145
295258095354201	6504719	E	Harris			Evangeline aquifer	12/1976	2/2016	1,480
295842095430201	6503101	F	Harris			Chicot aquifer	9/1955	1/2012	120
300146095510401	6058704	G	Harris			Chicot aquifer	1/1928	1/1991	297
300408095485701	6058501	H	Harris			Evangeline aquifer	10/1963	2/2020	1,160

Table 2. Wells with long-term groundwater-level measurements within the Gulf Coast aquifer system study area in southeast Texas.—Continued

[USGS well ID is the well identifier used by the U.S. Geological Survey (USGS; 2021b); TWDB well ID is the well identifier used by the Texas Water Development Board (TWDB; 2020b); bls, below land surface; --, not available; conf., confining]

USGS well ID	TWDB well ID	Identifier for long-term wells in this report (figs. 19–36, 51–52)	County	Groundwater-well groups (fig. 18)	Historical geographic area (fig. 18*B*)[1]	Hydrogeologic unit	Period of record (may contain gaps) (month/year)		Well depth, in feet bls[3]
							Begin[2]	End	
294747095444701	6511407	B	Harris	Western Harris County (fig. 23)	Katy area	Evangeline aquifer	5/1975	1/2020	1,210
294302095411801	6519201	C	Harris			Chicot aquifer	6/1950	1/2020	640
294726095351102	6512726	D	Harris			Evangeline aquifer	6/1974	2/2021	1,802
294726095351104	6512729	E	Harris			Chicot aquifer	10/1977	2/2021	237
294959095405501	6511508	F	Harris			Chicot and Evangeline aquifers	7/1975	1/2020	1,075
294201095355601	6520405	B	Harris	Southwestern Harris County (fig. 24)	Historical Houston area	Chicot and Evangeline aquifers	11/1969	1/2020	1,621
294002095351001	6520414	C	Harris			Chicot aquifer	12/1978	9/2020	1,038
293942095283101	6521701	D	Harris			Evangeline aquifer	5/1955	1/2020	1,735
294338095270401	6521201	E	Harris			Chicot aquifer	9/1953	9/2020	1,051
294348095270401	6521202	F	Harris			Evangeline aquifer	10/1953	9/2020	1,965
294216095301601	6520602	G	Harris			Chicot aquifer	12/1954	9/2020	972
294538095344601	[7]6512801	H	Harris			Chicot aquifer	4/1952	2/2020	467
294900095312101	6512619	I	Harris			Chicot and Evangeline aquifers	3/1964	1/2020	1,451
294518095254801	6513801	B	Harris	Central Harris County (fig. 25)	Historical Houston area	Chicot aquifer	12/1957	2/2005	1,227
294106095171201	6522618	C	Harris			Chicot aquifer	5/1937	1/2020	876
294415095165301	6522317	D	Harris			Chicot aquifer	8/1929	1/2020	900
294613095172601	6514912	E	Harris			Chicot aquifer	10/1929	1/2013	676
295201095173201	6514203	F	Harris			Chicot aquifer	6/1959	11/2007	870
295150095254601	6513214	G	Harris			Chicot and Evangeline aquifers	5/1968	1/2020	1,520
294901095221001	6514409	H	Harris			Chicot aquifer	1/1947	1/2020	1,152
294721095283201	6513701	I	Harris			Chicot and Evangeline aquifers	12/1954	1/2007	1,665

Table 2. Wells with long-term groundwater-level measurements within the Gulf Coast aquifer system study area in southeast Texas. —Continued

[USGS well ID is the well identifier used by the U.S. Geological Survey (USGS; 2021b); TWDB well ID is the well identifier used by the Texas Water Development Board (TWDB; 2020b); bls, below land surface; --, not available; conf., confining]

USGS well ID	TWDB well ID	Identifier for long-term wells in this report (figs. 19–36, 51–52)	County	Groundwater-well groups (fig. 18)	Historical geographic area (fig. 18*B*)[1]	Hydrogeologic unit	Period of record (may contain gaps) (month/year)		Well depth, in feet bls[3]
							Begin[2]	End	
293956095120801	6523809	B	Harris			Chicot aquifer	8/1965	1/2020	1,380
294237095093204	6523322	C	Harris			Burkeville conf. unit	10/1975	1/2021	2,831
294424095100401	6523221	D	Harris	South-central Harris County (fig. 26)	Pasadena area	Chicot and Evangeline aquifers	8/1951	1/2020	1,740
294425095100801	[8]6523220	E	Harris			Chicot aquifer	5/1951	1/2020	477
294445095141101	6523104	F	Harris			Chicot aquifer	9/1951	1/2020	1,350
294645095104401	6515806	G	Harris			Chicot aquifer	9/1958	1/2020	1,220
294930095125401	6515404	H	Harris			Chicot and Evangeline aquifers	5/1952	1/2020	1,500
294334095075001	6523302	I	Harris			Chicot aquifer	12/1953	1/2015	510
293348095070604	6532428	B	Harris	Southeastern Harris County (fig. 27)	Johnson Space Center area	Evangeline aquifer	5/1976	2/2021	3,072
293306095054101	6532401	C	Harris			Chicot aquifer	10/1962	2/2021	770
293446095033901	6532519	D	Harris			Chicot aquifer	7/1966	1/2020	660
293909095012201	6524902	E	Harris		Baytown area	Chicot aquifer	12/1951	1/2020	578
294158095024701	[9]6524501	F	Harris			Chicot aquifer	9/1947	12/2019	591
294527095014901	[10]6516904	G	Harris			Chicot aquifer	9/1952	7/2020	512
295817095065501	6508103	B	Harris	Eastern Harris County (fig. 28)	--	Chicot aquifer	11/1964	1/2020	555
295449095083401	6507902	C	Harris		--	Chicot aquifer	2/1954	7/2020	196
295449095084102	6507906	D	Harris		--	Evangeline aquifer	12/1979	7/2020	1,503
295449095084101	6507905	E	Harris		--	Jasper aquifer	11/1979	1/2021	2,592
294953095065601	6516401	F	Harris		--	Chicot aquifer	3/1956	1/2018	1,575
294932094551401	6409505	G	Harris		--	Chicot aquifer	5/1966	2/2020	375
291210095484001	6550504	B	Brazoria	Brazoria County (fig. 29)	--	Chicot aquifer	11/1946	2/2020	473
290834095384201	6551901	C	Brazoria		--	Chicot aquifer	10/1946	12/2019	659
285537095214001	8106408	D	Brazoria		--	Chicot aquifer	2/1958	12/2019	224
291201095200701	6554407	E	Brazoria		--	Chicot aquifer	8/1946	12/2019	960
292054095171901	6546301	F	Brazoria		--	Chicot aquifer	7/1946	12/2019	473
292204095281301	6545102	G	Brazoria		--	Chicot aquifer	1/1961	12/2019	923
292927095195801	[11]6538201	H	Brazoria		--	Chicot aquifer	7/1946	12/2019	480
293005095151801	6530902	I	Brazoria		--	Chicot aquifer	6/1946	12/2019	591

Table 2. Wells with long-term groundwater-level measurements within the Gulf Coast aquifer system study area in southeast Texas.—Continued

[USGS well ID is the well identifier used by the U.S. Geological Survey (USGS; 2021b); TWDB well ID is the well identifier used by the Texas Water Development Board (TWDB; 2020b); bls, below land surface; --, not available; conf., confining]

USGS well ID	TWDB well ID	Identifier for long-term wells in this report (figs. 19–36, 51–52)	County	Groundwater-well groups (fig. 18)	Historical geographic area (fig. 18*B*)[1]	Hydrogeologic unit	Period of record (may contain gaps) (month/year)		Well depth, in feet bls[3]
							Begin[2]	End	
292456095560101	[12]6533801	B	Fort Bend	Southern Fort Bend County (fig. 30)	--	Chicot aquifer	1/1953	1/2020	564
292459095451901	6534901	C	Fort Bend		--	Chicot aquifer	4/1947	1/2020	636
292903095375501	6535302	D	Fort Bend		--	Chicot aquifer	4/1956	1/2019	702
292951095335201	6536201	E	Fort Bend		--	Chicot aquifer	12/1948	1/2020	375
293453095283501	6529405	F	Fort Bend		--	Chicot aquifer	8/1968	1/2020	565
293628095312801	6528312	G	Fort Bend		--	Chicot and Evangeline aquifers	3/1975	2/2020	1,262
293717095380501	6527302	H	Fort Bend		--	Evangeline aquifer	3/1950	12/2016	1,565
293648095394601	6527322	I	Fort Bend		--	Chicot aquifer	1/1975	12/2015	407
293641095545001	[13]6525301	B	Fort Bend	Northern Fort Bend County (fig. 31)	Katy area	Chicot aquifer	1/1950	2/2015	438
293730095443301	6527107	C	Fort Bend			Chicot aquifer	8/1978	1/2020	314
293729095440301	6527106	D	Fort Bend			Evangeline aquifer	6/1978	2/2020	1,410
294400095505301	[14]6518103	E	Fort Bend			Chicot aquifer	3/1931	1/2005	628
300013094580901	6157703	B	Liberty	Liberty County (fig. 32)	--	Chicot aquifer	1/1960	2/2020	837
300748094554501	6149807	C	Liberty		--	Chicot aquifer	1/1967	2/2020	401
301411094432601	6151102	D	Liberty		--	Chicot aquifer	1/1960	2/2020	660
302353094593701	6133701	E	Liberty		--	Chicot and Evangeline aquifers	10/1955	2/2019	835
302040095050701	6048102	F	Liberty		--	Evangeline aquifer	1/1945	1/2018	845
291949095024801	6548502	B	Galveston	Northern Galveston County (fig. 33)	Alta Loma area	Chicot aquifer	5/1962	12/2019	756
292337094542801	[15]6433901	C	Galveston		Texas City area	Chicot aquifer	5/1957	12/2019	772
292913094584301	6433102	D	Galveston		--	Chicot aquifer	1/1964	12/2019	666
292338095063601	[16]6540707	E	Galveston		Alta Loma area	Chicot aquifer	1/1941	2/2021	870
--	8011201	B	Jackson	[17]Western part of the study area (fig. 34)	--	Chicot aquifer	3/1956	3/2018	579
--	6660401	C	Jackson		--	Chicot aquifer	3/1948	8/2018	286
--	8015402	D	Matagorda		--	Chicot aquifer	12/1957	1/2010	295
285903095575700	8101102	E	Matagorda		--	Chicot aquifer	4/1951	1/2018	1,032
--	6663105	F	Wharton		--	Chicot aquifer	8/1935	1/2018	342
--	6648404	G	Wharton		--	Chicot aquifer	3/1953	3/2013	760
--	6646402	H	Wharton		--	Chicot aquifer	3/1956	1/2018	366

Table 2. Wells with long-term groundwater-level measurements within the Gulf Coast aquifer system study area in southeast Texas. —Continued

[USGS well ID is the well identifier used by the U.S. Geological Survey (USGS; 2021b); TWDB well ID is the well identifier used by the Texas Water Development Board (TWDB; 2020b); bls, below land surface; --, not available; conf., confining]

USGS well ID	TWDB well ID	Identifier for long-term wells in this report (figs. 19–36, 51–52)	County	Groundwater-well groups (fig. 18)	Historical geographic area (fig. 18*B*)[1]	Hydrogeologic unit	Period of record (may contain gaps) (month/year)		Well depth, in feet bls[3]
							Begin[2]	End	
--	6635901	B	Lavaca	Northwestern part of the study area (fig. 35)	--	Evangeline aquifer	3/1956	1/2018	840
--	6637607	C	Colorado		--	Chicot aquifer	2/1959	1/2018	318
--	6620901	D	Colorado		--	Evangeline aquifer	3/1956	1/2018	800
294903096061401	6616407	E	Austin		--	Chicot aquifer	12/1966	1/2017	165
295442095542401	[18]6501905	F	Waller		Katy area	Evangeline aquifer	3/1941	1/2008	810
295213095532101	[19]6509307	G	Waller			Chicot aquifer	2/1931	1/2010	767
294521094545901	6409924	B	Chambers	Eastern part of the study area (fig. 36)	--	Chicot aquifer	11/1967	12/2019	409
293156094515501	6426701	C	Chambers		--	Chicot aquifer	11/1966	2/2019	683
294714094382001	[20]6411901	D	Chambers		--	Chicot aquifer	5/1941	2/2003	350
300503093450201	6258304	E	Orange		--	Chicot aquifer	8/1954	1/2017	719
302055094041301	[21]6148209	F	Jasper		--	Chicot aquifer	4/1956	12/2018	1,295
303948093541801	6217902	G	Jasper		--	Chicot aquifer	5/1942	5/2002	325
--	6739507	B	Lavaca	[17]Western part of the outcrop in the study area (fig. 51)	--	Jasper aquifer	8/1959	2/2017	245
--	6625203	C	Lavaca		--	Jasper aquifer	10/1966	1/2018	287
--	6618601	D	Colorado		--	Jasper aquifer	4/1937	1/2018	602
--	6604601	E	Austin		--	Evangeline aquifer	12/1965	1/2018	119
--	5961803	F	Austin		--	Jasper aquifer	11/1965	2/1998	725
--	6605604	G	Austin		--	Evangeline aquifer	9/1967	1/2000	160
302247096052201	5940707	H	Grimes		--	Jasper aquifer	8/1948	1/2018	272
--	6033103	I	Grimes		--	Catahoula conf. unit	12/1942	1/2018	611
302145095473901	6042206	B	Montgomery	Eastern part of the outcrop in the study area (fig. 52)	--	Jasper aquifer	2/1977	1/2020	760
302948095422501	--	C	Montgomery		--	Jasper aquifer	1/1953	11/2018	107
302558095343701	6036505	D	Montgomery		--	Jasper aquifer	5/1972	1/2020	640
--	6015803	E	San Jacinto		--	Jasper aquifer	10/1965	3/2018	360
304657094250800	6113802	F	Tyler		--	Jasper aquifer	1/1953	6/2020	582
303135093574700	6201701	G	Jasper		--	Catahoula conf. unit	3/1964	11/2018	1,004

[1]Modified from Gabrysch and Coplin (1990). The spatial areas of the groundwater-well groups in Harris and Galveston Counties (fig. 18) are spatially contiguous with the benchmark groups (fig. 70; table 4), and the Global Positioning System station groups (figs. 76–77; table 6).

[2]The period of record begin date may precede the data shown on figs. 19–36 and 51–52.

[3]The hydrogeologic unit assigned to each well is based on the well's screened interval(s); therefore, the well depth is listed to provide general information on well construction.

[4]A hydrograph for this well is presented on figure 10 in Baker (1986).

[5]A hydrograph for this well is presented on figure 16 in Popkin (1971) along with well 6045505 (TWDB, 2020b) from figure 14 and table 3.1 of this report. A hydrograph for this well is also presented on figure 6 in William F. Guyton and Associates, Inc. (1972).

[6]This well is also referenced as well 36 in William F. Guyton and Associates, Inc. (1972).

[7]A hydrograph for this well is presented on figure 14 in Williams and Ranzau (1987) and on figure 1 in Barbie and Locke (1993).

[8]Water-level data for this well are presented on figure 12 in Gabrysch (1982a), figure 8 in Gabrysch (1984), figure 16 in Williams and Ranzau (1987), and figure 4 in Barbie and Locke (1993).

[9]This well is also referred to as well 1100e in Gabrysch (1967). A hydrograph for this well is presented on figure 10 in Gabrysch (1967), figure 14 in Gabrysch (1982a), figure 17 in Williams and Ranzau (1987), and figure 5 in Barbie and Locke (1993).

[10]A hydrograph for this well is presented on figure 4 in Gabrysch and Bonnet (1974).

[11]A hydrograph for this well is presented on figure 18 in Sandeen and Wesselman (1973).

[12]This well is also referred to as well H-20, and water-level data for this well are presented in Rayner (1959) on page 43.

[13]This well is also referred to as well F-50 in Rayner (1959) and in Gabrysch (1967). A hydrograph for this well is presented on figure 13 in Gabrysch (1967).

[14]This well is also referred to as well 186 and B-7, and a hydrograph for this well is presented on figure 13 in Wood and Gabrysch (1965) and on figure 11 in Gabrysch (1967). This well is also listed in table 3.1.

[15]A hydrograph for this well is presented on figure 19 in Williams and Ranzau (1987).

[16]This well is also referred to as well E-93 and “City of Galveston test well #2” in Gabrysch (1967). A hydrograph for this well is presented on figure 14 in Gabrysch (1967), figure 17 in Gabrysch (1982a), figure 20 in Williams and Ranzau (1987), and figure 8 in Barbie and Locke (1993).

[17]These groundwater-well groups are not shown on figure 18.

[18]This well is also referred to as well F-11, and water-level data for this well are presented in Rayner (1959) on page 62.

[19]This well is also referred to as well F-25. Hydrographs for this well are presented in many publications, including Winslow and Fluellen (1952), Wood (1958a), Anders and Naftel (1962), Wood and Gabrysch (1965), Gabrysch (1967), and Gabrysch (1972). This well is also listed in table 3.1.

[20]This well is also referred to as well G-34, and water-level data for this well are presented in Rayner (1959) on page 8. A hydrograph for this well is also presented on figure 8 in Wesselman and Aronow (1971).

[21]A hydrograph for this well is presented on figure 18 in Wesselman (1967). Note this well was originally described as well 6148209B.

declines in the Evangeline aquifer in Harris County during 1943–67 were about 70 ft (fig. 14*G*) and 145 ft (fig. 21*F*) in the northern part of the county.

During 1965–75, groundwater levels in the historical Houston area declined by as much as 50 ft in the Chicot aquifer (or as much as 5 ft/yr) and as much as 130 ft in wells completed in the Evangeline aquifer (or as much as 13 ft/yr) (figs. 24–25) (Gabrysch, 1980a). Groundwater-level decreases in the Pasadena area were similar to those in the historical Houston area, with as much as 50 ft of decline in the Chicot aquifer and 100 ft of decline in the Evangeline aquifer during 1965–75 (fig. 26) (Gabrysch, 1980a). In the Johnson Space Center area, groundwater levels declined by as much as 80 ft and ranged from about 170 ft to about 260 ft bls (fig. 27) (Gabrysch, 1980a). In the Texas City area, the rate of groundwater-level decline was greater prior to 1970 than the rate of groundwater-level decline after 1970 (Gabrysch, 1980a). In the Katy area, groundwater-level declines in the Chicot aquifer ranged from less than 2 ft/yr to more than 4 ft/yr during 1965–75 (figs. 14–15, 21–23, 31, 35).

In Liberty County, Chicot aquifer groundwater levels in 1966 ranged from about 40 to 100 ft bls, and the mean groundwater level was about 60 ft bls (fig. 32). Groundwater levels in 1975 were generally not appreciably different from those in 1966 (fig. 32). Based on the groundwater levels from Deussen (1914), many wells were noted as flowing during the early part of the 20th century, and groundwater levels at many other wells generally were within 20 ft of land surface in Liberty County. The total groundwater-level decline in this county through 1966 was generally less than 100 ft (fig. 32).

In Montgomery County, an 1,800-ft-deep well measured in 1902 (well 6053502; fig. 13*A*; table 3.1) was still flowing in 1966, and the groundwater level in 1966 (the level to which water would rise above land surface in tightly cased well) was about 10 ft above land surface (Popkin, 1971). The mean groundwater-level decline in wells completed in the Jasper aquifer in Conroe was about 55 ft during 1965–75, and groundwater levels were generally between about 65–85 ft bls in 1975 (fig. 19).

Groundwater levels in the Chicot aquifer in Chambers County were about 85 to 120 ft bls in 1967, although levels in shallow wells were much nearer land surface (fig. 36). By 1974, groundwater levels in Chambers County near Harris County were at or near historical minimums (fig. 36).

Regulation and Post-Developed Conditions (1975–Present)

By 1975, groundwater levels in central, south-central, southeastern, and eastern Harris County were near historical minimums (figs. 25–28), coincident with the maximum groundwater use in the county the prior year. Groundwater levels in the Chicot and Evangeline aquifers during 1975–79 in the historical Houston area continued to decline in the western two-thirds of this area but rose in the eastern one-third (figs. 24–25) (Gabrysch, 1982a) as groundwater development continued northward, northwestward, and westward. In the Pasadena area during 1975–79, groundwater levels rose by a maximum of about 90 ft in the Chicot aquifer and 150 ft in the Evangeline aquifer (fig. 26) (Gabrysch, 1982a). A hydrograph from Gabrysch (1984) for the Pasadena area depicts a rapid groundwater-level recovery of about 65 ft during 1976–79 (fig. 26*E*; table 2), and the water-level recovery for a nearby well was about 130 ft (fig. 26*D*). In the Baytown area during 1975–79, groundwater levels rose by a maximum of about 110 ft in the Chicot aquifer (fig. 27*E–G*) and by a maximum of about 130 ft in the Evangeline aquifer (Gabrysch, 1982a). Similar to the recovery in the Pasadena area, the Baytown area had a rapid groundwater-level recovery of about 116 ft during 1977–79 (fig. 27*F*) (Gabrysch, 1984). In the Johnson Space Center area during 1975–79, groundwater levels rose between about 30 and 80 ft in the Chicot aquifer (fig. 27*C–D*) and between about 20 and 80 ft in the Evangeline aquifer (Gabrysch, 1982a).

Groundwater-level changes during 1975–79 in the greater Houston area other than Harris County included a range of declining and rising groundwater levels. In Fort Bend County, groundwater levels continued to decline during 1975–79. In the Katy area, Chicot aquifer groundwater levels declined by about 20 ft for most wells during this period (figs. 21–23, 31, 35), although groundwater levels declined in some individual wells by less than 10 ft and as much as 60 ft (Gabrysch, 1982a). Evangeline aquifer groundwater levels in the Katy area declined by less than 10 ft to about 70 ft during 1975–79 (figs. 21–23, 31, 35) (Gabrysch, 1982a). In the northern part of the Katy area, the Jasper aquifer groundwater level was about 6 ft bls in 1979 (fig. 21*H*). In the relatively undeveloped southwestern area of Fort Bend County, groundwater levels in the Chicot aquifer were within about 50 ft bls, but groundwater levels were about 100 ft bls in the eastern part of the county near Harris County (fig. 30). Evangeline aquifer groundwater levels in eastern Fort Bend County were about 215 to 250 ft bls during this period (fig. 30). Groundwater levels in Brazoria County were generally at or near historical minimums in some areas of the county about 1975, although further declines occurred in wells in the central to northern parts of the county (fig. 29). Groundwater-level changes in the Chicot aquifer in Brazoria County during this period ranged from about 10 ft of decline to about 45 ft of recovery (fig. 29). In Galveston County during 1975–79, groundwater levels in the Chicot aquifer rose by between 10 and 20 ft in the Texas City area and by about 20 ft in the Alta Loma area (fig. 33) (Gabrysch, 1982a). In Liberty County, groundwater-level minimums were generally reached during 1975–79 (fig. 32). In Chambers County, groundwater levels in the Chicot aquifer in 1979 either remained the same as those in 1975 or rose by as much as about 20 ft (fig. 36). In Montgomery County, groundwater levels in the Evangeline aquifer in The Woodlands were generally about 135 ft bls in 1979 (fig. 20). The groundwater level in the Jasper aquifer in this area was about 80 ft bls in 1981

(fig. 20). The mean groundwater-level decline in the Jasper aquifer near Conroe was about 30 ft during 1975–79, and the mean groundwater level was about 100 ft bls in 1979 (fig. 19).

During 1980–84, groundwater levels in the greater Houston area rose in Galveston County, Chambers County, and the central, south-central, southeastern, and eastern parts of Harris County (figs. 25–28) and declined in the northern, northwestern, and western parts of Harris County and in Montgomery County (figs. 19–23). During 1980–84, Chicot aquifer groundwater-level changes in the historical Houston area ranged from recoveries of as much as about 25 ft in the eastern part (fig. 25) to declines of as much as 15 ft in the southwestern part (fig. 24). Evangeline aquifer groundwater levels rose as much as about 10 ft in the eastern part of the historical Houston area (fig. 25) and declined by about 25 ft in the southwestern part of this area (fig. 24). During the 1980–84 period, some wells in the southwestern part of the historical Houston area had reached historical minimums, or nearly so (fig. 24). In the Pasadena and Baytown areas, groundwater levels rose in the Chicot and Evangeline aquifers as much as 60 ft during 1980–84 (figs. 26–27) (Williams and Ranzau, 1987). In the Johnson Space Center area, the groundwater-level recovery in the Chicot and Evangeline aquifers was less pronounced than the recovery in the Baytown and Pasadena areas, with recoveries of as much as 10–20 ft (fig. 27). In the Texas City and Alta Loma areas, groundwater-level recoveries were about 10–20 ft (fig. 33), although the groundwater level in one well in the Texas City area rose about 80 ft (Williams and Ranzau, 1987). In the Katy area during 1980–84, Chicot aquifer groundwater levels decreased by about 10 to 40 ft in the northern part (fig. 21) but were about the same elsewhere (figs. 21–23, 31, 35). Groundwater-level changes in the Evangeline aquifer in the Katy area during 1980–84 included declines of as much as about 130 ft figs. 21–23, 25, 31). In the northern part of the Katy area, the Jasper aquifer groundwater level was about 20 ft bls in 1984 (fig. 21). In Montgomery County, mean groundwater levels in the Evangeline aquifer in The Woodlands were about 175 ft bls in 1984, which was a decline of about 35 ft from the mean groundwater levels in 1980 (fig. 20). The Jasper aquifer groundwater level in The Woodlands was about 40 ft bls in 1984 (fig. 20), which is a recovery of about 35 ft from the 1981 level. Jasper aquifer groundwater-level declines in Conroe were about 20 ft during 1980–84, and the mean groundwater level was about 125 ft bls in 1984 (fig. 19). Evangeline aquifer groundwater levels in Conroe were about 120 ft bls in 1984 (fig. 19). In Liberty County, groundwater-level changes in the Chicot aquifer during this period were between about 15 ft of decline and about 10 ft of recovery (fig. 32). In Chambers County, groundwater levels in the Chicot aquifer rose by as much as 25 ft (fig. 36). Groundwater-level changes in the Chicot aquifer in Brazoria County during this period were between about 15 ft of decline and about 25 ft of recovery (fig. 29).

During 1985–89, groundwater-level changes varied across the greater Houston area. Groundwater levels generally rose in Galveston County and throughout most of the central, south-central, and southeastern parts of Harris County; however, declines continued in northern, northwestern, and western Harris County, in Montgomery County, and in some parts of Brazoria County. In the historical Houston area, historical minimums were reached in nearly all wells in the eastern part (fig. 25) and were approaching the historical minimums in some wells (fig. 24). In the Pasadena area, groundwater levels in the Chicot and Evangeline aquifers rose by as much as 40 ft and 20 ft, respectively, during 1985–89 (fig. 26) (Barbie and Locke, 1993). In the Johnson Space Center area, the groundwater-level recovery in the Chicot and Evangeline aquifers was less than 20 ft during 1985–89 (fig. 27) (Barbie and Locke, 1993). In the Texas City and Alta Loma areas, groundwater-level recoveries were less than 20 ft (fig. 33) (Barbie and Locke, 1993). Historical groundwater minimums were generally reached in southern Fort Bend County during 1985–89 (fig. 30). In the Katy area during 1985–89, Chicot aquifer groundwater levels decreased by about 10 to 40 ft in the northern part (fig. 21) but were about the same elsewhere (figs. 22–23, 31, 35). Groundwater-level changes in the Evangeline aquifer in the Katy area during 1980–84 include recoveries of as much as about 20 ft and declines of as much as about 70 ft (a mean decline of about 30 ft) (figs. 22–23, 25, 31). The Jasper aquifer groundwater level in the northern part of the Katy area was about 55 ft bls in 1989 (fig. 21). In Montgomery County, groundwater levels in the Evangeline aquifer in The Woodlands were generally about 200 ft bls in 1989, which was a decline of about 30 ft from 1984 (fig. 20). The groundwater level in the Jasper aquifer in this area was about 60 ft bls in 1989, which is a decline of about 20 ft from the 1984 level (fig. 20). During 1985–89, the mean groundwater-level declines in both the Evangeline and Jasper aquifers in Conroe were about 30 ft. By 1989, mean groundwater levels (measured as the depth to water in feet below land surface) in the Evangeline and Jasper aquifers were about 140 and 160 ft, respectively (fig. 19). In Liberty County, groundwater-level changes in the Chicot aquifer during 1985–89 included between about 10 ft of decline and about 5 ft of recovery (fig. 32). In Chambers County, groundwater levels in the Chicot aquifer were about the same during this period (fig. 36). Groundwater-level changes in the Chicot aquifer in Brazoria County during this period were between about 15 ft of decline and about 30 ft of recovery (fig. 29).

During 1990–99, groundwater levels generally rose in Brazoria, Fort Bend, Galveston, and Liberty Counties and throughout most of the southwestern, central, south-central, southeastern, and eastern parts of Harris County; however, declines generally continued in northern, northwestern, and western Harris County and in Montgomery County. Groundwater levels in southwestern Harris County rose as much as 80 ft in the Chicot aquifer and about 150 ft in the Evangeline aquifer (fig. 24). In northwestern and western Harris County, groundwater levels were at or near historical minimums in nearly all wells by 1999 (figs. 22–23). In western Harris County, a groundwater level of more than 600 ft bls was reached in 1996 and 1999 in one well (fig. 22*E*).

In northern Harris County, groundwater levels in wells closest to central Harris County were at or near historical minimums by 1999 (fig. 21*C–E*), while groundwater-level declines continued for wells closest to Montgomery County (fig. 21*B*, *G–H*). The decline in the Jasper aquifer groundwater level during 1990–99 in northern Harris County was about 65 ft and was measured at about 120 ft bls in 1999 (fig. 21). In Montgomery County, mean groundwater levels in the Evangeline aquifer in The Woodlands were about 275 ft bls in 1999, which was a decline of about 65 ft from the mean groundwater levels in 1990 (fig. 20). The groundwater level in the Jasper aquifer in this area was about 175 ft bls in 1999 (fig. 20), which is a decline of about 115 ft from the 1990 level. During 1990–99, the mean groundwater-level declines in the Evangeline and Jasper aquifers in Conroe were about 75 ft and 60 ft, respectively, and mean groundwater levels in 1999 in the Evangeline and Jasper aquifers were about 210 and 220 ft bls, respectively (fig. 19).

During 2000–09, groundwater levels generally rose in Brazoria, Galveston, and Liberty Counties, and throughout most of the western, southwestern, central, south-central, southeastern, and eastern parts of Harris County; however, declines generally continued in northern Harris County and in Montgomery County. In eastern Harris County, the groundwater level in the Jasper aquifer was below land surface beginning in summer 2006 and declined by about 60 ft during 2000–09 (fig. 28*E*). In northern Harris County, groundwater levels in wells closest to central Harris County rose by as much as about 50 ft during 2000–09 (fig. 21*C–E*). During 2000–09, groundwater levels in northern Harris County declined between about 35–160 ft for wells closest to Montgomery County, and historical minimums were approached by 2009 (fig. 21*B*, *G–H*). In Montgomery County, groundwater levels in the Evangeline and Jasper aquifers declined in The Woodlands by about 30–75 ft and 140 ft, respectively, during 2000–09 (fig. 20). Mean groundwater-level declines in the Evangeline and Jasper aquifers in Conroe during 2000–09 were about 75–85 ft (fig. 19). In Liberty County, groundwater-level changes were between about 7 ft of decline and 18 ft of recovery (fig. 32), and groundwater levels in Brazoria County generally rose by as much as 26 ft during this period (fig. 29).

During 2010–15, Chicot and Evangeline aquifer groundwater levels generally continued to recover in northern, northwestern, and western Harris County (figs. 21–23), coincident with a 2010 initial conversion to alternative water supplies for 30 percent (HGSD Regulatory Area 3; fig. 3) of total permitted water use. Groundwater levels generally continued to recover in Brazoria County, southern Fort Bend County, and Liberty County (figs. 29–30, 32). During this period, the mean groundwater-level recoveries in the Chicot and Evangeline aquifers in northern and northwestern Harris County were 25 ft and 17 ft, respectively (figs. 21–22). The groundwater level in the Jasper aquifer in northern Harris County declined by about 60 ft during 2010–15 (fig. 21). In eastern Harris County, the Jasper groundwater level declined by about 40 ft during this period (fig. 28). In Montgomery County, Evangeline and Jasper aquifer groundwater levels in Conroe and The Woodlands had reached historical minimums, and groundwater-level recoveries from these historical minimums had begun in some wells (fig. 19). This groundwater-level recovery was coincident with an alternative water-use conversion plan that was to be implemented in 2016 for large-volume groundwater users in Montgomery County, whereby groundwater use was generally limited to no more than 70 percent of total permitted use (LSGCD, 2013).

Colocated Groundwater Wells

Many colocated wells are in the study area, particularly in Harris County and Galveston County at borehole extensometer sites (hereinafter, "extensometer sites") which measure aquifer-system compaction (figs. 37–44). In Montgomery County, colocated wells are at public supply well sites (figs. 45–50). To illustrate the differences in groundwater levels at wells screened at differing vertical depths, hydrographs of groundwater levels for the wells at eight of the extensometer sites and six public supply sites were analyzed along with lithologic units and well screened intervals (figs. 37–50). Changes in groundwater levels in shallow wells generally are in response to changes in precipitation; the water table in shallow wells is at atmospheric pressure (unconfined conditions), and there is likely little hydraulic connection with the water in the deeper wells where the groundwater is under confined conditions. The patterns of groundwater-level changes in shallow wells are most evident when the depth to water is less than about 100 ft bls. Patterns in groundwater levels common to the wells at eight selected extensometer sites and six public supply sites include (1) minimal groundwater-level changes over time in the shallowest wells, and (2) a transition zone between about 100 and 250 ft bls, below which groundwater is generally under confined conditions and groundwater levels are primarily affected by groundwater withdrawals.

At the Pasadena extensometer site (hereinafter referred to as the "Pasadena site"), the groundwater levels (represented as depths to water in feet below land surface) in wells C and D (fig. 37; table 3) showed little association with water levels in the wells screened at greater depths (wells F through J) and were generally stable with less than 12 ft of change during the 1974–2015 period of record (hydrographs on fig. 37*D–J* generally span from 1975 to 2020). Wells C and D at this site are screened at depths of less than 100 ft, and the remaining wells are screened at progressively greater depths of more than 350 ft, representing regularly spaced intervals. Groundwater levels at wells C and D were similarly affected by changes in precipitation; for example, groundwater levels in wells C and D rose during periods of above-mean precipitation and declined during periods of below-mean precipitation (fig. 37*C–D*). Prior to about 1985, the pattern in groundwater levels over time in well E was similar to the pattern observed in wells C and D. However, after about 1990, the pattern in groundwater levels in well E was most similar to

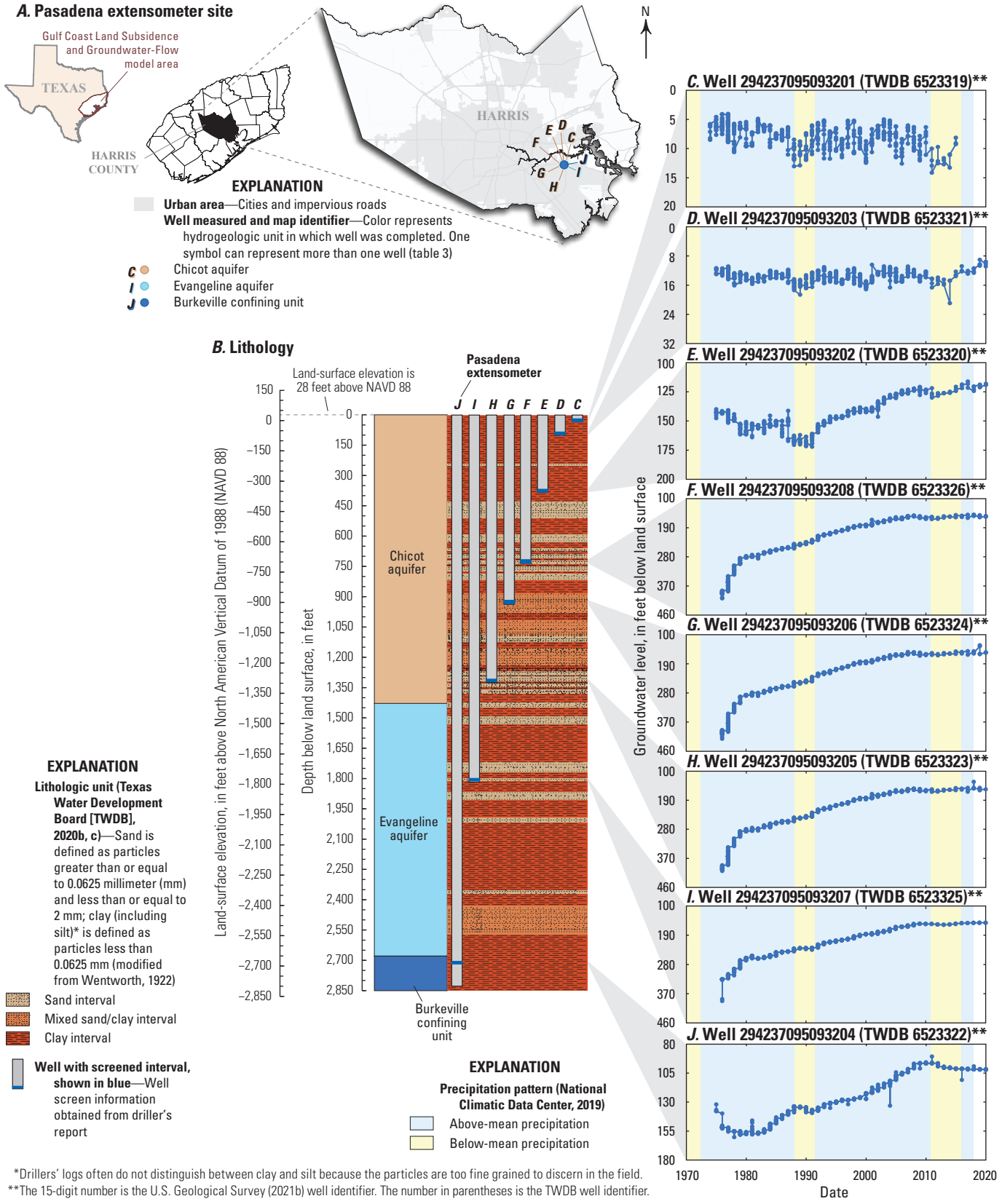

*Drillers' logs often do not distinguish between clay and silt because the particles are too fine grained to discern in the field.
**The 15-digit number is the U.S. Geological Survey (2021b) well identifier. The number in parentheses is the TWDB well identifier.

Figure 37. *A*, Map showing location of Pasadena extensometer site (extensometer 294237095093204) in Harris County within the Gulf Coast aquifer system study area in southeast Texas, and *B*, lithologic section with graphs *C*–*J* showing depths to groundwater (groundwater levels) and precipitation patterns during the periods of record between 1970 and 2020 at the colocated wells at the site.

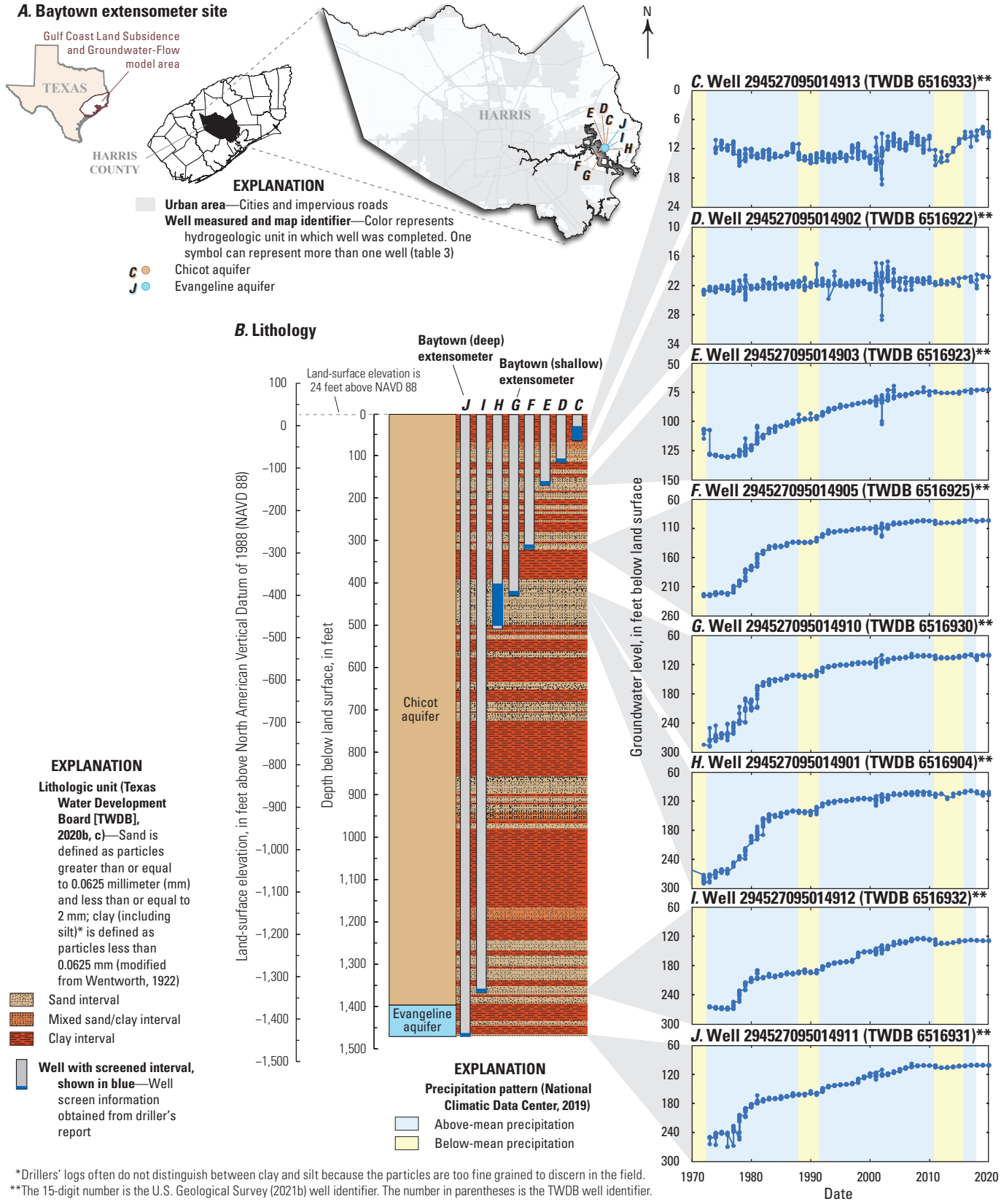

*Drillers' logs often do not distinguish between clay and silt because the particles are too fine grained to discern in the field.
**The 15-digit number is the U.S. Geological Survey (2021b) well identifier. The number in parentheses is the TWDB well identifier.

Figure 38. *A*, Map showing location of Baytown extensometer site (shallow extensometer 294527095014910 and deep extensometer 294527095014911) in Harris County within the Gulf Coast aquifer system study area in southeast Texas, and *B*, lithologic section with graphs *C*–*J* showing depths to groundwater (groundwater levels) and precipitation patterns during the periods of record between 1970 and 2020 at the colocated wells at the site.

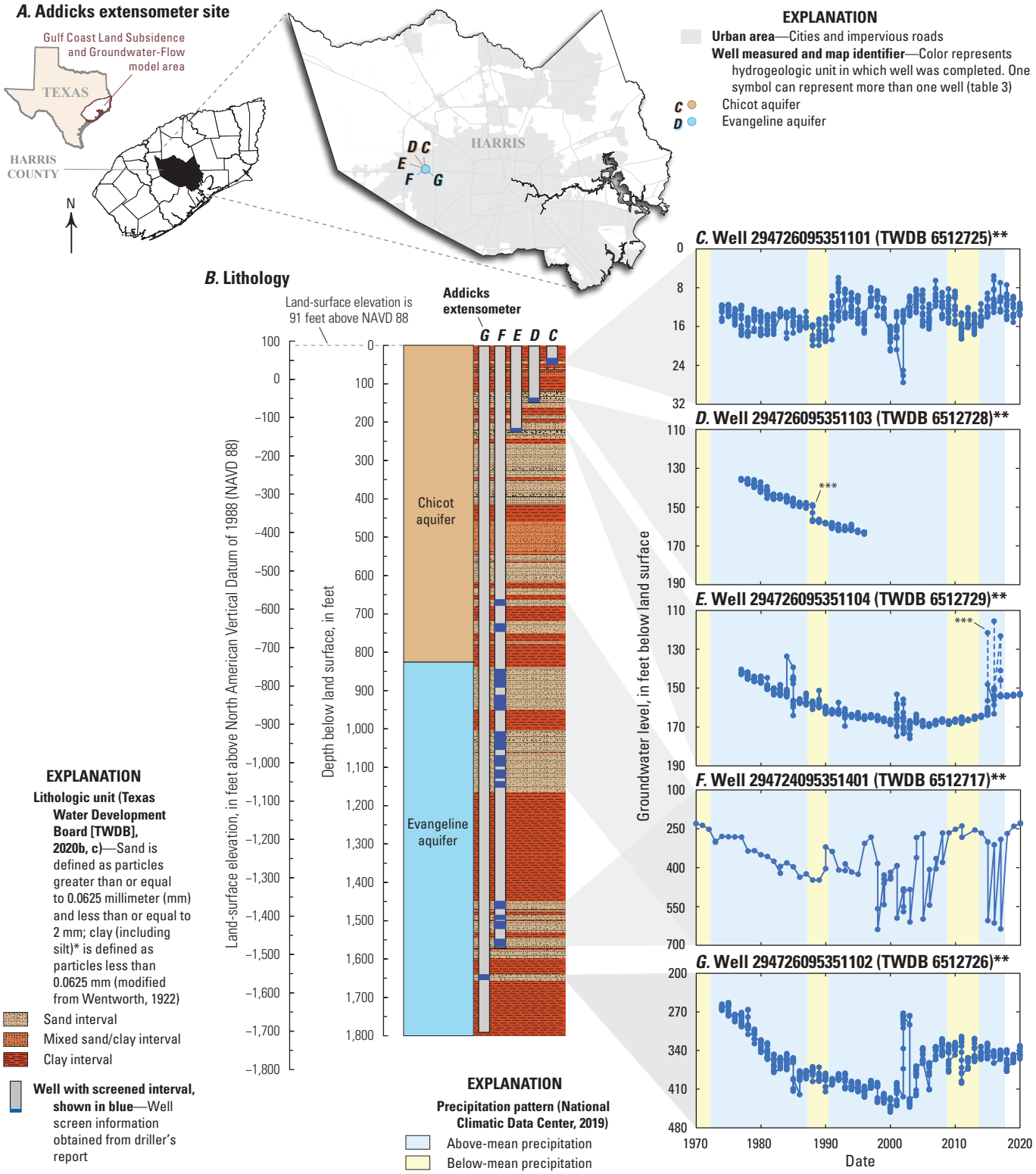

*Drillers' logs often do not distinguish between clay and silt because the particles are too fine grained to discern in the field.
**The 15-digit number is the U.S. Geological Survey (2021b) well identifier. The number in parentheses is the TWDB well identifier.
***The well casing could have been damaged during this period; therefore, water levels after this point have a greater uncertainty.

Figure 39. *A*, Map showing location of Addicks extensometer site (extensometer 294726095351102) in Harris County within the Gulf Coast aquifer system study area in southeast Texas, and *B*, lithologic section with graphs *C*–*G* showing depths to groundwater (groundwater levels) and precipitation patterns during the periods of record between 1970 and 2020 at the colocated wells at the site.

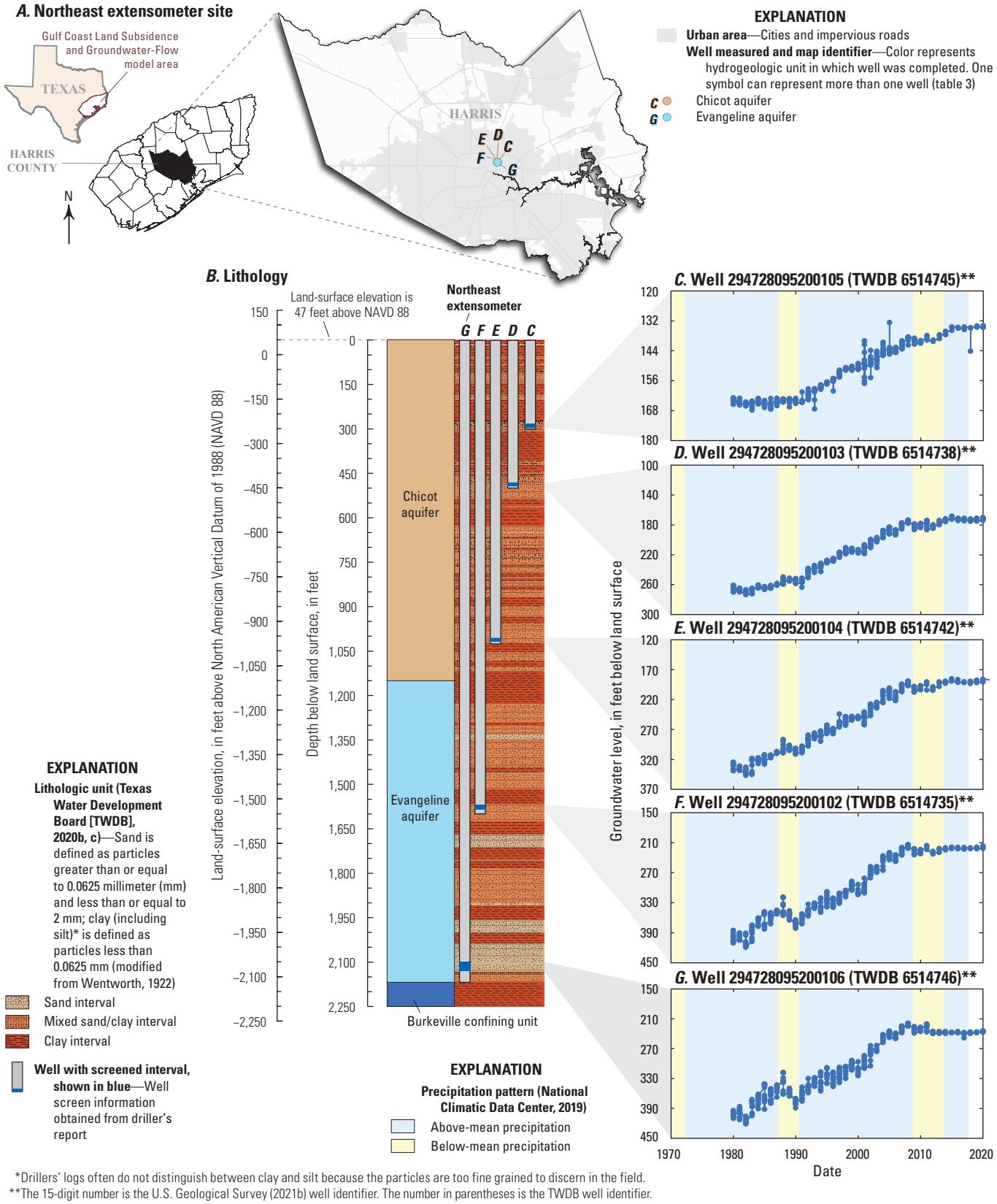

*Drillers' logs often do not distinguish between clay and silt because the particles are too fine grained to discern in the field.
**The 15-digit number is the U.S. Geological Survey (2021b) well identifier. The number in parentheses is the TWDB well identifier.

Figure 40. *A*, Map showing location of Northeast extensometer site (extensometer 294728095200106) in Harris County within the Gulf Coast aquifer system study area in southeast Texas, and *B*, lithologic section with graphs *C*–*G* showing depths to groundwater (groundwater levels) and precipitation patterns during the periods of record between 1970 and 2020 at the colocated wells at the site.

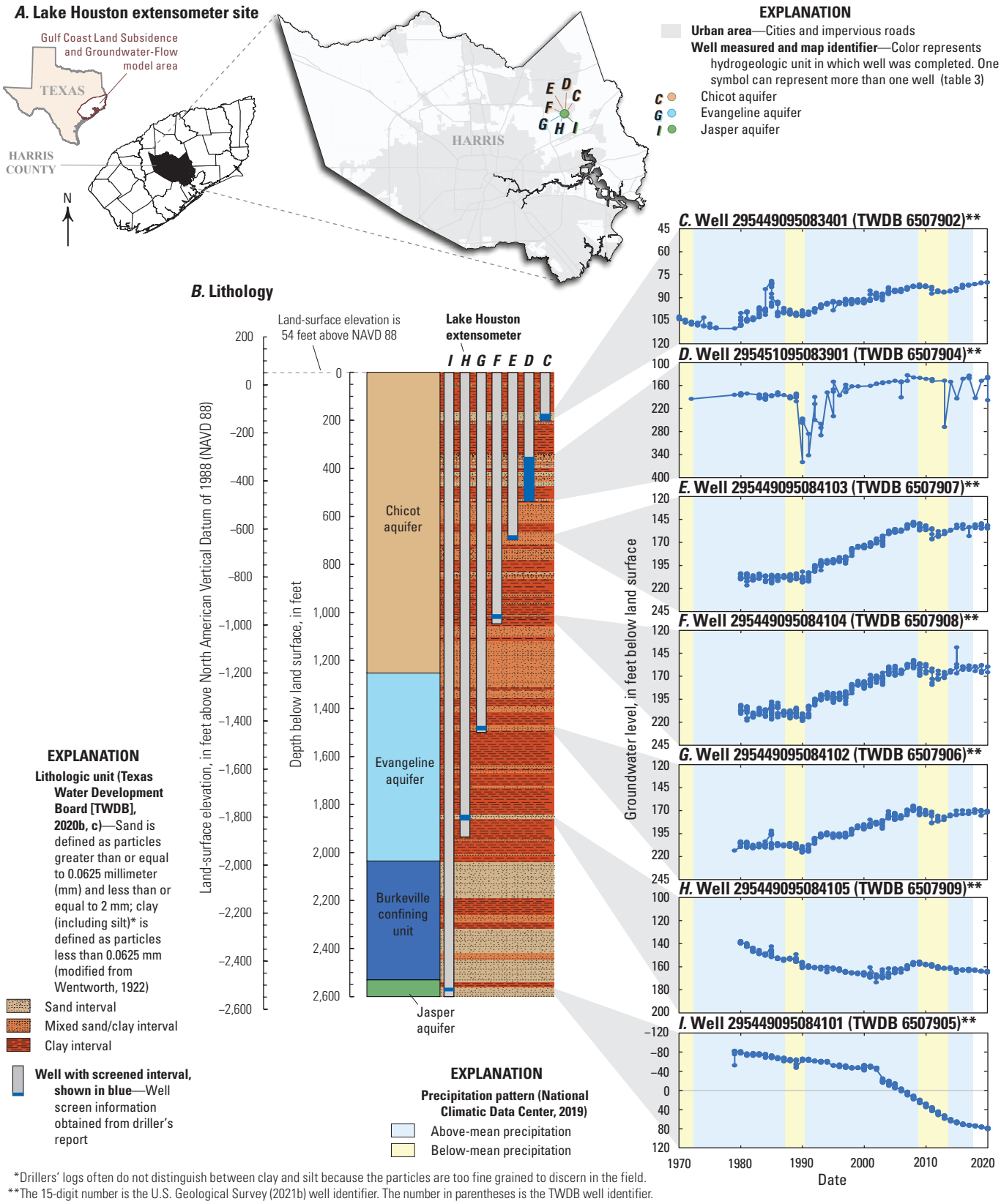

*Drillers' logs often do not distinguish between clay and silt because the particles are too fine grained to discern in the field.
**The 15-digit number is the U.S. Geological Survey (2021b) well identifier. The number in parentheses is the TWDB well identifier.

Figure 41. *A*, Map showing location of Lake Houston extensometer site (extensometer 295449095084105) in Harris County within the Gulf Coast aquifer system study area in southeast Texas, and *B*, lithologic section with graphs *C*–*I* showing depths to groundwater (groundwater levels) and precipitation patterns during the periods of record between 1970 and 2020 at the colocated wells at the site.

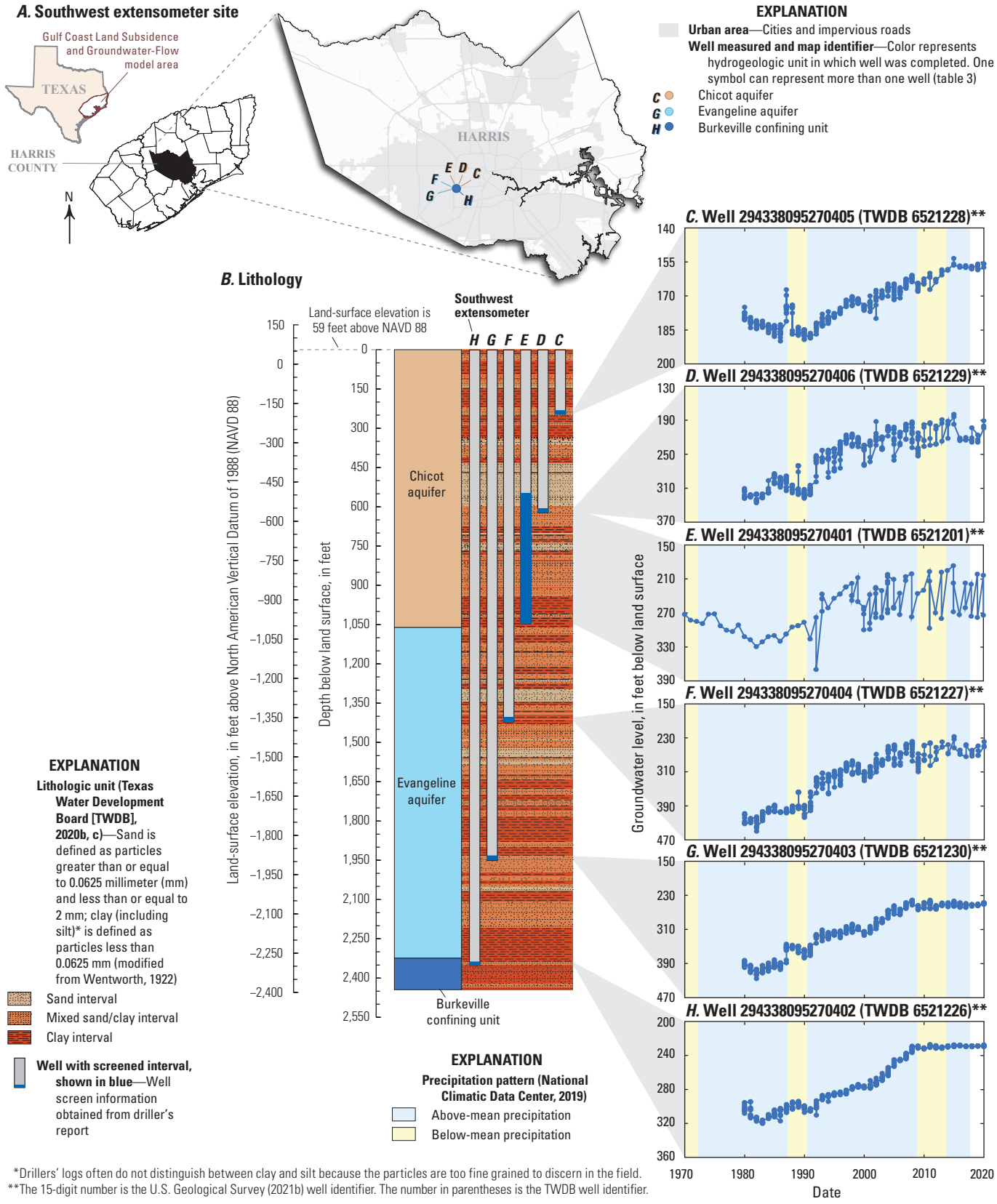

*Drillers' logs often do not distinguish between clay and silt because the particles are too fine grained to discern in the field.
**The 15-digit number is the U.S. Geological Survey (2021b) well identifier. The number in parentheses is the TWDB well identifier.

Figure 42. *A*, Map showing location of Southwest extensometer site (extensometer 294338095270402) in Harris County within the Gulf Coast aquifer system study area in southeast Texas, and *B*, lithologic section with graphs *C*–*H* showing depths to groundwater (groundwater levels) and precipitation patterns during the periods of record between 1970 and 2020 at the colocated wells at the site.

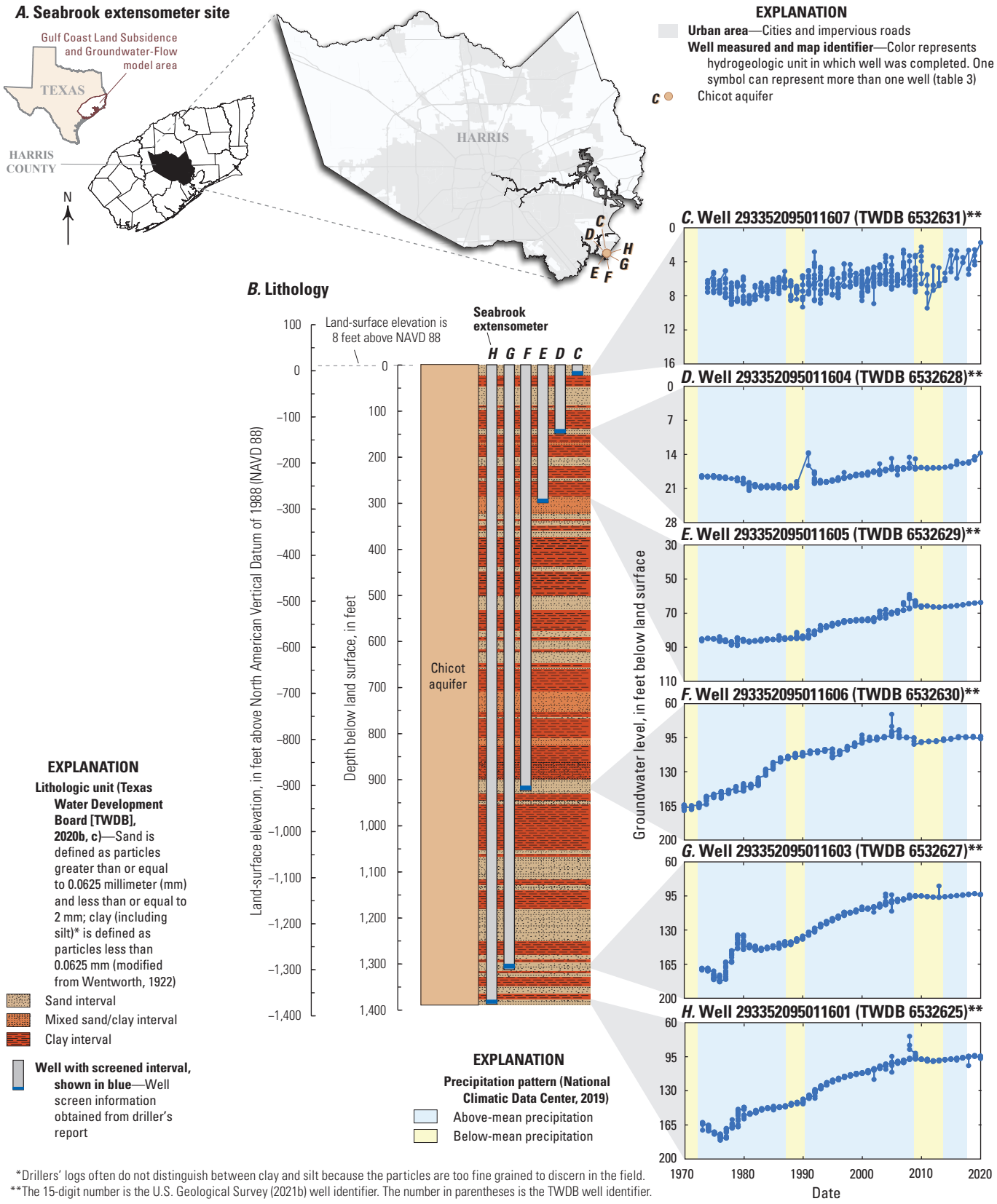

*Drillers' logs often do not distinguish between clay and silt because the particles are too fine grained to discern in the field.
**The 15-digit number is the U.S. Geological Survey (2021b) well identifier. The number in parentheses is the TWDB well identifier.

Figure 43. *A*, Map showing location of Seabrook extensometer site (extensometer 293352095011601) in Harris County within the Gulf Coast aquifer system study area in southeast Texas, and *B*, lithologic section with graphs *C*–*H* showing depths to groundwater (groundwater levels) and precipitation patterns during the periods of record between 1970 and 2020 at the colocated wells at the site.

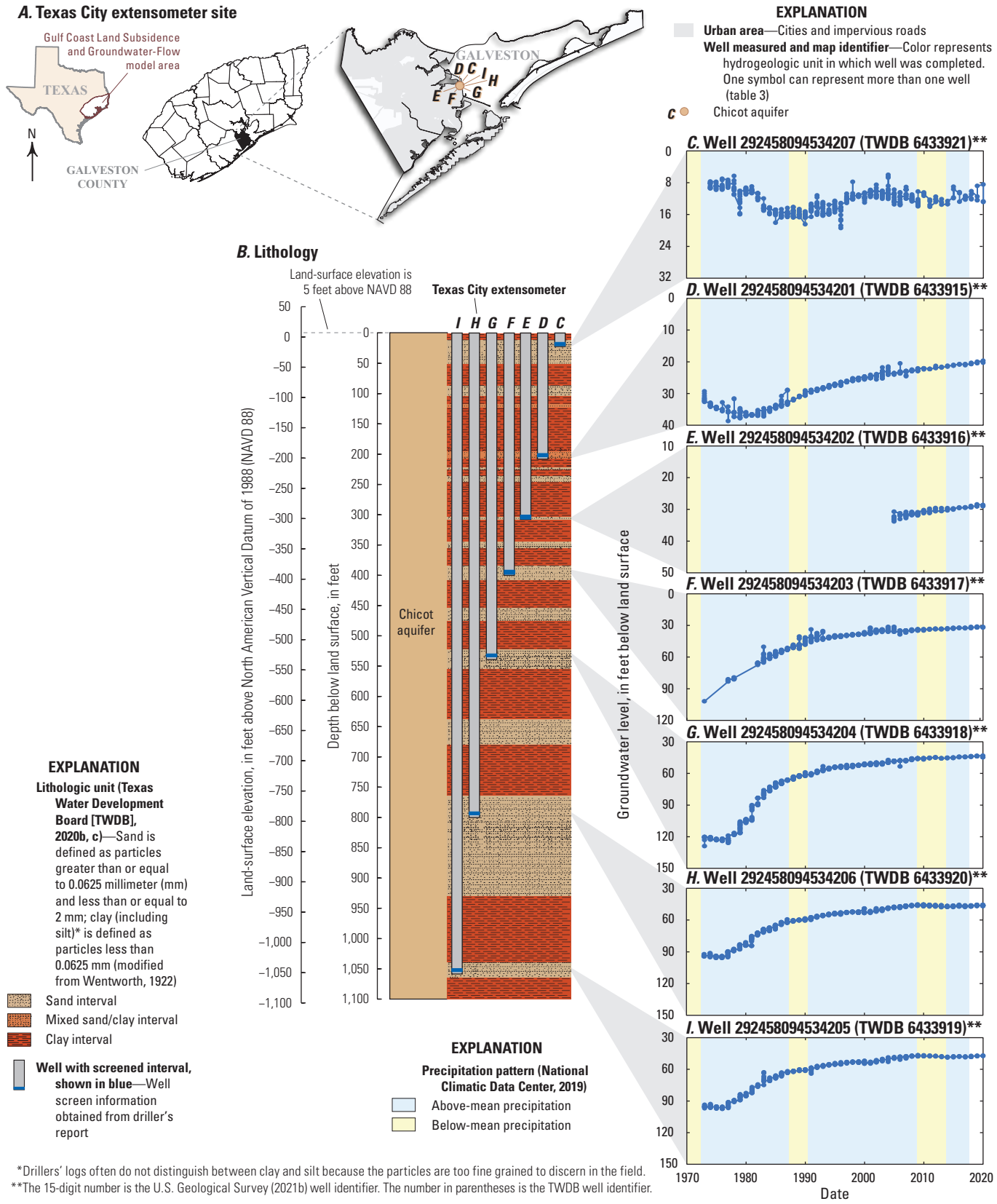

*Drillers' logs often do not distinguish between clay and silt because the particles are too fine grained to discern in the field.
**The 15-digit number is the U.S. Geological Survey (2021b) well identifier. The number in parentheses is the TWDB well identifier.

Figure 44. *A*, Map showing location of Texas City extensometer site (extensometer 292458094534205) in Harris County within the Gulf Coast aquifer system study area in southeast Texas, and *B*, lithologic section with graphs *C*–*I* showing depths to groundwater (groundwater levels) and precipitation patterns during the periods of record between 1970 and 2020 at the colocated wells at the site.

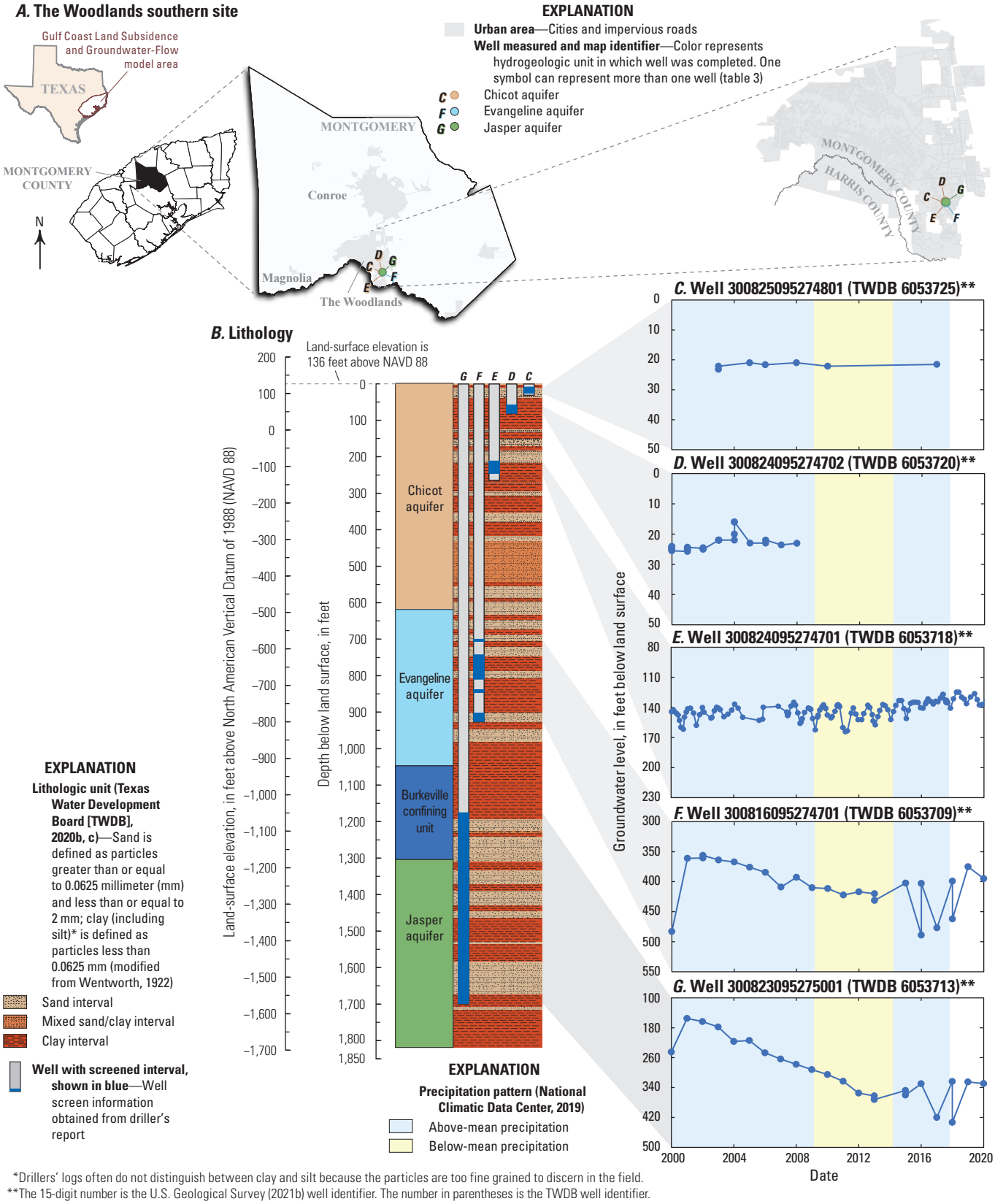

*Drillers' logs often do not distinguish between clay and silt because the particles are too fine grained to discern in the field.
**The 15-digit number is the U.S. Geological Survey (2021b) well identifier. The number in parentheses is the TWDB well identifier.

Figure 45. *A*, Map showing location of The Woodlands southern site in Montgomery County within the Gulf Coast aquifer system study area in southeast Texas, and *B*, lithologic section with graphs *C*–*G* showing depths to groundwater (groundwater levels) and precipitation patterns during the periods of record at the colocated wells at the site.

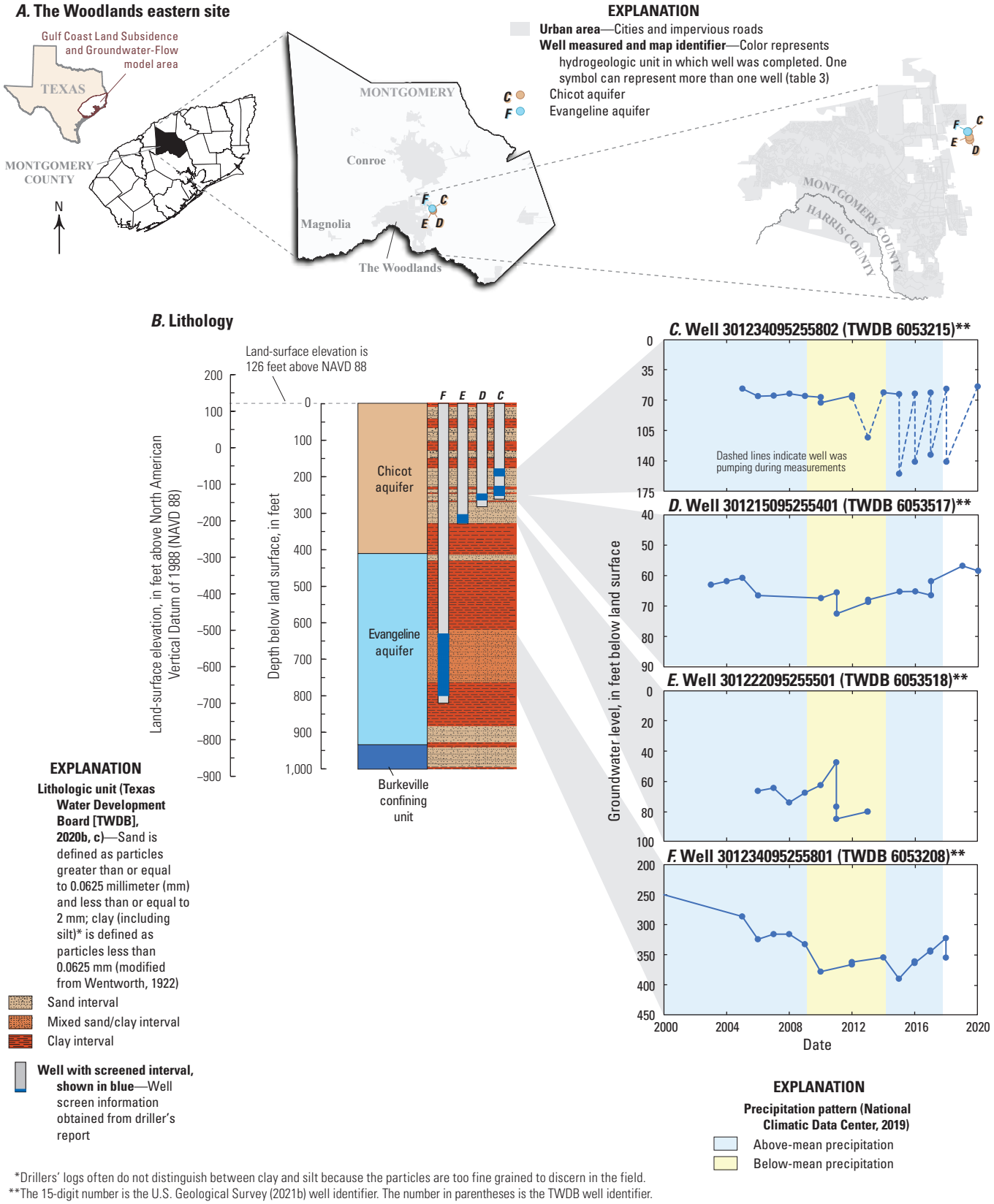

*Drillers' logs often do not distinguish between clay and silt because the particles are too fine grained to discern in the field.
**The 15-digit number is the U.S. Geological Survey (2021b) well identifier. The number in parentheses is the TWDB well identifier.

Figure 46. *A*, Map showing location of The Woodlands eastern site in Montgomery County within the Gulf Coast aquifer system study area in southeast Texas, and *B*, lithologic section with graphs *C*–*F* showing depths to groundwater (groundwater levels) and precipitation patterns during the periods of record at the colocated wells at the site.

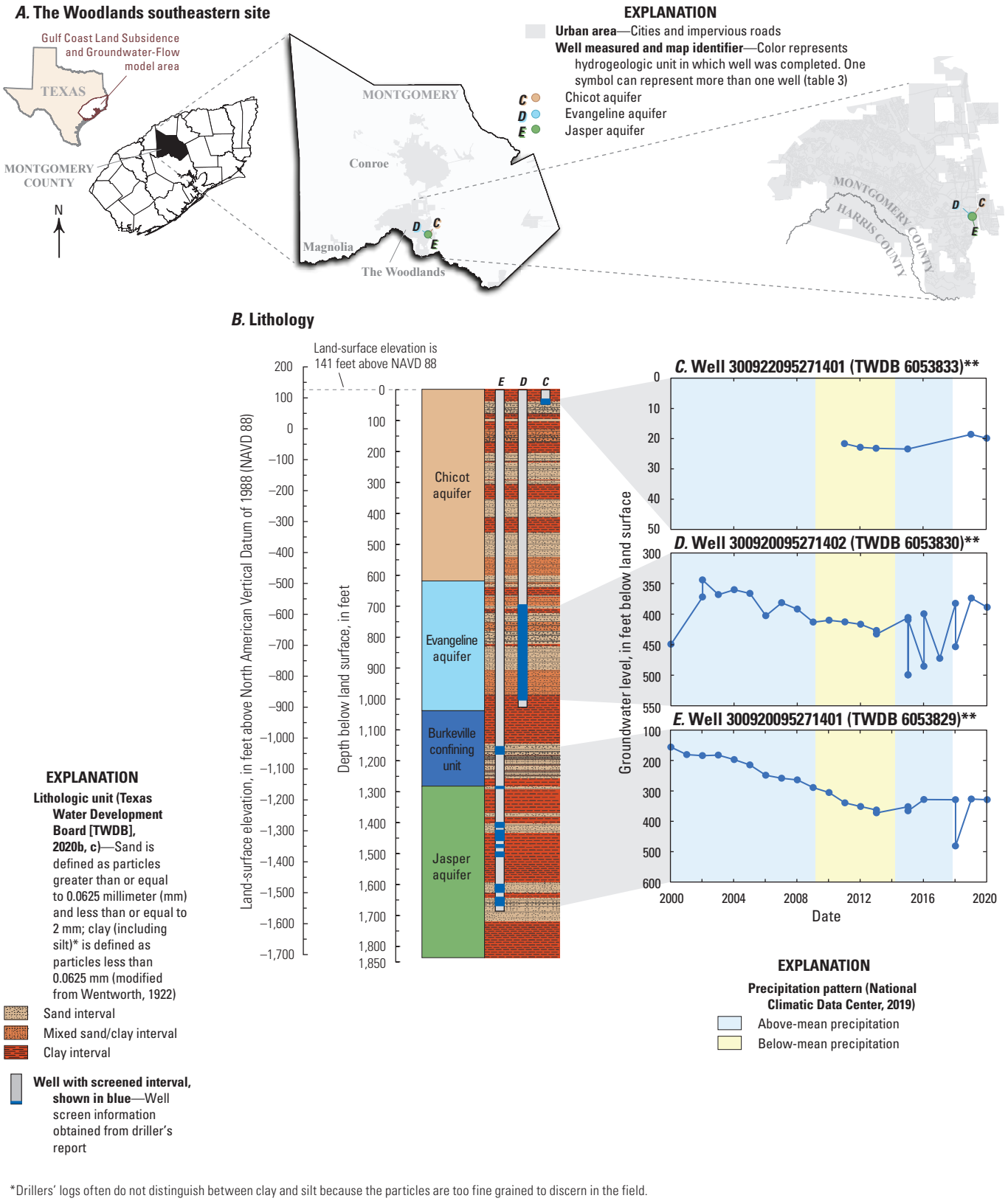

*Drillers' logs often do not distinguish between clay and silt because the particles are too fine grained to discern in the field.
**The 15-digit number is the U.S. Geological Survey (2021b) well identifier. The number in parentheses is the TWDB well identifier.

Figure 47. *A*, Map showing location of The Woodlands southeastern site in Montgomery County within the Gulf Coast aquifer system study area in southeast Texas, and *B*, lithologic section with graphs *C*–*E* showing depths to groundwater (groundwater levels) and precipitation patterns during the periods of record at the colocated wells at the site.

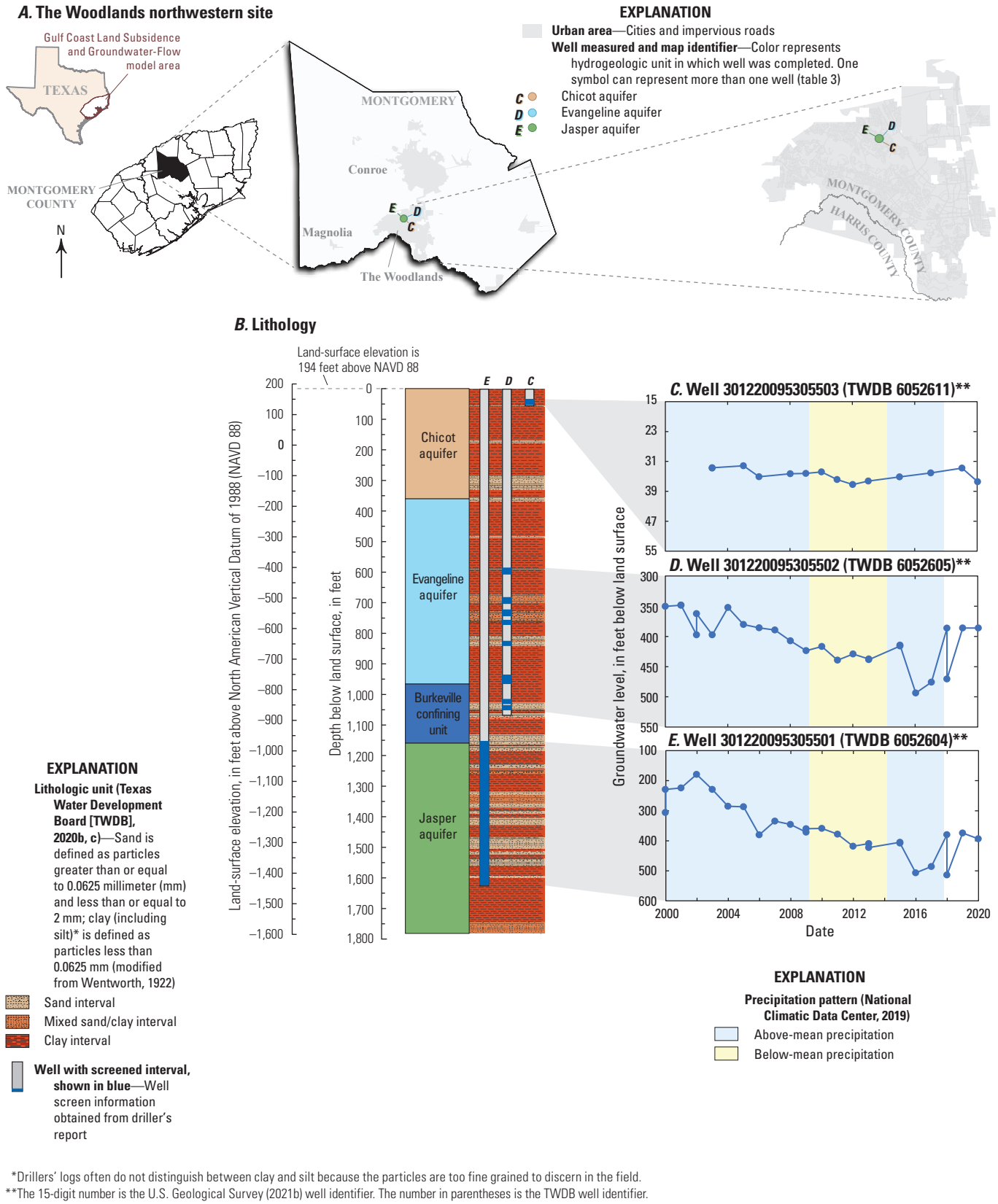

*Drillers' logs often do not distinguish between clay and silt because the particles are too fine grained to discern in the field.
**The 15-digit number is the U.S. Geological Survey (2021b) well identifier. The number in parentheses is the TWDB well identifier.

Figure 48. *A*, Map showing location of The Woodlands northwestern site in Montgomery County within the Gulf Coast aquifer system study area in southeast Texas, and *B*, lithologic section with graphs *C*–*E* showing depths to groundwater (groundwater levels) and precipitation patterns during the periods of record at the colocated wells at the site.

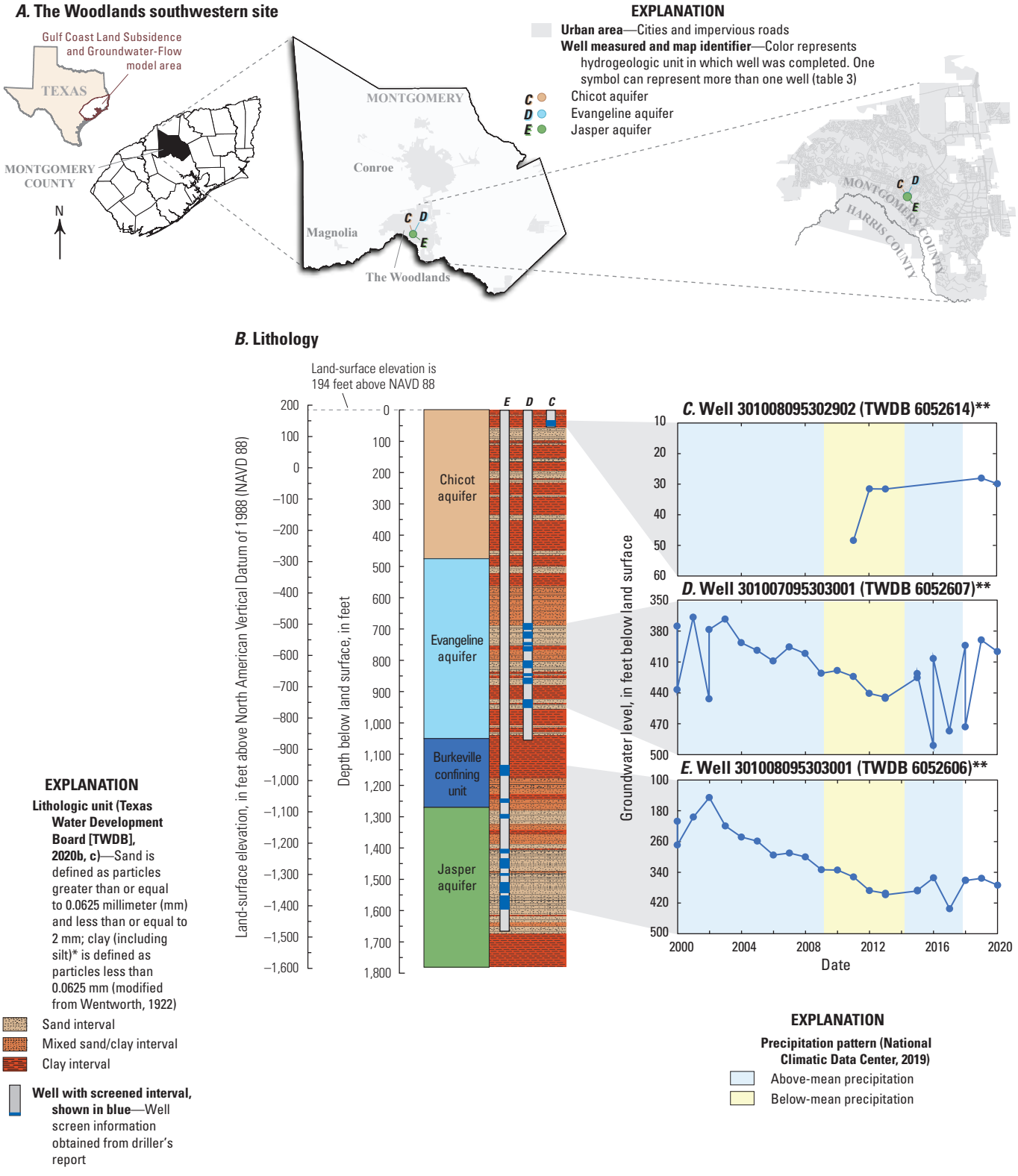

*Drillers' logs often do not distinguish between clay and silt because the particles are too fine grained to discern in the field.
**The 15-digit number is the U.S. Geological Survey (2021b) well identifier. The number in parentheses is the TWDB well identifier.

Figure 49. *A*, Map showing location of The Woodlands southwestern site in Montgomery County within the Gulf Coast aquifer system study area in southeast Texas, and *B*, lithologic section with graphs *C*–*E* showing depths to groundwater (groundwater levels) and precipitation patterns during the periods of record at the colocated wells at the site.

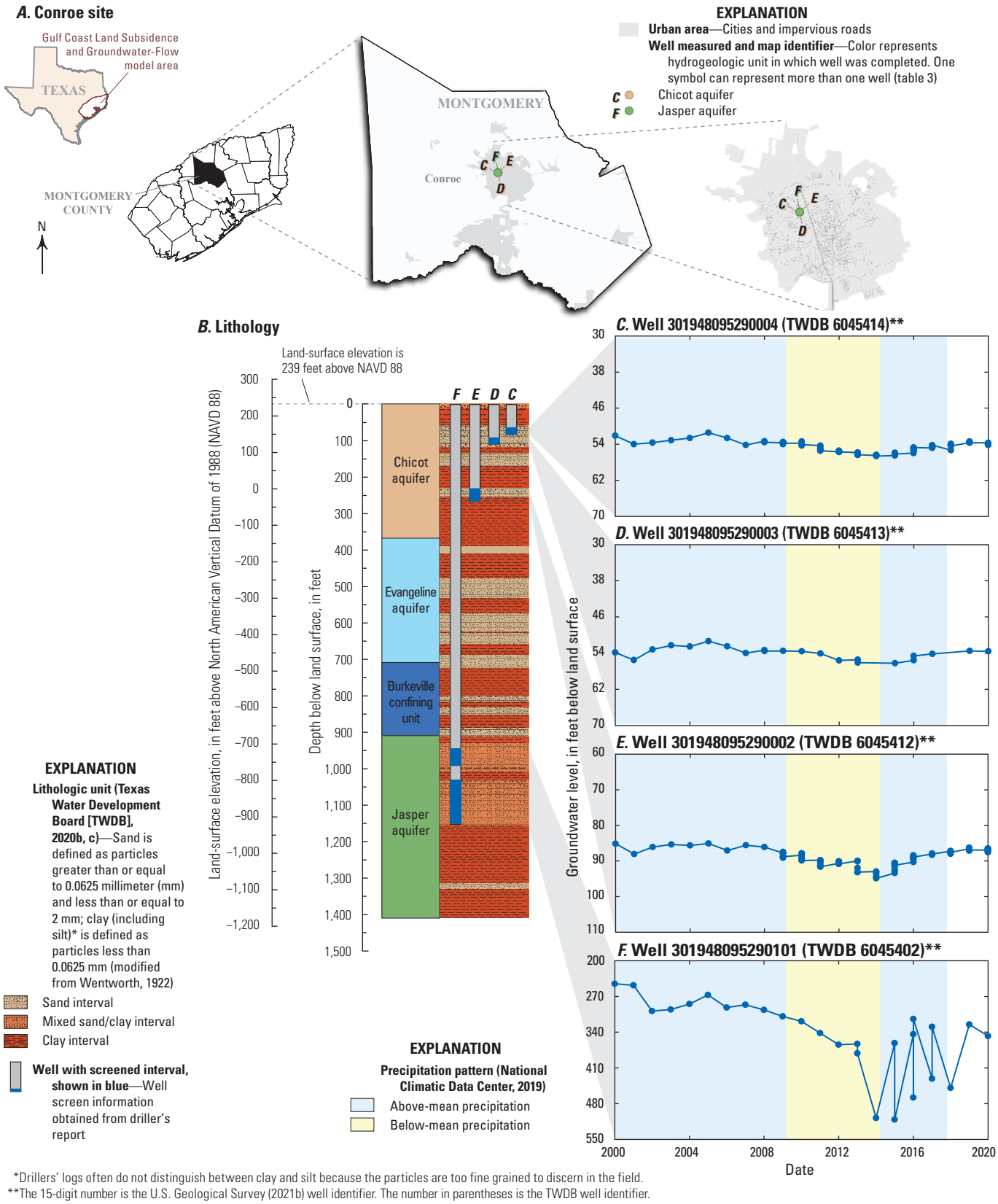

*Drillers' logs often do not distinguish between clay and silt because the particles are too fine grained to discern in the field.
**The 15-digit number is the U.S. Geological Survey (2021b) well identifier. The number in parentheses is the TWDB well identifier.

Figure 50. *A*, Map showing location of the Conroe site in Montgomery County within the Gulf Coast aquifer system study area in southeast Texas, and *B*, lithologic section with graphs *C*–*G* showing depths to groundwater (groundwater levels) and precipitation patterns during the periods of record at the colocated wells at the site.

Table 3. Wells with groundwater-level measurements located at extensometers and at colocated groundwater sites within the Gulf Coast aquifer system study area in southeast Texas.

[USGS well ID is the well identifier used by the U.S. Geological Survey (USGS; USGS, 2021b); TWDB well ID is the well identifier used by the Texas Water Development Board (TWDB; 2020b); ft, foot; bls, below land surface; --, not available]

USGS well ID	TWDB well ID	Identifier for colocated well in this report (figs. 37–50)[1]	Site name (figs. 37–50)	Aquifer unit[2] (figs. 37–50)	Well depth, in ft (figs. 37–50)	Top of screen (bls, in ft)[3]	Bottom of screen (bls, in ft)[3]	Top of screen (altitude, in ft)[3]	Bottom of screen (altitude, in ft)[3]
294237095093201	6523319	C	Pasadena extensometer site (fig. 37)	Chicot aquifer	34	24	34	4	−6
294237095093203	6523321	D		Chicot aquifer	100	90	100	−62	−72
294237095093202	6523320	E		Chicot aquifer	390	380	390	−352	−362
294237095093208	6523326	F		Chicot aquifer	730	715	725	−687	−697
294237095093206	6523324	G		Chicot aquifer	936	921	931	−893	−903
294237095093205	6523323	H		Chicot aquifer	1,328	1,313	1,323	−1,285	−1,295
294237095093207	6523325	I		Evangeline aquifer	1,817	1,802	1,812	−1,774	−1,784
294237095093204	6523322	J		Burkeville confining unit	2,831	2,707	2,717	−2,679	−2,689
294527095014913	6516933	C	Baytown extensometer site (fig. 38)	Chicot aquifer	60	30	60	−6	−36
294527095014902	6516922	D		Chicot aquifer	110	102	110	−78	−86
294527095014903	6516923	E		Chicot aquifer	170	162	170	−138	−146
294527095014905	6516925	F		Chicot aquifer	324	316	324	−292	−300
294527095014910	6516930	G		Chicot aquifer	431	420	430	−396	−406
294527095014901	6516904	H		Chicot aquifer	512	418	500	−394	−476
294527095014912	6516932	I		Chicot aquifer	1,365	1,355	1,365	−1,331	−1,341
294527095014911	6516931	J		Evangeline aquifer	1,475	1,455	1,465	−1,431	−1,441
294726095351101	6512725	C	Addicks extensometer site (fig. 39)	Chicot aquifer	49	29	49	61	41
294726095351103	6512728	D		Chicot aquifer	153	147	153	−57	−63
294726095351104	6512729	E		Chicot aquifer	237	231	237	−141	−147
294724095351401	6512717	F		Evangeline aquifer	1,575	664	1,565	−573	−1,474
294726095351102	6512726	G		Evangeline aquifer	1,802	1,643	1,653	−1,552	−1,562
294728095200105	6514745	C	Northeast extensometer site (fig. 40)	Chicot aquifer	298	283	293	−237	−247
294728095200103	6514738	D		Chicot aquifer	487	472	482	−426	−436
294728095200104	6514742	E		Chicot aquifer	1,035	1,020	1,030	−974	−984
294728095200102	6514735	F		Evangeline aquifer	1,596	1,567	1,577	−1,521	−1,531
294728095200106	6514746	G		Evangeline aquifer	2,170	2,099	2,119	−2,053	−2,073

Table 3. Wells with groundwater-level measurements located at extensometers and at colocated groundwater sites within the Gulf Coast aquifer system study area in southeast Texas.—Continued

[USGS well ID is the well identifier used by the U.S. Geological Survey (USGS; USGS, 2021b); TWDB well ID is the well identifier used by the Texas Water Development Board (TWDB; 2020b); ft, foot; bls, below land surface; --, not available]

USGS well ID	TWDB well ID	Identifier for colocated well in this report (figs. 37–50)[1]	Site name (figs. 37–50)	Aquifer unit[2] (figs. 37–50)	Well depth, in ft (figs. 37–50)	Top of screen (bls, in ft)[3]	Bottom of screen (bls, in ft)[3]	Top of screen (altitude, in ft)[3]	Bottom of screen (altitude, in ft)[3]
295449095083401	6507902	C	Lake Houston extensometer site (fig. 41)	Chicot aquifer	196	176	196	−126	−146
295451095083901	6507904	D		Chicot aquifer	540	350	535	−293	−478
295449095084103	6507907	E		Chicot aquifer	699	685	695	−631	−641
295449095084104	6507908	F		Chicot aquifer	1,048	1,033	1,043	−979	−989
295449095084102	6507906	G		Evangeline aquifer	1,503	1,488	1,498	−1,434	−1,444
295449095084105	6507909	H		Evangeline aquifer	1,940	1,861	1,871	−1,809	−1,819
295449095084101	6507905	I		Jasper aquifer	2,592	2,548	2,568	−2,494	−2,514
294338095270405	6521228	C	Southwest extensometer site (fig. 42)	Chicot aquifer	253	238	248	−182	−192
294338095270406	6521229	D		Chicot aquifer	627	612	622	−556	−566
294338095270401	6521201	E		Chicot aquifer	1,051	554	1,031	−498	−975
294338095270404	6521227	F		Evangeline aquifer	1,433	1,418	1,428	−1,362	−1,372
294338095270403	6521230	G		Evangeline aquifer	1,943	1,928	1,938	−1,872	−1,882
294338095270402	6521226	H		Burkeville confining unit	2,358	2,316	2,336	−2,257	−2,277
293352095011607	6532631	C	Seabrook extensometer site (fig. 43)	Chicot aquifer	24	16	21	−8	−13
293352095011604	6532628	D		Chicot aquifer	150	140	150	−132	−142
293352095011605	6532629	E		Chicot aquifer	300	290	300	−282	−292
293352095011606	6532630	F		Chicot aquifer	920	910	920	−902	−912
293352095011603	6532627	G		Chicot aquifer	1,308	1,298	1,308	−1,290	−1,300
293352095011601	6532625	H		Chicot aquifer	1,381	1,350	1,360	−1,342	−1,352
292458094534207	6433921	C	Texas City extensometer site (fig. 44)	Chicot aquifer	24	16	21	−11	−16
292458094534201	6433915	D		Chicot aquifer	210	200	210	−195	−205
292458094534202	6433916	E		Chicot aquifer	302	292	302	−287	−297
292458094534203	6433917	F		Chicot aquifer	400	390	400	−385	−395
292458094534204	6433918	G		Chicot aquifer	535	525	535	−520	−530
292458094534206	6433920	H		Chicot aquifer	800	780	790	−774	−784
292458094534205	6433919	I		Chicot aquifer	1,060	1,050	1,060	−1,045	−1,055

Table 3. Wells with groundwater-level measurements located at extensometers and at colocated groundwater sites within the Gulf Coast aquifer system study area in southeast Texas.—Continued

[USGS well ID is the well identifier used by the U.S. Geological Survey (USGS; USGS, 2021b); TWDB well ID is the well identifier used by the Texas Water Development Board (TWDB; 2020b); ft, foot; bls, below land surface; --, not available]

USGS well ID	TWDB well ID	Identifier for colocated well in this report (figs. 37–50)[1]	Site name (figs. 37–50)	Aquifer unit[2] (figs. 37–50)	Well depth, in ft (figs. 37–50)	Top of screen (bls, in ft)[3]	Bottom of screen (bls, in ft)[3]	Top of screen (altitude, in ft)[3]	Bottom of screen (altitude, in ft)[3]
300825095274801	6053725	C	The Woodlands southern site (fig. 45)	Chicot aquifer	39	26	36	111	101
300824095274702	6053720	D		Chicot aquifer	85	65	85	71	51
300824095274701	6053718	E		Chicot aquifer	246	226	246	−90	−110
300816095274701	6053709	F		Evangeline aquifer	944	700	934	−564	−798
300823095275001	6053713	G		Jasper aquifer	1,710	1,145	1,710	−1,008	−1,573
301234095255802	6053215	C	The Woodlands eastern site (fig. 46)	Chicot aquifer	256	190	256	−64	−130
301215095255401	6053517	D		Chicot aquifer	283	241	271	−113	−143
301222095255501	6053518	E		Chicot aquifer	330	310	330	−185	−205
301234095255801	6053208	F		Evangeline aquifer	820	625	805	−499	−679
300922095271401	6053833	C	The Woodlands southeastern site (fig. 47)	Chicot aquifer	48	38	48	102	92
300920095271402	6053830	D		Evangeline aquifer	1,025	695	1,025	−553	−883
300920095271401	6053829	E		Jasper aquifer	1,686	1,174	1,666	−1,033	−1,525
301220095305503	6052611	C	The Woodlands northwestern site (fig. 48)	Chicot aquifer	54	39	49	155	145
301220095305502	6052605	D		Evangeline aquifer	1,064	644	1,054	−450	−860
301220095305501	6052604	E		Jasper aquifer	1,630	1,150	1,630	−956	−1,436
301008095302902	6052614	C	The Woodlands southwestern site (fig. 49)	Chicot aquifer	73	60	73	106	93
301007095303001	6052607	D		Evangeline aquifer	1,052	690	1,032	−524	−866
301008095303001	6052606	E		Jasper aquifer	1,680	1,130	1,668	−963	−1,501
301948095290004	6045414	C	Conroe site (fig. 50)	Chicot aquifer	80	70	80	169	159
301948095290003	6045413	D		Chicot aquifer	110	100	110	142	132
301948095290002	6045412	E		Chicot aquifer	261	241	261	−2	−22
301948095290101	6045402	F		Jasper aquifer	1,393	930	1,140	−691	−901
294327095445201		--	Fort Bend extensometer site	Evangeline aquifer	2,000	1,930	1,950	−1,830	−1,850
294206095162602	6522623	--	East End extensometer site	Chicot aquifer	64	44	64	−13	−33
294206095162601	6522622	--		Chicot aquifer	995	975	995	−944	−964

Table 3. Wells with groundwater-level measurements located at extensometers and at colocated groundwater sites within the Gulf Coast aquifer system study area in southeast Texas.—Continued

[USGS well ID is the well identifier used by the U.S. Geological Survey (USGS; USGS, 2021b); TWDB well ID is the well identifier used by the Texas Water Development Board (TWDB; 2020b); ft, foot; bls, below land surface; --, not available]

USGS well ID	TWDB well ID	Identifier for colocated well in this report (figs. 37–50)[1]	Site name (figs. 37–50)	Aquifer unit[2] (figs. 37–50)	Well depth, in ft (figs. 37–50)	Top of screen (bls, in ft)[3]	Bottom of screen (bls, in ft)[3]	Top of screen (altitude, in ft)[3]	Bottom of screen (altitude, in ft)[3]
293348095070602	6532426	--	Clear Lake extensometer site	Chicot aquifer	392	377	387	−358	−368
293357095070801	6532410	--		Chicot aquifer	630	520	620	−500	−600
293348095070603	6532427	--		Chicot aquifer	957	942	952	−923	−933
293348095070601	6532425	--		Chicot aquifer	1,232	1,217	1,227	−1,198	−1,208
293349095070901	6532424	--		Evangeline aquifer	1,740	1,701	1,721	−1,681	−1,701
293348095070604	6532428	--		Evangeline aquifer	3,072	3,010	3,029	−2,992	−3,011
293306095054101	6532401	--	Johnson Space Center extensometer site[4]	Chicot aquifer	770	750	770	−730	−750

[1]Identifiers for colocated wells are not unique and are therefore always described in the context of a given extensometer site.

[2]Indicates the aquifer unit present at the screened interval of the well.

[3]Wells may have one or more screened intervals within this range as shown on figures 37–50.

[4]Originally named for the National Aeronautics and Space Administration Space Center, which was renamed the Johnson Space Center in February 1973.

the pattern observed in the groundwater levels measured in wells screened at greater depths (wells F through J), although the groundwater-level change in well E was less than about 55 ft compared to greater groundwater-level changes in the wells screened at greater depths, where groundwater-level changes ranged from about 70 to 289 ft. The patterns observed in groundwater levels for wells F through J were somewhat similar over time; however, the magnitudes of the changes in groundwater levels in wells F through I were much greater than the magnitude of the changes in groundwater levels in well J. An explanation for the differences in the magnitude of groundwater-level changes in wells F through I compared to well J is that well J is screened in the Burkeville confining unit and thus is surrounded by a substantial interval of fine-grained sediment (clay and silt) that decreases the hydraulic connection between well J and the overlying aquifer units. In most cases, drillers' logs obtained during the installation of wells do not distinguish between clay and silt because the particles are too fine grained to discern in the field and instead record all fine-grained sediment as clay. Fine-grained intervals are therefore referred to as clay intervals in figs. 37–50. After about 1990, the pattern of groundwater-level changes in well E was different from the pattern for wells C and D, indicating that a transition zone from a shallow zone where groundwater is under atmospheric pressure to a deeper zone where groundwater is generally under artesian pressure occurs at a depth of about 125–200 ft bls.

Groundwater-level patterns observed in wells at the Baytown extensometer site (hereinafter referred to as the "Baytown site") (fig. 38) were similar to the groundwater-level patterns observed at the Pasadena site (fig. 37). Unlike the wells at most of the other extensometer sites, the wells at the Baytown site are not screened at regularly spaced intervals by monitoring wells representing the full extent of the aquifer. Instead, six wells are screened between 30 and 500 ft bls, and two wells are screened between 1,355 and 1,465 ft bls (fig. 38; table 3). This is because most historical groundwater use in the Baytown area occurred from the Alta Loma Sand of Lang and others (1950) (fig. 10), including groundwater withdrawn by production wells. The Alta Loma Sand of Lang and others (1950) in the Baytown area is less than 600 ft bls, and nearly all of the production wells in the Baytown area are screened less than 600 ft bls (Wood, 1958a). Groundwater use in the Pasadena area was much greater than groundwater use in the adjacent Baytown area (fig. 11), and Baytown area groundwater levels in the Evangeline aquifer are appreciably affected by the extensive groundwater use in the Pasadena area (Gabrysch, 1967). In the Baytown area, groundwater levels in the Evangeline aquifer are monitored by the two deepest wells at the Baytown site (fig. 38*I–J*). Despite the large differences in screened-interval depths at the Baytown site, the groundwater-level patterns observed at all but the two shallowest wells (wells C and D) were similar, varying only in the amount of groundwater-level change. Groundwater levels between 1980 and 2020 in wells F through J at the Baytown site, representing the depth interval from 316 to 1,465 ft bls, generally differed by less than 30 ft (fig. 38*F–J*). Groundwater levels in the two shallowest wells at the Baytown site (wells C and D) reflected changes in precipitation patterns, whereas the groundwater level pattern in well E was similar to those in wells F though J (fig. 38*E–J*), differing only in the amount of groundwater-level change. Therefore, a transition zone from unconfined to confined conditions likely exists at a depth of about 125–150 ft bls.

At the Addicks extensometer site (hereinafter referred to as the "Addicks site"), the groundwater-level pattern in well C showed little relation to the groundwater levels in the progressively more deeply screened wells D through G (fig. 39*C–G*; table 3). The pattern of groundwater levels in wells D and E at this site was similar in terms of the magnitude of the groundwater-level declines and temporal changes in groundwater levels during 1977–97, the period when groundwater levels were recorded at both wells. During 1977–97, groundwater-level patterns observed in wells D and E at the Addicks site were also similar to the groundwater-level patterns observed in wells F and G, although the magnitude of the groundwater-level decline was much less in wells D and E than in wells F and G. On the basis of the groundwater-level data collected at the Addicks site, a transition zone from unconfined to confined conditions likely occurs at a depth of about 100–125 ft bls.

Groundwater-level data collected at five additional extensometer sites were similarly used to estimate the transition zone from unconfined to confined conditions. The transition zones were estimated as follows: 175–225 ft bls at the Northeast extensometer site (hereinafter referred to as the "Northeast site") (fig. 40); 100–150 ft bls at the Lake Houston extensometer site (hereinafter referred to as the "Lake Houston site") (fig. 41); 125–175 ft bls at the Southwest extensometer site (hereinafter referred to as the "Southwest site") (fig. 42); 125–175 ft bls at the Seabrook extensometer site (hereinafter referred to as the "Seabrook site") (fig. 43); and 120–150 ft bls at the Texas City extensometer site (hereinafter referred to as the "Texas City site") (fig. 44).

Colocated well sites in Montgomery County (five in and near The Woodlands and one in Conroe) (figs. 45–50; table 3) provide insights into patterns of groundwater-level variability during 2000–20 in this part of the study area. Water-level data from these collocated sites were also useful for estimating the depth range where the groundwater transitions from unconfined to confined groundwater conditions. Patterns of groundwater levels and insights regarding the transition zone are described for selected colocated well sites in Montgomery County.

During 2000–20, the groundwater levels at the two most shallowly screened wells at The Woodlands southern site varied by 2.2 and 9.8 ft, respectively (fig. 45*C–D*). The ranges of groundwater levels in wells C and D were much less compared to the ranges of groundwater levels in the more deeply screened wells at The Woodlands southern site (fig. 45*F–G*). During 2000–20, groundwater levels in well E varied by about 39 ft, which was greater than the ranges in groundwater

levels for wells C and D but less than the ranges of groundwater levels in the two deepest wells (wells F–G). Patterns of overall rising groundwater levels were observed during the last 6 years of the 2000–20 period in the three deepest wells (fig. 45*E–G*). Patterns of groundwater declines from about 2001 through 2014 were evident in the two deepest wells (fig. 45*F–G*). On the basis of the observed water-level range of well E, the transition zone from unconfined to confined groundwater conditions at The Woodlands southern site is likely about 200–250 ft bls.

The Woodlands eastern site includes three wells completed in the Chicot aquifer (wells C–E, fig. 46) screened between 190 and 330 ft bls (table 3), in the middle and lower parts of the Chicot aquifer. Excluding groundwater-level measurements made when groundwater was being withdrawn, the range of groundwater levels in well C at The Woodlands eastern site was about 19 ft during 2005–20, compared to the greater range of groundwater levels measured in colocated wells screened in deeper zones of the aquifer (fig. 46). The range in groundwater-level changes of about 19 ft during 2005–20 in well C at The Woodlands eastern site was slightly greater than the range in groundwater-level changes in the shallow wells at The Woodlands southern and Conroe sites (figs. 45, 50). The ranges of groundwater-level changes in wells D and E during 2000–20 were about 16 and 38 ft, respectively, compared to a range of about 140 ft in well F (fig. 46). Fewer water-level measurements were made at well E where the overall water-level record was from a shorter period compared to the length of the water-level record for other colocated wells at this site or other sites. The screen of well E is slightly less than 300 ft vertically from the top of the colocated production well (well F) (table 3). On the basis of a larger range of groundwater-level changes in well E compared to wells C and D and increasing similarity in the pattern of groundwater levels measured in well E to the pattern of groundwater levels measured in well F, the transition zone at The Woodlands eastern site is estimated to be about 250 ft bls, or near the screened intervals of well C. The groundwater levels from three other colocated sites near The Woodlands (The Woodlands southeastern, northwestern, and southwestern sites (figs. 47–49) followed similar patterns to the groundwater levels at The Woodlands southern and eastern sites (figs. 45–46).

At the Conroe site, groundwater levels varied by about 5 ft during 2000–20 for wells C and D, the two most shallowly screened wells (fig. 50*C–D*). The groundwater-level patterns observed in wells C and D and in well F (the production well) (fig. 50*F*) were somewhat similar. Any similarities in groundwater-level patterns may be coincidental, however, considering that groundwater levels in wells C and D only varied by about 5 ft during 2000–20, whereas groundwater levels varied by about 140 ft in well F (excluding groundwater levels during periods of active groundwater withdrawal). Likewise, a minor similarity in groundwater levels occurs between wells D and E, where the groundwater-level change in well E was about 10 ft during 2000–20. The other colocated sites in Montgomery County described previously (figs. 44–49) include a production well screened in the Evangeline aquifer, whereas the Conroe site has a production well screened exclusively in the Jasper aquifer. At the Conroe site, this increased vertical distance between the shallow monitoring wells (wells C–E) and the production well (well F) complicates the estimation of the transition zone. Based on the available data showing an increased similarity in the groundwater-level pattern between wells E and F, the transition zone likely occurs near the screened interval of well E (table 3). Therefore, this transition zone is estimated to be about 200–250 ft bls.

Hydrogeologic System Conceptualization

On the basis of patterns observed in the colocated well data at the extensometer sites (figs. 37–44), the mean transition zone is about 125–170 ft below land surface. The shallow depth intervals of the transition zones at these sites reflect the presence of the Beaumont Formation and associated substantial fine-grained sediment that generally creates confining conditions close to land surface in the part of the study area where these extensometer sites are located. This substantial amount of fine-grained sediment is shown on the lithologic sections at the extensometer sites (figs. 37–44). The transition zone between generally unconfined and confined conditions in the outcrop area at the colocated sites (figs. 45–50) probably occurs at a depth interval between about 200 and 250 ft bls in the outcrop area (fig. 8). Groundwater levels measured in shallow screened wells have remained relatively stable over time, even as groundwater levels steadily declined over time in adjacent deeply screened wells where the groundwater is under confined conditions. The groundwater levels above the transition to confined conditions closely reflect the effects of precipitation on the outcrop area, rising during periods of abundant precipitation and falling during periods of scant precipitation (White and others, 1944; Lang and others, 1950). Hereinafter, the depth interval above this transition zone generally representing water-table conditions is referred to as the "shallow groundwater system."

During the approximate 50-year period at the extensometer sites (1970–2020), groundwater-level patterns in the Chicot and Evangeline aquifers (below the shallow groundwater system) were similar (figs. 37–44). The similarity of groundwater-level patterns in the Chicot and Evangeline aquifers at different depth intervals for wells in the Houston-Galveston region was observed as far back as 1932 (in White and others, 1939) and 1937 (in White and others, 1944), respectively—about four decades prior to the installation of most of the extensometers. In 1932, the pattern of groundwater-level changes (rises and declines in groundwater levels) in all but the shallowest wells in the historical Houston area were observed to occur concurrently (White and others, 1939). In 1937, groundwater-level declines in wells near where the Pasadena site would be installed differed according to the depth of the screened intervals, with smaller declines in the more deeply screened wells and larger declines in the more shallowly screened wells (White and others, 1944). However,

the pattern of groundwater-level declines in all the wells at the Pasadena site was nearly the same even though thick beds of fine-grained sediments separate many of the water-production zones (White and others, 1944). Thus, there is a hydrologic connection between many of the water-production zones at various depth intervals (White and others, 1944), which is evident because of the similar groundwater-level patterns at the different depth intervals at the extensometer sites during about 1970–2020 and during the 1930s (as described in White and others, 1939, 1944). By comparison, few long-term water-level measurements are available from wells completed in the middle to lower parts of the Chicot aquifer in Montgomery County and adjacent counties. However, a confining unit does not separate the Chicot and Evangeline aquifers, thus allowing groundwater to flow between these two aquifers (Kasmarek and others, 2010; Oden and Truini, 2013; Liu and others, 2019). These aquifers are therefore hydraulically connected (Kearns and others, 2015) and can be considered to function as a single system in much of the study area (hereinafter, the "intermediate groundwater system") (Lang and others, 1950; Winslow and Wood, 1959). This intermediate groundwater system is generally similar to the groundwater system described in Kasmarek and Robinson (2004) and is synonymous with the Chicot and Evangeline aquifers (undifferentiated) presented in Braun and Ramage (2022).

Beneath the intermediate groundwater system, the Burkeville confining unit impedes the downward movement of water to the Jasper aquifer and Catahoula confining unit (fig. 9) (Turcan and others, 1966; Baker, 1986). Given the prevailing thickness of the Burkeville confining unit and its ability to impede the vertical movement of water, groundwater levels in the Jasper aquifer and Catahoula confining unit in much of the study area respond independently from groundwater levels in the overlying Chicot and Evangeline aquifers, although in the outcrop area (figs. 8–9), the thickness and confining properties of the Burkeville confining unit are less certain. Although the Catahoula confining unit is itself not classified as an aquifer, the shallow subsurface interval of this unit contains a high sand content (Baker, 1986), and wells screened in this high sand content layer produce water in some areas (fig. 12) (TWDB, 2020b). The hydraulic separation of the Jasper aquifer and Catahoula confining unit from the overlying units means that the Jasper aquifer and Catahoula confining unit can collectively be considered a deep groundwater system.

Hydrogeologic Unit Outcrop Areas

In the outcrop areas of the geologic units that contain the Evangeline aquifer, Burkeville confining unit, Jasper aquifer, and Catahoula confining unit (fig. 8), hydrographs of groundwater levels indicate that most groundwater levels generally are stable and have few long-term temporal patterns (figs. 51–52; table 2). Groundwater-level fluctuations for most wells are generally within a range of about plus or minus 20 ft. Sustained groundwater-level declines have occurred, however, for wells screened in the deeper parts of the outcrop area (fig. 9) (fig. 51*D, F, I*) independent of climate patterns in many of the wells measured during the study period. Thus, these groundwater-level declines have occurred because of long-term groundwater use in and near the outcrop area.

Streamflow and Base Flow

Most of the water that enters the Gulf Coast aquifer system infiltrates downward/downdip from the outcrop area (fig. 8) to the topographically controlled shallow groundwater system. Groundwater then flows horizontally to nearby streams where the water is discharged from the aquifer and forms the component of streamflow referred to as "base flow" (Winter and others, 1998). Groundwater discharges to streams in areas where the water table in the shallow aquifer system is higher relative to the elevation of nearby streambeds, and the amount of recharge going into the groundwater system exceeds the amount of water that can flow downdip into the intermediate and deep groundwater systems of the aquifer.

The base-flow component of streamflow was quantified at USGS streamgages in the study area (figs. 53–61) by using a base-flow separation code referred to as the base-flow index developed by Wahl and Wahl (1995) that has been integrated into the USGS Groundwater Toolbox (Barlow and others, 2015). The streamflow data were obtained from the NWIS database (USGS, 2021b). The base-flow separation method incorporated into the base-flow index code is used to identify the minimum streamflow for user-specified n-day moving increments and compares this streamflow to adjacent minimums to determine turning points on a base-flow hydrograph. The ratio of base flow to the total streamflow is the base-flow index. A base-flow index of 1 indicates that all streamflow originates from groundwater, and a base-flow index of 0 indicates that none of the streamflow originates from groundwater.

Base-flow computation at regulated streamgages can be complicated by reservoir releases and floodwater-retention structures because these releases (and the subsequent bank storage releases associated with them) are typically indistinguishable from naturally occurring base flow from the aquifer. As a result, hydrograph separation methods could overestimate base flows at regulated streamgages when these releases are present in the streamflow record. Although regulation can affect the results from base-flow separation computations, evaluation of the data from the selected streamgages in the study area indicates the base-flow values appear reasonable and do not indicate frequent patterns that are a result of upstream reservoir releases that overly disrupt the data. Each streamgage used for the analysis was in the outcrop area of study area geologic units (fig. 8) and was generally not regulated inside the study area, with the exception of USGS streamgage 08068000 West Fork San Jacinto River near Conroe, Tex. (fig. 55).

Data at streamgages in the outcrop area where there are unconfined groundwater-flow conditions show relatively stable base flow for most streamgages, and any patterns in the

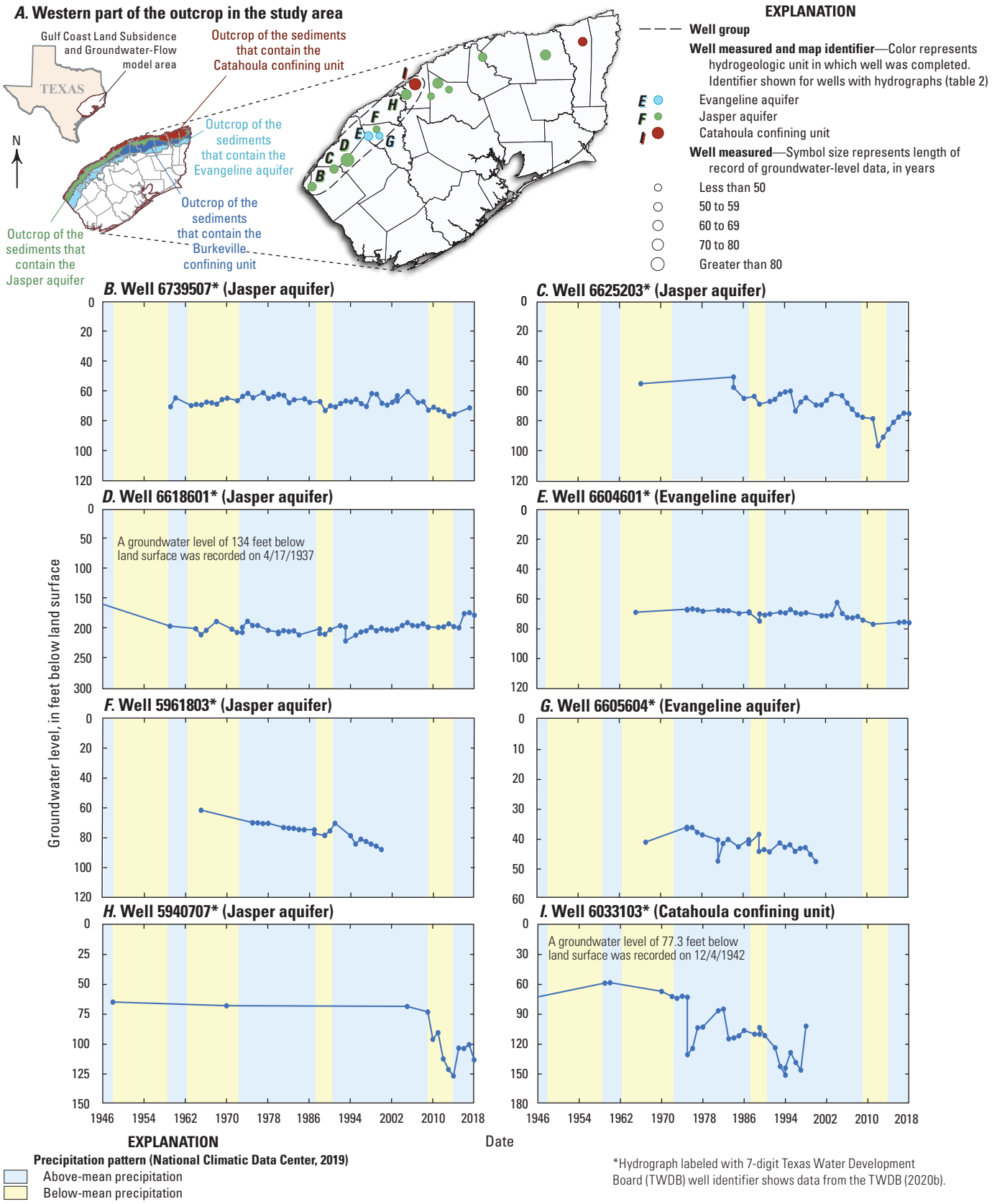

Figure 51. Depth to water for selected wells in and near the western outcrop area of hydrogeologic units in the Gulf Coast aquifer system study area.

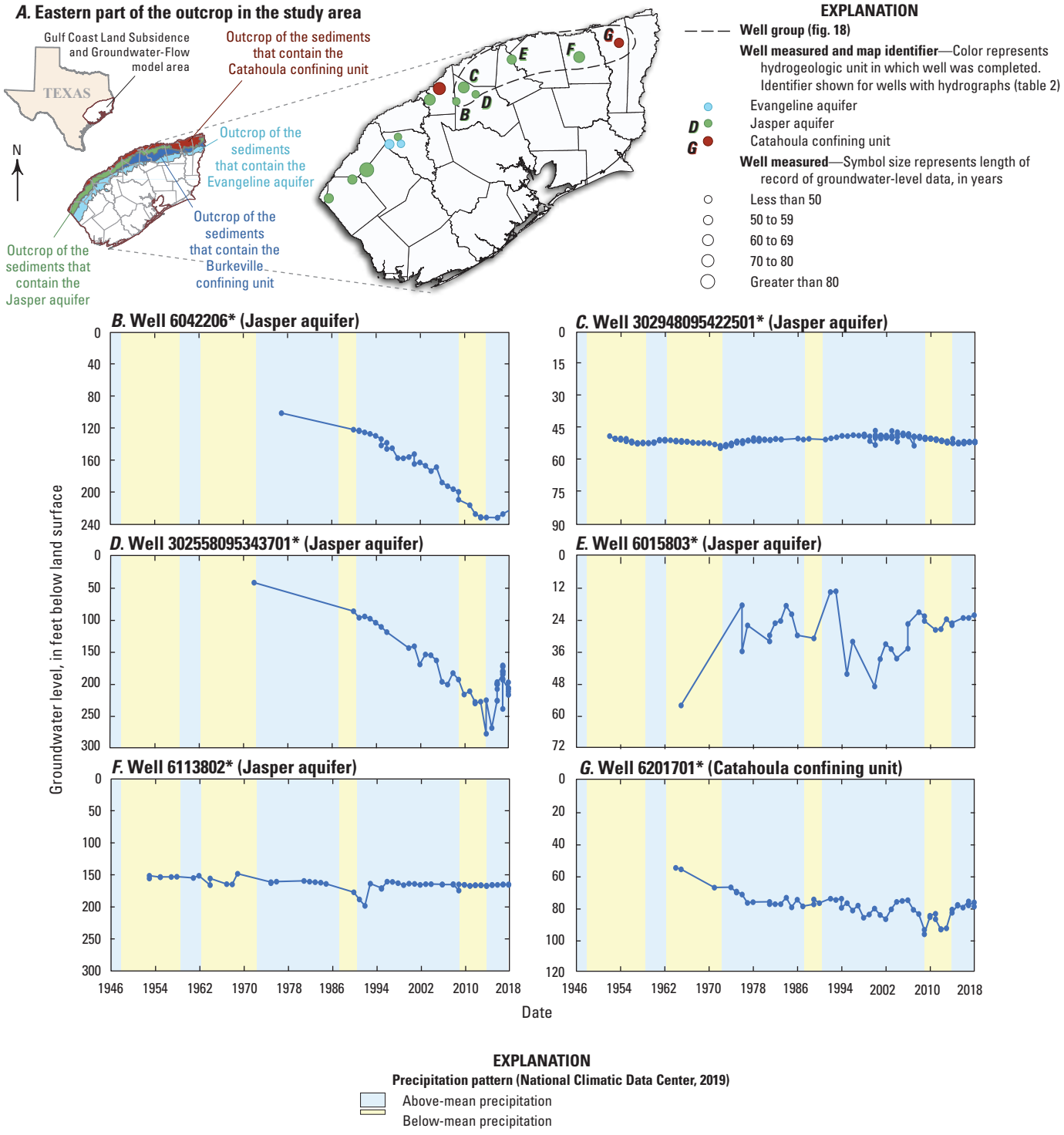

*Hydrograph labeled with 15-digit U.S. Geological Survey (USGS) well identifier shows data from the USGS (2021b). Hydrograph labeled with 7-digit Texas Water Development Board (TWDB) well identifier shows data from the TWDB (2020b).

Figure 52. Depth to water for selected wells in and near the eastern outcrop area of hydrogeologic units in the Gulf Coast aquifer system study area.

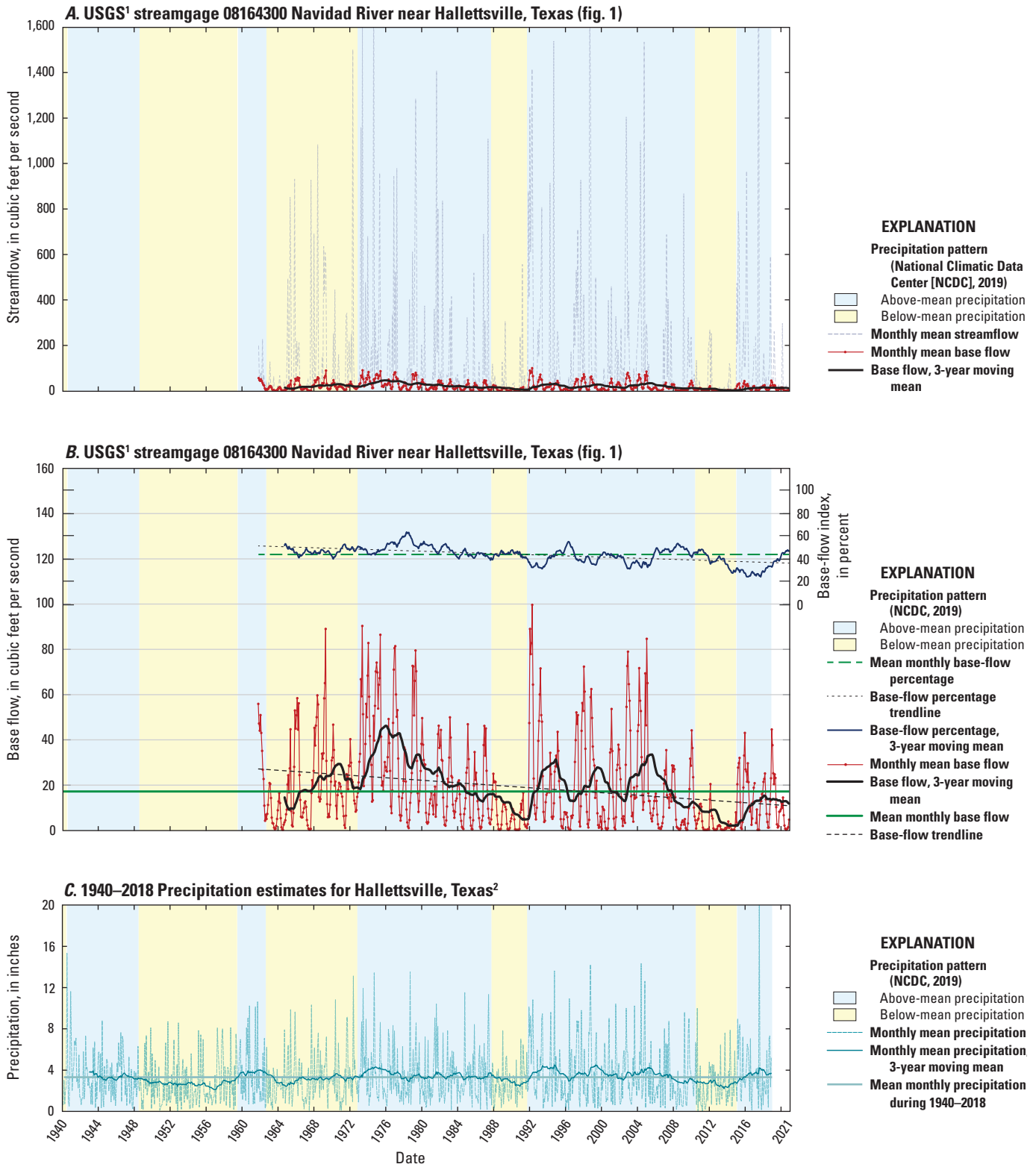

[1]U.S. Geological Survey.
[2]Interpolation of precipitation data from NCDC (2019). Climate stations are shown on fig. 62 and listed in table 4.1.

Figure 53. *A*, Streamflow, *B*, base flow, and *C*, precipitation at U.S. Geological Survey streamgage 08164300 Navidad River near Hallettsville, Texas.

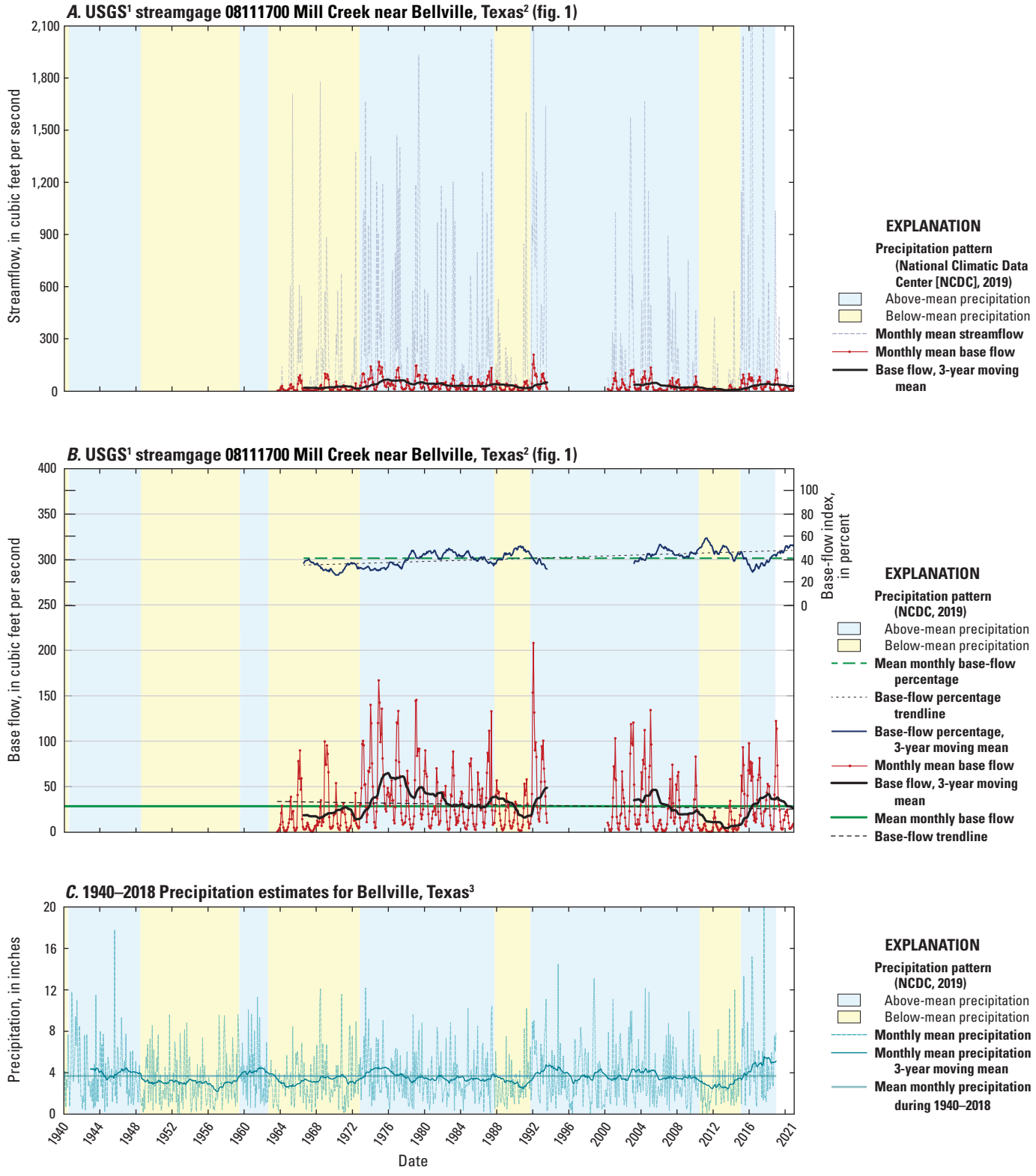

[1]U.S. Geological Survey.
[2]Streamgage operation was discontinued from October 1993 to March 2000 due to lack of funding.
[3]Interpolation of precipitation data from NCDC (2019). Climate stations are shown on fig. 62 and listed in table 4.1.

Figure 54. *A*, Streamflow, *B*, base flow, and *C*, precipitation at U.S. Geological Survey streamgage 08111700 Mill Creek near Bellville, Texas.

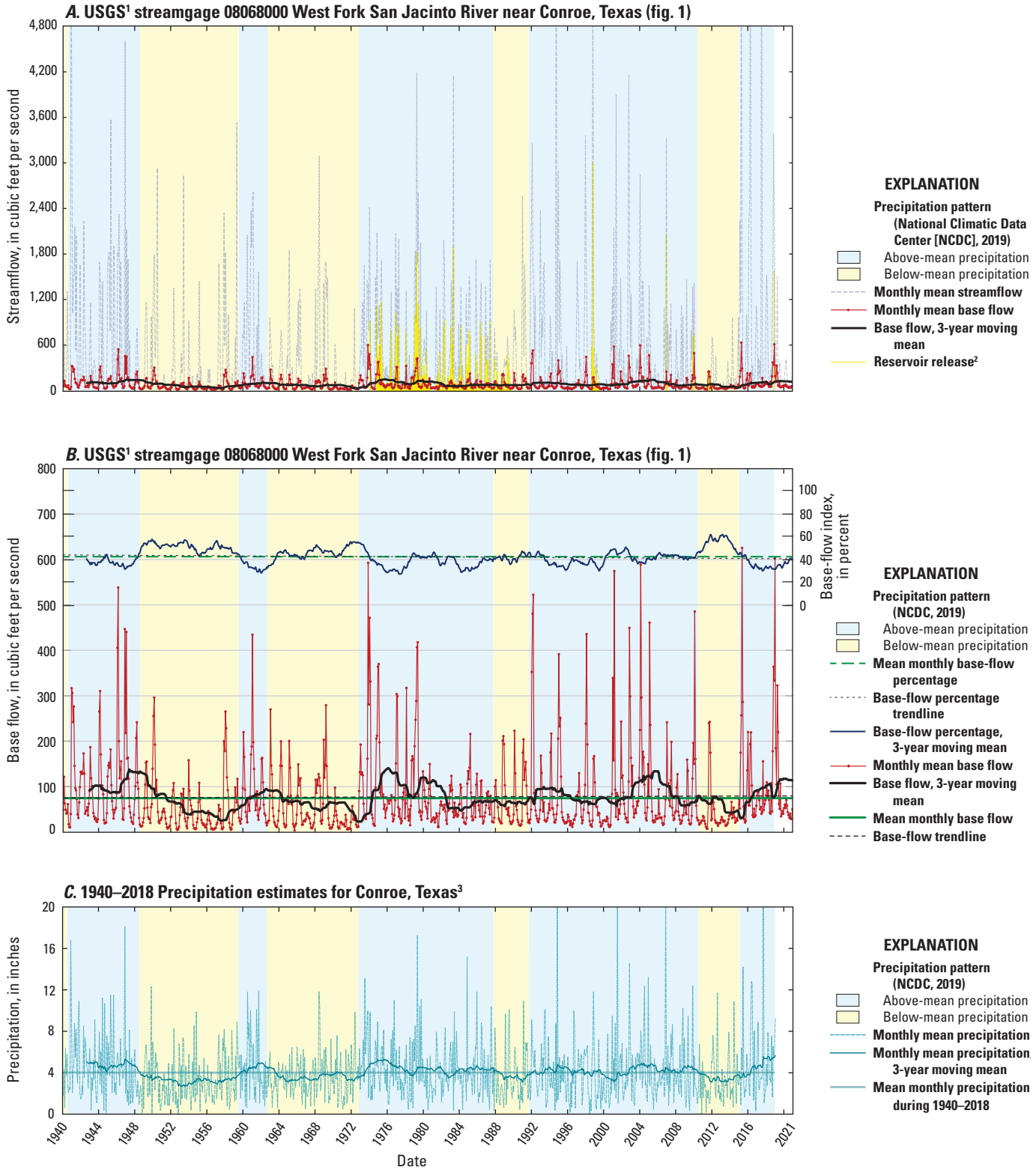

[1]U.S. Geological Survey.
[2]Releases from Lake Conroe measured at USGS streamgage 08067650 West Fork San Jacinto River below Lake Conroe near Conroe, Texas (fig. 1).
[3]Interpolation of precipitation data from NCDC (2019). Climate stations are shown on fig. 62 and listed in table 4.1.

Figure 55. *A*, Streamflow, *B*, base flow, and *C*, precipitation at U.S. Geological Survey streamgage 08068000 West Fork San Jacinto River near Conroe, Texas.

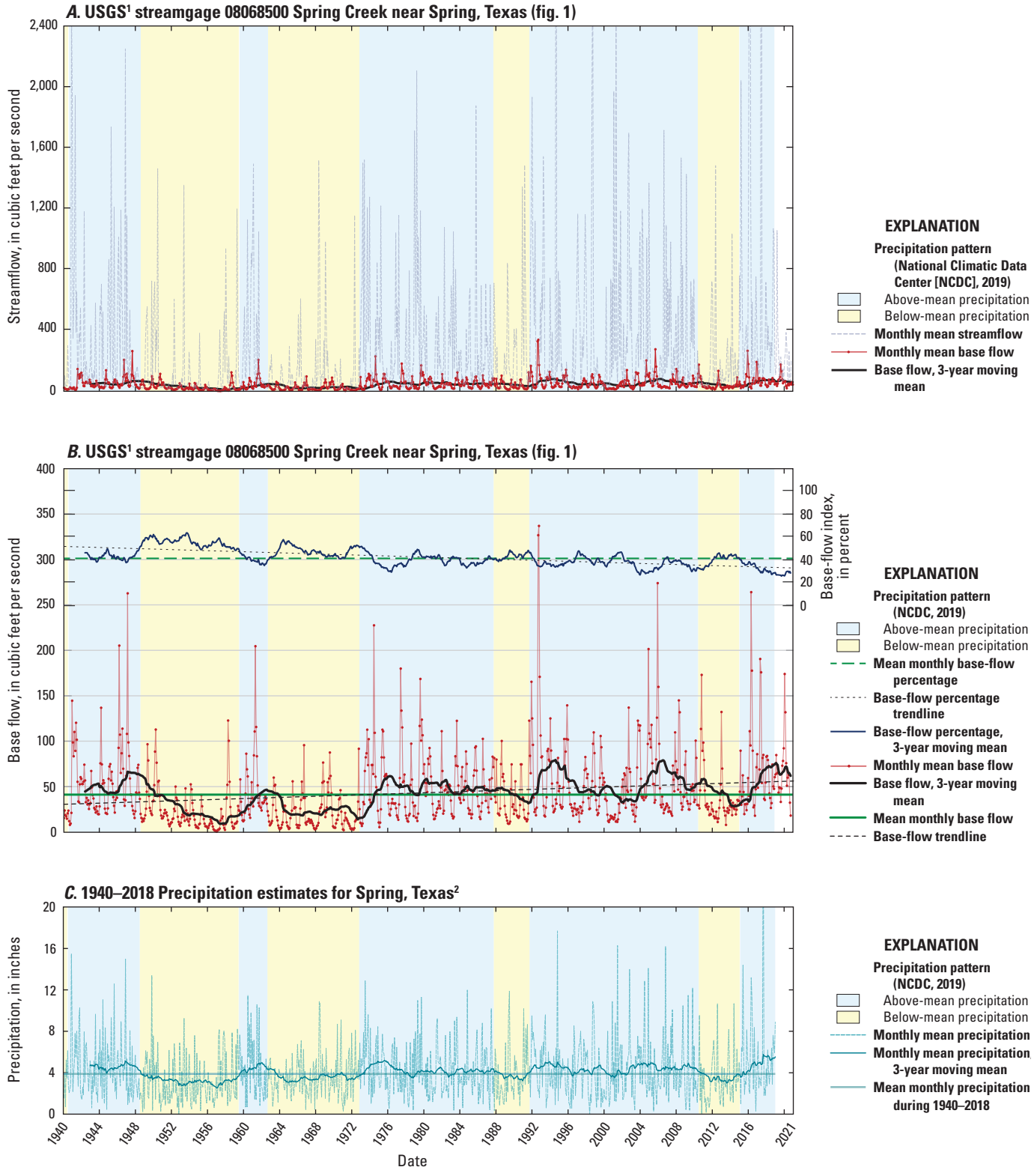

[1]U.S. Geological Survey.
[2]Interpolation of precipitation data from NCDC (2019). Climate stations are shown on fig. 62 and listed in table 4.1.

Figure 56. *A*, Streamflow, *B*, base flow, and *C*, precipitation at U.S. Geological Survey streamgage 08068500 Spring Creek near Spring, Texas.

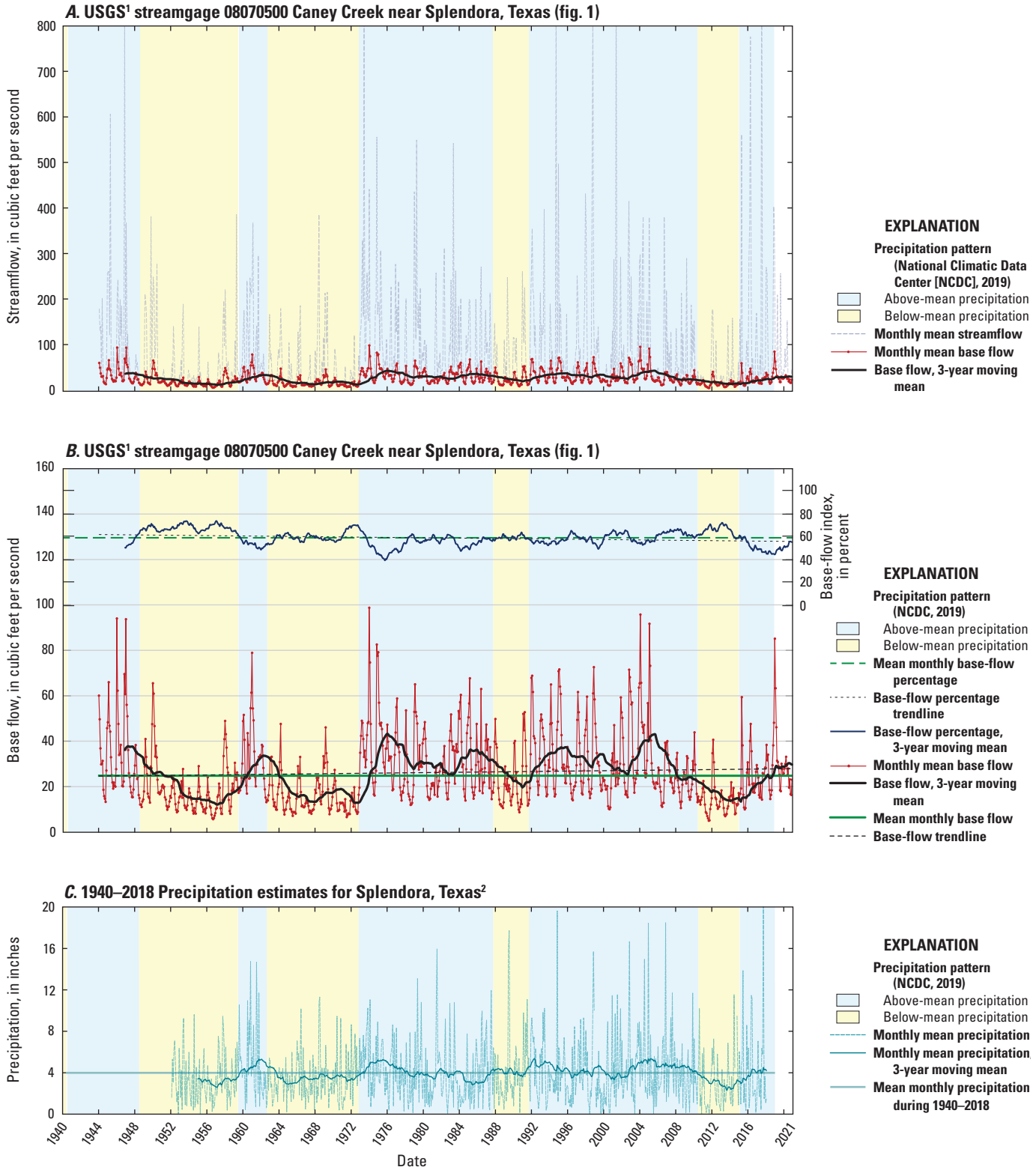

[1]U.S. Geological Survey.
[2]Interpolation of precipitation data from NCDC (2019). Climate stations are shown on fig. 62 and listed in table 4.1.

Figure 57. *A*, Streamflow, *B*, base flow, and *C*, precipitation at U.S. Geological Survey streamgage 08070500 Caney Creek near Splendora, Texas.

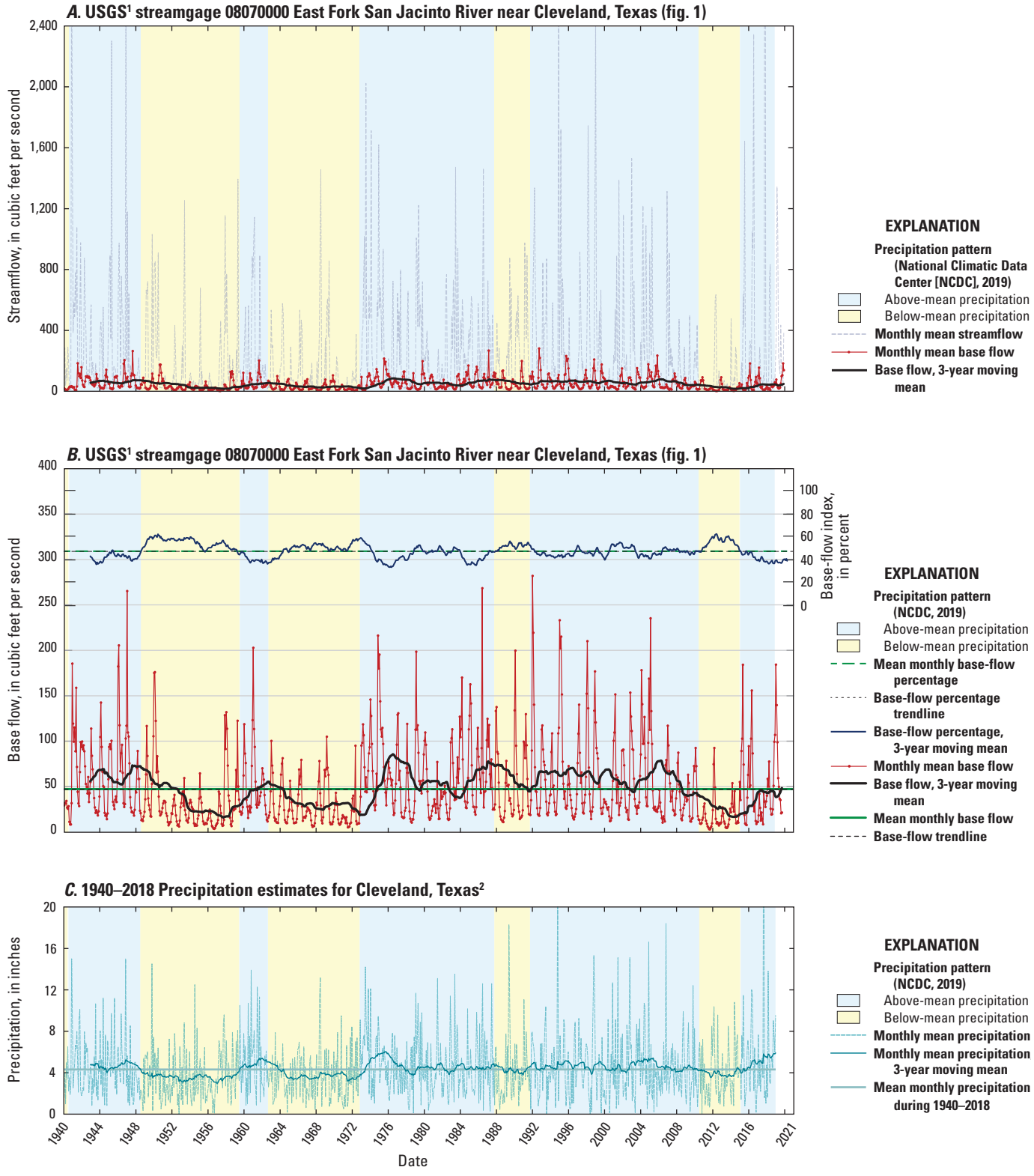

[1]U.S. Geological Survey.
[2]Interpolation of precipitation data from NCDC (2019). Climate stations are shown on fig. 62 and listed in table 4.1.

Figure 58. *A*, Streamflow, *B*, base flow, and *C*, precipitation at U.S. Geological Survey streamgage 08070000 East Fork San Jacinto River near Cleveland, Texas.

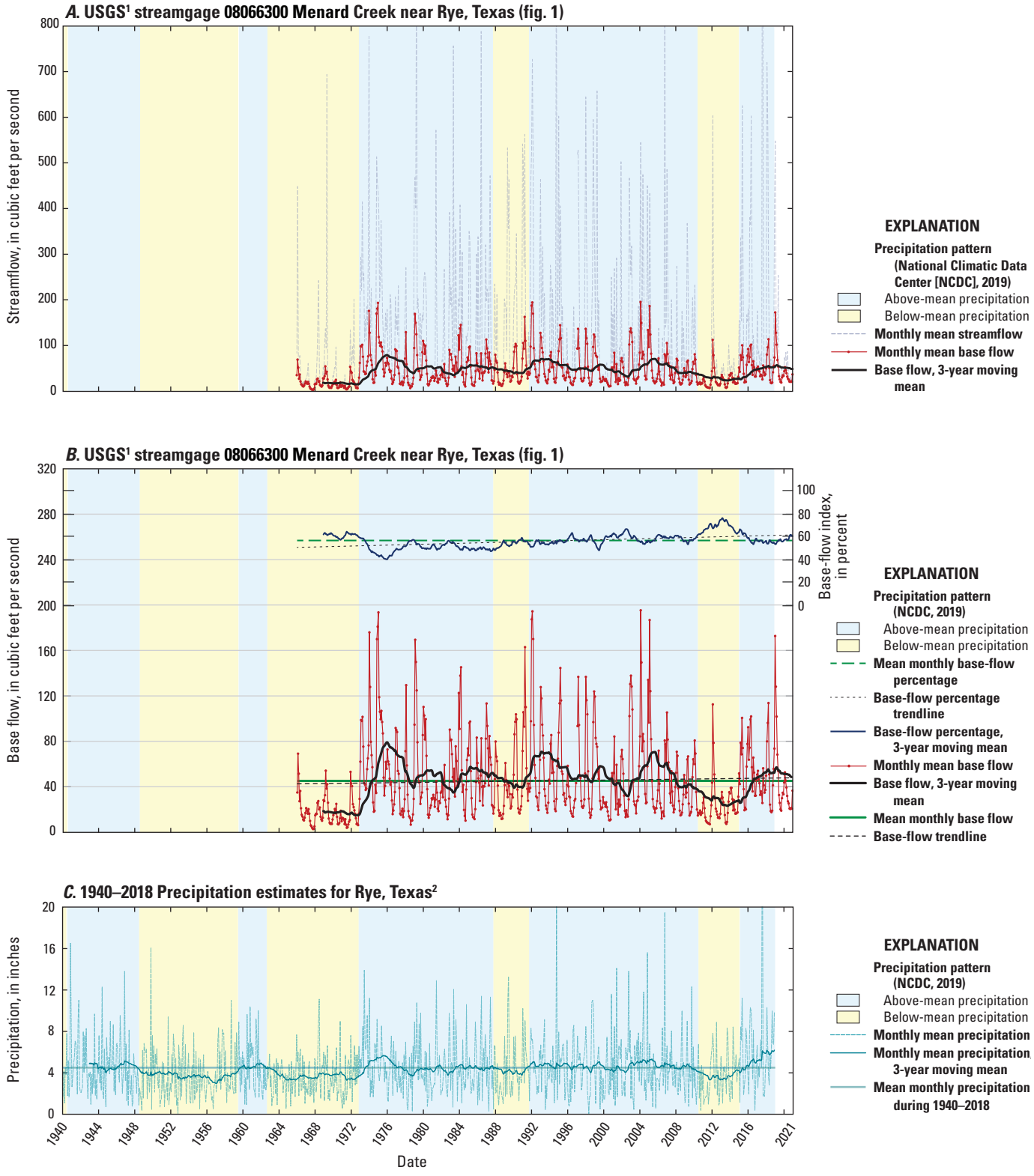

[1]U.S. Geological Survey.
[2]Interpolation of precipitation data from NCDC (2019). Climate stations are shown on fig. 62 and listed in table 4.1.

Figure 59. *A*, Streamflow, *B*, base flow, and *C*, precipitation at U.S. Geological Survey streamgage 08066300 Menard Creek near Rye, Texas.

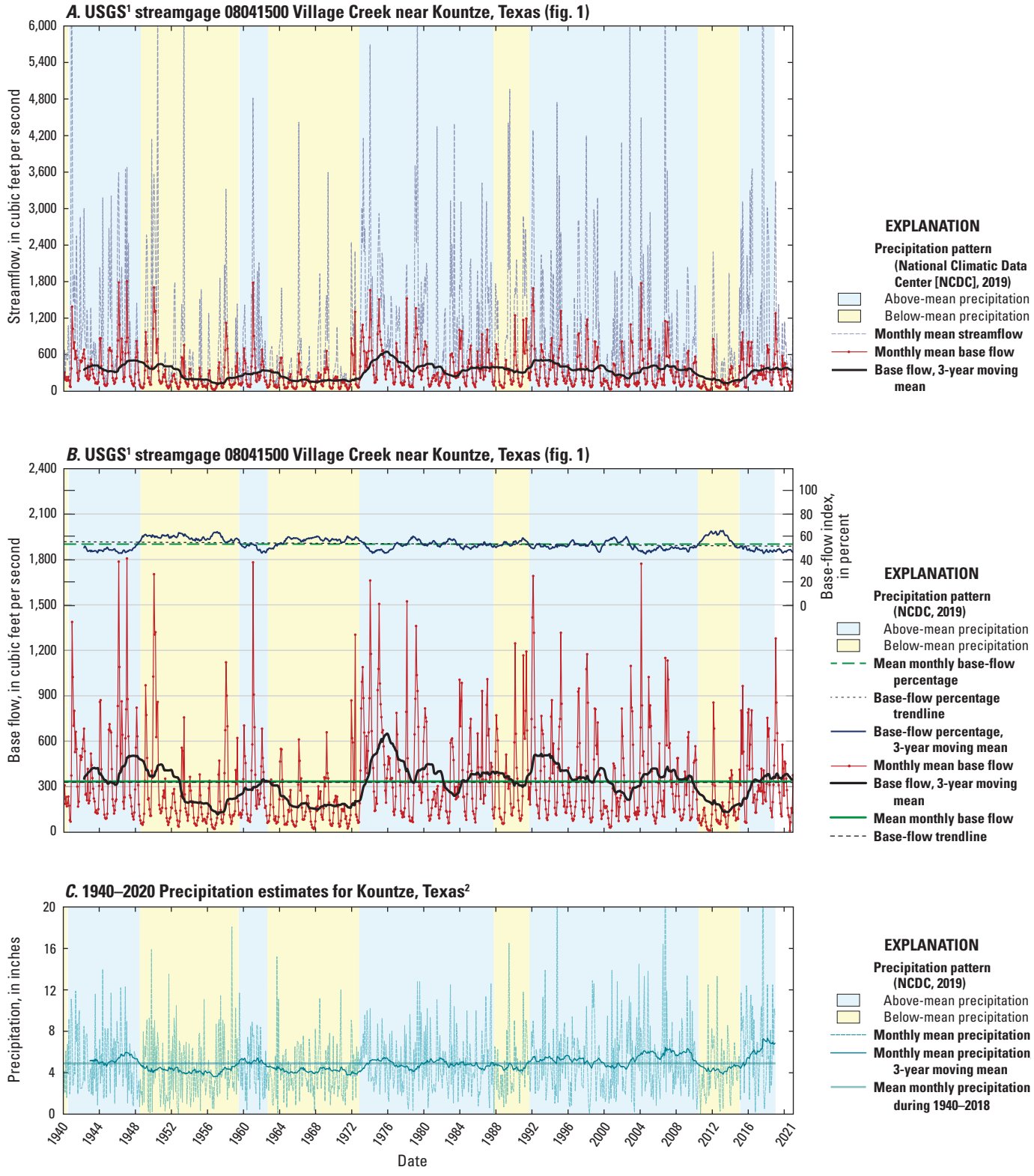

[1]U.S. Geological Survey.
[2]Interpolation of precipitation data from NCDC (2019). Climate stations are shown on fig. 62 and listed in table 4.1.

Figure 60. *A*, Streamflow, *B*, base flow, and *C*, precipitation at U.S. Geological Survey streamgage 08041500 Village Creek near Kountze, Texas.

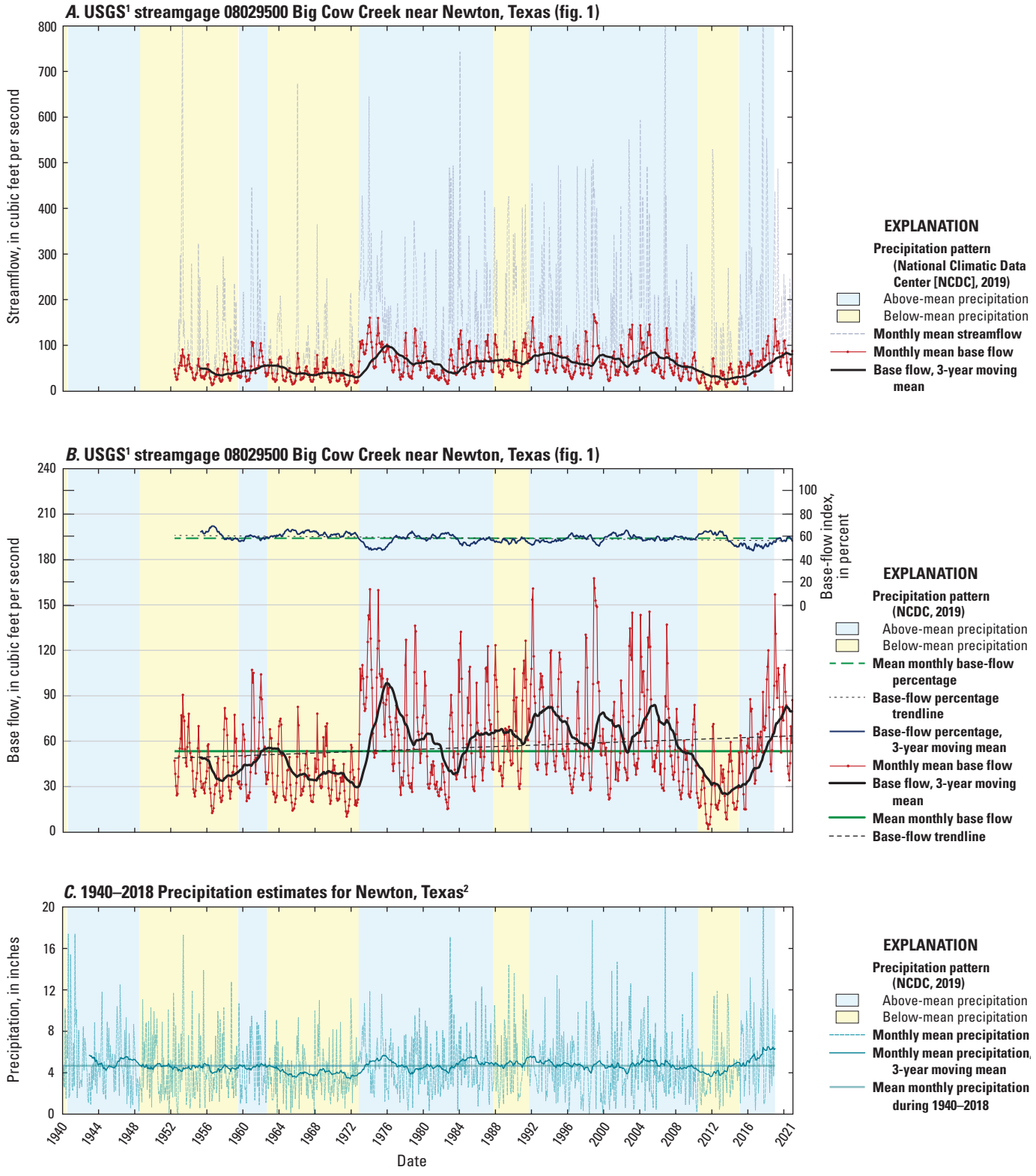

[1]U.S. Geological Survey.
[2]Interpolation of precipitation data from NCDC (2019). Climate stations are shown on fig. 62 and listed in table 4.1.

Figure 61. *A*, Streamflow, *B*, base flow, and *C*, precipitation at U.S. Geological Survey streamgage 08029500 Big Cow Creek near Newton, Texas.

streamflow and base flow appear to be predominantly climate related (figs. 53–61). Outcrop area groundwater levels in the shallow groundwater system have been relatively stable during the study period—a finding that was also reported in Wood (1958a) during a long period of below-mean precipitation in the 1950s (fig. 5). Additionally, because the majority of groundwater wells completed in the upper part of the Chicot aquifer are generally domestic or low-capacity wells, streamflow capture by groundwater withdrawals likely has not been substantial.

Recharge and Groundwater Flow

Groundwater recharge, in this report, is defined as water that infiltrates from the land surface through the unsaturated zone to the top of the water table (saturated zone) in the shallow groundwater system. Recharged water that subsequently flows from the shallow groundwater system to the intermediate and deep systems is described in terms of a "groundwater-flow rate." Recharge is one of the most challenging components of a groundwater budget to quantify because it cannot be measured directly aquifer-wide and therefore has to be estimated by using multiple methods (Delin and Falteisek, 2007). Recharge rates also are difficult to quantify because they can vary considerably both spatially and temporally. Furthermore, different approaches use a combination of different methods including mass-balance methods, streamflow-hydrograph techniques, environmental tracers, and physical measurements to estimate recharge rates, which can lead to different estimates (Scanlon and others, 2003). Estimates of recharge for the study area were obtained by using the Soil-Water-Balance (SWB) code (Westenbroek and others, 2010), a mass-balance method.

Conceptual Framework

Precipitation is the primary mechanism of recharge to the Gulf Coast aquifer system (Scanlon and others, 2003). Most of the water that recharges the Gulf Coast aquifer system infiltrates downward to the topographically controlled shallow saturated zone and flows horizontally to nearby streams, where the water is discharged as base flow. Recharge to local flow systems occurs in topographically high areas, and discharge occurs in nearby, topographically low areas. In this way, much of the recharge enters and exits the shallow groundwater system within relatively localized sections of the study area; however, a small portion of the groundwater in the outcrop area also flows downward into the intermediate and deep groundwater systems and moves laterally southeastward towards the coast. This water is also eventually discharged to streams or by upward leakage during predevelopment conditions (Ryder, 1996).

The subdivision of groundwater flow into shallow, intermediate, and deep systems (discussed in the "Hydrogeologic Unit Conceptualization" section) generally follows the method of Tóth (1963), although the intermediate groundwater system described in this report would probably be classified as a regional (deep) flow regime by Tóth (1963). The concept of recharge to the aquifer system and the subdivision of groundwater flow as described herein are simplifications, given the complexity of the numerous deposits of sand and interbedded fine-grained sediment and the heterogeneity of aquifers; however, the conceptual framework used for recharge and groundwater flow are believed to reasonably characterize conditions for the Gulf Coast aquifer system in accordance with published sources of information.

Recharge in the study area occurs primarily from precipitation that falls on the outcrop area (fig. 8) (White and others, 1939; Rose, 1943; Lang and others, 1950; Popkin, 1971; Gabrysch, 1977; Baker, 1986; Noble and others, 1996, Chowdhury and others, 2004; Oden and Truini, 2013), and the amount of recharge to the outcrop area is dependent on the type and slope of soil surfaces and geologic formations (Wilson, 1967). The outcrop area has a larger percentage of coarse-grained sediment than the downdip areas where the Beaumont Formation is present; therefore, the outcrop area receives greater amounts of recharge. The recharge area of the Chicot aquifer (fig. 8) is defined as the areal extent from Noble and others (1996)—which includes the Lissie Formation and Willis Sand—bounded by the updip limit of the Chicot aquifer from Casarez (2020).

Recharge to the outcrop area of Montgomery County and northern Harris County as well as laterally adjacent counties (fig. 8) supplies much of the water withdrawn in downdip areas (Popkin, 1971). The sediment in the outcrop area of the Chicot aquifer (fig. 8) is directly recharged by the downward movement of water, whereas the Beaumont Formation, present in the lower third to lower half of the study area (fig. 7), impedes the downward movement of recharge (Gabrysch, 1977; Chowdhury and others, 2004). Chemical concentrations and hydrogeochemical facies indicate that groundwater-flow paths begin in Montgomery and northern Harris Counties and in laterally adjacent counties, whereby groundwater moves towards the coast at angles consistent with the dip of the geologic formations (Young and others, 2014). An early recharge study using automated water-level recorders and lysimeters determined that recharge to the outcrop area (fig. 8) is substantial and produces a measurable rise in the water table of the shallow groundwater system during precipitation events (White and others, 1939). Where the water table underlies the streambed of study area streams, infiltration through the bed sediment to the water table could also contribute to aquifer recharge.

Prior to groundwater development, recharged water flowed from outcrop areas (fig. 8) to discharge areas in an approximate state of equilibrium, and groundwater-level changes were correlated to recharge from precipitation infiltration. Groundwater-level declines from groundwater use, however, have altered local and regional groundwater-flow patterns (Wood and Gabrysch, 1965; Oden and Truini, 2013). In the greater Houston area (fig. 18*A*), early groundwater-level declines for wells completed downdip from the Chicot aquifer outcrop (fig. 8) increased the hydraulic gradient between the outcrop area and the downdip areas (fig. 14).

Groundwater-level declines (figs. 37–50) have altered the hydraulic gradient and associated groundwater flow and have induced groundwater flow between the Chicot and Evangeline aquifers (Oden and Truini, 2013).

The decline in the groundwater levels and reduction of groundwater storage in the greater Houston area show an imbalance between the rate of groundwater flow to the intermediate and deep systems and the rate of groundwater use. Specifically, groundwater use in the intermediate and deep systems has exceeded the recharged water transmitted downdip from the outcrop area. This imbalance has persisted to varying degrees for many years based on the rate of groundwater development and generally has occurred earliest in time for the central, south-central, and southeastern parts of Harris County (figs. 14, 25–27) and Galveston County (figs. 16, 33), followed by northern, northwestern, and western Harris County (figs. 21–23) and Fort Bend County (figs. 15, 30–31), then in Montgomery County (figs. 13, 19–20) and adjacent counties.

Groundwater levels in wells completed in the shallow groundwater system generally are responsive to changes in precipitation patterns, have remained relatively stable over time for the greater Houston area (figs. 13, 37–50), and have not demonstrated any long-term patterns since groundwater development began (Noble and others, 1996; Ryder and Ardis, 2002). These characteristics of groundwater levels in the shallow groundwater system were observed as early as 1931 in White and others (1944) and in Lang and others (1950). The lack of any long-term patterns in groundwater levels in the shallow groundwater system is a result of the high volume of precipitation (figs. 5–6) that infiltrates as recharge. Thus, the shallow groundwater system functions more similarly to that of a "perched" system (White and others, 1939; White and others, 1944; Lang and others, 1950; Kasmarek and Strom, 2002), where groundwater levels in this system primarily are recharge and climate driven (figs. 37–50).

Groundwater use could capture groundwater that would otherwise flow to streams, thus reducing the base flow of streams. In the outcrop area (fig. 8), many shallow wells generally are low-capacity domestic wells, although higher capacity wells are present at greater depths (TWDB, 2020b, c). The base flow estimated at four streamgages in Montgomery and Liberty Counties (figs. 55–58) generally is stable, although surface-water diversions and impoundments can hinder the characterization of any base-flow decreases related to groundwater discharge. Groundwater-level changes over time for wells screened in the shallow groundwater system generally are small, and groundwater levels in this system are typically close to land surface (figs. 37–50). The lower capacity wells in the shallow system combined with the typically reliable large amounts of monthly precipitation across the study area (fig. 6) could explain the absence of base-flow decreases, although wells that are screened laterally and vertically adjacent to streams could locally capture some flow. The substantial fine-grained sediment thickness and heterogeneity (both laterally and vertically) between land-surface and water-production intervals (figs. 37–50) could additionally explain the absence of base-flow decreases that would normally be expected from downdip groundwater-level declines in the intermediate and deep systems (figs. 19–36).

A large amount of precipitation and associated infiltration occurs on the outcrop area; therefore, the available groundwater supply downdip from the outcrop areas is largely determined by the capacity of each aquifer to transmit flow from the outcrop areas to wells (White and others, 1939). The travel time of groundwater flow from the Chicot, Evangeline, and Jasper aquifer outcrops to Harris or Galveston Counties (or adjacent counties) is not fully known. Based on an analysis from Oden and Truini (2013), however, the median travel times from the Evangeline and Jasper outcrop areas to central and southern Montgomery County were about 5,350 and 30,000 years, respectively, although groundwater travel time in the Chicot aquifer had a median of 50 years. Preferential pathways based on localized variations in sand thickness and the presence of substantial heterogeneity of the aquifer units could reduce this travel time.

Infiltration from crop irrigation (also called irrigation return flows) could provide additional recharge in the western and southwestern parts of the study area (Williamson and others, 1990), where concentrated agriculture is present. Results of a groundwater model simulation from Jorgensen (1975) estimated that about 20 to 30 percent of the groundwater withdrawals in the Katy area returned to the Chicot aquifer through return flow. Similarly, return flow from rice irrigation—crops that are primarily in Colorado and Wharton Counties (fig. 4)—was estimated at 30 percent (from Tuck, 1974, in Loskot and others (1982). Wood and Gabrysch (1965) also mentioned that groundwater used for rice irrigation percolates to the water table.

Studies in Nebraska have found that irrigation increases groundwater recharge (Roark and Healy, 1998; McMahon and others, 2011), and recharge rates are greater in irrigated cropland areas compared to natural rangeland or nonirrigated cropland. Stanton and others (2010) described annual increases in recharge of 0.13–0.30 in/yr in irrigated cropland compared to nonirrigated cropland (Dugan and Zelt, 2000) and 1.3–1.6 in/yr in irrigated cropland compared to rangeland (McMahon and others, 2006). However, the soil properties (soil-water storage capacity and hydrologic soil group), irrigation methods, and irrigation rates in Nebraska differ from cropland areas in the Gulf Coast aquifer system.

Groundwater-Flow Rates to the Hydrogeologic Units

Little information is available on recharge or groundwater-flow rates to the various aquifers in Texas, and most available estimates are based on groundwater modeling studies such as Scanlon and others (2003). Additionally, many modeling studies of the Gulf Coast aquifer system in Texas only include a portion of the study area of this report. Therefore, the studies described in this report are primarily reproduced from Chowdhury and others (2004).

Ryder (1988) used a calibrated groundwater-flow rate of 0.74 inch per year (in/yr) to the Gulf Coast aquifer system in the GULF model documented in that report. Ryder and Ardis (2002) estimated a groundwater-flow rate to the aquifer system of about 0.12 in/yr across a 114,000-mi^2 area. Dutton and Richter (1990) estimated a groundwater-flow rate between 0.1 and 0.4 in/yr to the Chicot and Evangeline aquifers in Matagorda, Wharton, and Colorado Counties. Kasmarek and Robinson (2004) estimated that the groundwater-flow rate to the Chicot, Evangeline, and Jasper aquifers was about 0.9 percent of precipitation in 1977.

Soil-Water-Balance Code

Spatially distributed recharge to the Gulf Coast aquifer system was computed for each month of the study period by using the SWB code (Westenbroek and others, 2010). The SWB code is based on a modified Thornthwaite-Mather method (Thornthwaite and Mather, 1957) and requires gridded climatological and landscape-characteristic data inputs, including precipitation, temperature, soil-water storage capacity, hydrologic soil group, land-surface gradient, and land-cover type. The SWB code uses a mass-balance approach to compute gridded recharge as the difference between sources and sinks for each grid cell, while accounting for the cumulative effects of the change in soil moisture. The mass-balance equation (modified from Westenbroek and others, 2010) has the form:

$$R = (P + S + R_i) - (Int + R_o + P_{et}) - \Delta Sm \qquad (1)$$

where

R	is recharge,
P	is precipitation,
S	is snowmelt,
R_i	is surface runoff inflow,
Int	is plant interception,
R_o	is surface runoff outflow,
P_{et}	is potential evapotranspiration, and
ΔSm	is the change in soil moisture.

Daily climate data, including precipitation (P) and minimum and maximum air temperature, were obtained from 106 climate stations (National Climatic Data Center, 2019) (fig. 62; table 4.1) and interpolated to the GULF model area. Long-term climate data (more than 74 years) were available from 42 climate stations distributed across the study area (fig. 62; table 4.1). Temperature data (daily minimum, mean, and maximum) determine whether precipitation (P) is assumed to be immediately available for routing (in the form of rain) or stored temporarily above the surface (in the form of snow). Snowmelt (S) was calculated based on a temperature-index method. Surface runoff inflow (R_i) was not used. Plant interception (Int) occurs when precipitation is captured by vegetation prior to reaching the top of the soil profile, and Int was specified for each land-cover type during the growing season. Surface runoff outflow (R_o) was calculated by using Natural Resources Conservation Service curve numbers that relate precipitation and runoff (Westenbroek and others, 2010). Potential evapotranspiration (P_{et}) was calculated by using the Hargreaves and Samani (1985) method and represents the maximum rate at which groundwater could be evapotranspired with unlimited soil-moisture availability. The SWB code is used to compute the change in soil moisture (ΔSm) whereby P_{et} is subtracted from daily precipitation. If the resulting value is positive, A_{et} (actual evapotranspiration) equals P_{et}. If the resulting value is negative, A_{et} is limited to the ΔSm and is less than P_{et}.

Root-zone depths represent the maximum depth to which various types of vegetation will grow and are classified based on land cover and soil type. Greater plant root-zone depths result in the increased uptake of water in the soil-moisture zone, thus decreasing recharge, whereas smaller values result in an increased recharge to the water table (Westenbroek and others, 2010). Soil properties (soil-water storage capacity and hydrologic soil group) and land cover were derived from the Digital General Soil Map database (SSURGO; Natural Resources Conservation Service, 2019), which is an inventory of generalized soil characteristics at a scale between 1:12,000 and 1:63,360. Soils textures across much of the study area were predominantly fine sand to silt loam (fig. 63), although patterns in soil composition varied by county. The available water capacity associated with each soil type is the amount of water that a soil can store, which, when multiplied by the root-zone depth of the cell, results in the maximum soil water storage capacity. Any water added to the soil column in excess of this value will become recharge when using the SWB code (Westenbroek and others, 2010).

Soil infiltration rates were generally greatest, and thus overland flow potential was generally low, in the northern and northeastern parts of the study area (fig. 64), which coincides with the outcrop area of the Gulf Coast aquifer system hydrogeologic units (fig. 8). The greatest infiltration rates were generally associated with the streams in the study area and the outcrop of the Catahoula confining unit, and the lowest rates coincided with the location of the Beaumont Formation, approximately the lower third to lower half of the study area (figs. 7, 64).

SWB output includes 1,464 two-dimensional arrays of simulated monthly recharge from January 1897 through December 2018. To aid the GULF model simulation, and to remove unrealistic large values of simulated recharge, each SWB output array was processed with a low-pass filter (fig. 65). The filter's upper cutoff limit was calculated separately for each month of the year as the 97.5th-percentile value (corresponding to two standard deviations [2-sigma] above the mean) of an empirical cumulative distribution function, approximately corresponding to the upper limit of a 2-sigma probability distribution. The empirical cumulative distribution function was formed for each month by combining and sorting the SWB-simulated recharge rates in active model cells from all arrays representing a given month.

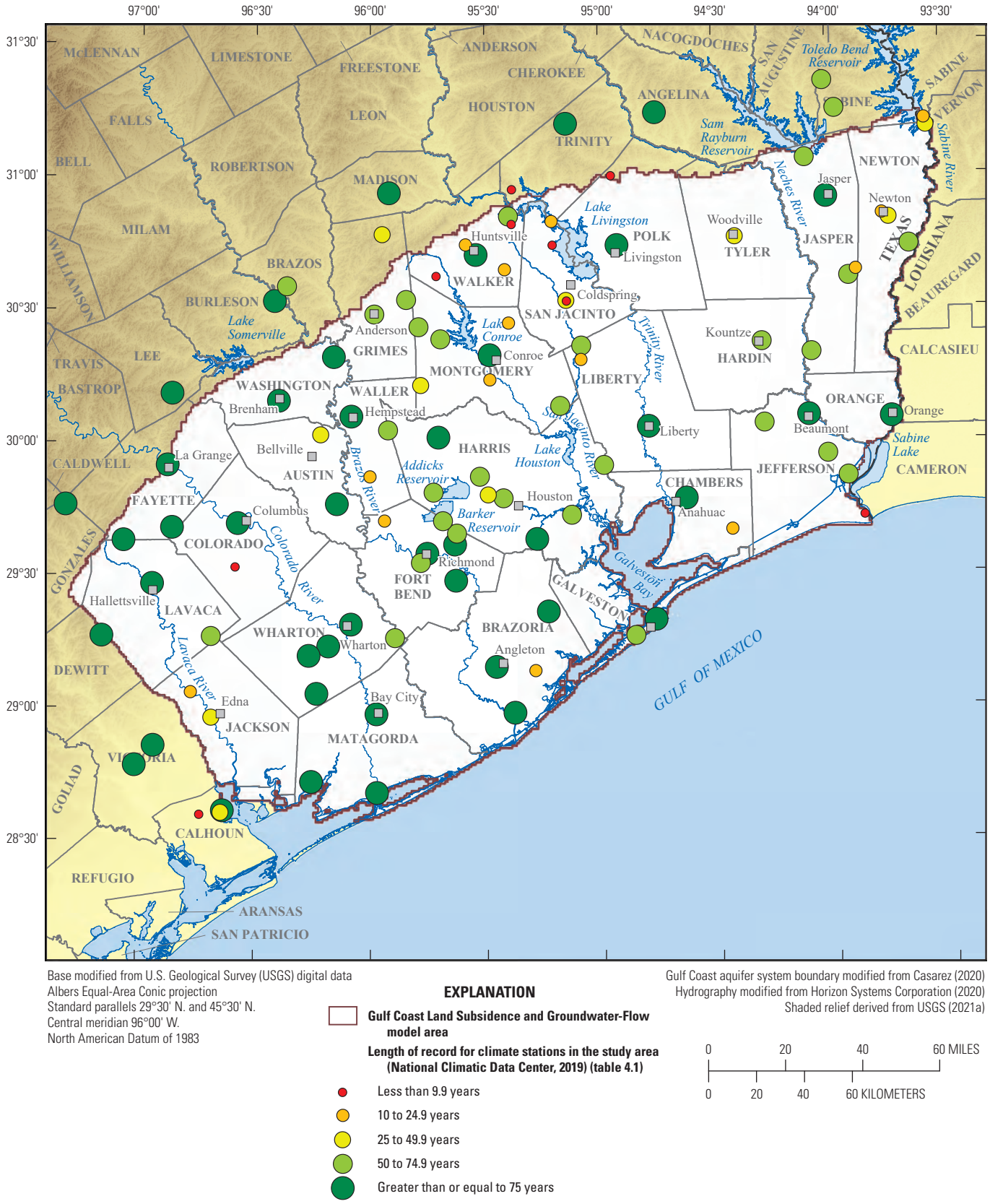

Figure 62. Spatial distribution of climate stations in and near the Gulf Coast aquifer system study area, southeast Texas.

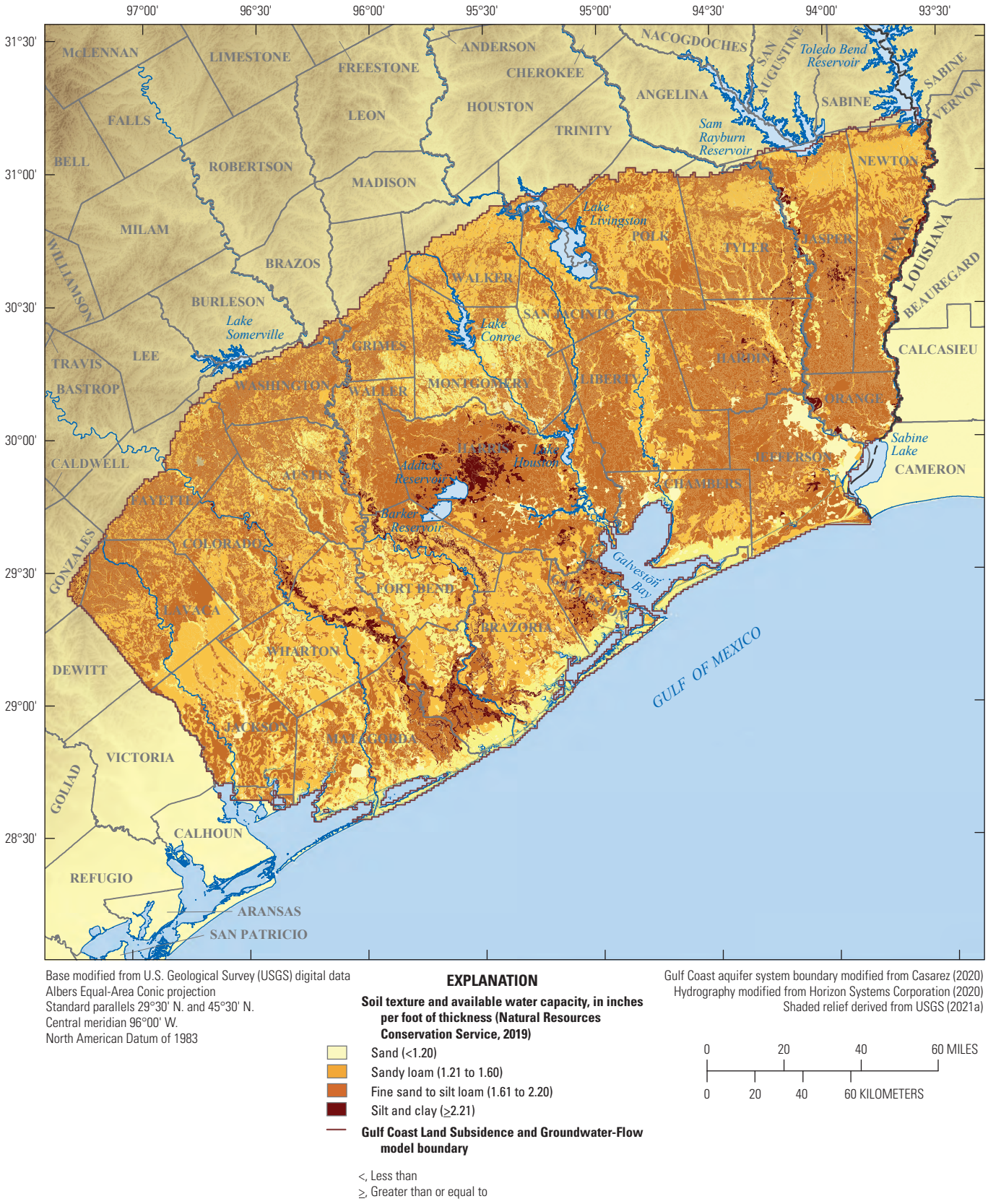

Figure 63. Spatial distribution of soil texture and available water capacity used for the estimation of recharge to the Gulf Coast aquifer within the study area in southeast Texas.

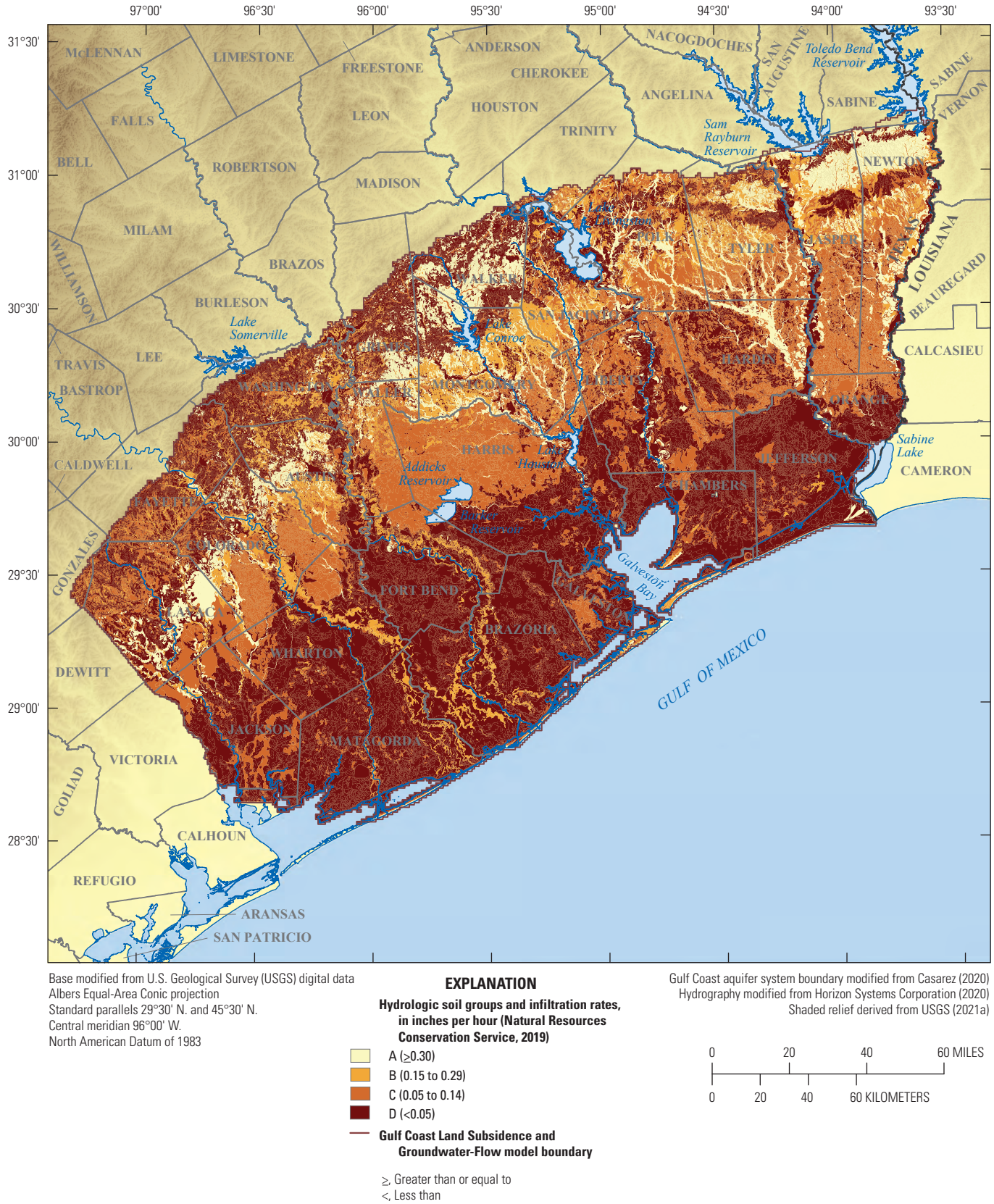

Base modified from U.S. Geological Survey (USGS) digital data
Albers Equal-Area Conic projection
Standard parallels 29°30' N. and 45°30' N.
Central meridian 96°00' W.
North American Datum of 1983

EXPLANATION

Hydrologic soil groups and infiltration rates, in inches per hour (Natural Resources Conservation Service, 2019)

- A (≥0.30)
- B (0.15 to 0.29)
- C (0.05 to 0.14)
- D (<0.05)

Gulf Coast Land Subsidence and Groundwater-Flow model boundary

≥, Greater than or equal to
<, Less than

Gulf Coast aquifer system boundary modified from Casarez (2020)
Hydrography modified from Horizon Systems Corporation (2020)
Shaded relief derived from USGS (2021a)

0 20 40 60 MILES
0 20 40 60 KILOMETERS

Figure 64. Spatial distribution of hydrologic soil groups and infiltration rates used for the estimation of recharge to the Gulf Coast aquifer within the study area in southeast Texas.

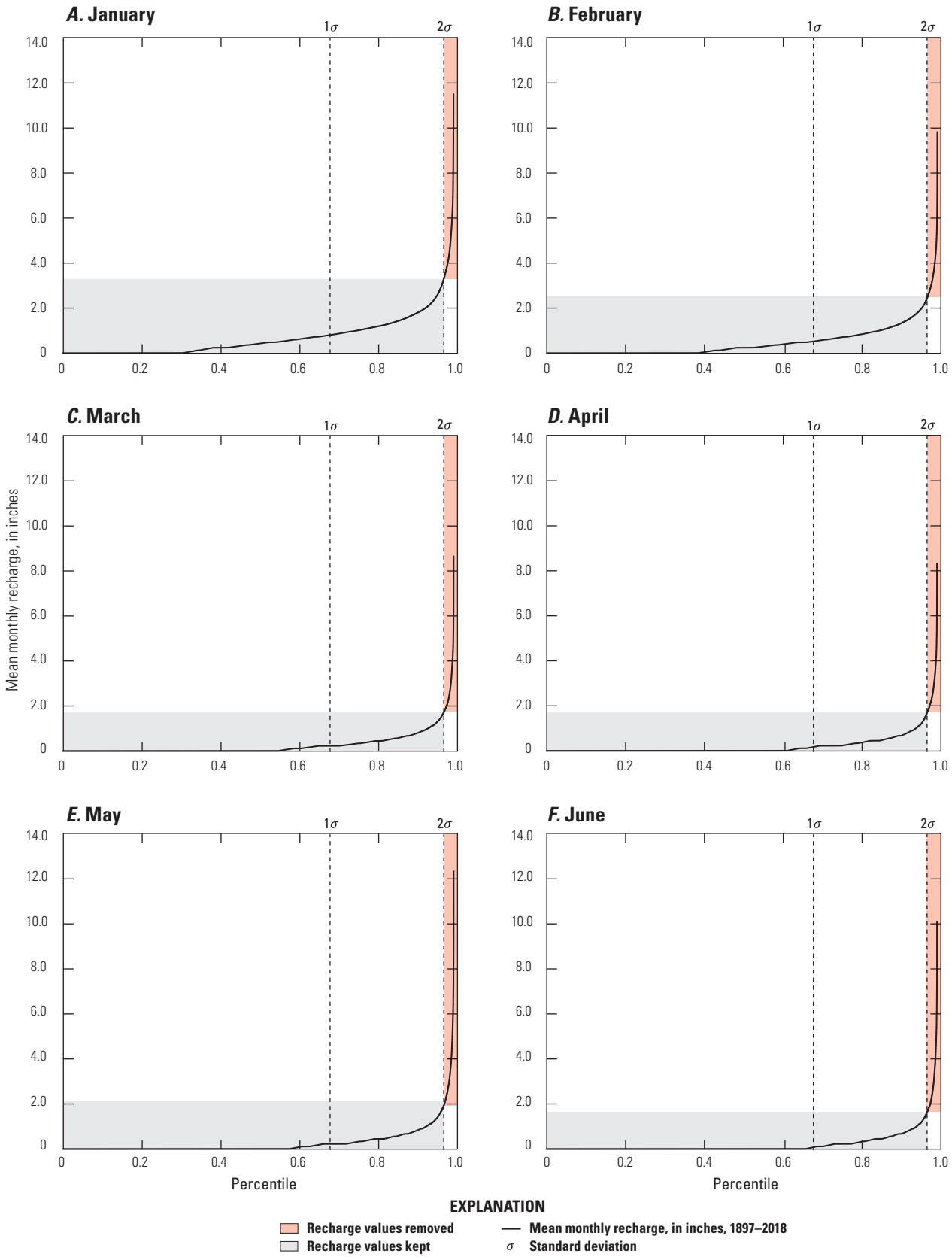

Figure 65. Mean monthly recharge estimates determined by using the Soil-Water-Balance (SWB) code and low-pass filtering (Westenbroek and others, 2010) for each SWB output array within the Gulf Coast aquifer system study area in southeast Texas for *A*, January, *B*, February, *C*, March, *D*, April, *E*, May, *F*, June, *G*, July, *H*, August, *I*, September, *J*, October, *K*, November, and *L*, December.

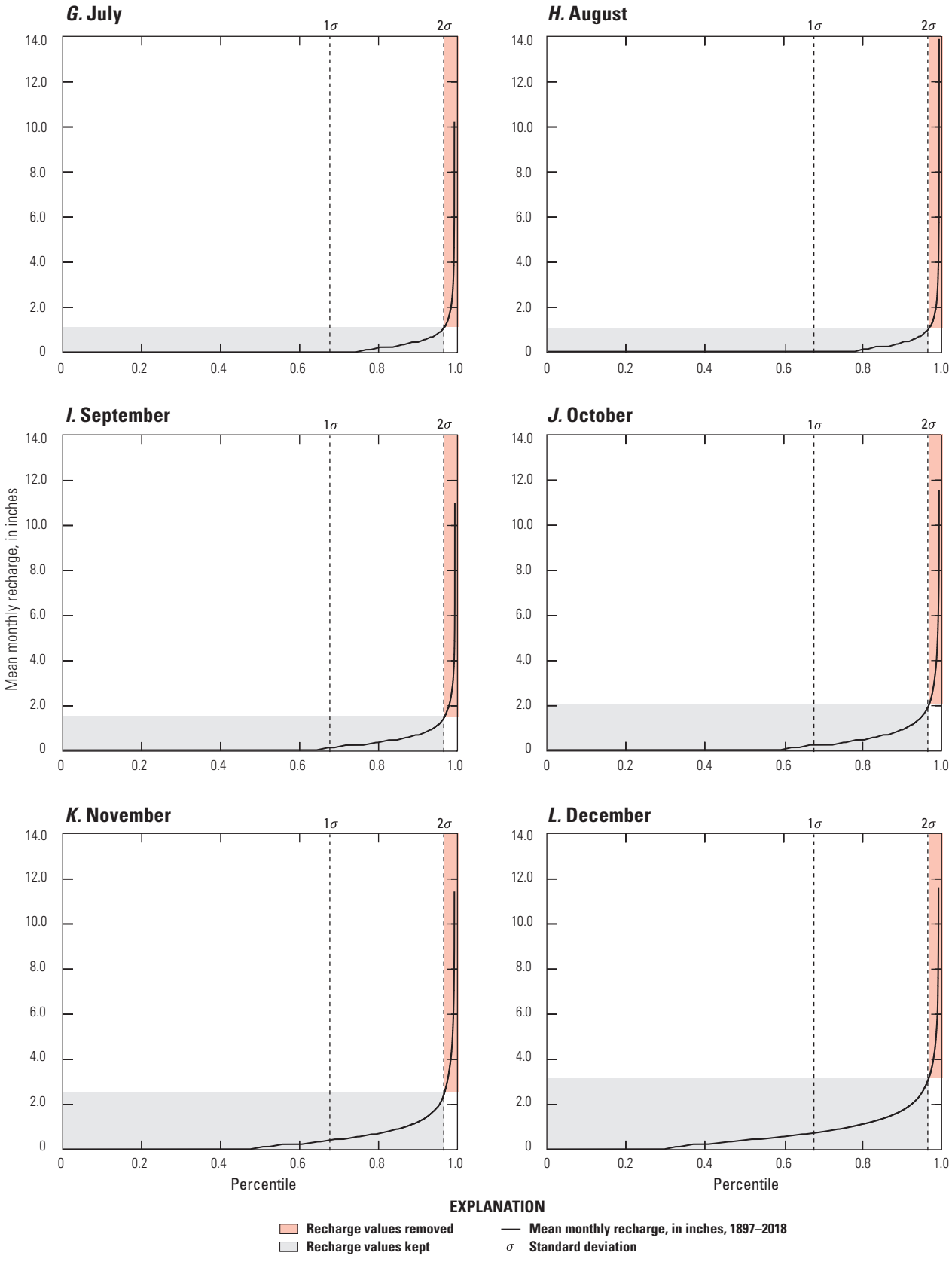

Figure 65.—Continued

The SWB-computed recharge was determined for the spatial extent of the study area and was computed without relation to the location or depth of the water table (or potentiometric surface) for the hydrogeologic units of the Gulf Coast aquifer system. The SWB-estimated mean annual recharge to the shallow groundwater system was about 4.1 in. or 8.7 percent of the mean annual precipitation of 47.5 in. (fig. 66*A*). The maximum annual mean recharge for the study period was 7.3 inches in 1973 (fig. 66*A*); during September 1–7, 1973, between 8 and 10 inches of precipitation fell on the study area from Tropical Storm Delia, contributing to the large annual mean recharge in 1973 (Hebert and Frank, 1974). The minimum annual mean recharge for the study period was 1.3 inches in 1917, coincident with the smallest annual amount of annual precipitation for the period of record (fig. 66*A*). Mean monthly recharge generally tended to be greatest during fall, winter, and spring (fig. 66*B*), consistent with Wilson (1967) who noted that precipitation duration during the cooler seasons tended to increase precipitation infiltration. Mean monthly recharge was least in July and August, the warmest months of summer (fig. 66*B*).

Spatially, mean annual recharge was greatest in the outcrop area, particularly in the northeastern part of the study area, which corresponds to the area of greatest soil infiltration rates and precipitation (figs. 67, 68). Recharge was least where the Beaumont Formation is present (figs. 7, 67). This spatial distribution generally agrees with the recharge estimated by Scanlon and others (2011), although the latter approach resulted in a spatial recharge distribution that is more closely aligned with precipitation rates than with soil properties. The recharge values computed by using the SWB code represent surficial recharge applied to the shallow groundwater system, much of which is discharged by study area streams and does not infiltrate to the intermediate and deep groundwater systems.

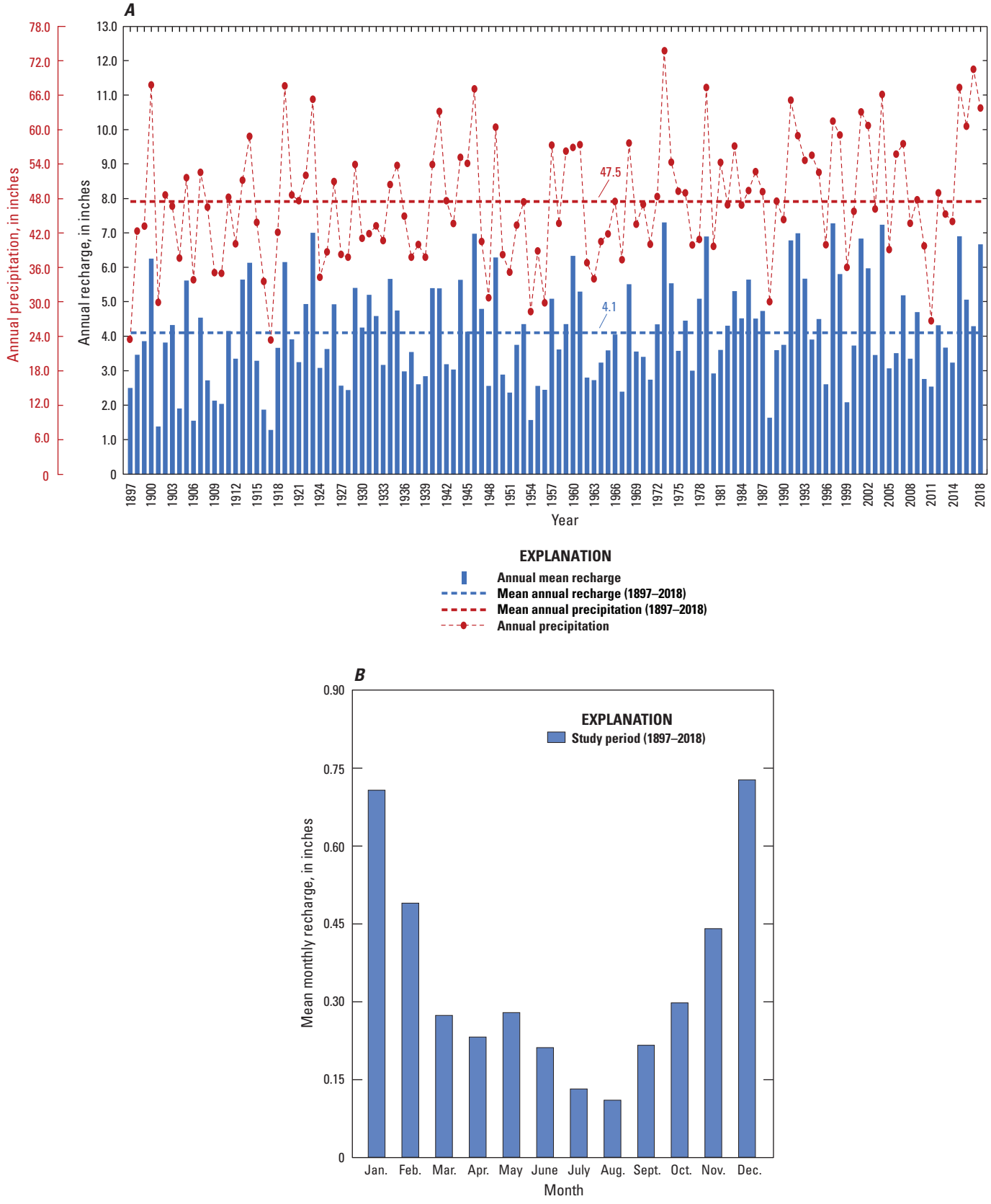

Figure 66. *A*, Annual recharge and precipitation and *B*, mean monthly recharge computed by using the Soil-Water-Balance code (Westenbroek and others, 2010) for the Gulf Coast aquifer system study area in southeast Texas.

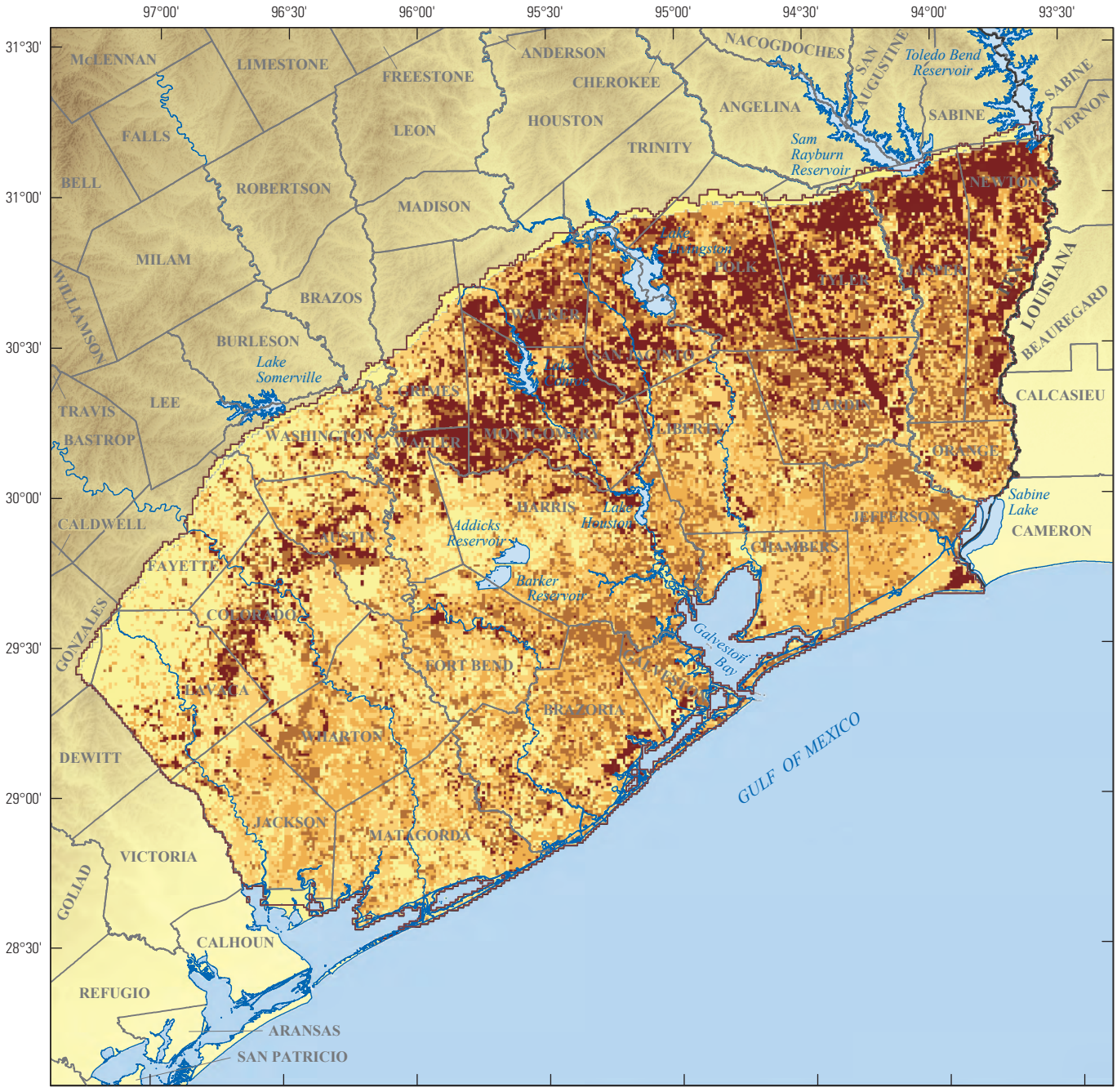

Base modified from U.S. Geological Survey (USGS) digital data
Albers Equal-Area Conic projection
Standard parallels 29°30' N. and 45°30' N.
Central meridian 96°00' W.
North American Datum of 1983

EXPLANATION

Mean annual recharge (1897–2018), in inches

- 0.01 to 0.9
- 1.0 to 1.9
- 2.0 to 2.9
- 3.0 to 4.9
- ≥ 5.00

Gulf Coast Land Subsidence and Groundwater-Flow model boundary

≥, Greater than or equal to

Gulf Coast aquifer system boundary modified from Casarez (2020)
Hydrography modified from Horizon Systems Corporation (2020)
Shaded relief derived from USGS (2021a)

0 20 40 60 MILES
0 20 40 60 KILOMETERS

The recharge values computed by using the Soil-Water-Balance code (Westenbroek and others, 2010) represent surficial recharge in the study area, much of which is discharged by study area streams and does not infiltrate into the deeper parts of the hydrogeologic units.

Figure 67. Mean annual recharge computed by using the Soil-Water-Balance code (Westenbroek and others, 2010) for the Gulf Coast aquifer system study area in southeast Texas, 1897–2018.

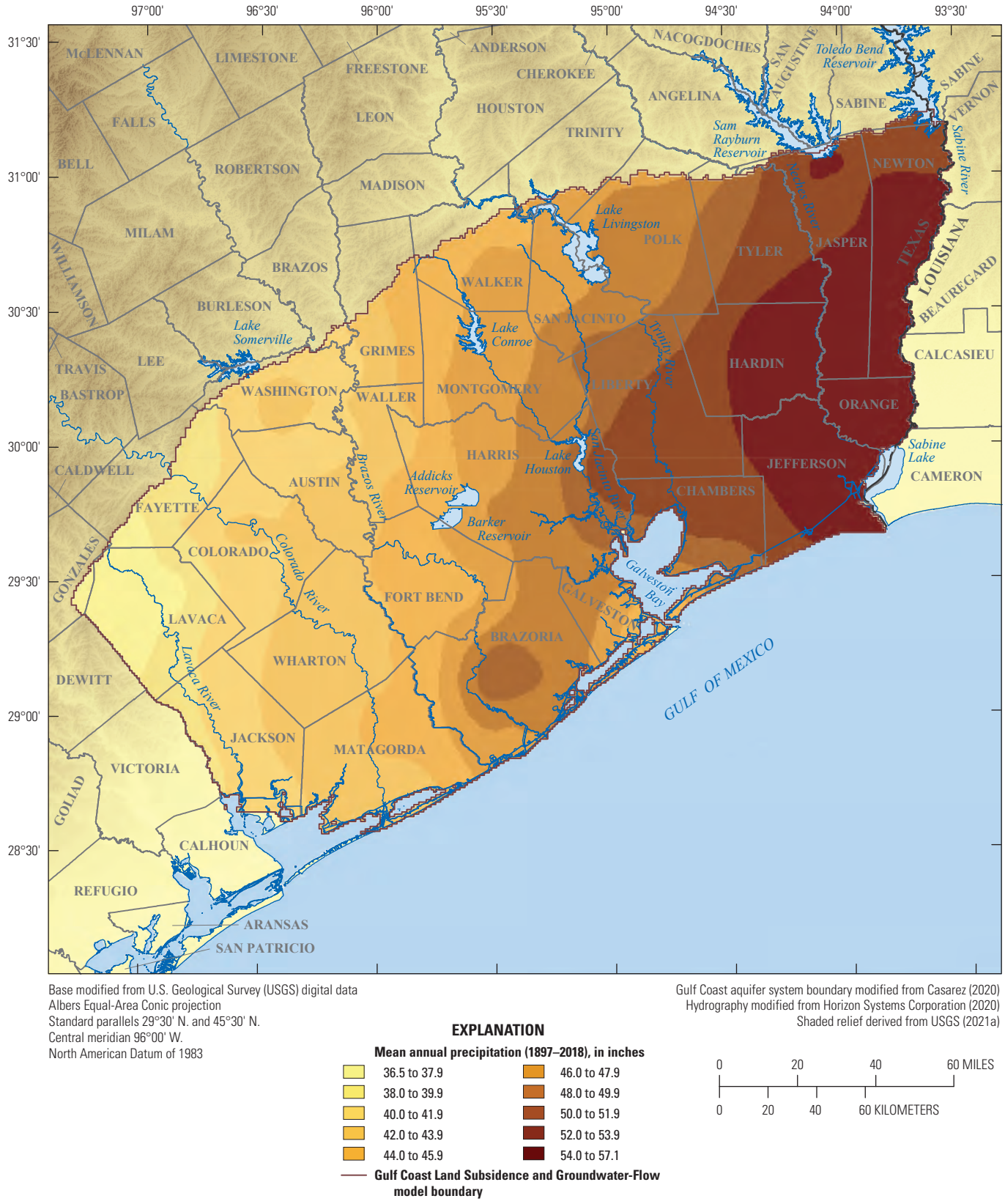

Base modified from U.S. Geological Survey (USGS) digital data
Albers Equal-Area Conic projection
Standard parallels 29°30' N. and 45°30' N.
Central meridian 96°00' W.
North American Datum of 1983

Gulf Coast aquifer system boundary modified from Casarez (2020)
Hydrography modified from Horizon Systems Corporation (2020)
Shaded relief derived from USGS (2021a)

EXPLANATION

Mean annual precipitation (1897–2018), in inches

36.5 to 37.9	46.0 to 47.9
38.0 to 39.9	48.0 to 49.9
40.0 to 41.9	50.0 to 51.9
42.0 to 43.9	52.0 to 53.9
44.0 to 45.9	54.0 to 57.1

Gulf Coast Land Subsidence and Groundwater-Flow model boundary

0 20 40 60 MILES
0 20 40 60 KILOMETERS

Figure 68. Mean annual precipitation for the Gulf Coast aquifer system study area in southeast Texas, 1897–2018.

Land-Surface Subsidence

The Houston-Galveston region forms part of one of the largest areas of land-surface-elevation change (subsidence) in the United States (Coplin and Galloway, 1999). Subsidence, which causes a decrease in land-surface elevation, has been extensively documented for more than 70 years in the Houston-Galveston region. Subsidence since at least the early 1930s resulted from groundwater-level declines, and earlier in the region's history, subsidence resulted from oil and gas extraction. Subsidence was first documented in 1918 in the Goose Creek oil field (fig. 1) by Pratt and Johnson (1926) in Galveston County. Subsidence has resulted in structural damage and flooding in low-lying areas along Galveston Bay in Baytown, Texas City, and Houston (Ashworth and Hopkins, 1995), and can lead to costly damage in coastal regions because of the relative rise of sea level, the associated landward shift of the coastline, and the increased risk of flooding from storm surges (Zilkoski and others, 2003).

Land can subside as a result of groundwater withdrawals in susceptible aquifer systems— typically unconsolidated alluvial or basin-fill aquifer systems comprising aquifers and fine-grained units that have undergone extensive groundwater development (Galloway and Burbey, 2011). The fine-grained units generally include two classes of low-permeability, thick and thin fine-grained deposits: (1) laterally discontinuous fine-grained sediments (or "interbeds") within the aquifers, and (2) laterally extensive fine-grained sediment (or "confining units") separating individual aquifers in the aquifer system (Poland, 1984). The interbeds and confining units are much less permeable and generally are substantially more compressible than the coarse-grained deposits constituting the aquifers, and they impede the vertical flow of water within and between the aquifers. Owing to their small lateral extent and typically smaller thickness, the interbeds are conceptually distinct from the confining units.

The relation between changes in pore-fluid pressure (which can be expressed in terms of an equivalent hydraulic head, assuming constant gravity and uniform fluid) and compression of the aquifer system is based on the principle of effective stress (Terzaghi, 1925) (fig. 69):

$$\sigma_e = \sigma_T - \rho \qquad (2)$$

where

σ_e is intergranular stress (or effective stress),
σ_T is total stress (or geostatic stress), and
ρ is the pore-fluid pressure (or hydrostatic stress).

The pore structure of a sedimentary aquifer system is supported by the granular skeleton of the aquifer system and the pore-fluid pressure of the groundwater that fills the intergranular pore space (Meinzer, 1928). When groundwater is withdrawn in quantities that result in reduced pore-fluid pressure, the reduction of the pore-fluid pressure support increases the intergranular stress, or effective stress, on the skeleton. An increase in effective stress compresses the skeleton. This deformation is sometimes inelastic (nonrecoverable), depending on the stress history of fine-grained sediment, resulting in a vertical decrease in thickness (or "compaction") of the aquifer system, a permanent reduction in aquifer-system storage capacity, and subsidence, illustrated in figure 69. Depending on the range of stress (elastic or inelastic), an aquifer-system skeleton that primarily consists of fine-grained sediments is potentially much more compressible than an aquifer-system skeleton that primarily consists of coarse-grained sediments, such as sand and gravel.

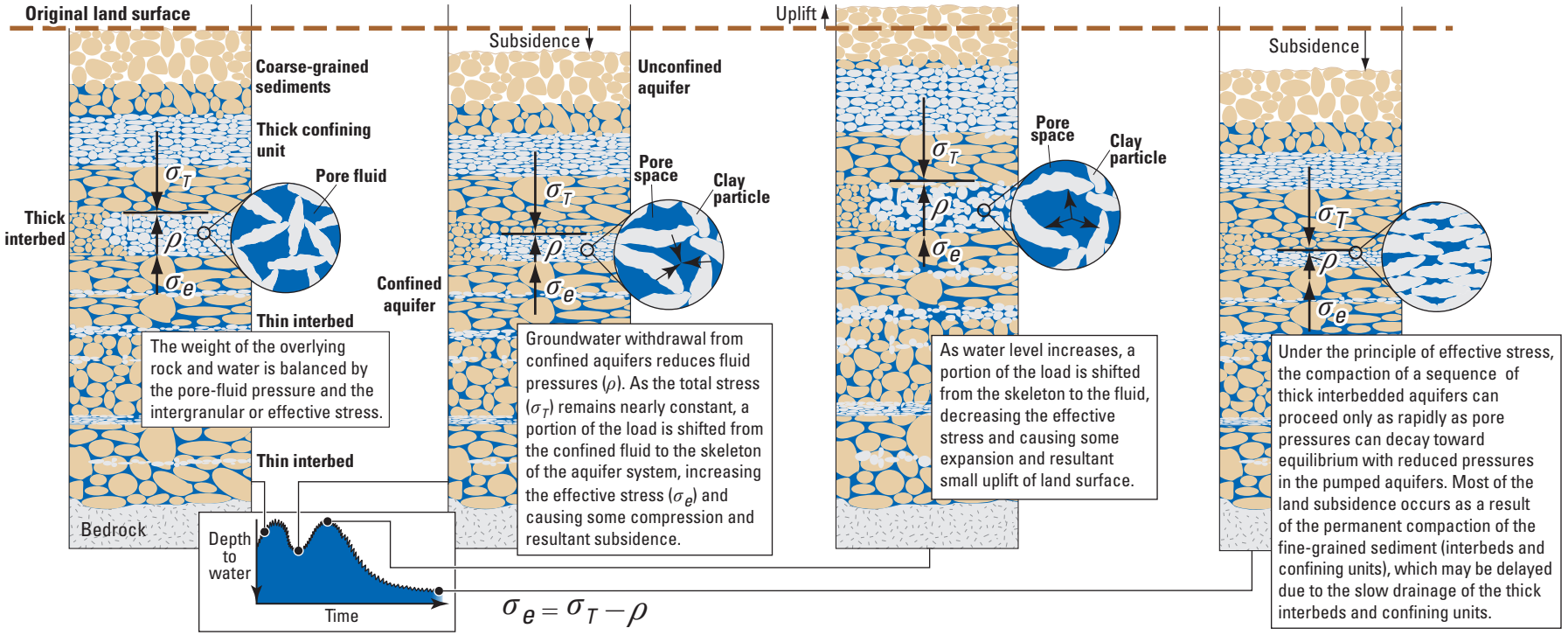

Figure 69. Illustration of the principle of effective stress.

Aquifer-system deformation can be elastic (recoverable) if the effective stress imposed on the skeleton is less than any previous maximum effective stress (Terzaghi, 1925). The greatest historical effective stress imposed on the aquifer system—sometimes the result of the lowest groundwater level—is the "preconsolidation stress," and the corresponding (lowest) groundwater level is the "preconsolidation head" (Leake and Prudic, 1991). If the effective stress does not exceed the preconsolidation stress, then the aquifer system undergoes elastic compression, which is recovered if groundwater levels (pore-fluid pressures) subsequently rise. Elastic compressibility, and thus elastic compaction, is small and generally similar or only slightly greater for fine-grained sediment than for coarse-grained sediment. If the effective stress within a confining unit or interbed exceeds the preconsolidation stress, the pore structure of the granular matrix of the fine-grained sediment is rearranged; this new configuration results in a reduction of pore volume and, thus, inelastic compaction of the aquifer system. The inelastic compressibility of the fine-grained sediment constituting a confining unit or interbed is generally 20 to more than 100 times greater than the elastic compressibility (Riley, 1998), and depending on the aggregate thickness of the fine-grained sediment, the resulting inelastic compaction can be large. Inelastic compaction of coarse-grained sediment generally is negligible (Ireland and others, 1984; Hanson, 1989; Sneed and Galloway, 2000).

The simple compaction model described herein does not account for delayed drainage from low-permeability fine-grained sediments in the form of interbeds or confining units in the aquifer system. Riley (1969) describes delayed drainage from low-permeability sediments in terms of the time-consolidation theory of soil mechanics and the delay in compaction resulting from the slow equilibration of pore pressures in interbeds and confining units in aquifer systems. For a developed aquifer system with an appreciable thickness of interbeds or confining units, only a part of the ultimate compaction that would occur under pore-pressure equilibration will be realized as excess pore pressures in these low-permeability units slowly dissipate and approach equilibrium with the pore-pressure declines in the adjacent aquifers. During this process, the difference between the ultimate compaction and the realized compaction for a specific pore-pressure decline in the adjacent aquifers is termed "residual compaction" (for example, see Sneed and Galloway, 2000). Thus, depending on the thickness and the vertical hydraulic diffusivity of a thick confining unit or interbed, compaction lags pore-pressure declines in the adjacent aquifers, and the associated compaction can require decades or more to ultimately be realized.

When an unconsolidated heterogeneous aquifer system undergoes groundwater development, the produced groundwater initially comes from storage in coarser grained sediment, interbeds, and margins of thicker confining units. After a period of groundwater development where vertical groundwater gradients have been established between the reduced groundwater levels in the coarse-grained fraction of the aquifer and the interior of the interbeds or confining units, groundwater flow occurs from these fine-grained units to the coarse-grained fraction of the aquifer. Where the groundwater-level decline and its areal extent are substantial, a large fraction of the water supplied to wells can be derived from groundwater released from storage in the interbeds or confining units, leading to inelastic compaction (Poland, 1984). Early estimates indicate that about 17 percent (Winslow and Doyel, 1954) to about 22 percent (Winslow and Wood, 1959) of the groundwater use in the greater Houston area was supplied by the fine-grained units. The water released from storage in interbeds and confining units during inelastic compaction represents a one-time mining of stored water and results in a generally small but potentially substantial nonrecoverable reduction in aquifer-system storage capacity (Riley, 1998; Sneed and Galloway, 2000).

For a more complete description of aquifer-system compaction as presented here, see Poland (1984). Holzer's paper entitled "History of the aquitard-drainage model" further describes the hydromechanical processes associated with interbeds and confining units (Holzer, 1998). For a review and selected case studies of subsidence caused by aquifer-system compaction in the United States, see Galloway and others (1999).

Estimation Methods

Aquifer-system compaction and subsidence data since as early as 1906 have been acquired throughout the greater Houston area by using the various methods described in this section; these data were used as model observations to aid in model history matching described in the "Simulation of Groundwater Flow and Land-Surface Subsidence" section. In this report, compaction is defined as a change in the vertical thickness of the aquifer system, whereas subsidence is defined as the lowering of the land-surface elevation as a result of aquifer-system compaction. Thus, an extensometer—which measures the distance between the base of the extensometer (bottom of a borehole) and a reference point on or near the surface—is used to measure compaction. Subsidence is calculated by differencing the repeated elevation measurements derived from spirit leveling (hereinafter referred to as "leveling"), or the repeated distance measurements between the ground and satellites using campaign Global Positioning System (GPS) surveying or interferometric synthetic aperture radar (InSAR). The GPS and leveling methods could be considered collectively because both use benchmarks, are carried out in a similar manner in terms of the number of measurements in space and time, and in many cases, are used conjunctively during a single geodetic survey (Sneed and Galloway, 2000). However, the leveling surveys in the greater Houston area were undertaken before the advent of GPS methods for determination of land subsidence; therefore, each method and associated data are discussed separately. In the following sections, each type of measurement that was used as

a model dataset is described, followed by a description of how these types of measurements were used together to improve the qualitative understanding and the quantitative simulations of aquifer-system mechanics. In this report, a decrease in the land-surface elevation (subsidence) and vertical thickness of the aquifer system (compaction) is described using positive values, whereas negative subsidence and compaction values indicate an increase in land-surface elevation (uplift) and vertical thickness of the aquifer system, respectively. The subsidence contour maps described in the "Subsidence Contour Maps" section of this report were developed from spirit-leveling data but are described separately for the convenience of the reader.

Spirit-Level Surveys

Leveling is the oldest method used to precisely measure elevation and was commonly performed along linear infrastructure including roads and railroad tracks as part of initial construction or ongoing maintenance (USGS, 2018). The installation of benchmarks (or "monumenting") in the region was first performed by the National Geodetic Survey (NGS) or the predecessor agency, the U.S. Coast and Geodetic Survey (Gabrysch and Coplin, 1990). The leveling technique allows the surveyor to carry an elevation from a known reference point (such as a benchmark) to other points by use of a precisely leveled telescope and a graduated rod resting vertically on temporary or permanent benchmarks. Repeated surveys of the same benchmarks over time yield a series of elevations from which elevation changes are calculated. Subsidence is then the net change in elevation of the land surface between the surveys.

An extensive network of benchmarks was monumented and resurveyed primarily by the NGS during 1906–87 in the greater Houston area. These benchmarks were generally based on first-order leveling surveys along primary roadways and railways, augmented by shorter second-order lines, that form the primary network of regional geodetic control. Information on these survey types and measurement uncertainty is available (Federal Geodetic Control Committee, 1984). In 1906, benchmarks were first established along a first-order line from La Grange, Tex. (about 100 mi west of Houston) to Galveston. In 1915, the USGS in cooperation with Harris County, established benchmarks along lines of third-order leveling surveys across a wide area of Harris County (documented in Marshall, 1916a and 1916b). Some of these benchmarks established by the USGS in 1915 were then incorporated into subsequent NGS leveling surveys. In 1918, another first-order line was established from Sinton, Tex., to New Orleans, Louisiana (Gabrysch and Coplin, 1990). During 1932–33, a line was established from Palestine, Tex., to Houston, by which additional first-order and some second-order lines were established, and the two lines established in 1906 and 1918 were releveled (Winslow and Wood, 1959). Also, during 1932–33, the existing leveling lines were adjusted to the National Geodetic Vertical Datum of 1929 (NGVD 29) (originally the Sea Level Datum of 1929) as part of the 1929 general adjustment (Winslow and Wood, 1959). During 1943, many second-order lines were established, and the previous lines were releveled (Winslow and Doyel, 1954). Further releveling was performed during 1951, at which point the regional nature of subsidence in the greater Houston area became known (Winslow and Wood, 1959). During 1954, many of the benchmarks were releveled, and in 1957, the entire benchmark network was readjusted (through a supplementary adjustment), through which leveled elevations at each benchmark (through 1954) were connected to previous leveling at points where little vertical movement was indicated between the leveling surveys (Winslow and Wood, 1959). Through this adjustment, the changes in all leveled elevations from 1906 to 1954 could be determined (Winslow and Wood, 1959). Subsequent adjustments used the methods from the 1957 adjustment except where the subsequent surveys were extended beyond the confines of previous surveys. The benchmark network was adjusted in 1959 and 1961 and releveled in 1964, which also included an adjustment of the existing leveling data. In 1971, part of the benchmark network in the Pasadena and Baytown areas was releveled by the U.S. Army Corps of Engineers (Gabrysch and Bonnet, 1974). In 1973, the entire benchmark network was again releveled after gaining municipal, city, and state-level financial support as well as funding from five federal agencies (National Oceanic and Atmospheric Administration [NOAA], 1980). In 1976, a single line from Galveston through Baytown and Houston to La Grange was releveled at the request of the HGSD. During this survey, the elevations of the inner pipe of the extensometers were also determined for the extensometers installed through 1976 (table 4). Further surveys of the entire benchmark network in the greater Houston area were conducted in 1978 (NOAA, 1980) and 1987 (NOAA, 2021a). Surveys in 1995 and 2000 were also performed at benchmarks monumented at many newly established GPS sites; thus, these surveys included only a small resurvey of historical benchmark locations.

Selected historical benchmark locations and elevations are shown on figure 70*A* and listed in table 4, respectively. The leveling surveys frequently were completed over multiple years but are referenced by one year per survey using the same single-year dates as Gabrysch (1980b, 1982b, 1984) and Gabrysch and others (1969). The benchmarks were selected based on leveling surveys through at least 1987 and the availability of leveled elevations during or prior to the 1943 survey. NGS leveling surveys account for nearly all the benchmark elevations listed in table 4 from the period 1906–87, even for benchmarks not monumented by the NGS. Surveys by the NGS account for some benchmark elevations listed in table 4 from the period 1995–2021; elevation data surveyed by other organizations met NGS "Blue Book" standards (described in NOAA, 2022). Benchmark elevations measured during 1906–73 (table 4) generally were not previously published. Observed subsidence during 1973–78, 1976–78, and 1963–78 is listed in NOAA (1980). Benchmark elevations from the 1987 survey and from the 1995–2021 surveys are available in NOAA (2021a).

The benchmark elevation data (table 4) are primarily based on first-order leveling and have an estimated vertical resolution of between 0.004 and 0.04 ft (Bawden and others, 2003). The 1973 survey used adjusted leveled elevations at each benchmark based on NGVD 1929 and incorporated prior revisions to the leveled elevations at each benchmark made in 1957, 1959, 1961, and 1964. The 1976 and 1978 surveys used similar adjustment methods as the 1973 benchmark elevation survey (NOAA, 1980). As a result of these adjustments, the stamped elevation on the benchmark will differ from the adjusted value determined on the date the benchmark was monumented. Benchmark elevation data in 1987 in table 4 (from NOAA, 2021a) are provided in reference to the NGVD 29 and to the NAVD 88 through the general adjustment of 1991. As a result of the general adjustment of 1991, the elevations reported in NAVD 88 for the 1987 survey listed in this report are dated as 1991 elevations on the NGS website (NOAA, 2021a).

Historical subsidence contour maps were used to estimate the rate and magnitude of subsidence in the greater Houston area. The benchmarks listed in table 4 are a subset of the benchmarks used to construct the subsidence contour maps during 1906–43, 1943–64, 1964–73, 1973–78, and 1978–87 that are described in this section of the report. These date ranges are produced herein verbatim from the historical reports; in the historical reports, the ending year of one date range is the beginning year of the next published date range, so that convention is followed in this section. The subsidence maps in Gabrysch and Bonnet (1975), Jorgensen (1975), Gabrysch (1980b), and Gabrysch and Coplin (1990) are based on differences in elevation at each of the benchmarks between the beginning and ending years of each period that correspond with the historical leveling surveys of the greater Houston area. In many cases, benchmarks established during earlier surveys had been destroyed prior to subsequent leveling surveys; in these cases, "contours of subsidence for other periods were added to supplement control data" (Gabrysch and Coplin, 1990, p. 18). For example, the subsidence contour map for 1906–78 would have been supplemented by the addition of contours from subsidence maps for 1906–43 and 1943–78.

Benchmark PTS 185 was monumented in 1915 by the U.S. Geological Survey (USGS) about 1,500 feet east of the Brownwood subdivision and about half a mile south of the Baytown extensometer site (fig. 70*A*). This benchmark was damaged during 1979–83 and was not leveled by the National Geodetic Survey after 1978 (fig. 95*C*; table 4). Benchmark PTS 185 is one of the few 1915 USGS benchmarks remaining in the greater Houston area. Photograph by Samuel Rendon, U.S. Geological Survey, July 7, 2022.

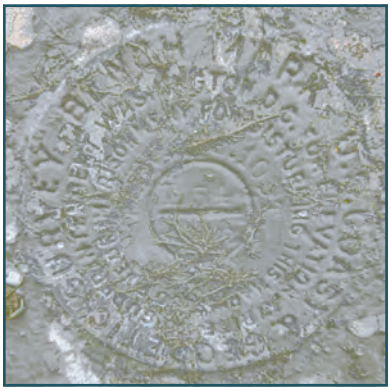

Benchmark L 54 was monumented in 1918 by the National Geodetic Survey (at the time of monument, the U.S. Coast and Geodetic Survey) on the side of the 1913 former Waddell House Furnishing Company warehouse foundation in downtown Houston, Texas (fig. 70*A*; table 4). Photograph by John Ellis, U.S. Geological Survey, July 20, 2022.

The method of supplementing benchmark-leveling data with contours from subsidence maps is not described in either Gabrysch and Bonnet (1975) or Gabrysch (1980b). However, because Gabrysch was lead author of each of these reports documenting subsidence in the Houston-Galveston region, it is likely that a method similar to the one described in Gabrysch and Coplin (1990) was used in the generation of subsidence maps in Gabrysch and Bonnet (1975) and Gabrysch (1980b).

Data from leveling surveys were not always available in some areas or time periods of interest because benchmark networks were established incrementally in the greater Houston area. Therefore, previously published contour maps (Gabrysch and Bonnet, 1975; Jorgensen, 1975; Gabrysch, 1980b; Gabrysch and Coplin, 1990) were used in describing general subsidence patterns over time during 1906–43, 1943–64, 1964–73, 1973–78, and 1978–87. Modifications to the 1906–43 and 1906–73 maps are described in appendix 5.

During 1906–43, most of the subsidence was confined to central, south-central, and southeastern Harris County and southeastern Galveston County (fig. 5.1). Measured subsidence in excess of 1.0 ft occurred in the historical Houston, Pasadena, Baytown, and Texas City areas, coincident with groundwater-level declines (figs. 14, 16) as a result of increases in groundwater use (fig. 11; table 1). As much as 2.4 ft of subsidence occurred in the Baytown area (fig. 5.1) at the site of a refinery. About 1.6 ft or more of subsidence occurred in and near the Texas City area generally during 1938–43 as a result of groundwater-level declines (wells D–H, fig. 16) caused by groundwater withdrawals mainly during 1935–43 (fig. 11; table 1) (Jorgensen, 1975). The largest amount of subsidence (greater than 3.2 ft) during this period was observed near the Goose Creek oil field, based on changes in elevation at USGS benchmarks monumented in 1915. The subsidence was "bowl shaped" and centered around the production zone wherein the greatest amount of subsidence and associated faulting was within 0.5 mi of the greatest oil production (Lockwood, 1954). Oil and gas were produced from this oil field as late as 1925 at a relatively shallow depth (for oil production)—between 1,000 and 4,100 ft bls (Gabrysch and Bonnet, 1974). Northwest of the Goose Creek oil field, groundwater levels declined in the adjacent Baytown area as a result of industrial groundwater use (fig. 11; table 1) (Gabrysch and Bonnet, 1975); these industrial groundwater withdrawals resulted in an estimated subsidence of greater than 2.4 ft by 1943 (fig. 5.1).

Benchmark V 305 was monumented in 1935 by the National Geodetic Survey (at the time of monument, the U.S. Coast and Geodetic Survey) on the side of the Santa Fe Consolidated High School foundation (now the Coastal Alternative Program building) in Santa Fe, Texas (fig. 70*A*; table 4). Photograph by John Ellis, U.S. Geological Survey, July 15, 2022.

Benchmark CONROE RM 1 was monumented in 1942 by the National Geodetic Survey (at the time of monument, the U.S. Coast and Geodetic Survey) in downtown Conroe, Texas (figs. 70*A*, 96*D*; table 4). Photograph by Samuel Rendon, U.S. Geological Survey, July 7, 2022.

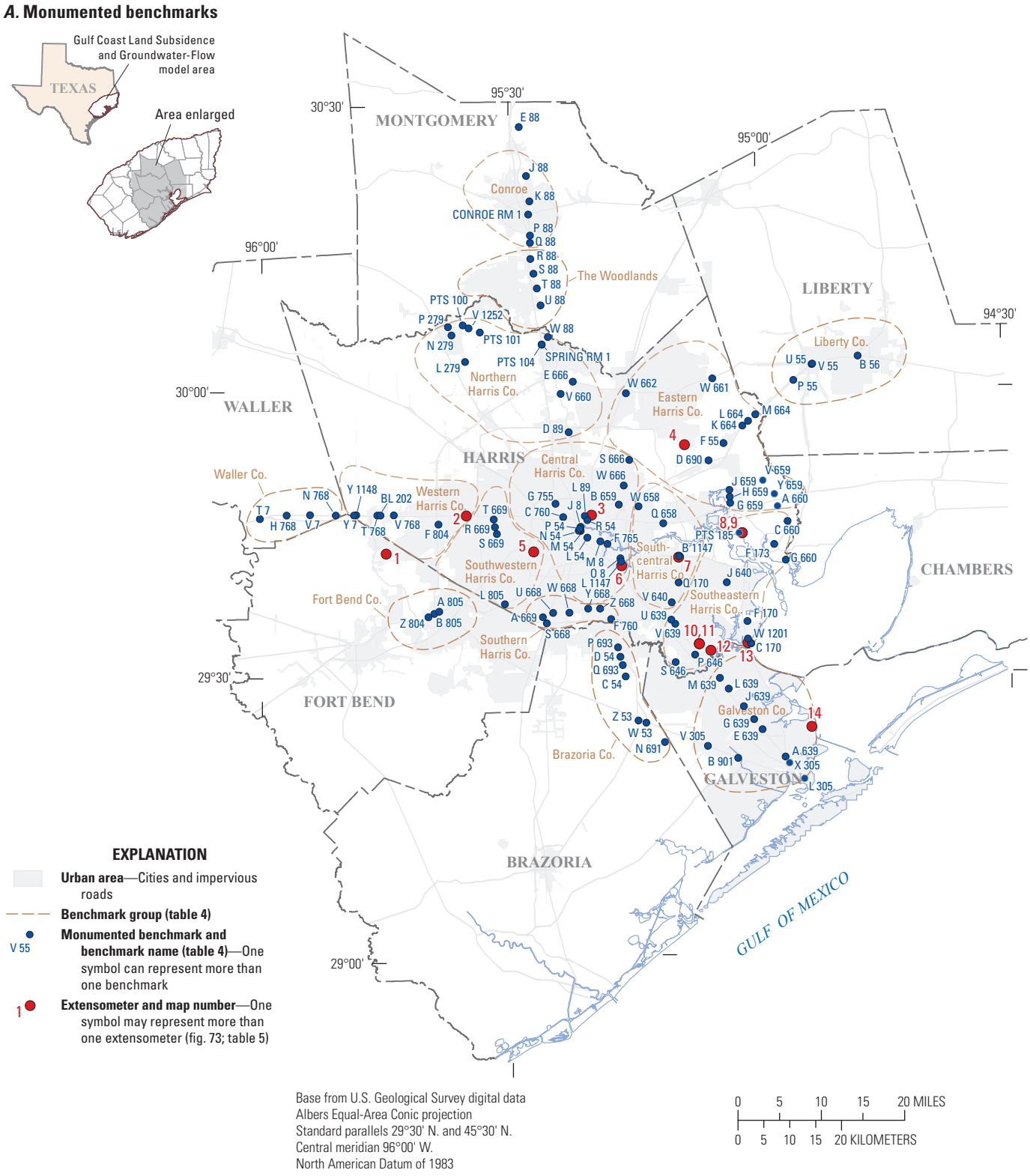

Figure 70. *A*, Locations of selected monumented benchmarks and extensometers and *B*, cumulative subsidence (1906–2021) contours in the greater Houston area, southeast Texas.

***B.* Cumulative subsidence (1906–2021) contours**

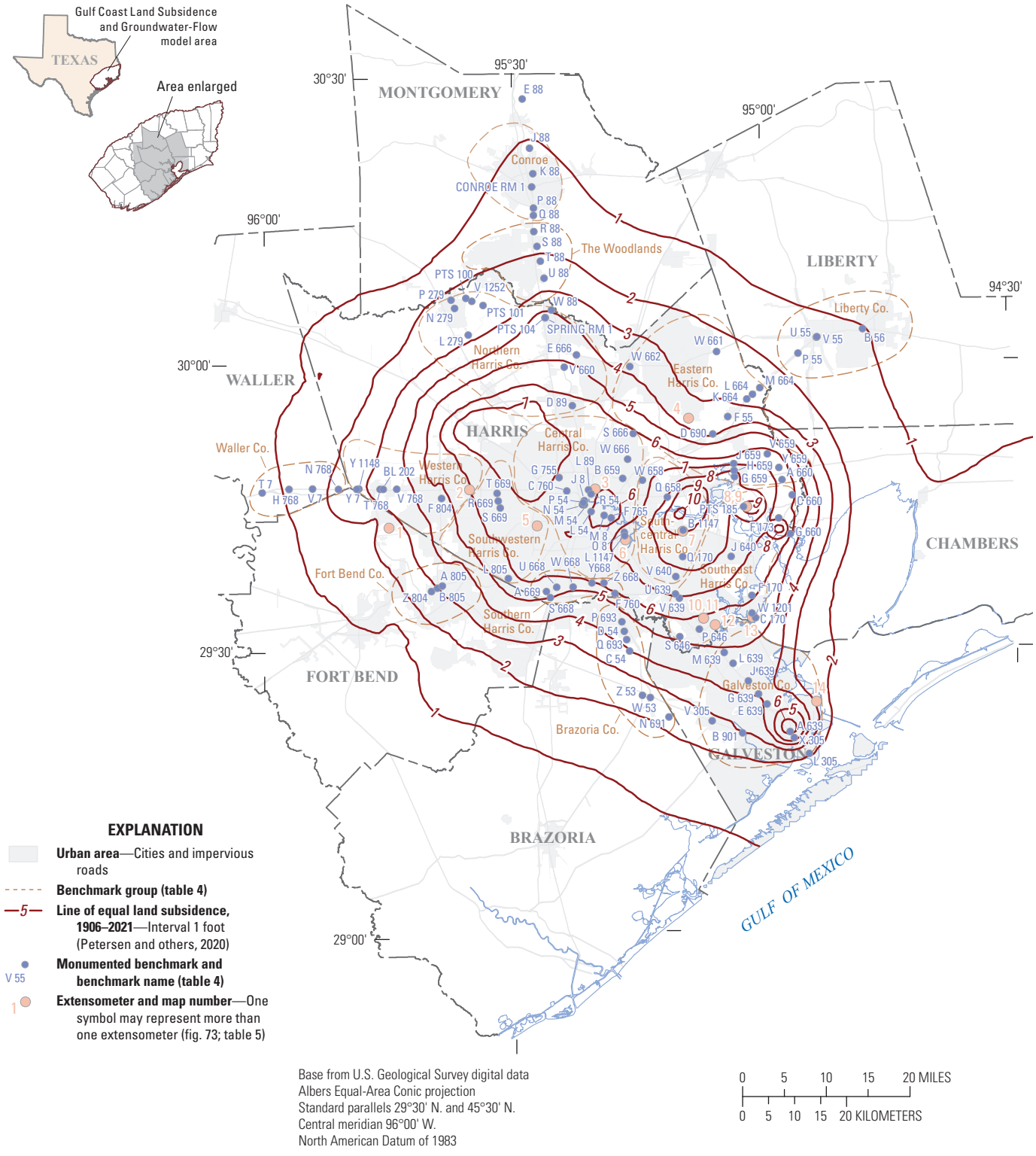

Figure 70.—Continued

Table 4. Monumented benchmarks and elevations in the Gulf Coast aquifer system study area in southeast Texas.

[NGVD 29, National Geodetic Vertical Datum of 1929; NAVD 88, North American Vertical Datum of 1988; USGS, U.S. Geological Survey; extensometer, borehole extensometer; subsidence, land-surface subsidence; --, not available; NGS, National Geodetic Survey; ft, foot]

Historical geographic area (fig. 18*B*)[1]	Benchmark name (fig. 70*A*)	Elevation, in feet above NGVD 29[1]											Elevation, in feet above NAVD 88[1]		
		1906, 1915, 1918[3]	1932–1936[4]	1943	1951	1954	1959	1964	1973	1976	1978	1987	1987	1995–2002[5]	2019–21
Benchmark group (fig. 70*A*)[2]															
Montgomery County															
--	E 88[6]	--	340.39	--	--	--	340.33	--	340.23	--	340.20	340.20	340.19	--	339.78
Montgomery County—Conroe (fig. 140)															
--	CONROE RM 1[6,7]	--	--	--	--	--	209.57	--	209.39	--	209.38	209.23	209.22	--	208.22
--	J 88	--	265.08	--	--	--	264.94	--	264.86	--	264.76	264.66	264.65	--	--
--	K 88[6,8]	--	232.61	--	--	--	232.49	--	232.25	--	232.26	232.14	232.13	--	231.40
--	P 88	--	141.39	--	--	--	141.26	--	141.01	--	141.01	140.83	140.82	--	--
--	Q 88[6]	--	130.72	--	--	--	--	--	130.33	--	130.33	130.16	130.16	--	129.33
Montgomery County—The Woodlands (fig. 141)															
--	R 88[6]	--	122.36	--	--	--	122.22	--	121.94	--	121.94	121.77	121.77	--	121.03
--	S 88	--	127.73	--	--	--	127.54	127.50	127.25	--	127.28	127.04	127.04	--	--
--	T 88	--	130.74	--	--	--	130.59	130.57	130.26	--	130.21	129.91	129.91	--	--
--	U 88	--	138.31	--	--	--	138.17	138.17	137.87	--	137.81	137.44	137.44	--	--
Northern Harris County (fig. 142)															
Katy area	D 89	--	82.72	82.64	82.25	82.07	81.72	81.32	80.20	--	79.44	78.14	78.15	77.18	77.15
	E 666	--	--	93.67	--	--	--	--	92.57	--	92.43	91.70	91.71	--	--
	L 279	--	153.65	--	--	153.40	--	--	152.96	--	152.78	152.46	152.48	--	--
	N 279	--	187.17	--	--	186.93	--	--	186.48	--	186.33	186.08	186.10	--	--
	P 279	--	191.38	--	--	191.10	--	--	190.66	--	190.50	190.24	190.25	--	--
	PTS 100	174.84	--	--	--	174.53	--	--	174.22	--	174.15	173.95	173.96	--	--
	PTS 101	150.98	--	--	--	150.63	--	--	150.39	--	150.34	150.07	150.08	--	--
	PTS 104	128.85	--	--	--	128.73	--	--	128.07	--	127.85	127.33	127.33	--	--
	SPRING RM 1[6]	--	--	--	--	128.35	--	--	127.65	--	127.50	126.88	126.88	--	124.20
	V 660	--	--	101.78	101.59	101.50	101.21	101.10	100.52	--	100.30	99.49	99.49	98.72	--
	V 1252[6,9]	--	--	--	--	--	--	--	--	--	151.38	151.11	151.12	--	149.73
	W 88	--	102.91	--	102.91	--	102.75	102.69	102.35	--	102.26	101.87	101.87	--	--

Table 4. Monumented benchmarks and elevations in the Gulf Coast aquifer system study area in southeast Texas.—Continued

[NGVD 29, National Geodetic Vertical Datum of 1929; NAVD 88, North American Vertical Datum of 1988; USGS, U.S. Geological Survey; extensometer, borehole extensometer; subsidence, land-surface subsidence; --, not available; NGS, National Geodetic Survey; ft, foot]

Historical geographic area (fig. 18*B*)[1]	Benchmark name (fig. 70*A*)	Elevation, in feet above NGVD 29[1]											Elevation, in feet above NAVD 88[1]		
		1906, 1915, 1918[3]	1932–1936[4]	1943	1951	1954	1959	1964	1973	1976	1978	1987	1987	1995–2002[5]	2019–21
Western Harris County (fig. 143)															
Katy area	BL 202	--	--	134.24	134.02	--	133.98	133.87	133.51	133.40	133.38	133.00	133.03	--	--
	F 804	--	--	82.32	82.11	--	--	81.65	81.04	--	80.63	79.88	79.90	--	--
	T 768	--	--	132.39	132.30	--	132.20	132.13	131.73	131.63	131.64	131.25	131.29	131.14	--
	V 768	--	--	125.30	125.23	--	125.09	124.94	124.53	124.44	124.42	123.94	123.97	--	--
	Y 7[6]	142.74	--	142.50	142.48	142.48	142.36	142.28	141.79	141.63	141.62	141.14	141.18	--	139.94
	Y 1148[6]	--	--	--	--	--	142.55	142.48	142.00	141.85	141.86	141.40	141.44	--	140.09
Southwestern Harris County (fig. 144)															
Historical Houston area	L 805	--	--	70.62	--	--	--	--	68.70	--	68.08	66.43	66.45	65.69	--
	R 669	--	--	75.32	--	75.04	74.47	74.03	72.85	--	72.10	70.79	70.81	--	--
	S 669	--	--	82.00	--	81.61	81.01	80.61	79.36	--	78.62	77.21	77.23	--	--
	T 669	--	--	84.22	--	83.83	83.23	82.82	81.37	--	80.49	78.84	78.86	--	--
Southern Harris County (fig. 145)															
Historical Houston area	A 669	--	--	59.97	--	--	58.87	58.44	57.20	--	56.51	55.18	55.20	--	--
	F 760	--	--	51.99	51.42	--	50.47	49.87	48.10	--	47.27	46.16	46.17	--	--
	S 668	--	--	62.95	--	--	--	--	60.67	--	60.08	58.88	58.89	--	--
	U 668	--	--	58.13	--	--	57.22	56.84	55.73	--	55.09	53.85	53.87	--	--
	W 668	--	--	61.86	--	--	60.83	60.25	58.66	--	57.86	56.74	56.75	--	--
	Y 668	--	--	52.83	52.46	52.46	51.78	51.26	49.89	--	49.17	48.19	48.20	--	--
	Z 668	--	--	55.34	--	54.90	54.04	53.41	51.83	--	51.06	50.04	50.06	--	--
Central Harris County (fig. 146)															
Historical Houston area	B 659	--	--	46.30	45.53	45.04	44.48	43.85	41.91	--	41.10	40.37	40.38	--	--
	C 760	--	--	57.47	56.90	56.51	56.21	55.73	53.94	53.49	53.13	52.14	52.16	51.76	--
	F 765	--	--	37.12	36.40	35.95	35.60	35.03	33.22	32.74	32.45	31.91	31.92	--	--
	G 755	--	--	71.55	70.84	70.38	--	--	67.28	--	66.41	65.26	65.28	--	--
	J 8	45.14	44.80	44.35	43.87	43.56	43.38	43.01	41.73	41.40	41.14	40.43	40.45	40.18	--
	L 54	52.23	51.76	51.18	50.51	--	49.73	49.15	47.31	46.82	46.48	45.68	45.69	--	--

Table 4. Monumented benchmarks and elevations in the Gulf Coast aquifer system study area in southeast Texas.—Continued

[NGVD 29, National Geodetic Vertical Datum of 1929; NAVD 88, North American Vertical Datum of 1988; USGS, U.S. Geological Survey; extensometer, borehole extensometer; subsidence, land-surface subsidence; --, not available; NGS, National Geodetic Survey; ft, foot]

Historical geographic area (fig. 18*B*)[1]	Benchmark name (fig. 70*A*)	Elevation, in feet above NGVD 29[1]											Elevation, in feet above NAVD 88[1]		
		1906, 1915, 1918[3]	1932–1936[4]	1943	1951	1954	1959	1964	1973	1976	1978	1987	1987	1995–2002[5]	2019–21
Central Harris County (fig. 146)—Continued															
Historical Houston area—Continued	L 89	--	53.47	--	52.27	51.83	51.39	50.78	48.86	--	48.06	47.23	47.24	46.94	--
	M 8	43.46	42.96	42.37	41.58	41.10	40.69	40.02	37.99	37.42	37.09	36.38	36.39	--	--
	M 54	54.75	54.36	53.82	53.13	--	52.29	51.67	49.78	49.30	48.94	48.08	48.09	--	--
	N 54	57.21	56.80	56.25	55.59	--	54.77	54.17	52.33	--	51.50	50.63	50.64	50.37	--
	O 8	37.62	37.11	36.50	--	34.92	34.29	33.48	31.07	30.47	30.14	29.51	29.52	--	--
	P 54	53.04	52.67	52.14	51.56	51.19	50.90	50.37	48.72	48.30	47.99	47.18	47.19	46.91	--
	R 54	52.99	52.55	52.00	51.26	50.83	50.45	49.90	48.14	--	47.34	46.48	46.50	--	--
	S 666	--	--	60.12	--	59.35	--	--	57.01	--	56.27	55.53	55.54	--	--
	W 666	--	--	48.59	47.99	47.59	--	--	44.63	--	43.86	43.11	43.12	--	--
South-central Harris County (fig. 147)															
Pasadena area	Q 170	--	40.80	40.20	--	38.52	--	36.78	--	--	32.87	32.62	32.63	--	--
	Q 658	--	--	30.43	--	28.99	28.31	27.51	25.10	--	24.37	24.22	24.22	--	--
	V 640	--	--	42.12	41.20	40.70	40.00	39.23	--	--	35.61	35.16	35.17	--	--
	W 658	--	--	42.19	41.24	40.86	40.41	39.80	--	--	37.33	36.69	36.70	--	--
Southeastern Harris County (fig. 148)															
Johnson Space Center area	C 170[10]	--	5.72	--	--	4.78	4.44	4.03	2.34	--	1.39	0.87	0.88	--	--
	F 170	--	17.68	--	--	16.44	16.00	15.40	13.37	--	12.29	11.84	11.85	--	--
	P 646	--	--	28.63	28.10	--	27.21	26.60	24.84	--	23.98	23.55	23.57	--	--
	S 646	--	--	28.25	27.79	--	27.16	26.66	25.13	--	24.37	23.96	23.98	--	--
	U 639	--	--	33.21	32.38	31.93	31.29	30.58	28.49	27.73	27.45	26.99	27.00	--	--
	V 639	--	--	40.45	39.45	38.92	38.26	37.52	35.38	34.62	34.35	33.91	33.92	--	--
Baytown area	C 660	--	--	29.67	--	29.02	28.48	27.89	--	--	25.74	25.68	25.68	--	--
	F 173	--	35.17	34.74	--	33.08	32.28	31.49	29.61	--	28.99	28.81	28.82	--	--
	G 660	--	--	24.02	--	23.28	22.72	22.08	20.70	--	20.26	20.08	20.08	--	--
	J 640	--	--	29.87	--	28.26	27.50	26.66	--	--	22.81	22.40	22.41	--	--
	PTS 185[11]	29.94	29.53	--	--	--	25.25	24.21	21.71	20.77	20.80	--	--	--	--

Table 4. Monumented benchmarks and elevations in the Gulf Coast aquifer system study area in southeast Texas.—Continued

[NGVD 29, National Geodetic Vertical Datum of 1929; NAVD 88, North American Vertical Datum of 1988; USGS, U.S. Geological Survey; extensometer, borehole extensometer; subsidence, land-surface subsidence; --, not available; NGS, National Geodetic Survey; ft, foot]

Historical geographic area (fig. 18*B*)[1]	Benchmark name (fig. 70*A*)	Elevation, in feet above NGVD 29[1]											Elevation, in feet above NAVD 88[1]		
		1906, 1915, 1918[3]	1932–1936[4]	1943	1951	1954	1959	1964	1973	1976	1978	1987	1987	1995–2002[5]	2019–21
Eastern Harris County (fig. 149)															
--	A 660	--	--	34.48	--	33.88	33.39	32.93	--	--	31.36	31.35	31.36	--	--
--	D 690	--	--	34.62	34.22	34.00	33.71	33.47	32.54	--	32.22	32.12	32.12	--	32.08
--	F 55	48.26	48.01	47.79	47.42	47.24	46.93	46.61	45.55	--	45.10	44.97	44.97	--	--
--	G 659	--	--	38.67	--	36.65	35.76	34.80	32.42	--	31.56	31.36	31.37	--	--
--	H 659	--	--	40.42	--	38.75	37.75	36.60	33.82	--	32.82	32.54	32.55	--	--
--	J 659	--	--	43.40	--	42.47	42.00	41.43	39.70	--	38.98	38.72	38.72	--	--
--	K 664	--	--	57.05	56.75	56.67	56.43	56.20	55.39	--	55.12	55.04	55.04	--	54.95
--	L 664	--	--	54.63	54.31	54.24	53.98	53.75	52.96	--	52.67	52.54	52.54	--	52.44
--	M 664	--	--	56.91	56.58	56.47	56.09	55.78	54.89	--	54.57	54.44	54.44	--	54.34
--	V 659	--	--	40.86	--	40.10	39.61	39.19		--	37.84	37.79	37.79	--	--
--	W 661	--	--	74.07	--	73.75	--	--	72.90	--	72.75	72.66	72.66	--	--
--	W 662	--	--	97.62	--	97.34	--	--	96.33	--	95.99	95.33	95.34	--	--
--	Y 659	--	--	38.27	--	37.33	36.84	36.46	--	--	35.10	35.11	35.12	--	--
Brazoria County (fig. 150)															
--	C 54	45.86	45.77	45.45	45.13	--	44.60	44.05	43.24	--	42.55	41.95	41.96	--	--
--	D 54	49.55	49.55	49.23	48.90	--	48.49	48.20	47.20	--	46.58	46.04	46.06	--	--
--	N 691	--	--	38.38	38.14	--	37.95	37.73	37.25	--	36.95	36.72	36.73	--	--
--	P 693	--	--	49.12	48.80	--	48.37	48.00	46.95	--	46.27	45.67	45.69	--	--
--	Q 693	--	--	46.61	46.30	--	45.84	45.40	44.49	--	43.67	43.17	43.18	--	--
--	W 53	42.84	--	42.41	42.20	--	41.88	41.69	40.94	--	40.52	40.03	40.04	--	--
--	Z 53	50.86	--	--	50.23	--	49.96	49.79	49.15	--	48.81	48.36	48.38	--	--
Liberty County (fig. 151)															
--	B 56	38.56	--	38.35	--	38.26	38.11	38.10	--	--	--	37.69	37.68	--	37.51
--	P 55	69.62	--	69.62	--	69.48	69.30	69.06	68.63	--	68.49	68.42	68.42	--	68.28
--	U 55	84.67	--	84.37	--	84.14	83.98	83.86	83.36	--	83.26	83.20	83.20	--	83.05
--	V 55	84.58	--	84.29	--	84.04	83.87	83.72	83.26	--	83.17	83.11	83.11	--	82.97

Table 4. Monumented benchmarks and elevations in the Gulf Coast aquifer system study area in southeast Texas.—Continued

[NGVD 29, National Geodetic Vertical Datum of 1929; NAVD 88, North American Vertical Datum of 1988; USGS, U.S. Geological Survey; extensometer, borehole extensometer; subsidence, land-surface subsidence; --, not available; NGS, National Geodetic Survey; ft, foot]

Historical geographic area (fig. 18*B*)[1]	Benchmark name (fig. 70*A*)	Elevation, in feet above NGVD 29[1]											Elevation, in feet above NAVD 88[1]		
		1906, 1915, 1918[3]	1932–1936[4]	1943	1951	1954	1959	1964	1973	1976	1978	1987	1987	1995–2002[5]	2019–21
Galveston County (fig. 152)															
Texas City area	A 639	--	--	13.23	10.85	10.29	9.89	9.50	8.29	7.92	7.79	7.62	7.63	--	--
	L 305	--	14.01	13.91	13.62	13.48	13.42	13.40	13.18	13.13	13.10	12.91	12.92	12.93	--
	X 305	--	10.32	9.95	8.00	7.47	7.10	6.71	5.66	5.34	5.26	5.11	5.12	5.15	--
--	B 901	--	--	20.04	19.61	--	19.15	18.99	18.34	--	18.08	17.70	17.71	--	--
--	E 639	--	--	15.75	15.23	15.05	14.83	14.58	13.79	13.47	13.30	12.89	12.90	12.62	--
--	G 639	--	--	19.31	18.85	18.68	18.45	18.18	17.40	17.11	16.97	16.53	16.54	16.34	--
--	J 639	--	--	22.19	21.72	21.54	21.25	20.95	20.00	19.63	19.45	19.00	19.01	18.85	--
--	L 639	--	--	21.50	21.14	20.98	20.75	20.48	19.45	18.96	18.71	18.19	18.20	18.12	--
--	M 639	--	--	25.90	25.45	25.21	24.75	24.23	22.60	21.98	21.75	21.23	21.24	21.14	--
Alta Loma area	V 305	--	31.53	31.22	31.08	--	30.77	30.57	30.01	--	29.77	29.42	29.43	--	--
Fort Bend County															
--	A 805	--	--	79.21	--	--	--	--	78.20	--	--	77.53	77.55	--	--
--	B 805	--	--	76.49	--	--	--	--	75.38	--	75.32	74.55	74.57	--	--
--	Z 804	--	--	79.11	--	--	--	--	78.15	--	--	77.52	77.54	--	--
Waller County															
--	H 768	--	--	161.27	--	161.27	161.16	161.14	--	160.60	160.60	160.34	160.40	--	--
--	N 768	--	--	145.74	145.74	--	145.64	145.58	145.09	144.89	144.87	144.29	144.33	--	--
--	T 7	120.39	--	120.39	--	--	120.23	--	119.93	--	119.78	119.46	119.52	--	--
--	V 7	157.43	--	157.29	--	--	157.15	156.99	156.63	156.40	156.34	155.88	155.92	--	--

Table 4. Monumented benchmarks and elevations in the Gulf Coast aquifer system study area in southeast Texas.—Continued

[NGVD 29, National Geodetic Vertical Datum of 1929; NAVD 88, North American Vertical Datum of 1988; USGS, U.S. Geological Survey; extensometer, borehole extensometer; subsidence, land-surface subsidence; --, not available; NGS, National Geodetic Survey; ft, foot]

Extensometer site (fig. 73; table 5)	Historical geographic area (fig. 18B)[1]	Benchmark name	Elevation, in feet above NGVD 29[2]											Elevation, in feet above NAVD 88		
			1906–1918[3]	1932–1936[4]	1943	1951	1954	1959	1964	1973	1976	1978	1987	1987	1995–2002[5]	2019–21
Benchmarks located at land surface onsite or near selected extensometer sites																
Addicks	Katy area	K 1226	--	--	--	--	--	--	--	--	91.82	91.61	90.19	90.21	--	--
Baytown	Baytown area	M 1201	--	--	--	--	--	--	--	23.22	22.61	22.77	22.36	22.37	--	--
Clear Lake (deep)	Johnson Space Center area	W 1226	--	--	--	--	--	--	--	--	19.55	19.36	18.91	18.92	18.81	--
		X 1226	--	--	--	--	--	--	--	--	20.02	19.83	19.36	19.37	19.17	--
Seabrook		W 1201	--	--	--	--	--	--	--	10.34	9.45	9.27	8.76	8.77	--	--
East End	Historical Houston area	L 1147	--	--	--	--	--	34.13	33.54	31.60	31.07	30.80	30.25	30.26	--	--
		D 1227	--	--	--	--	--	--	--	--	31.23	30.97	30.42	30.43	--	--
Northeast		V 1278	--	--	--	--	--	--	--	--	--	45.91	45.13	45.14	44.85	44.87
		W 1278	--	--	--	--	--	--	--	--	--	46.50	45.71	45.73	45.42	45.44
Lake Houston	--	P 1278	--	--	--	--	--	--	--	--	--	53.43	52.98	52.99	--	52.99
	--	Q 1278	--	--	--	--	--	--	--	--	--	53.70	53.24	53.25	--	53.25
Pasadena	Pasadena area	B 1147	--	--	--	--	--	32.57	31.53	28.18	27.33	27.27	27.10	27.11	27.20	--
		U 1244	--	--	--	--	--	--	--	--	--	28.79	28.62	28.63	--	--

Extensometer site (fig. 73; table 5)	Historical geographic area (fig. 18B)[1]	Benchmark name	Elevation, in feet above NGVD 29			Elevation, in feet above NAVD 88							
			1976	1978	1987	1987	1991	1995	1997	2012	2018	2019	2021
Benchmarks located on the inner pipe of the extensometers at selected extensometer sites													
Addicks	Katy area	ADDICKS 1795	95.00	95.01	94.91	94.94	--	--	--	--	--	--	--
		ADDICKS 1795 RESET 1991[6,12]	--	--	--	--	--	--	--	--	93.80	--	93.95 93.84
East End	Historical Houston area	EAST END 995	33.53	33.51	33.40	33.41	--	--	--	--	--	--	--
Northeast		NORTHEAST 2250[6]	--	--	49.26	49.27	--	--	--	--	--	--	49.41
		NORTHEAST 2250 RESET[6]	--	--	49.67	49.68	--	--	--	--	--	--	49.82
Lake Houston	--	LAKE HOUSTON 2050 RESET	--	--	56.43	56.44	--	--	--	--	--	56.43	--
Pasadena	Pasadena area	PASADENA 2831	30.36	30.40	30.25	30.26	--	--	--	--	--	--	--
Baytown (shallow)	Baytown area	BAYTOWN 430	26.35	26.34	26.16	26.17	--	--	--	--	--	--	--
Baytown (deep)		BAYTOWN 1465	26.60	26.60	26.54	26.55	--	--	--	--	--	--	--

Table 4. Monumented benchmarks and elevations in the Gulf Coast aquifer system study area in southeast Texas.—Continued

[NGVD 29, National Geodetic Vertical Datum of 1929; NAVD 88, North American Vertical Datum of 1988; USGS, U.S. Geological Survey; extensometer, borehole extensometer; subsidence, land-surface subsidence; --, not available; NGS, National Geodetic Survey; ft, foot]

Extensometer site (fig. 73; table 5)	Historical geographic area (fig. 18*B*)[1]	Benchmark name	Elevation, in feet above NGVD 29			Elevation, in feet above NAVD 88							
			1976	1978	1987	1987	1991	1995	1997	2012	2018	2019	2021
Benchmarks located on the inner pipe of the extensometers at selected extensometer sites—Continued													
Clear Lake (shallow)	Johnson Space Center area	CLEAR LAKE 740	21.86	21.85	21.75	21.76	--	--	--	--	--	--	--
		CLEAR LAKE 740 RESET	--	--	21.66	21.67	--	--	21.68	--	--	--	--
Clear Lake (deep)		CLEAR LAKE 3072[6]	21.42	21.41	21.30	21.31	--	--	--	--	--	--	21.57
		CLEAR LAKE 3072 RESET[6]	--	--	21.22	21.23	--	--	--	21.31	--	--	21.51
		CLEAR LAKE 3072 BASE ARP (TXEX)	--	--	--	--	--	--	--	33.50	--	--	--
Seabrook		SEABROOK 1360	11.65	11.71	11.59	11.61	--	--	--	--	--	--	--
Texas City	Texas City area	MOSES LAKE 790	11.68	11.66	11.57	11.58	--	--	--	--	--	--	--

[1]NGS leveling surveys account for nearly all the benchmark elevations listed in this table during 1906–87. NGS surveys account for some benchmark elevations during 1995–2021; elevation data surveyed by other organizations met NGS "Blue Book" standards (described in National Oceanic and Atmospheric Administration [NOAA], 2022). Benchmark elevations listed in this table that were measured during and prior to 1973 generally were not published. Subsidence measurements during 1973–78, 1976–78, and 1963–78 are listed in NOAA (1980). Benchmark elevations from the 1987 and 1995–2021 surveys are available in NOAA (2021a).

[2]The spatial areas of the benchmark groups in Harris and Galveston Counties (fig. 70*A*) are spatially contiguous with the groundwater-well groups (fig. 18; table 2) and the Global Positioning System station groups (figs. 76–77; table 6), with the exception of the Southern Harris County group listed in this table.

[3]Elevations for benchmarks J 8, M 8, O 8, T 7, and Y 7 are from 1906; elevations for PTS 100, PTS 101, PTS 104, and PTS 185 are from 1915 (monumented by USGS); all remaining elevations for benchmarks named with a single letter followed by a 2-digit number beginning with "5" are from 1918.

[4]Elevations from this period are from 1932 to 1933 except for the following: benchmark PTS 185, which was leveled in 1934; benchmarks L 279, L 305, N 279, P 279, V 305, and X 305, which were monumented in 1935; and benchmarks C 170, F 170, Q 170, and F 173, which were monumented in 1936.

[5]The dates when the benchmark elevations were taken for surveys between 1995 and 2002 are available on the NGS website (NOAA, 2021a).

[6]The 2021 elevations at these benchmarks were determined by using Global Navigation Satellite System equipment, discussed in the "Global Navigation Satellite System Surveys" section of this report and in appendix 6.

[7]Cumulative subsidence at benchmark CONROE RM 1 is 1.5 ft based on 1.4 ft of subsidence between 1958–59 and 2021 at this benchmark and about 0.1 ft of subsidence at benchmarks K 88 and P 88 between 1932–33 and 1958–59.

[8]At benchmark K 88, a leveled elevation of 232.61 ft above NGVD 29 was determined by NGS in 1947.

[9]The subsidence of 2.3 ft estimated at benchmark V 1252 is based on 0.7 ft of subsidence at benchmark PTS 100 from 1915 to 1978 and 1.6 ft of subsidence at V 1252 between 1978 and 2021.

[10]A 1971 leveled elevation of 3.03 ft was determined by the U.S. Army Corps of Engineers.

[11]A 1971 leveled elevation of 22.48 ft was determined by the U.S. Army Corps of Engineers.

[12]At ADDICKS 1795 RESET 1991, the second elevation in 2021 is the measurement documented by the NGS by another party. The USGS measurement in 2021 at this extensometer was used to determine the Global Navigation Satellite System measurement uncertainty (described in appendix 6); therefore, the 2021 elevation of 93.84 from NGS was used to determine subsidence between 1991 and 2021 described in this report.

During 1943–64, measured subsidence was substantially greater in magnitude and spatial extent than subsidence previously measured during 1906–43 (fig. 5.2; table 4). This subsidence was caused by steadily increasing groundwater-level declines (figs. 14–16, 21–33) resulting from greatly increasing groundwater use compared to earlier periods (fig. 11; table 1). In the Pasadena and Baytown areas, the 1943–64 center of subsidence (fig. 5.2) shifted northward as additional industries developed in these areas compared to 1906–43 (fig. 5.1). Most of the measured subsidence was still confined to central, south-central, and southeastern Harris County and southeastern Galveston County; however, by 1964, an area of 1,355 mi^2 had subsided more than 1.0 ft (Gabrysch and Bonnet, 1975). During 1943–64, more than 5.0 ft of subsidence was observed in a part of the Pasadena area, although the greatest amount of subsidence through about 1954 (about 4.4 ft) was measured in the Texas City area (Winslow and Doyel, 1954). In the southern part of Montgomery County, subsidence during 1943–64 was estimated at less than 0.5 ft (Popkin, 1971; William F. Guyton and Associates, Inc., 1972). Based on the benchmark data used to construct the contours presented in Gabrysch (1967), between 0.5 and 1.5 ft of subsidence was measured during 1943–64 in the northeastern area of Brazoria County (Sandeen and Wesselman, 1973). The subsidence contours in figure 5.2 are from Jorgensen (1975) where the 1.5-ft subsidence contour line borders but does not include Brazoria County. During 1943–64, subsidence in Liberty County was estimated to be between 0.81 and 0.86 ft in Dayton, Tex., and 0.46 ft in nearby Liberty, Tex. (fig. 1), both of which used a large amount of groundwater (Anders and others, 1968). Subsidence in Fort Bend County during 1943–64 exceeded 1 ft in a small southeastern area and was 0.5 ft in the eastern third of the county (Wesselman, 1972). Subsidence in western Chambers County during 1943–64 was 0.5 ft, although in small areas, subsidence might have been greater (Wesselman and Aronow, 1971).

During 1964–73, measured subsidence of greater than 1.0 ft primarily occurred in central, south-central, and southeastern Harris County. However, the area of subsidence expanded farther into Brazoria, Fort Bend, and Galveston Counties (fig. 5.3; table 4) in conjunction with population growth and decreases in groundwater levels in these areas (figs. 21–33) (Gabrysch and Bonnet, 1975). The largest amount of measured subsidence (greater than 3.5 ft) was centered in the eastern part of the Pasadena area (Gabrysch and Bonnet, 1975). This subsidence in the Pasadena area was the result of continued substantial groundwater-level declines (fig. 26); the period during 1964–73 included several years from the period of maximum historical groundwater use (1968–75) in this area (fig. 11; table 1). Although subsidence in the Pasadena and Baytown areas during 1964–73 was less than subsidence during 1943–64, measured subsidence was still as much as about 3.5 and 2.5 ft, respectively. In the Texas City area, most of the 1.0 ft of subsidence during 1943–64 had occurred by 1952. After 1952, subsidence was minimal because of a conversion from groundwater to surface water from the Brazos River in 1948, followed by a rapid rise in groundwater levels thereafter (wells D–H, fig. 16) (Lockwood, 1954; AMOCO, 1958). Subsidence in central Harris County during 1964–73 was similar to the subsidence during 1943–64. By the end of 1973, approximately 2,500 mi^2 had subsided greater than 1.0 ft (Gabrysch and Bonnet, 1975).

The period from 1973 to 1978 is much shorter than the three prior time periods; therefore, making direct comparisons with subsidence maps from prior time periods is difficult. In general, subsidence of between 0.75 and 1.25 ft principally occurred across central, south-central, and southeastern Harris County, and lesser amounts occurred in Brazoria, Chambers, Fort Bend, Galveston, Liberty, and Waller Counties (fig. 5.4; table 4). The maximum subsidence for this period was as much as 1.4 ft in the Pasadena area (Gabrysch, 1982b). As groundwater regulation was introduced after the establishment of the HGSD in 1975, water use moved northward and westward into the Katy area (fig. 11; table 1), resulting in continued groundwater-level declines in northern, northwestern, and western Harris County (figs. 21–23), whereas groundwater levels in south-central and southeastern Harris County rose towards the end of this period (figs. 26–27).

During 1978–87, the groundwater-level response to groundwater-use restrictions instituted by the HGSD in 1976 was more pronounced than in previous years. The associated water-level recovery in south-central and southeastern Harris County (figs. 26–27) resulted in a decrease in the effective stress; therefore, measured subsidence during this period in the Baytown and Pasadena areas was minimal and less than the measured subsidence in central, northern, northwestern, western, and southwestern Harris County (fig. 5.5; table 4). In the Pasadena area, maximum subsidence decreased to 0.3 ft during 1978–87 compared to 1.4 ft during 1973–78 (Gabrysch and Coplin, 1990). However, continued groundwater-level declines in northern, northwestern, western, and southwestern Harris County (figs. 21–24) continued to increase the effective stress on the aquifer; thus, the maximum observed subsidence (about 2 ft) during 1978–87 occurred in these parts of Harris County (Gabrysch and Coplin, 1990). Overall, subsidence continued to increase in northern Harris, southern Montgomery, eastern Fort Bend, and Waller Counties. The pattern of increasing subsidence in these counties (or parts of counties) coincided with ongoing groundwater-level declines. The groundwater-level declines were a result of population growth and increases in groundwater demands, which were prevalent to the west and north of Harris County (figs. 19–23, 31, and 35).

Borehole Extensometers

A borehole extensometer (hereinafter, "extensometer") is used to measure the one-dimensional thickness of a specified depth interval of an aquifer system. An extensometer is often described as a deep benchmark, in which changes in the vertical distance between the deep benchmark (bottom or anchor depth of the extensometer) and a surface reference point (a

concrete pad at land surface or the depth of the extensometer concrete pad piers, typically about 20 ft bls) are measured. Compaction in the aquifer system shortens this distance, and expansion lengthens this distance. Extensometers can measure compaction at a fine resolution, typically at or less than 0.004 inches (Bawden and others, 2003). Measurement precision varies somewhat depending on the type of extensometer, and the resolution of 0.004 in. or less described in Bawden and others (2003) is based on a lever arm and counterweight style of extensometer. The measurement precision for the different styles of extensometers used in the greater Houston area is likely similar to what Bawden and others (2003) reported.

To construct an extensometer well similar to those in the study area (fig. 71) (excepting the Fort Bend and early cable-based extensometers), a borehole is first drilled to a predetermined depth, generally below the depth of expected groundwater-level decline. A steel outer casing with one or more slip joints and a screened interval is installed in the previously drilled borehole. The slip joints help to prevent crumpling and collapse of the well casing as compaction of subsurface sediments occurs, and the screened interval allows groundwater to enter the casing of the piezometer, a type of small diameter well with a screened interval that is used to measure the groundwater level. A substantial cement plug is installed and set at the base of the extensometer, and after the cement plug hardens, the smaller diameter inner pipe is inserted downhole inside the outer casing and positioned to rest on the upper surface of the cement plug at depth. This rigid inner pipe therefore extends vertically from the top of the cement plug (the elevation of which is known as the "anchor depth") to slightly above land surface, thus providing a fixed reference elevation above land surface for measuring changes in land-surface elevation. At land surface, a concrete slab is poured that couples the piers and the slab. This construction design helps to eliminate the continuous shrink and swell associated with soil-moisture changes common in the upper 20 ft or so of fine-grained sediments. A metal gage house is constructed on the concrete slab, and a shaft encoder or clock-driven mechanical chart recorder (or "analog recorder") is mounted to a steel table that is attached to the concrete slab. A calibrated steel tape connects the recorder to the top of the inner pipe; because the steel table is anchored to the concrete slab, compaction can be accurately measured and recorded. These recorded values over time represent the cumulative compaction that has occurred at the extensometer site based on the decrease in the aggregate interbed and confining unit thickness that is propagated upward. Because the extensometer functions as a piezometer and an extensometer and is colocated along with a number of other piezometers screened at various depths, the cause-and-effect relation between the changes in groundwater level in the aquifer and the changes in land-surface elevation can be established. Detailed information on the scientific theory, construction, and operation of extensometers is presented in Gabrysch (1984).

A total of 14 extensometers at 12 sites were installed in the Houston-Galveston region to monitor compaction of subsurface sediment (figs. 72–73; table 5). Four of these sites (Addicks, Northeast, East End, and Southwest) are locations of current or former City of Houston municipal well fields (fig. 11*I*). The first extensometer in the greater Houston area was installed and instrumented in September 1959 at the East End extensometer site (fig. 72) (TWDB 6522615; table 3.1) and recorded almost no subsidence through September 1962 when the well casing collapsed. It was determined this extensometer might not have been working correctly (the minimal subsidence it recorded seemed unlikely), so reinstallation occurred in 1973 in a different well at the East End extensometer site. A second extensometer was installed in October 1962 in an existing well at the Johnson Space Center site. The Johnson Space Center extensometer was initially installed and recording of compaction began in 1962; however, the cable assembly at this site required a replacement in 1973; therefore, the compaction record at this extensometer was restarted in July 1973 at a value of 1.35 ft (fig. 74*K*), which was the cumulative compaction recorded prior to that date.

The East End extensometer enclosure. The first extensometer in the greater Houston area was installed and instrumented in September 1959 at the former East End well 1 (TWDB well 6522615; table 3.1). Because the well casing collapsed, this extensometer was reinstalled on July 20, 1973, in a purpose-built well located a short distance from the original well. Photograph by Matthew Barnes, U.S. Geological Survey, August 24, 2022.

The Pasadena extensometer enclosure. This extensometer was installed on October 8, 1975. Photograph by Alexandra Adams, U.S. Geological Survey, August 31, 2022.

The Texas City extensometer enclosure, installed on July 13, 1973. This was the third of 14 extensometers installed and is the southernmost extensometer in the greater Houston area. Photograph by Alexandra Adams, U.S. Geological Survey, August 31, 2022.

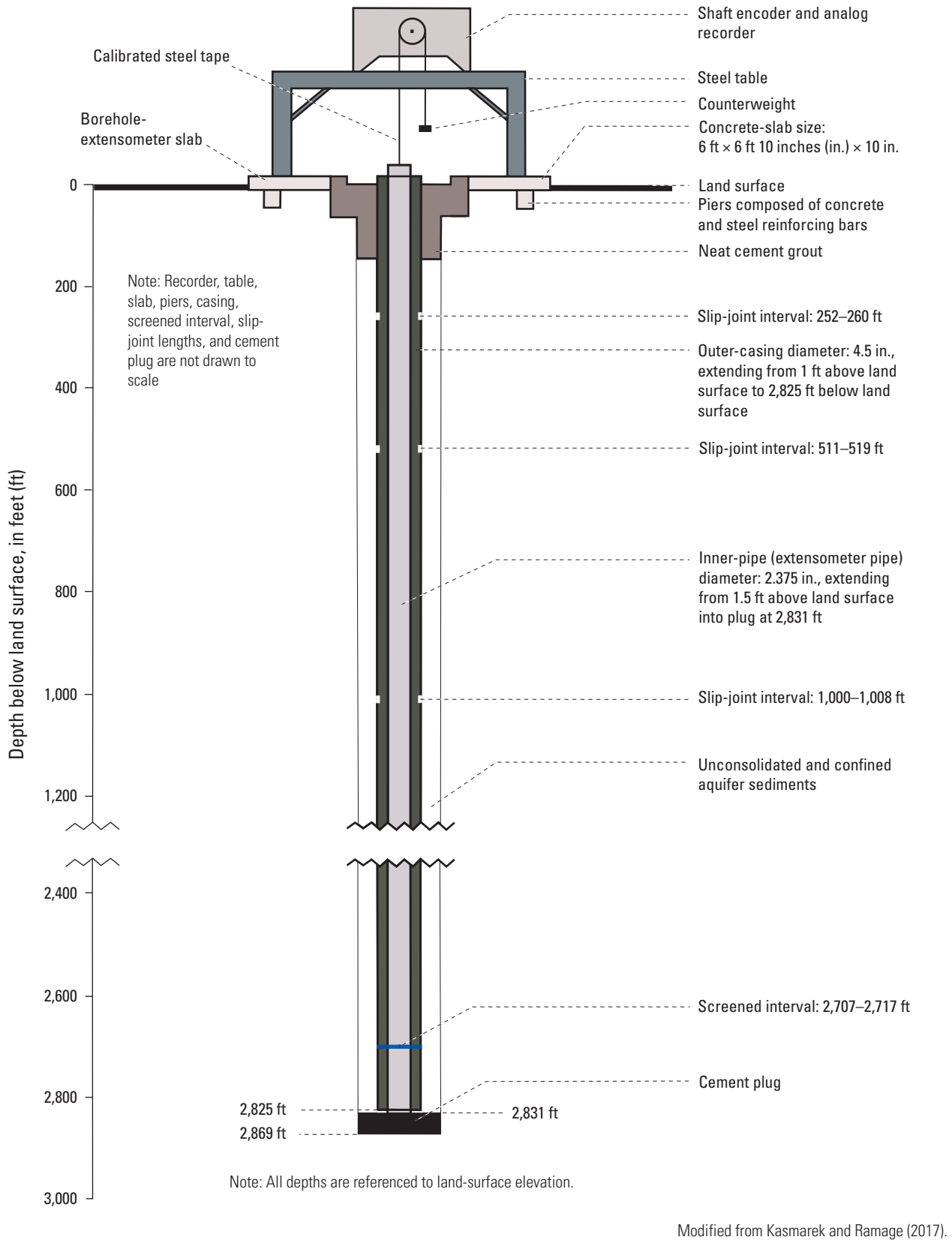

Figure 71. Diagram illustrating the Pasadena borehole extensometer (table 5).

The design of these first two extensometers (initial East End and Johnson Space Center extensometers) differed from the subsequent 11 extensometers installed in the study area because of the use of a steel cable weighted at the bottom of the borehole and counterweighted at the surface versus the use of a small-diameter solid inner pipe. After it was determined that the cable assembly at the East End and Johnson Space Center extensometers required replacement, these sites were converted to the "inner pipe" style of extensometer used at the other 11 extensometer sites.

The next 11 extensometers (fig. 72) were installed during 1973–80, including the reinstallation of the East End extensometer onsite at a newly drilled well in 1973. A total of six extensometers only record compaction in the Chicot aquifer, and seven record compaction in the Chicot and Evangeline aquifers (fig. 73). The Pasadena extensometer records compaction in the Chicot and Evangeline aquifers and in a small portion (initially estimated as about 15 ft) of the Burkeville confining unit (fig. 73) (Gabrysch, 1982b). At the Baytown site and the Clear Lake extensometer site (hereinafter, the "Clear Lake site"), two colocated extensometers anchored at different depths are used to directly monitor two depth intervals and indirectly monitor the depth interval between the anchor depths (fig. 73). The anchor depths at the Johnson Space Center extensometer site (hereinafter, the "Johnson Space Center site") and Clear Lake site (including the shallow and deep extensometers) were selected so that compaction information could be compared between these two sites (Gabrysch, 1982b) between the intervals of 750 ft, 1,722 ft, and 3,053 ft below NAVD 88. Compaction data collection from the extensometers began during 1973–80, providing an uninterrupted time series of aquifer-system compaction of nearly 50 years as of 2022. Compaction measurements are made about every 4 weeks, and the data are stored in the NWIS database (USGS, 2021b). Onsite at each extensometer, a number of monitoring wells are used to obtain groundwater levels at a number of depth intervals (figs. 37–44). The groundwater level is also monitored in the borehole of each extensometer through a 10-ft screened interval above the cement plug. This borehole groundwater level is shown alongside the compaction measured at each extensometer site on figure 74.

Near the Addicks site, substantial water-level declines had already occurred in the Chicot and Evangeline aquifers by the time of the extensometer installation. Groundwater levels in the colocated monitoring wells onsite show the continued decline of Chicot and Evangeline aquifer groundwater levels until the early 2000s, at which time a recovery began (fig. 39). Concurrent with the groundwater-level recovery in the early 2000s was a reduction in the compaction rate (fig. 74); the total additional compaction during 2005–20 was only 0.36 ft compared to 3.4 ft during 1974–2004. A production well (well F, fig. 39) is present onsite with a lower screened interval near the screened interval of the extensometer borehole, along with several other production wells within a 1-mile radius, which results in greater groundwater-level fluctuations at this site than at other extensometer sites.

For the Northeast and Southwest sites, which were installed approximately 1 week apart in 1980 (table 5), the historical groundwater-level minimums reached in about 1982 are generally similar (figs. 40, 42). However, about 0.7 ft more compaction occurred at the Southwest site compared to the Northeast site during 1982–87 (fig. 74). The additional 0.7 ft of compaction might be associated with the presence of an onsite production well (well E, fig. 42) and a cone of depression in the groundwater levels that forms near the site when large amounts of groundwater are withdrawn to meet periods of high demand. Groundwater levels for well E at the Southwest site were only measured two times outside of winter prior to 1998; one of these measurements was in 1992 and showed a substantial decline (fig. 42*E*). During 1982–87, groundwater levels during the summer at this well were likely lower than the static groundwater level and contributed to greater subsidence at the Southwest site compared to the Northeast site.

Compared to the other extensometer sites, the greatest decrease in the rate of compaction during the shortest period of time was recorded at the Pasadena site (fig. 74*F*). However, this substantial decrease in the rate of compaction at the Pasadena site did not coincide with a recovery of the groundwater level in the extensometer borehole (fig. 74*F*). Four colocated wells screened between 715 and 1,812 ft bls (wells F–I, fig. 37; table 3) show a rapid recovery of groundwater levels between 1976 and early 1979 (fig. 37). Thus, the decrease in effective stress in this interval more than offset the continued stress in the deepest interval of the extensometer site. The pressure changes in the coarse- and fine-grained sediment layers vary between different depth intervals, illustrating the need to monitor groundwater levels at multiple locations along the vertical depth profile (Gabrysch and Bonnet, 1974), particularly in water-production zones.

Along with the Pasadena extensometer, the Baytown extensometers are in an area with the greatest subsidence (fig. 70) and recorded among the greatest amounts of compaction of any extensometer in the greater Houston area initially after installation (fig. 74*G–H*). The compaction records at both Baytown extensometers include abrupt changes in subsidence during 1978–83 (fig. 74*G–H*) that are attributed by Gabrysch (1982b) to the shrinking and swelling of the soil at the site. This could have been caused by a lack of concrete piers supporting the concrete slab—an initial design consideration that was addressed in a modification to the original design in 1982 (Kasmarek and others, 2010). Compaction recorded at the Baytown (deep) extensometer was greater than the compaction recorded by the Baytown (shallow) extensometer through about 2010 (fig. 74*G–H*) (Kasmarek and others, 2016). Although about 80 percent of the compaction from 1973–2010 occurred above the anchor depth of the Baytown (shallow) extensometer, the remaining 20 percent was due to groundwater-level declines in the Evangeline aquifer largely as a result of groundwater use in the Pasadena area. During 2010–15, the compaction rate increased substantially for the Baytown (shallow) extensometer and increased to a lesser

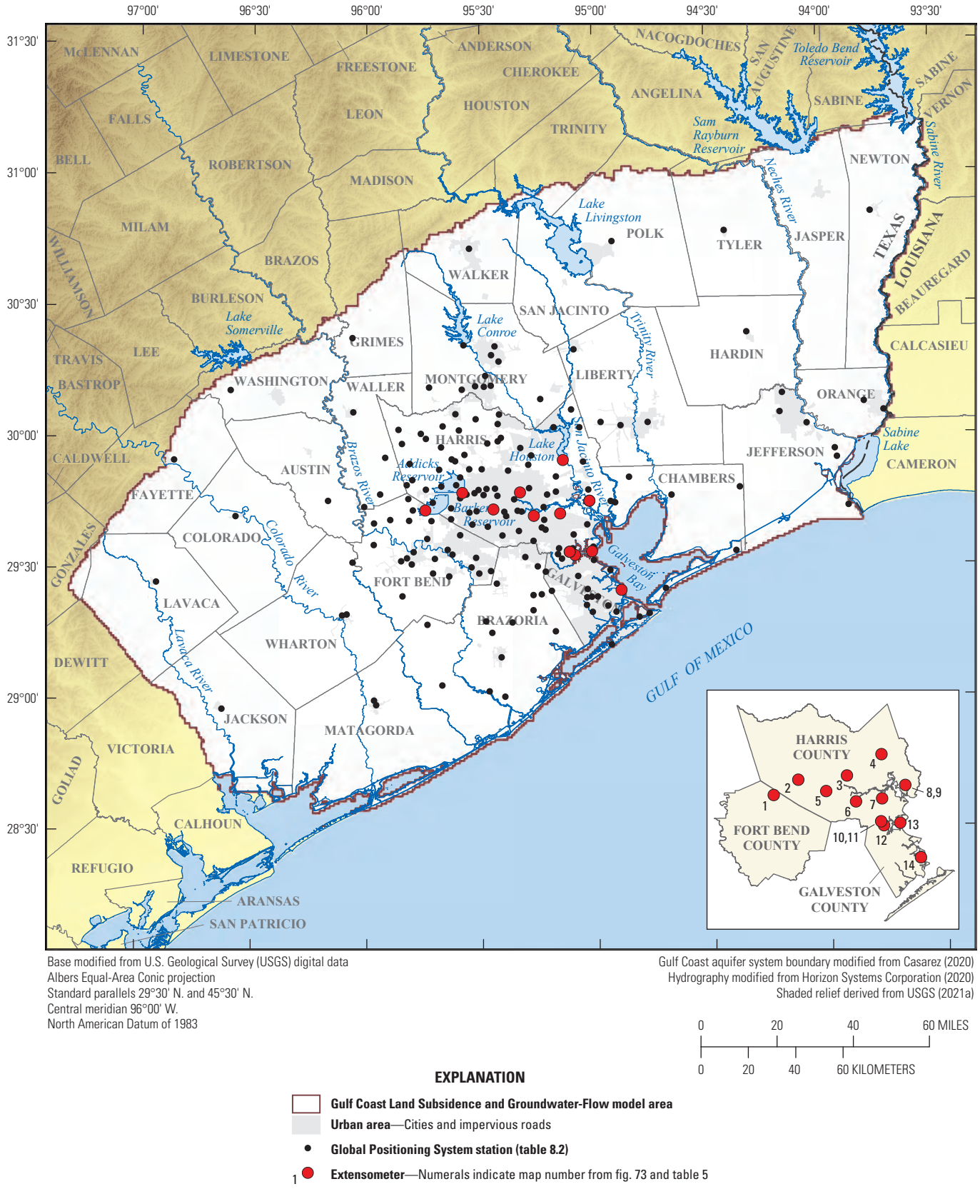

Figure 72. Locations of extensometers and selected Global Positioning System stations used to measure land-surface subsidence for the Gulf Coast aquifer system study area in southeast Texas.

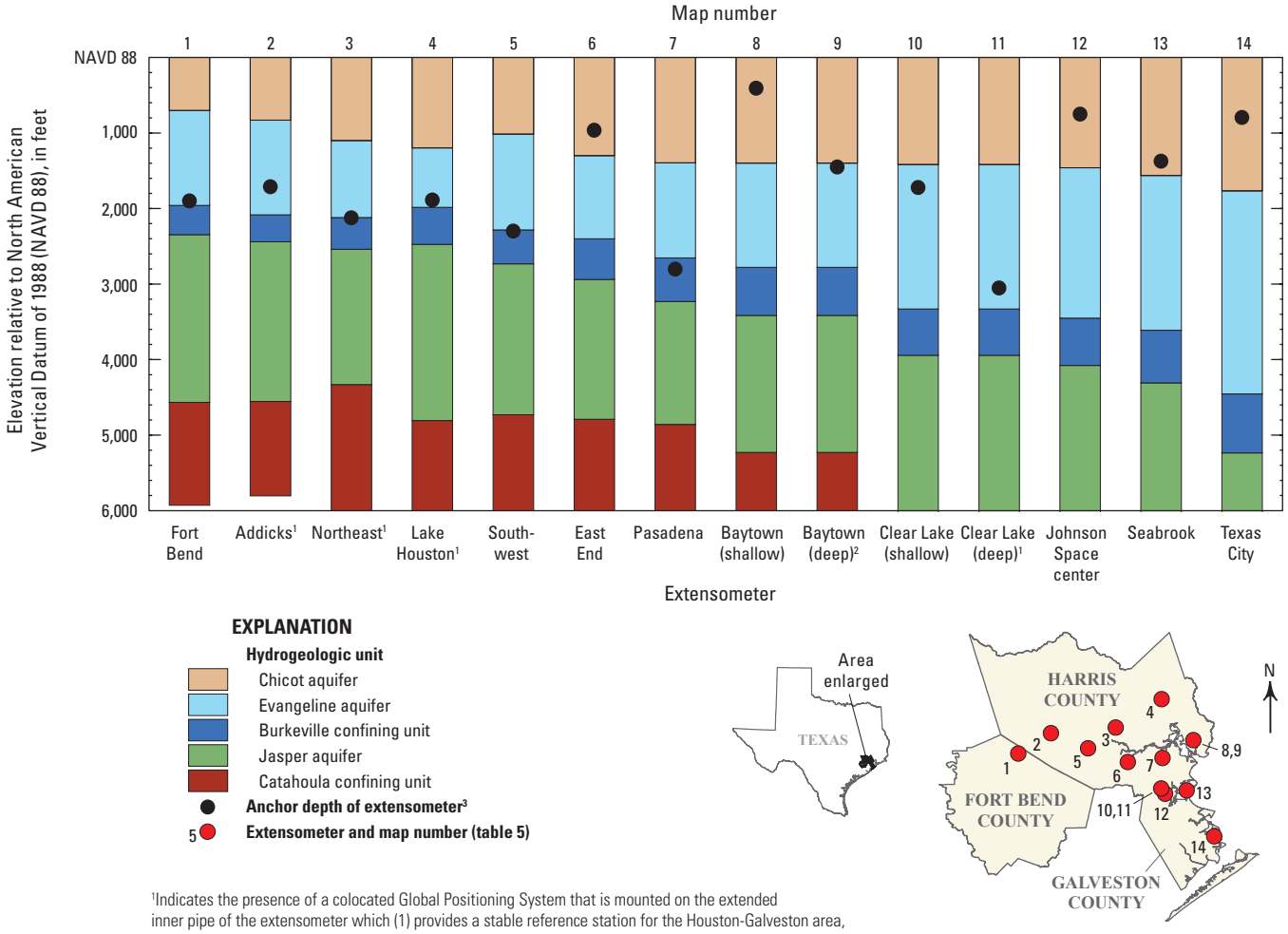

[1]Indicates the presence of a colocated Global Positioning System that is mounted on the extended inner pipe of the extensometer which (1) provides a stable reference station for the Houston-Galveston area, and (2) measures deep-seated compaction below the cement plug of the extensometer. These sites are referred to as Continuously Operating Reference Stations, or "CORS" sites.
[2]The Baytown (deep) extensometer is anchored about 75 feet into the Evangeline aquifer. However, considering this extensometer records compaction across about 1,400 feet of Chicot aquifer sediment (fig. 38), this extensometer is considered to record compaction only in the Chicot aquifer.
[3]The anchor depth of an extensometer is the depth at which the inner pipe rests on a concrete plug at the bottom of the borehole.

Figure 73. Depth intervals of extensometers installed in the greater Houston area.

extent at the Baytown (deep) extensometer; after 2015, the compaction rate for both extensometers was either approximately zero (for the deep site) or showed slight uplift (for the shallow site) (fig. 74*G–H*) (Kasmarek and others, 2016).

Similar to the groundwater levels at the other extensometer sites, groundwater levels had already declined substantially near the Lake Houston site when the extensometer was installed (fig. 26). Groundwater-level declines in the Chicot aquifer and upper part of the Evangeline aquifer ceased by the early 1990s (fig. 41), leading to a substantial reduction in compaction at this site (fig. 74*C*), although groundwater-level declines continued in the extensometer borehole anchored in the lower part of the Evangeline aquifer until about 2005 (figs. 41, 74*C*). Thus, similar to the Pasadena site, an understanding of compaction at the Lake Houston site requires analysis of the groundwater level at multiple depth intervals. Substantial groundwater-level declines occurred in the upper part of the Jasper aquifer from about 2000 through 2020 (fig. 41*I*). The extensometer at the Lake Houston site is anchored at 1,888 ft below NAVD 88 (table 5); therefore, water-level declines in the Jasper aquifer are not reflected in the compaction data. However, continued groundwater-level declines in the extensometer borehole have resulted in only minor continued subsidence at this site. A substantial thickness of fine-grained sediment separates the shallower wells (wells C–G) from the deeper wells (wells H–I) at the Lake Houston site (fig. 41). Additionally, groundwater use occurs in the Jasper aquifer to the west and more substantially to the northwest updip from this extensometer site. These factors could explain the groundwater-level declines in wells H–I at the Lake Houston site relative to the recovery of groundwater levels in the shallower wells at this site.

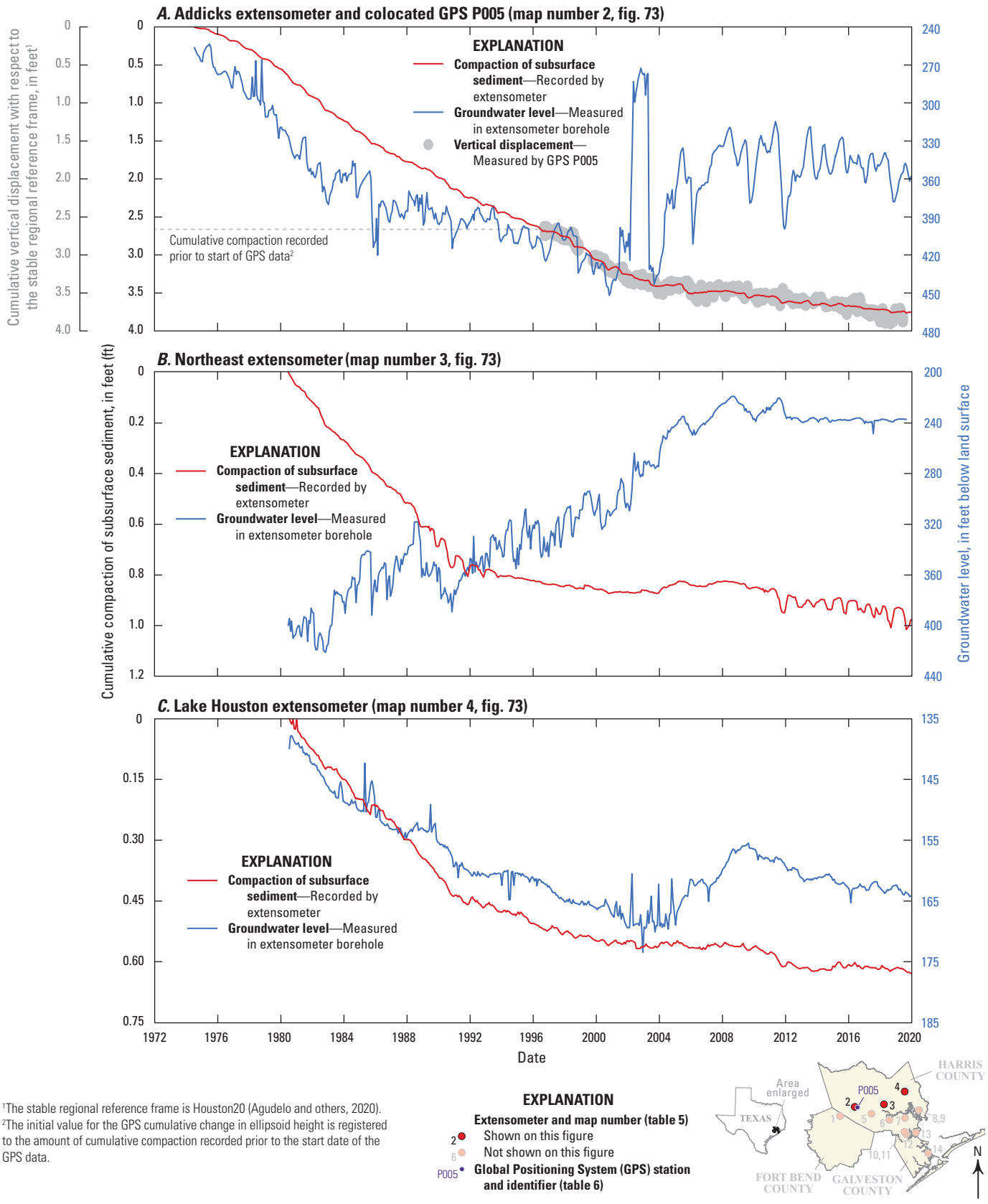

[1]The stable regional reference frame is Houston20 (Agudelo and others, 2020).
[2]The initial value for the GPS cumulative change in ellipsoid height is registered to the amount of cumulative compaction recorded prior to the start date of the GPS data.

Figure 74. Cumulative compaction and groundwater levels recorded at *A*, Addicks, *B*, Northeast, *C*, Lake Houston, *D*, Southwest, *E*, East End, *F*, Pasadena, *G*, Baytown (shallow), *H*, Baytown (deep), *I*, Clear Lake (shallow), *J*, Clear Lake (deep), *K*, Johnson Space Center, *L*, Seabrook, and *M*, Texas City extensometer sites in the Gulf Coast aquifer system study area in southeast Texas.

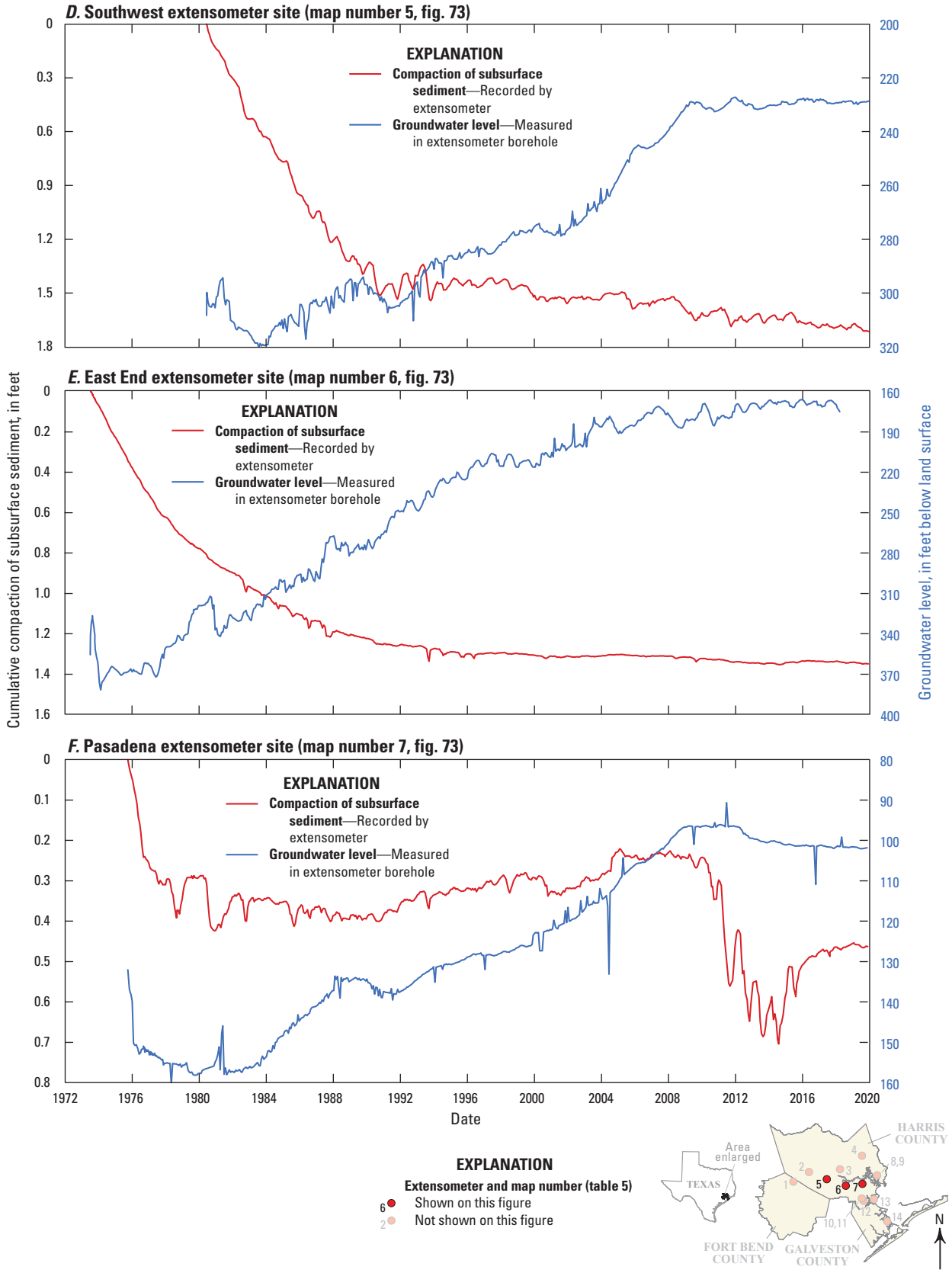

Figure 74.—Continued

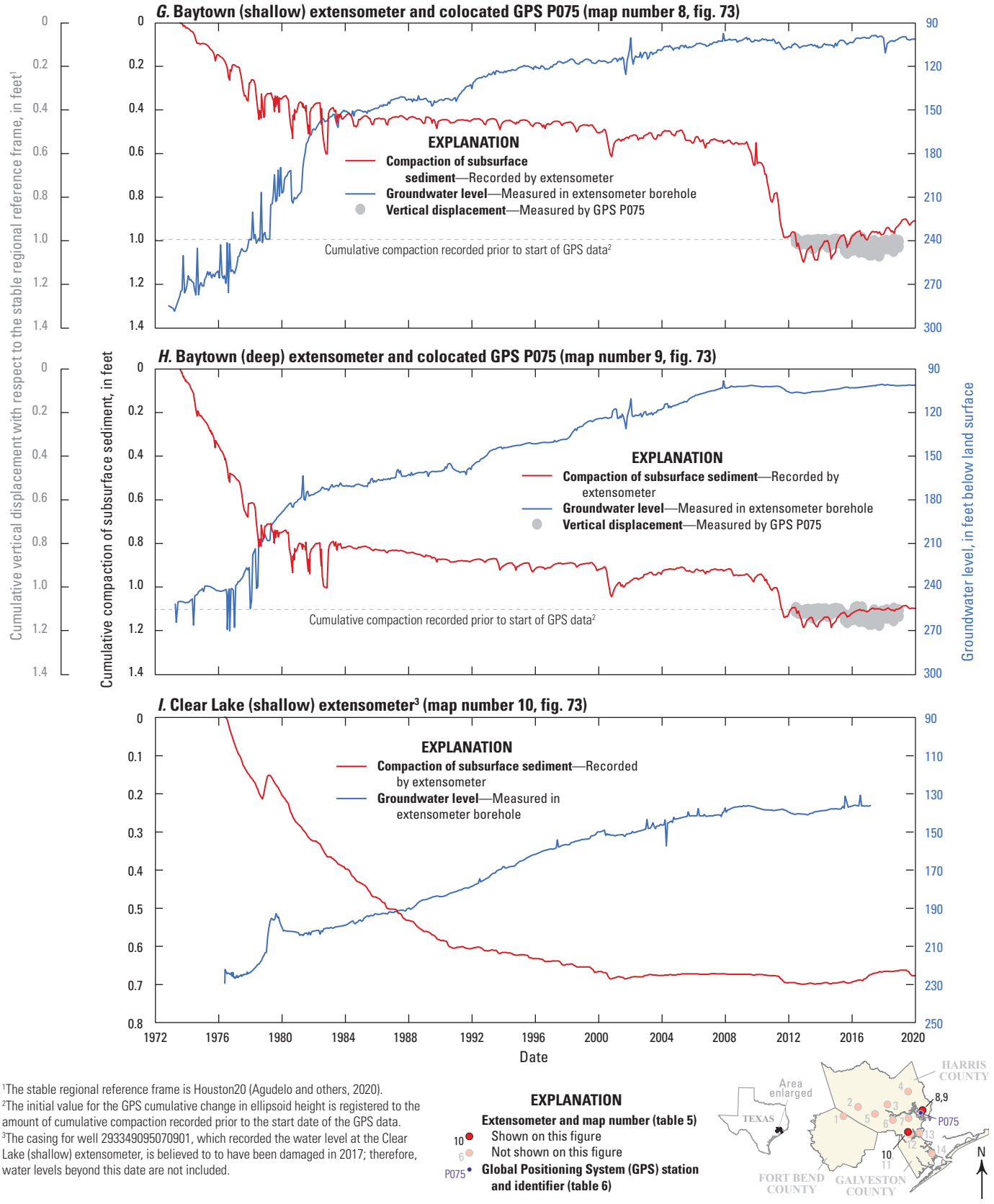

[1]The stable regional reference frame is Houston20 (Agudelo and others, 2020).
[2]The initial value for the GPS cumulative change in ellipsoid height is registered to the amount of cumulative compaction recorded prior to the start date of the GPS data.
[3]The casing for well 293349095070901, which recorded the water level at the Clear Lake (shallow) extensometer, is believed to to have been damaged in 2017; therefore, water levels beyond this date are not included.

Figure 74.—Continued

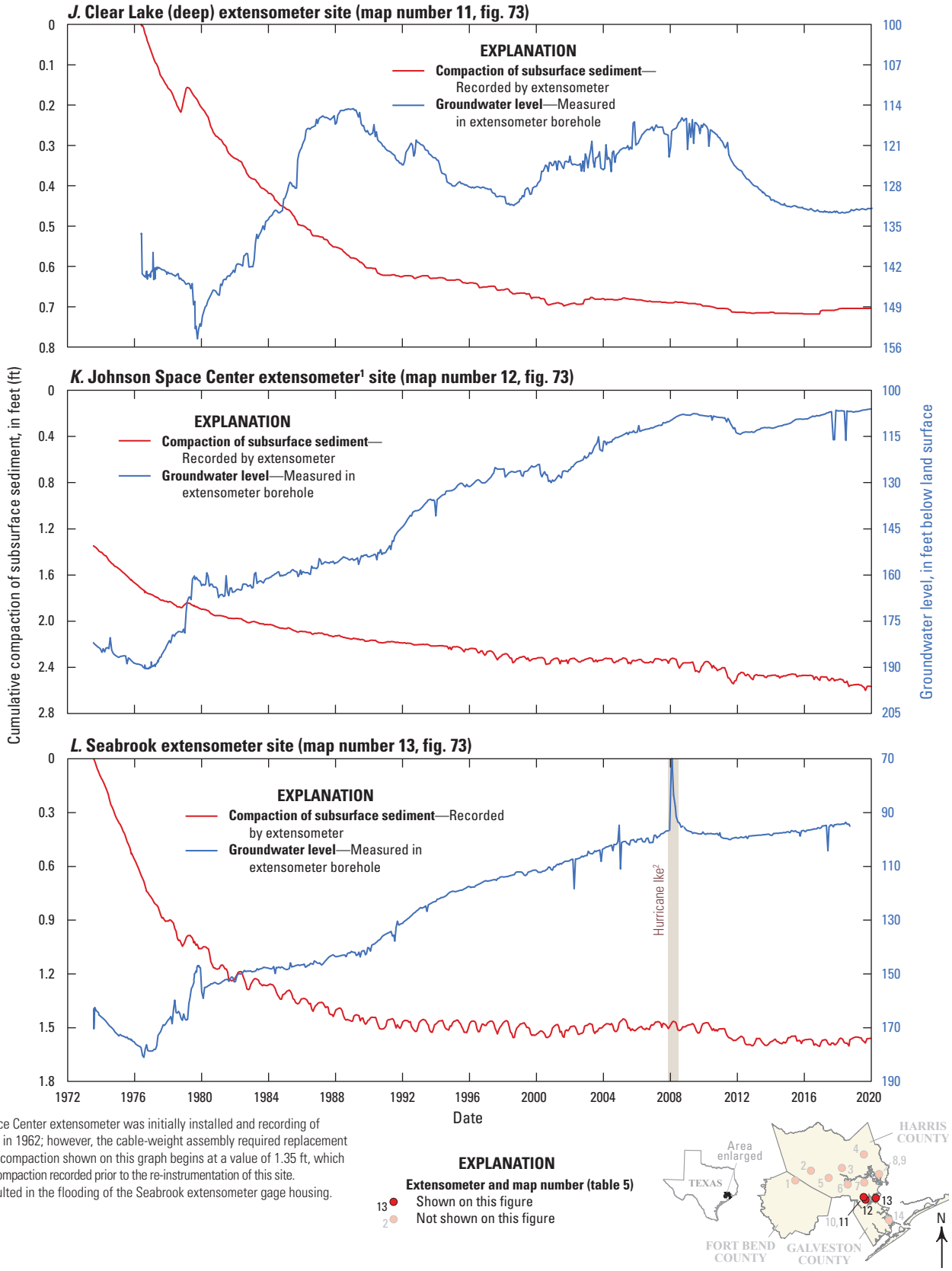

[1]The Johnson Space Center extensometer was initially installed and recording of compaction began in 1962; however, the cable-weight assembly required replacement in 1973. Thus, the compaction shown on this graph begins at a value of 1.35 ft, which is the cumulative compaction recorded prior to the re-instrumentation of this site.
[2]Hurricane Ike resulted in the flooding of the Seabrook extensometer gage housing.

Figure 74.—Continued

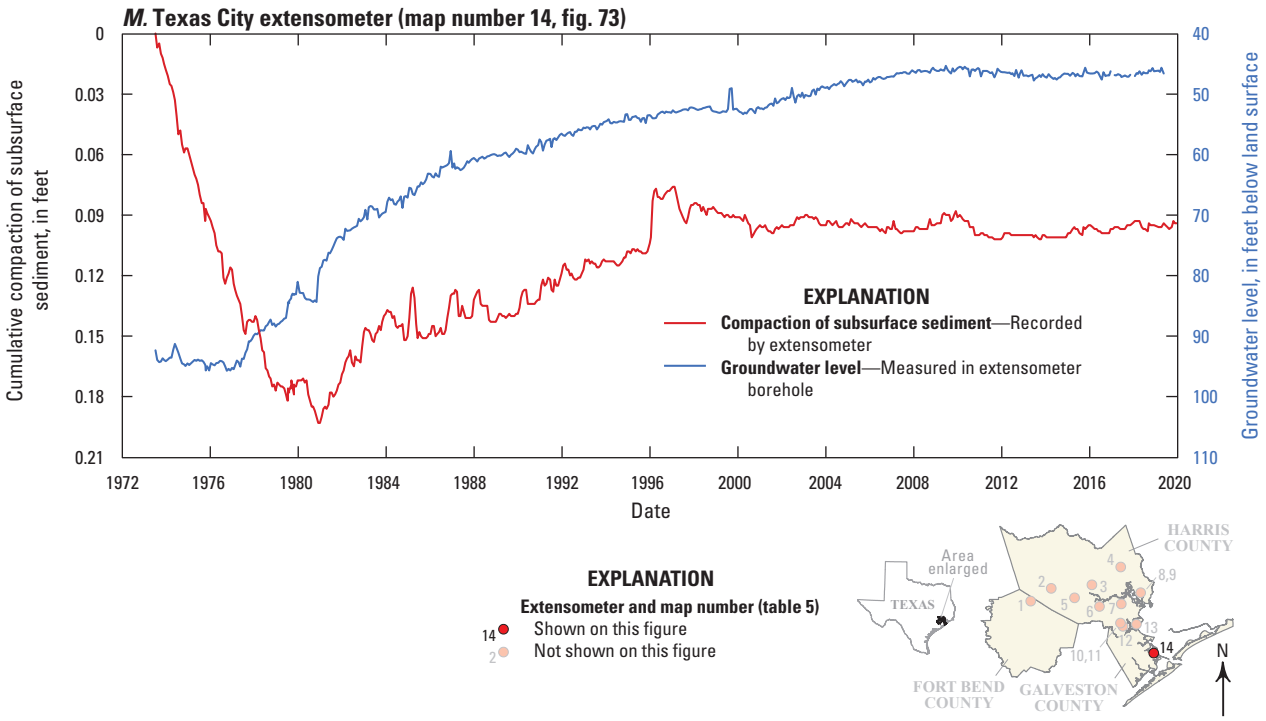

Figure 74.—Continued

The Johnson Space Center and Clear Lake sites are separated by approximately 1.6 mi; therefore, compaction patterns can be compared across a relatively short distance. Although the Johnson Space Center extensometer anchor elevation below NAVD 88 is relatively shallow (750 ft; table 5; fig. 73) compared to the Clear Lake shallow and deep sites (1,722 and 3,053 ft below NAVD 88, respectively; table 5; fig. 73), about 80 percent of the compaction during 1976–2019 occurred in the Chicot aquifer above the anchor depth of the Johnson Space Center extensometer.

The compaction rate at the Seabrook site decreased rapidly with the recovery of groundwater levels at this site to the point that the compaction rate was approximately zero by 1993 after groundwater levels had risen about 55 ft (figs. 43, 74*L*). The extensometer at Seabrook is anchored near the base of the Chicot aquifer (fig. 73). Most of the subsidence, however, is probably captured by the extensometer record at this site because (1) the approximately 1,373-ft thickness of the Chicot aquifer above the anchor depth of this extensometer means that few wells are completed in the Evangeline aquifer, (2) the similarity of the compaction measured at the nearby Clear Lake shallow and deep extensometers indicates that groundwater withdrawals and related drawdowns were likely above the anchor depth of 1,722 ft below NAVD 88 for the Clear Lake shallow extensometer, and (3) similar amounts of compaction (0.51 and 0.50 ft at the Seabrook and Clear Lake shallow extensometers, respectively) were determined during 1978–87 (Gabrysch and Coplin, 1990).

For all extensometer sites, the greatest rates of compaction were during the historical period of greatest groundwater use in the greater Houston area that culminated in the 1970s, when corresponding groundwater levels were at their lowest, generally in the initial years after installation of most extensometer sites. Likewise, the compaction rates declined substantially, coincident with a recovery in groundwater levels, which is most clearly evident in the compaction and groundwater-level data at the Southwest, East End, Baytown, Clear Lake, Johnson Space Center, and Seabrook sites (fig. 74). Although groundwater levels measured in onsite colocated wells either rose or did not further decline after the implementation of groundwater regulations and conversion to surface-water sources near a given site (figs. 37–44), substantial rates of compaction attributed to residual compaction continued at several sites, particularly the Northeast, East End, Clear Lake, and Seabrook sites (fig. 74). In the process of residual compaction, faster draining, generally fine-grained units compacted first, followed by the compaction of thicker and more slowly draining fine-grained units—even after groundwater levels stabilized and rose (fig. 74). Although groundwater levels have risen at the extensometer sites (figs. 37–44), the rates of compaction have leveled off. Despite the rise in groundwater levels, compressed interstitial pore spaces in the aquifer system have largely remained collapsed, preventing the land surface from rising (fig. 74) except at the Pasadena and Texas City sites which indicate some degree of elastic expansion (fig. 74*F, M*). Therefore, the majority of compaction recorded at the extensometer sites is inelastic (permanent) (fig. 74).

Table 5. Location, subsidence, and compaction data for borehole extensometer sites in the Gulf Coast aquifer system study area in southeast Texas.

[ID, identifier; USGS, U.S. Geological Survey; CORS, Continuously Operating Reference Station; NAVD 88, North American Vertical Datum of 1988; extensometer, borehole extensometer; subsidence, land-surface subsidence; --, not available; installation dates are given in month/day/year]

Map ID (figs. 72–73)	USGS site ID	Extensometer site	CORS ID (fig. 75)	Extensometer installation date	Anchor elevation, in feet above NAVD 88	Latitude, in decimal degrees	Longitude, in decimal degrees	Extensometer-measured-compaction (installation–2020), in feet	Subsidence prior to extensometer installation, in feet	Cumulative subsidence (1906–2020), in feet	Percent of subsidence prior to extensometer installation
1	294327095445201	Fort Bend	--	6/7/2018	−1,900	29.7242	−95.7478	0.01	--	0.01	--
2	294726095351102	Addicks (fig. 39)	ADKS	7/11/1974	−1,711	29.7907	−95.5861	3.75	2.33	6.08	38
3	294728095200106	Northeast (fig. 40)	NETP	6/24/1980	−2,124	29.7909	−95.3340	0.98	5.84	6.82	86
4	295449095084101	Lake Houston (fig. 41)	LKHU	7/22/1980	−1,888	29.9132	−95.1455	0.63	3.46	4.09	85
5	294338095270402	Southwest (fig. 42)	--	6/17/1980	−2,299	29.7270	−95.4508	1.71	4.74	6.45	73
6	294206095162601	East End[1]	--	7/20/1973	−964	29.7017	−95.2741	1.35	6.08	7.43	82
7	294237095093204	Pasadena (fig. 37)	--	10/8/1975	−2,803	29.7102	−95.1593	0.46	8.70	9.16	95
8	294527095014910	Baytown (shallow) (fig. 38)	--	7/24/1973	−407	29.7578	−95.0307	0.91	8.23	9.14	90
9	294527095014911	Baytown (deep) (fig. 38)	--	7/24/1973	−1,451	29.7578	−95.0307	1.10	8.23	9.33	88
10	293349095070901	Clear Lake (shallow)	--	5/26/1976	−1,722	29.5638	−95.1193	0.68	4.98	5.66	88
11	293348095070604	Clear Lake (deep)	TXEX	5/26/1976	−3,053	29.5634	−95.1189	0.71	4.98	5.69	88
12	293306095054101	Johnson Space Center[2,3]	--	7/24/1973	−750	29.5519	−95.0960	2.57	4.19	6.76	62
13	293352095011601	Seabrook (fig. 43)	--	7/20/1973	−1,373	29.5648	−95.0215	1.56	3.38	4.94	68
14	292458094534206	Texas City (fig. 44)	--	7/13/1973	−794	29.4163	−94.8950	0.09	1.80	1.89	95

[1]An extensometer at the East End site was first installed in 1959 (TWDB 6522615; table 3.1) but was only operated until 1962, when the well casing collapsed. Reinstallation occurred in 1973 in a different well.

[2]The Johnson Space Center extensometer was initially installed and recording of compaction began in 1962; however, the cable assembly at this site required a replacement in 1973; therefore, the compaction record at this extensometer was restarted in July 1973 at a value of 1.35 feet, which was the cumulative compaction recorded prior to that date.

[3]Originally named for the National Aeronautics and Space Administration Space Center, which was renamed the Johnson Space Center in February 1973.

Global Navigation Satellite System Surveys

A GPS survey, which is one component of the Global Navigation Satellite System (GNSS), uses a U.S. Department of Defense satellite-based navigation system designed to provide continuous worldwide positioning and navigation capability (Sneed and Brandt, 2020). GPS surveying is a method used to measure data from satellites and Earth-based reference stations to accurately determine the position and ellipsoid height of geodetic monuments (Sneed and others, 2001). The GPS technique allows the GPS surveyor to obtain elevations at specific locations autonomously, rather than carrying an elevation from a known reference point to other points like the leveling technique requires. Just like leveling, however, repeated GPS surveys of the same points over time yield a series of elevations from which elevation changes are calculated. The 95-percent confidence interval for the GPS survey data is described in Wang (2022).

A GPS station continuously measures the three-dimensional position of a point on or near the Earth's surface. Thousands of GPS stations in the United States are operated by various scientific research consortiums, government agencies, private industries, or other groups. GPS stations generally collect position information every 15 seconds to 5 minutes which can then be processed to produce a daily position. Several groups process GPS data and make it publicly available, including the Nevada Geodetic Laboratory at the University of Reno, Nevada (Blewitt and others, 2018).

GPS stations have been installed in various locations across southeast Texas to track vertical displacement since the 1990s—some of which are shown on figure 72. The dense network of GPS stations in the greater Houston area, referred to as HoustonNet (Agudelo and others, 2020; Wang and others, 2022), consists of a collaboration among the HGSD, FBSD, University of Houston, LSGCD, Brazoria County Groundwater Conservation District, NGS, USGS, City of Houston, and Texas Department of Transportation. HoustonNet has grown to more than 230 sites throughout the region (Petersen and others, 2020), and GPS surveying has superseded leveling surveys as the primary method of determining subsidence in the greater Houston area. A detailed description of the GPS stations is provided in Zilkoski and others (2003).

In the greater Houston area, GPS data are collected and recorded at monitoring stations and processed quarterly by the University of Houston. Position coordinates for these data are initially provided in the global International GNSS Service reference frame of 2014, then are transformed into a stable regional reference frame. A regional reference frame is used to ensure that localized and temporal ground deformations, such as subsidence and fault creeping, are not obscured or biased (Agudelo and others, 2020). This initial regional reference frame, known as Houston12 (Kearns and others, 2018), consisted of 10 GPS stations in 2013 (Wang and others, 2013). The regional reference frame was updated in 2014 to only include sites outside of the greater Houston area (Houston16; Kearns and others, 2018) and was further refined to a network of 25 stations known as the Houston20 stable regional reference frame that uses 25 continuously operating GPS stations which have a long history (greater than 8 years) (Agudelo and others, 2020; Petersen and others, 2020). In addition to the Houston20 stable regional reference frame, four GPS stations in the greater Houston area (Addicks [ADKS], Northeast [NETP], and Lake Houston [LKHU], and Clear Lake [deep; TXEX]) (fig. 75; table 5) are referred to as Continuously Operating Reference Stations (CORS), which are GPS stations that include an antenna mounted on the extended inner pipe of the Addicks, Northeast, Lake Houston, and Clear Lake (deep) extensometers, respectively. This arrangement provides a stable reference frame to measure subsidence at other GPS stations and measures deep-seated compaction. Vertical displacement, for the purposes of this report, is described as "subsidence" or "uplift" for a GPS station at land surface, and as "deep-seated compaction" or "uplift" for a CORS. Deep-seated compaction, for the purposes of this report, refers to compaction below the cement plug (fig. 71) of the extensometers in the study area (fig. 73), similar to the definition from Yu and others (2014).

Prior to the installation of the ADKS CORS in 1993, about 0.09 ft of deep-seated compaction occurred during 1976–87 in the sediment below the anchor depth of the Addicks extensometer (fig. 73) based on changes in elevation at a monumented benchmark located on the inner pipe of this extensometer (ADDICKS 1795, table 4). This 0.09 ft of deep-seated compaction during 1976–87, plus the 1.57 ft of

The Addicks extensometer enclosure, installed on July 11, 1974. Also shown at the top of the enclosure is the antenna array for the ADKS Continuously Operating Reference Station (fig. 75*A*). Photograph by Matthew Barnes, U.S. Geological Survey, July 28, 2022.

compaction recorded by the Addicks extensometer (fig. 74*A*) during the same period, about equals the 1.63 ft of subsidence measured during 1976–87 at an onsite benchmark at land surface (K 1226; table 4). The ADKS GPS data indicate a deep-seated compaction of about 0.05 ft from mid-1993 to 2020 (fig. 75) (HGSD, 2021). Therefore, the compaction below the extensometer anchor depth during 1976–2020 is about 0.14 ft.

About 0.13 ft of deep-seated compaction occurred during 1978–87 at the Northeast site based on the difference of the estimated extensometer compaction (0.66 ft) and changes in elevation at two onsite benchmarks at land surface (mean of 0.79 ft) (V 1278, W 1278; table 4). During 1987–2020, mean subsidence at land surface was 0.28 ft (V 1278, W 1278; table 4), and the compaction recorded at the Northeast extensometer was 0.51 ft (fig. 74*B*). This 0.51 ft of compaction, plus the mean 0.14 ft of deep-seated uplift recorded by two monumented benchmarks located on the inner pipe of this extensometer (NORTHEAST 2250, NORTHEAST 2250 RESET; table 4) during the same period, about equals the mean 0.28 ft of subsidence measured during 1987–2020 at the two onsite benchmarks at land surface. The NETP GPS data indicate a deep-seated uplift of about 0.04 ft from mid-1993 to 2020 (fig. 75) (HGSD, 2021); however, additional uplift could have occurred from 1987–93. Therefore, the uplift below the extensometer anchor depth during 1978–2020 is about 0.01 ft

At the Lake Houston site, about 0.05 ft of deep-seated compaction probably occurred during 1978–87 based on the difference between the estimated extensometer-measured-compaction (0.40 ft) and changes in elevation at two onsite benchmarks at land surface (0.45 ft) (P 1278, Q 1278; table 4) during the same period. During 1987–2018, a groundwater-level decline of about 140 ft occurred in the Jasper aquifer at the Lake Houston site, about 120 ft of which occurred after 2002 (fig. 41). Additionally, groundwater levels declined about 10 ft in the lower part of the Evangeline aquifer at this site during 1987–2018 (fig. 41). Groundwater levels in the Jasper aquifer also declined during this period in northern Harris County (fig. 21) and principally in Montgomery County (figs. 19–20) where many production wells are screened in the Jasper aquifer. At the Lake Houston site, the pattern of groundwater-level change in the lower part of the Evangeline aquifer (fig. 41*H*) is similar to the groundwater-level declines in the Jasper aquifer, in contrast with the recovery in wells screened in the upper parts of the Evangeline and Chicot aquifers (wells C–G, fig. 41). The 140 ft of groundwater-level decline in the Jasper aquifer and lesser groundwater-level decline in the extensometer borehole during 1987–2018 (fig. 41*H*) could be expected to result in compaction. However, during 1987–2019 only about 0.01 ft of deep-seated compaction was measured based on changes in elevation at a monumented benchmark located on the inner pipe of this extensometer (LAKE HOUSTON 2050 RESET) (table 4). The LKHU CORS data indicate a deep-seated uplift of about 0.07 ft from about 1993 to 2020 (fig. 75) (HGSD, 2021). Therefore, during 1978–2020, the deep-seated compaction at Lake Houston site was between 0.06 ft of compaction and 0.02 ft of uplift. The absence of a clear pattern of deep-seated compaction changes over time could be caused by the substantial depth of the Jasper aquifer at this site (the top of the Jasper aquifer at this site is about 2,475 ft below NAVD 88) (figs. 41, 75*B*).

At the Clear Lake (deep) extensometer, about 0.12 ft of deep-seated compaction occurred during 1976–87 based on changes in elevation at a monumented benchmark located on the inner pipe of this extensometer (CLEAR LAKE 3072; table 4). When the 0.12 ft of deep-seated compaction during 1976–87 is added to the 0.53 ft of compaction recorded by the Clear Lake (deep) extensometer during the same period (fig. 74*J*), the resulting sum of 0.65 ft of compaction equals the mean change in elevation of 0.65 ft at two onsite benchmarks at land surface (W 1226, X 1226; table 4) during 1976–87. A deep-seated uplift of 0.08 ft during 1987–2012 occurred based on changes in elevation at a second monumented benchmark located on the extensometer inner pipe (CLEAR LAKE 3072 RESET; table 4), which was re-surveyed in 2012 to establish the TXEX CORS antenna reference point. Deep-seated uplift of about 0.11 ft occurred during 2011–20 based on the TXEX CORS station data (fig. 75) (HGSD, 2021), resulting in a 1987–2020 uplift of 0.19 ft. Therefore, the deep-seated uplift during 1976–2020 at this extensometer site is about 0.07 ft.

The results discussed for the Addicks, Northeast, Lake Houston, and Clear Lake (deep) extensometers, and by extension the CORS, indicate that the sediment at and below the anchor depth of these extensometers generally have been stable after installation of the GPS antennas (fig. 75)—a finding also described in Yu and others (2014) and Kearns and others (2015). Vertical movement of the inner pipes of these extensometers attributed to deformation processes occurring below their anchor depths after the CORS installation is minimal compared to the substantial subsidence in parts of the greater Houston area in the 1960s and 1970s based on changes in elevation at monumented benchmarks (table 4).

GPS stations outside of the greater Houston area showed relatively small amounts of subsidence; therefore, a subset of 89 GPS stations was used to describe GPS vertical-displacement patterns across the greater Houston area (fig. 76). Because subsidence, and thus GPS-derived vertical displacement, is largely correlated to groundwater-level declines, the GPS stations and groundwater wells with long-term groundwater-level data were placed into spatially coincident groups (figs. 18, 76). Each group contains stations with between 5.3 and 26.8 years of vertical-displacement data and contains at least one station with more than 13 years of data (fig. 76; table 6). The high temporal resolution of the GPS station data facilitates detailed time-series analyses of subsidence patterns when these data are combined with the spatial coverage of the GPS station network (fig. 76). The 2016–20 annual vertical-displacement rates were obtained from HGSD (HGSD, 2021) (fig. 77; table 6).

The Clear Lake (deep) extensometer enclosure, installed on May 26, 1976. At the top of the enclosure is the antenna array for the TXEX Continuously Operating Reference Station (fig. 75*B*). Photograph by Alexandra Adams, U.S. Geological Survey, August 31, 2022.

The Lake Houston extensometer enclosure, installed on July 22, 1980. This was the final extensometer installed during the 1960–80 timeframe. Also shown at the top of the enclosure is the antenna array for the LKHU Continuously Operating Reference Station (fig. 75*B*). Photograph by Matthew Barnes, U.S. Geological Survey, August 24, 2022.

The Northeast extensometer enclosure, installed on June 24, 1980. At the top of the enclosure is the antenna array for the NETP Continuously Operating Reference Station (fig. 75*A*). Photograph by Matthew Barnes, U.S. Geological Survey, August 24, 2022.

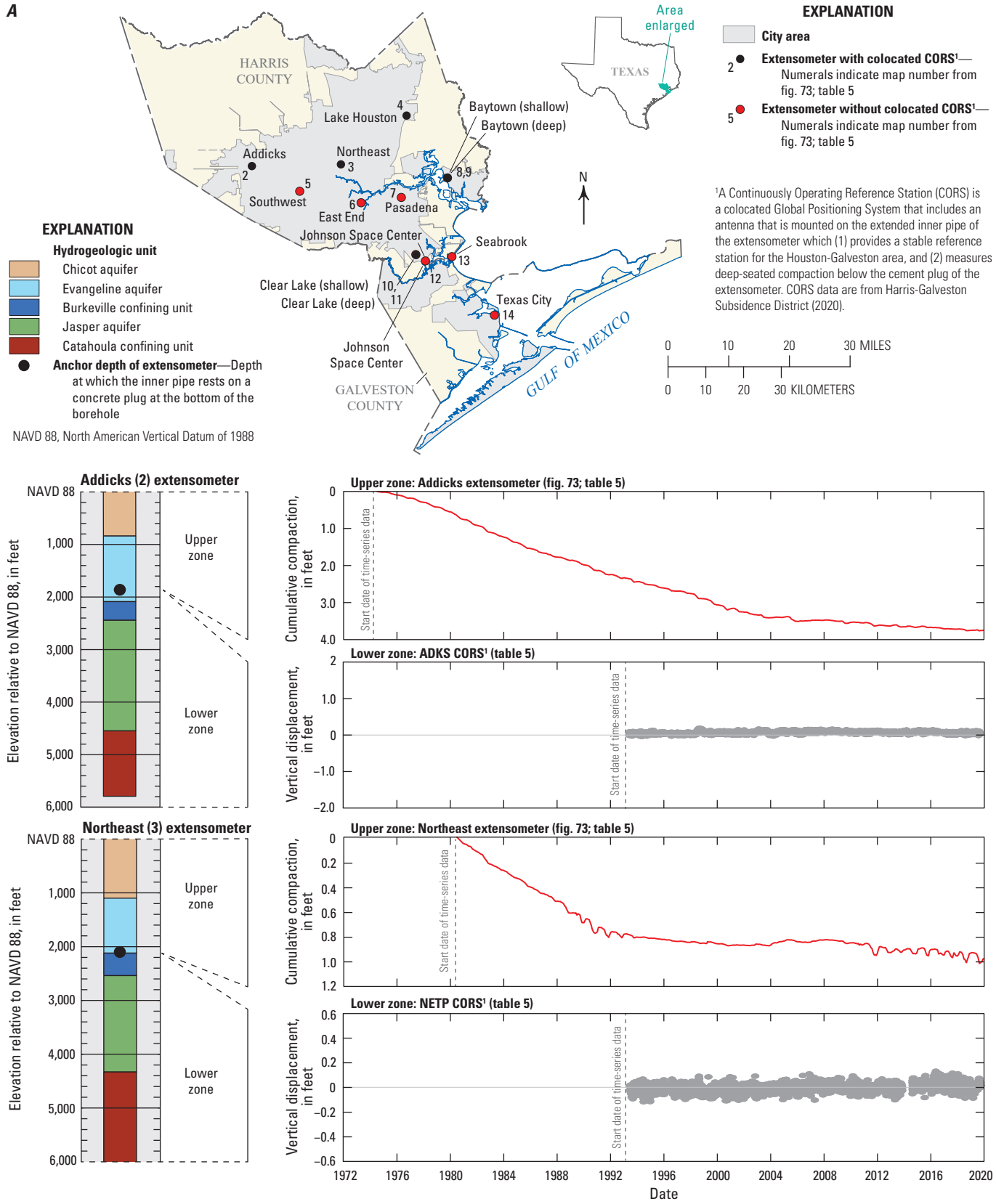

Figure 75. Cumulative compaction or vertical displacement measured at two depth intervals at four extensometers and colocated Continuously Operating Referencing Stations in the in the Gulf Coast aquifer system study area in southeast Texas.

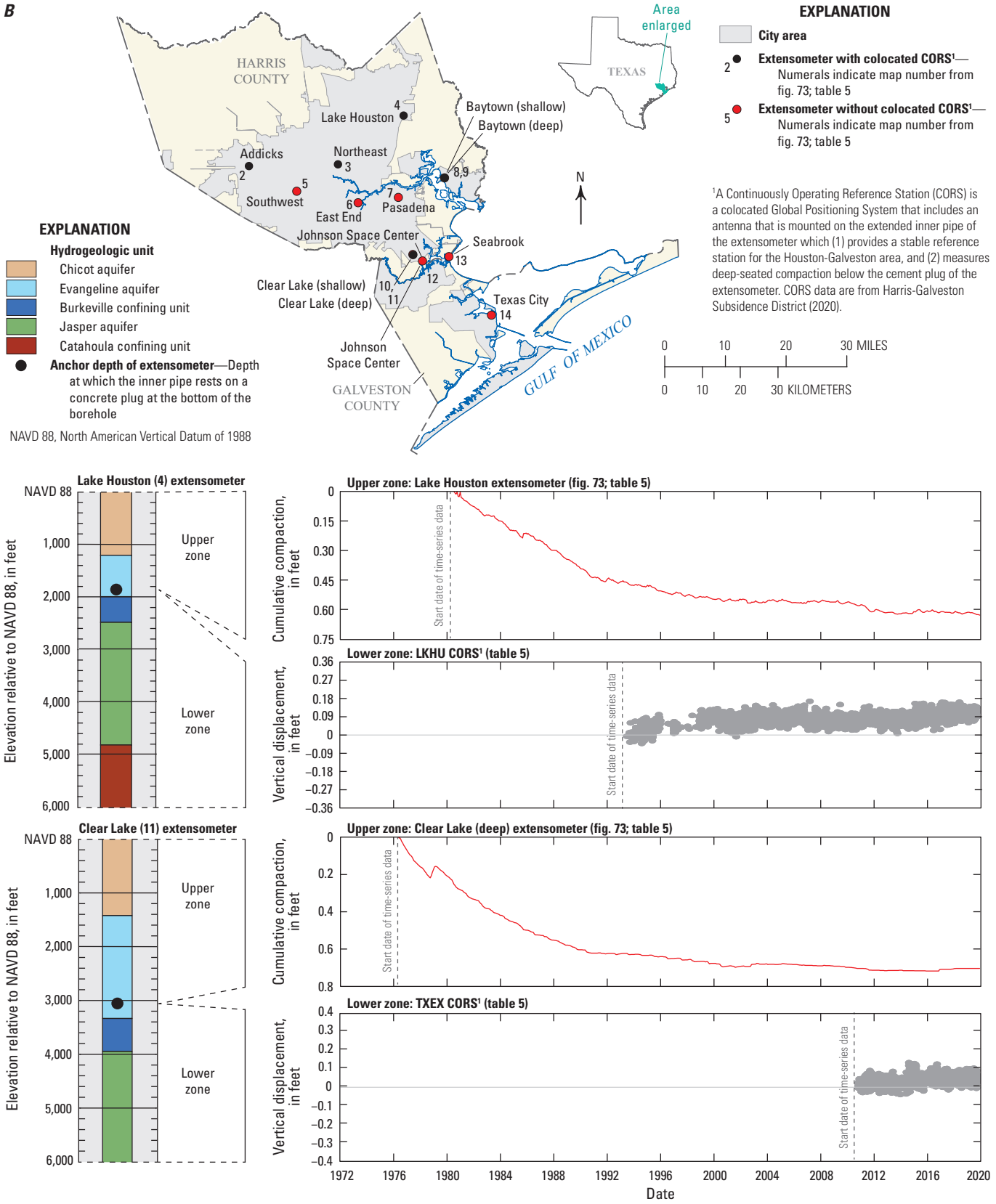

Figure 75.—Continued

The greatest amount of more recent subsidence has been measured in Montgomery County (figs. 77–79) and in northern, northwestern, and western Harris County (figs. 77, 80–82). During 2005–12, annual subsidence of as much as 2.5 centimeters (cm) occurred in northern Harris County and in The Woodlands, and as much as 2.0 cm occurred in western Harris County (Kearns and others, 2015). The subsidence rate at some stations in northern Harris County has slowed since 2010 as new groundwater regulations were enacted (Kearns and others, 2015). In Montgomery County, the subsidence rate has decreased since 2016, coincident with recoveries in groundwater levels (figs. 19–20) associated with the introduction of surface-water deliveries to the area from Lake Conroe (Wang and others, 2021). In western Harris County, the subsidence measured by GPS station P005 at the Addicks site during 1996–2012 matched the subsidence measured by the Addicks extensometer within 0.02 ft (fig. 74*A*) (Wang and others, 2014), which provides verification of the extensometer-measured-compaction record at this site between these dates. Subsidence rates in other parts of the study area are shown on figures 83–93.

Elevation data obtained from the NGS for benchmark reoccupations (in which the benchmark elevation is obtained through leveling or GNSS methods) during 2019–21 and elevation data from USGS benchmark reoccupations during 2021 were compared to elevation data from the 1987 leveling survey in order to determine subsidence in the greater Houston area. The available benchmark data obtained during 2019–21 generally were from a single transect between Houston and Liberty (fig. 1). Hence, eight land-surface benchmarks were reoccupied in 2021 using GNSS Level II survey methods from Rydlund and Densmore (2012). The reoccupied benchmarks (tables 4, 6.1) were selected based on locations in areas where greater rates of subsidence have occurred compared to other parts of the greater Houston area and based on GPS data. A Trimble R8 survey-grade GPS receiver (Trimble, 2022) in conjunction with the GNSS, and Trimble GRMS RTKnet managed by AllTerra, Inc. (2021), was used to record the positions of each of the benchmarks. The horizontal position was recorded in feet relative to the State Plane Coordinate System and the North American Datum of 1983 (NAD 83), and the elevation was recorded in feet relative to NAVD 88. Each of the nine benchmarks were visited at least twice on separate days, and two measurements were made during each visit by using the GPS receiver. If the two measured elevations differed by more than 0.1 ft on any given visit, or between separate visits, subsequent measurements were made until at least two measurements were within 0.1 ft. For benchmarks where direct occupation was not possible, temporary control points were positioned in nearby areas that were conducive to GPS measurements, and differential (indirect) leveling techniques described in Kenney (2010) were used to obtain the elevation at the benchmark (tables 4, 6.1).

Interferometric Synthetic Aperture Radar

Interferometric synthetic aperture radar (InSAR) is a satellite- or airborne-based remote sensing technique that can detect centimeter- to millimeter-level ground-surface deformation over a broad scale (Bawden and others, 2003; Qu and others, 2019). Synthetic aperture radar (SAR) imagery is produced by reflecting radar signals off a target area and measuring the two-way travel time back to the antenna. InSAR uses two SAR scenes of the same area made at different times and "interferes" (differences) them, resulting in maps called interferograms that show relative ground-elevation change (range change) between the two times.

The InSAR imagery has two components: amplitude and phase. The amplitude is the radar signal intensity returned to the satellite and depends on the varying reflective properties that delineate features of the landscape such as roads, mountains, and structures. The phase component is proportional to the line-of-sight distance from the ground to the satellite (range) and is the component used to measure land-surface displacement (subsidence or uplift). If the ground has moved away from the satellite (subsidence), a more distal phase portion of the waveform is reflected back to the satellite. Conversely, if the ground has moved closer to the satellite (uplift), a more proximal phase portion of the waveform is reflected back to the satellite. The phase difference, or shift, between the two SAR images is then calculated for each pixel. The map of phase shifts, or interferogram, can be depicted with a color scale that shows relative range change between the first and the second SAR acquisitions (Sneed and others, 2018).

Bawden and others (2012) described the use of InSAR data obtained for four overlapping scenes from remote sensing satellites to analyze subsidence in the Houston-Galveston region of Texas. The interferograms showed that the area of historical subsidence in downtown Houston along the Houston Ship Channel has stabilized and that recent subsidence has occurred in northern, northwestern, and western Harris County. Three areas of recent subsidence were delineated along a broad bow-shaped feature from Spring, Tex., southwest towards Cypress, Tex., and southward towards Sugar Land, Tex. Subsidence rates in these areas ranged from 0.05 ft/yr (15 millimeters per year [mm/yr]) to greater than 0.20 ft/yr (60 mm/yr). Additionally, multiyear interferograms near Seabrook, Tex., within the historical subsidence area and nearby Galveston Bay, showed about 0.28 ft (85 millimeters [mm]) of subsidence from January 1996 to December 1997 in the area, although some uncertainty exists regarding the subsidence in this area.

Similar to the Bawden and others (2012) study, other InSAR studies (Khan and others, 2014; Qu and others, 2015, 2019) have also noted (1) the more recent subsidence in northern, northwestern, and western Harris County concurrent with groundwater-level declines in these areas, and (2) land-surface uplift in south-central and southeastern Harris County after substantial groundwater-level recoveries in this area.

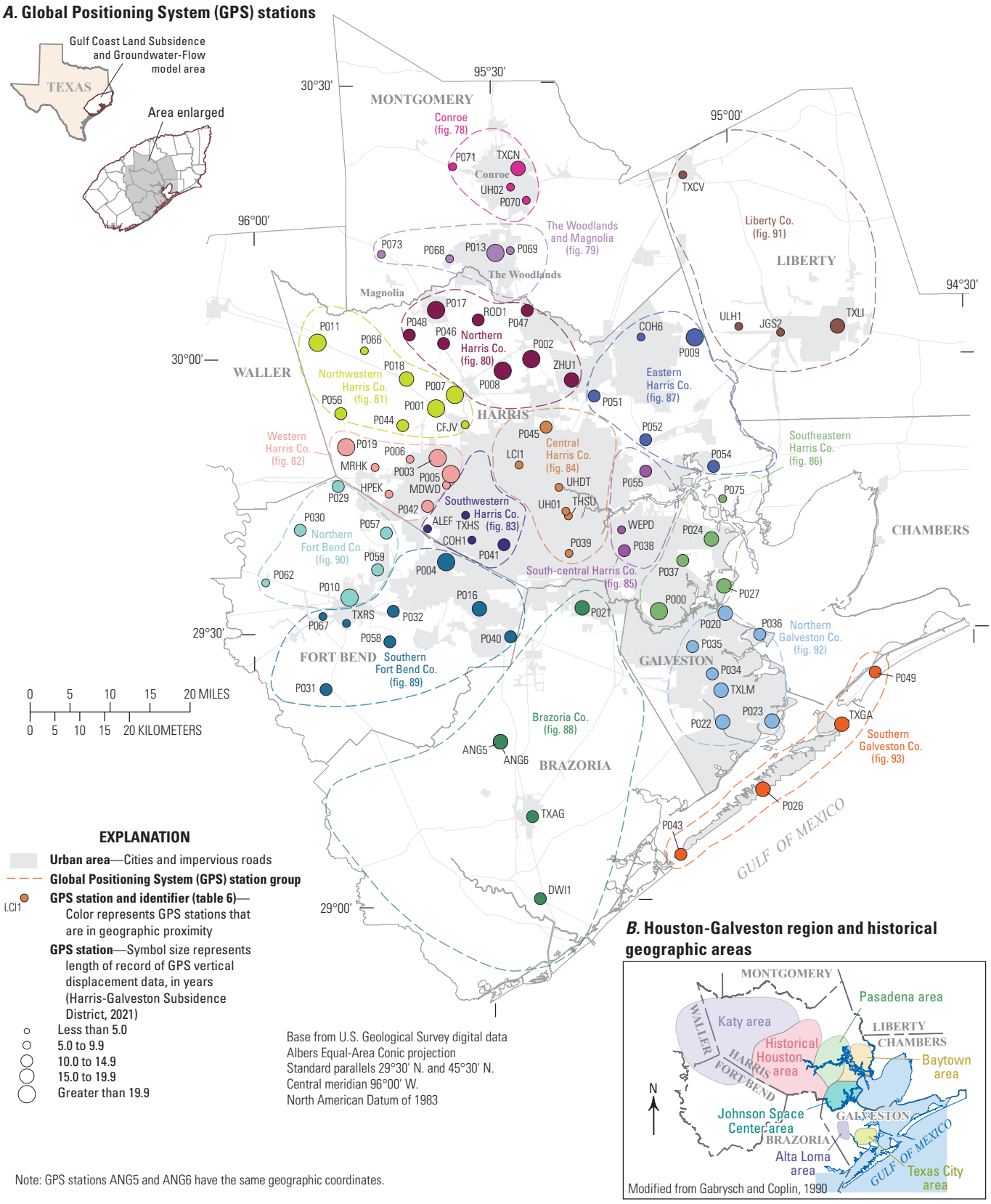

Note: GPS stations ANG5 and ANG6 have the same geographic coordinates.

Figure 76. Locations of selected Global Positioning System stations and duration of vertical-displacement data for the Gulf Coast aquifer system study area in southeast Texas.

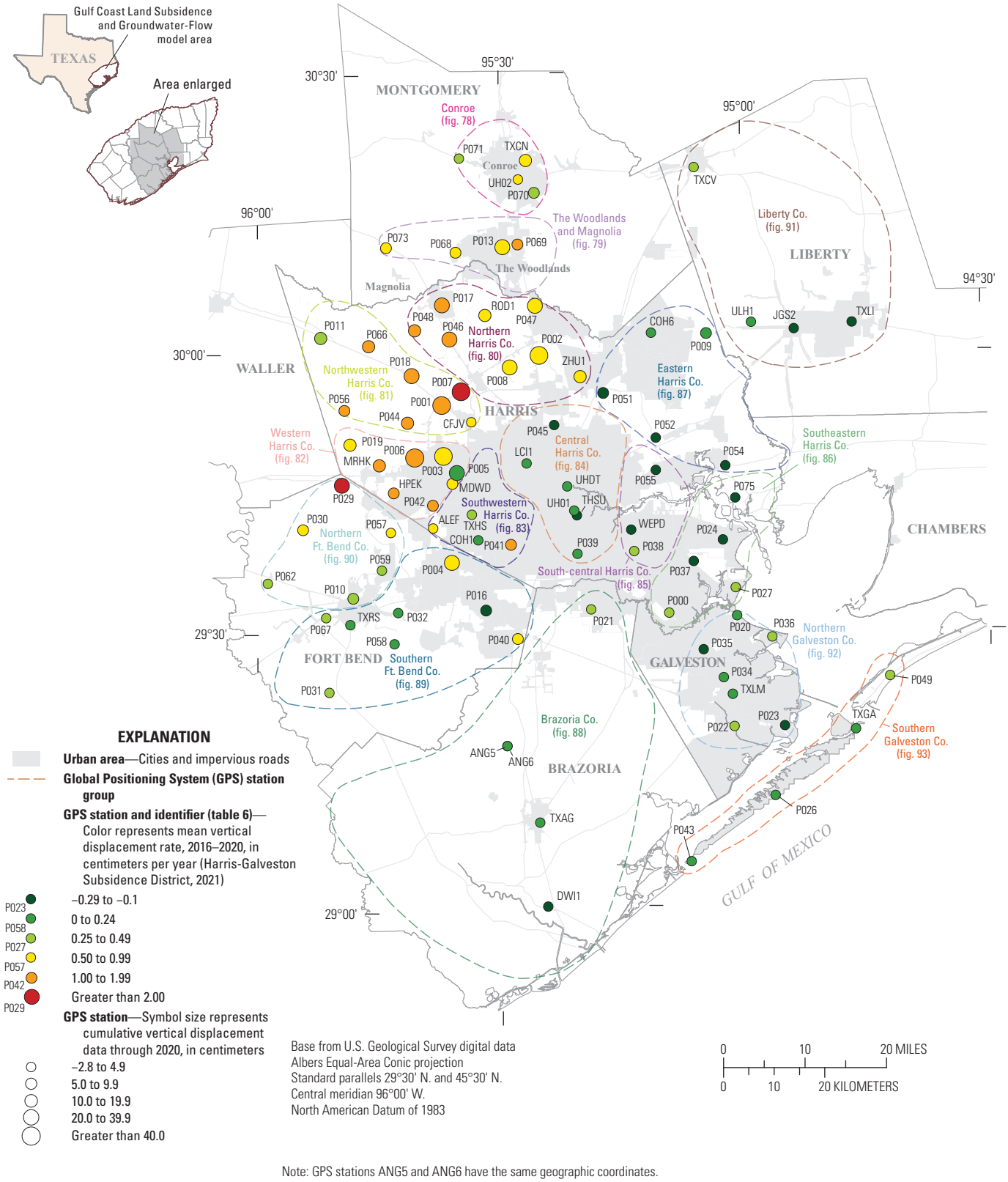

Note: GPS stations ANG5 and ANG6 have the same geographic coordinates.

Figure 77. Locations of selected Global Positioning System stations, mean rates of vertical displacement for 2016–20, and cumulative vertical displacement through 2020 used to estimate land-surface subsidence for the Gulf Coast aquifer system study area in southeast Texas.

Table 6. Location and period of record for selected Global Positioning System (GPS) stations in the Gulf Coast aquifer system study area in southeast Texas.

[ID, identifier; cm/yr, centimeter per year; cm, centimeter; --, not available]

GPS station group[1] (figs. 76–77)	Historical geographic area (fig. 18*B*)[1]	GPS station ID (figs. 76–93)	County	Installation date	Period of record (in years)	Mean vertical displacement rate, in cm/yr (2015–19)[2]	Mean vertical displacement rate, in cm/yr (2016–20)[2]	Cumulative vertical displacement (cm) through 2019[2]	Cumulative vertical displacement (cm) through 2020[2]
Conroe (fig. 78)	--	P070	Montgomery	2011	9.2	0.16	0.31	3.27	6.10
	--	P071	Montgomery	2011	9.2	0.92	0.31	4.66	4.13
	--	TXCN	Montgomery	2005	15.5	0.66	0.53	15.96	16.11
	--	UH02	Montgomery	2015	6.0	0.58	0.62	2.69	3.74
The Woodlands and Magnolia (fig. 79)	--	P013	Montgomery	2000	20.0	0.41	0.67	26.77	25.64
	--	P068	Montgomery	2011	9.2	1.13	0.94	8.21	9.29
	--	P069	Montgomery	2011	9.2	1.13	1.03	9.14	9.66
	--	P073	Montgomery	2012	8.9	0.99	0.65	7.60	7.41
Northern Harris County (fig. 80)	Katy area	P002	Harris	1994	26.7	1.28	0.70	62.29	63.25
		P008	Harris	1999	21.4	0.90	0.59	43.41	38.45
		P017	Harris	2000	20.1	1.14	1.30	31.34	33.13
		P046	Harris	2007	13.3	2.19	1.71	25.93	21.80
		P047	Harris	2007	13.6	0.95	0.87	22.26	26.17
		P048	Harris	2007	13.7	1.31	1.04	18.47	15.19
		ROD1	Harris	2007	14.0	0.59	0.64	15.11	16.94
		ZHU1	Harris	2003	18.0	0.60	0.56	11.83	12.59
Northwestern Harris County (fig. 81)		CFJV	Harris	2015	5.3	0.99	0.87	3.58	4.61
		P001	Harris	1994	26.8	2.54	1.71	71.80	70.15
		P007	Harris	1999	20.8	1.25	2.17	57.09	60.25
		P011	Harris	1999	21.7	0.55	0.25	15.08	11.34
		P018	Harris	2000	19.7	1.94	1.30	32.91	35.66
		P044	Harris	2007	13.6	1.91	1.49	15.97	18.72
		P056	Harris	2007	13.2	1.27	1.59	8.22	8.03
		P066	Harris	2011	9.8	2.22	1.37	15.10	13.58

Table 6. Location and period of record for selected Global Positioning System (GPS) stations in the Gulf Coast aquifer system study area in southeast Texas.—Continued

[ID, identifier; cm/yr, centimeter per year; cm, centimeter; --, not available]

GPS station group[1] (figs. 76–77)	Historical geographic area (fig. 18*B*)[1]	GPS station ID (figs. 76–93)	County	Installation date	Period of record (in years)	Mean vertical displacement rate, in cm/yr (2015–19)[2]	Mean vertical displacement rate, in cm/yr (2016–20)[2]	Cumulative vertical displacement (cm) through 2019[2]	Cumulative vertical displacement (cm) through 2020[2]
Western Harris County (fig. 82)	Katy area—Continued	HPEK	Harris	2014	6.2	1.30	1.24	7.14	8.61
		MDWD	Harris	2013	7.7	0.71	0.63	4.86	5.69
		MRHK	Harris	2014	6.6	1.70	1.69	9.37	11.80
		P019	Harris	2000	20.0	0.64	0.89	17.23	18.84
		P003	Harris	1994	26.6	1.17	0.78	59.82	55.12
		P005	Harris	1996	24.3	1.20	0.05	34.32	30.27
		P006	Harris	1997	6.6	2.34	1.86	57.31	57.31
		P042	Harris	2007	13.6	1.54	1.12	8.42	7.44
Southwestern Harris County (fig. 83)	Historical Houston area	ALEF	Harris	2014	6.8	0.84	0.62	3.00	3.88
		COH1	Harris	2009	8.7	1.07	0.00	2.92	2.98
		P041	Harris	2007	13.6	2.08	1.31	9.07	5.61
		TXHS	Harris	2012	8.6	0.69	0.46	4.98	5.04
Central Harris County (fig. 84)		LCI1	Harris	2012	8.6	0.36	0.14	2.50	2.37
		P039	Harris	2011	9.8	0.67	0.09	2.07	−1.80
		P045	Harris	2007	13.7	0.16	−0.26	3.75	3.31
		THSU	Harris	2013	8.1	0.08	−0.01	0.24	−0.02
		UH01	Harris	2012	7.3	0.21	0.15	-0.28	0.01
		UHDT	Harris	2013	7.5	0.20	0.07	0.45	0.52
South-central Harris County (fig. 85)	Pasadena area	P038	Harris	2007	13.6	0.61	0.30	−3.93	−5.17
		P055	Harris	2006	14.2	−0.28	−0.36	−2.83	−3.05
		WEPD	Harris	2014	7.0	−0.17	−0.08	−1.14	−1.34
Southeastern Harris County (fig. 86)	Johnson Space Center area	P000	Harris	1996	24.3	0.90	0.44	1.78	2.05
		P027	Harris	2002	18.5	0.70	0.42	4.80	4.41
		P037	Harris	2007	13.5	−0.30	−0.10	−3.57	−4.54
	Baytown area	P024	Harris	2002	18.8	−0.35	−0.43	−3.01	−4.48
		P075	Harris	2012	8.6	−0.30	−0.69	1.05	−0.27

Table 6. Location and period of record for selected Global Positioning System (GPS) stations in the Gulf Coast aquifer system study area in southeast Texas.—Continued

[ID, identifier; cm/yr, centimeter per year; cm, centimeter; --, not available]

GPS station group[1] (figs. 76–77)	Historical geographic area (fig. 18*B*)[1]	GPS station ID (figs. 76–93)	County	Installation date	Period of record (in years)	Mean vertical displacement rate, in cm/yr (2015–19)[2]	Mean vertical displacement rate, in cm/yr (2016–20)[2]	Cumulative vertical displacement (cm) through 2019[2]	Cumulative vertical displacement (cm) through 2020[2]
Eastern Harris County (fig. 87)	--	COH6	Harris	2009	6.5	0.00	0.00	4.02	4.02
	--	P009	Harris	1999	21.6	0.47	0.12	9.93	5.66
	--	P051	Harris	2007	13.6	0.30	−0.19	5.57	5.38
	--	P052	Harris	2007	13.6	−0.22	−0.67	0.71	−0.53
	--	P054	Harris	2006	14.2	−0.24	−0.07	0.50	−0.49
Brazoria County (fig. 88)	--	ANG5	Brazoria	2003	16.1	0.26	0.18	4.30	4.44
	--	ANG6	Brazoria	2003	16.1	0.08	0.02	4.23	4.31
	--	DWI1	Brazoria	2009	11.6	−0.04	−0.04	1.51	2.24
	--	P021	Brazoria	2002	18.9	0.84	0.46	2.44	−1.88
	--	TXAG	Brazoria	2005	15.0	−0.27	0.09	−0.34	1.54
Southern Fort Bend County (fig. 89)	--	P004	Fort Bend	1994	26.2	1.24	0.68	28.41	27.60
	--	P016	Fort Bend	2000	19.9	0.16	−0.04	7.12	6.30
	--	P031	Fort Bend	2007	13.6	0.13	0.39	−1.54	−2.42
	--	P032	Fort Bend	2007	13.6	0.23	0.06	0.07	0.32
	--	P040	Fort Bend	2007	13.6	1.11	0.57	7.75	6.66
	--	P058	Fort Bend	2010	10.3	0.39	0.24	4.34	2.17
	--	P067	Fort Bend	2011	9.8	0.61	0.30	4.22	2.24
	--	TXRS	Fort Bend	2011	9.6	0.34	0.23	5.48	3.89
Northern Fort Bend County (fig. 90)	Katy area	P029	Fort Bend	2007	13.5	1.95	2.16	21.52	21.47
		P030	Fort Bend	2007	13.5	0.51	0.66	5.28	5.19
		P057	Fort Bend	2009	11.7	0.47	0.66	5.30	3.34
	--	P010	Fort Bend	1999	21.7	0.64	0.34	7.62	7.33
	--	P059	Fort Bend	2010	10.3	0.80	0.32	3.58	−0.25
	--	P062	Fort Bend	2011	9.8	0.62	0.35	5.07	4.17
Liberty County (fig. 91)	--	JGS2	Liberty	2012	8.6	−0.08	−0.13	0.13	0.79
	--	TXCV	Liberty	2012	8.4	0.48	0.38	3.00	3.63
	--	TXLI	Liberty	2005	15.5	−0.06	−0.07	−1.19	−0.91
	--	UHL1	Liberty	2014	6.7	−0.01	0.04	−2.48	−1.60

Table 6. Location and period of record for selected Global Positioning System (GPS) stations in the Gulf Coast aquifer system study area in southeast Texas.—Continued

[ID, identifier; cm/yr, centimeter per year; cm, centimeter; --, not available]

GPS station group[1] (figs. 76–77)	Historical geographic area (fig. 18*B*)[1]	GPS station ID (figs. 76–93)	County	Installation date	Period of record (in years)	Mean vertical displacement rate, in cm/yr (2015–19)[2]	Mean vertical displacement rate, in cm/yr (2016–20)[2]	Cumulative vertical displacement (cm) through 2019[2]	Cumulative vertical displacement (cm) through 2020[2]
Northern Galveston County (fig. 92)	Texas City area	TXLM	Galveston	2005	15.5	0.13	0.04	3.62	3.37
		P022	Galveston	2002	19.0	0.90	0.31	4.24	3.98
	--	P020	Galveston	2002	19.0	0.04	0.16	−1.35	0.54
	--	P023	Galveston	2002	18.9	−0.03	−0.02	−1.27	−1.82
	--	P034	Galveston	2010	10.6	0.37	0.15	3.75	3.06
	--	P035	Galveston	2006	13.9	0.14	−0.06	−0.80	−3.92
	--	P036	Galveston	2007	14.0	1.04	0.36	2.36	0.55
Southern Galveston County (fig. 93)	--	P026	Galveston	2002	18.8	0.14	0.15	2.49	1.25
	--	P043	Galveston	2006	14.5	0.32	0.11	0.69	0.47
	--	P049	Galveston	2006	14.7	0.61	0.28	4.47	1.11
	--	TXGA	Galveston	2005	15.5	−0.19	0.17	1.86	3.69

[1]The spatial areas of the GPS station groups in Harris and Galveston Counties (figs. 76–77) are spatially contiguous with the benchmark groups (fig. 70; table 4), and the groundwater-well groups (fig. 18; table 2).

[2]The values were obtained from the Harris-Galveston Subsidence District (HGSD; 2020, 2021). In this report, positive values for vertical displacement indicate land subsidence, and negative values indicate uplift; however, HGSD (2020, 2021) use the inverse approach.

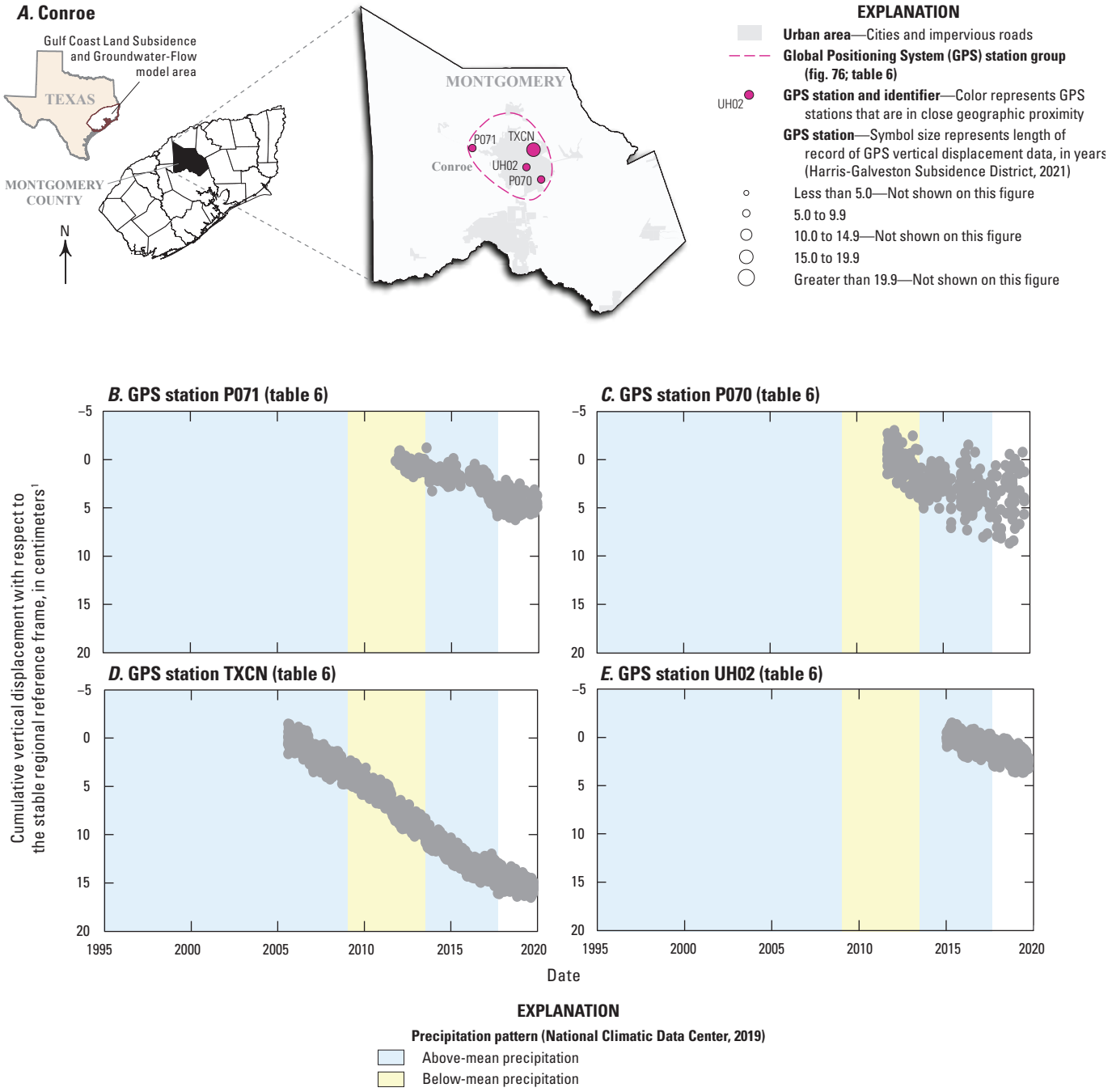

[1]The stable regional reference frame is Houston20 (Agudelo and others, 2020).

Figure 78. Cumulative vertical displacement measured at selected Global Positioning System stations used to estimate land-surface subsidence in and near Conroe, Texas.

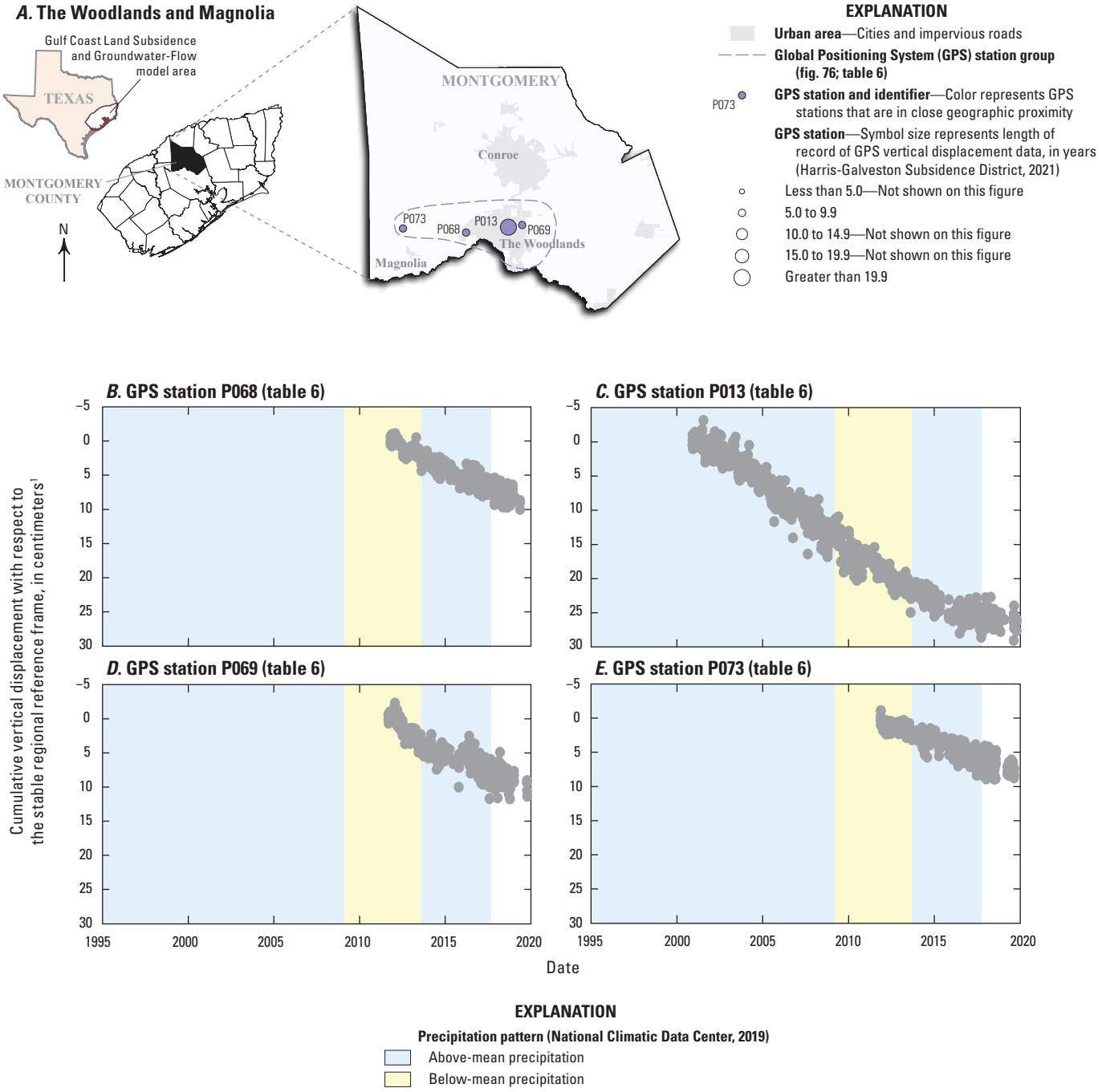

[1]The stable regional reference frame is Houston20 (Agudelo and others, 2020).

Figure 79. Cumulative vertical displacement measured at selected Global Positioning System stations used to estimate land-surface subsidence in and near The Woodlands and Magnolia, Texas.

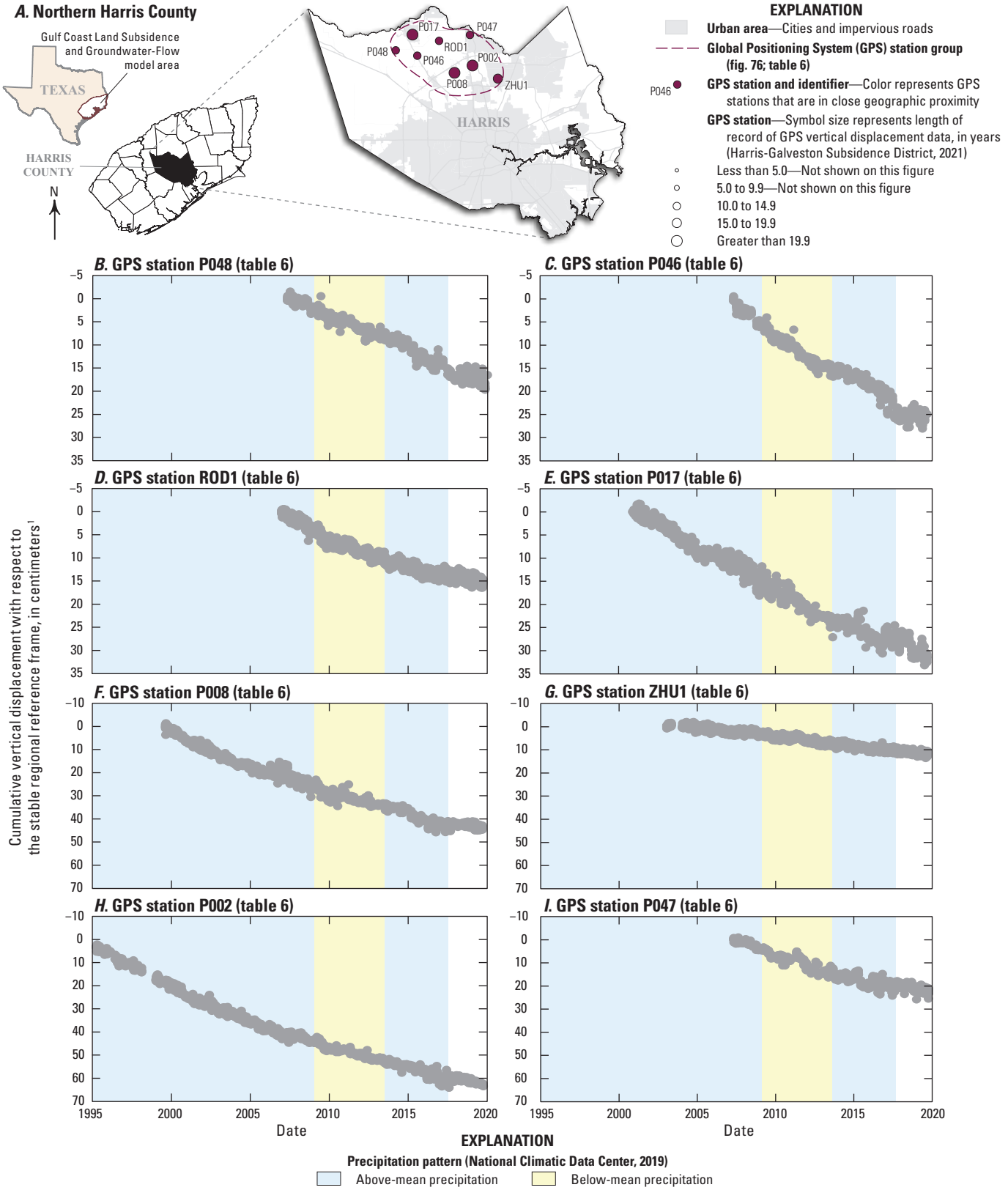

[1]The stable regional reference frame is Houston20 (Agudelo and others, 2020).

Figure 80. Cumulative vertical displacement measured at selected Global Positioning System stations used to estimate land-surface subsidence in and near northern Harris County, Texas.

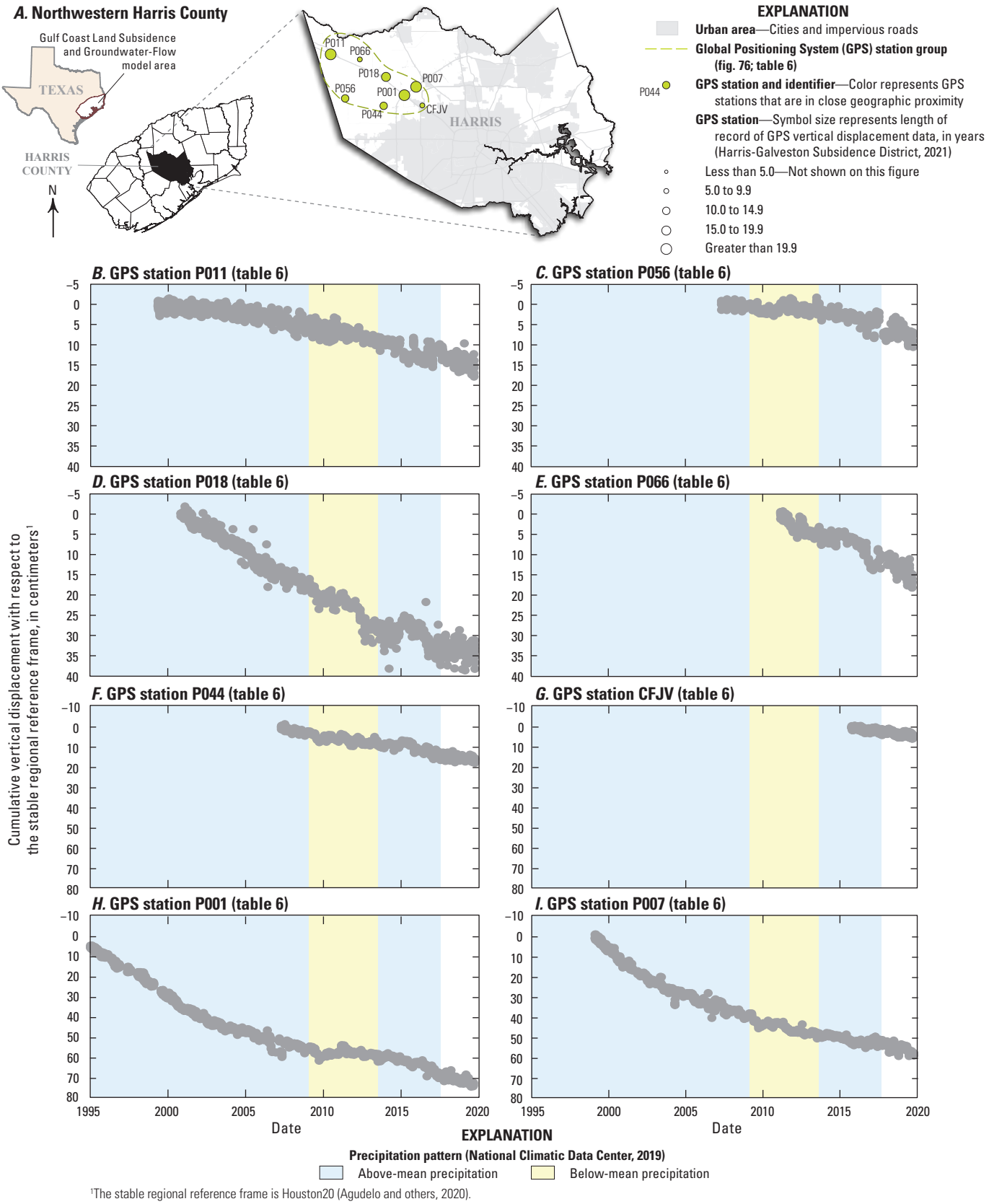

[1]The stable regional reference frame is Houston20 (Agudelo and others, 2020).

Figure 81. Cumulative vertical displacement measured at selected Global Positioning System stations used to estimate land-surface subsidence in and near northwestern Harris County.

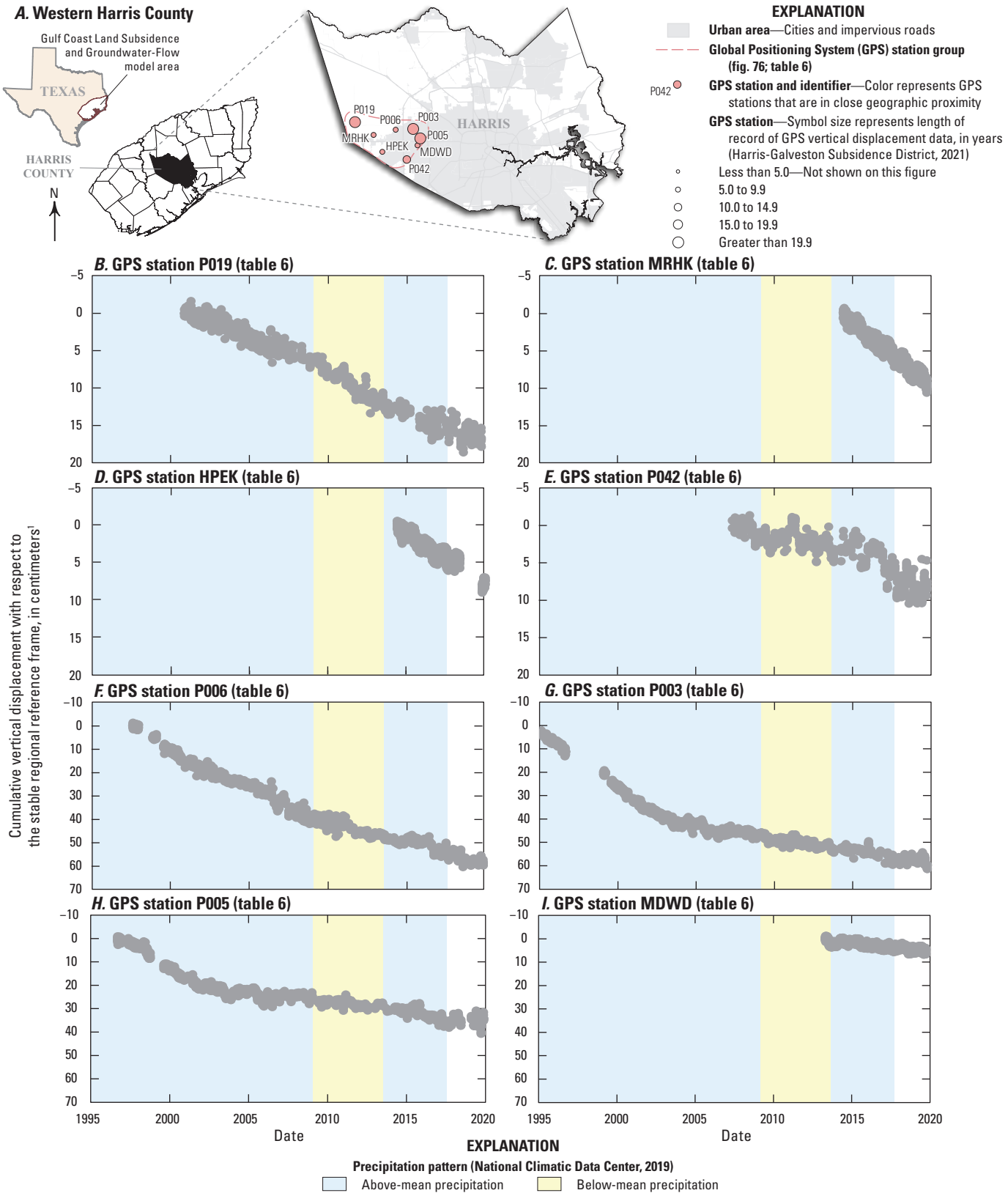

[1]The stable regional reference frame is Houston20 (Agudelo and others, 2020).

Figure 82. Cumulative vertical displacement measured at selected Global Positioning System stations used to estimate land-surface subsidence in and near western Harris County, Texas.

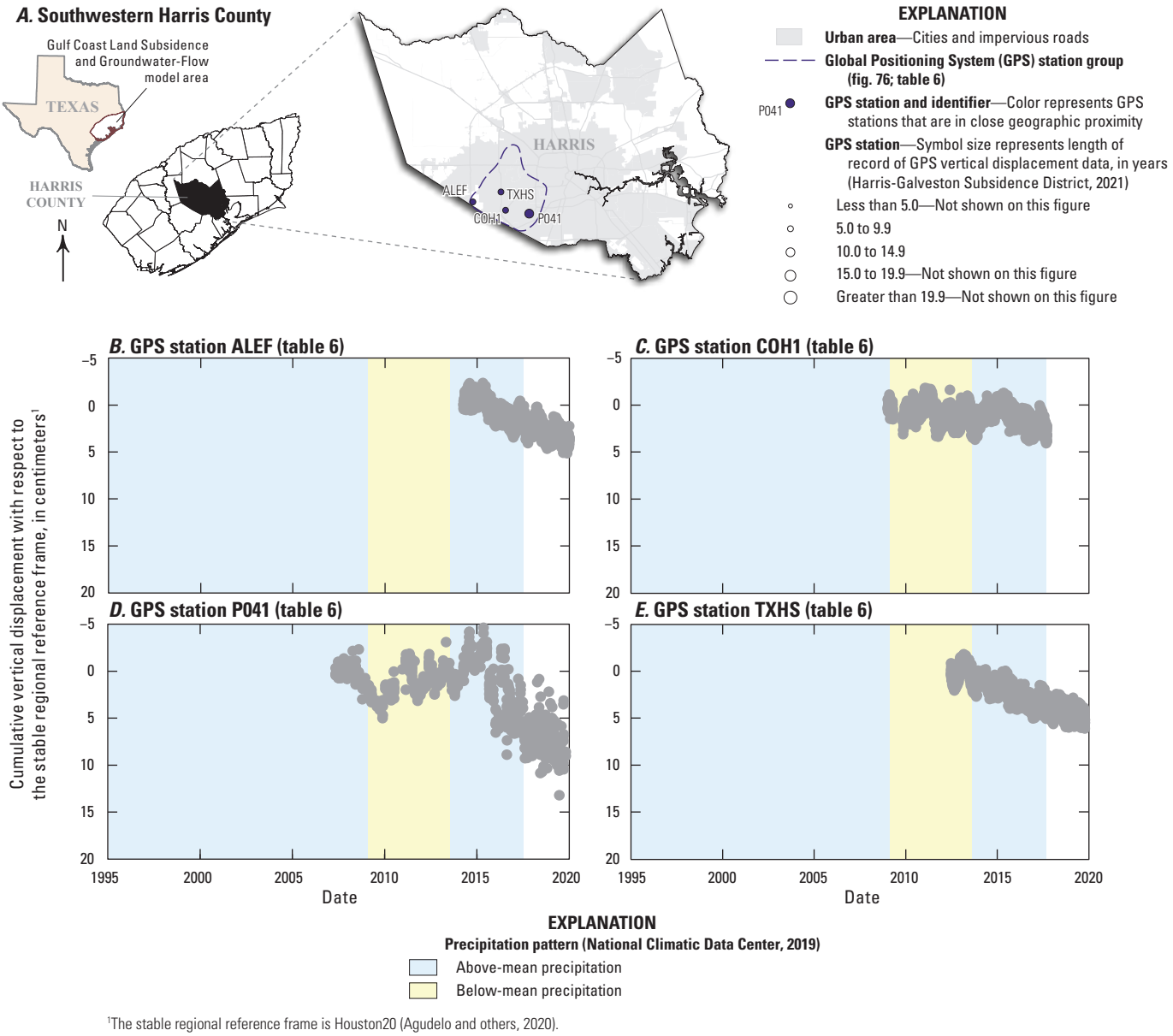

[1]The stable regional reference frame is Houston20 (Agudelo and others, 2020).

Figure 83. Cumulative vertical displacement measured at selected Global Positioning System stations used to estimate land-surface subsidence in and near southwestern Harris County, Texas.

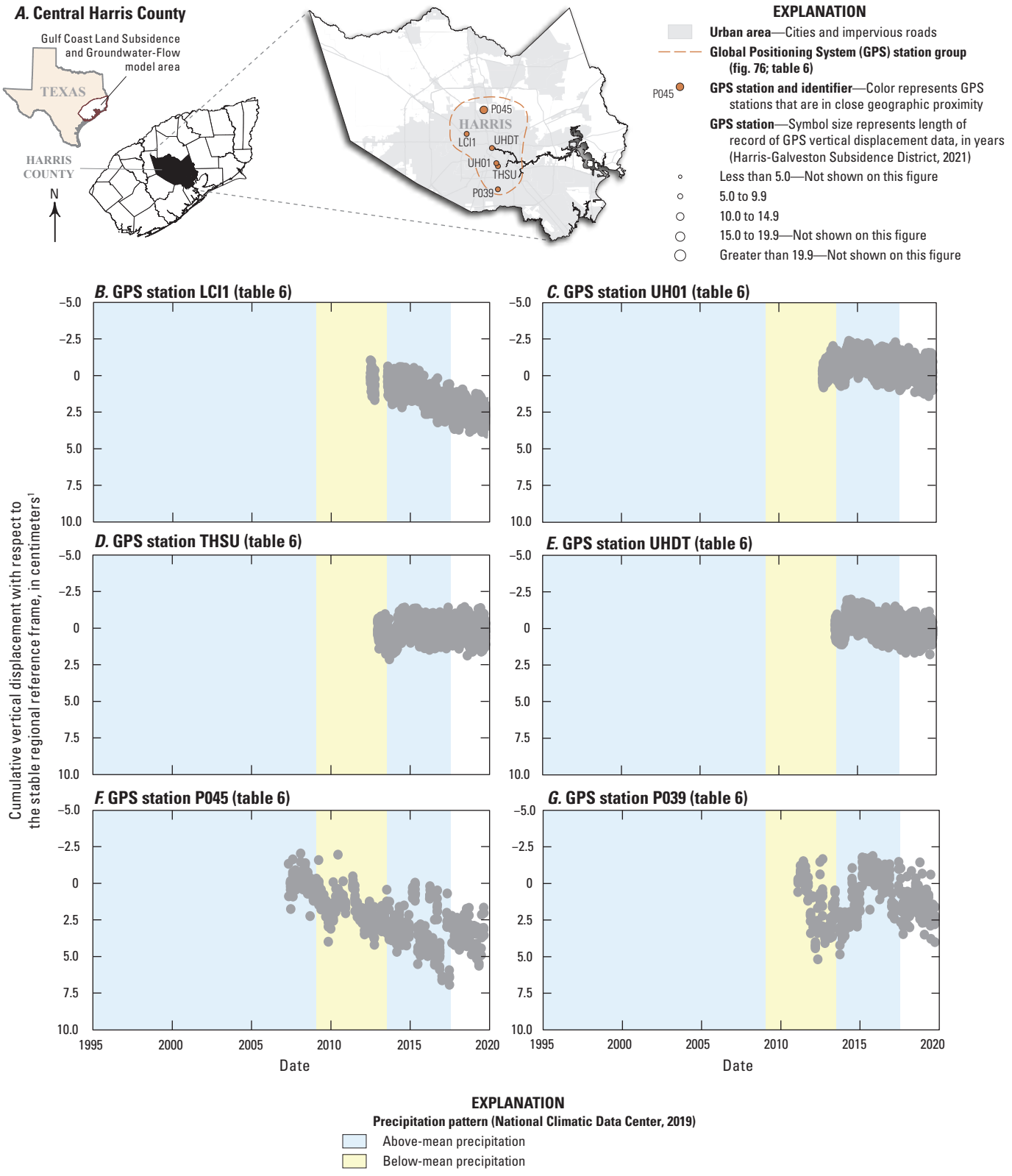

[1]The stable regional reference frame is Houston20 (Agudelo and others, 2020).

Figure 84. Cumulative vertical displacement measured at selected Global Positioning System stations used to estimate land-surface subsidence in and near central Harris County, Texas.

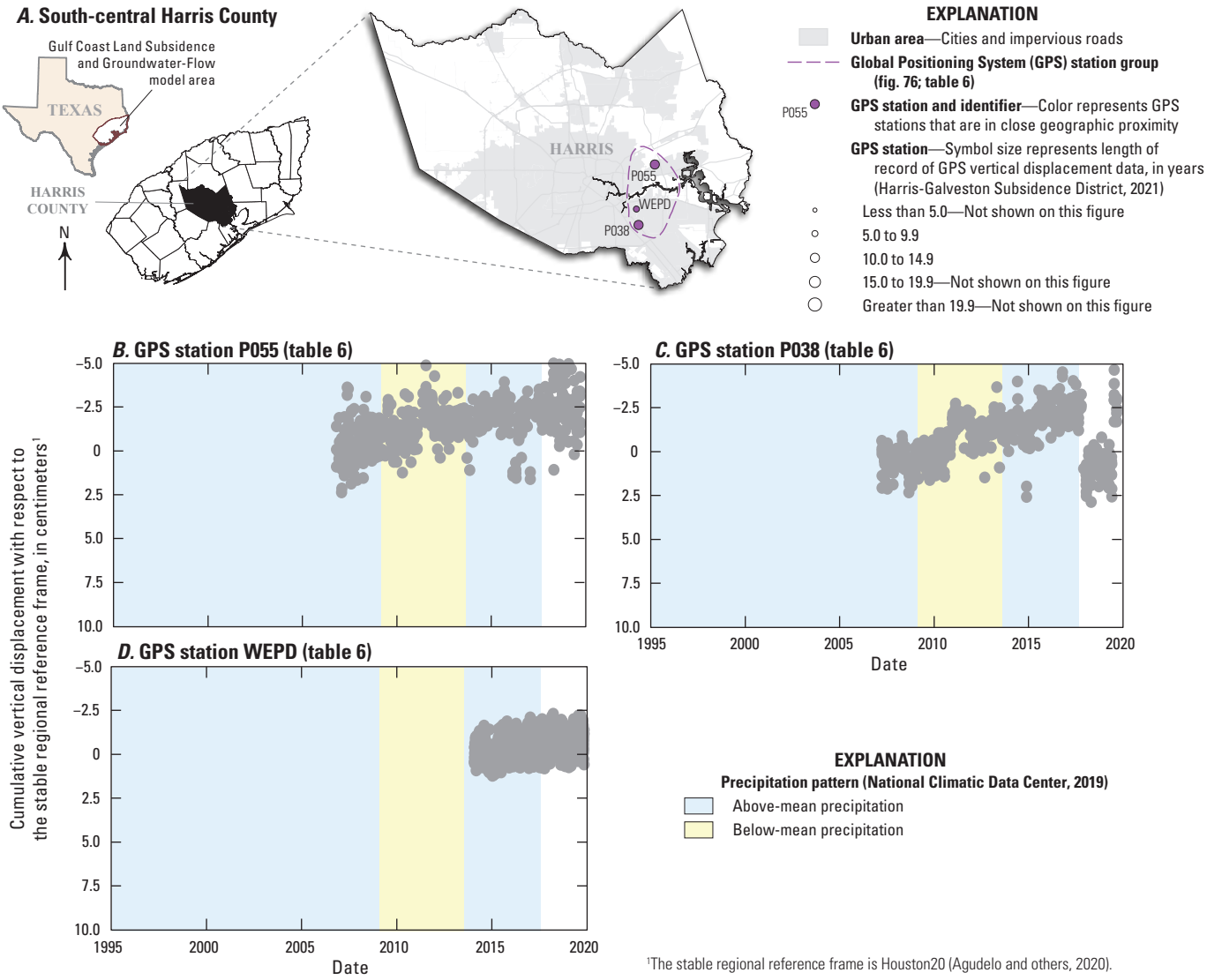

Figure 85. Cumulative vertical displacement measured at selected Global Positioning System stations used to estimate land-surface subsidence in and near south-central Harris County, Texas.

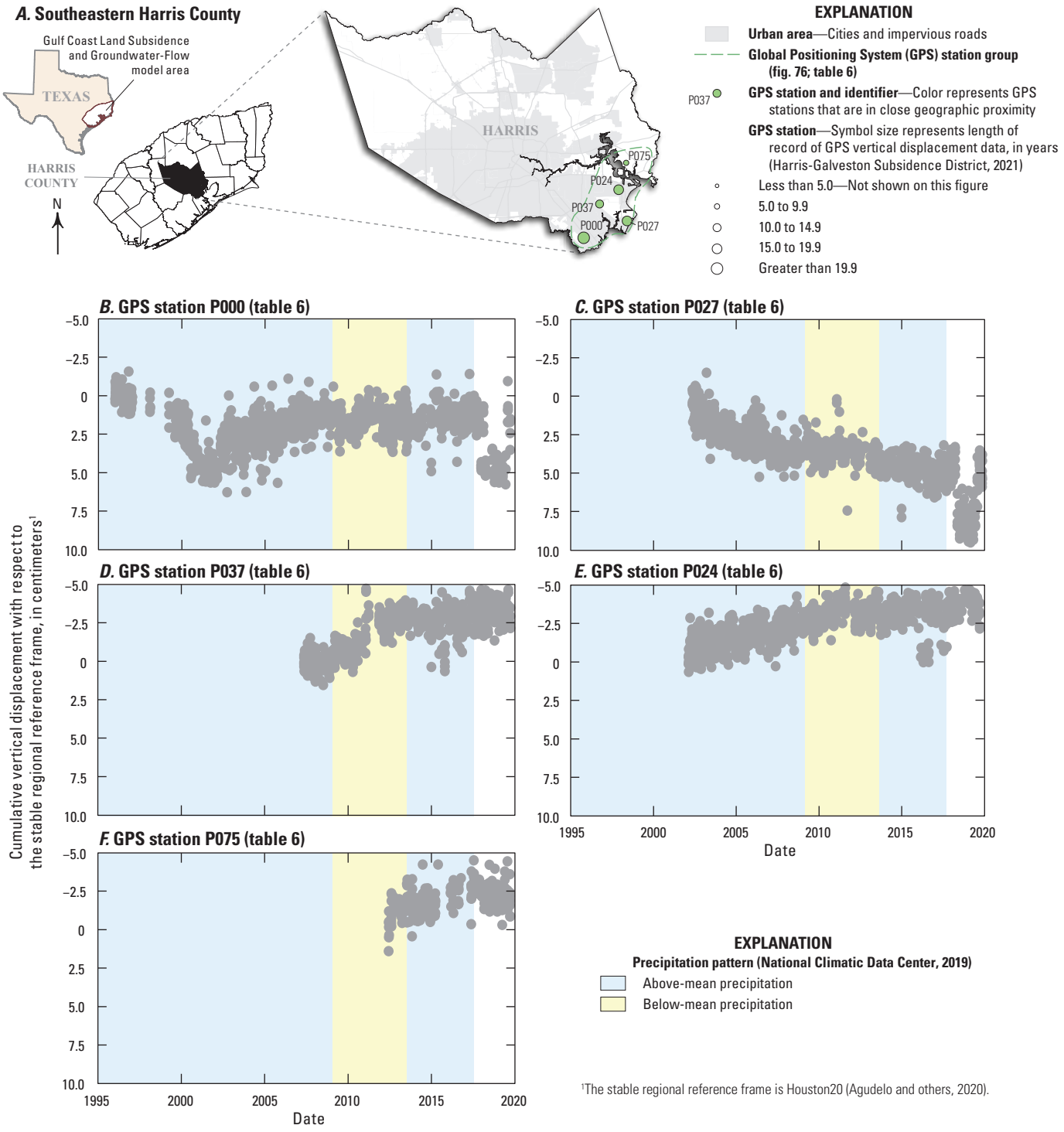

Figure 86. Cumulative vertical displacement measured at selected Global Positioning System stations used to estimate land-surface subsidence in and near southeastern Harris County, Texas.

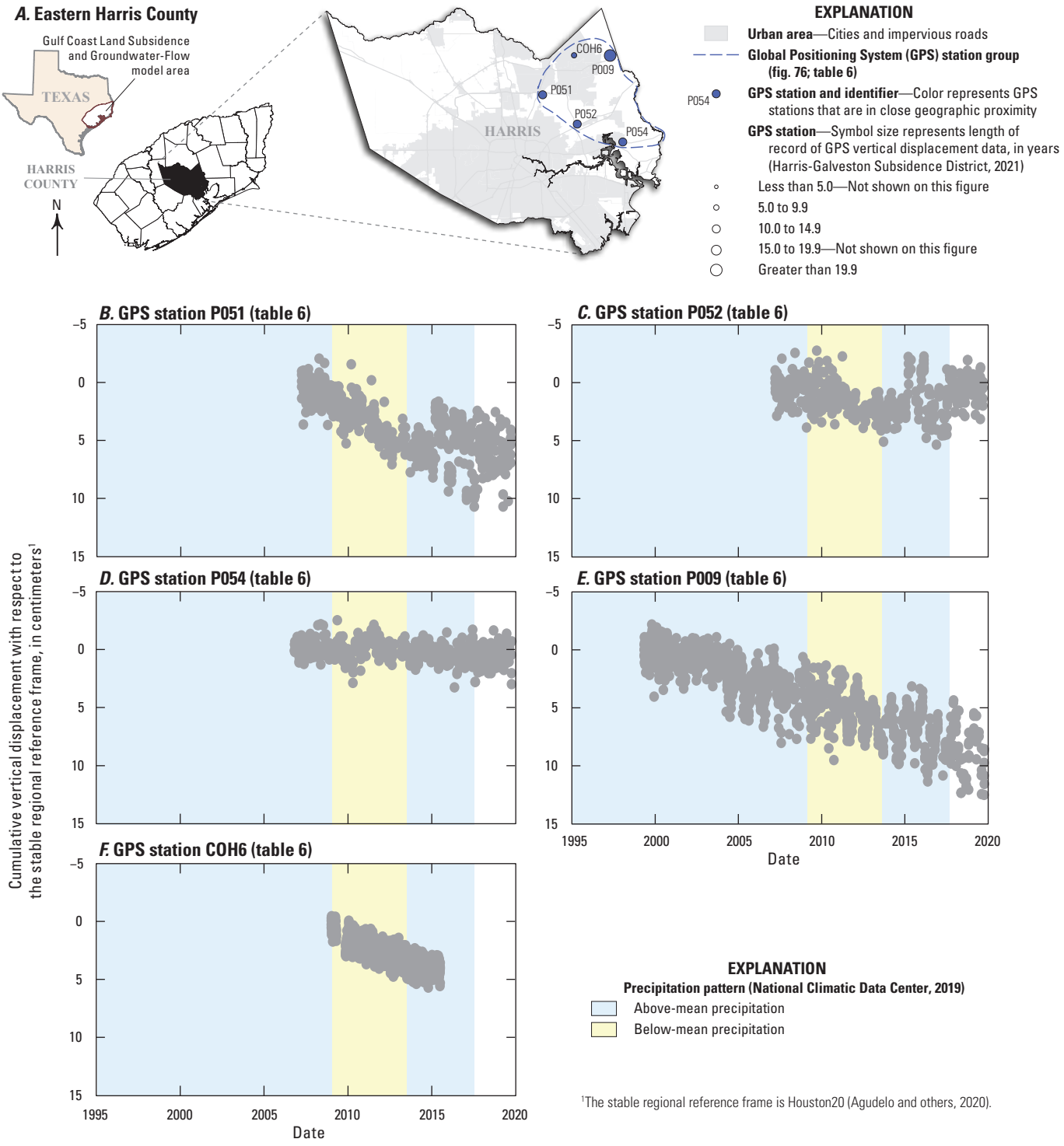

Figure 87. Cumulative vertical displacement measured at selected Global Positioning System stations used to estimate land-surface subsidence in and near eastern Harris County, Texas.

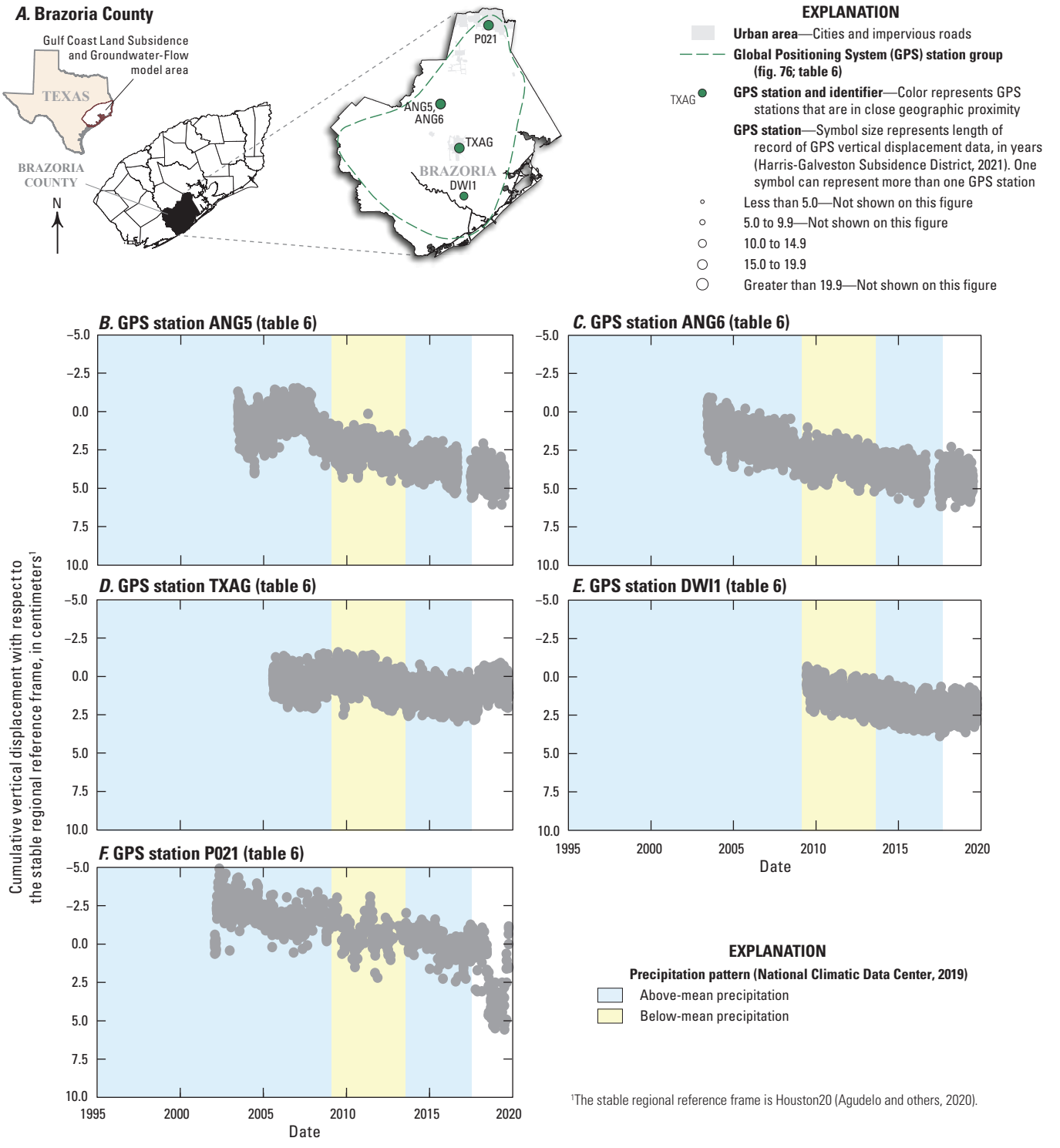

Figure 88. Cumulative vertical displacement measured at selected Global Positioning System stations used to estimate land-surface subsidence in and near Brazoria County, Texas.

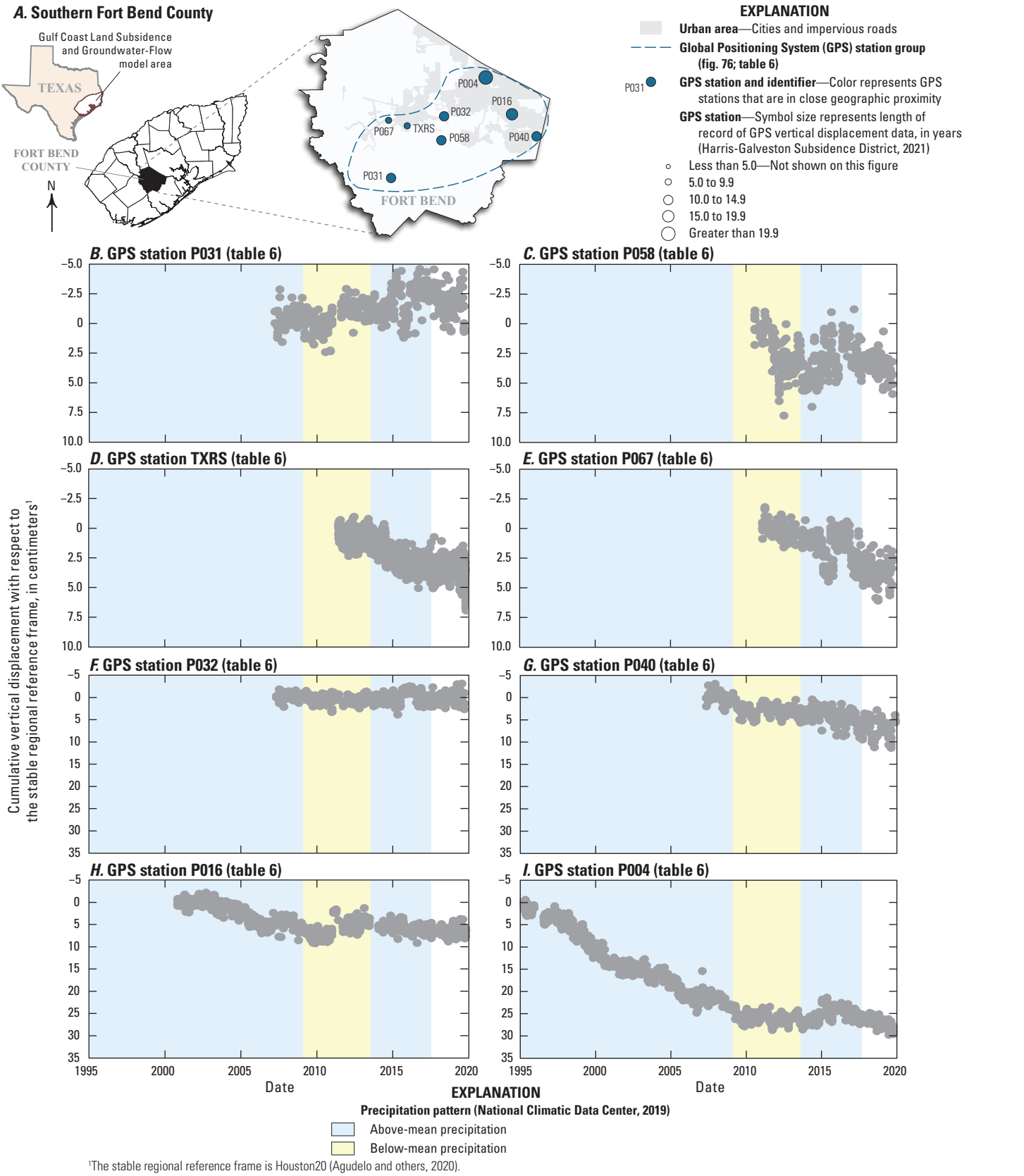

Figure 89. Cumulative vertical displacement measured at selected Global Positioning System stations used to estimate land-surface subsidence in and near southern Fort Bend County, Texas.

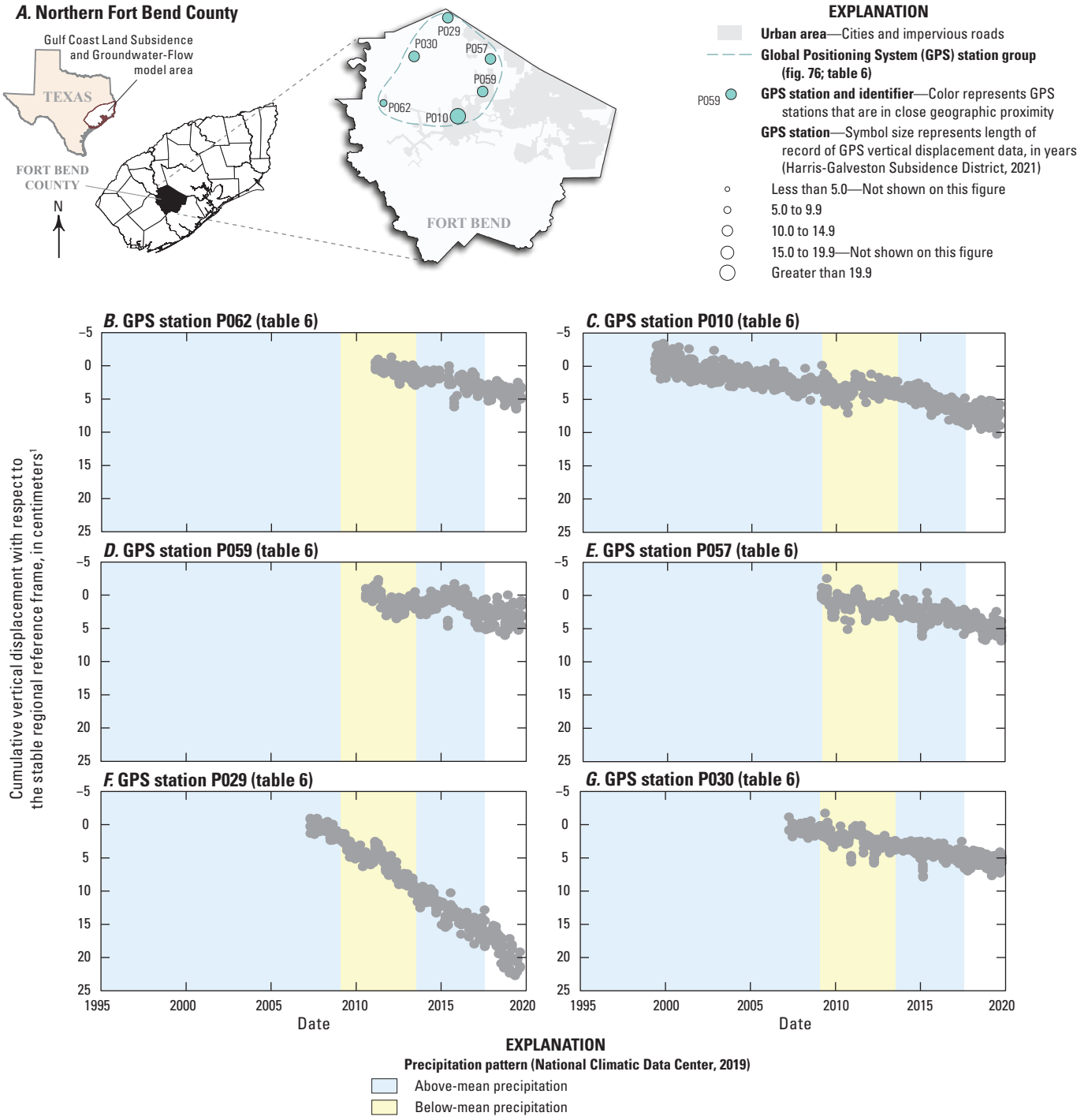

[1]The stable regional reference frame is Houston20 (Agudelo and others, 2020).

Figure 90. Cumulative vertical displacement measured at selected Global Positioning System stations used to estimate land-surface subsidence in and near northern Fort Bend County, Texas.

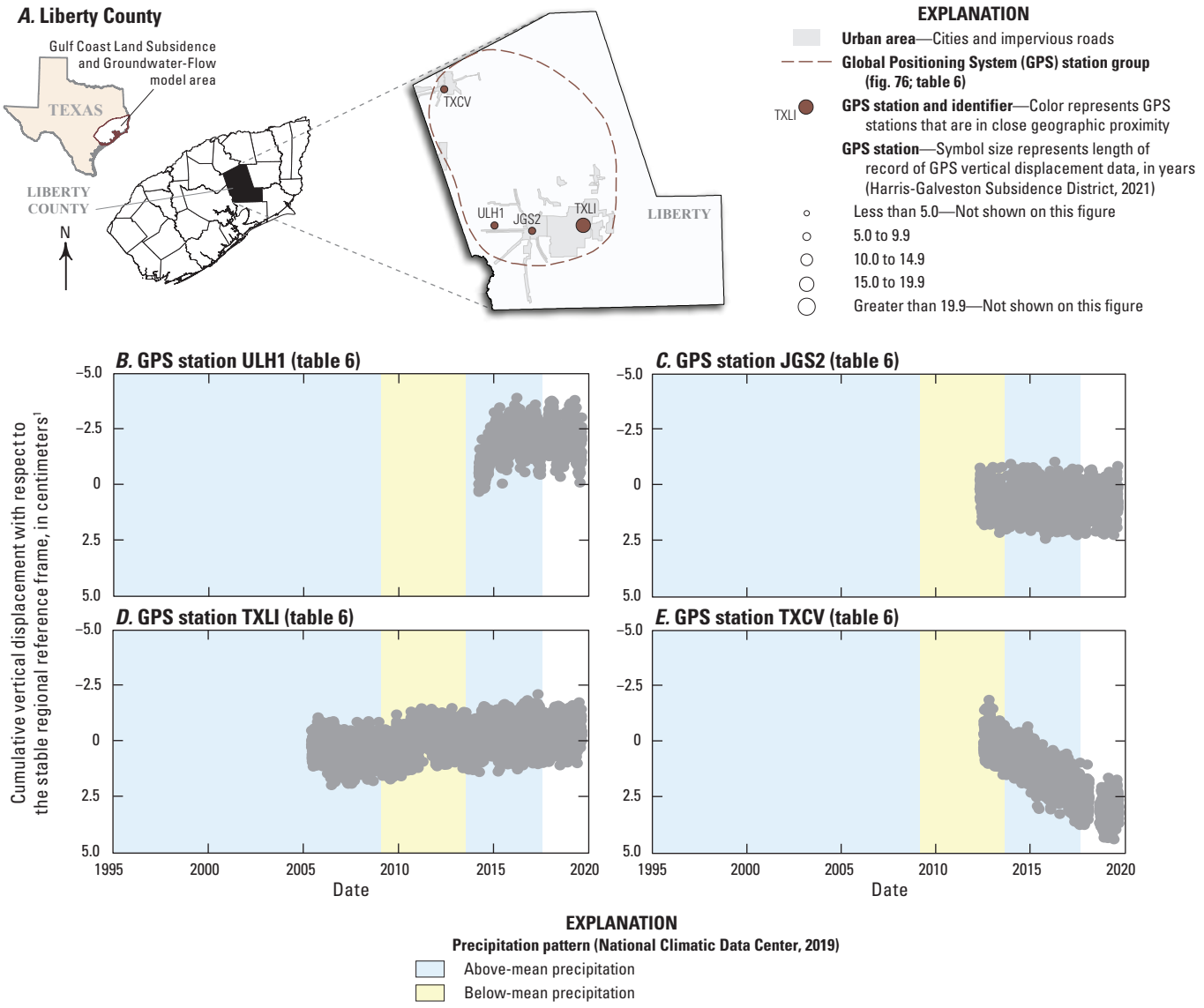

[1]The stable regional reference frame is Houston20 (Agudelo and others, 2020).

Figure 91. Cumulative vertical displacement measured at selected Global Positioning System stations used to estimate land-surface subsidence in and near Liberty County, Texas.

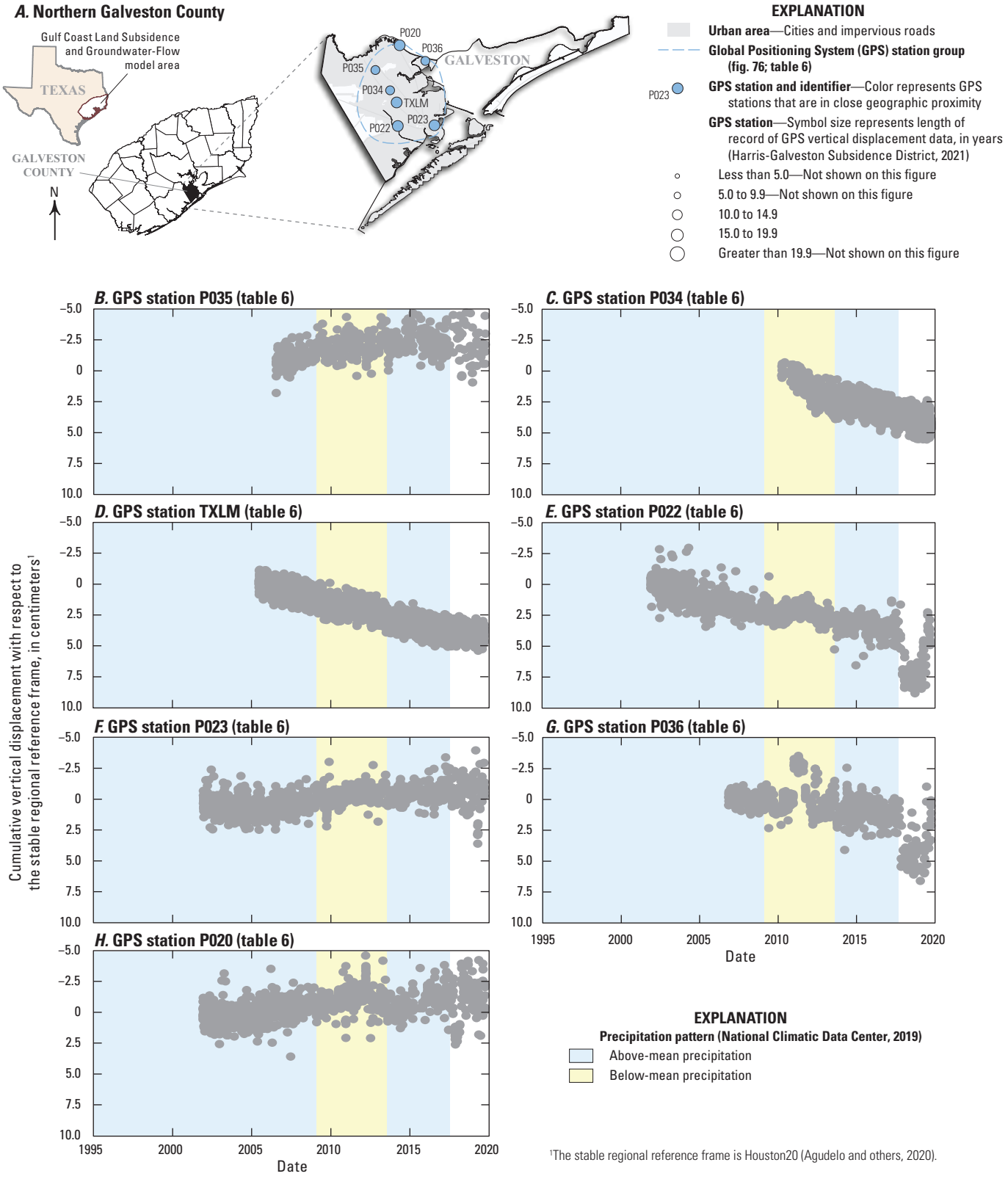

Figure 92. Cumulative vertical displacement measured at selected Global Positioning System stations used to estimate land-surface subsidence in and near northern Galveston County, Texas.

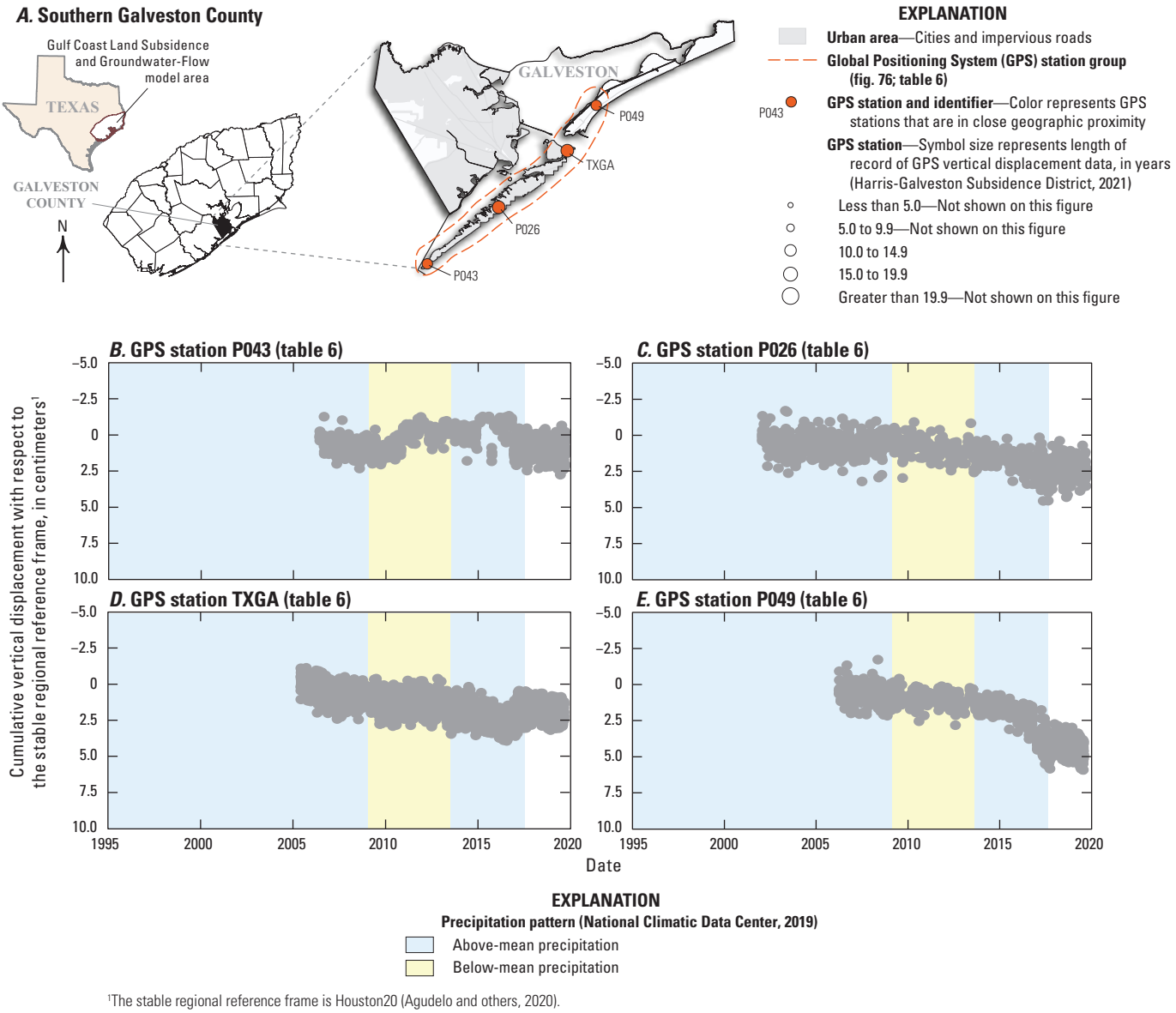

[1]The stable regional reference frame is Houston20 (Agudelo and others, 2020).

Figure 93. Cumulative vertical displacement measured at selected Global Positioning System stations used to estimate land-surface subsidence in and near southern Galveston County, Texas.

Computation of Subsidence Using Multiple Methods

Each measurement, and measurement type, is useful when used exclusively; however, the integration of the measurement types leverages the various temporal and spatial scales to help improve the understanding of compaction and subsidence processes in the greater Houston area. Some of the oldest subsidence determinations were made by repeat leveling surveys, which were followed by extensometer installations, then later by the installation of GPS stations. Although the spatial and temporal densities of measurements derived from the leveling surveys are fairly low, these data have provided the basis by which to compare later measurements of any type to determine subsidence locations and compute subsidence.

The historical subsidence contour maps (figs. 5.1–5.6) were based on leveling measurements at many benchmarks, whereas the InSAR-derived subsidence maps were based on measurements at millions of locations. Although InSAR data have the greatest spatial data density of all the measurement types, extensometer and GPS data have the highest temporal data densities. The substantial spatial density of InSAR data can be used to identify specific areas of surface deformation within broader regions to better position specialized instrumentation (such as extensometers and GPS sites) designed to precisely measure and monitor subsidence and compaction at specific locations. The temporal resolution of extensometer and GPS data permits detailed time-series analyses at many temporal scales to analyze aquifer-system responses to a range of processes: from monthly well operations to seasonal irrigation schedules to longer term changes in water deliveries, climate, and land use. The extensometer records (dating from 1973), the InSAR imagery (dating from the early 1990s), and the GPS records (generally dating from the mid-2000s) provide important time-series data over a range of time scales and spatial locations.

The various time-series compaction and subsidence measurements were integrated to assist with evaluating subsidence processes in the greater Houston area. Subsidence was estimated first by combining leveling and GNSS data (table 4). These data were then combined with either extensometer-measured-compaction (fig. 74; table 5) or GPS vertical displacement datasets (figs. 76–77) at selected locations in the study area. When paired with onsite or nearby groundwater-level data, a better understanding was attained regarding aquifer-system response to declining groundwater levels and the subsequent recovery during an approximately 80- to 100-year period.

Areas of Historical Subsidence

Historical subsidence in the greater Houston area primarily has occurred in six areas of substantial groundwater-level declines: the historical Houston area and the Pasadena, Baytown, Johnson Space Center, Texas City, and Katy areas (fig. 18). These areas correspond with historical population centers and areas where the rapid growth of groundwater use occurred.

The historical Houston area (fig. 18) was among the earliest areas where subsidence was recorded. Based on the elevation differences between benchmarks J 8, M 54, N 54, and P 54 monumented in 1906 and 1918 in this area, subsidence during 1906–18 was less than 0.1 ft (fig. 70*A*; table 4). Groundwater levels in the historical Houston area during 1917–18 were between about 20 ft above land surface and about 30 ft bls (table 3.1); therefore, minimal subsidence during 1906–18 was expected. By 1932, subsidence in this area was about 0.5 ft, concurrent with a groundwater-level decline to about 50–70 ft bls (figs. 14, 94; table 4). By 1943, subsidence in the historical Houston area was generally between about 0.8 and 1.1 ft (table 4), concurrent with a groundwater-level decline of about 40–70 ft, when groundwater levels were about 70–130 ft bls (figs. 14, 94, 95*A–B*). The availability of surface water from Lake Houston beginning in 1954 helped stabilize groundwater levels during 1954–59, but subsidence continued rapidly during this period (generally 0.3–0.6 ft; table 4). As groundwater levels in the historical Houston area continued to decline in the subsequent decades, the aquifer system reached a continually greater level of effective stress, thus resulting in inelastic compaction, as illustrated on figures 94 and 95*A–B*. By 1980, when groundwater levels were at or near historical minimums, subsidence determined by leveling was estimated at about 4.5–7.0 ft at the East End extensometer site (hereinafter the “East End site”), and the Southwest and Northeast sites (figs. 94, 95*A–B*). Although the groundwater level from a single screened interval is shown on figures 94 and 95*A–B*, the groundwater-level patterns at the colocated wells at the extensometers in the greater Houston area show a remarkable level of similarity across about 1,800–2,100 ft of heterogeneous aquifer sediment from 1980 to present (figs. 40, 42). As the groundwater level of the aquifers began to rise when groundwater withdrawals decreased with the advent of groundwater regulation and conversion to surface-water sources, the hydrostatic pressure increased and progressive equilibration of excess residual pore pressure decreased the rate of compaction (Kasmarek and others, 2010). However, because of the effects of residual compaction—where faster draining and generally thinner fine-grained units first compact, followed by thicker and more slowly draining fine-grained units—another 0.5–1.5 ft of compaction was recorded by the Northeast, Southwest, and East End extensometers during 1980–90 even after groundwater levels had stabilized and risen (figs. 94, 95*A–B*). Additionally, although the groundwater levels across each depth interval have since risen from the historical minimums (figs. 40, 42), it is unlikely they will recover fully to the predevelopment level, which was generally near land surface.

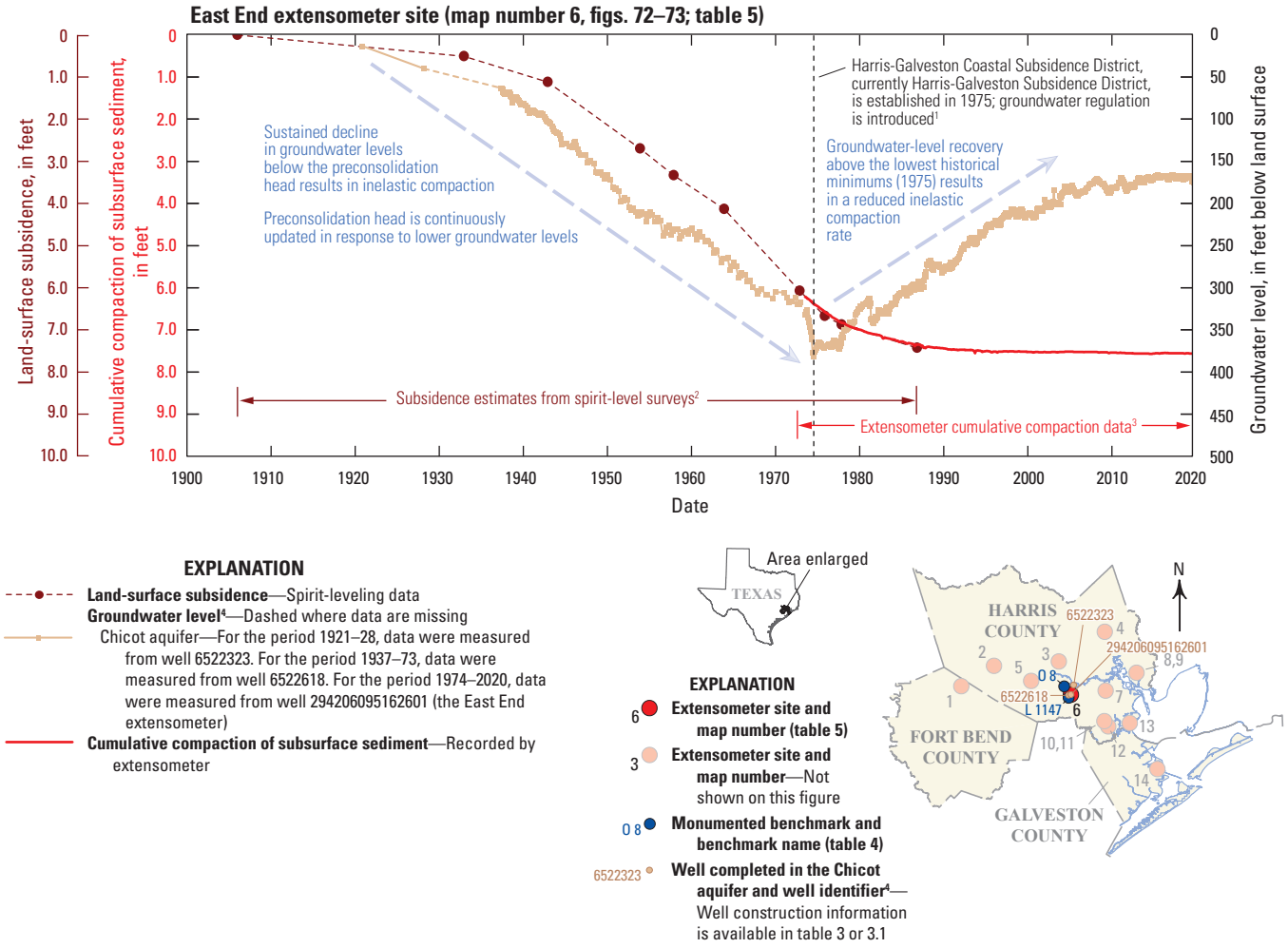

[1]Originally named the Harris-Galveston Coastal Subsidence District since its inception in 1975 and was renamed the Harris-Galveston Subsidence District in 2005.
[2]Spirit-leveling data are from benchmarks O 8 and L 1147 (fig. 70*A*; table 4).
[3]The initial value for cumulative compaction recorded by the extensometer is registered to the amount of cumulative subsidence estimated by spirit-level surveys prior to installation of the extensometer.
[4]The 7-digit Texas Water Development Board (TWDB) well identifier indicates data from TWDB (2020b). The 15-digit U.S. Geological Survey (USGS) well identifier indicates data from USGS (2021b).

Figure 94. Cumulative compaction at the East End extensometer site in the Gulf Coast aquifer system study area, southeast Texas.

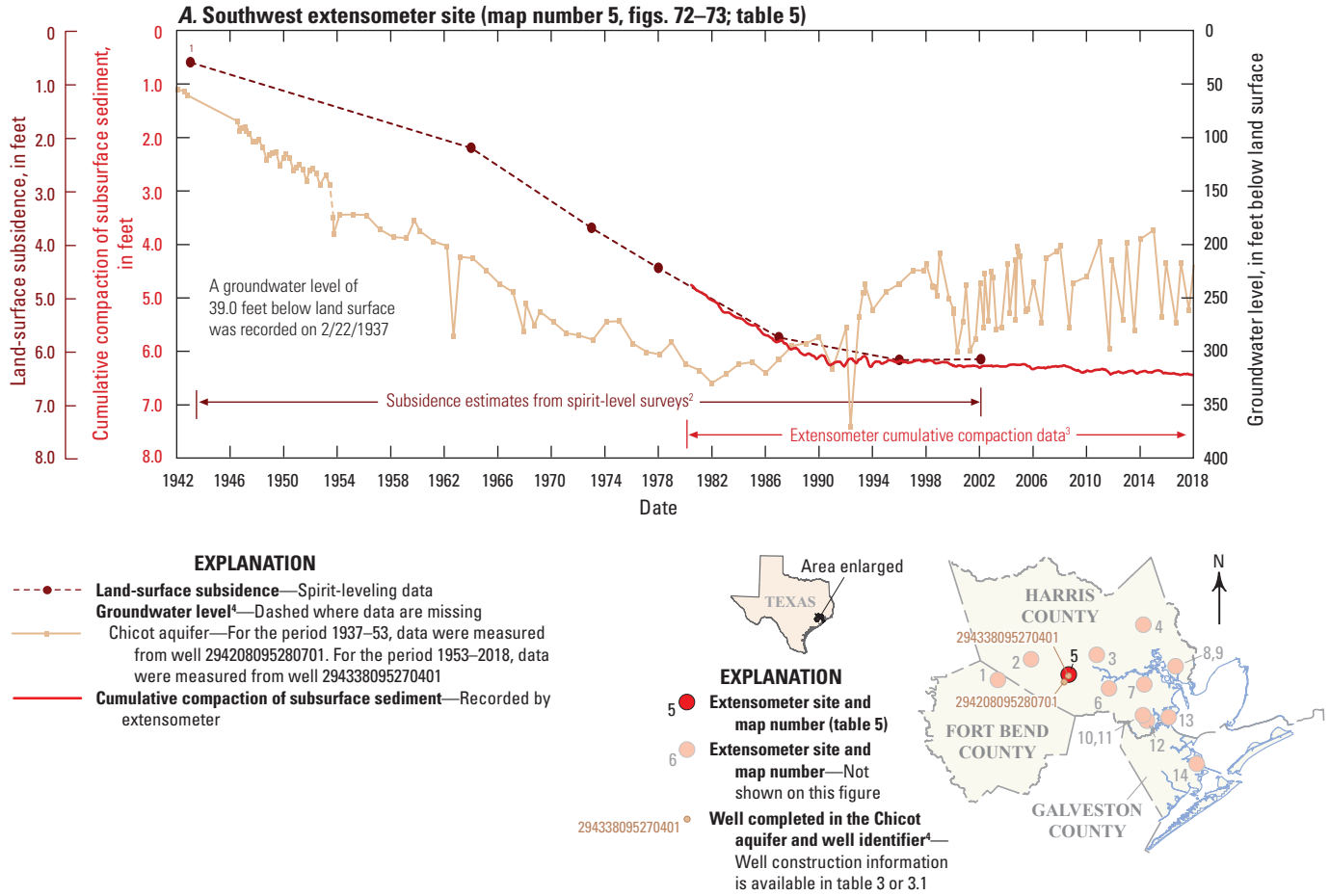

[1]A total of 0.60 foot of subsidence was estimated for the period 1906–43 based on interpolated subsidence contour maps described in appendix 5; therefore, this is the starting value for cumulative compaction shown on this figure in 1943.
[2]Spirit-leveling data based on contoured data from Gabrysch and Bonnet (1975), Jorgensen (1975), Gabrysch (1980b), and Gabrysch and Coplin (1990).
[3]The initial value for cumulative compaction recorded by the extensometer is registered to the amount of cumulative subsidence estimated by spirit-level surveys prior to installation of the extensometer.
[4]The 15-digit U.S. Geological Survey (USGS) well identifier indicates data from USGS (2021b).

Figure 95. Cumulative compaction at extensometer sites estimated from leveling contours, benchmarks, and extensometer time-series data at the *A*, Southwest, *B*, Northeast, *C*, Baytown, *D*, Pasadena, *E*, Clear Lake (deep), *F*, Johnson Space Center, *G*, Seabrook, *H*, Addicks, *I*, Lake Houston, and *J*, Texas City extensometer sites in the Gulf Coast aquifer system study area, southeast Texas.

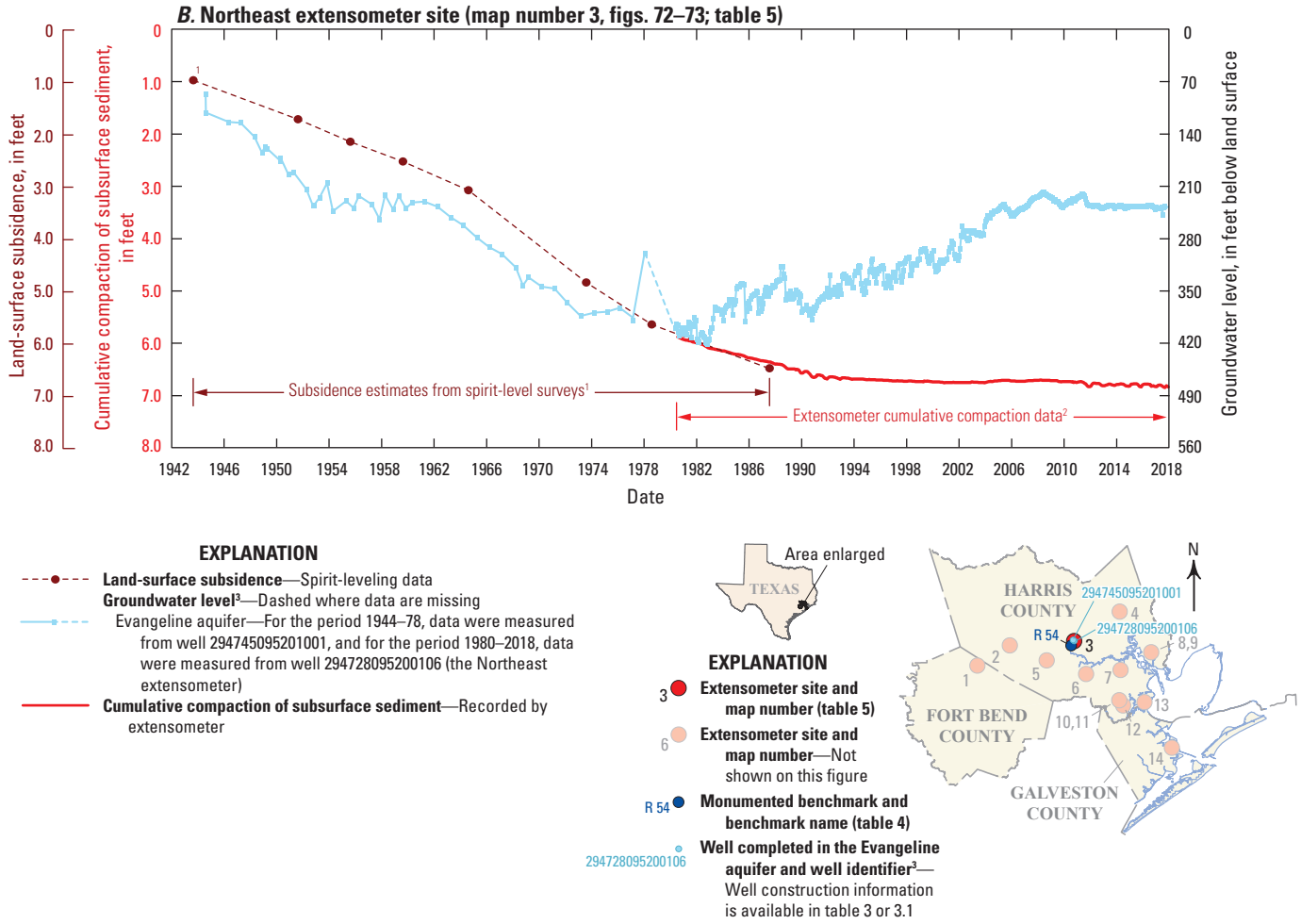

[1]Spirit-leveling data based on benchmark R 54 located approximately 1.2 miles southwest of the Northeast extensometer site (fig. 70*A*; table 4). A total of 0.99 foot of subsidence was estimated from 1918 to 1943 at this benchmark; therefore, this is the starting value for cumulative compaction shown on this figure in 1943.
[2]The initial value for cumulative compaction recorded by the extensometer is registered to the amount of cumulative subsidence estimated by spirit-level surveys prior to installation of the extensometer.
[3]The 15-digit U.S. Geological Survey (USGS) well identifier indicates data from USGS (2021b).

Figure 95.—Continued

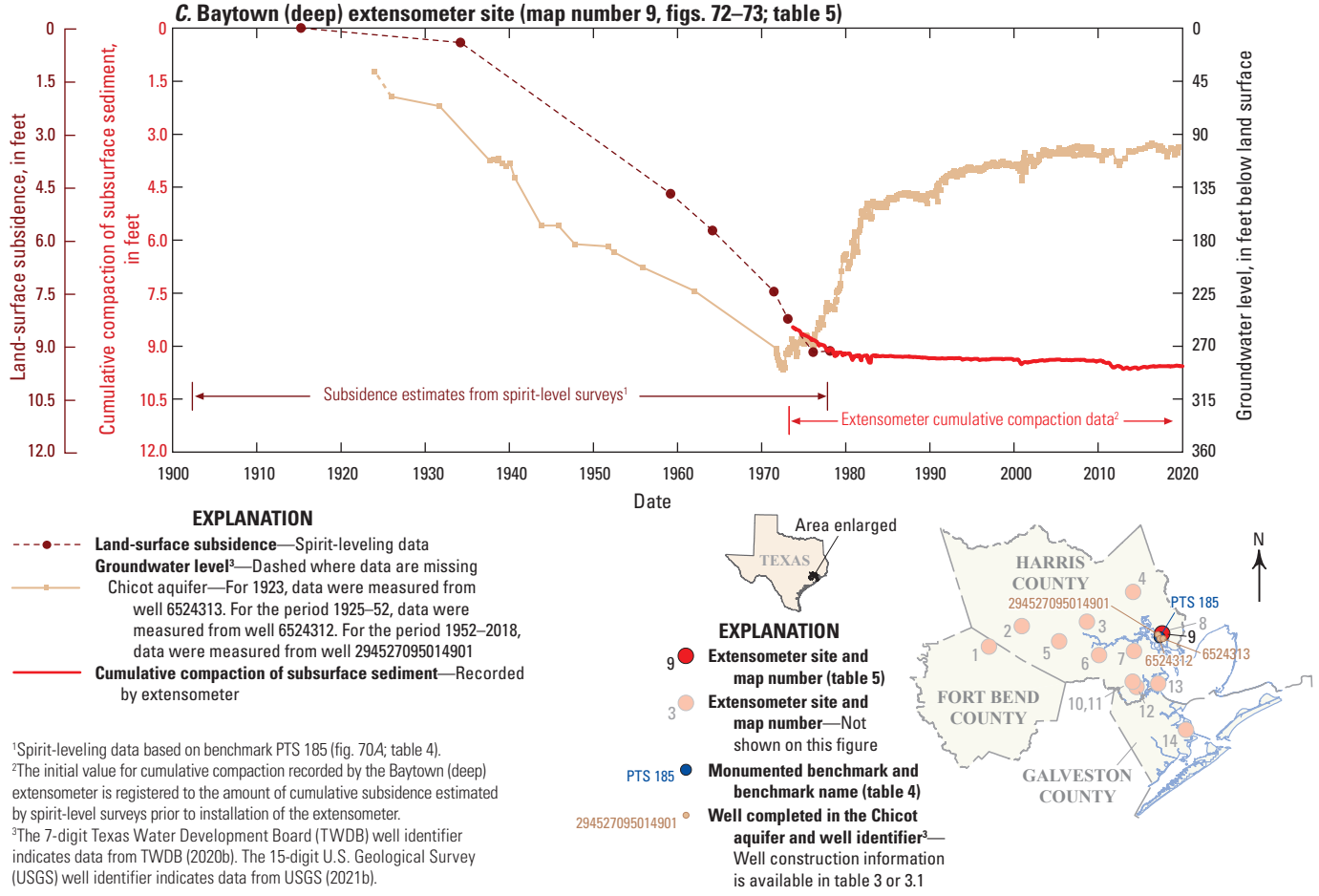

Figure 95.—Continued

Groundwater-level declines began in the Baytown area in about 1918 as a result of groundwater withdrawals from large industrial wells (fig. 11; table 1) (Gabrysch and Bonnet, 1975). Groundwater levels by 1934 were about 60–90 ft bls, and subsidence was estimated at 0.41 ft (figs. 14, 95*C*), similar to the groundwater levels in the historical Houston area (figs. 94, 95*A–B*). By 1943, groundwater levels in the Baytown area had declined between about 65 and 160 ft (figs. 14, 95*C*), resulting in the greatest amount of subsidence in the greater Houston area (excluding the Goose Creek oil field) at that time. Subsidence in 1943 was estimated at 2.4 ft near the future Baytown site and was 3.2 ft at the Goose Creek oil field (fig. 5.1). Subsidence of almost 3 ft occurred during 1943–64 at the Baytown site concurrent with groundwater-level declines of about 80–100 ft (figs. 14, 27, 95*C*). About 2.5 ft of subsidence occurred during 1964–73 at the Baytown site concurrent with groundwater-level declines of between about 50 and 80 ft (figs. 27, 95*C*). By 1973, subsidence of more than 8 ft had occurred in the Baytown area (fig. 95*C*; table 4) (Galloway and others, 1999), concurrent with groundwater levels that had declined to about 280 ft bls.

The leveling rod in the photograph is placed on benchmark PTS 185 (fig. 70*A*) in Baytown, Texas, located about 1,500 feet east of the former Brownwood subdivision, and about half a mile south of the Baytown extensometer site. Photograph by Samuel Rendon, U.S. Geological Survey, July 15, 2022.

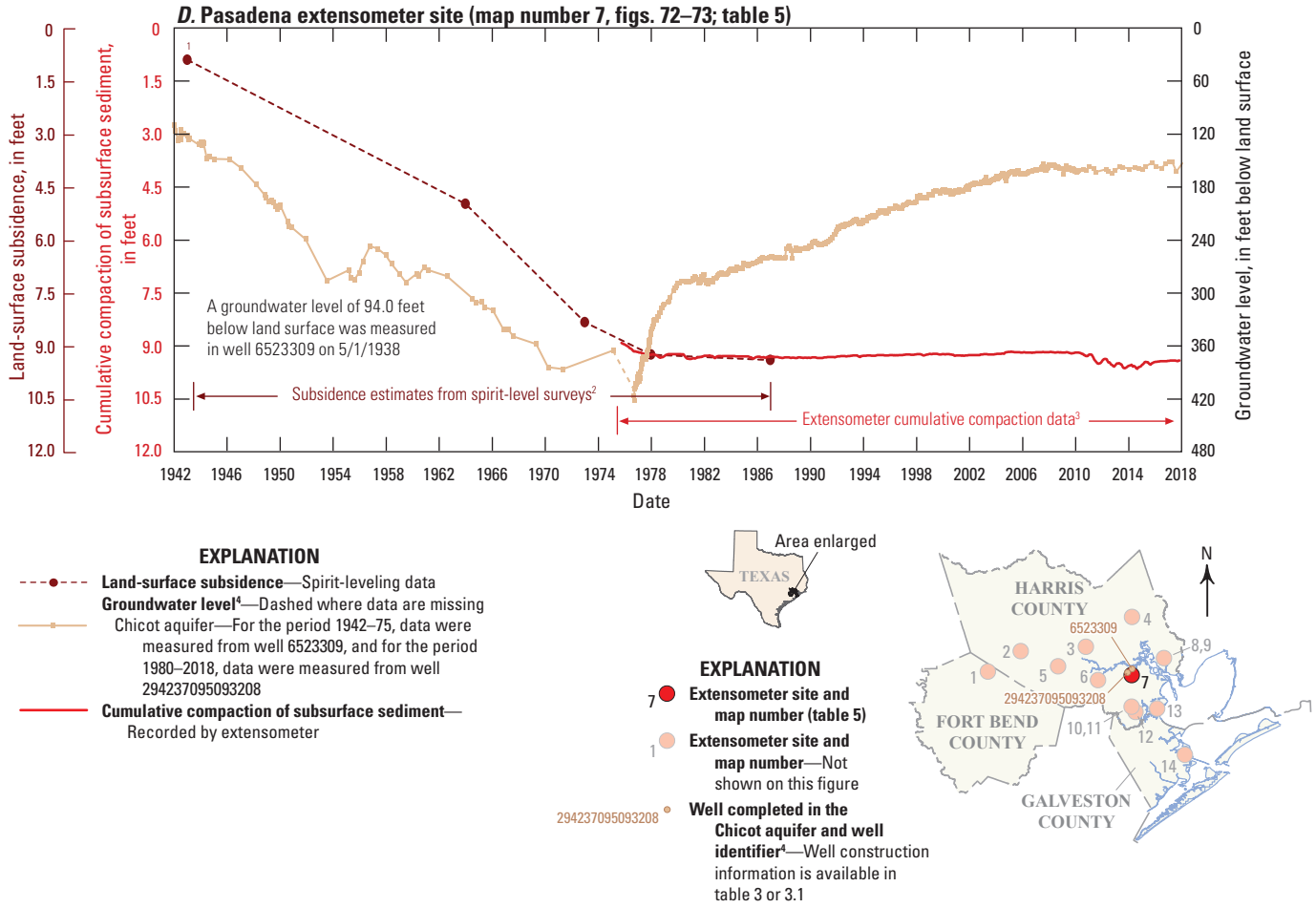

[1]A total of 0.85 foot of subsidence was estimated for the period 1906–43 based on interpolated subsidence contour maps described in appendix 5; therefore, this is the starting value for cumulative compaction shown on this figure in 1943.
[2]Spirit-leveling data based on contoured data from Gabrysch and Bonnet (1975), Jorgensen (1975), Gabrysch (1980b), and Gabrysch and Coplin (1990).
[3]The initial value for cumulative compaction recorded by the extensometer is registered to the amount of cumulative subsidence estimated by spirit-level surveys prior to installation of the extensometer.
[4]The 7-digit Texas Water Development Board (TWDB) well identifier indicates data from TWDB (2020b). The 15-digit U.S. Geological Survey (USGS) well identifier indicates data from USGS (2021b).

Figure 95.—Continued

This area of about 8 ft of subsidence included the Brownwood subdivision (fig. 1), which was about 1,500 ft northwest of benchmark PTS 185 and 0.75 mi southwest of the Baytown extensometer. The Brownwood subdivision initially was about 10.5 ft above sea level when construction began in 1938 (Galloway and others, 1999); however, the subdivision had subsided more than about 4 ft by 1959 (fig. 95*C*; table 4), which compounded the flooding in the subdivision during Hurricane Carla in 1961. As a result of the long-term subsidence in this area (figs. 95*C*, 5.1–5.6), more regular flooding occurred during 1969–78, which is described extensively in Bernal (2020). This subdivision was finally abandoned in 1983 in the aftermath of Hurricane Alicia after having subsided as much as 9.2 ft (fig. 95*C*; table 4). Groundwater levels rose rapidly during 1974–82 in the Baytown area (fig. 27) and at the Baytown site (fig. 95*C*), after which time the compaction rate decreased to approximately zero.

A similar pattern of historical groundwater-level declines and resulting subsidence, followed by groundwater-level recovery and reduction in the compaction rate, is observed at each extensometer site (figs. 94–95); the primary differences between each site are the magnitude of the groundwater-level decline and associated subsidence. The installation of most of the extensometers coincided with groundwater levels that approached historical minimums and the advent of groundwater regulation. As a result, by the time the extensometers were installed (table 5), a mean subsidence equal to about 80 percent of the compaction measured at each site from the date of installation to 2020 had already occurred (figs. 94–95; table 5).

Based on the combination of leveling and extensometer data, the greatest subsidence since 1906 present in the greater Houston area is 9.33 ft at the Baytown site (fig. 95*C*; table 5) and 9.16 ft at the Pasadena site (fig. 95*D*; table 5). The subsidence at the Baytown and Pasadena sites (fig. 70*B*) agrees with

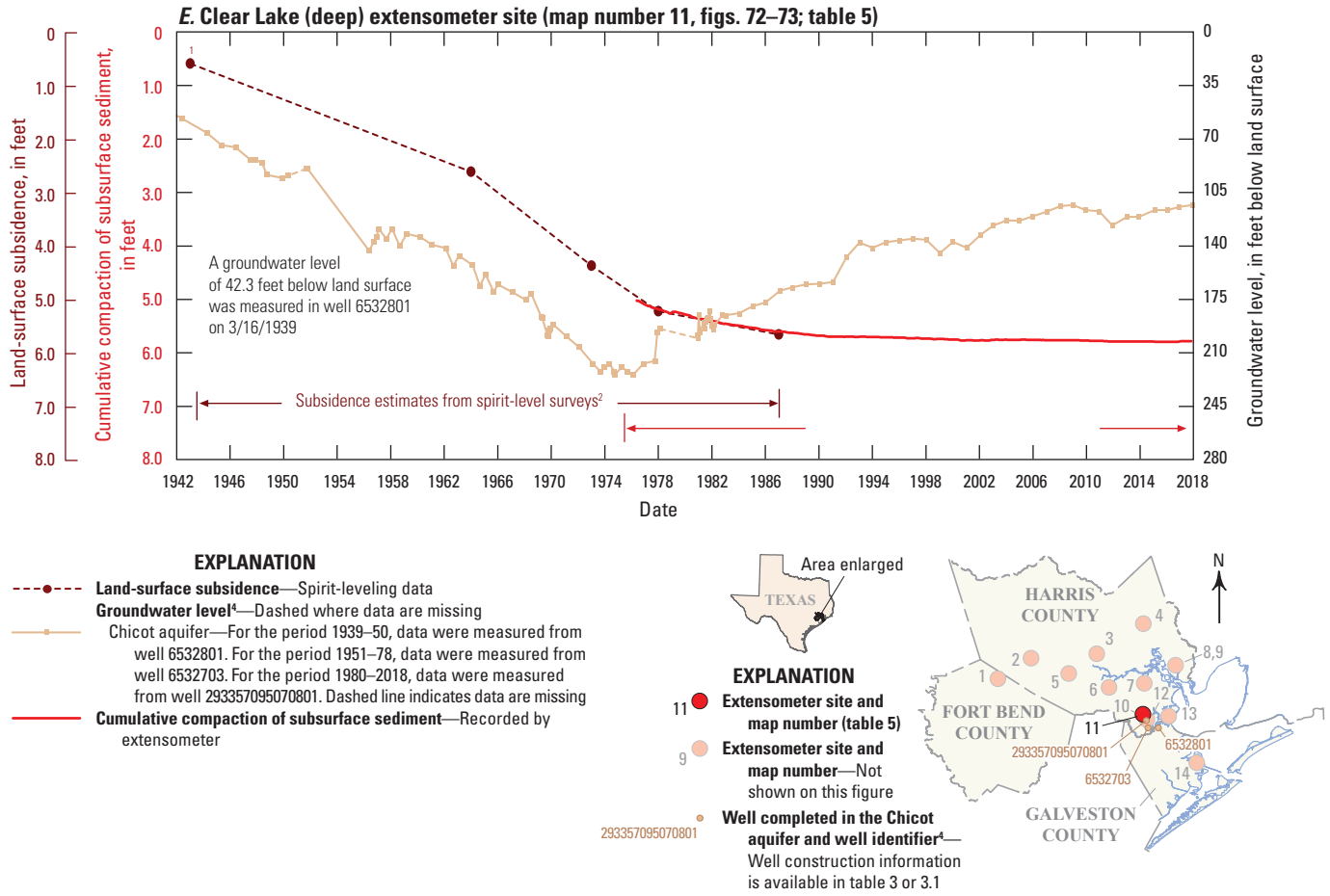

[1]A total of 0.60 foot of subsidence was estimated for the period 1906–43; therefore, this is the starting value for cumulative compaction shown on this figure in 1943.
[2]Spirit-leveling data based on contoured data from Gabrysch and Bonnet (1975), Jorgensen (1975), Gabrysch (1980b), and Gabrysch and Coplin (1990).
[3]The initial value for cumulative compaction recorded by the extensometer is registered to the amount of cumulative subsidence estimated by spirit-level surveys prior to installation of the extensometer.
[4]The 7-digit Texas Water Development Board (TWDB) well identifier indicates data from TWDB (2020b). The 15-digit U.S. Geological Survey (USGS) well identifier indicates data from USGS (2021b).

Figure 95.—Continued

the 1906–2016 subsidence from Petersen and others (2020). Because subsidence has been minimal at these sites since the early 1980s (figs. 95*C–D*), these subsidence estimates also agree with the 1906–2000 contour map from Gabrysch and Neighbors (2005).

The least amount of subsidence was estimated at the Texas City site (fig. 95*J*). Subsidence was first observed in the Texas City area at the Pan American Refinery about 3.5 mi southwest of the future extensometer site (fig. 70*A*). Leveling surveys of the benchmarks located on the refinery property proceeded normally until sometime between late 1938 and early 1940, when minor discrepancies began to occur in the survey results (AMOCO, 1958). Subsidence at the Pan American Refinery was about 1.6 ft by 1943 (fig. 5.1) and was much as 4.4 ft by 1952 after accounting for subsidence at the base monument (Lockwood, 1954; AMOCO, 1958). This subsidence was caused by declining groundwater levels measured onsite at the refinery (wells E–H, fig. 16) as a result of substantial groundwater withdrawals in a small area that included the refinery and nearby industrial plants (fig. 11; table 1) (Lockwood, 1954). At the neighboring Union Carbide Refinery, a subsidence of 1.2 ft was determined by 1945, and 2.4 ft by 1948, based on leveling surveys (Rose, 1949). Groundwater use in the Texas City area decreased from about 24 Mgal/d in 1945 to about 11.5 Mgal/d in 1952 (fig. 11*G*; table 1) after the delivery of surface water began in 1948 (Petitt and Winslow, 1955; AMOCO, 1958). After the introduction of surface-water sources, groundwater levels in the Texas City area (fig. 16*E–H*), and the subsidence rate at the Pan American Refinery rapidly decreased (AMOCO, 1958). Increases in groundwater use in this area after 1964 (fig. 11*G*; table 1) once again resulted in groundwater-level declines (fig. 33*C*), and an additional 1 ft of subsidence occurred near the Pan American Refinery during 1964–73 (Gabrysch and

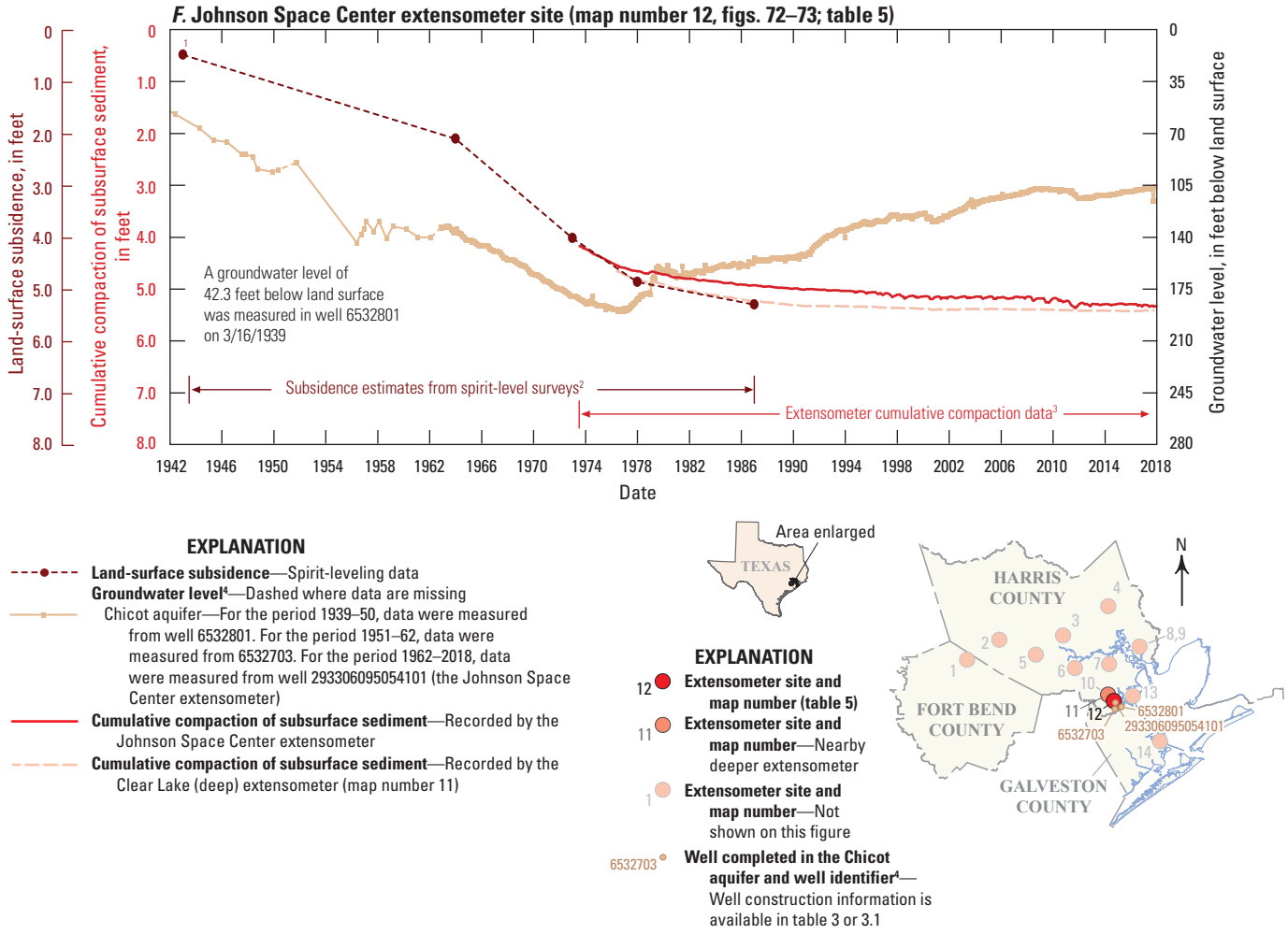

[1]A total of 0.33 foot (ft) of subsidence was estimated for the period 1906–43 based on interpolated subsidence contour maps described in appendix 5; therefore, this is the starting value for cumulative compaction shown on this figure in 1943.
[2]Spirit-leveling data based on contoured data from Gabrysch and Bonnet (1975), Jorgensen (1975), Gabrysch (1980b), and Gabrysch and Coplin (1990).
[3]The initial value for cumulative compaction recorded by the extensometer is registered to the amount of cumulative subsidence estimated by spirit-level surveys prior to installation of the extensometer. Some compaction may have occurred below the anchor elevation of the Johnson Space Center extensometer (750 ft below North American Vertical Datum of 1988 [NAVD 88]) that is observed at the Clear Lake (deep) extensometer (3,053 ft below NAVD 88), particularly between 1976 and 2012. By 2018, compaction differences between the two extensometers were minimal.
[4]The 7-digit Texas Water Development Board (TWDB) well identifier indicates data from TWDB (2020b). The 15-digit U.S. Geological Survey (USGS) well identifier indicates data from USGS (2021b).

Figure 95.—Continued

Bonnet, 1976a), prompting the installation of the Texas City extensometer in 1973. Groundwater use in the Texas City area subsequently decreased from 15.5 Mgal/d in 1971 to 9.7 Mgal/d in 1978 (fig. 11*G*; table 1) (Gabrysch, 1982a), which resulted in a groundwater-level recovery during this period and a reduction in the subsidence rate to approximately zero after 1978 (fig. 95*J*). The decrease in groundwater use, combined with the distance between the extensometer site and the general area of industrial groundwater withdrawals, resulted in only about 0.1 ft of subsidence being recorded by the extensometer since installation in 1973 (fig. 95*J*; table 5). Note that the groundwater-level declines shown on figure 95*J* prior to the extensometer installation in 1973 were recorded from wells located about 1.5 mi southwest of the extensometer; therefore, these declines were probably somewhat greater than the declines that would have occurred onsite at the extensometer. This extensometer site has undergone a slight rebound in land surface since 1981, indicating that some degree of elastic compaction has occurred.

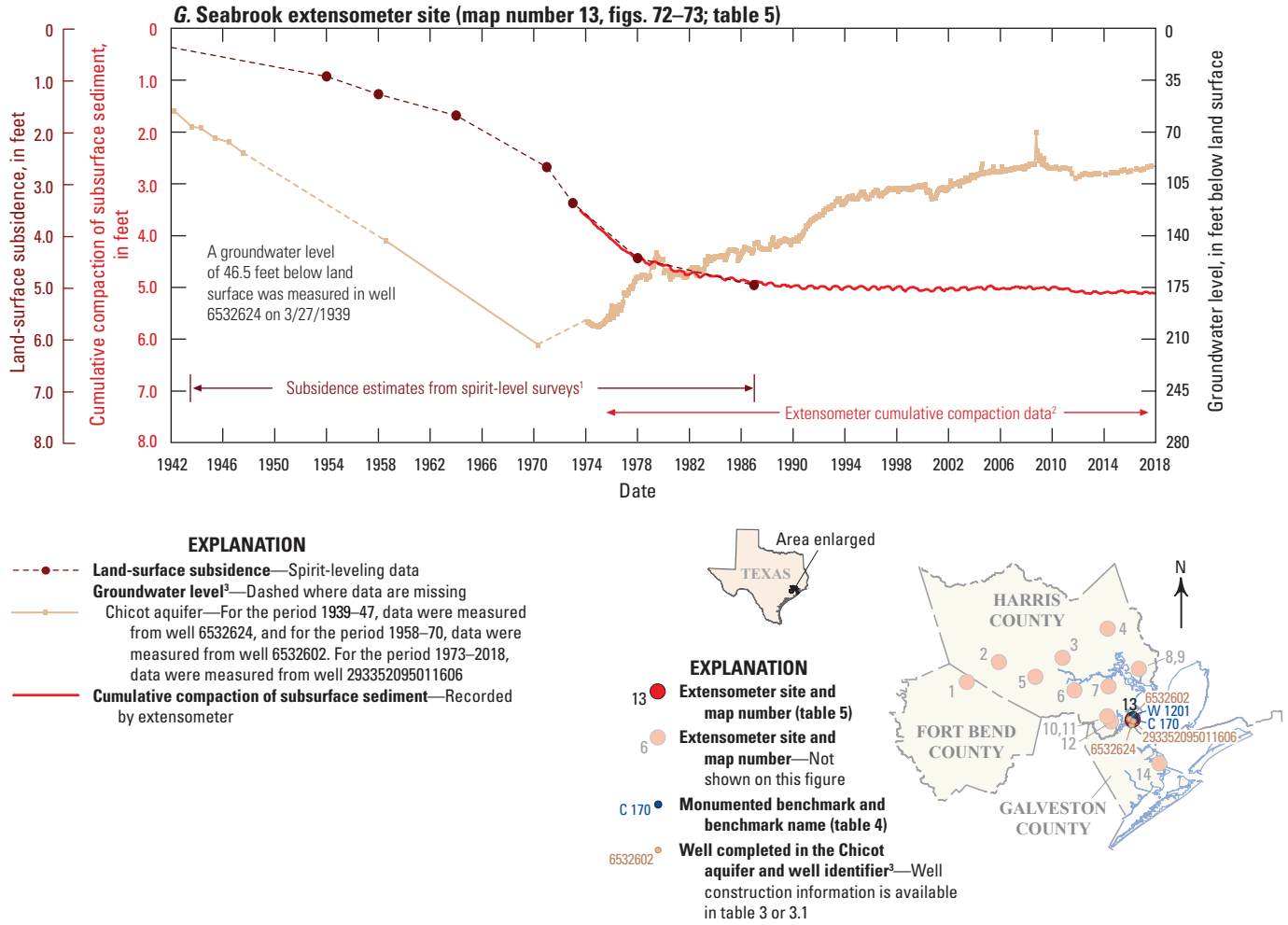

[1]Spirit-leveling data are from benchmarks C 170 and W 1201 (fig. 70*A;* table 4), which were monumented in 1936 and 1973, respectively.
[2]The initial value for cumulative compaction recorded by the extensometer is registered to the amount of cumulative subsidence estimated by spirit-level surveys prior to installation of the extensometer.
[3]The 7-digit Texas Water Development Board (TWDB) well identifier indicates data from TWDB (2020b). The 15-digit U.S. Geological Survey (USGS) well identifier indicates data from USGS (2021b).

Figure 95.—Continued

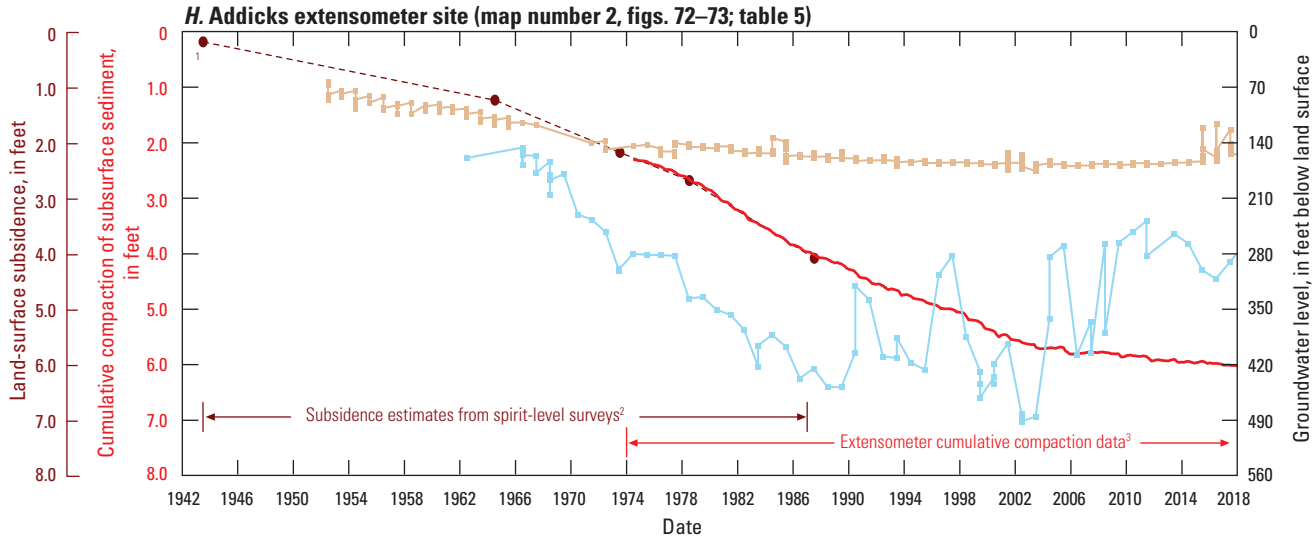

EXPLANATION

- **Land-surface subsidence**—Spirit-leveling data
- **Groundwater level**[4]
  - Chicot aquifer—For the period 1952–77, data were measured from well 294538095344601. For the period 1977–2018, data were measured from well 294726095351104
  - Evangeline aquifer—For the period 1962–68, data were measured from well 6512704. For the period 1968–2018, data were measured from well 294724095351401
- **Cumulative compaction of subsurface sediment**—Recorded by extensometer

Note: Summer pumping levels (not shown on this graph) for well 294724095351401 are as much as 639 feet below land surface. These summer pumping levels are shown on figure 39*F*.

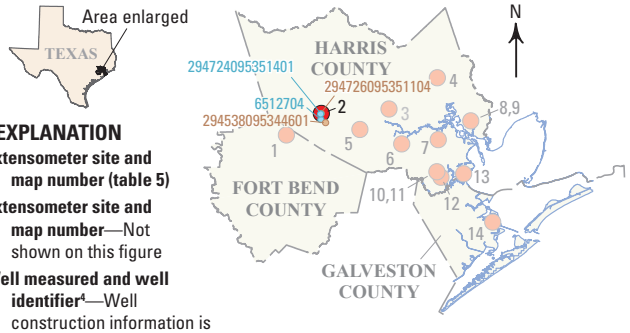

EXPLANATION

- 2 **Extensometer site and map number (table 5)**
- 6 **Extensometer site and map number**—Not shown on this figure
- **Well measured and well identifier**[4]—Well construction information is available in table 3 or 3.1
  - 294538095344601 Well completed in the Chicot aquifer
  - 6512704 Well completed in the Evangeline aquifer

[1]A total of 0.2 foot of subsidence was estimated from 1906 to 1943 based on interpolated subsidence contour maps described in appendix 5; therefore, this is the starting value for cumulative compaction shown on this figure in 1943.
[2]Spirit-leveling data based on contoured data from Gabrysch and Bonnet (1975), Jorgensen (1975), Gabrysch (1980b), and Gabrysch and Coplin (1990).
[3]The initial value for cumulative compaction recorded by the extensometer is registered to the amount of cumulative subsidence estimated by spirit-level surveys prior to installation of the extensometer.
[4]The 15-digit U.S. Geological Survey (USGS) well identifier indicates data from USGS (2021b). The 7-digit Texas Water Development Board (TWDB) well identifier indicates data from TWDB (2020b).

Figure 95.—Continued

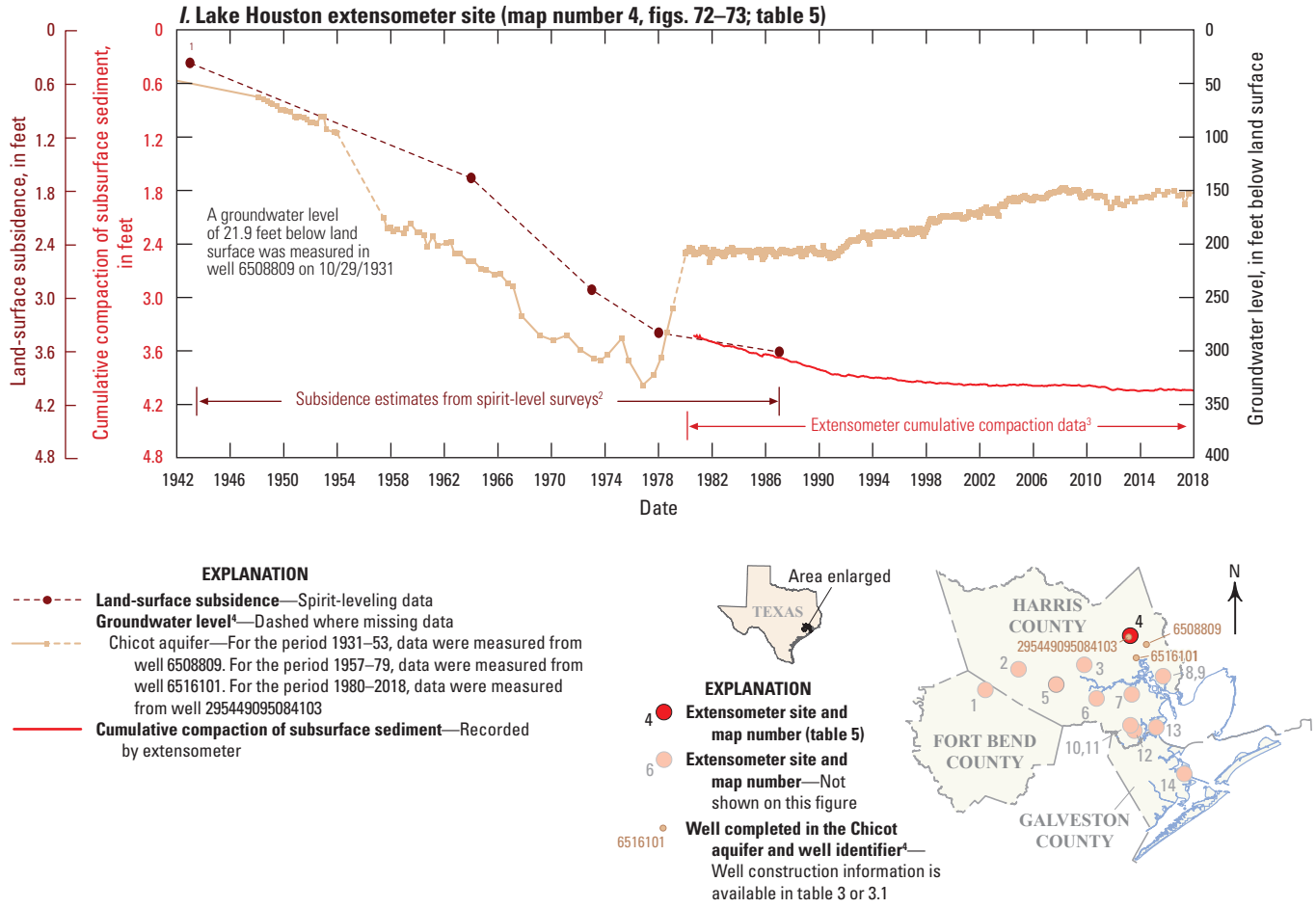

[1]A total of 0.4 foot of subsidence was estimated from 1906 to 1943 based on interpolated subsidence contour maps described in appendix 5; therefore, this is the starting value for cumulative compaction shown on this figure in 1943.
[2]Spirit-leveling data based on contoured data from Gabrysch and Bonnet (1975), Jorgensen (1975), Gabrysch (1980b), and Gabrysch and Coplin (1990).
[3]The initial value for cumulative compaction recorded by the extensometer is registered to the amount of cumulative subsidence estimated by spirit-level surveys prior to installation of the extensometer.
[4]The 7-digit Texas Water Development Board (TWDB) well identifier indicates data from TWDB (2020b). The 15-digit U.S. Geological Survey (USGS) well identifier indicates data from USGS (2021b).

Figure 95.—Continued

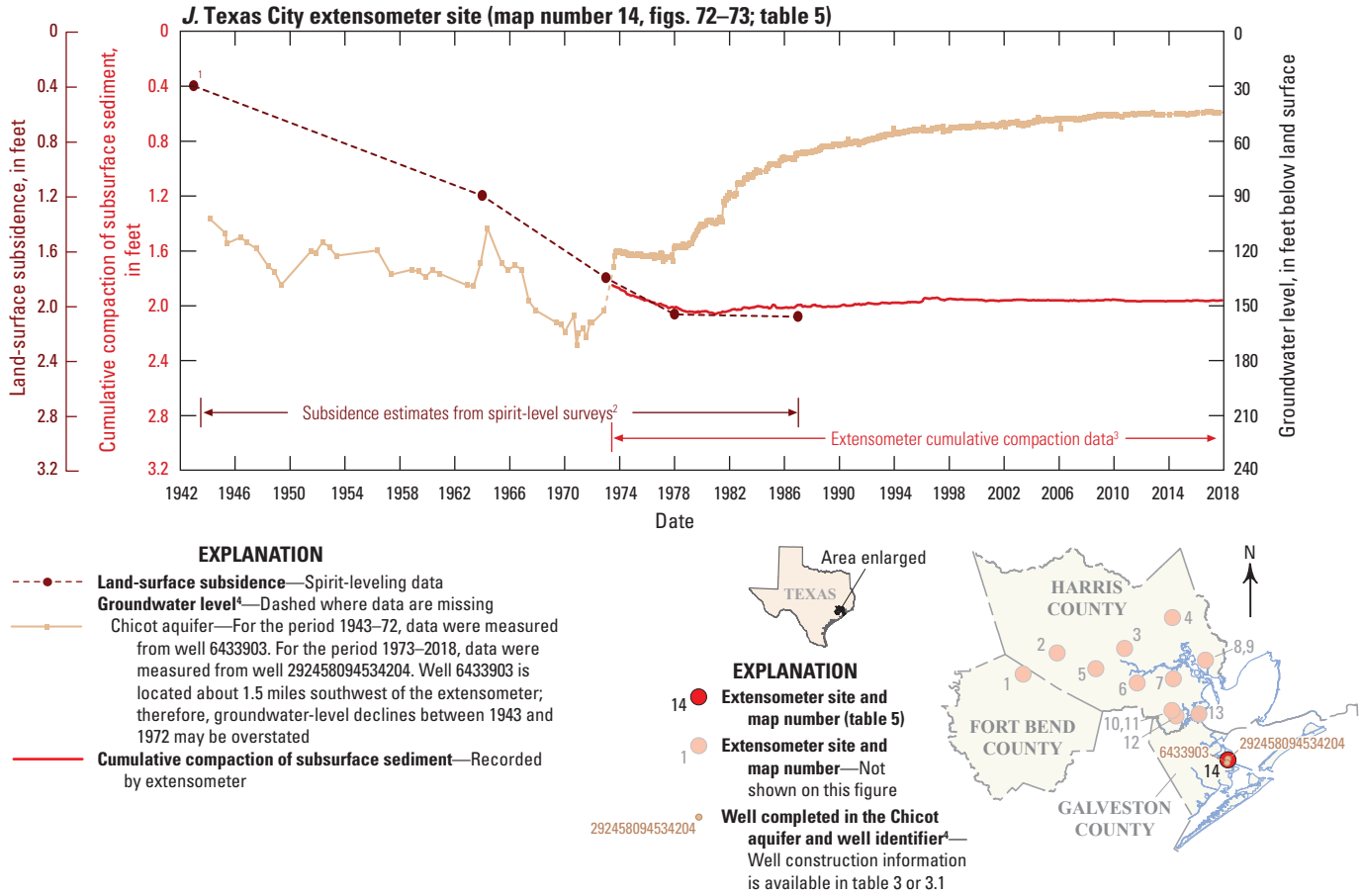

[1]A total of 0.4 foot of subsidence was estimated for the period 1906–43 based on interpolated subsidence contour maps described in appendix 5; therefore, this is the starting value for cumulative compaction shown on this figure in 1943.
[2]Spirit-leveling data based on contoured data from Gabrysch and Bonnet (1975), Jorgensen (1975), Gabrysch (1980b), and Gabrysch and Coplin (1990).
[3]The initial value for cumulative compaction recorded by the extensometer is registered to the amount of cumulative subsidence estimated by spirit-level surveys prior to installation of the extensometer.
[4]The 7-digit Texas Water Development Board (TWDB) well identifier indicates data from TWDB (2020b). The 15-digit U.S. Geological Survey (USGS) well identifier indicates data from USGS (2021b).

Figure 95.—Continued

The Land Surface–Groundwater Nexus: Brownwood, the Subdivision that Sank into the Sea

The predicament of Brownwood, a subdivision in Baytown, Texas, gained national attention after four hurricanes, two tropical storms, and numerous other rainfall events caused repeated flooding and eventually the demise of the neighborhood in 1983. This flooding was compounded by years of subsidence that began in the early 1930s because of rapid groundwater-level declines from concentrated groundwater development near where the Brownwood subdivision would be built. Construction in Brownwood began in the late 1930s on a peninsula surrounded by the Houston Ship Channel (fig. 1) after the purchase of the subdivision land by the Humble Oil and Refining Company. In 1915, the Brownwood land area was about 11.8 feet (ft) above a vertical control datum that approximates sea level. By 1953, however, Brownwood subsided by about 3.7 ft because of groundwater-level declines of about 165 ft in the local area. About 1.7 ft of this subsidence occurred during 1944–53, evident in the southern part of the subdivision where tideland and beachfront areas had become submerged. By 1959, about 4.7 ft of subsidence had occurred in Baytown and Brownwood (Gabrysch and Bonnet, 1974). That same year, minor flooding first occurred in Brownwood because of Hurricane Debra, and several houses were inundated with as much as 6 inches of water (Hartman, 1959). Although flooding from Hurricane Debra was minor, widespread flooding in Brownwood from Hurricane Carla in September 1961 resulted in $3.5 million worth of damages and an "almost complete loss" of the subdivision (Hartman, 1961). By 1962, subsidence of about 5.3 ft caused bay water to reach the subdivision's perimeter road and caused the submergence of marshland and beachfront areas on the southern and western parts of the subdivision. A levee was proposed to the U.S. Army Corps of Engineers the same year (1962) to protect the subdivision (Marsh, 1962), although funding for the levee was not obtained. By 1966, subsidence in the subdivision was about 6.2 ft, and the mean land elevation of about 5.6 ft was about half of the elevation in 1915. Hurricane Beulah resulted in flooding in the subdivision in September 1967 (Bernal, 2020). A month after the hurricane, the Baytown city council authorized a feasibility study on a proposed levee that would enclose the Brownwood subdivision and convert the bays adjacent to the subdivision to freshwater lakes (Holcomb, 1967). However, the levee had not been constructed by February 1969, when the subdivision flooded because of the Valentine's Day flood; about 150 homes were flooded, and damages were estimated at $250,000 (Boynton, 1969). During 1971–73, subsidence at Brownwood reached a peak of about 0.4 foot per year (ft/yr), coincident with the groundwater-level declines to a historical minimum of about 290 ft in December 1972. During this period, the subdivision flooded because of heavy precipitation in August 1970, Hurricane Fern in September 1971, and Tropical Storm Delia in September 1973 (Bernal, 2020). By 1973, subsidence of about 8.2 ft had resulted in bay water inundating both sides of the perimeter road. Additionally, bay water had also flooded the land surrounding a two-story house on the northwest side of the subdivision. That same year, the perimeter road that provided access to the subdivision was raised to an elevation of about 7.0 ft above sea level. The perimeter road continued to subside, however, along with the subdivision land, and the road's 7.0-ft elevation was similar to the elevation of the subdivision when Hurricanes Debra (1959) and Carla (1961) resulted in millions of dollars in damages to the subdivision. By 1978, a subsidence of 9.2 ft had resulted in a decrease in the mean land-surface elevation to only 2.6 ft and a loss of land area around the perimeter of Brownwood. A levee had been proposed in 1974 to the U.S. Army Corps of Engineers, who estimated the cost for the project to be about $70 million (Gabrysch, 1983). Although funds were approved by the U.S. Congress, a bond proposal by the City of Baytown required by the project did not pass on July 23, 1979 (Gabrysch, 1983). Two days later, 187 homes in Brownwood flooded due to the nearly 12 inches of precipitation that occurred from the landfall of Tropical Storm Claudette (Gabrysch, 1983; Bernal, 2020). The end of the neighborhood came after Hurricane Alicia resulted in $35 million worth of damages to 300 houses in the subdivision in August 1983 (Ocker, 1983; Bernal, 2020).

Because 5.7 ft of subsidence had resulted in a mean elevation for the subdivision of about 6.1 ft by 1964, the neighborhood was susceptible to flooding from even minor storm events—evidenced by the 12 flooding events during 1967–83 (Bernal, 2020). Additionally, due to the continuously declining groundwater levels, the subsidence rate during 1964–71 was about 0.25 ft/yr, which accelerated to about 0.4 ft/yr during 1971–73. This rapid subsidence rate, combined with the irreversible nature of the subsidence, rendered any land-based potential flood remediation projects as short-term solutions at best. Although the Brownwood subdivision could not be saved, the widely reported subsidence issues in that neighborhood helped pave the way for groundwater regulation beginning in the mid-1970s in Harris County.

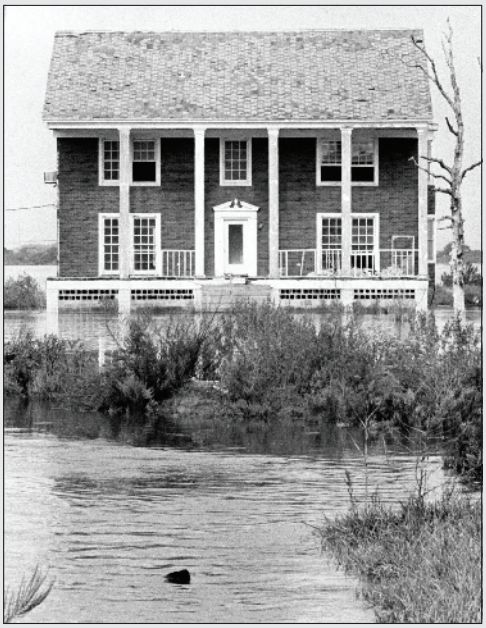

Photograph by Curtis McGee/copyright Houston Chronicle. Used with permission. This photograph was taken in 1976 and is republished from the following Houston Chronicle news article: https://www.chron.com/news/houston-texas/slideshow/Archive-photos-of-long-gone-Brownwood-Subdivision-130243.php.

Subsidence in the Brownwood subdivision resulted in the land underneath and around this house, located in the northwestern part of the subdivision, to sink into the bay by the late 1970s (see 1973 aerial photograph on page 183). The subsidence of the land on this property is visible in comparisons between the 1962 and 1973 aerial photographs.

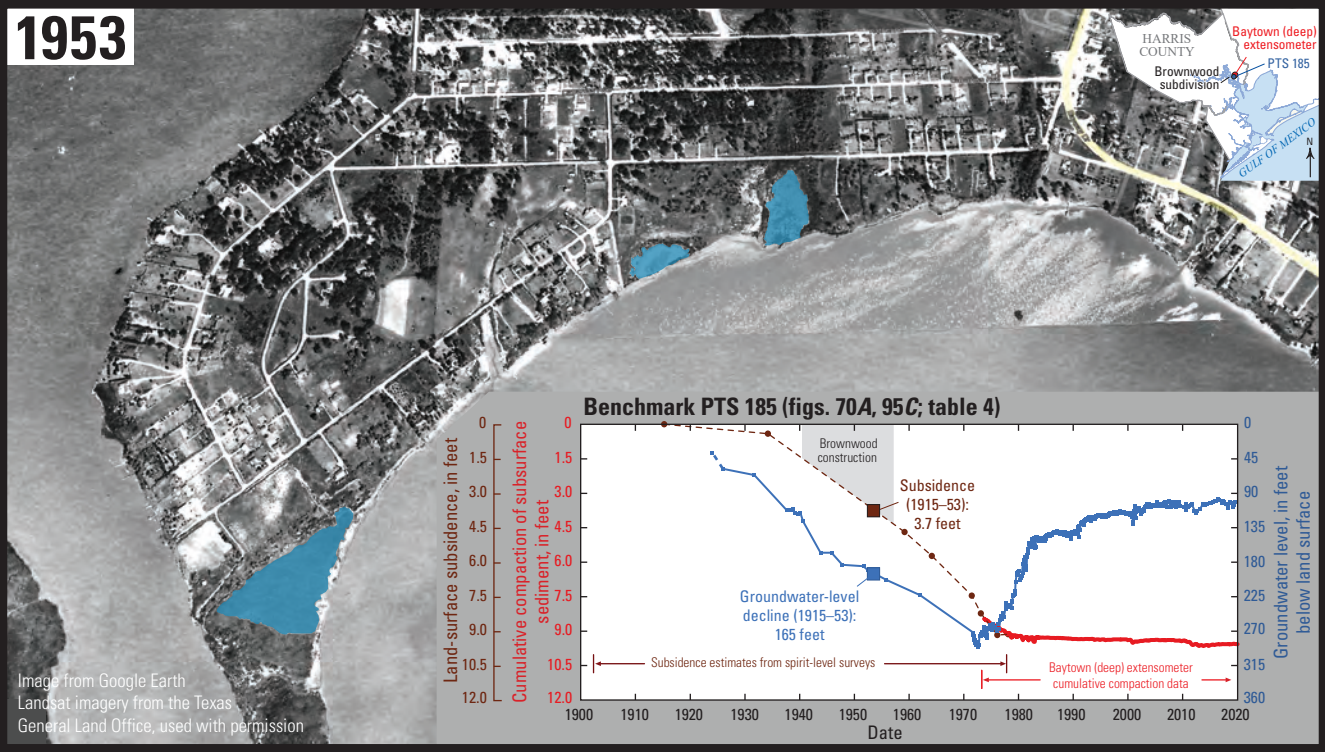

The Brownwood subdivision in 1953, after an estimated subsidence of about 3.7 feet during 1915–53 and about 1.7 feet during 1943–53 (fig. 95*C*). The estimated 1.7 feet of subsidence during 1943–53 is visible along the shoreline, as shown by the blue shaded areas.

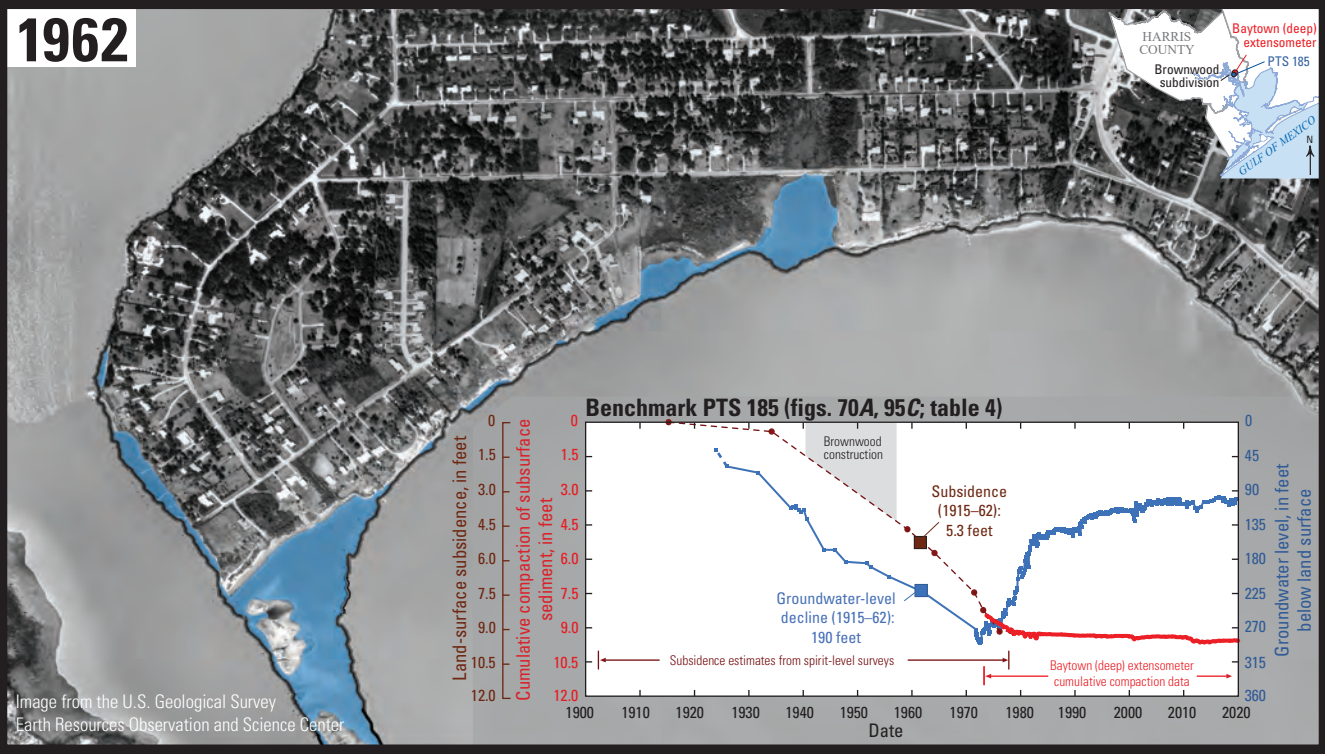

The Brownwood subdivision in 1962, after an estimated subsidence of about 5.3 feet during 1915–62 and about 3.3 feet during 1943–62 (fig. 95*C*). The estimated 3.3 feet of subsidence during 1943–62 is visible along the shoreline, as shown by the blue shaded areas and black outline.

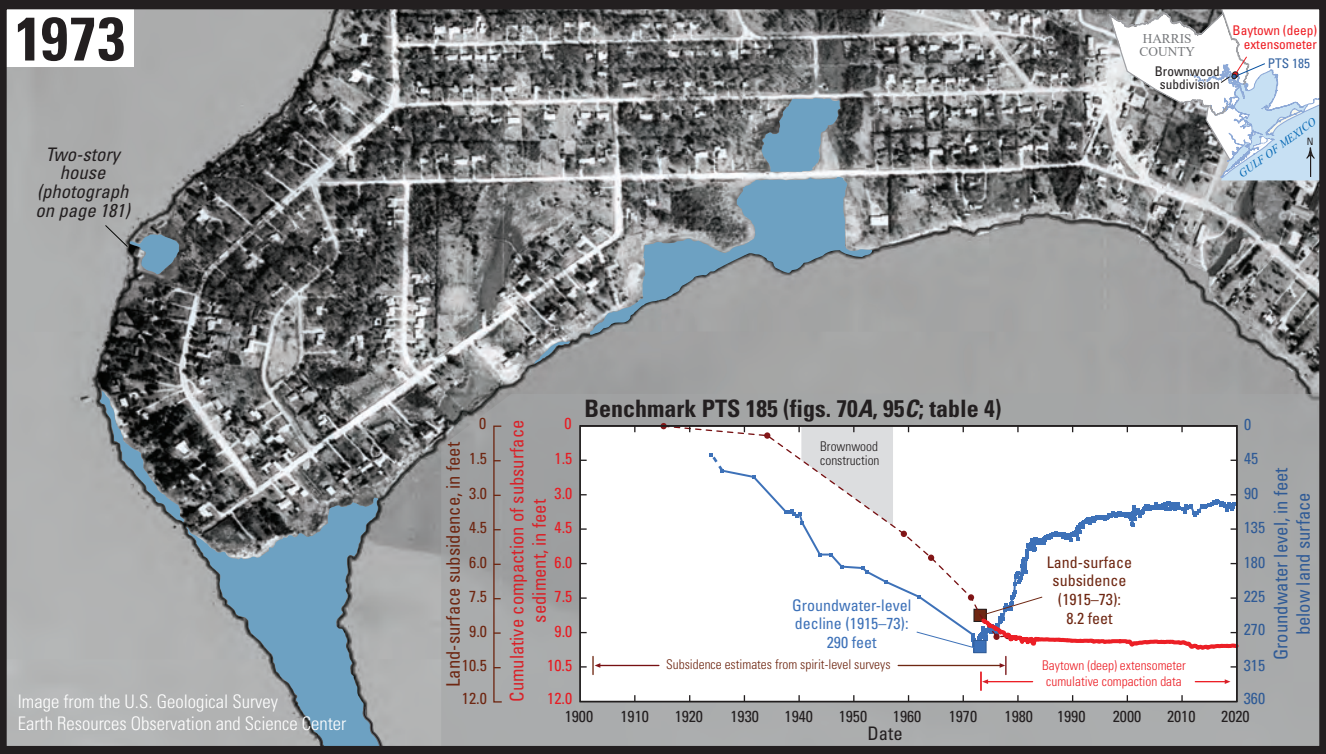

The Brownwood subdivision in 1973 after subsiding about 8.2 feet during 1915–73 and about 6.2 feet during 1943–73 (fig. 95*C*). The estimated 6.2 feet of subsidence during 1943–73 is visible along the shoreline, as shown by the blue shaded areas and black outline. Note that the two-story house shown on page 181 is located in the northwestern part of the Brownwood subdivision and surrounded by water in this photograph.

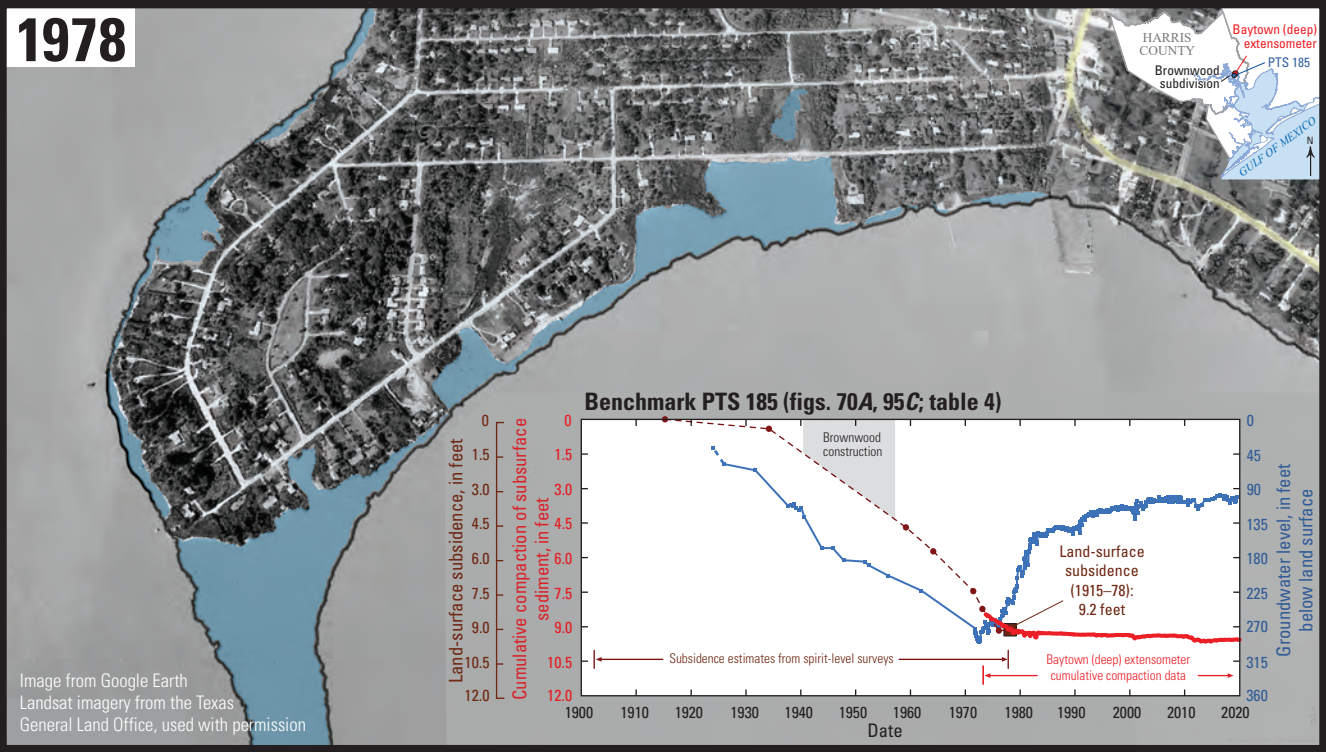

The Brownwood subdivision in 1978 after subsiding about 9.2 feet since 1915 and about 7.2 feet since 1943 (fig. 95*C*). During the period of greatest subsidence (1971–73) the subdivision was sinking more than 4.0 inches per year. The 1944 land area of the Brownwood subdivision is shown by the blue shaded area and black outline.

Areas of Recent and Continued Subsidence

Numerous studies have been conducted regarding subsidence in the greater Houston area. Few published studies describe subsidence in northern Harris County and in Montgomery County (fig. 70*B*), however, due in large part to the later onset of groundwater development and subsequent groundwater-level declines in these areas. Many of the benchmarks in these areas were not releveled in 1943 and 1964—the beginning and end dates of three widely circulated maps showing subsidence from 1906–43, 1943–64, and 1964–73 (appendix 5). Additionally, western Harris County and northern Fort Bend County and adjoining areas have undergone ongoing groundwater-level declines (figs. 23, 31). Based on GPS station data (fig. 77), much of the subsidence in the greater Houston area since the 2000s has taken place in areas of sustained groundwater declines in the northern and western parts of the greater Houston area (Kearns and others, 2015), as described in the "Groundwater Levels" section; therefore, a summary of historical subsidence and more recent subsidence in these areas is included below.

Subsidence in northern Harris County during 1906–78 was greatest at benchmark D 89 (3.3 ft, table 4) and least at benchmarks PTS 101 and W 88 (about 0.6 ft, table 4). In northern Harris County, groundwater levels in 1978 in the Chicot and Evangeline aquifers were about 80–250 ft and 200–220 ft bls, respectively (fig. 21). In Montgomery County, about 0.2–0.4 ft and 0.4–0.5 ft of subsidence occurred in Conroe and The Woodlands, respectively, during this period (fig. 5.6; table 4). An identical elevation (subsidence of 0.0 ft) was recorded in 1932 and 1947 for benchmark K 88 in Conroe (table 4). The groundwater level in the Jasper aquifer in Conroe during and prior to 1947–48 was at or above land surface (figs. 13, 19). Minimal subsidence in Conroe and The Woodlands occurred during 1973–78, including some slight uplift of about 0.03 ft at one site (S 88, table 4), which indicates some degree of elastic compaction during this period. Groundwater levels in Montgomery County in 1978 generally were 40 to 70 ft bls in the Chicot aquifer (TWDB, 2020b; USGS, 2021b), 100 to 150 ft bls in the Evangeline aquifer, and 70 to 130 ft bls in the Jasper aquifer (figs. 19–20). Subsidence in western Harris County during 1943–78 was between 0.75 and 1.7 ft (benchmark T 768 and F 804; table 4), and subsidence between 1906–78 was between 1.0 and 2.2 ft based on subsidence contours (fig. 5.6). In Waller County, subsidence during 1906–78 at benchmark V 7 was 1.1 ft (fig. 5.6; table 4). Groundwater levels in western Harris County in 1978 generally were 110 to 140 ft bls in the Chicot aquifer and about 300 ft bls in the Evangeline aquifer (fig. 23).

Subsidence in northern Harris County during 1978–87 was about 1.3 ft at benchmark D 89, and about 0.3–0.6 ft at most other benchmarks (fig. 5.5; table 4). During 1978–87, groundwater-level declines in northern Harris County were about 10 to 45 ft in the Chicot aquifer, about 60 to 90 ft in the Evangeline aquifer, and about 15 ft in the Jasper aquifer (fig. 21). In Montgomery County during 1978–87, about 0.1–0.2 ft and about 0.2–0.4 ft of subsidence occurred in Conroe and The Woodlands, respectively (fig. 5.5; table 4). During 1978–87, the groundwater-level declines in these areas were between about 40 and 80 ft in the Evangeline aquifer and between about 15 and 70 ft in the Jasper aquifer (figs. 19–20). Subsidence in western Harris County during 1973–87 was about 1.4 ft closest to central Harris County (Addicks extensometer, fig. 95*H*), about 0.8 ft at benchmark F 804 (fig. 5.5; table 4), and about 0.5 ft at the boundary of Harris, Waller, and Fort Bend Counties (benchmarks Y 7 and Y 1148) (fig. 5.5; table 4). In Waller County, subsidence at benchmark V 7 was also about 0.5 ft (fig. 5.5; table 4). During 1978–87, groundwater-level declines in the Chicot and Evangeline aquifers were about 10–15 ft and 0–80 ft, respectively, in western Harris County (fig. 23).

Subsidence in northern Harris County during 1987–2021 was about 1 ft at benchmark D 89, and between about 1.4 and 2.7 ft at two other benchmarks (SPRING RM 1, V 1252) (fig. 70*A*; table 4). At a third benchmark (V 660), there was about 2.9 ft of subsidence during this period based on the combination of leveling data during 1987–96 and data from GPS station P002 (fig. 80*H*; table 6). In this area, groundwater-level changes during 1987–2018 in the Chicot aquifer ranged from declines of about 45 ft to recoveries of about 7 ft (fig. 21). Evangeline aquifer groundwater-level changes during this period ranged from declines of about 85 ft to recoveries of between about 15 and 45 ft. The decline in groundwater levels in the Jasper aquifer during this period was about 315 ft (fig. 21*H*). Historical groundwater-level minimums in northern Harris County (excluding measurements made when a well was actively withdrawing groundwater) generally were reached earlier (about 2000) for wells closest to central Harris County (fig. 21*D, E*), and later (about 2010) for wells near the northern county boundary (fig. 21*B, G, H*).

In Montgomery County during 1987–2021, subsidence in Conroe was about 0.7–1.0 ft, and subsidence in the northern part of The Woodlands was about 0.7 ft (table 4). In the area that includes Conroe and The Woodlands, groundwater-level declines during 1987–2018 were between about 150 and 180 ft in the Evangeline aquifer and between about 185 and 230 ft in the Jasper aquifer for most wells (figs. 19–20). Historical groundwater-level minimums in Montgomery County generally were reached during 2012–15, and in subsequent years, groundwater levels in each aquifer rose somewhat (figs. 19–20). Subsidence in western Harris County during 1987–2018 was about 2.0 ft at the Addicks site (fig. 95*H*). Subsidence from 1987–2021 was about 1.2 to 1.4 ft at the boundary of Harris, Waller, and Fort Bend Counties (benchmarks Y 7 and Y 1148) (fig. 5.5; table 4). During this period, groundwater-level changes in the Chicot aquifer in western Harris County were between about 5 ft of recovery and 30 ft of decline. Groundwater-level changes in the Evangeline aquifer in western Harris County were between about 30 ft of recovery and 145 ft of decline (fig. 23). Historical minimums

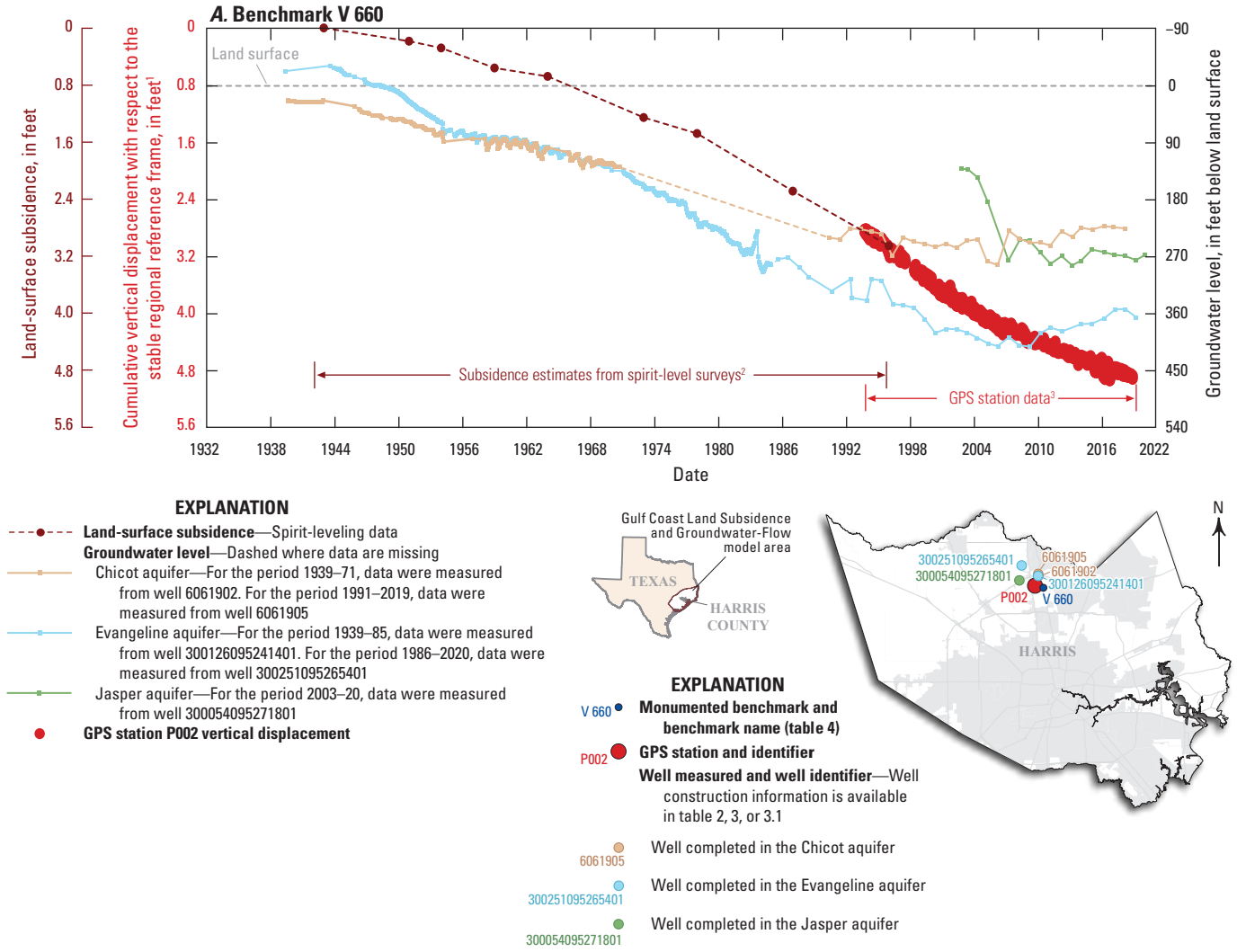

[1]The stable regional reference frame is Houston20 (Agudelo and others, 2020).
[2]Subsidence data for benchmark V 660 are available in table 4.
[3]The initial value for Global Positioning System (GPS) vertical-displacement data is registered to the amount of cumulative subsidence estimated by spirit-level surveys prior to installation of GPS station P002. GPS station P002 (figs. 76–77; table 6) is located approximately 1.2 miles from benchmark V 660 (fig. 70*A*; table 4).

Figure 96. Cumulative subsidence at selected benchmarks from leveling, Global Navigation Satellite System surveys, and Global Positioning System time-series data for benchmarks *A*, V 660, *B*, SPRING RM 1, *C*, T 88, *D*, CONROE RM 1, and *E*, Y 7 within the Gulf Coast aquifer system study area in southeast Texas.

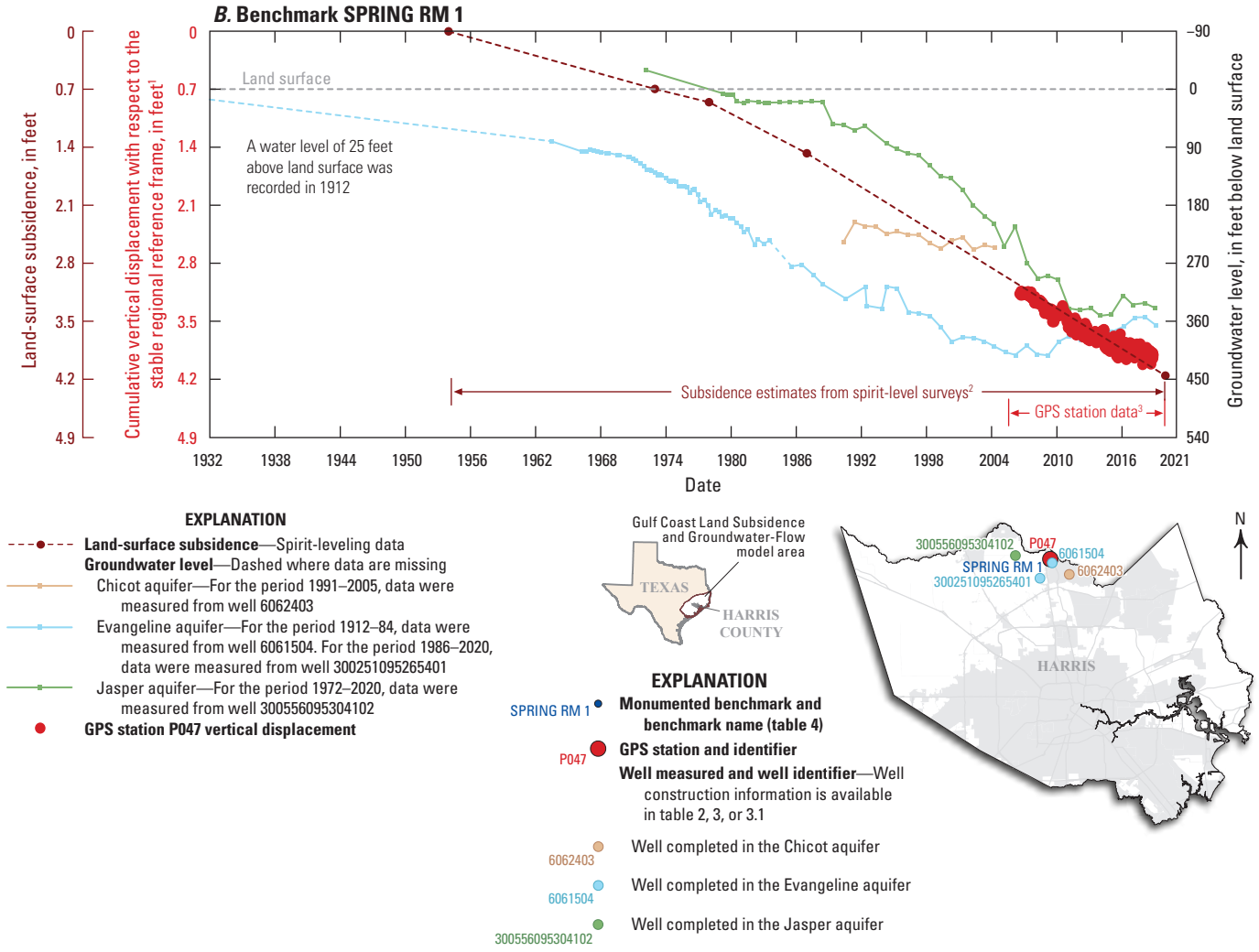

[1]The stable regional reference frame is Houston20 (Agudelo and others, 2020).
[2]Subsidence data for benchmark SPRING RM1 are available in table 4.
[3]The initial value for Global Positioning System (GPS) vertical-displacement data is registered to the amount of cumulative subsidence estimated by spirit-level surveys prior to installation of the GPS station. GPS station P047 (figs. 76–77; table 6) is located approximately 0.7 mile from benchmark SPRING RM 1 (fig. 70*A*; table 4).

Figure 96.—Continued

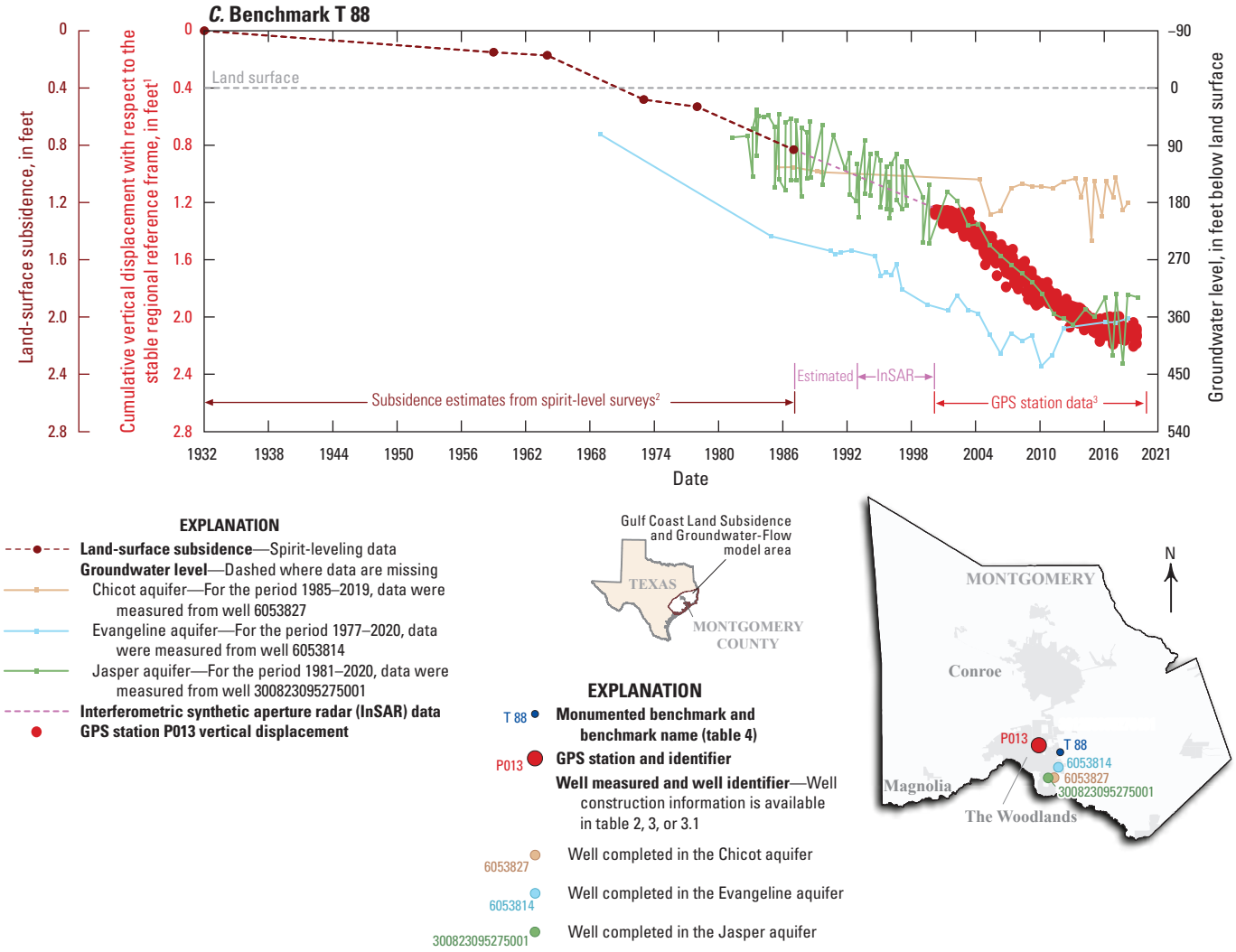

[1]The stable regional reference frame is Houston20 (Agudelo and others, 2020).
[2]Subsidence data for benchmark T 88 are available in table 4.
[3]The initial value for Global Positioning System (GPS) vertical-displacement data is registered to the amount of cumulative subsidence estimated by spirit-level surveys prior to installation of GPS station P013. GPS station P013 (figs. 76–77; table 6) is located approximately 2.9 miles from benchmark T 88 (fig. 70*A*; table 4).

Figure 96.—Continued

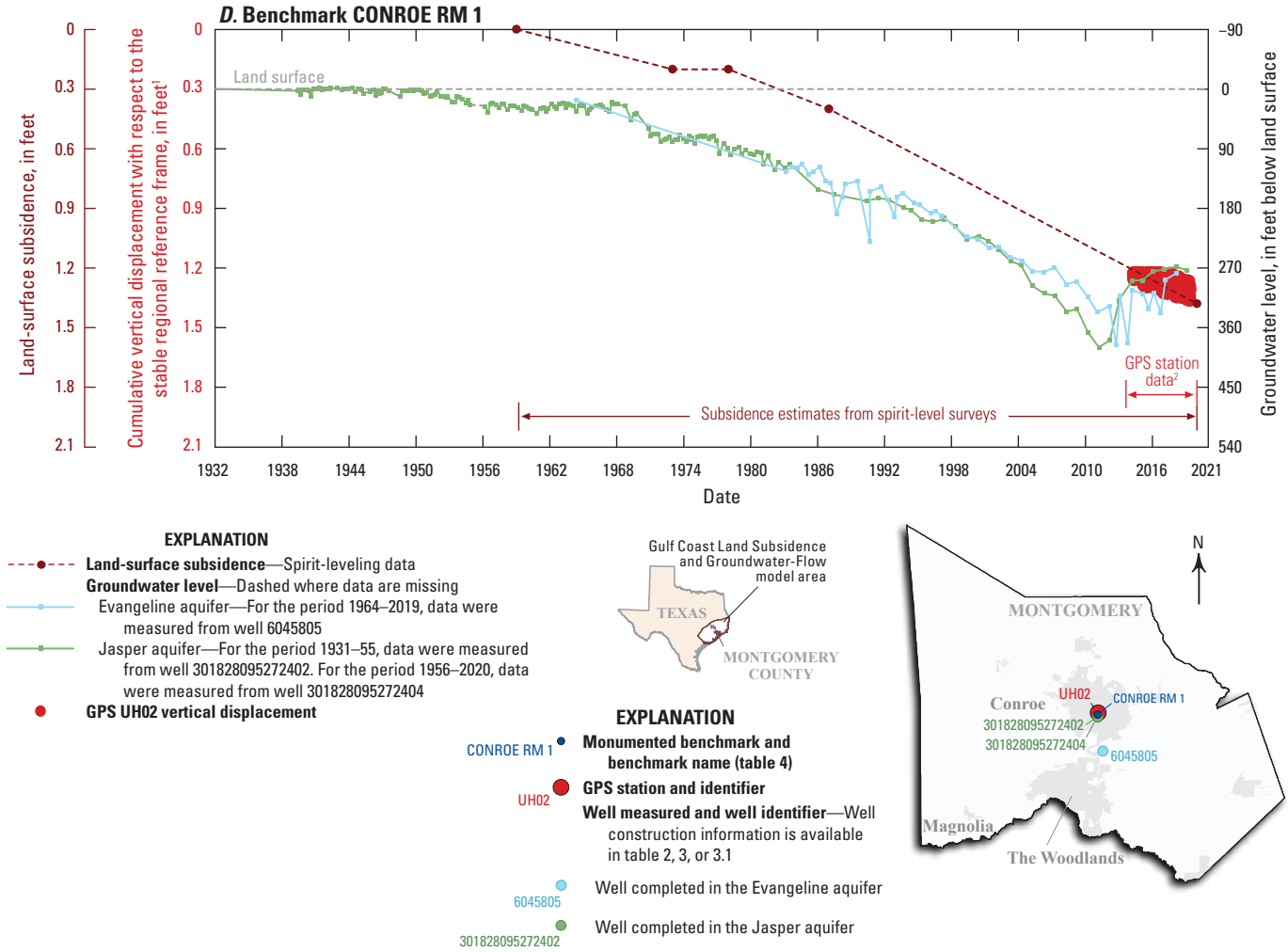

[1]The stable regional reference frame is Houston20 (Agudelo and others, 2020).
[2]Subsidence data for benchmark CONROE RM1 are available in table 4.
[3]The initial value for Global Positioning System (GPS) vertical-displacement data is registered to the amount of cumulative subsidence estimated by spirit-level surveys prior to installation of GPS station UH02. GPS station UH02 (figs. 76–77; table 6) is located approximately 0.2 mile from benchmark CONROE RM 1 (fig. 70*A*; table 4).

Figure 96.—Continued

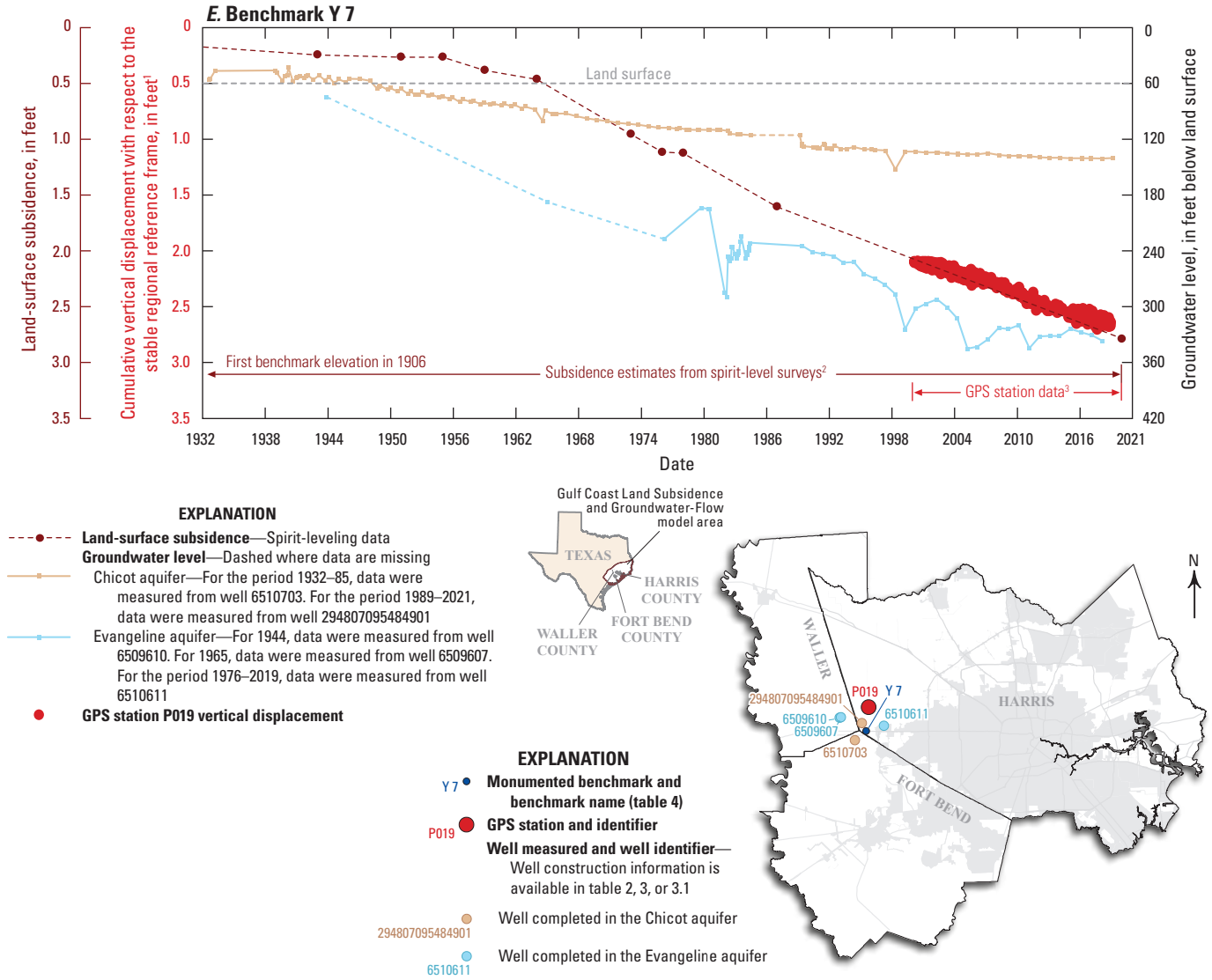

[1]The stable regional reference frame is Houston20 (Agudelo and others, 2020).
[2]Subsidence data for benchmark Y 7 are available in table 4.
[3]The initial value for Global Positioning System (GPS) vertical-displacement data is registered to the amount of cumulative subsidence estimated by spirit-level surveys prior to installation of the GPS station. GPS station P019 (figs. 76–77; table 6) is located approximately 3.9 miles from benchmark Y 7 (fig. 70*A*; table 4).

Figure 96.—Continued

in western Harris County generally were reached during 2000–06; since the early 2000s, groundwater levels in each aquifer have risen somewhat (fig. 23).

Based on the leveling and GNSS surveys at the benchmark sites in the study area, subsidence in northern Harris County through 2021 was about 5.5 ft at benchmark D 89, about 5.2 ft at benchmark V 660 (fig. 96*A*), about 4.2 ft at benchmark SPRING RM 1 (fig. 96*B*), and about 2.3 ft at benchmark V 1252 (fig. 70*B*; table 4). Subsidence at benchmark V 660 is based on a subsidence of about 3.1 ft during 1943–96 from leveling data (table 4) and a subsidence of about 2.1 ft during 1996–2020 at GPS station P002 (table 6) located about 1.2 mi west of benchmark V 660 (figs. 70*B*, 76, 96*A*). The subsidence of 2.3 ft estimated at benchmark V 1252 is based on 0.7 ft of subsidence at benchmark PTS 100 from 1915 to 1978 and 1.6 ft of subsidence at V 1252 during 1978–2021. Subsidence in western Harris County through 2020 was about 6.1 ft at the Addicks site (table 5) and about 2.8 ft at benchmark Y 7 through 2021 (figs. 70*B*, 96*E*), similar to the findings of Petersen and others (2020).

In Montgomery County, subsidence through 2021 was about 1.3 ft at benchmark R 88 (table 4) in the northern part of The Woodlands and about 2.5 ft at benchmark U 88 in the southern part of The Woodlands (fig. 70*B*). Subsidence of about 2.2 ft was estimated at benchmark T 88 through 2020 (fig. 96*C*). In The Woodlands near benchmark T 88, groundwater levels in the Evangeline aquifer declined by about 7 ft/yr during 1978–2001, and groundwater levels in the Jasper aquifer rose slightly during 1981–87 and declined about 8 ft/yr during 1987–2001 (fig. 96*C*). Thus, based on the groundwater-level changes during these periods, subsidence during 1987–2001 in The Woodlands at benchmark T 88 would be expected to be similar or somewhat greater than subsidence during 1978–87 (about 0.3 ft, or about 0.03 ft/yr; table 4). InSAR data from Bawden and others (2012) were available during 1993–2001, although the data quality near benchmark T 88 hindered analysis of the subsidence rate. However, based on a qualitative analysis of available InSAR interferograms combined with analysis of subsidence measured at nearby benchmarks, leveling data at benchmark T 88 prior to 1987 and GPS data at station P013 after 2001, about 0.5 ft of subsidence (or 0.04 ft/yr) occurred during 1987–2001 at benchmark T 88. Subsidence at benchmark T 88 was 0.83 ft from 1932 to 1987, was estimated at about 0.5 ft during 1987–2001 and was about 0.84 ft during 2001–2020 (tables 4, 6); therefore, subsidence at this site through 2020 is about 2.2 ft (fig. 70*B*).

In The Woodlands, benchmark R 88 was reoccupied in 2021 (table 4); thus, based on the percentage of subsidence at benchmarks T 88 and U 88 compared with subsidence at R 88 during 1978–87 (table 4), subsidence estimates at benchmarks T 88 and U 88 are probably about 2.1 and 2.5 ft, respectively (fig. 70*B*). Using this estimation method with SPRING RM 1 in place of R 88 yields the same results for subsidence through 2021 at T 88 and U 88. Thus, the 2.1 ft of subsidence at benchmark T 88 estimated by using this method agrees with the 2.2 ft of subsidence at this benchmark estimated from the combination of the leveling, InSAR, and GNSS datasets. These subsidence estimates for The Woodlands are consistent with (1) the general location of the 2-ft subsidence contour from Petersen and others (2020), and (2) the estimated 2 ft of subsidence for The Woodlands from William F. Guyton and Associates, Inc. (1972) based on predicted groundwater-level declines in that report that are similar to the measured declines in the Evangeline and Jasper aquifers in this area (fig. 20).

In Montgomery County, subsidence through 2021 was about 1.2–1.5 ft in Conroe based on data at three benchmarks (fig. 70*B*; table 4). Subsidence at benchmark CONROE RM 1 from leveling and GNSS surveys was 1.4 ft from 1959 through 2021 (fig. 96*D*). About 0.12–0.13 ft of subsidence occurred at benchmarks K 88 and P 88 during 1932–59; benchmarks K 88 and P 88 are a short distance (1.6 and 2.6 mi) north and south, respectively, of CONROE RM 1 (fig. 70*A*; table 4). Thus, subsidence at CONROE RM 1 is estimated at 1.5 ft.

The graph depicting subsidence at benchmark V 660 (fig. 96*A*) demonstrates the relation between the long-term rates of subsidence (and vertical displacement) and groundwater-level changes throughout much of the greater Houston area. The relation between subsidence and groundwater-level changes can be seen by the rate of subsidence through about 2006, which was highly responsive to the rate of groundwater-level declines, albeit with some delay. Starting about 2006, subsidence continued after groundwater-level declines slowed and reached historical minimums, similar to the pattern of subsidence in the period directly following installation of most of the extensometers (figs. 37–44, 94–95). At the extensometer sites where the groundwater-level recovery was most rapid after the decline to historical minimums (Pasadena and Baytown sites), compaction ceased within a relatively short period of time (figs. 37–38, 95*C–D*). However, at the Addicks site, where groundwater levels during about 1990–2004 (or later) remained at or near the historical minimum (fig. 39), a substantial compaction rate continued during this period (fig. 95*H*). This pattern of continued compaction absent a sustained groundwater-level recovery occurs at benchmark V 660, the Addicks site, and the other four benchmarks shown in figure 96. Subsidence will continue until pore pressures in the fine-grained interbeds and confining units reach equilibrium with the surrounding coarse-grained aquifer sediment (Poland, 1984; Bull and Poland, 1975)—a condition noted at the Addicks site by Yu and others (2014). Since 2005, the subsidence rates at benchmark V 660 and at many GPS sites in northern, northwestern, and western Harris County have decreased (figs. 80–82). This decrease in subsidence has been coincident with a recovery in groundwater levels (figs. 21–23) owing to decreases in groundwater use that occurred ahead of a 30-percent alternative water supplies conversion requirement in 2010 for these areas. More recently, the subsidence rate in Montgomery County has decreased since about 2016 (figs. 78–79), coincident with groundwater-level recoveries (figs. 19–20) resulting from decreases in groundwater use and increases in surface-water deliveries from Lake Conroe.

Compaction Properties

Fine-grained units (interbeds and confining units) within or adjacent to unconsolidated aquifers that undergo groundwater-level declines related to groundwater development are susceptible to aquifer-system compaction (Hughes and others, 2022). Although the compaction of a single interbed may not cause substantial subsidence, compaction of a sequence of numerous interbeds can result in appreciable subsidence (Kasmarek and Robinson, 2004). The compaction of these susceptible aquifer systems, and thereby subsidence, is largely dependent on various characteristics of the interbeds and confining units present in the aquifer system.

The thickness and vertical hydraulic conductivity (Kv) of a confining unit or interbed are important properties in determining the rate and duration of compaction, which occurs in these unconsolidated alluvial aquifer systems as the groundwater levels in the fine-grained units equilibrate with the groundwater levels in the surrounding aquifers (Kelley and others, 2018). The total interbed or confining unit thickness of the Gulf Coast aquifer system hydrogeologic units across the study area (fig. 97) was obtained from Young and others (2017). The thickness and spatial distribution of fine-grained sediment in each aquifer unit generally increase downdip from the northwest to the southeast (fig. 97) (Gabrysch, 1967). In the Chicot aquifer, the fine-grained unit thickness is about 100 ft or less in the northern part of the study area and increases to about 600 ft in the southern part of the study area (fig. 97*A*) (Gabrysch, 1984) where the Beaumont Formation is present (fig. 7). In the Evangeline aquifer, the fine-grained sediment thickness increases to about 2,500 ft along the Gulf of Mexico (fig. 97*B*) (Gabrysch, 1984). The lithology at the colocated well sites (figs. 37–50) generally reflects these fine-grained sediment thicknesses from Gabrysch (1984), although the variability in the amount and thickness of fine-grained sediment from site to site demonstrates the heterogeneity of the Gulf Coast aquifer system.

Depth-dependent Kv values for the Gulf Coast aquifer system units were estimated in Kelley and others (2018) on the basis of (1) core samples (and consolidation tests) collected at multiple vertical intervals at three field sites, as reported in Gabrysch and Bonnet (1974, 1976a, b), and (2) modeled Kv data for 26 sites in Harris, Galveston, and Fort Bend Counties. For various depths, the upper bound of the Kv value was estimated from Gabrysch and Bonnet (1974, 1976a, b), and the lower bound was the modeled value. The depth-dependent Kv values computed in Kelley and others (2018) are presented on figure 98*B*.

Groundwater supplied to wells actively withdrawing water from storage in confined aquifer systems comes from the expansion of the water and the compression of the sediments that constitute the skeleton of the aquifer system (Jacob, 1940). Water compressibility, skeletal compressibility, porosity, and thickness determine the storativity for each of the components of an aquifer system—aquifers, interbeds, and confining units. Aquifer-system storativity (S) is defined as the sum of the skeletal storativities (product of the skeletal compressibilities, unit weight of water, and thickness) of interbeds and confining units (S'_k), aquifers (S_k), and the storage from water compressibility (S_w) (Sneed and Galloway, 2000).

$$S = S'_k + S_k + S_w \tag{3}$$

where

S is the aquifer-system storativity,
S'_k is the skeletal storativity of the interbeds or confining units,
S_k is the skeletal storativity of the aquifer(s), and
S_w is the storage from water compressibility.

The skeletal storativity is defined for each of the elastic and inelastic stress conditions as the product of the elastic or inelastic skeletal specific storage (where specific storage is storativity divided by thickness) and the thickness of either the fine-grained units (interbeds or confining units) or the coarse-grained units (the aquifer).

$$S'_k \begin{cases} S'_{ske}(\sum b'),\ \sigma_e < \sigma_{e(\max)} \\ S'_{skv}(\sum b'),\ \sigma_e > \sigma_{e(\max)} \end{cases} \tag{4}$$

$$S_k = S_{ske}\,(\Sigma b) \tag{5}$$

where

S'_k is the skeletal storativity of the interbeds and confining units,
S'_{ske} is the elastic skeletal specific storage of the fine-grained units,
S'_{skv} is the inelastic skeletal specific storage of the fine-grained units,
$\Sigma b'$ is the thickness of the fine-grained units,
Σb is the thickness of the coarse-grained units,
$\sigma_e < \sigma_{e\ (\max)}$ where the effective stress is less than the past maximum effective stress (preconsolidation stress), and
$\sigma_e > \sigma_{e\ (\max)}$ where the effective stress is greater than the past maximum effective stress (preconsolidation stress).

Skeletal compressibilities (and therefore skeletal specific storativities) of interbeds and confining units can be substantially greater than skeletal compressibilities of coarse-grained units. These skeletal compressibilities are typically much greater than water compressibility. Thus, nearly all of the water derived from interbed and confining-unit storage is due to the compressibility of the granular skeleton. Furthermore,

the skeletal specific storativities of the interbeds and confining units and the drainage of these units largely govern the compaction magnitude and account for all but a negligible amount of the subsidence that often accompanies groundwater development in these aquifer systems (Hughes and others, 2022). To note, the coarse-grained aquifer material typically does not deform inelastically, and in the inelastic range of stress, the deformation of these materials is governed by the elastic skeletal compressibility of these units.

Consolidation tests were performed on core samples collected at multiple vertical intervals at three field sites, as reported in Gabrysch and Bonnet (1974, 1976a, b). The core samples were collected at elevations of about 1,208, 692, and 1,332 ft below NAVD 88 at the Baytown, Texas City, and Seabrook sites, respectively. These depth ranges approximate the sediment of the Chicot and Evangeline aquifer in Harris County (figs. 37–43) and laterally adjacent counties, and the Evangeline and Jasper aquifers in Montgomery County and laterally adjacent counties (figs. 45–50). These core-sample data were analyzed to estimate depth-dependent fine-grained sediment porosity and compressibility values, which were used to calculate inelastic specific storage, as documented in Kelley and others (2018). The elastic specific storage in that report was then calculated as the inelastic specific storage divided by a factor of 100, based on results presented by Holzer (1981) and Kasmarek (2012) for the Gulf Coast aquifer system near Houston. The depth-dependent values of porosity, vertical hydraulic conductivity, inelastic specific storage, and elastic specific storage are given in figure 98. Values for storage properties are smaller for deeply buried fine-grained sediment than for more shallow fine-grained sediment (fig. 98*C, D*). This is because the more deeply buried sediment is already partially compacted; therefore, less compaction is possible with increasing depth (Winslow and Doyel, 1954). An analysis of some depth-dependent compaction patterns based on extensometer data is presented in the "Deep-Seated Compaction" section.

In the greater Houston area (fig. 70*B*), the variability of the ratio of subsidence per 100 ft of water-level decline ranges from 0.5 ft to more than 2.5 ft (Gabrysch and others, 1969). Assuming a predevelopment groundwater level at land surface, during 1906–43 the subsidence per 100 ft of groundwater-level decline in the Texas City area was 1.8 ft, on the basis of a mean groundwater-level decline of about 90 ft (wells D–H, fig. 16) and subsidence of as much as 1.6 ft (fig. 5.1). Mean groundwater use in the Texas City area during 1920–43 was 9.2 Mgal/d (fig. 11; table 1). During 1906–43, subsidence amounts per 100 ft of groundwater-level decline in other areas of the Houston-Galveston region were as follows.

1. Baytown area: 1.8 ft on the basis of a mean of about 130 ft of groundwater-level decline and estimated subsidence of as much as 2.4 ft (figs. 14, 95*C*, 5.1). Mean groundwater use during 1920–43 was 11.5 Mgal/d (fig. 11; table 1). This estimate excludes the Goose Creek oil field subsidence prior to 1925 because groundwater-level declines in that area were not known.

2. Pasadena area: 0.8 ft on the basis of a mean of about 125 ft of groundwater-level decline and subsidence of as much as 1.0 ft (figs. 14, 95*D*, 5.1). Mean groundwater use during 1920–43 was 25.0 Mgal/d (fig. 11; table 1).

3. Historical Houston area: 1.0 ft on the basis of a mean of about 105 ft of groundwater-level decline (figs. 14, 94, 95*A–B*) and subsidence of as much as 1.1 ft (figs. 94, 95*A–B*, 5.1). Mean groundwater use during 1920–43 was 41.4 Mgal/d (fig. 11; table 1).

4. Katy area: 0.5 ft on the basis of a mean of about 55 ft of groundwater-level decline (fig. 15) and subsidence of as much as 0.3 ft (figs. 95*H*, 5.1). Mean groundwater use during 1920–43 was 30.2 Mgal/d (fig. 11; table 1).

Historical groundwater use in the Texas City area (fig. 11; table 1) occurred from wells screened in the Beaumont Formation above the Alta Loma Sand of Lang and others (1950) (fig. 10). These deposits compose the first 800-ft interval below land surface, which contains a substantial amount of fine-grained sediment (fig. 44). AMOCO (1958) describes a marked increase in subsidence at the Pan American Refinery in 1954 after a 0.21-Mgal/d increase in groundwater use from refinery well 2 (TWDB 6433811 on table 3.1; near well E, fig. 16), which is screened from 262 to 588 ft bls. Additionally, the Texas City area groundwater use during 1945–48 was particularly concentrated; during this period, 15 to 18 Mgal/d of groundwater use occurred in an area only 1.4 mi long by 0.36 mi wide at the Pan American and Union Carbide Refineries (fig. 16) (Rose, 1949). This concentrated groundwater use and abundance of fine-grained sediment resulted in localized differences in subsidence (or "differential subsidence") in the Texas City area (Winslow and Wood, 1959). Visible indications of this differential subsidence were cracks radiating from the pump foundations at Pan American wells 6–8 (wells F–H, fig. 16; table 3.1) across the floors to the four corners of each building (Rose, 1949). Differential subsidence at each of these wells (wells F–H, fig. 16) was as much as 1.6 ft within a horizontal distance of as little as 1,000 ft through December 1952 (Lockwood, 1954; AMOCO, 1958).

In Baytown, groundwater use through 1943 was similarly concentrated, with most of the groundwater withdrawn from wells at the Humble Oil Refinery in an area about 2 mi long by 2.5 mi wide. As a result, subsidence of greater than 2.4 ft occurred by 1943 and was centered on the refinery area (fig. 5.1) even though groundwater use in the Baytown area between 1920 and 1943 (11.5 Mgal/d) was substantially less than in the other areas in the Houston-Galveston region, except in the Texas City area (table 1). The amount of subsidence at the refinery decreased to about 0.8 ft within a distance of about 1.5 mi, which is shown by the closely spaced contour lines on fig. 5.1. Visible evidence of the subsidence in this area includes the protruding wellhead of the Burnet School well, about 1,500 ft west of the refinery (fig. 5.1) (fig. 3–6 in Garcia, 1991). Subsidence at the Goose Creek oil field was similarly concentrated, with 3 ft of subsidence during 1918–25 centered in an area approximately 2.5 mi long by 1.5 mi wide (fig. 5.1).

By contrast, much of the groundwater use in the historical Houston area was primarily from City of Houston municipal supply wells which were spatially distributed across an area of about 6 by 10 mi in the early 1930s (fig. 11*I*). Although the initial 65 wells drilled near the Central water plant and well field (fig. 11*I*) during 1886–1905 were concentrated inside a 14-acre tract, pumps were not required at some of these wells until about 1904 (Municipal Engineering Company, 1904); the flow rates per well were low, and many of these wells were subsequently replaced during 1910–20 by wells distributed among the Houston Heights, South End, and West End water plants (fig. 11*I*). As the Houston city area and groundwater demand increased, new well fields were also distributed across this expanding city area at a distance from existing well fields to cope with the subsidence issue (Lockwood, 1954) and lessen merged cones of depression around wellfields (Lang and others, 1950). Thus, the historical Houston area groundwater use has been less spatially dense than in the Pasadena, Baytown and Texas City areas where industrial groundwater use was heavily concentrated. As a result, the groundwater-level declines and resulting subsidence in the historical Houston area have been more uniform and widespread than in the Pasadena or Baytown areas (Winslow and Wood, 1959), and in the Texas City area.

The spacing of historical groundwater production wells in the Katy area was even wider than in the historical Houston area (and in the Pasadena, Baytown, and Texas City areas) (Winslow and Wood, 1959). This wider well spacing in the Katy area, when combined with the lesser amount of fine-grained sediment and proximity to the Chicot aquifer outcrop area, resulted in the smallest groundwater-level declines (figs. 15, 21–23, 31) and least subsidence (fig. 5.6) in the Houston-Galveston region (Kreitler, 1974; Gabrysch, 1972).

Deep-Seated Compaction

Estimated deep-seated compaction (or estimated uplift) was inferred based on changes in elevation at benchmarks located on the inner stem of the Lake Houston, Addicks, Northeast, and Clear Lake (deep) extensometers, and from CORS GPS station vertical-displacement data at these extensometers (fig. 75). To provide corroboration of the deep-seated compaction (or uplift) estimated at these sites (described in the "Global Navigation Satellite System Surveys" section), available changes in elevation at benchmarks located at land surface at these extensometer sites were compared to the sum of the extensometer-measured-compaction and deep-seated compaction. Deep-seated compaction estimates cannot be directly attributed to a specific hydrogeologic unit without installation of an extensometer penetrating the deeper units of the Gulf Coast aquifer system; however, compaction in the Jasper aquifer could possibly occur below the anchor depths of the extensometers because of groundwater withdrawals

Photograph by Darrell Davidson/copyright Houston Chronicle. Used with permission. This photograph was taken in 1971 and is republished from the following Houston Chronicle news article: https://www.chron.com/life/travel/slideshow/The-suburb-that-sank-58887.php.

The Burnet School well in 1971, located about 1,800 feet east of the Brownwood subdivision and about 1,000 feet east of benchmark PTS 185 (figs. 70*A*, 5.1).

A. **Thickness of fine-grained sediments (interbeds) in the Chicot aquifer**

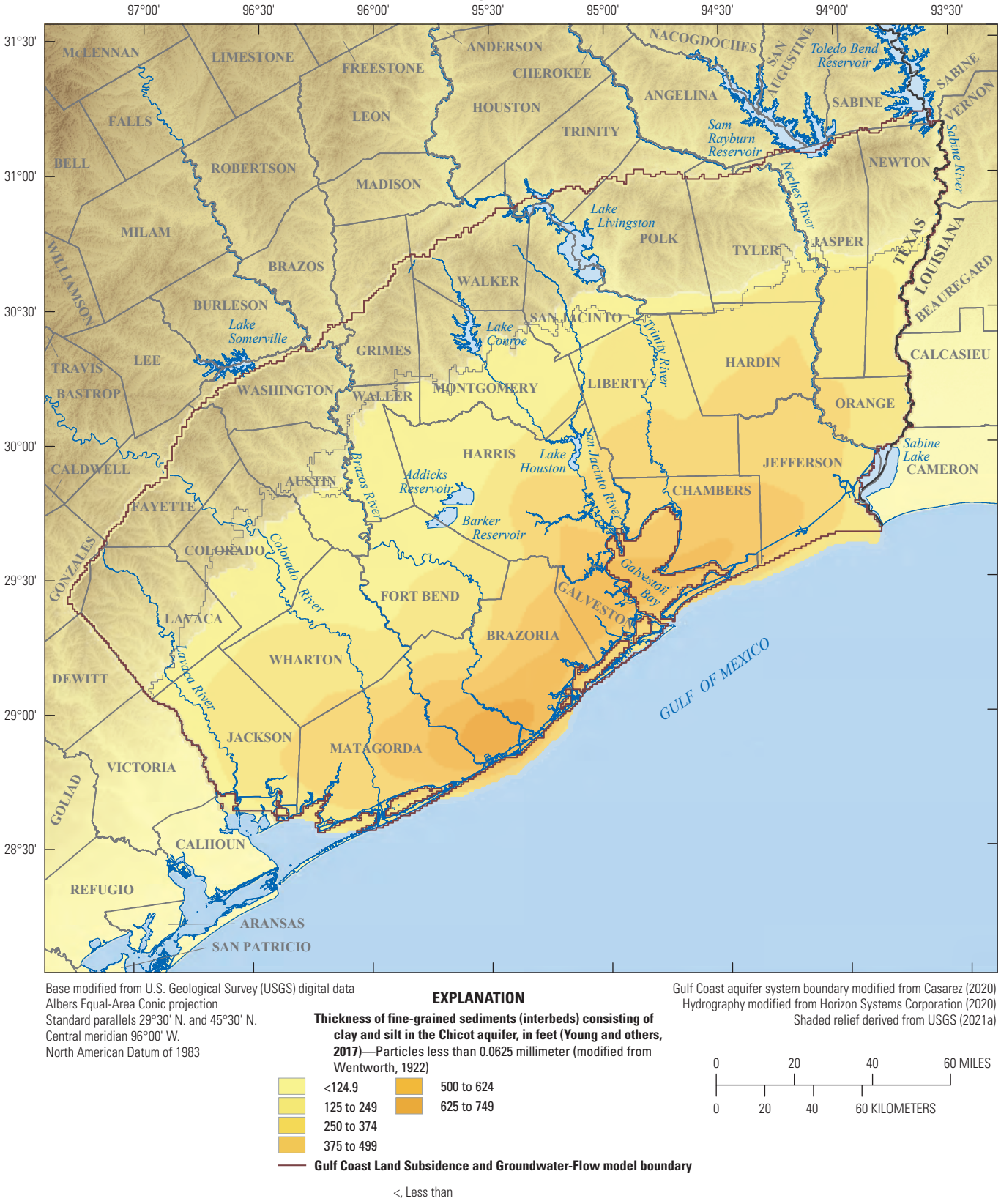

Base modified from U.S. Geological Survey (USGS) digital data
Albers Equal-Area Conic projection
Standard parallels 29°30' N. and 45°30' N.
Central meridian 96°00' W.
North American Datum of 1983

EXPLANATION

Thickness of fine-grained sediments (interbeds) consisting of clay and silt in the Chicot aquifer, in feet (Young and others, 2017)—Particles less than 0.0625 millimeter (modified from Wentworth, 1922)

- <124.9
- 125 to 249
- 250 to 374
- 375 to 499
- 500 to 624
- 625 to 749

Gulf Coast Land Subsidence and Groundwater-Flow model boundary

<, Less than

Gulf Coast aquifer system boundary modified from Casarez (2020)
Hydrography modified from Horizon Systems Corporation (2020)
Shaded relief derived from USGS (2021a)

0 20 40 60 MILES
0 20 40 60 KILOMETERS

Figure 97. Fine-grained unit thicknesses for the Gulf Coast aquifer system hydrogeologic units in the study area.

B. **Thickness of fine-grained sediments (interbeds) in the Evangeline aquifer**

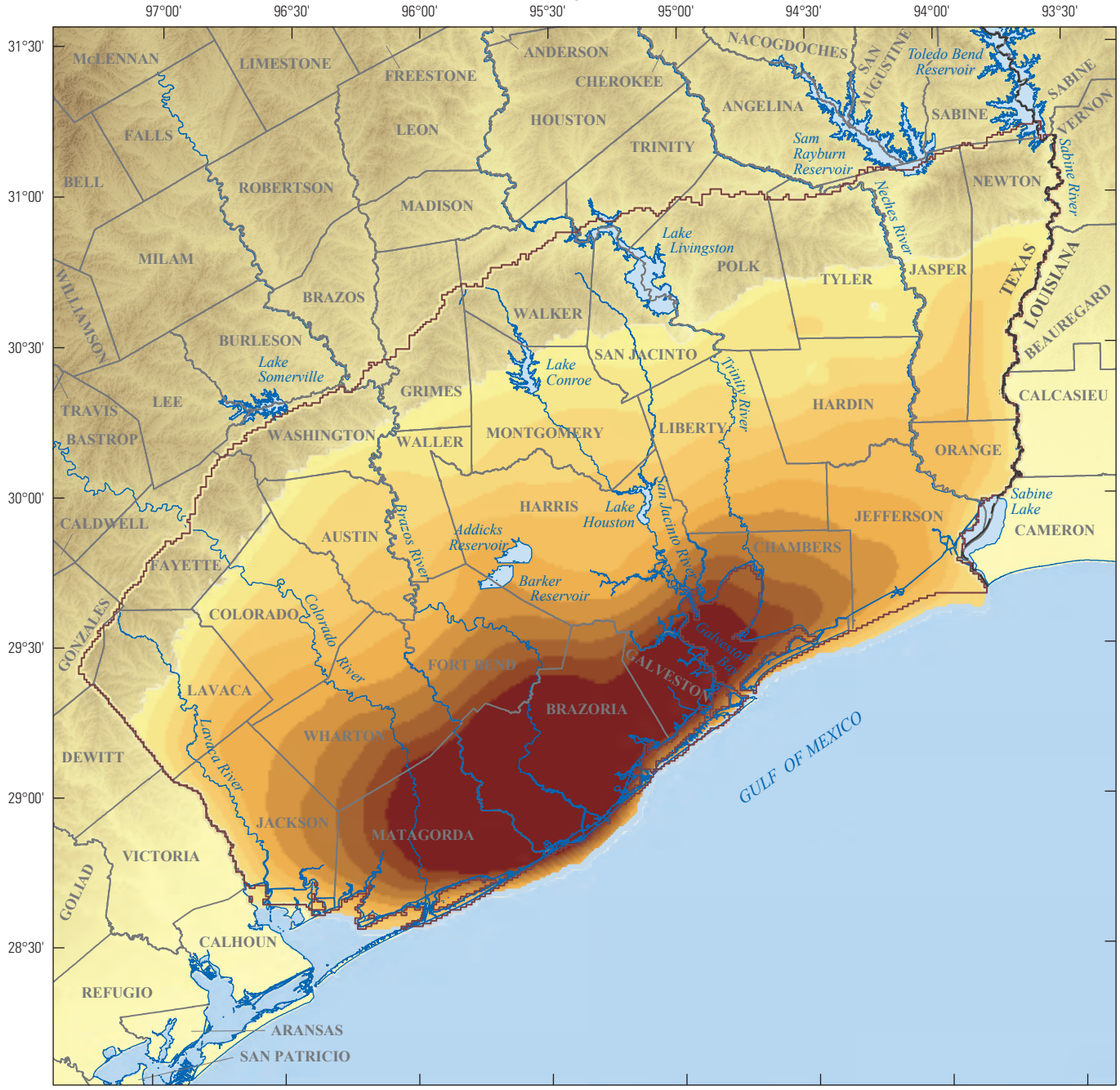

Base modified from U.S. Geological Survey (USGS) digital data
Albers Equal-Area Conic projection
Standard parallels 29°30' N. and 45°30' N.
Central meridian 96°00' W.
North American Datum of 1983

EXPLANATION

Thickness of fine-grained sediments (interbeds) consisting of clay and silt in the Evangeline aquifer, in feet (Young and others, 2017)—Particles less than 0.0625 millimeter (modified from Wentworth, 1922)

<124.9	500 to 624	1,000 to 1,124
125 to 249	625 to 749	1,125 to 1,249
250 to 374	750 to 874	≥1,250
375 to 499	875 to 999	

Gulf Coast Land Subsidence and Groundwater-Flow model boundary

<, Less than
≥, Greater than or equal to

Gulf Coast aquifer system boundary modified from Casarez (2020)
Hydrography modified from Horizon Systems Corporation (2020)
Shaded relief derived from USGS (2021a)

0 20 40 60 MILES
0 20 40 60 KILOMETERS

Figure 97.—Continued

C. **Thickness of fine-grained sediments (confining unit) in the Burkeville confining unit**

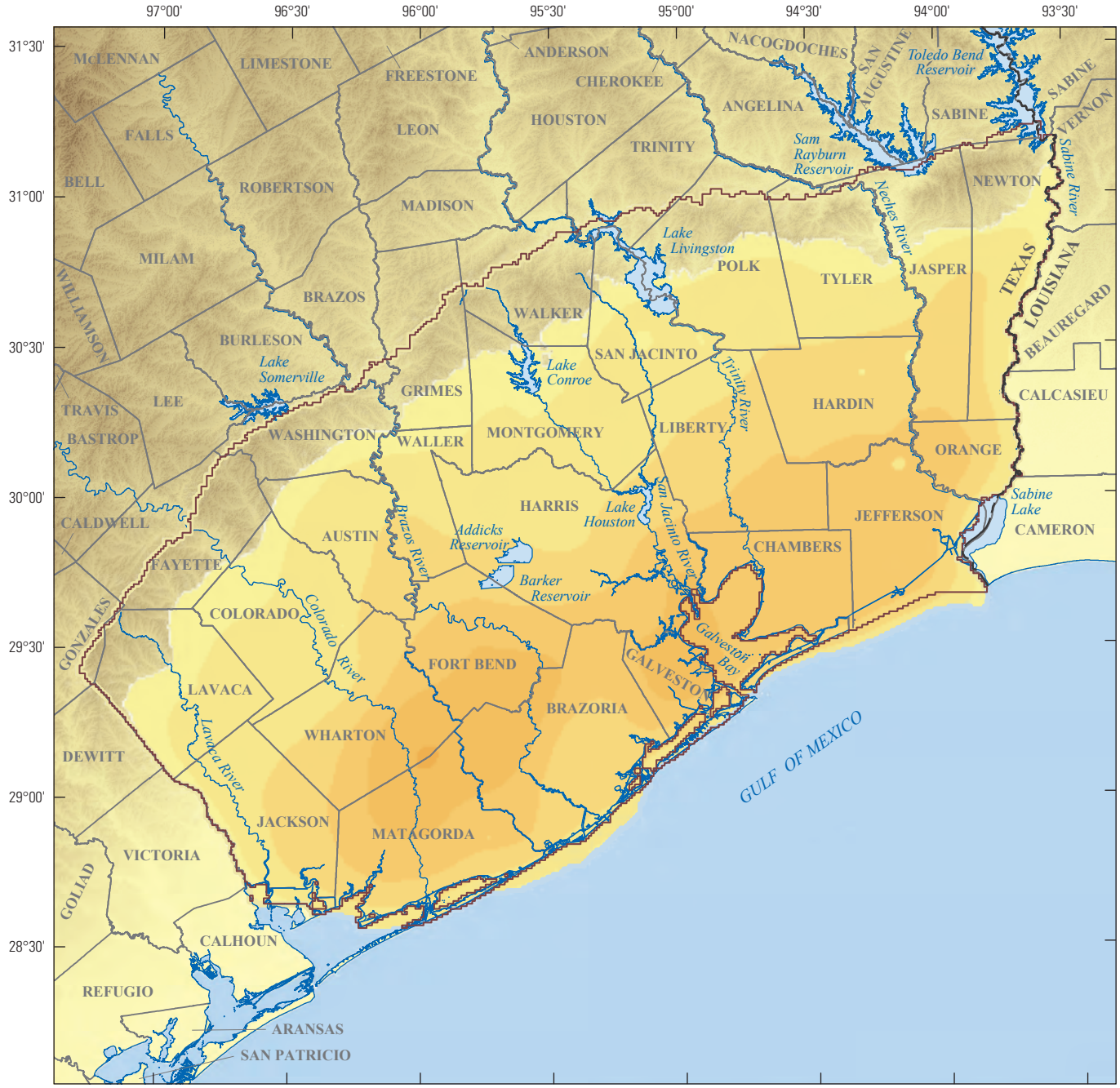

Base modified from U.S. Geological Survey (USGS) digital data
Albers Equal-Area Conic projection
Standard parallels 29°30' N. and 45°30' N.
Central meridian 96°00' W.
North American Datum of 1983

EXPLANATION

Thickness of fine-grained sediments (confining unit) consisting of clay and silt in the Burkeville confining unit, in feet (Young and others, 2017)—Particles less than 0.0625 millimeter (modified from Wentworth, 1922)

- <124.9
- 125 to 249
- 250 to 374
- 375 to 499
- 500 to 624
- 625 to 749

Gulf Coast Land Subsidence and Groundwater-Flow model boundary

<, Less than

Gulf Coast aquifer system boundary modified from Casarez (2020)
Hydrography modified from Horizon Systems Corporation (2020)
Shaded relief derived from USGS (2021a)

0 20 40 60 MILES
0 20 40 60 KILOMETERS

Figure 97.—Continued

***D.* Thickness of fine-grained sediments (interbeds) in the Jasper aquifer**

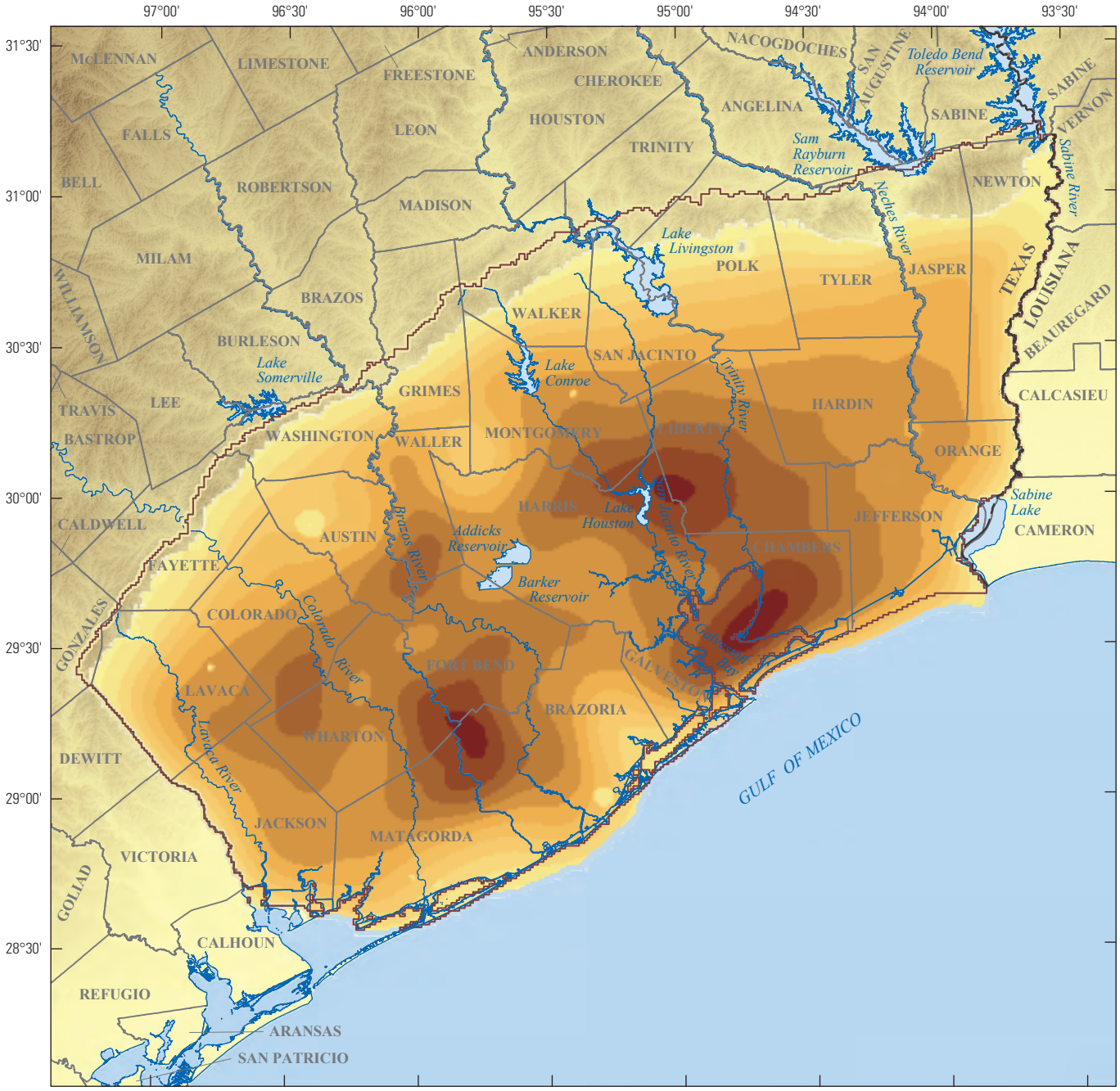

Base modified from U.S. Geological Survey (USGS) digital data
Albers Equal-Area Conic projection
Standard parallels 29°30' N. and 45°30' N.
Central meridian 96°00' W.
North American Datum of 1983

EXPLANATION

Thickness of fine-grained sediments (interbeds) consisting of clay and silt in the Jasper aquifer, in feet (Young and others, 2017)—Particles less than 0.0625 millimeter (modified from Wentworth, 1922)

<124.9	500 to 624	1,000 to 1,124
125 to 249	625 to 749	1,125 to 1,249
250 to 374	750 to 874	≥1,250
375 to 499	875 to 999	

Gulf Coast Land Subsidence and Groundwater-Flow model boundary

<, Less than
≥, Greater than or equal to

Gulf Coast aquifer system boundary modified from Casarez (2020)
Hydrography modified from Horizon Systems Corporation (2020)
Shaded relief derived from USGS (2021a)

0 20 40 60 MILES
0 20 40 60 KILOMETERS

Figure 97.—Continued

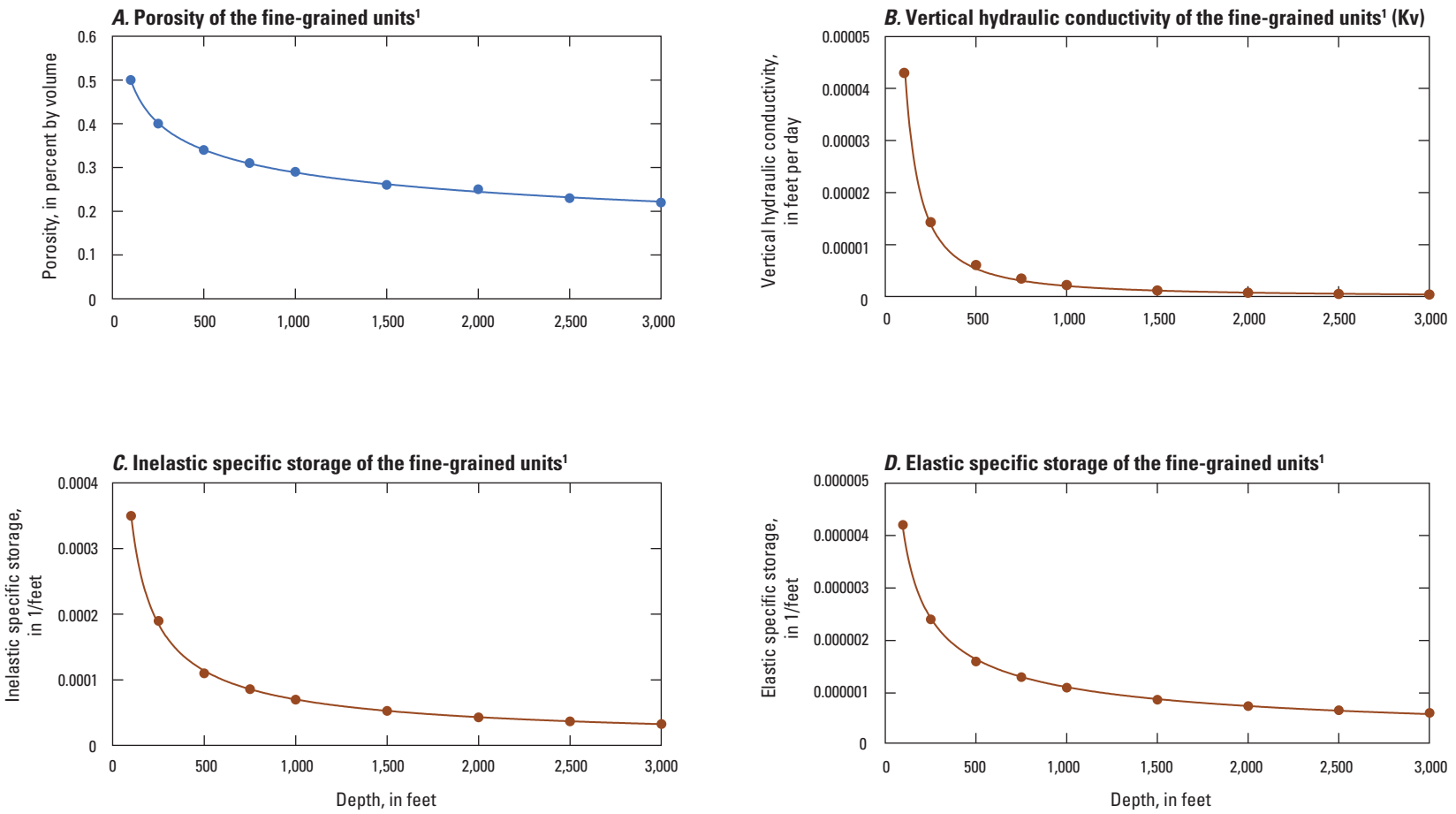

[1]Fine-grained units are defined as either (1) laterally discontinuous fine-grained sediment (or "interbeds") within the aquifers or (2) laterally extensive fine-grained sediment (or "confining units") separating individual aquifers in the aquifer system.

Figure 98. Compaction properties for the Gulf Coast aquifer system hydrogeologic units.

from this aquifer in northern Harris County and more substantially in Montgomery County. The Burkeville confining unit contains a thick sequence of fine-grained sediment from which few wells produce water and which would likely only slowly equilibrate with groundwater-level declines in adjacent aquifers. Therefore, minimal compaction is expected in the Burkeville confining unit.

From the data described in the "Global Navigation Satellite System Surveys" section, deep-seated compaction at the Northeast site during 1978–2021 did not occur—rather, there was about 0.01 ft of uplift. Deep-seated compaction at the Lake Houston site during 1978–2020 was between about 0.06 ft of compaction and 0.02 ft of uplift. Deep-seated compaction at the Clear Lake (deep) extensometer during 1978–2020 was about 0.07 ft. Deep-seated compaction at the Addicks extensometer during 1976–2021 was about 0.14 ft. Therefore, based on the similarity of burial depth of the Jasper aquifer at the Addicks (about 2,450 ft below NAVD 88; fig. 73), Northeast (2,550 ft below NAVD 88; fig. 73), and Lake Houston (2,470 ft below NAVD 88; fig. 73) extensometer sites, Jasper aquifer compaction is assumed to be zero at and downdip from these sites.

The absence of deeper subsidence and the depth-dependence of subsidence in the greater Houston area is also observed based on the differences of subsidence among the Clear Lake (shallow), Clear Lake (deep), and Johnson Space Center extensometers (fig. 74). During 1976–87, when most of the compaction measured at these extensometers occurred, about 75 percent of the compaction occurred between land surface and 750 ft below NAVD 88, about 22 percent occurred between 750 and 1,722 ft below NAVD 88, and only about 3 percent occurred in the interval between 1,722 and 3,053 ft below NAVD 88 (table 5) (Ramage and Shah, 2019). Similarly, Poland and Ireland (1965) determined that only about 0.01 ft of 1.2 ft of compaction occurred below a depth of 1,930 ft for an area in California. It was further observed by Gabrysch and Bonnet (1976b) that negligible compaction probably occurs in the Evangeline aquifer in the depth interval between 2,000 and 3,800 ft bls near the Seabrook extensometer. Based on this analysis, the Addicks, Northeast, and Lake Houston sites form a boundary approximately parallel to the coastline, beyond which in a coastward (downdip) direction, compaction in the Jasper aquifer is estimated to be approximately zero.

Simulation of Groundwater Flow and Land-Surface Subsidence

Groundwater flow and subsidence in the GULF model and ensemble were simulated by using MODFLOW 6 with the Newton-Raphson formulation (Langevin and others, 2021) which facilitates the improved solution of problems involving drying and rewetting of model cells. In the modular design of MODFLOW 6, each hydrologic boundary, such as stream seepage, recharge, or groundwater use, is included as a package that, when activated, adds new inflow and outflow terms to the groundwater-flow equation being solved. Model space is discretized into cells, and the cell size is the finest resolution at which spatially changing properties can be represented and varied. Model time is discretized into time steps within stress periods. The stress period length is the finest resolution at which temporally varying inflows and outflows could be represented and varied, and the time step length is the finest length of time for which model outputs could be written.

Previous Hydrogeologic Modeling

Nine previous publicly documented groundwater modeling studies, including three that simulated subsidence, have been completed in all or part of the study area. Although each model had varying spatial coverage of the Texas Gulf Coast area, all include the Houston-Galveston region, where the greatest groundwater-level declines have occurred. Below is a description of these models and associated subsidence packages included as part of the simulation.

The first groundwater model by Wood and Gabrysch (1965) covered about 5,000 mi^2 in the greater Houston area and surrounding counties (Austin, Brazoria, Chambers, Fort Bend, Galveston, Harris, Liberty, Montgomery, and Waller Counties) and was used to predict groundwater-level responses under various conditions. This electric-analog model used resistors and capacitors to simulate transmissibility and storage characteristics based on an analogy between Darcy's Law and Ohm's Law. The model used a resistor-capacitor analog network for two conceptualized layers: the Alta Loma Sand of Lang and others (1950) composing part of the Chicot aquifer, and the "heavily pumped layer," which included parts of the present-day Chicot and Evangeline aquifers. Groundwater use was simulated by using about 150 model wells that represented groundwater use from about 1,100 industrial, municipal, and irrigation wells for 5 stress periods to approximate groundwater use from 1890 through 1960 (Wood and Gabrysch, 1965). Results from the groundwater model indicated the need for improved aquifer delineation, a simulation that would allow hydraulic interaction between the Chicot and Evangeline aquifers, which were simulated independently in the groundwater model, and inclusion of agricultural groundwater use in the western part of the model area (Baker, 1986).

The second groundwater model (Jorgensen, 1975) covered about 9,100 mi^2 in the greater Houston area and again used an electric-analog approach to simulate the hydrologic system. Although the present-day hydrogeologic units formalized by Turcan and others (1966) were named in Jorgensen's study except for the Catahoula confining unit, the analog model simulated only the Chicot and Evangeline aquifers using one layer for each unit. The model used six stress periods to approximate groundwater use from 1890 through 1970. Use of the expanded modeled area compared to the 1965 study by Wood and Gabrysch allowed for the simulation of

large groundwater withdrawals, although the simulated cone of depression reached the boundaries of the modeled area by about 1970 (Jorgensen, 1975). The Jorgensen model incorporated several updates from the Wood and Gabrysch model, including allowances for the vertical movement of water between the two modeled aquifer units and an accounting for water contributed to the system from storage in fine-grained layers as groundwater use caused these layers to be depressurized and compact. However, the model did not directly simulate subsidence. Jorgensen (1975) documented needed improvements for the model, including (1) additional observation wells completed in only one aquifer unit (versus multiple aquifer units) to improve the fit to observations, (2) additional delineation of the water-bearing sands above the Alta Loma Sand of Lang and others (1950) (fig. 10), and (3) refinement of the fine-grained storage coefficients to improve the accuracy of simulating interbed compaction.

The third groundwater model (Meyer and Carr, 1979) used a modified form of the Trescott (1975) finite-difference code to simulate groundwater flow in a larger model area of about 27,000 mi^2 compared to the 9,100-mi^2 area of the analog model (Jorgensen, 1975). Compared to the first and second models, the expanded area of the third model provided more distance from areas of large groundwater use to the lateral model boundaries. Five layers using a 1- x 1-mi grid in the middle of the model area that expanded to a coarser grid towards the model extremities were used to simulate the Chicot and Evangeline aquifers. Layer 1 was used to simulate the Evangeline aquifer (sand thickness), layer 3 was used to simulate the Alta Loma Sand of Lang and others (1950) (fig. 10), and layer 5 was used as an upper boundary to simulate recharge (Meyer and Carr, 1979). Layers 2 and 4 were used to simulate the fine-grained sediment between the aquifer units. Through modification of Trescott's finite-difference code, by which the fine-grained sediment storage values were increased or decreased based on whether heads were lower than or higher than the preconsolidation head (critical head), respectively, subsidence was effectively simulated. The model simulated an initial, specified critical head that was adjusted to the simulated lowest antecedent head during the simulation. The model simulated groundwater-level response to groundwater use, fine-grained sediment storage change, elastic and inelastic compaction, and subsidence (Baker, 1986).

The fourth groundwater model (Carr and others, 1985) was not a single model, but rather four independent models of subregions extending from Louisiana along the Texas Gulf Coast nearly to Mexico. The layering, conceptual arrangement, and simulation code of these models were equivalent to those in Meyer and Carr (1979) described previously. The separate models were history matched in areas having historical water-level data from 1890 through 1975 for the Houston subregion and from 1900 through 1970 for all other subregions. As with the previous models, Carr and others (1985) simulated the groundwater-level response to groundwater use, fine-grained storage change, compaction, and subsidence.

The fifth (Williamson and others, 1990) and sixth (Ryder and Ardis, 2002) groundwater models were developed as a part of the USGS Regional Aquifer-System Analysis Program, and they simulated groundwater flow by using the Kuiper (1985) code. The models used similar conceptual arrangements and encompassed about 230,000 mi^2 in parts of Alabama, Arkansas, Florida, Illinois, Kentucky, Mississippi, Missouri, Tennessee, Texas, and all of Louisiana. In addition to the Gulf Coast aquifer system (included as a part of the larger multi-State Coastal lowlands aquifer system), the models also included the Mississippi embayment–Texas coastal uplands aquifer system. The Williamson and others (1990) model simulated flow in these two units by using 10 layers and a cell size of 10 x 10 mi, whereas the Ryder and Ardis (2002) model used 9 layers and a cell size of 5 x 5 mi.

The seventh groundwater model (Kasmarek and Strom, 2002) used the MODFLOW 1988 finite-difference code (McDonald and Harbaugh, 1988) to simulate groundwater flow in an area of about 18,100 mi^2 for the Chicot and Evangeline aquifers. MODFLOW was used with the Interbed-Storage package (IBS; Leake and Prudic, 1991) to simulate aquifer-system compaction and storage changes from 1891 to 1996. Layer 1 represented water-table conditions by using a specified head boundary, layer 2 represented the Chicot aquifer, and layer 3 represented the Evangeline aquifer. The grid was variably spaced: cells in the Houston-Galveston region were about 0.90 mi^2, whereas the cell size in the other model areas was about 4.5 mi^2.

The eighth groundwater model is the Northern Gulf Coast Groundwater Availability Model (NGC-GAM) (Kasmarek and Robinson, 2004). This model simulated subsidence in the Chicot and Evangeline aquifers by using the IBS package with a head-based formulation from 1891 to 2000. The NGC-GAM used a grid covering 33,565 mi^2 in southeast Texas with 1- x 1-mi cells and 4 layers.

The ninth and most recent model for the Gulf Coast aquifer system in Texas is the HAGM (Kasmarek, 2012), which was developed by the USGS in cooperation with the subsidence and groundwater conservation districts (including the HGSD, FBSD, and LSGCD). The HAGM was an update to the NGC-GAM and extended the model history-matching period through 2009. Additionally, the HAGM applied a newer subsidence code (SUB; Hoffmann and others, 2003) to simulate compaction in the Chicot, Evangeline, and Jasper aquifers and in the Burkeville confining unit from 1891 to 2000.

Baker (1986), although not included in the previous list of models because of the simulation of only one unit and the use of a two-dimensional model, documented a model of the Jasper aquifer by using the Trescott (1975) code. This model used cells varying between 5 x 10 mi and 10 x 10 mi to simulate groundwater flow in an area of about 25,000 mi^2 that coincides with much of the study area (fig. 1). The model was history matched to the estimated predevelopment potentiometric surface of the Jasper aquifer. Because of the simulation of only one aquifer unit, however, the net effects of stress from

groundwater withdrawals and interaction between the Jasper aquifer and the other hydrogeologic units of the Gulf Coast aquifer system were not simulated.

Modeling Strategy

Based on an evaluation of the previously published groundwater models, input from groundwater conservation and land subsidence districts (fig. 3), and preliminary model history matching from this study, the following design principles were implemented for the GULF model and ensemble: (1) the simulation of recharge by using a specified-flux boundary condition in conjunction with a code estimating spatially distributed recharge; (2) recompilation of the spatial and temporal distribution of groundwater use from historical use estimates; (3) use of an updated modeling code and subsidence package simulating delayed drainage of fine-grained interbeds; and (4) use of a Bayesian framework to estimate model-parameter and forecast uncertainty (Tarantola, 2005; Doherty and Simmons, 2013; Doherty, 2015; Hemmings and others, 2020) and to reduce this uncertainty through assimilating a wide range of historical observations of aquifer-system behavior.

A number of groundwater models have used a head-dependent boundary condition to simulate recharge (and discharge) in the Gulf Coast aquifer system. This type of boundary condition, typically applied by using the General-Head Boundary (GHB) package, simulates flow into or out of a cell from an external source in proportion to the difference between the head in the cell and the head assigned to the external source (Langevin and others, 2017). In the HAGM and NGC-GAM, the rate of recharge (or discharge) was then the product of a specified (vertical) conductance and the difference between the GHB-controlled potentiometric surface (groundwater levels specified as a constant in each model cell) and the simulated groundwater level that fluctuates over time in each layer.

The conceptual reasoning behind using the GHB package to apply recharge to the surface of the model area was the assumption that long-term groundwater-level declines were not observed in the outcrop area (fig. 8) and that this assumption generally held true elsewhere in the model area. This assumption was made due to the large amounts of recharge from precipitation infiltration that occurred in the outcrop area (figs. 67–68). Thus, the conductance specified in the GHB package for these models was greatest in the outcrop area and generally least in the downdip areas such as those areas overlain by the Beaumont Formation (fig. 7). Groundwater-level data shown on hydrographs indicate that groundwater levels in the shallow groundwater system (figs. 37–50; table 3) generally are stable and have few long-term temporal patterns. (By inference, the water table also is stable.) However, groundwater-level declines for wells screened in the intermediate and deep systems have occurred (figs. 19–52; tables 2–3) independent of climatic patterns in many of the wells measured during the model period. The GHB package provides an unlimited source of water for a specified conductance and groundwater level; therefore, the GHB cells in the locations of groundwater-level declines could potentially deliver substantial amounts of recharge to these model areas or in areas with the greatest amounts of groundwater use under sustained withdrawals simulated in a probabilistic model scenario. The amount of effective recharge supplied by the GHB package cells could exceed the amount of recharge that is expected based on recharge estimates for the study area (documented in Ryder, 1988; Dutton and Richter, 1990; Ryder and Ardis, 2002; Kasmarek and Robinson, 2004).

As explained in the Introduction section, the GULF model and ensemble were developed to provide an updated model for use as a GAM and are intended to serve as a decision-support tool; therefore, a robust recharge process was realized through the use of the SWB code (Westenbroek and others, 2010; described in the "Soil-Water-Balance Code" section) to estimate spatially distributed recharge and the use of the MODFLOW 6 Recharge package from Langevin and others (2021) to apply this recharge to the model domain. The GULF model and ensemble use a surficial layer to simulate the shallow groundwater system where the water table is largely stable over time (figs. 37–50; table 3). Simulating the shallow groundwater system in layer 1 allows for an explicitly defined and physically based recharge representation whereby recharge infiltrates this shallow groundwater system and primarily flows towards locations of discharge (modeled streams) along shallow flow paths, with a small amount of net recharge infiltrating to the intermediate and deep systems. The spatial distribution of the SWB-derived recharge generally agrees with published recharge patterns for the study area from Scanlon and others (2011). GHB-derived spatial recharge patterns do not resemble those of published estimates because the spatial distribution of the GHB-derived recharge in each cell is a function of the difference between the water level in the cell and the fixed water-level value assigned to the cell representing the water table. The SWB-derived recharge applied to the model surface in each stress period is independent of the simulated model state—that is, it is a specified flux applied to layer 1 in the model. A small portion of the specified flux applied to layer 1 will then flow to the underlying layers.

The groundwater use simulated in previous models of the study area was typically inherited from an earlier model and adapted based on changes in the spatial and temporal model structure. The groundwater use simulated in the HAGM was primarily derived from the NGC-GAM and was updated during 2000–09 in some counties and held constant at the year 2000 rate in others. The groundwater use in the NGC-GAM for the Chicot and Evangeline aquifers was primarily derived from Kasmarek and Strom (2002) and augmented with data from the TWDB during 1997–2000. Groundwater use during 1980–2000 for the Burkeville confining unit and the Jasper aquifer in that model was also obtained from the TWDB. Water-use records from predevelopment through 1979 did not exist for these hydrogeologic units; therefore,

municipal groundwater use was assumed to increase at the same rate as withdrawals from the Chicot and Evangeline aquifers. Groundwater use in the Kasmarek and Strom (2002) model was the same as the groundwater use in Carr and others (1985) for the overlapping model period (1891–1975). Groundwater use during 1976–96 in Kasmarek and Strom (2002) was obtained from the HGSD, FBSD, and TWDB and was the basis for simulated groundwater use during this period (1976–96) in the HAGM and NGC-GAM. Thus, although the water-use dataset used in models for the greater Houston area has been incrementally updated with each successive model for the simulation period between the end of the previous model simulation period and the subsequent model, the base dataset of groundwater use and simulated well locations used for the Chicot and Evangeline aquifers is more than 35 years old—first appearing in Carr and others (1985). This incremental approach to updating groundwater use can result in a misfit over time between the modeled and actual locations and quantities of groundwater use. Uncertainty in the historical spatial and temporal patterns of groundwater use can create problems with model history matching and, if not properly represented, can result in bias in the simulated outputs. The HAGM, NGC-GAM, and Kasmarek and Strom (2002) models were history matched to transient conditions only for part of the model period, possibly precluding the need to recomplete the modeled groundwater-use dataset. Preliminary history-matching analysis from this study demonstrated the need for the recompletion of the model groundwater-use dataset. Recognizing the need for updated groundwater-use information, Oliver and Harmon (2022) published updated historical estimates of groundwater use in the northern part of the Gulf Coast aquifer system from 1900 to 2018. To support successful history matching to the subsidence and groundwater-level observation datasets and facilitate groundwater-use uncertainty in the simulated results, the updated groundwater-use data provided in Oliver and Harmon (2022) were used in the GULF model and ensemble.

Previous groundwater models simulating subsidence in the Houston-Galveston region and the larger study area of this investigation have traditionally used a subsidence package that does not account for residual compaction—the delayed drainage response from low-permeability fine-grained sediment (interbeds and confining units in the aquifer system). Instead, an assumption was made with these subsidence packages that the groundwater levels in the interbeds and confining units are in instantaneous equilibrium with the groundwater levels in the surrounding coarse-grained sediment of the aquifer units. Depending on the thickness and the vertical hydraulic diffusivity of thick interbeds and confining units, however, fluid-pressure equilibration—and thereby compaction—could lag behind pressure (or hydraulic head) declines in the adjacent aquifers. Therefore, associated compaction could require many years or even centuries to fully respond to these changes and approach equilibrium (Galloway and others, 1999). This process of delayed compaction is observed in the time-series record of compaction and subsidence at most of the extensometer sites and benchmarks, respectively (figs. 74, 95, 96). This delayed compaction (figs. 74, 95, 96) occurs for a longer duration than the annual stress periods used in the model during 1970–99. Consequently, "delay interbeds" were incorporated into the modeled subsidence package to ensure a more accurate compaction simulation. The term "delay interbeds" is used to denote interbeds for which the time for equilibration of interbed and surrounding aquifer groundwater levels is substantially greater than the model time steps (Hughes and others, 2022).

Given the intended role of the GULF model as a decision-support tool for regional water management, it is essential to estimate the reliability of important simulated model outputs, such as forecasts of future water quantity and subsidence patterns. Uncertainty in these forecasts is a result of model-structure uncertainty, such as simplifications of the modeled natural system, spatial and temporal discretization, and uncertainty in the hydraulic parameter value estimates. Representing these sources of uncertainty requires a shift away from a traditional deterministic groundwater modeling workflow, where the modeling process uses a single set of model inputs, to a probabilistic or "stochastic" modeling workflow, where the focus is on generating multiple sets of model inputs (or an "ensemble"). In this way, the stochastic workflow can be used to identify and explore "nonuniqueness" and its effect on important simulated outputs to a greater degree than the more traditional deterministic groundwater modeling workflow (Moore and Doherty, 2005).

Spatial and Temporal Discretization

The GULF model grid was spatially discretized into a rectangular grid with 350 rows and 380 columns containing square cells 1 x 1 kilometer (km) without rotation of the grid. This grid is a subset of the larger National Hydrologic Grid (Clark and others, 2018), which encompasses the continental United States, and is a refinement of the larger cell size from the published models described in the "Previous Hydrogeologic Modeling" section. The lateral and updip extent of the model active area is the same as the extent defined in the "Study Area" section; however, the downdip extent was extended to a distance of about 4 mi offshore (figs. 99–100). Six layers were used to represent the modeled aquifer units in the Gulf Coast aquifer system, with one layer per unit, which follows previous model configurations for the Gulf Coast aquifer system, and a surficial top layer that includes part of each aquifer unit (figs. 99–100). The top layer (layer 1) was used to represent the shallow groundwater system where water-table conditions predominate, similar to the configuration in Kasmarek and Strom (2002). Although the shallow groundwater system typically extends to between about 70 and 300 ft bls as discussed in the "Colocated Groundwater Wells" section, layer 1 in the model is about 50 ft thick. The layer 1 land-surface elevation was estimated from a 10-meter (m) digital elevation model (USGS, 2021a).

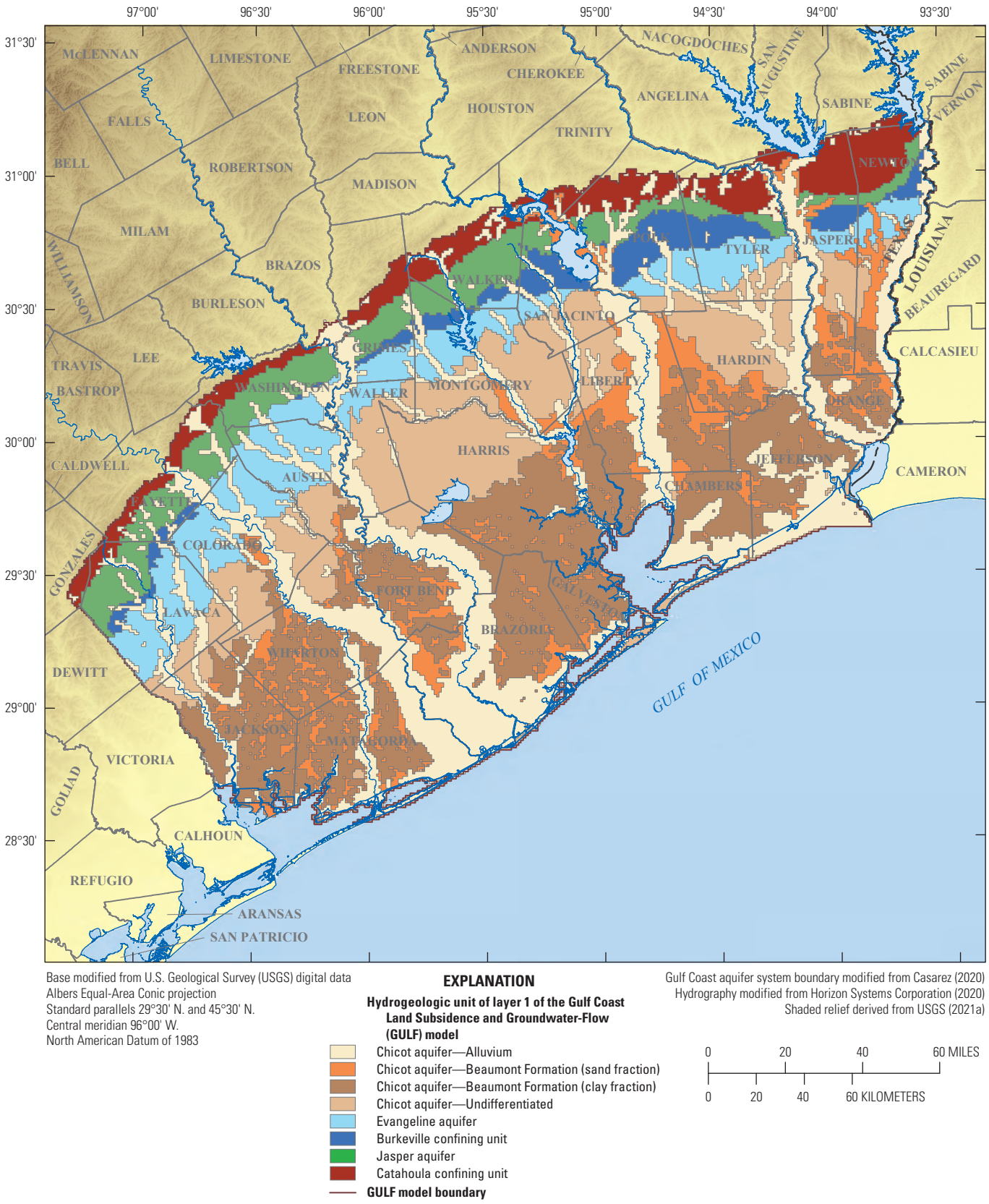

Base modified from U.S. Geological Survey (USGS) digital data
Albers Equal-Area Conic projection
Standard parallels 29°30' N. and 45°30' N.
Central meridian 96°00' W.
North American Datum of 1983

EXPLANATION

Hydrogeologic unit of layer 1 of the Gulf Coast Land Subsidence and Groundwater-Flow (GULF) model

- Chicot aquifer—Alluvium
- Chicot aquifer—Beaumont Formation (sand fraction)
- Chicot aquifer—Beaumont Formation (clay fraction)
- Chicot aquifer—Undifferentiated
- Evangeline aquifer
- Burkeville confining unit
- Jasper aquifer
- Catahoula confining unit
- **GULF model boundary**

Gulf Coast aquifer system boundary modified from Casarez (2020)
Hydrography modified from Horizon Systems Corporation (2020)
Shaded relief derived from USGS (2021a)

0 20 40 60 MILES
0 20 40 60 KILOMETERS

Figure 99. Geologic and hydrogeologic units in layer 1 of the Gulf Coast Land Subsidence and Groundwater-Flow model.

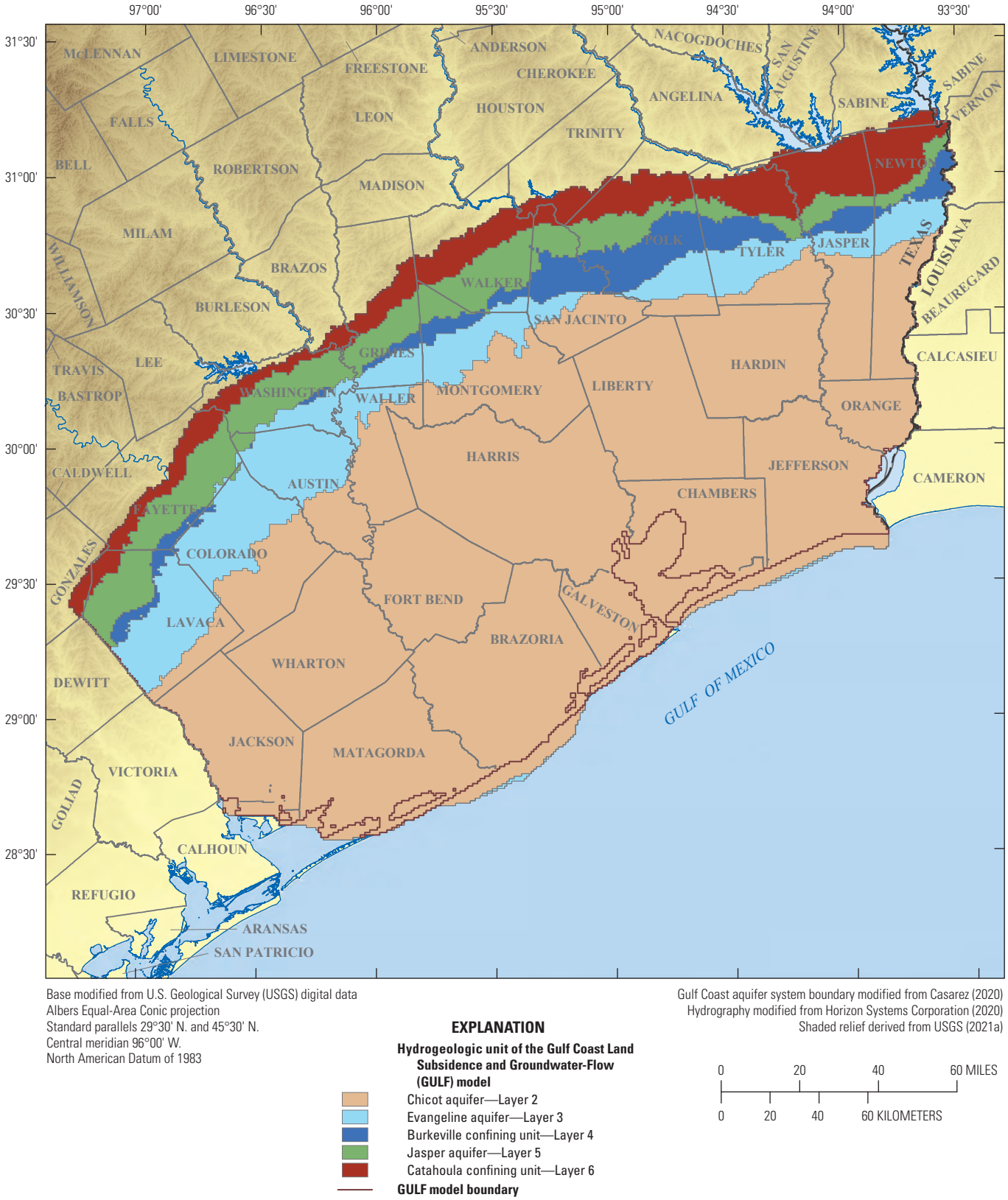

Base modified from U.S. Geological Survey (USGS) digital data
Albers Equal-Area Conic projection
Standard parallels 29°30' N. and 45°30' N.
Central meridian 96°00' W.
North American Datum of 1983

Gulf Coast aquifer system boundary modified from Casarez (2020)
Hydrography modified from Horizon Systems Corporation (2020)
Shaded relief derived from USGS (2021a)

EXPLANATION

Hydrogeologic unit of the Gulf Coast Land Subsidence and Groundwater-Flow (GULF) model

- Chicot aquifer—Layer 2
- Evangeline aquifer—Layer 3
- Burkeville confining unit—Layer 4
- Jasper aquifer—Layer 5
- Catahoula confining unit—Layer 6

GULF model boundary

0 20 40 60 MILES
0 20 40 60 KILOMETERS

Figure 100. Hydrogeologic units in layers 2–6 of the Gulf Coast Land Subsidence and Groundwater-Flow model.

Layer 1 includes the upper 50 ft of each of the following hydrogeologic units: the Chicot aquifer, Evangeline aquifer, Burkeville confining unit, Jasper aquifer, and Catahoula confining unit (fig. 99). Layer 1 was used to route local-scale recharge flow from the outcrop area to streams, much of which does not recharge the intermediate system (layers 2–3) and deep system (layers 5–6). Layer 2 represents the undifferentiated Chicot aquifer; layer 3 represents the Evangeline aquifer; layer 4 represents the Burkeville confining unit; layer 5 represents the Jasper aquifer; and layer 6 represents the Catahoula confining unit (fig. 100). The bottom elevations of layers 2–6 are based on surfaces interpolated as a part of this study that are described in appendix 1. These surfaces were created from the stratigraphic contacts described in Young and Draper (2020) and compiled in Teeple and others (2021). A specified minimum cell thickness in each layer was used to define the areal extent of the outcrop areas (other than the Catahoula confining unit). Barrier islands at the nearshore were not included in the simulation.

The spatial and temporal discretization used in the GULF model primarily differs from that of the HAGM, and generally also the NGC-GAM, in the following ways.

1. Layer 1 of the GULF model was used to represent the shallow groundwater system, alluvium, terrace, and the Beaumont Formation, as well as the outcrop area of the Gulf Coast aquifer system units.

2. The remainder of the Catahoula confining unit not previously included in the HAGM was included in layer 6 of the GULF model.

3. The Burkeville confining unit and Jasper aquifer were extended downdip to a distance of about 4 mi offshore without regard to any defined downdip limit of freshwater.

4. The GULF model grid uses a finer discretization of 1- x 1-km cells without rotation.

5. The GULF model uses monthly stress periods from January 2000 through December 2018, compared to monthly stress periods in the HAGM for only 1980, 1982, and 1988, with longer stress periods used for other years.

6. The GULF model layers have areas where the thickness of the geologic sediment differs compared to the HAGM based on updates to the stratigraphic contacts from Young and Draper (2020).

Furthermore, MODFLOW 6 includes the capability to permanently exclude inactive cells for the duration of the simulation and allow vertical flow between cells above and below these excluded cells. The GULF model used this capability to exclude inactive cells to directly simulate vertical flow between layer 1 and underlying layers, between which are layers representing the outcrop of geologic units that contain the hydrogeologic units.

The GULF model period (1897–2018) was temporally discretized into 1 steady-state stress period representing pre-1897 conditions and 267 transient stress periods with 1 time step each, representing January 1897 through December 2018 (appendix 7). Stress period lengths were refined from previous models and temporally decreased in length from predevelopment to present. Thus, 3 stress periods of approximately 14 years each were used for 1897–1939, 6 stress periods of 5 years each were used for 1940–1969, 30 annual stress periods were used for 1970–1999, and 228 monthly stress periods were used for 2000–18. An initial steady-state stress period was configured to represent mean annual predevelopment conditions to establish initial conditions for the transient period. Additionally, a 20-year forecast period was included at the end of the transient period, which was discretized into 20 stress periods of 1 year each. This forecast period uses the mean stresses from the last 3 years (36 stress periods) of the transient period.

Land-Surface Subsidence

To simulate subsidence in the Gulf Coast aquifer system, the numerical modeling code MODFLOW 6 was used with the Skeletal Storage, Compaction, and Subsidence package (CSUB; Hughes and others, 2022). The CSUB package simulates elastic compaction in coarse-grained sediment and both elastic and inelastic compaction in fine-grained sediment, as well as groundwater storage changes caused by the depressurization of interbeds (Hughes and others, 2022).

Subsidence in the GULF model was simulated for the Chicot, Evangeline, and Jasper aquifers and the Burkeville confining unit. Few studies have evaluated the compaction properties in the Catahoula confining unit; therefore, compaction in this unit was not simulated. The use of the CSUB package in the GULF model expands upon the capabilities of the SUB (Hoffmann and others, 2003) and SUB-WT (Leake and Galloway, 2007) packages. The SUB package uses a head-based formulation coupled with no-delay or delay interbeds, and the SUB-WT package uses an effective-stress-based formulation coupled with no-delay interbeds; however, the CSUB package can couple either the head-based or effective-stress-based formulations with either delay or no-delay interbeds. Similar to previous subsidence packages (SUB, SUB-WT, IBS), subsidence simulated with the CSUB package does not affect the simulation of the water table in comparison to the top of a model cell where simulated subsidence has occurred. Additionally, calculations are not made for the subsidence package during the first stress period representing predevelopment conditions, although data from the simulated groundwater levels in this stress period could be relevant to subsidence in subsequent stress periods as a representation of previous maximum stress (Hughes and others, 2022).

The GULF model uses the head-based formulation in which the geostatic stress (also referred to as “total stress”) remains constant and a unit increase in effective stress results

from a unit decline in groundwater levels. In the head-based formulation, changes in effective stress are caused only by changes in fluid pore pressure, and elastic and inelastic skeletal specific-storage values are constant (temporally invariant, that is they do not vary with changes in effective stress). Thus, use of the head-based formulation results in effectively the same representation of the interbeds as the SUB package (Hughes and others, 2022). Coupled with the head-based formulation is the use of delay interbeds (or "delay beds") to simulate the delayed drainage response from low-permeability fine-grained sediment. These delay beds were used in the Evangeline and Jasper aquifers and Burkeville confining unit where overlain by the Chicot aquifer. Delay beds in the Chicot aquifer were used where the cell thickness was greater than about 650 ft. Volumetric storage contributions from a system of delay interbeds are scaled by using the cell saturation in convertible (unconfined or confined) cells with at least one delay interbed; however, if the saturated thickness of a convertible model cell is less than the delay interbed thickness, the simulation will terminate (Hughes and others, 2022). Additionally, when using confined cells, the simulation will terminate if the groundwater level in a cell decreases to below the top of the cell when at least one delay interbed is present.

Depth-dependent values specified for interbed elastic and inelastic specific storage, as well as porosity and interbed vertical hydraulic conductivity (Kv) in the CSUB package, were obtained from Kelley and others (2018) as discussed in the "Compaction Properties" section. Exponential functions were fit to the provided paired depth and property values (fig. 98) and used to interpolate property values to individual model cells based on simulated depth from model top to the midpoint of each cell.

CSUB input values for representative interbed thickness ("thick_frac") and representative number of interbeds ("rnb") were derived from observed percentages of sand and fine-grained sediment in each hydrogeologic unit at 316 borehole locations. The property values were spatially interpolated from the borehole locations to all active model cells representing each hydrogeologic unit. A Gaussian (normal distribution) filter (SciPy, 2020) was then applied to the resulting property arrays to partially reduce high-frequency spatial variability.

The auxiliary parameter "clay_frac" was used to simulate varying ratios of fine-grained sediment (interbeds or confining units) to coarse-grained sediment in each cell during history matching. The initial value of clay_frac in every CSUB-enabled model cell is calculated as the product of the representative interbed thickness and representative number of interbeds, divided by total cell thickness. A domain-wide global multiplier and a multiplier interpolated from pilot point locations modify the initial value within a range of 0.75–1.25. The parameterized value of clay_frac is limited by ultimate bounds of 0.1 and 0.9 and is used to reverse-calculate the value of thick_frac that must be specified in CSUB input data. The corresponding thick_frac input value is calculated as the product of clay_frac and total cell thickness, divided by a representative number of interbeds. This indirect method of parameterization is necessary to prevent combinations of CSUB input values that could result in the simulation of total interbed thickness greater than the cell thickness.

The specified initial preconsolidation head in the CSUB package controls the onset of inelastic compaction. Similar to the operation in the SUB package, the preconsolidation head is subsequently updated to the effective stress (represented in terms of the height of an equivalent column of water) at the end of each time step when the preconsolidation stress has been exceeded. The initial preconsolidation head is specified as a drawdown below the groundwater level in the first stress period (steady state), and the application of elastic or inelastic storage coefficients then occurs based on the relation between modeled groundwater level and the current preconsolidation head.

The initial preconsolidation head was estimated at benchmarks and extensometer sites where long-term groundwater-level and subsidence datasets are available. A rough estimate of the initial preconsolidation head can be derived from the groundwater level at which the rate of subsidence first markedly increased (Holzer, 1981; Galloway and Burbey, 2011). This analysis assumes a predevelopment groundwater level at land surface unless early-time groundwater-level data was available, which is a conservative estimate given that during predevelopment to early development conditions artesian pressure was often sufficient to sustain groundwater levels between 15 and 30 ft above land surface in some areas. The subsidence per 100 ft of groundwater-level decline at selected sites in the greater Houston area was approximated for different areas as follows.

1. The area near the East End extensometer: 0.68 ft, based on 0.51 ft of subsidence and about 75.0 ft of Chicot aquifer groundwater-level decline by 1932, and 1.04 ft, based on 1.12 ft of subsidence and 108 ft of Chicot aquifer groundwater-level decline by 1943 (fig. 94; table 3.1). The greater subsidence ratio after 1932 indicates that the initial preconsolidation head was probably reached in 1932 when Chicot aquifer groundwater levels had declined by about 65.0 ft.

2. The area near the Baytown extensometer: 0.53 ft, based on 0.41 ft of subsidence and a mean of 77.0 ft of Chicot aquifer groundwater-level decline by 1934 (figs. 14, 95*C*), and 2.20 ft, based on 4.69 ft of subsidence and 213 ft of Chicot aquifer groundwater-level decline by 1959 (fig. 95*C*). The greater subsidence ratio after 1934 indicates that the initial preconsolidation head was probably reached in 1934 when Chicot aquifer groundwater levels had declined by about 77.0 ft.

3. The area near benchmark V 660:

    A. Chicot aquifer: 0.31 ft, based on 0.28 ft of subsidence and 89.0 ft of Chicot aquifer groundwater-level decline by 1954, and 0.66 ft, based on 0.56 ft of subsidence and 85.0 ft of Chicot aquifer groundwater-level decline by 1959 (fig. 96*A*).

B. Evangeline aquifer: 0.29 ft, based on 0.28 ft of subsidence and 96.0 ft of Evangeline aquifer groundwater-level decline by 1954, and 0.64 ft, based on 0.56 ft of subsidence and 109 ft of Evangeline aquifer groundwater-level decline by 1959 (fig. 96*A*).

The greater subsidence ratios after 1954 indicate that the initial preconsolidation head was probably reached by 1954 when Chicot and Evangeline aquifer groundwater levels had declined by about 89.0 and 96.0 ft, respectively.

4. The area near benchmark CONROE RM 1:

A. Evangeline aquifer: 0.21 ft, based on 0.20 ft of subsidence and 96.0 ft of estimated Evangeline aquifer groundwater-level decline by 1978, and 0.28 ft, based on 0.40 ft of subsidence and 141.0 ft of Evangeline aquifer groundwater-level decline by 1987 (fig. 96*D*); because there were no groundwater-level data from about 1976 to about 1980 for Evangeline aquifer in the area near benchmark CONROE RM 1, the amount of water-level decline in 1978 was estimated by linear regression from data collected before and after that year.

B. Jasper aquifer: 0.23 ft, based on 0.20 ft of subsidence and 88.0 ft of Jasper aquifer groundwater-level decline by 1978, and 0.26 ft, based on 0.40 ft of subsidence and 155.0 ft of Evangeline aquifer groundwater-level decline by 1987 (fig. 96*D*).

The greater subsidence ratio after 1978 indicates that the initial preconsolidation head was probably reached in 1978 when Evangeline and Jasper aquifer groundwater levels had declined by about 96.0 and 88.0 ft, respectively.

The ratio of subsidence to groundwater-level decline depends on various characteristics of the fine-grained units, such as the thickness, compressibility, and permeability (Holzer, 1981). Additionally, the rate of groundwater-level decline at these sites was not entirely constant, which is preferred during the analysis period for preconsolidation head (Holzer, 1981); therefore, the initial preconsolidation head estimates for each of these four sites (East End and Baytown extensometers and benchmarks V 660 and CONROE RM 1) are generalized.

The initial preconsolidation head also was estimated in Kelley and others (2018) (termed the "drawdown at preconsolidation stress") partially on the basis of USGS consolidometer tests reported in Gabrysch and Bonnet (1974, 1976a, b). Using a linear regression, Kelley and others (2018) determined that the preconsolidation head was 104 ft at land surface and 0 ft at a depth of 423 ft bls based on analysis of 12 clay samples Gabrysch and Bonnet (1974, 1976a, b). The preconsolidation head was 75 ft at land surface and 0 ft at a depth of 870 ft bls (Kelley and others, 2018). The preconsolidation head value of 0 ft at a depth of 870 ft bls is the 90th-percentile value based on model-simulation results at 26 sites (Kelley and others, 2018).

Unlike previous modeling reports where an initial preconsolidation head of about 70 ft was used across the model domain (Meyer and Carr, 1979; Carr and others, 1985; Kasmarek and Strom, 2002; Kasmarek and Robinson, 2004; Kasmarek, 2012), the GULF model used the depth-dependent relation established in Kelley and others (2018). The input preconsolidation head array specified in the CSUB package was based on this relation and is relative to the steady-state groundwater level in the first stress period of the model. The preconsolidation head used in each model cell is relative to the midpoint value of the elevation of each cell; therefore, the preconsolidation head value varies spatially across the model domain. In general, the preconsolidation head is greatest in the outcrop areas and least in the downdip areas where the Beaumont Formation is present (fig. 7).

Hydraulic Properties

Based on available published data describing the hydraulic properties of the Gulf Coast aquifer system, the Chicot, Evangeline, and Jasper aquifers and the Catahoula confining unit are assumed to be under water-table conditions in the respective outcrop areas (fig. 8). Additionally, based on colocated groundwater-level data (discussed in the "Colocated Groundwater Wells" section), it is estimated that unconfined conditions generally exist in the shallow groundwater system to a depth of less than a few hundred feet (figs. 37–50). With increases in depth towards the coast, however, the interbedded accumulation of fine-grained sediment generally results in a transition to confined conditions (Carr and others, 1985).

The simulation of confined conditions can be challenging when using a coarse vertical discretization by which the Chicot and Evangeline aquifers are each simulated with a single model layer. When groundwater levels decrease below the tops of cells in each respective aquifer, a conversion from confined to unconfined conditions results if convertible layers are used in the model downdip from the outcrop area. MODFLOW 6 uses a combination of specific-storage and specific-yield values to calculate storage changes in convertible cells. Under confined conditions, only specific storage is used, whereas under unconfined conditions, both specific storage and specific yield are used. When a transition from confined to unconfined conditions occurs, the much larger specific-yield value largely governs the calculation of the amount of water released from storage, which is substantially greater than under confined conditions where only the smaller specific-storage value (albeit, multiplied by the saturated thickness) is applied. As a result, this conversion between confined and unconfined conditions can change the pattern of the simulated drawdown. The single-layer approach per aquifer unit used in the GULF model contrasts with simulating the Chicot aquifer

with multiple layers, whereby the upper layers could convert between unconfined and confined conditions, but the deeper layers, where most groundwater use is present, could remain under confined conditions. To account for these dynamics with a single layer per hydrogeologic unit, all areas of layers 1 and 2 in the model were simulated as convertible, and layers 3, 5, and 6 are set as convertible only in the outcrop area (fig. 8). Layer 4, which represents the Burkeville confining unit, was simulated as nonconvertible everywhere for purposes of model stability and runtime efficiency. Nonconvertible conditions were effectively imposed in layer 2 (Chicot aquifer) by gradationally decreasing specific yield from updip to downdip to simulate the transition from unconfined to confined conditions (fig. 101). A specific-yield value of 0.200 was used in the outcrop area of this layer, and the value gradually decreases to zero towards the coast where the midpoint depth of each cell is greater than about 650 ft below the model top surface. This 650-ft threshold was based on the assumption that the hydrogeologic units are under confined conditions below this depth—a conservative value based on the analysis presented in the "Hydrogeologic System Conceptualization" section. Therefore, the transition from unconfined conditions to confined conditions can be simulated by using a single layer for each hydrogeologic unit. Specific-storage values specified in the MODFLOW 6 STO package (Langevin and others, 2021) are disregarded when using CSUB, even in layers where the subsidence package is not active; therefore, these values are set to zero in the STO package and are specified in the CSUB package.

Based on the analysis presented in the "Hydrogeologic System Conceptualization" section, a hydrologic connection generally exists across the water-production zones at various depth intervals of the intermediate groundwater system. However, the vertical movement of groundwater is slowed by the substantial amount of interbedded fine-grained sediment in this groundwater system. As a result, although the groundwater-level pattern at different depth intervals in the intermediate groundwater system is similar at each extensometer site between 1970 and 2020, the groundwater levels are generally dissimilar for wells screened above an elevation of between about 250 and 730 ft bls (figs. 37–44). Therefore, an initial vertical anisotropy of 0.0001 was used for layers 2 and 3 (Chicot and Evangeline aquifers, respectively) where the depth of the midpoint of the model cells was less than about 650 ft below the model top surface. The initial vertical anisotropy of 0.0001 is similar to the average of the Chicot and Evangeline vertical anisotropy values (0.00008) from Ryder and Ardis (2002).

Hydrologic Boundaries

Hydrologic boundaries in the groundwater model represent the locations where the inflow or outflow of groundwater to and from the model could occur and include specified-flux and head-dependent boundaries. For a specified-flux boundary, a user-specified rate governs groundwater exchange at that boundary. Simulated specified-flux boundaries include groundwater use (fig. 12) and recharge (fig. 67). Based on an analysis of available groundwater-level data, the northeast and southwest lateral active model boundaries are located at a considerable distance from the potentiometric surface declines caused by groundwater use in the greater Houston area. In the absence of large groundwater withdrawals or changing hydraulic gradients near these boundaries, little flow across the boundaries is likely; therefore, the lateral boundaries were specified as no-flow—a type of specified-flux boundary. A no-flow boundary was also established at the bottom of layer 6. A head-dependent boundary simulates flow based on the difference between a user-specified groundwater level at the boundary and the simulated groundwater level in model cells. Head-dependent boundaries were used to simulate surface-water/groundwater exchange and groundwater flow to and from the Gulf of Mexico.

Recharge

Areally distributed recharge derived from the SWB code was simulated as a specified-flux boundary by using the Recharge package (Langevin and others, 2021) in the GULF model. MODFLOW 6 computes the volume of water added to the model for each stress period as the product of the specified recharge rates at each node and the cell area. Transient recharge was calculated as the mean of all filtered monthly SWB output arrays (fig. 65) within the time span of each stress period. The Recharge package input for the steady-state simulation was calculated as the mean of all filtered monthly SWB output arrays from January 1897 through December 2018. Spatial adjustment of recharge occurred during history matching to obtain better matches between simulated and observed history-matching targets.

Two options are available with the MODFLOW 6 Recharge package to apply recharge in the model: (1) assignment of recharge to the highest active cell (the default setting) and (2) assignment of recharge only to cells in layer 1 ("FIXED_CELL" option). Shallow groundwater levels in the outcrop areas generally have remained relatively stable over time; therefore, it is expected that the shallow groundwater system is continually recharged by precipitation infiltration in these areas. By comparison, because of the presence of the Beaumont Formation (fine-grained fraction; fig. 7), areal recharge in the downdip areas is expected to be much less, and little of this recharge is expected to percolate vertically downward below the shallow groundwater system. Much of the recharge applied to layer 1 remains in the shallow groundwater system and is discharged to local streams, and only a small fraction of this recharge enters the deeper system.

To enable these two forms of recharge applications, two recharge packages were used in the GULF model. One recharge package for the area of the hydrogeologic unit outcrops and adjacent alluvium and terrace deposits (figs. 8–9) applies recharge to the highest active cell. The other recharge

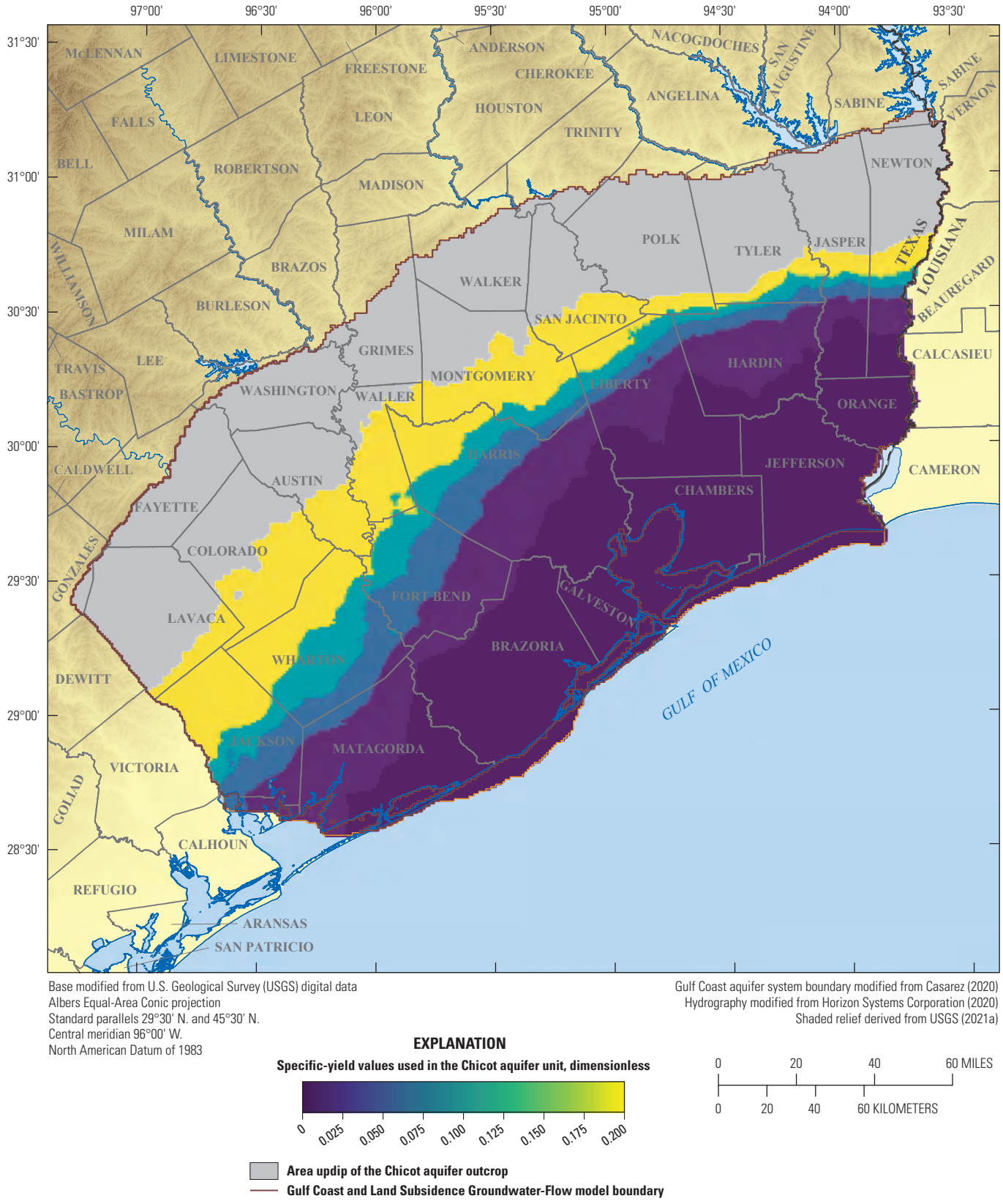

Figure 101. Specific-yield configuration used in layer 2 (Chicot aquifer) of the Gulf Coast Land Subsidence and Groundwater-Flow model.

package used the "FIXED_CELL" option for the downdip area of the model where the Beaumont Formation is present (fig. 7).

Layer 1 in the GULF model was used to simulate the shallow groundwater system; therefore, net groundwater flow between layer 1 and layers 2 and 3 is described as "net groundwater flow" to the Chicot and Evangeline aquifers, respectively, and net groundwater flow between layer 1 and layers 5 and 6 is described as net groundwater flow to the Jasper aquifer and Catahoula confining unit, respectively. This "net groundwater flow" is also similar to "deep recharge" described in some published reports.

Discharge

Discharge from the Gulf Coast aquifer system offshore to the Gulf of Mexico was simulated by using the GHB package (fig. 102) (Langevin and others, 2021). This package uses a linear relation between the water-table altitude and a user-specified reference groundwater level and conductance. Conductance is defined as the product of hydraulic conductivity of the sediment between the model cell at the boundary and the reference groundwater-level boundary condition and the cross-sectional area perpendicular to flow, divided by the distance between the GHB and the model cell. Water flows into the groundwater model when the simulated groundwater level is lower than the reference groundwater level. Water flows out of the groundwater model when the simulated groundwater level is higher than the reference groundwater level. GHBs were used in each layer at the downdip boundary of the model, which extends about 4 mi offshore (figs. 99–100). This arrangement allows for groundwater interaction with the Gulf of Mexico and the simulation of submarine groundwater discharge. The reference groundwater level for each GHB cell representing Galveston Bay and the Gulf of Mexico was set to 0 ft. GHB cells were used in each layer of the model at the nearshore interface and in layer 1 near Galveston Bay.

Surface-water/groundwater interaction was simulated by using a combination of the River and Drain packages (Langevin and others, 2021); the River package cells simulate the largest stream features in the model area, and the Drain package cells simulate the intermittent stream systems (fig. 102). Flow between the aquifer and drain cells is similar to the flow in the GHB package, except that (1) water does not flow to the drain from the aquifer when the groundwater level in the aquifer is less than the elevation of the drain and (2) water does not flow from the drain to the aquifer.

The extent of the simulated streams (fig. 102) was modified from the National Hydrography Dataset Plus (Horizon Systems Corporation, 2020), a 1:100,000-scale geospatial dataset of surface-water features. River package streambed elevations were based on a 30-m digital elevation model (USGS, 2021a) and specified to be incised about 30 ft in relation to the top of layer 1 in the model. The specified stream stage was set about 15 ft above the streambed, and all stream segments were assigned to layer 1 of the model. In this way, the simulated flow was predominantly towards the stream and out of the model domain, which follows the conceptual understanding of surface-water/groundwater exchange in the region. Initial streambed conductance was set at about 1,075 square feet per day (ft^2/d) and was adjusted during history matching. Lakes and reservoirs are not simulated in the model.

Groundwater Use

The withdrawal of groundwater (fig. 2.1) was simulated as a specified-flux boundary by using the Well package (Langevin and others, 2021). Historical groundwater use for the model area was obtained from estimates presented in Oliver and Harmon (2022). A flow chart (fig. 3–1 in Oliver and Harmon [2022]) shows the implementation process for groundwater withdrawals, and table 2–1 in that same report summarizes the primary data sources. The methods used to estimate groundwater use in Oliver and Harmon (2022) are summarized below.

Historical groundwater-use estimates during 1900–74 for municipal, rural domestic, manufacturing/industrial, irrigation, livestock, mining, and power generation use types were based on published sources, many of which are listed in the "References Cited" section of this report. Municipal and rural domestic water use (from surface water and groundwater) were estimated based on population estimates from the U.S. Census Bureau, population density distributions, and assumed per capita use rates. Total county water use was the product of the urban and rural estimated population and the per capita use rates. Municipal groundwater use was then estimated based on the total county water use multiplied by the fraction of groundwater use in 1974—the first year in which these estimates were available. Livestock groundwater use was based on U.S. Department of Agriculture livestock populations and an assumed per animal use. Irrigation groundwater use was based on a multistep process through which mean irrigation depths in each county were estimated based on the irrigated acreage and the applied groundwater volume from the TWDB (2001). A mean water budget was then constructed based on the mean irrigation depths and precipitation data and was used to estimate an irrigation depth for years when only applied groundwater volume estimates were available. Total irrigation water use (both surface water and groundwater) was then calculated as the product of the irrigation depth and the irrigation acreage. Irrigated groundwater use by county was then obtained as the product of total irrigation water use multiplied by the fraction of groundwater use in 1974.

Historical groundwater-use estimates during 1974–2018 for municipal, manufacturing, irrigation, livestock, mining, and power generation were obtained from the TWDB water-use survey database (TWDB, 2020a). Domestic groundwater use was estimated based on census data and the same method used for 1900–74. Metered groundwater-use data from the HGSD, FBSD, and LSGCD, which were first available in 1976, 1990, and 2002, respectively, were integrated with the TWDB groundwater-use estimates. In Harris, Galveston, and

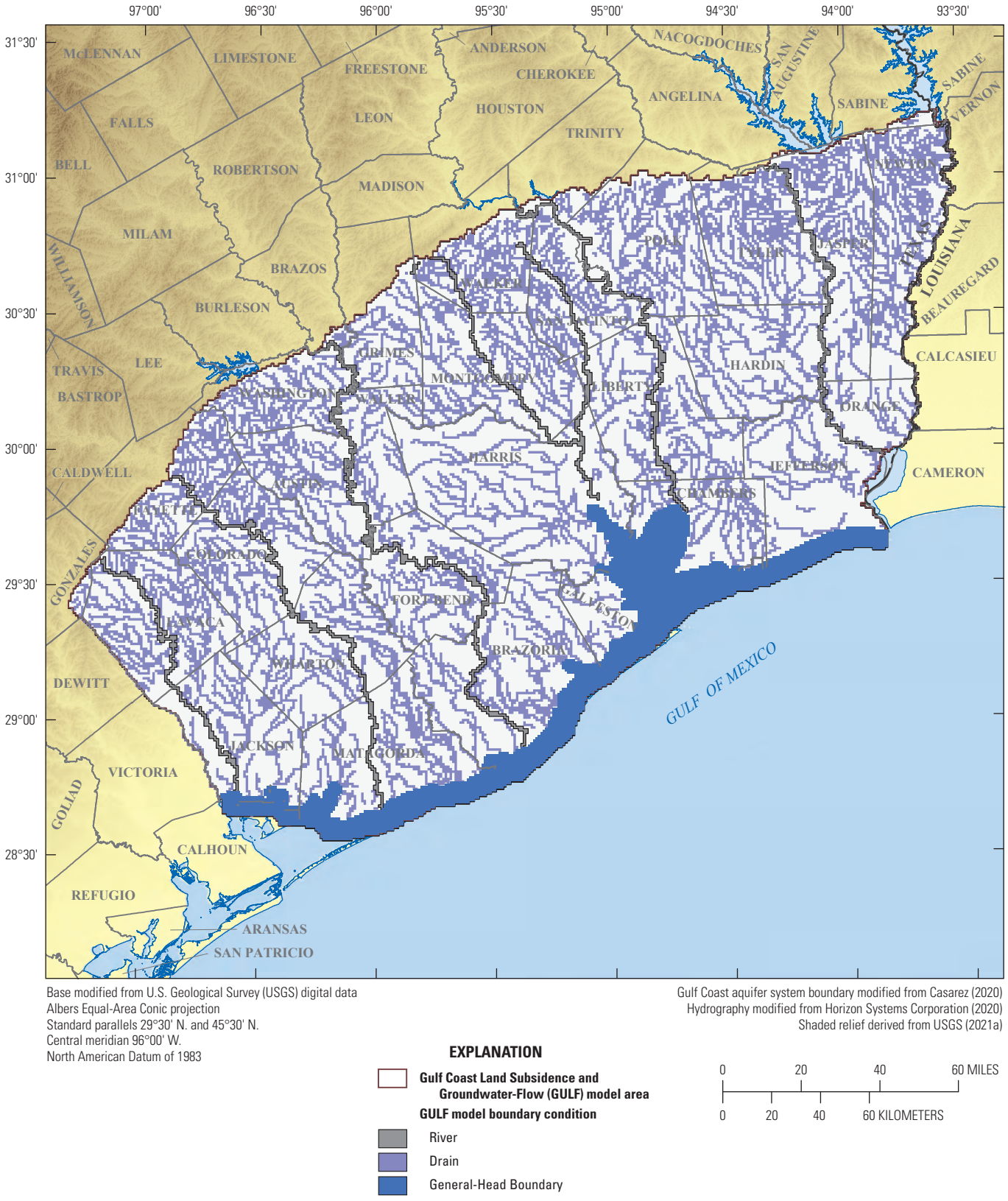

Base modified from U.S. Geological Survey (USGS) digital data
Albers Equal-Area Conic projection
Standard parallels 29°30' N. and 45°30' N.
Central meridian 96°00' W.
North American Datum of 1983

Gulf Coast aquifer system boundary modified from Casarez (2020)
Hydrography modified from Horizon Systems Corporation (2020)
Shaded relief derived from USGS (2021a)

EXPLANATION

- **Gulf Coast Land Subsidence and Groundwater-Flow (GULF) model area**
- **GULF model boundary condition**
  - River
  - Drain
  - General-Head Boundary

0 20 40 60 MILES
0 20 40 60 KILOMETERS

Figure 102. Subset of boundary conditions of the Gulf Coast Land Subsidence and Groundwater-Flow model.

Fort Bend Counties, the metered groundwater withdrawals and information from the individual well schedules were used to directly incorporate groundwater withdrawal information to vertically distribute groundwater use into each model layer. In counties where metered data were unavailable, groundwater use was distributed to wells based on well yields from the TWDB (2020b, 2020c) or were estimated by using a linear regression.

Historical irrigation groundwater-use estimates from Oliver and Harmon (2022) used in the GULF model were simulated in a separate Well package included in MODFLOW 6. The simulation of historical irrigation groundwater use was done to facilitate parameterization, which reflects the higher degree of uncertainty in the spatial and temporal variation of irrigation use compared to other use types simulated in the model. The uncertainty with irrigation use is related to the division of irrigation water use between surface-water and groundwater sources, and to a lesser degree, irrigation return flows in areas with a large agricultural component (fig. 4). Historical water-use estimates by Oliver and Harmon (2022) included model cell locations of irrigation wells with drill dates and abandonment dates. Groundwater withdrawal rates assigned to these cells within the applicable time ranges were simulated in the irrigation-specific Well package and removed from the general Well package. An urban (developed) land-cover dataset was overlain with the model grid for cross-checking purposes to ensure that model cells that included municipal groundwater use were not moved into the irrigation-specific Well package.

Initial attempts were made to calculate rates of irrigation return flows based on estimated withdrawals and to apply these as positive fluxes to model cells containing irrigated acreage. The approach was found to be overly complex, however, given the substantial uncertainties surrounding the timing and rates of actual irrigation groundwater use. Instead, irrigation groundwater use in the GULF model was simulated by using adjusted net withdrawal rates that account for the portion of estimated irrigation groundwater use that was potentially fulfilled by surface-water deliveries and irrigation return flows.

History Matching and Uncertainty Quantification

To aid decision-making purposes underlying the use of the GULF model, a Bayesian framework (Tarantola, 2005; Doherty and Simmons, 2013; Doherty, 2015; Hemmings and others, 2020) was used to represent uncertainty in model parameters and simulated outputs of interest. History matching is the process of changing model stresses and parameters to acceptably fit historical information such as hydraulic-head observations and stream-leakage estimates and is performed to allow the model to better address a range of hydrologic problems. The term "history matching" is used to describe reservoir modeling in the petroleum industry and avoids the implication of parameterization finality. The history-matching approach used in this study incorporates a Monte Carlo approach for determining the parameter values and avoids the implications of a traditional "calibrated" model having arrived at a finalized dataset of exactly known parameter values given that there are any number of differing parameter value datasets that could potentially be used (Doherty and Simmons, 2013). Model history matching and uncertainty quantification were performed by using the iterative ensemble smoother PESTPP-IES (White, 2018), included in the PEST++ software suite (Welter and others, 2015; White and others, 2020a), in conjunction with the open-source Python packages FloPy (Bakker and others, 2016) and pyEMU (White and others, 2016a, b). The combination of these software tools allows much of the history matching and uncertainty quantification workflow to be performed programmatically, which provides transparency and reproducibility (White and others, 2020a, b; Fienen and others, 2021).

The iterative ensemble smoother (IES) algorithm is available through the open-source PEST++ software suite (White and others, 2020a). IES provides two important advantages over the more frequently used deterministic parameter estimation algorithms: reduced computational demand for highly parameterized models and an accessible way to estimate uncertainty of forecasts that depend on a high number of parameters (White and others, 2020a, b).

The IES algorithm substantially reduces the computational demand of parameter estimation for highly parameterized models by using a Monte Carlo approach to approximate the first-order relation between model inputs (parameters) and outputs (simulated equivalents of historical observations and forecasted conditions). This approximation allows the number of model runs required in each iteration of the IES process to be substantially fewer than the number of adjustable parameters (White, 2018). The GULF model ensemble includes 183,207 adjustable parameters, and the parameter estimation process implemented for the GULF model ensemble used less than 300 sets of possible random parameter values (or "realizations" of parameter values) in each iteration of the algorithm.

The IES approach also provides the benefit of a built-in uncertainty analysis. The result of the IES algorithm is an ensemble of realizations (the "posterior parameter ensemble") that show similar success in simulating historical conditions using different combinations of parameter values. This represents a level of nonuniqueness in aquifer properties that exists after assimilating historical observations of groundwater levels and subsidence/compaction. This posterior ensemble is used to estimate uncertainty in future aquifer-system conditions by evaluating this ensemble with scenarios of future water use. Appendix 7 contains a description of the parameter estimation and uncertainty analysis workflow and options used in the implementation of PESTPP-IES.

Historical Observations

The model is designed to simulate the groundwater-level and subsidence response to stress patterns in a temporally meaningful way and is primarily focused on simulating long-term changes in these quantities at regional to subregional spatial scales. Historical observations of groundwater levels and subsidence were used for history matching. (The term "subsidence" is used in this section to also include compaction and vertical displacement processes.)

Groundwater Levels

Groundwater-level observations for the GULF model (fig. 103; table 8.1) were obtained from the NWIS database (USGS, 2021b) and the TWDB Groundwater Database (TWDB, 2020b). An initial observation filtering process was performed, followed by a spatial and temporal observation declustering process to ensure that disparate groundwater levels did not occur in an area with spatially dense observations and that all model areas were represented during model history matching. The remaining groundwater levels were then smoothed temporally (for example, fig. 104), and target observations were created from the smoothed observation values nearest the end of each stress period. A 5-year moving mean filter was applied to groundwater-level observations prior to 2000, and a 2-year moving mean filter was used during 2000–18. In this way, much of the high-frequency noise associated with these observations was removed, but the important patterns expected to be matched by the model, such as long-term changes in groundwater levels, were retained. Observation targets of temporal differences in groundwater levels were created for each location by calculating the difference between smoothed groundwater levels assigned to consecutive stress periods.

Groundwater levels in shallow groundwater-system wells are generally under water-table conditions and are primarily controlled by surficial processes that do not affect the intermediate or deeper systems. Although layer 1 is only about 50 ft thick, the shallow groundwater system defined in this report is about the first 200–300-ft interval below land surface in the outcrop area (fig. 8) and about the first 70–175-ft interval below land surface in the confined area, as discussed in the "Colocated Groundwater Wells" section. Therefore, wells screened in the entirety of the shallow groundwater system, which includes layer 1 and the upper part of layer 2 at or above the intervals described previously, were not included in the groundwater-level observation dataset.

A total of 19,508 groundwater levels at 724 wells (TWDB, 2020b; USGS, 2021b) distributed across the model area (fig. 103; table 8.1) were used for model history matching. The vertical distribution of these wells and observations included the following: Chicot aquifer (369 wells, 10,987 groundwater levels); Evangeline aquifer (212 wells; 5,204 groundwater levels); Burkeville confining unit (16 wells; 583 groundwater levels); Jasper aquifer (100 wells; 2,079 groundwater levels); and Catahoula confining unit (27 wells; 655 groundwater levels). Approximately 455 of the 724 wells are located in the greater Houston area (fig. 18) and are part of a network of wells whose groundwater levels are measured annually. Of the wells used for history matching, 15 wells are at extensometer sites where 3,028 groundwater levels were measured.

In the counties nearest the coastline, most wells are screened in the sediments that compose the Chicot aquifer (fig. 103) because the geologic units underlying the Chicot aquifer are buried at a substantial depth of often more than about 1,500 ft below NAVD 88 as the units approach the Texas coast (fig. 9); in contrast, groundwater-level observations from the Evangeline and Jasper aquifers predominate in the updip areas where the geologic units underlying the Chicot aquifer are shallowly buried at depths of less than about 500 ft below NAVD 88. Fewer groundwater-level observations were available in the eastern part of the model than in the central and western parts (fig. 103). For the model period, a median of 20 groundwater-level observations are available for each observation well; however, most observations were made between November and February as a part of an annual groundwater-level measurement program (fig. 105*A*). A greater number of groundwater-level observations are available after 2000 when the annual USGS groundwater-measurement program was expanded (fig. 105*B*). Therefore, a tendency towards best reproducing the post-2000 period groundwater levels and subsidence is inherent in the model (fig. 105*B*); however, this tendency was mitigated by the use of multiple observation groups with a balanced weighting approach for different groups of wells representing different time periods during history matching.

Wells were separated into four groups for the purpose of history matching, depending on the following characteristics in the data obtained at each well: (1) the historical minima reached for the water-level measurements in each well, (2) groundwater-level differences between stress periods, (3) wells measured annually, and (4) all other groundwater-level measurements. The latter two groups were further divided among model layer/aquifer designations.

Subsidence

Subsidence observations for the GULF model history-matching process included differencing of leveled elevations at benchmarks (fig. 70*A*; table 4), subsidence from contour maps (appendix 5), compaction recorded at extensometers (fig. 74), and vertical displacement at GPS stations (fig. 72; table 6.1). The objective function (eq. 6; table 7.2) included a total of 485 subsidence observations from benchmarks, 413 grid-scale contour map subsidence observations, 3,907 extensometer-measured-compaction observations, and 29,910 GPS vertical-displacement observations. Similar to the approach for the groundwater-level observations, the subsidence observations were programmatically prepared for model history matching. Initial observation filtering (for GPS data) was followed

by spatial observation declustering (for benchmark and GPS data) and temporal observation declustering (for GPS data). A 5-year (prior to 2000) or 365-day (during and after 2000) moving mean was then applied to the GPS data to ensure a focus on the long-term pattern of the vertical-displacement data. The finalized subsidence time-series datasets were then temporally shifted to coincide with the end date of the corresponding stress period described in the "Spatial and Temporal Discretization" section.

Two types of observation groups were defined for the subsidence observations: one for the measurements and one for the temporal differences between stress periods. Temporal difference observations were used for the subsidence contour maps, benchmarks, extensometers, and GPS stations.

Subsidence Contour Maps

The subsidence contour maps for 1906–43 (fig. 5.1), 1906–78 (fig. 5.6), and 1906–2021 (fig. 70*B*) were used for history matching. Contour values from the subsidence maps were interpolated and applied to the model grid. Nonzero-weighted observations of subsidence in 1943 and 1978 were created in every model cell that also contained an observation in any model time step of extensometer-measured-compaction, benchmark subsidence, or GPS-measured subsidence. Zero-weighted observations of subsidence in 2021 were also created at these same model cell locations for visual inspection of history-matching performance in late-model time.

Bilinear interpolation of contour values to overlie on the model grid introduces error from spatial approximation, particularly in places where contours are close together and occur within the same 1- x 1-km model cell. Furthermore, the contours on the original subsidence maps are an approximation, based on many measurements at point locations. Subsidence presented in the 1906–43 contour map was assigned as an observation to the nearest model stress period end date of January 1, 1945. For parameter estimation through history matching, the most important contribution of the subsidence contour maps is to constrain the level of simulated subsidence that occurs before the other observation types (extensometers or GPS stations) have available data.

Benchmarks

Benchmark subsidence observations used in history matching include those listed in table 4. Subsidence began in many parts of the greater Houston area prior to 1943 (fig. 5.1), the date when the first large-scale leveling lines were run by NGS. Although 24 benchmarks used in this study were monumented during 1906, 1915, or 1918 (table 4), many more would have been needed to estimate subsidence between 1906–43 across the greater Houston area. Therefore, the 1906–43 subsidence contour map (fig. 5.1) was used to represent 1906–43 elevation changes at benchmarks located in the contoured area that did not have elevations from leveling surveys during or prior to 1943. Subsidence outside of the contoured area was assumed to be zero during and prior to the monumenting of each benchmark unless elevation data were available at a nearby benchmark during this period. Subsidence observations for the model were generated as the difference between the leveled elevations at these benchmarks during each survey listed in table 4. Some benchmarks from table 4 were not used, generally due to colocation in the same or an adjacent model cell as another benchmark, and were therefore removed during the observation declustering process.

Extensometers

The GULF model was history matched to time-series compaction observations from 13 extensometers located at 12 sites (figs. 72–73) (the Fort Bend extensometer was not included because it was installed in 2017, the second to last year included in the model simulation). The depth to anchor at each site was used to calculate the percentage of each model layer intersected by the extensometer. Model-simulated compaction in each layer was multiplied by these percentages and summed to produce depth-integrated values of compaction consistent with extensometer-measured compaction. Compaction data are estimated monthly at each extensometer compared to the much greater temporal density of the GPS station data; therefore, temporal smoothing of the compaction data was not required. Model-simulated compaction on the start date of each extensometer observation time series was subtracted from all subsequent simulated values for consistency with observed values.

It is estimated from interpolations of the subsidence contour maps that a mean of 80 percent of subsidence occurred at the extensometer sites prior to their installation (table 5). Therefore, these sites were history matched to (1) either the interpolated subsidence contour map data or to nearby benchmarks with long-term subsidence datasets, and (2) to the extensometer time-series compaction record. Additionally, subsidence from the interpolated subsidence contour maps for 1943–64, 1964–73, 1973–78, and 1978–87 (figs. 5.1–5.5) was used as a zero-weighted history-matching target for visual inspection only. In this way, the model could be history matched to subsidence from 1906 to 2018.

Global Positioning System Stations

A total of 178 GPS stations were used for GULF model history matching (fig. 72; table 8.2). These stations were selected from among the 256 GPS stations in the model area, then filtered to remove stations that had less than 3 years of data or stations that had shorter durations compared to nearby stations. GPS height solutions vary from day to day, which is likely the result of variable atmospheric conditions, random walk noise, and other effects not directly related to land-surface-elevation change (Zerbini and others, 2001; Williams and others, 2004; Langbein, 2008). To minimize this high-frequency noise and to enable better comparison between changes in GPS heights and simulated results, a 365-day moving mean was applied to the GPS time-series observations.

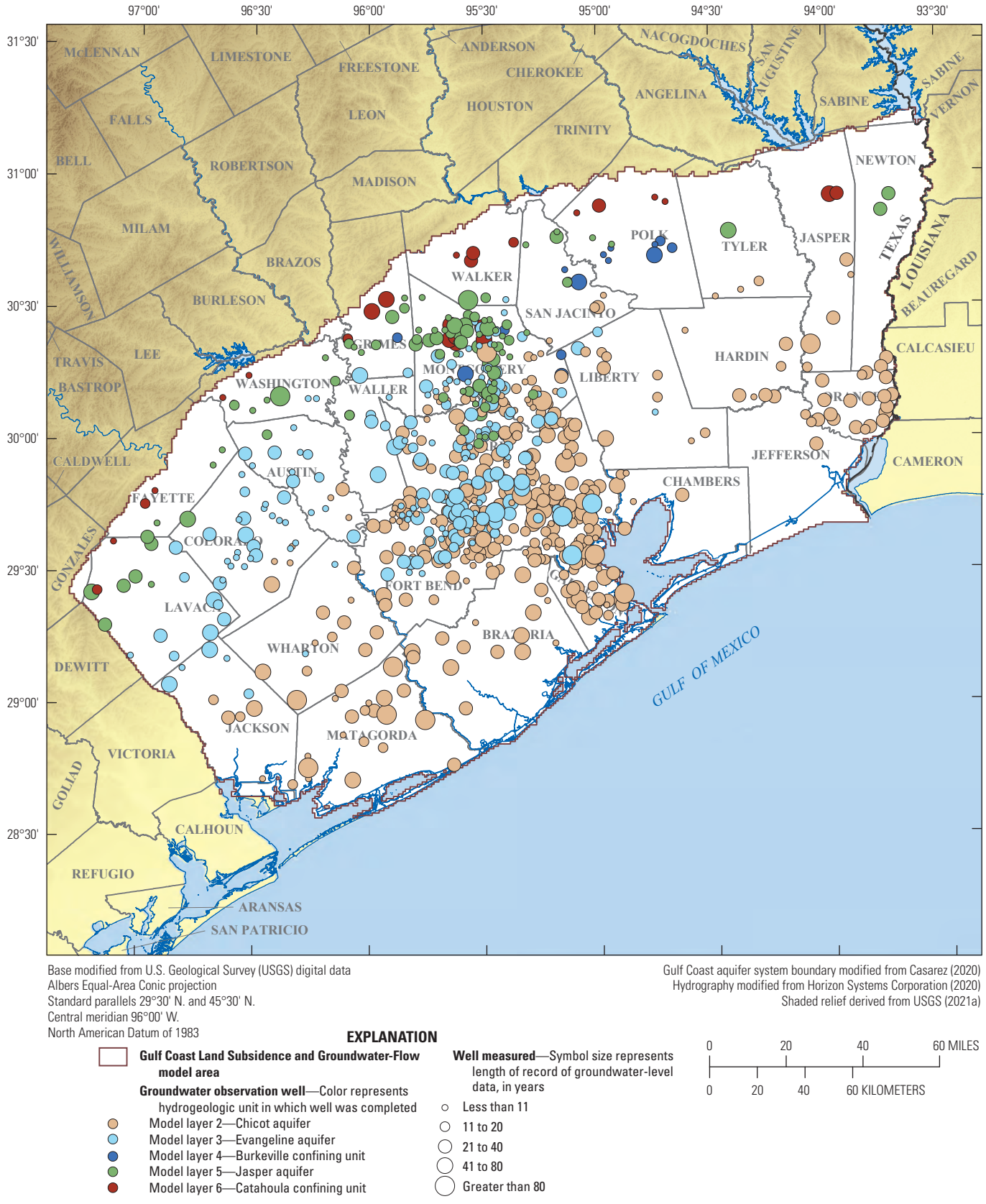

Base modified from U.S. Geological Survey (USGS) digital data
Albers Equal-Area Conic projection
Standard parallels 29°30' N. and 45°30' N.
Central meridian 96°00' W.
North American Datum of 1983

Gulf Coast aquifer system boundary modified from Casarez (2020)
Hydrography modified from Horizon Systems Corporation (2020)
Shaded relief derived from USGS (2021a)

EXPLANATION

Gulf Coast Land Subsidence and Groundwater-Flow model area

Groundwater observation well—Color represents hydrogeologic unit in which well was completed

- Model layer 2—Chicot aquifer
- Model layer 3—Evangeline aquifer
- Model layer 4—Burkeville confining unit
- Model layer 5—Jasper aquifer
- Model layer 6—Catahoula confining unit

Well measured—Symbol size represents length of record of groundwater-level data, in years

- Less than 11
- 11 to 20
- 21 to 40
- 41 to 80
- Greater than 80

0 20 40 60 MILES
0 20 40 60 KILOMETERS

Figure 103. Spatial distribution of groundwater-level observations for the Gulf Coast Land Subsidence and Groundwater-Flow model.

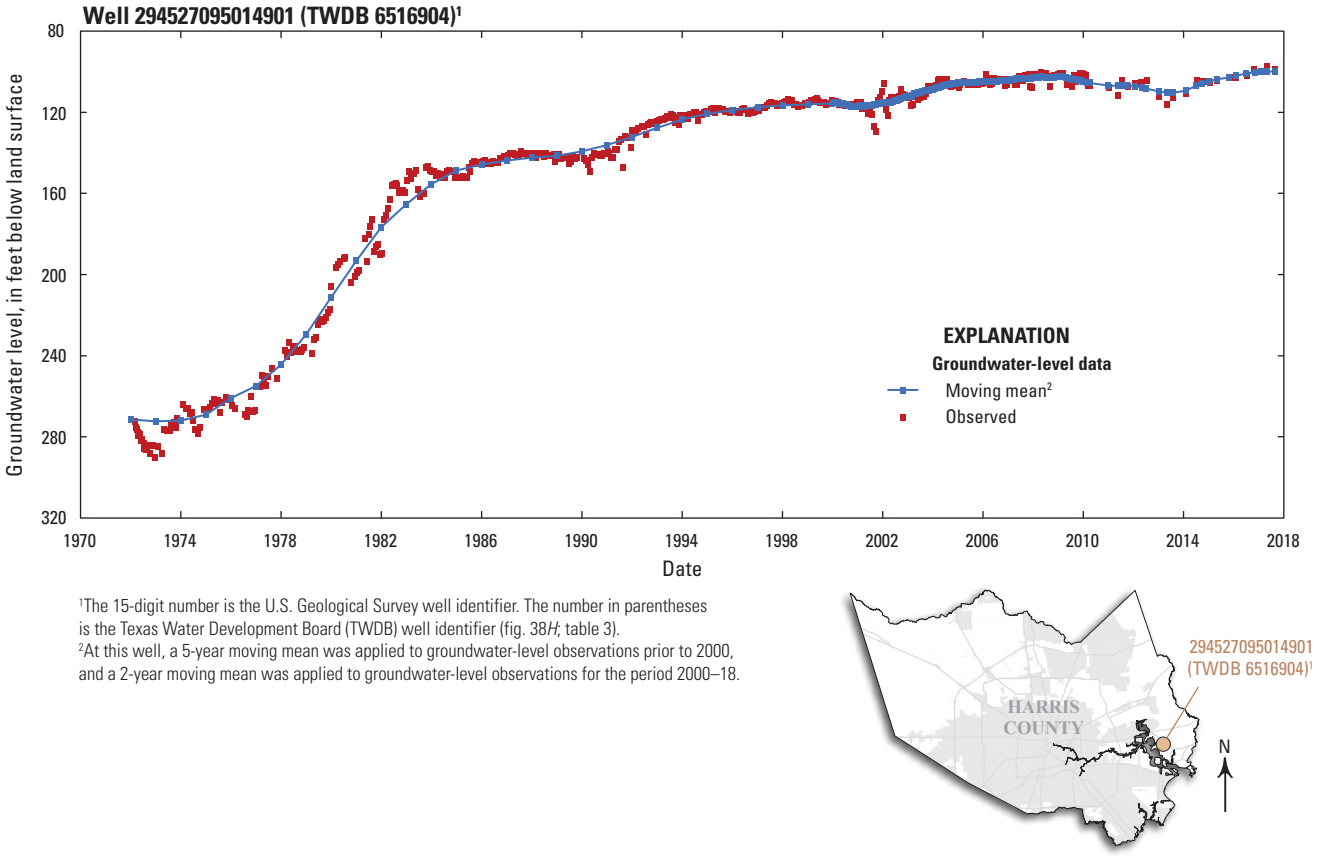

Figure 104. Temporal smoothing of groundwater-level observations for the Gulf Coast Land Subsidence and Groundwater-Flow model.

The removal of the day-to-day variations in GPS heights did not remove seasonal or long-term deformation patterns and therefore facilitated a more meaningful comparison with simulated results.

Prior Parameter Distribution

In the Bayesian framework used herein, the prior parameter distribution is a multivariate Gaussian (normal) distribution that represents existing uncertainty in the model inputs (represented by parameters) before history matching (White and others, 2016a, b). That is, the prior parameter distribution is derived a priori (before) the history-matching process and, therefore, does not formally include any insights gained from examining the historical observations. Instead, the prior parameter distribution is based only on knowledge of the hydrologic system, literature values, and expert knowledge of the groundwater model (White and others, 2016a, b). Models are simplistic simulators of highly complex and largely unseen natural systems. Therefore, models have inherent limitations derived from the simplification of the real-world complex systems to a numerical approximation, constructed of components, each based on unique assumptions (White and others, 2014). Consequently, the prior parameter distribution must be defined by using the current understanding of the Gulf Coast aquifer system, values of aquifer properties from literature, and an understanding derived from previous groundwater-flow models in the modeled area, such that the prior parameter distribution represents an unbiased and conservative representation of what is known and unknown regarding the model inputs. The prior parameter distribution is the basis for the prior parameter ensemble (hereinafter referred to as "the Prior"), which represents samples of the prior parameter distribution and is roughly analogous to a suite of model parameters, each of which is equally likely with respect to the preexisting understanding of the aquifer.

A spatial and temporal parameterization arrangement of pilot point parameters, grid-scale parameters, and spatially uniform parameters was used to stochastically account for recognized sources of model-input uncertainty. The pilot points, the values of which are geostatistically interpolated to each cell, were spaced 10 cells apart and represent expected broad-scale heterogeneity and uncertainty (fig. 106). The grid-scale parameters, which are individually applied to each cell programmatically, represent local-scale heterogeneity and uncertainty. The constant domain-wide parameters, which are single values applied to the entirety of the model area, represent domain-scale uncertainty. Additionally, multiplier parameters, whereby the base values are multiplied by a value

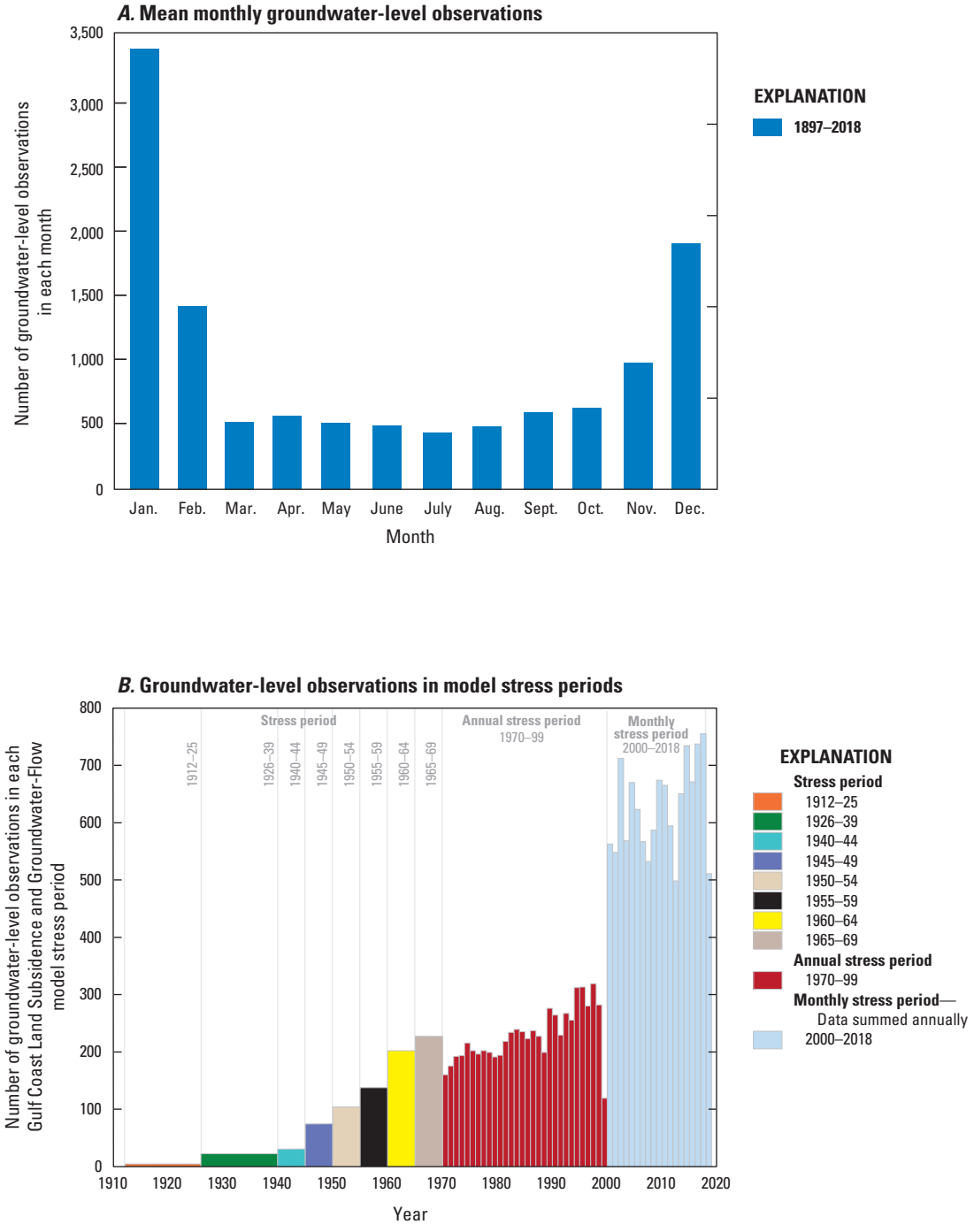

Figure 105. *A*, Mean monthly distribution of groundwater-level observations and *B*, number of groundwater-level observations in model stress periods for the Gulf Coast Land Subsidence and Groundwater-Flow model.

selected within a parameter range, were used to represent uncertainty in recharge, groundwater use, and conductance for the River and Drain packages (Langevin and others, 2021).

Geostatistical variograms define spatial covariance among groups of pilot point and grid-scale parameter values. A summary of the spatial and temporal scales at which the multiplier parameters modify the underlying aquifer properties in the parameter estimation process and the range of multiplier values affecting each property type is presented on table 7. Temporally static, spatially distributed aquifer properties (horizontal hydraulic conductivity [Kh], vertical anisotropy, specific yield, and specific storage) were modified during history matching by the combined effects of a domain-wide multiplier and a multiplier interpolated to each cell from surrounding pilot point locations. Absolute upper and lower limits were assigned to each model property to prevent the

simulation of physically unrealistic property values resulting from the modification of base values by the cumulative effects of several multipliers.

Specified fluxes simulated with the Well and Recharge packages (Langevin and others, 2021) were parameterized spatially and temporally to represent incomplete knowledge of historical water-use patterns and uncertainty in the disposition of natural recharge, respectively. Each well in the Well package was parameterized with a temporally constant multiplier within the range 0.66 to 1.33 (table 7) to account for the variability and uncertainty in the spatial distribution of groundwater use. A domain-wide global multiplier selected for each stress period from within the same range compounds this variability and is applied uniformly to all specified Well package fluxes. Simulated groundwater use in each aquifer is tracked by stress period at a county scale during history matching to ensure a reasonable fit to expected total county groundwater use.

Spatially distributed recharge rate inputs were modified by multipliers interpolated from pilot point parameterization, temporally constant individual cell multipliers, and a domain-wide global multiplier estimated for each stress period. The range of all multipliers for recharge is from 0.9 to 1.1. Although substantial uncertainty exists with regard to the spatial and temporal variability of natural recharge rates, which belies the small multiplier range, the model fit to observations was not particularly sensitive to recharge adjustments. This is largely due to the aquifer-system configuration, where recharge occurs updip and recharged water slowly travels downdip towards water-use centers.

The conductance for Drain cells representing the intermittent streams in the model area was parameterized by using individual-cell-scale multipliers between 0.01 and 100 acting on a uniform initial value of 10,764 square feet (ft^2). The conductance for River cells representing the largest perennial streams in the model area was similarly parameterized with a multiplier range of 0.1–10 acting on a uniform initial value of 1,076 ft^2. GHB cells representing groundwater interaction with the Gulf of Mexico were parameterized with a domain-wide global multiplier between 0.1 and 10 acting on an initial value of about 5 ft^2.

History Matching with PESTPP-IES

Model history matching is the process of adjusting initial model parameter values to improve the fit between model-simulated data and the historical observations (observed or estimated data used as history-matching targets). In a stochastic framework, the parameter values in the Prior are adjusted to new values that reduce the discrepancy, or residual, between the historical observations and their simulated equivalents for each realization in the ensemble. In a Bayesian framework, history matching combines two sources of information: (1) the aquifer-specific information provided by historical observations and (2) the knowledge of the aquifer system encapsulated in the Prior distribution (White and others, 2016a, b). By using PESTPP-IES, history matching was done to propagate the Prior through a series of iterative upgrades and thus improve fit between model-simulated outputs and observed data, resulting in a posterior parameter ensemble (hereinafter referred to as "the Posterior") that can be used to forecast future hydrologic conditions. The term "posterior" is a Bayesian concept referring to a statistical distribution resulting from the combination of different sources of information (White and others, 2016a, b).

The ensemble-based history-matching algorithm used in PESTPP-IES measures the fit between model-simulated outputs and historical observations by a sum of squared weighted residuals, or objective function (ϕ) (table 7.2). The objective function is expressed as

$$\Phi = \sum_{i=1}^{n} [\omega_i (s_i - o_i)]^2 \quad (6)$$

where

n is the number of observations,
ω_i is the observation weight,
s_i is the simulated value, and
o_i is the observed or estimated value.

In PESTPP-IES, the observed values in equation 6 are combined with additive measurement noise derived from a normal distribution with a mean of zero and specified standard deviation or derived from the reciprocal of the observation weight. This creates an ensemble of observation realizations that are paired individually with parameter realizations for the iterative parameter upgrade process, such that the Posterior reflects both parameter and measurement noise uncertainty. PESTPP-IES automates history matching by running the model in parallel as many times as needed to apply an ensemble-based Bayesian conditioning algorithm. This rigorous approach allows for many parameters to be estimated simultaneously with much greater efficiency and in more conceptually coherent ways compared to a traditional manual history-matching approach.

The objective function is composed of several data types (table 7.2) and was largely based on historical observations of groundwater levels, subsidence, and compaction discussed in the "Historical Observations" section. Additionally, estimated groundwater use and expected recharge were included in the objective function to ensure that Posterior-simulated groundwater use and recharge patterns did not stray unduly from the Prior patterns. In a decision-support setting, where this model is used to represent a more complex natural system, the objective function is best formed in a way that closely reproduces the aspects of the historical observations that most resemble important simulated outputs (Anderson and others, 2015; Doherty, 2015). Thus, the observation weights in equation 6 corresponding to the various historical observation types, were specified for use in history matching so that the contribution of a given observation type best aligns with the stated decision-support purposes of the model.

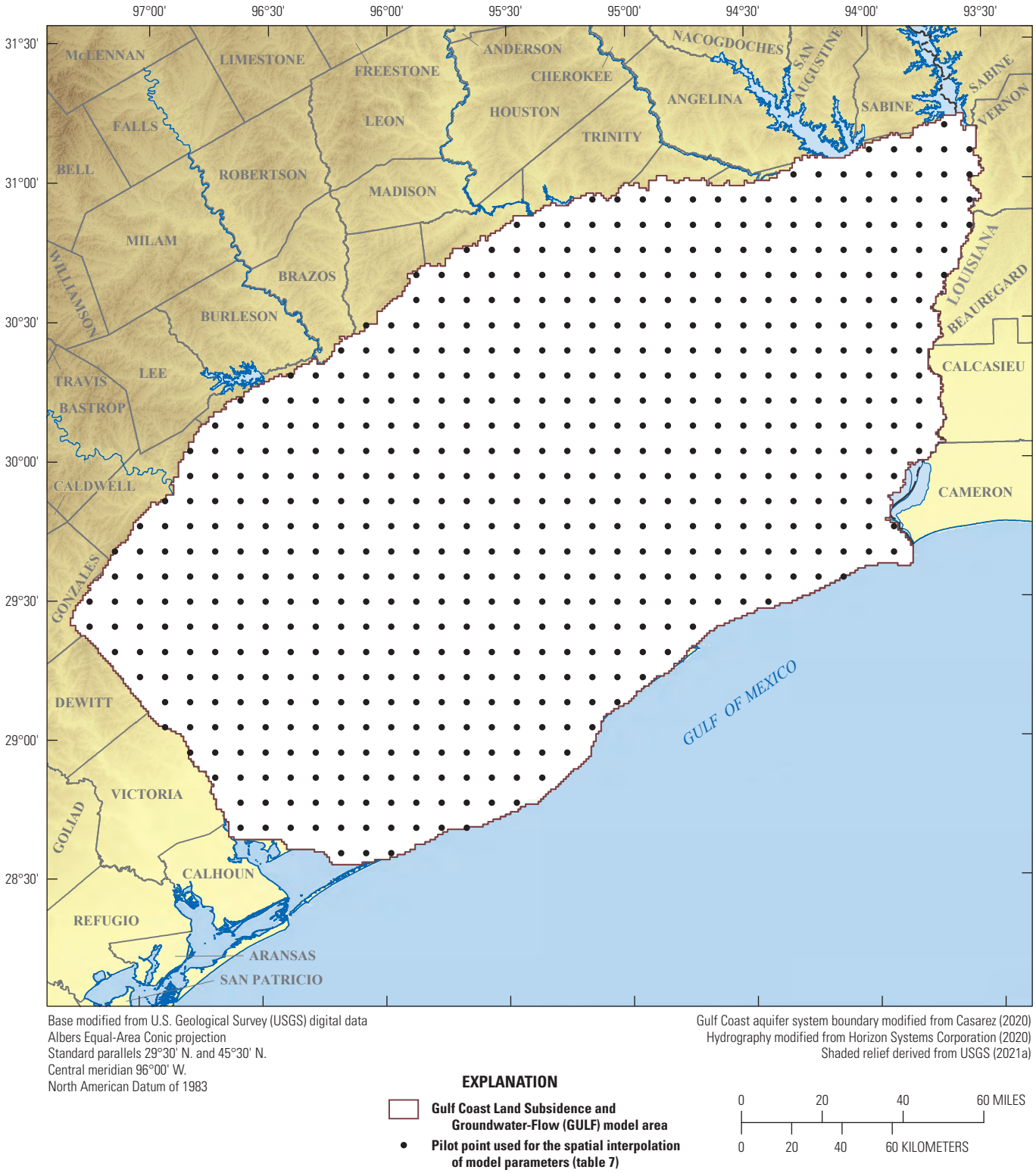

Figure 106. Location of pilot points for the Gulf Coast Land Subsidence and Groundwater-Flow model.

Table 7. Aquifer parameters and mean prior parameter distribution multiplier range.

[--, not applicable]

Model parameter	Multiplier parameter				
	Domain-scale multiplier	Pilot point multiplier	Individual cell (grid-scale) multiplier	Temporal variation	Lower and upper limits for each multiplier
Recharge	X	X	X	X	0.9–1.1
Groundwater use (all use types except irrigation)	--	--	X	X	0.66–1.33
Groundwater use (irrigation)	--	--	X	X	0.001–1
General-Head Boundary conductance	X	--	--	--	0.1–10
River streambed conductance	--	--	X	--	0.1–10
Drain conductance	--	--	X	--	0.01–100
Horizontal hydraulic conductivity (layer 1)	X	X	--	--	0.1–10
Horizontal hydraulic conductivity (layer 2)	X	X	--	--	0.1–10
Horizontal hydraulic conductivity (layer 3)	X	X	--	--	0.1–10
Horizontal hydraulic conductivity (layer 4)	X	X	--	--	0.1–10
Horizontal hydraulic conductivity (layer 5)	X	X	--	--	0.1–10
Horizontal hydraulic conductivity (layer 6)	X	X	--	--	0.1–10
Vertical to horizontal hydraulic conductivity ratio (all layers)	X	X	--	--	0.1–10
Specific yield (all layers)	X	X	--	--	0.75–1.25
Interbed elastic specific storage[1]	X	X	--	--	0.1–2
Interbed inelastic specific storage[1]	X	X	--	--	0.1–2
Coarse-grained elastic specific storage[1]	X	X	--	--	0.1–2
Interbed vertical hydraulic conductivity[1]	X	X	--	--	0.5–2
Coarse-grained porosity[1]	X	X	--	--	0.5–1.5
Interbed porosity[1]	X	X	--	--	0.5–2
Interbed clay thickness as fraction of model layer[1,2]	X	X	--	--	0.75–1.25

[1]These model parameters are specified in the Skeletal Storage, Compaction, and Subsidence (CSUB) package (Hughes and others, 2022). The CSUB package is not active in layers 1 and 6. An interbed is a laterally discontinuous unit composed of fine-grained sediments.

[2]This parameter was created to modify the CSUB parameter for representative interbed thickness in accordance with the CSUB parameter for the representative number of interbeds (layers of clays and silts, which are commonly referred to as "fine-grained sediments").

Observation groups (table 7.2) were formed by the type of observation and, in some cases, were further refined by relative importance, geographic location, or aquifer setting. Groundwater-level observations were grouped by aquifer, and observations from wells that are part of a formalized annual measurement campaign were placed into separate groups with greater relative weights. Evangeline aquifer wells in this higher weighted group that are located in Montgomery County were further divided into subgroups. Groundwater temporal difference observations and minimum level observations were calculated from the higher weighted groups and combined into a separate group. All the subgroups representing subsidence and compaction were assigned equal importance except for extensometer-measured-compaction, which was assigned a higher relative weight due to the observations representing compaction at discrete depth intervals. The combined relative importance of observation groups related to groundwater levels was set equal to the combined relative importance of observation groups related to subsidence. That is, before parameter estimation through history matching, the contribution to the objective function from the groundwater-level groups was equal to the contribution from the subsidence observations.

The parameter estimation algorithm of PESTPP-IES was run through 3 iterations requiring about 900 forward model runs (fig. 107). The ensemble resulting from the first iteration was chosen based on the model residuals and the statistical and spatial distribution of parameter values. As expected, the model fit to observations in iterations 2 and 3 was improved compared to iteration 1 (fig. 108). However, the spatial distribution of parameter values from these later iterations resulted in increased heterogeneity, and the statistical variance of the parameter ensemble decreased substantially. Given the regional, water-planning scope of the model and

the importance of conservatively estimating uncertainty in that setting, it was decided that maintaining parameter variance was of greater importance than reproducing historical observations to the levels yielded by iterations 2 and 3. Recent publications have shown that seeking an overly good reproduction of historical observations with a necessarily simplified model can lead to bias in important model-simulated outcomes (Knowling and others, 2020a, b).

Running the initial ensemble of 600 model realizations drawn from the prior parameter distribution resulted in 286 completed realizations. Before starting the first upgrade iteration, PESTPP-IES was used to identify and remove 19 of the 286 completed realizations based on a user-specified option ("bad_phi_sigma") to automatically remove realizations with an objective function greater than the mean objective function of the ensemble plus two standard deviations. The remaining 267 model realizations were run through the first upgrade iteration, in which 29 realizations failed to run to completion, and an additional 2 were removed by applying the "bad_phi_sigma" criteria in PESTPP-IES, leaving 236 completed realizations for use in the Posterior.

Based on visual inspection, the objective function distribution yielded by the Posterior had an approximately Gaussian distribution but with a tail extending towards higher objective function values. Therefore, the ensemble was conditioned to remove model realizations with an objective function equal to or greater than the 95th percentile. This resulted in a conditioned posterior ensemble of 224 model realizations out of the initial 236 model realizations for use in the Posterior.

A single realization (which is the GULF model) was selected from the Posterior, which represents the maximum a priori realization. That is, this realization represents the mean of the Prior and therefore is also near the Posterior mean. Conceptually, this realization represents the model inputs with minimum prior heterogeneity and is also the closest ensemble-method equivalent to the minimum error variance solution (Moore and Doherty, 2005; Doherty, 2015). However, it is best to minimize inferences drawn from and decisions based on this single realization (even if the realization is the minimum error variance) and instead base inferences on the simulated outcomes derived from evaluation with the Posterior, the results of which provide critical context related to the reliability of simulated outcomes.

Posterior Parameter Ensemble

The history-matched parameter values for the Posterior (figs. 7.1–7.7; table 8) represent updates to the initial values estimated in the Prior. In general, the history-matched parameter values were within the ranges of previously published values from Jacob (1941), Rose and others (1944), White and others (1944), Guyton and Rose (1945), Rorabaugh (1949), and Lang and others (1950) and agree with the current (2023) understanding of the spatial and temporal patterns of parameter uncertainty for the Gulf Coast aquifer system. These values were based on the Posterior, which was composed of

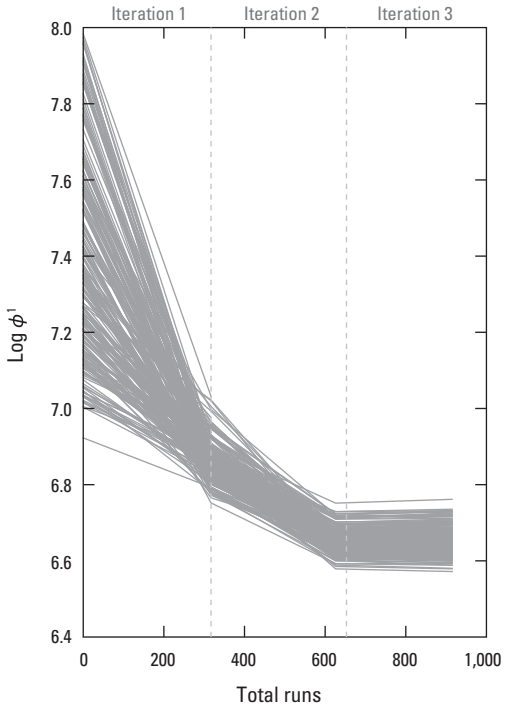

[1]The objective function (ϕ) is the sum of squared weighted residuals.

Figure 107. The posterior parameter ensemble objective function reduction over three iterations.

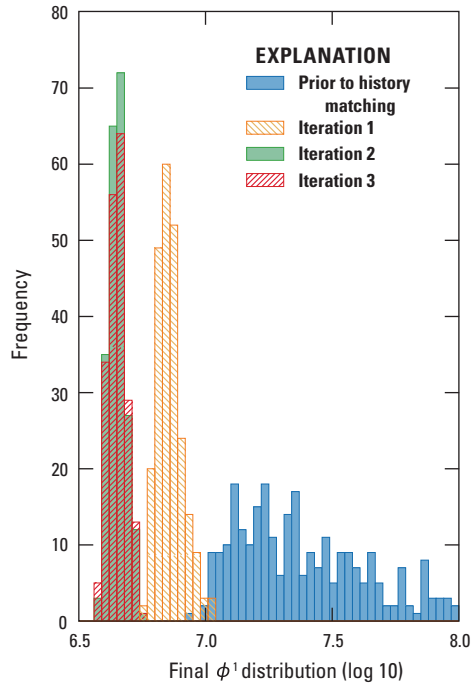

[1]The objective function (ϕ) is the sum of squared weighted residuals.

Figure 108. The posterior parameter ensemble distribution.

224 realizations drawn from the posterior parameter distribution; the GULF model is one of these realizations. Aquifer hydraulic conductivity and storage parameter values pertaining to the Posterior and to the GULF model are described in table 8.

The history-matched Posterior parameter values are shown on a set of violin plots in the following sections of this report. A violin plot is essentially a box plot that displays information about the underlying distribution of the plotted data, adding a rotated kernel density plot on each side (Hintze and Nelson, 1998; National Institute of Standards and Technology, 2015). The width of the violin plot shows the frequency of values, and the length of the violin plot shows the numerical range of values.

Hydraulic Conductivity and Vertical Anisotropy

The Posterior Kh values for all model layers are within the corresponding Prior range for each of the summary statistics (fig. 109). The parameter distributions generally were not at the upper or lower bounds (table 8), indicating that the history-matching process maintained the understanding of Kh encapsulated in the Prior. Of all the model layers, the Kh uncertainty in model layer 2 (Chicot aquifer) was reduced the most through the history-matching process, evidenced by the decreased range of values for the 25th, 50th, and 75th quantiles (fig. 109*B*). The Posterior vertical anisotropy also falls largely within the corresponding Prior range (fig. 110). The mean Posterior vertical anisotropy values for layer 1 (shallow groundwater system, fig. 110*A*) increased slightly compared to the Prior values, as did anisotropy for layer 3 (Evangeline aquifer, fig. 110*C*). However, expected variability in the Posterior anisotropy is maintained for each layer (figs. 110, 7.2).

Storage Parameters

The Posterior interbed storage and subsidence-related properties generally display expected and reasonable statistical and spatial patterns. The Posterior summary statistics show that the Posterior specific yield is largely in agreement with the corresponding Prior; the range of values spanned and the number of parameter values at or near the upper and lower bounds are similar for all model layers. Layer 2 specific-yield Prior and Posterior summary statistics display the confined/unconfined storage transition contained in this layer (figs. 111, 7.3). The gradational decrease in specific yield in layer 2 reflects the transition from unconfined to confined conditions where specific yield is set to zero.

The Posterior interbed (skeletal) elastic specific storage for model layers 2–5 did not change much from the Prior; however, the values decreased somewhat during history matching (fig. 112). The Posterior interbed (skeletal) inelastic storage for model layers 2–5 reveals a substantial reduction in variance compared to the prior parameter distribution (fig. 113) and maintains a reasonable spatial variation similar to that of the interbed elastic specific storage (figs. 7.4–7.5). The Posterior summary statistics for these quantities are approximately centered within the Prior range, indicating the Posterior mean is similar to the Prior mean (figs. 112–113). Interbed vertical hydraulic conductivity also did not change much from the Prior (fig. 114). The mean Posterior interbed porosity for layer 3 generally decreased across the model domain compared to that of the Prior, whereas the interbed porosity for model layer 4 generally increased (fig. 115). However, these Prior-to-Posterior changes are within the physically plausible range, with a few Posterior parameter values at or near a parameter bound.

In general, the fraction of fine-grained sediment for all model layers increased in the Posterior compared to the Prior. This indicates that, in general, a higher proportion of fine-grained sediment, yielding a larger equivalent interbed, could be needed to better reproduce historical groundwater-level and subsidence/compaction observations.

Groundwater Use

The Posterior groundwater-use parameters yielded simulation results that generally agree with the county-scale estimates of Oliver and Harmon (2022) (fig. 2.1). In counties where a substantial portion of the groundwater withdrawals were for irrigation, the simulated groundwater use differed from the estimated use. As described in the “Groundwater Use” section, however, irrigation groundwater-use estimates contain a high degree of uncertainty. Simulated groundwater use during the earlier stress periods was reduced (fig. 2.1) in order to delay the onset of simulated subsidence until stress period 3 (1912–25), towards the end of which is generally the time period when subsidence was first estimated to occur based on benchmark data (table 4). Otherwise, simulated subsidence would have begun about 1905, thus overpredicting the amount of subsidence through the remaining stress periods.

Net Groundwater Flow

Annual net groundwater flow in the Posterior to the Chicot aquifer was between 0.0 and 0.49 in. (fig. 116), most of which occurred in the northern third of the model area. Posterior groundwater flow to this unit was less than 0.06 in. during 1926 but increased to between 0.18 and 0.49 in. during 1975 (fig. 116). Posterior groundwater flow to this unit after 1975 was generally between 0.18 and 0.40 in. (fig. 116). By comparison, net groundwater flows to the Chicot aquifer in the NGC-GAM were 0.40 inch and 0.55 in. during 1977 and 2000, respectively (Kasmarek and Robinson, 2004), and 0.56 in. in the HAGM in 2009 (Kasmarek, 2012). In the GULF model, annual Posterior groundwater flow to the Chicot aquifer was 0.31 in. Annual groundwater flow to the Chicot aquifer in the GULF model progressively increased from less than 0.03 in. during 1926 to about 0.37 in. during 1977, after which annual groundwater flow was between 0.32 and 0.36 in. (fig. 116). The increase in simulated groundwater flow to the Chicot aquifer coincided with increases in the simulated hydraulic gradient resulting from a substantial increase in groundwater use between the 1940s and the 1970s (fig. 11; table 1). Offsetting this increase in simulated groundwater flow in the

Table 8. Hydraulic conductivity and storage parameter values pertaining to the GULF model and Posterior parameter distribution.

[ft/d, foot per day; GULF model, Gulf Coast Land Subsidence and Groundwater-Flow model; --, not available; 2.96E−06 means $2.96\times10^{-6} = 0.00000296$]

Aquifer property	Layer	Hydrogeologic unit (figs. 99–100)	Posterior parameter distribution				
			GULF model mean	GULF model 5th percentile	GULF model 95th percentile	Posterior parameter ensemble 5th percentile	Posterior parameter ensemble 95th percentile
Horizontal hydraulic conductivity (ft/d) (figs. 109, 7.1)	Layer 1	Shallow groundwater system[1]	14.79	3.95	33.55	1.46	43.55
	Layer 2	Chicot aquifer	11.06	4.12	20.39	2.76	30.19
	Layer 3	Evangeline aquifer	5.42	2.06	12.91	1.16	15.88
	Layer 4	Burkeville confining unit	0.06	0.03	0.11	0.01	0.21
	Layer 5	Jasper aquifer	0.62	0.27	1.15	0.16	2.16
	Layer 6	Catahoula confining unit	1.83	1.01	3.03	0.42	5.11
Vertical to horizontal hydraulic conductivity ratio (vertical anisotropy)[2] (figs. 110, 7.2)	Layer 1	Shallow groundwater system[1]	2.96E−06	1.46E−06	5.26E−06	8.49E−07	1.11E−05
	Layer 2	Chicot aquifer	9.01E−03	1.33E−04	3.39E−02	5.49E−05	6.12E−02
	Layer 3	Evangeline aquifer	2.59E−03	2.86E−05	1.22E−02	2.12E−05	1.67E−02
	Layer 4	Burkeville confining unit	2.05E−05	1.17E−05	3.41E−05	4.82E−06	7.91E−05
	Layer 5	Jasper aquifer	5.53E−03	2.52E−03	9.21E−03	1.21E−03	2.40E−02
	Layer 6	Catahoula confining unit	7.22E−03	3.66E−03	1.18E−02	1.71E−03	3.60E−02
Specific yield (unitless)[2] (figs. 111, 7.3)	Layer 1	Shallow groundwater system[1]	0.19	0.18	0.20	0.16	0.20
	Layer 2	Chicot aquifer	0.06	0.001	0.20	0.001	0.20
	Layer 3	Evangeline aquifer	0.20	0.19	0.20	0.17	0.20
	Layer 4	Burkeville confining unit	0.20	0.19	0.20	0.18	0.20
	Layer 5	Jasper aquifer	0.19	0.18	0.20	0.16	0.20
	Layer 6	Catahoula confining unit	0.19	0.17	0.20	0.16	0.20
Interbed (skeletal) elastic specific storage[3] (1/foot) (figs. 112, 7.4)	Layer 1	Shallow groundwater system[1]	--	--	--	--	--
	Layer 2	Chicot aquifer	2.33E−06	1.38E−06	4.43E−06	7.96E−07	5.81E−06
	Layer 3	Evangeline aquifer	1.56E−06	7.03E−07	3.96E−06	4.30E−07	4.59E−06
	Layer 4	Burkeville confining unit	1.39E−06	6.60E−07	3.77E−06	3.84E−07	4.25E−06
	Layer 5	Jasper aquifer	1.33E−06	6.52E−07	3.72E−06	3.63E−07	4.13E−06
	Layer 6	Catahoula confining unit	--	--	--	--	--

Table 8. Hydraulic conductivity and storage parameter values pertaining to the GULF model and Posterior parameter distribution.—Continued

[ft/d, foot per day; GULF model, Gulf Coast Land Subsidence and Groundwater-Flow model; --, not available; 2.96E−06 means $2.96\times10^{-6} = 0.00000296$]

Aquifer property	Layer	Hydrogeologic unit (figs. 99–100)	Posterior parameter distribution				
			GULF model mean	GULF model 5th percentile	GULF model 95th percentile	Posterior parameter ensemble 5th percentile	Posterior parameter ensemble 95th percentile
Interbed (skeletal) inelastic specific storage[3] (1/foot) (figs. 113, 7.5)	Layer 1	Shallow groundwater system[1]	--	--	--	--	--
	Layer 2	Chicot aquifer	6.15E−05	2.78E−05	1.20E−04	2.41E−05	1.38E−04
	Layer 3	Evangeline aquifer	3.65E−05	1.15E−05	1.07E−04	1.01E−05	1.12E−04
	Layer 4	Burkeville confining unit	3.17E−05	1.10E−05	1.08E−04	9.01E−06	1.06E−04
	Layer 5	Jasper aquifer	2.95E−05	1.04E−05	9.80E−05	8.51E−06	9.87E−05
	Layer 6	Catahoula confining unit	--	--	--	--	--
Interbed vertical hydraulic conductivity[3] (ft/d) (figs. 114, 7.6)	Layer 1	Shallow groundwater system[1]	--	--	--	--	--
	Layer 2	Chicot aquifer	6.62E−06	2.52E−06	2.08E−05	2.12E−06	2.17E−05
	Layer 3	Evangeline aquifer	4.34E−06	2.35E−06	1.23E−05	1.90E−06	1.27E−05
	Layer 4	Burkeville confining unit	3.94E−06	2.35E−06	1.11E−05	1.88E−06	1.03E−05
	Layer 5	Jasper aquifer	3.91E−06	2.33E−06	1.04E−05	1.86E−06	1.01E−05
	Layer 6	Catahoula confining unit	--	--	--	--	--
Interbed porosity[3] (unitless) (figs. 115, 7.7)	Layer 1	Shallow groundwater system[1]	--	--	--	--	--
	Layer 2	Chicot aquifer	0.37	0.27	0.49	0.21	0.56
	Layer 3	Evangeline aquifer	0.29	0.19	0.43	0.16	0.47
	Layer 4	Burkeville confining unit	0.27	0.18	0.43	0.14	0.46
	Layer 5	Jasper aquifer	0.26	0.18	0.41	0.14	0.44
	Layer 6	Catahoula confining unit	--	--	--	--	--
Coarse-grained elastic specific storage[3] (1/foot)	Layer 1	Shallow groundwater system[1]	9.53E−07	6.75E−07	1.35E−06	3.53E−07	2.08E−06
	Layer 2	Chicot aquifer	1.15E−06	8.10E−07	1.53E−06	4.79E−07	2.42E−06
	Layer 3	Evangeline aquifer	1.96E−06	1.28E−06	2.84E−06	8.70E−07	3.79E−06
	Layer 4	Burkeville confining unit	1.55E−06	1.07E−06	2.19E−06	6.31E−07	3.73E−06
	Layer 5	Jasper aquifer	1.27E−06	9.01E−07	1.68E−06	4.99E−07	2.72E−06
	Layer 6	Catahoula confining unit	7.81E−07	5.57E−07	1.05E−06	3.14E−07	1.82E−06

Table 8. Hydraulic conductivity and storage parameter values pertaining to the GULF model and Posterior parameter distribution.—Continued

[ft/d, foot per day; GULF model, Gulf Coast Land Subsidence and Groundwater-Flow model; --, not available; 2.96E−06 means $2.96\times10^{-6} = 0.00000296$]

Aquifer property	Layer	Hydrogeologic unit (figs. 99–100)	Posterior parameter distribution				
			GULF model mean	GULF model 5th percentile	GULF model 95th percentile	Posterior parameter ensemble 5th percentile	Posterior parameter ensemble 95th percentile
Coarse-grained porosity[3] (unitless)	Layer 1	Shallow groundwater system[1]	0.13	0.11	0.15	0.09	0.18
	Layer 2	Chicot aquifer	0.14	0.13	0.17	0.10	0.20
	Layer 3	Evangeline aquifer	0.12	0.10	0.13	0.08	0.15
	Layer 4	Burkeville confining unit	0.19	0.16	0.23	0.13	0.28
	Layer 5	Jasper aquifer	0.13	0.11	0.16	0.09	0.19
	Layer 6	Catahoula confining unit	0.16	0.13	0.18	0.11	0.22

[1]Layer 1 represents the upper 50 feet of each hydrogeologic unit and is used to route local-scale recharge flow from the outcrop area to model area streams.

[2]See the "Hydraulic Properties" section of the report for additional information.

[3]These model parameters are specified in the Skeletal Storage, Compaction, and Subsidence (CSUB) package (Hughes and others, 2022). The CSUB package is not active in layers 1 and 6. An interbed is a laterally discontinuous unit composed of fine-grained sediments.

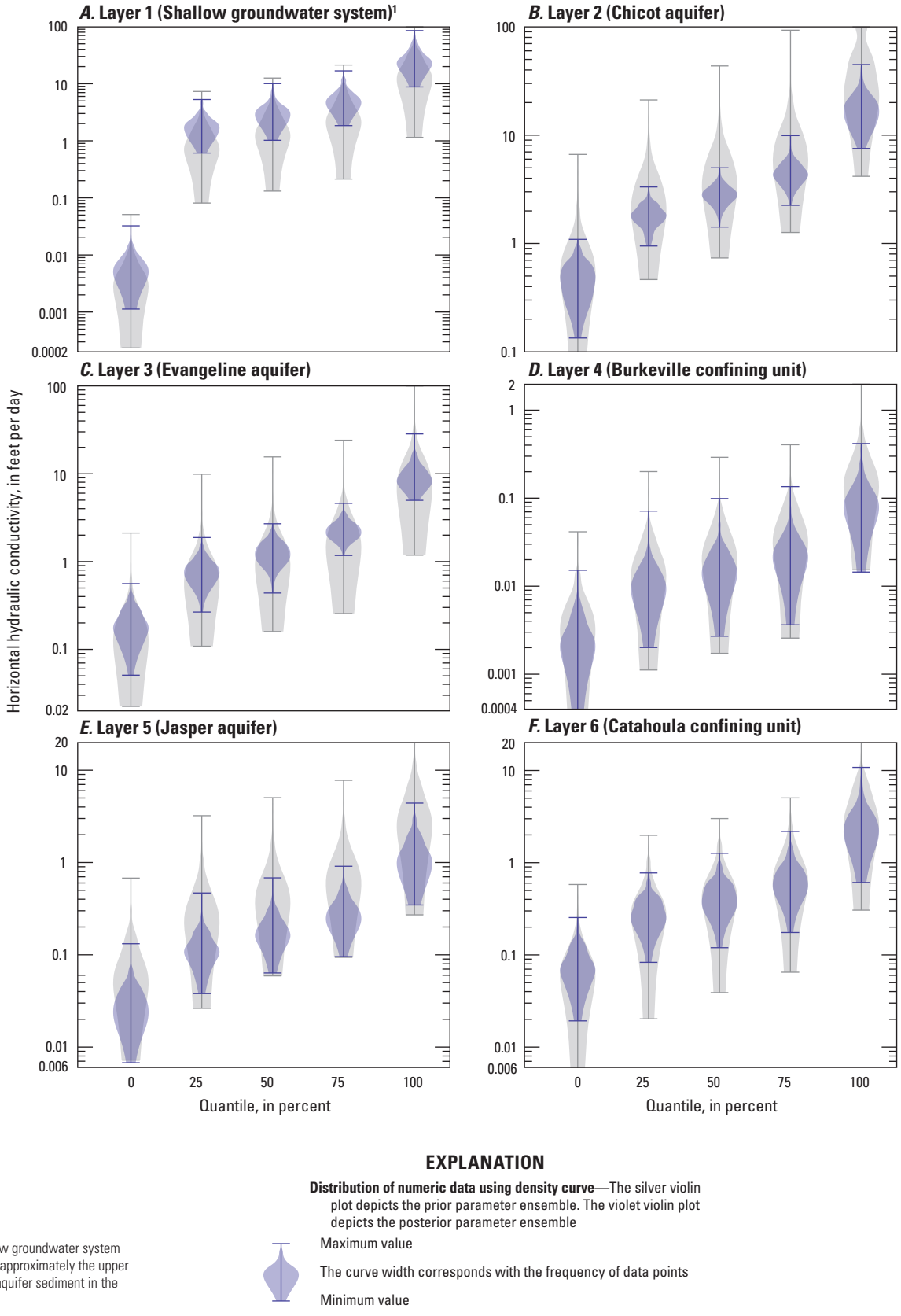

Figure 109. Violin plots showing the prior and posterior parameter ensemble horizontal hydraulic conductivity of *A*, Layer 1 (the shallow groundwater system), *B*, Layer 2 (the Chicot aquifer), *C*, Layer 3 (the Evangeline aquifer), *D*, Layer 4 (the Burkeville confining unit), *E*, Layer 5 (the Jasper aquifer), and *F*, Layer 6 (the Catahoula confining unit).

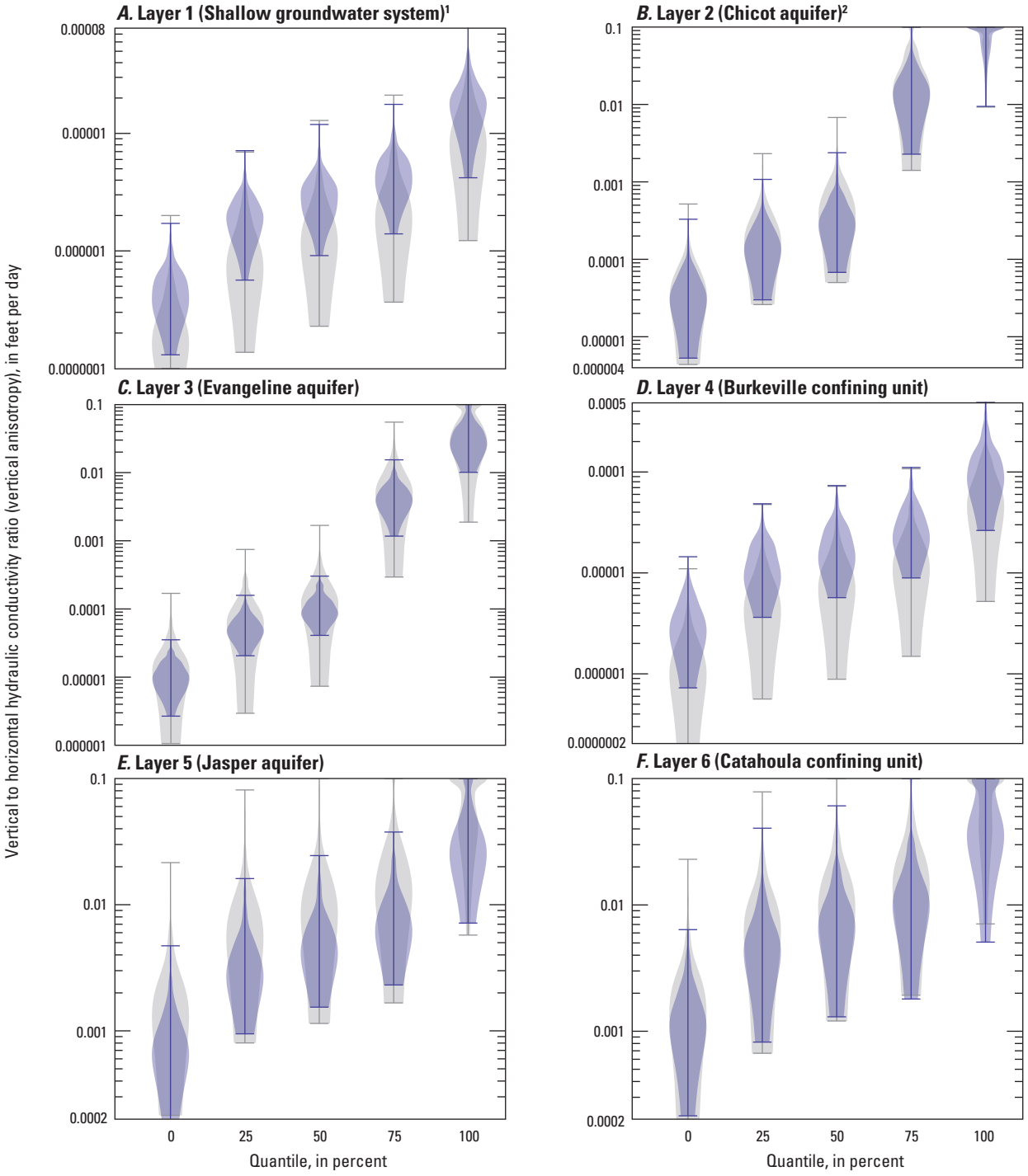

Figure 110. Violin plots showing the prior and posterior parameter ensemble vertical to horizontal hydraulic conductivity ratio of *A*, layer 1 (the shallow groundwater system), *B*, layer 2 (the Chicot aquifer), *C*, layer 3 (the Evangeline aquifer), *D*, layer 4 (the Burkeville confining unit), *E*, layer 5 (the Jasper aquifer), and *F*, layer 6 (the Catahoula confining unit).

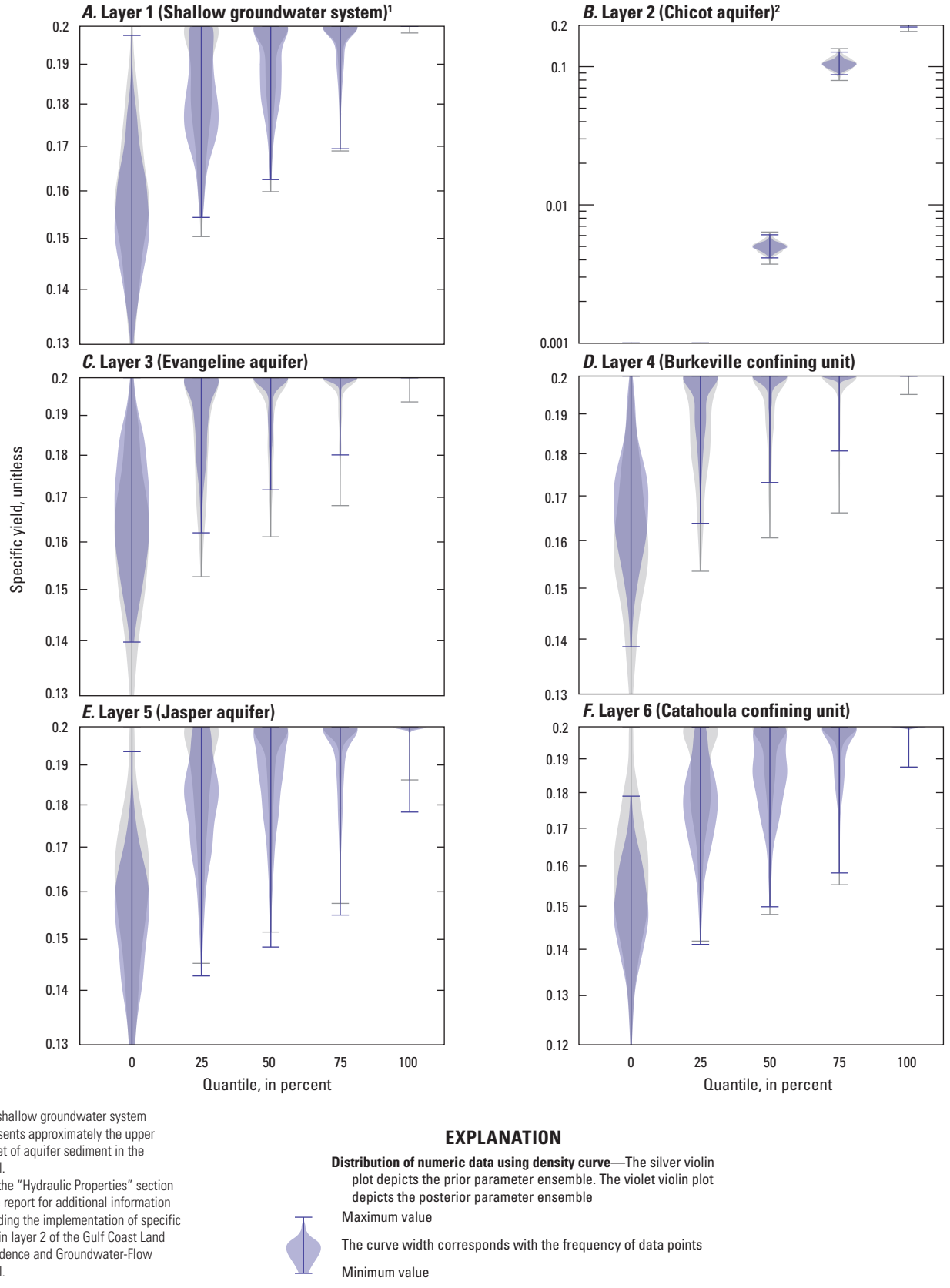

Figure 111. Violin plots showing the prior and posterior parameter ensemble specific yield of *A*, layer 1 (the shallow groundwater system), *B*, layer 2 (the Chicot aquifer), *C*, layer 3 (the Evangeline aquifer), *D*, layer 4 (the Burkeville confining unit), *E*, layer 5 (the Jasper aquifer), and *F*, layer 6 (the Catahoula confining unit).

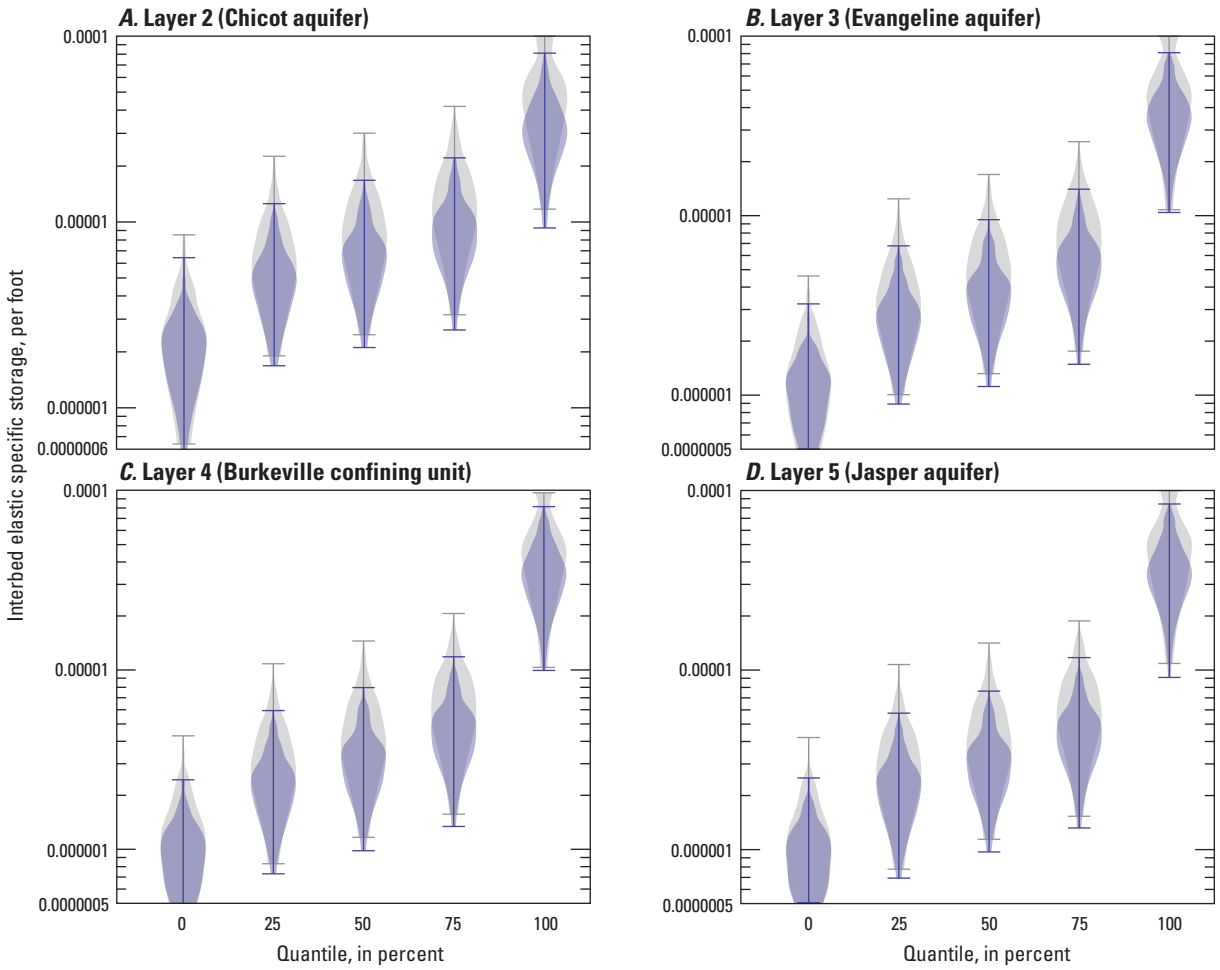

Figure 112. Violin plots showing the prior and posterior parameter ensemble interbed elastic specific storage of *A*, layer 2 (the Chicot aquifer), *B*, layer 3 (the Evangeline aquifer), *C*, layer 4 (the Burkeville confining unit), and *D*, layer 5 (the Jasper aquifer).

Chicot aquifer during this period was a decrease in simulated flow to the model area streams during this period. The stability of the observed groundwater levels in the shallow groundwater system was documented as early as 1931 in White and others (1944), and data at streamgages show relatively stable base-flow patterns that appear to be predominantly climate related (figs. 53–61). However, the actual rate of increased groundwater flow downdip that is caused by increased groundwater use may be small enough that the observed groundwater levels in the shallow groundwater system and base flow may be not altered.

Annual net groundwater flow in the Posterior to the Evangeline aquifer was between 0.09 and 0.33 in. (fig. 116). Posterior groundwater flow to this unit was between 0.10 and 0.25 in. prior to 1926, which increased to between 0.11 and 0.32 in. by the end of the simulation (fig. 116). By comparison, annual simulated groundwater-flow rates to the surficial exposure of the Evangeline aquifer in the NGC-GAM were 0.12 and 0.11 in. in 1977 and 2000, respectively (Kasmarek and Robinson, 2004), and 0.23 in. in the HAGM in 2009 (Kasmarek, 2012). In the GULF model, annual groundwater flow to the Evangeline aquifer in the GULF model slowly

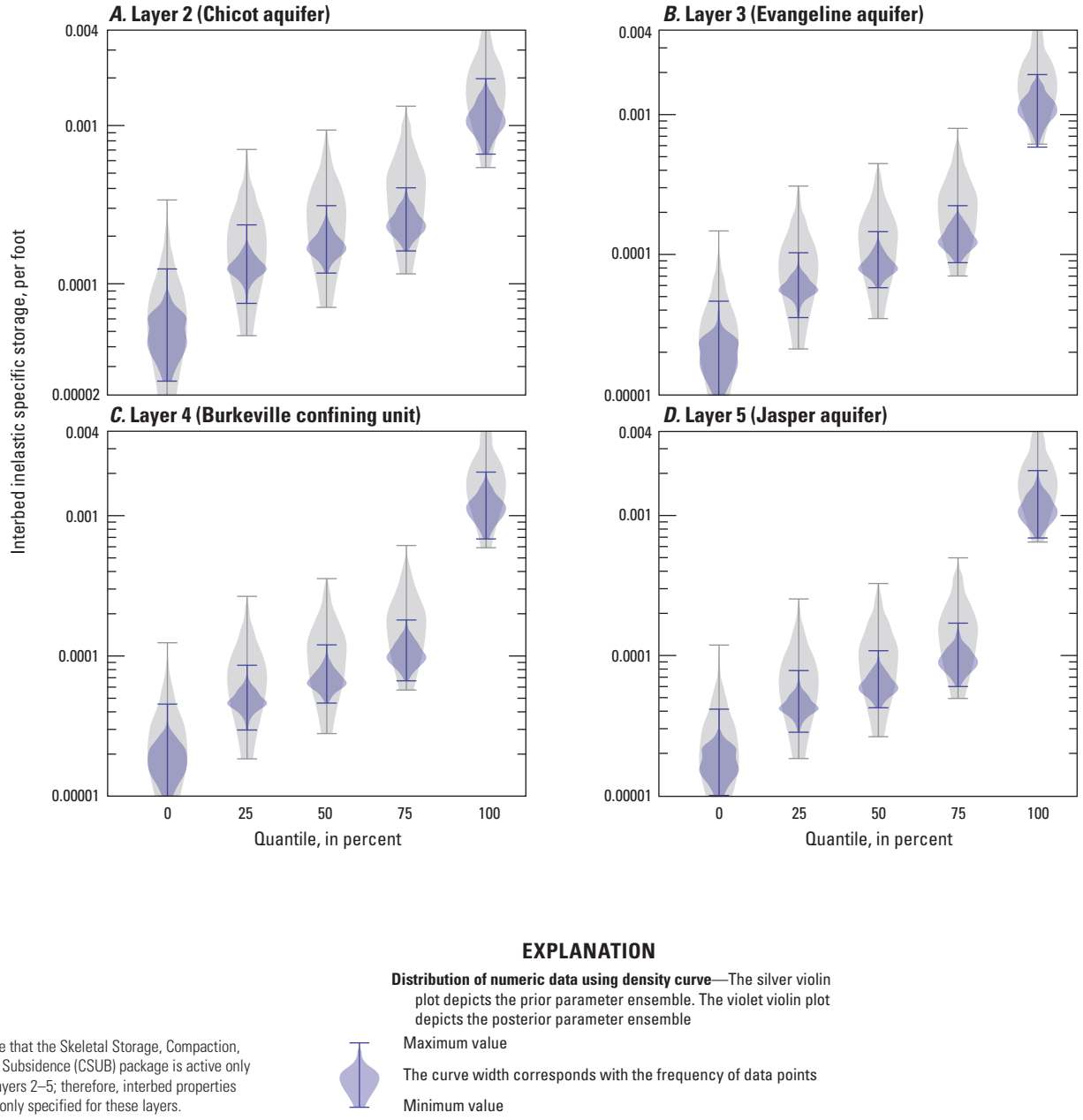

Figure 113. Violin plots showing the prior and posterior parameter ensemble interbed inelastic specific storage of *A*, layer 2 (the Chicot aquifer), *B*, layer 3 (the Evangeline aquifer), *C*, layer 4 (the Burkeville confining unit), and *D*, layer 5 (the Jasper aquifer).

increased from 0.16 in. prior to 1929 to 0.2 in. at the end of the simulation in 2018, and variations between stress periods were relatively minimal.

Annual net groundwater flow in the Posterior to the Jasper aquifer was between 0.01 and 0.07 in. (fig. 116). By comparison, the simulated groundwater-flow rates to the surficial exposure of the Jasper aquifer in the NGC-GAM were 0.06 and 0.07 in. in 1977 and 2000, respectively (Kasmarek and Robinson, 2004), and 0.07 in. in the HAGM in 2009 (Kasmarek, 2012). In the GULF model, the annual groundwater-flow rate to the Jasper aquifer was between 0.02 and 0.03 in., and variations between stress periods were minimal.

Annual net groundwater flow in the Posterior to the Catahoula confining unit was between 0.01 and 0.05 in. (fig. 116). In the GULF model, annual groundwater flow to the Catahoula confining unit was 0.03 in., and variations between stress periods were relatively minimal (fig. 116). The Catahoula confining unit has not been simulated in previous publicly available models; therefore, few comparisons can be made with other groundwater-flow estimates.

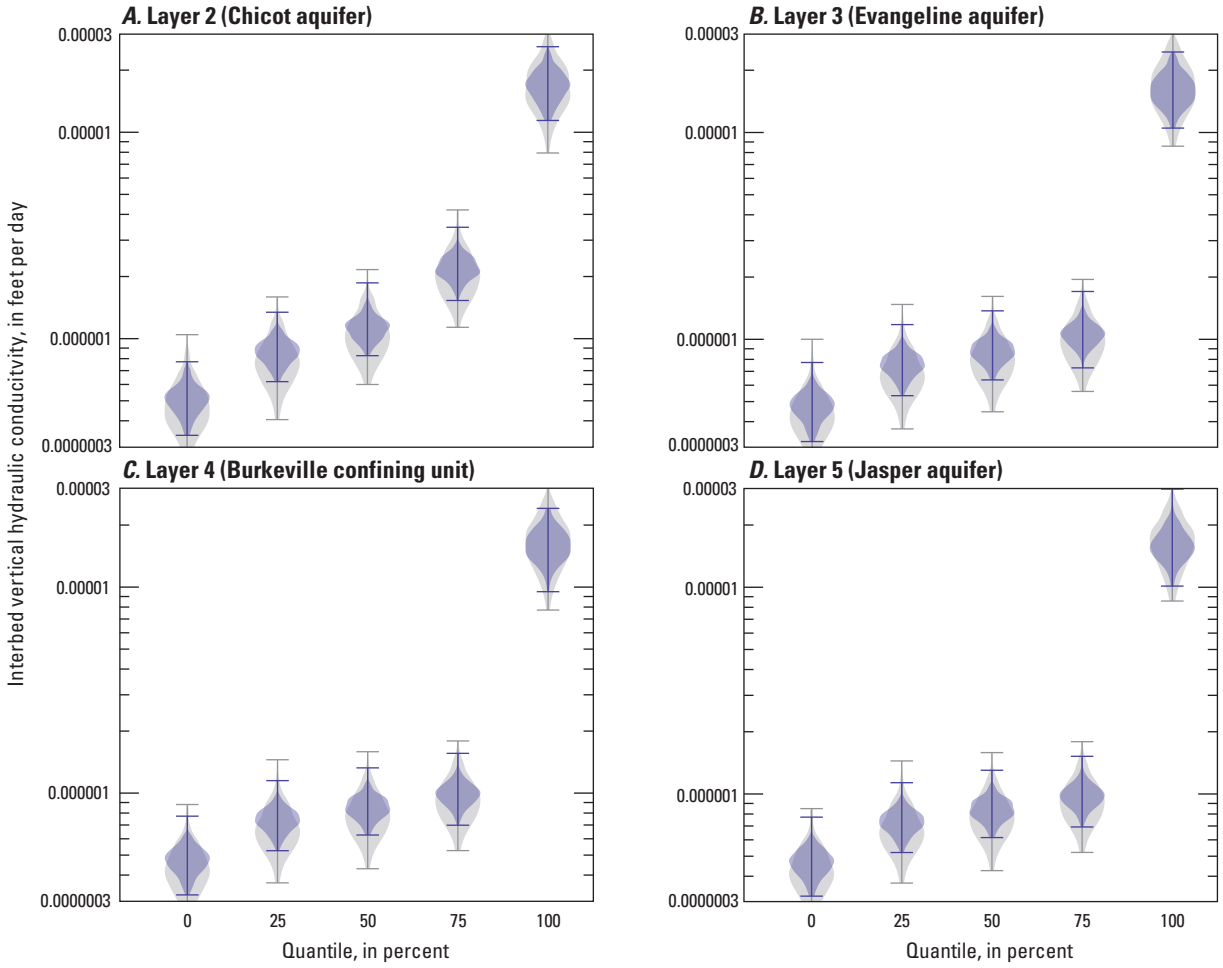

Figure 114. Violin plots showing the prior and posterior parameter ensemble interbed vertical hydraulic conductivity of *A*, layer 2 (the Chicot aquifer), *B*, layer 3 (the Evangeline aquifer), *C*, layer 4 (the Burkeville confining unit), and *D*, layer 5 (the Jasper aquifer).

The Posterior groundwater flow to the hydrogeologic units was relatively insensitive to adjustments to the recharge packages. This relative insensitivity resulted from the distance between the outcrop area where the majority of recharge occurs and the downdip area, combined with the low Kh, which was generally less than 30 ft/d in most areas and substantially less in many areas of the model.

Model Fit to Observations

The history-matched GULF model and ensemble fit to observations was evaluated based on the reduction of residuals between historical observations and the simulated equivalents. When plotting simulated groundwater levels or subsidence against measured groundwater levels or observed (or estimated) subsidence, all the points would plot on the one-to-one (1:1) correlation line if the simulated results perfectly matched the measured data. Similarly, when plotting the residuals

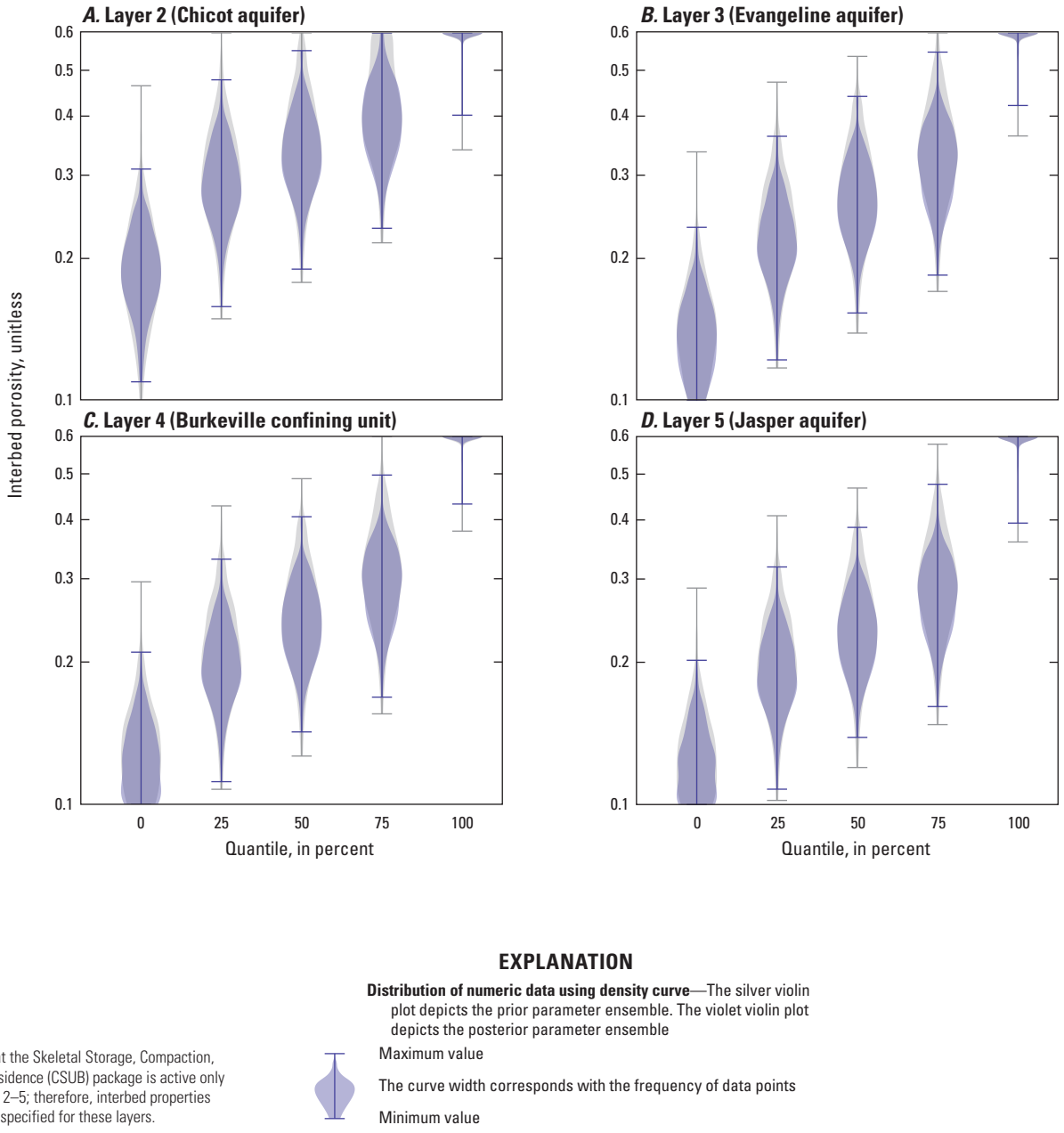

Figure 115. Violin plots showing the prior and posterior parameter ensemble interbed porosity of *A*, layer 2 (the Chicot aquifer), *B*, layer 3 (the Evangeline aquifer), *C*, layer 4 (the Burkeville confining unit), and *D*, layer 5 (the Jasper aquifer).

against the simulated groundwater levels, the residual between the measured data and simulated results would be zero if the simulated results matched the measured data perfectly. Additionally, when the simulated results are evaluated based on calculated mean residuals, a mean residual closest to zero indicates less model bias. Residuals were calculated as observed minus simulated values; positive residuals indicate lower simulated than observed values (undersimulated), and negative residuals indicate higher simulated than observed values (oversimulated). Note the 1:1 correlation and residual distribution plots refer only to the GULF model, whereas the observed and simulated plots present both the GULF model and Posterior results.

Groundwater Levels

A good agreement between the observed and GULF-model-simulated groundwater levels (fig. 117; table 7.3) was obtained, particularly at simulated wells in the greater Houston area (fig. 118). Most simulated groundwater levels in the Chicot and Evangeline aquifers plotted on or near the 1:1 line (fig. 117*A*,*C*), and the residuals follow a Gaussian

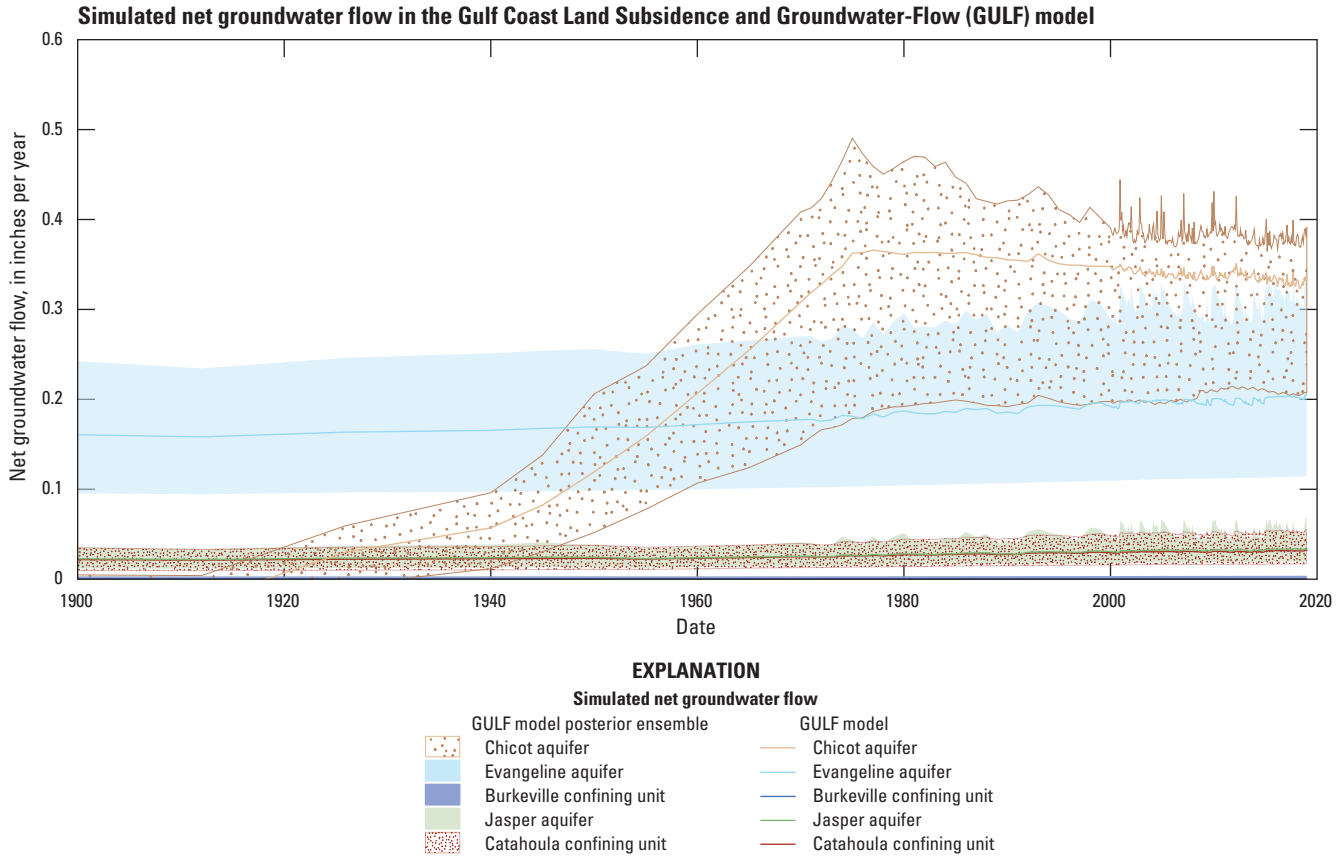

Figure 116. Temporal history-matched net groundwater flow to layer 2 (Chicot aquifer), layer 3 (the Evangeline aquifer), layer 4 (the Burkeville confining unit), and layer 5 (the Jasper aquifer), and layer 6 (the Catahoula confining unit).

distribution (fig. 117*B,D*). Jasper aquifer groundwater levels in the GULF model were generally oversimulated in much of the greater Houston area (figs. 119–121) but undersimulated in the northeastern model area (figs. 132, 138), shown by the greater frequency of values above the 1:1 line and negative residuals (fig. 117*E–F*). Catahoula confining unit groundwater levels in the GULF model were generally undersimulated in much of the model area (fig. 137–138), shown by the many values below the 1:1 line and negative residuals (fig. 117*I–J*). Relatively few groundwater measurements have been made in the Burkeville confining unit relative to the Chicot, Evangeline, and Jasper aquifers (table 7.2). Because this unit is not a major source of groundwater in the model area, and the adjustment of parameter values did not yield substantial changes in the simulated groundwater levels in this layer, further calibration in this layer was not attempted.

The ranges of simulated groundwater levels in the hydrographs produced by the Posterior realizations generally bracket historical groundwater-level observations at most of the groundwater wells included in the model (figs. 119–138). The simulated groundwater levels from the predevelopment period through 2018 generally matched the pattern of the observed groundwater levels. Selected wells from figures 17–36 and 51–52 were not included in the model observation dataset if they were near another well or if the screened interval of the well intersected multiple geologic units and thus withdrew water from more than one aquifer. Wells that are included on three related sets of figures (figs. 19–36, 51–52, 119–138) share the same letter identifiers (for example, well 292337094542801 is referred to as well "C" on figures 33 and 133; table 8.1).

Groundwater levels in the Jasper aquifer, and to a lesser degree in the Evangeline aquifer, were generally oversimulated in Montgomery County and in northern Harris County (figs. 120–122). Simulated groundwater levels were similar to observed groundwater levels in the Jasper aquifer in these areas during 1980–90; however, the substantial groundwater-level decline after 1990 was only partially reproduced in the simulation. The history matching to groundwater levels in the Jasper aquifer was complicated by the use of one model layer per hydrogeologic unit in the GULF model. The lower part of the geologic units that contain the Jasper aquifer consist of a greater percentage of fine-grained sediment compared to the upper part (Popkin, 1971); thus, most groundwater is withdrawn from the upper part of the Jasper aquifer. This could explain the difficulty of matching to observed groundwater levels in the Jasper aquifer, where the simulated values were generally greater than the observed values (figs. 120–122).

In northwestern Harris County and in Waller County, groundwater levels in the Evangeline aquifer (where groundwater-level observations were available) were undersimulated through most of the model period (1897–2018;

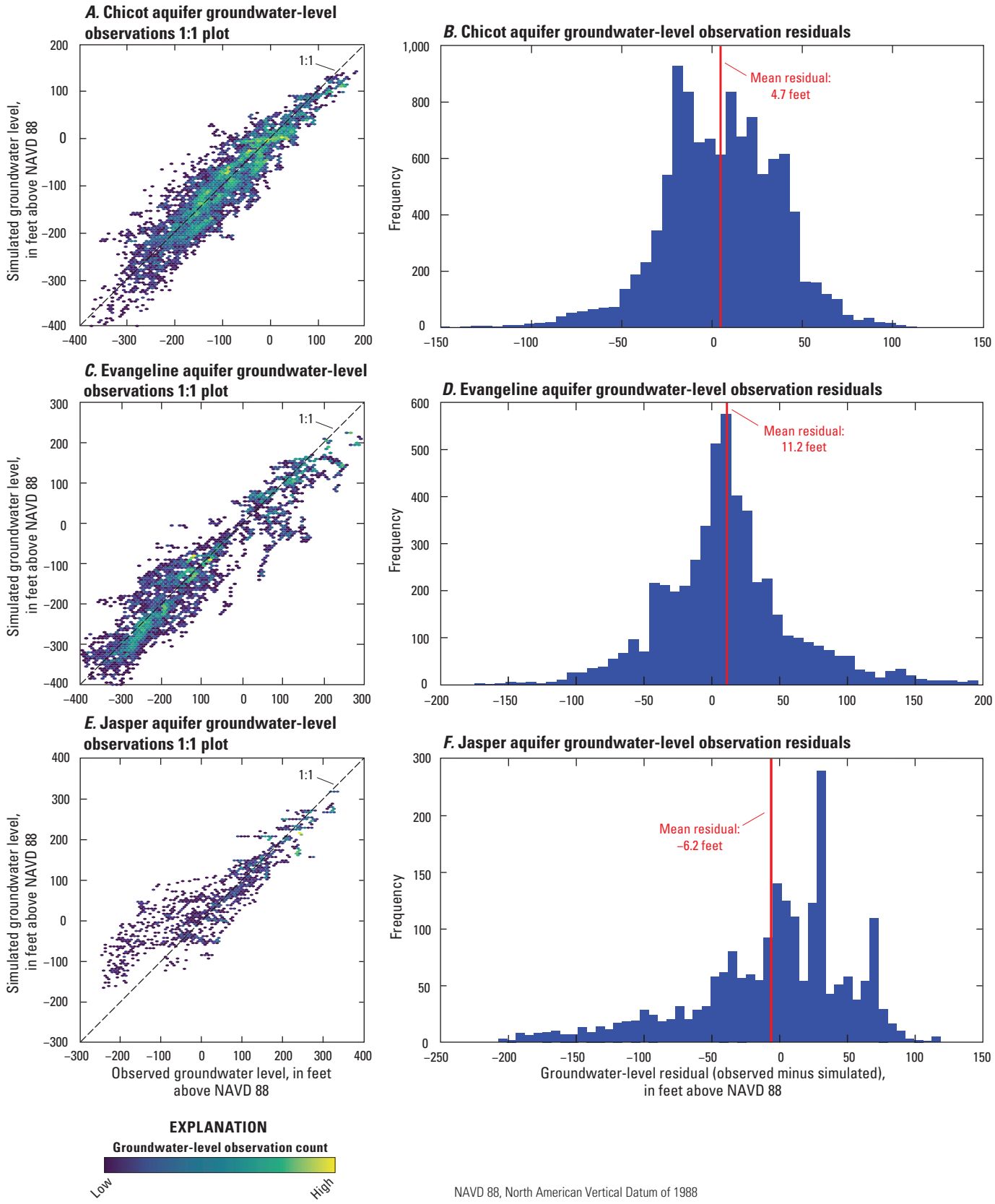

Figure 117. *A*, Chicot aquifer (layer 2) observed and simulated groundwater levels and *B*, groundwater-level residual distributions; *C*, Evangeline aquifer (layer 3) observed and simulated groundwater levels and *D*, groundwater-level residual distributions; *E*, Jasper aquifer (layer 5) observed and simulated groundwater levels and *F*, groundwater-level residual distributions; *G*, Burkeville confining unit (layer 4) observed and simulated groundwater levels and *H*, groundwater-level residual distributions; *I*, Catahoula confining unit (layer 6) observed and simulated groundwater levels and *J*, groundwater-level residual distributions, Gulf Coast Land Subsidence and Groundwater-Flow model.

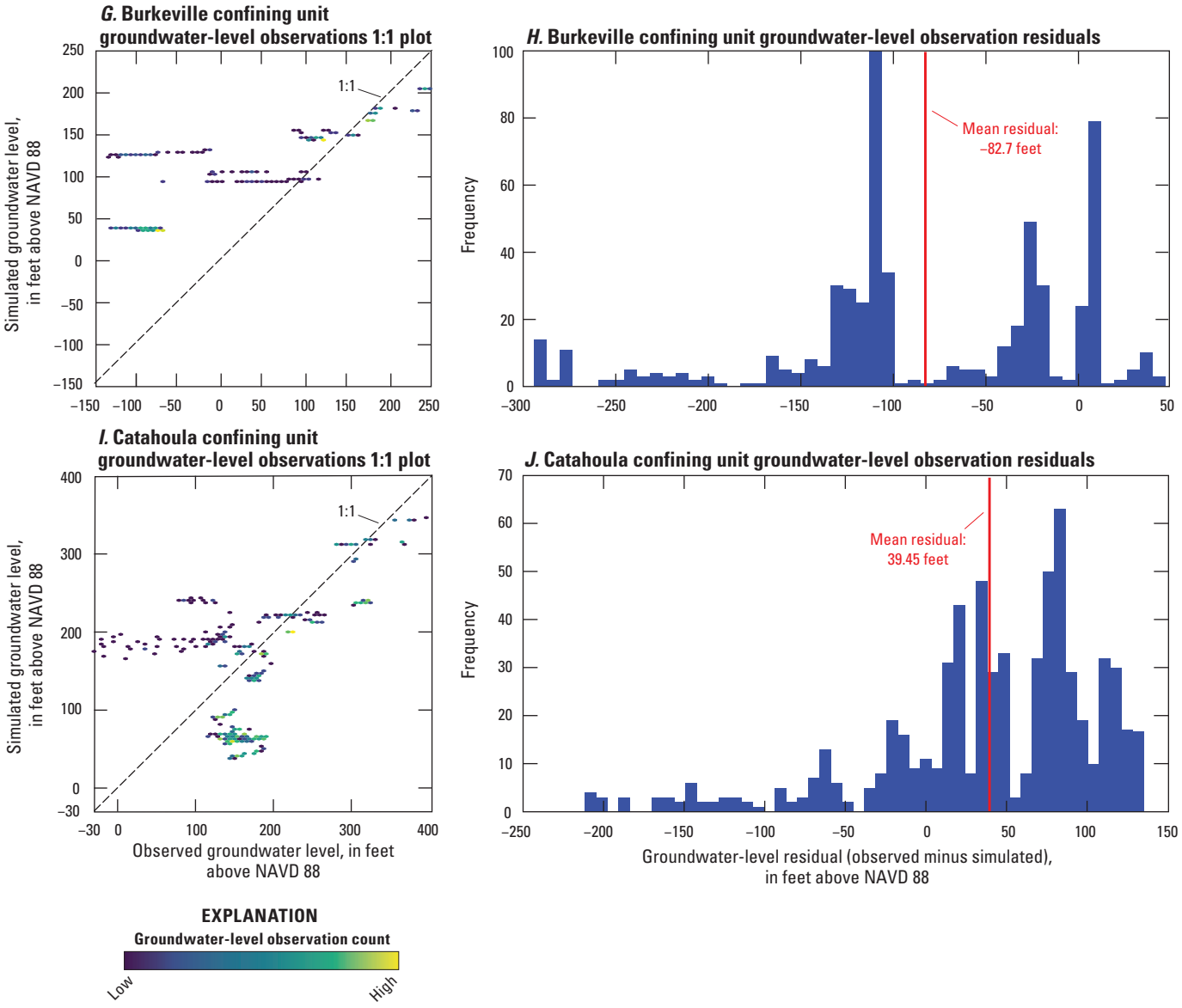

NAVD 88, North American Vertical Datum of 1988

Figure 117.—Continued

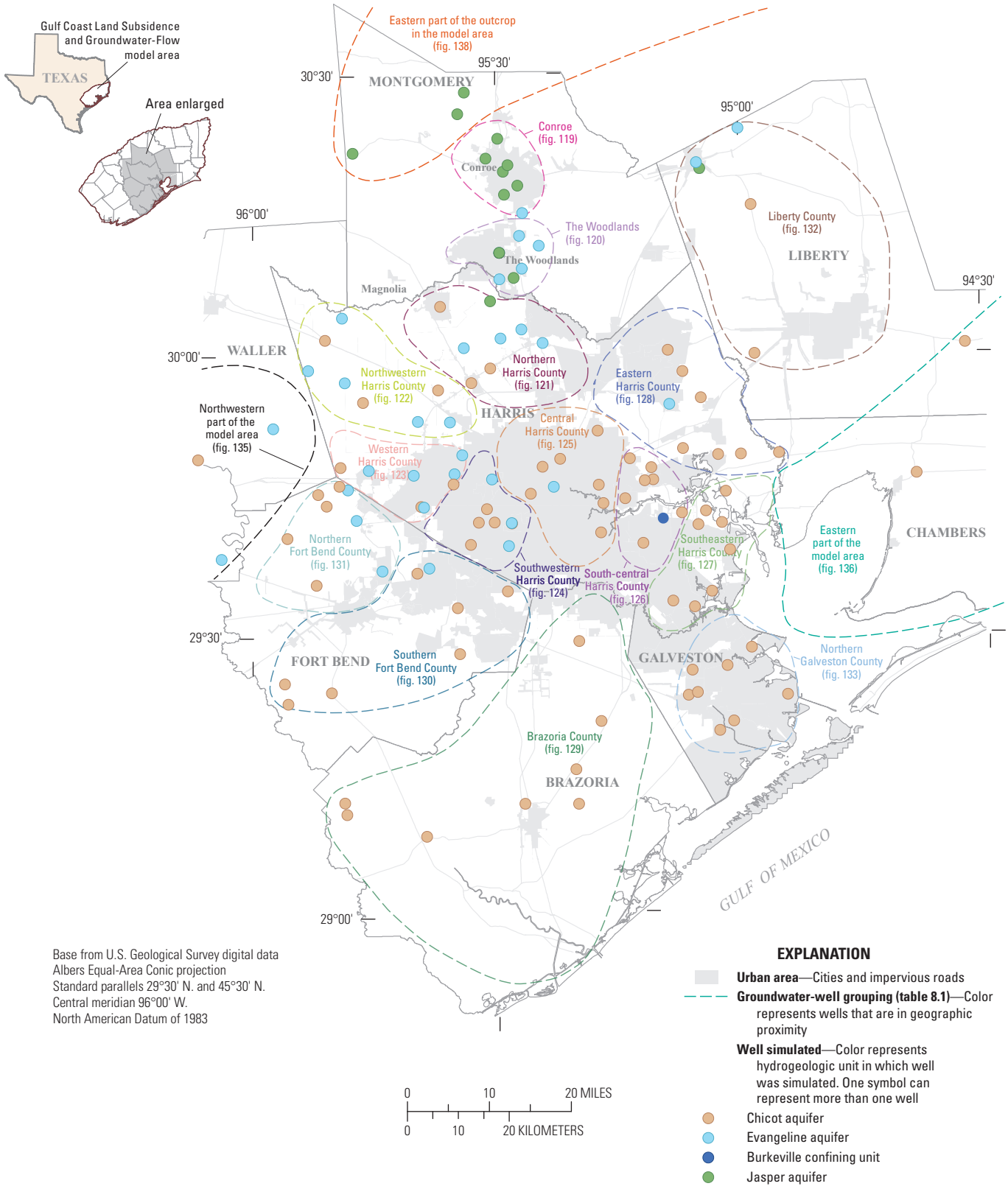

Figure 118. Locations of groundwater wells used for simulation in the Gulf Coast Land Subsidence and Groundwater-Flow model, in the greater Houston area.

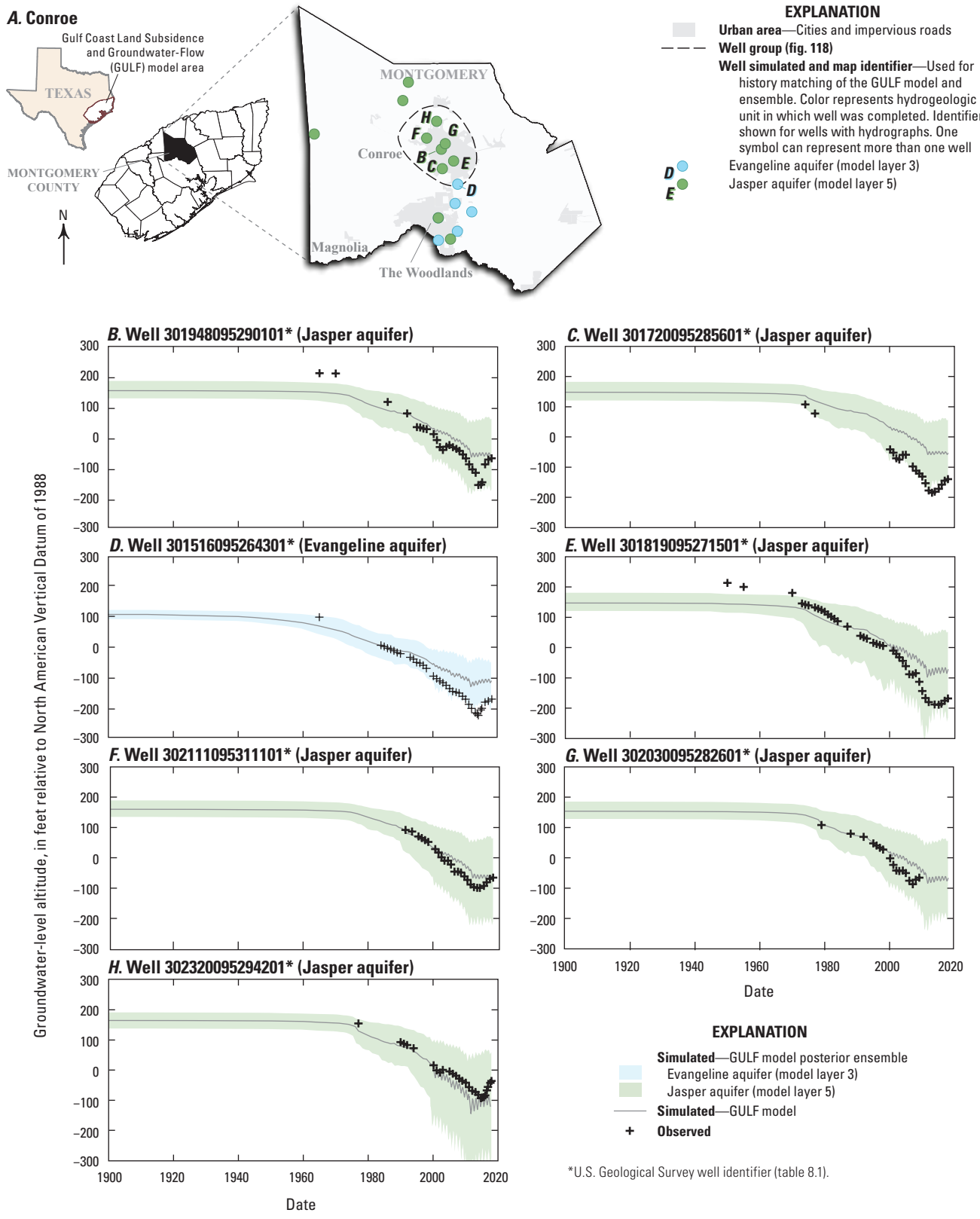

Figure 119. Observed and simulated groundwater levels in and near Conroe, Texas.

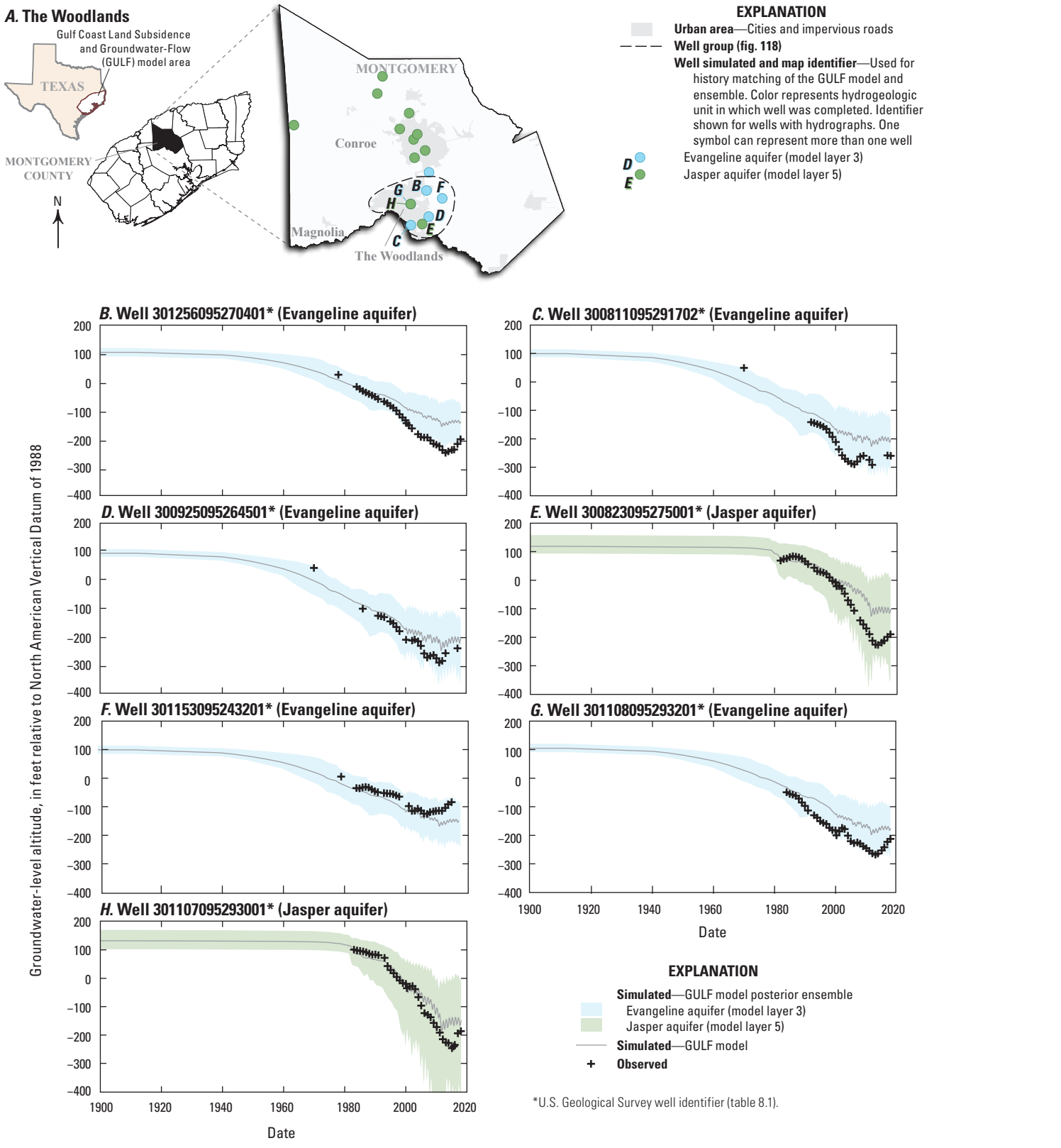

Figure 120. Observed and simulated groundwater levels in and near The Woodlands in Montgomery County, Texas.

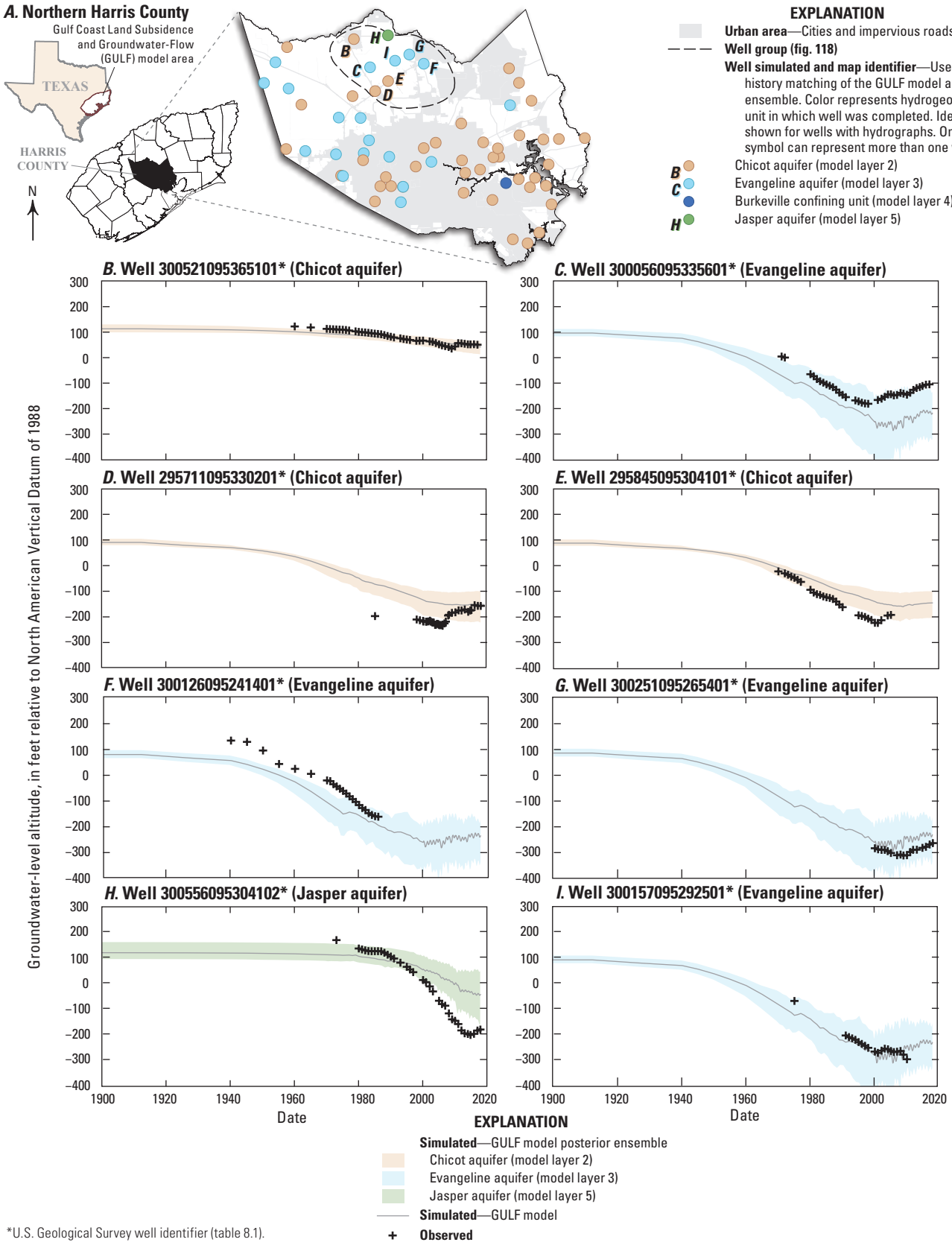

*U.S. Geological Survey well identifier (table 8.1).

Figure 121. Observed and simulated groundwater levels in and near northern Harris County in southeast Texas.

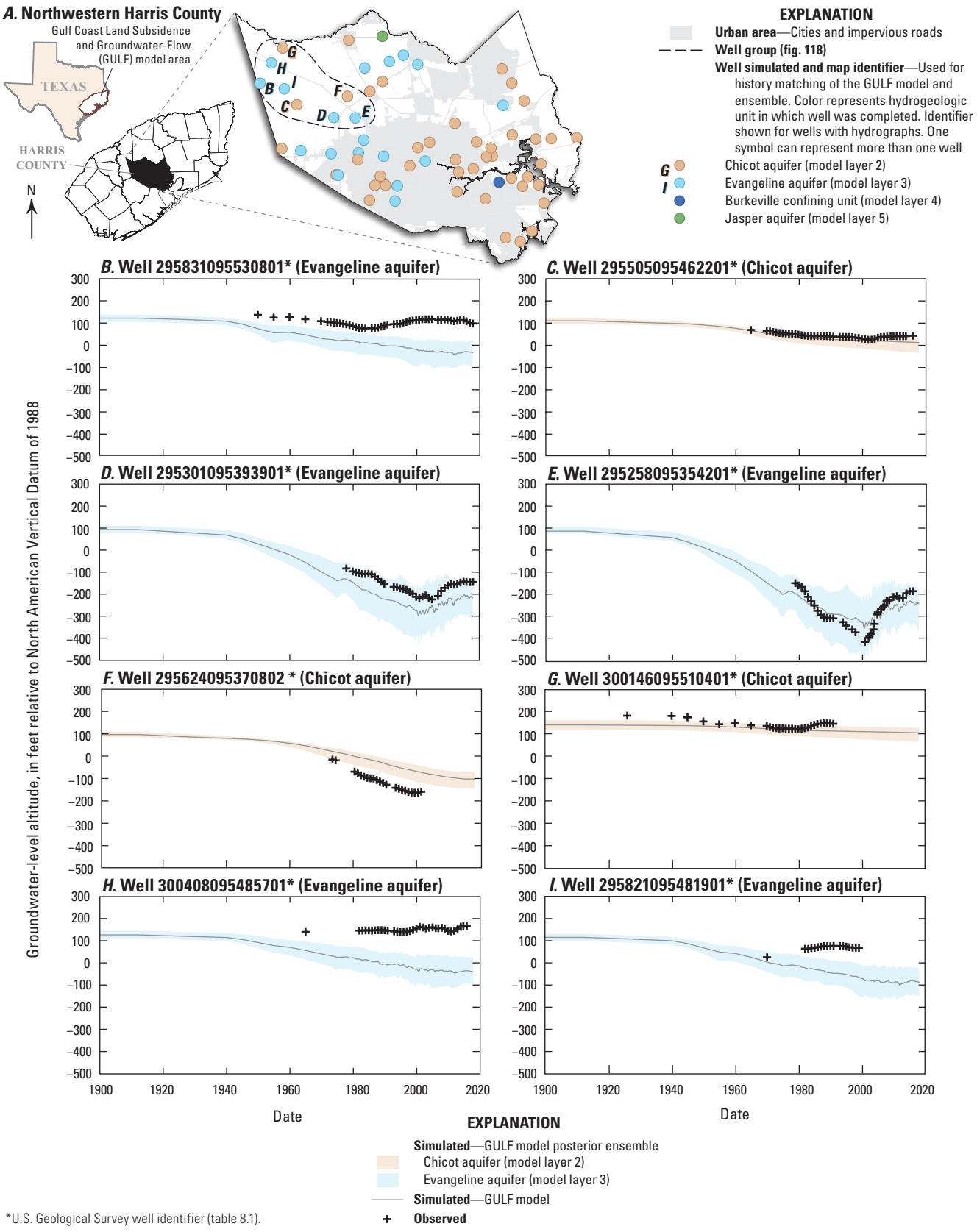

*U.S. Geological Survey well identifier (table 8.1).

Figure 122. Observed and simulated groundwater levels in and near northwestern Harris County in southeast Texas.

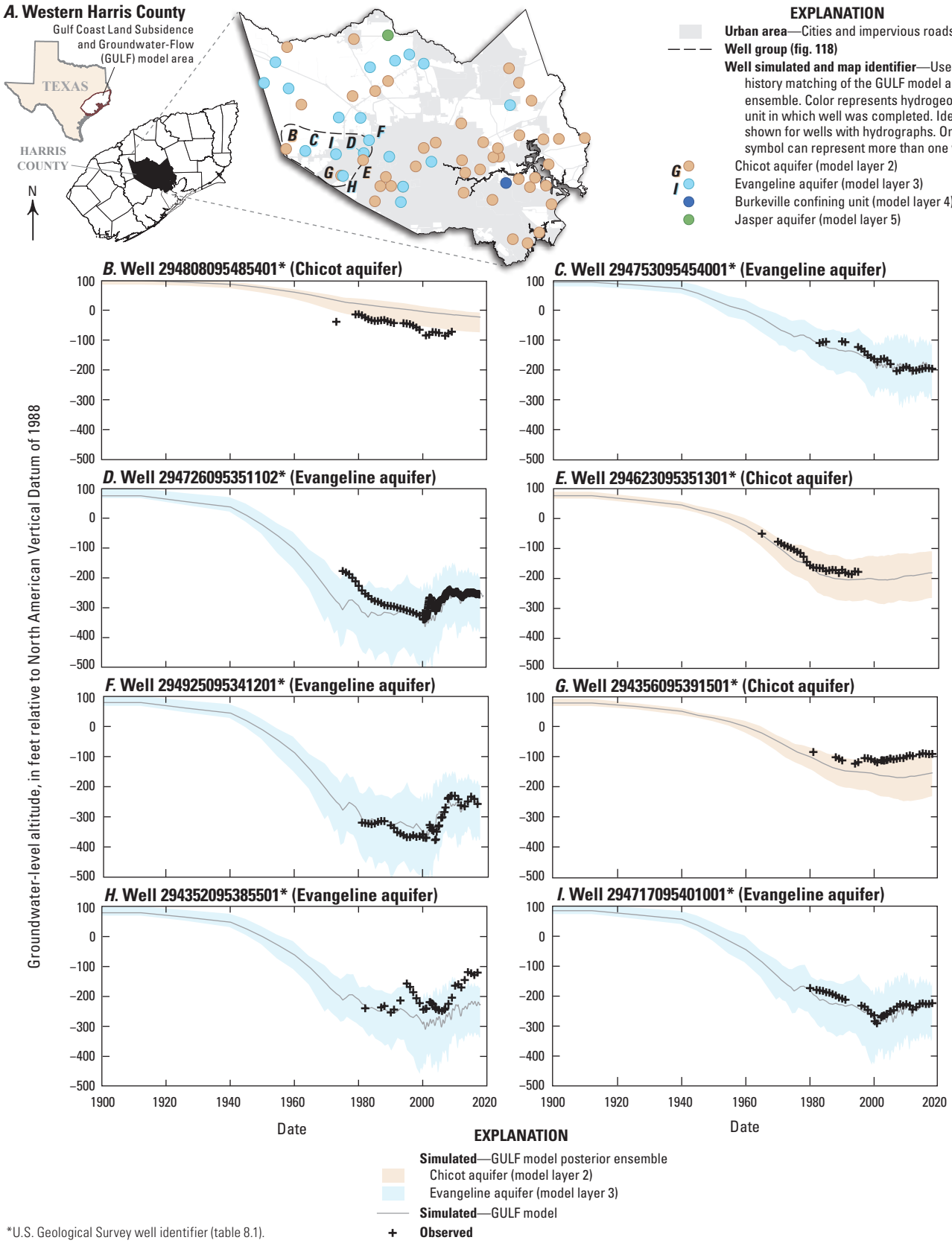

Figure 123. Observed and simulated groundwater levels in and near western Harris County in southeast Texas.

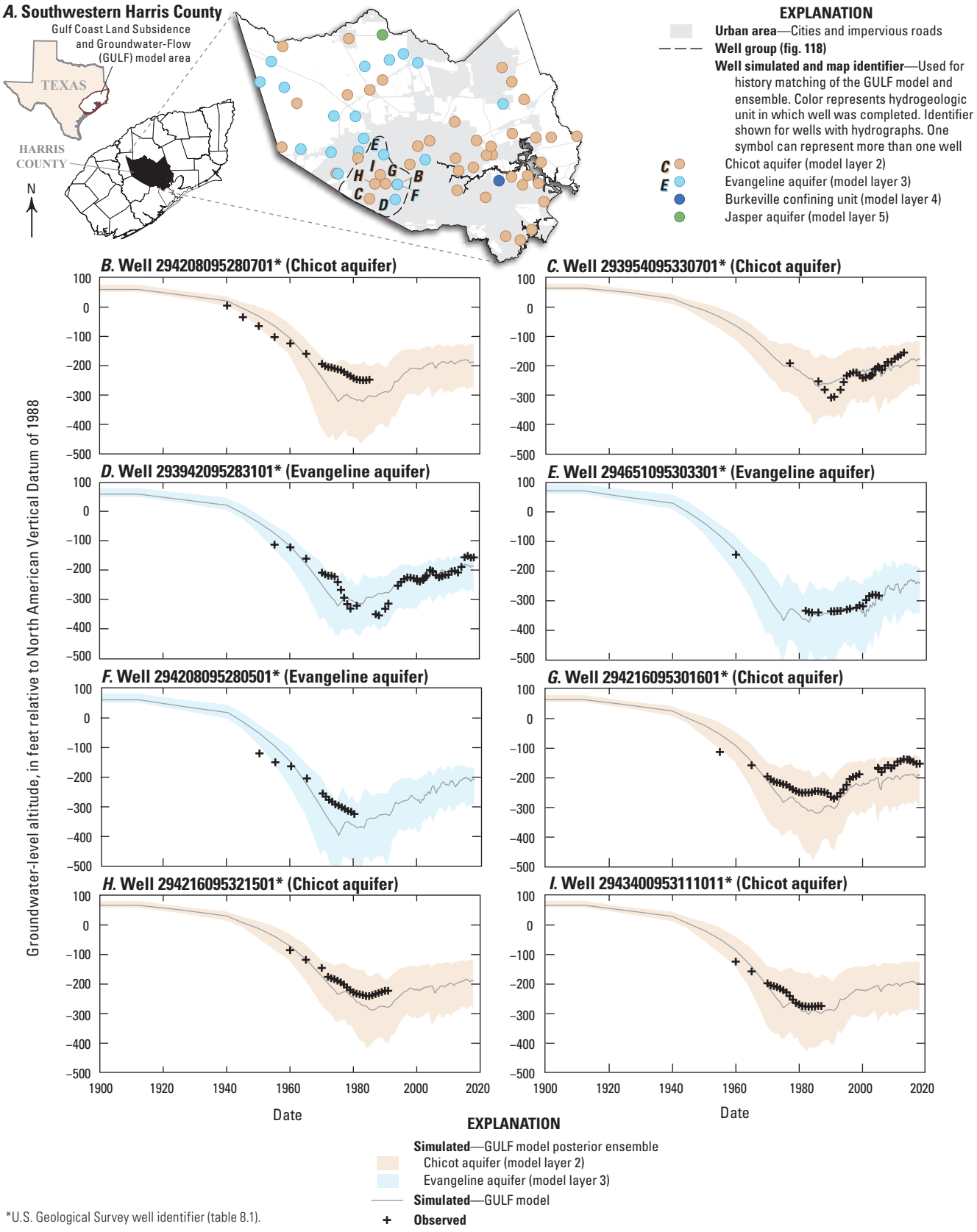

*U.S. Geological Survey well identifier (table 8.1).

Figure 124. Observed and simulated groundwater levels in and near southwestern Harris County in southeast Texas.

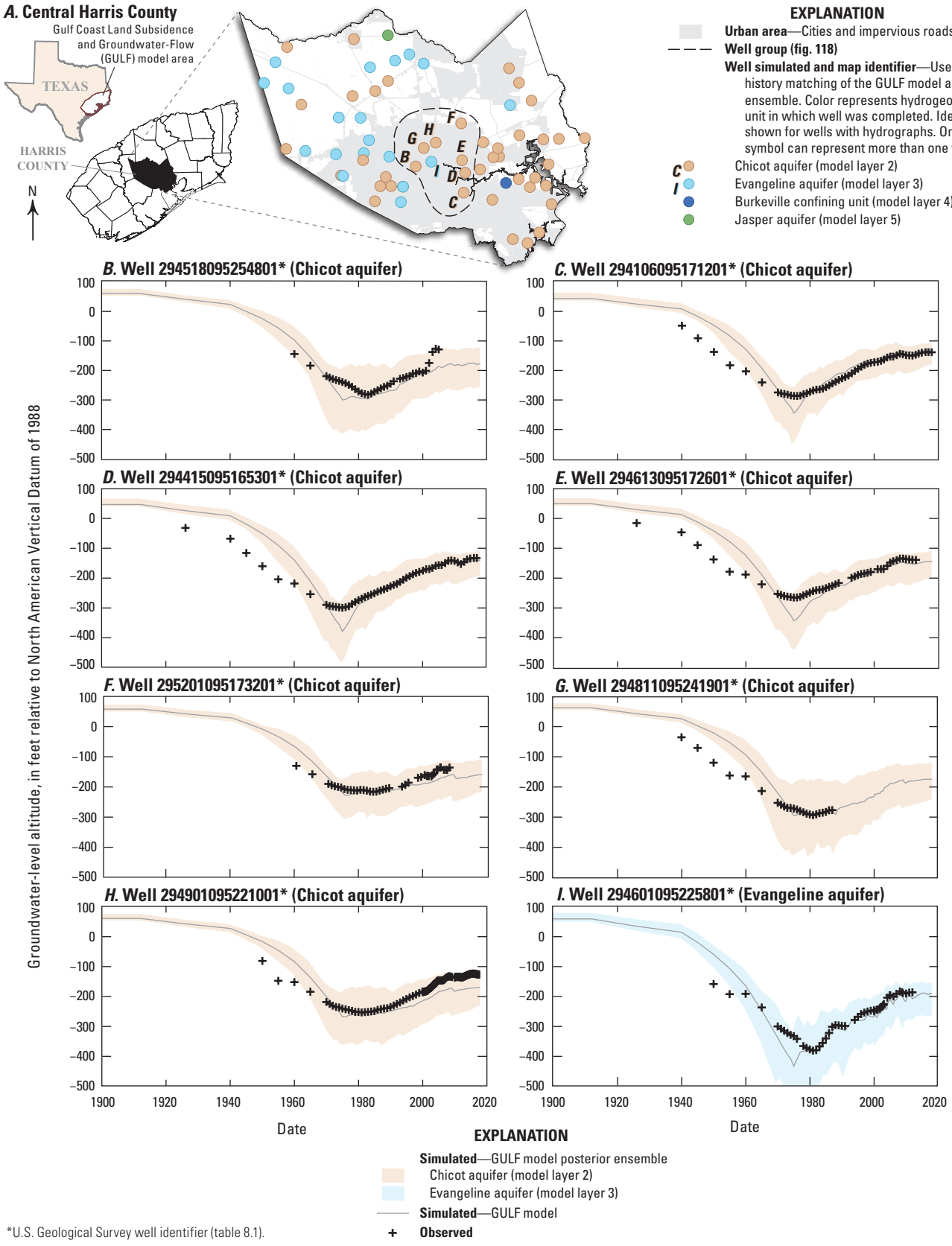

Figure 125. Observed and simulated groundwater levels in and near central Harris County in southeast Texas.

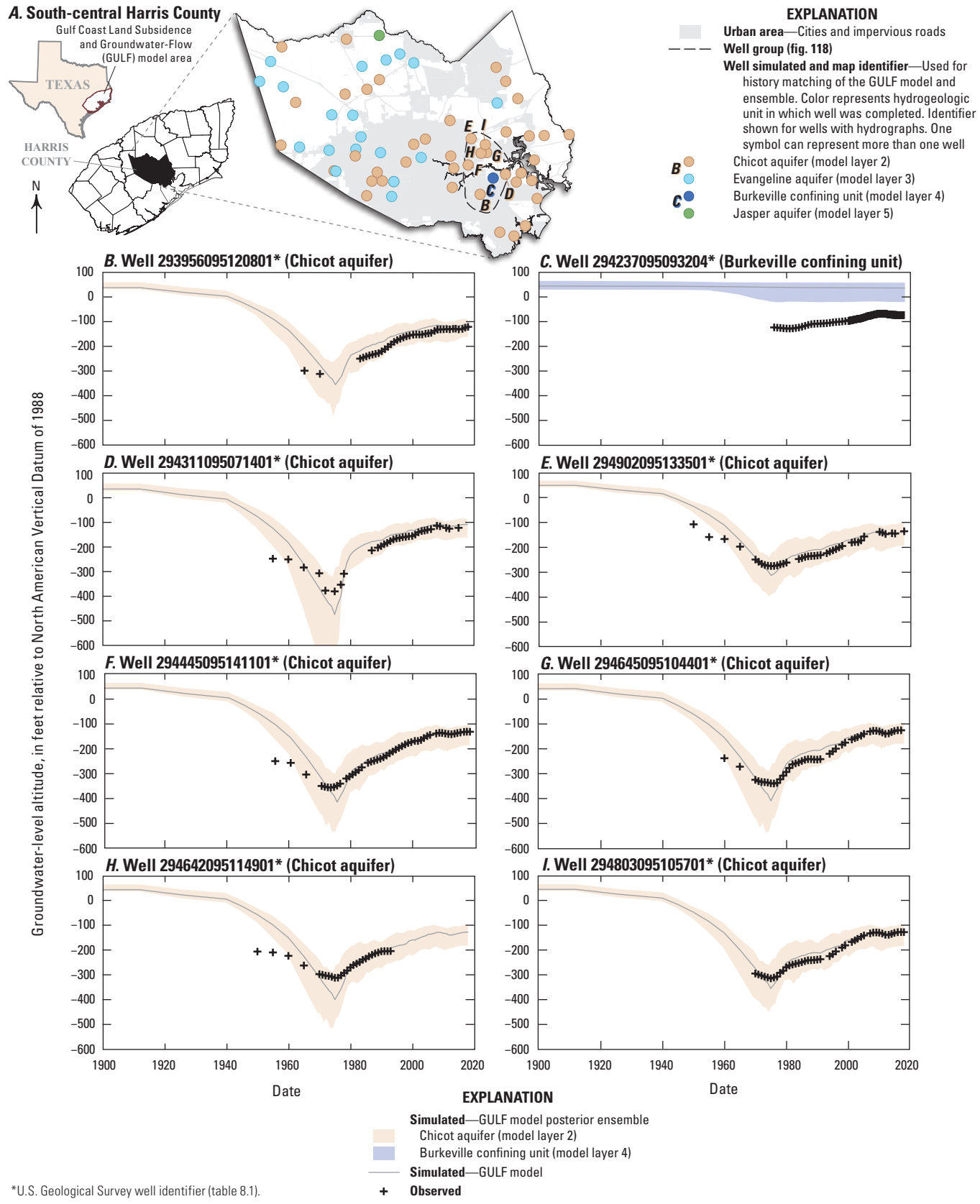

Figure 126. Observed and simulated groundwater levels in and near south-central Harris County in southeast Texas.

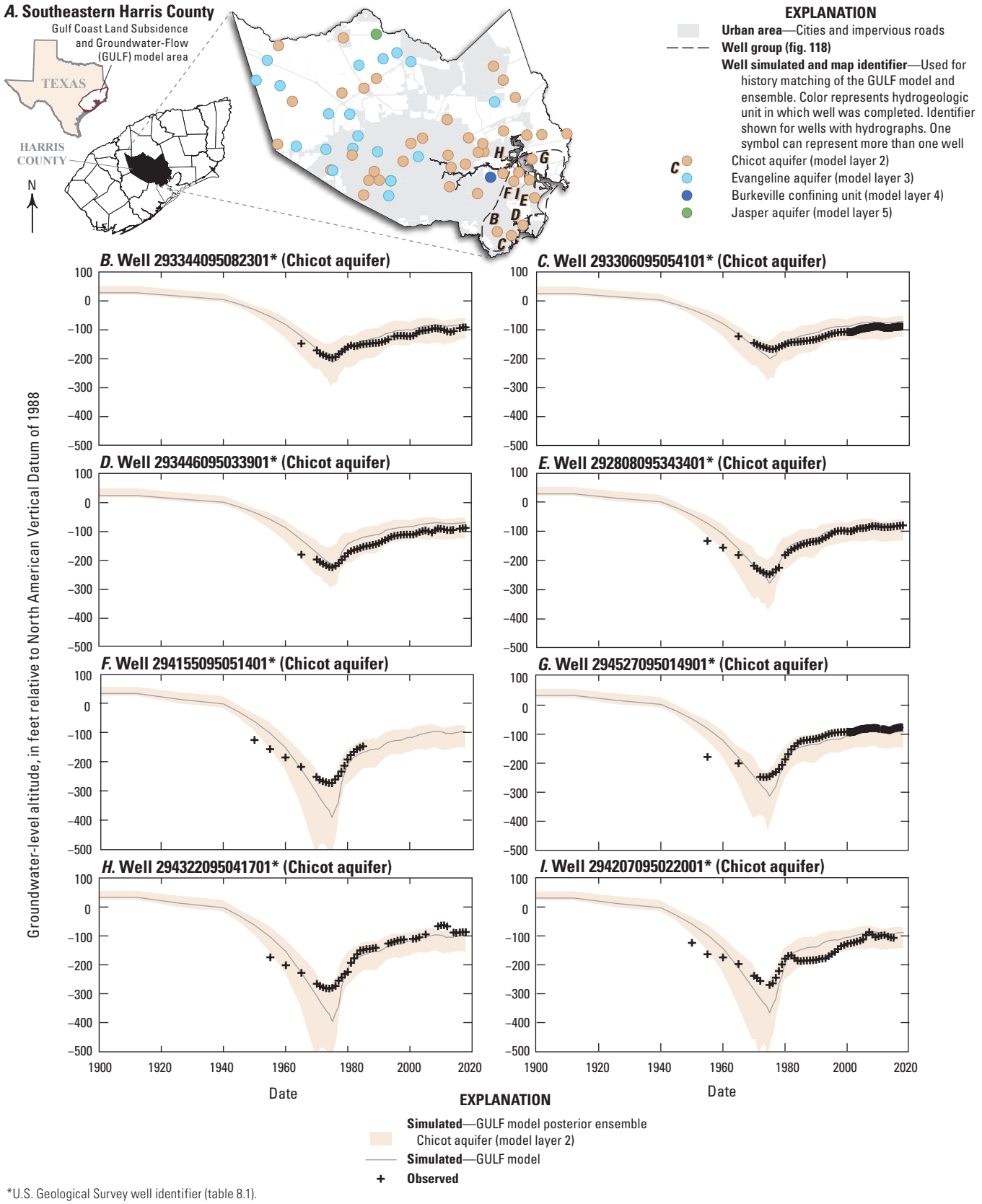

*U.S. Geological Survey well identifier (table 8.1).

Figure 127. Observed and simulated groundwater levels in and near southeastern Harris County in southeast Texas.

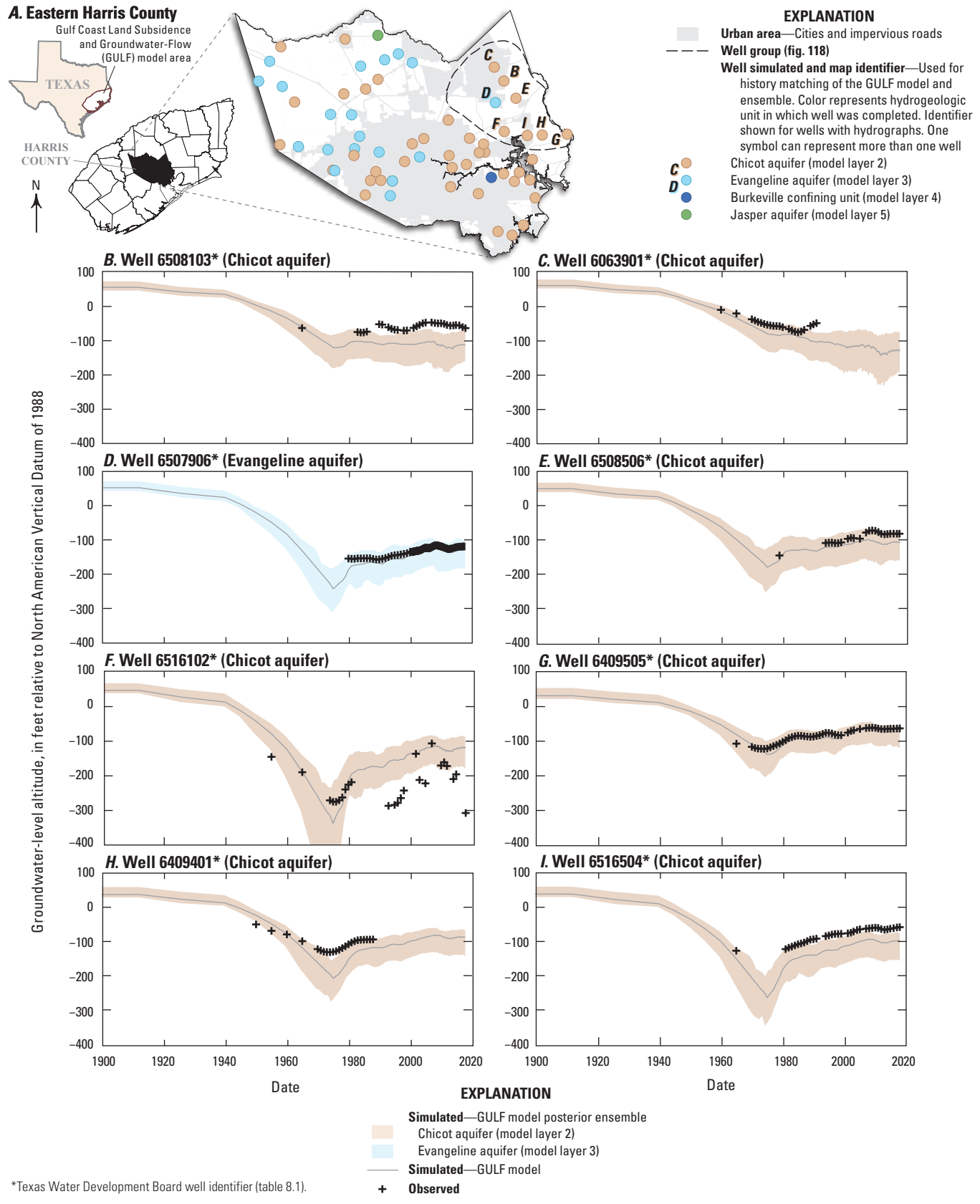

*Texas Water Development Board well identifier (table 8.1).

Figure 128. Observed and simulated groundwater levels in and near eastern Harris County in southeast Texas.

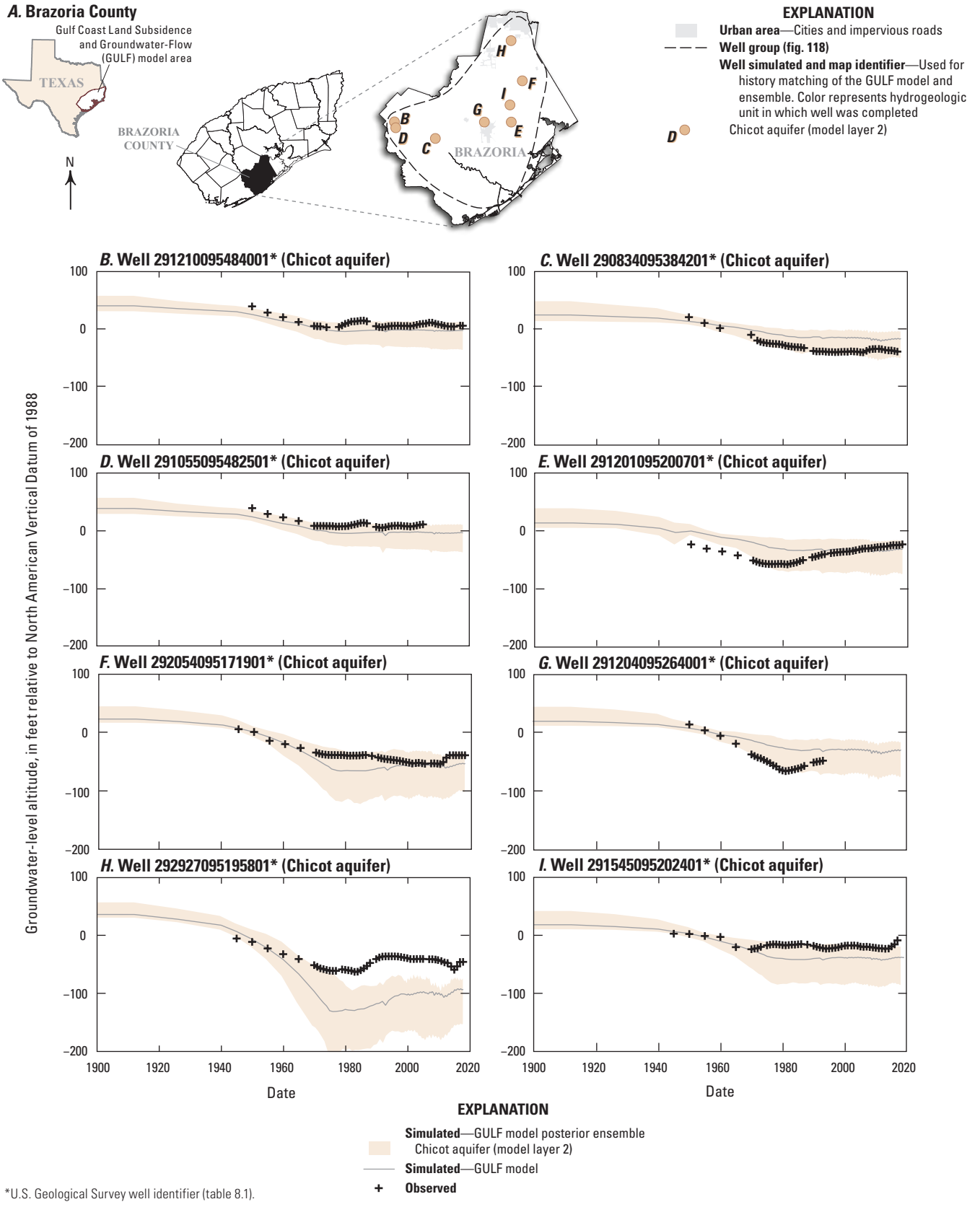

*U.S. Geological Survey well identifier (table 8.1).

Figure 129. Observed and simulated groundwater levels in and near Brazoria County in southeast Texas.

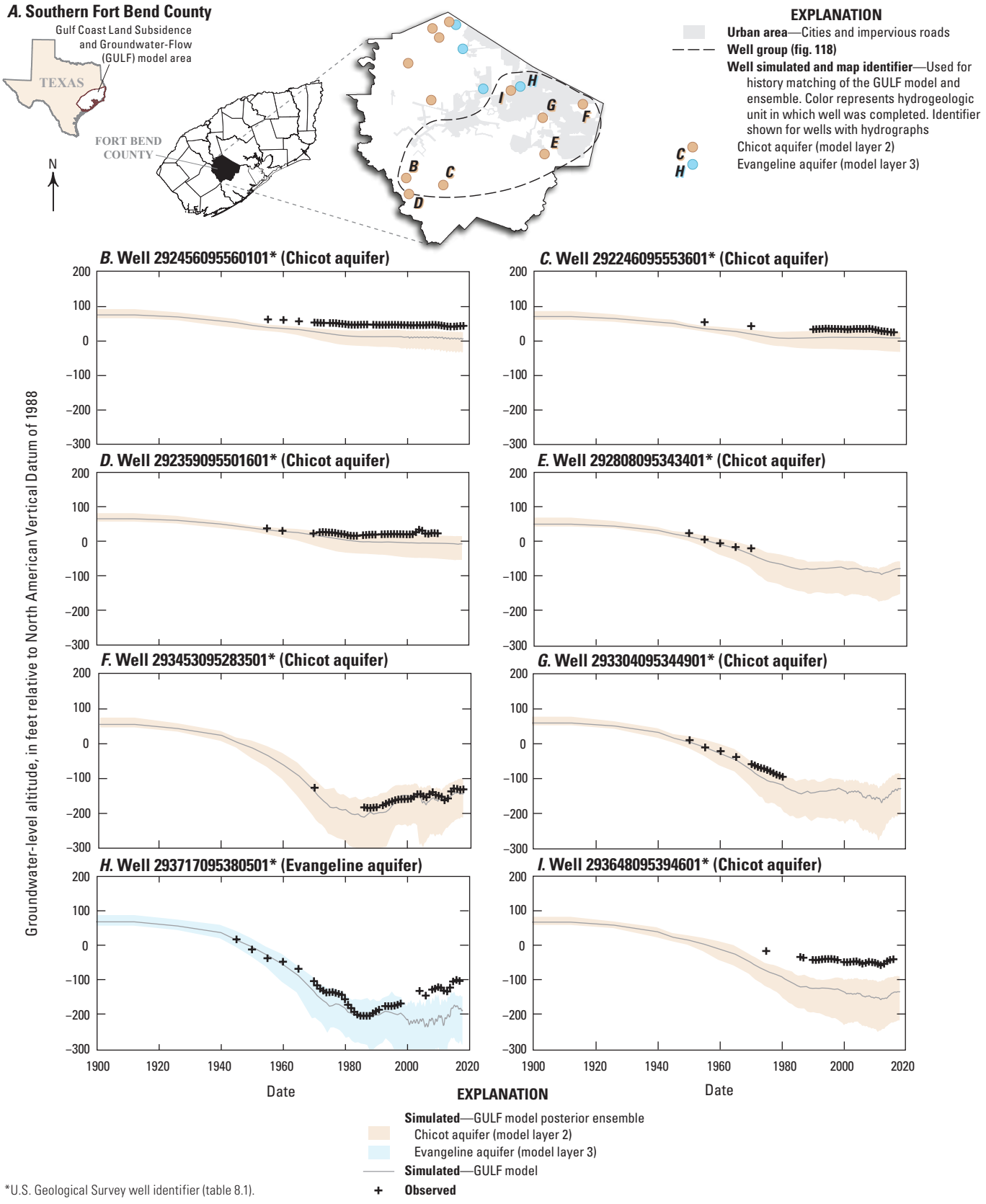

*U.S. Geological Survey well identifier (table 8.1).

Figure 130. Observed and simulated groundwater levels in and near southern Fort Bend County in southeast Texas.

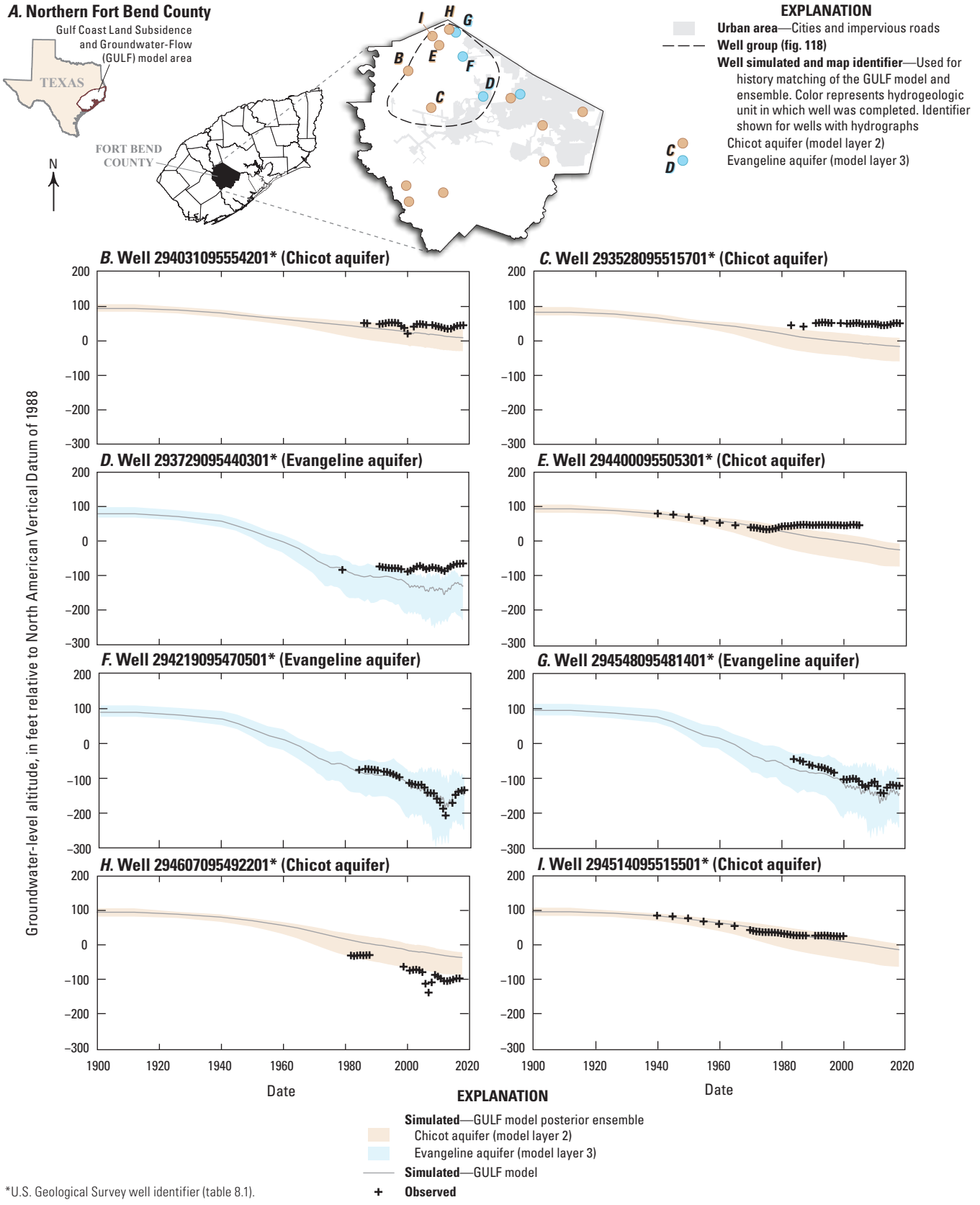

Figure 131. Observed and simulated groundwater levels in and near northern Fort Bend County in southeast Texas.

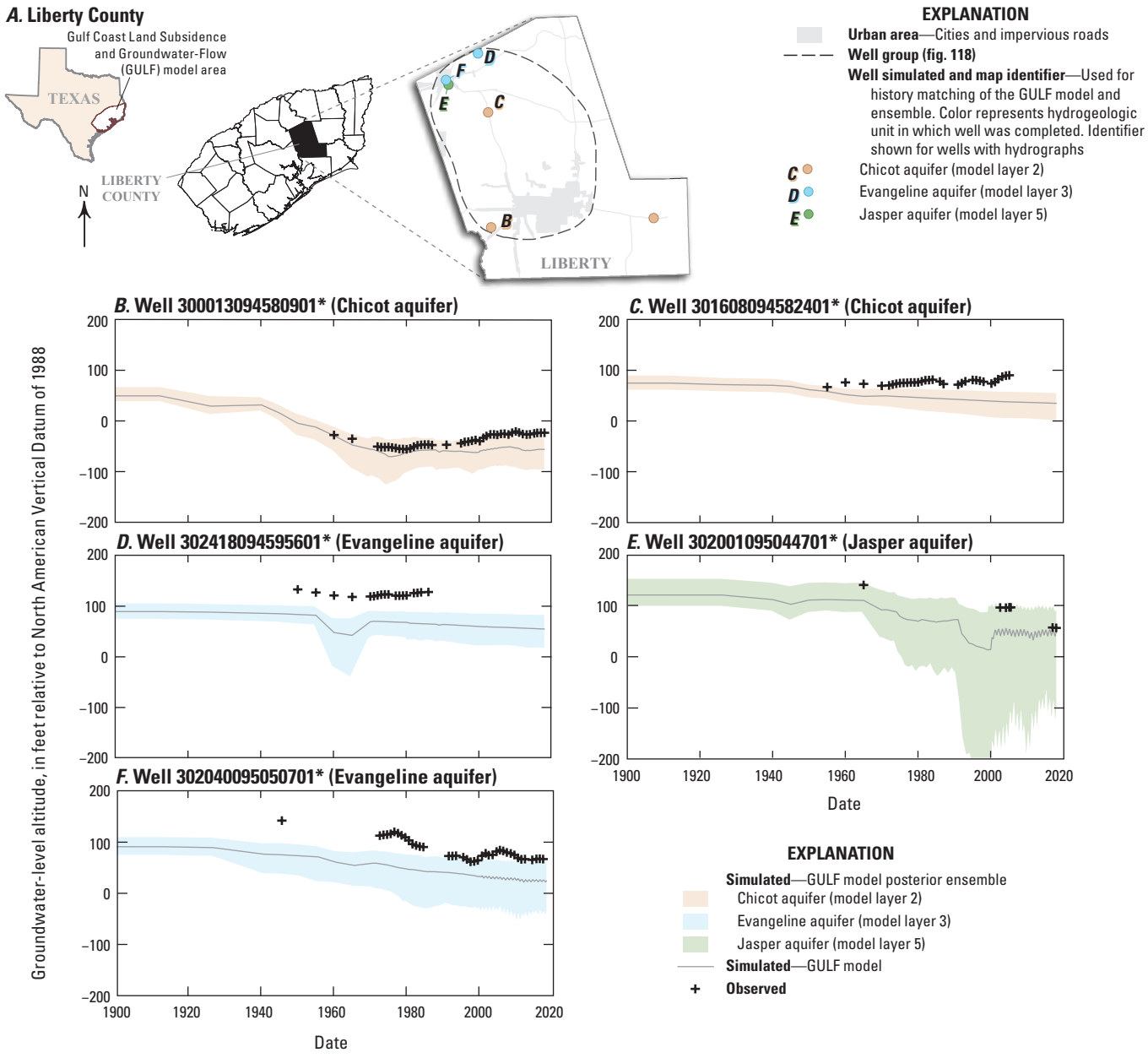

*U.S. Geological Survey well identifier (table 8.1).

Figure 132. Observed and simulated groundwater levels in and near Liberty County in southeast Texas.

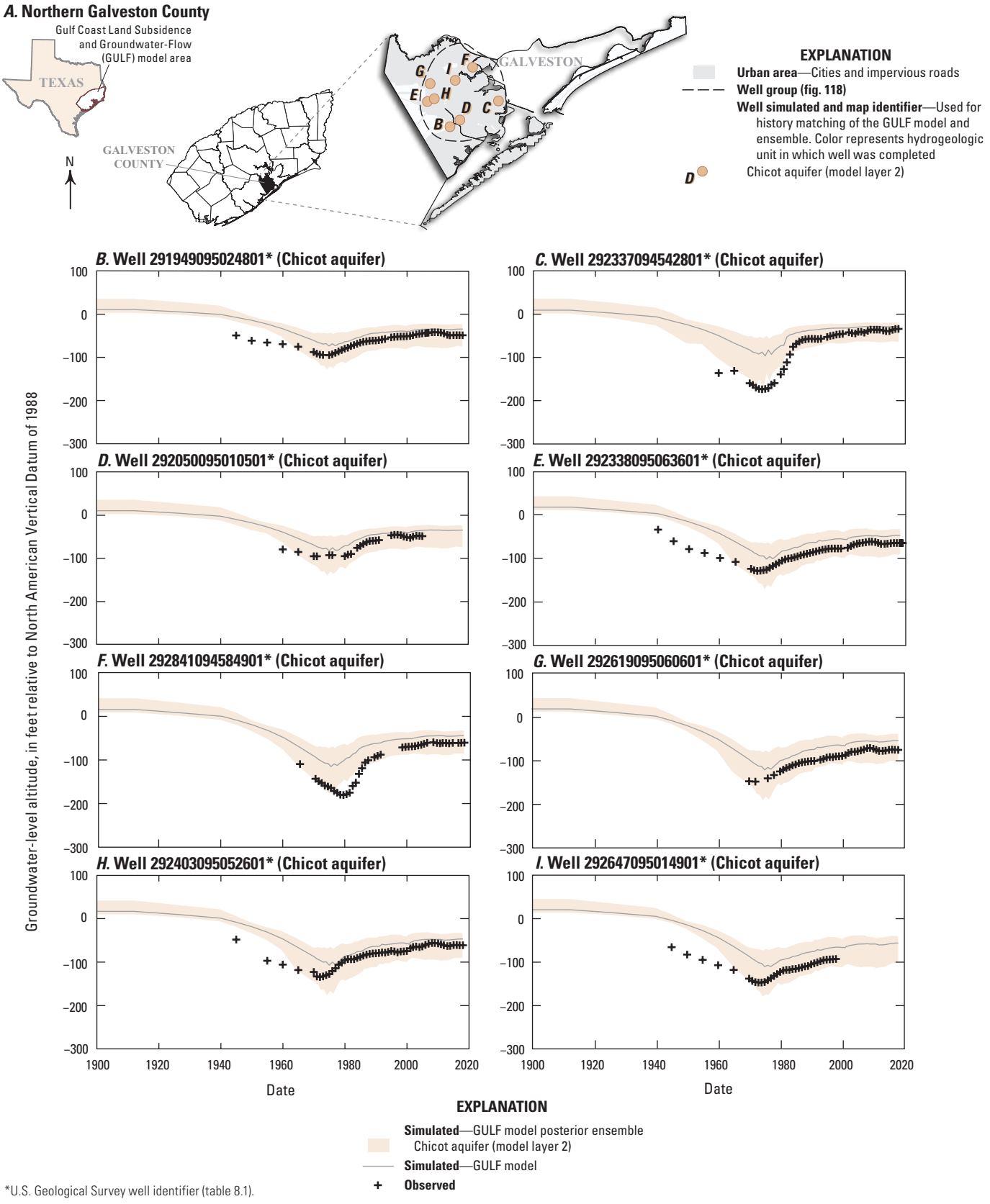

*U.S. Geological Survey well identifier (table 8.1).

Figure 133. Observed and simulated groundwater levels in and near northern Galveston County in southeast Texas.

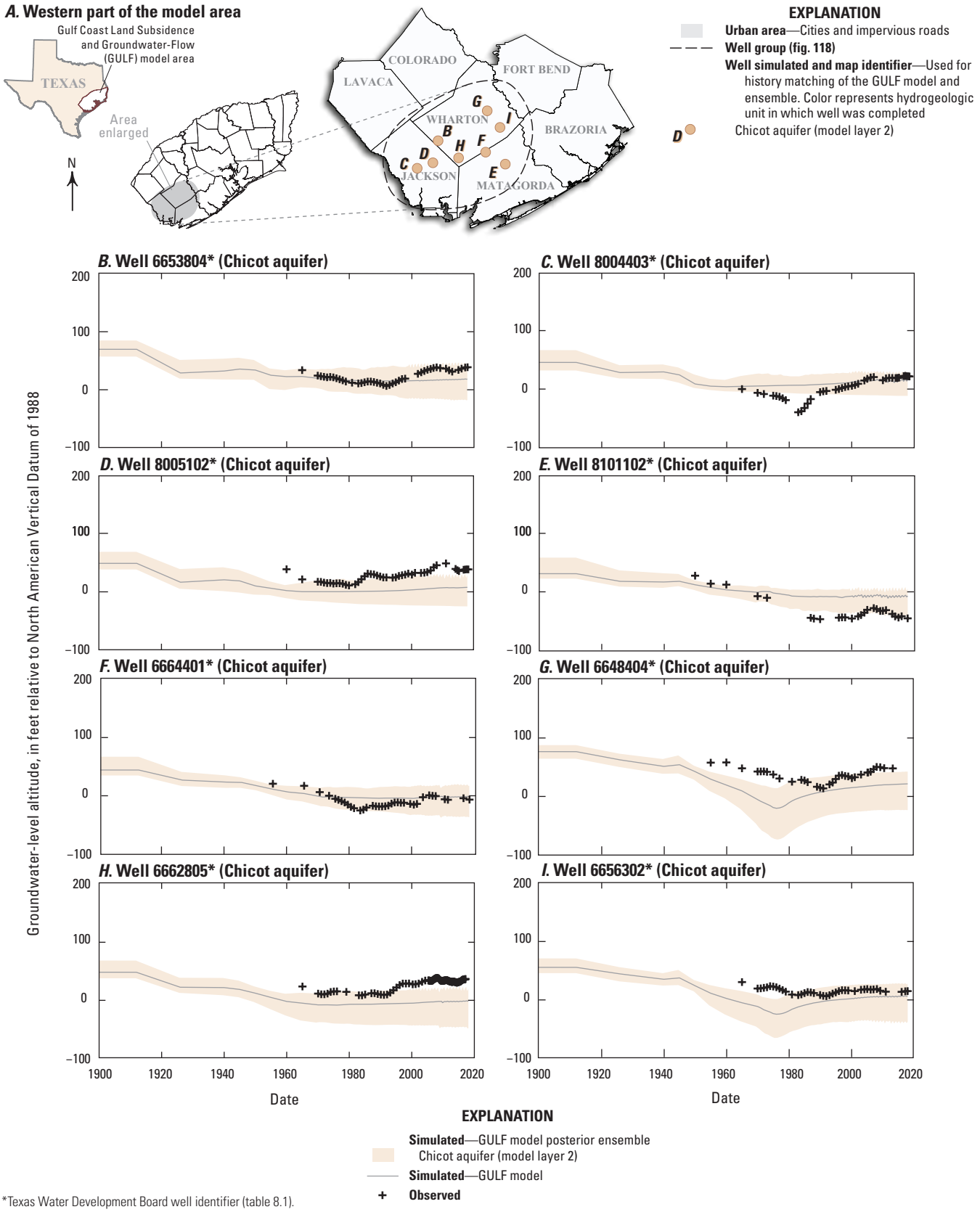

*Texas Water Development Board well identifier (table 8.1).

Figure 134. Observed and simulated groundwater levels in and near the western part of the Gulf Coast aquifer system model area in southeast Texas.

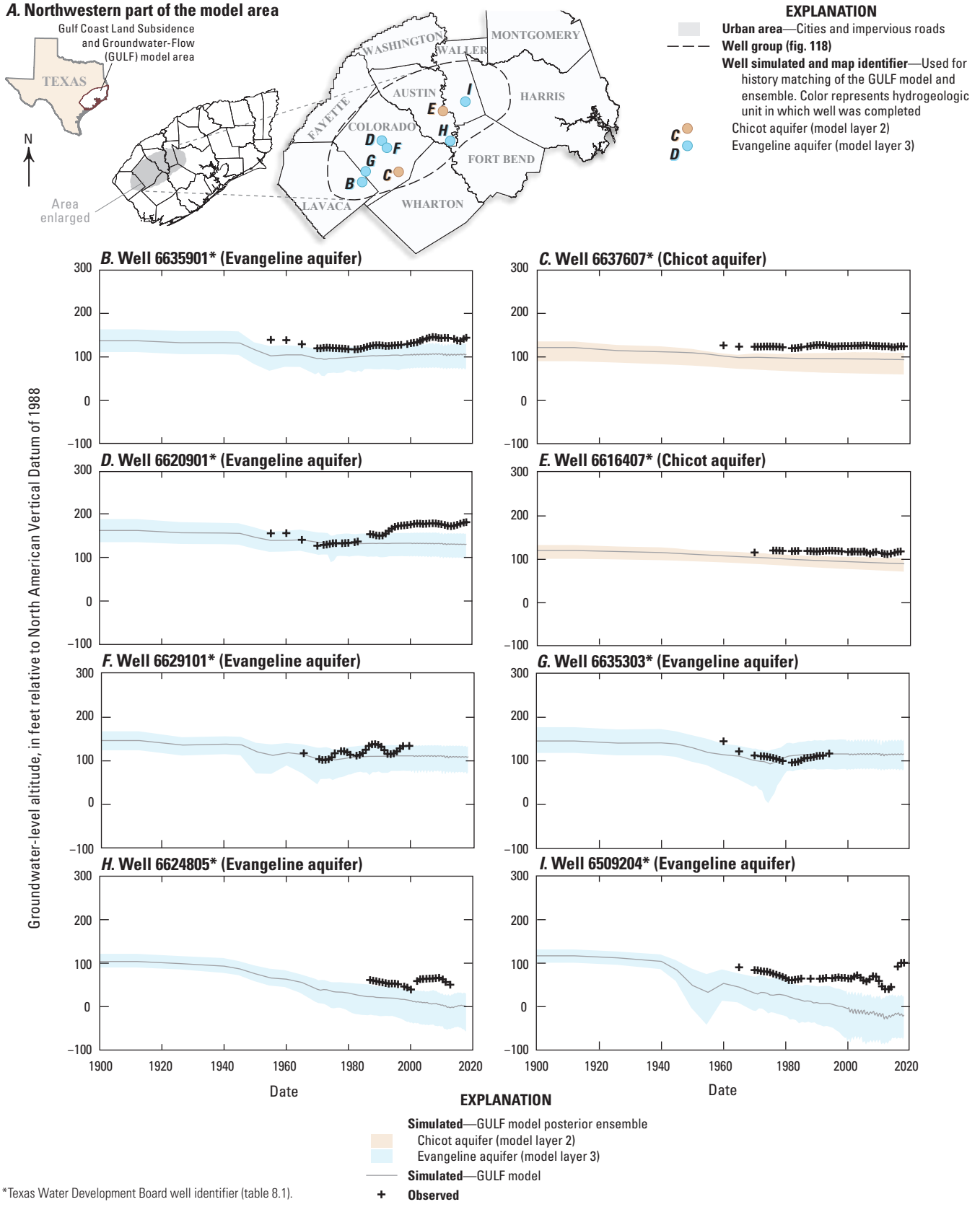

Figure 135. Observed and simulated groundwater levels in and near the northwestern part of the Gulf Coast aquifer system model area in southeast Texas.

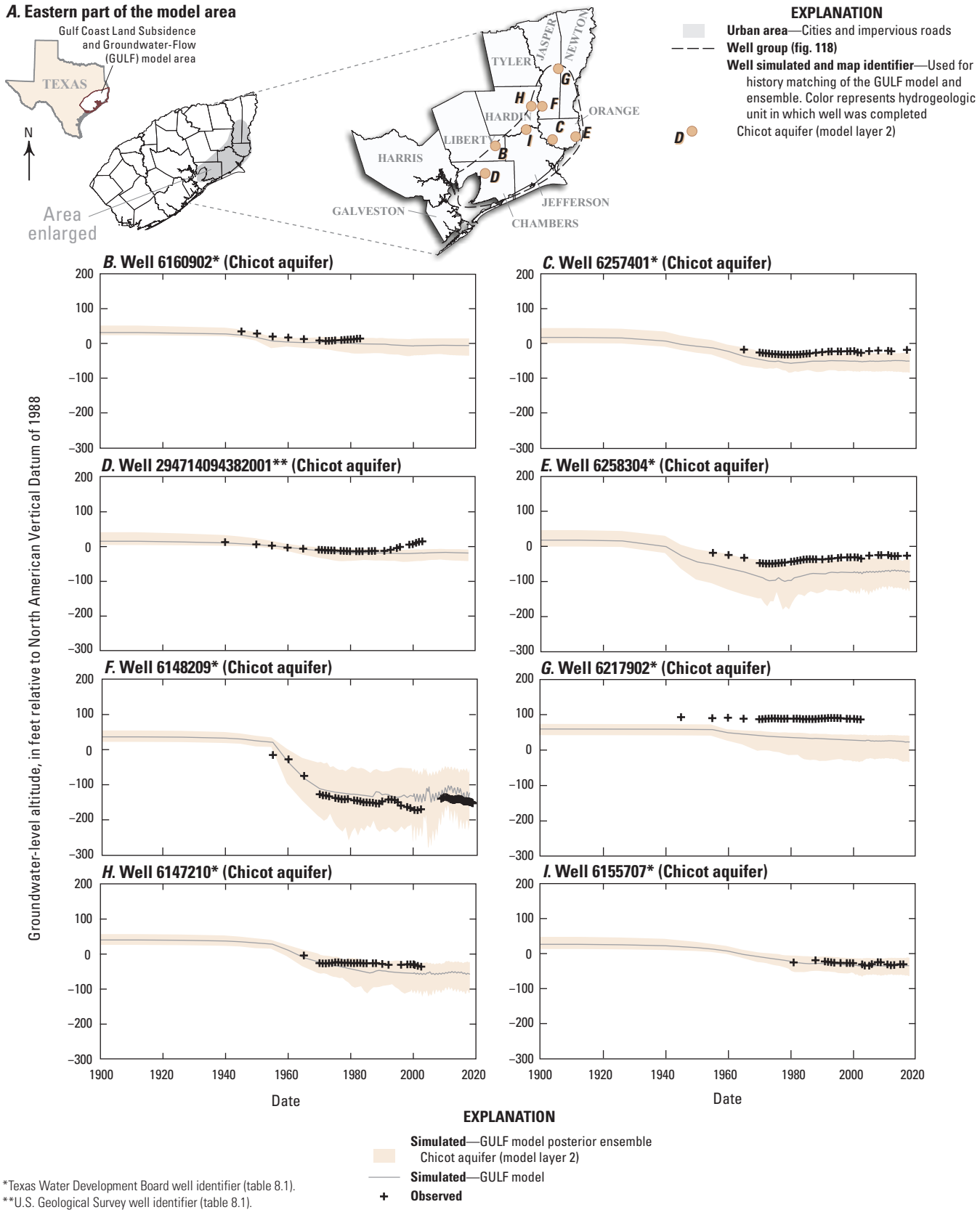

*Texas Water Development Board well identifier (table 8.1).
**U.S. Geological Survey well identifier (table 8.1).

Figure 136. Observed and simulated groundwater levels in and near the eastern part of the Gulf Coast aquifer system model area in southeast Texas.

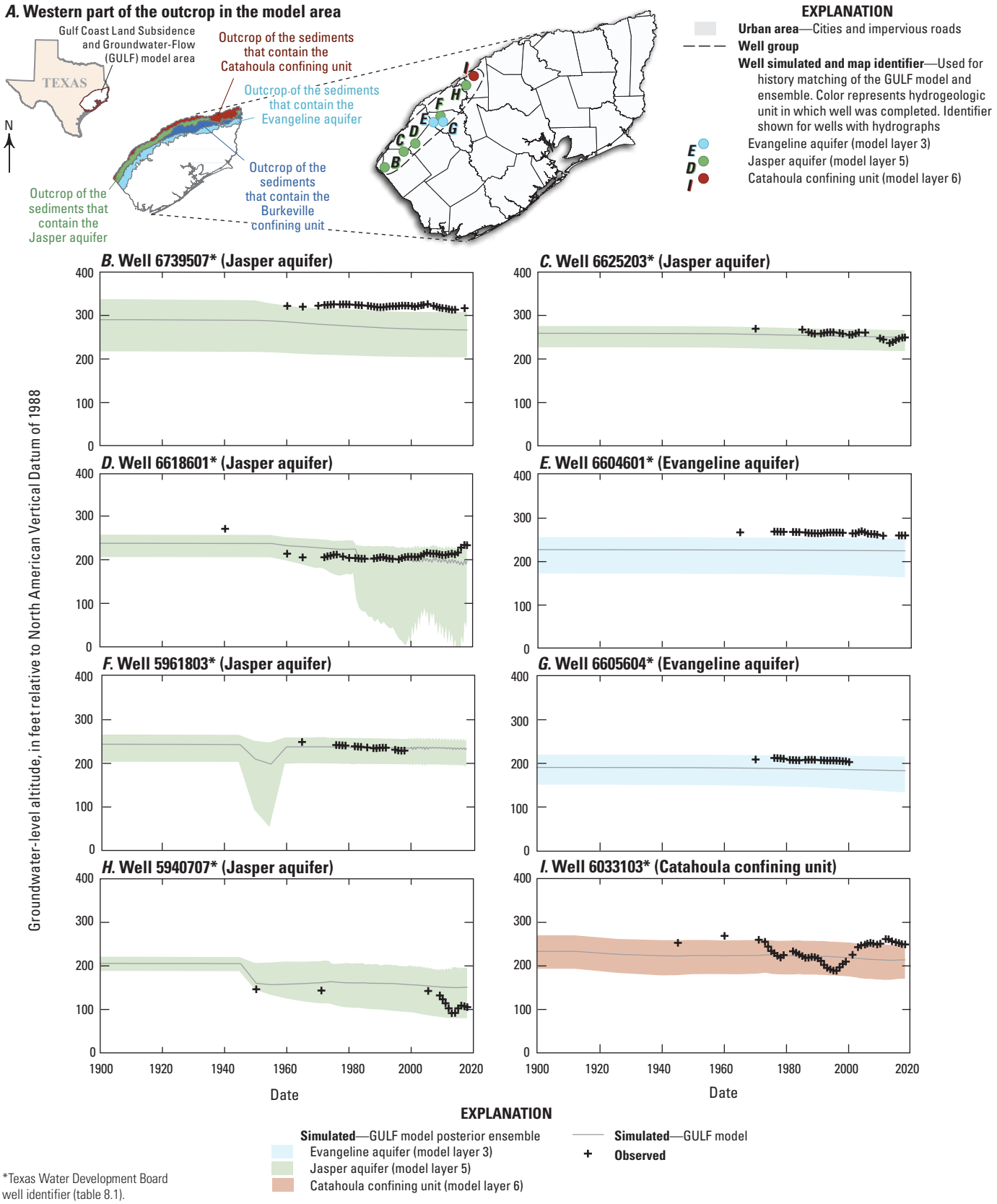

Figure 137. Observed and simulated groundwater levels in and near the hydrogeologic outcrop area in the western part of the Gulf Coast aquifer system model area in southeast Texas.

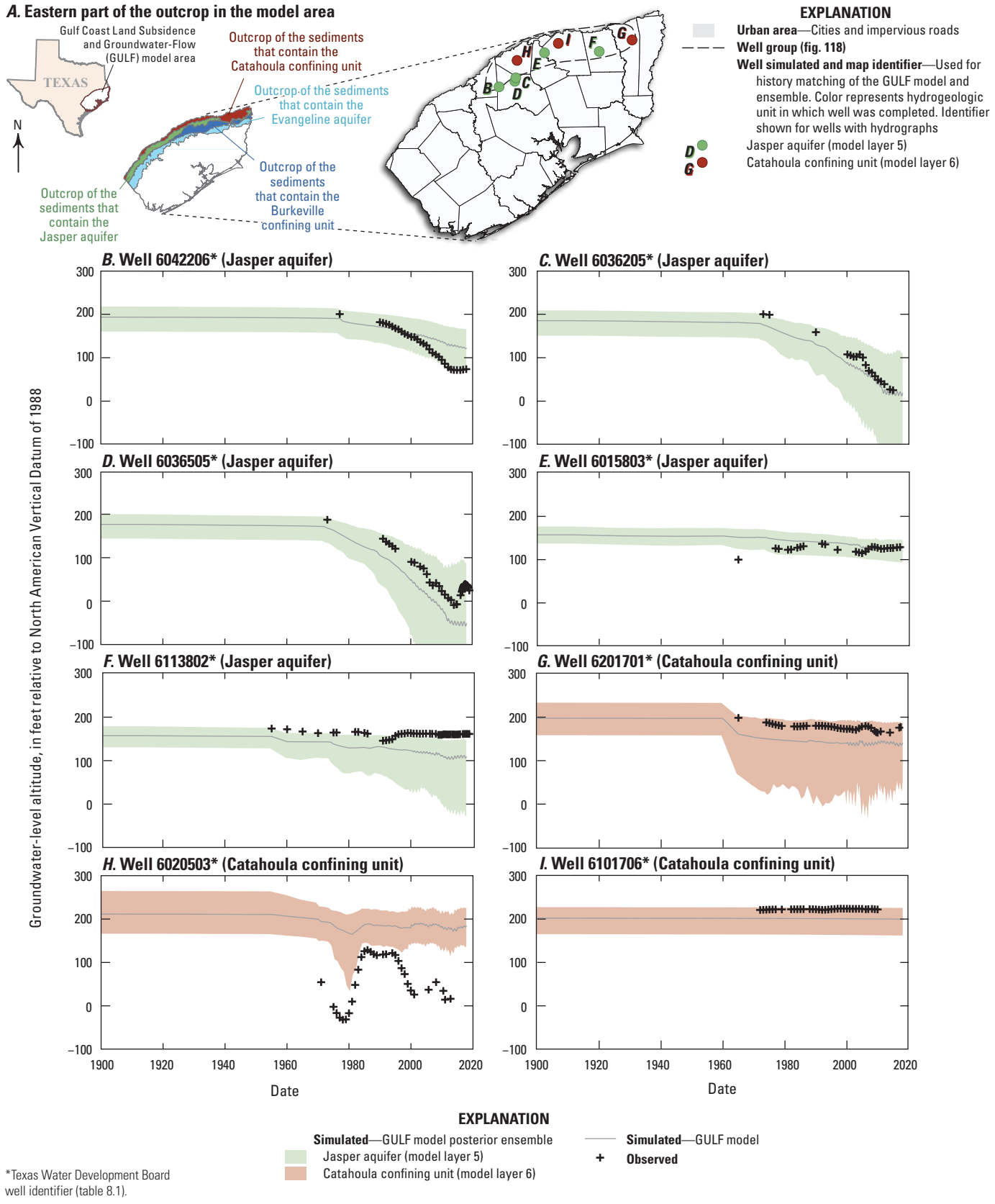

*Texas Water Development Board well identifier (table 8.1).

Figure 138. Observed and simulated groundwater levels in and near the hydrogeologic outcrop area in the eastern part of the Gulf Coast aquifer system model area in southeast Texas.

figs. 122, 135). Substantial irrigation groundwater use in this area occurred during 1940–70, and nearly all of this groundwater was from the Evangeline aquifer (Wilson, 1967). Irrigation return flow in this area may account for the simulated groundwater level that was consistently less than the observed level. Near wells D–E of figure 122, where the groundwater-use type was primarily municipal versus irrigation, simulated Evangeline aquifer groundwater levels more closely matched observed groundwater levels.

Groundwater-level historical minimums at most of the wells were generally well fit, particularly in south-central and southeastern Harris County (Pasadena, Baytown, and Johnson Space Center areas, respectively), where the greatest historical declines occurred prior to 1980 (figs. 126–127). Groundwater-level historical minimums in Galveston County were not entirely matched, particularly in the Texas City area (fig. 133).

Subsidence

Generally, the observed subsidence and simulated vertical-displacement values at benchmarks and GPS stations, respectively, are in good agreement. When these data are plotted on the same graph, most values plot on or near the 1:1 line, and the residuals (differences between the observed subsidence and vertical displacement) follow a Gaussian distribution (fig. 139*A–B, E–F*). Compaction at the extensometers was generally undersimulated, as indicated by the greater frequency of residuals below the 1:1 line and negative residuals (fig. 139*C–D*).

Benchmarks

The range of simulated time-series subsidence produced by the Posterior and GULF model generally bracket historical subsidence observations and estimations at most of the benchmarks included in the model (figs. 140–152), indicating that the Posterior can reproduce many aspects of the observed historical subsidence processes. Subsidence was generally undersimulated at benchmarks in central (fig. 146) south-central (fig. 147) and southeastern (fig. 148) Harris County—the location of the greatest amount of subsidence in the model area. Subsidence was slightly undersimulated in northern Harris County (fig. 142; table 9) as a result of oversimulated groundwater levels in the Evangeline and Jasper aquifers. Simulated subsidence was similar to observed and estimated values of subsidence at The Woodlands at benchmarks T 88 and U 88 (fig. 141; table 9) and was oversimulated at benchmarks in Conroe (table 9; fig. 140). Subsidence was also generally oversimulated in western Harris County (fig. 143). In eastern Harris County, simulated subsidence was undersimulated at benchmark G 659 (fig. 149) and was oversimulated to the north at benchmark D 690. Subsidence in eastern Harris County varied considerably, from greater than 8 ft at benchmark G 659 to less than 4 ft at benchmark D 690, indicating a large subsidence gradient between these two benchmarks (fig. 70*B*). At the Goose Creek oil field in southeastern Harris County, much of the subsidence at the Goose Creek oil field documented by Pratt and Johnson (1926) occurred prior to 1926 and before the installation of monumented benchmarks in the area (fig. 148; table 4). Although the model reproduces the observed subsidence at nearby benchmarks F 173 and G 660 (fig. 148), subsidence before the installation of monumented benchmarks was not recorded and therefore not simulated by the model. Overall, the Posterior and GULF model still capture the temporal pattern in subsidence from the benchmark observations in Harris County.

In Galveston County, the simulated subsidence at benchmark A 639, which was monumented prior to most of the observed subsidence in the area, was less than the observed subsidence (fig. 152). The undersimulation of subsidence at this site was the result of the rapid subsidence increase over a short distance that could not easily be simulated owing to (1) the relatively coarse size (1 by 1 km) of the model grid cells, and (2) the use of mean subsidence observation targets in these model grid cells because of the closely spaced subsidence contour lines (fig. 70*B*). The simulated subsidence was similar to the observed subsidence at most other benchmarks in Galveston County (fig. 152).

The spread of the Posterior values widens as a function of the magnitude of the simulated subsidence increases. This is attributed to a larger subsidence magnitude effectively "activating" more parameters that contribute to the simulated subsidence at observation locations. That is, as simulated subsidence increases in the model, more model parameters representing a range of interbed properties are used, resulting in the upper and lower bounds of the Posterior expanding substantially.

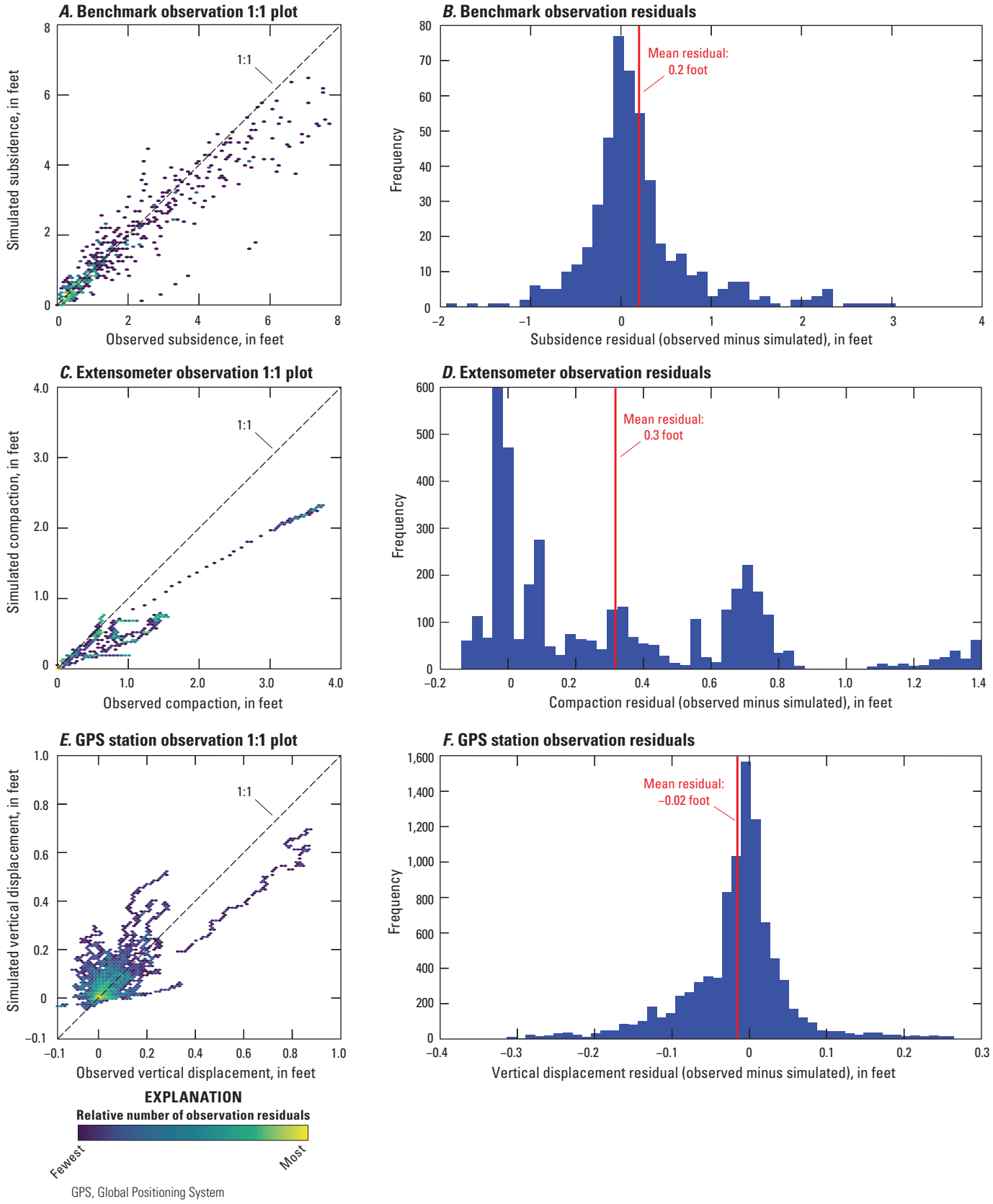

Figure 139. Observed and simulated subsidence at benchmarks and subsidence residual distributions; observed and simulated compaction at extensometers and compaction residual distributions; observed and simulated vertical displacement at Global Positioning System stations and vertical-displacement residual distributions.

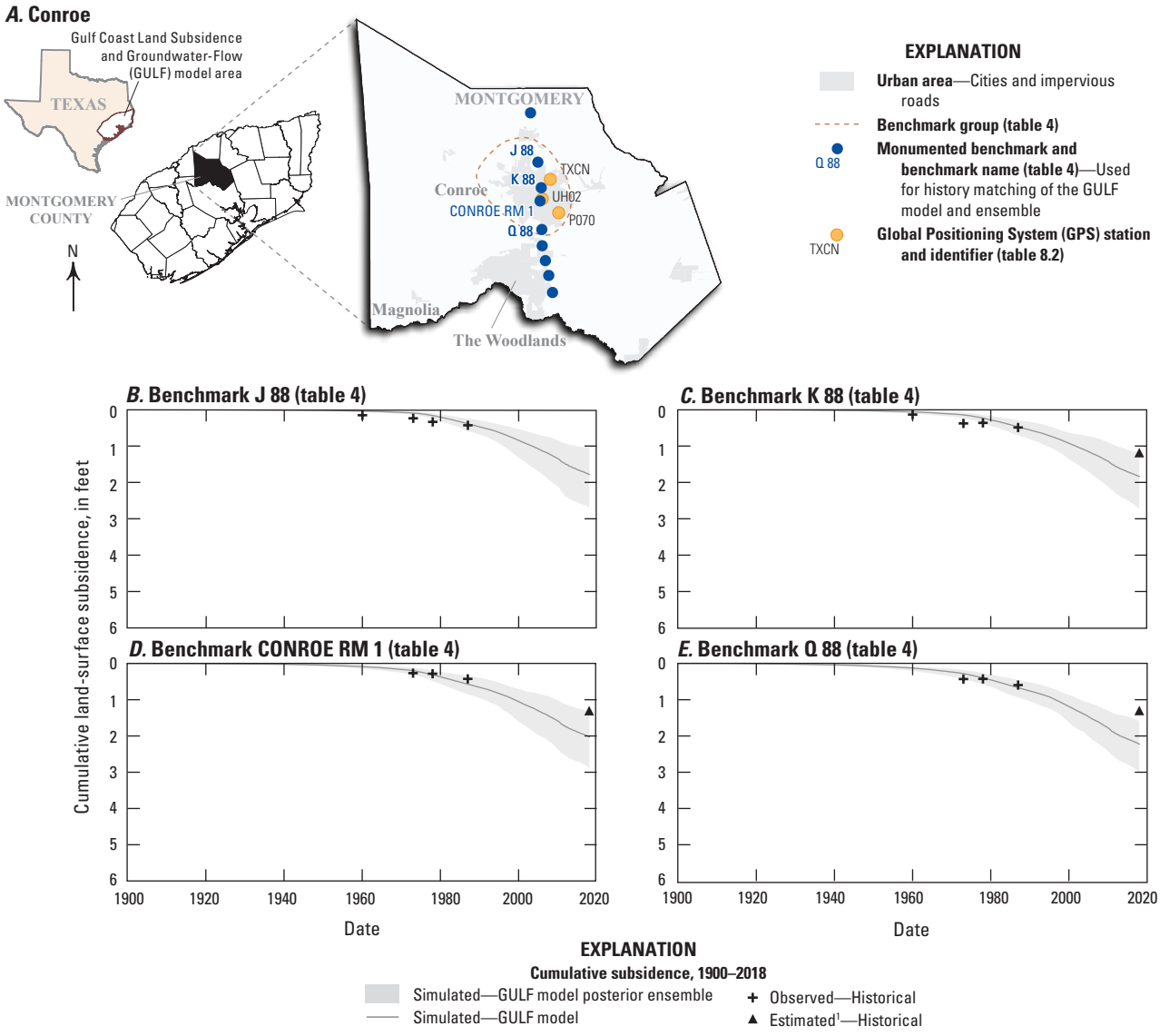

[1]The estimated subsidence through 2018 at benchmarks K 88, CONROE RM 1, and Q 88 was calculated based on the methods described in table 9 using vertical-displacement data from GPS stations TXCN, UH02, and P070, respectively.

Figure 140. Observed and simulated subsidence at benchmarks in and near Conroe, Texas.

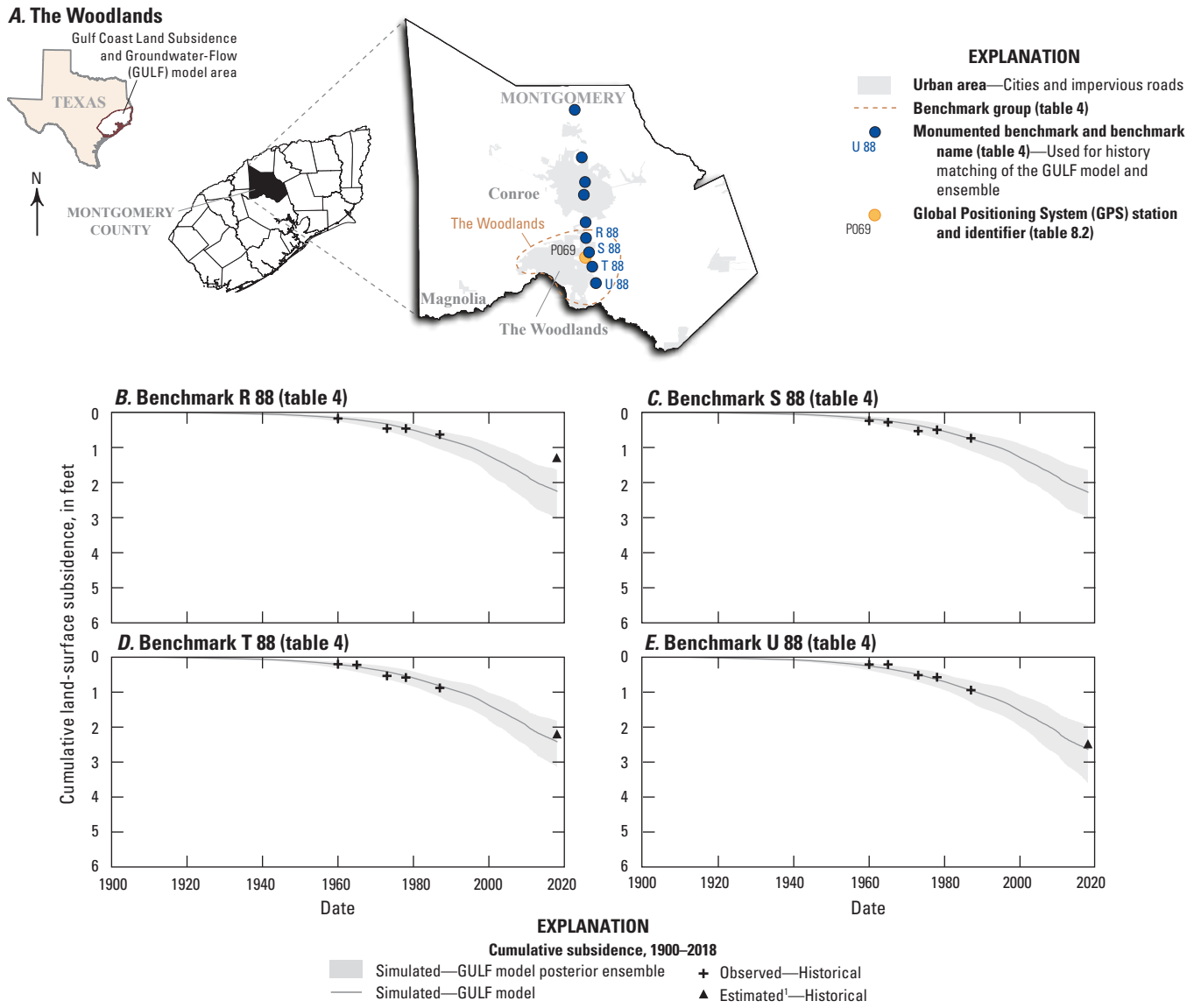

[1]The estimated subsidence through 2018 at benchmarks R 88, T 88, and U 88 was calculated based on the methods described in table 9 using vertical-displacement data from GPS station P069.

Figure 141. Observed and simulated subsidence at benchmarks in and near The Woodlands, Texas.

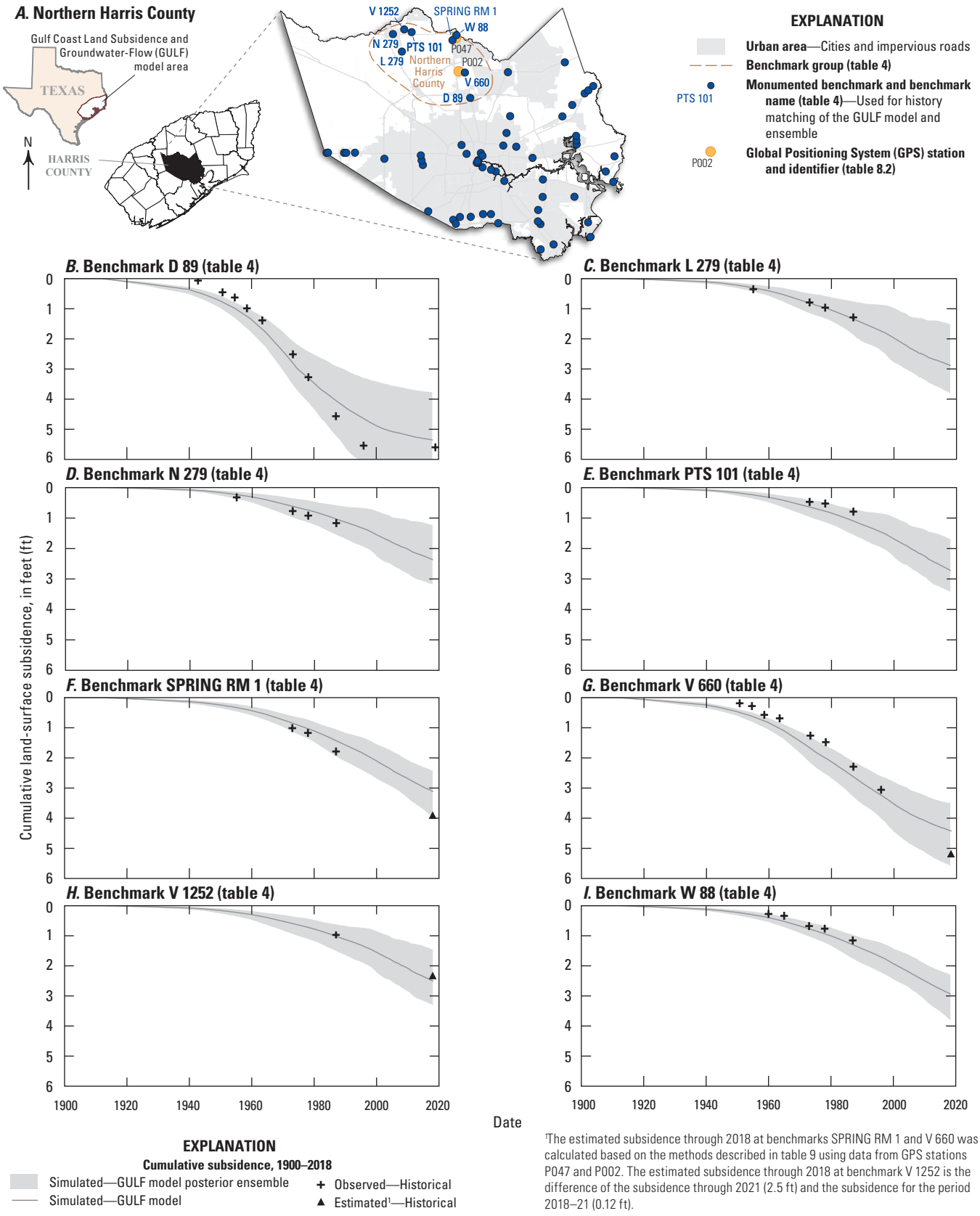

[1]The estimated subsidence through 2018 at benchmarks SPRING RM 1 and V 660 was calculated based on the methods described in table 9 using data from GPS stations P047 and P002. The estimated subsidence through 2018 at benchmark V 1252 is the difference of the subsidence through 2021 (2.5 ft) and the subsidence for the period 2018–21 (0.12 ft).

Figure 142. Observed and simulated subsidence at benchmarks in and near northern Harris County in southeast Texas.

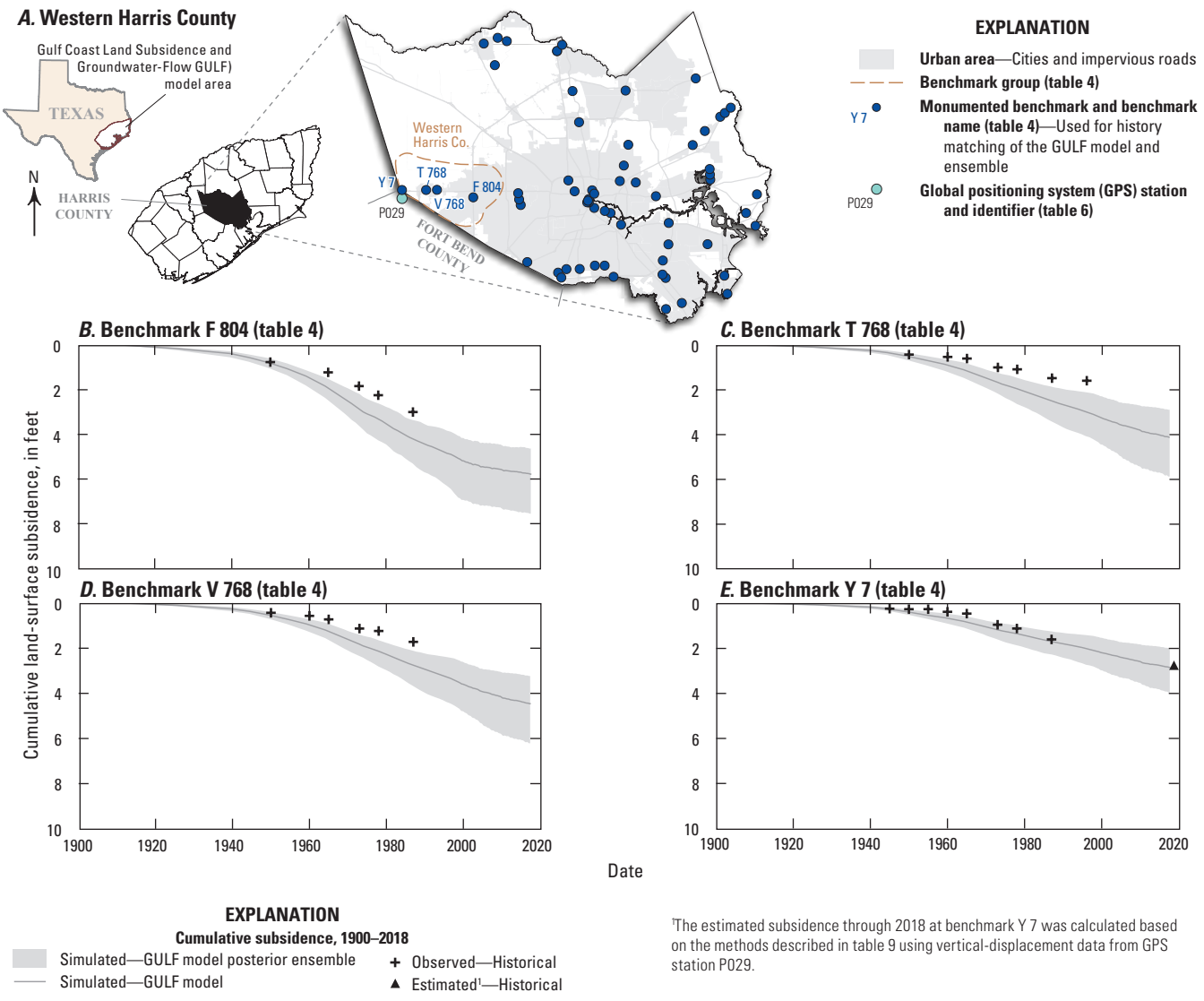

Figure 143. Observed and simulated subsidence at benchmarks in and near western Harris County in southeast Texas.

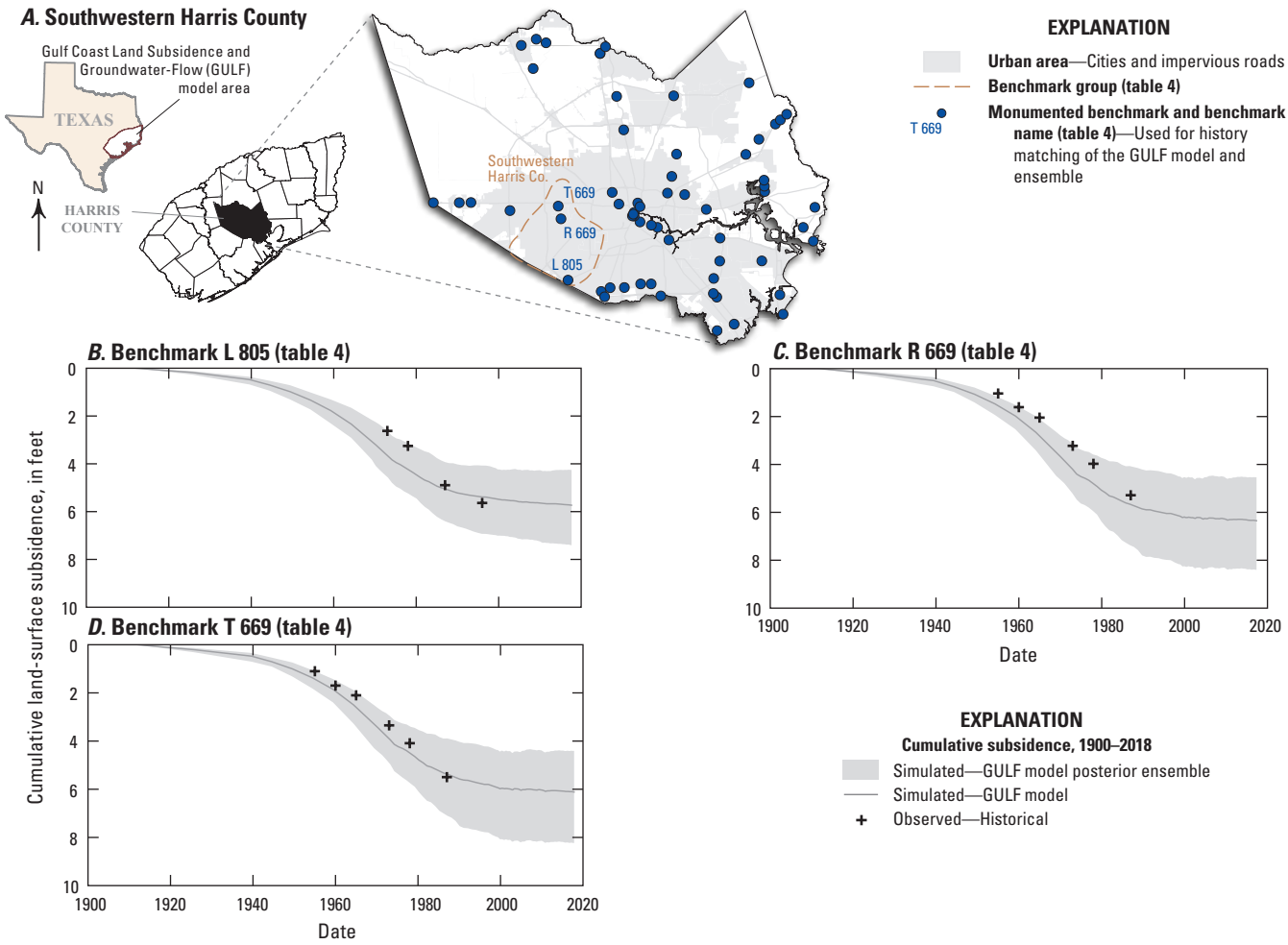

Figure 144. Observed and simulated subsidence at benchmarks in and near southwestern Harris County in southeast Texas.

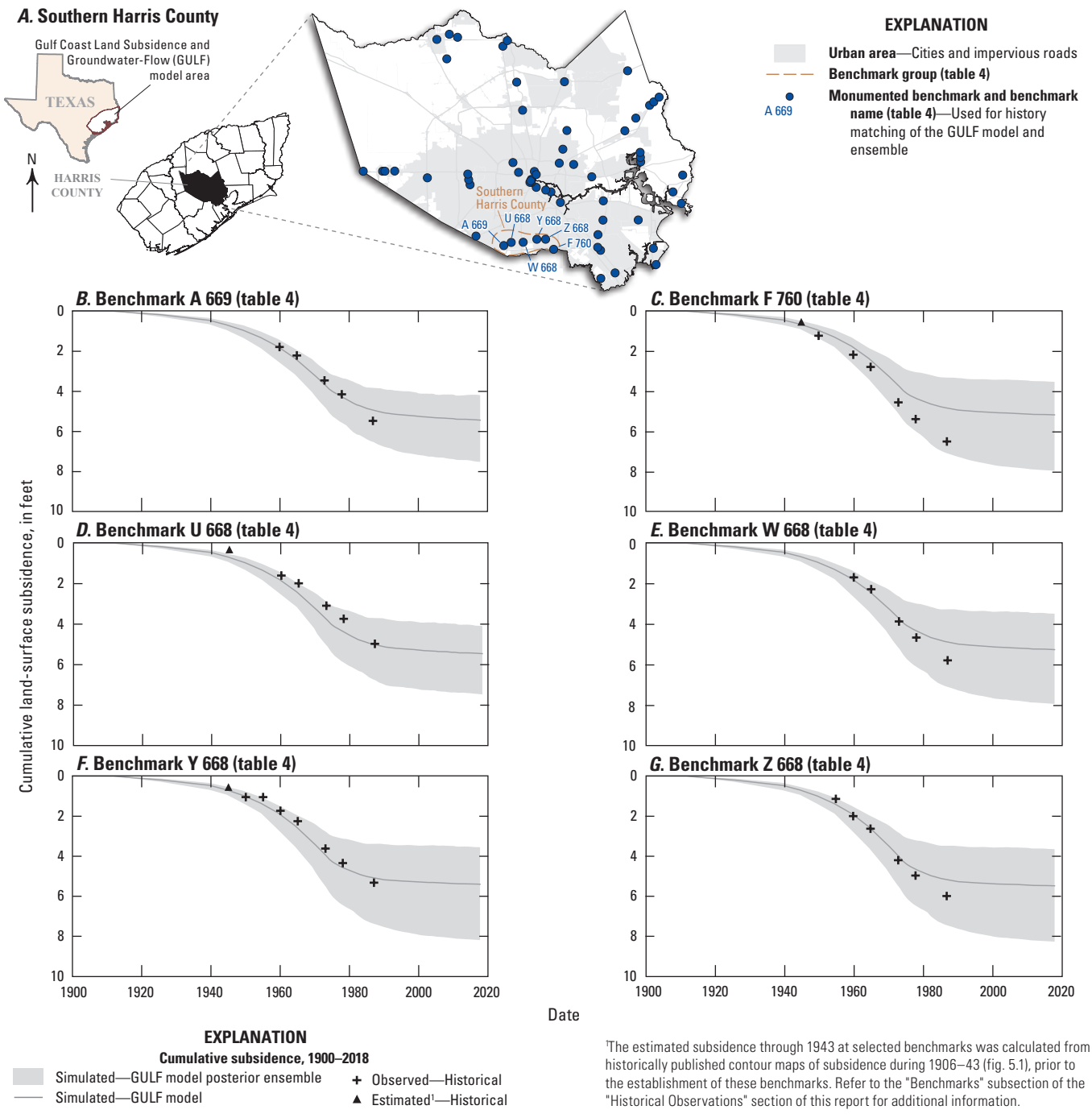

[1]The estimated subsidence through 1943 at selected benchmarks was calculated from historically published contour maps of subsidence during 1906–43 (fig. 5.1), prior to the establishment of these benchmarks. Refer to the "Benchmarks" subsection of the "Historical Observations" section of this report for additional information.

Figure 145. Observed and simulated subsidence at benchmarks in and near southern Harris County in southeast Texas.

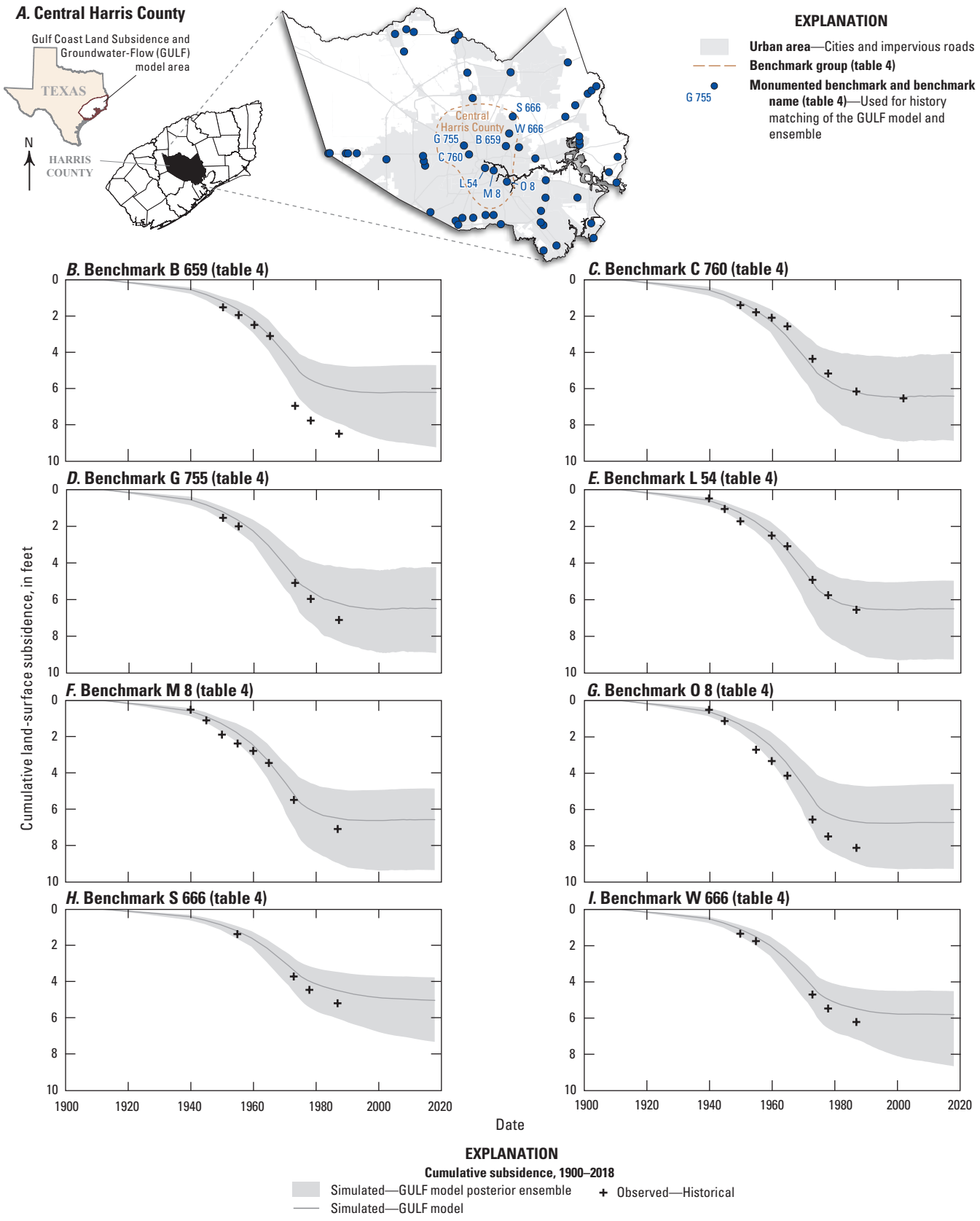

Figure 146. Observed and simulated subsidence at benchmarks in and near central Harris County in southeast Texas.

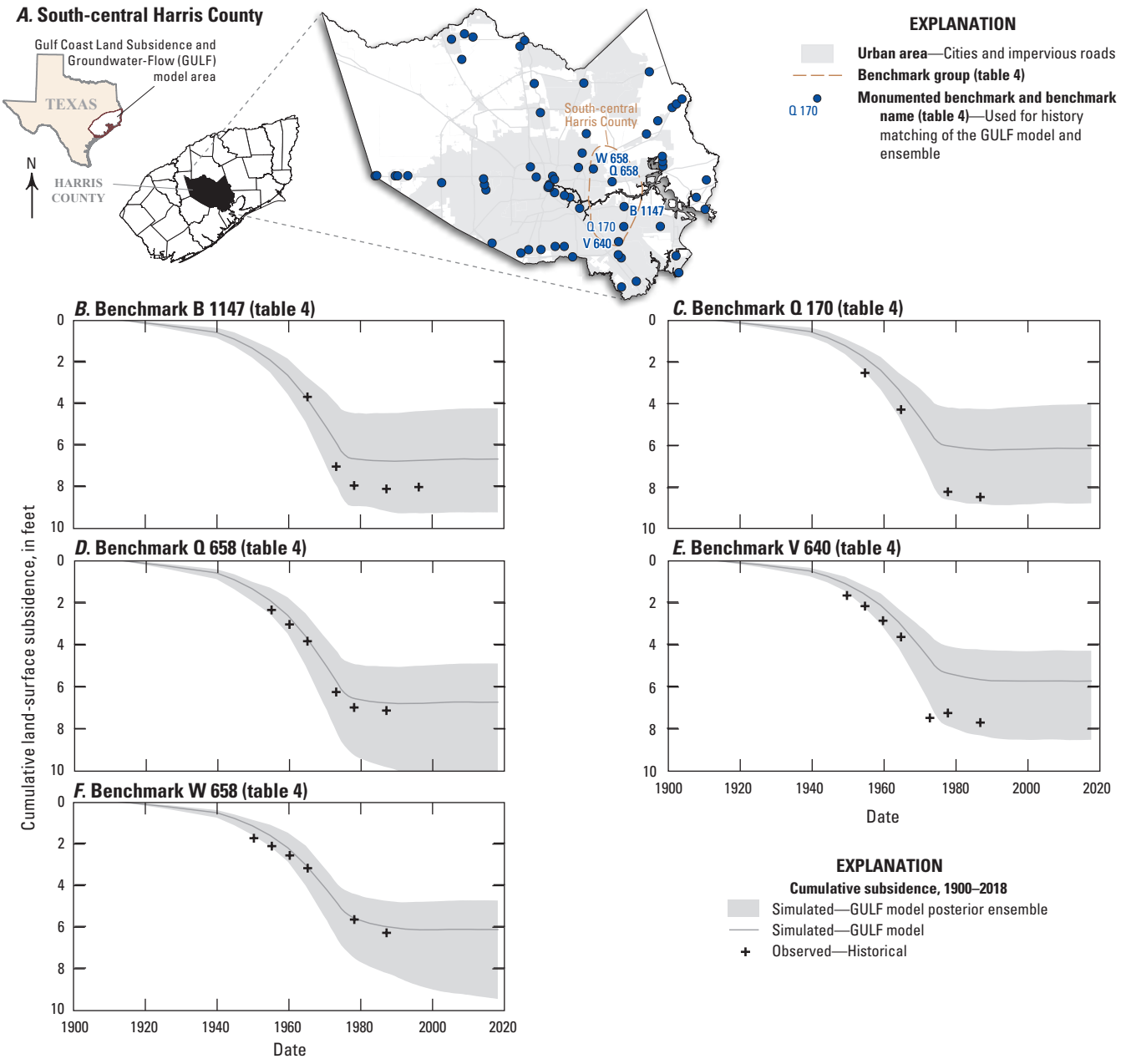

Figure 147. Observed and simulated subsidence at benchmarks in and near south-central Harris County in southeast Texas.

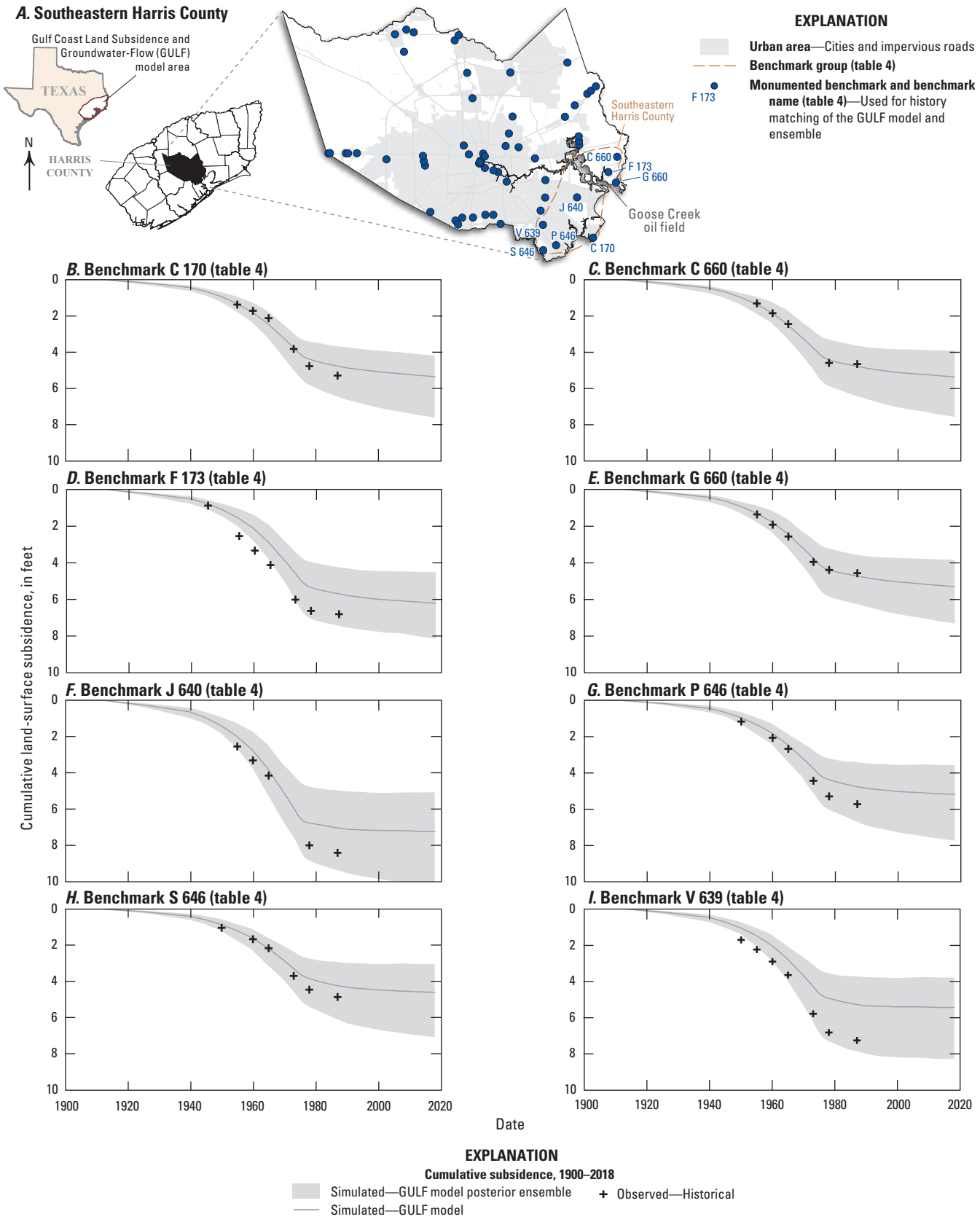

Figure 148. Observed and simulated subsidence at benchmarks in and near southeastern Harris County in southeast Texas.

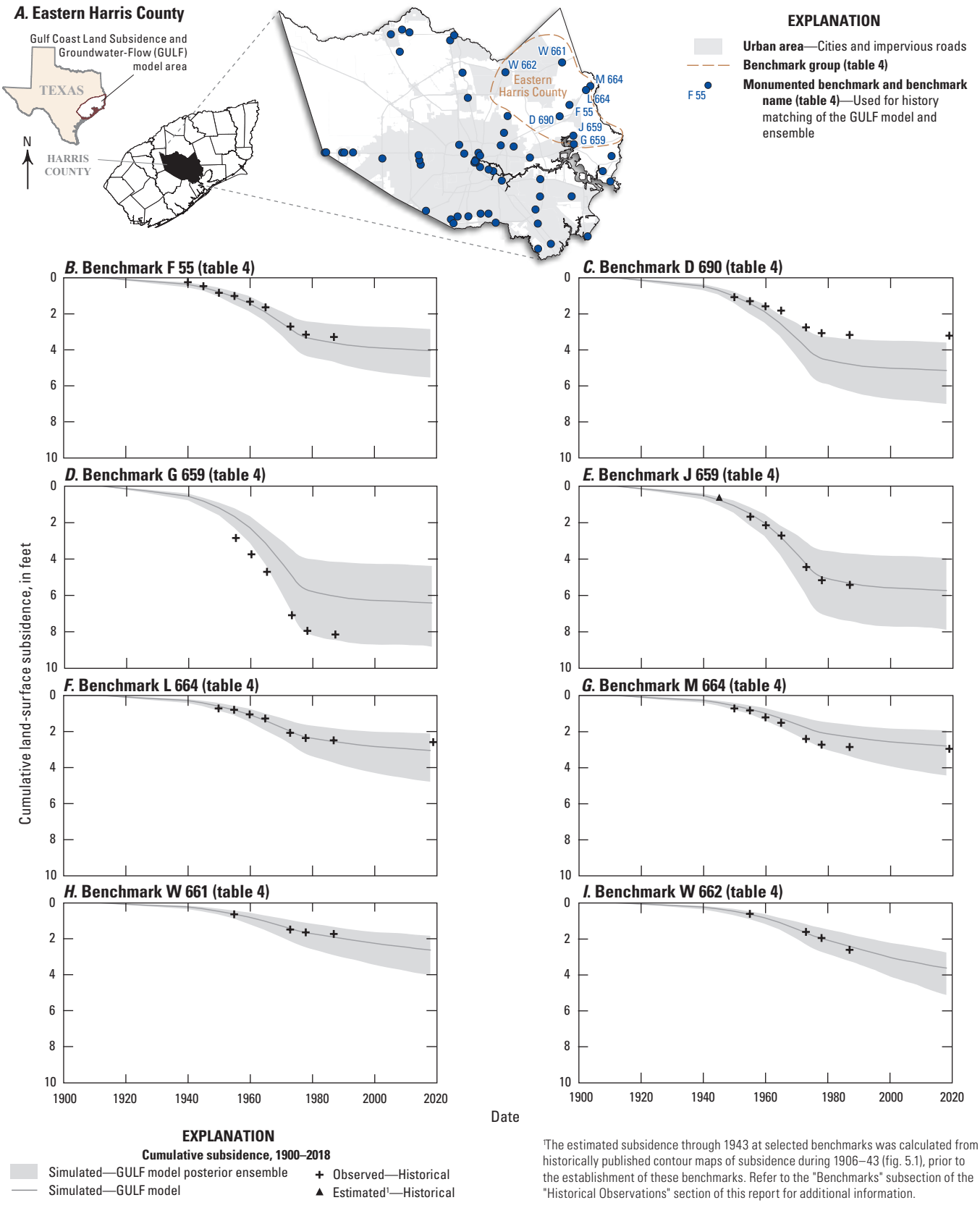

Figure 149. Observed and simulated subsidence at benchmarks in and near eastern Harris County in southeast Texas.

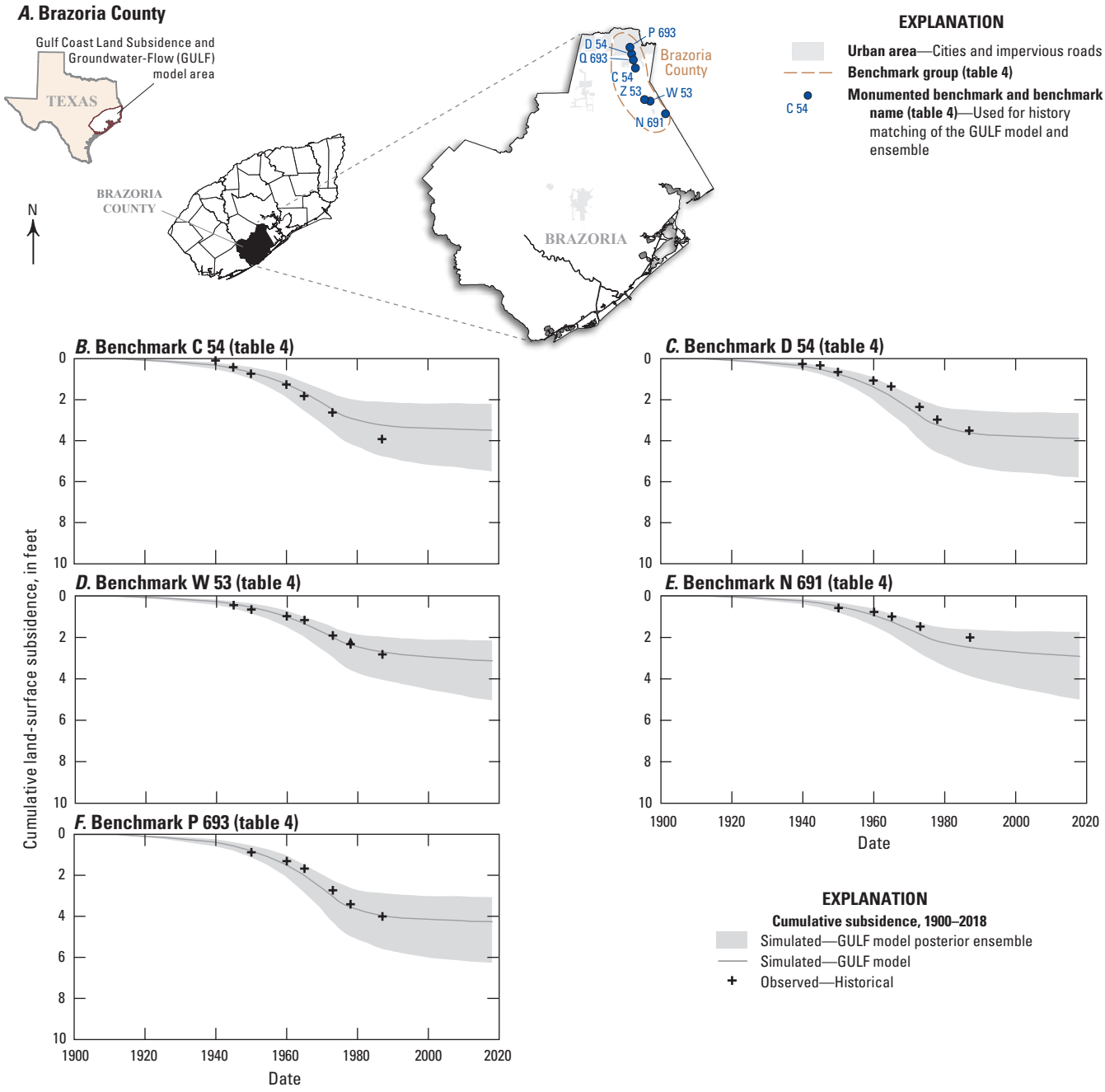

Figure 150. Observed and simulated subsidence at benchmarks in and near Brazoria County in southeast Texas.

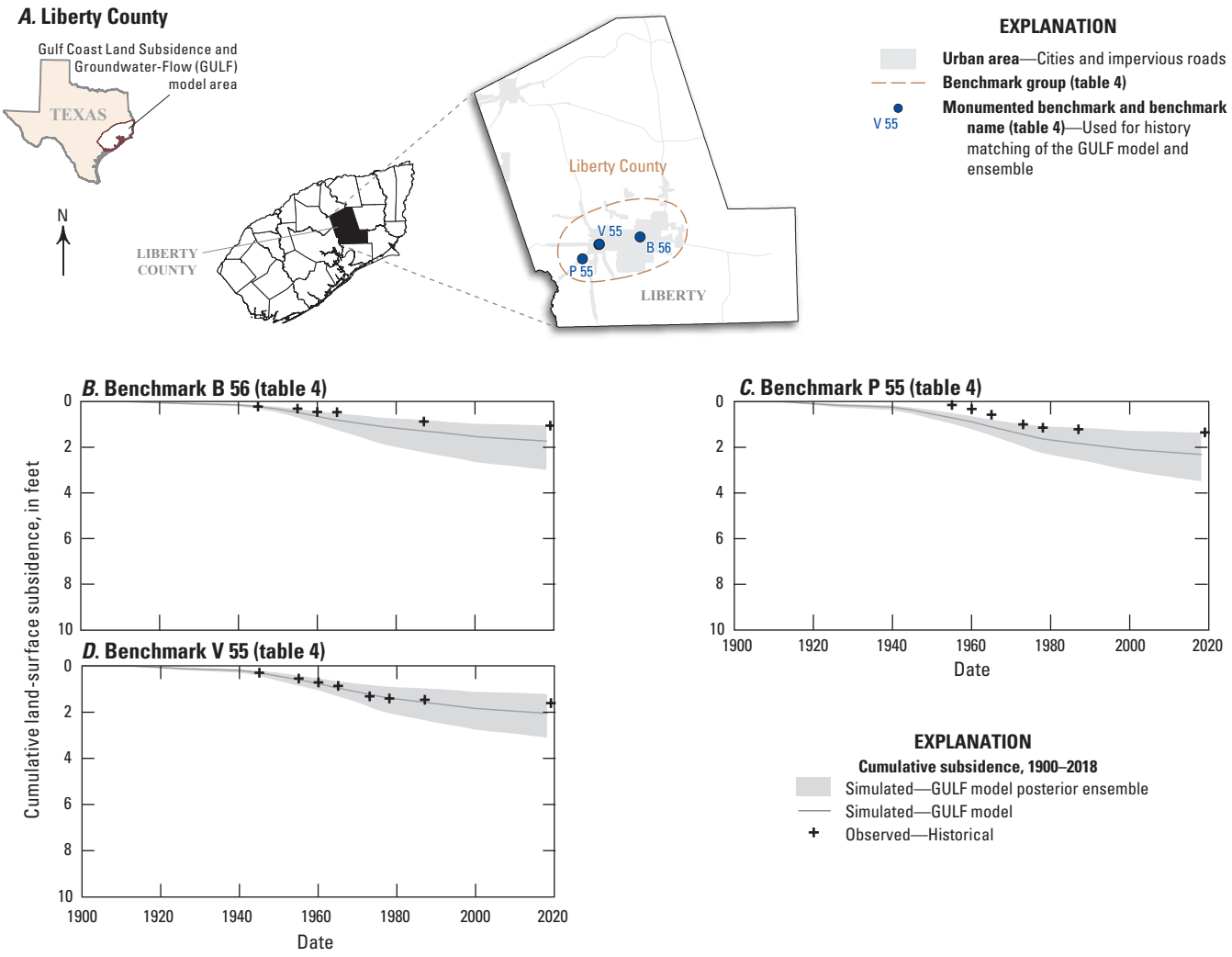

Figure 151. Observed and simulated subsidence at benchmarks in and near Liberty County in southeast Texas.

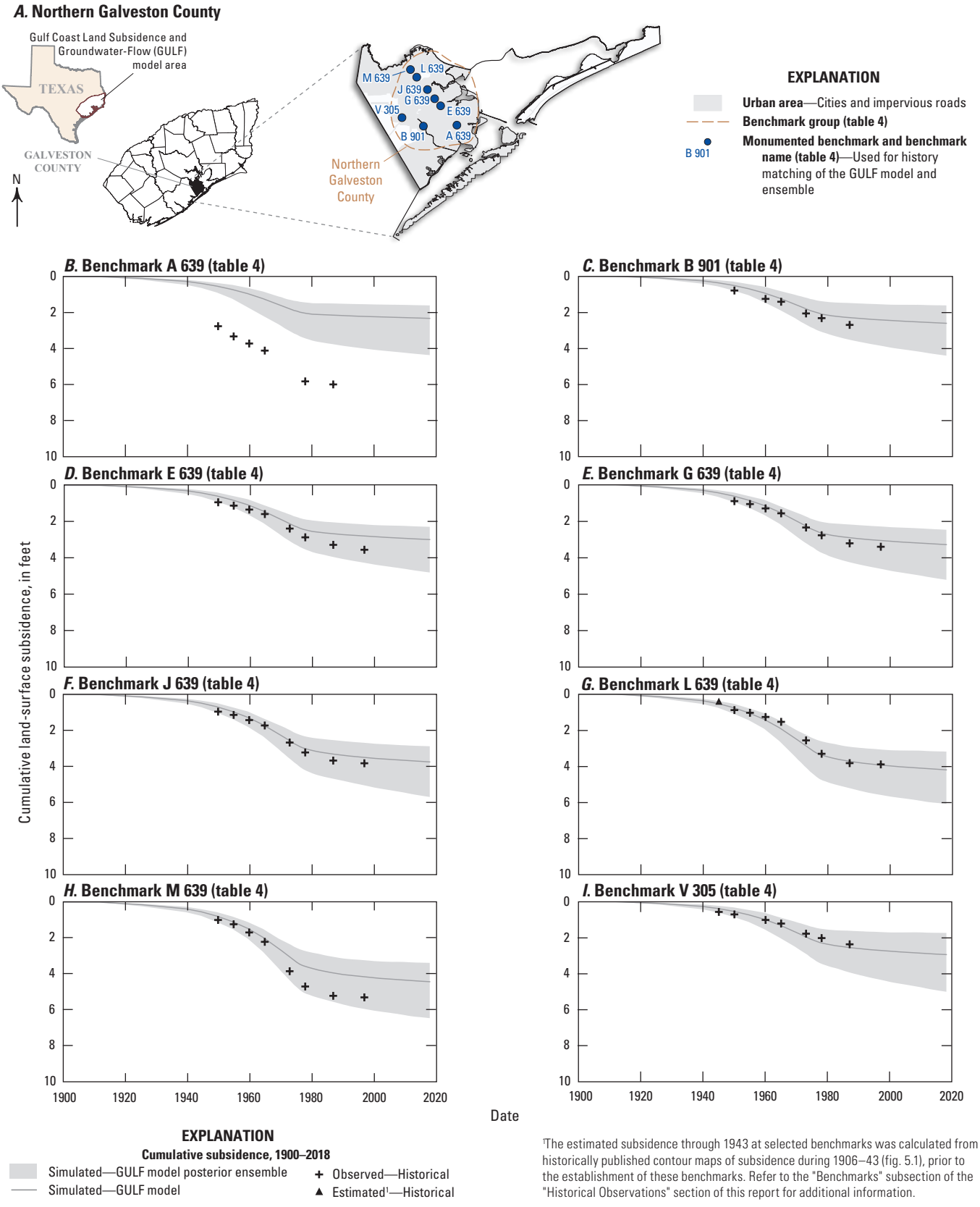

Figure 152. Observed and simulated subsidence at benchmarks in and near northern Galveston County in southeast Texas.

Table 9. Simulated compaction by model layer and land-surface subsidence at selected benchmarks in 2018, and simulated compaction by model layer as a percentage of simulated land-surface subsidence at selected benchmarks in Montgomery and northern Harris Counties, Texas.

[GULF model, Gulf Coast Land Subsidence and Groundwater-Flow model; GPS, Global Positioning System]

Benchmark group	Benchmark (fig. 70*A*)	County	GULF-model-simulated hydrogeologic unit compaction in 2018, in feet				GULF-model-simulated land-surface subsidence through 2018, in feet (figs. 172–174)	Estimated land-surface subsidence through 2018, in feet[1]	Observed or estimated land-surface subsidence through 2021, in feet (fig. 96; table 4)	GULF-model-simulated hydrogeologic unit compaction as a percentage of simulated land-surface subsidence[3]			
			Layer 2 (Chicot aquifer)	Layer 3 (Evangeline aquifer)	Layer 4 (Burkeville confining unit)	Layer 5 (Jasper aquifer)				Layer 2 (Chicot aquifer)	Layer 3 (Evangeline aquifer)	Layer 4 (Burkeville confining unit)	Layer 5 (Jasper aquifer)
Conroe (fig. 174)	K 88	Montgomery	0.01	0.6	0.03	1.2	1.8	1.2	[2]1.2	0.6	33	1.7	67
	CONROE RM 1	Montgomery	0.02	0.8	0.04	1.2	2.1	1.4	1.5	1.0	38	1.9	57
	Q 88	Montgomery	0.05	1.2	0.05	0.9	2.2	1.3	[2]1.4	2.3	55	2.3	41
The Woodlands (fig. 173)	R 88	Montgomery	0.08	1.3	0.05	0.8	2.2	1.3	[2]1.3	3.6	59	2.3	36
	T 88	Montgomery	0.1	1.4	0.07	0.8	2.4	2.2	2.2	4.2	58	2.9	33
	U 88	Montgomery	0.1	1.5	0.07	0.9	2.6	2.5	[2]2.5	3.8	58	2.7	35
Northern Harris County (fig. 172)	SPRING RM 1	Harris	0.5	2.0	0.08	0.5	3.1	3.9	4.2	16	65	2.6	16
	V 660	Harris	1.4	2.7	0.09	0.2	4.4	5.1	5.2	32	61	2.0	4.5

[1]Land-surface subsidence through 2018 was estimated by (1) multiplying the difference of the vertical displacement through 2019 and through 2020 at the closest GPS station (fig. 76; table 6) by 2 to account for the period 2018–20, then (2) differencing the subsidence through 2020–21 at the benchmark (table 4) and the value from (1).

[2]Not included in figure 96.

[3]Percentages may not sum to 100 because of rounding differences.

Extensometers

The range of simulated compaction and subsidence produced by the Posterior and GULF model generally bracket the observed compaction and observed or estimated subsidence at each extensometer site (figs. 153–156). The greatest compaction residuals occurred at the Addicks site where simulated compaction was several feet less than observed compaction despite the Posterior bracketing the compaction observations (figs. 153). However, subsidence at this site was oversimulated, generally due to the onset of subsidence early in the model simulation (prior to about 1920), which resulted in the general oversimulation of subsidence through the remainder of the model period (fig. 153). As seen with the benchmark fit to observations, subsidence was undersimulated at the extensometers in southeastern Harris County but was slightly oversimulated at the extensometers in central and south-central Harris County (figs. 153–156).

Global Positioning System Stations

The Posterior and GULF model both reproduce most GPS observation data across the model domain, indicating the historical subsidence processes represented in the GPS observations is well represented (figs. 157–171). Because of the kilometer-sized (1-km x 1-km) model grid cells, the GULF model cannot easily reproduce the millimeter-scale vertical-displacement changes common from year-to-year in some areas; therefore, figures 157–171 register the initial value for the vertical-displacement data to the amount of simulated subsidence prior to installation of the GPS stations. In this way, the GPS vertical-displacement data can be considered in the context of the overall estimated subsidence near each GPS site.

Simulated Compaction at Selected Benchmarks

In the greater Houston area, the GULF model was used to estimate compaction in each hydrogeologic unit, with a focus on the geologic units that contain the Jasper aquifer, at selected benchmarks in northern Harris County and in Montgomery County. Most groundwater withdrawals from the Jasper aquifer are in Montgomery County, and a smaller amount of withdrawals are in northern Harris County. These areas coincide with the areas where subsidence has occurred (fig. 70*B*) as described in the "Land-Surface Subsidence" section. Compaction in each aquifer unit is described herein and in table 9, along with subsidence at selected benchmarks. Percentages of compaction in each hydrogeologic unit may not sum to 100 because of rounding differences (table 9).

Simulated Jasper aquifer compaction in northern Harris County in 2018 near benchmark V 660 was about 0.2 ft, or about 5 percent of the simulated subsidence of 4.4 ft through 2018 (fig. 172). Subsidence at this benchmark was undersimulated by 0.7 ft (table 9). Near benchmark V 660, large declines in groundwater levels in the Jasper aquifer occurred years later compared to when they occurred in the Chicot and Evangeline aquifers (fig. 96*A*). Additionally, the elevation of the top of the Jasper aquifer at benchmark V 660 is about 1,650 ft below NAVD 88, below which little compaction is expected to occur as explained in the "Deep-Seated Compaction" section. Therefore, little subsidence stemming from declining water levels in the Jasper aquifer was expected. Comparatively, compaction amounts in the Chicot and Evangeline aquifers and Burkeville confining unit at this site were 1.4 ft, 2.7 ft, and 0.09 ft, or about 32 percent, 61 percent, and 2.0 percent, respectively, of simulated subsidence (fig. 172; table 9). The Chicot aquifer groundwater level near this benchmark has risen somewhat (fig. 96*A*) and is slowly approaching the 120–180 ft bls range common to many Chicot aquifer wells in central, south-central, and southeastern Harris County where groundwater levels have risen for a longer period (figs. 25–27). Greater groundwater-level declines occurred in the Evangeline aquifer near this benchmark than declines in the Chicot aquifer; however, the Evangeline aquifer groundwater level has risen somewhat. Some subsidence in the Chicot and Evangeline aquifers at this benchmark is likely to continue, reflected in the modeled results, as pore pressures in the fine-grained interbeds continue to reach equilibrium with the surrounding aquifer sediment.

Simulated Jasper aquifer compaction in northern Harris County in 2018 near benchmark SPRING RM 1 (fig. 70*A*) was about 0.5 ft, or about 16 percent of the simulated subsidence of 3.1 ft through 2018 (fig. 172). Subsidence at this benchmark was undersimulated by about 0.8 ft (table 9). Comparatively, compaction amounts in the Chicot and Evangeline aquifers and Burkeville confining unit were 0.5 ft, 2.0 ft, and 0.08 ft, or about 16 percent, 65 percent, and 2.6 percent, respectively, of simulated subsidence (fig. 172; table 9). Jasper aquifer groundwater-level declines near benchmark SPRING RM 1 were greater than the groundwater-level declines near benchmark V 660 during 2003–20 (fig. 96*B*), and the elevation of the top of the Jasper aquifer is about 1,350 ft below NAVD 88 at this benchmark (SPRING RM 1) compared to about 1,650 ft below NAVD 88 at V 660. The increased compaction of the sediments that contain the Jasper aquifer at benchmark SPRING RM 1 compared to V 660 likely results from differences in the interbed and confining-unit storage properties at each benchmark. Interbed and confining-unit storage properties (fig. 98) are somewhat greater for the less deeply buried sediment at benchmark SPRING RM 1 compared to the more deeply buried sediment at benchmark V 660, and the more deeply buried sediment at benchmark V 660 was already partially compacted prior to 2003, reducing additional compaction at this site.

Simulated Jasper aquifer compaction in The Woodlands in 2018 near benchmark T 88 (fig. 70*A*) was about 0.8 ft, or about 33 percent of the simulated subsidence of 2.4 ft through 2018 (fig. 173), which is the same ratio estimated in Wang and others (2021). Subsidence at this benchmark was oversimulated by about 0.2 ft compared to the estimated subsidence (table 9). Simulated Jasper aquifer compaction (greater than 0.25 ft) began during 1998–99 concurrent with substantial groundwater-level declines (fig. 20). Comparatively, compaction amounts in the Chicot and Evangeline aquifers and Burkeville confining unit were 0.1 ft, 1.4 ft, and 0.07 ft, or

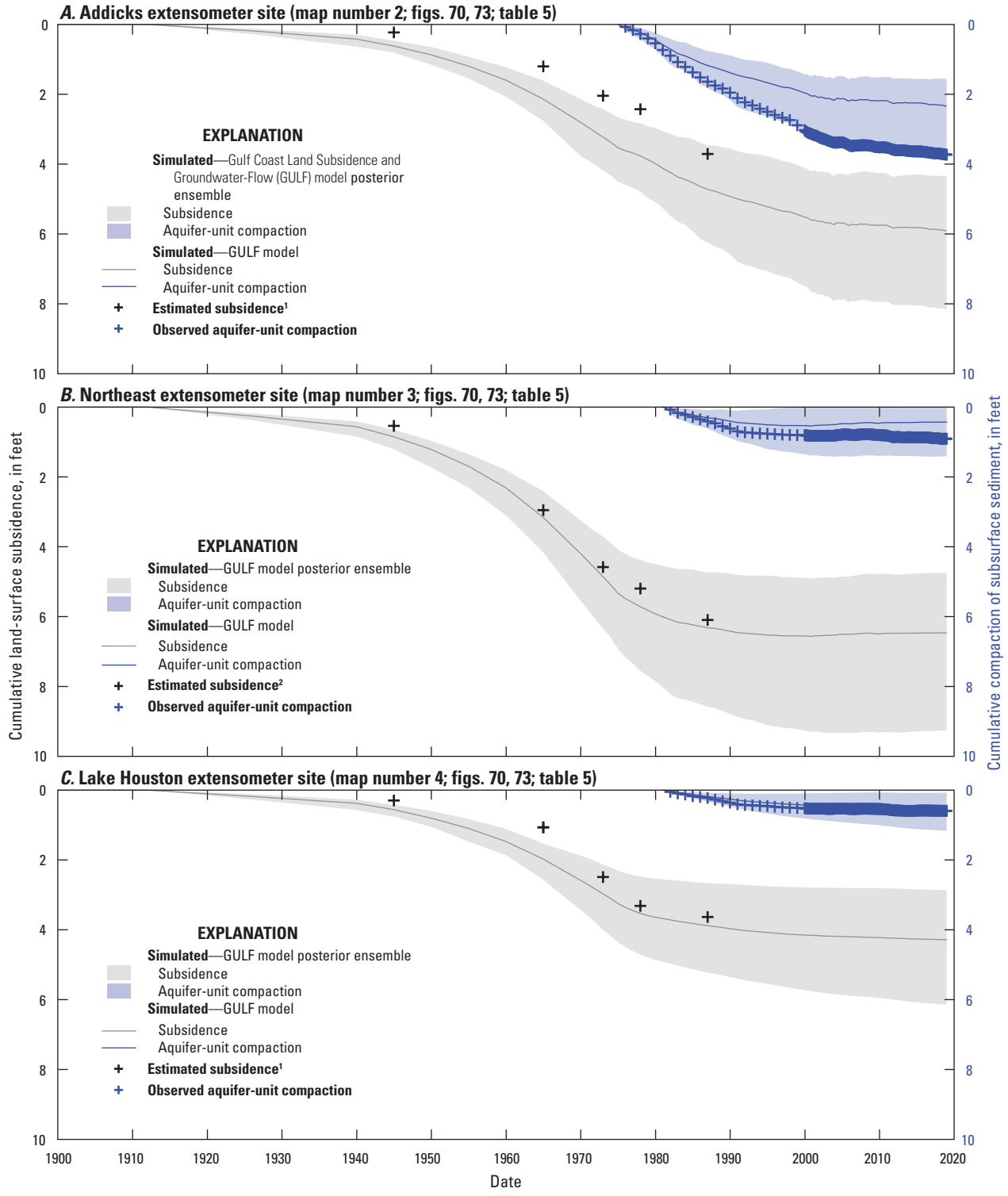

[1]Based on interpolated subsidence contour maps described in appendix 5.
[2]Based on spirit-level data at benchmark R 54 (figure 70*A*; table 4) located approximately 1.2 miles southwest of the Northeast extensometer site.

Figure 153. Temporal history-matched subsidence and compaction at the *A*, Addicks, *B*, Northeast, and *C*, Lake Houston extensometer sites for the Gulf Coast Land Subsidence and Groundwater-Flow model in southeast Texas.

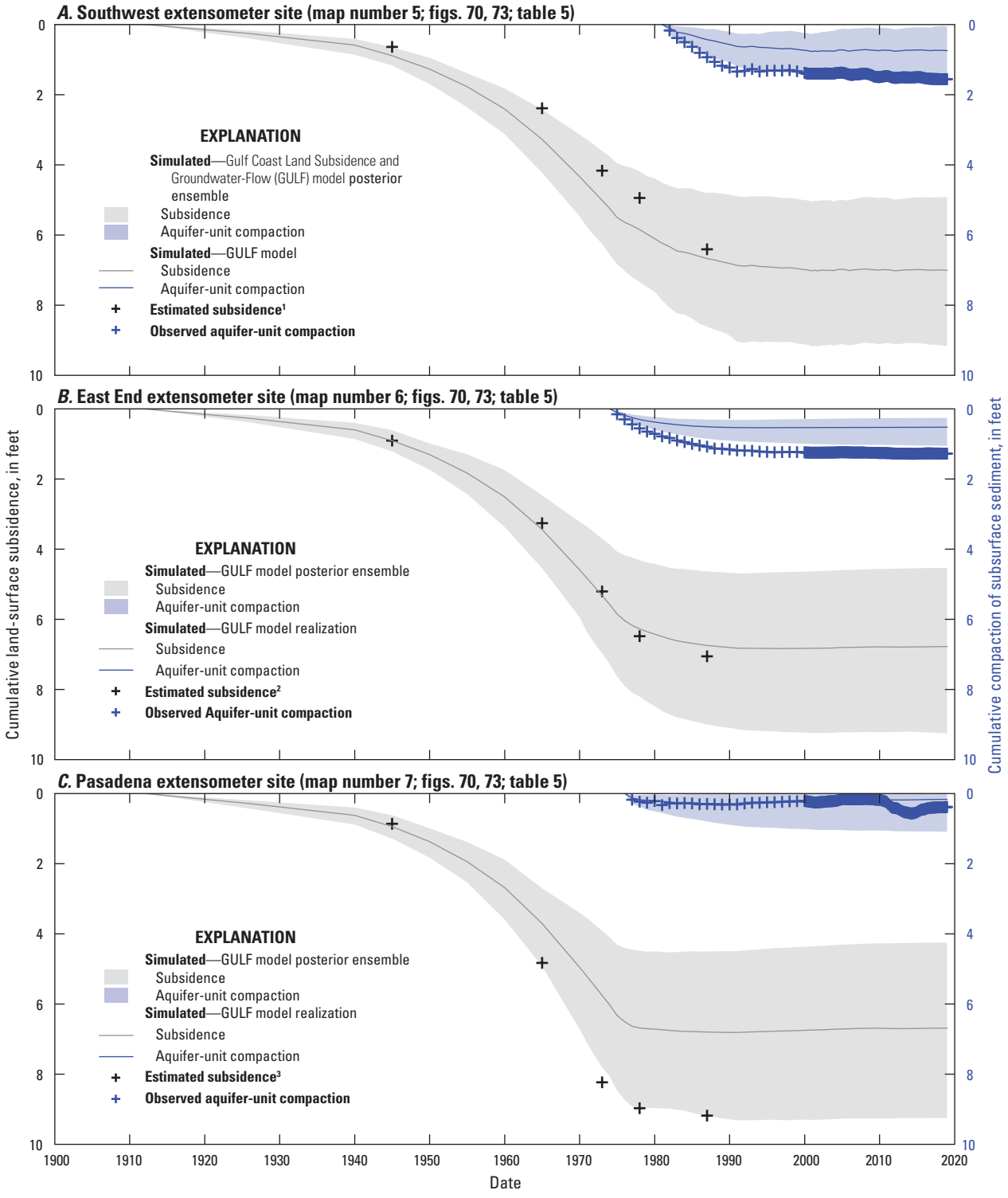

[1]Based on interpolated subsidence contour maps described in appendix 5.
[2]Based on spirit-level data at benchmark O 8 (figure 70*A*; table 4) located approximately 0.5 mile northwest of the East End extensometer site.
[3]Estimated subsidence prior to 1964 is based on interpolated subsidence contour maps described in appendix 5. Observed subsidence from 1964 to 1987 is based on spirit-level data at benchmark B 1147 (figure 70*A*; table 4) located approximately 0.1 mile northwest of the Pasadena extensometer site.

Figure 154. Temporal history-matched subsidence and compaction at the *A*, Southwest, *B*, East End, and *C*, Pasadena extensometer sites for the Gulf Coast Land Subsidence and Groundwater-Flow model in southeast Texas.

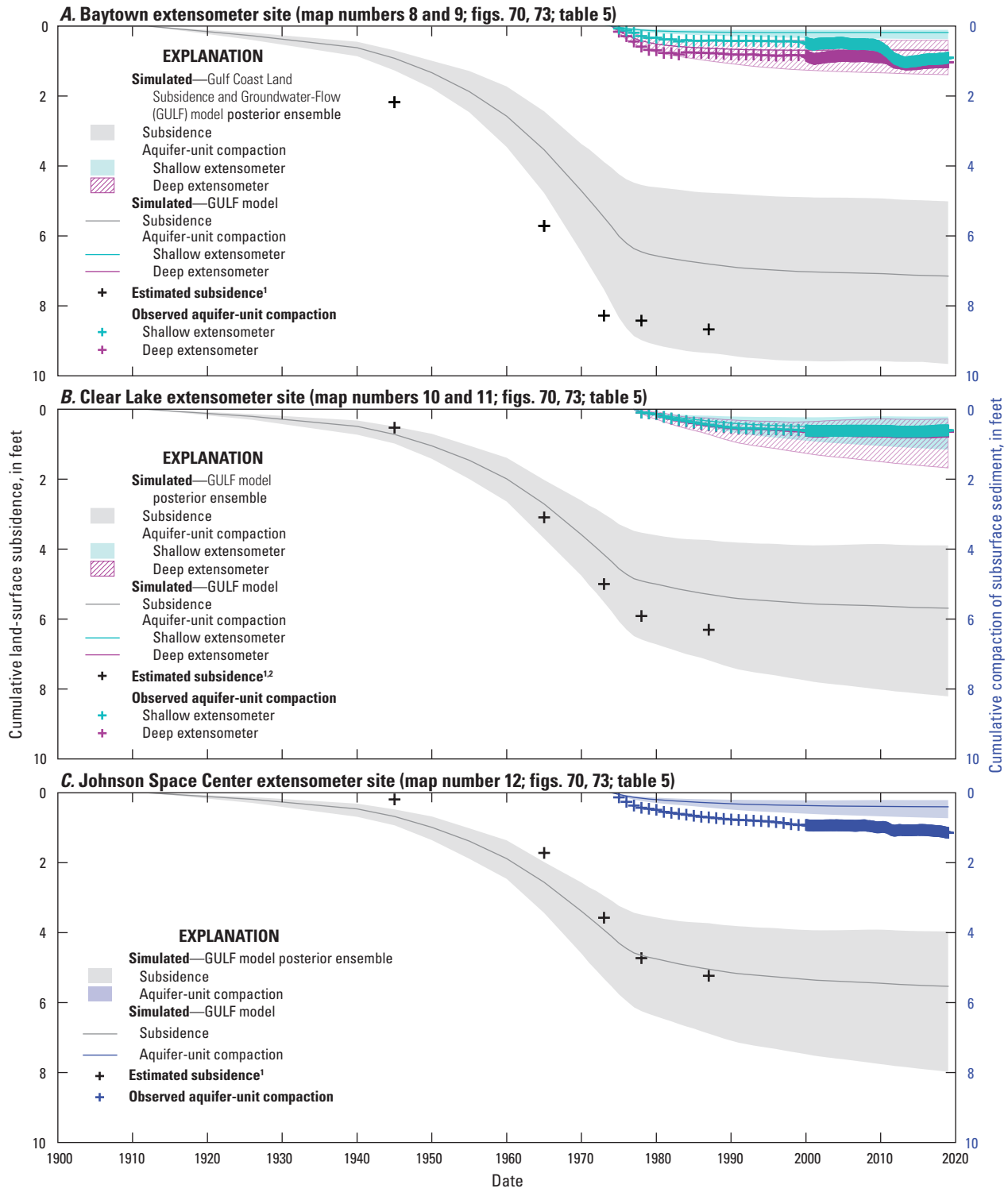

[1]Based on interpolated subsidence contour maps described in appendix 5.
[2]Observed subsidence from 1943 to 1987 is based on spirit-level data at benchmark P 646 (figure 70*A*; table 4) located approximately 2.2 miles southwest of the Clear Lake extensometer site.

Figure 155. Temporal history-matched subsidence and compaction at the *A*, Baytown, *B*, Clear Lake, and *C*, Johnson Space Center extensometer sites for the Gulf Coast Land Subsidence and Groundwater-Flow model in southeast Texas.

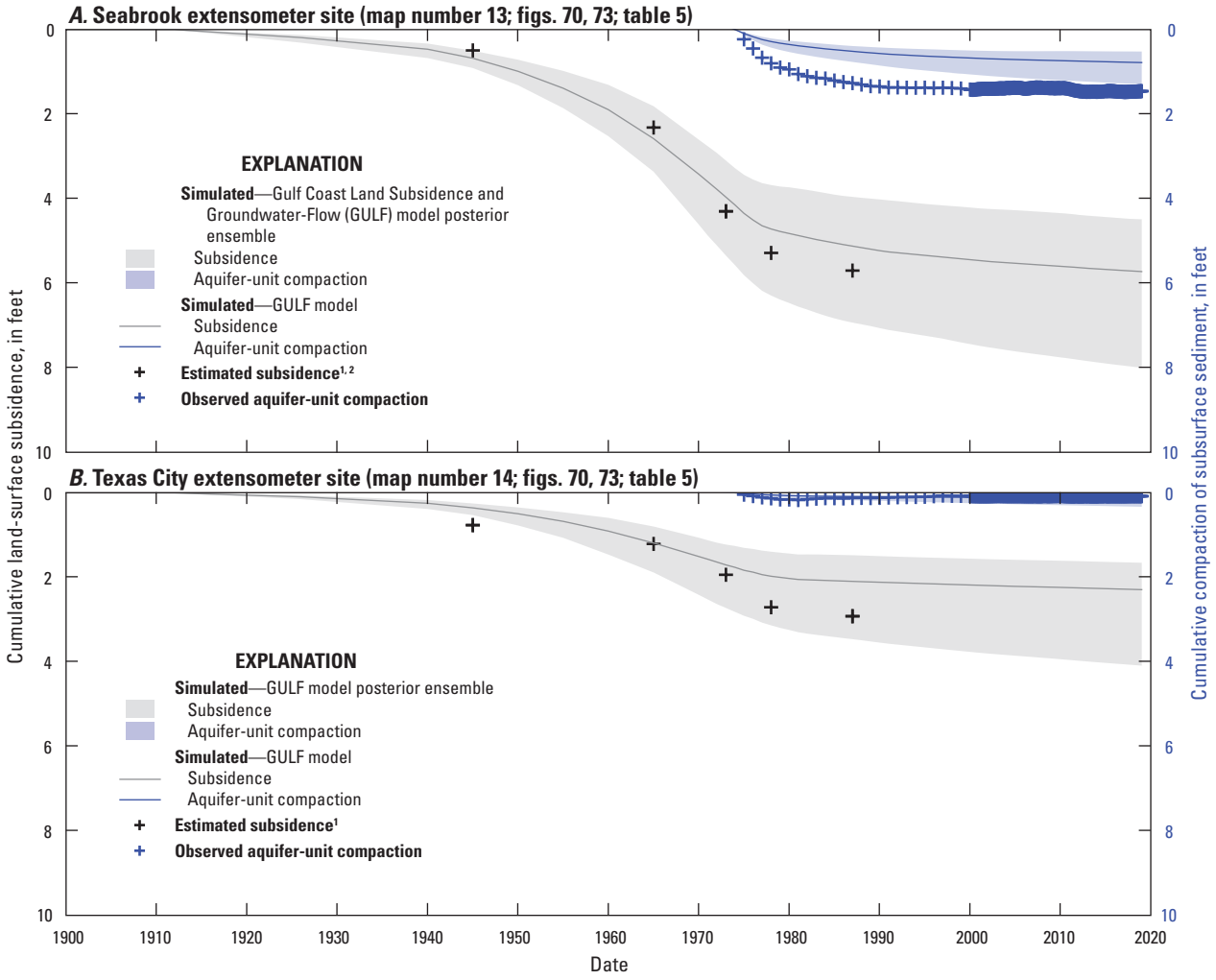

[1]Based on interpolated subsidence contour maps described in appendix 5.
[2]Observed subsidence from 1932 to 1987 is based on spirit-level data at benchmark C 170 (figure 70*A*; table 4) located approximately 0.6 mile southeast of the Seabrook extensometer site.

Figure 156. Temporal history-matched subsidence and compaction at the *A*, Seabrook and *B*, Texas City extensometer sites for the Gulf Coast Land Subsidence and Groundwater-Flow model in southeast Texas.

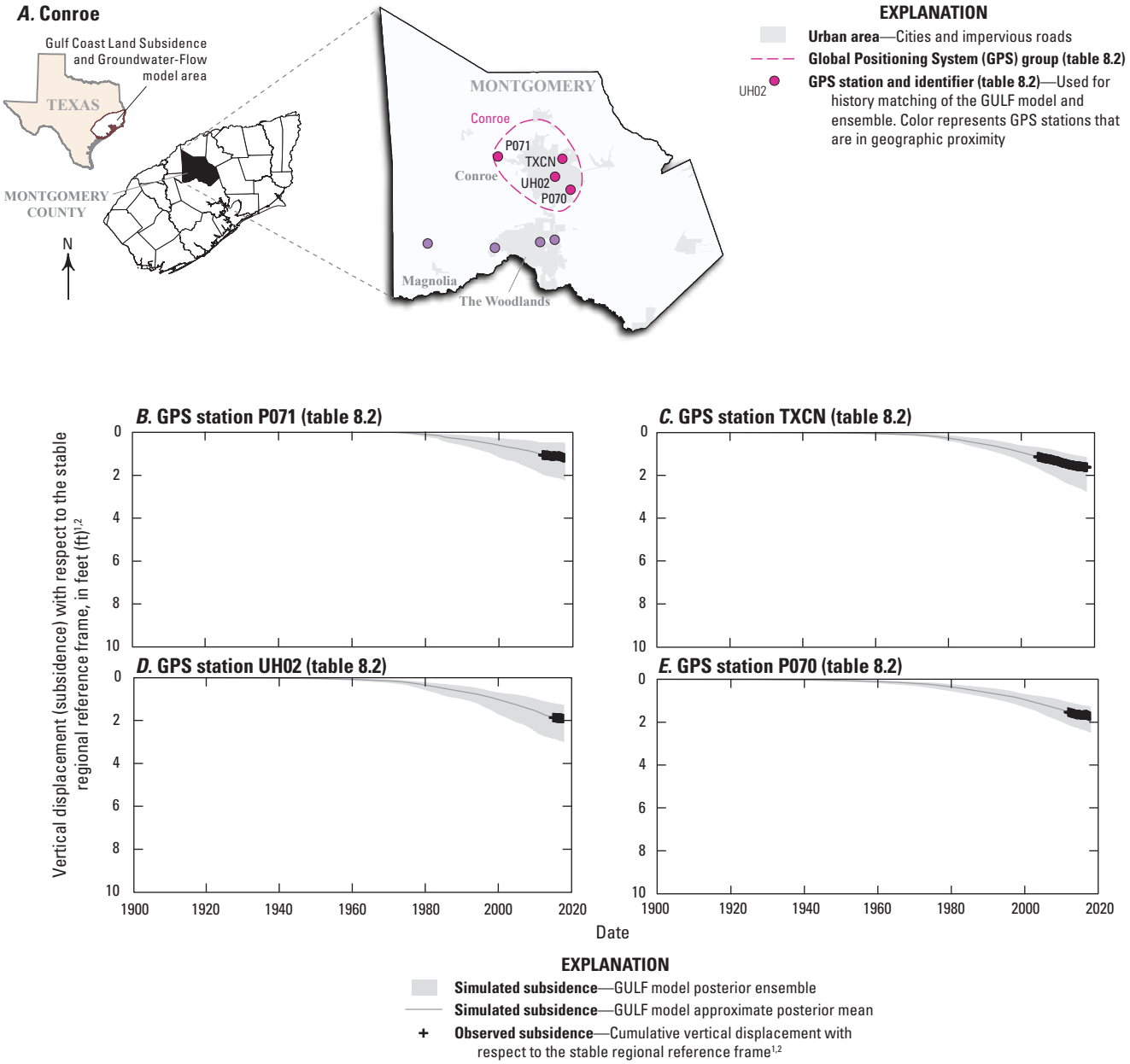

[1]The stable regional reference frame is Houston20 (Agudelo and others, 2020).
[2]The initial value for GPS vertical-displacement data is registered to the amount of simulated subsidence prior to installation of the GPS station.

Figure 157. Observed and simulated vertical displacement at Global Positioning System stations in and near Conroe, Texas.

about 4.2 percent, 58 percent, and 2.9 percent, respectively, of simulated subsidence (fig. 173; table 9). The minimal compaction of the Chicot aquifer sediment in this area was expected because of the small percentage (2–3 percent) of groundwater withdrawals from this aquifer relative to total annual groundwater withdrawals in Montgomery County (Wang and others, 2021). Jasper aquifer declines near benchmark T 88 generally were between 10.0 and 30.0 ft greater than downdip Jasper aquifer declines near benchmark SPRING RM 1 (figs. 96*B*–*C*). Additionally, the top of the Jasper aquifer is about 1,100 ft below NAVD 88 at this benchmark compared to about 1,350 ft below NAVD 88 at SPRING RM 1. Therefore, an increase in Jasper aquifer subsidence was expected at this benchmark compared to benchmarks SPRING RM 1 and V 660 owing to the less deeply buried sediment and greater Jasper aquifer groundwater use in this area.

Simulated compaction in the Jasper aquifer in 2018 near benchmark CONROE RM 1 (fig. 70*A*) was about 1.2 ft, or about 57 percent of the simulated subsidence of 2.1 ft through 2018 (fig. 174). Subsidence at this benchmark was

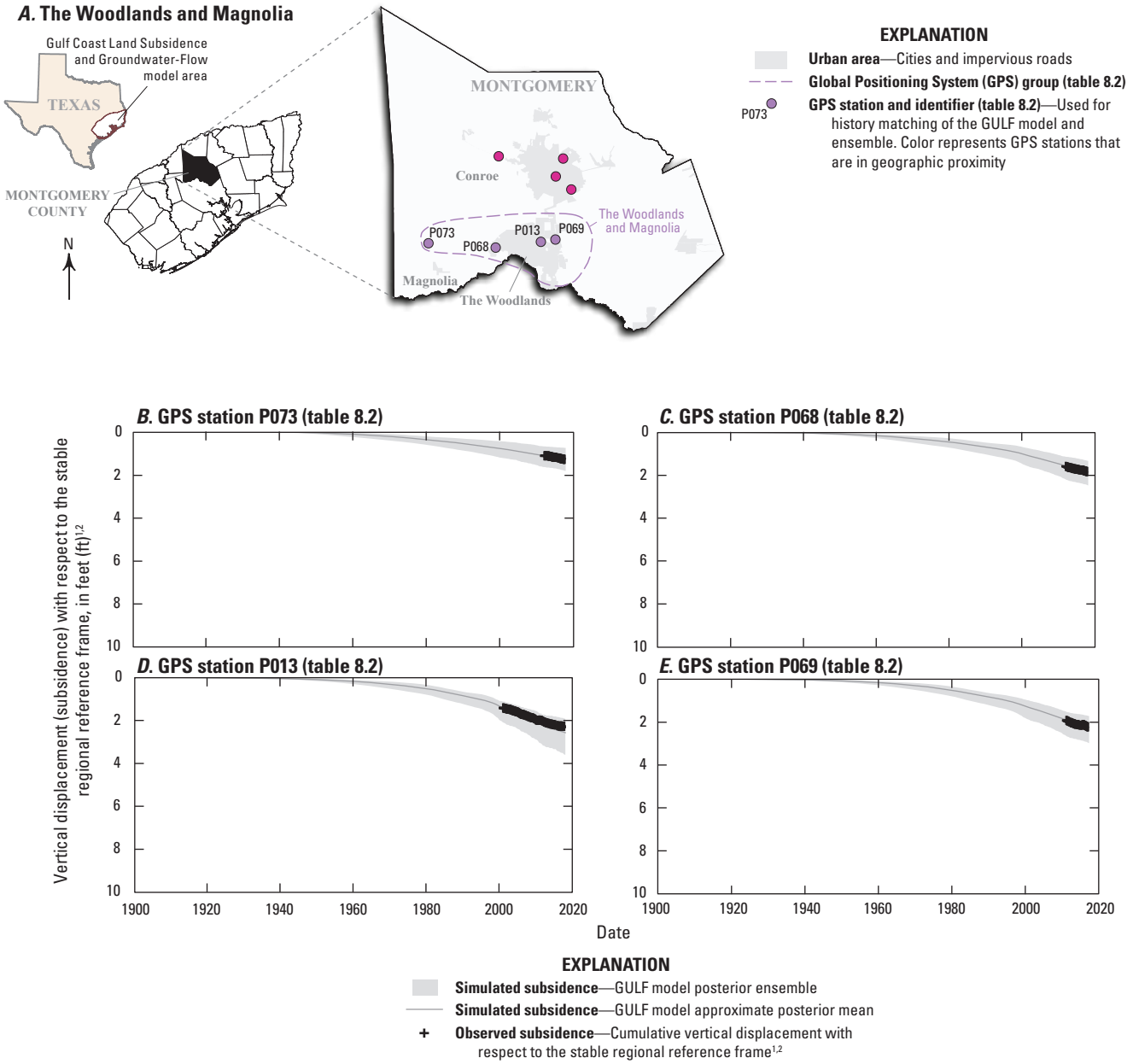

[1]The stable regional reference frame is Houston20 (Agudelo and others, 2020).
[2]The initial value for GPS vertical-displacement data is registered to the amount of simulated subsidence prior to installation of the GPS station.

Figure 158. Observed and simulated vertical displacement at Global Positioning System stations in and near The Woodlands and Magnolia, Texas.

oversimulated by about 0.7 ft (table 9). Most of the withdrawals from the Jasper aquifer for groundwater use in Conroe are made at an elevation of between about 650 ft and 1,100 ft below NAVD 88 (one site shown on fig. 50), compared to the deeper withdrawals made at about 1,000 ft to 1,500 ft below NAVD 88 in The Woodlands (figs. 45–49; table 3). The Jasper aquifer production zone in Conroe (650 ft to 1,100 ft below NAVD 88) is similar to the Evangeline aquifer production zone in The Woodlands of about 450 ft to 850 ft below NAVD 88 (figs. 45–49; table 3), and groundwater-level declines are similar in the Jasper aquifer in Conroe (fig. 96*D*) and in the Evangeline aquifer in The Woodlands (figs. 19–20, 96*C*). Therefore, the ratio of Jasper aquifer compaction to subsidence at CONROE RM 1 (57 percent, table 9) was comparable to the ratio of Evangeline aquifer compaction to subsidence at T 88 (58 percent, table 9) (figs. 172–173). Compaction amounts in the Chicot and Evangeline aquifers and Burkeville confining unit at CONROE RM 1 were 0.02 ft, 0.8 ft, and 0.04 ft, or about 1.0 percent, 38 percent, and 1.9 percent, respectively, of simulated subsidence (fig. 174; table 9).

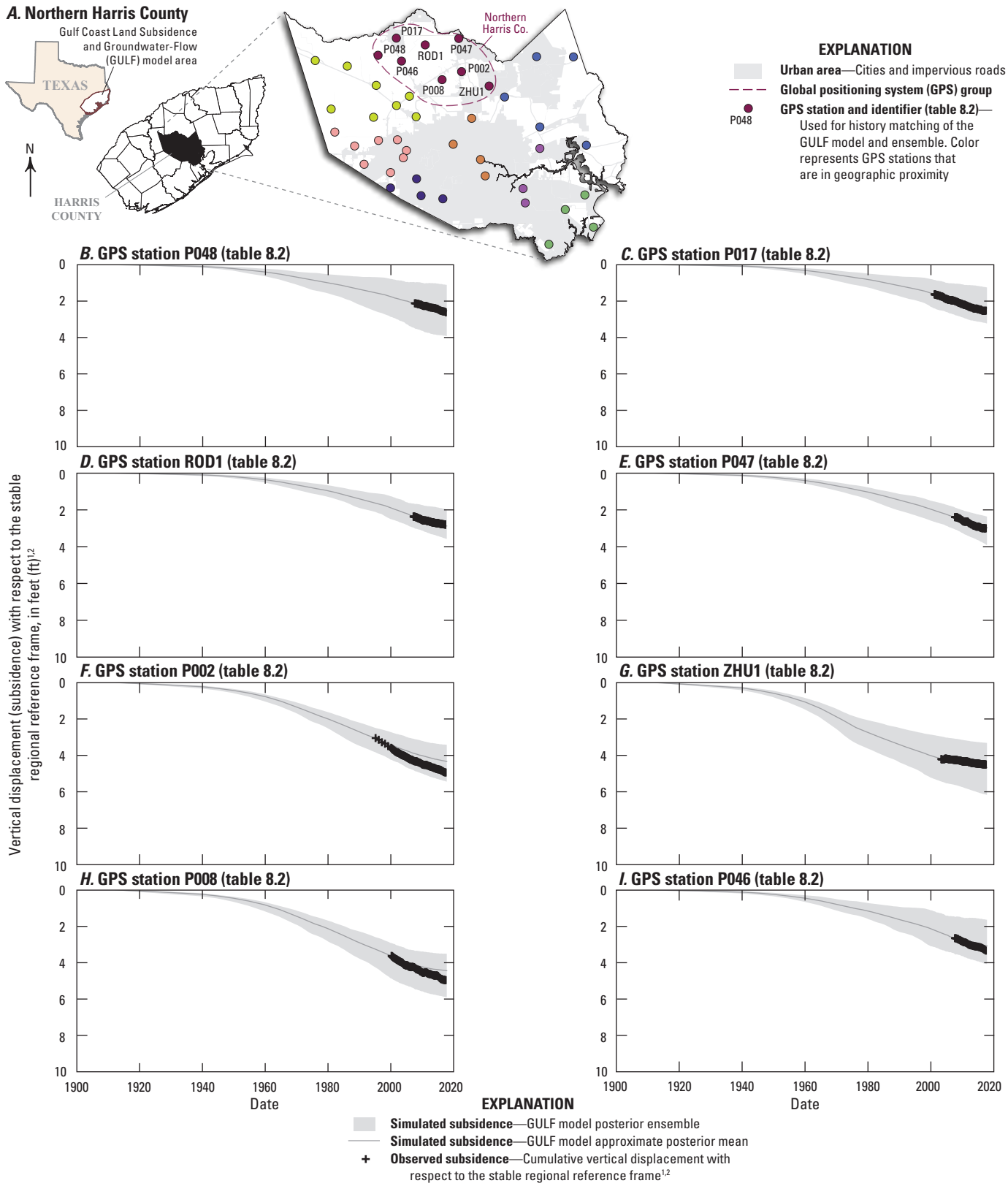

[1]The stable regional reference frame is Houston20 (Agudelo and others, 2020).
[2]The initial value for GPS vertical-displacement data is registered to the amount of simulated subsidence prior to installation of the GPS station.

Figure 159. Observed and simulated vertical displacement at Global Positioning System stations in and near northern Harris County in southeast Texas.

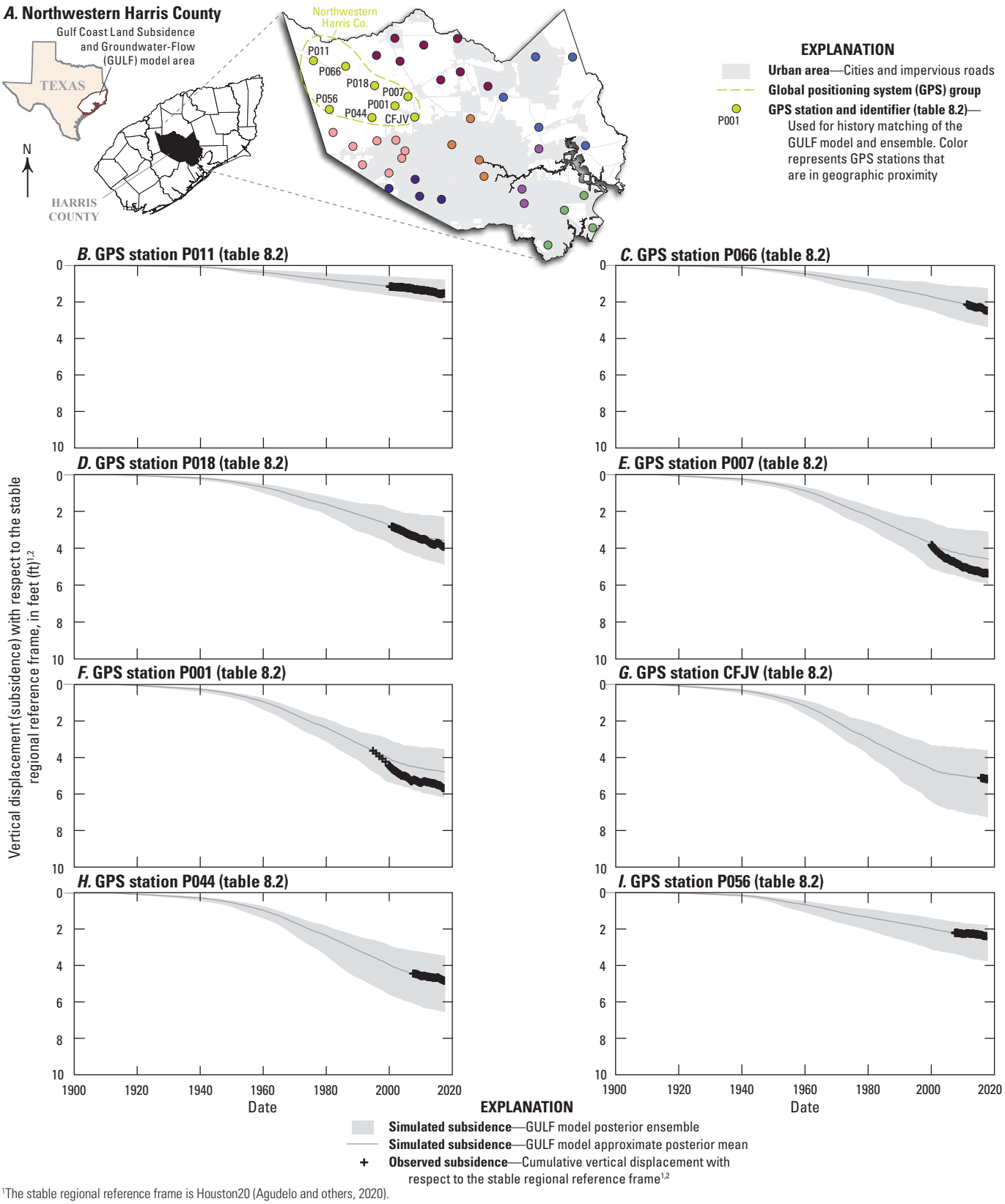

[1]The stable regional reference frame is Houston20 (Agudelo and others, 2020).
[2]The initial value for GPS vertical-displacement data is registered to the amount of simulated subsidence prior to installation of the GPS station.

Figure 160. Observed and simulated vertical displacement at Global Positioning System stations in and near northwestern Harris County in southeast Texas.

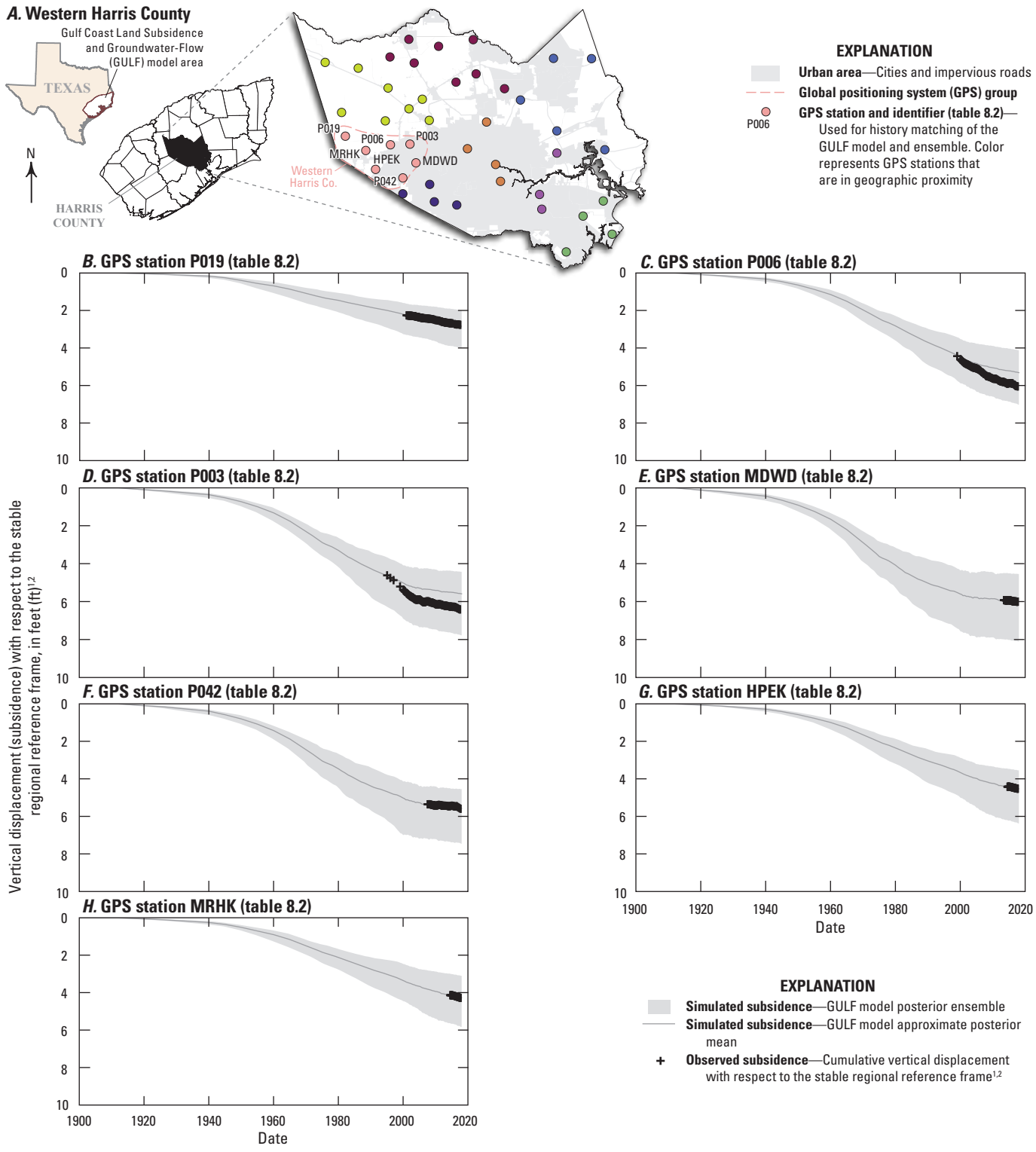

[1]The stable regional reference frame is Houston20 (Agudelo and others, 2020).
[2]The initial value for GPS vertical-displacement data is registered to the amount of simulated subsidence prior to installation of the GPS station.

Figure 161. Observed and simulated vertical displacement at Global Positioning System stations in and near western Harris County in southeast Texas.

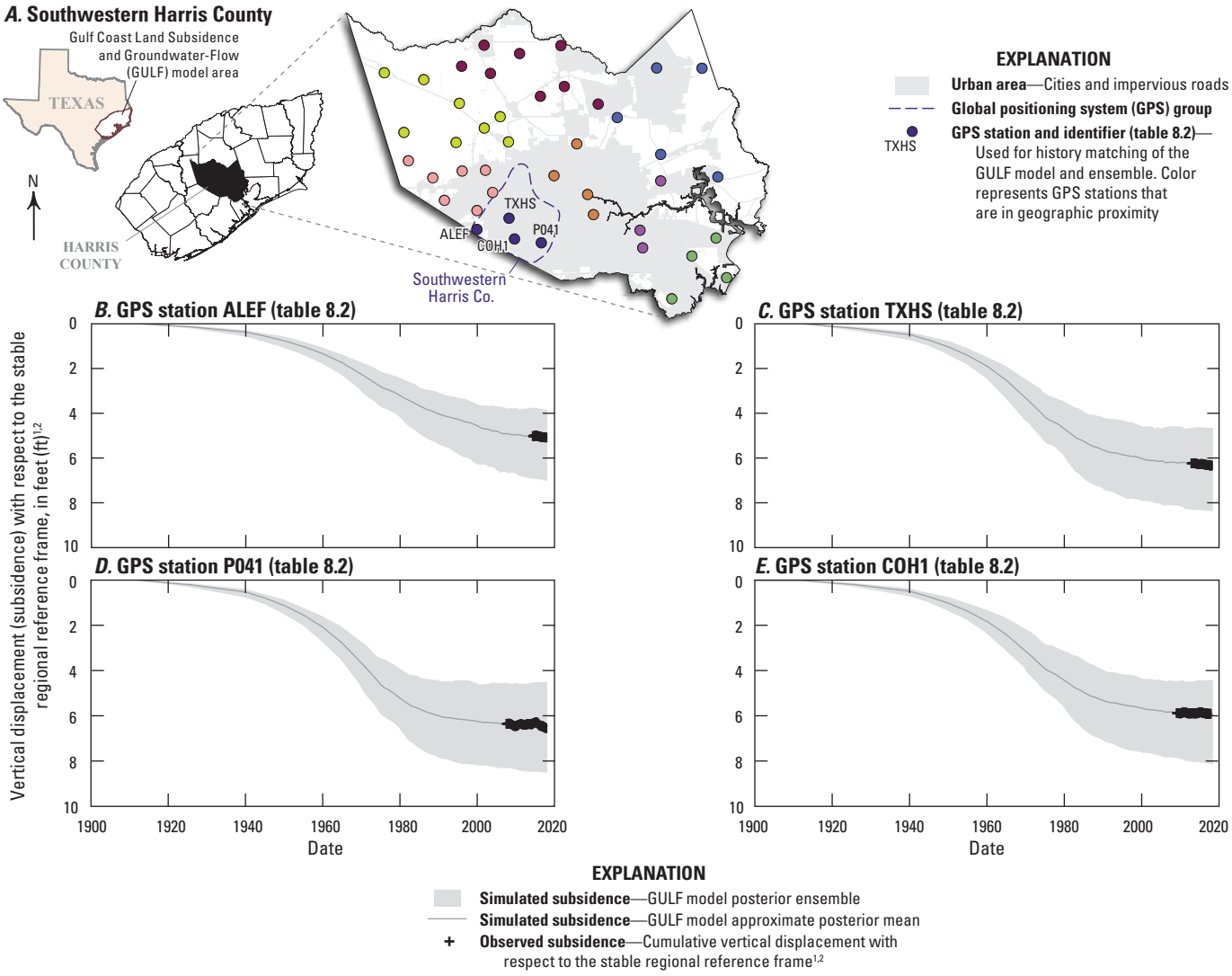

[1]The stable regional reference frame is Houston20 (Agudelo and others, 2020).
[2]The initial value for GPS vertical-displacement data is registered to the amount of simulated subsidence prior to installation of the GPS station.

Figure 162. Observed and simulated vertical displacement at Global Positioning System stations in and near southwestern Harris County in southeast Texas.

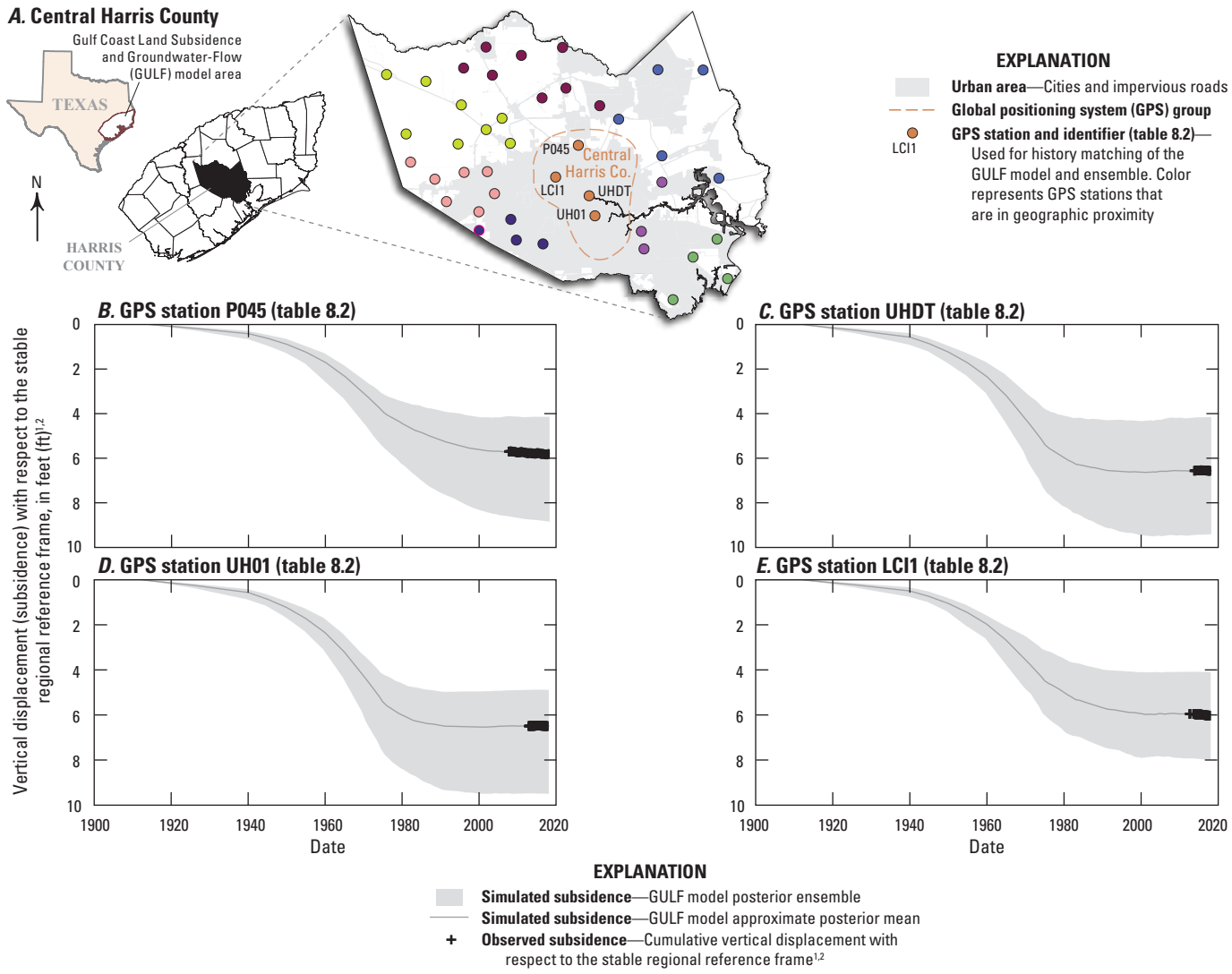

[1]The stable regional reference frame is Houston20 (Agudelo and others, 2020).
[2]The initial value for GPS vertical-displacement data is registered to the amount of simulated subsidence prior to installation of the GPS station.

Figure 163. Observed and simulated vertical displacement at Global Positioning System stations in and near central Harris County in southeast Texas.

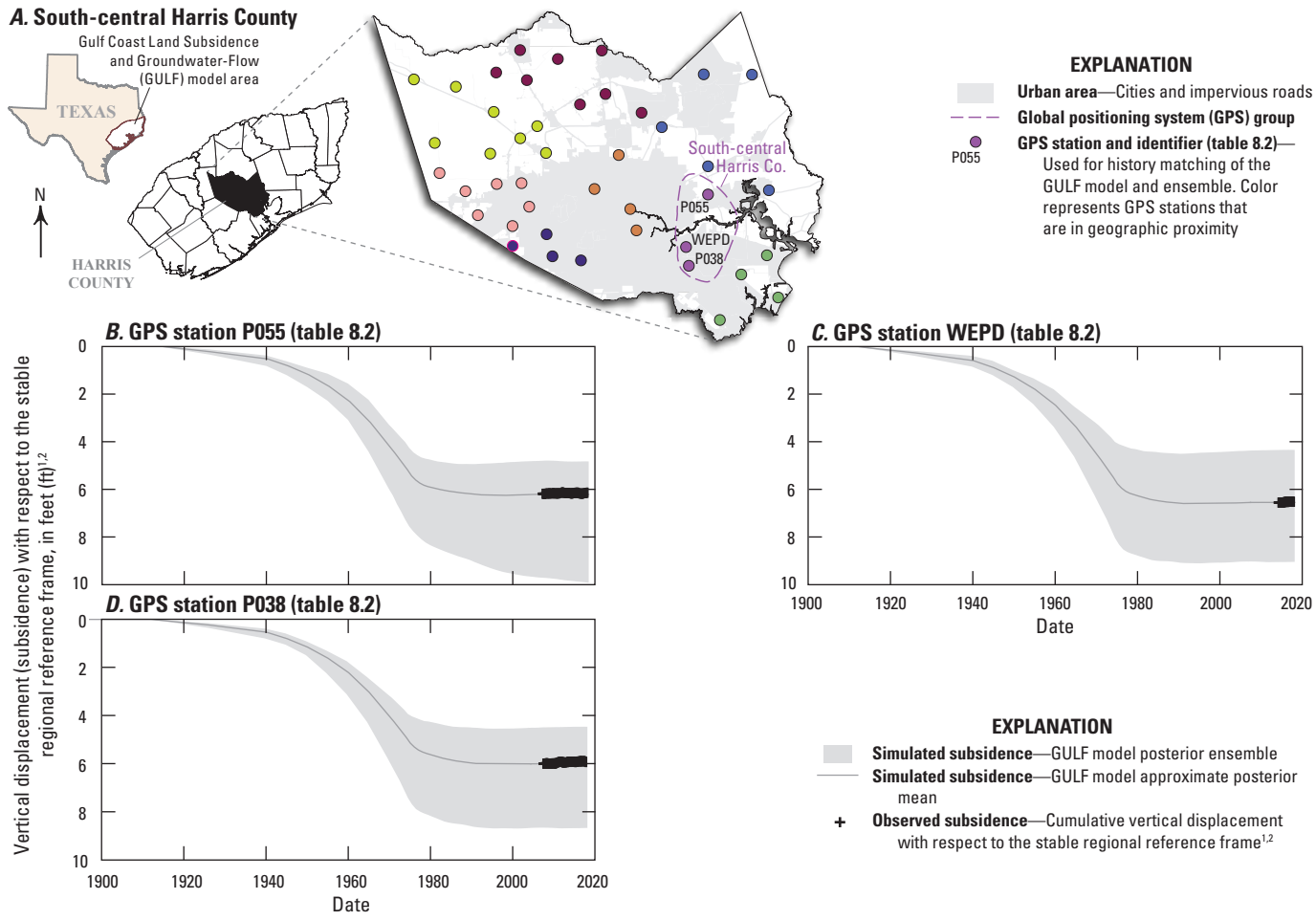

[1]The stable regional reference frame is Houston20 (Agudelo and others, 2020).
[2]The initial value for GPS vertical-displacement data is registered to the amount of simulated subsidence prior to installation of the GPS station.

Figure 164. Observed and simulated vertical displacement at Global Positioning System stations in and near south-central Harris County in southeast Texas.

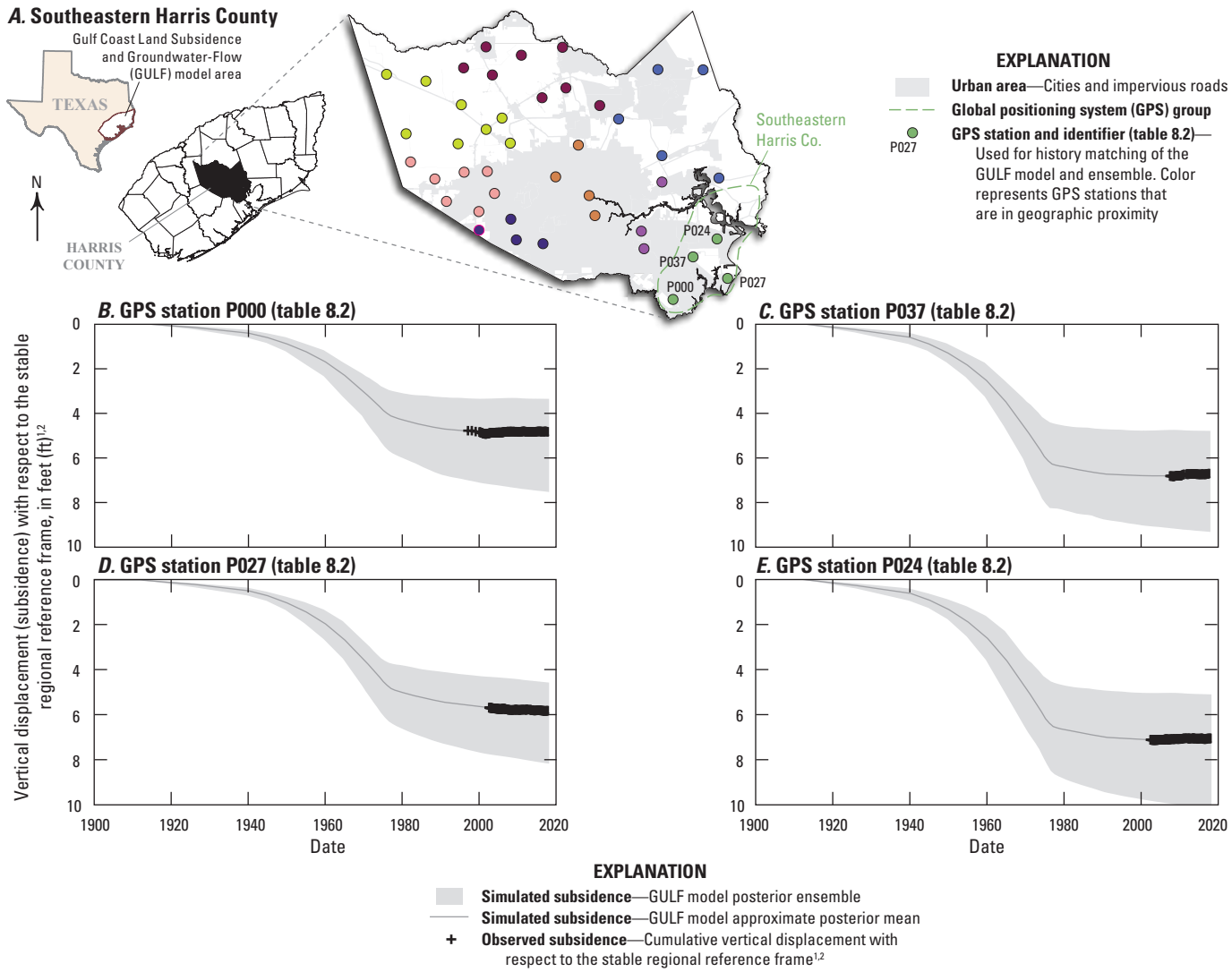

[1]The stable regional reference frame is Houston20 (Agudelo and others, 2020).
[2]The initial value for GPS vertical-displacement data is registered to the amount of simulated subsidence prior to installation of the GPS station.

.

Figure 165. Observed and simulated vertical displacement at Global Positioning System stations in and near southeastern Harris County in southeast Texas.

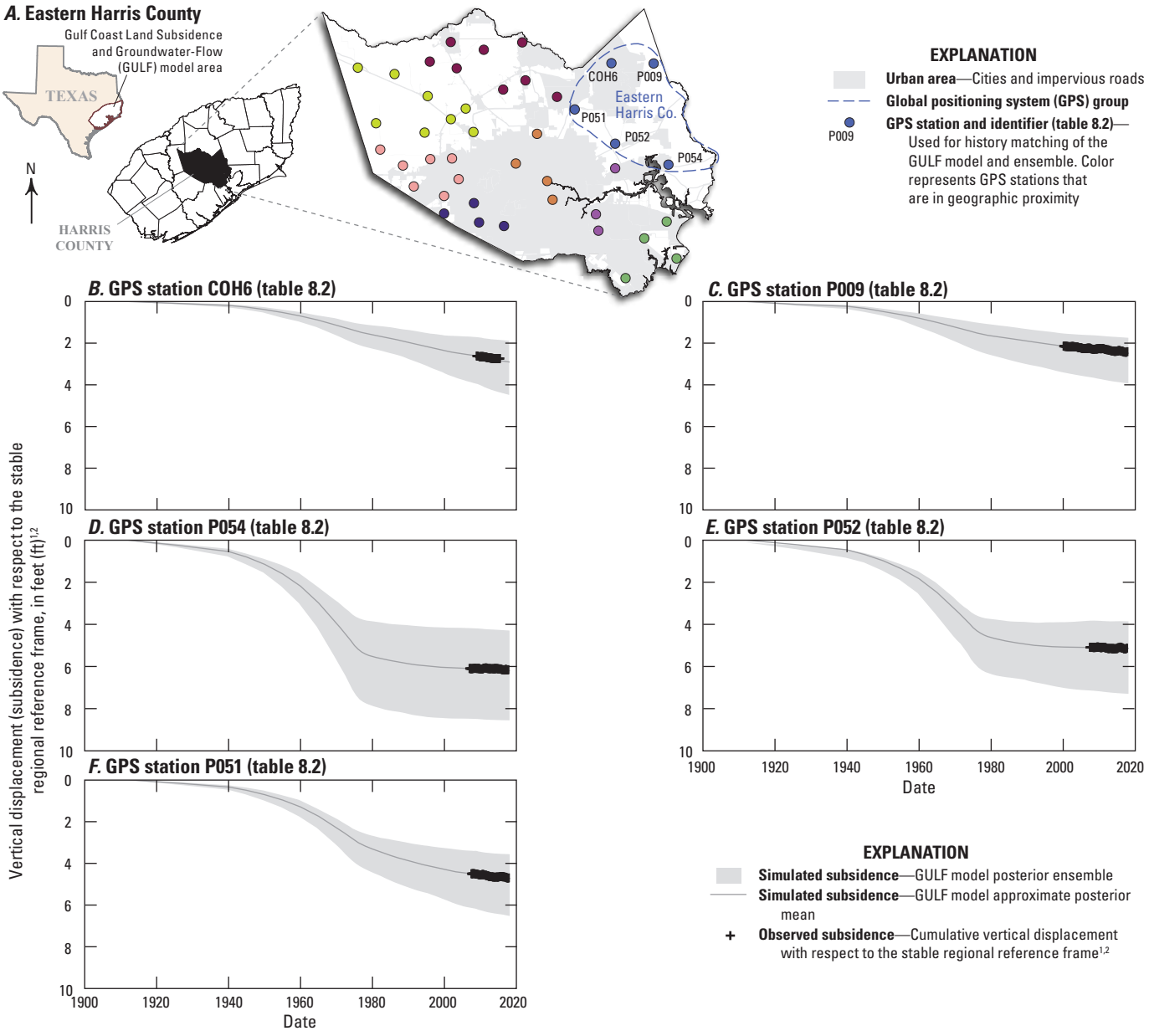

[1]The stable regional reference frame is Houston20 (Agudelo and others, 2020).
[2]The initial value for GPS vertical-displacement data is registered to the amount of simulated subsidence prior to installation of the GPS station.

Figure 166. Observed and simulated vertical displacement at Global Positioning System stations in and near eastern Harris County in southeast Texas.

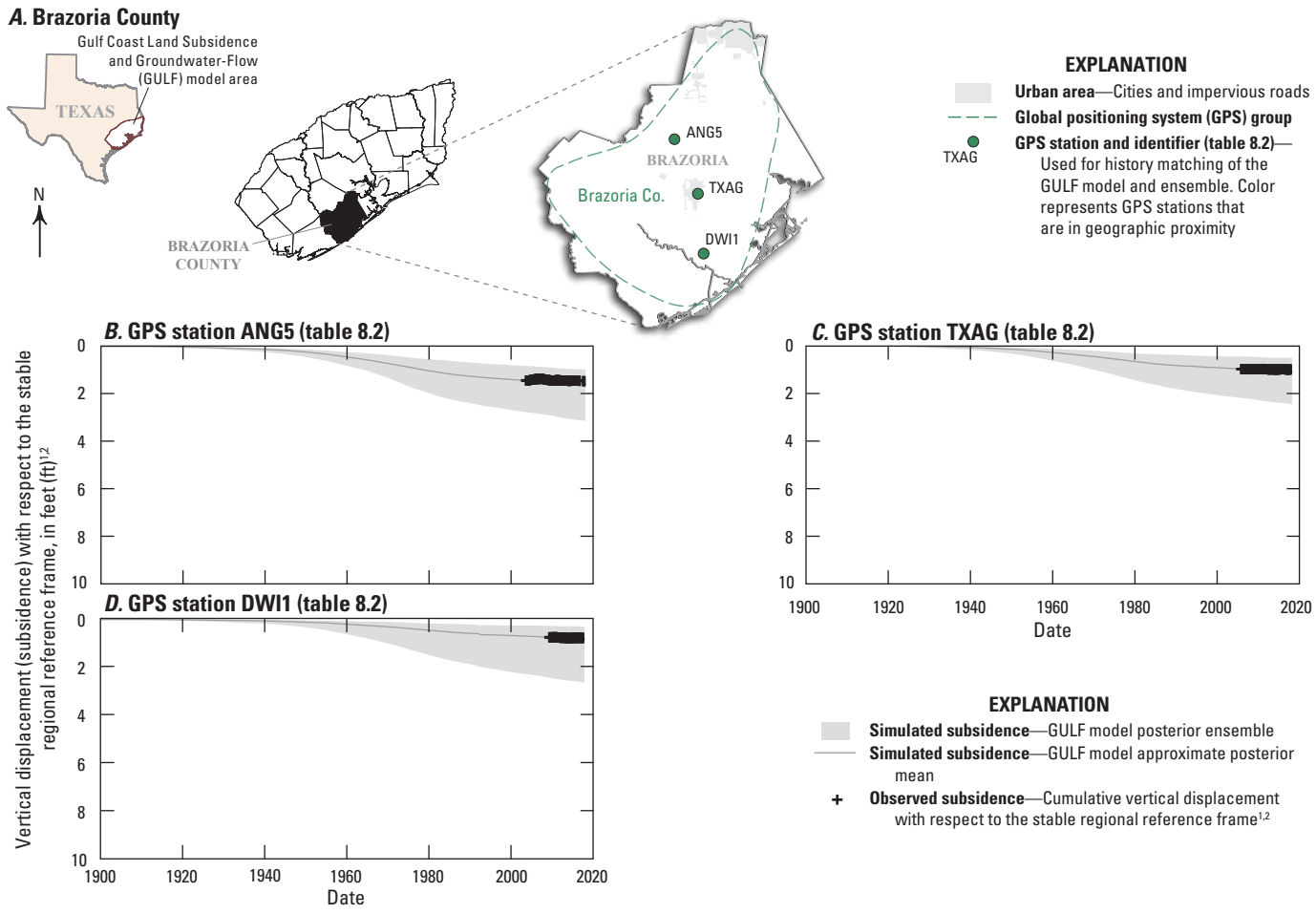

[1]The stable regional reference frame is Houston20 (Agudelo and others, 2020).
[2]The initial value for GPS vertical-displacement data is registered to the amount of simulated subsidence prior to installation of the GPS station.

Figure 167. Observed and simulated vertical displacement at Global Positioning System stations in and near Brazoria County in southeast Texas.

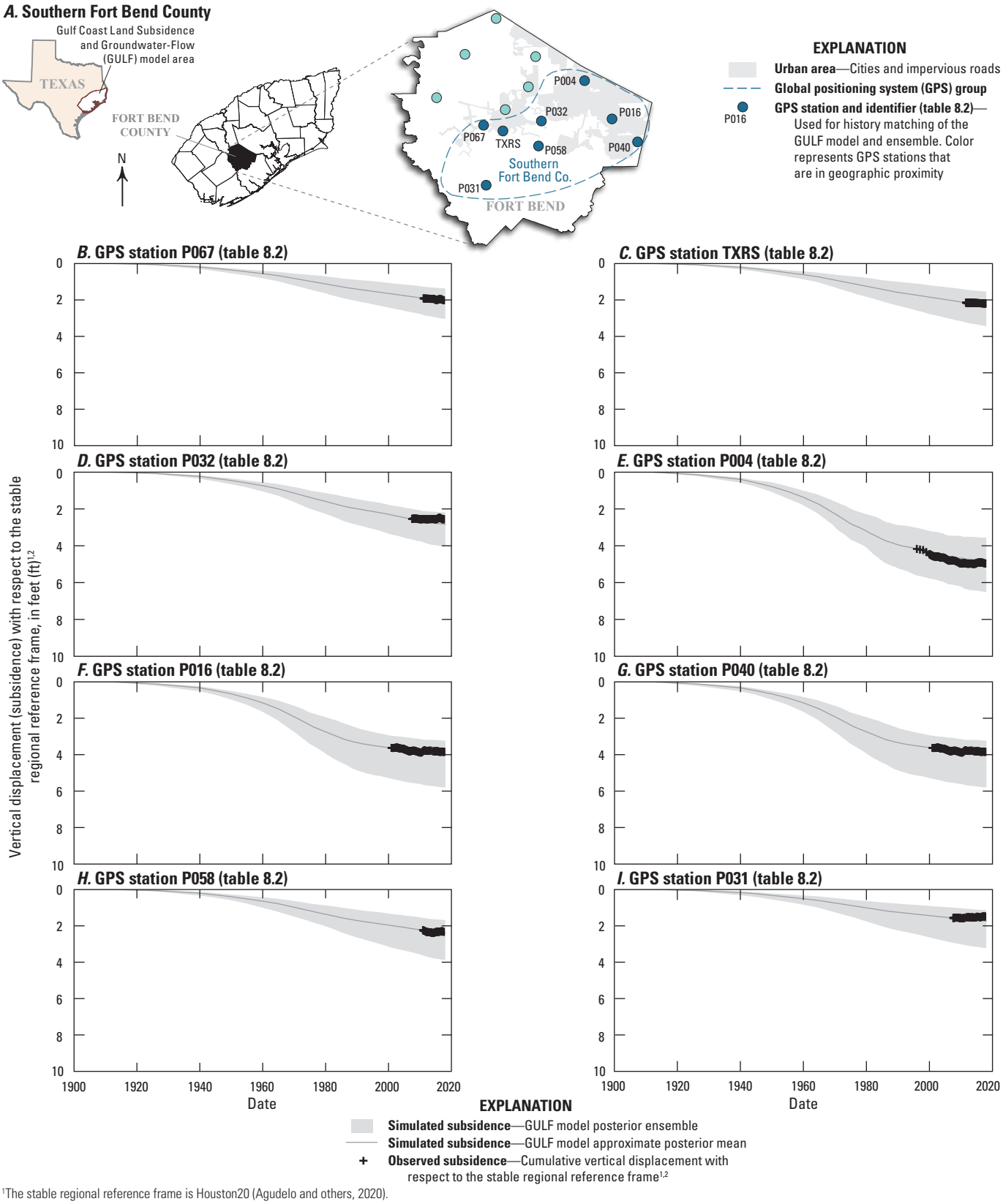

[1]The stable regional reference frame is Houston20 (Agudelo and others, 2020).
[2]The initial value for GPS vertical-displacement data is registered to the amount of simulated subsidence prior to installation of the GPS station.

Figure 168. Observed and simulated vertical displacement at Global Positioning System stations in and near southern Fort Bend County in southeast Texas.

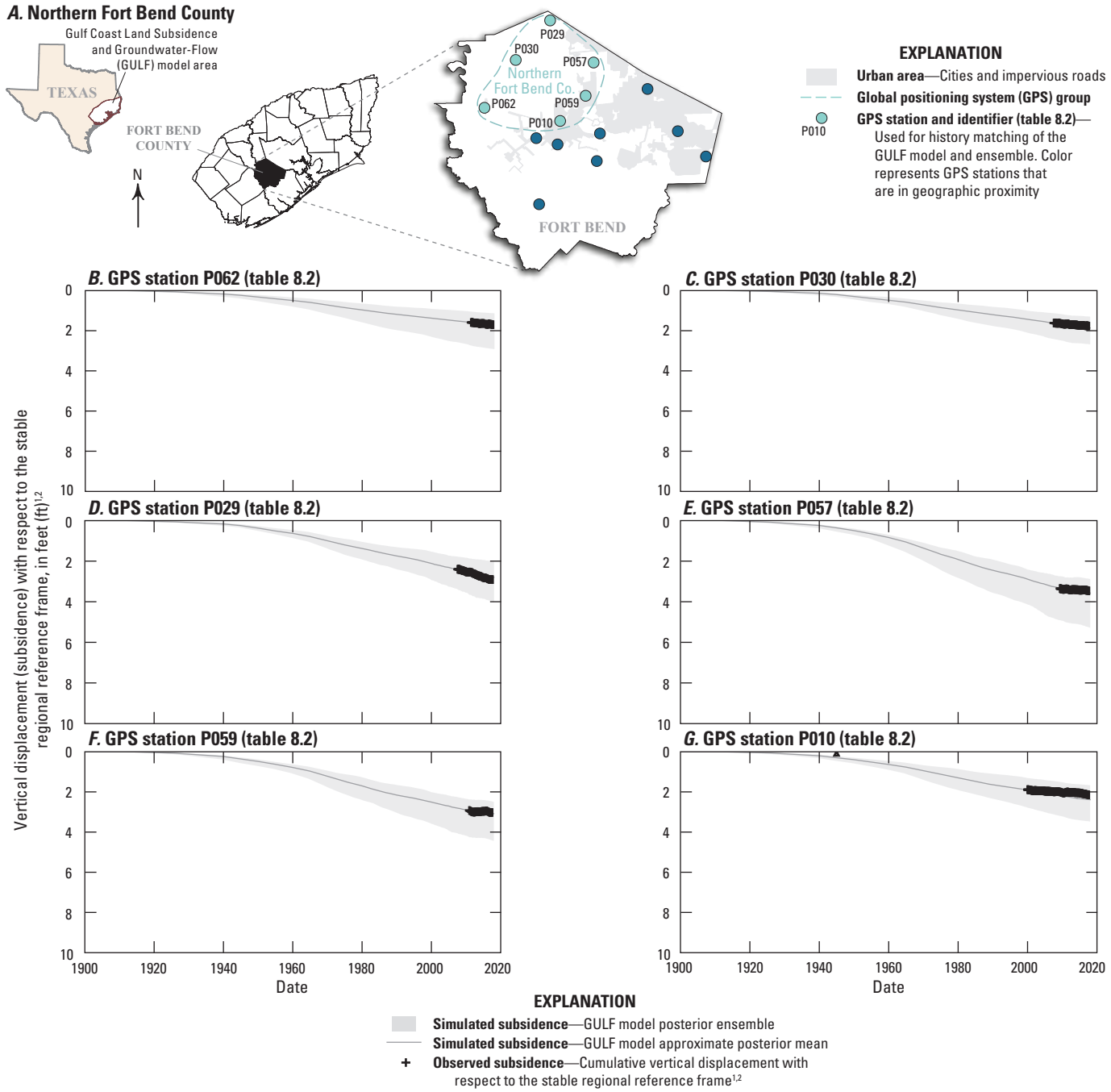

[1]The stable regional reference frame is Houston20 (Agudelo and others, 2020).
[2]The initial value for GPS vertical-displacement data is registered to the amount of simulated subsidence prior to installation of the GPS station.

Figure 169. Observed and simulated vertical displacement at Global Positioning System stations in and near northern Fort Bend County in southeast Texas.

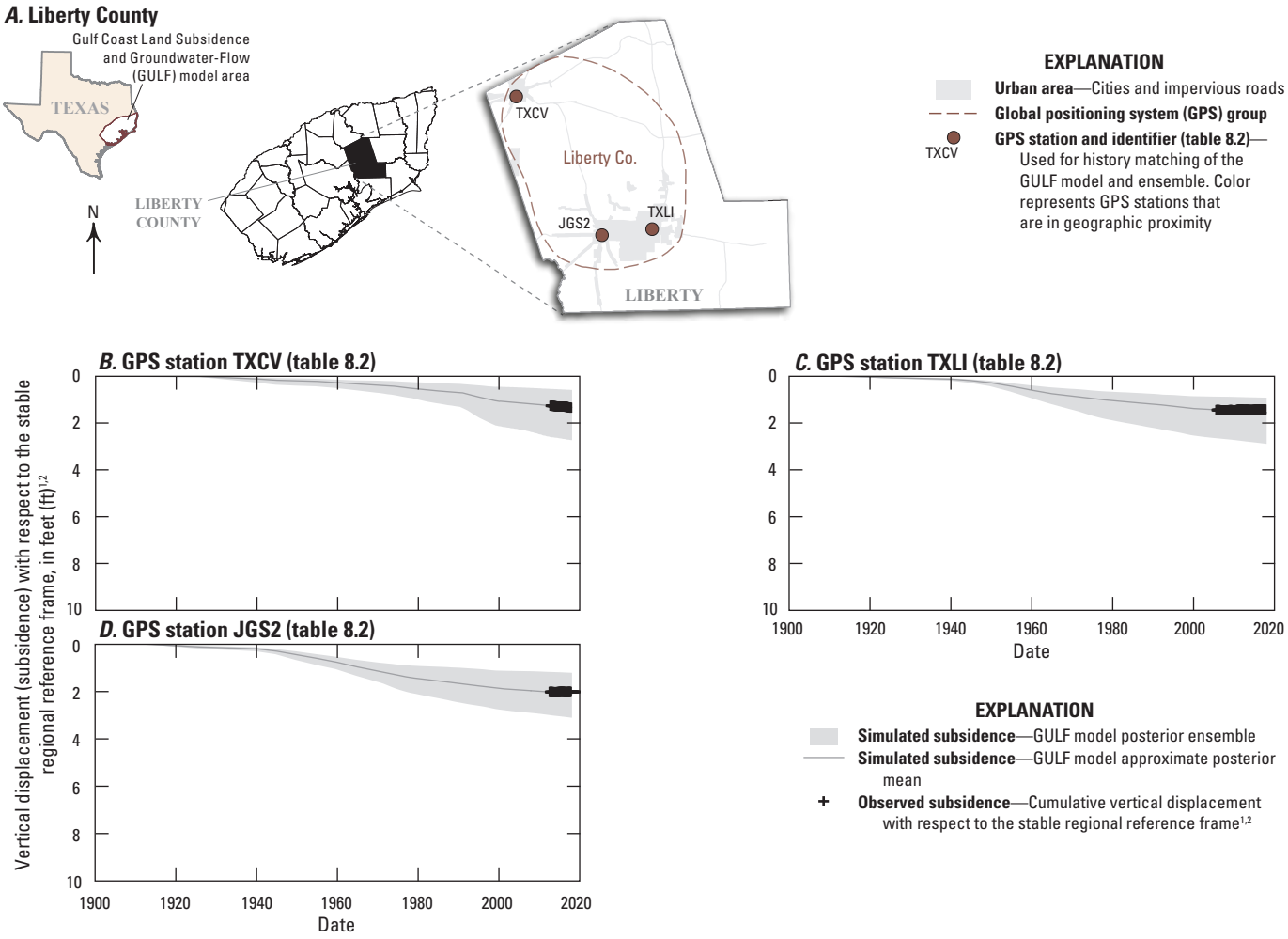

[1]The stable regional reference frame is Houston20 (Agudelo and others, 2020).
[2]The initial value for GPS vertical-displacement data is registered to the amount of simulated subsidence prior to installation of the GPS station.

Figure 170. Observed and simulated vertical displacement at Global Positioning System stations in and near Liberty County in southeast Texas.

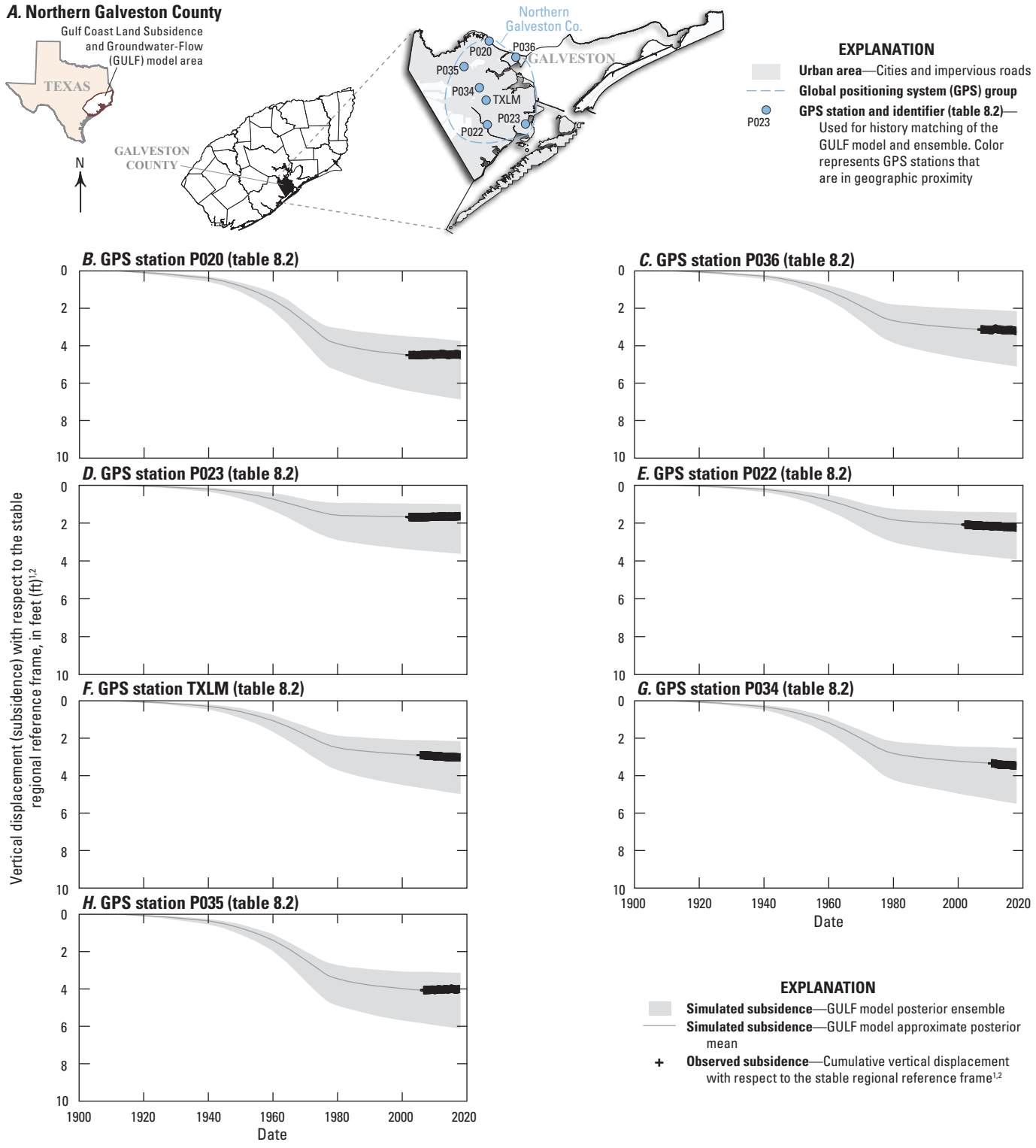

[1]The stable regional reference frame is Houston20 (Agudelo and others, 2020).
[2]The initial value for GPS vertical-displacement data is registered to the amount of simulated subsidence prior to installation of the GPS station.

Figure 171. Observed and simulated vertical displacement at Global Positioning System stations in and near northern Galveston County in southeast Texas.

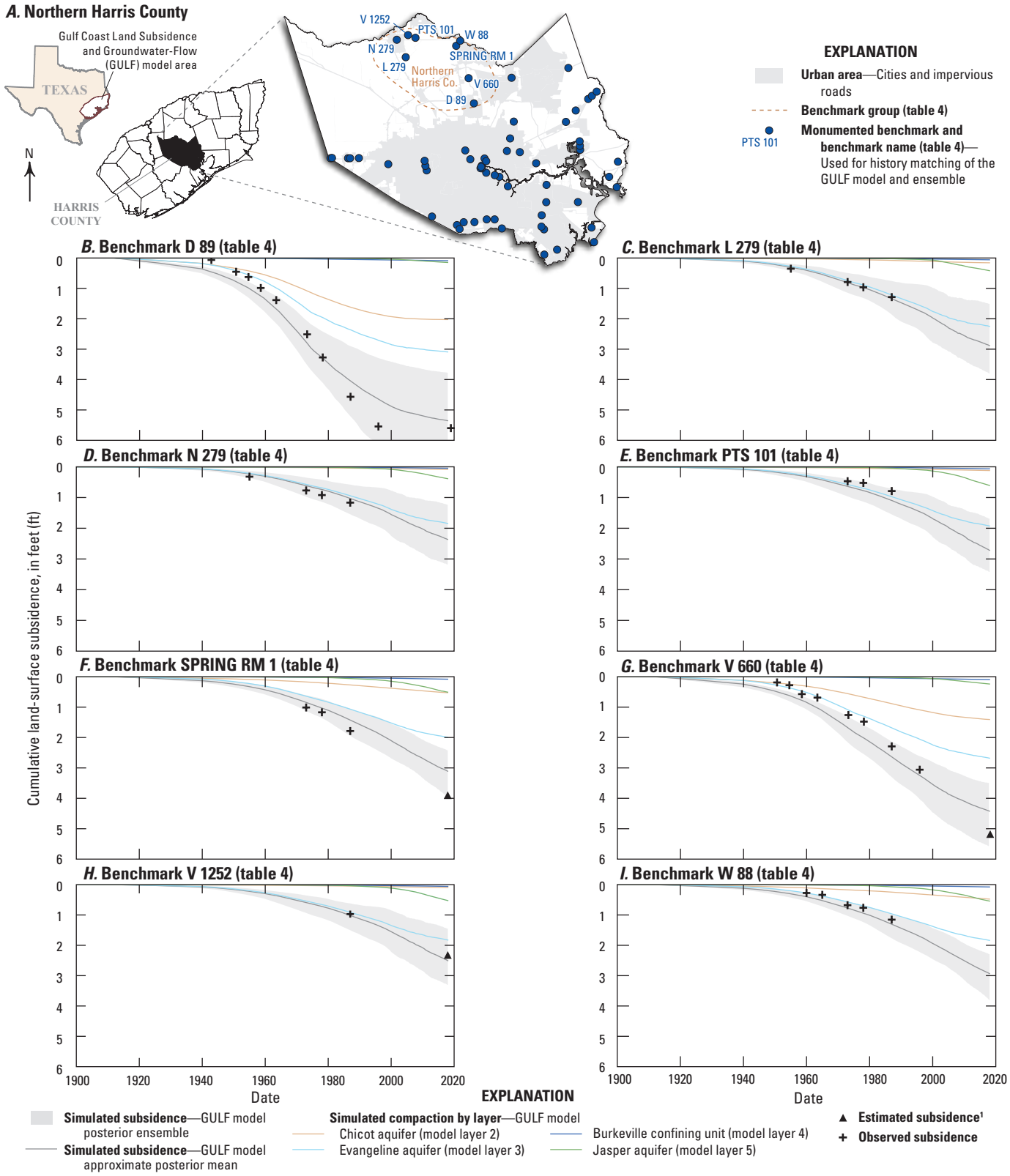

[1]The estimated subsidence through 2018 at benchmarks SPRING RM 1 and V 660 was calculated based on the methods described in table 9. The subsidence of 2.2 ft estimated at benchmark V 1252 during 1915–2018 is based on: (1) 0.7 ft of subsidence at benchmark PTS 100 from 1915 to 1978, (2) 1.6 ft of subsidence at V 1252 between 1978 and 2021, and (3) 0.1 ft of subsidence at V 1252 between 2018 and 2021.

Figure 172. Observed and simulated subsidence by model layer at benchmarks in northern Harris County in southeast Texas.

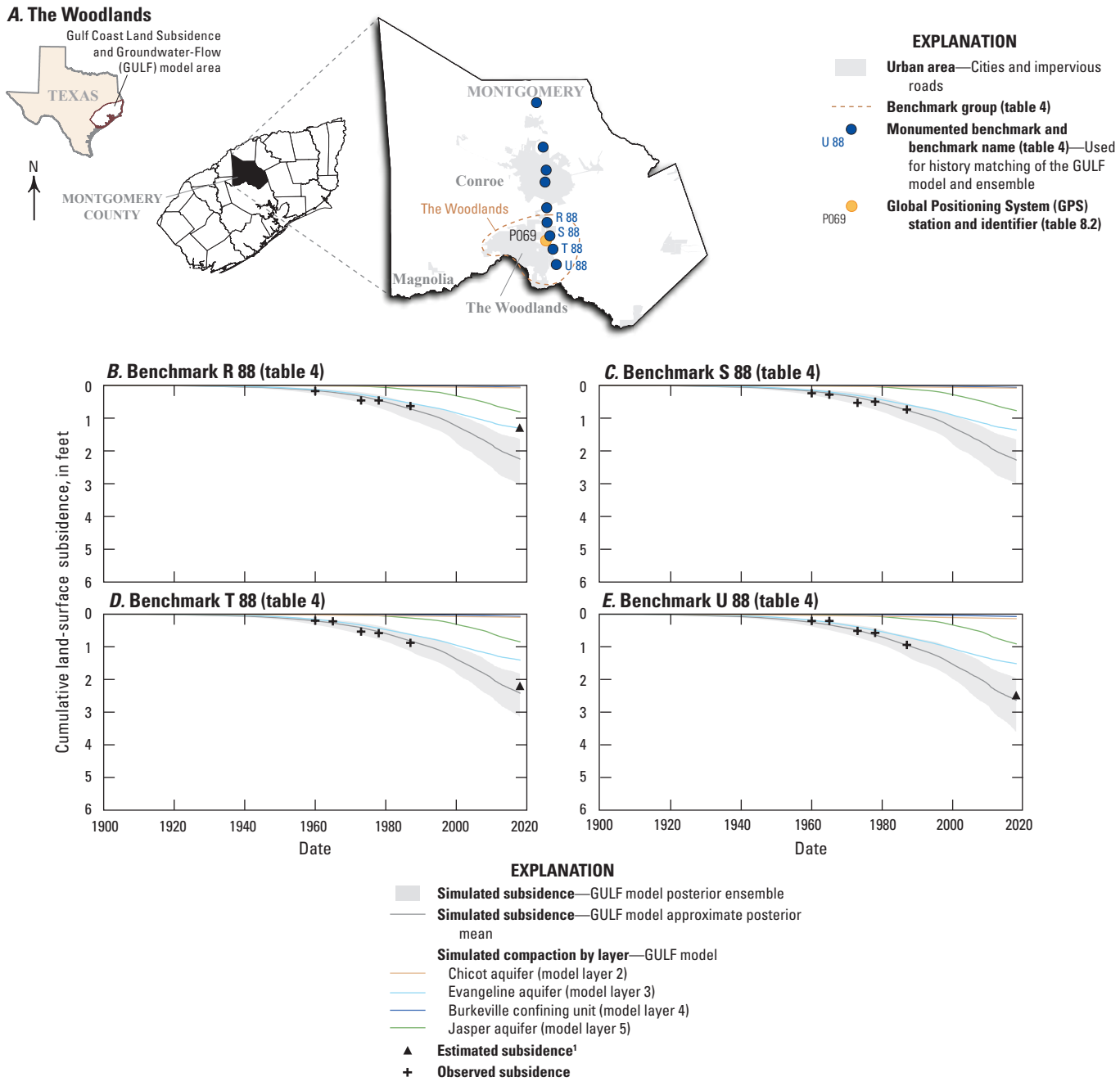

[1]The estimated subsidence through 2018 at benchmarks R 88, T 88, and U 88 was calculated based on the methods described in table 9 using vertical-displacement data from GPS station P069.

Figure 173. Observed and simulated subsidence by model layer at benchmarks in and near The Woodlands, Texas.

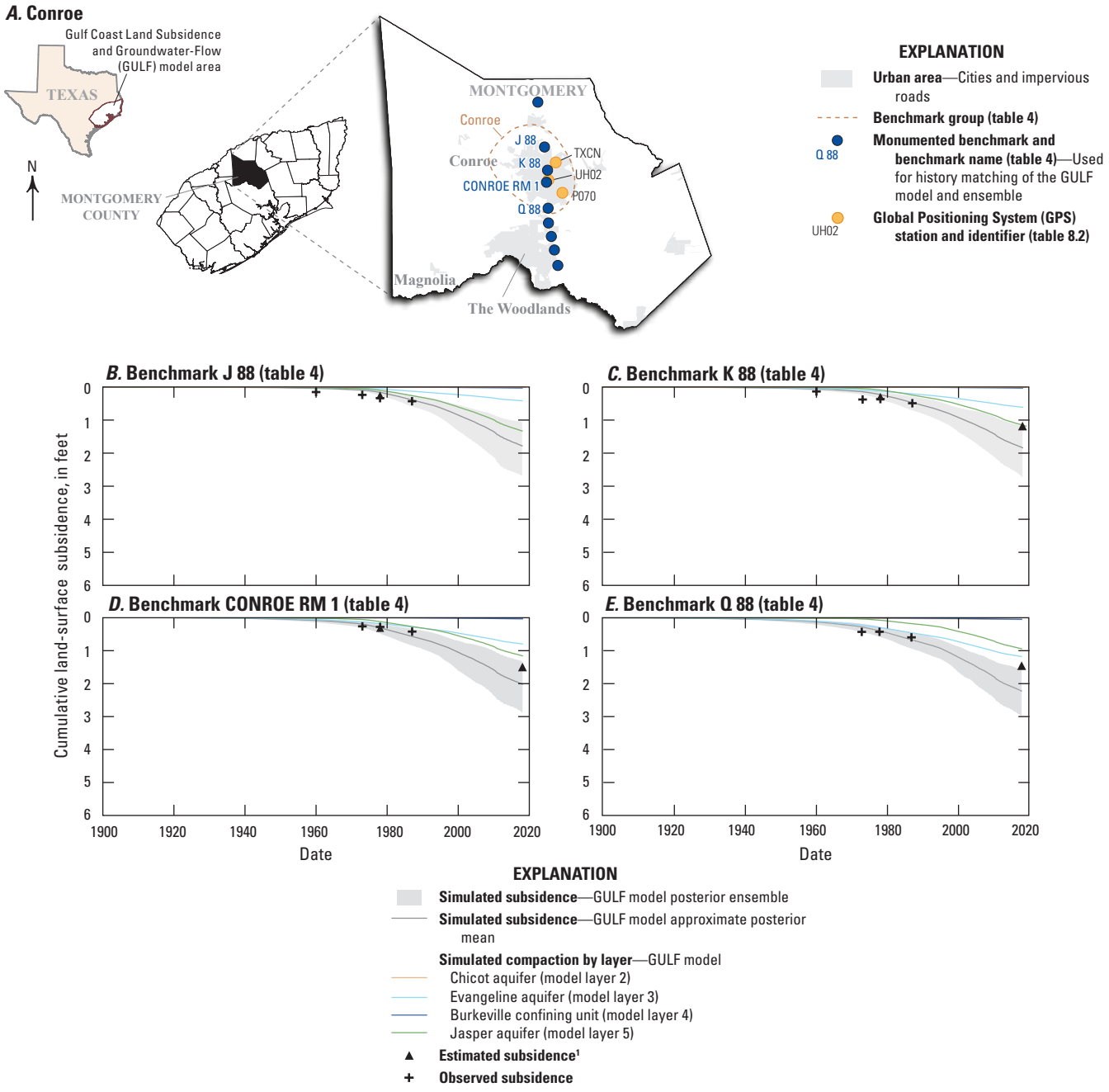

[1]The estimated subsidence through 2018 at benchmarks CONROE RM 1, K 88, and Q 88 was calculated based on the methods described in table 9. Data from GPS station TXCN were used for K 88, data from GPS station UH02 were used for CONROE RM 1, and data from GPS station P070 were used for Q 88.

Figure 174. Observed and simulated subsidence by model layer at benchmarks in and near Conroe, Texas.

Water Budget

The history-matched water budget for the Gulf Coast aquifer system in the GULF model (fig. 175; table 10) includes mean annual inflows, outflows, and the net change in storage for the model period. The simulated recharge to the outcrop area was the largest inflow (75 percent), and recharge to other areas was 25 percent of the model inflow. Simulated outflows include (1) net surface-water/groundwater exchange with model area streams (including the River and Drain packages) (50 percent), (2) groundwater use (49 percent), and (3) net surface-water/groundwater exchange with the Gulf of Mexico (1 percent).

The sum of the simulated values of the outflows (1,041,973 acre-feet per year [acre-ft/yr]) and the elastic expansion of the fine-grained sediment and numerical solver error (339 acre-ft/yr) minus the inflows (654,172 acre-ft/yr) represents the reduction of storage from the Gulf Coast aquifer system (388,140 acre-ft/yr). Most of the storage depletion is the result of the long-term groundwater-level declines described in the "Groundwater Levels" section. The magnitude and duration of these groundwater-level declines have resulted in predominantly inelastic compaction; therefore, only a small percentage of water was derived from elastic compaction during the model period (fig. 176; table 10). The reduction of storage was generally greatest between the mid-1960s and mid-1970s (fig. 176), concurrent with when groundwater levels were near or at historical minimums (figs. 25–28) in the greater Houston area. In 1974, which is the year of greatest simulated groundwater use (fig. 176), the release of water from interbeds caused by inelastic compaction was about 346,000 acre-feet, or about 30 percent of total groundwater use. As groundwater levels have risen concurrently with a reduction in groundwater use since the mid-1970s, the volume of water derived from inelastic compaction by 2018 had decreased to approximately the same volume simulated in 1945 (fig. 176).

Based on the groundwater use (514,952 acre-ft/yr) and the volume of water derived from inelastic compaction (132,462 acre-ft/yr), about 26 percent of the mean annual groundwater use in the model area represents water that had been stored in the fine-grained sediment. The simulated volume of water from the fine-grained sediment was greatest during 1970–74 (about 31 percent) when groundwater levels were near or at historical minimums. This simulated volume of water from inelastic compaction decreased after 1974 to about 20 percent by 1995 and was about 16 percent at the end of the transient model period in 2018. The GULF-model-simulated volume of water from the fine-grained sediment as a percentage of the mean annual groundwater use is similar to the following estimates: (1) 17 percent from Winslow and Doyel (1954); (2) 22 percent from Winslow and Wood (1959); (3) between 16 and 31 percent estimated using a numerical model in Carr and others (1985); (4) between 21 percent (for 1977) and 8 percent (for 2000) in the NGC-GAM (Kasmarek and Robinson, 2004); and (5) 8 percent (for 2009) in the HAGM (Kasmarek, 2012).

Model Uses, Limitations, and Assumptions

The GULF model was created for the purposes of fulfilling the role of a GAM, whereby the model design, boundary conditions, subsidence package, and uncertainty framework are appropriate to effectively simulate a variety of probabilistic and management scenarios, such as the simulation or estimation of modeled available groundwater (for example, pursuant to Texas Water Code §36.1132), at regional to subregional spatial scales. The appropriate use of this model in this context includes the limitations and assumptions described in this section.

The model grid was spatially discretized with a cell size of 1 x 1 km, and hydraulic properties are uniform in each cell. The GULF model incorporates a finer grid spacing than the grid spacing in many previous models of the model area and represents some localized features. However, hydraulic properties that change over a short distance, such as horizontal and vertical hydraulic conductivity, are generalized and could not be fully represented, especially given the heterogeneity of the Gulf Coast aquifer system. The use of one model layer to simulate each hydrogeologic unit in the Gulf Coast aquifer system follows the configuration of many previous models. However, this 1- x 1-km grid size is not sufficiently fine for the model to be used to rigorously evaluate localized hydrologic processes, such as the relation between local-scale drawdown and aquifer-system compaction and accompanying subsidence. The stress periods used in the GULF model were assumed to provide an adequate temporal resolution to assess changes in storage, groundwater levels, and base flows in streams. However, the uncertainty in model results is greater for earlier time periods because of the coarser temporal discretization used for earlier time periods (1897–1939 and 1940–69, which were discretized into about 14- and 5-year stress periods, respectively) compared to the finer temporal discretization used for later periods (1970–99 and 2000–18, which were discretized into 1-year and monthly stress periods, respectively). Thus, simulation of transient processes that take substantially less time than the lengths of the stress periods would require model refinement.

The use of the CSUB package in the GULF model to simulate the hydro-mechanical coupling of pore-fluid pressure (equivalent hydraulic head) and aquifer-system compaction is based on solely one-dimensional (vertical) stress and strain (thereby, displacement or compaction). Therefore, the use of the GULF model for applications where horizontal stress or displacement is of interest is not recommended. However, the model could be used to explore areas prone to large gradients of head, compaction, and subsidence, such as near faults acting as barriers to groundwater flow, and where substantial horizontal stresses and displacements may occur (as described in Galloway and Burbey, 2011). Additionally, the interbeds in each model cell generally are assumed to be uniformly distributed vertically—a simplification of the substantial

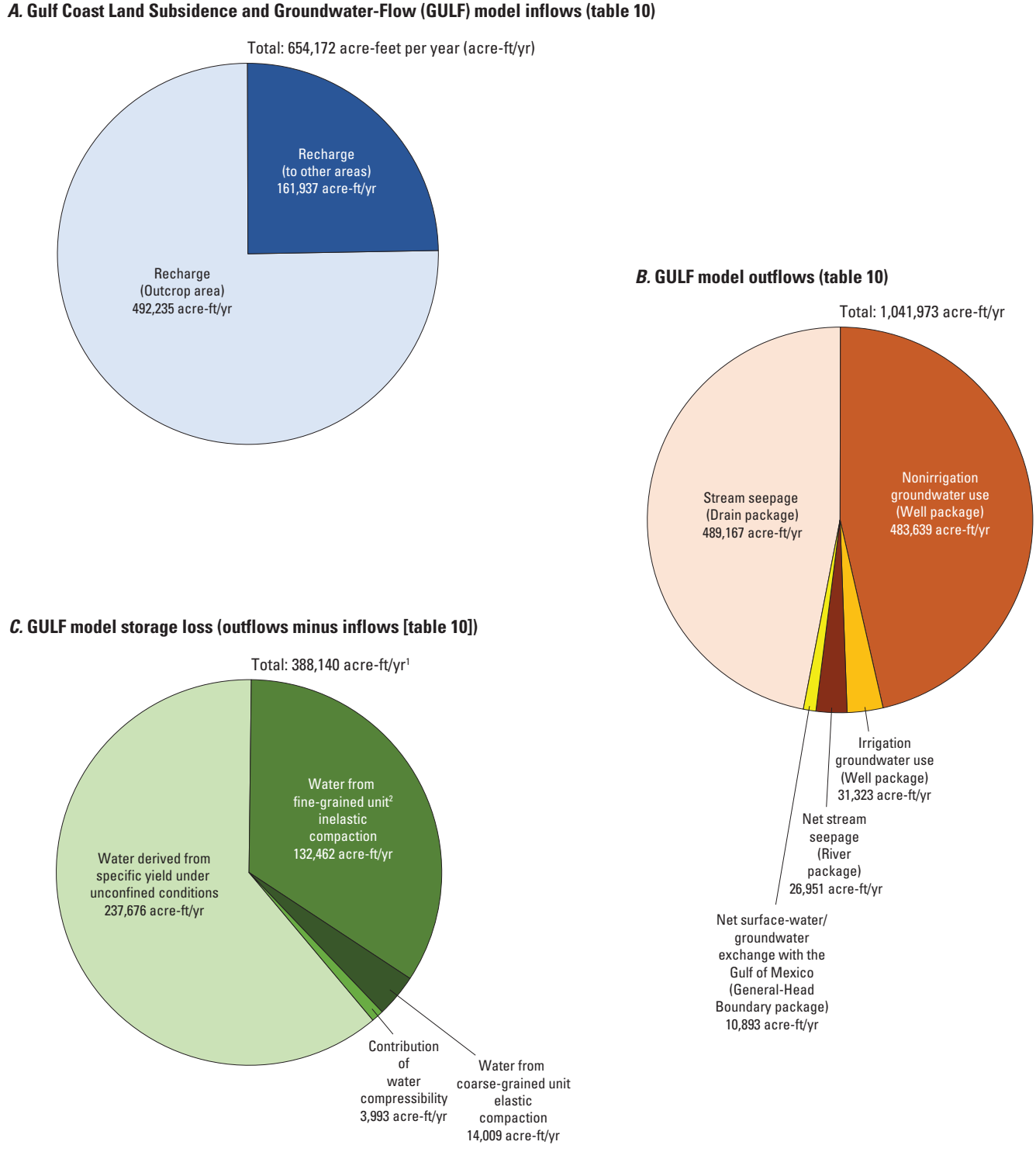

[1]The sum of the simulated values of the outflows (1,041,973 acre-feet per year [acre-ft/yr]) and the elastic expansion of the fine-grained sediment and numerical solver error (339 acre-ft/yr) minus the inflows (654,172 acre-ft/yr) represents the reduction of storage from the Gulf Coast aquifer system (388,140 acre-ft/yr).
[2]Fine-grained units are defined as either (1) laterally discontinuous fine-grained sediment (or "interbeds") within the aquifers or (2) laterally extensive fine-grained sediment (or "confining units") separating individual aquifers in the aquifer system.

Figure 175. Mean annual history-matched water budget for the Gulf Coast Land Subsidence and Groundwater-Flow model.

Table 10. Mean annual water budget for the Gulf Coast Land Subsidence and Groundwater-Flow model.

[The net change in storage is calculated as outflow minus inflow and reported in acre-feet per year and as a percentage of the water budget]

Water-budget category	Amount (in acre-feet per year)	Percentage of water budget
Inflow		
Recharge (outcrop area)[1]	492,235	75
Recharge (to other areas)[1]	161,937	25
Total inflow	**654,172**	**100**
Outflow		
Stream seepage (Drain package)[2]	489,167	47
Groundwater use (nonirrigation)	483,639	46
Groundwater use (irrigation)	31,323	3.0
Net stream seepage (River package)[3]	26,951	2.6
Net surface-water/groundwater exchange with the Gulf of Mexico (General-Head Boundary package)[4]	10,893	1.0
Total outflow	**1,041,973**	**100**
Net change in storage		
Water derived from specific yield under unconfined conditions	237,676	61
Water from fine-grained unit inelastic compaction[5]	132,462	34
Water from coarse-grained unit elastic compaction	14,009	3.6
Contribution of water compressibility	3,993	1.0
Total storage change[6]	**388,140**	**100**

[1]Includes recharge to the shallow groundwater system, most of which does not infiltrate to underlying layers. Recharge from layer 1 to the underlying layers is shown on figure 116.

[2]The Drain package represents small model area streams.

[3]The River package represents large model area streams.

[4]The General-Head Boundary package represents exchange of water between the Gulf Coast aquifer system and the Gulf of Mexico.

[5]Fine-grained units are defined as either (1) laterally discontinuous fine-grained sediment (or "interbeds") within the aquifers or (2) laterally extensive fine-grained sediment (or "confining units") separating individual aquifers in the aquifer system.

[6]The sum of the simulated values of the outflows (1,041,973 acre-feet per year [acre-ft/yr]) and the elastic expansion of the fine-grained sediment and numerical solver error (339 acre-ft/yr) minus the inflows (654,172 acre-ft/yr) represents the reduction of storage from the Gulf Coast aquifer system (388,140 acre-ft/yr).

heterogeneity in each hydrogeologic unit. Thus, CSUB-computed stress changes at the cell center are representative of mean conditions for the entire cell thickness where this package is active. Because the model layers have substantial thickness and contain multiple geologic units, this assumption might not be completely realistic; therefore, additional model layer discretization might warrant consideration. However, the use of one model layer per hydrogeologic unit, which has been used previously, was considered to be appropriate for use with the subsidence simulation. Additionally, a finer discretization could complicate the use of delay beds in thinner cells when using the CSUB package as released.

The GULF model uses the head-based formulation through which the geostatic stress remains constant, and a unit increase in effective stress results from a unit decline in groundwater levels. That is, (1) changes in effective stress are only caused by changes in pore-fluid pressure, and (2) elastic and inelastic skeletal specific-storage values are constant (temporally invariant, which means that they do not vary with changes in effective stress). The CSUB package is not active in layer 1 of the GULF model, which simulates the uppermost (about) 50 ft of the shallow groundwater system. Furthermore, the Burkeville confining unit is simulated by using a single layer similar to some previous models. Because the hydraulic conductivity in confining units is very small, fluid pressure changes in the confining unit resulting from declines in groundwater levels in the surrounding aquifer are initially limited to the periphery of the confining unit, and only later in time do they propagate towards the center of fine-grained units. Therefore, to simulate compaction in the Burkeville confining unit throughout the thickness of this unit, at least three layers in the model would be needed, including thin layers at the upper and lower surfaces of this unit; preferably, five or more layers would be used.

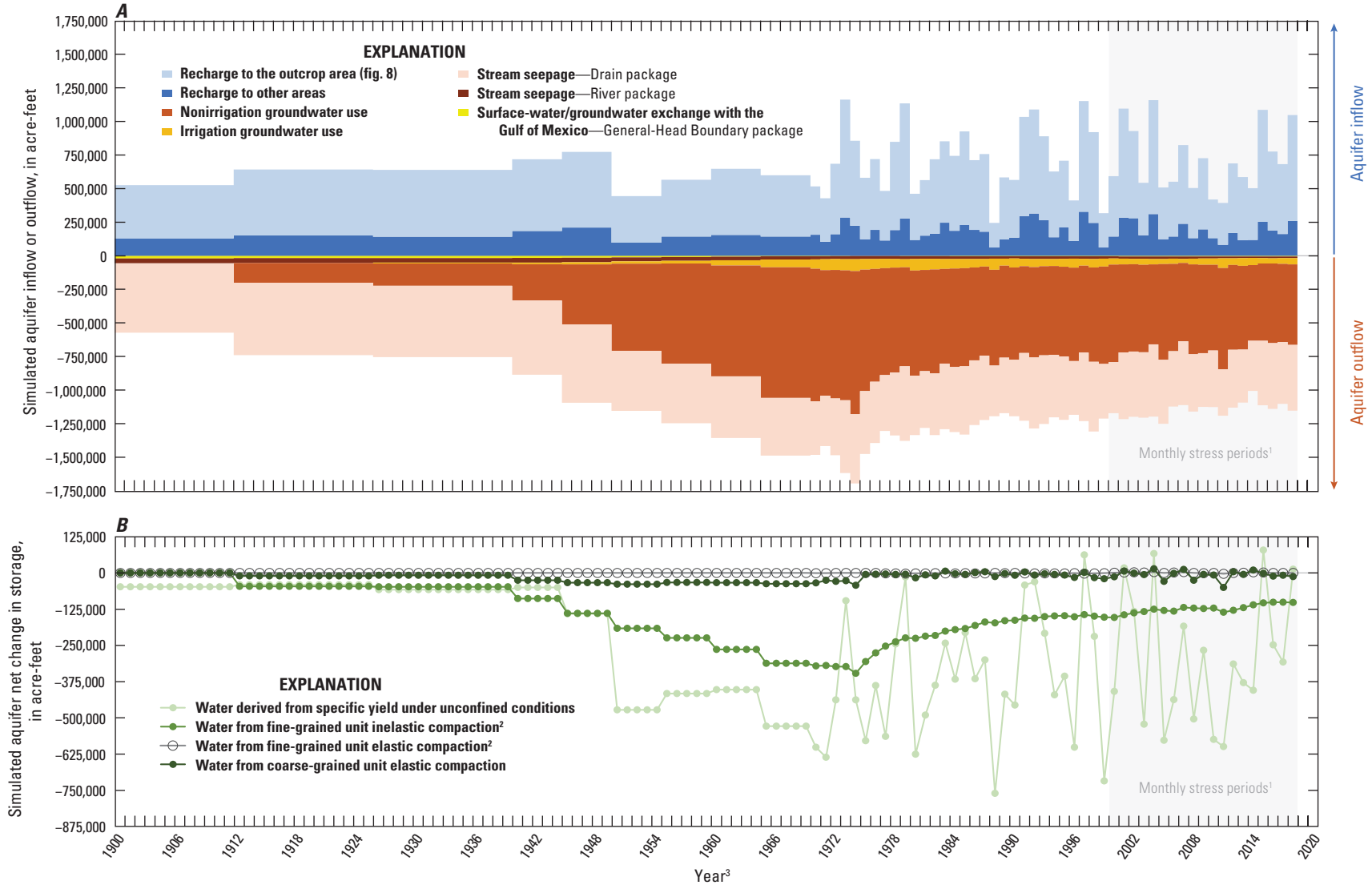

[1]The water budget for the monthly stress periods beginning January 1, 2000, is shown as an annual average.
[2]Fine-grained units are defined as either (1) laterally discontinuous fine-grained sediment (or "interbeds") within the aquifers or (2) laterally extensive fine-grained sediment (or "confining units") separating individual aquifers in the aquifer system.
[3]The model transient period is 1897–2018; however, the graphs begin at 1900 to simplify the x-axis.

Figure 176. Simulated inflows and outflows for the Gulf Coast Land Subsidence and Groundwater-Flow model.

The onset of inelastic subsidence begins based on the value of the preconsolidation head specified in each model cell in relation to the simulated steady-state groundwater level representing predevelopment conditions. The predevelopment groundwater levels were approximated for the Chicot, Evangeline, and Jasper aquifers based on historical reports describing groundwater levels for the greater Houston area and early-time groundwater levels compiled in this report (table 3.1). For predevelopment, exact groundwater levels are unknown except for those in a small number of wells; therefore, uncertainty exists in the simulated steady-state groundwater level, and by extension, the onset of subsidence in the model area from the specified preconsolidation head values used. Additionally, based on long-term groundwater levels, subsidence, and compaction datasets at the extensometer sites (figs. 94, 95), the preconsolidation head varies spatially. Although the GULF model uses a depth-dependent relation for preconsolidation head established in Kelley and others (2018), the spatial variability of the preconsolidation head could be greater than the variability simulated in the model. Furthermore, the depth-dependent relation of preconsolidation head is considered to be conservative for modeling the Jasper aquifer in the downdip areas (Kelley and others, 2018).

The GULF model was history matched to subsidence observations obtained from previously published historical subsidence contour maps, benchmark data, compaction observations at extensometers, and vertical-displacement observations at GPS stations. Although the combined subsidence dataset (where the term "subsidence" is generally used to also include compaction and vertical-displacement processes) contains a greater number of subsidence observations than in those previous groundwater models, some temporal and spatial data gaps exist. Most of the subsidence observations in the dataset are in the greater Houston area; therefore, greater uncertainty exists in the remaining model areas, particularly prior to the installation of the GPS stations. In the greater Houston area, the largest amount of more recent subsidence (generally since the 1990s) has occurred in northwestern Harris County (fig. 77). However, benchmarks were generally not monumented in the northwestern Harris County area until the 1951 leveling survey. Therefore, benchmarks in this area were not included in the benchmark dataset (fig. 70*A*) and the historical subsidence contour datasets (appendix 5) could not entirely account for all the subsidence prior to the installation of the GPS stations in this area. As a result, although the model was reasonably fit to the GPS subsidence observations in this area, uncertainty exists for the years prior where only a partial dataset was available.

Likewise, although the spatial distribution of groundwater-level and subsidence observations was reasonable, fewer observations were available for the eastern to northeastern areas of the model—particularly in Tyler, Hardin, Chambers, Jasper, and Newton Counties—compared to the central area of the model (figs. 72, 103); therefore, more uncertainty exists in the eastern to northeastern parts of the modeled area than in the central part of the of modeled area. Additionally, layer 1 did not contain any groundwater-level observations and was not history matched. Although the simulated water table in the eastern to northeastern areas of the model was in an expected range, more site-specific and local history-matching target data would facilitate an improved characterization of groundwater flow in these areas.

The NGS-derived leveled elevations at each benchmark listed in table 4 were adjusted in 1957, 1959, 1964, and 1973 to determine the changes in elevations of benchmarks from previous leveling surveys. During these adjustments, the leveled elevations based on the NGVD 29 were held fixed at the boundary point—generally at or beyond the perimeter of the greater Houston area. Leveling completed during different surveys was connected at benchmarks that remained stable between the dates of the leveling surveys. In this way, the adjusted benchmark elevations can be compared to the elevations obtained in previous years (NOAA, 1980) and represent the best available data for use in this study.

The benchmark elevation data (table 4) are primarily based on first-order leveling and have an estimated vertical resolution of between 0.004 and 0.04 ft (Bawden and others, 2003). However, this vertical resolution does not account for the uncertainty that occurs from adjustments to the leveled elevations. Surface-fitting methods were used by Holdahl and others (1989) to quantify and interpolate subsidence and estimate a correction to the leveled elevations in the greater Houston area, which can be distorted by the selection of adjustment constraints and network design (Holdahl and others, 1989). Annual subsidence rates during 1973–78 and 1978–87 at seven benchmarks from this study (R 88, J 8, F 55, W 661, D 54, Z 53, and L 305) were compared with the surface-fitting-derived subsidence rates from Holdahl and others (1989). During 1973–78 and 1978–87, annual subsidence rates based on the adjusted leveled elevations at five of the seven benchmarks were within the uncertainty range published in Holdahl and others (1989), although the differences between the Holdahl and others (1989) surface-fitting-derived annual subsidence rate and the annual subsidence rate in other parts of the greater Houston area and for time periods prior to 1973 have not been published. The uncertainty due to the adjustment constraints and network design is generally proportional to the cumulative subsidence recorded at study-area benchmarks. As a result, the uncertainty is greater in the historical Houston, Pasadena, Baytown, and Texas City areas and is lesser in the areas closer to the boundaries of the greater Houston area.

The transient model period (1897–2018) included substantial hydrologic and climatic variability; however, results from the groundwater model may not entirely be representative of future climatic variability. For probabilistic scenarios where sustained, substantial below-mean or above-mean recharge are simulated (extreme future conditions), the results warrant careful evaluation, and preferably, the model ensemble would be run to generate forecast uncertainty in order to assess simulated results for extreme future conditions in the context of an uncertainty framework.

The GULF model uses a simplified approach to the simulation of surface-water/groundwater exchange through use of the River and Drain packages, as compared to use of a more advanced package such as the Streamflow-Routing package (Langevin and others, 2021), whereby streamflow is routed through the model domain by a network of modeled rectangular channels. The Streamflow-Routing package is a more comprehensive approach that can explicitly simulate surface-water diversions, connections with simulated lakes and reservoirs, overland runoff, direct precipitation, and evapotranspiration. Thus, any use cases where these features would reasonably be required may not represent an appropriate use of the GULF model. The stream network used in the GULF model is a simplification of the actual stream geometry and hydraulic properties. More work could be done to refine the stream channel width, characterize the channel geometry, and estimate the streambed conductance and stream seepage exchange with the aquifer; these properties can vary substantially at the local scale. Additionally, the River package used in the model does not route streamflow; rather, it uses a simplified system to exchange water with the modeled groundwater system.

The GULF model includes a 20-year forecast period discretized into 1-year stress periods; the 20-year forecast period incorporates the mean of the last 3 years of the model transient period. A limitation of any forecast model is that the further out the model forecasts, the greater the uncertainty. A large degree of this uncertainty is associated with possible future changes in groundwater use, particularly in the greater Houston area, where continued and future conversions from groundwater to alternative water supplies are planned. The included 20-year forecast period can therefore be used as a baseline from which to simulate future groundwater-use scenarios that can then be modified to include refined groundwater-use estimations that account for these water supply conversions. Otherwise, the baseline outputs warrant careful consideration with the understanding that they are based on mean groundwater-use data from January 2016 through December 2018.

Groundwater levels obtained by the USGS and TWDB were measured during winter and spring when the least water use was expected during the year. Because (1) the withdrawal status of nearby wells was not always known, and (2) production wells could not remain inactive for a long enough period for the groundwater level to fully recover, these measurements could not always reflect the true static groundwater level. When all the measurements in an area were considered, however, any individual discrepancies tended to offset one another, and the mean groundwater-level decline or recovery among these wells is considered a reasonable estimate of groundwater-level patterns.

Caution is warranted when interpreting the effect of adding simulated groundwater use in layer 1 on modeled storage in the intermediate and deep groundwater systems. Layer 1 represents the shallow groundwater system of the Gulf Coast aquifer system hydrogeologic units. Similar to real-world conditions, the majority of simulated recharge in the model is discharged to modeled streams, whereas a much smaller amount of recharged water enters the deeper aquifer system. Because much of the groundwater in the shallow groundwater system is in transit to model area streams where it is discharged, the effect to the water budget of the intermediate and deeper systems is lessened by groundwater withdrawals that intercept groundwater in the shallow groundwater system. Therefore, it is not appropriate to use the GULF model to simulate groundwater use in layer 1.

The SWB-derived recharge values used in the GULF model are similar to other values estimated for the model area from previously published reports (Scanlon and others, 2011). Most of this recharge is applied in the model outcrop area (fig. 8), a small portion of which travels downdip into the intermediate and deep groundwater systems. Thus, the reliability of the recharge used in the model partially depends on the accuracy of the simulated hydraulic conductivity values, as discussed in Scanlon and others (2011). Additionally, some uncertainties exist for input data used to estimate recharge for the Gulf Coast aquifer system with the SWB code. Soil and land-cover properties, such as available water capacity and root-zone depth, influence model results but are not precisely known at the model scale.

Soil properties from the SSURGO database used with the SWB code are generalized and may not be representative of soil properties at a fine scale. Additionally, although the climate stations and associated data were reasonably distributed spatially and temporally, this distribution was not completely uniform. Thus, uncertainty exists in the interpolated climate data used to estimate recharge. The SWB code also does not account for delay between precipitation and recharge caused by the distance between the plant root zone and the water-table surface. In the Gulf Coast aquifer system, other than in the outcrop area, the water-table altitude is commonly more than 75 ft below the land-surface elevation. Therefore, the travel time for recharge to reach the water-table surface, which could be substantial in some areas, is not considered. Additionally, the SWB code may not provide accurate estimates of recharge where the water table is near land surface; thus, recharge could be overestimated in these areas. As a result of these uncertainties, although the SWB-derived recharge is comparable with other estimates, the overall distribution of recharge from this method could be more accurate than the magnitude of the recharge values estimated at any given location.

Exact amounts of annual groundwater use are unknown because not all groundwater wells are metered, particularly irrigation wells, and groundwater-use data, particularly prior to 1975, were not compiled annually, but instead sourced from a series of groundwater studies. Irrigation groundwater use in the western model area in Colorado, Wharton, Matagorda, and Jackson Counties was especially difficult to estimate given the uncertainty in discerning the source of this water (from groundwater or surface water).

Summary

This report describes the hydrogeology of the northern part of the Gulf Coast aquifer system in Texas and documents the Gulf Coast Land Subsidence and Groundwater-Flow model (hereinafter, the "GULF model") and ensemble. This groundwater-flow model and ensemble were used to simulate groundwater flow and land-surface subsidence caused by aquifer-system compaction in the northern part of the Gulf Coast aquifer system in Texas under transient conditions from 1897 through 2018. Since the release of the previous groundwater model for the greater Houston area in 2012 there have been changes to the distribution of groundwater withdrawals and advances in modeling tools. To reflect these changes and simulate more recent conditions, the GULF model was developed by the U.S. Geological Survey, in cooperation with the Harris-Galveston and Fort Bend Subsidence Districts, to provide an updated model for use as a Groundwater Availability Model.

The study area consists of about 22,770 square miles (14.6 million acres) of Gulf Coast aquifer system sedimentary deposits primarily in 28 counties, and includes 2 subsidence districts and 11 groundwater conservation districts. The northern boundary of the study area is the outcrop of the Catahoula confining unit; the northeastern boundary is the Texas–Louisiana boundary; the southwestern boundary is the western extent of Lavaca and Jackson Counties; and the southern boundary is the nearshore area of the Gulf of Mexico.

In a generalized conceptual model of the Gulf Coast aquifer system, water enters the groundwater system in topographically high outcrops of the hydrogeologic units in the northwestern part of the aquifer system. Groundwater that does not discharge to streams flows to intermediate and deep zones of the aquifer system southeastward of the outcrop areas where it is discharged by wells and by upward leakage in topographically low areas near the coast. The uppermost parts of the aquifer system, which include outcrop areas, are under water-table conditions. As depth increases in the aquifer system and interbedded, low-permeability fine-grained sediment accumulates, water-table conditions evolve into confined conditions.

Since the early 1900s, most of the groundwater withdrawals in the study area have been from three of the hydrogeologic units that compose the Gulf Coast aquifer system—the Chicot, Evangeline, and Jasper aquifers, and, more recently, from the Catahoula confining unit. Withdrawals from these units are used for municipal supply, commercial and industrial use, and irrigation purposes. Withdrawals of large quantities of groundwater in the greater Houston area have caused widespread groundwater-level declines (where "groundwater level" in this report is synonymous with "groundwater head") in the Chicot, Evangeline, and Jasper aquifers of more than 300 feet (ft). Early development of the aquifer system, which began before 1900, resulted in nearly 50 percent of the eventual historical groundwater-level minimums having been reached as early as 1946 in some parts of the greater Houston area. The greatest sustained annual groundwater-level declines during the study period occurred in the historical Houston area and Pasadena area during 1937–52, averaging 10–14 feet per year (ft/yr), compared to the declines of about 8 ft/yr during 1962–72, generally the second greatest period of sustained annual declines.

Groundwater-level data from colocated wells indicate (1) minimal groundwater-level changes over time in the shallowest wells that generally are climate and recharge driven, and (2) a transition zone between about 100 and 250 ft below land surface (bls), below which groundwater is generally under confined conditions and groundwater levels are primarily affected by groundwater withdrawals. A substantial degree of similarity is observed in the groundwater-level patterns from colocated wells at the borehole extensometer sites which are under confined conditions.

Substantial groundwater-level declines have caused more than 9 ft of land-surface subsidence from depressurization and compaction principally of fine-grained sediments interbedded in the aquifer system. Subsidence prior to 1978 was generally concentrated in central, south-central, and southeastern Harris County and in Galveston County. More recent subsidence has occurred in northern, northwestern, and western Harris County, in Montgomery County, and in northern Fort Bend County. Subsidence in the greater Houston area has generally occurred on a broad scale, although substantial subsidence gradients across relatively short distances occurred in the Baytown and Texas City areas. Observed rates of subsidence generally correspond to the rates of groundwater-level declines, and absent a sustained groundwater-level recovery, compaction has continued to occur in some areas as pore pressures (equivalent hydraulic heads) in the fine-grained units slowly equilibrate with groundwater levels in the surrounding higher permeability coarse-grained aquifer material. Based on a combination of benchmark and Global Positioning System data at the Addicks, Northeast, and Lake Houston sites, these sites form a downdip boundary approximately parallel to the coastline where compaction in the Jasper aquifer is approximately zero.

Groundwater flow and land-surface subsidence in the GULF model and ensemble were simulated by using the MODFLOW 6 code with the Skeletal Storage, Compaction, and Subsidence package. The model consists of six layers, one for each of the five hydrogeologic units (layers 2–6: Chicot and Evangeline aquifers, Burkeville confining unit, Jasper aquifer, and the Catahoula confining unit, respectively) in the northern part of the Gulf Coast aquifer system and a surficial top layer (layer 1: shallow groundwater system) that includes part of each hydrogeologic unit. Transient groundwater flow was simulated during 1897–2018 by using a combination of multiyear, annual, and monthly stress periods. An initial steady-state stress period was configured to represent predevelopment mean annual inflows and outflows. The Skeletal Storage, Compaction, and Subsidence package uses a head-based subsidence formulation that simulates the delayed

drainage response from low-permeability fine-grained sediment (interbeds and confining units) to changes in groundwater levels.

The GULF model and ensemble were history matched to groundwater-level observations at selected wells, land-surface subsidence at benchmarks, aquifer-system compaction at borehole extensometers, and vertical displacement from Global Positioning System stations. A Bayesian framework was used to represent uncertainty in modeled parameters and simulated outputs of interest. History matching and uncertainty quantification were performed by using a Monte Carlo approach enabled through iterative ensemble smoother software to produce an ensemble of models fit to historical data. The iterative ensemble smoother substantially reduced the computation demand of parameter estimation by approximating the first-order relation between model inputs and outputs, thereby allowing 183,207 adjustable parameters to be used for history matching at a relatively low computational and time cost.

The history-matched parameter values are within the ranges of previously published values and agree with the current understanding of the spatial and temporal patterns of parameter uncertainty for the Gulf Coast aquifer system. A good agreement between the observed (or estimated) and simulated groundwater levels, land-surface subsidence, compaction, and vertical displacement was obtained across the modeled area based on qualitative and quantitative comparisons.

Ensemble mean annual groundwater-flow rates to the Chicot, Evangeline, and Jasper aquifers and the Catahoula confining unit were 0.0–0.49 inch, 0.09–0.33 inch, 0.01–0.07 inch, and 0.01–0.05 inch, respectively. GULF model mean annual groundwater-flow rates to the Chicot, Evangeline, and Jasper aquifers and the Catahoula confining unit were 0.31 inch, 0.19 inch, 0.03 in., and 0.03 inch, respectively. These groundwater-flow rates are similar to the groundwater-flow rates of the two most recent groundwater-flow models developed for the study area.

The simulated recharge to the outcrop area was the largest inflow (75 percent), and recharge to other areas was 25 percent of the model inflow. Simulated outflows included (1) net surface-water/groundwater exchange with study area streams (50 percent), (2) groundwater use (49 percent), and (3) net surface-water/groundwater exchange with the Gulf of Mexico (1 percent). The sum of the simulated values of the outflows (1,041,973 acre-feet per year [acre-ft/yr]) and the elastic expansion of the fine-grained sediment and numerical solver error (339 acre-ft/yr) minus the inflows (654,172 acre-ft/yr) represents the reduction of storage from the Gulf Coast aquifer system (388,140 acre-ft/yr). Most of the storage depletion is caused by long-term groundwater-level declines. The magnitude and duration of these groundwater-level declines have resulted in predominantly inelastic compaction; therefore, only a small percentage of water was derived from elastic compaction during the model period. This loss of storage was generally greatest between the mid-1960s and mid-1970s, concurrent with groundwater levels near or at historical minimums in the greater Houston area.

The GULF model was used to estimate Jasper aquifer compaction at selected benchmarks in Montgomery County and northern Harris County, which are the primary locations of Jasper aquifer groundwater use. Simulated Jasper aquifer compaction in northern Harris County near benchmark V 660 was about 0.2 ft, or about 5 percent of the simulated subsidence of 4.4 ft at the benchmark location. Simulated Jasper aquifer compaction in Montgomery County at CONROE RM 1 was about 1.2 ft, or about 57 percent of the simulated subsidence of 2.1 ft at the benchmark location.

References Cited

Agudelo, G., Wang, G., Liu, Y., Bao, Y., and Turco, M.J., 2020, GPS geodetic infrastructure for subsidence and fault monitoring in Houston, Texas, USA, *in* Proceedings from the Tenth International Symposium on Land Subsidence: International Association of Hydrological Sciences, v. 382, p. 11–18, accessed January 5, 2021, at https://piahs.copernicus.org/articles/382/11/2020/.

Alexander, W.H., Jr., 1950, Ground-water resources of Liberty County, Texas, *with a section on* Stream runoff, by S.D. Breeding: U.S. Geological Survey Water-Supply Paper 1079–A, 61 p., accessed October 19, 2019, at https://doi.org/10.3133/wsp1079A.

AllTerra, Inc., 2021, A Trimble VRS network: AllTerra, Inc., accessed August 18, 2021, at https://allterracentral.com/rtknet-tx-ok.

American Oil Company [AMOCO], 1958, Refinery ground subsidence at Texas City: American Oil Company, Plant Engineering Department, Report TR58-1, 58 p., accessed October 17, 2019, at http://www.twdb.texas.gov/groundwater/docs/Subsidence_AmericanOilCompany_1958.pdf.

Anders, R.B., McAdoo, G.D., and Alexander, W.H., Jr., 1968, Ground-water resources of Liberty County, Texas: Texas Water Development Board Report 72, prepared by U.S. Geological Survey, 140 p., accessed October 17, 2019, at https://www.twdb.texas.gov/publications/reports/numbered_reports/doc/R72/Report72.asp.

Anders, R.B., and Naftel, W.L., 1962, Pumpage of ground water and fluctuation of water levels in the Houston District and the Baytown-La Porte area, Texas, 1957–61: Texas Water Commission Bulletin 6211, 45 p., accessed October 17, 2019, at http://www.twdb.texas.gov/publications/reports/bulletins/doc/B6211/B6211.pdf.

Anders, R.B., and Naftel, W.L., 1963, Pumpage of ground water and changes in water levels in Galveston County, Texas, 1958–62: Texas Water Commission Bulletin 6303, 32 p., accessed October 17, 2019, at http://www.twdb.texas.gov/publications/reports/bulletins/doc/B6303.pdf.

Anderson, M.P., Woessner, W.W., and Hunt, R.J., 2015, Applied groundwater modeling—Simulation of flow and advective transport (2d ed.): Amsterdam, The Netherlands, Elsevier, 610 p.

Archaeological & Historical Commission, 2015, Protected landmark designation report: Archaeological & Historical Commission, City of Houston, 12 p., accessed October 17, 2019, at https://www.houstontx.gov/planning/HistoricPres/landmarks/15PL123_Heights_Water_Works.pdf.

Ashworth, J.B., and Hopkins, J., 1995, Aquifers of Texas: Texas Water Development Board Report 345, 69 p., accessed October 17, 2019, at https://www.twdb.texas.gov/publications/reports/numbered_reports/doc/R345/R345Complete.pdf.

Baker, E.T., Jr., 1965, Ground-water resources of Jackson County, Texas: Texas Water Development Board Report 1, 90 p., accessed October 17, 2019, at https://www.twdb.texas.gov/publications/reports/numbered_reports/doc/R1/report1.asp.

Baker, E.T., Jr., 1979, Stratigraphic and hydrogeologic framework of part of the Coastal Plain of Texas: Texas Department of Water Resources Report 236, prepared by U.S. Geological Survey, 43 p., accessed October 17, 2019, at https://www.twdb.texas.gov/publications/reports/numbered_reports/doc/R236/Report236.asp.

Baker, E.T., Jr., 1986, Hydrology of the Jasper aquifer in the southeast Texas Coastal Plain: Texas Water Development Board Report 295, prepared by U.S. Geological Survey, 64 p., accessed October 17, 2019, at https://www.twdb.texas.gov/publications/reports/numbered_reports/doc/R295/Report295.asp.

Baker, E.T., Jr., Follett, C.R., McAdoo, G.D., and Bonnet, C.W., 1974, Ground-water resources of Grimes County, Texas: Texas Water Development Board Report 186, prepared by U.S. Geological Survey, 103 p., accessed October 17, 2019, at https://www.twdb.texas.gov/publications/reports/numbered_reports/doc/R186/R186.pdf?d=10091.545000090264.

Baker, M.N., 1891, The manual of American water-works: The Engineering News Publishing Company, v. 3, 384 p., accessed May 10, 2021, at https://www.google.com/books/edition/Manual_of_American_Water_works/TFJBAAAAMAAJ?gbpv=0#f=false.

Baker, M.N., 1897, The manual of American water-works: The Engineering News Publishing Company, v. 4, 698 p., accessed May 10, 2021, at https://www.google.com/books/edition/The_Manual_of_American_Water_works/ILIOAAAAYAAJ?hl=en&gbpv=1&pg=PA518&printsec=frontcover#v=onepage&q&f=false.

Bakker, M., Post, V., Langevin, C.D., Hughes, J.D., White, J.T., Starn, J.J., and Fienen, M.N., 2016, Scripting MODFLOW model development using Python and FloPy: Groundwater, v. 54, no. 5, p. 733–739, accessed May 10, 2022, at https://doi.org/10.1111/gwat.12413.

Barbie, D.L., and Locke, G.L., 1993, Ground-water withdrawals, water levels, and ground-water quality in the Houston district, Texas, with emphasis on 1985–89: U.S. Geological Survey Water-Resources Investigations Report 92–4180, 28 p., accessed October 17, 2019, at https://doi.org/10.3133/wri924180.

Barlow, P.M., Cunningham, W.L., Zhai, T., and Gray, M., 2015, U.S. Geological Survey Groundwater Toolbox, a graphical and mapping interface for analysis of hydrologic data (version 1.0)—User guide for estimation of base flow, runoff, and groundwater recharge from streamflow data: U.S. Geological Survey Techniques and Methods, book 3, chap. B10, 27 p., accessed October 17, 2019, at https://doi.org/10.3133/tm3B10.

Bawden, G.W., Johnson, M.R., Kasmarek, M.C., Brandt, J., and Middleton, C.S., 2012, Investigation of land subsidence in the Houston-Galveston region of Texas by using the Global Positioning System and interferometric synthetic aperture radar, 1993–2000: U.S. Geological Survey Scientific Investigations Report 2012–5211, 88 p., accessed October 17, 2019, at https://doi.org/10.3133/sir20125211.

Bawden, G.W., Sneed, M., Stork, S.V., and Galloway, D.L., 2003, Measuring human-induced land subsidence from space: U.S. Geological Survey Fact Sheet 069–03, 4 p., accessed October 17, 2019, at https://doi.org/10.3133/fs06903.

Bernal, L., 2020, Brownwood—Baytown's most historic neighborhood: University of Houston, M.S. thesis, 330 p., accessed December 15, 2020, at https://uh-ir.tdl.org/bitstream/handle/10657/6754/BERNAL-THESIS-2020.pdf?sequence=1&isAllowed=y.

Blewitt, G., Hammond W.C., and Kreemer, C., 2018, Harnessing the GPS data explosion for interdisciplinary science: Eos, v. 99, accessed October 17, 2019, at https://doi.org/10.1029/2018EO104623.

Borchert, J.R., 1954, The surface water supply of American municipalities: Annals of the Association of American Geographers v. 44, no. 1, p. 15–32, accessed May 10, 2022, at https://www.jstor.org/stable/2561112?seq=1.

Boynton, J., 1969, Levee study sure, city to pay part: The Baytown Sun, v. 47, no. 130, ed. 1, Sunday, February 16, 1969, p. 1, accessed June 12, 2022, at https://texashistory.unt.edu/ark:/67531/metapth1056936.

Braun, C.L., and Ramage, J.K., 2022, Status of water-level altitudes and long-term water-level changes in the Chicot and Evangeline (undifferentiated) and Jasper aquifers, greater Houston area, Texas, 2021: U.S. Geological Survey Scientific Investigations Report 2022–5065, 25 p., accessed August 5, 2022, at https://doi.org/10.3133/sir20225065.

Bull, W.B., and Poland, J.F., 1975, Land subsidence due to ground-water withdrawal in the Los Banos–Kettleman City area, California—Part 3. Interrelations of water-level change, change in aquifer-system thickness, and subsidence: U.S. Geological Survey Professional Paper 437–G, 62 p., accessed October 17, 2019, at https://doi.org/10.3133/pp437G.

Bumgarner, J.R., Stanton, G.P., Teeple, A.P., Thomas, J.V., Houston, N.A., Payne, J.D., and Musgrove, M., 2012, A conceptual model of the hydrogeologic framework, geochemistry, and groundwater-flow system of the Edwards-Trinity and related aquifers in the Pecos County region, Texas (revised July 10, 2012): U.S. Geological Survey Scientific Investigations Report 2012–5124, 74 p., accessed October 17, 2019, at https://doi.org/10.3133/sir20125124.

Carr, J.E., Meyer, W.E., Sandeen, W.M., and McLane, I.R., 1985, Digital models for simulation of ground-water hydrology of the Chicot and Evangeline aquifers along the Gulf Coast of Texas: Texas Department of Water Resources Report 289, 101 p., accessed October 17, 2019, at https://www.twdb.texas.gov/publications/reports/numbered_reports/doc/R289/Report289.asp.

Casarez, I.R., 2020, Aquifer extents in the Coastal lowlands aquifer system regional groundwater availability study area in Texas, Louisiana, Mississippi, Alabama, and Florida: U.S. Geological Survey data release, accessed December 15, 2020, at https://doi.org/10.5066/P9BH2KG2.

Chen, Y., and Oliver, D.S., 2013, Levenberg–Marquardt forms of the iterative ensemble smoother for efficient history matching and uncertainty quantification: Computational Geosciences, v. 17, no. 4, p. 689–703.

Chowdhury, A.H., and Turco, M.J., 2006, Geology of the Gulf Coast aquifer, Texas, *in* Mace, R.E., Davidson, S.C., Angle, E.S., and Mullican, W.F., III, eds., Aquifers of the Gulf Coast of Texas: Texas Water Development Board Report 365, chap. 2, p. 23–50, accessed October 17, 2019, at http://www.twdb.texas.gov/publications/reports/numbered_reports/doc/r365/r365_composite.pdf.

Chowdhury, A.H., Wade, S., Mace, R.E., and Ridgeway, C., 2004, Groundwater availability model of the central Gulf Coast aquifer system—Numerical simulations through 1999: Texas Water Development Board, 108 p., accessed October 17, 2019, at https://www.twdb.texas.gov/groundwater/models/gam/glfc_c/glfc_c.asp.

Clark, B.R., Barlow, P.M., Peterson, S.M., Hughes, J.D., Reeves, H.W., and Viger, R.J., 2018, National-scale grid to support regional groundwater availability studies and a national hydrogeologic database: U.S. Geological Survey data release, accessed October 17, 2019, at https://doi.org/10.5066/F7P84B24.

Coplin, L.S., and Galloway, D., 1999, Houston-Galveston, Texas—Managing coastal subsidence, *in* Galloway, D., Jones, D.R., and Ingebritsen, S.E., eds., Land subsidence in the United States: U.S. Geological Survey Circular 1182, p. 35–48, accessed October 17, 2019, at https://doi.org/10.3133/cir1182.

Darton, N.H., Stephenson, L.W., and Gardner, J., 1937, Geologic map of Texas: U.S. Geological Survey, scale 1:500,000, accessed October 17, 2019, at https://doi.org/10.3133/70210881.

Delin, G.N., and Falteisek, J.D., 2007, Ground-water recharge in Minnesota: U.S. Geological Survey Fact Sheet 2007–3002, 6 p., accessed October 17, 2019, at https://doi.org/10.3133/fs20073002.

Deussen, A., 1914, Geology and underground waters of the southeastern part of the Texas Coastal Plain: U.S. Geological Survey Water-Supply Paper 335, 365 p., accessed October 17, 2019, at https://doi.org/10.3133/wsp335.

Doering, J.A., 1935, Post-Fleming surface formations of coastal southeast Texas and south Louisiana: American Association of Petroleum Geologists Bulletin, v. 19, p. 651–688, accessed October 17, 2019, at https://archives.datapages.com/data/bulletns/1931-37/images/pg/00190005/0650/06510.pdf.

Doherty, J., and Simmons, C.T., 2013, Groundwater modelling in decision support—Reflections on a unified conceptual framework: Hydrogeology Journal, 21, p. 1531–1537, accessed October 17, 2019, at https://doi.org/10.1007/s10040-013-1027-7.

Doherty, J.E., 2015, Calibration and uncertainty analysis for complex environmental models: Brisbane, Australia, Watermark Numerical Computing, 237 p.

Dowell, C.L., 1964, Dams and reservoirs in Texas—Historical and descriptive information: Texas Water Commission Bulletin 6408, 248 p., 1 pl., accessed April 7, 2022, at https://www.twdb.texas.gov/publications/reports/bulletins/doc/B6408.pdf.

Doyel, W.W., Winslow, A.G., and Naftel, W.L., 1954, Pumpage of ground water and decline of artesian pressure in the Houston district, Texas, during 1951 and 1952: Texas Board of Water Engineers Bulletin 5401, prepared in cooperation with the U.S. Geological Survey, 34 p., accessed October 17, 2019, at https://www.twdb.texas.gov/publications/reports/bulletins/doc/B5401.pdf.

Dugan, J.T., and Zelt, R.B., 2000, Simulation and analysis of soil-water conditions in the Great Plains and adjacent areas, central United States, 1951–80: U.S. Geological Survey Water-Supply Paper 2427, 81 p., accessed October 17, 2019, at https://doi.org/10.3133/wsp2427.

Dumble, E.T., 1894, The Cenozoic deposits of Texas: Journal of Geology, v. 2, p. 555–556.

Dutton, A.R., and Richter, B.C., 1990, Regional hydrogeology of the Gulf Coast aquifer in Matagorda and Wharton Counties, Texas—Development of a numerical model to estimate the impact of water-management strategies: Report prepared for the Lower Colorado River Authority under contract (88-89) 0910, Bureau of Economic Geology, University of Texas at Austin, 118 p. [Also available at https://www.beg.utexas.edu/files/publications/cr/CR1990-DuttonA-1-QAe5623.pdf.]

Federal Geodetic Control Committee, 1984, Standards and specifications for Geodetic Control Networks: National Oceanic and Atmospheric Administration Technical Publication, [variously paged; 34 p.], accessed October 17, 2019, at https://www.ngs.noaa.gov/FGCS/tech_pub/1984-stds-specs-geodetic-control-networks.pdf.

Fienen, M.N., Corson-Dosch, N.T., White, J.T., Leaf, A.T., and Hunt, R.J., 2021, Risk-based wellhead protection decision support—A repeatable workflow approach: Groundwater, v. 60, no. 1, p. 71–86, accessed March 23, 2022, at https://doi.org/10.1111/gwat.13129.

Fienen, M.N., D'Oria, M., Doherty, J.E., and Hunt, R.J., 2013, Approaches in highly parameterized inversion—bgaPEST, a Bayesian geostatistical approach implementation with PEST—Documentation and instructions: U.S. Geological Survey Techniques and Methods, book 7, section C9, 86 p., accessed October 17, 2019, at https://doi.org/10.3133/tm7C9.

Follett, C.R., 1947, Ground-water resources of Brazoria County, Texas: Texas Board of Water Engineers, 101 p., accessed October 17, 2019, at https://www.twdb.texas.gov/publications/reports/historic_groundwater_reports/doc/M019.pdf.

Follett, C.R., and Cumley, J.C., 1943, Records of wells, drillers' logs, water analyses, and map showing location of wells in Jackson County, Texas: Texas State Board of Water Engineers, 49 p., 1 pl., accessed October 17, 2019, at http://doi.org/10.26153/tsw/4816.

Fort Bend Subsidence District [FBSD], 2013, Fort Bend Subsidence District 2013 regulatory plan: Fort Bend Subsidence District, 14 p., accessed October 17, 2019, at http://fbsubsidence.org/wp-content/uploads/2020/07/FBSD-Regulatory-Plan-Amended-2013.pdf.

Freeze, R.A., and Cherry, J.A., 1979, Groundwater: Englewood Cliffs, N.J., Prentice Hall, 604 p.

Fugate, G.L., 1941, Development of Houston's water supply: Journal of the American Water Works Association, v. 33, no. 10, p. 1768–1777, accessed October 17, 2019, at https://www.jstor.org/stable/41233249?seq=1.

Gabrysch, R.K., 1967, Development of ground water in the Houston district, Texas, 1961–65: Texas Water Development Board Report 63, prepared by the U.S. Geological Survey, 35 p., accessed October 17, 2019, at https://www.twdb.texas.gov/publications/reports/numbered_reports/doc/R63/Report63.asp.

Gabrysch, R.K., 1972, Development of ground water in the Houston district, Texas, 1966–69: Texas Water Development Board Report 152, prepared by U.S. Geological Survey, 24 p., accessed October 17, 2019, at https://www.twdb.texas.gov/publications/reports/numbered_reports/doc/R152/Report152.asp.

Gabrysch, R.K., 1977, Approximate areas of recharge to the Chicot and Evangeline aquifer systems in the Houston-Galveston area, Texas: U.S. Geological Survey Open-File Report 77–754, 1 sheet, accessed October 17, 2019, at https://doi.org/10.3133/ofr77754.

Gabrysch, R.K., 1980a, Development of ground water in the Houston district, Texas, 1970–74: Texas Department of Water Resources Report 241, prepared by U.S. Geological Survey, 49 p., accessed October 17, 2019, at https://www.twdb.texas.gov/publications/reports/numbered_reports/doc/R241/R241.pdf.

Gabrysch, R.K., 1980b, Approximate land-surface subsidence in the Houston-Galveston region, Texas, 1906–78, 1943–78, and 1973–78: U.S. Geological Survey Open-File Report 80–338, 3 pls., accessed October 17, 2019, at https://doi.org/10.3133/ofr80338.

Gabrysch, R.K., 1982a, Ground-water withdrawals and changes in water levels in the Houston district, Texas, 1975–79: U.S. Geological Survey Open-File Report 82–431, 39 p., 10 pls., accessed October 17, 2019, at https://doi.org/10.3133/ofr82431.

Gabrysch, R.K., 1982b, Ground-water withdrawals and land-surface subsidence in the Houston-Galveston region, Texas, 1906–80: U.S. Geological Survey Open-File Report 82–571, 68 p., accessed October 17, 2019, at https://doi.org/10.3133/ofr82571.

Gabrysch, R.K., 1983, The impact of land-surface subsidence, *in* Impact of Science on Society, Managing our freshwater resources: United Nations Educational, Scientific and Cultural Organization, no. 1, p. 117–123, accessed October 19, 2019, at https://unesdoc.unesco.org/ark:/48223/pf0000054873.

Gabrysch, R.K., 1984, Ground-water withdrawals and land-surface subsidence in the Houston-Galveston region, Texas, 1906–80: Texas Department of Water Resources Report 287, prepared by U.S. Geological Survey, 64 p., accessed October 17, 2019, at https://www.twdb.texas.gov/publications/reports/numbered_reports/doc/R287/report287.asp.

Gabrysch, R.K., and Bonnet, C.W., 1974, Land-surface subsidence in the area of Burnett, Scott, and Crystal Bays near Baytown, Texas: U.S. Geological Survey Water-Resources Investigations Report 21–74, 54 p., accessed October 17, 2019, at https://doi.org/10.3133/wri7421.

Gabrysch, R.K., and Bonnet, C.W., 1975, Land-surface subsidence in the Houston-Galveston region, Texas: Texas Water Development Board Report 188, prepared by U.S. Geological Survey, 19 p., accessed October 17, 2019, at https://www.twdb.texas.gov/publications/reports/numbered_reports/doc/R188.pdf.

Gabrysch, R.K., and Bonnet, C.W., 1976a, Land-surface subsidence in the area of Moses Lake near Texas City, Texas: U.S. Geological Survey Water-Resources Investigations Report 76–32, 42 p., accessed October 17, 2019, at https://doi.org/10.3133/wri7632.

Gabrysch, R.K., and Bonnet, C.W., 1976b, Land-surface subsidence at Seabrook, Texas: U.S. Geological Survey Water-Resources Investigations Report 76–31, 53 p., accessed October 17, 2019, at https://doi.org/10.3133/wri7631.

Gabrysch, R.K., and Coplin, L.S., 1990, Land-surface subsidence resulting from ground-water withdrawals in the Houston-Galveston region, Texas, through 1987: U.S. Geological Survey Report of Investigations 90–01, 53 p., accessed October 17, 2019, at https://doi.org/10.3133/1391.

Gabrysch, R.K., McAdoo, G.D., and Bonnet, C.W., 1970, Records of water-level measurements in wells in Galveston County, Texas, 1894–1969: Texas Water Development Board Report 123, prepared by U.S. Geological Survey, 105 p., accessed October 17, 2019, at https://www.twdb.texas.gov/publications/reports/numbered_reports/doc/R123/report123.asp.

Gabrysch, R.K., Naftel, W.L., and McAdoo, G.D., 1969, Records of water-level measurements in observation wells in Harris County, Texas: Texas Water Development Board Report 103, prepared by U.S. Geological Survey, 256 p., accessed October 17, 2019, at https://www.twdb.texas.gov/publications/reports/numbered_reports/doc/R103.pdf.

Gabrysch, R.K., and Neighbors, R.J., 2005, Measuring a century of subsidence in the Houston-Galveston region, Texas, USA, *in* Zhang, A., Gong, S., Carbognin, L., and Johnson, A.I., eds., Land subsidence—Proceedings of the 7th International Symposium on Land Subsidence, [Shanghai, China, October 2005]: Shanghai Scientific & Technical Publishers, v. 1, p. 379–387, accessed October 17, 2019, at https://www.landsubsidence-unesco.org/wp-content/uploads/2019/03/Proceedings_Shangai_2005.pdf.

Galloway, D., Jones, D.R., and Ingebritsen, S.E., eds., 1999, Land subsidence in the United States: U.S. Geological Survey Circular 1182, 177 p., accessed October 17, 2019, at https://doi.org/10.3133/cir1182.

Galloway, D.L., and Burbey, T.J., 2011, Review—Regional land subsidence accompanying groundwater extraction: Hydrogeology Journal, v. 19, no. 8, p. 1459–1486, accessed October 17, 2019, at https://link.springer.com/article/10.1007/s10040-011-0775-5.

Garcia, T.D., 1991, Subsidence and surface faulting at San Jacinto Monument, Goose Creek oil field, and Baytown, Texas, *in* Field trip guidebook on environmental impact of clays along the upper Texas Coast—Clay Minerals Society, 28th Annual Meeting, 1991, accessed October 17, 2019, at https://adsabs.harvard.edu/pdf/1991LPICo.773A..33G.

Goines, W.H., Winslow, A.G., and Barnes, J.R., 1951, Water supply of the Houston Gulf Coast region: Texas Board of Water Engineers Bulletin 5101, [variously paged; 44 p.], accessed October 17, 2019, at https://www.twdb.texas.gov/publications/reports/bulletins/doc/B5101.pdf.

Guyton, W.F., and Rose, N.A., 1945, Quantitative analysis of some artesian aquifers in Texas: Economic Geology, v. 40, no. 3, p. 193–226.

Hammond, W.W., Jr., 1969, Ground-water resources of Matagorda County, Texas: Texas Water Development Board Report 91, 163 p., accessed October 17, 2019, at https://www.twdb.texas.gov/publications/reports/numbered_reports/doc/R91/Report91.asp.

Hanson, R.T., 1989, Aquifer-system compaction, Tucson basin and Avra Valley, Arizona: U.S. Geological Survey Water-Resources Investigations Report 88–4172, 69 p., accessed October 17, 2019, at https://doi.org/10.3133/wri884172.

Hargreaves, G.H., and Samani, Z.A., 1985, Reference crop evapotranspiration from temperature: Applied Engineering in Agriculture, v. 1, no. 2, p. 96–99, accessed October 17, 2019 at https://doi.org/10.13031/2013.26773.

Harris-Galveston Subsidence District [HGSD], 2013, Regulatory plan 2013: Harris-Galveston Subsidence District, 14 p., accessed October 17, 2019, at http://hgsubsidence.org/wp-content/uploads/2013/07/HGSD-2013-Regulatory-Plan-with-Amendment.pdf.

Harris-Galveston Subsidence District [HGSD], 2020, Subsidence rates in Harris and surrounding counties, 2015–2019: Harris-Galveston Subsidence District web page, accessed October 17, 2020, at https://www.arcgis.com/home/webmap/viewer.html?webmap=a3e7214071f6421fb745d9866e2d3985&extent=-96.7596,28.7813,-93.7274,30.4716.

Harris-Galveston Subsidence District [HGSD], 2021, Subsidence rates in Harris and surrounding counties, 2015–2019: Harris-Galveston Subsidence District web page, accessed October 30, 2021, at https://www.arcgis.com/home/webmap/viewer.html?webmap=061405d3fc794d298af0415d245ae44e&extent=-97.4811,28.5499,-92.9685,30.7693.

Hartman, F., 1959, Storm bulletins: The Baytown Sun, 1959, v. 38, no. 296, ed. 1, Sunday, July 26, 1959, accessed June 12, 2022, at https://texashistory.unt.edu/ark:/67531/metapth1105349.

Hartman, F., 1961, Brownwood almost complete loss: The Baytown Sun, 1961, v. 42, no. 299, ed. 1, Thursday, September 14, 1961, accessed June 12, 2022, at https://texashistory.unt.edu/ark:/67531/metapth1056930.

Hayes, C.W., and Kennedy, W., 1903, Oil fields of the Texas–Louisiana Gulf Coastal Plain: U.S. Geological Survey Bulletin 212, 174 p., accessed October 17, 2019, at https://doi.org/10.3133/b212.

Hebert, P.J., and Frank, N.L., 1974, Atlantic hurricane season of 1973: Monthly Weather Review, v. 102, p. 280–295, accessed June 7, 2022, at https://www.aoml.noaa.gov/hrd/hurdat/mwr_pdf/1973.pdf.

Hemmings, B., Knowling, M.J., and Moore, C.R., 2020, Early uncertainty quantification for an improved decision support modeling workflow—A streamflow reliability and water quality example: Frontiers in Earth Science, v. 8, 22 p., accessed November 27, 2020, at https://doi.org/10.3389/feart.2020.565613.

Hintze, J.L., and Nelson, R.D., 1998, Violin plots—A box plot-density trace synergism: The American Statistician, v. 52, no. 2, p. 181–184, accessed October 17, 2019, at https://doi.org/10.1080/00031305.1998.10480559.

Hoffmann, J., Leake, S.A., Galloway, D.L., and Wilson, A.M., 2003, MODFLOW-2000 ground-water model—User guide to the Subsidence and Aquifer-System Compaction (SUB) package: U.S. Geological Survey Open-File Report 03–233, 46 p., accessed October 17, 2019, at https://pubs.usgs.gov/of/2003/ofr03-233/pdf/ofr03233.pdf.

Holcomb, H., 1967, Levee study sure, city to pay part: The Baytown Sun, v. 45, no. 75, ed. 1, Friday, October 20, 1967, p. 1, accessed June 12, 2022, at https://texashistory.unt.edu/ark:/67531/metapth1061350.

Holdahl, S.R., Holzschuh, J.C., and Zilkoski, D.B., 1989, Subsidence at Houston, Texas 1973–78: National Oceanic and Atmospheric Administration Technical Report NOS 131 NGS 44, 21 p., accessed October 17, 2019, at https://geodesy.noaa.gov/library/pdfs/NOAA_TR_NOS_0131_NGS_0044.pdf.

Holzer, T.L., 1981, Preconsolidation stress of aquifer systems in areas of induced land subsidence: Water Resources Research, v. 17, no. 3 p. 693–704.

Holzer, T.L., 1998, History of the aquitard-drainage model, *in* Borchers, J.W., ed., Land subsidence case studies and current research—Proceedings of the Dr. Joseph F. Poland Symposium on Land Subsidence: Association of Engineering Geologists Special Publication 8: 7–12.

Horizon Systems Corporation, 2020, National Hydrography Dataset Plus (NHDPlus): Horizon Systems Corporation, accessed October 17, 2020, at http://www.horizon-systems.com/nhdplus/.

Hosman, R.L., 1996, Regional stratigraphy and subsurface geology of Cenozoic deposits, Gulf Coastal Plain, south-central United States: U.S. Geological Survey Professional Paper 1416–G, 35 p., accessed October 17, 2019, at https://doi.org/10.3133/pp1416G.

Howson, L.R., 1938, Well water problems of Houston: Journal of American Water Works Association, v. 30, no. 7, p. 1092–1102.

Hughes, J.D., Leake, S.A., Galloway, D.L., and White, J.T., 2022, Documentation for the Skeletal Storage, Compaction, and Subsidence (CSUB) package of MODFLOW 6: U.S. Geological Survey Techniques and Methods, book 6, chap. A62, 57 p., accessed April 25, 2022, at https://doi.org/10.3133/tm6A62.

Ireland, R.L., Poland, J.F., and Riley, F.S., 1984, Land subsidence in the San Joaquin Valley, California, as of 1980: U.S. Geological Survey Professional Paper 437–1, 93 p., 1 pl., accessed October 17, 2019, at https://doi.org/10.3133/pp437I.

Isaaks, E.H., and Srivastava, R.M., 1989, An introduction to applied geostatistics: New York, Oxford University Press, 561 p.

Jacob, C.E., 1940, On the flow of water in an elastic artesian aquifer: Eos, Transactions, American Geophysical Union, v. 21, no. 2, p. 574–586, accessed May 10, 2022, at https://doi.org/10.1029/TR021i002p00574.

Jacob, C.E., 1941, Coefficients of storage and transmissibility obtained from pumping tests in the Houston district, Texas: Eos, Transactions, American Geophysical Union, v. 22, no. 3, p. 744–756, accessed October 17, 2019, at https://doi.org/10.1029/TR022i003p00744.

Jones, P.H., Turcan, A.N., Jr., and Skibitzke, H.E., 1954, Geology and groundwater resources of southwestern Louisiana: Louisiana Geological Survey Bulletin 30, 285 p.

Jorgensen, D.G., 1975, Analog-model studies of ground-water hydrology in the Houston district, Texas: Texas Water Development Board Report 190, 84 p., accessed October 17, 2019, at https://www.twdb.texas.gov/publications/reports/numbered_reports/doc/R190/Report190.asp.

Kasmarek, M.C., 2012, Hydrogeology and simulation of groundwater flow and land-surface subsidence in the northern part of the Gulf Coast aquifer system, Texas, 1891–2009 (ver. 1.1, December 2013): U.S. Geological Survey Scientific Investigations Report 2012–5154, 55 p., accessed October 17, 2019, at https://doi.org/10.3133/sir20125154.

Kasmarek, M.C., Johnson, M.R., and Ramage, J.K., 2010, Water-level altitudes 2010 and water-level changes in the Chicot, Evangeline, and Jasper aquifers and compaction 1973–2009 in the Chicot and Evangeline aquifers, Houston-Galveston region, Texas: U.S. Geological Survey Scientific Investigations Map 3138, 16 p., 17 sheets, accessed October 17, 2019, at https://doi.org/10.3133/sim3138.

Kasmarek, M.C., and Ramage, J.K., 2017, Water-level altitudes 2017 and water-level changes in the Chicot, Evangeline, and Jasper aquifers and compaction 1973–2016 in the Chicot and Evangeline aquifers, Houston-Galveston region, Texas: U.S. Geological Survey Scientific Investigations Report 2017–5080, 32 p., accessed October 17, 2019, at https://doi.org/10.3133/sir20175080.

Kasmarek, M.C., Ramage, J.K., and Johnson, M.R., 2016, Water-level altitudes 2016 and water-level changes in the Chicot, Evangeline, and Jasper aquifers and compaction 1973–2015 in the Chicot and Evangeline aquifers, Houston-Galveston region, Texas: U.S. Geological Survey Scientific Investigations Map 3365, 39-p. pamphlet, 16 sheets, scale 1:100,000, accessed October 17, 2019, at http://doi.org/10.3133/sim3365.

Kasmarek, M.C., and Robinson, J.L., 2004, Hydrogeology and simulation of ground-water flow and land-surface subsidence in the northern part of the Gulf Coast aquifer system, Texas: U.S. Geological Survey Scientific Investigations Report 2004–5102, 103 p., accessed October 17, 2019, at https://doi.org/10.3133/sir20045102.

Kasmarek, M.C., and Strom, E.W., 2002, Hydrogeology and simulation of ground-water flow and land-surface subsidence in the Chicot and Evangeline aquifers, Houston area, Texas: U.S. Geological Survey Water-Resources Investigations Report 02–4022, 61 p., accessed October 17, 2019, at https://doi.org/10.3133/wri024022.

Kearns, T.J., Wang, G., Bao, Y., Jiang, J., and Lee, D., 2015, Current land subsidence and groundwater level changes in the Houston metropolitan area (2005–2012): Journal of Surveying Engineering, v. 141, no. 4, p. 05015002-1–05015002-16.

Kearns, T.J., Wang, G., Turco, M., Welch, J., Tsibanos, V., and Liu, H., 2018, Houston16—A stable geodetic reference frame for subsidence and faulting study in the Houston metropolitan area, Texas, U.S.: Geodesy and Geodynamics, v. 10, no5p. 382–393, accessed October 17, 2019, at https://doi.org/10.1016/j.geog.2018.05.005.

Kelley, V., Deeds., N., Young, S.C., and Pinkard, J., 2018, Subsidence risk assessment and regulatory considerations for the brackish Jasper aquifer: Prepared by INTERA Incorporated for the Harris-Galveston and Fort Bend Subsidence Districts, 69 p., accessed October 17, 2019, at https://hgsubsidence.org/wp-content/uploads/2021/11/HGSD-Scientific-Report-2018-002_SUBSIDENCE-RISK-ASSESSMENT-AND-REGULATORY-CONSIDERATIONS-FOR-THE-BRACKISH-JASPER-AQUIFER.pdf.

Kennedy, W., 1892, A section from Terrell, Kaufman County, to Sabine Pass on the Gulf of Mexico: Texas Geological Survey 3d Annual Report, p. 45, 62.

Kenney, T.A., 2010, Levels at gaging stations: U.S. Geological Survey Techniques and Methods, book 3, chap. A19, 60 p., accessed October 17, 2019, at https://doi.org/10.3133/tm3A19.

Khan, S.D., Huang, Z., and Karacay, A., 2014, Study of ground subsidence in northwest Harris County using GPS, LiDAR, and InSAR techniques: Natural Hazards, v. 73, p. 1143–1173, accessed October 17, 2019, at https://link.springer.com/article/10.1007/s11069-014-1067-x.

Knight, J.E., Ellis, J.H., White, J.T., Sneed, M., Hughes, J.D., Ramage, J.K., Braun, C.L., Teeple, A.P., Foster, L., Rendon, S.H., Brandt, J., Duncan, L.L., Traylor, J.P., and Pattison, C.N., 2023, MODFLOW 6 model and ensemble used in the simulation of groundwater flow and land-surface subsidence in the northern part of the Gulf Coast aquifer system, 1897–2018: U.S. Geological Survey data release, https://doi.org/10.5066/P9XM8A1P.

Knowling, M.J., White, J.T., McDonald, G.W., Kim, J.H., Moore, C.R., and Hemmings, B., 2020b, Disentangling environmental and economic contributions to hydro-economic model output uncertainty—An example in the context of land-use change impact assessment: Environmental Modelling & Software, v. 127, article 104653, accessed October 17, 2021, at https://doi.org/10.1016/j.envsoft.2020.104653.

Knowling, M.J., White, J.T., Moore, C.R., Rakowski, P., and Hayley, K., 2020a, On the assimilation of environmental tracer observations for model-based decision support: Hydrology and Earth System Sciences, v. 24, p. 1677–1689, accessed December 17, 2020, at https://doi.org/10.5194/hess-24-1677-2020.

Kreitler, C.W., 1974, Land-surface subsidence and active faulting in the Texas Coastal Zone: Bureau of Economic Geology—Texas House of Representatives special interim committee on water supply and waste disposal in metropolitan areas, 23 p., accessed December 9, 2022, at https://www.beg.utexas.edu/files/publications/contract-reports/CR1974-Kreitler-1.pdf.

Kreitler, C.W., Guevera, E., Granata, G., and McKalips, D., 1977, Hydrogeology of Gulf Coast aquifers, Houston-Galveston area, Texas: Bureau of Economic Geology, Geologic Circular 77–4, p. 72–89, accessed October 17, 2019, at https://www.beg.utexas.edu/files/publications/cr/CR1977-Kreitler-1-QAe5600.pdf.

Kuiper, L.K., 1985, Documentation of a numerical code for the simulation of variable density ground-water flow in three dimensions: U.S. Geological Survey Water-Resources Investigations Report 84–4302, [variously paged; 94 p.], accessed October 17, 2019, at https://doi.org/10.3133/wri844302.

Lang, J.W., and Sundstrom, R.W., 1946, Ground-water resources of the Houston district, Texas: Texas Board of Water Engineers progress report for 1946 (Memorandum 138), 34 p., accessed October 17, 2019, at https://www.twdb.texas.gov/publications/reports/historic_groundwater_reports/doc/M138.pdf.

Lang, J.W., Winslow, A.G., and White, W.N., 1950, Geology and ground-water resources of the Houston district, Texas: Texas State Board of Water Engineers, Bulletin 5001, prepared by the U.S. Geological Survey, 56 p., 3 pls., accessed October 17, 2019, at https://www.twdb.texas.gov/publications/reports/bulletins/doc/B5001.pdf.

Langbein, J., 2008, Noise in GPS displacement measurements from Southern California and Southern Nevada: Journal of Geophysical Research, v. 113, no. B5, 12 p., accessed October 17, 2019, at https://agupubs.onlinelibrary.wiley.com/doi/full/10.1029/2007JB005247.

Langevin, C.D., Hughes, J.D., Banta, E.R., Niswonger, R.G., Panday, S., and Provost, A.M., 2017, Documentation for the MODFLOW 6 Groundwater Flow Model: U.S. Geological Survey Techniques and Methods, book 6, chap. A55, 197 p., accessed October 17, 2019, at https://doi.org/10.3133/tm6A55.

Langevin, C.D., Hughes, J.D., Banta, E.R., Provost, A.M., Niswonger, R.G., and Panday, S., 2021, MODFLOW 6 Modular Hydrologic Model version 6.2.1: U.S. Geological Survey Software Release, February 18, 2021, accessed October 17, 2021, at https://doi.org/10.5066/F76Q1VQV.

Leake, S.A., and Galloway, D.L., 2007, MODFLOW ground-water model—User guide to the Subsidence and Aquifer-System Compaction package (SUB-WT) for water-table aquifers: U.S. Geological Survey Techniques and Methods, book 6, chap. A23, 42 p., accessed October 17, 2019, at https://doi.org/10.3133/tm6A23.

Leake, S.A., and Prudic, D.E., 1991, Documentation of a computer program to simulate aquifer-system compaction using the modular finite-difference ground-water flow model: U.S. Geological Survey Techniques of Water-Resources Investigations, book 6, chap. A2, 68 p., accessed October 17, 2019, at https://doi.org/10.3133/twri06A2.

Liu, Y., Li, J., and Fang, Z.N., 2019, Groundwater level change management on control of land subsidence supported by borehole extensometer compaction measurements in the Houston-Galveston region, Texas: Geosciences, v. 9, no. 5, 19 p. [Also available at https://www.mdpi.com/2076-3263/9/5/223.]

Livingston, P., 1937, Fort Bend County, Texas (west of the Brazos River)—Records of wells, drillers' logs, and water analyses, and maps showing location of wells: State Board of Water Engineers Report 85, 14 p., accessed October 19, 2019, at https://www.twdb.texas.gov/publications/reports/historic_groundwater_reports/doc/M085.pdf.

Livingston, P., 1939a, Fort Bend County, Texas (east of the Brazos River)—Records of wells, drillers' logs, water analyses, and map showing location of wells: State Board of Water Engineers Report 86, 14 p., accessed October 19, 2019, at https://www.twdb.texas.gov/publications/reports/historic_groundwater_reports/doc/M086.pdf.

Livingston, P., 1939b, Montgomery County, Texas—Records of wells, drillers' logs, water analyses, and map showing location of wells: State Board of Water Engineers Report 191, 15 p., accessed October 19, 2019, at https://www.twdb.texas.gov/publications/reports/historic_groundwater_reports/doc/M191.pdf.

Lockwood, M.G., 1954, Subsidence from declining artesian pressure can no longer be ignored in Houston area, Texas—American Society of Civil Engineers, Texas Section Spring Meeting, April 1954, accessed December 9, 2022, at https://www.twdb.texas.gov/publications/reports/other_reports/doc/Lockwood_1954.pdf.

Lone Star Groundwater Conservation District [LSGCD], 2013, Groundwater management plan, 139 p., accessed October 17, 2019, at https://www.twdb.texas.gov/groundwater/docs/GCD/lsgcd/lsgcd_mgmt_plan2013.pdf.

Loskot, C.L., Sandeen, W.M., and Follett, C.R., 1982, Groundwater resources of Colorado, Lavaca, and Wharton Counties, Texas: Texas Department of Water Resources Report 270, prepared by U.S. Geological Survey, 240 p., accessed October 17, 2019, at https://www.twdb.texas.gov/publications/reports/numbered_reports/doc/R270/R270.pdf.

Marsh, J., 1962, Bay area levee data heard by engineers: The Baytown Sun, v. 43, no. 132, ed. 1, Tuesday, March 6, 1962, p. 1, accessed June 12, 2022, at https://texashistory.unt.edu/ark:/67531/metapth1057970.

Marshall, R.B., 1916a, Spirit leveling in Texas, 1896 to 1915, inclusive: U.S. Geological Survey Bulletin 637, 254 p., accessed October 17, 2019, at https://doi.org/10.3133/b637.

Marshall, R.B., 1916b, Triangulation and primary traverse, 1913–1915: U.S. Geological Survey Bulletin 644–P, p. 521–597, accessed August 23, 2022, at https://doi.org/10.3133/b644P.

McDonald, M.G., and Harbaugh, A.W., 1988, A modular three-dimensional finite-difference ground-water flow model: U.S. Geological Survey Techniques of Water-Resources Investigations, book 6, chap. A1, 586 p., accessed October 17, 2019, at https://doi.org/10.3133/twri06A1.

McDougal, S., 2018, Galveston's 30th Street Pump Station—A written history of the city water system in Galveston, Texas, and the 30th Street Pump Station water storage tanks: McDoux Preservation LLC, [variously paged; 74 p.], accessed October 17, 2019, at https://www.galvestontx.gov/DocumentCenter/View/7018/30th-Street-Pump-Station---A-History-of-the-Citys-Water-System-PDF.

McMahon, P.B., Dennehy, K.F., Bruce, B.W., Böhlke, J.K., Michel, R.L., Gurdak, J.J., and Hurlbut, D.B., 2006, Storage and transit time of chemicals in thick unsaturated zones under rangeland and irrigated cropland, High Plains, United States: Water Resources Research, v. 42, no. 3, 18 p., accessed October 19, 2017, at https://doi.org/10.1029/2005WR004417.

McMahon, P.B., Plummer, L.N., Böhlke, J.K., Shapiro, S.D., and Hinkle, S.R., 2011, A comparison of recharge rates in aquifers of the United States based on groundwater-age data: Hydrogeology Journal, v. 19, p. 779–800, accessed June 22, 2017, at https://doi.org/10.1007/s10040-011-0722-5.

Meinzer, O.E., 1928, Compressibility and elasticity of artesian aquifers: Economic Geology, v. 23, no. 3, p. 263–291, accessed October 17, 2019, at https://doi.org/10.2113/gsecongeo.23.3.263.

Meyer, W.R., and Carr, J.E., 1979, A digital model for simulation of ground-water hydrology in the Houston area, Texas: Texas Department of Water Resources Limited Publication LP–103, prepared by U.S. Geological Survey, [variously paged], accessed October 17, 2019, at http://www.twdb.texas.gov/publications/reports/limited_printing/doc/LP-103/LP-103%20a.pdf.

Moore, C., and Doherty, J., 2005, Role of the calibration process in reducing model predictive error: Water Resources Research, v. 41, no. 5, 14 p., accessed October 17, 2019, at https://agupubs.onlinelibrary.wiley.com/doi/full/10.1029/2004WR003501.

Moré, J.J., 1978, The Levenberg-Marquardt algorithm—Implementation and theory, *in* Watson, G.A., ed., Numerical analysis: Berlin, Heidelberg, Springer, p. 105–116.

Municipal Engineering Company, 1904, Municipal Engineering Index: Municipal Engineering Company, v. 25, 500 p.

National Agricultural Statistics Service, 2021, CropScape—Cropland data layers, 2010–15, accessed February 2021 at https://nassgeodata.gmu.edu/CropScape/.

National Climatic Data Center [NCDC], 2019, Climate Data Online: National Oceanic and Atmospheric Administration database, accessed October 14, 2021, at https://www7.ncdc.noaa.gov/CDO/CDODivisionalSelect.jsp. [Database moved prior to time of publication; accessed April 6, 2022, at https://www.ncdc.noaa.gov/cdo-web/; search interface and search parameters did not change.]

National Institute of Standards and Technology, 2015, Violin plot: National Institute of Standards and Technology web page, accessed January 5, 2022, at https://www.itl.nist.gov/div898/software/dataplot/refman1/auxillar/violplot.htm.

National Oceanic and Atmospheric Administration [NOAA], 1980, The 1978 Houston–Galveston and Texas Gulf Coast vertical control surveys: NOAA Technical Memorandum NOS NGS 27, 61 p., accessed October 17, 2019, at https://www.ngs.noaa.gov/PUBS_LIB/The1978Houston_Galveston_and_Texas_GulfCoast_VerticalControlSurveys_TM_NOS_NGS27.pdf.

National Oceanic and Atmospheric Administration [NOAA], 2021a, Finding survey marks and datasheets: NOAA, National Geodetic Survey, accessed March 10, 2021, at https://geodesy.noaa.gov/datasheets/.

National Oceanic and Atmospheric Administration [NOAA], 2021b, NGS suppresses height information for southeast Texas: NOAA, National Geodetic Survey, accessed March 10, 2021, at https://geodesy.noaa.gov/web/news/southeast-texas-height-suppression.shtml.

National Oceanic and Atmospheric Administration [NOAA], 2021c, Southeast TX valid orthometric heights: NOAA, National Geodetic Survey, accessed March 10, 2021, at https://geodesy.noaa.gov/datasheets/southeastTXValidHeights/index.html.

National Oceanic and Atmospheric Administration [NOAA], 2022, FGCS Blue Book: NOAA, National Geodetic Survey, accessed June 6, 2022, at https://geodesy.noaa.gov/FGCS/BlueBook/.

Natural Resources Conservation Service, 2019, Geospatial Data Gateway, accessed September 10, 2019, at https://datagateway.nrcs.usda.gov/.

Noble, J.E., Bush, P.W., Kasmarek, M.C., and Barbie, D.L, 1996, Estimated depth to the water table and estimated rate of recharge in outcrops of the Chicot and Evangeline aquifers near Houston, Texas: U.S. Geological Survey Water-Resources Investigations Report 96–4018, 19 p., 1 pl., accessed October 17, 2019, at https://doi.org/10.3133/wri964018.

Ocker, L., 1983, Brownwood reconstruction opposed by city authorities: The Baytown Sun, v. 61, no. 253, ed. 1, Tuesday, August 23, 1983, p. 1, accessed June 12, 2022, at https://texashistory.unt.edu/ark:/67531/metapth1154000.

Oden, T.D., and Truini, M., 2013, Estimated rates of groundwater recharge to the Chicot, Evangeline, and Jasper aquifers by using environmental tracers in Montgomery and adjacent counties, Texas, 2008 and 2011 (revised May 31, 2013): U.S. Geological Survey Scientific Investigations Report 2013–5024, 50 p., accessed October 17, 2019, at https://doi.org/10.3133/sir20135024.

Oliver, W., and Harmon, R., 2022, Estimation of historical pumping for the northern part of the Gulf Coast aquifer, 1900 to 2018, prepared for the Harris–Galveston Subsidence District, 81 p., accessed July 22, 2022, at https://hgsubsidence.org/wp-content/uploads/2022/10/GULF2023_PumpingFile_Report_2022-07-03_FINAL.pdf.

Petersen, C., Greuter, A., and Thompson, R., 2020, Determination of groundwater withdrawal and effects on subsidence—2019: Harris-Galveston Subsidence District Report 2020–01, 27 p., accessed October 17, 2020, at https://hgsubsidence.org/wp-content/uploads/2020/06/2019-HGSD-2020-001-AGR-Discussion.pdf.

Petitt, B.M., Jr., and Winslow, A.G., 1955, Geology and ground-water resources of Galveston County, Texas: Texas Water Development Board bulletin 5502, 157 p., accessed October 17, 2019, at https://www.twdb.texas.gov/publications/reports/bulletins/doc/B5502.pdf.

Poland, J.F., ed., 1984, Guidebook to studies of land subsidence due to ground-water withdrawal: Paris, France, United Nations Educational, Scientific and Cultural Organization (UNESCO), Studies and reports in hydrology, v. 40, 305 p., 5 app., accessed October 17, 2019, at https://wwwrcamnl.wr.usgs.gov/rgws/Unesco/.

Poland, J.F., and Ireland, R.L., 1965, Shortening and protrusion of a well casing due to compaction of sediments in a subsiding area in California, *in* Geological Survey Research 1965: U.S. Geological Survey Professional Paper 525–B, p. B180–B183, accessed October 17, 2019, at https://doi.org/10.3133/pp525B.

Popkin, B.P., 1971, Ground-water resources of Montgomery County, Texas: Texas Water Development Board Report 136, prepared by U.S. Geological Survey, 149 p., accessed October 17, 2019, at https://www.twdb.texas.gov/publications/reports/numbered_reports/doc/R136/Report136.asp.

Plummer, F.B., 1932, Cenozoic systems in Texas, *in* The geology of Texas, v. 1, stratigraphy: University of Texas Bulletin 3232 [1933], p. 519–818.

Pratt, W., and Johnson, D., 1926, Local subsidence of the Goose Creek oil field, Journal of Geology v. 34, no. 7, p. 577–590.

Qu, F., Lu, Z., Kim, J-W., and Zheng, W., 2019, Identify and monitor growth faulting using InSAR over northern greater Houston, Texas, USA: Remote Sensing, v. 11, no. 12, article 1498, 23 p., accessed October 17, 2019, at https://doi.org/10.3390/rs11121498.

Qu, F., Lu, Z., Zhang, Q., Bawden, G.W., Kim, J-W., Zhao, C., and Qu, W., 2015, Mapping ground deformation over Houston–Galveston, Texas using multi-temporal InSAR: Remote Sensing of Environment, v. 169, p. 290–306. [Also available at https://doi.org/10.1016/j.rse.2015.08.027.]

Ramage, J.K., and Shah, S.D., 2019, Cumulative compaction of subsurface sediments in the Chicot and Evangeline aquifers in the Houston-Galveston region, Texas (ver. 2.0, June 2020): U.S. Geological Survey data release, accessed October 17, 2019, at https://doi.org/10.5066/P9YGUE2V.

Rayner, F.A., 1959, Records of water-level measurements in Chambers, Liberty, and Montgomery Counties, Texas, 1931 through April 1958: Texas Board of Water Engineers Bulletin 5901, 33 p., accessed October 17, 2019, at https://www.twdb.texas.gov/publications/reports/bulletins/doc/B5901.pdf.

Riley, F.S., 1969, Analysis of borehole extensometer data from central California, *in* Tison, L.J., ed., Land subsidence, Volume 2: International Association of Scientific Hydrology Publication 89, p. 423–431.

Riley, F.S., 1998, Mechanics of aquifer systems—The scientific legacy of Joseph F. Poland, *in* Borchers, J.W., ed., Land subsidence case studies and current research—Proceedings of the Dr. Joseph F. Poland Symposium on Land Subsidence: Association of Engineering Geologists Special Publication no. 8, p. 13–27.

Roark, D.M., and Healy, D.F., 1998, Quantification of deep percolation from two flood-irrigated alfalfa fields, Roswell Basin, New Mexico: U.S. Geological Survey Water-Resources Investigations Report 98–4096, 32 p., accessed October 17, 2019, at https://doi.org/10.3133/wri984096.

Rorabaugh, M.I., 1949, Memorandum on multiple-step drawdown tests, Southwest well field, Houston, Texas, February 1949: U.S. Geological Survey Memorandum 139, 14 p., accessed October 17, 2019, at https://www.twdb.texas.gov/publications/reports/historic_groundwater_reports/doc/m139.pdf.

Rose, N.A., 1943, Ground water and relation of geology to its occurrence in the Houston district, Texas: American Association of Petroleum Geologists Bulletin, v. 27, no. 8, p. 1081–1101, accessed September 8, 2023, at https://doi.org/10.1306/3D9335F8-16B1-11D7-8645000102C1865D.

Rose, N.A., 1949, Subsidence in the Texas City area—Proceedings from the Annual Meeting for the Society of Economic Geology, February 1949, accessed December 9, 2022, at https://www.twdb.texas.gov/publications/reports/other_reports/doc/Rose_1949.pdf.

Rose, N.A., and Alexander, W.H., Jr., 1944, Progress report on the ground-water resources of the Houston district: Texas State Board of Water Engineers Memorandum 137, 40 p., accessed October 17, 2019, at https://www.twdb.texas.gov/publications/reports/historic_groundwater_reports/doc/M137.pdf.

Rose, N.A., White, W.N., and Livingston, P., 1944, Exploratory water-well drilling in the Houston district, Texas: U.S. Geological Survey Water-Supply Paper 889–D, 32 p., accessed October 17, 2019, at https://doi.org/10.3133/wsp889D.

Ryder, P.D., 1988, Hydrogeology and predevelopment flow in the Texas Gulf Coast aquifer systems: U.S. Geological Survey Water-Resources Investigations Report 87–4248, 109 p., accessed October 17, 2019, at https://doi.org/10.3133/wri874248.

Ryder, P.D., 1996, Ground water atlas of the United States—Segment 4, Oklahoma and Texas: U.S. Geological Survey Hydrologic Atlas 730–E, accessed October 17, 2019, at https://doi.org/10.3133/ha730E.

Ryder, P.D., and Ardis, A.F., 1991, Hydrology of the Texas Gulf Coast aquifer systems: U.S. Geological Survey Open-File Report 91–64, 147 p., accessed October 17, 2019, at https://doi.org/10.3133/ofr9164.

Ryder, P.D., and Ardis, A.F., 2002, Hydrology of the Texas Gulf Coast aquifer systems: U.S. Geological Survey Professional Paper 1416–E, 77 p., accessed October 17, 2019, at https://doi.org/10.3133/pp1416E.

Rydlund, P.H., Jr., and Densmore, B.K., 2012, Methods of practice and guidelines for using survey-grade Global Navigation Satellite Systems (GNSS) to establish vertical datum in the United States Geological Survey: U.S. Geological Survey Techniques and Methods, book 11, chap. D1, 102 p. with appendixes, accessed October 17, 2019, at https://doi.org/10.3133/tm11D1.

Sandeen, W.M., and Wesselman, J.B., 1973, Groundwater resources of Brazoria County, Texas: Texas Water Development Board Report 163, prepared by U.S. Geological Survey, 175 p., accessed October 17, 2019, at https://www.twdb.texas.gov/publications/reports/numbered_reports/doc/R163/report163.asp.

Scanlon, B.R., Dutton, A., and Sophocleous, M., 2003, Groundwater recharge in Texas: Bureau of Economic Geology, The University of Texas at Austin, submitted to Texas Water Development Board, 80 p., accessed October 17, 2019, at https://www.beg.utexas.edu/files/content/beg/research/swr/pubs/TWDBRechRept.pdf.

Scanlon, B.R., Reedy, R.C., Strassberg, G., Huang, Y., and Senay, G., 2011, Estimation of groundwater recharge to the Gulf Coast aquifer in Texas, USA: The University of Texas at Austin, Bureau of Economic Geology, Final Contract Report [variously paged], accessed October 17, 2019, at https://www.twdb.texas.gov/groundwater/docs/studies/TWDB%20Gulf%20Coast%20Recharge.pdf.

SciPy, 2020, API reference—Gaussian filter: SciPy web page, accessed January 15, 2020, at https://docs.scipy.org/doc/scipy/reference/generated/scipy.ndimage.gaussian_filter.html.

Seequent, 2021, Geosoft Technical Workshop—Topics in gridding: Broomfield, Calif., Seequent, accessed October 27, 2021, at https://files.seequent.com/MySeequent/technical-papers/topicsingriddingworkshop.pdf.

Sellards, E.H., Adkins, W.S., and Plummer, F.B., 1932, The geology of Texas, volume 1—Stratigraphy: The University of Texas Bulletin 3232, 1,007 p., 1 sheet, accessed October 17, 2019, at https://repositories.lib.utexas.edu/handle/2152/24040.

Singley, J.A., 1893, Preliminary report on the artesian wells of the Gulf Coastal slope: Texas Geological Survey, 4th annual report.

Sneed, M., and Brandt, J.T., 2020, Detection and measurement of land subsidence and uplift using Global Positioning System surveys and interferometric synthetic aperture radar, Coachella Valley, California, 2010–17: U.S. Geological Survey Scientific Investigations Report 2020–5093, 74 p., accessed October 17, 2020, at https://doi.org/10.3133/sir20205093.

Sneed, M., Brandt, J.T., and Solt, M., 2018, Land subsidence along the California Aqueduct in west-central San Joaquin Valley, California, 2003–10: U.S. Geological Survey Scientific Investigations Report 2018–5144, 67 p., accessed October 17, 2019, at https://doi.org/10.3133/sir20185144.

Sneed, M., and Galloway, D.L., 2000, Aquifer-system compaction and land subsidence—Measurements, analyses, and simulations—The Holly site, Edwards Air Force Base, Antelope Valley, California: U.S. Geological Survey Water-Resources Investigations Report 2000–4015, 65 p., accessed October 17, 2019, at https://doi.org/10.3133/wri20004015.

Sneed, M., Ikehara, M.E., Galloway, D.L., and Amelung, F., 2001, Detection and measurement of land subsidence using Global Positioning System and interferometric synthetic aperture radar, Coachella Valley, California, 1996–98: U.S. Geological Survey Water-Resources Investigations Report 01–4193, 26 p., accessed October 17, 2019, at https://doi.org/10.3133/wri014193.

Stanton, J.S., Peterson, S.M., and Fienen, M.N., 2010, Simulation of groundwater flow and effects of groundwater irrigation on stream base flow in the Elkhorn and Loup River Basins, Nebraska, 1895–2055—Phase two: U.S. Geological Survey Scientific Investigations Report 2010–5149, 78 p., accessed October 17, 2019, at https://doi.org/10.3133/sir20105149.

Stoeser, D.B., Green, G.N., Morath, L.C., Heran, W.D., Wilson, A.B., Moore, D.W., and Van Gosen, B.S., 2005, Preliminary integrated geologic map databases for the United States—Central States—Montana, Wyoming, Colorado, New Mexico, North Dakota, South Dakota, Nebraska, Kansas, Oklahoma, Texas, Iowa, Missouri, Arkansas, and Louisiana: U.S. Geological Survey Open-File Report 2005–1351, accessed September 26, 2022, at https://doi.org/10.3133/ofr20051351.

Strom, E.W., Houston, N.A., and Garcia, C.A., 2003a, Selected hydrogeologic datasets for the Chicot aquifer, Texas: U.S. Geological Survey Open-File Report 03–297, 1 CD–ROM.

Strom, E.W., Houston, N.A., and Garcia, C.A., 2003b, Selected hydrogeologic datasets for the Evangeline aquifer, Texas: U.S. Geological Survey Open-File Report 03–298, 1 CD–ROM.

Strom, E.W., Houston, N.A., and Garcia, C.A., 2003c, Selected hydrogeologic datasets for the Jasper aquifer, Texas: U.S. Geological Survey Open-File Report 03–299, 1 CD–ROM.

Tarantola, A., 2005, Inverse problem theory and methods for model parameter estimation: Philadelphia, Pa., Society for Industrial and Applied Mathematics, 342 p.

Taylor, T.U., 1907, Underground waters of Coastal Plain of Texas: U.S. Geological Survey Water-Supply and Irrigation Paper 190, 73 p., accessed October 17, 2019, at https://doi.org/10.3133/wsp190.

Teeple, A.P., Foster, L.K., Lindaman, M.A., Duncan, L.L., and Casarez, I., 2021, Hydrogeologic data for the development of the hydrogeologic framework of the Coastal lowlands aquifer system regional groundwater availability study area in Texas, Louisiana, Mississippi, Alabama, and Florida: U.S. Geological Survey data release, accessed October 17, 2021, at https://doi.org/10.5066/P9PEFY11.

Terzaghi, K., 1925, Principles of soil mechanics, IV—Settlement and consolidation of clay: Engineering News-Record, v. 95, no. 22, p. 874–878.

Texas Historical Commission, 2022, Details for 1879 Houston Waterworks (Atlas Number 2076002037): Texas Historical Commission—Texas Historic Sites Atlas, accessed June 27, 2022, at https://atlas.thc.state.tx.us/Details/2076002037.

Texas Water Development Board [TWDB], 1998, System operation of surface water supply sources in the Houston area, accessed October 4, 2022, at https://www.twdb.texas.gov/publications/reports/contracted_reports/doc/TransTXSEr.pdf.

Texas Water Development Board [TWDB], 2001, Surveys of irrigation in Texas: Texas Water Development Board Report 347, 102 p., accessed October 17, 2019, at https://www.twdb.texas.gov/publications/reports/numbered_reports/doc/R347/Report347.asp.

Texas Water Development Board [TWDB], 2019, Groundwater Conservation Districts, accessed October 10, 2019, at https://www.twdb.texas.gov/groundwater/conservation_districts/.

Texas Water Development Board [TWDB], 2020a, Historical water use estimates, accessed October 5, 2020, at http://www.twdb.texas.gov/waterplanning/waterusesurvey/estimates/index.asp.

Texas Water Development Board [TWDB], 2020b, Groundwater Database (GWDB) reports, accessed September 10, 2020, at https://www3.twdb.texas.gov/apps/waterdatainteractive/groundwaterdataviewer.

Texas Water Development Board [TWDB], 2020c, Submitted driller well reports, accessed September 10, 2020, at https://www3.twdb.texas.gov/apps/WaterDataInteractive/GroundwaterDataViewer/?map=sdr.

Thornthwaite, C.W., and Mather, J.R., 1957, Instructions and tables for computing potential evapotranspiration and the water balance: Centerton, N.J., Drexel Institute of Technology, Laboratory of Climatology, Publications in Climatology, v. 10, no. 3, p. 185–311.

Tóth, J., 1963, A theoretical analysis of ground-water flow in small drainage basins: Journal of Geophysical Research, v. 68, no. 16, p. 4795–4812.

Trescott, P.C., 1975, Documentation of finite-difference model for simulation of three-dimensional ground-water flow: U.S. Geological Survey Open-File Report 75–438, [variously paged; 107 p.], accessed October 17, 2019, at https://doi.org/10.3133/ofr75438.

Trimble, 2022, Trimble R8s Integrated GNSS System, accessed April 28, 2022, at A Trimble R8 survey-grade GPS receiver, accessed October 17, 2019, at https://geospatial.trimble.com/sites/geospatial.trimble.com/files/2019-03/Datasheet%20-%20Trimble%20R8s%20GNSS%20System%20-%20English%20A4%20-%20Screen.pdf.

Tuck, C.A., 1974, Rice irrigation return flow study, Brookshire and Garwood projects, Texas, interim report, 1969–73: Texas Water Development Board file report, 48 p.

Turcan, A.N., Jr., Wesselman, J.B., and Kilburn, C., 1966, Interstate correlation of aquifers, southwestern Louisiana and southeastern Texas: U.S. Geological Survey Professional Paper 550–D, p. D231–D236, accessed October 17, 2019, at https://pubs.usgs.gov/pp/0550d/report.pdf.

Turner, S.F., 1939, Brazoria County, Texas (west of the Brazos River)—Records of wells, drillers' logs, and water analyses, and map showing location of wells: State Board of Water Engineers Report 17, 45 p., accessed October 19, 2019, at https://www.twdb.texas.gov/publications/reports/historic_groundwater_reports/doc/M017.pdf.

Turner, S.F., and Livingston, P., 1939, Brazoria County, Texas (east of the Brazos River)—Records of wells, drillers' logs, water analyses, and map showing location of wells: State Board of Water Engineers Report 18, 15 p., accessed October 19, 2019, at https://www.twdb.texas.gov/publications/reports/historic_groundwater_reports/doc/M018.pdf.

U.S. Census Bureau, 2020, Texas—2020 Census: U.S. Census Bureau, accessed June 3, 2022, at https://www.census.gov/library/stories/state-by-state/texas-population-change-between-census-decade.html.

U.S. Geological Survey [USGS], 2018, Spirit leveling: U.S. Geological Survey, accessed June 7, 2022, at https://www.usgs.gov/centers/land-subsidence-in-california/science/spirit-leveling.

U.S. Geological Survey [USGS], 2019, National Geologic Map Database—The U.S. Geologic Names Lexicon ("Geolex"), a National compilation of names and descriptions of geologic units, accessed October 17, 2019, at https://ngmdb.usgs.gov/Geolex/search.

U.S. Geological Survey [USGS], 2021a, National Elevation Dataset, accessed January 15, 2021, at https://ned.usgs.gov/index.html.

U.S. Geological Survey [USGS], 2021b, USGS water data for the Nation: U.S. Geological Survey National Water Information System database, accessed January 15, 2021, at http://doi.org/10.5066/F7P55KJN.

Veatch, A.C., 1906, Geology and underground water resources of northern Louisiana and southern Arkansas: U.S. Geological Survey Professional Paper 46, 422 p., accessed October 17, 2019, at https://doi.org/10.3133/pp46.

Wahl, K.L., and Wahl, T.L., 1995, Determining the flow of Comal Springs at New Braunfels, Texas, *in* Proceedings of Texas Water '95, A Component Conference of the First International Conference on Water Resources Engineering, San Antonio, Texas, August 16–17, 1995: American Society of Civil Engineers, p. 77–86.

Wang, G., 2022, The 95% confidence interval for GNSS-derived site velocities: Journal of Surveying Engineering, v. 148, no. 1, 17 p., accessed November 19, 2021, at http://doi.org/10.1061/(ASCE)SU.1943-5428.0000390.

Wang, G., Greuter, A., Petersen, C.M., Turco, M.J., 2022, Houston GNSS network for subsidence and faulting monitoring—Data analysis methods and products: Journal of Surveying Engineering, v. 148, no. 4, 26 p., accessed June 26, 2022, at https://hgsubsidence.org/wp-content/uploads/2022/07/2022_HoustonNet_Data_Processing.pdf.

Wang, G., Yu, J., Kearns, T.J., and Ortega, J., 2014, Assessing the accuracy of long-term subsidence derived from borehole extensometer data using GPS observations—Case study in Houston, Texas: Journal of Surveying Engineering, v. 140, no. 3, 7 p.

Wang, G., Yu, J., Ortega, J., Saenz, G., Burrough, T., and Neill, R., 2013, A stable reference frame for the study of ground deformation in the Houston metropolitan area, Texas: Journal of Geodetic Science, v. 3, no. 3, p. 188–202, accessed October 17, 2019, at http://doi.org/10.2478/jogs-2013-0021.

Wang, K., Wang, G., Cornelison, B., Liu, H., and Bao, Y., 2021, Land subsidence and aquifer compaction in Montgomery County, Texas, U.S.—2000–2020: Geoenvironmental Disasters, v. 8, article 28, 24 p., accessed December 12, 2021, at https://link.springer.com/article/10.1186/s40677-021-00199-7.

Welter, D.E., White, J.T., Hunt, R.J., and Doherty, J.E., 2015, Approaches in highly parameterized inversion—PEST++ Version 3, a Parameter ESTimation and uncertainty analysis software suite optimized for large environmental models: U.S. Geological Survey Techniques and Methods, book 7, chap. C12, 54 p., accessed October 17, 2019, at https://doi.org/10.3133/tm7C12.

Wentworth, C.K., 1922, A scale of grade and class terms for clastic sediments: The Journal of Geology, v. 30, no. 5, p. 377–392, accessed April 5, 2022, at https://doi.org/10.1086/622910.

Wesselman, J.B., 1967, Ground-water resources of Jasper and Newton Counties, Texas: Texas Water Development Board Report 59, Prepared by U.S. Geological Survey, 167 p., accessed October 17, 2019, at https://www.twdb.texas.gov/publications/reports/numbered_reports/doc/R59/R59.pdf.

Wesselman, J.B., 1972, Ground-water resources of Fort Bend County, Texas: Texas Water Development Board Report 155, Prepared by U.S. Geological Survey, 40 p., accessed October 17, 2019, at https://www.twdb.texas.gov/publications/reports/numbered_reports/doc/R155/report155.asp.

Wesselman, J.B., and Aronow, S., 1971, Ground-water resources of Chambers and Jefferson Counties, Texas: Texas Water Development Board Report 133, 144 p., accessed October 17, 2019, at https://www.twdb.texas.gov/publications/reports/numbered_reports/doc/R133/Report133.asp.

Westenbroek, S.M., Kelson, V.A., Dripps, W.R., Hunt, R.J., and Bradbury, K.R., 2010, SWB—A modified Thornthwaite-Mather Soil-Water-Balance code for estimating groundwater recharge: U.S. Geological Survey Techniques and Methods, book 6, chap. A31, 59 p., accessed October 17, 2019, at https://doi.org/10.3133/tm6A31.

White, J.T., 2018, A model-independent iterative ensemble smoother for efficient history-matching and uncertainty quantification in very high dimensions: Environmental Modelling & Software, v. 109, p. 191–201, accessed October 17, 2019, at https://doi.org/10.1016/j.envsoft.2018.06.009.

White, J.T., Doherty, J.E., and Hughes, J.D., 2014, Quantifying the predictive consequences of model error with linear subspace analysis: Water Resources Research, v. 50, no. 2, p. 1152–1173, accessed October 17, 2019, at https://doi.org/10.1002/2013WR014767.

White, J.T., Fienen, M.N., and Doherty, J.E., 2016a, A Python framework for environmental model uncertainty analysis: Environmental Modeling Software, v. 85, p. 217–228.

White, J.T., Fienen, M.N., and Doherty, J.E., 2016b, pyEMU—A Python framework for environmental model uncertainty analysis, version .01: U.S. Geological Survey software release, accessed October 17, 2019, at https://dx.doi.org/10.5066/F75D8Q01.

White, J.T., Foster, L.K., Fienen, M.N., Knowling, M.J., Hemmings, B., and Winterle, J.R., 2020b, Toward reproducible environmental modeling for decision support—A worked example: Frontiers of Earth Science, v. 8, 11 p., accessed November 17, 2020, at https://doi.org/10.3389/feart.2020.00050.

White, J.T., Hunt, R.J., Fienen, M.N., and Doherty, J.E., 2020a, Approaches to highly parameterized inversion—PEST++ Version 5, a software suite for parameter estimation, uncertainty analysis, management optimization and sensitivity analysis: U.S. Geological Survey Techniques and Methods, book 7, chap. C26, 52 p., accessed November 9, 2020, at https://doi.org/10.3133/tm7C26.

White, W.N., Livingston, P.P., and Turner, S.F., 1939, Groundwater resources of the Houston-Galveston area and adjacent region, Texas: Texas Board of Water Engineers Report 130, 300 p., accessed October 17, 2019, at https://www.twdb.texas.gov/publications/reports/historic_groundwater_reports/doc/M130.pdf.

White, W.N., Rose, N.A., and Guyton, W.F., 1944, Groundwater resources of the Houston district, Texas: U.S. Geological Survey Water-Supply Paper 889–C, accessed October 17, 2019, at https://doi.org/10.3133/wsp889C.

William F. Guyton and Associates, Inc., 1972, Ground-water conditions in the vicinity of The Woodlands, Montgomery County, Texas: Prepared for The Woodlands Development Corporation, Houston, Texas, 53 p.

Williams, J.F., III, and Ranzau, C.E., Jr., 1987, Ground-water withdrawals and changes in ground-water levels, groundwater quality, and land-surface subsidence in the Houston district, Texas, 1980–84: U.S. Geological Survey Water-Resources Investigations Report 87–4153, 56 p., accessed October 17, 2019, at https://doi.org/10.3133/wri874153.

Williams, S.D.P., Bock, Y., Fang, P., Jamason, P., Nikolaidis, R.M., Prawirodirdjo, L., Miller, M., and Johnson, D.J., 2004, Error analysis of continuous GPS position time series: Journal of Geophysical Research, v. 109, B03412, 19 p.

Williamson, A.K., Grubb, H.F., and Weiss, J.S., 1990, Groundwater flow in the Gulf Coast aquifer systems, south central United States—A preliminary analysis: U.S. Geological Survey Water-Resources Investigations Report 89–4071, 124 p., 4 pls., accessed October 17, 2019, at https://doi.org/10.3133/wri894071.

Wilson, C.A., 1967, Ground-water resources of Austin and Waller Counties, Texas: Texas Water Development Board Report 68, prepared by U.S. Geological Survey, 201 p., accessed October 17, 2019, at https://www.twdb.texas.gov/publications/reports/numbered_reports/doc/R68/report68.asp.

Winslow, A.G., and Doyel, W.W., 1954, Land-surface subsidence and its relation to the withdrawal of ground water in the Houston–Galveston region, Texas: Economic Geology, v. 49, no. 4, p. 413–422.

Winslow, A.G., and Fluellen, T.R., Jr., 1952, The Houston district, Texas, pumpage and decline of artesian pressure during 1950–51: Texas Board of Water Engineers Bulletin 5201, 28 p., accessed October 17, 2019, at https://www.twdb.texas.gov/publications/reports/bulletins/doc/B5201.pdf.

Winslow, A.G., and Wood, L.A., 1959, Relation of land subsidence to ground-water withdrawals in the upper Gulf Coast region, Texas: Mining Engineering, v. 11, p. 1030–1034.

Winter, T.C., Harvey, J.W., Franke, O.L., and Alley, W.M., 1998, Ground water and surface water—A single resource: U.S. Geological Survey Circular 1139, 79 p., accessed April 24, 2022, at https://doi.org/10.3133/cir1139.

Wood, L.A., 1956, Pumpage of ground water and changes in artesian pressure in the Houston district and Baytown-La Porte area, Texas, 1953–55: Texas Board of Water Engineers Bulletin 5602, 38 p., accessed October 17, 2019, at http://www.twdb.texas.gov/publications/reports/bulletins/doc/B5602.pdf.

Wood, L.A., 1958a, Pumpage of ground water and fluctuations of water levels in the Houston district and Baytown-La Porte area, Texas, 1955–57: Texas Board of Water Engineers Bulletin 5805, 57 p., accessed October 17, 2019, at https://www.twdb.texas.gov/publications/reports/bulletins/doc/B5805.pdf.

Wood, L.A., 1958b, Pumpage of ground water and changes in water levels in Galveston County, Tex., 1952–57: Texas Board of Water Engineers Bulletin 5808, 27 p., accessed October 17, 2019, at https://www.twdb.texas.gov/publications/reports/bulletins/doc/B5808.pdf.

Wood, L.A., and Gabrysch, R.K., 1965, Analog model study of ground water in the Houston district, Texas: Texas Water Commission Bulletin 6508, prepared by U.S. Geological Survey, 103 p., accessed October 18, 2019, at https://www.twdb.texas.gov/publications/reports/bulletins/doc/B6508/B6508.pdf.

Wood, L.A., Gabrysch, R.K., and Marvin, R., 1963, Reconnaissance investigation of the ground-water resources of the Gulf Coast region, Texas: Texas Water Commission Bulletin 6305, 114 p., prepared by U.S. Geological Survey, accessed October 17, 2019, at https://www.twdb.texas.gov/publications/reports/bulletins/doc/B6305/B6305.pdf.

Young, S.C., Budge, T., Knox, P.R., Kalbouss, R., Baker, E., Hamlin, S., Galloway, B., and Deeds, N., 2010, Hydrostratigraphy of the Gulf Coast aquifer from the Brazos River to the Rio Grande (Final Report): Texas Water Development Board, 203 p., accessed October 17, 2019, at https://www.twdb.texas.gov/publications/reports/contracted_reports/doc/0804830795_Gulf_coast_hydrostratigraphy_wcover.pdf.

Young, S.C., and Draper, C., 2020, The delineation of the Burkeville confining unit and the base of the Chicot aquifer to support the development of the GULF 2023 groundwater model: INTERA Incorporated, [variously paged; 72 p.], accessed November 10, 2020, at https://hgsubsidence.org/wp-content/uploads/2021/06/Final_HGSD_FBSD_Burkeville_Report_final.pdf.

Young, S.C., Ewing, T., Hamlin, S., Baker, E., and Lupton, D., 2012, Final report updating the hydrogeologic framework for the northern portion of the Gulf Coast aquifer system: Prepared for the Texas Water Development Board, [variously paged; 285 p.], accessed October 17, 2019, at https://www.twdb.texas.gov/publications/reports/contracted_reports/doc/1004831113_GulfCoast.pdf.

Young, S.C., Kelley, V., Deeds, N., Hudson, C., Piemonti, D., Ewing, T.E., Banerji, D., Seifert, J., and Lyman, P., 2017, Report on the delineation of fresh, brackish and saline groundwater resources based on interpretation of geophysical logs: Harris-Galveston Subsidence District Scientific Research Report 2018–001, prepared by INTERA, Inc., LBG-Guyton Associates, and the University of Texas Bureau of Economic Geology, [variously paged; 216 p.], accessed June 3, 2022, at https://hgsubsidence.org/wp-content/uploads/2021/11/HGSD-Scientific-Report-2018-001_Report-on-the-Delineation-of-Fresh-Brackish-and-Saline-Groundwater-Resources-Based-on-Interpretation-of-Geophysical-Logs.pdf.

Young, S.C., Pinkard, J., Bassett, R.L., and Chowdhury, A.H., 2014, Hydrogeochemical evaluation of the Texas Gulf Coast aquifer system and implications for developing groundwater availability models: Prepared for the Texas Water Development Board, [variously paged; 375 p.], accessed October 17, 2019, at https://www.twdb.texas.gov/publications/reports/contracted_reports/doc/1148301233.pdf.

Yu, J., Wang, G., Kearns, T.J., and Yang, L., 2014, Is there deep-seated subsidence in the Houston-Galveston area?: International Journal of Geophysics, v. 2014, 11 p., accessed October 17, 2019, at https://doi.org/10.1155/2014/942834.

Zerbini, S., Richter, B., Negusini, M., Romagnoli, C., Simon, D., Domenichini, F., and Schwahn, W., 2001, Height and gravity variations by continuous GPS, gravity and environmental parameter observations in the southern Po Plain, near Bologna, Italy: Earth and Planetary Science Letters, v. 192, no. 3, p. 267–279, accessed May 4, 2022, at https://doi.org/10.1016/S0012-821X(01)00445-9.

Zilkoski, D., Hall, L., Mitchell, G., Kammula, V., Singh, A., Chrismer, W., and Neighbors, R., 2003, The Harris-Galveston Coastal Subsidence District/National Geodetic Survey Automated GPS Subsidence Monitoring Project, *in* Prince, K.R., and Galloway, D.L., eds., U.S. Geological Survey Subsidence Interest Group Conference, Proceedings of the Technical Meeting, Galveston, Texas, November 27–29, 2001: U.S. Geological Survey Open-File Report 03–308, p. 13–28, accessed October 17, 2019, at https://doi.org/10.3133/ofr03308.

Appendixes

Appendix 1. Model Grid Construction

The hydrogeologic framework for the Gulf Coast aquifer system was developed by using datasets compiled in Teeple and others (2021). The resulting dataset was used to define the extents and thicknesses of the Chicot aquifer, Evangeline aquifer, Burkeville confining unit, Jasper aquifer, and Catahoula confining unit. The following sections describe the compilation of the hydrogeologic data and the gridding of the hydrogeologic unit contacts.

Data Compilation

Hydrogeologic data and interpretative information pertaining to the Gulf Coast aquifer system hydrogeologic units were compiled from previous studies done by various local, State, and Federal agencies and primarily include the reports listed in the "Geologic and Hydrogeologic Units" section. Published hydrogeologic unit contact information from more than 13,300 wells was compiled for the study area to assess spatial variations of the Chicot aquifer, Evangeline aquifer, Burkeville confining unit, Jasper aquifer, and Catahoula confining unit and any correlative units (Teeple and others, 2021). Where possible, data available only in hard copy were digitized and combined with existing digital data before being entered into the database (Teeple and others, 2021). Hydrogeologic and lithologic descriptions (Deussen, 1914; Sellards and others, 1932; Darton and others, 1937; Baker, 1979; Carr and others, 1985) were used to help characterize correlative hydrogeologic units to those used for the study (fig. 10).

Data were referenced by elevation and spatial location for correlation among neighboring wells to create a regional network of correlated points. The various horizontal datums were reprojected into the Albers Equal-Area Conic projection with the World Geodetic System of 1984 (WGS 84) datum in meters. The various vertical datums were converted into depths below land surface in meters by using the source's original vertical datum. Because vertical datums are required to convert the data from an elevation to a depth below land surface, if the source's original vertical datum was not available, the datum was assumed to be land surface above the National Geodetic Vertical Datum of 1929. Land-surface elevations were determined from a digital elevation model (USGS, 2021a) for all well locations by using the horizontal coordinates to provide consistency and improve accuracy with values being referenced above the North American Vertical Datum of 1988 (NAVD 88). Depths to hydrogeologic unit contacts were converted to elevations by subtracting the depths from the well's land-surface elevation.

Control points were added to the dataset to constrain the hydrogeologic units to land surface (surficial control points) where the surficial extent of the hydrogeologic unit had been previously mapped or where data gaps (interpolated control points) were found within the dataset. Using the surficial geologic extents defined by Casarez (2020), surficial control points were placed approximately every 10 kilometers along the surficial extent of each hydrogeologic unit, and the land-surface value was noted for hydrogeologic units located at the contact point. A predetermined grid was developed with an interpolated control point located every 25 kilometers throughout the study area. During the gridding process, gaps within the hydrogeologic dataset were identified and filled in with the evenly spaced interpolated control points. The elevation value used at these interpolated control points was an interpolated value based on elevations from nearby wells. The surficial geologic extents were also used to identify and remove any picks that were located outside of the updip extent of each hydrogeologic unit. Picks that occurred outside of the updip extent of the hydrogeologic unit were most likely a result of poor locational information.

Gridding Hydrogeologic Unit Contacts

The tops and bases of the hydrogeologic units from all the data released in Teeple and others (2021) were used to create hydrogeologic unit surface grids. Hydrogeologic unit surface grids were created by using Oasis montaj (Seequent, 2021) and kriging interpolation techniques. Kriging is a geostatistical interpolation method that determines the most probable value at each grid node (1,000 meters by 1,000 meters for this study) based on a statistical analysis of the entire dataset (Isaaks and Srivastava 1989). The grid cell size was set to match the cell size of the numerical model. A variogram model was created to optimize the kriging results. A variogram is a statistical analysis chart showing variance against distance between each paired point within the selected dataset (Isaaks and Srivastava, 1989). Based on the observed data, a model (variogram model) is fit to best represent the data. This model is then used in the gridding process to estimate the cell values in the grid and to calculate the variance for that cell. Anisotropy, or spatial patterns of the data, could occur within a dataset. Any patterns within the selected dataset were identified and incorporated into the kriging process. Variance maps developed during the kriging process were used to evaluate the uncertainty in hydrogeologic unit surface grids in the planning of additional data-collection tasks. Generally, as the distance between data points became greater, correlation between points lessened, and uncertainty in areas between points increased (Isaaks and Srivastava, 1989). Additional information on kriging is available in Isaaks and Srivastava (1989).

Preliminary grids were used to identify outliers and areas requiring review. To aid in identifying outliers, the residual was calculated as the difference between the hydrogeologic unit contact elevation at each well and the interpolated grid value (Bumgarner and others, 2012). Residuals were evaluated

after each iteration of the gridding process. Residuals greater than 10 percent of the maximum absolute residual (rounded up to the nearest whole number) were evaluated through a correlation process to determine data-point uncertainty. The correlation process involved the comparison of the hydrogeologic unit contact elevation at a given site to the hydrogeologic unit contact elevation at nearby sites to determine if it "correlated." If the hydrogeologic unit contact elevation was verified to be different from that of the nearby sites, it was removed from the final grid. The correlation process was finished when the maximum absolute residual was the same value between successive iterations and all hydrogeologic unit contact elevations were verified to correlate with each other within the dataset.

Appendix 2. Groundwater Use

Temporal estimated groundwater use by historical geographic area described in the "Groundwater Development" section is included in table 1 and figure 2.1. The sources of data for this estimated groundwater use include the following references that are sorted by groundwater-use period.

Predevelopment to early development period: White and others (1939), Rose (1943), Rose and Alexander (1944), White and others (1944), Rose (1949), Lang and Sundstrom (1946), Lang and others (1950), Goines and others (1951), Petitt and Winslow (1955), American Oil Company (1958), Wood and Gabrysch (1965), Gabrysch (1967), Anders and others, (1968), Wesselman and Aronow (1971), Popkin (1971), Sandeen and Wesselman (1973), Gabrysch and Bonnet (1974), Gabrysch and Bonnet (1976a), and Gabrysch and Coplin (1990).

Transition to developed conditions: Lang and others (1950), Goines and others (1951), Winslow and Fluellen (1952), Doyel and others (1954), Wood (1956), Wood (1958a, b), Anders and Naftel (1962), Wood and Gabrysch (1965), Gabrysch (1967), Gabrysch (1972), Gabrysch and Bonnet (1976a), Gabrysch (1980a), and Gabrysch (1984).

Regulation and post-developed conditions: Gabrysch (1982a), Gabrysch (1984), Williams and Ranzau (1987), Gabrysch and Coplin (1990), and Barbie and Locke (1993).

The estimated total county groundwater use is based on groundwater-use data from Oliver and Harmon (2022) that were used during the history matching of the GULF model. Note that the GULF model contains the full extent of several counties but only parts of some counties; therefore, the groundwater-use estimates from figure 2.1 include only counties where mean annual groundwater use during the study period is greater than 1 Mgal/d. In these counties, the groundwater use is only representative of the areas simulated in the model.

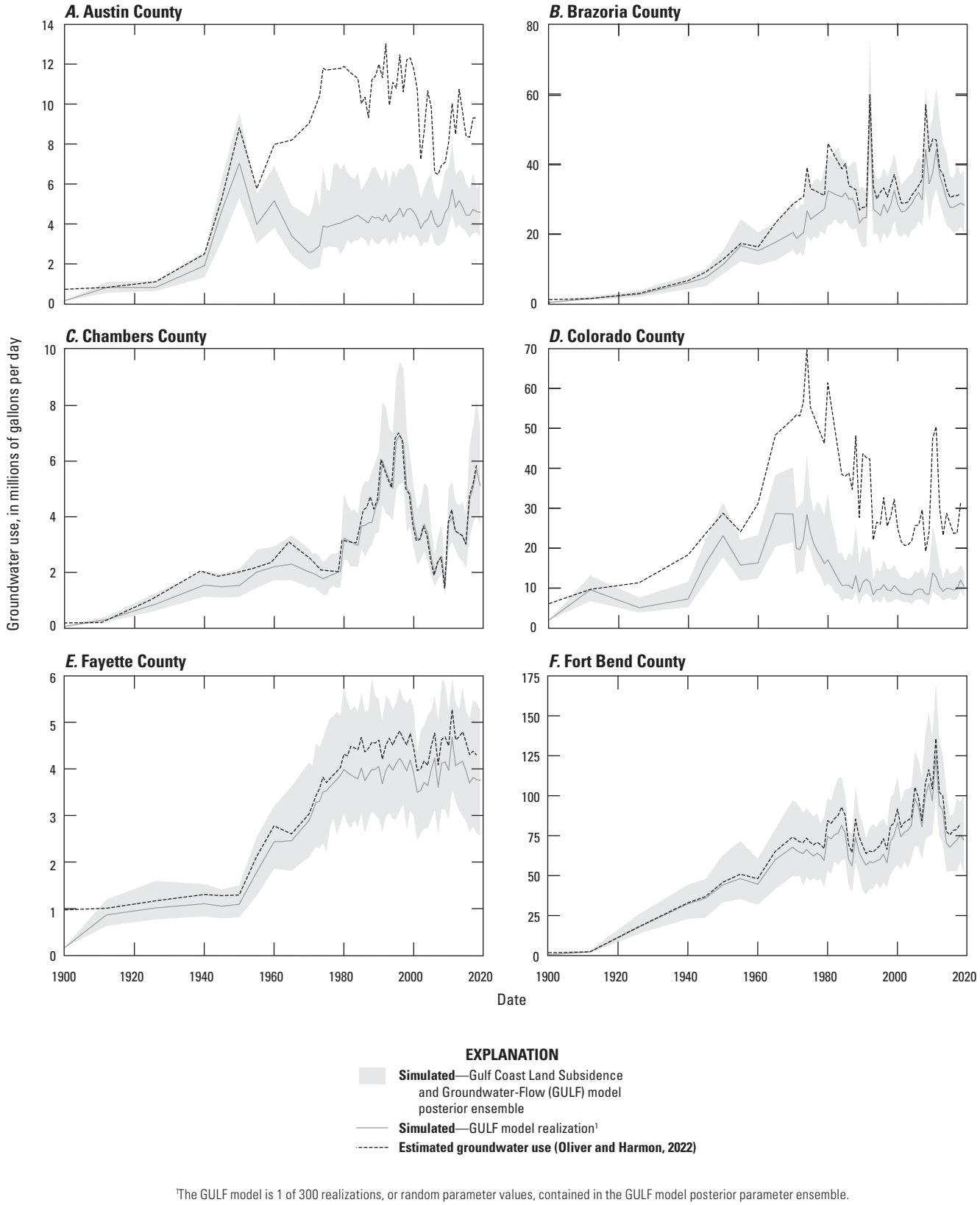

[1]The GULF model is 1 of 300 realizations, or random parameter values, contained in the GULF model posterior parameter ensemble.

Figure 2.1. Temporal distribution of groundwater use by county for the Gulf Coast aquifer system study area in southeast Texas, 1900–2020.

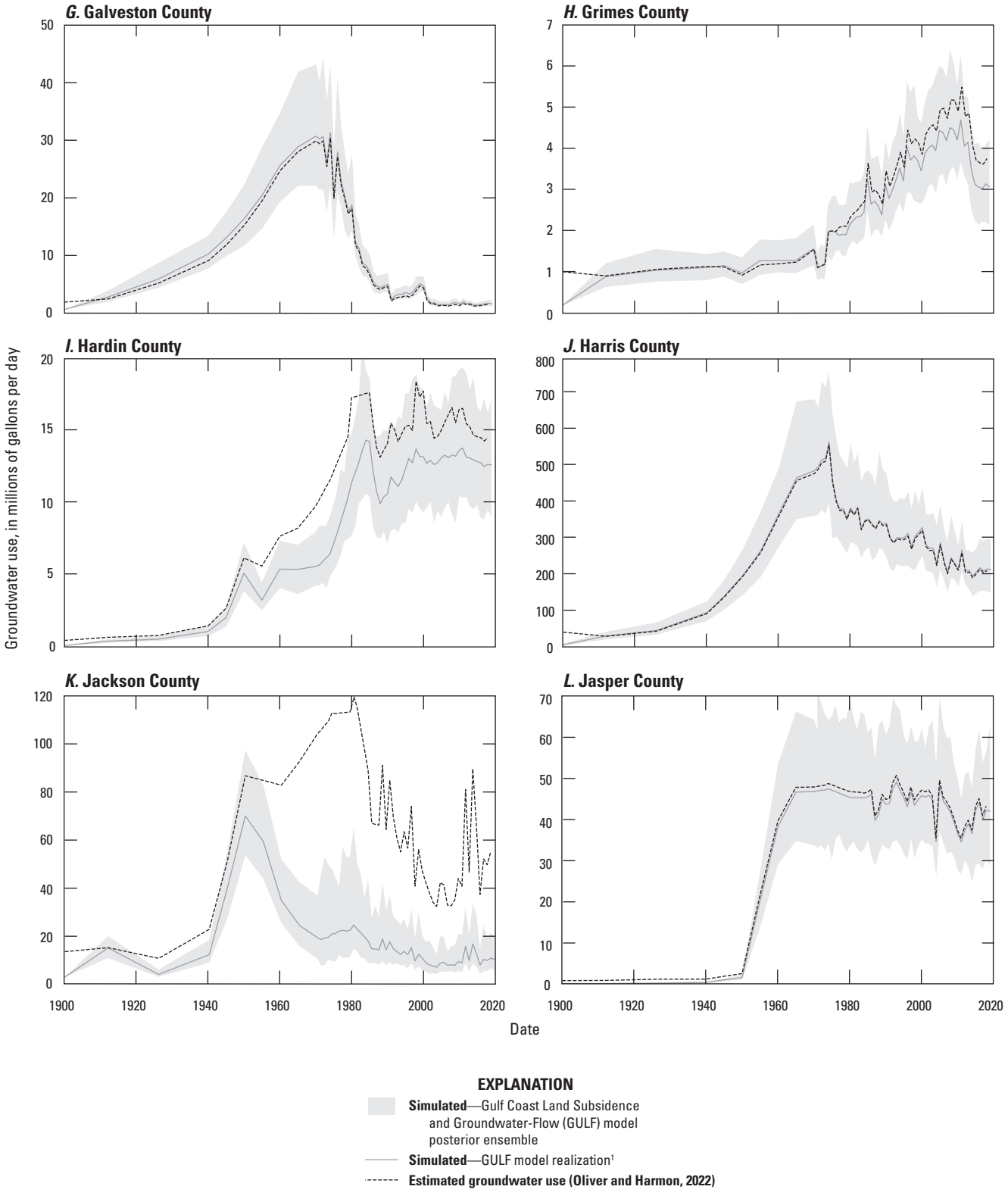

[1]The GULF model is 1 of 300 realizations, or random parameter values, contained in the GULF model posterior parameter ensemble.

Figure 2.1.—Continued

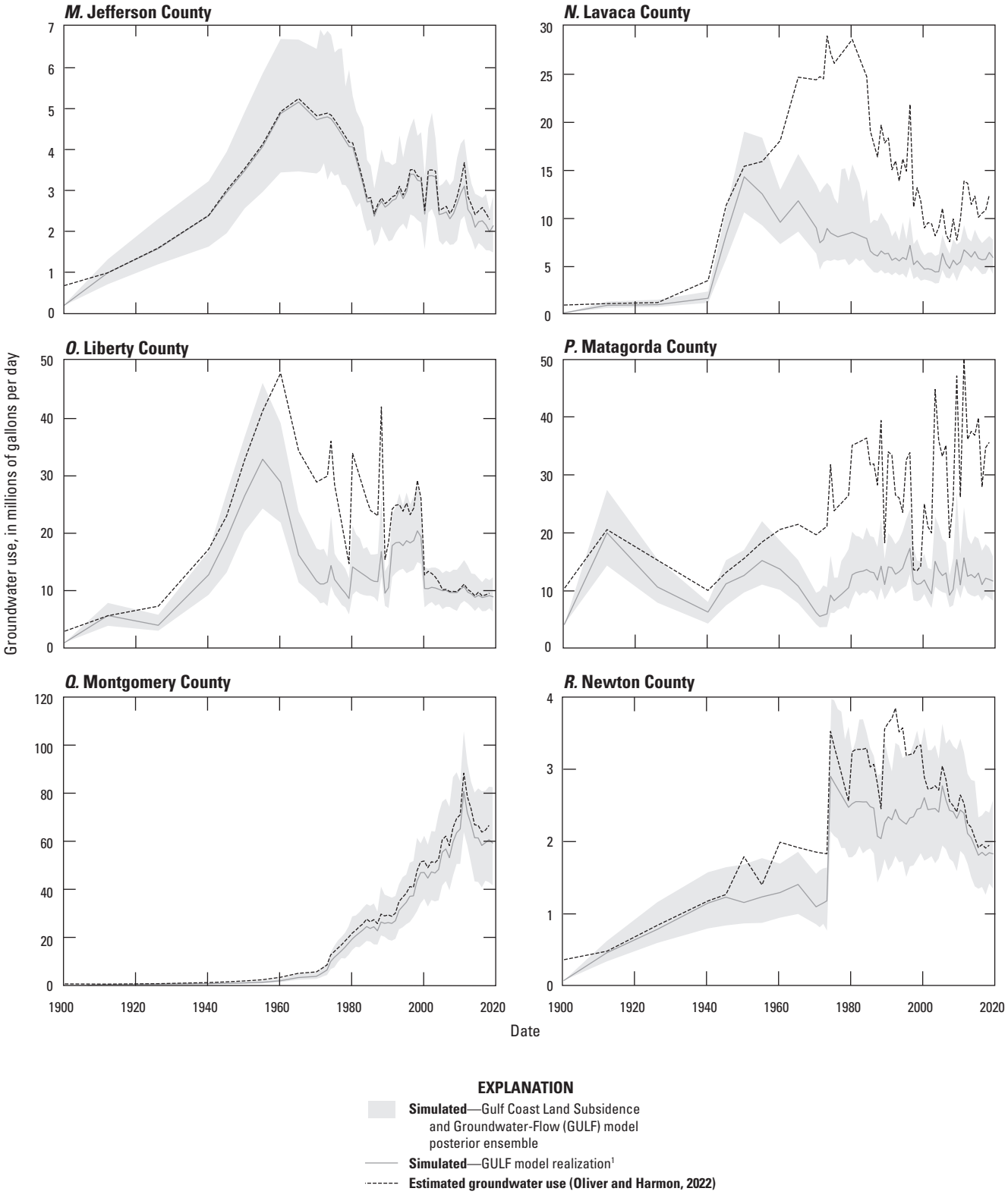

[1]The GULF model is 1 of 300 realizations, or random parameter values, contained in the GULF model posterior parameter ensemble.

Figure 2.1.—Continued

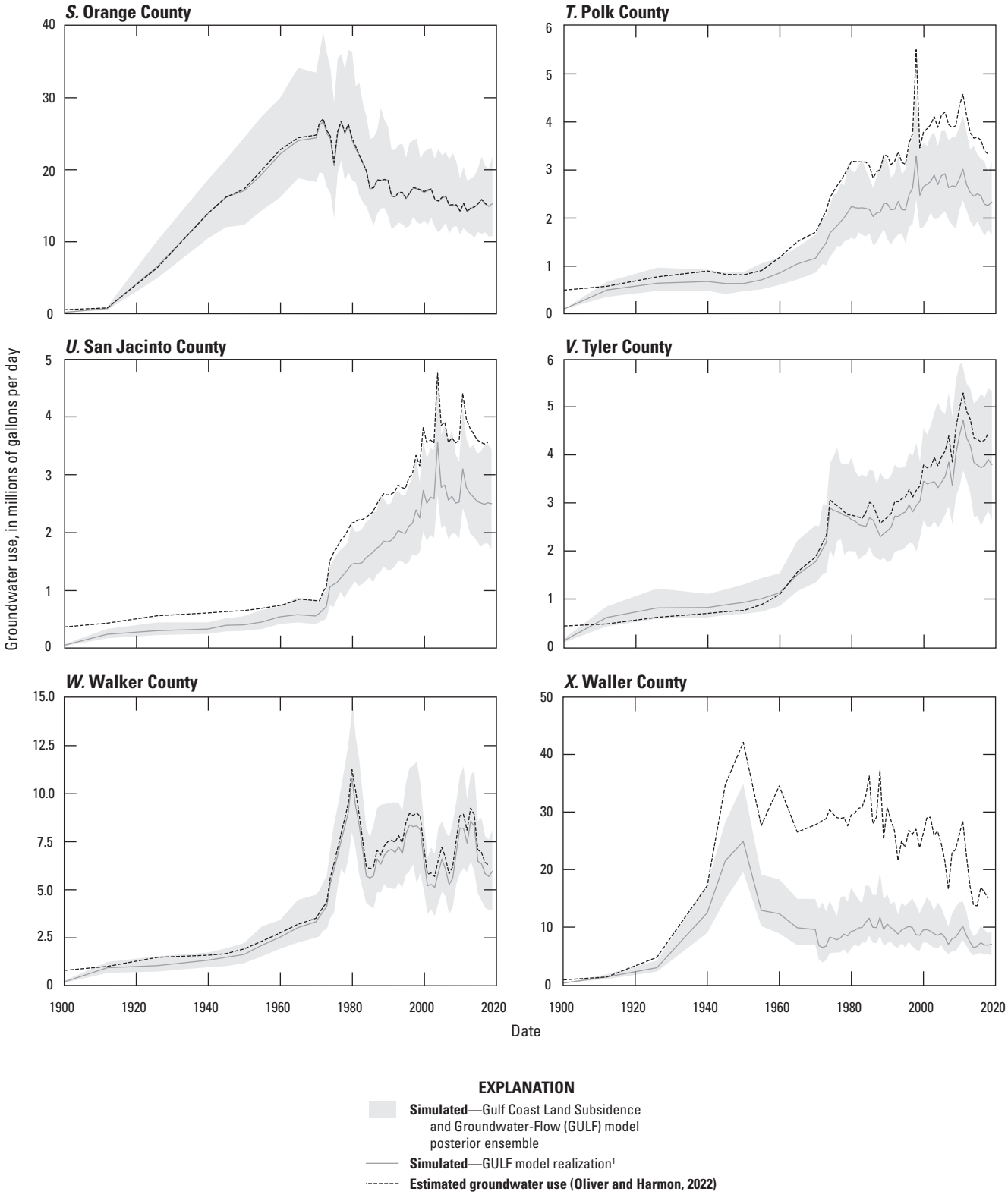

[1]The GULF model is 1 of 300 realizations, or random parameter values, contained in the GULF model posterior parameter ensemble.

Figure 2.1.—Continued

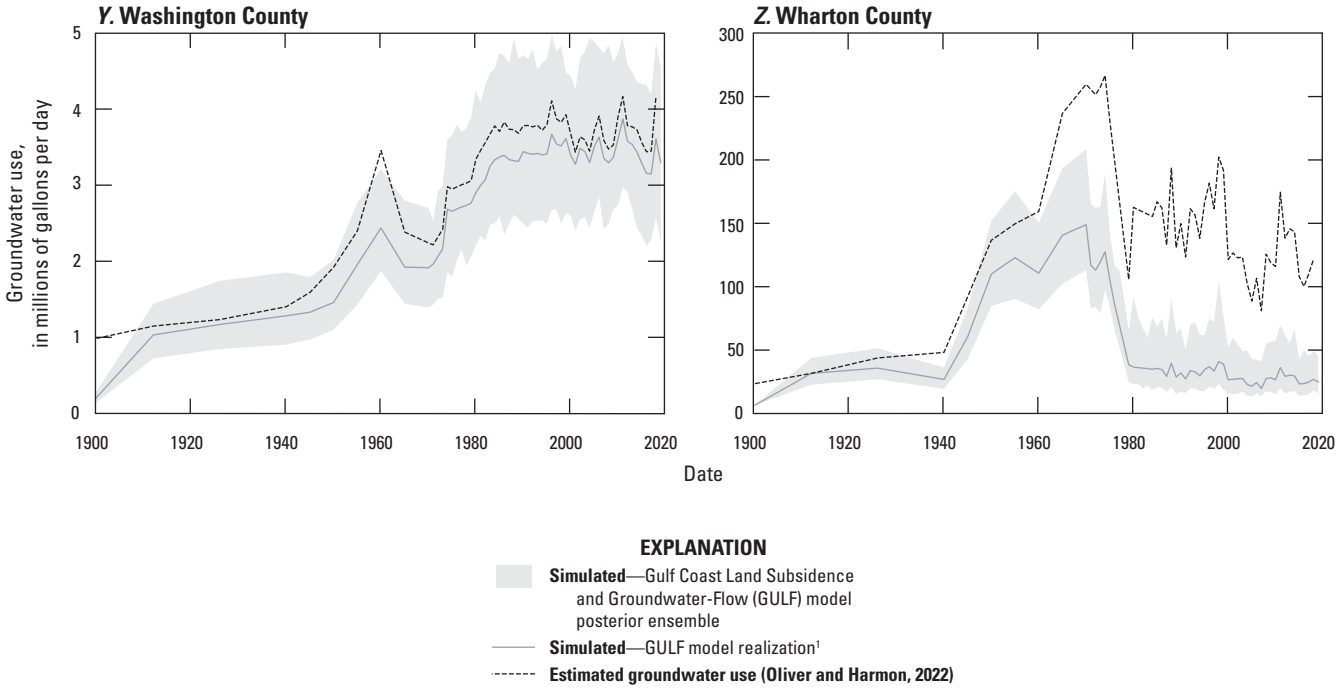

[1]The GULF model is 1 of 300 realizations, or random parameter values, contained in the GULF model posterior parameter ensemble.

Figure 2.1.—Continued

Appendix 3. Predevelopment to Early Development Groundwater-Level Measurements

From the early 1900s until about 1930, periodic measurements of groundwater levels were documented in the Houston-Galveston region. More substantial groundwater-level datasets generally were available beginning about 1931 when the first USGS groundwater measurement surveys began in cooperation with the Texas State Board of Water Engineers (predecessor to the Texas Water Commission) (White and others, 1939). These measurement surveys were undertaken to investigate the rapid development of groundwater resources between 1930 and 1940. Selected groundwater levels from these surveys at are listed in table 3.1.

Table 3.1. Wells in selected counties with groundwater-level data generally during the predevelopment to early development period (1897–1945) in the greater Houston area, Texas.

[USGS well ID is the well identifier used by the U.S. Geological Survey (USGS; 2021b); TWDB well ID is the well identifier used by the Texas Water Development Board (TWDB; 2020b); M/D/Y, month/day/year; A groundwater level above land surface is indicated by a negative number; -- not available]

USGS well ID	TWDB well ID	Historical identifier (TWDB or USGS)[1]	Other identifier	Map identifier (figs. 13–16)	County and figure, where applicable	Historical geographic area (fig. 18*B*)	Land-surface elevation (feet)	Period of record (may contain gaps) or single measurement date (M/D/Y)		Groundwater level below land surface (date of first measurement)[1]	Well or hole depth, in feet below land surface
								Begin	End		
Wells with groundwater-level data generally prior to 1940											
285555095333301	8104502			--	Brazoria	--	6.4	1/1/1920	1/1/1920	22.0	550
292545095294101	6537403			--	Brazoria	--	61.0	4/10/1931	4/10/1931	8.0	220
292556095290201	6537404			--	Brazoria	--	60.2	4/10/1931	4/10/1931	18.0	300
292344095284701	6537704	77		--	Brazoria	--	59.9	4/13/1931	4/13/1931	15.0	300
291252095281901	6553103	101		--	Brazoria	--	35.6	4/14/1931	4/14/1931	1.0	635
285808095322401	8104309			--	Brazoria	--	12.1	10/30/1936	10/30/1936	0.0	478
291117095371601	6552406			--	Brazoria	--	34.0	11/6/1936	11/6/1936	18.7	135
285909095342501	8104205			--	Brazoria	--	12.2	6/1/1937	6/1/1937	9.0	98
292358095323801	6536801			--	Brazoria	--	51.3	1/1/1939	1/1/1939	12.0	655
291346095205101	6554103			--	Brazoria	--	23.9	5/18/1939	5/18/1939	22.2	600
294743094535801	6409610			--	Chambers	--	24.2	1895	4/2/1941	−30.0	305
294314094525001	6417306			--	Chambers	--	28.4	1/1/1917	4/8/1941	20.0	110
295031094482201	6410206			--	Chambers	--	22.1	1/1/1926	1/1/1940	10.0	370
294149094545301	6417604			--	Chambers	--	8.0	1/1/1926	3/1/1948	25.0	550
293944094534201	6417906			--	Chambers	--	24.8	1/1/1926	4/1/1941	20.0	600
294323094545501	6417308			--	Chambers	--	26.2	11/1/1926	11/1/1926	24.0	97
294416094501001	6418105			--	Chambers	--	22.0	1/1/1928	4/5/1956	21.0	240
294452094554401	6417212			--	Chambers	--	13.5	1/1/1929	4/5/1941	25.0	346
294549094355201	6412706			--	Chambers	--	19.6	1/1/1931	1/1/1931	13.0	340
294420094552401	6417209			--	Chambers	--	11.4	1/1/1931	4/15/1954	20.0	410
294033094521301	6418407			--	Chambers	--	20.2	1/1/1931	3/20/1941	30.0	755
294839094494601	6410503			--	Chambers	--	26.6	1/1/1933	3/5/1941	21.0	120
294754094510201	6410408			--	Chambers	--	29.6	1/1/1933	3/5/1941	18.0	143
294801094514001	6410410			--	Chambers	--	32.3	1/1/1933	4/9/1941	20.0	175
294637094540101	6409911			--	Chambers	--	20.8	1/1/1934	1/1/1934	25.0	292

Table 3.1. Wells in selected counties with groundwater-level data generally during the predevelopment to early development period (1897–1945) in the greater Houston area, Texas.—Continued

[USGS well ID is the well identifier used by the U.S. Geological Survey (USGS; 2021b); TWDB well ID is the well identifier used by the Texas Water Development Board (TWDB; 2020b); M/D/Y, month/day/year; A groundwater level above land surface is indicated by a negative number; -- not available]

USGS well ID	TWDB well ID	Historical identifier (TWDB or USGS)[1]	Other identifier	Map identifier (figs. 13–16)	County and figure, where applicable	Historical geographic area (fig. 18*B*)	Land-surface elevation (feet)	Period of record (may contain gaps) or single measurement date (M/D/Y)		Groundwater level below land surface (date of first measurement)[1]	Well or hole depth, in feet below land surface
								Begin	End		
294816094392401	6411602			--	Chambers	--	20.3	1/1/1935	1/1/1935	22.0	115
294936094481801	6410511			--	Chambers	--	32.2	1/1/1935	4/18/1941	17.0	501
295051094375501	6411305			--	Chambers	--	29.9	1/1/1936	7/1/1941	14.0	94
294800094510201	6410409			--	Chambers	--	30.3	1/1/1936	1/1/1936	30.0	183
294330094510601	6418111			--	Chambers	--	25.9	1/1/1936	1/1/1936	25.0	196
294820094502401	6410405			--	Chambers	--	24.3	1/1/1936	3/5/1941	8.0	488
293934094535601	6417904			--	Chambers	--	23.1	1/1/1936	1/1/1936	30.0	630
294938094480701	6410513			--	Chambers	--	23.7	1/1/1937	4/8/1941	33.0	125
293152094460801	6426902			--	Chambers	--	5.0	1/1/1937	1/1/1937	4.0	127
294820094503301	6410407			--	Chambers	--	24.0	1/1/1937	1/1/1937	20.0	150
294413094524001	6417312			--	Chambers	--	24.6	1/1/1937	1/1/1937	22.0	180
294618094513401	6410704			--	Chambers	--	34.9	1/1/1937	1/1/1937	40.0	556
294457094510201	6418108			--	Chambers	--	33.2	1/1/1938	1/1/1938	18.0	140
295144094373701	6411302			--	Chambers	--	30.0	1/1/1938	6/6/1941	8.0	185
295125094533701	6409321			--	Chambers	--	53.3	1/1/1938	1/1/1938	73.0	304
294106094515901	6418405			--	Chambers	--	16.1	5/12/1938	5/12/1938	22.5	438
294548094510501	6410703			--	Chambers	--	29.1	10/1/1938	3/28/1974	38.0	443
295214094344101	6412204			--	Chambers	--	35.0	1/1/1939	1/1/1939	10.0	34
294557094341701	6412801			--	Chambers	--	21.8	1/1/1939	1/1/1939	10.0	40
294418094551901	6417206			--	Chambers	--	13.4	1/1/1939	1/1/1939	17.0	90
294825094500601	6410403			--	Chambers	--	25.7	1/1/1939	10/13/1955	18.0	125
294339094504801	6418110			--	Chambers	--	25.9	1/1/1939	1/1/1939	20.0	192
293741094404101	6419806			--	Chambers	--	4.6	1/1/1939	1/1/1939	−0.5	216
294600094380401	6411908			--	Chambers	--	16.6	1/1/1939	1/1/1939	6.0	345
293949094543701	6417910			--	Chambers	--	20.1	1/1/1939	10/13/1955	55.0	550
294435094502201	6418107			--	Chambers	--	25.5	1/1/1939	1/1/1939	0.0	634
294004094553501	6417504			--	Chambers	--	5.9	7/1/1939	7/1/1939	18.0	93

Table 3.1. Wells in selected counties with groundwater-level data generally during the predevelopment to early development period (1897–1945) in the greater Houston area, Texas.—Continued

[USGS well ID is the well identifier used by the U.S. Geological Survey (USGS; 2021b); TWDB well ID is the well identifier used by the Texas Water Development Board (TWDB; 2020b); M/D/Y, month/day/year; A groundwater level above land surface is indicated by a negative number; -- not available]

USGS well ID	TWDB well ID	Historical identifier (TWDB or USGS)[1]	Other identifier	Map identifier (figs. 13–16)	County and figure, where applicable	Historical geographic area (fig. 18*B*)	Land-surface elevation (feet)	Period of record (may contain gaps) or single measurement date (M/D/Y)		Groundwater level below land surface (date of first measurement)[1]	Well or hole depth, in feet below land surface
								Begin	End		
294041094552501	6417501			--	Chambers	--	19.2	7/1/1939	7/1/1939	52.0	429
294558094501601	6410707			--	Chambers	--	25.5	10/1/1939	3/28/1941	38.0	429
294552095502601	6510703			B	Fort Bend (fig. 15)	Katy area	138.4	8/11/1932	1/22/1985	55.8	170
294444095510001	6518105			C	Fort Bend (fig. 15)	Katy area	140.7	3/24/1931	3/15/1954	51.8	172
294400095505301	6518103			D	Fort Bend (fig. 15)	Katy area	139.4	3/24/1931	1/5/2005	53.2	628
294156095483101	6518501			E	Fort Bend (fig. 15)	Katy area	121.3	3/24/1931	3/9/1956	39.4	250
294259095495801	6518204			--	Fort Bend	Katy area	132.1	5/1/1926	3/11/1952	63.6	586
294308095483401	6518203	19		--	Fort Bend	Katy area	122.2	3/24/1931	4/14/1947	34.5	545
294220095504201	6518401	18		--	Fort Bend	Katy area	134.5	3/24/1931	3/24/1931	49.2	723
294418095522201	6518106	16		--	Fort Bend	Katy area	146.4	8/25/1931	4/14/1947	62.8	337
294225095411801	6519507			--	Fort Bend	Katy area	93.9	1/1/1932	1/1/1932	8.0	260
294223095475701	6518503			--	Fort Bend	Katy area	117.6	3/18/1933	3/18/1933	39.0	250
294438095551001	6517205			--	Fort Bend	Katy area	158.8	4/1/1936	12/2/1957	92.7	334
294514095515501	6510702			--	Fort Bend	Katy area	146.7	3/15/1939	2/3/2000	57.8	346
294326095533701	6517304	6		--	Fort Bend	Katy area	147.4	3/15/1939	12/17/1968	63.1	596
292901095371601	6536103	422		--	Fort Bend	--	70.1	4/4/1936	4/4/1936	49.0	209
293335095484001	6526517	242		--	Fort Bend	--	104.9	7/15/1905	7/15/1905	28.0	298
293337095482702	6526510	51		--	Fort Bend	--	103.9	7/24/1913	7/24/1913	32.0	351
293717095380101	[2]6527312	54		--	Fort Bend	--	74.8	1/1/1920	1/1/1920	1.8	1,606
293242095560801	6525502	119		--	Fort Bend	--	113.6	1/1/1923	1/1/1923	22.0	85
292145095523701	6541301	340		--	Fort Bend	--	80.0	1/1/1924	1/1/1924	20.0	90
293016095290001	6529703	90		--	Fort Bend	--	66.9	12/1/1925	12/1/1925	18.0	271
293149095455201	6526902	277		--	Fort Bend	--	92.2	1/1/1928	1/1/1928	20.0	106

Table 3.1. Wells in selected counties with groundwater-level data generally during the predevelopment to early development period (1897–1945) in the greater Houston area, Texas.—Continued

[USGS well ID is the well identifier used by the U.S. Geological Survey (USGS; 2021b); TWDB well ID is the well identifier used by the Texas Water Development Board (TWDB; 2020b); M/D/Y, month/day/year; A groundwater level above land surface is indicated by a negative number; -- not available]

USGS well ID	TWDB well ID	Historical identifier (TWDB or USGS)[1]	Other identifier	Map identifier (figs. 13–16)	County and figure, where applicable	Historical geographic area (fig. 18*B*)	Land-surface elevation (feet)	Period of record (may contain gaps) or single measurement date (M/D/Y)		Groundwater level below land surface (date of first measurement)[1]	Well or hole depth, in feet below land surface
								Begin	End		
293025095473501	6526802	281		--	Fort Bend	--	88.6	1/1/1930	4/23/1930	20.0	80
293030095482901	6526803	283		--	Fort Bend	--	91.7	1/1/1930	4/23/1930	30.0	85
293654095395801	6527314			--	Fort Bend	--	79.8	10/23/1930	10/23/1930	19.0	257
293437095374301	6527605			--	Fort Bend	--	70.0	6/27/1931	6/27/1931	16.0	160
293420095375001	6527606			--	Fort Bend	--	69.9	7/9/1931	7/9/1931	14.3	353
294217095584201	6517406	1		--	Fort Bend	--	115.5	9/11/1931	10/1/1940	27.4	205
292831095591201	6533106	155		--	Fort Bend	--	103.9	1/1/1933	1/1/1933	27.0	85
292752095512901	6534102	302		--	Fort Bend	--	95.3	1/1/1933	1/1/1933	16.0	116
293331095481802	6526516	244		--	Fort Bend	--	103.0	11/28/1934	11/28/1934	41.0	515
293218095265501	6529801			--	Fort Bend	--	71.7	1/1/1935	1/1/1938	35.0	450
293458095454302	6526604			--	Fort Bend	--	90.8	7/3/1935	7/3/1935	28.2	331
293005095542101	6525906	138		--	Fort Bend	--	110.6	4/8/1936	4/8/1936	20.0	22
292245095484501	6534802	345		--	Fort Bend	--	84.5	1/1/1936	1/1/1936	20.0	24
292538095465501	6534608	324		--	Fort Bend	--	80.3	1/1/1936	1/1/1936	14.0	26
292726095464302	6534605	321		--	Fort Bend	--	75.6	1/1/1936	1/1/1936	11.0	30
293106095590301	6525706	113		--	Fort Bend	--	113.2	1/1/1936	1/1/1936	15.0	32
292455095485801	6534811	331		--	Fort Bend	--	85.8	1/1/1936	1/1/1936	26.0	38
292350095445201	6535706	349		--	Fort Bend	--	67.9	1/1/1936	1/1/1936	18.0	40
292101095531301	6541302	178		--	Fort Bend	--	75.2	1/1/1936	1/1/1936	22.0	48
293422095464501	6526607	252		--	Fort Bend	--	99.2	4/13/1936	4/13/1936	48.8	50
292656095594501	6533402	166		--	Fort Bend	--	96.8	1/1/1936	1/1/1936	20.0	60
292551095464301	6534607	323		--	Fort Bend	--	80.0	1/1/1936	1/1/1936	14.0	67
293147095514901	6526706	229		--	Fort Bend	--	108.8	1/1/1936	4/8/1936	26.0	76
293142095580701	6525708	114		--	Fort Bend	--	112.1	1/1/1936	1/1/1936	35.0	82
293223095465001	6526901	276		--	Fort Bend	--	95.4	4/23/1936	4/23/1936	21.0	82
293348095471001	6526608	249		--	Fort Bend	--	100.0	1/1/1936	1/1/1936	40.0	82

Table 3.1. Wells in selected counties with groundwater-level data generally during the predevelopment to early development period (1897–1945) in the greater Houston area, Texas.—Continued

[USGS well ID is the well identifier used by the U.S. Geological Survey (USGS; 2021b); TWDB well ID is the well identifier used by the Texas Water Development Board (TWDB; 2020b); M/D/Y, month/day/year; A groundwater level above land surface is indicated by a negative number; -- not available]

USGS well ID	TWDB well ID	Historical identifier (TWDB or USGS)[1]	Other identifier	Map identifier (figs. 13–16)	County and figure, where applicable	Historical geographic area (fig. 18*B*)	Land-surface elevation (feet)	Period of record (may contain gaps) or single measurement date (M/D/Y)		Groundwater level below land surface (date of first measurement)[1]	Well or hole depth, in feet below land surface
								Begin	End		
293127095523801	6525902	225		--	Fort Bend	--	109.9	1/1/1936	1/1/1936	24.0	84
292745095413401	6535202	429		--	Fort Bend	--	73.4	5/1/1936	5/1/1936	15.0	85
292900095561001	6533204	145		--	Fort Bend	--	103.2	1/1/1936	1/1/1936	40.0	86
293453095461001	6526606	256		--	Fort Bend	--	100.4	1/1/1936	1/1/1936	30.0	86
292648096000101	6640602	165		--	Fort Bend	--	99.4	1/1/1936	1/1/1936	30.0	90
293117095502701	6526704	291		--	Fort Bend	--	98.4	5/11/1936	5/11/1936	40.0	90
293027095535901	6525905	136		--	Fort Bend	--	107.8	1/1/1936	1/1/1936	35.0	96
293319095484901	6526508	240		--	Fort Bend	--	102.9	1/1/1936	1/1/1936	23.0	97
292033095465701	6542305	356		--	Fort Bend	--	73.9	1/1/1936	1/1/1936	20.0	100
292552095464401	6534606	322		--	Fort Bend	--	80.0	1/1/1936	1/1/1936	14.0	100
292802095551501	6533205	173		--	Fort Bend	--	99.8	1/1/1936	1/1/1936	40.0	100
292906095570401	6533202	149		--	Fort Bend	--	105.2	1/1/1936	1/1/1936	40.0	100
292351095500301	6534704	334		--	Fort Bend	--	91.0	1/1/1936	1/1/1936	20.0	103
293227095591701	6525707	110		--	Fort Bend	--	116.6	1/1/1936	1/1/1936	25.0	105
293047095534001	6525904	134		--	Fort Bend	--	108.2	1/1/1936	1/1/1936	30.0	110
293255095540401	6525603	127		--	Fort Bend	--	110.0	1/1/1936	1/1/1936	38.0	112
292935095502401	6534104	305		--	Fort Bend	--	89.4	1/1/1936	1/1/1936	30.0	125
293151095490501	6526804	287		--	Fort Bend	--	95.6	1/1/1936	4/27/1936	35.0	132
292241095513601	6534707	341		--	Fort Bend	--	84.9	1/1/1936	1/1/1936	20.0	135
293045095452401	6526903	270		--	Fort Bend	--	83.5	1/1/1936	3/7/1936	25.0	140
292808095364401	6536104	420		--	Fort Bend	--	69.0	1/1/1936	1/1/1936	20.0	185
292955095353401	6536102	414		--	Fort Bend	--	64.2	1/1/1936	1/1/1936	20.0	420
293710095582701	6525103	11		--	Fort Bend	--	125.7	3/18/1936	3/18/1936	32.0	139
293802095571001	6517805	15		--	Fort Bend	--	129.2	3/19/1936	3/19/1936	52.0	371
293049095422901	6527801	269		--	Fort Bend	--	77.9	4/1/1936	4/1/1936	40.0	79
293151095390201	6527904	406		--	Fort Bend	--	75.8	4/2/1936	4/2/1936	17.0	179
293252095545501	6525601	124		--	Fort Bend	--	114.8	4/7/1936	4/7/1936	34.0	64

Table 3.1. Wells in selected counties with groundwater-level data generally during the predevelopment to early development period (1897–1945) in the greater Houston area, Texas.—Continued

[USGS well ID is the well identifier used by the U.S. Geological Survey (USGS; 2021b); TWDB well ID is the well identifier used by the Texas Water Development Board (TWDB; 2020b); M/D/Y, month/day/year; A groundwater level above land surface is indicated by a negative number; -- not available]

USGS well ID	TWDB well ID	Historical identifier (TWDB or USGS)[1]	Other identifier	Map identifier (figs. 13–16)	County and figure, where applicable	Historical geographic area (fig. 18*B*)	Land-surface elevation (feet)	Period of record (may contain gaps) or single measurement date (M/D/Y)		Groundwater level below land surface (date of first measurement)[1]	Well or hole depth, in feet below land surface
								Begin	End		
293247095495501	6526509	233		--	Fort Bend	--	102.4	4/8/1936	4/8/1936	30.0	82
293221095504201	6526705	231		--	Fort Bend	--	103.7	4/8/1936	4/8/1936	30.0	86
293025095505401	6526703	294		--	Fort Bend	--	99.6	4/27/1936	4/27/1936	35.0	82
293324095471901	6526609	245		--	Fort Bend	--	99.8	4/27/1936	4/27/1936	45.0	82
293305095482701	6526507	289		--	Fort Bend	--	101.0	4/27/1936	4/27/1936	30.0	92
292650095570601	6533507	171		--	Fort Bend	--	95.6	4/27/1936	4/27/1936	21.0	105
292948096001001	6640309	158		--	Fort Bend	--	109.3	5/4/1936	5/4/1936	28.0	33
292631095501701	6534404	327		--	Fort Bend	--	90.0	5/6/1936	5/6/1936	18.0	52
292310095384301	6535902	434		--	Fort Bend	--	64.2	5/6/1936	5/6/1936	20.0	130
292104095504801	6542102	358		--	Fort Bend	--	76.6	5/18/1936	5/18/1936	18.9	23
292551095585601	6533404	168		--	Fort Bend	--	89.8	5/22/1936	5/22/1936	14.0	19
293502095571401	6525210			--	Fort Bend	--	115.6	8/1/1937	8/1/1937	43.0	236
293510095571201	6525213			--	Fort Bend	--	115.3	8/1/1937	8/1/1937	43.0	244
293458095570001	6525503			--	Fort Bend	--	116.5	9/1/1937	9/1/1937	43.0	214
293503095565601	6525212			--	Fort Bend	--	116.6	9/1/1937	9/1/1937	43.0	247
293720095380501	6527315			--	Fort Bend	--	76.0	11/1/1938	11/1/1938	30.0	733
293449095303701	6528601			--	Fort Bend	--	75.4	12/6/1938	12/6/1938	30.6	297
293453095275401	6529403			--	Fort Bend	--	66.5	12/6/1938	6/17/1955	45.3	665
292209095042801	6548209	L-64	well 2	B	Galveston (fig. 16)	Alta Loma area	19.1	9/23/1932	1/7/2003	34.3	855
--	[3]6548222	L-44	well 5-N	--	Galveston	Alta Loma area	22.0	12/10/1907	7/11/1947	2.4	797
--	[3]6548221	L-43	well 7-N	--	Galveston	Alta Loma area	21.0	12/10/1907	4/19/1944	2.3	797
--	6548227	L-50	well 8-S	--	Galveston	Alta Loma area	23.0	9/23/1932	5/28/1940	31.8	796
--	[3]6548220	L-42	well 9-N	--	Galveston	Alta Loma area	20.0	12/10/1907	5/16/1945	0.6	797
--	[3]6548223	L-51	well 10-S	--	Galveston	Alta Loma area	23.0	12/10/1907	6/10/1946	1.6	797
--	[3]6548224	L-54	well 16-S	--	Galveston	Alta Loma area	23.0	12/10/1907	5/16/1945	0.5	800
--	[3]6540807	E-104	well 17-N	--	Galveston	Alta Loma area	18.0	12/10/1907	5/11/1954	−2.9	793

Table 3.1. Wells in selected counties with groundwater-level data generally during the predevelopment to early development period (1897–1945) in the greater Houston area, Texas.—Continued

[USGS well ID is the well identifier used by the U.S. Geological Survey (USGS; 2021b); TWDB well ID is the well identifier used by the Texas Water Development Board (TWDB; 2020b); M/D/Y, month/day/year; A groundwater level above land surface is indicated by a negative number; -- not available]

USGS well ID	TWDB well ID	Historical identifier (TWDB or USGS)[1]	Other identifier	Map identifier (figs. 13–16)	County and figure, where applicable	Historical geographic area (fig. 18*B*)	Land-surface elevation (feet)	Period of record (may contain gaps) or single measurement date (M/D/Y)		Groundwater level below land surface (date of first measurement)[1]	Well or hole depth, in feet below land surface
								Begin	End		
--	[3]6524225	L-56	well 20-S	--	Galveston	Alta Loma area	23.0	12/10/1907	6/10/1946	−2.2	795
--	[3]6548226	L-57	well 22-S	--	Galveston	Alta Loma area	24.0	12/10/1907	4/19/1944	−2.0	795
292210095044501	6548206	L-60	well 1	--	Galveston	Alta Loma area	24.6	9/1/1914	1/26/1981	10.0	840
292155095041001	6548211	L-66	well 4	--	Galveston	Alta Loma area	20.0	1/1/1916	1/3/2003	14.0	873
292203095043201	6548213	L-62	well 7	--	Galveston	Alta Loma area	23.7	11/1/1927	1/3/2003	28.5	843
292236094580401	6433702	F-34	GH & H RR	D	Galveston (fig. 16)	Texas City area	15.0	4/15/1931	5/10/1976	4.2	914
--	[4]6433812	F-55	Pan Am refining well 3	E	Galveston (fig. 16)	Texas City area	14.0	11/1/1933	1/1/1958	8.0	965
292235094562701	[5]6433810	F-53	Pan Am refining well 6	F	Galveston (fig. 16)	Texas City area	13.3	3/1/1936	1/22/1985	18.0	1,000
--	[6]6441216	M-28	Pan Am refining well 7	G	Galveston (fig. 16)	Texas City area	15.0	4/1/1936	1/22/1985	25.0	1,024
--	[7]6441208	M-29	Pan Am refining well 8	H	Galveston (fig. 16)	Texas City area	15.0	6/1/1937	5/11/1953	44.0	1,000
--	[8]6433811	F-54	Pan Am refining well 2	--	Galveston	Texas City area	14.0	8/1/1933	5/9/1952	45.0	610
--	[9]6441217	M-30	Pan Am refining well 4	--	Galveston	Texas City area	15.0	5/1/1934	10/1/1947	37.0	974
--	[10]6441218	M-31	Pan Am refining well 5	--	Galveston	Texas City area	15.0	3/1/1934	7/1/1948	40.0	965
--	6433906	F-60	AMOCO	--	Galveston	Texas City area	9.0	2/22/1939	5/14/1959	66.6	801
--	6433913	228		--	Galveston	Texas City area	9.0	10/22/1931	5/5/1961	7.2	740
293039095053201	6532714	B-40		--	Galveston	--	15.4	4/15/1931	1/11/1994	25.3	560
292611095012601	6540602	E-68	Oilfield Salvage Co.	C	Galveston (fig. 16)	--	17.2	9/7/1932	11/2/1976	15.1	526
--	6540215	109		--	Galveston	--	12.5	4/15/1931	10/26/1933	13.4	230
--	6540212	E-35	GH&H RR	--	Galveston	--	14.0	4/15/1931	10/5/1948	17.9	750
--	6433709	203	TxDOT	--	Galveston	--	14.4	4/15/1931	10/26/1933	2.2	860
--	6433813	206		--	Galveston	--	9.6	4/15/1931	3/15/1941	6.3	926
--	6532725	B-37	GH&H RR	--	Galveston	--	15.0	4/15/1931	12/19/1938	11.9	1,020

Table 3.1. Wells in selected counties with groundwater-level data generally during the predevelopment to early development period (1897–1945) in the greater Houston area, Texas.—Continued

[USGS well ID is the well identifier used by the U.S. Geological Survey (USGS; 2021b); TWDB well ID is the well identifier used by the Texas Water Development Board (TWDB; 2020b); M/D/Y, month/day/year; A groundwater level above land surface is indicated by a negative number; -- not available]

USGS well ID	TWDB well ID	Historical identifier (TWDB or USGS)[1]	Other identifier	Map identifier (figs. 13–16)	County and figure, where applicable	Historical geographic area (fig. 18*B*)	Land-surface elevation (feet)	Period of record (may contain gaps) or single measurement date (M/D/Y)		Groundwater level below land surface (date of first measurement)[1]	Well or hole depth, in feet below land surface
								Begin	End		
--	6531705	A-5		--	Galveston	--	32.7	9/11/1931	2/28/1936	38.8	600
--	6531818	A-17		--	Galveston	--	26.2	9/11/1931	5/5/1952	33.1	763
--	6540507	E-20		--	Galveston	--	9.3	9/20/1932	5/6/1953	6.7	240
--	6540210	E-32		--	Galveston	--	15.6	9/20/1932	5/10/1945	14.4	504
--	6441206	M-5		--	Galveston	--	10.8	9/21/1932	2/18/1952	7.4	117
--	6548315	300		--	Galveston	--	13.5	9/22/1932	12/19/1938	10.9	500
292050095010801	6548302	L-13		--	Galveston	--	16.3	9/22/1932	10/14/1982	12.0	720
--	6548228	283		--	Galveston	--	19.2	9/23/1932	1/2/1937	11.3	720
--	6548314	286		--	Galveston	--	15.5	9/23/1932	12/19/1938	11.9	720
--	6548306	L-19		--	Galveston	--	10.1	10/7/1932	1/4/1938	5.0	790
292819095133201	6539101	D-1		--	Galveston	--	36.0	2/27/1939	2/27/1939	43.7	800
--	[11]6513824	602	River Oaks Country Club well 1	B	Harris (fig. 14)	Historical Houston area	56.0	1/19/1931	2/18/1966	46.5	887
--	6522119	856	Scott Street well 1	--	Harris	Historical Houston area	45.0	6/25/1925	9/10/1941	46.8	866
--	[12]6522118	855	Scott Street well 2	C	Harris (fig. 14)	Historical Houston area	45.0	1/1/1926	3/6/1959	22.0	1,521
--	6522120	857	Scott Street well 3	--	Harris	Historical Houston area	45.0	8/1/1928	2/14/1964	62.0	1,350
--	6522121	858	Scott Street well 4	--	Harris	Historical Houston area	45.0	5/1/1931	2/28/1955	58.0	1,756
--	6522106	--	Scott Street well 5	--	Harris	Historical Houston area	44.0	11/15/1938	3/14/1963	97.4	957
294415095165301	[13]6522317	878	Gulf Atlantic Warehouse	D	Harris (fig. 14)	Historical Houston area	15.0	8/3/1929	2/3/2021	42.0	900
294613095172601	6514912	757	Layne Bowler Co.	E	Harris (fig. 14)	Historical Houston area	41.7	10/19/1929	1/18/2013	54.0	676
294536095223201	[14]6513927	619	Lincoln Swimming Pool	F	Harris (fig. 14)	Historical Houston area	42.4	1/30/1931	12/22/1983	53.5	625

Table 3.1. Wells in selected counties with groundwater-level data generally during the predevelopment to early development period (1897–1945) in the greater Houston area, Texas.—Continued

[USGS well ID is the well identifier used by the U.S. Geological Survey (USGS; 2021b); TWDB well ID is the well identifier used by the Texas Water Development Board (TWDB; 2020b); M/D/Y, month/day/year; A groundwater level above land surface is indicated by a negative number; -- not available]

USGS well ID	TWDB well ID	Historical identifier (TWDB or USGS)[1]	Other identifier	Map identifier (figs. 13–16)	County and figure, where applicable	Historical geographic area (fig. 18*B*)	Land-surface elevation (feet)	Period of record (may contain gaps) or single measurement date (M/D/Y)		Groundwater level below land surface (date of first measurement)[1]	Well or hole depth, in feet below land surface
								Begin	End		
--	6514747	688	Central well C-16	--	Harris	Historical Houston area	35.0	7/10/1925	3/19/1948	48.0	1,535
--	[15]6514707	--	Central well C-18	--	Harris	Historical Houston area	25.0	8/20/1945	1/12/1988	136.4	2,035
--	6513925	617	Central well F-1	--	Harris	Historical Houston area	42.0	4/1/1927	3/3/1953	27.0	1,540
--	6513924	616	Central well F-5	--	Harris	Historical Houston area	42.0	5/21/1927	3/3/1966	47.0	1,456
--	6513926	618	Central well F-10	--	Harris	Historical Houston area	30.0	11/17/1938	2/24/1961	89.4	1,320
--	6513932	624	Central well F-11	--	Harris	Historical Houston area	30.0	7/30/1935	3/3/1966	83.0	953
--	6513933	625	Central well F-12	--	Harris	Historical Houston area	43.0	9/11/1935	9/11/1953	53.0	2,025
--	6513613	590	Heights well 2	--	Harris	Historical Houston area	68.0	3/5/1923	8/26/1936	19.5	1,362
--	6513614	591	Heights well 3	--	Harris	Historical Houston area	68.0	1/20/1938	1/20/1987	76.9	1,039
--	6513606	589	Heights well 5	--	Harris	Historical Houston area	67.0	11/14/1938	2/13/1964	63.6	1,858
--	6513605	1410	Heights well 6	--	Harris	Historical Houston area	68.0	11/14/1938	1/10/1980	87.7	1,232
--	6513608	1412	Heights well 7	--	Harris	Historical Houston area	69.0	11/14/1938	2/8/1977	84.7	1,458
--	6513607	1411	Heights well 8	--	Harris	Historical Houston area	67.0	11/14/1938	2/17/1970	88.4	1,252
--	6521319	792	South End well 1	--	Harris	Historical Houston area	52.0	4/1/1917	4/1/1917	13.0	1,394
--	6521322	795	South End well 2	--	Harris	Historical Houston area	50.0	1/1/1917	3/7/1955	29.0	830

Table 3.1. Wells in selected counties with groundwater-level data generally during the predevelopment to early development period (1897–1945) in the greater Houston area, Texas.—Continued

[USGS well ID is the well identifier used by the U.S. Geological Survey (USGS; 2021b); TWDB well ID is the well identifier used by the Texas Water Development Board (TWDB; 2020b); M/D/Y, month/day/year; A groundwater level above land surface is indicated by a negative number; -- not available]

USGS well ID	TWDB well ID	Historical identifier (TWDB or USGS)[1]	Other identifier	Map identifier (figs. 13–16)	County and figure, where applicable	Historical geographic area (fig. 18*B*)	Land-surface elevation (feet)	Period of record (may contain gaps) or single measurement date (M/D/Y)		Groundwater level below land surface (date of first measurement)[1]	Well or hole depth, in feet below land surface
								Begin	End		
	6521323	796	South End well 3	--	Harris	Historical Houston area	51.0	5/23/1933	5/23/1933	47.3	1,127
	6521321	794	South End well 4	--	Harris	Historical Houston area	50.0	11/16/1938	9/18/1953	78.2	777
--	6521320	793	South End well 5	--	Harris	Historical Houston area	51.0	1/1/1932	2/16/1966	76.0	1,618
--	6513915	601	West End well 1	--	Harris	Historical Houston area	59.0	11/25/1918	11/25/1918	−18.0	1,465
--	6513914	600	West End well 2	--	Harris	Historical Houston area	59.0	10/19/1928	10/19/1928	20.0	558
--	6522226	879	Magnolia Park well 2	--	Harris	Historical Houston area	36.0	6/1/1925	4/27/1959	41.0	1,033
--	[16]6522615	895	East End well 1	--	Harris	Historical Houston area	34.0	10/28/1930	12/1/1965	48.7	1,651
--	[17]6514727	744	Northeast well 1	--	Harris	Historical Houston area	49.0	3/12/1932	3/9/1962	15.0	1,876
--	6514759	1395	Northeast well 2	--	Harris	Historical Houston area	49.0	11/16/1938	1/28/1982	92.4	1,291
294106095171201	6522618	913		--	Harris	Historical Houston area	38.0	5/27/1937	1/22/2020	62.8	876
--	6522212	868	Hughes Tool Co. well 1	--	Harris	Historical Houston area	40.0	1/8/1931	3/16/1945	49.3	694
--	6522211	869	Hughes Tool Co. well 2	--	Harris	Historical Houston area	40.0	5/3/1926	6/1/1956	31.0	1,096
--	6522214		Houston Golf Club	--	Harris	Historical Houston area	33.0	1/16/1931	2/6/1964	51.2	697
--	6522323	892	Lone Star Cement Co.	--	Harris	Historical Houston area	35.0	1/1/1921	6/1/1956	13.0	1,283
--	6514809			--	Harris	Historical Houston area	50.0	5/1/1925	5/1/1925	30.0	947

Table 3.1. Wells in selected counties with groundwater-level data generally during the predevelopment to early development period (1897–1945) in the greater Houston area, Texas.—Continued

[USGS well ID is the well identifier used by the U.S. Geological Survey (USGS; 2021b); TWDB well ID is the well identifier used by the Texas Water Development Board (TWDB; 2020b); M/D/Y, month/day/year; A groundwater level above land surface is indicated by a negative number; -- not available]

USGS well ID	TWDB well ID	Historical identifier (TWDB or USGS)[1]	Other identifier	Map identifier (figs. 13–16)	County and figure, where applicable	Historical geographic area (fig. 18*B*)	Land-surface elevation (feet)	Period of record (may contain gaps) or single measurement date (M/D/Y)		Groundwater level below land surface (date of first measurement)[1]	Well or hole depth, in feet below land surface
								Begin	End		
--	6521324	797		--	Harris	Historical Houston area	52.0	1/24/1931	6/12/1951	66.9	910
--	6514908	751	Texas Pipeline Co	--	Harris	Historical Houston area	44.0	3/19/1931	2/3/1966	50.1	540
--	6513916			--	Harris	Historical Houston area	60.0	1/23/1931	6/12/1968	69.6	340
--	6521217	801	Southside Place well 1	--	Harris	Historical Houston area	56.0	1/24/1931	11/23/1935	38.9	610
--	6521218		Southside Place well 2	--	Harris	Historical Houston area	56.0	9/1/1935	1/18/1946	50.0	988
--	6513918	606	Henke and Pillot	--	Harris	Historical Houston area	55.0	1/22/1931	6/10/1948	74.7	571
--	6514914			--	Harris	Historical Houston area	42.0	2/26/1931	6/6/1957	56.9	569
--	6521220	804	Historical production well 2	--	Harris	Historical Houston area	57.0	11/3/1931	8/5/1940	42.4	650
--	6514413	656	Texas Creosoting Co	--	Harris	Historical Houston area	64.0	1/9/1931	2/10/1966	57.7	666
--	6514425			--	Harris	Historical Houston area	53.0	1/14/1931	6/2/1947	62.9	834
--	6514733			--	Harris	Historical Houston area	50.0	1/29/1931	10/24/1939	51.3	1,638
--	6514737			--	Harris	Historical Houston area	45.0	1/21/1931	10/11/1940	73.1	873
--	6513732			--	Harris	Historical Houston area	50.0	7/8/1934	2/27/1958	−34.0	1,996
295836095233301	[18]6505309	264		G	Harris (fig. 14)	Katy area	98.4	5/29/1931	2/8/1985	3.0	1,130
300146095510401	6058704	31		H	Harris (fig. 14)	Katy area	224.0	1/7/1928	1/15/1991	42.8	297
--	6510606			I	Harris (fig. 14)	Katy area	143.0	1/1/1905	3/11/1966	27.0	500

Table 3.1. Wells in selected counties with groundwater-level data generally during the predevelopment to early development period (1897–1945) in the greater Houston area, Texas.—Continued

[USGS well ID is the well identifier used by the U.S. Geological Survey (USGS; 2021b); TWDB well ID is the well identifier used by the Texas Water Development Board (TWDB; 2020b); M/D/Y, month/day/year; A groundwater level above land surface is indicated by a negative number; -- not available]

USGS well ID	TWDB well ID	Historical identifier (TWDB or USGS)[1]	Other identifier	Map identifier (figs. 13–16)	County and figure, where applicable	Historical geographic area (fig. 18*B*)	Land-surface elevation (feet)	Period of record (may contain gaps) or single measurement date (M/D/Y)		Groundwater level below land surface (date of first measurement)[1]	Well or hole depth, in feet below land surface
								Begin	End		
294948095441001	6511405	385		--	Harris	Katy area	136.6	3/17/1933	1/10/2001	35.8	359
300450095250501	[19]6061504	42		--	Harris	Katy area	120.8	1/1/1912	2/8/1984	−25.0	1,072
295814095415301	6503204	171		--	Harris	Katy area	150.7	4/3/1931	1/7/1985	6.5	72
300707095354801	6060104	71		--	Harris	Katy area	174.6	3/1/1923	3/1/1923	36.0	65
294704095461601	6510907			--	Harris	Katy area	132.6	3/12/1931	3/12/1931	36.3	609
300027095274802	6061703			--	Harris	Katy area	117.2	3/27/1931	3/27/1931	19.7	24
295704095250901	6505506	255		--	Harris	Katy area	92.8	3/27/1931	1/20/1981	9.7	41
300027095274801	6061704			--	Harris	Katy area	117.2	3/27/1931	3/27/1931	24.4	142
300318095551302	6057503	6		--	Harris	Katy area	250.3	4/13/1931	4/13/1931	10.0	30
300322095550501	6057502	5		--	Harris	Katy area	268.1	4/13/1931	4/13/1931	36.5	42
300303095532801	6057607	14		--	Harris	Katy area	258.2	4/13/1931	4/13/1931	50.3	122
300315095550101	6057501			--	Harris	Katy area	263.5	5/13/1931	5/13/1931	3.5	20
295458095371401	6504704	202		--	Harris	Katy area	127.9	5/19/1931	5/19/1931	9.4	48
300528095260501	6061207			--	Harris	Katy area	133.9	6/1/1931	6/1/1931	26.1	33
300459095261401	6061503	92		--	Harris	Katy area	130.6	6/1/1931	6/1/1931	22.8	35
300111095492501	6058805			--	Harris	Katy area	212.6	11/3/1931	11/3/1931	21.0	22
300552095543201	6057303			--	Harris	Katy area	269.0	11/5/1931	11/5/1931	20.1	60
300302095544301	6057606			--	Harris	Katy area	263.5	11/5/1931	11/5/1931	43.1	--
300356095541201	6057605	3		--	Harris	Katy area	279.1	11/6/1931	11/6/1931	50.5	71
300009095253701	6061806	106		--	Harris	Katy area	107.5	11/9/1931	11/9/1931	14.0	17
300327095253601	6061505	95		--	Harris	Katy area	111.8	11/9/1931	11/9/1931	26.0	32
300111095253901	6061805			--	Harris	Katy area	112.3	11/9/1931	11/9/1931	16.4	45
300106095253801	6061804			--	Harris	Katy area	110.4	11/9/1931	11/9/1931	28.3	155
300117095241101	6061901	105		--	Harris	Katy area	105.6	11/18/1931	11/18/1931	16.7	21
300438095253801	6061501			--	Harris	Katy area	122.3	8/1/1932	8/1/1932	18.0	365
300045095281101	6061702			--	Harris	Katy area	115.2	9/28/1932	9/28/1932	24.3	556
300444095401001	6059502			--	Harris	Katy area	178.4	6/1/1933	6/1/1933	25.0	156

Table 3.1. Wells in selected counties with groundwater-level data generally during the predevelopment to early development period (1897–1945) in the greater Houston area, Texas.—Continued

[USGS well ID is the well identifier used by the U.S. Geological Survey (USGS; 2021b); TWDB well ID is the well identifier used by the Texas Water Development Board (TWDB; 2020b); M/D/Y, month/day/year; A groundwater level above land surface is indicated by a negative number; -- not available]

USGS well ID	TWDB well ID	Historical identifier (TWDB or USGS)[1]	Other identifier	Map identifier (figs. 13–16)	County and figure, where applicable	Historical geographic area (fig. 18*B*)	Land-surface elevation (feet)	Period of record (may contain gaps) or single measurement date (M/D/Y)		Groundwater level below land surface (date of first measurement)[1]	Well or hole depth, in feet below land surface
								Begin	End		
300403095392101	6059603			--	Harris	Katy area	172.9	6/1/1933	6/1/1933	24.0	234
300432095375701	6059604			--	Harris	Katy area	175.3	7/1/1933	7/1/1933	60.0	864
300352095370801	6060402	74		--	Harris	Katy area	159.7	8/4/1933	8/4/1933	16.3	23
300316095364301	6060403	75		--	Harris	Katy area	162.7	8/4/1933	8/4/1933	21.7	30
300304095543101	6057604			--	Harris	Katy area	262.8	1/1/1938	1/1/1938	37.0	211
300107095254001	6061803			--	Harris	Katy area	110.7	2/6/1938	2/6/1938	16.2	20
295910095443501	6503104			--	Harris	Katy area	155.4	5/8/1938	1/3/2008	8.0	499
295416095410801	6503806			--	Harris	Katy area	141.0	1/3/1939	1/3/1939	28.5	239
300126095241401	6061903			--	Harris	Katy area	109.7	5/31/1939	8/23/1985	−22.6	1,052
300124095241401	6061902			--	Harris	Katy area	107.4	8/31/1939	2/24/1971	23.5	793
--	[20]6523139	1170	Houston Lighting and Power Co. [well 3]	K	Harris (fig. 14)	Pasadena area	18.0	2/25/1931	2/27/1961	54.8	836
294336095082101	[21]6523309	1125	Shell Oil Refinery well 6	L	Harris (fig. 14)	Pasadena area	29.5	2/1/1938	2/10/2011	108.0	913
--	6523314	1198	Shell Oil Refinery well 2	M	Harris (fig. 14)	Pasadena area	26.0	1/1/1929	1/1/1965	41.0	790
--	6523315	1199	Shell Oil Refinery well 3	--	Harris	Pasadena area	33.0	1/1/1929	11/1/1951	41.0	860
--	6523311		Shell Oil Refinery well 4	--	Harris	Pasadena area	35.0	1/1/1929	12/29/1947	51.0	1,284
293954095111201	[22]6523805	1230	Test well 9	N	Harris (fig. 14)	Pasadena area	34.5	7/2/1939	5/28/1997	91.4	1,419
--	[23]6523804	1229	Test well 8	--	Harris	Pasadena area	40.0	7/1/1939	3/24/1966	93.0	1,680
--	6523147		Texaco well 5	--	Harris	Pasadena area	19.0	12/14/1929	9/9/1953	35.0	1,376
294351095130401	6523148	1174	Texaco east well	--	Harris	Pasadena area	17.4	3/25/1931	1/21/2005	43.1	802
--	[24]6515406	933	Champion Paper Mill well 3, later Houston Lighting and Power	--	Harris	Pasadena area	40.0	7/1/1938	2/7/1966	48.2	890
--	[25]6523233	1129	Champion Paper Mill well D-1	--	Harris	Pasadena area	29.0	8/11/1937	8/11/1937	75.0	515
--	[25]6523234	1130	Champion Paper Mill well D-3	--	Harris	Pasadena area	29.0	8/12/1937	8/12/1937	201.0	1,481

Table 3.1. Wells in selected counties with groundwater-level data generally during the predevelopment to early development period (1897–1945) in the greater Houston area, Texas.—Continued

[USGS well ID is the well identifier used by the U.S. Geological Survey (USGS; 2021b); TWDB well ID is the well identifier used by the Texas Water Development Board (TWDB; 2020b); M/D/Y, month/day/year; A groundwater level above land surface is indicated by a negative number; -- not available]

USGS well ID	TWDB well ID	Historical identifier (TWDB or USGS)[1]	Other identifier	Map identifier (figs. 13–16)	County and figure, where applicable	Historical geographic area (fig. 18*B*)	Land-surface elevation (feet)	Period of record (may contain gaps) or single measurement date (M/D/Y)		Groundwater level below land surface (date of first measurement)[1]	Well or hole depth, in feet below land surface
								Begin	End		
--	[25]6523235	1131	Champion Paper Mill well B-1	--	Harris	Pasadena area	34.0	3/5/1937	3/5/1937	67.0	960
--	[25]6523236	1132	Champion Paper Mill well B-2	--	Harris	Pasadena area	30.0	2/6/1937	2/6/1937	70.0	1,840
--	[25]6523237	1133	Champion Paper Mill well B-3	--	Harris	Pasadena area	30.0	2/10/1937	2/10/1937	174.0	1,399
--	[25]6523122	1135	Champion Paper Mill well A-1	--	Harris	Pasadena area	31.0	1/26/1937	1/26/1937	63.0	974
--	[25]6523123	1136	Champion Paper Mill well A-2	--	Harris	Pasadena area	29.0	1/18/1937	1/18/1937	56.0	1,275
--	[25]6523124	1137	Champion Paper Mill well A-3	--	Harris	Pasadena area	28.0	1/17/1937	1/17/1937	42.0	1,927
293724095115901	6531211			--	Harris	Pasadena area	40.5	4/3/1931	1/31/2007	47.1	832
294227095061401	6524403			--	Harris	Pasadena area	29.0	4/2/1931	6/3/1949	55.0	900
294333095073301	6523312			--	Harris	Pasadena area	23.4	9/13/1935	9/13/1935	71.0	1,329
--	6523151	1187	Historical production well 1	--	Harris	Pasadena area	27.0	9/22/1937	6/7/1951	111.7	834
294445095001001	6524313	1057	Humble Oil and Refining Co. well 7	O	Harris (fig. 14)	Baytown area	22.3	12/1/1923	9/5/1963	37.0	515
294321095005401	[26]6524316	1067	Humble Oil and Refining Co. well 10	P	Harris (fig. 14)	Baytown area	13.6	4/4/1925	5/1/1957	20.0	545
294452095010501	6524312	1051	Humble Oil and Refining Co. well 12	Q	Harris (fig. 14)	Baytown area	28.0	12/15/1925	1/1/1952	58.0	558
294432095002301	6524319	1058	Humble Oil and Refining Co. well 13	--	Harris	Baytown area	23.2	12/8/1925	12/8/1925	77.0	509
294437095003801	6524318	1054	Humble Oil and Refining Co. well 15	--	Harris	Baytown area	22.3	6/5/1926	1/1/1948	76.0	571
294427095011801	6524310	1053	Humble Oil and Refining Co. well 19	--	Harris	Baytown area	19.5	10/1/1929	9/9/1963	87.0	974

Table 3.1. Wells in selected counties with groundwater-level data generally during the predevelopment to early development period (1897–1945) in the greater Houston area, Texas.—Continued

[USGS well ID is the well identifier used by the U.S. Geological Survey (USGS; 2021b); TWDB well ID is the well identifier used by the Texas Water Development Board (TWDB; 2020b); M/D/Y, month/day/year; A groundwater level above land surface is indicated by a negative number; -- not available]

USGS well ID	TWDB well ID	Historical identifier (TWDB or USGS)[1]	Other identifier	Map identifier (figs. 13–16)	County and figure, where applicable	Historical geographic area (fig. 18*B*)	Land-surface elevation (feet)	Period of record (may contain gaps) or single measurement date (M/D/Y)		Groundwater level below land surface (date of first measurement)[1]	Well or hole depth, in feet below land surface
								Begin	End		
294408095003101	6524315		Humble Oil and Refining Co. well 20	--	Harris	Baytown area	21.4	12/10/1935	1/10/1966	114.0	516
294420095000401	6524314		Humble Oil and Refining Co. well 21	--	Harris	Baytown area	21.5	8/28/1936	1/13/1966	126.0	568
294452095010201	6524311		Humble Oil and Refining Co. well 22	--	Harris	Baytown area	21.8	5/1/1937	1/11/1966	58.0	998
294352095002801	6524317		Humble Oil and Refining Co. well 1	--	Harris	Baytown area	18.5	10/1/1931	5/8/1952	42.0	743
--	6524914	1104	Historical production well 1	R	Harris (fig. 14)	Baytown area	27.0	4/1/1930	12/4/1956	40.0	570
294936094563801	6409502	960		--	Harris	Baytown area	30.8	1/1/1932	1/1/1932	34.0	344
--	6531601	1322	Humble West Ranch	--	Harris	Johnson Space Center area	32.0	1/1/1927	2/2/1966	16.0	806
295045094574701	6409101	952		--	Harris (fig. 14)	--	31.6	1/22/1932	1/22/1932	10.0	88
294914094585501	6409402			--	Harris (fig. 14)	--	36.8	1/22/1932	1/22/1932	10.0	100
301049094485700	6134503			--	Liberty	--	30.1	1/1/1908	1/1/1908	−30.0	659
300254094530800	6157605			--	Liberty	--	82.5	11/1/1929	11/1/1929	45.0	399
302336094590400	6133703			--	Liberty	--	155.2	12/29/1936	12/29/1936	−5.0	1,200
300540094384901	6159301			--	Liberty	--	65.0	1/1/1938	3/14/1967	17.0	255
295924094354700	6404101			--	Liberty	--	50.1	1/1/1938	4/7/1950	14.0	406
301828095272402	[27]6045505	22	Historical production well 1	B	Montgomery (fig. 13)	--	213.0	6/3/1931	2/4/1955	−0.6	1,464
301707095272201	[28]6045803	29		C	Montgomery (fig. 13)	--	177.2	11/18/1931	9/11/1992	24.4	26
301041095262701	6053503	45		D	Montgomery (fig. 13)	--	129.2	11/18/1931	6/22/1953	16.2	27
301031095270501	6053504	46		E	Montgomery (fig. 13)	--	161.5	6/2/1931	6/10/1958	29.8	40
301018095253901	[29]6053502	48		--	Montgomery	--	120.9	1902	8/1/1966	−46.0	1,800

Table 3.1. Wells in selected counties with groundwater-level data generally during the predevelopment to early development period (1897–1945) in the greater Houston area, Texas.—Continued

[USGS well ID is the well identifier used by the U.S. Geological Survey (USGS; 2021b); TWDB well ID is the well identifier used by the Texas Water Development Board (TWDB; 2020b); M/D/Y, month/day/year; A groundwater level above land surface is indicated by a negative number; -- not available]

USGS well ID	TWDB well ID	Historical identifier (TWDB or USGS)[1]	Other identifier	Map identifier (figs. 13–16)	County and figure, where applicable	Historical geographic area (fig. 18*B*)	Land-surface elevation (feet)	Period of record (may contain gaps) or single measurement date (M/D/Y)		Groundwater level below land surface (date of first measurement)[1]	Well or hole depth, in feet below land surface
								Begin	End		
301938095095701	6047607			--	Montgomery	--	170.8	3/1/1914	1/26/1966	−10.0	809
302612095360801	6036401			--	Montgomery	--	202.0	1/1/1924	1/1/1924	55.0	2,500
300912095273301	6053706			--	Montgomery	--	144.6	6/2/1931	6/2/1931	24.2	173
301623095272401	6045801			--	Montgomery	--	135.1	6/3/1931	10/4/1940	26.2	33
302103095290202	6045106			--	Montgomery	--	265.7	11/13/1931	8/3/1939	16.0	50
301843095271401	6045510			--	Montgomery	--	221.3	1/1/1932	1/1/1932	64.0	220
302716095294101	6037408			--	Montgomery	--	307.8	1/1/1934	1/1/1934	100.0	300
302320095420501	6035809			--	Montgomery	--	299.4	9/1/1935	9/1/1935	83.0	110
302254095420001	6035805			--	Montgomery	--	305.8	9/1/1935	9/1/1935	68.0	566
301912095343401	6044501			--	Montgomery	--	271.6	6/1/1936	6/1/1936	85.0	546
301402095093201	6055301			--	Montgomery	--	130.4	7/1/1936	7/1/1936	35.0	130
301913095275201	6045409			--	Montgomery	--	191.4	11/18/1938	7/3/1941	32.4	34
301719095271801	6045806			--	Montgomery	--	164.6	11/18/1938	12/19/1939	3.6	210
302300095394501	6035901			--	Montgomery	--	303.9	1/1/1939	1/1/1939	71.0	606
295213095532101	[30]6509307	223	well F-25	--	Waller	--	177.2	2/10/1931	1/5/2010	48.2	767
294703095513700	6510708	234		--	Waller	--	149.9	3/12/1931	3/12/1931	48.5	545
295147095533300	6509308			--	Waller	--	172.9	3/15/1939	3/15/1939	55.6	641
Wells with early-time groundwater-level data used in figures 94–96. Wells may be duplicated from the list above.											
--	6522323	892	Lone Star Cement Co.	--	Harris (fig. 94)	Houston area	35.0	1/1/1921	6/1/1956	13.0	1,283
294106095171201	6522618	913		--	Harris (fig. 94)	Houston area	38.0	5/27/1937	1/1/2020	62.8	876
294208095280701	6521413	840		--	Harris (fig. 95*A*)	Houston area	59.0	2/1/1937	1/17/1985	39.0	712
294745095201001	6514406		Northeast well 3	--	Harris (fig. 95*B*)	Houston area	57.4	6/12/1944	1/4/1978	87.6	1,993
294452095010501	6524312	1051	Humble Oil and Refining Co. well 12	--	Harris (fig. 95*C*)	Baytown area	28.0	12/15/1925	1/1/1952	58.0	558
294445095001001	6524313	1057	Humble Oil and Refining Co. well 7	--	Harris (fig. 95*C*)	Baytown area	22.3	12/1/1923	9/5/1963	37.0	515
294336095082101	6523309	1125	Shell Oil Refinery well 6	--	Harris (fig. 95*D*)	Pasadena area	31.0	2/1/1938	2/10/2011	108.0	913

Table 3.1. Wells in selected counties with groundwater-level data generally during the predevelopment to early development period (1897–1945) in the greater Houston area, Texas.—Continued

[USGS well ID is the well identifier used by the U.S. Geological Survey (USGS; 2021b); TWDB well ID is the well identifier used by the Texas Water Development Board (TWDB; 2020b); M/D/Y, month/day/year; A groundwater level above land surface is indicated by a negative number; -- not available]

USGS well ID	TWDB well ID	Historical identifier (TWDB or USGS)[1]	Other identifier	Map identifier (figs. 13–16)	County and figure, where applicable	Historical geographic area (fig. 18*B*)	Land-surface elevation (feet)	Period of record (may contain gaps) or single measurement date (M/D/Y)		Groundwater level below land surface (date of first measurement)[1]	Well or hole depth, in feet below land surface
								Begin	End		
--	6532801			--	Harris (fig. 95*E*, *F*)	Johnson Space Center area	12.0	3/16/1939	11/17/1952	42.3	570
293207095061501	6532703			--	Harris (fig. 95*E*, *F*)	Johnson Space Center area	19.0	9/1/1951	1/25/2007	90.0	664
--	6532624			--	Harris (fig. 95*G*)	Johnson Space Center area	17.0	3/27/1939	7/9/1947	46.5	545
--	6532602			--	Harris (fig. 95*G*)	Johnson Space Center area	16.0	7/24/1958	6/8/1976	144.0	610
294538095344601	6512801		Lakeside Country Club 2	--	Harris (fig. 95*H*)	--	75.0	4/29/1952	2/1/2020	63.2	467
294623095351401	6512704		Memorial West well 1	--	Harris (fig. 95*H*)	--	84.0	8/3/1962	1/9/1990	159.0	1,310
--	6508809	326		--	Harris (fig. 95*I*)	--	47.0	10/29/1931	12/18/1959	21.9	533
295003095063901	6516101			--	Harris (fig. 95*I*)	--	45.0	12/1/1955	5/10/2010	190.0	1,520
292352094543001	6433903			--	Harris (fig. 95*J*)	Texas City area	8.0	2/22/1944	6/1/1975	103.0	778
300124095241401	6061902			--	Harris (fig. 96*A*)	--	107.4	8/31/1939	2/24/1971	23.5	793
300146095241801	6061905			--	Harris (fig. 96*A*)	--	89.0	4/12/1966	1/29/2019	92.0	560
300126095241401	6061903			--	Harris (fig. 96*A*)	--	109.7	5/31/1939	8/23/1985	−22.6	1,052
300054095271801	6061841			--	Harris (fig. 96*A*)	--	89.0	2/3/2005	2/6/2019	145.2	2,204
300312095221601	6062403			--	Harris (fig. 96*B*)	--	103.0	1/16/1991	2/2/2005	235.7	615
300450095250501	[19]6061504	42		--		--	120.8	1/1/1912	2/8/1984	−25.0	1,072
300826095270801	6053827			--	Harris (fig. 96*B*)	--	139.0	12/31/1985	2/14/2019	125.0	570
301828095272402	[27]6045505	22	Historical production well 1	--	Montgomery (fig. 96*D*)	--	213.0	6/3/1931	2/4/1955	−0.6	1,464
294552095502601	6510703			--	Fort Bend (fig. 96*E*)	Katy area	138.4	8/11/1932	1/22/1985	55.8	170
294807095484901	6510518			--	Fort Bend (fig. 96*E*)	Katy area	146.0	10/10/1989	2/7/2019	115.5	240

Table 3.1. Wells in selected counties with groundwater-level data generally during the predevelopment to early development period (1897–1945) in the greater Houston area, Texas.—Continued

[USGS well ID is the well identifier used by the U.S. Geological Survey (USGS; 2021b); TWDB well ID is the well identifier used by the Texas Water Development Board (TWDB; 2020b); M/D/Y, month/day/year; A groundwater level above land surface is indicated by a negative number; -- not available]

USGS well ID	TWDB well ID	Historical identifier (TWDB or USGS)[1]	Other identifier	Map identifier (figs. 13–16)	County and figure, where applicable	Historical geographic area (fig. 18*B*)	Land-surface elevation (feet)	Period of record (may contain gaps) or single measurement date (M/D/Y)		Groundwater level below land surface (date of first measurement)[1]	Well or hole depth, in feet below land surface
								Begin	End		
--	6509610			--	Fort Bend (fig. 96*E*)	Katy area	163.0	1/1/1944	1/1/1944	74.0	808
--	6509607			--	Fort Bend (fig. 96*E*)	Katy area	163.0	6/1/1965	6/1/1965	187.0	812
294753095454001	6510611			--	Fort Bend (fig. 96*E*)	Katy area	132.0	9/17/1976	2/12/2019	227.0	1,170

[1]Groundwater-level data and well information used in this table and on figures 13–16 are from Livingston (1937, 1939a, 1939b) Turner (1939), Turner and Livingston (1939), White and others (1939), White and others (1944), Lang and others (1950), Petitt and Winslow (1955), Gabrysch and others (1969, 1970), Popkin (1971), TWDB (2020b), and USGS (2021b). The well historical identifier used in this table may differ from those in Deussen (1914). Negative values indicate groundwater levels above land surface and refer to the level to which water would rise above land surface in a tightly cased well.

[2]A hydrograph for this well is presented on figure 17 in Wesselman (1972).

[3]These wells compose the original wellfield that was drilled in 1893–94 that is described in Petitt and Winslow (1955).

[4]The other identifier (Pan Am refining well 3) is used in Rose (1949), Petitt and Winslow (1955), and American Oil Company (1958). The groundwater levels are supplied as furnished records.

[5]The other identifier (Pan Am refining well 6) is used in Rose (1943), Petitt and Winslow (1955), and American Oil Company (1958). The groundwater levels are supplied as furnished records.

[6]The other identifier (Pan Am refining well 7) is used in Rose (1943), Petitt and Winslow (1955), and American Oil Company (1958). The groundwater levels are supplied as furnished records.

[7]The other identifier (Pan Am refining well 8) is used in Rose (1943), Petitt and Winslow (1955), and American Oil Company (1958). The groundwater levels are supplied as furnished records.

[8]The other identifier (Pan Am refining well 2) is used in Rose (1949), Petitt and Winslow (1955), and American Oil Company (1958). The groundwater levels are supplied as furnished records.

[9]The other identifier (Pan Am refining well 4) is used in Rose (1949), Petitt and Winslow (1955), and American Oil Company (1958). The groundwater levels are supplied as furnished records.

[10]The other identifier (Pan Am refining well 5) is used in Rose (1949), Petitt and Winslow (1955), and American Oil Company (1958). The groundwater levels are supplied as furnished records.

[11]Hydrographs for this well are presented in many publications, including White and others (1939), Lang and others (1950), Winslow and Fluellen (1952), Wood (1956), and Gabrysch (1967).

[12]A hydrograph for this well is presented on figure 5 in Doyel and others (1954).

[13]A hydrograph for this well is presented on figure 19 in Anders and Naftel (1962).

[14]Hydrographs for this well are presented in many publications, including White and others (1939), Rose and Alexander (1944), White and others (1944), Lang and others (1950), Winslow and Fluellen (1952), Wood and Gabrysch (1965), Gabrysch (1967), and Gabrysch (1972).

[15]This well was located at the site of the Houston Water Works plant (later the city Central water plant; fig. 11*I*), established in 1879 and where the first groundwater well in the Houston area was drilled in 1886. The Houston Water Works plant is on the National Register of Historic Places (Texas Historical Commission, 2022).

[16]The first East End extensometer was installed in this well in 1958. Hydrographs for this well are presented on figure 6 in Winslow and Fluellen (1952), figure 5 in Doyel and others (1954) and Wood (1956), and figure 7 in Wood (1958a) and Anders and Naftel (1962).

[17]Hydrographs for this well are presented on figure 6 in Winslow and Fluellen (1952) and figure 7 in Wood (1958a). Some reports list the hole depth (2,150 feet) as the well depth.

[18]A hydrograph for this well is presented on figure 9 in White and others (1944).

[19]A hydrograph for this well is presented on figure 6 in William F. Guyton and Associates, Inc. (1972).

[20]Hydrographs for this well are presented in many publications, including White and others (1939), Fugate (1941), Rose and Alexander (1944), White and others (1944), Lang and others (1950), Wood (1956), Wood (1958a), Anders and Naftel (1962), Wood and Gabrysch (1965), Gabrysch (1967), and Gabrysch (1972).

[21]Groundwater-level data for this well are displayed on figure 95*D*.

[22]Hydrographs for this well are presented in many publications, including Fugate (1941), White and others (1944), Lang and others (1950), Winslow and Fluellen (1952), Wood (1958a), Wood and Gabrysch (1965), Gabrysch (1967), and Gabrysch (1972).

[23]Hydrographs for this well are presented on figure 3 in Fugate (1941) and figure 5 in White and others (1944).

[24]Hydrographs for this well are presented on figure 16 in Wood (1958a) and Wood and Gabrysch (1965) and figure 15 in Anders and Naftel (1962).

[25]These eight wells were located at the Champion Paper Mill that began operations in 1937, described in White and others (1944). A ninth well was drilled at this site, however a well record does not exist.

[26]Hydrographs for this well are presented on figure 27 in Wood (1958a) and figure 19 in Wood and Gabrysch (1965).

[27]Hydrographs for this well are presented on figure 16 in Popkin (1971) and figure 6 in William F. Guyton and Associates, Inc. (1972).

[28]Hydrographs are presented on figure 14 in Lang and others (1950), figure 23 in Wood (1958a), and figure 20 in Popkin (1971).

[29]A picture of this well flowing in 1966 is provided on figure 5 in Popkin (1971).

[30]Hydrographs for this well are presented in many publications, including Winslow and Fluellen (1952), Wood (1958a), Anders and Naftel (1962), Wood and Gabrysch (1965), Gabrysch (1967), and Gabrysch (1972).

Appendix 4. Climate Stations In and Near the Gulf Coast Aquifer System Study Area

Spatially distributed recharge to the Gulf Coast aquifer system was computed for each month of the study period by using the Soil-Water-Balance (SWB) code (Westenbroek and others, 2010). Use of the SWB code requires gridded climatological data inputs, including precipitation and temperature data. Daily climate data, including precipitation and minimum and maximum air temperature, were obtained from 106 climate stations (National Climatic Data Center, 2019) (fig. 62; table 4.1) and interpolated to the groundwater model. Climate stations with long-term data were well distributed across the study area where a total of 30 stations had greater than 90 years of climate data (fig. 62).

Table 4.1. Climate stations in and near the Gulf Coast Land Subsidence and Groundwater-Flow model study area, southeast Texas.

[Dates are in month/day/year format]

Station identifier[1]	Station name	Latitude, in decimal degrees	Longitude, in decimal degrees	Period of record (may contain gaps)		
				Begin	End	Duration (in years)
USC00410204	ALVIN, TX US	29.36530	−95.23370	6/1/1898	11/30/2010	112.6
USR0000TANA	ANAHUAC NWR TEXAS, TX US	29.66920	−94.43830	6/6/1994	3/6/2019	24.8
USC00410235	ANAHUAC, TX US	29.78780	−94.63430	6/1/1909	2/1/2019	109.7
USC00410244	ANDERSON, TX US	30.48333	−95.98333	5/18/1914	9/30/1972	58.4
USC00410257	ANGLETON 2 W, TX US	29.15730	−95.45930	6/1/1895	12/31/2018	123.7
USC00410569	BAY CITY WATERWORKS, TX US	28.97980	−95.97490	10/1/1909	12/31/2018	109.3
USC00410586	BAYTOWN, TX US	29.91420	−94.99080	6/15/1946	12/31/2018	72.6
USC00410613	BEAUMONT RESRCH CTR, TX US	30.06880	−94.29270	9/1/1947	9/19/2019	72.1
USC00410611	BEAUMONT CITY, TX US	30.09690	−94.09970	11/1/1901	11/6/2019	118.1
USC00410635	BEDIAS, TX US	30.78333	−95.95000	3/8/1940	12/31/1985	45.8
USC00410655	BELLVILLE 6 NNE, TX US	30.03160	−96.21660	11/1/1978	3/6/2019	40.4
USC00410917	BON WIER, TX US	30.73333	−93.65000	1/1/1914	6/30/1988	74.5
USR0000TBRA	BRAZORIA NWR TEXAS, TX US	29.14170	−95.29170	6/6/1994	3/6/2019	24.8
USC00411048	BRENHAM, TX US	30.15910	−96.39720	1/1/1897	9/19/2019	122.8
USC00411094	BRONSON, TX US	31.35000	−94.01667	7/1/1924	12/31/1979	55.5
US1TXWL0009	BROOKSHIRE 6.9 NNW, TX US	29.87290	−96.00300	6/17/1998	11/17/2018	20.4
USC00411470	CARMONA, TX US	31.00000	−94.95000	8/1/1907	11/30/1915	8.3
USC00411810	CLEVELAND, TX US	30.36370	−95.08400	6/1/1954	3/31/2018	63.9
USC00411838	CLODINE, TX US	29.70670	−95.68780	1/1/1943	11/22/2011	68.9
US1TXSJ0003	COLDSPRING 4.3 SSW, TX US	30.53090	−95.14760	1/23/2012	2/1/2014	2.0
USC00411870	COLDSPRING 5 SSW, TX US	30.53333	−95.15000	6/1/1954	2/28/2002	47.8
USR0000TCLD	COLDSPRINGS TEXAS, TX US	30.31060	−95.08670	11/21/2001	3/6/2019	17.3
USW00003904	COLLEGE STATION EASTERWOOD FIELD, TX US	30.58917	−96.36472	8/1/1951	3/6/2019	67.6
USC00411888	COLLEGE STATION 6 SW, TX US	30.53333	−96.41667	5/1/1882	5/31/1984	102.2
USC00411911	COLUMBUS, TX US	29.69900	−96.57300	9/30/1903	9/12/2019	116.0
USR0000TCON	CONROE TEXAS, TX US	30.23640	−95.48280	1/1/1995	3/3/2019	24.2
USC00411956	CONROE, TX US	30.33020	−95.48310	8/16/1897	12/31/2018	121.5
USC00412206	CYPRESS, TX US	30.02100	−95.70690	1/1/1943	12/31/2018	76.0
USC00412218	DACUS, TX US	30.43640	−95.79190	6/1/1954	9/3/2012	58.3
USC00412266	DANEVANG 1 W, TX US	29.05670	−96.23190	3/1/1896	11/4/2019	123.8
USC00412770	EDNA 7 NW, TX US	29.06230	−96.77140	12/1/1995	5/28/2016	20.5

Table 4.1. Climate stations in and near the Gulf Coast Land Subsidence and Groundwater-Flow model study area, southeast Texas.—Continued

[Dates are in month/day/year format]

Station identifier[1]	Station name	Latitude, in decimal degrees	Longitude, in decimal degrees	Period of record (may contain gaps)		
				Begin	End	Duration (in years)
USC00412768	EDNA HIGHWAY 59 BRIDGE, TX US	28.96667	−96.68333	3/1/1968	11/30/1995	27.8
USC00413000	EVADALE, TX US	30.33333	−94.08333	8/24/1944	3/31/2004	59.6
USC00412786	EL CAMPO, TX US	29.20000	−96.26540	10/1/1941	11/6/2019	78.2
USC00413183	FLATONIA 4 SE, TX US	29.63400	−97.06450	1/1/1908	9/18/2019	111.8
USC00413298	FOUR NOTCH GUARD STATION, TX US	30.65000	−95.41667	7/1/1940	12/31/1964	24.5
USC00413340	FREEPORT 2 NW, TX US	28.98450	−95.38090	1/1/1931	3/6/2019	88.2
US1TXFB0032	FULSHEAR 2.7 WNW, TX US	29.70740	−95.93970	6/17/1998	12/18/2017	19.5
USW00012944	GALVESTON, TX US	29.33333	−94.77167	1/1/1897	3/31/2011	114.3
USW00012923	GALVESTON SCHOLES FIELD, TX US	29.27330	−94.85920	8/1/1946	11/6/2019	73.3
USC00413525	GIDDINGS 5 E, TX US	30.18720	−96.85940	3/1/1940	7/31/2019	79.5
USC00413778	GROVETON, TX US	31.19639	−95.14611	7/1/1923	6/30/2004	81.1
USC00414080	HEMPSTEAD, TX US	30.10000	−96.08333	9/30/1903	9/30/1978	75.1
USC00413873	HALLETTSVILLE 2 N, TX US	29.47050	−96.93970	1/1/1893	11/6/2019	126.9
USC00414313	HOUSTON BARKER, TX US	29.81420	−95.72760	1/1/1943	11/30/2013	71.0
USC00414315	HOUSTON DEER PARK, TX US	29.72833	−95.13056	8/1/1945	3/27/2011	65.7
USC00414321	HOUSTON HEIGHTS, TX US	29.79139	−95.42611	6/1/1948	2/19/2012	63.8
USC00414327	HOUSTON NORTH HOUSTON, TX US	29.87320	−95.52740	9/1/1947	12/31/2018	71.4
USC00414331	HOUSTON SPRING BRCH, TX US	29.80417	−95.49139	4/1/1954	12/31/2000	46.8
USC00414325	HOUSTON WESTBURY, TX US	29.66000	−95.62750	6/1/1948	3/3/2019	70.8
USW00012918	HOUSTON WILLIAM P HOBBY AIRPORT, TX US	29.63806	−95.28194	8/1/1930	3/3/2019	88.6
US1TXWK0003	HUNTSVILLE 11.5 WSW, TX US	30.62560	−95.71480	5/9/2009	3/3/2019	9.8
US1TXWK0004	HUNTSVILLE 12.3 NE, TX US	30.81940	−95.38510	5/9/2009	3/3/2019	9.8
USW00053903	HUNTSVILLE MUNICIPAL AIRPORT, TX US	30.74389	−95.58611	2/2/1997	3/2/2019	22.1
USR0000THUN	HUNTSVILLE TEXAS, TX US	30.45000	−95.40000	12/1/2000	9/3/2019	18.8
USC00414382	HUNTSVILLE, TX US	30.70650	−95.54210	1/1/1903	3/2/2019	116.2
USC00414563	JASPER, TX US	30.91520	−94.00970	9/20/1878	9/19/2019	141.1
USC00414575	JEDDO 3 S, TX US	29.76630	−97.31630	3/1/1940	12/31/2017	77.9
US1TXJS0003	KIRBYVILLE 1.5 SE, TX US	30.64050	−93.88510	12/8/2007	9/19/2019	11.8
USC00414819	KIRBYVILLE, TX US	30.61667	−93.91667	1/1/1929	2/28/1999	70.2
USC00414878	KOUNTZE, TX US	30.37500	−94.29940	6/1/1948	1/31/2019	70.7
USC00414903	LA GRANGE, TX US	29.91760	−96.87690	6/6/1910	12/26/2014	104.6
USC00415196	LIBERTY, TX US	30.05910	−94.79490	10/1/1903	12/31/2018	115.3
USC00415271	LIVINGSTON 2 NNE, TX US	30.73940	−94.92560	3/1/1937	10/29/2018	81.7
USW00093987	LUFKIN ANGELINA CO AIRPORT, TX US	31.23611	−94.75444	10/1/1906	9/18/2019	113.0
USC00415477	MADISONVILLE, TX US	30.93920	−95.92040	9/1/1918	3/6/2019	100.6
USC00415496	MAGNOLIA 1 W, TX US	30.21667	−95.78333	6/1/1954	6/30/1986	32.1
USC00415659	MATAGORDA 2, TX US	28.68350	−95.97330	7/1/1910	9/30/2018	108.3
USC00416024	MONTGOMERY, TX US	30.39070	−95.69700	6/1/1954	3/3/2019	64.8
USC00416280	NEW CANEY 2 E, TX US	30.13740	−95.17830	1/1/1952	12/5/2017	66.0
USC00416286	NEW GULF, TX US	29.26667	−95.89500	6/1/1946	2/28/1999	52.8

Table 4.1. Climate stations in and near the Gulf Coast Land Subsidence and Groundwater-Flow model study area, southeast Texas.—Continued

[Dates are in month/day/year format]

Station identifier[1]	Station name	Latitude, in decimal degrees	Longitude, in decimal degrees	Period of record (may contain gaps)		
				Begin	End	Duration (in years)
USC00416339	NEWTON, TX US	30.85000	−93.76667	1/1/1966	3/31/1977	11.3
USC00416341	NEWTON, TX US	30.83300	−93.73690	1/1/1980	9/30/2013	33.8
USC00416664	ORANGE, TX US	30.08580	−93.74160	1/1/1897	8/31/2018	121.7
USW00012935	PALACIOS MUNICIPAL AIRPORT, TX US	28.72472	−96.25361	2/1/1943	3/5/2019	76.1
USC00417020	PIERCE 1 E, TX US	29.23530	−96.18160	5/1/1904	9/30/2014	110.5
USC00417040	PINELAND, TX US	31.24470	−93.96570	1/23/1965	5/23/2019	54.4
US1TXSJ0011	POINT BLANK 0.7 ESE, TX US	30.74070	−95.20720	10/12/2014	3/2/2019	4.4
US1TXSJ0010	POINT BLANK 5.8 N, TX US	30.83040	−95.21160	6/17/1998	3/2/2019	20.7
USC00417173	PORT ARTHUR WEATHER BUREAU CITY, TX US	29.86667	−93.93333	3/1/1911	12/31/1967	56.9
USW00012917	PORT ARTHUR SE TX REGIONAL AIRPORT, TX US	29.95056	−94.02056	10/1/1947	3/6/2019	71.5
USC00417182	PORT LAVACA 2, TX US	28.61667	−96.63333	2/1/1901	2/29/1988	87.1
US1TXCLH012	PORT LAVACA 6.8 W, TX US	28.60040	−96.73140	7/3/2012	9/18/2019	7.2
USC00417183	PORT LAVACA, TX US	28.60790	−96.64160	2/1/1982	10/5/2015	33.7
USC00417586	RICHARDS, TX US	30.53810	−95.84580	6/1/1954	7/31/2013	59.2
USC00417594	RICHMOND, TX US	29.58380	−95.75520	6/1/1919	3/6/2019	99.8
USC00417651	RIVERSIDE, TX US	30.85000	−95.40000	7/27/1903	1/31/1970	66.6
USC00417693	ROCK ISLAND, TX US	29.53333	−96.58333	1/1/1899	10/31/1907	8.8
USC00417756	ROSENBERG, TX US	29.55000	−95.78333	9/1/1900	2/29/1960	59.5
USC00417875	SABINE, TX US	29.71667	−93.86667	11/10/1898	12/31/1903	5.1
USC00417936	SAM RAYBURN DAM, TX US	31.06190	−94.10110	1/1/1968	9/19/2019	51.8
USC00418126	SCHULENBURG, TX US	29.68250	−96.85630	1/1/1926	9/17/2019	93.8
USC00418160	SEALY, TX US	29.77139	−96.14556	10/1/1910	3/31/2003	92.6
USC00418519	SPEAKS 2, TX US	29.27280	−96.68580	1/1/1967	7/31/2019	52.6
USC00418728	SUGAR LAND, TX US	29.61833	−95.63583	4/1/1893	6/21/2013	120.3
USC00418996	THOMPSONS 3 WSW, TX US	29.48210	−95.63140	2/1/1942	8/31/2019	77.6
USC00419068	TOLEDO BEND DAM, TX US	31.17500	−93.56528	7/1/1975	11/30/2004	29.4
USC00169074	TOLEDO BEND LAKE, LA US	31.20210	−93.57260	12/1/2004	9/19/2019	14.8
USC00419139	TRINITY, TX US	30.95000	−95.38333	5/1/1900	5/31/1907	7.1
USC00419365	VICTORIA CP AND L, TX US	28.78750	−97.01056	1/1/1893	3/31/2003	110.3
USW00012912	VICTORIA REGIONAL AIRPORT, TX US	28.86140	−96.93030	11/4/1941	9/18/2019	77.9
USC00419448	WALLER, TX US	30.04861	−95.92500	1/1/1943	4/30/1999	56.4
USC00419491	WASHINGTON STATE PARK, TX US	30.32370	−96.15940	4/1/1915	2/26/2019	104.0
USC00419655	WHARTON, TX US	29.31770	−96.08470	5/1/1902	2/24/2019	116.9
USC00419898	WOODVILLE, TX US	30.76770	−94.41160	9/1/1988	5/31/2019	30.8
USC00419952	YOAKUM, TX US	29.27380	−97.15550	7/1/1917	9/19/2019	102.3

[1]Climate stations and data used for running the Soil-Water-Balance code are from National Climatic Data Center (2019).

Appendix 5. Historical Subsidence Contour Maps

Historical contour maps were used to estimate the rate and magnitude of subsidence in the greater Houston area. The general process for converting these contour maps into subsidence target data involved first downloading subsidence contour maps in portable document format (PDF) for the periods of interest from the source publications, which consisted of the 1906–43 and 1943–64 maps from Jorgensen (1975), the 1964–73 map from Gabrysch and Bonnet (1975), the 1973–78 and 1906–78 maps from Gabrysch (1980b), and the 1978–87 map from Gabrysch and Coplin (1990). The PDFs associated with each subsidence contour map were then clipped to remove extraneous information from the map (explanation, figure title, etc.) before exporting each map as a high-resolution (600 pixels per inch) image in tagged image file format (TIFF). Each subsidence contour map was then fit to a display in ArcMap, with a shapefile of county boundaries in the Houston area as a background layer. A minimum of four control points (typically county boundary intersections distributed outside the area of interest, if possible) common to both the non-georeferenced subsidence contour map in question and the shapefile of county boundaries were selected so that each of these points in the contour map could be linked to the corresponding point in the shapefile of county boundaries. Once the control points were linked, the subsidence contour map was transformed, thereby georeferencing it to the same projection as the shapefile of county boundaries. Once the TIFFs corresponding to the six subsidence contour maps used as source data in conjunction with the modeling effort (1906–43, 1943–64, 1964–73, 1973–78, 1978–87, and 1906–78) were georeferenced, the subsidence contours on each of the maps were digitized such that the resulting shapefiles were also georeferenced. A shapefile containing extensometer locations was then used to evaluate the subsidence during each of the six periods of interest (1906–43, 1943–64, 1964–73, 1973–78, 1978–87, and 1906–78; figs. 5.1–5.6) at each extensometer location and then compared to nearby benchmark data.

The 1906–43 and 1906–78 subsidence contour maps were modified from the published maps through the inclusion of additional contour intervals of subsidence in these maps. This was performed to capture minor amounts of subsidence for these periods to estimate subsidence during the model period (1897–2018).

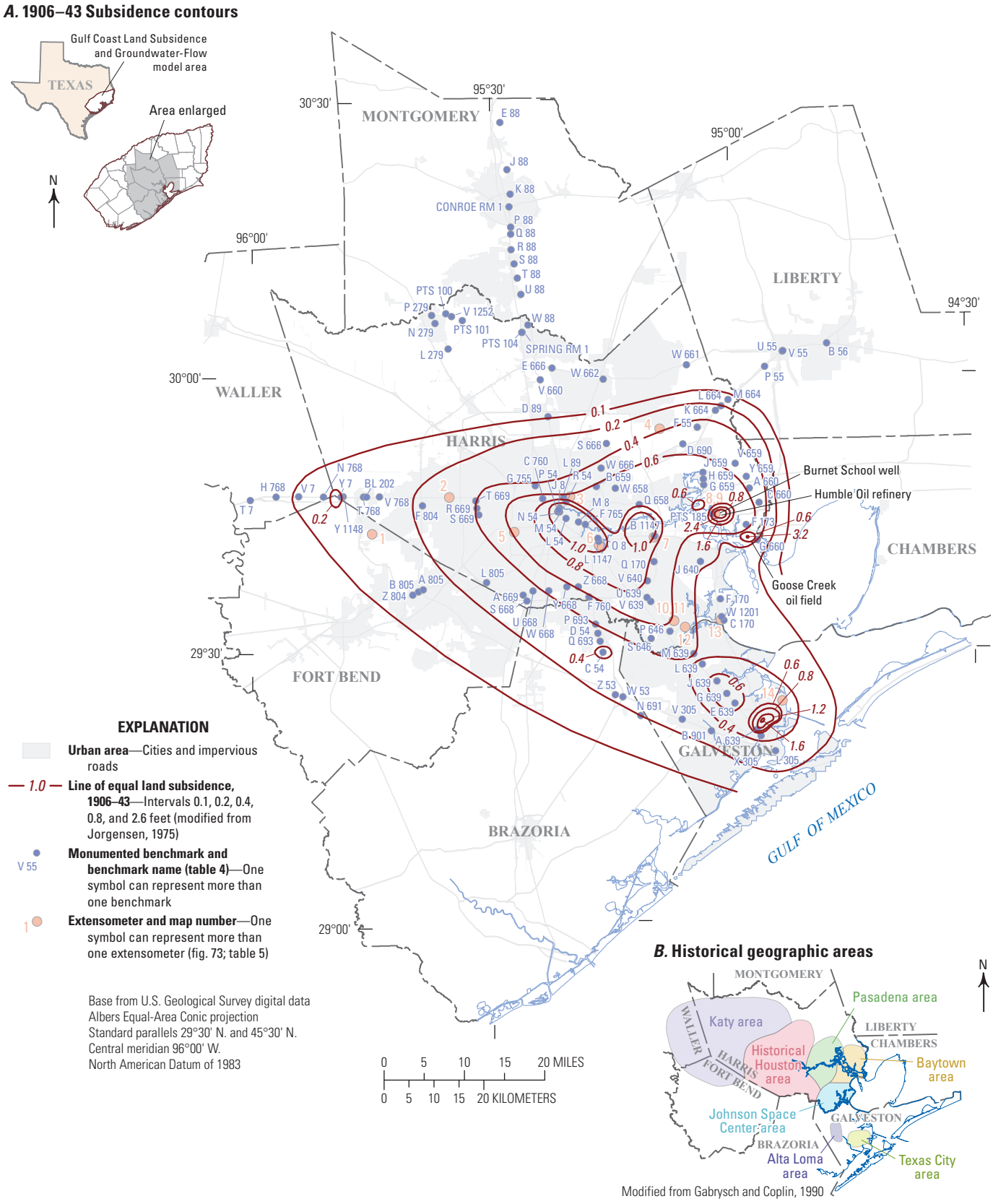

Figure 5.1. *A*, Approximate land-surface subsidence, 1906–43, and *B*, historical geographic areas in the greater Houston area, Gulf Coast aquifer system study area, southeast Texas.

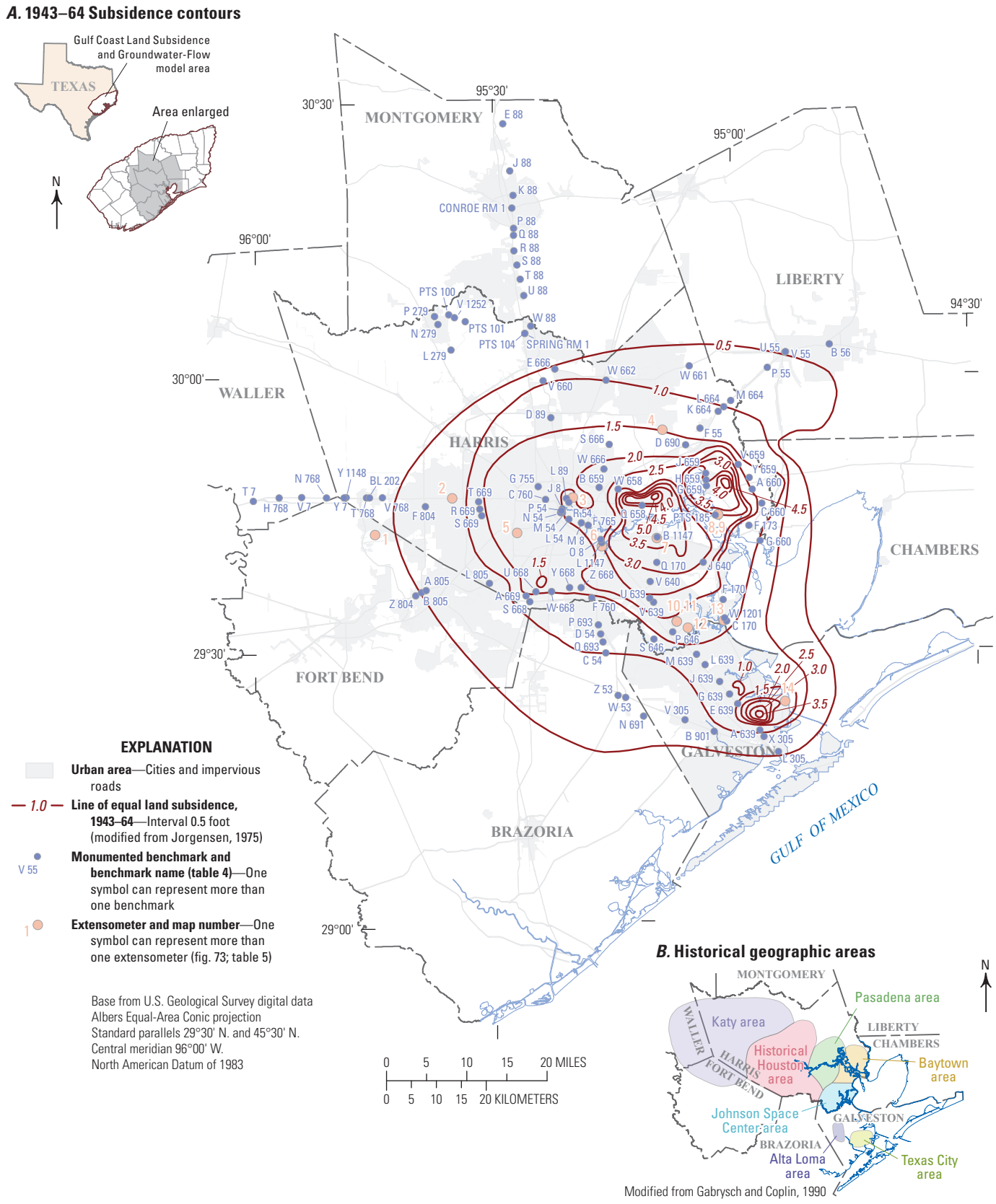

Figure 5.2. *A*, Approximate land-surface subsidence, 1943–64, and *B*, historical geographic areas in the greater Houston area, Gulf Coast aquifer system study area, southeast Texas.

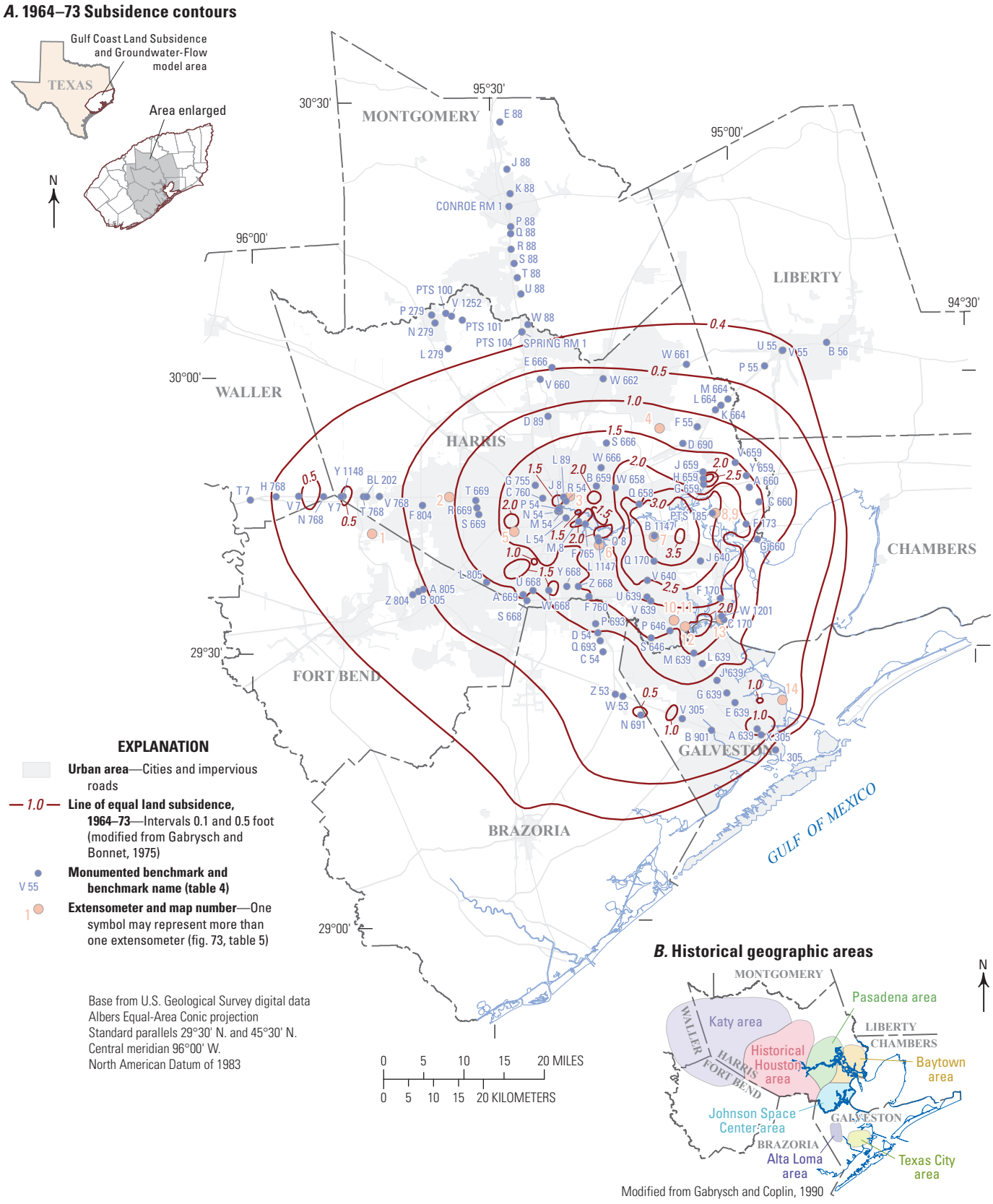

Figure 5.3. *A*, Approximate land-surface subsidence, 1964–73, and *B*, historical geographic areas in the greater Houston area, Gulf Coast aquifer system study area, southeast Texas.

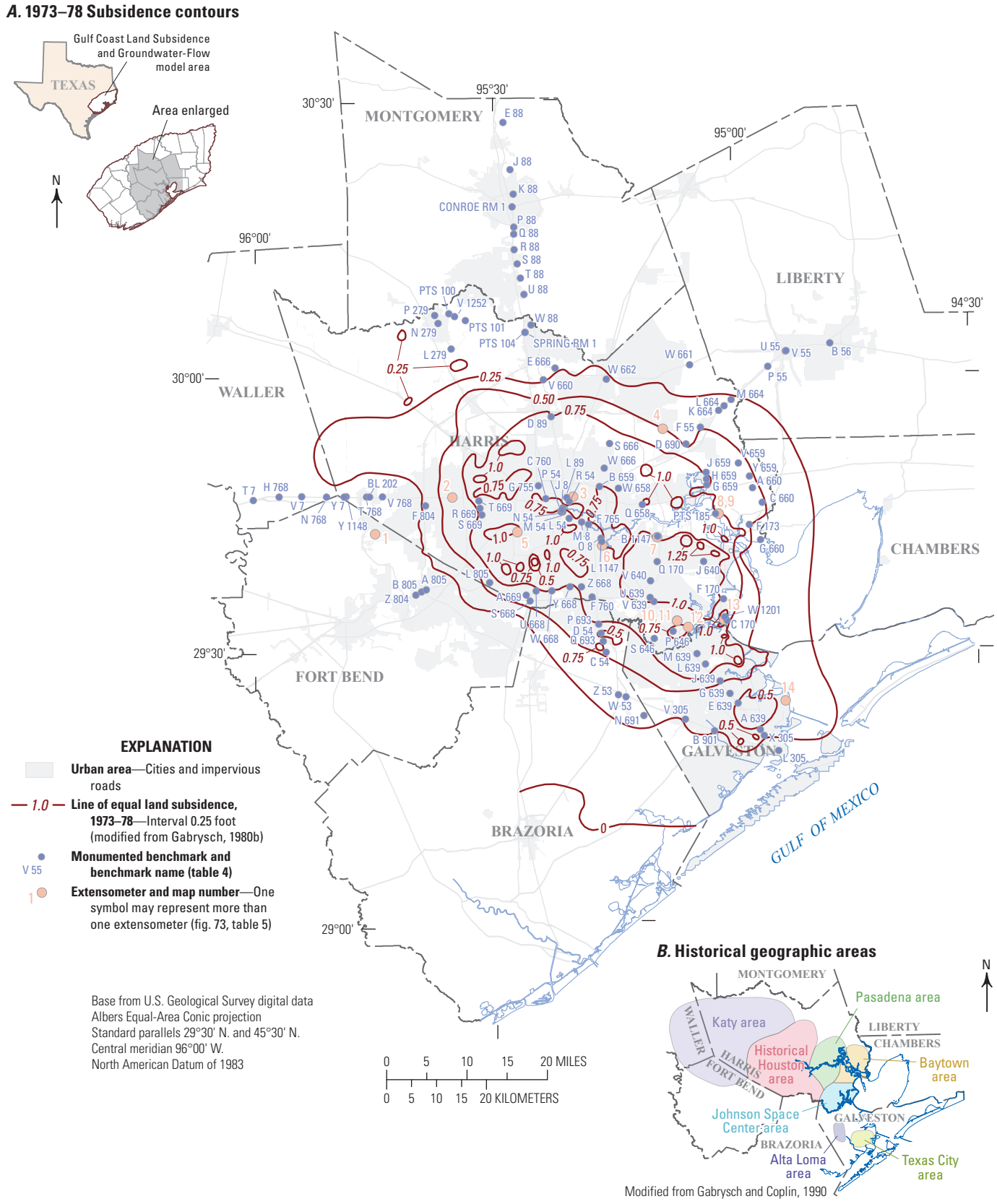

Figure 5.4. *A*, Approximate land-surface subsidence, 1973–78, and *B*, historical geographic areas in the greater Houston area, Gulf Coast aquifer system study area, southeast Texas.

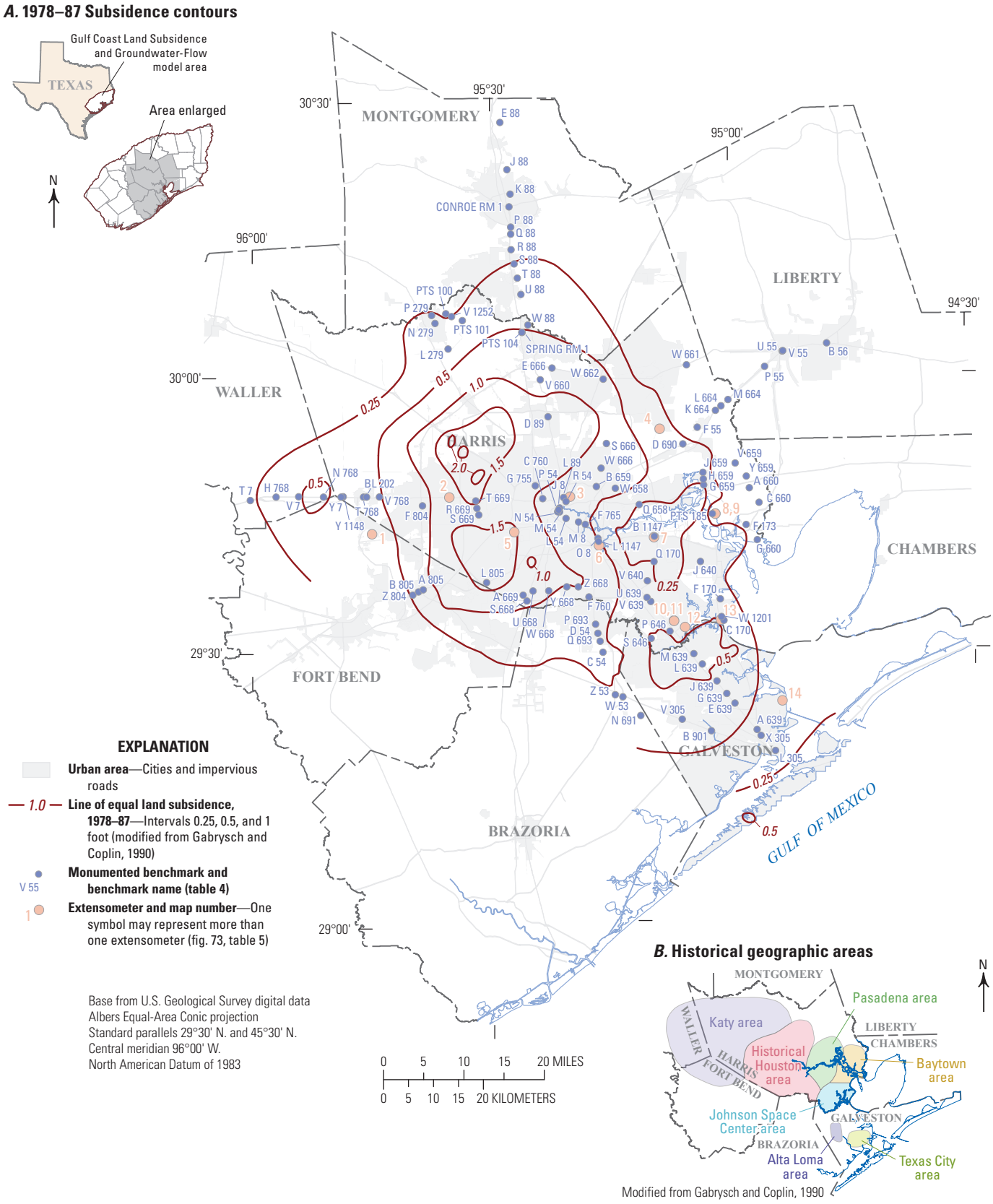

Figure 5.5. *A*, Approximate land-surface subsidence, 1978–87, and *B*, historical geographic areas in the greater Houston area, Gulf Coast aquifer system study area, southeast Texas.

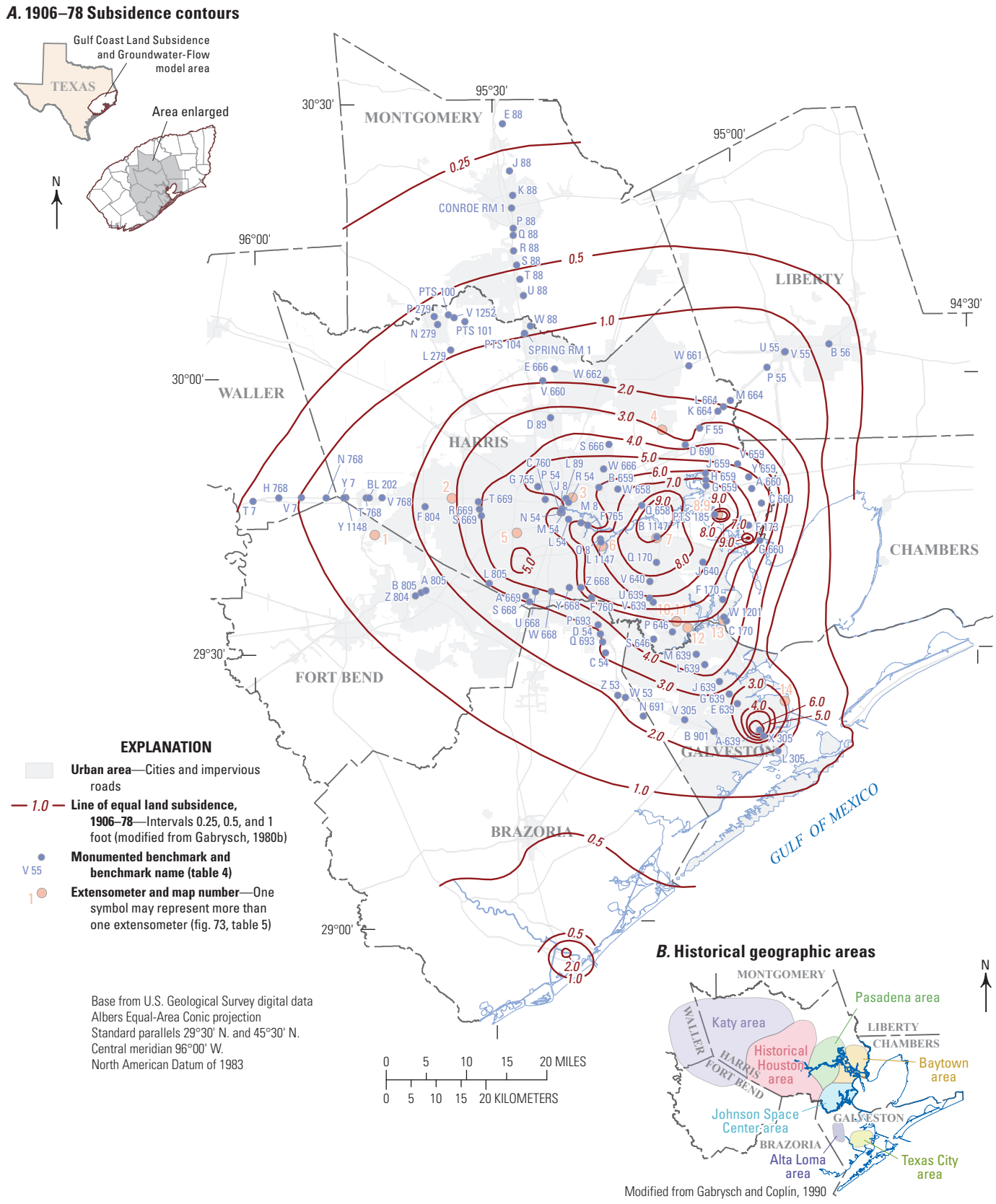

Figure 5.6. *A*, Approximate land-surface subsidence, 1906–78, and *B*, historical geographic areas in the greater Houston area, Gulf Coast aquifer system study area, southeast Texas.

Appendix 6. Global Navigation Satellite System Survey Uncertainty

An important component of the use of a Global Positioning System (GPS) for high accuracy vertical positioning surveys is establishing the measurement uncertainty through comparison with the elevation at a stable benchmark. The greater Houston area has undergone considerable subsidence through 2021, prompting the National Geodetic Survey (NGS) to suppress height information at benchmarks for this area beginning in March 2021 (NOAA, 2021b) except for a limited number of sites that are listed on the Southeast Texas Valid Orthometric Heights web page (NOAA, 2021c). This NOAA web page includes three of the four Continuously Operating Reference Station GPS sites (ADKS, NETP, and LHKU; fig. 75) with GPS receivers mounted on the inner stem of the Addicks, Northeast, and Lake Houston extensometers, respectively. Thus, the measurement uncertainty of the GPS equipment was assessed at monumented benchmarks located on the inner stem of the Addicks and Northeast extensometers and is documented in tables 6.1 and 6.2.

The first measurement uncertainty test was conducted at the Addicks extensometer (fig. 73, table 5) at monumented benchmark ADDICKS 1795 RESET 1991 (table 4) by using GPS measurements in conjunction with differential leveling techniques. Minor subsidence and uplift of the sediment below the inner stem of this extensometer have occurred between 1976 and 2021, as discussed in the "Global Navigation Satellite System Surveys" section. However, this benchmark was reoccupied in January 2021, which was 7 months prior to this measurement accuracy test. Thus, any discrepancies resulting from this 7-month period were expected to be minor. Additionally, the January 2021 benchmark reoccupation elevation provided was referenced to NAVD 88; therefore, any error resulting from a datum conversion was minimized. A temporary control point was set up and an elevation measurement was made by using the GPS in order to compare the GPS-derived elevation to the January 2021 known elevation at the monumented benchmark. By using a combination of a Trimble R8 survey-grade GPS receiver and a total station, the difference between the January 2021 elevation of the inner-stem benchmark (93.84 feet [ft]; table 4) and the USGS reoccupation control point (93.95 ft) was 0.11 ft. Using a combination of a Trimble R8 survey-grade GPS receiver and a level resulted in the same 0.11-ft difference compared to ADDICKS 1795 RESET 1991.

A second measurement uncertainty test was performed at the Northeast extensometer (fig. 73, table 5) at two monumented benchmarks (NORTHEAST 2250, NORTHEAST 2250 RESET; table 4) by using the same procedures as used at the Addicks site. The Northeast extensometer was installed in 1980 (table 5); therefore, the elevation of the extensometer inner stem was not determined during the 1976 leveling survey. As a result, only a single measurement for this benchmark was available in 1987. In 1987, the benchmark elevations at this site available from the NGS were 49.27 ft and 49.68 ft at benchmarks NORTHEAST 2250 and NORTHEAST 2250 RESET, respectively (table 4). The NETP GPS station data indicate an inner stem elevation uplift of 0.04 ft during 1993–2020 (HGSD, 2021); therefore, the 2021 elevations of these benchmarks are expected to be about 49.31 ft and 49.72 ft, respectively, although changes in elevation are not known between 1987 and 1993. By using a combination of a Trimble R8 survey-grade GPS receiver and a level, the difference between the estimated 2021 elevations at the benchmarks (49.31 ft and 49.72 ft, respectively) and the USGS reoccupation control points (49.41 ft and 49.82 ft, respectively; table 4) was 0.10 ft for both benchmarks.

The GPS method uncertainty estimated at these two extensometer sites is between 0.10 and 0.11 ft, which is similar to the vertical precision of 0.16 ft for a Level II survey from Rydlund and Densmore (2012). This 0.10–0.11-ft uncertainty was thus applied to the 2021 elevations at the benchmarks reoccupied by the USGS listed in table 4 determined using GNSS methods.

Table 6.1. Real-Time Network direct surveys of selected benchmarks in the study area in southeast Texas.

[PID, permanent identifier; ft, foot; RMSE, root mean square error; PDOP, position dilution of precision; dates are in month/day/year format]

PID, measurement number	Date	Latitude, in decimal degrees	Longitude, in decimal degrees	Ellipsoid height (ft)	Elevation (ft)	Mean elevation (ft)[1]	Horizontal precision (ft)	Vertical precision (ft)	RMSE (ft)	PDOP	Number of positions	Number of satellites observed	Antenna height (ft)[2]
CONROE RM 1 (fig. 70*A*)													
BL1256-1	7/26/2021	30.31228	−95.45913	117.91	208.22	208.22	0.015	0.03	28.95	2.1	303	8	6.939
BL1256-2	7/26/2021	30.31228	−95.45913	117.94	208.24		0.013	0.02	10.92	1.3	303	9	6.939
BL1256-1	8/20/2020	30.31228	−95.45913	117.91	208.22		0.009	0.02	10.34	1.1	193	15	6.119
BL1256-2	8/20/2020	30.31228	−95.45913	117.91	208.21		0.008	0.02	14.76	1.5	187	14	6.119
K 88 (fig. 70*A*)													
BL1260-1	7/26/2021	30.33530	−95.45654	141.14	231.40	231.40	0.011	0.02	12.42	1.9	306	10	6.939
BL1260-2	7/26/2021	30.33530	−95.45654	141.12	231.38		0.01	0.02	9.18	1.2	309	10	6.939
BL1260-1	8/20/2020	30.33530	−95.45654	141.17	231.43		0.017	0.04	22.49	1.6	186	16	6.119
BL1260-2	8/20/2020	30.33530	−95.45654	141.12	231.38		0.019	0.04	16.11	1.5	184	16	6.119
BL1260-3	8/20/2020	30.33530	−95.45654	141.22	231.48		0.015	0.03	22.40	2.0	184	11	6.119
BL1260-4	8/20/2020	30.33530	−95.45654	141.09	231.35		0.014	0.02	13.62	2.1	183	11	6.119
Q 88 (fig. 70*A*)													
BL1166-1	4/7/2021	30.26264	−95.45592	38.95	129.31	129.32	0.031	0.07	41.00	2.4	219	11	6.119
BL1166-2	4/7/2021	30.26264	−95.45592	38.97	129.33		0.027	0.06	46.51	2.3	188	12	6.119
BL1166-1	7/26/2021	30.26264	−95.45592	38.79	129.15	129.17	0.034	0.08	35.35	2.8	305	10	6.939
BL1166-2	7/26/2021	30.26264	−95.45592	38.83	129.19		0.016	0.03	31.77	2.9	304	10	6.939
R 88 (fig. 70*A*)													
BL1169-1	4/7/2021	30.23429	−95.45557	30.62	120.98	121.03	0.021	0.04	16.63	1.8	194	14	6.119
BL1169-2	4/7/2021	30.23429	−95.45557	30.64	121.01		0.025	0.05	21.11	1.7	184	14	6.119
BL1169-1	7/26/2021	30.23429	−95.45557	30.69	121.06		0.024	0.04	18.19	1.7	305	13	6.939
BL1169-2	7/26/2021	30.23429	−95.45557	30.68	121.05		0.019	0.03	23.17	1.5	317	13	6.939
V 1252 (fig. 70*A*)													
B1877-3	4/16/2021	30.11339	−95.58102	58.86	149.73	149.73	0.024	0.05	40.11	2.1	183	15	6.562
B1877-4	4/16/2021	30.11339	−95.58102	58.85	149.73		0.022	0.04	32.77	1.7	182	14	6.562
BL1877-1	9/2/2021	30.11339	−95.58102	59.25	149.72		0.031	0.06	23.73	2.3	298	10	6.562
BL1877-2	9/2/2021	30.11339	−95.58102	59.37	149.75		0.015	0.03	19.25	2.4	305	10	6.562
SPRING RM 1 (fig. 70*A*)													
B1291-1	4/16/2021	30.08404	−95.43364	33.56	124.18	124.18	0.018	0.04	13.51	2.3	182	10	6.562
B1291-2	4/16/2021	30.08404	−95.43364	33.56	124.18		0.02	0.04	11.34	1.7	190	10	6.562

Table 6.1. Real-Time Network direct surveys of selected benchmarks in the study area in southeast Texas.—Continued

[PID, permanent identifier; ft, foot; RMSE, root mean square error; PDOP, position dilution of precision; dates are in month/day/year format]

PID, measurement number	Date	Latitude, in decimal degrees	Longitude, in decimal degrees	Ellipsoid height (ft)	Elevation (ft)	Mean elevation (ft)[1]	Horizontal precision (ft)	Vertical precision (ft)	RMSE (ft)	PDOP	Number of positions	Number of satellites observed	Antenna height (ft)[2]
Y 7 (fig. 70*A*)													
AW0134-1	8/23/2021	29.78596	−95.81980	49.83	140.01	139.99	0.023	0.05	32.31	1.8	192	12	6.562
AW0134-2	8/23/2021	29.78596	−95.81980	49.78	139.96		0.024	0.05	22.85	2.4	299	13	6.562
AW0134-1	8/24/2021	29.78596	−95.81980	49.99	140.18	140.09	0.036	0.06	28.24	2.0	301	13	7.382
AW0134-2	8/24/2021	29.78596	−95.81980	49.81	140.00		0.025	0.05	48.57	1.8	307	12	7.382
Y 1148 (fig. 70*A*)													
AW0135-1	8/23/2021	29.78649	−95.81541	49.93	140.82	140.85	0.028	0.06	49.05	2.4	291	11	6.562
AW0135-2	8/23/2021	29.78649	−95.81541	49.92	140.88		0.022	0.04	35.54	2.3	299	12	6.562
AW0135-1	8/24/2021	29.78649	−95.81542	50.64	140.11	140.11	0.027	0.05	84.64	1.9	264	11	7.382
AW0135-2	8/24/2021	29.78649	−95.81542	50.70	140.11		0.024	0.05	39.67	1.9	302	11	7.382

[1]For sites where three or more measurements (each on separate days) were taken, the elevation value specified in table 4 was determined as the mean of two measurements with the closest elevations. As an example, for benchmark Q 88, the elevation of 129.33 ft listed in table 4 is the mean of the measurements taken on 4/7/21 from this table (129.32 ft) and 8/30/21 from table 6.2 (129.33 ft).

[2]Antenna height is measured for quality control regarding the potential for systematic error.

Table 6.2. Real-Time Network indirect surveys of selected benchmarks in the study area in southeast Texas.

[PID, permanent identifier; ft, foot; RMSE, root mean square error; PDOP, position dilution of precision; dates are in month/day/year format]

PID, measurement number	Date	Latitude, in decimal degrees	Longitude, in decimal degrees	Ellipsoid height (ft)	Horizontal precision (ft)	Vertical precision (ft)	RMSE (ft)	PDOP	Number of positions	Number of satellite views	Antenna height (ft)[1]	Control point 1 elevation (ft)[2]	Elevation mean (ft)[2]	Back shot (ft)[2]	Instrument elevation (ft)[2]	Front shot (ft)[2]	Benchmark elevation (ft)[2]
E 88 (fig. 70*A*)																	
BL1278-1	8/30/2021	30.46568	−95.47752	244.97	0.01	0.03	14.75	1.8	634.0	14	6.56	334.85	334.85	6.00	340.85	1.12	339.73
BL1278-2	8/30/2021	30.46568	−95.47752	244.97	0.02	0.03	34.12	1.6	299.0	12	6.56	334.85					
BL1278-1	9/2/2021	30.46571	−95.47749	244.80	0.02	0.04	31.00	1.6	302.0	14	6.56	334.69	334.69	6.61	341.29	1.47	339.82
BL1278-2	9/2/2021	30.46571	−95.47749	244.80	0.02	0.03	23.14	1.5	326.0	13	6.56	334.68					
Q 88 (fig. 70*A*)																	
BL1166-1	8/30/2021	30.26333	−95.4558	40.49	0.02	0.03	16.57	1.5	308.0	12	6.56	130.85	130.86	2.72	133.57	4.24	129.33
BL1166-2	8/30/2021	30.26333	−95.4558	40.50	0.01	0.03	15.59	1.6	326.0	12	6.56	130.86					
SPRING RM 1 (fig. 70*A*)																	
BL1291-1	8/30/2021	30.08417	−95.43368	34.35	0.01	0.02	13.83	1.8	299.0	14	6.56	124.57	124.57	4.44	129.01	4.80	124.21
BL1291-2	8/30/2021	30.08417	−95.43368	34.35	0.01	0.01	10.00	0.8	300.0	14	6.56	124.57					
Y 7 (fig. 70*A*)																	
AW0134-1	8/30/2021	29.78593	−95.81953	49.94	0.02	0.04	18.57	1.7	298.0	12	6.56	140.13	140.15	4.49	144.64	4.74	139.90
AW0134-2	8/30/2021	29.78593	−95.81953	49.97	0.02	0.03	24.43	1.7	304.0	12	6.56	140.16					
Y 1148 (fig. 70*A*)																	
AW0135-1	8/30/2021	29.78628	−95.81533	49.77	0.02	0.03	24.23	2.0	331.0	13	6.56	139.96	139.97	4.69	144.65	4.92	139.73
AW0135-2	8/30/2021	29.78628	−95.81533	49.79	0.01	0.02	10.54	1.7	299.0	14	6.56	139.97					
AW0135-1	9/2/2021	29.78629	−95.81533	50.03	0.02	0.04	17.98	1.9	302.0	11	6.56	140.21	140.19	4.53	144.71	4.64	140.07
AW0135-2	9/2/2021	29.78629	−95.81533	49.97	0.02	0.03	22.73	1.9	330.0	12	6.56	140.16					
ADDICKS 1795 RESET 1991 (fig. 70*A*)																	
AA9583-1	8/5/2021	29.79078	−95.58665	−0.31	0.016	0.02	12.85	2.0	532.0	11	6.56	89.74	89.74	4.51	94.24	0.29	93.95
AA9583-2	8/5/2021	29.79078	−95.58665	−0.32	0.011	0.02	14.44	1.8	303.0	11	6.56	89.73					
CLEAR LAKE 3072 (fig. 70*A*)																	
AW1090	8/2/2021	29.56366	−95.11933	−71.117	0.012	0.02	15.17	2.1	331.0	12	6.56	17.77	17.77	5.89	23.66	2.15	21.51
CLEAR LAKE 3072 RESET (fig. 70*A*)																	
AW5587	8/2/2021	29.56366	−95.11919	−71.117	0.012	0.02	15.17	2.1	331.0	12	6.56	17.77	17.77	5.89	23.66	2.09	21.57
NORTHEAST 2250 (fig. 70*A*)																	
AW4835-1	8/10/2021	29.79118	−95.33421	−42.86	0.016	0.024	11.13	1.8	310.0	10	6.56	46.85	46.85	4.66	51.51	2.10	49.41

Table 6.2. Real-Time Network indirect surveys of selected benchmarks in the study area in southeast Texas.—Continued

[PID, permanent identifier; ft, foot; RMSE, root mean square error; PDOP, position dilution of precision; dates are in month/day/year format]

PID, measurement number	Date	Latitude, in decimal degrees	Longitude, in decimal degrees	Ellipsoid height (ft)	Horizontal precision (ft)	Vertical precision (ft)	RMSE (ft)	PDOP	Number of positions	Number of satellite views	Antenna height (ft)[1]	Control point 1 elevation (ft)[2]	Elevation mean (ft)[2]	Back shot (ft)[2]	Instrument elevation (ft)[2]	Front shot (ft)[2]	Benchmark elevation (ft)[2]
NORTHEAST 2250 RESET (fig. 70*A*)																	
AW5561-1	8/10/2021	29.79118	−95.33421	−42.86	0.016	0.024	11.13	1.8	310.0	10	6.56	46.85	46.85	4.66	51.50	1.68	49.82

[1]Antenna height is measured for quality control regarding the potential for systematic error.

[2]The values for the control point (and thus the elevation mean), back shot, and front shot on this table are rounded to two decimal places based on the field data. Therefore, the instrument elevation and (or) the benchmark elevation may differ slightly from the sum of the elevation mean and back shot (for the instrument elevation) and the sum of the instrument elevation and the front shot (for the benchmark elevation). For sites where three or more measurements (each on separate days) were taken, the elevation value specified in table 4 was determined as the mean of two measurements with the closest elevations. As an example, for benchmark Q 88, the benchmark elevation of 129.33 ft listed in table 4 is the mean of the measurements taken on 4/7/21 from this table (129.32 ft) and 8/30/21 from table 6.2 (129.33 ft).

Appendix 7. Model Temporal Discretization, History Matching, and Uncertainty Analysis with PESTPP-IES

The Gulf Coast Land Subsidence and Groundwater-Flow model (GULF model) was discretized into 288 stress periods: a steady-state stress period, 267 historical transient stress periods, and 20 forecast transient stress periods. Owing to the relatively few groundwater-level measurements available in the early 1900s, the first three transient stress periods (2–4, table 7.1) are 14 or 15 years in length. The model simulates 5-year transient stress periods (5–10, table 7.1) from January 1940 to December 1969 because of the increased availability of groundwater-level data during this period. Annual stress periods (11–40, table 7.1) are used from January 1970 to December 1999, and monthly stress periods (41–268, table 7.1) are used from January 2000 to December 2018.

Workflow Summary

History matching and uncertainty analysis of the GULF model was performed by using PESTPP-IES, which is included in the PEST++ software suite (White and others, 2020a). Pre- and postprocessing were performed by using the Python packages FloPy (Bakker and others, 2016) and pyEMU (White and others, 2016b). All software packages used in this analysis are open source and publicly available. Software executable files, input files, and helper scripts used to produce the results of this report are available in a supplementary data release (Knight and others, 2023).

The following is an outline of the workflow and a description of the primary software options to select that lead to the results presented in this report.

1. Parameterize model inputs.
2. Develop a prior parameter distribution.
3. Build and run a prior ensemble of models (the "Prior") containing parameter values drawn from the prior parameter distribution.
4. Evaluate the modeled results and condition the Prior.
5. Starting with the Prior, use an iterative algorithm that evaluates model fit to historical observations to develop an updated history-matched posterior model distribution.
6. Condition the posterior ensemble of models (the "Posterior") on the basis of evaluation of model fit and reasonableness of parameter values.
7. Use the Posterior to simulate future withdrawal and enhanced recharge scenarios.

Model Parameterization

The Python package pyEMU was used to build a PEST++ control file and associated template and control files to serve as an interface to parameterize model inputs. Adjustable parameters included multipliers that modify the underlying original model property values. The upper and lower limits of the multiplier parameters implied the uncertainty of the underlying original model property values at different spatial or temporal scales. This Python package was also used to define the prior parameter distribution and build the Prior to draw parameter values from the distribution. A large number of model realizations were drawn from the prior parameter distribution according to the defined mean and covariance of the parameters.

Prior Parameter Ensemble

Uncertainties in model parameters and outputs can be obtained by using a Bayesian uncertainty framework (Fienen and others, 2013). This requires the definition of a Prior that is based on expert knowledge and previous modeling results. The Prior includes a mean value and variance for every adjustable model parameter. The Prior for the GULF model is defined by using a truncated, multivariate Gaussian distribution. Model outputs were evaluated and compared to understand model behavior and sensitivities. History matching of transient groundwater-level observations was used to update the mean value and variance of the adjustable parameters, which resulted in the posterior parameter distribution. The Posterior consists of realizations (individual models) built with parameters drawn from this posterior parameter distribution.

Posterior Model Ensemble

PESTPP-IES (White, 2018) implements a form of the iterative ensemble smoother (IES) algorithm (Chen and Oliver, 2013), which minimizes a least-squares objective function (table 7.2) in high dimensions. PESTPP-IES accomplishes this in a manner similar to the Gauss-Levenberg-Marquardt (GLM) algorithm (Moré, 1978), but instead of filling a complete Jacobian matrix representing the first-order relation between every adjustable parameter and every observation, PESTPP-IES empirically estimates the Jacobian matrix from an ensemble of random parameter values. The Jacobian matrix contains the derivatives of each observation with respect to each parameter.

Table 7.1. Listing of stress periods for the Gulf Coast Land Subsidence and Groundwater-Flow model.

[NSTP, number of time steps; TSMULT, time step multiplier. All stress periods are transient except the first stress period. Dates are in month/day/year format]

Stress period[1,2]	Start date	End date	Stress period length, in days	NSTP	TSMULT
1	1896	1896	1	1	1
2	1/1/1897	12/31/1911	5,477	1	1
3	1/1/1912	12/31/1925	5,114	1	1
4	1/1/1926	12/31/1939	5,113	1	1
5	1/1/1940	12/31/1944	1,827	1	1
6	1/1/1945	12/31/1949	1,826	1	1
7	1/1/1950	12/31/1954	1,826	1	1
8	1/1/1955	12/31/1959	1,826	1	1
9	1/1/1960	12/31/1964	1,827	1	1
10	1/1/1965	12/31/1969	1,826	1	1
11	1/1/1970	12/31/1970	365	1	1
12	1/1/1971	12/31/1971	365	1	1
13	1/1/1972	12/31/1972	366	1	1
14	1/1/1973	12/31/1973	365	1	1
15	1/1/1974	12/31/1974	365	1	1
16	1/1/1975	12/31/1975	365	1	1
17	1/1/1976	12/31/1976	366	1	1
18	1/1/1977	12/31/1977	365	1	1
19	1/1/1978	12/31/1978	365	1	1
20	1/1/1979	12/31/1979	365	1	1
21	1/1/1980	12/31/1980	366	1	1
22	1/1/1981	12/31/1981	365	1	1
23	1/1/1982	12/31/1982	365	1	1
24	1/1/1983	12/31/1983	365	1	1
25	1/1/1984	12/31/1984	366	1	1
26	1/1/1985	12/31/1985	365	1	1
27	1/1/1986	12/31/1986	365	1	1
28	1/1/1987	12/31/1987	365	1	1
29	1/1/1988	12/31/1988	366	1	1
30	1/1/1989	12/31/1989	365	1	1
31	1/1/1990	12/31/1990	365	1	1
32	1/1/1991	12/31/1991	365	1	1
33	1/1/1992	12/31/1992	366	1	1
34	1/1/1993	12/31/1993	365	1	1
35	1/1/1994	12/31/1994	365	1	1
36	1/1/1995	12/31/1995	365	1	1
37	1/1/1996	12/31/1996	366	1	1
38	1/1/1997	12/31/1997	365	1	1
39	1/1/1998	12/31/1998	365	1	1
40	1/1/1999	12/31/1999	365	1	1
41	1/1/2000	1/31/2000	31	1	1
42	2/1/2000	2/29/2000	29	1	1
43	3/1/2000	3/31/2000	31	1	1
44	4/1/2000	4/30/2000	30	1	1
45	5/1/2000	5/31/2000	31	1	1
46	6/1/2000	6/30/2000	30	1	1
47	7/1/2000	7/31/2000	31	1	1
48	8/1/2000	8/31/2000	31	1	1
49	9/1/2000	9/30/2000	30	1	1
50	10/1/2000	10/31/2000	31	1	1
51	11/1/2000	11/30/2000	30	1	1
52	12/1/2000	12/31/2000	31	1	1
53	1/1/2001	1/31/2001	31	1	1
54	2/1/2001	2/28/2001	28	1	1
55	3/1/2001	3/31/2001	31	1	1
56	4/1/2001	4/30/2001	30	1	1
57	5/1/2001	5/31/2001	31	1	1
58	6/1/2001	6/30/2001	30	1	1
59	7/1/2001	7/31/2001	31	1	1
60	8/1/2001	8/31/2001	31	1	1
61	9/1/2001	9/30/2001	30	1	1
62	10/1/2001	10/31/2001	31	1	1
63	11/1/2001	11/30/2001	30	1	1
64	12/1/2001	12/31/2001	31	1	1
65	1/1/2002	1/31/2002	31	1	1
66	2/1/2002	2/28/2002	28	1	1
67	3/1/2002	3/31/2002	31	1	1
68	4/1/2002	4/30/2002	30	1	1
69	5/1/2002	5/31/2002	31	1	1
70	6/1/2002	6/30/2002	30	1	1
71	7/1/2002	7/31/2002	31	1	1
72	8/1/2002	8/31/2002	31	1	1
73	9/1/2002	9/30/2002	30	1	1
74	10/1/2002	10/31/2002	31	1	1
75	11/1/2002	11/30/2002	30	1	1
76	12/1/2002	12/31/2002	31	1	1
77	1/1/2003	1/31/2003	31	1	1
78	2/1/2003	2/28/2003	28	1	1
79	3/1/2003	3/31/2003	31	1	1
80	4/1/2003	4/30/2003	30	1	1
81	5/1/2003	5/31/2003	31	1	1
82	6/1/2003	6/30/2003	30	1	1

Table 7.1. Listing of stress periods for the Gulf Coast Land Subsidence and Groundwater-Flow model.—Continued

[NSTP, number of time steps; TSMULT, time step multiplier. All stress periods are transient except the first stress period. Dates are in month/day/year format]

Stress period[1,2]	Start date	End date	Stress period length, in days	NSTP	TSMULT
83	7/1/2003	7/31/2003	31	1	1
84	8/1/2003	8/31/2003	31	1	1
85	9/1/2003	9/30/2003	30	1	1
86	10/1/2003	10/31/2003	31	1	1
87	11/1/2003	11/30/2003	30	1	1
88	12/1/2003	12/31/2003	31	1	1
89	1/1/2004	1/31/2004	31	1	1
90	2/1/2004	2/29/2004	29	1	1
91	3/1/2004	3/31/2004	31	1	1
92	4/1/2004	4/30/2004	30	1	1
93	5/1/2004	5/31/2004	31	1	1
94	6/1/2004	6/30/2004	30	1	1
95	7/1/2004	7/31/2004	31	1	1
96	8/1/2004	8/31/2004	31	1	1
97	9/1/2004	9/30/2004	30	1	1
98	10/1/2004	10/31/2004	31	1	1
99	11/1/2004	11/30/2004	30	1	1
100	12/1/2004	12/31/2004	31	1	1
101	1/1/2005	1/31/2005	31	1	1
102	2/1/2005	2/28/2005	28	1	1
103	3/1/2005	3/31/2005	31	1	1
104	4/1/2005	4/30/2005	30	1	1
105	5/1/2005	5/31/2005	31	1	1
106	6/1/2005	6/30/2005	30	1	1
107	7/1/2005	7/31/2005	31	1	1
108	8/1/2005	8/31/2005	31	1	1
109	9/1/2005	9/30/2005	30	1	1
110	10/1/2005	10/31/2005	31	1	1
111	11/1/2005	11/30/2005	30	1	1
112	12/1/2005	12/31/2005	31	1	1
113	1/1/2006	1/31/2006	31	1	1
114	2/1/2006	2/28/2006	28	1	1
115	3/1/2006	3/31/2006	31	1	1
116	4/1/2006	4/30/2006	30	1	1
117	5/1/2006	5/31/2006	31	1	1
118	6/1/2006	6/30/2006	30	1	1
119	7/1/2006	7/31/2006	31	1	1
120	8/1/2006	8/31/2006	31	1	1
121	9/1/2006	9/30/2006	30	1	1
122	10/1/2006	10/31/2006	31	1	1
123	11/1/2006	11/30/2006	30	1	1
124	12/1/2006	12/31/2006	31	1	1
125	1/1/2007	1/31/2007	31	1	1
126	2/1/2007	2/28/2007	28	1	1
127	3/1/2007	3/31/2007	31	1	1
128	4/1/2007	4/30/2007	30	1	1
129	5/1/2007	5/31/2007	31	1	1
130	6/1/2007	6/30/2007	30	1	1
131	7/1/2007	7/31/2007	31	1	1
132	8/1/2007	8/31/2007	31	1	1
133	9/1/2007	9/30/2007	30	1	1
134	10/1/2007	10/31/2007	31	1	1
135	11/1/2007	11/30/2007	30	1	1
136	12/1/2007	12/31/2007	31	1	1
137	1/1/2008	1/31/2008	31	1	1
138	2/1/2008	2/29/2008	29	1	1
139	3/1/2008	3/31/2008	31	1	1
140	4/1/2008	4/30/2008	30	1	1
141	5/1/2008	5/31/2008	31	1	1
142	6/1/2008	6/30/2008	30	1	1
143	7/1/2008	7/31/2008	31	1	1
144	8/1/2008	8/31/2008	31	1	1
145	9/1/2008	9/30/2008	30	1	1
146	10/1/2008	10/31/2008	31	1	1
147	11/1/2008	11/30/2008	30	1	1
148	12/1/2008	12/31/2008	31	1	1
149	1/1/2009	1/31/2009	31	1	1
150	2/1/2009	2/28/2009	28	1	1
151	3/1/2009	3/31/2009	31	1	1
152	4/1/2009	4/30/2009	30	1	1
153	5/1/2009	5/31/2009	31	1	1
154	6/1/2009	6/30/2009	30	1	1
155	7/1/2009	7/31/2009	31	1	1
156	8/1/2009	8/31/2009	31	1	1
157	9/1/2009	9/30/2009	30	1	1
158	10/1/2009	10/31/2009	31	1	1
159	11/1/2009	11/30/2009	30	1	1
160	12/1/2009	12/31/2009	31	1	1
161	1/1/2010	1/31/2010	31	1	1
162	2/1/2010	2/28/2010	28	1	1
163	3/1/2010	3/31/2010	31	1	1
164	4/1/2010	4/30/2010	30	1	1

Table 7.1. Listing of stress periods for the Gulf Coast Land Subsidence and Groundwater-Flow model.—Continued

[NSTP, number of time steps; TSMULT, time step multiplier. All stress periods are transient except the first stress period. Dates are in month/day/year format]

Stress period[1,2]	Start date	End date	Stress period length, in days	NSTP	TSMULT
165	5/1/2010	5/31/2010	31	1	1
166	6/1/2010	6/30/2010	30	1	1
167	7/1/2010	7/31/2010	31	1	1
168	8/1/2010	8/31/2010	31	1	1
169	9/1/2010	9/30/2010	30	1	1
170	10/1/2010	10/31/2010	31	1	1
171	11/1/2010	11/30/2010	30	1	1
172	12/1/2010	12/31/2010	31	1	1
173	1/1/2011	1/31/2011	31	1	1
174	2/1/2011	2/28/2011	28	1	1
175	3/1/2011	3/31/2011	31	1	1
176	4/1/2011	4/30/2011	30	1	1
177	5/1/2011	5/31/2011	31	1	1
178	6/1/2011	6/30/2011	30	1	1
179	7/1/2011	7/31/2011	31	1	1
180	8/1/2011	8/31/2011	31	1	1
181	9/1/2011	9/30/2011	30	1	1
182	10/1/2011	10/31/2011	31	1	1
183	11/1/2011	11/30/2011	30	1	1
184	12/1/2011	12/31/2011	31	1	1
185	1/1/2012	1/31/2012	31	1	1
186	2/1/2012	2/29/2012	29	1	1
187	3/1/2012	3/31/2012	31	1	1
188	4/1/2012	4/30/2012	30	1	1
189	5/1/2012	5/31/2012	31	1	1
190	6/1/2012	6/30/2012	30	1	1
191	7/1/2012	7/31/2012	31	1	1
192	8/1/2012	8/31/2012	31	1	1
193	9/1/2012	9/30/2012	30	1	1
194	10/1/2012	10/31/2012	31	1	1
195	11/1/2012	11/30/2012	30	1	1
196	12/1/2012	12/31/2012	31	1	1
197	1/1/2013	1/31/2013	31	1	1
198	2/1/2013	2/28/2013	28	1	1
199	3/1/2013	3/31/2013	31	1	1
200	4/1/2013	4/30/2013	30	1	1
201	5/1/2013	5/31/2013	31	1	1
202	6/1/2013	6/30/2013	30	1	1
203	7/1/2013	7/31/2013	31	1	1
204	8/1/2013	8/31/2013	31	1	1
205	9/1/2013	9/30/2013	30	1	1
206	10/1/2013	10/31/2013	31	1	1
207	11/1/2013	11/30/2013	30	1	1
208	12/1/2013	12/31/2013	31	1	1
209	1/1/2014	1/31/2014	31	1	1
210	2/1/2014	2/28/2014	28	1	1
211	3/1/2014	3/31/2014	31	1	1
212	4/1/2014	4/30/2014	30	1	1
213	5/1/2014	5/31/2014	31	1	1
214	6/1/2014	6/30/2014	30	1	1
215	7/1/2014	7/31/2014	31	1	1
216	8/1/2014	8/31/2014	31	1	1
217	9/1/2014	9/30/2014	30	1	1
218	10/1/2014	10/31/2014	31	1	1
219	11/1/2014	11/30/2014	30	1	1
220	12/1/2014	12/31/2014	31	1	1
221	1/1/2015	1/31/2015	31	1	1
222	2/1/2015	2/28/2015	28	1	1
223	3/1/2015	3/31/2015	31	1	1
224	4/1/2015	4/30/2015	30	1	1
225	5/1/2015	5/31/2015	31	1	1
226	6/1/2015	6/30/2015	30	1	1
227	7/1/2015	7/31/2015	31	1	1
228	8/1/2015	8/31/2015	31	1	1
229	9/1/2015	9/30/2015	30	1	1
230	10/1/2015	10/31/2015	31	1	1
231	11/1/2015	11/30/2015	30	1	1
232	12/1/2015	12/31/2015	31	1	1
233	1/1/2016	1/31/2016	31	1	1
234	2/1/2016	2/29/2016	29	1	1
235	3/1/2016	3/31/2016	31	1	1
236	4/1/2016	4/30/2016	30	1	1
237	5/1/2016	5/31/2016	31	1	1
238	6/1/2016	6/30/2016	30	1	1
239	7/1/2016	7/31/2016	31	1	1
240	8/1/2016	8/31/2016	31	1	1
241	9/1/2016	9/30/2016	30	1	1
242	10/1/2016	10/31/2016	31	1	1
243	11/1/2016	11/30/2016	30	1	1
244	12/1/2016	12/31/2016	31	1	1
245	1/1/2017	1/31/2017	31	1	1
246	2/1/2017	2/28/2017	28	1	1

Table 7.1. Listing of stress periods for the Gulf Coast Land Subsidence and Groundwater-Flow model.—Continued

[NSTP, number of time steps; TSMULT, time step multiplier. All stress periods are transient except the first stress period. Dates are in month/day/year format]

Stress period[1,2]	Start date	End date	Stress period length, in days	NSTP	TSMULT	Stress period[1,2]	Start date	End date	Stress period length, in days	NSTP	TSMULT
247	3/1/2017	3/31/2017	31	1	1	268	12/1/2018	12/31/2018	31	1	1
248	4/1/2017	4/30/2017	30	1	1	269	1/1/2019	12/31/2019	365	1	1
249	5/1/2017	5/31/2017	31	1	1	270	1/1/2020	12/31/2020	366	1	1
250	6/1/2017	6/30/2017	30	1	1	271	1/1/2021	12/31/2021	365	1	1
251	7/1/2017	7/31/2017	31	1	1	272	1/1/2022	12/31/2022	365	1	1
252	8/1/2017	8/31/2017	31	1	1	273	1/1/2023	12/31/2023	365	1	1
253	9/1/2017	9/30/2017	30	1	1	274	1/1/2024	12/31/2024	366	1	1
254	10/1/2017	10/31/2017	31	1	1	275	1/1/2025	12/31/2025	365	1	1
255	11/1/2017	11/30/2017	30	1	1	276	1/1/2026	12/31/2026	365	1	1
256	12/1/2017	12/31/2017	31	1	1	277	1/1/2027	12/31/2027	365	1	1
257	1/1/2018	1/31/2018	31	1	1	278	1/1/2028	12/31/2028	366	1	1
258	2/1/2018	2/28/2018	28	1	1	279	1/1/2029	12/31/2029	365	1	1
259	3/1/2018	3/31/2018	31	1	1	280	1/1/2030	12/31/2030	365	1	1
260	4/1/2018	4/30/2018	30	1	1	281	1/1/2031	12/31/2031	365	1	1
261	5/1/2018	5/31/2018	31	1	1	282	1/1/2032	12/31/2032	366	1	1
262	6/1/2018	6/30/2018	30	1	1	283	1/1/2033	12/31/2033	365	1	1
263	7/1/2018	7/31/2018	31	1	1	284	1/1/2034	12/31/2034	365	1	1
264	8/1/2018	8/31/2018	31	1	1	285	1/1/2035	12/31/2035	365	1	1
265	9/1/2018	9/30/2018	30	1	1	286	1/1/2036	12/31/2036	366	1	1
266	10/1/2018	10/31/2018	31	1	1	287	1/1/2037	12/31/2037	365	1	1
267	11/1/2018	11/30/2018	30	1	1	288	1/1/2038	12/31/2038	365	1	1

[1]Model time is discretized into time steps within stress periods. The stress period length is the finest resolution at which temporally varying inflows and outflows can be represented and varied.

[2]Stress periods 269–288 represent a 20-year forecast period discretized into 1-year stress periods; the 20-year forecast period incorporates the mean stresses of the last 3 years of the model transient period.

The IES algorithm substantially reduces the computational demand for highly parameterized models compared to the GLM algorithm. In each iteration of the GLM algorithm, the forward model must be run at least once for each adjustable parameter. IES approximates the Jacobian matrix by using a specified number of realizations, so the number of model runs required in each iteration of the parameter estimation process can be far fewer than the number of adjustable parameters. The GULF model included 183,207 adjustable parameters, but only a few hundred realizations were used to empirically estimate the Jacobian matrix.

A potential downside of using an ensemble with fewer model runs than the number of parameters is the potential for substantial error in estimated cross-covariance between each parameter and observation, which can lead to spurious correlation. This is addressed through an approach called localization, which injects expert knowledge or obvious physical limitations on the magnitude of correlation between specific parameters and observations. PESTPP-IES includes an option to automate this approach, called automatic adaptive localization. Automatic adaptive localization compares the empirical correlation coefficient between each parameter and observation to a background level of correlation calculated by repeated circular shifting of the observation vector relative to the parameter vector. Correlations greater than one standard deviation from the mean background correlation are deemed statistically significant and retained. The remainder of the correlations are set to zero (White and others, 2020a).

The use of ensembles in the IES algorithm provides the benefit of built-in uncertainty analysis. Instead of upgrading a single set of parameters based on a single set of residuals, IES adjusts an ensemble of parameters based on an ensemble of residuals. The spread of these ensembles provides an empirical estimation of the uncertainty associated with each parameter value.

Table 7.2. Observation group weights used for history matching of the Gulf Coast Land Subsidence and Groundwater-Flow model.

[GPS, Global Positioning System; --, not available]

Observation group	Model layer	Hydrogeologic unit (figs. 99–100)	Number of nonzero-weighted observations	Contribution to initial objective function (percent)	Total observations in each group	Group contribution (percent)
Groundwater-level observations						
Groundwater levels, general	Layer 2	Chicot aquifer	2,703	1	5,253	5
	Layer 3	Evangeline aquifer	988	1		
	Layer 4	Burkeville confining unit	187	1		
	Layer 5	Jasper aquifer	731	1		
	Layer 6	Catahoula confining unit	644	1		
Groundwater levels[1]	Layer 2	Chicot aquifer	8,036	8	13,510	20
	Layer 3	Evangeline aquifer	3,795	8		
	Layer 4	Burkeville confining unit	389	1		
	Layer 5	Jasper aquifer	1,280	3		
	Layer 6	Catahoula confining unit[2]	10	--		
Groundwater levels, in the northern part of the model area	Layer 3	Evangeline aquifer	301	5	301	5
Groundwater levels, temporal difference observations	--	--	13,800	10	13,800	10
Minimum observed groundwater level[1]	--	--	444	10	444	10
Subsidence observations						
Benchmarks	--	--	485	5	485	5
Subsidence maps[3]	--	--	413	5	413	5
Extensometers	--	--	3,907	20	3,907	20
Extensometers, temporal difference observations	--	--	3,906	5	3,906	5
GPS, outcrop area[4]	--	--	5,522	5	5,522	5
GPS, confined area	--	--	9,433	5	9,433	5
GPS, temporal difference observations	--	--	14,955	5	14,955	5
				100	71,929	100

[1]At annual measurement sites.

[2]Each observation in the Catahoula confining unit was assigned a nominal weight of 1.0.

[3]The 1906–43 and 1906–78 subsidence maps from Gabrysch and Bonnet (1975) and Gabrysch (1980b) were used for history matching.

[4]The extents of the outcrop areas of the geologic units that contain the Gulf Coast aquifer system are displayed on figure 8.

The parameter estimation process implemented in IES typically narrows the distribution of parameters drawn from the prior parameter ensemble to ranges that best replicate historical observations (figs. 109–115). The parameter estimation process begins with a wide distribution to avoid prior data conflicts, the condition of a nonzero-weighted observation falling outside the range of simulated equivalents produced by the ensemble of models. As implemented here, IES removes data with prior data conflicts by assigning a zero weight to observations falling outside the range of simulated equivalents before the first upgrade iteration. Attempting to match such observations would require model realizations comprising extreme parameter values or unreasonable combinations of parameters compared to realizations producing outputs that bracket the remainder of the (nonconflicted) observations.

PESTPP-IES produces an ensemble of simulated results in each iteration of the algorithm with typically lower objective function values as it seeks to minimize the weighted least-squares objective function. Occasionally a model realization will produce an outlier result with an objective function much greater than the mean of the remaining realizations. For the GULF model, the "bad_phi_sigma" option was set to 2.0, which removes selected model realizations that yield realization objective functions greater than the mean plus two times the standard deviation of all realization objective functions in the current iteration. This helps focus the parameter estimation process by rejecting realizations unlikely to produce a good fit.

Based on visual inspection, the objective function distribution yielded by the Posterior has an approximately Gaussian distribution but with a tail extending towards higher objective function values. Therefore, the Posterior was conditioned to remove model realizations with an objective function equal to or greater than the 95th percentile (fig. 108), resulting in the removal of 12 realizations. This resulted in a conditioned Posterior of 224 model realizations. Spatial parameter distributions are shown on figures 7.1–7.7. A statistical summary of the groundwater-level residuals is listed in table 7.3.

Table 7.3. Statistical summary of groundwater-level residuals for the numerical groundwater-flow model of the Gulf Coast Land Subsidence and Groundwater-Flow model.

[RMSE, root-mean-square error]

Time period	Aquifer unit (model layer)	Observation count	Mean residual, in feet	Minimum residual, in feet	Maximum residual, in feet	75th-percentile residual range, in feet	RMSE, in feet
Transient period (1897–2018)	Chicot aquifer (layer 2)	10,739	4.7	−163.0	131.2	36.6	33.2
	Evangeline aquifer (layer 3)	5,084	11.2	−174.8	203.8	48.4	49.8
	Burkeville confining unit (layer 4)	576	−82.7	−294.4	54.0	121.5	115.2
	Jasper aquifer (layer 5)	2,011	−6.2	−207.4	118.8	64.5	58.9
	Catahoula confining unit (layer 6)	654	39.5	−211.6	135.4	93.5	80.0
End of transient period (2018)	Chicot aquifer (layer 2)	182	8.8	−74.1	78.1	40.4	29.1
	Evangeline aquifer (layer 3)	121	4.0	−118.2	173.4	30.9	41.7
	Burkeville confining unit (layer 4)	41	−39.8	−116.8	54.0	110.1	65.1
	Jasper aquifer (layer 5)	86	18.8	−194.5	89.6	74.3	64.7
	Catahoula confining unit (layer 6)	76	72.9	−22.1	111.6	92.3	78.3

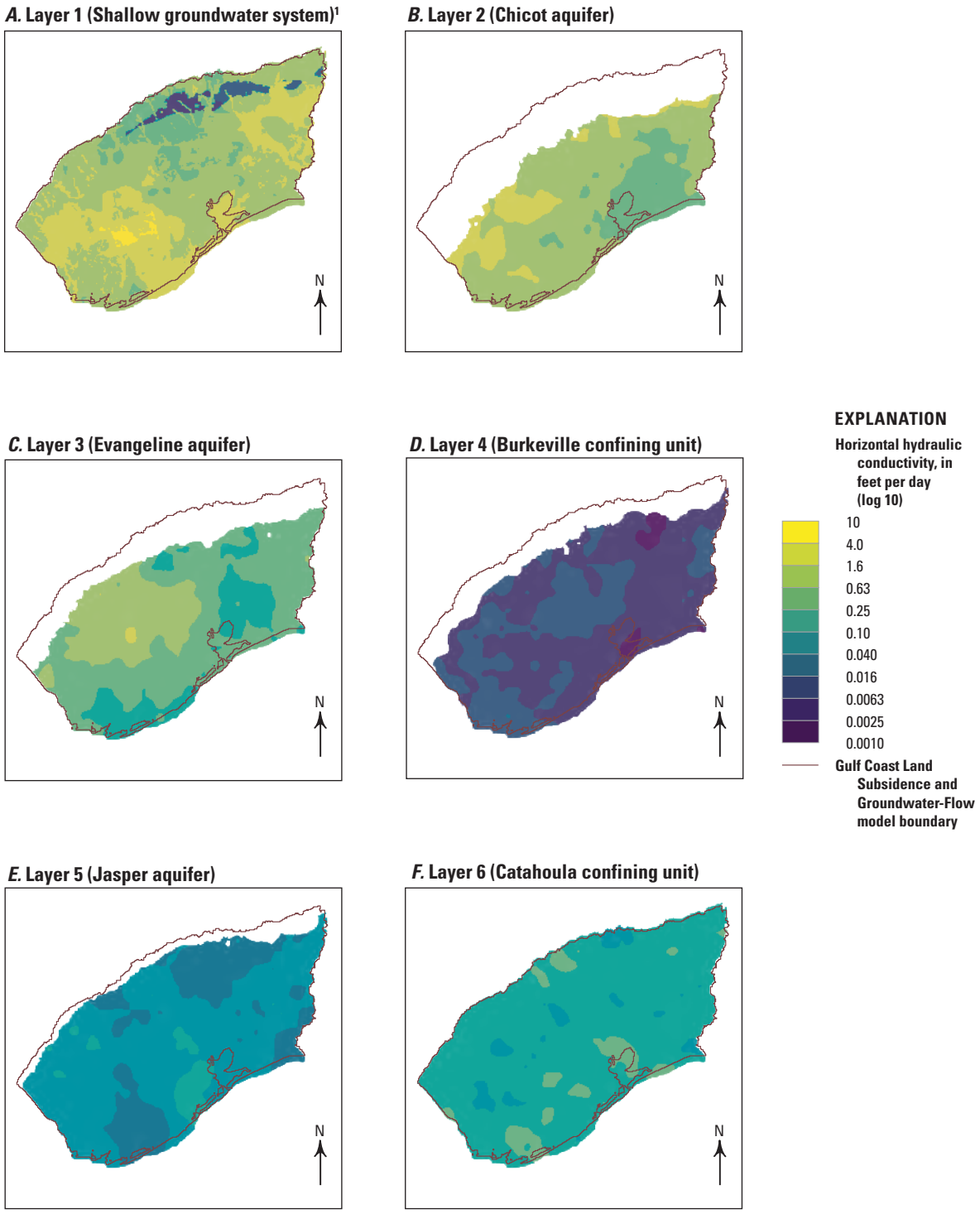

[1]The shallow groundwater system represents about the upper 50 feet of aquifer sediment in the model.

Figure 7.1. Spatial parameter distributions of horizontal hydraulic conductivity in the Gulf Coast Land Subsidence and Groundwater-Flow model.

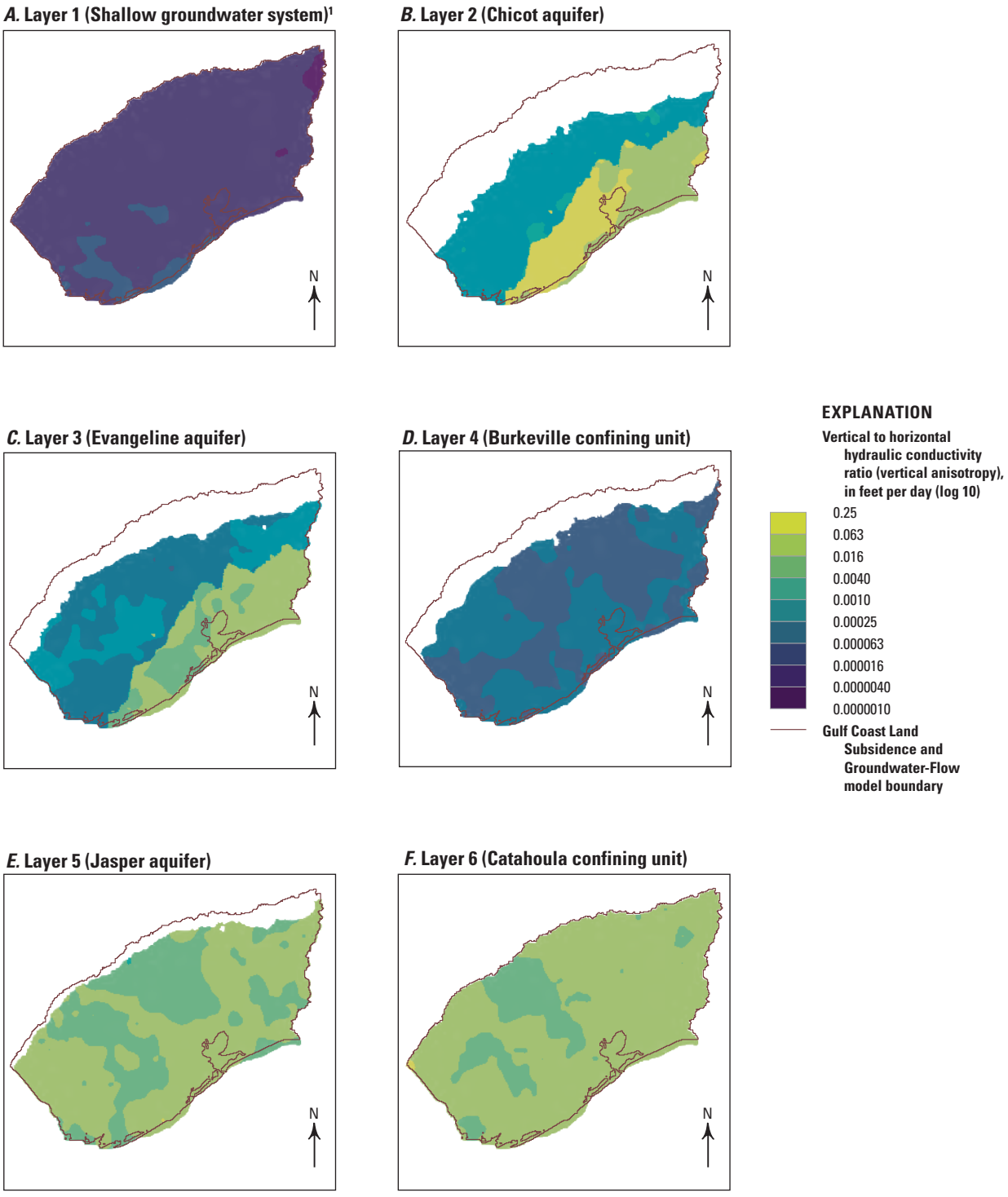

[1]The shallow groundwater system represents about the upper 50 feet of aquifer sediment in the model.

Figure 7.2. Spatial parameter distributions of vertical to horizontal hydraulic conductivity ratio (anisotropy) in the Gulf Coast Land Subsidence and Groundwater-Flow model.

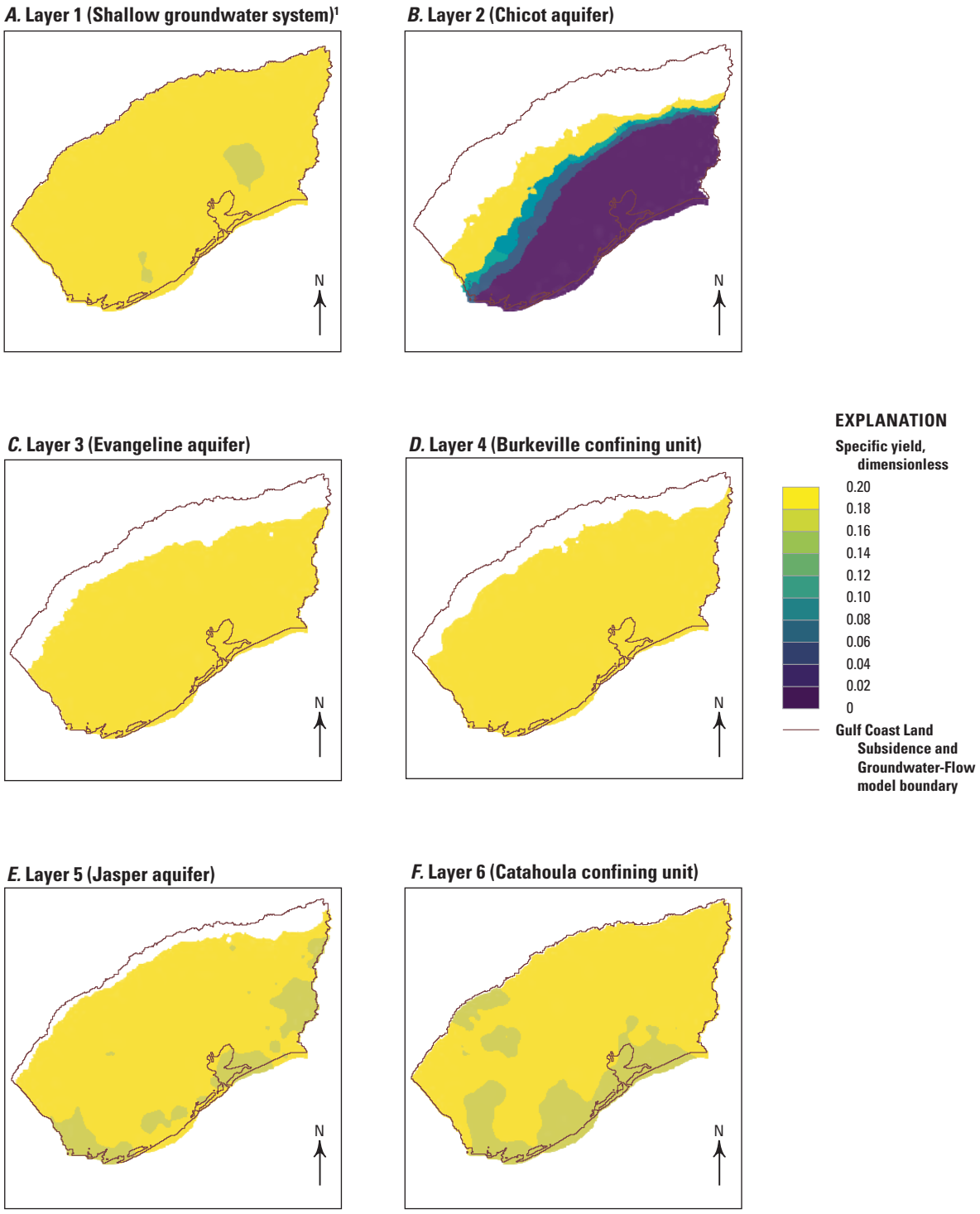

[1]The shallow groundwater system represents about the upper 50 feet of aquifer sediment in the model.

Figure 7.3. Spatial parameter distributions of specific yield (dimensionless) in the Gulf Coast Land Subsidence and Groundwater-Flow model.

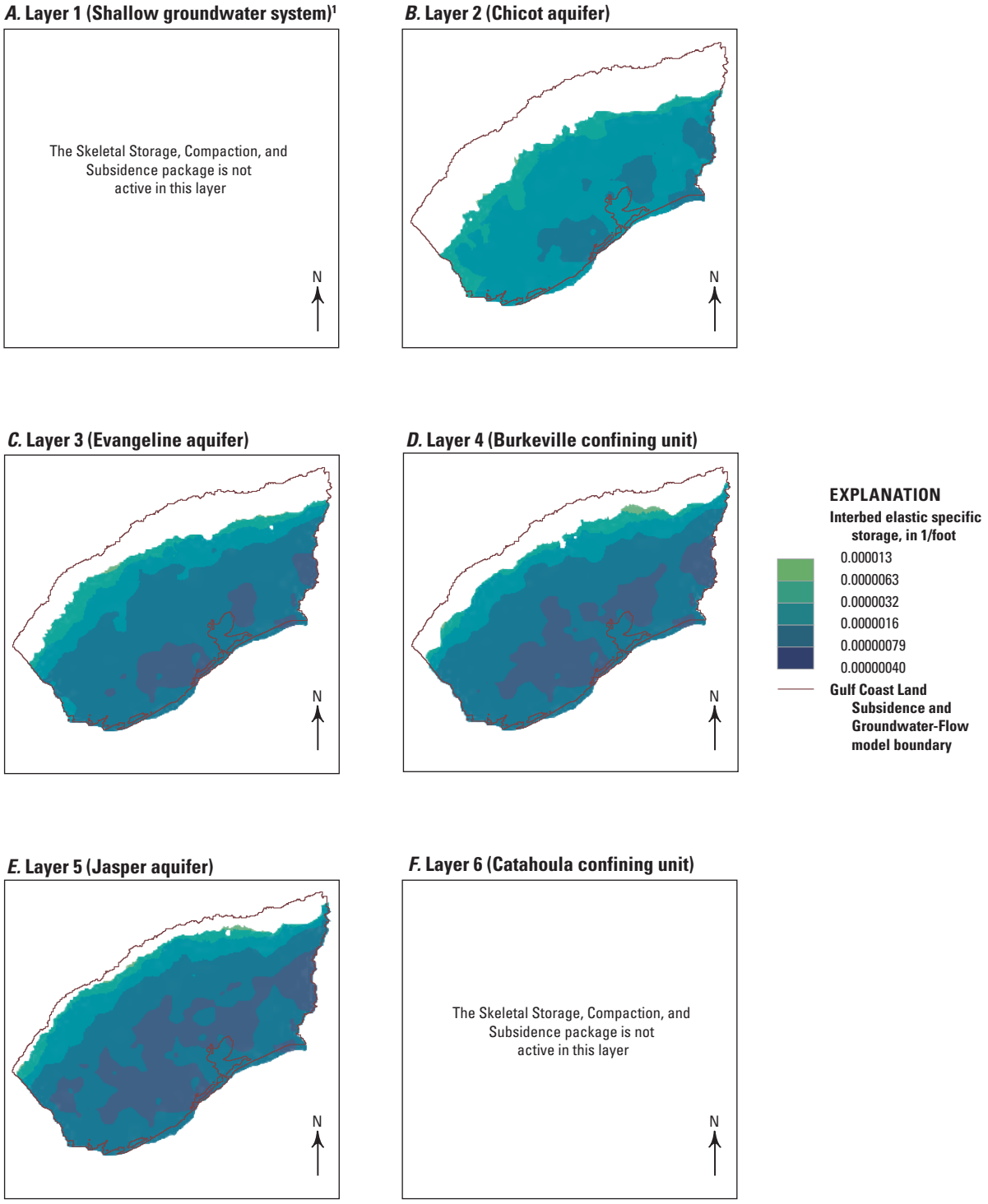

[1]The shallow groundwater system represents about the upper 50 feet of aquifer sediment in the model.

Figure 7.4. Spatial parameter distributions of Interbed elastic specific storage in the Gulf Coast Land Subsidence and Groundwater-Flow model.

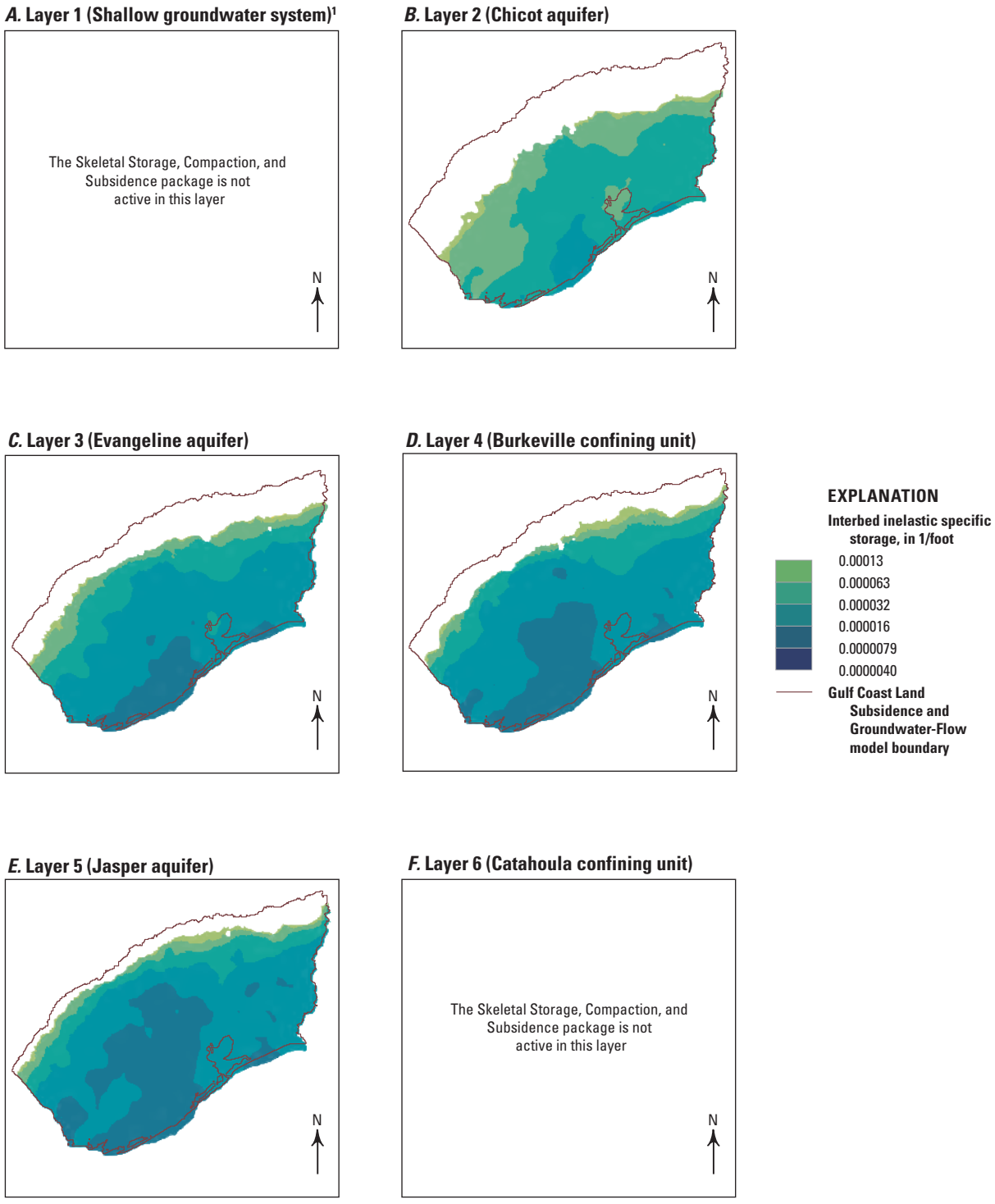

[1]The shallow groundwater system represents about the upper 50 feet of aquifer sediment in the model.

Figure 7.5. Spatial parameter distributions of interbed inelastic specific storage in the Gulf Coast Land Subsidence and Groundwater-Flow model.

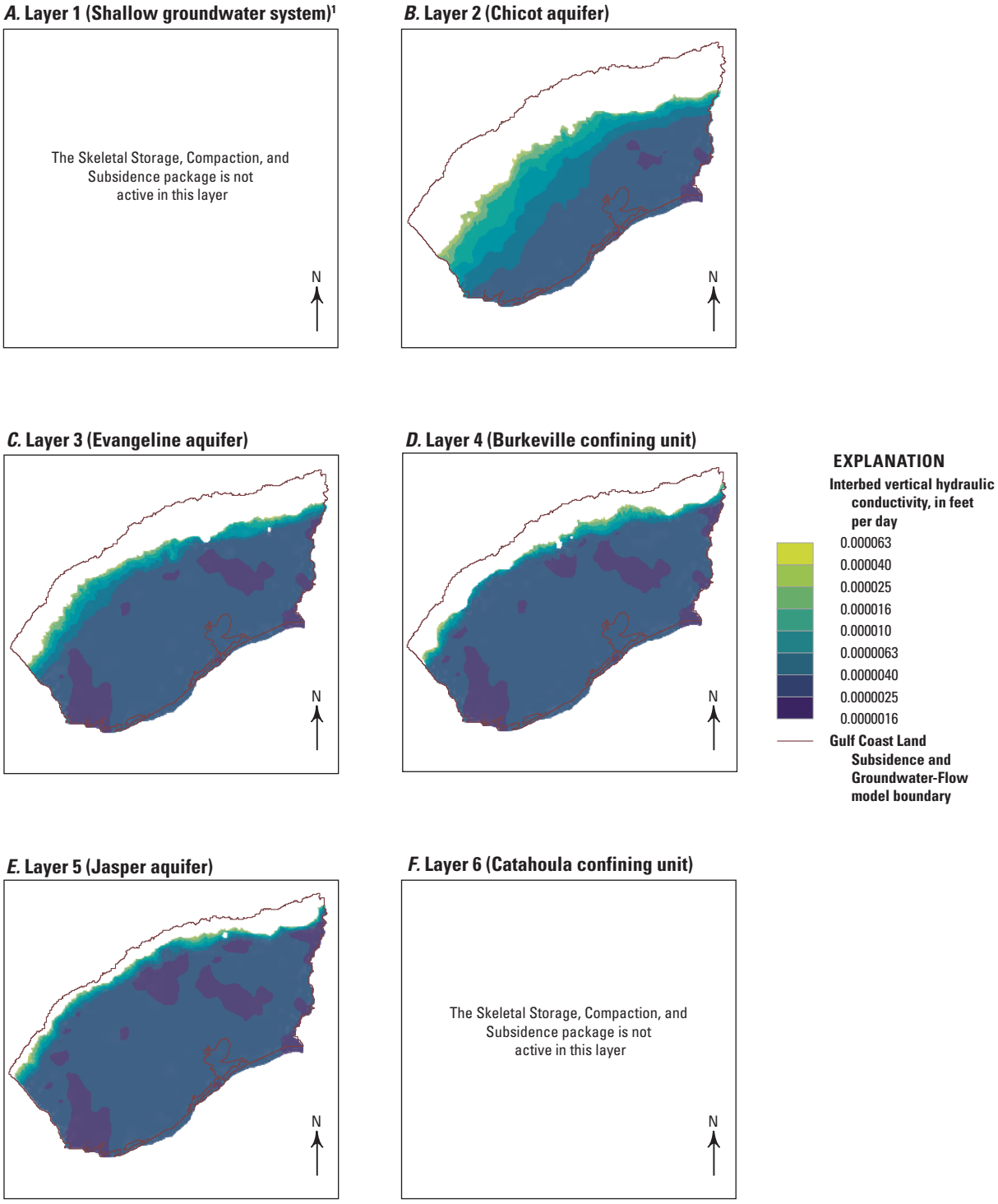

[1]The shallow groundwater system represents about the upper 50 feet of aquifer sediment in the model.

Figure 7.6. Spatial parameter distributions of interbed vertical hydraulic conductivity in the Gulf Coast Land Subsidence and Groundwater-Flow model.

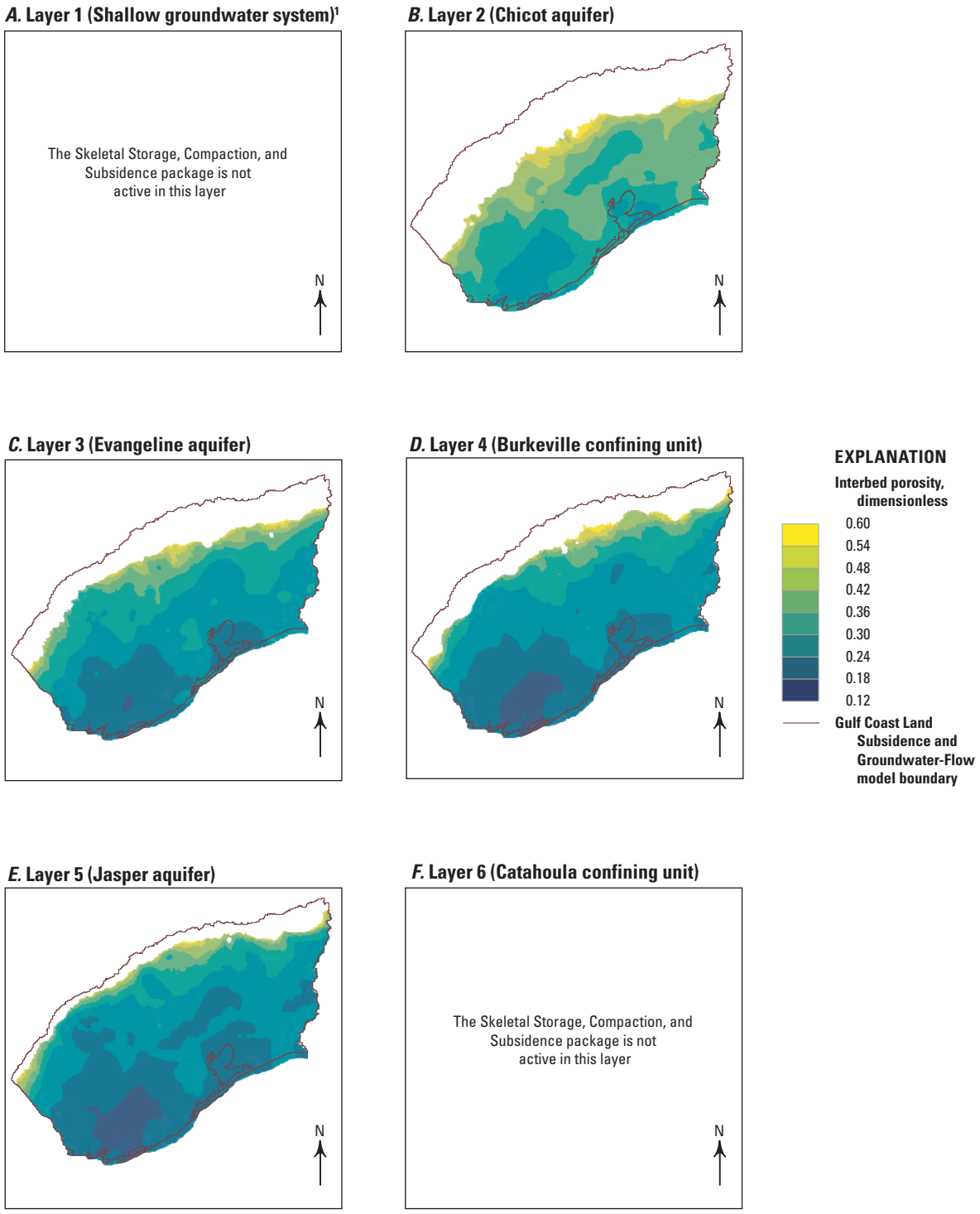

[1]The shallow groundwater system represents about the upper 50 feet of aquifer sediment in the model.

Figure 7.7. Spatial parameter distributions of interbed porosity in the Gulf Coast Land Subsidence and Groundwater-Flow model.

Appendix 8. Groundwater Model Observations and Water Budgets

Observation processing for the Gulf Coast Land Subsidence and Groundwater-Flow model (GULF model) was performed programmatically, with the goal to extract and amplify information that informs the likelihood of model input distributions. Observation noise was reduced by spatially declustering observations and smoothing and resampling temporal data. Multiple types of observations were used, including measurements of groundwater levels, land subsidence, and aquifer-system compaction. Summary estimates of recharge to each unit and groundwater use from each county were also used to constrain multiscale input parameter values. Tables 8.1 and 8.2 contain information on observation wells and Global Positioning System stations used for history matching of the GULF model and ensemble.

Detailed model water budgets are provided in this section, including budgets by county, individual layer by county, and by groundwater conservation district for steady state (1896) and the last year of the transient period (2018) (tables 8.3–8.8). Although the steady-state stress period is 1 day in length in the model, the water budget is shown as a year-long period for comparability to the transient water budget.

Table 8.1. Wells with groundwater-level observations used for history matching in the Gulf Coast Land Subsidence and Groundwater-Flow model (GULF model), southeast Texas.

[USGS well ID is the well identifier used by the U.S. Geological Survey (USGS; 2021b); TWDB well ID is the well identifier used by the Texas Water Development Board (TWDB; 2020b); obs., observations; --, not included in the GULF model; conf. unit, confining unit]

USGS well ID	TWDB well ID	Model observation name[1]	Identifier for observation well in this report[2]		County	Groundwater-well groups (figs. 19–36, 51–52, 119–138)	Hydrogeologic unit	Model layer	Model row	Model column	Number of obs.
			Figures 19–36, 51–52	Figures 119–138							
301948095290101	6045402	hds_04_114_183	B	B	Montgomery	Conroe (figs. 19, 119)	Jasper aquifer	5	115	184	28
301720095285601	6045712	hds_04_118_183	C	C	Montgomery		Jasper aquifer	5	119	184	20
301516095264301	6045805	hds_02_122_187	D	D	Montgomery		Evangeline aquifer	3	123	188	35
301819095271501	6045507	hds_04_116_186	E	E	Montgomery		Jasper aquifer	5	117	187	39
302111095311101	6044318	hds_04_111_180	--	F	Montgomery		Jasper aquifer	5	112	181	25
302030095282601	6045111	hds_04_112_184	--	G	Montgomery		Jasper aquifer	5	113	185	17
302320095294201	6037711	hds_04_107_182	H	H	Montgomery		Jasper aquifer	5	108	183	27
301256095270401	6053209	hds_02_126_186	B	B	Montgomery	The Woodlands (figs. 20, 120)	Evangeline aquifer	3	127	187	35
300811095291702	6053708	hds_02_135_182	C	C	Montgomery		Evangeline aquifer	3	136	183	23
300925095264501	6053814	hds_02_133_187	--	D	Montgomery		Evangeline aquifer	3	134	188	23
300823095275001	6053713	hds_04_135_185	E	E	Montgomery		Jasper aquifer	5	136	186	37
301153095243201	6053608	hds_02_128_190	F	F	Montgomery		Evangeline aquifer	3	129	191	30
301108095293201	6053407	hds_02_130_182	--	G	Montgomery		Evangeline aquifer	3	131	183	35
301107095293001	6053406	hds_04_130_182	--	H	Montgomery		Jasper aquifer	5	131	183	37
300521095365101	6060103	hds_01_140_171	B	B	Harris	Northern Harris County (figs. 21, 121)	Chicot aquifer	2	141	172	46
300056095335601	6060804	hds_02_149_175	C	C	Harris		Evangeline aquifer	3	150	176	36
295711095330201	6504526	hds_01_155_177	--	D	Harris		Chicot aquifer	2	156	178	38
295845095304101	6504310	hds_01_153_181	--	E	Harris		Chicot aquifer	2	154	182	28
300126095241401	6061903	hds_02_148_191	F	F	Harris		Evangeline aquifer	3	149	192	23
300251095265401	6061528	hds_02_145_187	G	G	Harris		Evangeline aquifer	3	146	188	17
300556095304102	6060306	hds_04_139_181	H	H	Harris		Jasper aquifer	5	140	182	35
300157095292501	6061715	hds_02_147_183	--	I	Harris		Evangeline aquifer	3	148	184	20

Table 8.1. Wells with groundwater-level observations used for history matching in the Gulf Coast Land Subsidence and Groundwater-Flow model (GULF model), southeast Texas.—Continued

[USGS well ID is the well identifier used by the U.S. Geological Survey (USGS; 2021b); TWDB well ID is the well identifier used by the Texas Water Development Board (TWDB; 2020b); obs., observations; --, not included in the GULF model; conf. unit, confining unit]

USGS well ID	TWDB well ID	Model observation name[1]	Identifier for observation well in this report[2]		County	Groundwater-well groups (figs. 19–36, 51–52, 119–138)	Hydrogeologic unit	Model layer	Model row	Model column	Number of obs.
			Figures 19–36, 51–52	Figures 119–138							
295831095530801	6501302	hds_02_153_145	B	B	Harris	Northwestern Harris County (figs. 22, 122)	Evangeline aquifer	3	154	146	49
295505095462201	6502612	hds_01_159_155	C	C	Harris		Chicot aquifer	2	160	156	46
295301095393901	6503906	hds_02_163_166	D	D	Harris		Evangeline aquifer	3	164	167	37
295258095354201	6504719	hds_02_163_173	E	E	Harris		Evangeline aquifer	3	164	174	40
295624095370802	6504416	hds_01_157_170	--	F	Harris		Chicot aquifer	2	158	171	22
300146095510401	6058704	hds_01_147_148	G	G	Harris		Chicot aquifer	2	148	149	29
300408095485701	6058501	hds_02_143_151	H	H	Harris		Evangeline aquifer	3	144	152	35
295821095481901	6502208	hds_02_153_152	--	I	Harris		Evangeline aquifer	3	154	153	18
294808095485401	6510516	hds_01_172_151	--	B	Harris	Western Harris County (figs. 23, 123)	Chicot aquifer	2	173	152	28
294753095454001	6510611	hds_02_173_157	--	C	Harris		Evangeline aquifer	3	174	158	28
294726095351102	6512726	hds_02_174_174	D	D	Harris		Evangeline aquifer	3	175	175	237
294623095351301	6512705	hds_01_176_173	--	E	Harris		Chicot aquifer	2	177	174	27
294925095341201	6512520	hds_02_170_175	--	F	Harris		Evangeline aquifer	3	171	176	49
294356095391501	6519317	hds_01_180_167	--	G	Harris		Chicot aquifer	2	181	168	31
294352095385501	6519319	hds_02_180_167	--	H	Harris		Evangeline aquifer	3	181	168	36
294717095401001	6511804	hds_02_174_165	--	I	Harris		Evangeline aquifer	3	175	166	39
294208095280701	6521413	hds_01_183_185	--	B	Harris	Southwestern Harris County (figs. 24, 124)	Chicot aquifer	2	184	186	22
293954095330701	6520807	hds_01_188_177	--	C	Harris		Chicot aquifer	2	189	178	32
293942095283101	6521701	hds_02_188_184	D	D	Harris		Evangeline aquifer	3	189	185	49
294651095303301	6512904	hds_02_175_181	--	E	Harris		Evangeline aquifer	3	176	182	19
294208095280501	6521402	hds_02_183_185	--	F	Harris		Evangeline aquifer	3	184	186	15
294216095301601	6520602	hds_01_183_181	G	G	Harris		Chicot aquifer	2	184	182	48
294216095321501	6520603	hds_01_183_178	--	H	Harris		Chicot aquifer	2	184	179	23
294340095311101	6520307	hds_01_180_180	--	I	Harris		Chicot aquifer	2	181	181	20

Table 8.1. Wells with groundwater-level observations used for history matching in the Gulf Coast Land Subsidence and Groundwater-Flow model (GULF model), southeast Texas.—Continued

[USGS well ID is the well identifier used by the U.S. Geological Survey (USGS; 2021b); TWDB well ID is the well identifier used by the Texas Water Development Board (TWDB; 2020b); obs., observations; --, not included in the GULF model; conf. unit, confining unit]

USGS well ID	TWDB well ID	Model observation name[1]	Identifier for observation well in this report[2]		County	Groundwater-well groups (figs. 19–36, 51–52, 119–138)	Hydrogeologic unit	Model layer	Model row	Model column	Number of obs.
			Figures 19–36, 51–52	Figures 119–138							
294518095254801	6513801	hds_01_177_189	B	B	Harris	Central Harris County (figs. 25, 125)	Chicot aquifer	2	178	190	37
294106095171201	6522618	hds_01_185_203	C	C	Harris		Chicot aquifer	2	186	204	55
294415095165301	6522317	hds_01_179_203	D	D	Harris		Chicot aquifer	2	180	204	56
294613095172601	6514912	hds_01_176_202	E	E	Harris		Chicot aquifer	2	177	203	47
295201095173201	6514203	hds_01_165_202	F	F	Harris		Chicot aquifer	2	166	203	43
294811095241901	6513614	hds_01_172_191	--	G	Harris		Chicot aquifer	2	173	192	24
294901095221001	6514409	hds_01_170_194	H	H	Harris		Chicot aquifer	2	171	195	226
294601095225801	6513904	hds_02_176_193	--	I	Harris		Evangeline aquifer	3	177	194	52
293956095120801	6523809	hds_01_187_211	B	B	Harris	South-central Harris County (figs. 26, 126)	Chicot aquifer	2	188	212	39
294237095093204	6523322	hds_03_182_215	C	C	Harris		Burkeville conf. unit	4	183	216	236
294311095071401	6524114	hds_01_181_219	--	D	Harris		Chicot aquifer	2	182	220	32
294902095133501	6515403	hds_01_170_208	--	E	Harris		Chicot aquifer	2	171	209	40
294445095141101	6523104	hds_01_178_207	F	F	Harris		Chicot aquifer	2	179	208	49
294645095104401	6515806	hds_01_175_213	G	G	Harris		Chicot aquifer	2	176	214	45
294642095114901	6515802	hds_01_175_211	--	H	Harris		Chicot aquifer	2	176	212	28
294803095105701	6515507	hds_01_172_212	--	I	Harris		Chicot aquifer	2	173	213	44
293344095082301	6531605	hds_01_199_217	--	B	Harris	Southeastern Harris County (figs. 27, 127)	Chicot aquifer	2	200	218	48
293306095054101	6532401	hds_01_200_221	C	C	Harris		Chicot aquifer	2	201	222	246
293446095033901	6532519	hds_01_197_225	D	D	Harris		Chicot aquifer	2	198	226	49
293909095012201	6524902	hds_01_188_228	E	E	Harris		Chicot aquifer	2	189	229	53
294155095051401	6524401	hds_01_183_222	--	F	Harris		Chicot aquifer	2	184	223	20
294527095014901	6516904	hds_01_177_227	G	G	Harris		Chicot aquifer	2	178	228	174
294322095041701	6524202	hds_01_181_223	--	H	Harris		Chicot aquifer	2	182	224	42
294207095022001	6524606	hds_01_183_226	--	I	Harris		Chicot aquifer	2	184	227	48

Table 8.1. Wells with groundwater-level observations used for history matching in the Gulf Coast Land Subsidence and Groundwater-Flow model (GULF model), southeast Texas.—Continued

[USGS well ID is the well identifier used by the U.S. Geological Survey (USGS; 2021b); TWDB well ID is the well identifier used by the Texas Water Development Board (TWDB; 2020b); obs., observations; --, not included in the GULF model; conf. unit, confining unit]

USGS well ID	TWDB well ID	Model observation name[1]	Identifier for observation well in this report[2]		County	Groundwater-well groups (figs. 19–36, 51–52, 119–138)	Hydrogeologic unit	Model layer	Model row	Model column	Number of obs.
			Figures 19–36, 51–52	Figures 119–138							
295817095065501	6508103	hds_01_153_219	B	B	Harris		Chicot aquifer	2	154	220	30
300037095084801	6063901	hds_01_149_216	--	C	Harris		Chicot aquifer	2	150	217	22
295449095084102	6507906	hds_02_160_216	D	D	Harris		Evangeline aquifer	3	161	217	169
295529095043501	6508506	hds_01_158_222	--	E	Harris	Eastern Harris County (figs. 28, 128)	Chicot aquifer	2	159	223	23
295005095070301	6516102	hds_01_168_219	--	F	Harris		Chicot aquifer	2	169	220	25
294932094551401	6409505	hds_01_169_238	G	G	Harris		Chicot aquifer	2	170	239	47
294926094595501	6409401	hds_01_169_230	--	H	Harris		Chicot aquifer	2	170	231	23
294924095024301	6516504	hds_01_170_226	--	I	Harris		Chicot aquifer	2	171	227	35
291210095484001	6550504	hds_01_239_152	B	B	Brazoria		Chicot aquifer	2	240	153	47
290834095384201	6551901	hds_01_245_168	C	C	Brazoria		Chicot aquifer	2	246	169	48
291055095482501	6550505	hds_01_241_152	--	D	Brazoria		Chicot aquifer	2	242	153	38
291201095200701	6554407	hds_01_239_198	E	E	Brazoria	Brazoria County (figs. 29, 129)	Chicot aquifer	2	240	199	51
292054095171901	6546301	hds_01_222_203	F	F	Brazoria		Chicot aquifer	2	223	204	52
291204095264001	6553504	hds_01_239_188	--	G	Brazoria		Chicot aquifer	2	240	189	26
292927095195801	6538201	hds_01_207_198	H	H	Brazoria		Chicot aquifer	2	208	199	51
291545095202401	6546702	hds_01_232_198	--	I	Brazoria		Chicot aquifer	2	233	199	52
292456095560101	6533801	hds_01_215_140	B	B	Fort Bend		Chicot aquifer	2	216	141	50
292246095553601	6533803	hds_01_219_141	--	C	Fort Bend		Chicot aquifer	2	220	142	29
292359095501601	6534701	hds_01_217_149	--	D	Fort Bend		Chicot aquifer	2	218	150	40
292808095343401	6536203	hds_01_209_175	--	E	Fort Bend	Southern Fort Bend County (figs. 30, 130)	Chicot aquifer	2	210	176	5
293453095283501	6529405	hds_01_197_184	F	F	Fort Bend		Chicot aquifer	2	198	185	34
293304095344901	6528501	hds_01_200_174	--	G	Fort Bend		Chicot aquifer	2	201	175	15
293717095380501	6527302	hds_02_192_169	H	H	Fort Bend		Evangeline aquifer	3	193	170	45
293648095394601	6527322	hds_01_193_166	I	I	Fort Bend		Chicot aquifer	2	194	167	29

Table 8.1. Wells with groundwater-level observations used for history matching in the Gulf Coast Land Subsidence and Groundwater-Flow model (GULF model), southeast Texas.—Continued

[USGS well ID is the well identifier used by the U.S. Geological Survey (USGS; 2021b); TWDB well ID is the well identifier used by the Texas Water Development Board (TWDB; 2020b); obs., observations; --, not included in the GULF model; conf. unit, confining unit]

USGS well ID	TWDB well ID	Model observation name[1]	Identifier for observation well in this report[2]		County	Groundwater-well groups (figs. 19–36, 51–52, 119–138)	Hydrogeologic unit	Model layer	Model row	Model column	Number of obs.
			Figures 19–36, 51–52	Figures 119–138							
294031095554201	6517505	hds_01_186_140	--	B	Fort Bend	Northern Fort Bend County (figs. 31, 131)	Chicot aquifer	2	187	141	28
293528095515701	6526105	hds_01_196_146	--	C	Fort Bend		Chicot aquifer	2	197	147	27
293729095440301	6527106	hds_02_193_159	D	D	Fort Bend		Evangeline aquifer	3	194	160	28
294400095505301	6518103	hds_01_180_148	E	E	Fort Bend		Chicot aquifer	2	181	149	42
294219095470501	6518609	hds_02_183_154	--	F	Fort Bend		Evangeline aquifer	3	184	155	30
294548095481401	6510811	hds_02_177_152	--	G	Fort Bend		Evangeline aquifer	3	178	153	30
294607095492201	6510812	hds_01_176_151	--	H	Fort Bend		Chicot aquifer	2	177	152	26
294514095515501	6510702	hds_01_178_147	--	I	Fort Bend		Chicot aquifer	2	179	148	35
300013094580901	6157703	hds_01_149_233	B	B	Liberty	Liberty County (figs. 32, 132)	Chicot aquifer	2	150	234	43
301608094582401	6141701	hds_01_120_232	--	C	Liberty		Chicot aquifer	2	121	233	32
302418094595601	6133708	hds_02_105_230	--	D	Liberty		Evangeline aquifer	3	106	231	18
302001095044701	6048202	hds_04_113_222	--	E	Liberty		Jasper aquifer	5	114	223	7
302040095050701	6048102	hds_02_112_221	F	F	Liberty		Evangeline aquifer	3	113	222	39
291949095024801	6548502	hds_01_224_226	B	B	Galveston	Northern Galveston County (figs. 33, 133)	Chicot aquifer	2	225	227	53
292337094542801	6433901	hds_01_217_240	C	C	Galveston		Chicot aquifer	2	218	241	48
292050095010501	6548301	hds_01_222_229	--	D	Galveston		Chicot aquifer	2	223	230	28
292338095063601	6540707	hds_01_217_220	E	E	Galveston		Chicot aquifer	2	218	221	62
292841094584901	6433103	hds_01_208_232	--	F	Galveston		Chicot aquifer	2	209	233	41
292619095060601	6540411	hds_01_212_221	--	G	Galveston		Chicot aquifer	2	213	222	42
292403095052601	6540704	hds_01_216_222	--	H	Galveston		Chicot aquifer	2	217	223	53
292647095014901	6540601	hds_01_211_228	--	I	Galveston		Chicot aquifer	2	212	229	17

Table 8.1. Wells with groundwater-level observations used for history matching in the Gulf Coast Land Subsidence and Groundwater-Flow model (GULF model), southeast Texas.—Continued

[USGS well ID is the well identifier used by the U.S. Geological Survey (USGS; 2021b); TWDB well ID is the well identifier used by the Texas Water Development Board (TWDB; 2020b); obs., observations; --, not included in the GULF model; conf. unit, confining unit]

USGS well ID	TWDB well ID	Model observation name[1]	Identifier for observation well in this report[2]		County	Groundwater-well groups (figs. 19–36, 51–52, 119–138)	Hydrogeologic unit	Model layer	Model row	Model column	Number of obs.
			Figures 19–36, 51–52	Figures 119–138							
--	6653804	hds_01_247_089	--	B	Wharton	Western part of the model area (figs. 34, 134)	Chicot aquifer	2	248	90	43
--	8004403	hds_01_266_075	--	C	Jackson		Chicot aquifer	2	267	76	40
--	8005102	hds_01_262_086	--	D	Jackson		Chicot aquifer	2	263	87	46
285903095575700	8101102	hds_01_263_136	E	E	Matagorda		Chicot aquifer	2	264	137	26
290318096064800	6664401	hds_01_255_122	--	F	Matagorda		Chicot aquifer	2	256	123	36
--	6648404	hds_01_226_123	G	G	Wharton		Chicot aquifer	2	227	124	34
--	6662805	hds_01_259_104	--	H	Wharton		Chicot aquifer	2	260	105	171
--	6656302	hds_01_238_132	--	I	Wharton		Chicot aquifer	2	239	133	40
--	6635901	hds_02_217_069	B	B	Lavaca	Northwestern part of the model area (figs. 35, 135)	Evangeline aquifer	3	218	70	49
--	6637607	hds_01_211_093	C	C	Colorado		Chicot aquifer	2	212	94	48
--	6620901	hds_02_190_082	D	D	Colorado		Evangeline aquifer	3	191	83	46
294903096061401	6616407	hds_01_171_123	E	E	Austin		Chicot aquifer	2	172	124	39
--	6629101	hds_02_195_086	--	F	Colorado		Evangeline aquifer	3	196	87	28
--	6635303	hds_02_210_071	--	G	Colorado		Evangeline aquifer	3	211	72	23
--	6624805	hds_02_191_127	--	H	Austin		Evangeline aquifer	3	192	128	24
295218095572701	6509204	hds_02_165_138	--	I	Waller		Evangeline aquifer	3	166	139	44
300110094320901	6160902	hds_01_147_275	--	B	Liberty	Eastern part of the model area (figs. 36, 136)	Chicot aquifer	2	148	276	17
300353093583801	6257401	hds_01_141_328	--	C	Orange		Chicot aquifer	2	142	329	34
294714094382001	6411901	hds_01_173_265	D	D	Chambers		Chicot aquifer	2	174	266	30
300503093450201	6258304	hds_01_138_350	E	E	Orange		Chicot aquifer	2	139	351	39
302055094041301	6148209	hds_01_110_319	F	F	Jasper		Chicot aquifer	2	111	320	124
303948093541801	6217902	hds_01_075_334	G	G	Jasper		Chicot aquifer	2	76	335	35
302100094104102	6147210	hds_01_110_308	--	H	Hardin		Chicot aquifer	2	111	309	28
--	6155707	hds_01_132_304	--	I	Jefferson		Chicot aquifer	2	133	305	21

Table 8.1. Wells with groundwater-level observations used for history matching in the Gulf Coast Land Subsidence and Groundwater-Flow model (GULF model), southeast Texas.—Continued

[USGS well ID is the well identifier used by the U.S. Geological Survey (USGS; 2021b); TWDB well ID is the well identifier used by the Texas Water Development Board (TWDB; 2020b); obs., observations; --, not included in the GULF model; conf. unit, confining unit]

USGS well ID	TWDB well ID	Model observation name[1]	Identifier for observation well in this report[2]		County	Groundwater-well groups (figs. 19–36, 51–52, 119–138)	Hydrogeologic unit	Model layer	Model row	Model column	Number of obs.
			Figures 19–36, 51–52	Figures 119–138							
--	6739507	hds_04_214_018	B	B	Lavaca	Western part of the outcrop in the model area (figs. 51, 137)	Jasper aquifer	5	215	19	43
--	6625203	hds_04_194_043	C	C	Lavaca		Jasper aquifer	5	195	44	25
--	6618601	hds_04_183_058	D	D	Colorado		Jasper aquifer	5	184	59	44
--	6604601	hds_02_156_082	E	E	Austin		Evangeline aquifer	3	157	83	34
--	5961803	hds_04_148_091	F	F	Austin		Jasper aquifer	5	149	92	18
--	6605604	hds_02_155_094	G	G	Austin		Evangeline aquifer	3	156	95	23
302247096052201	5940707	hds_04_108_125	H	H	Grimes		Jasper aquifer	5	109	126	13
--	6033103	hds_05_096_135	I	I	Grimes		Catahoula conf. unit	6	97	136	44
302145095473901	6042206	hds_04_110_153	B	B	Montgomery	Eastern part of the outcrop in the model area (figs. 52, 138)	Jasper aquifer	5	111	154	30
302817095334301	6036205	hds_04_098_175	--	C	Montgomery		Jasper aquifer	5	99	176	18
302558095343701	6036505	hds_04_102_174	D	D	Montgomery		Jasper aquifer	5	103	175	49
--	6015803	hds_04_065_212	E	E	San Jacinto		Jasper aquifer	5	66	213	27
304657094250800	6113802	hds_04_062_284	F	F	Tyler		Jasper aquifer	5	63	285	48
303135093574700	6201701	hds_05_047_327	G	G	Jasper		Catahoula conf. unit	6	48	328	41
304042095330101	6020503	hds_05_075_177	--	H	Walker		Catahoula conf. unit	6	76	178	31
--	6101706	hds_05_052_230	--	I	Polk		Catahoula conf. unit	6	53	231	35
294658096094200	6615902	hds_01_174_118	--	--	Austin	--	Chicot aquifer	2	175	119	3
--	6624102	hds_01_183_125	--	--	Austin	--	Chicot aquifer	2	184	126	2
--	5962501	hds_02_145_102	--	--	Austin	--	Evangeline aquifer	3	146	103	10
294440096111300	6623201	hds_02_179_116	--	--	Austin	--	Evangeline aquifer	3	180	117	3
--	6623101	hds_02_181_110	--	--	Austin	--	Evangeline aquifer	3	182	111	7
295130096124300	6615101	hds_02_166_113	--	--	Austin	--	Evangeline aquifer	3	167	114	14
--	6606501	hds_02_155_105	--	--	Austin	--	Evangeline aquifer	3	156	106	8
--	6614204	hds_02_167_102	--	--	Austin	--	Evangeline aquifer	3	168	103	26
--	6606614	hds_02_156_108	--	--	Austin	--	Evangeline aquifer	3	157	109	18
--	6606802	hds_02_164_102	--	--	Austin	--	Evangeline aquifer	3	165	103	8
--	6604904	hds_02_161_085	--	--	Austin	--	Evangeline aquifer	3	162	86	3

Table 8.1. Wells with groundwater-level observations used for history matching in the Gulf Coast Land Subsidence and Groundwater-Flow model (GULF model), southeast Texas.—Continued

[USGS well ID is the well identifier used by the U.S. Geological Survey (USGS; 2021b); TWDB well ID is the well identifier used by the Texas Water Development Board (TWDB; 2020b); obs., observations; --, not included in the GULF model; conf. unit, confining unit]

USGS well ID	TWDB well ID	Model observation name[1]	Identifier for observation well in this report[2]		County	Groundwater-well groups (figs. 19–36, 51–52, 119–138)	Hydrogeologic unit	Model layer	Model row	Model column	Number of obs.
			Figures 19–36, 51–52	Figures 119–138							
293416095170701	6530601	hds_01_198_203	--	--	Brazoria	--	Chicot aquifer	2	199	204	46
285919095344701	8104202	hds_01_262_174	--	--	Brazoria	--	Chicot aquifer	2	263	175	37
291510095405201	6543803	hds_01_233_165	--	--	Brazoria	--	Chicot aquifer	2	234	166	22
293253095141001	6531402	hds_01_200_208	--	--	Brazoria	--	Chicot aquifer	2	201	209	16
291843095321401	6544607	hds_01_227_178	--	--	Brazoria	--	Chicot aquifer	2	228	179	9
293000095171201	6530615	hds_01_200_206	--	--	Brazoria	--	Chicot aquifer	2	201	207	15
293243095165201	6530604	hds_01_200_203	--	--	Brazoria	--	Chicot aquifer	2	201	204	25
292335095133501	6539705	hds_01_217_209	--	--	Brazoria	--	Chicot aquifer	2	218	210	5
292603095150901	6538609	hds_01_213_206	--	--	Brazoria	--	Chicot aquifer	2	214	207	24
291305095352201	6552103	hds_01_237_173	--	--	Brazoria	--	Chicot aquifer	2	238	174	27
293040095260001	6529802	hds_01_204_188	--	--	Brazoria	--	Chicot aquifer	2	205	189	16
293431095191201	6530533	hds_01_197_199	--	--	Brazoria	--	Chicot aquifer	2	198	200	4
291359095113401	6555205	hds_01_235_212	--	--	Brazoria	--	Chicot aquifer	2	236	213	5
294548094510501	6410703	hds_01_176_245	--	--	Chambers	--	Chicot aquifer	2	177	246	7
293946094532701	6417901	hds_01_187_241	--	--	Chambers	--	Chicot aquifer	2	188	242	32
295156094542001	6409302	hds_01_165_239	--	--	Chambers	--	Chicot aquifer	2	166	240	18
295217094525201	6409336	hds_01_164_242	--	--	Chambers	--	Chicot aquifer	2	165	243	2
--	6630201	hds_01_195_102	--	--	Colorado	--	Chicot aquifer	2	196	103	3
--	6630701	hds_01_202_101	--	--	Colorado	--	Chicot aquifer	2	203	102	3
--	6629603	hds_01_201_094	--	--	Colorado	--	Chicot aquifer	2	202	95	3
--	6630101	hds_02_196_101	--	--	Colorado	--	Evangeline aquifer	3	197	102	6
--	6628502	hds_02_197_079	--	--	Colorado	--	Evangeline aquifer	3	198	80	4
--	6635301	hds_02_209_073	--	--	Colorado	--	Evangeline aquifer	3	210	74	4
--	6621601	hds_02_184_096	--	--	Colorado	--	Evangeline aquifer	3	185	97	4
--	6622402	hds_02_185_099	--	--	Colorado	--	Evangeline aquifer	3	186	100	3
--	6628901	hds_02_203_082	--	--	Colorado	--	Evangeline aquifer	3	204	83	3
--	6628402	hds_02_201_075	--	--	Colorado	--	Evangeline aquifer	3	202	76	8

Table 8.1. Wells with groundwater-level observations used for history matching in the Gulf Coast Land Subsidence and Groundwater-Flow model (GULF model), southeast Texas.—Continued

[USGS well ID is the well identifier used by the U.S. Geological Survey (USGS; 2021b); TWDB well ID is the well identifier used by the Texas Water Development Board (TWDB; 2020b); obs., observations; --, not included in the GULF model; conf. unit, confining unit]

USGS well ID	TWDB well ID	Model observation name[1]	Identifier for observation well in this report[2]		County	Groundwater-well groups (figs. 19–36, 51–52, 119–138)	Hydrogeologic unit	Model layer	Model row	Model column	Number of obs.
			Figures 19–36, 51–52	Figures 119–138							
--	6629401	hds_02_198_087	--	--	Colorado	--	Evangeline aquifer	3	199	88	23
--	6621201	hds_02_179_090	--	--	Colorado	--	Evangeline aquifer	3	180	91	10
--	6612201	hds_02_165_081	--	--	Colorado	--	Evangeline aquifer	3	166	82	3
--	6614703	hds_02_174_098	--	--	Colorado	--	Evangeline aquifer	3	175	99	32
--	6620602	hds_02_183_082	--	--	Colorado	--	Evangeline aquifer	3	184	83	27
--	6626202	hds_02_195_053	--	--	Colorado	--	Evangeline aquifer	3	196	54	33
--	6613801	hds_02_177_090	--	--	Colorado	--	Evangeline aquifer	3	178	91	3
--	6620505	hds_02_183_079	--	--	Colorado	--	Evangeline aquifer	3	184	80	3
--	6628509	hds_02_199_078	--	--	Colorado	--	Evangeline aquifer	3	200	79	2
--	6628605	hds_02_200_084	--	--	Colorado	--	Evangeline aquifer	3	201	85	2
--	6628703	hds_02_203_076	--	--	Colorado	--	Evangeline aquifer	3	204	77	2
--	6621301	hds_02_182_093	--	--	Colorado	--	Evangeline aquifer	3	183	94	3
--	6630203	hds_02_193_103	--	--	Colorado	--	Evangeline aquifer	3	194	104	3
--	6619804	hds_02_190_067	--	--	Colorado	--	Evangeline aquifer	3	191	68	34
--	6612603	hds_02_172_082	--	--	Colorado	--	Evangeline aquifer	3	173	83	11
--	6609502	hds_05_171_044	--	--	Fayette	--	Catahoula conf. unit	6	172	45	7
--	6609707	hds_05_177_040	--	--	Fayette	--	Catahoula conf. unit	6	178	41	17
295416096402500	6603804	hds_04_161_069	--	--	Fayette	--	Jasper aquifer	5	162	70	3
--	6617602	hds_04_185_045	--	--	Fayette	--	Jasper aquifer	5	186	46	6
--	6603303	hds_04_154_072	--	--	Fayette	--	Jasper aquifer	5	155	73	6
--	6617807	hds_04_191_041	--	--	Fayette	--	Jasper aquifer	5	192	42	31
294439095530301	6517306	hds_01_179_145	--	--	Fort Bend	--	Chicot aquifer	2	180	146	4
293141095283601	6529702	hds_01_203_184	--	--	Fort Bend	--	Chicot aquifer	2	204	185	2
294045095584201	6517407	hds_01_186_136	--	--	Fort Bend	--	Chicot aquifer	2	187	137	22
293647095325701	6528201	hds_01_193_177	--	--	Fort Bend	--	Chicot aquifer	2	194	178	13
293719095381601	6527303	hds_01_192_169	--	--	Fort Bend	--	Chicot aquifer	2	193	170	38
292354095430201	6535711	hds_01_217_161	--	--	Fort Bend	--	Chicot aquifer	2	218	162	18

Table 8.1. Wells with groundwater-level observations used for history matching in the Gulf Coast Land Subsidence and Groundwater-Flow model (GULF model), southeast Texas.—Continued

[USGS well ID is the well identifier used by the U.S. Geological Survey (USGS; 2021b); TWDB well ID is the well identifier used by the Texas Water Development Board (TWDB; 2020b); obs., observations; --, not included in the GULF model; conf. unit, confining unit]

USGS well ID	TWDB well ID	Model observation name[1]	Identifier for observation well in this report[2]		County	Groundwater-well groups (figs. 19–36, 51–52, 119–138)	Hydrogeologic unit	Model layer	Model row	Model column	Number of obs.
			Figures 19–36, 51–52	Figures 119–138							
292859095380501	6535304	hds_01_208_169	--	--	Fort Bend	--	Chicot aquifer	2	209	170	37
293144095392201	6527901	hds_01_203_167	--	--	Fort Bend	--	Chicot aquifer	2	204	168	3
293337095482701	6526501	hds_01_199_152	--	--	Fort Bend	--	Chicot aquifer	2	200	153	9
293458095454301	6526603	hds_01_197_157	--	--	Fort Bend	--	Chicot aquifer	2	198	158	32
293527095271501	6529209	hds_01_196_186	--	--	Fort Bend	--	Chicot aquifer	2	197	187	32
294322095533901	6517307	hds_01_181_144	--	--	Fort Bend	--	Chicot aquifer	2	182	145	3
293321095550901	6525506	hds_01_199_141	--	--	Fort Bend	--	Chicot aquifer	2	200	142	27
293959095380401	6519907	hds_01_187_169	--	--	Fort Bend	--	Chicot aquifer	2	188	170	16
293434095311501	6528604	hds_01_197_180	--	--	Fort Bend	--	Chicot aquifer	2	198	181	21
293424095330702	6528508	hds_01_198_177	--	--	Fort Bend	--	Chicot aquifer	2	199	178	33
294144095410001	6519509	hds_01_184_164	--	--	Fort Bend	--	Chicot aquifer	2	185	165	21
294155095533701	6517612	hds_01_184_144	--	--	Fort Bend	--	Chicot aquifer	2	185	145	2
293245095414801	6527505	hds_01_201_163	--	--	Fort Bend	--	Chicot aquifer	2	202	164	28
293606095315401	6528313	hds_01_194_179	--	--	Fort Bend	--	Chicot aquifer	2	195	180	23
293328095301401	6528605	hds_01_199_182	--	--	Fort Bend	--	Chicot aquifer	2	200	183	3
293001095274601	6529709	hds_01_206_186	--	--	Fort Bend	--	Chicot aquifer	2	207	187	25
293642095361901	6528108	hds_01_193_172	--	--	Fort Bend	--	Chicot aquifer	2	194	173	17
294043095504201	6518404	hds_01_186_149	--	--	Fort Bend	--	Chicot aquifer	2	187	150	19
293338095451901	6526613	hds_01_199_157	--	--	Fort Bend	--	Chicot aquifer	2	200	158	30
293455095375701	6527609	hds_01_197_169	--	--	Fort Bend	--	Chicot aquifer	2	198	170	28
294140095425701	6519407	hds_01_184_161	--	--	Fort Bend	--	Chicot aquifer	2	185	162	7
293704095440401	6527108	hds_01_193_159	--	--	Fort Bend	--	Chicot aquifer	2	194	160	13
293321095311401	6528607	hds_01_200_180	--	--	Fort Bend	--	Chicot aquifer	2	201	181	13
293758095365801	6520715	hds_01_191_171	--	--	Fort Bend	--	Chicot aquifer	2	192	172	7
294321095472801	6518307	hds_01_181_154	--	--	Fort Bend	--	Chicot aquifer	2	182	155	3
293523095483702	6526205	hds_01_196_152	--	--	Fort Bend	--	Chicot aquifer	2	197	153	7
293140095325001	6528810	hds_01_203_177	--	--	Fort Bend	--	Chicot aquifer	2	204	178	8

Table 8.1. Wells with groundwater-level observations used for history matching in the Gulf Coast Land Subsidence and Groundwater-Flow model (GULF model), southeast Texas.—Continued

[USGS well ID is the well identifier used by the U.S. Geological Survey (USGS; 2021b); TWDB well ID is the well identifier used by the Texas Water Development Board (TWDB; 2020b); obs., observations; --, not included in the GULF model; conf. unit, confining unit]

USGS well ID	TWDB well ID	Model observation name[1]	Identifier for observation well in this report[2]		County	Groundwater-well groups (figs. 19–36, 51–52, 119–138)	Hydrogeologic unit	Model layer	Model row	Model column	Number of obs.
			Figures 19–36, 51–52	Figures 119–138							
294142095515301	6518406	hds_01_184_147	--	--	Fort Bend	--	Chicot aquifer	2	185	148	6
293431095341801	6528513	hds_01_197_175	--	--	Fort Bend	--	Chicot aquifer	2	198	176	6
293647095325801	6528202	hds_02_193_177	--	--	Fort Bend	--	Evangeline aquifer	3	194	178	3
293219095485701	6526812	hds_02_202_151	--	--	Fort Bend	--	Evangeline aquifer	3	203	152	28
293237095504801	6526406	hds_02_201_148	--	--	Fort Bend	--	Evangeline aquifer	3	202	149	29
293830095373201	6519904	hds_02_190_170	--	--	Fort Bend	--	Evangeline aquifer	3	191	171	32
293736095365501	6520711	hds_02_192_171	--	--	Fort Bend	--	Evangeline aquifer	3	193	172	28
293855095395501	6519906	hds_02_189_166	--	--	Fort Bend	--	Evangeline aquifer	3	190	167	4
293226095471601	6526908	hds_02_201_154	--	--	Fort Bend	--	Evangeline aquifer	3	202	155	29
292944095550101	6533210	hds_02_206_142	--	--	Fort Bend	--	Evangeline aquifer	3	207	143	30
293332095411301	6527506	hds_02_199_164	--	--	Fort Bend	--	Evangeline aquifer	3	200	165	21
293340095400501	6527507	hds_02_199_166	--	--	Fort Bend	--	Evangeline aquifer	3	200	167	21
294442095450801	6518309	hds_02_179_157	--	--	Fort Bend	--	Evangeline aquifer	3	180	158	13
293921095441601	6519708	hds_02_189_159	--	--	Fort Bend	--	Evangeline aquifer	3	190	160	12
293546095374901	6527326	hds_02_195_169	--	--	Fort Bend	--	Evangeline aquifer	3	196	170	15
293740095410201	6519811	hds_02_192_164	--	--	Fort Bend	--	Evangeline aquifer	3	193	165	6
292953095460301	6534309	hds_02_206_156	--	--	Fort Bend	--	Evangeline aquifer	3	207	157	6
293006095492501	6526817	hds_02_206_151	--	--	Fort Bend	--	Evangeline aquifer	3	207	152	7
294326095492301	6518212	hds_02_181_151	--	--	Fort Bend	--	Evangeline aquifer	3	182	152	6
294004095404901	6519517	hds_02_187_164	--	--	Fort Bend	--	Evangeline aquifer	3	188	165	6
294511095512901	6510714	hds_02_178_147	--	--	Fort Bend	--	Evangeline aquifer	3	179	148	6
294305095511301	6518114	hds_02_182_148	--	--	Fort Bend	--	Evangeline aquifer	3	183	149	6
294209095494701	6518505	hds_02_183_150	--	--	Fort Bend	--	Evangeline aquifer	3	184	151	5
294408095483001	6518211	hds_02_179_152	--	--	Fort Bend	--	Evangeline aquifer	3	180	153	5
292205095043701	6548207	hds_01_220_223	--	--	Galveston	--	Chicot aquifer	2	221	224	34
293032095064301	6532716	hds_01_204_220	--	--	Galveston	--	Chicot aquifer	2	205	221	17
292542095082301	6539601	hds_01_213_217	--	--	Galveston	--	Chicot aquifer	2	214	218	34

Table 8.1. Wells with groundwater-level observations used for history matching in the Gulf Coast Land Subsidence and Groundwater-Flow model (GULF model), southeast Texas.—Continued

[USGS well ID is the well identifier used by the U.S. Geological Survey (USGS; 2021b); TWDB well ID is the well identifier used by the Texas Water Development Board (TWDB; 2020b); obs., observations; --, not included in the GULF model; conf. unit, confining unit]

USGS well ID	TWDB well ID	Model observation name[1]	Identifier for observation well in this report[2]		County	Groundwater-well groups (figs. 19–36, 51–52, 119–138)	Hydrogeologic unit	Model layer	Model row	Model column	Number of obs.
			Figures 19–36, 51–52	Figures 119–138							
293223095010701	6532901	hds_01_201_229	--	--	Galveston	--	Chicot aquifer	2	202	230	14
292007094575401	6441114	hds_01_224_234	--	--	Galveston	--	Chicot aquifer	2	225	235	11
293044095001601	6532904	hds_01_204_230	--	--	Galveston	--	Chicot aquifer	2	205	231	3
293222095020301	6532902	hds_01_201_227	--	--	Galveston	--	Chicot aquifer	2	202	228	29
292233094541501	6433912	hds_01_219_240	--	--	Galveston	--	Chicot aquifer	2	220	241	39
292240095001301	6540901	hds_01_219_230	--	--	Galveston	--	Chicot aquifer	2	220	231	4
292327094575901	6433710	hds_01_217_234	--	--	Galveston	--	Chicot aquifer	2	218	235	39
292617095065501	6540412	hds_01_212_219	--	--	Galveston	--	Chicot aquifer	2	213	220	32
292350095002201	6540903	hds_01_217_230	--	--	Galveston	--	Chicot aquifer	2	218	231	31
292458094534204	6433918	hds_01_215_241	--	--	Galveston	--	Chicot aquifer	2	216	242	175
292941094563001	6433213	hds_01_206_236	--	--	Galveston	--	Chicot aquifer	2	207	237	22
292923095091601	6539310	hds_01_207_215	--	--	Galveston	--	Chicot aquifer	2	208	216	19
292231094581701	6433713	hds_01_219_233	--	--	Galveston	--	Chicot aquifer	2	220	234	2
302315095522301	6034702	hds_03_107_146	--	--	Grimes	--	Burkeville conf. unit	4	108	147	18
302301096052301	5940708	hds_05_108_125	--	--	Grimes	--	Catahoula conf. unit	6	109	126	11
303203095551800	6025804	hds_05_091_141	--	--	Grimes	--	Catahoula conf. unit	6	92	142	43
301445096020901	5956301	hds_02_123_130	--	--	Grimes	--	Evangeline aquifer	3	124	131	46
301518095494001	6042803	hds_02_122_150	--	--	Grimes	--	Evangeline aquifer	3	123	151	18
302207096050600	5948106	hds_04_110_125	--	--	Grimes	--	Jasper aquifer	5	111	126	12
302949095503300	6034102	hds_04_095_149	--	--	Grimes	--	Jasper aquifer	5	96	150	13
302138095575901	6041105	hds_04_110_137	--	--	Grimes	--	Jasper aquifer	5	111	138	16
302800095534501	6033302	hds_04_099_144	--	--	Grimes	--	Jasper aquifer	5	100	145	21
303214095502801	6026707	hds_04_091_149	--	--	Grimes	--	Jasper aquifer	5	92	150	8
302107096034101	5948207	hds_04_111_128	--	--	Grimes	--	Jasper aquifer	5	112	129	8
301956096014801	5948605	hds_04_114_131	--	--	Grimes	--	Jasper aquifer	5	115	132	3
--	6153907	hds_01_131_289	--	--	Hardin	--	Chicot aquifer	2	132	290	22
301554094120201	6147804	hds_01_119_306	--	--	Hardin	--	Chicot aquifer	2	120	307	16

Table 8.1. Wells with groundwater-level observations used for history matching in the Gulf Coast Land Subsidence and Groundwater-Flow model (GULF model), southeast Texas.—Continued

[USGS well ID is the well identifier used by the U.S. Geological Survey (USGS; 2021b); TWDB well ID is the well identifier used by the Texas Water Development Board (TWDB; 2020b); obs., observations; --, not included in the GULF model; conf. unit, confining unit]

USGS well ID	TWDB well ID	Model observation name[1]	Identifier for observation well in this report[2]		County	Groundwater-well groups (figs. 19–36, 51–52, 119–138)	Hydrogeologic unit	Model layer	Model row	Model column	Number of obs.
			Figures 19–36, 51–52	Figures 119–138							
302426094370101	6136705	hds_01_104_266	--	--	Hardin	--	Chicot aquifer	2	105	267	3
--	6154805	hds_01_132_295	--	--	Hardin	--	Chicot aquifer	2	133	296	8
293546095101501	6531207	hds_01_195_214	--	--	Harris	--	Chicot aquifer	2	196	215	14
293724095115901	6531211	hds_01_192_211	--	--	Harris	--	Chicot aquifer	2	193	212	40
294258095372501	6520111	hds_01_182_170	--	--	Harris	--	Chicot aquifer	2	183	171	22
--	6513932	hds_01_176_194	--	--	Harris	--	Chicot aquifer	2	177	195	4
293643095101901	6531202	hds_01_193_214	--	--	Harris	--	Chicot aquifer	2	194	215	15
293903095270601	6521805	hds_01_189_187	--	--	Harris	--	Chicot aquifer	2	190	188	20
293917095191301	6522803	hds_01_188_199	--	--	Harris	--	Chicot aquifer	2	189	200	19
294101095122901	6523502	hds_01_185_210	--	--	Harris	--	Chicot aquifer	2	186	211	4
294403095141801	6523103	hds_01_180_207	--	--	Harris	--	Chicot aquifer	2	181	208	51
294742095160101	6514602	hds_01_173_204	--	--	Harris	--	Chicot aquifer	2	174	205	33
295150095352101	6512101	hds_01_165_173	--	--	Harris	--	Chicot aquifer	2	166	174	20
293207095061501	6532703	hds_01_202_220	--	--	Harris	--	Chicot aquifer	2	203	221	27
293717095240501	6529301	hds_01_192_191	--	--	Harris	--	Chicot aquifer	2	193	192	14
294358094573501	6417103	hds_01_179_234	--	--	Harris	--	Chicot aquifer	2	180	235	2
294410095322001	6520309	hds_01_180_178	--	--	Harris	--	Chicot aquifer	2	181	179	19
294637095022901	6516905	hds_01_175_226	--	--	Harris	--	Chicot aquifer	2	176	227	36
294812095013001	6516602	hds_01_172_228	--	--	Harris	--	Chicot aquifer	2	173	229	34
294932095293501	6513408	hds_01_170_182	--	--	Harris	--	Chicot aquifer	2	171	183	22
295018095171101	6514301	hds_01_168_202	--	--	Harris	--	Chicot aquifer	2	169	203	4
295227095200501	6514112	hds_01_164_198	--	--	Harris	--	Chicot aquifer	2	165	199	14
293638095164801	6530304	hds_01_193_203	--	--	Harris	--	Chicot aquifer	2	194	204	17
293738095260501	6521807	hds_01_192_188	--	--	Harris	--	Chicot aquifer	2	193	189	15
293910095135601	6523708	hds_01_189_208	--	--	Harris	--	Chicot aquifer	2	190	209	16
294004095275801	6521404	hds_01_187_185	--	--	Harris	--	Chicot aquifer	2	188	186	19
294028095305701	6520617	hds_01_186_180	--	--	Harris	--	Chicot aquifer	2	187	181	18

Table 8.1. Wells with groundwater-level observations used for history matching in the Gulf Coast Land Subsidence and Groundwater-Flow model (GULF model), southeast Texas.—Continued

[USGS well ID is the well identifier used by the U.S. Geological Survey (USGS; 2021b); TWDB well ID is the well identifier used by the Texas Water Development Board (TWDB; 2020b); obs., observations; --, not included in the GULF model; conf. unit, confining unit]

USGS well ID	TWDB well ID	Model observation name[1]	Identifier for observation well in this report[2]		County	Groundwater-well groups (figs. 19–36, 51–52, 119–138)	Hydrogeologic unit	Model layer	Model row	Model column	Number of obs.
			Figures 19–36, 51–52	Figures 119–138							
294107095323801	6520507	hds_01_185_178	--	--	Harris	--	Chicot aquifer	2	186	179	4
294619095142701	6515703	hds_01_175_207	--	--	Harris	--	Chicot aquifer	2	176	208	40
294745095331101	6512502	hds_01_173_177	--	--	Harris	--	Chicot aquifer	2	174	178	22
295312095173301	6506802	hds_01_163_202	--	--	Harris	--	Chicot aquifer	2	164	203	19
295758095494301	6502201	hds_01_154_150	--	--	Harris	--	Chicot aquifer	2	155	151	16
300308095071402	6064403	hds_01_144_218	--	--	Harris	--	Chicot aquifer	2	145	219	48
293636095133801	6531108	hds_01_193_208	--	--	Harris	--	Chicot aquifer	2	194	209	18
294105095070001	6524404	hds_01_185_219	--	--	Harris	--	Chicot aquifer	2	186	220	13
294735095023401	6516509	hds_01_173_226	--	--	Harris	--	Chicot aquifer	2	174	227	18
295153095281401	6513110	hds_01_165_185	--	--	Harris	--	Chicot aquifer	2	166	186	4
--	6512916	hds_01_176_178	--	--	Harris	--	Chicot aquifer	2	177	179	7
293543095134201	6531109	hds_01_195_208	--	--	Harris	--	Chicot aquifer	2	196	209	8
293644095045501	6532203	hds_01_193_222	--	--	Harris	--	Chicot aquifer	2	194	223	23
293732095044101	6524804	hds_01_191_223	--	--	Harris	--	Chicot aquifer	2	192	224	20
293958095221401	6522711	hds_01_187_194	--	--	Harris	--	Chicot aquifer	2	188	195	11
294517095084101	6515912	hds_01_177_216	--	--	Harris	--	Chicot aquifer	2	178	217	29
294548095455101	6510906	hds_01_177_156	--	--	Harris	--	Chicot aquifer	2	178	157	14
295333095433801	6503703	hds_01_162_160	--	--	Harris	--	Chicot aquifer	2	163	161	15
295813095343601	6504207	hds_01_154_174	--	--	Harris	--	Chicot aquifer	2	155	175	7
300231095133501	6063404	hds_01_145_208	--	--	Harris	--	Chicot aquifer	2	146	209	28
293709095024802	6532207	hds_01_192_226	--	--	Harris	--	Chicot aquifer	2	193	227	19
293938095351001	6520706	hds_01_188_174	--	--	Harris	--	Chicot aquifer	2	189	175	31
294601095041901	6516814	hds_01_176_223	--	--	Harris	--	Chicot aquifer	2	177	224	45
295101095140601	6515101	hds_01_167_207	--	--	Harris	--	Chicot aquifer	2	168	208	19
294659095375802	6511919	hds_01_174_169	--	--	Harris	--	Chicot aquifer	2	175	170	5
300133095065101	6064713	hds_01_147_219	--	--	Harris	--	Chicot aquifer	2	148	220	51
293741095010101	6524920	hds_01_191_229	--	--	Harris	--	Chicot aquifer	2	192	230	10

Table 8.1. Wells with groundwater-level observations used for history matching in the Gulf Coast Land Subsidence and Groundwater-Flow model (GULF model), southeast Texas.—Continued

[USGS well ID is the well identifier used by the U.S. Geological Survey (USGS; 2021b); TWDB well ID is the well identifier used by the Texas Water Development Board (TWDB; 2020b); obs., observations; --, not included in the GULF model; conf. unit, confining unit]

USGS well ID	TWDB well ID	Model observation name[1]	Identifier for observation well in this report[2]		County	Groundwater-well groups (figs. 19–36, 51–52, 119–138)	Hydrogeologic unit	Model layer	Model row	Model column	Number of obs.
			Figures 19–36, 51–52	Figures 119–138							
295619095171001	6506616	hds_01_157_202	--	--	Harris	--	Chicot aquifer	2	158	203	42
294206095162601	6522622	hds_01_183_204	--	--	Harris	--	Chicot aquifer	2	184	205	236
294500095073401	6515914	hds_01_178_218	--	--	Harris	--	Chicot aquifer	2	179	219	38
293352095011606	6532630	hds_01_198_228	--	--	Harris		Chicot aquifer	2	199	229	174
293732095300601	6520911	hds_01_192_182	--	--	Harris	--	Chicot aquifer	2	193	183	47
293949095024301	6524811	hds_01_187_226	--	--	Harris	--	Chicot aquifer	2	188	227	18
294237095093206	6523324	hds_01_182_215	--	--	Harris	--	Chicot aquifer	2	183	216	167
295522095291902	6505404	hds_01_159_183	--	--	Harris	--	Chicot aquifer	2	160	184	27
294338095270406	6521229	hds_01_180_187	--	--	Harris	--	Chicot aquifer	2	181	188	154
294728095200104	6514742	hds_01_173_198	--	--	Harris	--	Chicot aquifer	2	174	199	164
295449095084104	6507908	hds_01_160_216	--	--	Harris	--	Chicot aquifer	2	161	217	170
300018095225701	6061914	hds_01_149_193	--	--	Harris	--	Chicot aquifer	2	150	194	26
294849095034701	6516502	hds_01_171_224	--	--	Harris	--	Chicot aquifer	2	172	225	16
294329095284603	6521150	hds_01_181_184	--	--	Harris	--	Chicot aquifer	2	182	185	37
300624095302001	6060307	hds_01_138_181	--	--	Harris	--	Chicot aquifer	2	139	182	11
295644095261001	6505517	hds_01_156_188	--	--	Harris	--	Chicot aquifer	2	157	189	29
300447095444101	6059405	hds_01_142_158	--	--	Harris	--	Chicot aquifer	2	143	159	9
294402095294701	6521151	hds_01_180_182	--	--	Harris	--	Chicot aquifer	2	181	183	19
295605095184701	6506530	hds_01_157_200	--	--	Harris	--	Chicot aquifer	2	158	201	30
294237095342301	6520224	hds_01_182_175	--	--	Harris	--	Chicot aquifer	2	183	176	23
294237095351901	6520118	hds_01_182_173	--	--	Harris	--	Chicot aquifer	2	183	174	4
294921095312907	6512633	hds_01_170_179	--	--	Harris	--	Chicot aquifer	2	171	180	44
295130095241203	6513323	hds_01_166_191	--	--	Harris	--	Chicot aquifer	2	167	192	5
295957095460901	6502312	hds_01_150_156	--	--	Harris	--	Chicot aquifer	2	151	157	15
295252095300401	6504901	hds_01_163_182	--	--	Harris	--	Chicot aquifer	2	164	183	45
300146095241801	6061905	hds_01_147_191	--	--	Harris	--	Chicot aquifer	2	148	192	28
300239095212601	6062401	hds_01_145_195	--	--	Harris	--	Chicot aquifer	2	146	196	26

Table 8.1. Wells with groundwater-level observations used for history matching in the Gulf Coast Land Subsidence and Groundwater-Flow model (GULF model), southeast Texas.—Continued

[USGS well ID is the well identifier used by the U.S. Geological Survey (USGS; 2021b); TWDB well ID is the well identifier used by the Texas Water Development Board (TWDB; 2020b); obs., observations; --, not included in the GULF model; conf. unit, confining unit]

USGS well ID	TWDB well ID	Model observation name[1]	Identifier for observation well in this report[2]		County	Groundwater-well groups (figs. 19–36, 51–52, 119–138)	Hydrogeologic unit	Model layer	Model row	Model column	Number of obs.
			Figures 19–36, 51–52	Figures 119–138							
300111095132302	6063714	hds_01_148_208	--	--	Harris	--	Chicot aquifer	2	149	209	41
300007095354701	6060712	hds_01_150_172	--	--	Harris	--	Chicot aquifer	2	151	173	18
295518095240201	6505606	hds_01_159_191	--	--	Harris	--	Chicot aquifer	2	160	192	6
295616095195803	6506532	hds_01_157_198	--	--	Harris	--	Chicot aquifer	2	158	199	9
295204095261301	6513225	hds_01_165_188	--	--	Harris	--	Chicot aquifer	2	166	189	29
295651095083501	6507601	hds_01_156_217	--	--	Harris	--	Chicot aquifer	2	157	218	20
293539095054201	6532104	hds_01_195_221	--	--	Harris	--	Chicot aquifer	2	196	222	22
300321095060201	6064407	hds_01_144_220	--	--	Harris	--	Chicot aquifer	2	145	221	33
295411095174601	6506804	hds_01_161_202	--	--	Harris	--	Chicot aquifer	2	162	203	17
300359095122902	6063513	hds_01_143_210	--	--	Harris	--	Chicot aquifer	2	144	211	22
300403095125402	6063512	hds_01_143_212	--	--	Harris	--	Chicot aquifer	2	144	213	22
294844095342401	6512522	hds_01_171_175	--	--	Harris	--	Chicot aquifer	2	172	176	25
295424095240001	6505955	hds_01_161_191	--	--	Harris	--	Chicot aquifer	2	162	192	2
300211095350102	6060409	hds_01_146_174	--	--	Harris	--	Chicot aquifer	2	147	175	15
300249095355701	6060407	hds_01_145_172	--	--	Harris	--	Chicot aquifer	2	146	173	15
300101095211301	6062716	hds_01_148_196	--	--	Harris	--	Chicot aquifer	2	149	197	13
300928095324401	6052810	hds_01_133_177	--	--	Harris	--	Chicot aquifer	2	134	178	3
294909095121101	6515514	hds_01_170_211	--	--	Harris	--	Chicot aquifer	2	171	212	10
300355095093501	6063602	hds_01_143_214	--	--	Harris	--	Chicot aquifer	2	144	215	15
294606095383901	6511921	hds_01_176_168	--	--	Harris	--	Chicot aquifer	2	177	169	8
294716095401201	6511809	hds_01_174_165	--	--	Harris	--	Chicot aquifer	2	175	166	3
295842095361201	6504109	hds_02_153_172	--	--	Harris	--	Evangeline aquifer	3	154	173	27
294253095352701	6520110	hds_02_182_173	--	--	Harris	--	Evangeline aquifer	3	183	174	68
295836095233301	6505309	hds_02_153_192	--	--	Harris	--	Evangeline aquifer	3	154	193	19
293854095270701	6521804	hds_02_189_187	--	--	Harris	--	Evangeline aquifer	3	190	188	15
294214095155501	6522602	hds_02_183_205	--	--	Harris	--	Evangeline aquifer	3	184	206	20
294909095200301	6514403	hds_02_170_198	--	--	Harris	--	Evangeline aquifer	3	171	199	48

Table 8.1. Wells with groundwater-level observations used for history matching in the Gulf Coast Land Subsidence and Groundwater-Flow model (GULF model), southeast Texas.—Continued

[USGS well ID is the well identifier used by the U.S. Geological Survey (USGS; 2021b); TWDB well ID is the well identifier used by the Texas Water Development Board (TWDB; 2020b); obs., observations; --, not included in the GULF model; conf. unit, confining unit]

USGS well ID	TWDB well ID	Model observation name[1]	Identifier for observation well in this report[2]		County	Groundwater-well groups (figs. 19–36, 51–52, 119–138)	Hydrogeologic unit	Model layer	Model row	Model column	Number of obs.
			Figures 19–36, 51–52	Figures 119–138							
295019095240801	6513304	hds_02_168_191	--	--	Harris	--	Evangeline aquifer	3	169	192	47
295029095200101	6514103	hds_02_168_198	--	--	Harris	--	Evangeline aquifer	3	169	199	41
295944095155801	[3]6506302	hds_02_151_204	--	--	Harris	--	Evangeline aquifer	3	152	205	19
294409095105501	6523214	hds_02_179_213	--	--	Harris	--	Evangeline aquifer	3	180	214	20
294122095265601	6521504	hds_02_185_187	--	--	Harris	--	Evangeline aquifer	3	186	188	22
294320095231901	6521304	hds_02_181_193	--	--	Harris	--	Evangeline aquifer	3	182	194	33
294548095310701	6512930	hds_02_177_180	--	--	Harris	--	Evangeline aquifer	3	178	181	3
295155095282401	6513111	hds_02_165_184	--	--	Harris	--	Evangeline aquifer	3	166	185	36
295830095333501	6504210	hds_02_153_176	--	--	Harris	--	Evangeline aquifer	3	154	177	6
300053095271901	6061824	hds_02_149_186	--	--	Harris	--	Evangeline aquifer	3	150	187	6
294452095354501	6520104	hds_02_178_173	--	--	Harris	--	Evangeline aquifer	3	179	174	39
294527095014911	6516931	hds_02_177_227	--	--	Harris	--	Evangeline aquifer	3	178	228	243
295647095343901	6504518	hds_02_156_174	--	--	Harris	--	Evangeline aquifer	3	157	175	14
294605095383001	6511913	hds_02_176_168	--	--	Harris	--	Evangeline aquifer	3	177	169	17
295621095324701	6504517	hds_02_157_177	--	--	Harris	--	Evangeline aquifer	3	158	178	4
300551095330401	6060203	hds_02_139_177	--	--	Harris	--	Evangeline aquifer	3	140	178	23
293349095070901	6532424	hds_02_198_219	--	--	Harris	--	Evangeline aquifer	3	199	220	235
294326095321001	6520322	hds_02_181_178	--	--	Harris	--	Evangeline aquifer	3	182	179	7
300159095311301	6060912	hds_02_147_180	--	--	Harris	--	Evangeline aquifer	3	148	181	3
294237095093207	6523325	hds_02_182_215	--	--	Harris	--	Evangeline aquifer	3	183	216	168
300053095292601	6061728	hds_02_149_182	--	--	Harris	--	Evangeline aquifer	3	150	183	16
300138095475701	6058811	hds_02_147_153	--	--	Harris	--	Evangeline aquifer	3	148	154	2
294338095270403	6521230	hds_02_181_187	--	--	Harris	--	Evangeline aquifer	3	182	188	234
294306095371801	6520123	hds_02_182_170	--	--	Harris	--	Evangeline aquifer	3	183	171	30
294215095301502	6520626	hds_02_183_181	--	--	Harris	--	Evangeline aquifer	3	184	182	36
295544095462401	6502603	hds_02_158_155	--	--	Harris	--	Evangeline aquifer	3	159	156	35
295932095514701	6502101	hds_02_151_147	--	--	Harris	--	Evangeline aquifer	3	152	148	26

Table 8.1. Wells with groundwater-level observations used for history matching in the Gulf Coast Land Subsidence and Groundwater-Flow model (GULF model), southeast Texas.—Continued

[USGS well ID is the well identifier used by the U.S. Geological Survey (USGS; 2021b); TWDB well ID is the well identifier used by the Texas Water Development Board (TWDB; 2020b); obs., observations; --, not included in the GULF model; conf. unit, confining unit]

USGS well ID	TWDB well ID	Model observation name[1]	Identifier for observation well in this report[2]		County	Groundwater-well groups (figs. 19–36, 51–52, 119–138)	Hydrogeologic unit	Model layer	Model row	Model column	Number of obs.
			Figures 19–36, 51–52	Figures 119–138							
295553095191201	6506528	hds_02_158_199	--	--	Harris	--	Evangeline aquifer	3	159	200	38
294414095364202	6520126	hds_02_179_171	--	--	Harris	--	Evangeline aquifer	3	180	172	36
294723095370501	6512730	hds_02_174_170	--	--	Harris	--	Evangeline aquifer	3	175	171	46
294301095341801	6520226	hds_02_182_175	--	--	Harris	--	Evangeline aquifer	3	183	176	32
295240095375601	6503915	hds_02_164_169	--	--	Harris	--	Evangeline aquifer	3	165	170	37
295609095233801	6505618	hds_02_157_192	--	--	Harris	--	Evangeline aquifer	3	158	193	3
295703095245101	6505619	hds_02_155_190	--	--	Harris	--	Evangeline aquifer	3	156	191	23
294127095342502	6520519	hds_02_185_175	--	--	Harris	--	Evangeline aquifer	3	186	176	25
295228095263101	6513222	hds_02_164_187	--	--	Harris	--	Evangeline aquifer	3	165	188	31
294731095414201	6511514	hds_02_173_163	--	--	Harris	--	Evangeline aquifer	3	174	164	27
294113095361701	6520421	hds_02_185_172	--	--	Harris	--	Evangeline aquifer	3	186	173	26
295027095312301	6512328	hds_02_168_180	--	--	Harris	--	Evangeline aquifer	3	169	181	35
295929095432201	6503111	hds_02_151_160	--	--	Harris	--	Evangeline aquifer	3	152	161	2
295555095344601	6504534	hds_02_158_174	--	--	Harris	--	Evangeline aquifer	3	159	175	2
300342095282201	6061415	hds_02_143_184	--	--	Harris	--	Evangeline aquifer	3	144	185	6
295955095502601	6502109	hds_02_151_149	--	--	Harris	--	Evangeline aquifer	3	152	150	2
293933095342101	6520813	hds_02_188_175	--	--	Harris	--	Evangeline aquifer	3	189	176	10
300819095315501	6052903	hds_02_135_178	--	--	Harris	--	Evangeline aquifer	3	136	179	9
300049095305801	6060921	hds_04_149_180	--	--	Harris	--	Jasper aquifer	5	150	181	5
300044095293201	6061727	hds_04_149_182	--	--	Harris	--	Jasper aquifer	5	150	183	7
300211095350101	6060408	hds_04_146_174	--	--	Harris	--	Jasper aquifer	5	147	175	14
300054095271801	6061841	hds_04_149_186	--	--	Harris	--	Jasper aquifer	5	150	187	14
295915095311501	6504320	hds_04_152_180	--	--	Harris	--	Jasper aquifer	5	153	181	12
300814095300001	6052902	hds_04_135_178	--	--	Harris	--	Jasper aquifer	5	136	179	8
284153096193000	8022501	hds_01_294_102	--	--	Jackson	--	Chicot aquifer	2	295	103	20
290059096395300	6659901	hds_01_259_069	--	--	Jackson	--	Chicot aquifer	2	260	70	15
--	8021214	hds_01_292_089	--	--	Jackson	--	Chicot aquifer	2	293	90	1

Table 8.1. Wells with groundwater-level observations used for history matching in the Gulf Coast Land Subsidence and Groundwater-Flow model (GULF model), southeast Texas.—Continued

[USGS well ID is the well identifier used by the U.S. Geological Survey (USGS; 2021b); TWDB well ID is the well identifier used by the Texas Water Development Board (TWDB; 2020b); obs., observations; --, not included in the GULF model; conf. unit, confining unit]

USGS well ID	TWDB well ID	Model observation name[1]	Identifier for observation well in this report[2]		County	Groundwater-well groups (figs. 19–36, 51–52, 119–138)	Hydrogeologic unit	Model layer	Model row	Model column	Number of obs.
			Figures 19–36, 51–52	Figures 119–138							
--	8004504	hds_01_266_080	--	--	Jackson	--	Chicot aquifer	2	267	81	17
--	6651505	hds_02_238_067	--	--	Jackson	--	Evangeline aquifer	3	239	68	49
--	6650801	hds_02_245_056	--	--	Jackson	--	Evangeline aquifer	3	246	57	3
291032096363500	6652407	hds_02_242_074	--	--	Jackson	--	Evangeline aquifer	3	243	75	6
--	6658402	hds_02_252_050	--	--	Jackson	--	Evangeline aquifer	3	253	51	43
--	6660613	hds_02_256_084	--	--	Jackson	--	Evangeline aquifer	3	257	85	19
--	6201803	hds_05_047_330	--	--	Jasper	--	Catahoula conf. unit	6	48	331	26
301537094051301	6148701	hds_01_120_317	--	--	Jasper	--	Chicot aquifer	2	121	318	20
303622093531701	6225308	hds_01_081_336	--	--	Jasper	--	Chicot aquifer	2	82	337	8
302642093580701	6233409	hds_01_099_328	--	--	Jasper	--	Chicot aquifer	2	100	329	24
300345094024001	6164509	hds_01_142_322	--	--	Jefferson	--	Chicot aquifer	2	143	323	24
--	6164505	hds_01_143_319	--	--	Jefferson	--	Chicot aquifer	2	144	320	11
--	6408201	hds_01_152_321	--	--	Jefferson	--	Chicot aquifer	2	153	322	30
300933094161601	6154902	hds_01_131_300	--	--	Jefferson	--	Chicot aquifer	2	132	301	28
--	6164405	hds_01_139_317	--	--	Jefferson	--	Chicot aquifer	2	140	318	16
--	6739517	hds_05_213_020	--	--	Lavaca	--	Catahoula conf. unit	6	214	21	14
--	6732106	hds_05_192_027	--	--	Lavaca	--	Catahoula conf. unit	6	193	28	3
--	6650401	hds_02_241_052	--	--	Lavaca	--	Evangeline aquifer	3	242	53	11
--	6635902	hds_02_219_071	--	--	Lavaca	--	Evangeline aquifer	3	220	72	12
--	6644402	hds_02_225_073	--	--	Lavaca	--	Evangeline aquifer	3	226	74	34
--	6643803	hds_02_231_067	--	--	Lavaca	--	Evangeline aquifer	3	232	68	43
--	6641903	hds_02_232_047	--	--	Lavaca	--	Evangeline aquifer	3	233	48	37
--	6634207	hds_02_208_057	--	--	Lavaca	--	Evangeline aquifer	3	209	58	16
--	6756605	hds_02_240_034	--	--	Lavaca	--	Evangeline aquifer	3	241	35	3
--	6633507	hds_04_211_043	--	--	Lavaca	--	Jasper aquifer	5	212	44	10
--	6740503	hds_04_211_031	--	--	Lavaca	--	Jasper aquifer	5	212	32	31
--	6740301	hds_04_207_036	--	--	Lavaca	--	Jasper aquifer	5	208	37	34

Table 8.1. Wells with groundwater-level observations used for history matching in the Gulf Coast Land Subsidence and Groundwater-Flow model (GULF model), southeast Texas.—Continued

[USGS well ID is the well identifier used by the U.S. Geological Survey (USGS; 2021b); TWDB well ID is the well identifier used by the Texas Water Development Board (TWDB; 2020b); obs., observations; --, not included in the GULF model; conf. unit, confining unit]

USGS well ID	TWDB well ID	Model observation name[1]	Identifier for observation well in this report[2]		County	Groundwater-well groups (figs. 19–36, 51–52, 119–138)	Hydrogeologic unit	Model layer	Model row	Model column	Number of obs.
			Figures 19–36, 51–52	Figures 119–138							
--	6747607	hds_04_227_023	--	--	Lavaca	--	Jasper aquifer	5	228	24	30
295924094354700	6404101	hds_01_150_269	--	--	Liberty	--	Chicot aquifer	2	151	270	1
301417094442301	6151111	hds_01_123_255	--	--	Liberty	--	Chicot aquifer	2	124	256	20
301948095030701	6048505	hds_01_113_225	--	--	Liberty	--	Chicot aquifer	2	114	226	15
301938094585501	6141411	hds_01_114_231	--	--	Liberty	--	Chicot aquifer	2	115	232	15
300921094442901	6151717	hds_01_132_255	--	--	Liberty	--	Chicot aquifer	2	133	256	20
301840094574501	6141409	hds_01_115_233	--	--	Liberty	--	Chicot aquifer	2	116	234	16
300555094450501	6158305	hds_02_138_254	--	--	Liberty	--	Evangeline aquifer	3	139	255	1
--	8109201	hds_01_279_140	--	--	Matagorda	--	Chicot aquifer	2	280	141	12
--	6558401	hds_01_255_148	--	--	Matagorda	--	Chicot aquifer	2	256	149	26
284257096040400	8024201	hds_01_293_127	--	--	Matagorda	--	Chicot aquifer	2	294	128	44
--	8014606	hds_01_283_108	--	--	Matagorda	--	Chicot aquifer	2	284	109	5
290131096084100	6663901	hds_01_258_120	--	--	Matagorda	--	Chicot aquifer	2	259	121	9
290854095533800	6549901	hds_01_245_144	--	--	Matagorda	--	Chicot aquifer	2	246	145	144
284319096153000	8022302	hds_01_292_109	--	--	Matagorda	--	Chicot aquifer	2	293	110	2
285315096063500	8008701	hds_01_274_123	--	--	Matagorda	--	Chicot aquifer	2	275	124	8
285837096005400	8008302	hds_01_263_132	--	--	Matagorda	--	Chicot aquifer	2	264	133	15
290028095594700	6557702	hds_01_260_134	--	--	Matagorda	--	Chicot aquifer	2	261	135	10
--	8016301	hds_01_277_132	--	--	Matagorda	--	Chicot aquifer	2	278	133	15
--	8008504	hds_01_266_127	--	--	Matagorda	--	Chicot aquifer	2	267	128	21
284659095371600	8111901	hds_01_286_169	--	--	Matagorda	--	Chicot aquifer	2	287	170	35
--	8101205	hds_01_265_141	--	--	Matagorda	--	Chicot aquifer	2	266	142	116
--	8102605	hds_01_267_157	--	--	Matagorda	--	Chicot aquifer	2	268	158	110
--	8014903	hds_01_287_108	--	--	Matagorda	--	Chicot aquifer	2	288	109	109
290141095554400	6557802	hds_01_258_140	--	--	Matagorda	--	Chicot aquifer	2	259	141	47
301443095091801	6055313	hds_03_123_214	--	--	Montgomery	--	Burkeville conf. unit	4	124	215	31
301505095343704	6044807	hds_03_122_174	--	--	Montgomery	--	Burkeville conf. unit	4	123	175	65

Table 8.1. Wells with groundwater-level observations used for history matching in the Gulf Coast Land Subsidence and Groundwater-Flow model (GULF model), southeast Texas.—Continued

[USGS well ID is the well identifier used by the U.S. Geological Survey (USGS; 2021b); TWDB well ID is the well identifier used by the Texas Water Development Board (TWDB; 2020b); obs., observations; --, not included in the GULF model; conf. unit, confining unit]

USGS well ID	TWDB well ID	Model observation name[1]	Identifier for observation well in this report[2]		County	Groundwater-well groups (figs. 19–36, 51–52, 119–138)	Hydrogeologic unit	Model layer	Model row	Model column	Number of obs.
			Figures 19–36, 51–52	Figures 119–138							
301911095092901	6047602	hds_03_115_214	--	--	Montgomery	--	Burkeville conf. unit	4	116	215	17
302452095242001	6037909	hds_03_104_191	--	--	Montgomery	--	Burkeville conf. unit	4	105	192	18
302208095365702	6044124	hds_05_109_170	--	--	Montgomery	--	Catahoula conf. unit	6	110	171	50
302248095294401	6037718	hds_05_108_182	--	--	Montgomery	--	Catahoula conf. unit	6	109	183	48
302251095384501	6035915	hds_05_108_168	--	--	Montgomery	--	Catahoula conf. unit	6	109	169	46
302332095370001	6036710	hds_05_107_170	--	--	Montgomery	--	Catahoula conf. unit	6	108	171	46
302609095382601	6035604	hds_05_102_168	--	--	Montgomery	--	Catahoula conf. unit	6	103	169	47
302522095284301	6037418	hds_05_103_184	--	--	Montgomery	--	Catahoula conf. unit	6	104	185	38
302534095300401	6036615	hds_05_103_181	--	--	Montgomery	--	Catahoula conf. unit	6	104	182	41
300534095112801	6063205	hds_01_139_211	--	--	Montgomery	--	Chicot aquifer	2	140	212	22
301853095180701	6046505	hds_01_115_201	--	--	Montgomery	--	Chicot aquifer	2	116	202	20
300742095244301	6053902	hds_01_136_190	--	--	Montgomery	--	Chicot aquifer	2	137	191	31
300831095173401	6054804	hds_01_134_202	--	--	Montgomery	--	Chicot aquifer	2	135	203	12
300637095240801	6061307	hds_01_138_191	--	--	Montgomery	--	Chicot aquifer	2	139	192	22
301124095242501	6053609	hds_01_128_190	--	--	Montgomery	--	Chicot aquifer	2	129	191	9
301328095171801	6054306	hds_01_125_202	--	--	Montgomery	--	Chicot aquifer	2	126	203	14
300602095145501	6063109	hds_01_139_206	--	--	Montgomery	--	Chicot aquifer	2	140	207	20
301124095152901	6054612	hds_01_129_204	--	--	Montgomery	--	Chicot aquifer	2	130	205	12
--	6053110	hds_01_124_185	--	--	Montgomery	--	Chicot aquifer	2	125	186	7
301420095093201	6055315	hds_01_124_214	--	--	Montgomery	--	Chicot aquifer	2	125	215	21
301948095290002	6045412	hds_01_114_183	--	--	Montgomery	--	Chicot aquifer	2	115	184	107
300824095274701	6053718	hds_01_135_185	--	--	Montgomery	--	Chicot aquifer	2	136	186	147
300806095130201	6055712	hds_01_135_209	--	--	Montgomery	--	Chicot aquifer	2	136	210	20
300849095143301	6055710	hds_01_134_206	--	--	Montgomery	--	Chicot aquifer	2	135	207	145
301254095270401	6053212	hds_01_126_186	--	--	Montgomery	--	Chicot aquifer	2	127	187	7
300849095412601	6051811	hds_01_134_163	--	--	Montgomery	--	Chicot aquifer	2	135	164	2
300720095165701	6062305	hds_01_137_203	--	--	Montgomery	--	Chicot aquifer	2	138	204	7

Table 8.1. Wells with groundwater-level observations used for history matching in the Gulf Coast Land Subsidence and Groundwater-Flow model (GULF model), southeast Texas.—Continued

[USGS well ID is the well identifier used by the U.S. Geological Survey (USGS; 2021b); TWDB well ID is the well identifier used by the Texas Water Development Board (TWDB; 2020b); obs., observations; --, not included in the GULF model; conf. unit, confining unit]

USGS well ID	TWDB well ID	Model observation name[1]	Identifier for observation well in this report[2]		County	Groundwater-well groups (figs. 19–36, 51–52, 119–138)	Hydrogeologic unit	Model layer	Model row	Model column	Number of obs.
			Figures 19–36, 51–52	Figures 119–138							
300838095244701	6053903	hds_01_134_190	--	--	Montgomery	--	Chicot aquifer	2	135	191	16
301234095255802	6053215	hds_01_127_188	--	--	Montgomery	--	Chicot aquifer	2	128	189	15
300658095443101	6059102	hds_01_137_158	--	--	Montgomery	--	Chicot aquifer	2	138	159	12
300907095182301	6054808	hds_01_133_200	--	--	Montgomery	--	Chicot aquifer	2	134	201	9
301136095212101	6054406	hds_01_129_195	--	--	Montgomery	--	Chicot aquifer	2	130	196	13
300954095421101	6051816	hds_01_132_162	--	--	Montgomery	--	Chicot aquifer	2	133	163	10
301350095383801	6051308	hds_01_125_168	--	--	Montgomery	--	Chicot aquifer	2	126	169	9
300906095392001	6051909	hds_01_134_167	--	--	Montgomery	--	Chicot aquifer	2	135	168	9
300915095343701	6052811	hds_01_133_174	--	--	Montgomery	--	Chicot aquifer	2	134	175	11
301837095164001	6046605	hds_01_116_203	--	--	Montgomery	--	Chicot aquifer	2	117	204	2
301139095393801	6051603	hds_01_129_166	--	--	Montgomery	--	Chicot aquifer	2	130	167	9
301931095145301	6047408	hds_01_114_206	--	--	Montgomery	--	Chicot aquifer	2	115	207	9
300643095214301	6062101	hds_01_138_195	--	--	Montgomery	--	Chicot aquifer	2	139	196	7
301002095251401	6053520	hds_01_132_189	--	--	Montgomery	--	Chicot aquifer	2	133	190	9
300439095202201	6062404	hds_01_142_197	--	--	Montgomery	--	Chicot aquifer	2	143	198	7
301047095104801	6055512	hds_01_130_212	--	--	Montgomery	--	Chicot aquifer	2	131	213	7
301310095190201	6054209	hds_01_126_199	--	--	Montgomery	--	Chicot aquifer	2	127	200	7
302522095284201	6037401	hds_02_103_184	--	--	Montgomery	--	Evangeline aquifer	3	104	185	9
--	6053205	hds_02_124_187	--	--	Montgomery	--	Evangeline aquifer	3	125	188	4
300816095274701	6053709	hds_02_135_185	--	--	Montgomery	--	Evangeline aquifer	3	136	186	36
301234095255801	6053208	hds_02_127_188	--	--	Montgomery	--	Evangeline aquifer	3	128	189	21
302511095300001	6036611	hds_02_104_181	--	--	Montgomery	--	Evangeline aquifer	3	105	182	22
301904095414801	6043511	hds_02_115_163	--	--	Montgomery	--	Evangeline aquifer	3	116	164	31
302125095310001	6044315	hds_02_111_180	--	--	Montgomery	--	Evangeline aquifer	3	112	181	4
300419095154301	6062604	hds_02_142_205	--	--	Montgomery	--	Evangeline aquifer	3	143	206	38
302130095280201	6045112	hds_02_110_185	--	--	Montgomery	--	Evangeline aquifer	3	111	186	2
301616095293801	6045714	hds_02_120_182	--	--	Montgomery	--	Evangeline aquifer	3	121	183	6

Table 8.1. Wells with groundwater-level observations used for history matching in the Gulf Coast Land Subsidence and Groundwater-Flow model (GULF model), southeast Texas.—Continued

[USGS well ID is the well identifier used by the U.S. Geological Survey (USGS; 2021b); TWDB well ID is the well identifier used by the Texas Water Development Board (TWDB; 2020b); obs., observations; --, not included in the GULF model; conf. unit, confining unit]

USGS well ID	TWDB well ID	Model observation name[1]	Identifier for observation well in this report[2]		County	Groundwater-well groups (figs. 19–36, 51–52, 119–138)	Hydrogeologic unit	Model layer	Model row	Model column	Number of obs.
			Figures 19–36, 51–52	Figures 119–138							
301052095265501	6053514	hds_02_130_187	--	--	Montgomery	--	Evangeline aquifer	3	131	188	15
302331095283101	6037713	hds_02_107_184	--	--	Montgomery	--	Evangeline aquifer	3	108	185	5
302436095263501	6037806	hds_02_105_187	--	--	Montgomery	--	Evangeline aquifer	3	106	188	14
300801095393701	6051907	hds_02_135_166	--	--	Montgomery	--	Evangeline aquifer	3	136	167	13
--	6036811	hds_02_105_176	--	--	Montgomery	--	Evangeline aquifer	3	106	177	8
300446095121901	6063507	hds_02_141_210	--	--	Montgomery	--	Evangeline aquifer	3	142	211	29
301104095422001	6051513	hds_02_130_162	--	--	Montgomery	--	Evangeline aquifer	3	131	163	10
301218095445401	6051409	hds_02_128_158	--	--	Montgomery	--	Evangeline aquifer	3	129	159	22
--	6044216	hds_02_112_176	--	--	Montgomery	--	Evangeline aquifer	3	113	177	6
--	6037310	hds_02_097_190	--	--	Montgomery	--	Evangeline aquifer	3	98	191	7
--	6044117	hds_02_111_173	--	--	Montgomery	--	Evangeline aquifer	3	112	174	3
--	6035704	hds_02_108_160	--	--	Montgomery	--	Evangeline aquifer	3	109	161	8
301220095305502	6052605	hds_02_127_180	--	--	Montgomery	--	Evangeline aquifer	3	128	181	27
302323095194201	6038806	hds_02_107_198	--	--	Montgomery	--	Evangeline aquifer	3	108	199	17
301034095283802	6053409	hds_02_131_184	--	--	Montgomery	--	Evangeline aquifer	3	132	185	21
301614095284201	6045716	hds_02_120_184	--	--	Montgomery	--	Evangeline aquifer	3	121	185	13
301135095290102	6053417	hds_02_129_184	--	--	Montgomery	--	Evangeline aquifer	3	130	185	19
301103095334302	6052502	hds_02_130_176	--	--	Montgomery	--	Evangeline aquifer	3	131	177	20
301039095092901	6055605	hds_02_130_215	--	--	Montgomery	--	Evangeline aquifer	3	131	216	14
300544095231501	6061308	hds_02_140_193	--	--	Montgomery	--	Evangeline aquifer	3	141	194	14
301931095355801	6044411	hds_02_114_172	--	--	Montgomery	--	Evangeline aquifer	3	115	173	6
301311095335701	6052215	hds_02_126_175	--	--	Montgomery	--	Evangeline aquifer	3	127	176	6
302644095320601	6036614	hds_02_101_178	--	--	Montgomery	--	Evangeline aquifer	3	102	179	2
301711095381201	[4]6043902	hds_02_119_168	--	--	Montgomery	--	Evangeline aquifer	3	120	169	11
301051095322402	6052613	hds_02_130_178	--	--	Montgomery	--	Evangeline aquifer	3	131	179	11
301020095442801	6051415	hds_02_131_158	--	--	Montgomery	--	Evangeline aquifer	3	132	159	8
300621095225201	6061309	hds_02_138_193	--	--	Montgomery	--	Evangeline aquifer	3	139	194	11

Table 8.1. Wells with groundwater-level observations used for history matching in the Gulf Coast Land Subsidence and Groundwater-Flow model (GULF model), southeast Texas.—Continued

[USGS well ID is the well identifier used by the U.S. Geological Survey (USGS; 2021b); TWDB well ID is the well identifier used by the Texas Water Development Board (TWDB; 2020b); obs., observations; --, not included in the GULF model; conf. unit, confining unit]

USGS well ID	TWDB well ID	Model observation name[1]	Identifier for observation well in this report[2]		County	Groundwater-well groups (figs. 19–36, 51–52, 119–138)	Hydrogeologic unit	Model layer	Model row	Model column	Number of obs.
			Figures 19–36, 51–52	Figures 119–138							
301106095351101	6052410	hds_02_130_173	--	--	Montgomery	--	Evangeline aquifer	3	131	174	9
301318095364501	6052113	hds_02_126_171	--	--	Montgomery	--	Evangeline aquifer	3	127	172	8
301250095400701	6051310	hds_02_127_166	--	--	Montgomery	--	Evangeline aquifer	3	128	167	6
301412095302101	6052309	hds_02_124_181	--	--	Montgomery	--	Evangeline aquifer	3	125	182	7
301021095153501	6054614	hds_02_131_205	--	--	Montgomery	--	Evangeline aquifer	3	132	206	6
301335095385001	6051311	hds_02_125_167	--	--	Montgomery	--	Evangeline aquifer	3	126	168	7
300923095282601	6053727	hds_02_133_184	--	--	Montgomery	--	Evangeline aquifer	3	134	185	3
302522095284202	6037402	hds_04_103_184	--	--	Montgomery	--	Jasper aquifer	5	104	185	59
302416095182701	6038801	hds_04_105_200	--	--	Montgomery	--	Jasper aquifer	5	106	201	2
302338095361601	6036705	hds_04_107_171	--	--	Montgomery	--	Jasper aquifer	5	108	172	19
301902095365101	6044408	hds_04_114_170	--	--	Montgomery	--	Jasper aquifer	5	115	171	7
302240095440101	6035703	hds_04_108_159	--	--	Montgomery	--	Jasper aquifer	5	109	160	30
302412095382101	6035907	hds_04_106_168	--	--	Montgomery	--	Jasper aquifer	5	107	169	17
302105095255601	6045207	hds_04_111_188	--	--	Montgomery	--	Jasper aquifer	5	112	189	16
302557095372201	6036409	hds_04_102_170	--	--	Montgomery	--	Jasper aquifer	5	103	171	64
302311095450501	6035812	hds_04_107_162	--	--	Montgomery	--	Jasper aquifer	5	108	163	26
302444095340802	6036810	hds_04_105_175	--	--	Montgomery	--	Jasper aquifer	5	106	176	27
302450095263601	6037805	hds_04_104_187	--	--	Montgomery	--	Jasper aquifer	5	105	188	6
301220095305501	6052604	hds_04_127_180	--	--	Montgomery	--	Jasper aquifer	5	128	181	28
302208095365701	6044115	hds_04_109_170	--	--	Montgomery	--	Jasper aquifer	5	110	171	6
302753095320601	6036305	hds_04_099_178	--	--	Montgomery	--	Jasper aquifer	5	100	179	20
301516095270801	6045813	hds_04_122_186	--	--	Montgomery	--	Jasper aquifer	5	123	187	21
301849095225701	6045615	hds_04_115_193	--	--	Montgomery	--	Jasper aquifer	5	116	194	9
302715095281401	6037416	hds_04_100_184	--	--	Montgomery	--	Jasper aquifer	5	101	185	6
301034095283801	6053408	hds_04_131_184	--	--	Montgomery	--	Jasper aquifer	5	132	185	21
300920095271401	6053829	hds_04_133_186	--	--	Montgomery	--	Jasper aquifer	5	134	187	19
302332095245201	6037910	hds_04_107_190	--	--	Montgomery	--	Jasper aquifer	5	108	191	9

Table 8.1. Wells with groundwater-level observations used for history matching in the Gulf Coast Land Subsidence and Groundwater-Flow model (GULF model), southeast Texas.—Continued

[USGS well ID is the well identifier used by the U.S. Geological Survey (USGS; 2021b); TWDB well ID is the well identifier used by the Texas Water Development Board (TWDB; 2020b); obs., observations; --, not included in the GULF model; conf. unit, confining unit]

USGS well ID	TWDB well ID	Model observation name[1]	Identifier for observation well in this report[2]		County	Groundwater-well groups (figs. 19–36, 51–52, 119–138)	Hydrogeologic unit	Model layer	Model row	Model column	Number of obs.
			Figures 19–36, 51–52	Figures 119–138							
301613095283701	6045704	hds_04_120_184	--	--	Montgomery	--	Jasper aquifer	5	121	185	7
300943095402501	6051815	hds_04_132_165	--	--	Montgomery	--	Jasper aquifer	5	133	166	14
301103095334301	6052501	hds_04_130_176	--	--	Montgomery	--	Jasper aquifer	5	131	177	15
302608095234301	6037603	hds_04_102_192	--	--	Montgomery	--	Jasper aquifer	5	103	193	17
301917095413101	6043514	hds_04_114_164	--	--	Montgomery	--	Jasper aquifer	5	115	165	17
301133095273401	6053418	hds_04_129_186	--	--	Montgomery	--	Jasper aquifer	5	130	187	15
302500095464901	6034605	hds_04_104_155	--	--	Montgomery	--	Jasper aquifer	5	105	156	9
303222095455301	6026901	hds_04_090_156	--	--	Montgomery	--	Jasper aquifer	5	91	157	8
301016095165501	6054613	hds_04_131_203	--	--	Montgomery	--	Jasper aquifer	5	132	204	14
300728095292901	6061104	hds_04_136_182	--	--	Montgomery	--	Jasper aquifer	5	137	183	12
302456095423701	6035707	hds_04_104_161	--	--	Montgomery	--	Jasper aquifer	5	105	162	3
302138095265501	6045213	hds_04_110_186	--	--	Montgomery	--	Jasper aquifer	5	111	187	8
302708095293201	6037417	hds_04_100_182	--	--	Montgomery	--	Jasper aquifer	5	101	183	7
302233095230701	6037911	hds_04_108_193	--	--	Montgomery	--	Jasper aquifer	5	109	194	12
302747095385901	6035303	hds_04_099_167	--	--	Montgomery	--	Jasper aquifer	5	100	168	9
302216095354201	6044122	hds_04_109_172	--	--	Montgomery	--	Jasper aquifer	5	110	173	24
301105095351401	6052409	hds_04_130_173	--	--	Montgomery	--	Jasper aquifer	5	131	174	10
301254095270301	6053217	hds_04_126_186	--	--	Montgomery	--	Jasper aquifer	5	127	187	9
302500095395201	6035913	hds_04_104_166	--	--	Montgomery	--	Jasper aquifer	5	105	167	9
302356095305501	6036908	hds_04_106_180	--	--	Montgomery	--	Jasper aquifer	5	107	181	7
301929095243201	6045616	hds_04_114_190	--	--	Montgomery	--	Jasper aquifer	5	115	191	5
300922095282701	6053726	hds_04_133_184	--	--	Montgomery	--	Jasper aquifer	5	134	185	5
302252095471701	6034906	hds_04_108_154	--	--	Montgomery	--	Jasper aquifer	5	109	155	19
301732093443001	6243406	hds_01_115_350	--	--	Newton	--	Chicot aquifer	2	116	351	33
--	6242909	hds_01_119_348	--	--	Newton	--	Chicot aquifer	2	120	349	30
305104093450000	6210309	hds_04_053_348	--	--	Newton	--	Jasper aquifer	5	54	349	30
--	6203704	hds_04_047_351	--	--	Newton	--	Jasper aquifer	5	48	352	34

Table 8.1. Wells with groundwater-level observations used for history matching in the Gulf Coast Land Subsidence and Groundwater-Flow model (GULF model), southeast Texas.—Continued

[USGS well ID is the well identifier used by the U.S. Geological Survey (USGS; 2021b); TWDB well ID is the well identifier used by the Texas Water Development Board (TWDB; 2020b); obs., observations; --, not included in the GULF model; conf. unit, confining unit]

USGS well ID	TWDB well ID	Model observation name[1]	Identifier for observation well in this report[2]		County	Groundwater-well groups (figs. 19–36, 51–52, 119–138)	Hydrogeologic unit	Model layer	Model row	Model column	Number of obs.
			Figures 19–36, 51–52	Figures 119–138							
300309093454401	6258609	hds_01_142_349	--	--	Orange	--	Chicot aquifer	2	143	350	22
300623093443601	6259101	hds_01_136_351	--	--	Orange	--	Chicot aquifer	2	137	352	40
300200093490301	6258809	hds_01_144_344	--	--	Orange	--	Chicot aquifer	2	145	345	22
300453093592201	6257409	hds_01_139_327	--	--	Orange	--	Chicot aquifer	2	140	328	27
300809094005501	6156901	hds_01_133_324	--	--	Orange	--	Chicot aquifer	2	134	325	21
300906093431301	6251707	hds_01_131_353	--	--	Orange	--	Chicot aquifer	2	132	354	30
301300093444101	6251103	hds_01_124_350	--	--	Orange	--	Chicot aquifer	2	125	351	22
301410093495101	6250201	hds_01_122_342	--	--	Orange	--	Chicot aquifer	2	123	343	26
300148093524601	6257904	hds_01_145_338	--	--	Orange	--	Chicot aquifer	2	146	339	27
300754093541101	6249904	hds_01_134_335	--	--	Orange	--	Chicot aquifer	2	135	336	35
300818093492101	6250807	hds_01_133_343	--	--	Orange	--	Chicot aquifer	2	134	344	25
301237094012301	6156315	hds_01_125_324	--	--	Orange	--	Chicot aquifer	2	126	325	26
300115093502602	6258709	hds_01_146_342	--	--	Orange	--	Chicot aquifer	2	147	343	15
300842093451401	6250911	hds_01_132_350	--	--	Orange	--	Chicot aquifer	2	133	351	22
301334093510002	6250107	hds_01_123_340	--	--	Orange	--	Chicot aquifer	2	124	341	20
--	6117201	hds_03_070_235	--	--	Polk	--	Burkeville conf. unit	4	71	236	5
--	6119103	hds_03_067_256	--	--	Polk	--	Burkeville conf. unit	4	68	257	12
--	6119210	hds_03_070_261	--	--	Polk	--	Burkeville conf. unit	4	71	262	12
--	6117410	hds_03_073_232	--	--	Polk	--	Burkeville conf. unit	4	74	233	8
--	6117511	hds_03_075_234	--	--	Polk	--	Burkeville conf. unit	4	76	235	6
--	6119104	hds_03_068_254	--	--	Polk	--	Burkeville conf. unit	4	69	255	5
--	6119417	hds_03_073_253	--	--	Polk	--	Burkeville conf. unit	4	74	254	65
--	6103806	hds_05_050_258	--	--	Polk	--	Catahoula conf. unit	6	51	259	3
--	6103720	hds_05_048_253	--	--	Polk	--	Catahoula conf. unit	6	49	254	3
--	6016103	hds_05_055_221	--	--	Polk	--	Catahoula conf. unit	6	56	222	5
--	6117219	hds_04_068_235	--	--	Polk	--	Jasper aquifer	5	69	236	3
--	6016902	hds_04_066_227	--	--	Polk	--	Jasper aquifer	5	67	228	5

Table 8.1. Wells with groundwater-level observations used for history matching in the Gulf Coast Land Subsidence and Groundwater-Flow model (GULF model), southeast Texas.—Continued

[USGS well ID is the well identifier used by the U.S. Geological Survey (USGS; 2021b); TWDB well ID is the well identifier used by the Texas Water Development Board (TWDB; 2020b); obs., observations; --, not included in the GULF model; conf. unit, confining unit]

USGS well ID	TWDB well ID	Model observation name[1]	Identifier for observation well in this report[2]		County	Groundwater-well groups (figs. 19–36, 51–52, 119–138)	Hydrogeologic unit	Model layer	Model row	Model column	Number of obs.
			Figures 19–36, 51–52	Figures 119–138							
303537095073001	6031318	hds_03_084_217	--	--	San Jacinto	--	Burkeville conf. unit	4	85	218	11
303826095082401	6023907	hds_03_079_216	--	--	San Jacinto	--	Burkeville conf. unit	4	80	217	4
--	6032219	hds_03_084_222	--	--	San Jacinto	--	Burkeville conf. unit	4	85	223	70
302957094594701	6133102	hds_01_094_230	--	--	San Jacinto	--	Chicot aquifer	2	95	231	32
303000095002001	6040315	hds_01_095_228	--	--	San Jacinto	--	Chicot aquifer	2	96	229	15
--	6125410	hds_01_090_232	--	--	San Jacinto	--	Chicot aquifer	2	91	233	8
--	6047103	hds_01_109_209	--	--	San Jacinto	--	Chicot aquifer	2	110	210	6
303536095074501	6031317	hds_04_084_217	--	--	San Jacinto	--	Jasper aquifer	5	85	218	20
--	6022215	hds_04_068_199	--	--	San Jacinto	--	Jasper aquifer	5	69	200	6
--	6015810	hds_04_063_213	--	--	San Jacinto	--	Jasper aquifer	5	64	214	5
--	6130303	hds_01_084_297	--	--	Tyler	--	Chicot aquifer	2	85	298	20
--	6129704	hds_01_090_279	--	--	Tyler	--	Chicot aquifer	2	91	280	1
--	6130405	hds_01_087_289	--	--	Tyler	--	Chicot aquifer	2	88	290	1
--	6020603	hds_05_072_177	--	--	Walker	--	Catahoula conf. unit	6	73	178	22
304441095214601	6022101	hds_05_067_194	--	--	Walker	--	Catahoula conf. unit	6	68	195	12
304155095365201	6020401	hds_05_073_170	--	--	Walker	--	Catahoula conf. unit	6	74	171	3
--	6029904	hds_02_091_191	--	--	Walker	--	Evangeline aquifer	3	92	192	3
303212095291201	6029707	hds_04_091_183	--	--	Walker	--	Jasper aquifer	5	92	184	12
303143095334801	6028802	hds_04_092_175	--	--	Walker	--	Jasper aquifer	5	93	176	153
300543095592001	6057103	hds_02_140_135	--	--	Waller	--	Evangeline aquifer	3	141	136	14
300318095553401	6057506	hds_02_144_141	--	--	Waller	--	Evangeline aquifer	3	145	142	15
300419095591101	6057402	hds_02_142_135	--	--	Waller	--	Evangeline aquifer	3	143	136	28
300947095543401	6049908	hds_02_132_142	--	--	Waller	--	Evangeline aquifer	3	133	143	4
300542096045401	5964207	hds_02_140_126	--	--	Waller	--	Evangeline aquifer	3	141	127	16
300542096045403	5964206	hds_04_140_126	--	--	Waller	--	Jasper aquifer	5	141	127	19
--	5952308	hds_05_123_084	--	--	Washington	--	Catahoula conf. unit	6	124	85	6
--	5951904	hds_05_132_073	--	--	Washington	--	Catahoula conf. unit	6	133	74	5

Table 8.1. Wells with groundwater-level observations used for history matching in the Gulf Coast Land Subsidence and Groundwater-Flow model (GULF model), southeast Texas.—Continued

[USGS well ID is the well identifier used by the U.S. Geological Survey (USGS; 2021b); TWDB well ID is the well identifier used by the Texas Water Development Board (TWDB; 2020b); obs., observations; --, not included in the GULF model; conf. unit, confining unit]

USGS well ID	TWDB well ID	Model observation name[1]	Identifier for observation well in this report[2]		County	Groundwater-well groups (figs. 19–36, 51–52, 119–138)	Hydrogeologic unit	Model layer	Model row	Model column	Number of obs.
			Figures 19–36, 51–52	Figures 119–138							
--	5952706	hds_05_135_077	--	--	Washington	--	Catahoula conf. unit	6	136	78	8
--	5954913	hds_02_133_108	--	--	Washington	--	Evangeline aquifer	3	134	109	7
--	5955705	hds_02_133_112	--	--	Washington	--	Evangeline aquifer	3	134	113	6
301358096085400	5955301	hds_04_126_120	--	--	Washington	--	Jasper aquifer	5	127	121	12
300954096230800	5953915	hds_04_132_097	--	--	Washington	--	Jasper aquifer	5	133	98	200
--	5952806	hds_04_136_077	--	--	Washington	--	Jasper aquifer	5	137	78	14
--	5953812	hds_04_133_091	--	--	Washington	--	Jasper aquifer	5	134	92	7
--	5960304	hds_04_138_085	--	--	Washington	--	Jasper aquifer	5	139	86	7
--	5947505	hds_04_116_116	--	--	Washington	--	Jasper aquifer	5	117	117	6
--	6655103	hds_01_235_111	--	--	Wharton	--	Chicot aquifer	2	236	112	3
--	6654906	hds_01_247_108	--	--	Wharton	--	Chicot aquifer	2	248	109	18
--	6632809	hds_01_204_128	--	--	Wharton	--	Chicot aquifer	2	205	129	28
--	6647904	hds_01_233_118	--	--	Wharton	--	Chicot aquifer	2	234	119	17
--	6640803	hds_01_217_126	--	--	Wharton	--	Chicot aquifer	2	218	127	3
--	6541707	hds_01_231_137	--	--	Wharton	--	Chicot aquifer	2	232	138	21
--	6647201	hds_01_222_115	--	--	Wharton	--	Chicot aquifer	2	223	116	22
--	6654603	hds_02_240_107	--	--	Wharton	--	Evangeline aquifer	3	241	108	4
--	6631906	hds_02_202_120	--	--	Wharton	--	Evangeline aquifer	3	203	121	7

[1]The observation names follow the format hds_[layer]_[row]_[column]. These values are zero-based compared to the values in the "Model layer," "Model row," and "Model column," columns, which are one-based.

[2]Identifiers for colocated wells are not unique and are therefore always described in the context of a given extensometer site.

[3]Well 6506302 was plugged back to 290 feet below land surface; therefore, in NWIS (USGS, 2021b), this well is completed in the Chicot aquifer.

[4]Well 6043902 is screened in the Chicot aquifer; therefore, the classification on this table was determined to be incorrect.

Table 8.2. Global Positioning System stations used for history matching of the Gulf Coast Land Subsidence and Groundwater-Flow model (GULF model), southeast Texas.

[GPS, Global Positioning System; The following GPS stations are included on figures 76–77 and table 6 but were not included in the model: ANG6, P005, P043, P075, THSU, and UHL1. The GULF model does not include barrier islands; therefore, GPS stations P026, P043, P049, and TXGA were not included in the model]

GPS station identifier (figs. 76–92; figs. 157–171)	Model GPS observation name[1]	GPS station group (figs. 76–92; figs. 157–171)	GPS installation date	Model row	Model column	Number of observations
P070	gps_00_118_189	Conroe (figs. 78, 157)	2011	119	190	59
P071	gps_00_111_174		2011	112	175	61
TXCN	gps_00_112_187		2005	113	188	162
UH02	gps_00_115_186		2015	116	187	49
P013	gps_00_129_183	The Woodlands and Magnolia (figs. 79, 158)	2000	130	184	165
P068	gps_00_130_173		2011	131	174	64
P069	gps_00_128_186		2011	129	187	64
P073	gps_00_129_159		2012	130	160	62
P002	gps_00_150_190	Northern Harris County (figs. 80, 159)	1994	151	191	178
P008	gps_00_153_184		2000	154	185	173
P017	gps_00_140_171		2000	141	172	161
P046	gps_00_147_172		2007	148	173	84
P047	gps_00_140_189		2007	141	190	89
P048	gps_00_145_165		2007	146	166	82
ROD1	gps_00_142_179		2007	143	180	142
ZHU1	gps_00_154_198		2003	155	199	183
CFJV	gps_00_163_176	Northwestern Harris County (figs. 81, 160)	2015	164	177	39
P001	gps_00_160_171		1994	161	172	175
P007	gps_00_157_174		1999	158	175	170
P011	gps_00_147_147		2000	148	148	168
P018	gps_00_154_165		2000	155	166	159
P044	gps_00_164_164		2007	165	165	88
P056	gps_00_161_151		2007	162	152	91
P066	gps_00_148_156		2011	149	157	52
HPEK	gps_00_178_161	Western Harris County (figs. 82, 161)	2014	179	162	49
MDWD	gps_00_176_173		2013	177	174	69
MRHK	gps_00_172_158		2014	173	159	54
P003	gps_00_170_171		1994	171	172	171
P006	gps_00_171_165		1998	172	166	179
P019	gps_00_168_152		2000	169	153	148
P042	gps_00_180_169		2007	181	170	86
ALEF	gps_00_185_169	Southwestern Harris County (figs. 83, 162)	2014	186	170	57
COH1	gps_00_187_178		2009	188	179	101
P041	gps_00_188_184		2007	189	185	98
TXHS	gps_00_182_177		2012	183	178	77

Table 8.2. Global Positioning System stations used for history matching of the Gulf Coast Land Subsidence and Groundwater-Flow model (GULF model), southeast Texas.—Continued

[GPS, Global Positioning System; The following GPS stations are included on figures 76–77 and table 6 but were not included in the model: ANG6, P005, P043, P075, THSU, and UHL1. The GULF model does not include barrier islands; therefore, GPS stations P026, P043, P049, and TXGA were not included in the model]

GPS station identifier (figs. 76–92; figs. 157–171)	Model GPS observation name[1]	GPS station group (figs. 76–92; figs. 157–171)	GPS installation date	Model row	Model column	Number of observations
LCI1	gps_00_172_187	Central Harris County (figs. 84, 163)	2012	173	188	70
P039	gps_00_190_198		2011	191	199	56
P045	gps_00_164_193		2007	165	194	82
UH01	gps_00_181_197		2012	182	198	76
UHDT	gps_00_176_195		2013	177	196	66
P038	gps_00_189_209	South-central Harris County (figs. 85, 164)	2007	190	210	93
P055	gps_00_173_213		2006	174	214	92
WEPD	gps_00_185_208		2014	186	209	60
P000	gps_00_201_216	Southeastern Harris County (figs. 86, 165)	1996	202	217	177
P027	gps_00_196_229		2002	197	230	144
P037	gps_00_191_221		2007	192	222	85
P024	gps_00_187_226		2002	188	227	148
COH6	gps_00_146_212	Eastern Harris County (figs. 87, 166)	2009	147	213	74
P009	gps_00_146_223		2000	147	224	178
P051	gps_00_158_203		2007	159	204	87
P052	gps_00_166_213		2007	167	214	86
P054	gps_00_172_227		2006	173	228	89
ANG5	gps_00_228_184	Brazoria County (figs. 88, 167)	2003	229	185	177
DWI1	gps_00_260_192		2009	261	193	110
P021[2]	gps_00_201_200		2002	202	201	148
TXAG	gps_00_243_190		2005	244	191	162
P004	gps_00_191_173	Southern Fort Bend County (figs. 89, 168)	1995	192	174	174
P016	gps_00_201_179		2000	202	180	162
P031	gps_00_217_148		2007	218	149	85
P032	gps_00_201_162		2007	202	163	86
P040	gps_00_206_186		2007	207	187	93
P058	gps_00_208_161		2010	209	162	66
P067	gps_00_202_148		2011	203	149	59
TXRS	gps_00_204_152		2011	205	153	91
P010	gps_00_198_153	Northern Fort Bend County (figs. 90, 169)	1999	199	154	169
P029	gps_00_176_151		2007	177	152	86
P030	gps_00_185_143		2007	186	144	90
P057	gps_00_185_160		2009	186	161	73
P059	gps_00_193_159		2010	194	160	58
P062	gps_00_196_136		2011	197	137	56
JGS2	gps_00_145_240	Liberty County (figs. 91, 170)	2012	146	241	78
TXCV	gps_00_113_221		2012	114	222	71
TXLI	gps_00_143_252		2005	144	253	162

Table 8.2. Global Positioning System stations used for history matching of the Gulf Coast Land Subsidence and Groundwater-Flow model (GULF model), southeast Texas.—Continued

[GPS, Global Positioning System; The following GPS stations are included on figures 76–77 and table 6 but were not included in the model: ANG6, P005, P043, P075, THSU, and UHL1. The GULF model does not include barrier islands; therefore, GPS stations P026, P043, P049, and TXGA were not included in the model]

GPS station identifier (figs. 76–92; figs. 157–171)	Model GPS observation name[1]	GPS station group (figs. 76–92; figs. 157–171)	GPS installation date	Model row	Model column	Number of observations
P020	gps_00_202_229	Northern Galveston County (figs. 92, 171)	2002	203	230	142
P022	gps_00_224_229		2002	225	230	144
P023	gps_00_224_239		2002	225	240	154
P034	gps_00_214_227		2010	215	228	101
P035	gps_00_208_223		2006	209	224	91
P036	gps_00_206_236		2007	207	237	89
TXLM	gps_00_217_228		2005	218	229	162
ALVN	gps_00_217_204	--	2012	218	205	58
AULT	gps_00_151_158	--	2015	152	159	40
CFHS	gps_00_159_169	--	2015	160	170	39
COH2	gps_00_191_191	--	2009	192	192	115
COH4	gps_00_174_209	--	2009	175	210	29
COTM	gps_00_217_231	--	2015	218	232	48
DEN1	gps_00_204_205	--	2011	205	206	67
DISD	gps_00_229_159	--	2015	230	160	43
FSFB	gps_00_200_169	--	2014	201	170	56
GSEC	gps_00_128_179	--	2015	129	180	40
KKES	gps_00_167_173	--	2015	168	174	41
KPCD	gps_00_159_141	--	2016	160	142	32
LCBR	gps_00_130_076	--	2010	131	77	67
LGC1	gps_00_144_319	--	2013	145	320	66
ME01	gps_00_194_204	--	2015	195	205	27
MEPD	gps_00_188_207	--	2014	189	208	60
OKEK	gps_00_181_153	--	2014	182	154	52
P014	gps_00_209_168	--	2000	210	169	157
P028	gps_00_177_238	--	2002	178	239	142
P033	gps_00_207_209	--	2006	208	210	99
P050	gps_00_167_244	--	2007	168	245	95
P053	gps_00_160_225	--	2007	161	226	84
P060	gps_00_185_151	--	2012	186	152	49
P061	gps_00_186_136	--	2011	187	137	59
P063	gps_00_205_177	--	2011	206	178	57
P065	gps_00_138_220	--	2012	139	221	51
P072	gps_00_134_206	--	2012	135	207	52
P074	gps_00_179_208	--	2012	180	209	53
P076	gps_00_221_226	--	2012	222	227	46
P077	gps_00_153_148	--	2013	154	149	41
P078	gps_00_179_132	--	2014	180	133	33
P079	gps_00_257_185	--	2014	258	186	50

Table 8.2. Global Positioning System stations used for history matching of the Gulf Coast Land Subsidence and Groundwater-Flow model (GULF model), southeast Texas.—Continued

[GPS, Global Positioning System; The following GPS stations are included on figures 76–77 and table 6 but were not included in the model: ANG6, P005, P043, P075, THSU, and UHL1. The GULF model does not include barrier islands; therefore, GPS stations P026, P043, P049, and TXGA were not included in the model]

GPS station identifier (figs. 76–92; figs. 157–171)	Model GPS observation name[1]	GPS station group (figs. 76–92; figs. 157–171)	GPS installation date	Model row	Model column	Number of observations
P080	gps_00_197_214	--	2014	198	215	50
P081	gps_00_199_214	--	2014	200	215	51
P083	gps_00_232_213	--	2016	233	214	27
P084	gps_00_228_195	--	2016	229	196	26
P085	gps_00_223_204	--	2016	224	205	24
P086	gps_00_233_186	--	2016	234	187	23
P087	gps_00_255_165	--	2016	256	166	23
P088	gps_00_212_188	--	2016	213	189	21
P090	gps_00_182_215	--	2016	183	216	32
P091	gps_00_174_183	--	2016	175	184	30
P092	gps_00_163_182	--	2016	164	183	27
P093	gps_00_215_211	--	2017	216	212	15
P094	gps_00_181_180	--	2017	182	181	20
P095	gps_00_171_202	--	2017	172	203	21
RPFB	gps_00_207_181	--	2014	208	182	52
SESG	gps_00_152_189	--	2014	153	190	53
SHSG	gps_00_144_188	--	2014	145	189	52
SISD	gps_00_177_117	--	2015	178	118	44
SPBH	gps_00_172_180	--	2013	173	181	69
TDAM	gps_00_226_249	--	2013	227	250	66
TMCC	gps_00_183_192	--	2003	184	193	179
TSFT	gps_00_172_184	--	2013	173	185	68
TXAC	gps_00_174_262	--	2011	175	263	95
TXAV	gps_00_216_207	--	2017	217	208	23
TXB2	gps_00_139_308	--	2012	140	309	73
TXB6	gps_00_177_236	--	2012	178	237	70
TXBC	gps_00_261_136	--	2009	262	137	116
TXBH	gps_00_174_139	--	2017	175	140	23
TXBM	gps_00_131_309	--	1996	132	310	167
TXCM	gps_00_183_078	--	2010	184	79	101
TXED	gps_00_265_072	--	2009	266	73	114
TXH2	gps_00_198_289	--	2016	199	290	36
TXHA	gps_00_211_044	--	2009	212	45	116
TXHE	gps_00_139_127	--	2005	140	128	162
TXHU	gps_00_175_188	--	1996	176	189	96
TXHV	gps_00_070_176	--	2015	71	177	43
TXKO	gps_00_105_293	--	2011	106	294	88
TXKY	gps_00_170_150	--	2012	171	151	57
TXLG	gps_00_159_052	--	2010	160	53	98

Table 8.2. Global Positioning System stations used for history matching of the Gulf Coast Land Subsidence and Groundwater-Flow model (GULF model), southeast Texas.—Continued

[GPS, Global Positioning System; The following GPS stations are included on figures 76–77 and table 6 but were not included in the model: ANG6, P005, P043, P075, THSU, and UHL1. The GULF model does not include barrier islands; therefore, GPS stations P026, P043, P049, and TXGA were not included in the model]

GPS station identifier (figs. 76–92; figs. 157–171)	Model GPS observation name[1]	GPS station group (figs. 76–92; figs. 157–171)	GPS installation date	Model row	Model column	Number of observations
TXLQ	gps_00_221_235	--	2013	222	236	72
TXLV	gps_00_067_237	--	2011	68	238	88
TXMG	gps_00_263_137	--	2013	264	138	60
TXNE	gps_00_054_346	--	2013	55	347	70
TXNV	gps_00_108_127	--	2012	109	128	79
TXO1	gps_00_138_351	--	2012	139	352	79
TXOR	gps_00_134_343	--	2011	135	344	87
TXPH	gps_00_158_332	--	2015	159	333	45
TXPT	gps_00_154_331	--	2011	155	332	94
TXRN	gps_00_201_150	--	2015	202	151	46
TXSP	gps_00_178_337	--	2016	179	338	30
TXTG	gps_00_162_201	--	2015	163	202	43
TXWH	gps_00_225_123	--	2010	226	124	104
TXWI	gps_00_171_291	--	2015	172	292	43
TXWN	gps_00_225_125	--	2015	226	126	49
TXWO	gps_00_062_284	--	2013	63	285	68
UHC2	gps_00_218_226	--	2014	219	227	57
UHCL	gps_00_197_220	--	2014	198	221	55
UHCR	gps_00_181_157	--	2014	182	158	56
UHEB	gps_00_203_127	--	2014	204	128	54
UHEP	gps_00_181_199	--	2014	182	200	56
UHF1	gps_00_124_183	--	2014	125	184	56
UHRI	gps_00_181_191	--	2014	182	192	57
UHSL	gps_00_198_167	--	2014	199	168	56
UHWL	gps_00_143_232	--	2014	144	233	57
UTEX	gps_00_174_175	--	2012	175	176	79
WDVW	gps_00_174_179	--	2013	175	180	68

[1]The observation names follow the format gps_[00]_[row]_[column]. These values are zero-based compared to the values in the "Model layer," "Model row," and "Model column," columns, which are one-based.

[2]This GPS station is not shown on figure 167.

Table 8.3. Steady-state (1896) predevelopment water budget by county for the Gulf Coast Land Subsidence and Groundwater-Flow model.

[All units are in acre-feet per year and are net totals. Positive values indicate net inflow, and negative values indicate net outflow. The steady-state water budget is shown as a year-long period for comparability to the transient water budget]

County[1]	Recharge[2]	Drain	River	Lateral flow
Austin	18,841	−11,890	−520	−6,432
Brazoria	24,355	−36,400	−1,252	13,291
Chambers	10,197	−14,030	−259	4,091
Colorado	24,673	−9,317	−2,110	−13,246
Fayette	12,542	−7,714	−1,173	−3,654
Fort Bend	14,964	−12,445	−3,811	1,291
Galveston	5,577	−7,788	0	2,210
Grimes	18,635	−14,728	−428	−3,479
Hardin	23,024	−23,643	−562	1,180
Harris	32,815	−31,402	−2,291	876
Jackson	11,476	−14,051	−2,223	4,798
Jasper	41,719	−38,872	−1,743	−1,105
Jefferson	17,630	−20,579	−291	3,238
Lavaca	21,571	−12,310	−1,862	−7,398
Liberty	21,861	−20,031	−2,322	491
Matagorda	15,227	−21,708	−1,014	7,493
Montgomery	51,732	−44,289	−2,941	−4,502
Newton	47,540	−44,297	−1,301	−1,944
Orange	6,718	−9,226	−563	3,070
Polk	27,505	−21,896	−2,933	−2,676
San Jacinto	52,321	−48,047	−884	−3,390
Tyler	47,817	−42,100	−780	−4,937
Walker	32,851	−28,426	−2,184	−2,240
Waller	17,343	−11,699	−1,555	−4,089
Washington	15,383	−11,292	−734	−3,357
Wharton	16,929	−12,868	−713	−3,348

[1]Only a small percentage of the land area of Brazos, Calhoun, Gonzales, Sabine, and Trinity Counties is included in the model area; therefore, these counties are not included in this table.

[2]The recharge included in this table includes the sum of recharge applied from the two recharge packages documented on report page 208.

Table 8.4. Water budget by county for the Gulf Coast Land Subsidence and Groundwater-Flow model, 2018.

[All units are in acre-feet per year and are net totals. WEL, water derived from well pumping for either irrigation or nonirrigation purposes; STO-SY, water derived from specific yield under unconfined conditions; CSUB-inelastic, water from fine-grained unit inelastic compaction; CSUB-elastic, water from fine-grained unit elastic compaction; CSUB-cgelastic, water from coarse-grained elastic compaction; CSUB-watercomp, contribution of water compressibility. Positive values indicate net inflow, and negative values indicate net outflow]

County[1]	Recharge[2]	Drain	River	WEL (nonirrigation)	WEL (irrigation)	Lateral flow	STO-SY	CSUB-inelastic	CSUB-elastic	CSUB-cgelastic	CSUB-watercomp
Austin	28,004	−10,722	113	−4,424	−1,008	−22,576	8,345	1,932	0	261	76
Brazoria	33,269	−4,567	1,950	−31,915	−619	−8,817	4,342	5,972	6	191	188
Chambers	23,574	−10,921	−53	−8,232	−19	901	−9,137	3,122	29	598	139
Colorado	30,720	−8,158	−1,496	−9,585	−4,162	−22,265	12,483	2,246	4	159	55
Fayette	16,945	−7,571	−1,086	−4,176	−115	−3,527	−664	189	−1	4	3
Fort Bend	16,570	−55	6,019	−78,485	−1,371	22,902	24,282	8,537	15	1,294	293
Galveston	7,780	−1,802	0	−1,515	0	−4,465	−1,576	1,536	−5	10	37
Grimes	29,815	−16,175	−378	−3,533	−119	−8,986	−1,343	486	3	183	48
Hardin	44,643	−17,727	−238	−14,377	−77	−3,251	−14,122	4,861	2	168	119
Harris	54,651	−4,996	−388	−239,791	−704	132,517	35,002	18,435	46	4,258	971
Jackson	11,924	−5,990	−1,020	−2,181	−9,612	6,419	−865	1,016	30	229	48
Jasper	67,514	−38,375	−1,440	−47,512	−18	25,444	−9,203	3,200	12	243	134
Jefferson	35,986	−18,864	−88	−2,105	−53	−6,438	−12,492	3,692	0	275	88
Lavaca	22,869	−11,447	−1,630	−6,554	−1,214	−11,552	8,536	849	11	98	33
Liberty	47,893	−15,103	−1,875	−10,152	−95	−12,861	−15,852	7,156	20	631	238
Matagorda	21,008	−8,729	−126	−8,455	−5,224	1,024	−3,195	3,542	−1	100	57
Montgomery	82,701	−48,758	−2,466	−70,442	−358	−13,098	33,625	15,480	6	2,459	852
Newton	69,414	−44,322	−1,181	−2,121	−7	−11,297	−12,364	1,642	1	177	58
Orange	13,645	−2,645	71	−16,535	−5	9,158	−5,368	1,625	0	27	26
Polk	42,718	−24,488	−2,991	−2,561	−12	−8,462	−6,525	1,911	1	309	100
San Jacinto	100,143	−61,669	−867	−3,419	−35	−5,579	−29,276	680	−1	15	9
Tyler	93,215	−52,416	−712	−4,273	−38	−11,294	−25,764	1,121	3	119	40
Walker	53,993	−34,706	−2,227	−4,936	−8	−6,828	−5,663	302	−1	53	21
Waller	27,198	−11,607	−1,235	−6,292	−1,616	−26,666	15,709	3,657	0	685	168
Washington	23,658	−11,510	−663	−3,822	−35	−5,308	−2,652	282	0	40	10
Wharton	16,143	−278	2,588	−9,549	−20,667	73	5,636	5,519	−11	437	109

[1]Only a small percentage of the land area of Brazos, Calhoun, Gonzales, Sabine, and Trinity Counties is included in the model area; therefore, these counties are not included in this table.

[2]The recharge included in this table includes the sum of recharge applied from the two recharge packages documented on report page 208.

Table 8.5. Steady-state (1896) predevelopment water budget by county and layer for the Gulf Coast Land Subsidence and Groundwater-Flow model.

[All units are in acre-feet per year and are net totals. Positive values indicate net inflow, and negative values indicate net outflow. The steady-state water budget is shown as a year-long period for comparability to the transient water budget. --, not applicable]

County[1]	Hydrogeologic unit (model layer)	Recharge[2]	Drain	River	Lateral flow
Austin	Surficial layer (layer 1)	2,997	−6,484	−520	4,007
	Chicot aquifer (layer 2)	11,200	−3,587	0.0	−7,612
	Evangeline aquifer (layer 3)	4,512	−1,758	0.0	−2,755
	Burkeville confining unit (layer 4)	0.0	0.0	0.0	0.0
	Jasper aquifer (layer 5)	133	−61	0.0	−71
	Catahoula confining unit (layer 6)	0.0	0.0	0.0	0.1
Brazoria	Surficial layer (layer 1)	24,327	−36,217	−1,252	13,142
	Chicot aquifer (layer 2)	28	−182	0	155
	Evangeline aquifer (layer 3)	0.0	0.0	0.0	0.2
	Burkeville confining unit (layer 4)	0.0	0.0	0.0	0.0
	Jasper aquifer (layer 5)	0.0	0.0	0.0	−0.9
	Catahoula confining unit (layer 6)	0.0	0.0	0.0	−4.2
Chambers	Surficial layer (layer 1)	10,145	−13,922	−259	4,036
	Chicot aquifer (layer 2)	52	−108	0.0	56
	Evangeline aquifer (layer 3)	0.0	0.0	0.0	−0.2
	Burkeville confining unit (layer 4)	0.0	0.0	0.0	0.0
	Jasper aquifer (layer 5)	0.0	0.0	0.0	−0.2
	Catahoula confining unit (layer 6)	0.0	0.0	0.0	−0.9
Colorado	Surficial layer (layer 1)	6,089	−6,553	−2,337	2,801
	Chicot aquifer (layer 2)	15,279	−2,335	227	−13,171
	Evangeline aquifer (layer 3)	3,306	−430	0.0	−2,876
	Burkeville confining unit (layer 4)	0.0	0.0	0.0	0.0
	Jasper aquifer (layer 5)	0.0	0.0	0.0	0.1
	Catahoula confining unit (layer 6)	0.0	0.0	0.0	0.2
Fayette	Surficial layer (layer 1)	1,432	−4,606	−1,223	4,397
	Chicot aquifer (layer 2)	--	--	--	--
	Evangeline aquifer (layer 3)	2,411	−404	0	−2,008
	Burkeville confining unit (layer 4)	0.0	0.0	0.0	0.0
	Jasper aquifer (layer 5)	6,274	−1,170	49	−5,153
	Catahoula confining unit (layer 6)	2,425	−1,535	0.0	−890
Fort Bend	Surficial layer (layer 1)	14,269	−12,347	−3,811	1,889
	Chicot aquifer (layer 2)	695	−98	0.0	−597
	Evangeline aquifer (layer 3)	0.0	0.0	0.0	−0.2
	Burkeville confining unit (layer 4)	0.0	0.0	0.0	0.0
	Jasper aquifer (layer 5)	0.0	0.0	0.0	−0.2
	Catahoula confining unit (layer 6)	0.0	0.0	0.0	−0.6
Galveston	Surficial layer (layer 1)	5,577	−7,788	0	2,211
	Chicot aquifer (layer 2)	0.0	0.0	0.0	0.0
	Evangeline aquifer (layer 3)	0.0	0.0	0.0	0.0
	Burkeville confining unit (layer 4)	0.0	0.0	0.0	0.0
	Jasper aquifer (layer 5)	0.0	0.0	0.0	−0.4
	Catahoula confining unit (layer 6)	0.0	0.0	0.0	−0.9

Table 8.5. Steady-state (1896) predevelopment water budget by county and layer for the Gulf Coast Land Subsidence and Groundwater-Flow model.—Continued

[All units are in acre-feet per year and are net totals. Positive values indicate net inflow, and negative values indicate net outflow. The steady-state water budget is shown as a year-long period for comparability to the transient water budget. --, not applicable]

County[1]	Hydrogeologic unit (model layer)	Recharge[2]	Drain	River	Lateral flow
Grimes	Surficial layer (layer 1)	1,393	−3,834	−452	2,893
	Chicot aquifer (layer 2)	5,543	−2,766	0.0	−2,777
	Evangeline aquifer (layer 3)	2,051	−1,793	0.0	−258
	Burkeville confining unit (layer 4)	726	−717	0.0	−10
	Jasper aquifer (layer 5)	6,209	−3,604	0.0	−2,605
	Catahoula confining unit (layer 6)	2,713	−2,014	24	−722
Hardin	Surficial layer (layer 1)	10,956	−15,705	−562	5,311
	Chicot aquifer (layer 2)	12,068	−7,938	0.0	−4,130
	Evangeline aquifer (layer 3)	0.0	0.0	0.0	−0.2
	Burkeville confining unit (layer 4)	0.0	0.0	0.0	0.0
	Jasper aquifer (layer 5)	0.0	0.0	0.0	0.0
	Catahoula confining unit (layer 6)	0.0	0.0	0.0	−0.4
Harris	Surficial layer (layer 1)	26,113	−28,354	−2,291	4,532
	Chicot aquifer (layer 2)	6,702	−3,048	0.0	−3,654
	Evangeline aquifer (layer 3)	0.0	0.0	0.0	−1.0
	Burkeville confining unit (layer 4)	0.0	0.0	0.0	0.0
	Jasper aquifer (layer 5)	0.0	0.0	0.0	−0.2
	Catahoula confining unit (layer 6)	0.0	0.0	0.0	−0.8
Jackson	Surficial layer (layer 1)	10,078	−13,854	−2,289	6,065
	Chicot aquifer (layer 2)	1,398	−197	66	−1,268
	Evangeline aquifer (layer 3)	0.0	0.0	0.0	0.4
	Burkeville confining unit (layer 4)	0.0	0.0	0.0	0.0
	Jasper aquifer (layer 5)	0.0	0.0	0.0	−0.1
	Catahoula confining unit (layer 6)	0.0	0.0	0.0	−0.2
Jasper	Surficial layer (layer 1)	12,386	−20,006	−1,310	8,930
	Chicot aquifer (layer 2)	4,637	−1,342	−63	−3,232
	Evangeline aquifer (layer 3)	2,825	−1,430	0	−1,396
	Burkeville confining unit (layer 4)	3,255	−3,166	0	−88
	Jasper aquifer (layer 5)	4,576	−4,707	0	131
	Catahoula confining unit (layer 6)	14,039	−8,221	−370	−5,449
Jefferson	Surficial layer (layer 1)	17,419	−20,245	−293	3,119
	Chicot aquifer (layer 2)	211	−335	2	121
	Evangeline aquifer (layer 3)	0.0	0.0	0.0	−0.3
	Burkeville confining unit (layer 4)	0.0	0.0	0.0	0.0
	Jasper aquifer (layer 5)	0.0	0.0	0.0	−0.4
	Catahoula confining unit (layer 6)	0.0	0.0	0.0	−1.2
Lavaca	Surficial layer (layer 1)	1,747	−4,960	−1,471	4,684
	Chicot aquifer (layer 2)	8,280	−1,959	−284	−6,037
	Evangeline aquifer (layer 3)	8,750	−4,715	−229	−3,806
	Burkeville confining unit (layer 4)	0.0	0.0	0.0	0.0
	Jasper aquifer (layer 5)	2,705	−677	194	−2,222
	Catahoula confining unit (layer 6)	89	0.0	−73	−16

Table 8.5. Steady-state (1896) predevelopment water budget by county and layer for the Gulf Coast Land Subsidence and Groundwater-Flow model.—Continued

[All units are in acre-feet per year and are net totals. Positive values indicate net inflow, and negative values indicate net outflow. The steady-state water budget is shown as a year-long period for comparability to the transient water budget. --, not applicable]

County[1]	Hydrogeologic unit (model layer)	Recharge[2]	Drain	River	Lateral flow
Liberty	Surficial layer (layer 1)	18,794	−19,195	−2,322	2,723
	Chicot aquifer (layer 2)	3,067	−836	0	−2,232
	Evangeline aquifer (layer 3)	0.0	0.0	0.0	−0.4
	Burkeville confining unit (layer 4)	0.0	0.0	0.0	0.0
	Jasper aquifer (layer 5)	0.0	0.0	0.0	0.2
	Catahoula confining unit (layer 6)	0.0	0.0	0.0	0.3
Matagorda	Surficial layer (layer 1)	15,223	−21,708	−1,014	7,499
	Chicot aquifer (layer 2)	3.8	0.0	0.0	−3.6
	Evangeline aquifer (layer 3)	0.0	0.0	0.0	0.3
	Burkeville confining unit (layer 4)	0.0	0.0	0.0	0.0
	Jasper aquifer (layer 5)	0.0	0.0	0.0	−0.1
	Catahoula confining unit (layer 6)	0.0	0.0	0.0	−2.2
Montgomery	Surficial layer (layer 1)	11,585	−14,909	−2,629	5,953
	Chicot aquifer (layer 2)	28,036	−18,952	0.0	−9,084
	Evangeline aquifer (layer 3)	6,751	−5,946	−312	−493
	Burkeville confining unit (layer 4)	2,763	−2,740	0.0	−23
	Jasper aquifer (layer 5)	2,598	−1,742	0.0	−856
	Catahoula confining unit (layer 6)	0.0	0.0	0.0	0.8
Newton	Surficial layer (layer 1)	13,769	−16,992	−1,294	4,517
	Chicot aquifer (layer 2)	1,464	−656	0.0	−809
	Evangeline aquifer (layer 3)	5,926	−3,697	0.0	−2,230
	Burkeville confining unit (layer 4)	1,758	−1,710	0.0	−48
	Jasper aquifer (layer 5)	15,110	−14,874	0.0	−236
	Catahoula confining unit (layer 6)	9,512	−6,367	−6.9	−3,138
Orange	Surficial layer (layer 1)	6,712	−9,204	−563	3,055
	Chicot aquifer (layer 2)	5.8	−22	0.0	15.6
	Evangeline aquifer (layer 3)	0.0	0.0	0.0	−0.3
	Burkeville confining unit (layer 4)	--	--	--	--
	Jasper aquifer (layer 5)	0.0	0.0	0.0	−0.1
	Catahoula confining unit (layer 6)	0.0	0.0	0.0	−0.3
Polk	Surficial layer (layer 1)	4,412	−5,990	−2,692	4,269
	Chicot aquifer (layer 2)	13,452	−7,380	31	−6,103
	Evangeline aquifer (layer 3)	1,161	−803	0.0	−358
	Burkeville confining unit (layer 4)	7,258	−7,132	−25	−100
	Jasper aquifer (layer 5)	1,223	−576	−6.6	−640
	Catahoula confining unit (layer 6)	0.0	−14	−241	256
San Jacinto	Surficial layer (layer 1)	7,442	−15,324	−872	8,754
	Chicot aquifer (layer 2)	2,823	−1,184	0.0	−1,639
	Evangeline aquifer (layer 3)	10,458	−5,159	0.0	−5,299
	Burkeville confining unit (layer 4)	16,722	−16,385	−3.7	−333
	Jasper aquifer (layer 5)	8,104	−3,370	−8.8	−4,725
	Catahoula confining unit (layer 6)	6,773	−6,624	0.0	−149

Table 8.5. Steady-state (1896) predevelopment water budget by county and layer for the Gulf Coast Land Subsidence and Groundwater-Flow model.—Continued

[All units are in acre-feet per year and are net totals. Positive values indicate net inflow, and negative values indicate net outflow. The steady-state water budget is shown as a year-long period for comparability to the transient water budget. --, not applicable]

County[1]	Hydrogeologic unit (model layer)	Recharge[2]	Drain	River	Lateral flow
Tyler	Surficial layer (layer 1)	5,817	−13,059	−534	7,776
	Chicot aquifer (layer 2)	4,706	−1,784	−99	−2,823
	Evangeline aquifer (layer 3)	12,704	−8,580	0.0	−4,124
	Burkeville confining unit (layer 4)	10,052	−9,839	0.0	−213
	Jasper aquifer (layer 5)	9,065	−5,841	−26	−3,197
	Catahoula confining unit (layer 6)	5,473	−2,997	−121	−2,355
Walker	Surficial layer (layer 1)	3,973	−4,742	−1,471	2,240
	Chicot aquifer (layer 2)	388	−72	0.0	−316
	Evangeline aquifer (layer 3)	1,453	−1,267	0.0	−186
	Burkeville confining unit (layer 4)	13,146	−12,769	−259	−118
	Jasper aquifer (layer 5)	8,380	−5,896	−42	−2,441
	Catahoula confining unit (layer 6)	5,511	−3,679	−412	−1,419
Waller	Surficial layer (layer 1)	2,529	−3,087	−1,555	2,112
	Chicot aquifer (layer 2)	14,814	−8,612	0.0	−6,202
	Evangeline aquifer (layer 3)	0.0	0.0	0.0	0.3
	Burkeville confining unit (layer 4)	0.0	0.0	0.0	0.0
	Jasper aquifer (layer 5)	0.0	0.0	0.0	0.0
	Catahoula confining unit (layer 6)	0.0	0.0	0.0	0.2
Washington	Surficial layer (layer 1)	1,693	−3,286	−768	2,361
	Chicot aquifer (layer 2)	--	--	--	--
	Evangeline aquifer (layer 3)	3,849	−1,689	0	−2,160
	Burkeville confining unit (layer 4)	0.0	0.0	0.0	0.0
	Jasper aquifer (layer 5)	7,664	−3,787	34	−3,910
	Catahoula confining unit (layer 6)	2,177	−2,529	0.0	352
Wharton	Surficial layer (layer 1)	14,909	−12,297	−713	−1,899
	Chicot aquifer (layer 2)	2,020	−571	0.0	−1,449
	Evangeline aquifer (layer 3)	0.0	0.0	0.0	0.1
	Burkeville confining unit (layer 4)	0.0	0.0	0.0	0.0
	Jasper aquifer (layer 5)	0.0	0.0	0.0	0.0
	Catahoula confining unit (layer 6)	0.0	0.0	0.0	−0.1

[1]Only a small percentage of the land area of Brazos, Calhoun, Gonzales, Sabine, and Trinity Counties is included in the model area; therefore, these counties are not included in this table.

[2]The recharge included in this table includes the sum of recharge applied from the two recharge packages documented on report page 208.

Table 8.6. Water budget by county and layer for the Gulf Coast Land Subsidence and Groundwater-Flow model, 2018.

[All units are in acre-feet per year and are net totals. WEL, water derived from well pumping for either irrigation or nonirrigation purposes; STO-SY, water derived from specific yield under unconfined conditions; CSUB-inelastic, water from fine-grained unit inelastic compaction; CSUB-elastic, water from fine-grained unit elastic compaction; CSUB-cgelastic, water from coarse-grained elastic compaction; CSUB-watercomp, contribution of water compressibility. Positive values indicate net inflow, and negative values indicate net outflow; --, not applicable]

County[1]	Hydrogeologic unit (model layer)	Recharge[2]	Drain	River	WEL (nonirrigation)	WEL (irrigation)	Lateral flow	STO-SY	CSUB-inelastic	CSUB-elastic	CSUB-cgelastic	CSUB-watercomp
Austin	Surficial layer (layer 1)	4,230	−5,306	113	0.0	0.0	1,227	−263	0.0	0.0	0.0	−0.1
	Chicot aquifer (layer 2)	16,524	−3,530	0.0	−1,016	−174	−13,961	2,067	90	0.0	−1.7	2.3
	Evangeline aquifer (layer 3)	7,060	−1,820	0.0	−2,594	−775	−9,948	6,471	1,437	0.0	132	38
	Burkeville confining unit (layer 4)	0.0	0.0	0.0	0.0	0.0	−70	0.0	66	0.0	3.1	1.3
	Jasper aquifer (layer 5)	190	−66	0.0	−814	−59	248	71	339	0.1	74	17
	Catahoula confining unit (layer 6)	0.0	0.0	0.0	0.0	0.0	−72	0.0	0.0	0.0	53	18
Brazoria	Surficial layer (layer 1)	33,233	−4,538	1,950	0.0	0.0	−34,977	4,333	0.0	0.0	−1.4	0.1
	Chicot aquifer (layer 2)	35	−29	0.0	−31,614	−619	30,582	9.2	1,559	0.1	45	31
	Evangeline aquifer (layer 3)	0.0	0.0	0.0	−301	0.0	−4,016	0.0	4,229	6.4	−28	109
	Burkeville confining unit (layer 4)	0.0	0.0	0.0	0.0	0.0	−61	0.0	53	0.0	5.5	2.4
	Jasper aquifer (layer 5)	0.0	0.0	0.0	0.0	0.0	−181	0.0	131	0.0	40	11
	Catahoula confining unit (layer 6)	0.0	0.0	0.0	0.0	0.0	−164	0.0	0.0	0.0	129	35
Chambers	Surficial layer (layer 1)	23,452	−10,904	−53	0.0	0.0	−3,322	−9,174	0.0	0.0	1.4	−0.3
	Chicot aquifer (layer 2)	123	−17	0.0	−7,333	−19	5,610	37	1,391	15	134	58
	Evangeline aquifer (layer 3)	0.0	0.0	0.0	−900	0.0	−1,125	0.0	1,594	14	365	52
	Burkeville confining unit (layer 4)	0.0	0.0	0.0	0.0	0.0	−20	0.0	19	0.0	0.5	0.4
	Jasper aquifer (layer 5)	0.0	0.0	0.0	0.0	0.0	−158	0.0	118	0.0	32	7.2
	Catahoula confining unit (layer 6)	0.0	0.0	0.0	0.0	0.0	−85	0.0	0.0	0.0	64	21
Colorado	Surficial layer (layer 1)	7,386	−5,422	−1,725	0	0	61	−300	0	0.0	0.0	−0.1
	Chicot aquifer (layer 2)	18,968	−2,288	229	−3,145	−1,058	−19,354	6,521	129	0.0	−3.6	2.8
	Evangeline aquifer (layer 3)	4,367	−448	0	−6,065	−3,099	−2,830	6,257	1,674	12	96	35
	Burkeville confining unit (layer 4)	0.0	0.0	0.0	0.0	0.0	−120	0.0	112	0.0	5.7	2.0
	Jasper aquifer (layer 5)	0.0	0.0	0.0	−375	−6.1	18	5.1	332	−8.4	28	6.6
	Catahoula confining unit (layer 6)	0.0	0.0	0.0	0.0	0.0	−41	0.0	0.0	0.0	32	10
Fayette	Surficial layer (layer 1)	1,950	−4,433	−1,141	0.0	0.0	4,059	−436	0.0	0.0	0.0	−0.1
	Chicot aquifer (layer 2)	--	--	--	--	--	--	--	--	--	--	--
	Evangeline aquifer (layer 3)	3,119	−405	0.0	−24	0.0	−2,206	−484	0.8	0.0	0.1	−0.1
	Burkeville confining unit (layer 4)	0.0	0.0	0.0	0.0	0.0	−3.5	0.0	3.3	0.0	0.1	0.0
	Jasper aquifer (layer 5)	8,658	−1,182	55	−1,644	−12	−6,236	170	185	−1.0	4.0	2.5
	Catahoula confining unit (layer 6)	3,218	−1,551	0.0	−2,508	−104	860	85	0.0	0.0	0.0	0.5

Table 8.6. Water budget by county and layer for the Gulf Coast Land Subsidence and Groundwater-Flow model, 2018.—Continued

[All units are in acre-feet per year and are net totals. WEL, water derived from well pumping for either irrigation or nonirrigation purposes; STO-SY, water derived from specific yield under unconfined conditions; CSUB-inelastic, water from fine-grained unit inelastic compaction; CSUB-elastic, water from fine-grained unit elastic compaction; CSUB-cgelastic, water from coarse-grained elastic compaction; CSUB-watercomp, contribution of water compressibility. Positive values indicate net inflow, and negative values indicate net outflow; --, not applicable]

County[1]	Hydrogeologic unit (model layer)	Recharge[2]	Drain	River	WEL (nonirrigation)	WEL (irrigation)	Lateral flow	STO-SY	CSUB-inelastic	CSUB-elastic	CSUB-cgelastic	CSUB-watercomp
Fort Bend	Surficial layer (layer 1)	15,769	−55	6,019	0.0	0.0	−39,347	17,619	0.0	0.0	−5.0	1.1
	Chicot aquifer (layer 2)	801	0.0	0.0	−40,736	−1,350	34,168	6,664	483	−56	62	−37
	Evangeline aquifer (layer 3)	0.0	0.0	0.0	−37,689	−21	28,702	0.0	7,633	71	1,039	265
	Burkeville confining unit (layer 4)	0.0	0.0	0.0	0.0	0.0	−135	0.0	124	0.0	7.0	4.1
	Jasper aquifer (layer 5)	0.0	0.0	0.0	−52	0.0	−266	0.0	296	−0.2	11	11
	Catahoula confining unit (layer 6)	0.0	0.0	0.0	−8.2	0.0	−219	0.0	0.0	0.0	180	48
Galveston	Surficial layer (layer 1)	7,780	−1,802	0	0.0	0.0	−4,392	−1,585	0.0	0.0	0.2	0.0
	Chicot aquifer (layer 2)	0.0	0.0	0.0	−1,515	0.0	1,042	9.0	469	−0.8	−9.4	4.8
	Evangeline aquifer (layer 3)	0.0	0.0	0.0	0.0	0.0	−964	0.0	997	−4.4	−42	14
	Burkeville confining unit (layer 4)	0.0	0.0	0.0	0.0	0.0	−19	0.0	18	0.0	0.4	0.4
	Jasper aquifer (layer 5)	0.0	0.0	0.0	0.0	0.0	−77	0.0	52	0.0	22	4.2
	Catahoula confining unit (layer 6)	0.0	0.0	0.0	0.0	0.0	−53	0.0	0.0	0.0	40	14
Grimes	Surficial layer (layer 1)	2,170	−3,750	−394	0.0	0.0	2,632	−658	0.0	0.0	0.1	−0.2
	Chicot aquifer (layer 2)	8,931	−3,337	0.0	0.0	0.0	−2,939	−2,656	0.3	0.0	0.5	−0.9
	Evangeline aquifer (layer 3)	3,286	−1,937	0.0	−409	−14	−3,874	2,900	57	0.0	−12	2.1
	Burkeville confining unit (layer 4)	1,167	−869	0.0	0.0	0.0	−23	−289	12	0.0	1.4	0.3
	Jasper aquifer (layer 5)	9,853	−4,024	0.0	−2,149	−85	−3,798	−309	417	3	76	16
	Catahoula confining unit (layer 6)	4,407	−2,258	16	−975	−20	−984	−332	0.0	0.0	117	30
Hardin	Surficial layer (layer 1)	21,486	−11,612	−238	0.0	0.0	−1,963	−7,674	0.0	0.0	1.1	−0.5
	Chicot aquifer (layer 2)	23,157	−6,115	0.0	−13,745	−77	730	−6,448	2,457	0.9	−10	51
	Evangeline aquifer (layer 3)	0.0	0.0	0.0	−633	0.0	−1,627	0.0	2,136	0.8	82	41
	Burkeville confining unit (layer 4)	0.0	0.0	0.0	0.0	0.0	−37	0.0	35	0.0	1.0	0.9
	Jasper aquifer (layer 5)	0.0	0.0	0.0	0.0	0.0	−278	0.0	233	0.0	36	9.1
	Catahoula confining unit (layer 6)	0.0	0.0	0.0	0.0	0.0	−75	0.0	0.0	0.0	57	18
Harris	Surficial layer (layer 1)	44,468	−4,366	−388	0.0	0.0	−42,950	3,237	0.0	0.0	−1.9	0.3
	Chicot aquifer (layer 2)	10,182	−630	0.0	−115,749	−563	73,715	31,764	1,398	−116	0.3	−0.3
	Evangeline aquifer (layer 3)	0.0	0.0	0.0	−117,650	−141	103,151	0.0	11,429	162	2,615	434
	Burkeville confining unit (layer 4)	0.0	0.0	0.0	0.0	0.0	−820	0.0	770	0.0	27	23
	Jasper aquifer (layer 5)	0.0	0.0	0.0	−6,391	0.0	808	0.0	4,838	0.2	544	200
	Catahoula confining unit (layer 6)	0.0	0.0	0.0	−0.2	0.0	−1,387	0.0	0.0	0.0	1,073	314

Table 8.6. Water budget by county and layer for the Gulf Coast Land Subsidence and Groundwater-Flow model, 2018.—Continued

[All units are in acre-feet per year and are net totals. WEL, water derived from well pumping for either irrigation or nonirrigation purposes; STO-SY, water derived from specific yield under unconfined conditions; CSUB-inelastic, water from fine-grained unit inelastic compaction; CSUB-elastic, water from fine-grained unit elastic compaction; CSUB-cgelastic, water from coarse-grained elastic compaction; CSUB-watercomp, contribution of water compressibility. Positive values indicate net inflow, and negative values indicate net outflow; --, not applicable]

County[1]	Hydrogeologic unit (model layer)	Recharge[2]	Drain	River	WEL (nonirrigation)	WEL (irrigation)	Lateral flow	STO-SY	CSUB-inelastic	CSUB-elastic	CSUB-cgelastic	CSUB-watercomp
Jackson	Surficial layer (layer 1)	10,678	−5,927	−1,105	0.0	0.0	−3,594	−51	0.0	0.0	−0.3	0.0
	Chicot aquifer (layer 2)	1,246	−63	85	−1,576	−5,362	6,423	−814	10	4.4	38	6.4
	Evangeline aquifer (layer 3)	0.0	0.0	0.0	−605	−3,984	3,430	0.0	936	25	164	35
	Burkeville confining unit (layer 4)	0.0	0.0	0.0	0.0	0.0	−34	0.0	29	0.0	3.6	1.1
	Jasper aquifer (layer 5)	0.0	0.0	0.0	0.0	0.0	−48	0.0	41	0.9	4.3	1.7
	Catahoula confining unit (layer 6)	0.0	0.0	0.0	0.0	−266	242	0.0	0.0	0.0	19	4.6
Jasper	Surficial layer (layer 1)	22,456	−16,649	−999	0.0	0.0	2,144	−6,953	0.0	0.0	1.2	−0.7
	Chicot aquifer (layer 2)	7,740	−1,265	−56	−24,635	−5.7	15,993	872	1,337	6	−42	56
	Evangeline aquifer (layer 3)	4,650	−1,721	0.0	−14,199	−0.8	10,073	−463	1,437	5	180	39
	Burkeville confining unit (layer 4)	5,258	−4,143	0.0	0.0	0.0	−133	−1,027	43	0.0	1.3	0.6
	Jasper aquifer (layer 5)	7,046	−5,466	0.0	−811	0.0	−214	−980	383	1.6	31	9.0
	Catahoula confining unit (layer 6)	20,364	−9,131	−386	−7,867	−11	−2,420	−652	0.0	0.0	72	31
Jefferson	Surficial layer (layer 1)	35,609	−18,657	−96	0.0	0.0	−4,493	−12,364	0.0	0.0	1.7	−0.3
	Chicot aquifer (layer 2)	377	−208	7.5	−2,105	−53	133	−127	1,880	0.0	65	31
	Evangeline aquifer (layer 3)	0.0	0.0	0.0	0.0	0.0	−1,958	0	1,751	0.0	162	46
	Burkeville confining unit (layer 4)	0.0	0.0	0.0	0.0	0.0	−25	0	23	0.0	1.1	0.7
	Jasper aquifer (layer 5)	0.0	0.0	0.0	0.0	0.0	−62	0	38	0.0	20	3.9
	Catahoula confining unit (layer 6)	0.0	0.0	0.0	0.0	0.0	−32	0	0.0	0.0	26	6.3
Lavaca	Surficial layer (layer 1)	1,706	−4,452	−1,350	0.0	0.0	3,874	222	0.0	0.0	−0.1	0.0
	Chicot aquifer (layer 2)	8,334	−1,746	−214	−623	−1.2	−8,167	2,385	33	0.0	−0.9	0.6
	Evangeline aquifer (layer 3)	9,841	−4,668	−206	−2,408	−998	−5,413	3,369	430	11	30	12
	Burkeville confining unit (layer 4)	0.0	0.0	0.0	0.0	0.0	−42	0	39	0.0	2.5	0.8
	Jasper aquifer (layer 5)	2,914	−580	214	−1,659	−134	−3,111	1,958	346	0.5	40	11
	Catahoula confining unit (layer 6)	74	0.0	−73	−1,864	−80	1,307	601	0.0	0.0	27	8.9
Liberty	Surficial layer (layer 1)	42,078	−14,429	−1,875	0.0	0.0	−7,478	−18,297	0	0.0	2.7	−1.3
	Chicot aquifer (layer 2)	5,815	−674	0.0	−8,086	−94	−1,952	2,446	2,452	8.6	32	52
	Evangeline aquifer (layer 3)	0.0	0.0	0.0	−1,314	−1.3	−2,401	0.0	3,464	8.2	186	59
	Burkeville confining unit (layer 4)	0.0	0.0	0.0	0.0	0.0	−94	0.0	90	0.0	2.5	1.7
	Jasper aquifer (layer 5)	0.0	0.0	0.0	−752	0.0	−548	0.0	1,150	3.5	110	36
	Catahoula confining unit (layer 6)	0.0	0.0	0.0	0.0	0.0	−388	0.0	0.0	0.0	297	91

Table 8.6. Water budget by county and layer for the Gulf Coast Land Subsidence and Groundwater-Flow model, 2018.—Continued

[All units are in acre-feet per year and are net totals. WEL, water derived from well pumping for either irrigation or nonirrigation purposes; STO-SY, water derived from specific yield under unconfined conditions; CSUB-inelastic, water from fine-grained unit inelastic compaction; CSUB-elastic, water from fine-grained unit elastic compaction; CSUB-cgelastic, water from coarse-grained elastic compaction; CSUB-watercomp, contribution of water compressibility. Positive values indicate net inflow, and negative values indicate net outflow; --, not applicable]

County[1]	Hydrogeologic unit (model layer)	Recharge[2]	Drain	River	WEL (nonirrigation)	WEL (irrigation)	Lateral flow	STO-SY	CSUB-inelastic	CSUB-elastic	CSUB-cgelastic	CSUB-watercomp
Matagorda	Surficial layer (layer 1)	20,999	−8,729	−126	0.0	0.0	−9,234	−2,911	0.0	0.0	0.4	−0.1
	Chicot aquifer (layer 2)	8.7	0.0	0.0	−8,455	−5,103	12,835	−284	1,012	−0.7	−16	3.2
	Evangeline aquifer (layer 3)	0.0	0.0	0.0	0.0	−121	−2,498	0.0	2,469	0.0	101	50
	Burkeville confining unit (layer 4)	0.0	0.0	0.0	0.0	0.0	−34	0.0	31	0.0	2.0	0.9
	Jasper aquifer (layer 5)	0.0	0.0	0.0	0.0	0.0	−33	0.0	30	0.1	2.4	0.9
	Catahoula confining unit (layer 6)	0.0	0.0	0.0	0.0	0.0	−12	0.0	0.0	0.0	10	2.0
Montgomery	Surficial layer (layer 1)	18,532	−14,398	−2,145	0.0	0.0	2,978	−4,967	0.0	0.0	0.7	−0.8
	Chicot aquifer (layer 2)	44,250	−20,977	0.0	−18,860	−201	−30,841	25,735	912	0.0	−46	28
	Evangeline aquifer (layer 3)	11,194	−7,352	−321	−24,905	−116	3,333	11,900	5,849	2.2	284	132
	Burkeville confining unit (layer 4)	4,570	−3,791	0	0.0	0.0	−585	−756	518	0.0	28	15
	Jasper aquifer (layer 5)	4,154	−2,241	0	−26,476	−41	13,436	1,694	8,202	3.7	931	336
	Catahoula confining unit (layer 6)	0.0	0.0	0.0	−201	0.0	−1,419	19	0.0	0.0	1,260	342
Newton	Surficial layer (layer 1)	23,243	−14,970	−1,171	0.0	0.0	−69	−7,033	0.0	0.0	1.0	−0.6
	Chicot aquifer (layer 2)	2,407	−562	0.0	−757	−6.3	−2,682	1,007	574	0.0	4	14
	Evangeline aquifer (layer 3)	9,106	−4,199	0.0	−318	−1.1	−4,010	−1,474	792	0.0	85	19
	Burkeville confining unit (layer 4)	2,532	−1,932	0.0	0.0	0.0	−81	−553	31	0.0	2.2	0.8
	Jasper aquifer (layer 5)	19,776	−15,813	0.0	−364	0.0	−446	−3,428	244	0.7	23	6.4
	Catahoula confining unit (layer 6)	12,350	−6,847	−9.5	−683	0.0	−4,009	−883	0.0	0.0	61.9	20
Orange	Surficial layer (layer 1)	13,632	−2,645	71	0.0	0.0	−5,697	−5,361	0.0	0.0	0.8	−0.1
	Chicot aquifer (layer 2)	13	0.0	0.0	−16,535	−5	15,745	−6.6	782	0.1	−1.4	7.6
	Evangeline aquifer (layer 3)	0.0	0.0	0.0	0.0	0.0	−826	0.0	801	0.3	10	14
	Burkeville confining unit (layer 4)	0.0	0.0	0.0	0.0	0.0	−24	0.0	22	0.0	1.4	0.7
	Jasper aquifer (layer 5)	0.0	0.0	0.0	0.0	0.0	−29	0.0	20	0.0	7.5	1.5
	Catahoula confining unit (layer 6)	0.0	0.0	0.0	0.0	0.0	−11	0.0	0.0	0.0	8.7	2.1
Polk	Surficial layer (layer 1)	7,510	−6,196	−2,749	0.0	0.0	3,995	−2,560	0.0	0.0	0.5	−0.4
	Chicot aquifer (layer 2)	20,861	−8,341	25	−648	−5.2	−9,209	−2,769	85	0.0	−0.6	0.9
	Evangeline aquifer (layer 3)	1,830	−970	0.0	−387	−5.7	−1,133	265	380	0.0	15	5.5
	Burkeville confining unit (layer 4)	10,570	−8,319	−26	0.0	0.0	−137	−2,105	27	0.0	−8.6	−1.2
	Jasper aquifer (layer 5)	1,947	−648	−4.4	−1,398	−1.5	−2,051	575	1,418	0.6	122	39
	Catahoula confining unit (layer 6)	0.0	−13	−236	−128	0.0	72	68	0.0	0.0	181	57

Table 8.6. Water budget by county and layer for the Gulf Coast Land Subsidence and Groundwater-Flow model, 2018.—Continued

[All units are in acre-feet per year and are net totals. WEL, water derived from well pumping for either irrigation or nonirrigation purposes; STO-SY, water derived from specific yield under unconfined conditions; CSUB-inelastic, water from fine-grained unit inelastic compaction; CSUB-elastic, water from fine-grained unit elastic compaction; CSUB-cgelastic, water from coarse-grained elastic compaction; CSUB-watercomp, contribution of water compressibility. Positive values indicate net inflow, and negative values indicate net outflow; --, not applicable]

County[1]	Hydrogeologic unit (model layer)	Recharge[2]	Drain	River	WEL (nonirrigation)	WEL (irrigation)	Lateral flow	STO-SY	CSUB-inelastic	CSUB-elastic	CSUB-cgelastic	CSUB-watercomp
San Jacinto	Surficial layer (layer 1)	14,897	−16,905	−858	0.0	0.0	8,705	−5,839	0.0	0.0	1.2	−1.0
	Chicot aquifer (layer 2)	5,652	−1,394	0.0	−332	−0.2	−3,140	−840	54	0.0	−0.7	0.7
	Evangeline aquifer (layer 3)	20,529	−7,115	0.0	−546	−13	−5,959	−7,011	113	0.0	2.7	−0.3
	Burkeville confining unit (layer 4)	31,922	−24,105	−3.5	0.0	0.0	−412	−7,301	6.0	−0.1	−88	−18
	Jasper aquifer (layer 5)	14,906	−4,265	−5.6	−1,034	−22	−5,567	−4,574	507	−0.5	45	10
	Catahoula confining unit (layer 6)	12,237	−7,886	0.0	−1,506	0.0	794	−3,711	0.0	0.0	55	17
Tyler	Surficial layer (layer 1)	11,102	−13,341	−473	0.0	0.0	6,549	−3,837	0.0	0.0	0.7	−0.5
	Chicot aquifer (layer 2)	8,768	−1,906	−86	−333	0.0	−6,937	206	281	0.0	3.2	4.7
	Evangeline aquifer (layer 3)	25,474	−11,039	0.0	−1,006	−35	−5,089	−8,670	355	0.0	7.9	2.2
	Burkeville confining unit (layer 4)	20,498	−15,062	0.0	0.0	0.0	−228	−5,218	15	0.0	−2.6	−2.1
	Jasper aquifer (layer 5)	17,470	−7,393	−23	−1,725	−0.6	−2,986	−5,871	470	2.9	46	10
	Catahoula confining unit (layer 6)	9,903	−3,676	−129	−1,209	−1.9	−2,603	−2,373	0.0	0.0	64	25
Walker	Surficial layer (layer 1)	6,738	−4,932	−1,468	0.0	0.0	1,931	−2,270	0.0	0.0	0.6	−0.6
	Chicot aquifer (layer 2)	600	−99	0.0	0.0	0.0	−324	−177	0.0	0.0	0.1	−0.1
	Evangeline aquifer (layer 3)	2,396	−1,533	0.0	−103	−1.1	−244	−516	1.4	0.0	−0.2	−0.1
	Burkeville confining unit (layer 4)	21,035	−16,771	−284	0.0	0.0	−129	−3,841	6.8	0.0	−13	−3.1
	Jasper aquifer (layer 5)	13,912	−7,293	−49	−1,476	−6.6	−7,046	1,641	294	−0.6	16	8.5
	Catahoula confining unit (layer 6)	9,312	−4,078	−427	−3,357	0.0	−1,016	−499	0.0	0	49	16
Waller	Surficial layer (layer 1)	3,931	−2,368	−1,235	0.0	0.0	337	−665	0.0	0.0	0.1	−0.2
	Chicot aquifer (layer 2)	23,267	−9,239	0.0	−2,212	−475	−22,049	10,483	232	0.0	−14	6.8
	Evangeline aquifer (layer 3)	0.0	0.0	0.0	−3,792	−1,142	−3,957	5,891	2,611	0.1	325	63
	Burkeville confining unit (layer 4)	0.0	0.0	0.0	0.0	0.0	−74	0.0	68	0.0	3.7	1.8
	Jasper aquifer (layer 5)	0.0	0.0	0.0	−288	0.0	−671	0.0	746	0.2	173	40
	Catahoula confining unit (layer 6)	0.0	0.0	0.0	0.0	0.0	−253	0.0	0.0	0.0	196	57
Washington	Surficial layer (layer 1)	2,579	−3,239	−701	0.0	0.0	2,095	−735	0.0	0.0	0.2	−0.2
	Chicot aquifer (layer 2)	--	--	--	--	--	--	--	--	--	--	--
	Evangeline aquifer (layer 3)	6,356	−1,780	0.0	−739	−13	−3,604	−343	117	0.0	5.2	1.6
	Burkeville confining unit (layer 4)	0.0	0.0	0.0	0.0	0.0	−11	0.0	9.7	0.0	0.7	0.2
	Jasper aquifer (layer 5)	11,780	−3,943	37	−1,788	−12	−4,715	−1,544	156	0.4	24	5.0
	Catahoula confining unit (layer 6)	2,944	−2,549	0.0	−1,294	−10	926	−30	0.0	0.0	10	3.8

Table 8.6. Water budget by county and layer for the Gulf Coast Land Subsidence and Groundwater-Flow model, 2018.—Continued

[All units are in acre-feet per year and are net totals. WEL, water derived from well pumping for either irrigation or nonirrigation purposes; STO-SY, water derived from specific yield under unconfined conditions; CSUB-inelastic, water from fine-grained unit inelastic compaction; CSUB-elastic, water from fine-grained unit elastic compaction; CSUB-cgelastic, water from coarse-grained elastic compaction; CSUB-watercomp, contribution of water compressibility. Positive values indicate net inflow, and negative values indicate net outflow; --, not applicable]

County[1]	Hydrogeologic unit (model layer)	Recharge[2]	Drain	River	WEL (nonirrigation)	WEL (irrigation)	Lateral flow	STO-SY	CSUB-inelastic	CSUB-elastic	CSUB-cgelastic	CSUB-watercomp
Wharton	Surficial layer (layer 1)	14,355	−278	2,588	0.0	0.0	−26,318	9,654	0.0	0.0	−2.5	0.7
	Chicot aquifer (layer 2)	1,788	0.0	0.0	−7,446	−17,425	27,090	−4,019	39	−25	8.6	−11
	Evangeline aquifer (layer 3)	0.0	0.0	0.0	−2,103	−3,242	−466	0.0	5,304	14	386	107
	Burkeville confining unit (layer 4)	0.0	0.0	0.0	0.0	0.0	−70	0.0	64	0.0	4.5	1.7
	Jasper aquifer (layer 5)	0.0	0.0	0.0	0.0	0.0	−129	0.0	112	0.1	13	3.8
	Catahoula confining unit (layer 6)	0.0	0.0	0.0	0.0	0.0	−34	0.0	0.0	0.0	27	6.6

[1]Only a small percentage of the land area of Brazos, Calhoun, Gonzales, Sabine, and Trinity counties is included in the model area; therefore, these counties are not included in this table.

[2]The recharge included in this table includes the sum of recharge applied from the two recharge packages documented on report page 208.

Table 8.7. Steady-state (1896) predevelopment water budget by district for the Gulf Coast Land Subsidence and Groundwater-Flow model.

[All units are in acre-feet per year and are net totals. GCD, Groundwater Conservation District. Positive values indicate net inflow, and negative values indicate net outflow. The steady-state water budget is shown as a year-long period for comparability to the transient water budget]

District[1]	Recharge[2]	Drain	River	Lateral flow
Bluebonnet GCD	87,693	−66,743	−4,686	−16,264
Brazoria County GCD	24,355	−36,400	−1,252	13,291
Coastal Bend GCD	16,929	−12,868	−713	−3,348
Coastal Plains GCD	15,227	−21,708	−1,014	7,493
Colorado County GCD	24,651	−9,317	−2,110	−13,224
Fayette County GCD	12,562	−7,714	−1,173	−3,674
Fort Bend Subsidence District	14,964	−12,445	−3,811	1,291
Harris Galveston Subsidence District	38,364	−39,215	−2,291	3,138
Lone Star GCD	51,732	−44,289	−2,941	−4,502
Lower Trinity GCD	79,827	−69,942	−3,817	−6,066
Southeast Texas GCD	160,099	−148,912	−4,386	−6,806
Texana GCD	11,483	−14,051	−2,223	4,791

[1]Only a small percentage of the land area of Brazos, Calhoun, Gonzales, Sabine, and Trinity Counties is included in the model area; therefore, the GCDs representing Brazos, Calhoun, Gonzales, Sabine, and Trinity Counties are not included in this table. Slight differences are present in some budget terms between this table and the sum of the budget terms for counties comprising a GCD.

[2]The recharge included in this table includes the sum of recharge applied from the two recharge packages documented on report page 208.

Table 8.8. Water budget by district for the Gulf Coast Land Subsidence and Groundwater-Flow model, 2018.

[All units are in acre-feet per year and are net totals. WEL, water derived from well pumping for either irrigation or nonirrigation purposes; STO-SY, water derived from specific yield under unconfined conditions; CSUB-inelastic, water from fine-grained unit inelastic compaction; CSUB-elastic, water from fine-grained unit elastic compaction; CSUB-cgelastic, water from coarse-grained elastic compaction; CSUB-watercomp, contribution of water compressibility; GCD, Groundwater Conservation District. Positive values indicate net inflow, and negative values indicate net outflow]

District[1]	Recharge[2]	Drain	River	WEL (nonirrigation)	WEL (irrigation)	Lateral flow	STO-SY	CSUB-inelastic	CSUB-elastic	CSUB-cgelastic	CSUB-watercomp
Bluebonnet GCD	139,047	−73,210	−3,727	−19,186	−2,751	−65,101	17,051	6,381	3	1,181	313
Brazoria County GCD	33,269	−4,567	1,950	−31,915	−619	−8,817	4,342	5,972	6	191	188
Coastal Bend GCD	16,143	−278	2,588	−9,549	−20,667	73	5,636	5,519	−11	437	109
Coastal Plains GCD	21,008	−8,729	−126	−8,455	−5,224	1,024	−3,195	3,542	−1	100	57
Colorado County GCD	30,695	−8,158	−1,496	−9,584	−4,162	−22,235	12,477	2,246	4	159	55
Fayette County GCD	16,973	−7,571	−1,086	−4,177	−115	−3,555	−664	189	−1	4	3
Fort Bend Subsidence District	16,570	−55	6,019	−78,485	−1,371	22,902	24,282	8,537	15	1,294	293
Harris Galveston Subsidence District	62,386	−6,824	−388	−241,305	−704	128,130	33,426	19,964	41	4,267	1,008
Lone Star GCD	82,701	−48,758	−2,466	−70,442	−358	−13,098	33,625	15,480	6	2,459	852
Lower Trinity GCD	142,861	−86,157	−3,858	−5,980	−48	−14,041	−35,802	2,591	0	324	109
Southeast Texas GCD	274,785	−152,840	−3,570	−68,284	−140	−398	−61,453	10,823	17	708	352
Texana GCD	11,929	−5,990	−1,020	−2,181	−9,612	6,407	−859	1,017	30	229	48

[1]Only a small percentage of the land area of Brazos, Calhoun, Gonzales, Sabine, and Trinity Counties is included in the model area; therefore, the GCDs representing Brazos, Calhoun, Gonzales, Sabine, and Trinity Counties are not included in this table. Slight differences are present in some budget terms between this table and the sum of the budget terms for counties comprising a GCD.

[2]The recharge included in this table includes the sum of recharge applied from the two recharge packages documented on report page 208.

For more information about this publication, contact
Director, Oklahoma-Texas Water Science Center
U.S. Geological Survey
1505 Ferguson Lane
Austin, TX 78754-4501

For additional information, visit
https://www.usgs.gov/centers/ot-water

Publishing support provided by
Lafayette Publishing Service Center

ISSN 2330-7102 (online)
https://doi.org/10.3133/pp1877